Experience mineralogy at its best in South Africa at IMA 2014

21st General Meeting of IMA
South Africa 2014

1 - 5 September 2014 - Sandton Convention Centre, Johannesburg, Gauteng, South Africa

SOUTH AFRICA ima 2014

DELVING DEEPER
MINERALS AS MINES OF INFORMATION

Hosted by

MINSA
Mineralogical Association of South Africa
A division of the GSSA

GSSA
Geological Society of South Africa

ABSTRACT VOLUME

www.ima2014.co.za

21st meeting of the International Mineralogical Association

1-5 September 2014

Johannesburg, South Africa

ABSTRACTS

Edited by:

Deshenthree Chetty (Chief Editor)
Lesley Andrews
Johan de Villiers
Roger Dixon
Paul Nex
Wolf Uwe Reimold
Jill Richards
Bertus Smith
Craig Smith
Sabine Verryn
Fanus Viljoen

A joint publication of the Geological Society of South Africa and the Mineralogical Association of South Africa

ISBN: 978-0-620-60082-8

Abstracts for the IMA2014 conference were collated into 58 topical sessions convened after proposals for sessions were approved. All abstracts were subjected to a review process by convenors, prior to editing and collation of the abstract volume. The sessions were grouped into ten themes. Themes, sessions, codes and convenors are listed as follows:

Code	Session	Convenors
	CLAY SCIENCE	
CS1	General Session: Clay science	Birgit Schampera, Rosa Torres, Sabine Verryn, Jean-Louis Robert, Maguy Jaber
CS2	Scientific and industrial applications of green rust related compounds and layered double hydroxides	Andrew Christy, Jean-Marie Genin, Stuart Mills
CS3	Structural characterisation of lamellar compounds	Bruno Lansen, Eric Ferrage, Douglas McCarty
	DEEP EARTH	
DE1	Cratons and diamonds	Thomas Stachel, Graham Pearson, Fanus Viljoen
DE2	Fluid in the Earth	Pei Ni, Ronald J. Bakker (IMA-WGIM)
DE3	Mineralogy in the Deep Earth	Catherine McCammon, Toru Inoue, Paola Comodi, Eiji Ohtani, Fanus Viljoen (IMA-CPM)
DE4	Theoretical and Compositional mineral physics for Deep Earth	Taku Tsuchiya, Razvan Caracas, Jun Tsuchiya (IMA-CPM)
DE5	Water and hydrous phases in the Earth's interior: geological, geophysical and geodynamic implications	Istvan Kovacs, Jannick Ingrin, Qunke Xia
	ECONOMIC GEOLOGY/MINERALOGY, APPLIED MINERALOGY	
EG1	Critical metals and Rare earth elements	Frances Wall, Kathryn Moore, Judith Kinnaird, Kathryn Goodenough (Critical Metals Alliance; Applied Mineralogy Group, Mineralogical Society of Great Britain and Ireland)
EG2	General Session: Applied Mineralogy	Hans-Joachim Kleebe, Lesley Andrews
EG3	General Session: Economic Geology/Mineralogy	Paul Nex, Judith Kinnaird, Brian Hoal, Thomas Oberthür, Frank Melcher (SEG)
EG4	Gold deposits	Lynnette Greyling, Hartwig Frimmel (SGA)
EG5	Non-sulphide Pb-Zn deposits	Maria Boni, Suzanne Paradis
EG6	Platinum group minerals (PGMs) from the mantle to the crust	Federica Zaccarini, Maryse Ohnenstetter, Anna Vymazalova (IMA-COM, SGA)
EG7	Process Mineralogy and Geometallurgy	Dee Bradshaw, Megan Becker (IMA-CAM)
EG8	Sediment-hosted ore deposits	Bertus Smith, Lynnette Greyling, Jens Gutzmer
EG9	Sulphide mineralogy and Geochemistry	Nigel Cook, Martin Reich, Joël Brugger (IAGOD, IMA-COM)
EG10	Zeolites and porous materials	Maria Giovanna Vezzalini, Thomas Armbruster, Rosella Arletti

ENVIRONMENTAL MINERALOGY/GEOCHEMISTRY

EM1	Applied Geochemistry and Geomicrobiology for the Remediation of inorganic pollutants	Manuel A. Caraballo, Esta van Heerden, Harish Veeramani, Julio Castillo
EM2	CO_2 storage: Mineralogical Implications	Jordi Cama, Linda Luquot, Sebastian Fischer
EM3	Environmental mineralogy and geochemistry of mine waste	Juraj Majzlan, Karen Hudson-Edwards, Dogan Paktunc
EM4	Environmental Mineralogy and the Carbon Cycle	Ben Gilbert, Glenn Waychunas
EM5	General Session: Environmental Mineralogy and Geochemistry	Christian Mavris, Mihály Pósfai, Theophilus Davies, Benjamin Mapani, Hassina Mouri, Tsutomo Sato
EM6	Inorganic fibres, biosphere, and risk assessment	Elena Belluso, Alessandro Gualtieri, Mickey Gunter, Caterina Rinaudo
EM7	Mineralogy on Radioactive waste disposal, decontamination of radioactively contaminated sites and decommissioning of nuclear power plants	Tsutomo Sato, Anhuai Lu, Jordi Cama (IMA-WGEMG)
EM8	Minerals and Microbes	Anhuai Lu, Hailiang Dong
EM9	Role of Mineralogical Sciences in Sustainable Cement-based materials	Gilberto Artioli, Joseph Biernacki, Luca Valentini

GEOCHEMISTRY AND PETROLOGY

GP1	Africa-A Mecca of kimberlite, alkaline rock and carbonatite geology	Frances Wall, Craig Smith
GP2	Aqueous and carbonic fluids in ultramafic rocks: From vein precipitation to channeled and pervasive wall-rock reaction	Walter Maresch, Hans-Peter Schertl, George Harlow
GP3	Dating Metamorphic Processes: Promise and Pitfalls of Geochronology	Hao Cheng, Tatsuki Tsujimori, Patrick O'Brien, Hafiz UrRehman
GP4	General Session: Geochemistry and Petrology	Paul Nex, Jean-Louis Robert
GP5	Geologic fluids in the deep crust and upper mantle	Dirk van Reenen, Oleg Safonov, Daniel Harlov (IMA-WGME)
GP6	Magma differentiation and ore formation processes	Ilya Veksler, Rais Latypov, Jakob Keidling
GP7	Magma mixing - from macro to micro scale	Ewa Slaby, Diego Perugini
GP8	Magmas and Melts under extreme conditions	Grant Henderson, Daniel Neuville, Roberto Moretti (IMA-CPM)
GP9	Mineral Inclusions - their genesis and fate	Alexander Proyer, Shah Wali Faryad, Tzen-Fu Yui
GP10	Pegmatites, and pegmatite mineralogy	Paul Nex, Robert Martin, William 'Skip' Simmons
GP11	Petrologic Pathfinders: Trace elements and stable isotopes in tourmaline, rutile and other accessory minerals	Robert Trumbull, Horst Marschall
GP12	The Geology of Gems and their Geographical Origin	Gaston Giuliani, Lee Groat, Daniel Ichangi (IMA-CGM)
GP13	Timing and genesis of mineralisations: the isotope record	Axel Gerdes, Dirk Frei

METHODS AND APPLICATIONS

MA1	Computed tomography – pushing frontiers in imaging of the third and fourth dimensions	Deshenthree Chetty, Cecil Churms, David Reid (IMA-CAM)
MA2	General Session - methods and applications	Sabine Verryn, Simon Clark, Klaus-Dieter Grevel, Artur Benisek
MA3	Mineral microanalysis	Michael Wiedenbeck, Roger Dixon
MA4	Remote mapping of minerals	Eric Pirard, VDM Van der Meer, Erick Ramanaidou, Paul Linton (IMA-CAM)

MINERALOGICAL CRYSTALLOGRAPHY

MC1	Crystallography and its importance in applied mineralogy	Volker Kahlenberg, Johan de Villiers (IMA-CAM)
MC2	General Session: Mineralogical Crystallography	Johan de Villiers
MC3	Modular aspects of mineral structures	Massimo Nespolo, Marco Pasero, Sergey Krivovichev
MC4	Physics, Chemistry and Crystallography of Minerals	Stefan Stöber, Christoph Berthold (German Minerological Society, Section: Physics, Chemistry and Crystallography of Minerals)
MC5	Recent progress in the crystal chemistry of minerals: systematising mineral properties and behaviour	Georges Calas, Frank Hawthorne

MINERALS, MUSEUMS, CULTURE AND HISTORY

MM1	Archaeometry and Geosciences: facing the cultural heritage challenges	Corina Ionescu, Gilberto Artioli, Patrik Degryse, Ãkos Torok, Richard Prikryl
MM2	General Session: Minerals, museums, culture and history	Roger Dixon, Bruce Cairncross, Peter Davidson, Suzanne Miller, Eric Pirard (IMA-CM)

OPEN THEME

OT1	Education and skills development	Megan Becker, Gillian Drennan, Rene Toerien (IMA-CAM)
OT2	New minerals, nomenclature and classification	Stuart Mills, Frédéric Hatert, Peter Williams (IMA-CNMNC)
OT3	General Session: Open Theme	Deshenthree Chetty

PLANETARY AND COSMIC MINERALOGY

PC1	Challenges in Asteroidal, Lunar and Martian mineralogy	Jesús Martínez-Frías, Fernando Rull-Pérez
PC2	General Session: Planetary and cosmic mineralogy	Uwe Reimold, Ansgar Greshake, Razvan Caracas
PC3	Impact cratering, high pressure shock metamorphism and luminescence studies	Uwe Reimold, Roger L Gibson, Ansgar Greshake, Jörg Fritz, Arnold Gucsik
PC4	Mineralogical Co-evolution of the Geosphere and Biosphere	Edward Grew, Robert Hazen, Axel Hofmann

IMA 2014 ORGANISATION

CONFERENCE CHAIR: Sabine Verryn, XRD Analytical Consulting, South Africa

Vice Chair: Deshenthree Chetty, Mintek, South Africa

Vice Chair: Craig Smith, GSSA, South Africa

Organising bodies:

Mineralogical Association of South Africa (MINSA)

The Geological Society of South Africa (GSSA)

LOCAL ORGANISING COMMITTEE

Scientific Programme Committee:

Deshenthree Chetty (Chair)	Mintek, South Africa
Lesley Andrews	Private Consultant, South Africa
Johan de Villiers	University of Pretoria, South Africa
Roger Dixon	University of Pretoria, South Africa
Paul Nex	University of the Witwatersrand, South Africa
Wolf Uwe Reimold	Museum für Naturkunde and Humboldt Universität zu Berlin, Germany
Jill Richards	Exxaro Resources, South Africa
Bertus Smith	University of Johannesburg, South Africa
Craig Smith	Geological Society of South Africa
Sabine Verryn	XRD Analytical and Consulting, South Africa
Fanus Viljoen	University of Johannesburg, South Africa

Sponsorship, Marketing and Exhibition Committee:

David Long (Chair)	Sci-Ba, South Africa
Siksha Bramdeo	Anglo American, South Africa
Deshenthree Chetty	Mintek, South Africa
Annegret Lombard	SGS Minerals Services, South Africa
Chazanne Long	Sci-Ba, South Africa
Craig Smith	Geological Society of South Africa
Darren Tiddy	Anglo American, South Africa
Sabine Verryn	XRD Analytical and Consulting, South Africa

Bursary Committee:

Bertus Smith (Chair)	University of Johannesburg, South Africa
Megan Becker	University of Cape Town, South Africa
Grant Bybee	University of Witwatersrand, South Africa
Annegret Lombard	SGS, South Africa
Luke Longridge	VMIC, South Africa
Jodie Miller	University of Stellenbosch, South Africa
Hervé Wabo	University of Johannesburg, South Africa

Field trips:

Judith Kinnaird, University of the Witwatersrand, South Africa

Finance:

Craig Smith, Geological Society of South Africa

Social Events:

Wiebke Grote, University of Pretoria, South Africa

Additional LOC members:

Erica Barton	Nelson Mandela Metropolitan University, South Africa
Byron Bezuidenhout	Anglo American, South Africa
Grant Cawthorn	University of the Witwatersrand, South Africa
Louise Coney	De Beers, South Africa
John Dunlevey	University of Limpopo, South Africa
Christoph Gauert	University of the Free State, South Africa
Johan Krynauw	Consultant, South Africa
Hassina Mouri	University of Johannesburg, South Africa
Musarrat Safi	Anglo American, South Africa
Igor Tonzetic	Consultant, South Africa
Brandon Youlton	SGS, South Africa

CONFERENCE SECRETARIAT: Scatterlings Conference and Events

Carolyn Ackerman	Project manager
Jeanne Day-Spriesterbach	Programme, speakers, field trips
Shelley-Ann Abrahams	Registration
Carina du Plessis	Sponsorship and Exhibition
Rowan Moss	Technical
Juanita Males	Speaker preparation room

INTERNATIONAL ADVISORY COMMITTEE:

Walter V. Maresch	President of the International Mineralogical Association, Ruhr Universität Bochum, Germany
Dee Bradshaw	University of Queensland, Australia
Georges Calas	Université Pierre et Marie Curie, France
Jens Gutzmer	Helmholtz Institute Freiberg for Resource Technology, Germany
Hannah Horsch	Hazen Research, Inc., USA
Sergey Krivovichev	St. Petersburg State University, Russia
Anhuai Lu	Peking University, China
Stuart J Mills	Geosciences Museum Victoria, Australia
Aberra Mogessie	President of the Geological Society of Africa (GSAf), Karl-Franzens-Universität Graz, Austria
Massimo Nespolo	Université de Lorraine, France
Eric Pirard	Université de Liège, Belgium
Herbert Pöllmann	University of Halle-Saale, Germany
Wolf Uwe Reimold	Museum für Naturkunde and Humboldt Universität zu Berlin, Germany
Ekkehart Tillmanns	Universität Wien, Austria
Frances Wall	University of Exeter, UK
Peter A. Williams	University of Western Sydney, Australia

CONTENTS

PLENARY		1
SPECIAL TALK		5
CLAY SCIENCE		
CS1	General Session: Clay science	6
CS2	Scientific and industrial applications of green rust related compounds and layered double hydroxides	13
CS3	Structural characterisation of lamellar compounds	16
DEEP EARTH		
DE1	Cratons and diamonds	20
DE2	Fluid in the Earth	33
DE3	Mineralogy in the Deep Earth	37
DE4	Theoretical and Compositional mineral physics for Deep Earth	45
DE5	Water and hydrous phases in the Earth's interior: geological, geophysical and geodynamic implications	49
ECONOMIC GEOLOGY/MINERALOGY, APPLIED MINERALOGY		
EG1	Critical metals and Rare earth elements	57
EG2	General Session: Applied Mineralogy	66
EG3	General Session: Economic Geology/Mineralogy	73
EG4	Gold deposits	86
EG5	Non-sulphide Pb-Zn deposits	97
EG6	Platinum group minerals (PGMs) from the mantle to the crust	101
EG7	Process Mineralogy and Geometallurgy	113
EG8	Sediment-hosted ore deposits	125
EG9	Sulphide mineralogy and Geochemistry	129
EG10	Zeolites and porous materials	138
ENVIRONMENTAL MINERALOGY/GEOCHEMISTRY		
EM1	Applied Geochemistry and Geomicrobiology for the Remediation of inorganic pollutants	143
EM2	CO_2 storage: Mineralogical Implications	149
EM3	Environmental mineralogy and geochemistry of mine waste	154
EM4	Environmental Mineralogy and the Carbon Cycle	161
EM5	General Session: Environmental Mineralogy and Geochemistry	163
EM6	Inorganic fibres, biosphere, and risk assessment	174
EM7	Mineralogy on Radioactive waste disposal, decontamination of radioactively contaminated sites and decommissioning of nuclear power plants	179
EM8	Minerals and Microbes	183
EM9	Role of Mineralogical Sciences in Sustainable Cement-based materials	188

GEOCHEMISTRY AND PETROLOGY

GP1	Africa-A Mecca of kimberlite, alkaline rock and carbonatite geology	192
GP2	Aqueous and carbonic fluids in ultramafic rocks: From vein precipitation to channeled and pervasive wall-rock reaction	197
GP3	Dating Metamorphic Processes: Promise and Pitfalls of Geochronology	204
GP4	General Session: Geochemistry and Petrology	208
GP5	Geologic fluids in the deep crust and upper mantle	218
GP6	Magma differentiation and ore formation processes	229
GP7	Magma mixing - from macro to micro scale	237
GP8	Magmas and Melts under extreme conditions	241
GP9	Mineral Inclusions - their genesis and fate	245
GP10	Pegmatites, and pegmatite mineralogy	253
GP11	Petrologic Pathfinders: Trace elements and stable isotopes in tourmaline, rutile and other accessory minerals	271
GP12	The Geology of Gems and their Geographical Origin	278
GP13	Timing and genesis of mineralisations: the isotope record	286

METHODS AND APPLICATIONS

MA1	Computed tomography – pushing frontiers in imaging of the third and fourth dimensions	292
MA2	General Session - methods and applications	301
MA3	Mineral microanalysis	310
MA4	Remote mapping of minerals	315

MINERALOGICAL CRYSTALLOGRAPHY

MC1	Crystallography and its importance in applied mineralogy	319
MC2	General Session: Mineralogical Crystallography	323
MC3	Modular aspects of mineral structures	327
MC4	Physics, Chemistry and Crystallography of Minerals	333
MC5	Recent progress in the crystal chemistry of minerals: systematising mineral properties and behaviour	345

MINERALS, MUSEUMS, CULTURE AND HISTORY

MM1	Archaeometry and Geosciences: facing the cultural heritage challenges	353
MM2	General Session: Minerals, museums, culture and history	361

OPEN THEME

OT1	Education and skills development	369
OT2	New minerals, nomenclature and classification	372
OT3	General Session: Open Theme	380

PLANETARY AND COSMIC MINERALOGY

PC1	Challenges in Asteroidal, Lunar and Martian mineralogy	382
PC2	General Session: Planetary and cosmic mineralogy	389
PC3	Impact cratering, high pressure shock metamorphism and luminescence studies	393
PC4	Mineralogical Co-evolution of the Geosphere and Biosphere	402

IMA2014 SPONSORS AND EXHIBITORS 410

AUTHOR INDEX 423

Where abstracts have multiple authors, the presenting author is underlined

The valuable role of process mineralogy in the future of the mining industry

Bradshaw D

Julius Kruttschnitt Mineral Research Centre, University of Queensland, Australia
d.bradshaw@uq.edu.au

Process mineralogy is at the centre or heart of the Mining Industry, where its very purpose or 'raison d'etre' is to extract value from the defined ore deposit. Each deposit is made up of a distinct set of minerals; their location, type, abundance, association and texture are determined by its formation. In the past, as noted by early twentieth century authors, a working knowledge of applied mineralogy was intrinsic to effective extraction and value creation and so was a skill acquired by any metallurgist or mineral processor.

As the years progressed, processes were to some extent standardised, company structures became formalised, with different disciplines and groups becoming more specialised and less integrated and 'professional silos' were created. With notable exceptions of course, less mineralogical knowledge became inherent to mineral processing, which has resulted in the steady weakening of the discipline's position and contribution of value to the industry.

While at first this did not diminish success, this has all changed recently and unexpected surprises resulting from inadequate ore body knowledge have resulted in reduced economic returns for the Mining Industry. More and more, ores have become complex and lower grade, containing more deleterious elements, resources such as energy and water need to be conserved, and skills shortages have resulted in a wider range of people entering the industry, often with inadequate preparation and less equipped to deal with the more difficult operating environment.

For the future of the Mining Industry to be sustained, the discipline 'Process Mineralogy' needs to be returned to its central, core position. This will provide foundational support for mineral processing circuit design and optimisation, appropriate research and technology development, as well as effective waste and tailings disposal strategies. This requires an articulation of the value as well as the appropriate education and training at all levels to establish and develop our 'Process Mineralogy' communities of practice.

Cross-fertilization of mineralogy and crystallography: a tribute to the International Year of Crystallography at IMA 2014

Depmeier W

Institute of Geosciences, University of Kiel, Germany wd@min.uni-kiel.de

It goes without saying that mineralogy as a scientific discipline depends strongly on crystallographic knowledge, techniques and methods, such as structure determination, refinement of site occupancies, or indexing of crystal faces. On the other hand, it is clear that crystallography has its roots in mineralogy, although it is fair to say that nowadays much crystallographic work pertains to objects related to biology.

In this contribution several examples shall be described and discussed where *sine qua non* conditions between mineralogy and crystallography, or vice versa, have been decisive for substantial progress in one of the two fields to be made. Examples include, but are not necessarily restricted to, boracite, charoite, icosahedrite and calaverite.

The type locality of boracite, $Mg_3B_7O_{13}Cl$, is Lüneburger Kalkberg, Lüneburg, Lower Saxony, Germany where it occurs within the gypsum cap rock of a salt dome. The story has it that the children of Lüneburg liked to play dice with the cube-shaped boracite crystals. Idiomorphic quartz crystals occur together with boracite in this deposit and since both minerals show similar hardness and lustre, boracite was described as "cubic quartz" before it was discovered that it contains boron (hence the name). Later this mineral played a notable role in crystal physics, because it was one of the materials on which J. and P. Curie first demonstrated piezoelectricity. The structure of boracite, in both its cubic and orthorhombic phase, had been determined in the 1950s and it is characterized by chains of corner-sharing asymmetric O_4Cl_2-octahedra around the Mg^{2+} ions running along all three cubic <100> directions. Note that a variant of boracite, named ericaite, exists where Fe^{2+} substitutes for Mg^{2+}. In the sixties of the last century the question was raised whether materials exist, which are simultaneously ferroelectric and ferromagnetic. There were no reasons based on symmetry considerations why such materials should be forbidden. At that time it was believed that a "good" ferroelectric material, such as certain perovskites, should contain d^0 cations (Ti^{4+}, Nb^{5+}, etc.), e.g. at the centre of symmetric octahedra in the structure of perovskite. Obviously, d^0 cations do not allow for ferromagnetism. In order to overcome this dilemma scientists proposed to prepare materials containing paramagnetic cations in an asymmetric octahedral environment. First attempts with oxyfluorides failed. Input from mineralogy drew the attention to boracites and after a long and arduous way the first ferroelectric - ferromagnetic, i.e. multiferroic material, Ni-I-boracite, could be prepared. This is how mineralogy helped crystallography.

Likewise, the recent confirmation of a natural quasicrystal, icosahedrite, was only possible with the help of mineralogy. On the other hand, the 50 years old enigma of the structure of charoite could only be solved with the help of a newly developed method of electron crystallography. Another long-standing enigma in mineralogy, namely the indexing of the crystal faces of calaverite, succeeded after application of superspace group theory.

Petrography in 3D: using X-ray computed tomography to amplify geological intuition

Ketcham R A

Jackson School of Geosciences, University of Texas at Austin, USA
ketcham@jsg.utexas.edu

Three-dimensional imaging using high-resolution X-ray computed tomography (CT) transforms petrographic analysis. An early and persistent critique of X-ray CT for geological applications was that it only produced "pretty pictures", and great progress has been made developing tools to extract 3D quantitative data from voxel data sets. However, the opportunities inherent in doing fundamental petrography in 3D through visualization and geological intuition have remained relatively overlooked. Three examples of the power of CT are presented from the fields of planetary geology and igneous petrology, featuring insights derived from 3D visualization and leveraged by 3D image analysis.

In the first, 3D analysis of a fragment of the famous Murchison meteorite reveals a flattening texture in the chondrules [1]. This flattening may be caused by impact events or a more steady process akin to sediment compaction. Volumetric imagery allows investigation for textural clues of which process may be responsible, and provides a unique opportunity to estimate porosity loss, which may be responsible for the divergent densities of asteroids and meteorites derived from them.

Next, CT analysis of vesicles and phenocryst fragments within pumice provides a fresh look at pre-eruption dynamics [2]. The discovery of welded pumice with vesicles and phenocrysts aligned in a planar fabric that cross-cuts the weld suggests a sequence of fragmentation, welding, strain, and re-fragmentation that is more complex than previously proposed simple end-members for the eruption process. 3D interrogation allows vesicles formed by explosive decrepitation to be easily distinguished from those formed by nucleation of vapour bubbles and enables *in situ* access to fragment size distributions, providing further insight into the development of eruptive textures.

Finally, 3D inspection of a 27-carat carbonado provides numerous insights critical to unraveling the origin of this enigmatic diamond variety [3]. CT data reveal a texture in the porosity that evolves across the sample, suggesting a link between the through-going porosity and the patinaed surface on the specimen. A shear fabric in the pores suggests a shearing event immediately prior to solidification. *In-situ* examination of the unusual inclusion suite indicative of crustal conditions (e.g., kaolinite, hematite, florencite, etc.), normally accessed by crushing specimens, shows that they all have textures indicating disequilibrium formation. Abundant pseudomorphs reveal a megacrystic euhedral dodecahedral phase (Figure 1) never previously described in carbonado, which has been entirely eradicated but may have provided the raw materials for REE- and U-rich inclusions.

These examples point to the tremendous potential for scientific discovery with more widespread dissemination and utilization of CT data, and the importance of lowering the technical, educational, and financial barriers to it.

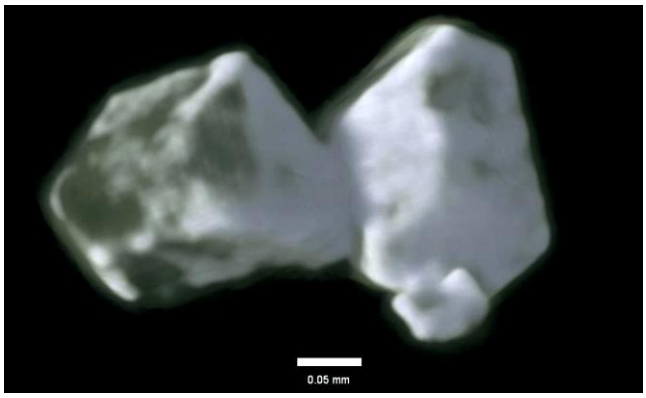

Figure 1: 3D visualization of dodecahedral pseudomorphs in carbonado diamond.

[1] Hanna R.D. and Ketcham R.A. (2013). *Ann. Meet. Meteor. Soc.*, 75, abstract #5031.

[2] Ketcham R.A., Gardner J.E. and Abbott S. (2011). *Am. Geophys. Union Fall Meet.*, abstract EP52C-05.

[3] Ketcham R.A. and Koeberl C. (2013). *Geosphere*, 9 (5), 1336-1347.

Photoelectrons from the mineral and microbial world: a new perspective on the interactions between the geosphere and biosphere

Lu A

School of Earth and Space Sciences, Peking University, China ahlu@pku.edu.cn

The Earth surface is a multiple open system. It is obvious that the interaction among solar light, semiconducting minerals, photoelectrons/photoholes, organics, inorganics, valence electrons and microorganisms occurs continuously on our planet. Semiconducting minerals, including most metal oxides and sulfides, absorb visible light of the solar spectrum. Microorganisms evolve varied pathways to obtain carbon and energy sources. In a recent study [1], evidence was presented demonstrating solar energy mediated by semiconducting mineral photocatalysis, acting as energy source, promoting the growth of some non-photosynthetic bacteria. This revealed that the ternary system of microorganisms, minerals and solar light has played a critical role in the history of life on our planet. In a simulated system, under simulated solar light, semiconducting minerals generate photoelectrons that could be used by non-phototrophic microorganisms to support their metabolisms. The growth of microorganisms was closely related to photon quantity and energy and the microorganism growth and mineral light absorption spectra were fitted well under different light wavelengths. The overall energy efficiency from photon to biomass was 0.13‰ to 1.9‰. Further studies revealed that in natural soil systems, semiconducting mineral photocatalysis could influence the microbial population. Solar energy utilization pathways by non-phototrophic microorganisms, mediated by semiconducting mineral photocatalysis, provide a new concept to evaluate the origin and evolution of life. Semiconducting minerals are ubiquitous on Earth's surface and widely participate in redox reactions following photoelectron-photohole pairs excited by solar light. As photoholes can be easily scavenged by environmental reductive substances and microorganisms possess multiple strategies to utilize extracellular electrons, the highly reductive photoelectrons serve as potential energy source for microbial life. The discovery of this pathway extends our knowledge on the use of solar energy by nonphototrophic microorganisms, and provides important clues to evaluate life on the early Earth. Microorganisms, minerals and solar light constitute a complex but important ternary system through Earth history. The discovery of the novel energy conversion pathway in this system demonstrates how non-phototrophic microorganisms directly or indirectly utilized photoelectrons as the solar energy source. The full comprehension of non-phototrophic bacterial solar energy utilization conducted by semiconducting minerals in present environments will greatly help us to better understand the energy transform mechanism among interfaces of lithosphere, pedosphere, hydrosphere and biosphere.

[1] Lu A. *et al*. (2012). Growth of non-phototrophic microorganisms using solar energy through mineral photocatalysis. *Nature Communications*, 3(4), 768-775.

To be or not to be an eclogite, that is the question: the amphibolite-eclogite transition revisited

Maresch W

Institute of Geology, Mineralogy and Geophysics, Ruhr-University Bochum

IUGS guidelines recommend that the term eclogite be used only for rocks of basic composition, in which garnet + sodic pyroxene exceed 75 vol%. Consequently, the eclogite facies is a *P-T* region in which eclogite is stable. It is a broad field clearly characterized by high pressures but also highly variable temperatures. Thus the eclogite facies grades into the blueschist, the epidote-amphibolite, the amphibolite and the granulite facies with rising temperatures. However, typical compositions of garnet and sodic pyroxene in low-temperature basaltic eclogites often lead to modal amounts of garnet + pyroxene much less than 75%. Therefore significant amounts of additional amphibole, epidote-group mineral, mica, etc. are common [1]. According to IUGS, these are not eclogite *sensu stricto*, but "amphibole-eclogite", "zoisite-amphibole eclogite", etc. Although the geodynamic significance of the high-pressure rock eclogite is immense, the precise *P-T* definition of eclogite facies boundaries is not straightforward. Exhumation from great depths often dismembers coherent high-pressure rock sequences. Basic rocks as evidence of eclogite formation may only constitute minor fragments of these units. Ambiguity of the role of water fugacity adds uncertainty.

This presentation analyzes a case study of a rare metamorphic array spanning the transition between the epidote-amphibolite and eclogite facies as exposed in a coherent 15 km sequence of tholeiitic rocks on Margarita Island, Venezuela. From south to north, the following assemblages are encountered in low-variance metabasaltic rocks (Ab = albite; Bar = barroisite; Chl = chlorite; Ep = epidote; Czo = clinozoisite; Grt = garnet; Omp = omphacite; Pg = paragonite; Qtz = quartz):

Bar + Grt + Ep/Czo + Ab + Chl + Qtz (Omp,Pg absent)

Bar + Grt + Ep/Czo + Ab + Pg + Qtz (Omp,Chl absent)

Bar + Grt + Ep/Czo + Omp + Pg + Qtz (Ab, Chl absent)

where the assemblages (Omp,Pg) and (Ab,Chl) represent the epidote-amphibolite and eclogite facies, respectively. The assemblage (Omp,Chl) corresponds to the paragonite amphibolite stage discussed by Konzett and Hoinkes [2] as a transitional stage towards the eclogite facies. The reaction leading to eclogite, or in IUGS compatible terminology Ep/Czo-amphibole eclogite, can be formulated by mass balance from the Margaritan array as Bar + Ab + Ep/Czo => Omp + Pg + Grt + Fluid and is essentially analogous to a reaction derived by Molina and Poli [3] from phase petrological considerations. In the present analysis, the two reactions linking the three assemblages by mass balance are strongly pressure dependent, with low d*P*/d*T* slopes, and indicate dehydration with increasing pressure. Best estimates for the exposed metamorphic array suggest 500 - 550°C and 10 to 14 kbar, with the eclogite-forming reaction located at approximately 12 kbar. Conspicuous reequilibration textures of omphacite, paragonite and garnet (essentially a reversal of the S - N metamorphic array), as well as Ca-rich overgrowths on barroisite, monitor a return to epidote-amphibolite conditions during exhumation. This metamorphic array is thought to have been produced in young oceanic crust during closure and subduction of a back-arc basin, followed by arc-continent collision and exhumation.

[1] Schliestedt M. (1990). *in*, Carswell, ed., *Eclogite Facies Rocks*, Blackie, 160-179.

[2] Konzett J. and Hoinkes G. (1996). *J. met. Geol.*, 14, 85-101.

[3] Molina J.F. and Poli S. (1998). *J. Petrology*, 39, 1325-1346.

Feldspars on the inside: reading their record

Parsons I

School of Geoscience, University of Edinburgh, UK ian.parsons@ed.ac.uk

Alkali feldspar is the third most abundant mineral in the continental crust, growing from magma, during metamorphism, and in hydrothermal systems and diagenesis. Individual grains exhibit a range of intracrystal microtextures, unique in the mineral world, that record both, their thermal history and replacive fluid-feldspar reaction events, sometimes multiple, that they have experienced over geological time. This talk will concentrate on the characterization and interpretation of the microtextures from the standpoint of the petrologist or geochemist.

Only rare, very rapidly cooled volcanic crystals, and some near end-member grains that grew at low *T*, are strictly single crystals that can be described by a single lattice. Most 'single crystals' are complex intergrowths based on many lattices. The geometrical relationships within the microtextures, many of which are sub-optical, were established in the 1950s in pioneering single-crystal X-ray diffraction work by W.S. MacKenzie and J.V. Smith. Since the 1970s, transmission and scanning electron microscopy, in combination with electron probe analysis, experimental work on diffusion rates, two-feldspar geothermometry and observations on crystals from well-constrained geological settings, have allowed the mechanisms of microtexture formation and their thermochronology to be deduced. The most complex crystals known contain 8 chemically distinct phases, some twinned in 4 different orientations.

Factors leading to the microtextures are exsolution (giving perthitic intergrowths), framework Si-Al ordering (leading to the sanidine-microcline phase transition, with orthoclase as a metastable intermediate structure, and to high- and low-albite) and the shearing phase transition in albite. A nanoscale peristerite intergrowth has been found recently in a mesoperthite. Perthitic intergrowths formed wholly by diffusion are initially coherent (have a continuous Si-Al-O framework) and have regular morphologies constrained by minimization of elastic coherency strain energy, which defines the orientation of exsolution lamellae and repeated twinning. Misfit dislocations sometimes develop during cooling and these are important in replacement reactions and weathering. Preservation of elastic strain in coherent intergrowths is a robust indicator of structure that has remained chemically (and isotopically) undisturbed since the microtexture formed. Their periodicity has been used to calculate cooling rates in volcanic rocks using experimental diffusion coefficients and to estimate relative cooling rates in plutonic rocks. The coarsest coherent intergrowths have periodicities (~10 µm) in order-of-magnitude agreement with measured diffusivities.

Plutonic crystals are usually mixtures of coherent and replacive microtextures. Replacive textures are coarser, relatively irregular, with 'patch' or 'vein' morphology, and are associated with the development of optical turbidity, caused by µm-scale micropores. At the electron microscope scale they have a sub-grain microtexture on scales from 10s of nm to >100 µm. In some examples replacement reactions have occurred twice and in evolved igneous rocks some euhedral primocrysts are entirely pseudomorphs. Cathodoluminescence has revealed extraordinary concentric oscillatory zoning of trace-elements in sub-grains. Replacement may be isochemical (driven only by decrease of coherency strain energy) or non-isochemical, a common feature widely ignored by petrologists and geochemists. Replacive microtextures have recently been produced experimentally. Vein intergrowths are sometimes periodic, on scales >100 µm, but for kinetic reasons cannot have formed by diffusion, and cannot be used to estimate cooling rates. The cause of their regularity is an enigma. Once formed, all microtextures exercise a strong control on feldspar dissolution and mechanical degradation during sedimentary transport, diagenesis and soil formation. Microtextures can be used as provenance indicators in clastic sedimentary rocks. Misfit dislocations, enlarged by dissolution to form networks of 'nanotunnels', would have provided ideal reactors for the emergence of life.

Natural controls of platinum group mineral formation and distribution: new insights from recent advances in nanomineralogical analysis

Reid D L

Department of Geological Sciences, University of Cape Town, South Africa
david.reid@uct.ac.za

Recently developed techniques in high resolution mineralogical analysis include Focussed Ion Beam and High Resolution Transmission Electron Microscopy (FIB/HRTEM) [1] and microfocus X-Ray Computed Tomography (XRCT) [2]. Both approaches have been driven primarily by the search for new materials and industrial applications, but as is often encountered in science, provide the opportunity for returning full circle to studies of a more fundamental nature. The platinum group metals are immensely important in numerous technologies and thus have received much attention from a wide spectrum of industries. Their strategic importance and high cost have motivated numerous efforts at gaining a better understanding of their properties, more effective usage and ensuring a continuous and sustainable supply. We review recent research using these techniques developed by the materials industry on seeking a better understanding of the natural controls that govern the concentration and distribution of platinum group elements (PGE) in the world's largest repository of these strategic metals in the Bushveld Complex of South Africa.

Despite a voluminous literature on PGE chemistry, geology, exploration, mining, beneficiation and recovery, we still debate some of the most fundamental features of the fabulous Bushveld deposits, including the perennial question of how they acquired their incredibly high concentrations that range between a thousand to a million times typical crustal levels. Previous research has highlighted the relationship between base metal (Cu-Ni-Fe) sulphides and the PGE, which has led to the popular theory involving preferential concentration in sulphide melts due to their chalcophile and siderophile nature. Not so obvious from this theory is an explanation for the close relationship between PGE and chromite, since this oxide seemingly possesses no tendency to accommodate base and precious metals into its internal structure. Thus the traditional orthomagmatic collection model suffers from serious deficiencies in its successful application to the Bushveld ores, which has led to alternatives that challenge the assumption of simple thermodynamic partitioning between sulphide, silicate and oxide phases. One such alternative highlights the potential for the PGE to experience an early phase of atomic scale aggregation into nanometre-sized crystalline and non-crystalline particles or clusters, even under conditions of extreme undersaturation [3]. Should this occur in natural magmatic systems then the distribution of PGE between silicate, sulphide and even metal melts will be controlled by the surface properties of the nano-associations, more so than by the chemical properties of the elements and conventional mineral species.

Experimental work designed to explore the behaviour of the PGE in magmatic systems has produced results confirming the self-organisation into nanoparticles, well before the melt has reached elemental concentrations at which discrete minerals become stable phases [4]. Similar to minerals crystallizing from aqueous solutions, magmatic minerals may nucleate by using pre-existing nanophases and nanoparticles as building blocks. The importance of As in the experimental Fe-Cu-S melts was emphasized, as this component was responsible for the preferential aggregation of Pt.

Preservation of very similar PGE-bearing arsenide and sulphide nanocrystals in host base metal sulphides has been reported in a recent FIB/HRTEM study of the Merensky Reef [5]. This particular population of PGE-bearing phases has never been detected before and could prove to be crucial to the concentration of precious metals in not only the Bushveld ores but also other deposits.

[1] Wirth R. (2009). *Chemical Geology*, 261 (3-4), 217-229.

[2] Godel B. (2013). *Economic Geology*, 108 (8), 2005-2019.

[3] Tredoux M. *et al*. (1995). *South African Journal Geology*, 98, 157-167.

[4] Helmy H.M. *et al*. (2013). *Nature Communications*, 4, 2405

[5] Wirth R. *et al*. (2013). *Canadian Mineralogist*, 51, 143-155.

Ultrahigh pressure mineralogy of the continental lithosphere

Sobolev N

Institute of Geology and Mineralogy, Siberian Branch of the Russian Academy of Sciences, Russia sobolev@igm.nsc.ru

Coesite and diamond are principal index minerals of ultrahigh pressure (UHP) metamorphic and igneous rocks equilibrated at depths greater than 100 km. In spite of a long time knowledge of both minerals associated with silicates and oxides in kimberlites and their eclogite xenoliths, their occurrence *in situ* in crustal metamorphic rocks was detected relatively recently in 1984 (Italian Alps and Norway for coesite) and in 1990 (Kokchetav massif, Kazakhstan for diamond). Following these discoveries, an intense search was performed and resulted in numerous new findings. Zircon is shown to be the best and perfect container of coesite, diamond and coexisting minerals in UHP metamorphic rocks since the early 1990's and successfully used to date almost for all new UHP localities. Nitrogen isotope data and negative $\delta^{13}C$ values of metamorphic diamonds as well as oxygen isotope data of coexisting minerals indicate the metasedimentary origin of coesite and diamond bearing metamorphic rocks. Eclogite (E-type) diamonds and associated minerals (e.g., Na-bearing garnets and K- bearing clinopyroxenes) of several kimberlitic and placer localities worldwide demonstrate similar specific compositional features, probably caused by subduction. Diamond occupies a unique position in discussion on the igneous and metamorphic aspects of the Earth's carbon cycle. This talk will also review research on naturally occurring diamonds and their mineral and fluid inclusions. Comparison of mineralogical features of coesite- bearing UHP crustal and mantle rocks will be performed and relative significance of subducted and deep mantle assemblages of the continental lithosphere will be estimated. We conclude that only through careful investigation and interpretation of often sub-millimetre and even sub-micrometre scale observations it is possible to derive large-scale orogenetic processes.

Hypatia: from unusual carbonado to cometary nucleus

Andreoli M[1*], Belyanin G[2], Block D[3], Kramers J[2], Pischedda V[4], Sigalas J[3], Westraad J[5]

1 – Necsa, South Africa *marco.andreoli@necsa.co.za 2 - University of Johannesburg, South Africa 3 - University of the Witwatersrand, South Africa 4 - University of Lyon, France 5 - Nelson Mandela Metropolitan University, South Africa

Of all rocks on earth, carbonados consisting of polycrystalline diamond, found in Brazil and the Central African Republic, are arguably the only ones for which their ultimate place of origin, this world or the stars, remains open to discussion. Stimulated by the controversy, research was initiated in the early 1980s at the University of the Witwatersrand on stones supplied by the late Prof H Meyer of Purdue University. Two features of carbonado attract special attention, namely porosity and the fact they tend to host elements in native or in highly reduced state (i.e. TiN, Ni). These features have been considered to point unquestionably to a cosmic origin. However, doubt about this arose from observing the similarly porous nature of the spherical, radially textured "ballas" recovered from kimberlite pipes, and the occurrence of TiN (osbornite) inclusions in chromite from an ophiolite in Tibet [1]. Later on, an expanding collaboration with scientists working on the enigmatic Libyan Desert Glass found in SW Egypt led to the study of a new carbonado-like stone previously collected by Dr Aly Barakat in that region. Petrographic, mineralogical and isotopic studies of subsamples of this stone (named Hypatia) have shown that it only superficially resembles carbonados. The latter are extremely tough yet porous, with diamond the only carbon mineral present, whereas Hypatia lacks porosity, is pervaded by open fractures that make the stone exceedingly brittle, and most of the carbon is in an amorphous, glassy state (Figure 1) hosting graphite and containing appreciable oxygen and nitrogen. Further, carbonados have $\delta^{13}C$ values between -30 and -20 ‰ (PDB) like organic matter, whereas Hypatia's value is close to 0 ‰. If carbonado failed so far to provide unequivocal diagnostic signatures of its origin, a growing list of isotopic and mineralogical features brand Hypatia as uniquely cometary in origin. Noble gas analyses provided crucial evidence. $^{40}Ar/^{36}Ar$ ratios range down to 30, between the atmospheric value of 298 and all meteoritic material, which has $^{40}Ar/^{36}Ar$ ratios <1. This betrayed an extra-terrestrial object that had captured atmospheric gases before impact, in accord with the presence of high pressure atmospheric gas inclusions in the stone. Other noble gases (neon, krypton and xenon) yielded more subtle indications of a material very different from chondritic meteorites [2]. Further differences from all known meteorites are the major element chemistry dominated by carbon (the most carbon-rich carbonaceous chondrites have only 3% carbon) and the $\delta^{13}C$ value mentioned above, which differs from the range of -25 to -10 found in chondrites. Last but not least, the non-carbon mineralogy of Hypatia is totally different from that in all known meteorites [3], and from sediments close to Hypatia's discovery site grains of metallic Ti were recovered, which may be regarded as debris from exploded parts of the bolide [4]. We thus conclude that Hypatia represents part of an impacted fragment of a cometary nucleus that exploded over the SW Egyptian desert, causing the surface melting that produced the Libyan Desert Glass, and that shock-induced modification of the matrix led to its extraordinary preservation.

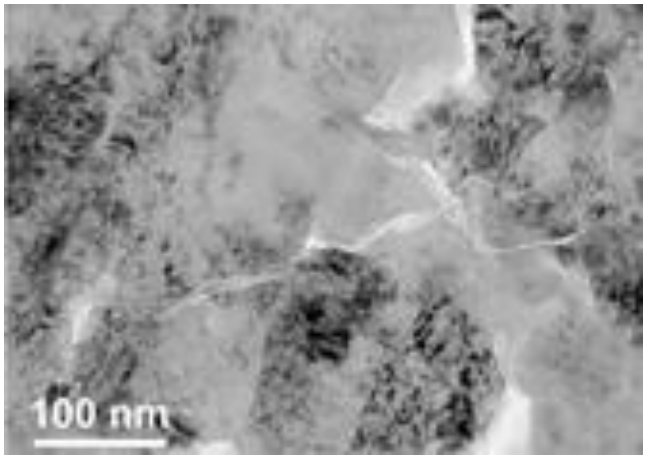

Figure 1: Bright-field transmission electron microscope image from Hypatia; "dark" specs: cubic diamond domains (in non-diamond carbon matrix) oriented to produce electron diffraction. Lamellar nature of the domains is reminiscent of shock diamonds from the Popigai impact site [5].Image by Johan Westraadt.

[1] Dobrzhinetskaya *et al*. (2009). PNAS-0905514106.

[2] Kramers *et al*. (2014). IMA2014 abstracts volume.

[3] Belyanin *et al*. (2014). IMA2014 abstracts volume.

[4] Andreoli *et al*. (2014). IMA2014 abstracts volume.

[5] Koeberl *et al*. (1997). Diamonds from the Popigai impact structure, Russia. *Geology*, 25, 867-890.

Clay stratigraphy at the Vaalputs low level radioactive waste disposal site, Namaqualand, South Africa

Andreoli M[1*], Clarke C[2], Cloete M[3], Evans M[4], Harris C[5], Logue A[1], Majodina O[2], McCarthy T[4], Netterberg F[6], Stengel I[7], van Blerk J[8], van Rooy L[9]

1 - Necsa *marco.andreoli@necsa.co.za 2 - University of Stellenbosch 3 - Council for Geoscience 4 - University of the Witwatersrand 5 - University of Cape Town 6 - Private Consultant 7 - Private Consultant, Windhoek; Polytechnic of Namibia 8 - AquiSim Consulting 9 - University of Pretoria

The first nuclear power station in Africa is situated at Koeberg, near Cape Town and has been a reliable producer of electricity to the South African power grid since 1984. Whereas the spent fuel is currently stored at the utility, the low level radioactive waste is trucked over 600 km north to Vaalputs, a licensed facility located in Bushmanland being a sub-arid and sparsely populated area. Over the past 30 years Vaalputs has been the site of continuous, detailed investigations of most aspects of the earth and environmental sciences. In simple outline, the geology of the area consists of a sequence of Late Mesozoic to Cenozoic continental clastic sediments of the informally termed Koa Plateau Group (KPG) overlying a Mesoproterozoic granitic-granulitic basement. Mesozoic igneous activity at the site is represented by numerous explosive pipes of melilitite and non-diamondiferous kimberlite ~67 Ma in age. The KPG comprises three formations, the oldest being the Dasdap (fluvial conglomerate and arkosic sandstone) followed by the Lower Vaalputs Formation (lacustrine siltstone) and later by the Upper Vaalputs formation (unconsolidated, argillaceous fluvial sediments). Sedimentation occurred under changing climate conditions in shallow basins developed eastward of the receding Great Escarpment, which was initiated by the breakaway of South America ca.130 Ma ago. The Dasdap sediments are saprolitic and kaolinite-rich as a result of a prolonged hot and humid Cretaceous episode. Little is known of the unexposed Lower Vaalputs Formation, but much research has been conducted on the Upper Vaalputs Formation, which is exposed in the 8 m deep trenches in which the radioactive waste is placed. Most trenches show a subdivision of the Upper Vaalputs Formation in a beige, pebbly bottom member and a light grey, gritty member above. The most distinctive clay mineral of the pebbly member is palygorskite. When this mineral coats the surface of peds, it gives the impression of a white bed at the base of the trenches (see A, Figure1). Illite is, instead, the characteristic clay of the overlying gritty member (B, Figure 1). In the top 2 to 3 m of the trenches the gritty member is increasingly fractured, with fractures stained red by Fe oxides. Veins of calcium carbonate and, less frequently, gypsum become common, locally coalescing into thick calcrete duricrusts (C, Figure. 1). However, up to 40 percent of what appears to be calcrete is actually a sepiolite duricrust or sepiocrete, and nodules of this mineral are common near the base of a thin, near surface siliceous and ferruginous duripan, locally called dorbank, within which barite-bearing veins also occur. Dorbank also fills funnel-shaped karstic embayments within the calcrete (D, Figure. 1). Finally, a thin veneer of unconsolidated to semiconsolidated, weathered red sand is draped over these palaeosols (E, Figure 1). Silt and clay-size material derived from the excavations is used to backfill the trenches once packed with radioactive waste drums. Ongoing studies of the Vaalputs geohydrology and sediments, their mineralogy, age and palaeoenvironmental significance are aimed to assess the overall safety of the disposal operations for the current and future generations.

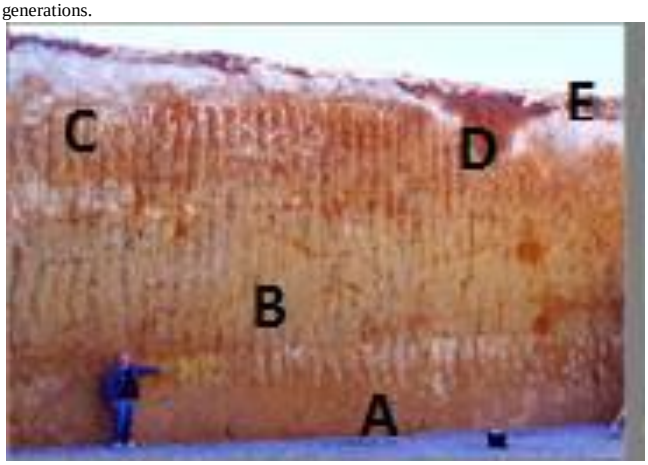

Figure 1: Photo of the NE wall of trench B.

Origin and petrophysical behaviour of clay minerals in faults affecting deeply buried reservoirs: example of Annot sandstones (Southern Alps, France)

Buatier M[1*], Cavailhes T[2], Leclère H[3], Lerat J[4], Charpentier D[1], Sizun J[1], Labaume P[5], Gout C[6]

1 - Chrono-Environnement, UFC Besançon *martine.buatier@univ-fcomte.fr

2 - DNO International ASA, Norway 3 - University of Liverpool, UK 4 - Université de Nancy, France5 - Geosciences Montpellier, France 6 - TOTAL Pau, France

Clay minerals are ubiquitous minerals in fault zones in a broad range of geological contexts, particularly in sedimentary basins. The presence of clay minerals in fault zones and their structural arrangement can play a critical role on fault mechanics and on fluid-flow properties of faults.

The present study focuses on clay mineral assemblages from two normal faults located in the Annot sandstones, a Priabonian-Rupelian turbidite succession of the Alpine foredeep, SE France. The Annot sandstones were buried below the front of Alpine nappes soon after their deposition and exhumed during the middle-late Miocene.

The studied faults are located in the internal part of the basin (Moutière-Restefond area), where the sandstone formation reached 8-10 km burial depth attested by vitrinite reflectance. The faults affect arkosic sandstone alternating with pelitic layers, and display throws of a few cm to tens of meters.

A mineralogical investigation (XRD, optical and SEM observations) combined with chemical analyses (microprobe analyses) has been performed to investigate the origin of clay minerals and their conditions of formation. Shear deformation of sandstone beds in fault zones is mainly achieved by the combination of pressure-solution (and precipitation) of quartz and alteration of feldspar giving rise to the formation of illite. The foliation in the fault core zone of the faults is underlined by preferentially oriented newly-formed phyllosilicates (illite and chlorite) and cross-cut by mineralized veins of quartz and calcite. Chemical analyses of chlorites and thermodynamic calculations suggest that fault deformation occurred at temperatures around 220-250°C in accordance with the peak temperature of the host rock estimated from vitrinite reflectance. These data suggest that synkinematic clay minerals registered the early stages of the fault deformation close to the maximal burial of the sandstones between 6.5 and 8 km, assuming a mean geothermal gradient between 25 and 30 °C/km. One of the two studied faults (Point Vert) displays a core zone including intensely foliated sandstones bounding a corridor of gouge about 20 cm thick. The gouge samples have a higher illite crystallinity index than the foliated sandstones, which could be explained by a reactivation of the fault at lower temperature.

The petrophysical properties of sandstones from the core zone and the hanging and foot walls of the fault were determined on drilled plugs following three spatial directions. The permeability of the highly-deformed sandstone from the core zone is anisotropic, about one order of magnitude higher than in the host rock in the direction parallel to the foliation. This permeability increase is explained by the occurrence of well-connected micropores localized between platy phyllosilicates. This study shows that the fault petrophysical properties are mostly controlled by the precipitation of synkinematic phyllosilicates under deep burial conditions.

Mineralogical characterization of clays involved in the Termini-Nerano slow moving landslide (southern Italy)

Cesarano M[1*], Bish D[2], Cappelletti P[3], Belviso C[4], Cavalcante F[4], Fiore S[4]

1 - Dipartimento di Scienze della Terra, dell'Ambiente e delle Risorse *mara.cesarano@unina.it 2 - Indiana University 3 - DiSTAR - Università degli Studi di Napoli Federico II 4 - Institute of Methodologies for Environmental Analysis-CNR

"Slow moving landslides" are downslope movements of rock masses, characterized by low rates of displacement (some mm to 1/2 m per year). External phenomena, such as long-duration rainfall or earthquakes, can increase their velocity (which can reach 50 cm/hour - 5 m/day) and consequently their hazard. These slope movements in southern Italy involve sedimentary formations characterized by arenaceous and clayey successions. Physical-chemical weathering, which alters shallow zones of these rock masses, favours the development of slow moving landslides. Another factor promoting these phenomena is their water content (i.e., groundwater). Both weathering and water cause a general decrease in material strength [1]. The occurrence of weathering-related clay minerals (e.g., smectites), able to trap significant quantities of water, has been generally considered a triggering factor of these landslides [2]. The main goal of this research was to carry out a mineralogical characterization of clay minerals occurring in the Termini-Nerano landslide (Massalubrense, Naples) in order to assess this statement.

Five bore holes were drilled in the study area on the rocks involved in the landslide. Several samples were selected at different depths along the cores and were analyzed by quantitative X-ray powder diffraction (QXRPD) to investigate their mineralogical composition. Bulk-rock chemical analyses were used to calibrate the quantitative mineralogical analyses. Samples were also treated to separate the clay fraction from the more coarse-grained mineral phases.

The material involved in the landslide is an association of sandstone and siltstone, mainly constituted by quartz, mica, feldspars and variable amounts of clay minerals. Calcareous sandstone layers are also frequent. Quantitative analysis of the bulk samples showed that the clay fraction is on average the 50 wt.% of the material involved in the landslide. Specific analysis of the clay fraction revealed kaolinite, chlorite, mixed-layer illite/smectite (I/S), and mixed-layer chlorite/smectite (C/S). Using the Moore and Reynolds approach [3], the percentage of illite in the mixed-layer illite/smectite and the stacking order, R, were determined. The amount of illite in the mixed-layer I/S had a mean value of 57% and varied between 21% and 83%. The stacking order of the I/S was R0 and R1.

According to literature data [4], the total amount of clays, and specifically the amount of smectite in the mixed-layer I/S, could have played an important role in the landslide development.

A geotechnical study on these samples is ongoing, to investigate any possible relationships between the clay mineral properties and the geomechanical parameters of materials.

[1] Taylor K.R. and Cripps J.C. (1987). Weathering effects: slopes in mudrocks and over consolidated clays. p.40. In Slope Stability: Geotechnical Engineering and Geomorphology (M.G. Anderson and K.S. Richards, editors). Wiley, New York.

[2] Calcaterra D., Calò P. Cappelletti, de' Gennaro M., Di Martire D., Parise M. and Ramondini M. (2007). Mineralogical and geotechnical characterization of a large earthflow in weathered structurally complex terrains of the Molise region, Italy-Geophysical Research Abstracts, Vol.9.

[3] Moore D.M. and Reynolds R.C., Jr. (1997). X-Ray Diffraction and the Identification and Analysis of Clay Minerals, 2nd ed. XVII + 378 pp.

[4] Uneno H., Jige M., Sakamoto T., Balce G.R., Deguchi I. (2008). Geology and clay mineralogy of the landslides area in Guisaugon, southern Leyte Island, Philippines. University Bulletin of Chiba Institute of Schenze, No 1, 9 pp.

Asbestiform sepiolite wrapped by aliphatic hydrocarbons from Perletoa, Aosta Valley (Western Alps, Italy): characterization, genesis and possible hazards

Giustetto R[1*], Seenivasan K[2], Belluso E[3]

1 - Department of Earth Sciences, University of Turin (Italy) roberto.giustetto@unito.it 2 - NIS, Centre of Excellence, Turin 3 - University of Torino

An atypical asbestiform sepiolite was found in the Gressoney Valley (Italian Western Alps), with exceptionally long fibres coated by an aliphatic hydrocarbons sheath - an association never reported before in literature. This sepiolite was characterized with a multi-analytical approach with the aim to infer its genesis, the role of its organic coating and its potential noxiousness for human health.

Microscopic and FT-IR analyses proved that these fibres, apparently up to several cm long, are formed by bundles of thinner fibrils (average length: 150 mm) potentially dispersible in the environment. When observed with TEM, these fibrils show a rhomboidal to parallelogram cross section (< 1 mm) with surfaces covered mostly by a thin film of aliphatic hydrocarbons (Figure 1).

The sepiolite fibrils and their organic coating originated in sequential steps from precipitation of Si/Mg rich hydrothermal fluids, resulting from serpentinization of olivine and clinopyroxene and Fischer-Tropsch-type reaction in the Combin Zone (Aosta Valley). Presence of a hydrocarbons sheath implies serious consequences on the sepiolite habit: the organic matter, in fact, interacts with the fibrils surface reducing the amount of adsorbed water and favouring fragmentation of thicker units into thinner ones, due to an 'opening' process implying separation along *z* and cleavage on (110). Similar mechanisms were observed in several sections of amphibole asbestos and fibrous serpentine wrapped by organic matter.

This progressive 'defibrillation' of the Perletoa sepiolite, triggered by the hydrocarbons sheath, not only causes a significant increase in the interfibrillar (open) porosity but also affects the fibre morphology enhancing its aspect ratio (length vs. thickness) from 'high' to 'very high'. The thinner and exceptionally long fibrils (rods and/or laths), therefore, potentially become more dangerous for human health due to their carcinogenic potential if dispersed in air and breathed in high doses.

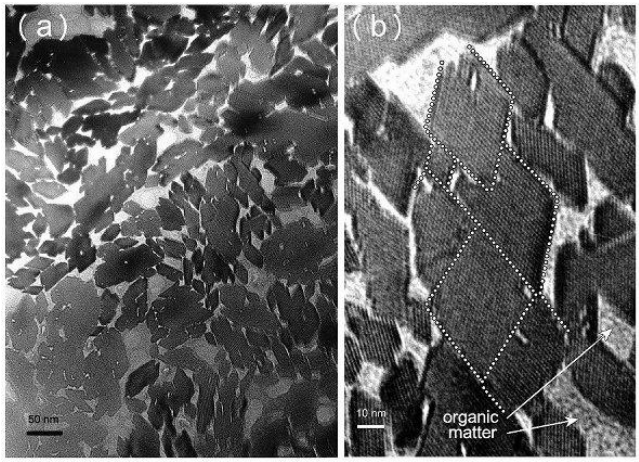

Figure 1: TEM micrographs of sepiolite fibres in cross section, observed along [001]. a) At medium magnification, fibrils show a rhomboidal to parallelogram-like contour and a large open texture. (b) At high magnification the incipient 'opening' process is evident (split surfaces: dashed white lines); a roughly continuous and scarcely electron-dense organic film (indicated by arrows) surrounds the fibres.

Quantitative mineral analysis of complex mineral assemblages – the Reynolds Cup round robins in clay analysis

Ploetze M

ETH Zurich. ploetzel@ethz.ch

The quantification of clays with phases having stacking faults like turbostratic disorder (e.g. smectite), with interstratified minerals (e.g. I/S), and with their strong tendency to preferred orientation in sample preparation has always been a big problem. The traditional methods like internal standard or RIR do not provide a satisfactory solution and also the Rietveld method is not able to fit the pattern with the same accuracy as for other phases.

In 2000 the Reynolds Cup, a biennial competition in quantitative mineral analysis was established. The Cup is supported by the Clay Minerals Society and open to anyone interested in quantitative mineral analysis with particular emphasis on clay mineralogy. The main goal is to promote and improve quantitative mineral analysis, but in a sportive spirit! Unlike in other round robins, mixtures of pure mineral standards that represent realistic sedimentary rock compositions were used. Although the choice of analytical approaches is free, the most commonly applied method is the XRD with Rietveld analysis.

The presentation deals with developments in analytical approaches in the decade of the Reynolds Cups. Results of the last (the 7th) Reynolds Cup in 2014 will be reported including specialties of the provided mixtures and details of their preparation as well as the analytical techniques used by the participants, particularly those used by the top three contestants.

Clay composition of bole layers of gilded Portuguese baroc retables

Rocha F[1*], Barata C[2], Andrejkovičová S[3], Reguer S[4], Cardoso A[5]

1 - Geobiotec/University of Aveiro *tavares.rocha@ua.pt 2 - Geobiotec, Conservation Dep, Cathol. Univ. Porto, Portugal 3 - Geosciences Dep., Geobiotec Res. Centre, Univ. Aveiro 4 - Synchrotron SOLEIL Diffabs, 91190 Saint Aubin, France 5 - HERCULES, Univ. Évora, 7000-809 Évora, Portugal

Boles were healing clays administered mainly orally as antacids, gastrointestinal protectors and antidiarrhoeaics. The red and yellow varieties were also used as a base in water gilding (protein based binder). Traditionally, it is designated as Armenian bole, in accordance with the best known origin (Armenia) and from which the best quality material was obtained. Probably due to its high cost, however, it was frequently adulterated. Furthermore, it has been clearly extracted in other regions, namely in Portugal, where good quality boles were obtained. Very little is known about the materials and techniques used in Portuguese gilded retables from the Baroque, although it had great symbolic importance in this period. For this reason, it is still not possible to characterize regional characteristics and their evolutionary processes. The main goal of this experiment was to characterize the geological source of the boles used, by comparison with samples collected from known Portuguese deposits analysed under the same experimental conditions. 18 erudite pieces belonging to Oporto (an important artistic centre during the Baroque) and 16 popular ones from the rural surroundings were selected. Boles elemental analyses were undertaken by SEM-EDS on cross sections. Bole layers show a homogeneous matrix, apparently without additives. A first scan of the bole layer has been followed by point analysis where rare earth elements were detected. Micro-FTIR and XRD analysis were also performed. On a second stage, we used SR-XRD (at synchrotron SOLEIL Diffabs, Saclay, France) for the analysis of a selection of samples taken from each one of the retables under research. The obtained results showed differences on the bole clay composition, both qualitative (presence/absence of certain clay minerals, such as kaolinite, illite and smectite) and semi-quantitative (namely, different predominant clay mineral). These results will assess if local clays were used in rural areas instead of boles available in the main trade centres.

Retardation capacity for ions and non-polar compounds by bentonite and functionalized organo-bentonites

Schampera B[1*], Solc R[2], Tunega D[2], Dultz S[1]

1 - Leibniz University of Hannover *schampera@ifbk.uni-hannover.de 2 - University of Natural Resources and Life Sciences (BOKU)

Clays are used in barrier systems to minimise pollutant discharge. Their most important properties include cation exchange capacity (CEC), plasticity, and the ability to impede diffusion. A challenge is how to improve the low anion exchange capacity (AEC) and sorption capacity of non-polar compounds, because pollutants such as anions and organics are of high environmental concern. Improvement is possible by modification with organic cations. The organo-clays have been shown to increase the AEC and to sorb anions and cations simultaneously as well as non-polar compounds.

For detailed characterization of material properties influencing retardation of ion transport in compacted clays (MX-80 bentonite, Wyoming), two organic cations, Hexadecylpyridinium ($HDPy^+$) and Hexadecyl-trimethylammonium ($HDTMA^+$) were used. Parameters controlling the retardation of NO_3^-, SeO_3^{2-} or phenanthrene were measured. The surface charge shifted from negative (-94 $mmol_c/kg$) to positive values (+385 $mmol_c/kg$) with increasing amount of organic cations that also highly affected their wettability (from hydrophilic to hydrophobic). The diffusion coefficient, e.g. for NO_3^- decreases from 7.5 x 10^{-9} m^2/s for the self-diffusion to 1.69 x 10^{-11} m^2/s for the sample with the high content of $HDTMA^+$.

Molecular dynamic (MD) simulations on the models corresponding to the experimental samples were performed to better understand the diffusion processes of ions (Na^+, Cl^-, I^-, NO_3^-). A surface coverage in models ranged from 0.125 to 1.5 $HDTMA^+$ ion/A_{uc} (unit cell area). The simulations were performed by the LAMMPS package [1]. Inter- and intramolecular interactions in the organo-clay models were described by the CLAYFF and OPLS-AA force fields. Decreasing diffusion coefficients of ions with increasing density of the organic cations were observed in accord with experimental observations. The surface properties of organo-clay have a strong impact on the retardation capacity that is higher for organo-clays than for natural clay. Therefore, organo-clays are prospective materials for engineered barriers.

[1] Plimpton S. (1995). Fast parallel logarithms for short-range molecular dynamics, Journal of Computational Physics, 117, 1-19. http://lammps.sandia.gov.

Swelling clay in artificial and natural anhydritic claystone

Wangler T*, Shahab A, Flatt R

ETH Zürich Institute for Building Materials. *wangler@ifb.baug.ethz.ch

The anhydritic claystones of the Gipskeuper in Switzerland and southwest Germany present a unique engineering problem for the road and rail tunnels through this formation. The relatively high amounts of anhydrite and swelling clays have caused repeated floor heave events and subsequent expensive repairs for these tunnels over the past few decades, due to the crystallization pressure of the anhydrite to gypsum transformation as well as the swelling of the clay [1, 2]. Systematic studies of this problem are difficult for a number of reasons, chief among them the coupling of the two phenomena and the relatively long time scales of the process, with experiments expected to span years and even decades [3]. A strategy that has been employed to generate faster results as well as higher reproducibility is to press samples of anhydrite and clay for swelling experiments [4, 5]. Additionally, it is known that above temperatures of about 40 °C, anhydrite becomes thermodynamically more stable than gypsum, effectively shutting off the anhydrite to gypsum transformation [6]. In this study, we use this thermodynamic "switch" to decouple the two swelling phenomena and examine swelling clays in isolation in artificially generated samples as well as natural samples.

[1] Grob H. (1975). Swelling and heave in Swiss tunnels. *Bull. Int. Assoc. Eng. Geol. - Bull. Assoc. Int. Géologie Ing.*, 14, 55-60.
[2] Anagnostou G., Pimentel E. and Serafeimidis K. (2010). Swelling of sulphatic claystones - some fundamental questions and their practical relevance /. Quellen von sulfatführenden Tonsteinen - Themen der Grundlagenforschung und ihre praktische Bedeutung. *Geomech. Tunn.*, 3, 567-572.
[3] Pimentel E. and Anagnostou G. (2013). New Apparatus and Experimental Setup for Long-Term Swelling Tests on Sulphatic Claystones. *Rock Mech. Rock Eng.*, 46, 1271-1285.
[4] Thuro K. (1993). DerPulver-Quellversuch - ein neuer Quellhebungsversuch. *Geotechnik*, 16.
[5] Azam S. and Abduljauwad S. (2000). Influence of Gypsification on Engineering Behavior of Expansive Clay. *J. Geotech. Geoenvironmental Eng.*, 126, 538-542.
[6] Charola A.E., Pühringer J. and Steiger M. (2007). Gypsum: a review of its role in the deterioration of building materials. *Environ. Geol.*, 52, 339-352.

Supported ionic liquids on montmorillonite as catalysts for cobalt-based Fischer-Tropsch synthesis

Zhang B, Su H*, Xing H

School of Chemistry and Chemical Engineering, Inner Mongolia University, Inner Mongolia Key Laboratory of Coal Chemistry, Hohhot 010021, P.R.China.
*haiquansu@yahoo.com

The Fischer-Tropsch synthesis (FTS) is a key gas to liquid (GTL) process that converts synthesis gas to clean environment-friendly liquid fuels. Immobilization of ionic liquids onto solid supports as catalytic materials has attracted significant attention. Here, supported ionic liquids on montmorillonite (MMT) as novel supports are first applied to cobalt-based Fischer-Tropsch synthesis.

In the experiments, an oligomer ionic liquid with excellent thermal stability anchored onto the montmorillonite was designed to prevent the active Co components and phases generated during catalytic reaction from being oxidized when they are exposed to air. A schematic representation of this amber-inspired approach is shown in Figure 1. Consequently, the changes of the active species such as ε-Co to hcp Co and ε-Co to fcc Co phase transformation, Co nanoparticle growth, reoxidation during reaction, and the structure-property relationship of FTS catalysts were revealed clearly.

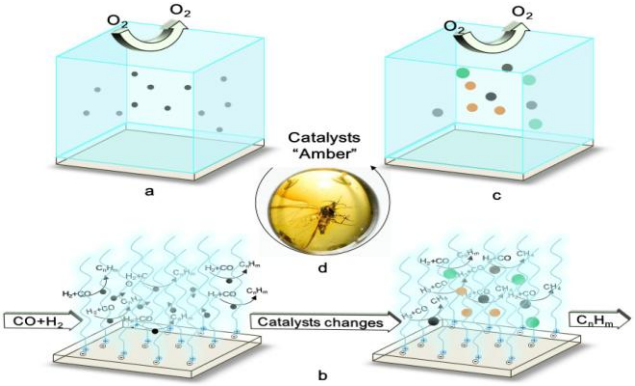

Figure 1: Schematic representation of the supported ionic liquid on montmorillonite as catalyst to trap the working state of active nanoparticles.

Moreover, a series of imidazolium and phosphonium ionic liquids modified montmorillonite supports and their corresponding catalysts were prepared and the FTS catalytic performance was investigated. Figure 2 shows that the imidazolium modified catalyst displayed a significantly improved catalytic activity compared with pure montmorillonite as carrier. On the contrary, the phosphonium modified catalyst deteriorated the catalytic activity.

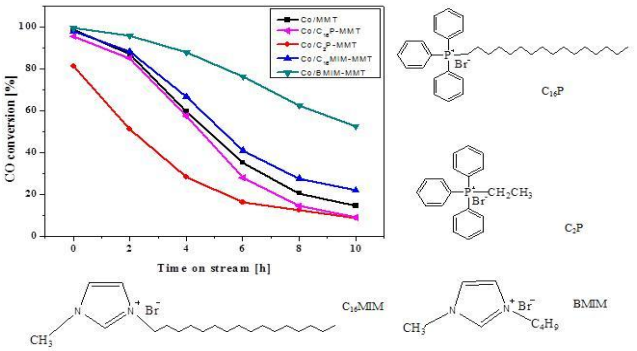

Figure 2: Variation of CO conversion with time on stream over the catalysts with different ionic liquids modification.

Acknowledgement: Project supported by the National Natural Science Foundation of China (grant no.20661001) and the Inner Mongolia University high-level scientific research foundation for the introduction of talent (grant no. 135128).

Sodium modification of Ca-bentonites by tri-roller grinder

Miao M, Zhang B, Su H*

School of Chemistry and Chemical Engineering, Inner Mongolia University
*haiquansu@yahoo.com

Sodium bentonites have several advantages over calcium bentonites, especially in expansibility, cation exchange capacity (CEC), cohesive force, dispersibility etc. Compared with conventional screw extrusion, tri-roller grinder provides an alternative method for sodium modification of Ca-bentonites.

In this paper, the mineralogical composition of bentonite was determined by XRD technique. The XRD patterns of natural Ca-bentonite and bentonite samples with different extrusion times (Figure 1) show that the d-spacing of montmorillonite decreases from 1.52 nm (2θ = 5.80°) to 1.24 nm (2θ = 7.16°), demonstrating that Ca-montmorillonite was completely converted to Na-montmorillonite after sodium-modification. The thermoanalysis results (Figure 2) demonstrate that the typical two endothermic peaks of Ca-montmorillonite were changed to one endothermic peak of Na-montmorillonite, which also confirmed the formation of Na-montmorillonite. The tri-roller grinder provided a convenient and effective method for sodium modification of Ca-bentonites.

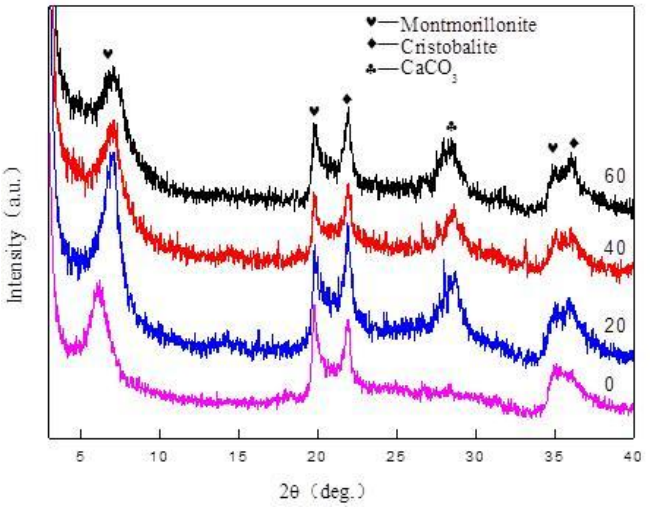

Figure 1: XRD patterns of the bentonite samples with different rolling times (the numbers represent the rolling times).

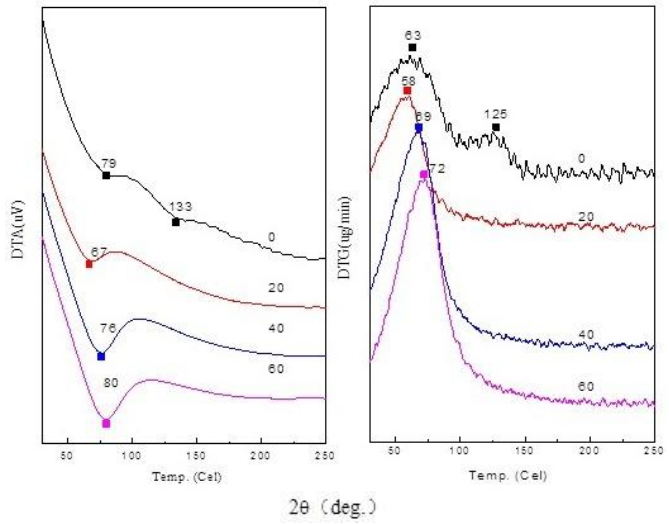

Figure 2: DTA (left) and DTG (right) curves of the bentonite samples with different rolling times (the numbers represent the rolling times).

Acknowledgements: Project supported by the science and technology innovation team of high efficiency and clean conversion technology for superior resources in Inner Mongolia (grant no. 21020101) and the Inner Mongolia University high-level scientific research foundation for the introduction of talent (grant no. 135128).

The hydrothermal synthesis of crystalline layered calcium manganese oxide using Mn residues and its transformation into Ca-OMS-2

Pöllmann H[1*], Miranda Figueiro B[2], da Costa M[2]

1 - Martin Luther University, Halle-Saale *herbert.poellmann@geo.uni-halle.de
2 - University of Belem

This work describes the synthesis of octahedral layered manganese oxide with Ca^{2+} as interlayer cations (Ca-OL-2) and its conversion to the octahedral molecular sieve (Ca-OMS-2) employing manganese oxides from old residue disposal in Carajás (northern Brazil). Due to its clay and zeolite-like structures, much interest has been focused on synthetic manganese oxides, since these materials can exhibit excellent cation exchange, catalytic and adsorptive properties. Firstly, a Na-birnessite-type structure (Na-OL-1) was obtained from Mn residues using the method reported [1]. Afterwards, a sample of 0.1 g of Na-OL-1 was treated with 1 mol.L^{-1} solution of $CaCl_2.2.H_2O$ at 25 ºC to obtain a Ca-buserite-type structure (Ca-OL-2, expanded birnessite to 10 Å). Ca-OL-2 was filtered and washed with deionized water followed by hydrothermal treatment in a Teflon-lined stainless steel autoclave between 120-160 ºC for 2 days at pH 4.5 for buffer solution. The synthesized solid (Ca-OMS-2) was thoroughly washed with deionized water and then dried at 40º C for 6 hours. The products have been characterized using X-ray powder diffraction (XRD), infrared spectroscopy (FTIR) and scanning electron microscopy (SEM-EDS). The XRD results clearly showed the transformation from Mn residues into a lamellar structure with basal spacing around 7 Å. When the hydrothermal treatment was conducted at 150 ºC, Ca-OL-2 was converted to an OMS-2 type structure. FTIR bands around 410, 475, 510, 524 and 710 cm^{-1} were observed and are diagnostics of manganese oxides with either layered and tunnel structures, respectively. The SEM images of the synthesized lamellar phase (Na-OL-1) showed a typical hexagonal platy morphology (Figure 1a) or fibrous-like one for Ca-OMS-2 (Figure 1b). These results have indicated that Mn residues can be excellent raw materials for the synthesis of lamellar and octahedral molecular sieve structure.

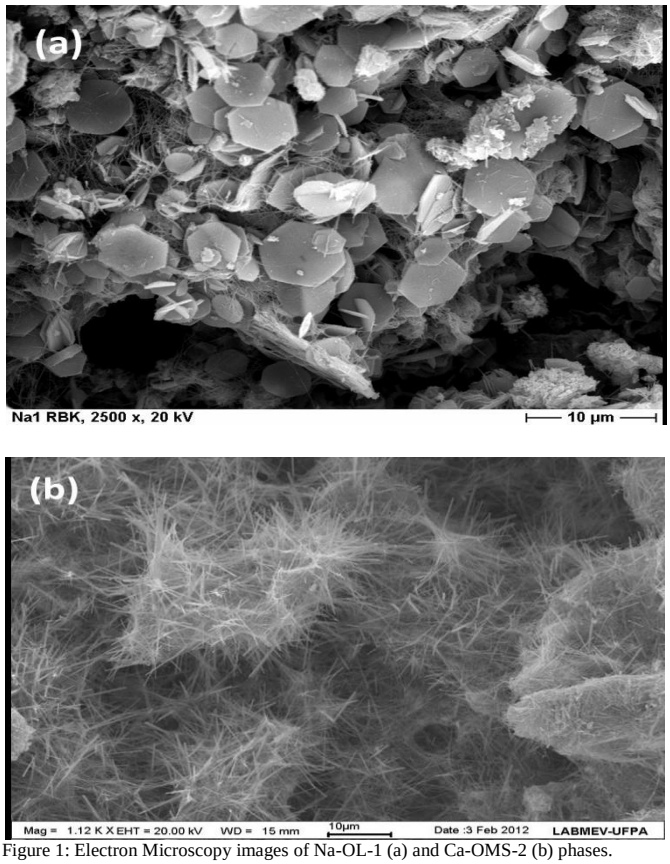

Figure 1: Electron Microscopy images of Na-OL-1 (a) and Ca-OMS-2 (b) phases.

Keywords: Mn residues, hydrothermal synthesis, Na-OL-1, Ca-OL-2, Ca-OMS-2

[1] Cornell R.M. and Giovanoli R. (1988). Transformation of hausmannite into birnessite in alkaline media. *Clays and Clay Minerals*, 36, 249-257.

Effect of layer charge on the swelling of Na^{+}, K^{+}, Cs^{+} and Ca^{2+}-montmorillonites: a molecular dynamics simulation

Seppala A*, Puhakka E, Tanhua-Tyrkkö M
VTT Technical Research Centre of Finland *anniina.seppala@vtt.fi

Bentonite buffer is an essential component planned in the KBS-3 concept for safe disposal of spent nuclear fuel. It limits mass flow to and from the copper canister to prevent corrosion, and in the case of canister failure, it retards transport of radionuclides to bedrock, and it protects the canister in the case of large dislocations of bedrock caused by e.g. tectonic movement. Bentonite consists of montmorillonite, which is the clay's main and functional component, some dissolved salts and accessory minerals. Montmorillonite is a swelling clay mineral that consists of 1 nm thick and approximately 200-400 nm wide negatively charged layers and charge compensating cations near the mineral surfaces. It has the ability to absorb water molecules into the interlayer space, resulting in swelling of the mineral, and the ability to change its cationic composition. Bentonite's beneficial properties are based on nano level reactions and structures, and therefore molecular level studies are needed regarding long term performance studies of spent fuel disposal.

The aim of this work is to study the effect of layer charge on montmorillonite's swelling properties. Three different layer charges are applied to four montmorillonites (Na, Ca, K and Cs) with 16 different water contents (from 1-16 molecules per unit cell), which means about 1-3 water layers in the interlayer space. Larger basal spacings are observed with lower layer charges of Na- and Ca- montmorillonites, and swelling is greater with lower charges. Results for K- and Cs-montmorillonites will be reported later. Molecular dynamics calculations are performed on a one-layered montmorillonite particle in a periodic simulation box. The objective is to determine the interlayer thickness at equilibrium state in each case. Calculations are done using the molecular dynamics software LAMMPS[1] with the CLAYFF[2] interaction potential. As a result, swelling curves with respect to the number of water molecules per unit cell are determined (the swelling curves of Na-montmorillonite are presented in Figure 1). Comparisons to the sample system density (contribution only from mineral layer and interlayer) and the number of interlayer water layers are made.

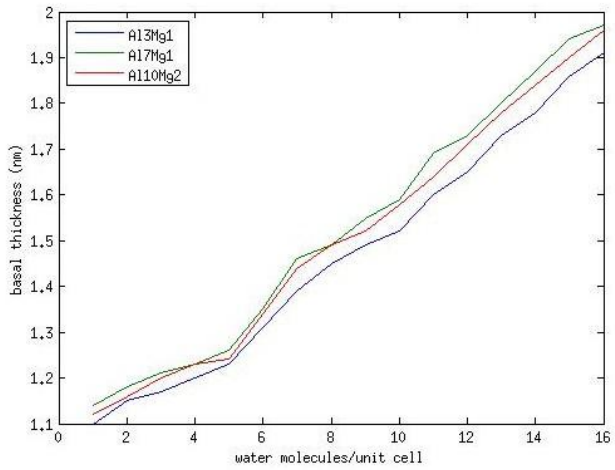

Figure 1: Swelling curves of Na-montmorillonites with varying number of octahedral substitutions (aluminum to magnesium).

[1] Plimpton S. (1995). Fast Parallel Algorithms for Short-Range Molecular Dynamics, *J Comp Phys*, 117, 1-19. http://lammps.sandia.gov.

[2] Cygan R.T. *et al.* (2004). Molecular Models of Hydroxide, Oxyhydroxide, and Clay Phases and the Development of a General Force Field, *J Phys Chem B*, 108, 1255-1266.

Structure and occurrences of green rust related new minerals of the fougérite group, trébeurdenite and mössbauerite, belonging to the hydrotalcite supergroup; how Mössbauer spectroscopy helps XRD

Genin J[1*], Christy A[2], Ruby C[3], Mills S[4]

1 - Institut Jean Barriol-ESSTIN -Université de Lorraine
*jean-marie.genin@univ-lorraine.fr 2 - Australian National University 3 - Institut Jean Barriol (FR2843), ESSTIN-Université de Lorraine 4 - Museum Victoria

Fe^{II-III} compounds often called "green rusts" were studied since the eighties to explain the corrosion of steels in E_h-pH diagrams. Part of the layered double hydroxides family (LDH) where divalent and trivalent cations belong to iron, present outstanding redox properties. Whereas X-ray diffraction (XRD) reveals stacking of $[Fe^{II}_{(1-x)}\ Fe^{III}_x\ (OH)_2]^{x+}$ layers and $[(x/n)A^{n-} \bullet m(H_2O)]^{x-}$ interlayers, Mössbauer spectroscopy determines the ferric ionic ratio $x = \{[Fe^{III}] / Fe_{total}]\}$ that lies within the range [1/4, 1/3]. Quadrupole doublets at 78 K; D_1 and D_2 with large splitting are due to Fe^{II} ions where D_2 is in register to an anion, whereas D_3 of small splitting is due to Fe^{III} ions. Three x values 1/4, 2/7 and 1/3 insure that each Fe^{III} is surrounded by six Fe^{II} cations. Cation order depends on the charge, size and shape of anions in interlayers as testified by the cases of oxalate, methanoate and carbonate.

In 1996, Mössbauer spectroscopy designated the mineral responsible for the bluish color of gleys in samples from Fougères (Brittany). Similar to "green rusts", it was named "fougérite" displaying an x ratio in the range [1/3, 2/3], whereas the synthetic sample had a ratio equal to 1/3. A "green rust" presents two modes of oxidation, (i) classically, it dissolves and an orange-brownish ferric oxyhydroxide precipitates, (ii) an in situ oxidation by deprotonation occurs in conditions such as fast oxidation keeping its global structure unchanged. A product where x >1/3 is obtained by bacterial reduction of ferric oxyhydroxide in anoxic conditions. In 2010, gleys extracted from maritime marshes in Trébeurden (Brittany) and Mont-Saint Michel Bay showed x ratio in the [2/3, 1] range. But it is a mixture of distinct minerals with similarities and topotaxical relationships and IMA accepted them as **fougèrite, trébeurdenite and mössbauerite** for x values of 1/3, 2/3 and 1.

In green rusts with CO_3^{2-} anions, the minerals constitute the fougèrite group where the structure stays globally unchanged; a difference comes from deprotonation of OH^- ions at the apices of octahedrons occupied by cations and Fe^{II} become Fe^{III}. The centered rectangular mesh comprises four CO_3^{2-} ions in configurations and presenting a 2D long range order with primitive rhombic mesh $\sqrt{12} \times \sqrt{12}$; the hexagonal mesh in Fe layers is $\sqrt{3} \times \sqrt{3}$ for fougèrite and trébeurdenite. Synchrotron XRD patterns display different stacking sequences in mössbauerite and fougèrite where prevailing polytypes are compatible with a short range coupling.

Industrial applications of green rusts related minerals, fougérite, trébeurdenite and mössbauerite: from steel corrosion to water purification

Genin J[1*], Ona-Nguema G[2], Ruby C[3]

1 - Institut Jean Barriol-ESSTIN -Université de Lorraine
*jean-marie.genin@univ-lorraine.fr 2 - Institut de Minéralogie & Physique des Milieux Condensés, 3 - Institut Jean Barriol (FR2843), ESSTIN-Université de Lorraine

Fe^{II-III} hydroxysalts were originally studied in the eighties to understand the corrosion of iron-based materials and steels since they are intermediate compounds between metallic iron and ferric oxyhydroxide end products; therefore, they are called commonly green rusts because of their color. They belong to the double layered hydroxide family and own unchallenged redox properties since both divalent and trivalent cations come from the same iron element, where Mössbauer spectroscopy allows us to determine very easily the molar ferric ratio $x = \{[Fe^{III}]/ ([Fe^{II}] + [Fe^{III}])\}$. The discovery in 1996 of a green rust related mineral in the gleys of hydromorphic soils of aquifers opened a new field of potential applications since synthetic green rusts are able to reduce oxidized pollutants.

An explanation of what occurs in the field was found by oxidizing carbonated green rust with H_2O_2 as demonstrated by Mössbauer spectroscopy. The oxidation proceeded by in situ deprotonation of OH^- ions making us think that a phase Fe^{II-III} oxyhydroxycarbonate with formula $Fe^{II}_{6(1-x)}\ Fe^{III}_{6x}\ O_{12}\ H_{2(7-3x)}\ CO_3 \bullet 3H_2O$ does exist instead of dissolving in solution for precipitating a usual ferric oxyhydroxide FeOOH as it does with oxygen. Any average value of x ratio comes from mixing domains of the "fougèrite group" that transform topotaxicaly during the redox reaction as explained elsewhere in this volume [1].

Firstly, a comparison of the E_h-pH diagrams between the dissolution-precipitation oxidation and the in situ deprotonation modes explains the remarkable properties of weathering (CORTEN®) steels which were empirically discovered in the sixties; the protection of these steels comes from the in situ deprotonation of the green rust layer that forms at the steel surface giving the ferric mössbauerite. Another development is currently investigated; the minerals found in gleysols of characteristic bluish-green shade come from the bacterial reduction of natural ferric oxyhydroxides in anoxic conditions under the water table of aquifers. Results from the development of a tertiary treatment for waste water denitrification will be presented. Finally, the landscaping of "watered areas with reinforced iron purification" (WARIP) which is starting in Brittany for large scale treatment in the field will be discussed. This development is intended to solve in the long term the devastating proliferation of algae at the mouth of coastal rivers and beaches due to intense agricultural activity.

[1] Genin J., Christy A., Ruby C. and Mills S. (2014). Structure and occurrences of green rust related new minerals of the fougèrite group, trébeurdenite and mössbauerite, belonging to the hydrotalcite supergroup; how Mössbauer spectroscopy helps XRD. *IMA2014 abstract volume*.

Possible biogenesis for the occurrences of the trébeurdenite-mössbauerite minerals in salt marshes

Guerin O[1], Genin J[2*]

1 - EPHE laboratoire de Geomorphologie * jean-marie.genin@univ-lorraine.fr 2 - Institut Jean Barriol-ESSTIN -Université de Lorraine

Samples of sediments where trébeurdenite and mössbauerite were identified for the first time were obtained from ancient salt marshes under present beaches, pebbles and/or sand, in Northern Brittany (France). Some of them are older than 3000 years and others more recent (Middle ages). Their identification is easy, because of their very fine grain size (<20mm) similar to clay and by their bluish color that is very homogeneous. These formations are found in bays where hydrodynamic conditions are met, i.e. weak current, swell protection, due to dune or pebble ridges.

However, they are also found in present sedimentary deposits in large bays such as Mont-Saint Michel Bay into which one million m^3 of sediments enter each year from the erosion of the western coast, essentially granitic arena and quaternary loess, which are both rich in iron. Present deposits in Mont Saint Michel Bay are presently forming in the western part close to Cancale where currents are weak and rotary. The formation of the mixture of the two minerals is efficient when the sediments are depositing; this suggests that it would be done during the transport with a possible intervention of marine organisms. The presence of these sediments in deep sea beds has also been reported. It is clear that this presentation opens up a large field of further studies all over the planet.

Synthesis and in situ X-ray investigation of manganeous Layered Double Hydroxides (LDHs) intercalated with inorganic anions

König U[1*], Pöllmann H[2]

1 - PANalytical B.V., Almelo, The Netherlands *uwe.konig@panalytical.com

2 - Martin Luther University, Halle-Saale, Germany

Layered double hydroxides, LDHs, also known as mixed-metal layered hydroxides (MMLHs) and hydrotalcite-like compounds (HTs) are an important class of materials with permanent anion exchange capacity [1]. The natural and synthetic compounds are important for a wide field of applications, such as catalysis, environmental remediation, medicine and the hydration of cements. In order to use such compounds in an optimal and efficient way for technical purposes, the formation and properties need to be understand and investigated.

XRD was used to follow the precipitation and dehydration of manganeous LDHs with the inorganic anions Cl^-, NO_3^-, Br^-, I^- and ClO_4^-. We will show the optimal conditions for the synthesis and discuss the properties of the different compounds. Synthesis and characterization of SO_4^{2-} intercalated manganeous LDHs from the shigaite type will be discussed in a separate paper.

In situ XRD in combination with other techniques and statistical evaluation of the data (PCA analysis) was the main tool to describe the thermal behaviour of $[Mn_6Al_3(OH)_{18}][Cl{\cdot}4H_2O]$. Characterization of the crystallinity and shape of the synthesized LDHs was done using Cryo-SEM, enabling the analysis of water containing components that are not stable under ambient vacuum conditions.

[1] Cavani F., Trifiro F. and Vaccari A. (1991). Catalysis Today, Vol. 11, 173-301.

Properties and synthesis of alkali-substituted shigaite

König U[1*], Pöllmann H[2]

1 - PANalytical.B.V., Almelo, The Netherlands *uwe.konig@panalytical.com

2 - Martin Luther University, Halle-Saale, Germany

Synthetic manganeous Layered Double Hydroxides of the Shigaite-type were prepared by the co precipitation method. The thermal behaviour of the compounds, $[Mn_6Al_3(OH)_{18}]$ $[(SO_4)_2X*12H_2O]$ with X = Li, Na, K, Rb, Cs, NH_4^+ was investigated by several experimental techniques. Different conditions were used for the synthesis. The influence of temperature (20°C, 40°C, 60°C), pH (7, 8, 9, 10, 11), reaction time (1d, 4d, 7d, 14d, 21d) and varying manganese/aluminium ratios were examined. Thermal analysis and in-situ X-ray diffractometry show several dehydration stages of the synthesis products in the temperature range of 25 <T <170°C followed by decomposition at temperatures above 200°C.

Synthetic Shigaite-like compounds have a structure consisting of brucite-like octahedral layers. The net positive charge of the brucite-like octahedral layers is balanced by an equal negative charge from the interlayer anions. Water molecules occupy residual space and additional space with the compensating anions in the interlayer region.

The main results are as follows: (1) Alkali-substituted shigaite-like compounds were synthesised under CO2 exclusion (glove box under nitrogen) under defined conditions (Table 1). (2) Thermal behaviour was investigated with thermal analysis and in-situ X-ray investigation using the PANalytical X´Celerator module. Dehydration is carried out at two stages (60°C and 90-120°C).

Table 1 Synthesized alkali-substituted Shigaites.

Shigaite-Na	$[Mn_2Al(OH)_6]_3$ $[(SO_4)_2Na(H_2O)_6(H_2O)_6]$
Shigaite-Li	$[Mn_2Al(OH)_6]_3$ $[(SO_4)_2Li(H_2O)_6(H_2O)_6]$
Shigaite-K	$[Mn_2Al(OH)_6]_3$ $[(SO_4)_2K(H_2O)_6(H_2O)_6]$
Shigaite-Rb	$[Mn_2Al(OH)_6]_3$ $[(SO_4)_2Rb(H_2O)_6(H_2O)_6]$
Shigaite-Cs	$[Mn_2Al(OH)_6]_3$ $[(SO_4)_2Cs(H_2O)_6(H_2O)_6]$
Shigaite-NH_4^+	$[Mn_2Al(OH)_6]_3$ $[(SO_4)_2NH_4(H_2O)_6(H_2O)_6]$

Fougerite group minerals from the bottom sediments of the freshwater lakes of the Ilmen State Reserve (South Urals, Russia)

Shcherbakova E[1*], Nikandrova N[2], Valizer P[3], Nikandrov A[3], Nikandrov S[3]

1 - Institute of Mineralogy *founds@ilmeny.ac.ru 2 - Institute of Mineralogy of Ural Branch RAS, Miass, Russia 3 - Ilmen State Reserve of UB RAS, Miass, Russia

Green rust (GR) compounds close to fougerite group minerals (FGM) have been found in the bottom sediments of the freshwater lakes of the Ilmensky Reserve (South Urals, Russia) [1, 2].

Fougerite group minerals are localized in the lacustrine marls composing the lower horizons of lake sediments or on the Fe-Mn-Ni substrates of unknown origin. In the lacustrine marls, fougerite group minerals crystallize on the particles of phyllosilicates, mainly micas, forming micro- and nanoscale epitaxial growths.

The problems of diagnostics of fougerite group minerals in the presence of other Fe-containing phases (illite, chlorite, pyrite) as well as accordance of real compositions of FGM and their ideal formulas are discussed.

[1] Genin J-M.R. *et al*. (2012). Hyperfine interactions, 71-81.

[2] Valizer P. *et al*. (2013). Vestnik IG Komi SC RAS, 5, 6-8 (in Russian).

Crystal-chemical controls on smectite hydration

Lanson B[1*], Dazas B[1], Ferrage E, Delville A[2]

1 - ISTerre - CNRS / Univ. Grenoble * bruno.lanson@obs.ujf-grenoble.fr 2 - CRMD - CNRS / Univ. Orléans

Swelling clay minerals such as smectites are ubiquitous at the Earth surface and possess major hydration ability and contaminant uptake/retention capacity. As a consequence smectites exert a pivotal influence on elemental transfers in surficial environments. These properties are especially relevant also when smectites are used as sealant in engineered or geological barriers for waste disposal facilities. As interlayer H_2O molecules account for more than 80% of smectite water in undersaturated conditions, characterization of H_2O organization and dynamics in smectites interlayers is essential to determining the geometrical and dynamical properties of clay barriers for waste disposal and to predicting the mobility of contaminant whose principal vector is water.

Within this general framework, the main goal of the present talk is to review the influence of structural parameters such as the amount and location of layer charge deficit and the chemical composition (and more especially the presence of structural fluorine/hydroxyl) on smectite hydration properties. A set of samples covering the whole compositional range of swelling phyllosilicates has thus been synthesized and characterized chemically and structurally. Special attention was paid to determining the amount (water vapor sorption isotherms) and the distribution (X-ray diffraction) of interlayer water.

Molecular modeling allowed unraveling the origin of the contrasting behaviors observed experimentally and to determine the influence of the different crystal-chemical parameters on smectite hydration. This step is essential for the prediction of smectite reactivity in the environment from a limited number of crystal-chemical parameters.

^{23}Na, ^{27}Al and ^{29}Si NMR-MAS investigation of synthetic saponites and sodium micas

Sanz J[1], Sobrados I[1], Robert J-L[2*]

1 - Instituto de Ciencia de Materiales, CSIC, Cantoblanco, 28049 Madrid, Spain

2 - IMPMC (UMR 7590), Université Pierre et Marie Curie, CNRS, IRD, MNHM, 4 place Jussieu, 75252 Paris Cedex 05, France. *jean-louis.robert@impmc.upmc.fr

Saponite solid solutions synthesised at 400°C, 0.1 GPa, for 4 weeks with the composition $Na_xMg_3(Si_{4-x}Al_x)O_{10}(OH)_2.nH_2O$, with $0.33 \leq x \leq 1$, and trioctahedral sodium mica solid solutions, which belong to the aspidolite $NaMg_3(Si_3Al)O_{10}(OH)_2.nH_2O$ - preiswerkite $Na(Mg_2Al)(Si_2Al_2)O_{10}(OH)_2$ join with general formula $Na(Mg_{3-y}Al_y)(Si_{3-y}Al_{1+y})O_{10}(OH)_2 .nH_2O$, prepared at 500°C, 0.1 GPa for 3 weeks, have been studied by NMR-MAS of ^{23}Na, ^{27}Al and ^{29}Si, in their wet and the dry forms. All saponites exhibit the two-layer hydrated form ($5H_2O$ per Na) with d_{001} = 15 Å. In Na-micas the one layer hydrate ($2H_2O$ per Na, d_{001} = 12 Å) is dominant for low y values, and anhydrous phases (d_{001} = 10 Å) are observed for high Al contents. These different hydration states generate distinct bands in ^{23}Na NMR spectra, at 0, -9 and -20 ppm respectively. In dry samples, only the last one persists. One of the salient results is the effect of the interlayer charge, from 0.33 to 1, on chemical shifts of the four ^{29}Si components, Q_0 [Si(3Si)], Q_1 [Si(2Si, 1Al)], Q_2 [Si(1Si, 2Al)] and Q_3 [Si(3Al)]. This effect is significantly superior to that of the commonly admitted ditrigonal distortions of the tetrahedral layer. NMR spectra of ^{29}Si and ^{27}Al change considerably with the hydration of the interlayer sodium in saponites and sodium micas. In hydrated samples, the Na^+ cation mainly interacts with water molecules and the chemical shifts are averaged as a consequence of interlayer water and of mobility of compensating cations. In anhydrous saponites, where Na^+ is close to the basal oxygens of tetrahedra, the NMR components split as a consequence of the different Na^+ occupancy of the three interlayer sites adjacent to a given (TO_4) tetrahedron. In Na micas, NMR spectra of Si are formed by addition of one-layer and anhydrous phases, with all ditrigonal holes occupied by Na^+ cations.

Keywords: NMR-MAS, 29Si, 27Al, 23Na, smectites, micas, hydration

Influence of composition on the configuration of tetrahedra in 2:1 layer silicates

Robert J-L

CNRS-UPMC, Paris IMPMC (UMR 7590), Université Pierre et Marie Curie, CNRS, IRD, MNHM, 4 place Jussieu, 75252 Paris Cedex 05, France.
jean-louis.robert@impmc.upmc.fr

Analysis of T-O distances in layer silicates shows that tetrahedra with ideal T_d symmetry are exceptional, most (TO_4) tetrahedra having much lower symmetry. A predictive model, based on bond valences is proposed. In talc, each (SiO_4) tetrahedron is adjacent to three identical (SiO_4) tetrahedra and to three octahedra occupied by Mg^{2+}. The charge balance on all oxygens is obeyed without distortions of polyhedra and the (SiO_4) tetrahedron exhibits four equal Si-O bonds, 1.624 Å. This results in a single FTIR absorption band, at ~1030 cm^{-1}, in the antisymmetric Si-O_b-Si_{as} (i.e. Si-O parallel) and Si-O_{apical} (i.e. Si-O perpendicular) region. In phyllosilicates with charge generated in octahedra only, like hectorites $Na_x(Mg_{3-x}Li_x)Si_4O_{10}(OH,F)_2$, the tetrasilicic magnesium mica $K(Mg_{2.5}v_{0.5})Si_4O_{10}(OH)_2$, where v stands for a vacant site and the tetrasilicic Li-micas tainiolite $K(Mg_2Li)Si_4O_{10}(OH,F)_2$ and polylithionite $K(Li_2Al)Si_4O_{10}(OH,F)_2$, the compensating cation induces a local charge excess on basal oxygens. The structure accommodates this local charge imbalance by modifying the tetrahedral configuration with three long Si-O_b (around 1.63 Å) and one short Si-O_{apical} (close to 1.60 Å) bonds. This results in a splitting of Si-O bands, with a low-intensity band at 1100 cm^{-1} due to the Si-O_{apical} vibration, and a high-intensity one at 950 cm^{-1}. The intensity ratio of these bands is near 3/1 and reflects the proportion of Si-O bond species. These bands are complex and can be decomposed in elementary Gaussians whose positions and intensities reflect local fluctuations of the octahedral composition. The introduction of Al^{3+} or another low-valence cation in the tetrahedral layer induces the opposite effect. The basal T-O_b bonds become shorter and the T-O_{apical} one increases in length. The tetrahedral regularity, initially observed for talc, is reached again for the composition $A^+(Mg_{2.5}Al_{0.5})(Si_{2.5}Al_{1.5})O_{10}(OH)_2$, with $A^+ = Na^+$ or K^+, but the band position is shifted towards low wavenumbers (35 cm^{-1}). In more aluminous compositions, typically disilicic phases, like preiswerkite, $Na(Mg_2Al)(Si_2Al_2)O_{10}(OH)_2$ or ephesite $Na(Al_2Li)(Si_2Al_2)O_{10}(OH)_2$, the trend is similar, and basal T-O_b bonds become shorter than the T-O_{apical} one. In this case, the T-O_{apical} stretching band is observed at a lower value of ~900 cm^{-1}. Overall, the shift of this band is therefore considerable, from 1100 cm^{-1} in tetrasilicic 2:1 layer silicates to 900 cm^{-1} in disilicic ones. The use of FTIR data as fingerprints in the T-O stretching range may thus be misleading for phyllosilicates.

Key-words: tetrahedral configuration, FTIR, charge balance, talc, micas, smectites

Cation occupation study for a chromium bearing montmorillonite

Nuertai M[1], Tuersun M[1], Cai Y[1*], Wang H[2], Pan Y[1]

1 - State Key Laboratory of Metal Ore Deposits, School of Earth Sciences and Engineering, Nanjing University *caiyf@nju.edu.cn

2 - Key Laboratory of Surficial Geochemistry, Ministry of Education. School of Earth Sciences and Engineering, Nanjing University

The purified montmorillonite with trace amounts of quartz was equilibrated with different concentration chromium sulphate solutions for one week cation exchange. The obtained chromium bearing montmorillonites were verified and tested using powder X-ray diffractometry (XRD), X-ray Fluorescence (XRF), Electron Spin Resonance (ESR) spectrometry and Fourier Transform Infrared (FTIR) spectroscopy to explore the occupation site of chromium. Compared to the FTIR spectra of purified montmorillonite, the octahedral hydroxyl bands, such as Al_2OH, showed a less than two cm^{-1} shift to the higher band sides in both of the lower and middle bands, and a ~20 cm^{-1} shift to a lower band sides of the Si-OH vibrations in the FTIR spectra of chromium bearing ones. However, the MgAlOH band was almost unshifted. These results might suggest the substitution of chromium for the octahedral aluminium. ESR spectra strongly differ before and after chromium exchange, the disappearance of the signals of both Mn^{2+} and free Fe^{3+}, and the new signals from the chromium suggesting several occupational sites for chromium. However, the intensity of the Fe^{3+} in the tetrahedron of the TOT unit of the montmorillonite is stable suggesting that no Cr^{3+} substitutes the ferric iron in tetrahedral sites. However, the signal near this ferric cation disappeared after the substitution, suggesting that the chromium entered this kind of structural sites. Furthermore, based on the XRD analysis and the calculation of the size of the interlayer space, two types of montmorillonites with different kinds of hydration cations were inferred to be present in 0.2M chromium sulphate solutions exchanged ones. The hydration cation might be the $[Cr(H_2O)_6]^{3+}$ and $[Cr(H_2O)_3O_3]^{3+}$, respectively. This may suggest that the species of hydration cation is constrained by the concentration of the chromium solution.

In summary, the results comprehensively suggested that the Cr^{3+} can exchange the cation in octahedral sites, such as Mn^{2+}, Al^{3+} in octahedra, Al^{3+} in tetrahedra and the cation adsorbed on the surface of clay grains, as well as the cations in the interlayer space of montmorillonite, such as Ca^{2+}, K^+ and Na^+ etc.

Acknowledgements: This study was supported by NSFC Project (41272055) and grant (G1210284013) from the ability of innovating and Entrepreneurship training programme (Nanjing University).

Structural and mechanical properties of silicate ceramics shaped by tape-casting

Houta N

Laboratoire Groupe d'Etude des Matériaux Hétérogènes (GEMH), France

nadia.houta@etu.unilim.fr

Phyllosilicates are abundant raw materials offering a wide range of applications, from traditional ceramics (e.g. tableware) to functional high-added value ceramics (e.g. filtration membranes). If individual kaolin and smectite aqueous suspensions have been extensively investigated, few studies deal with the behavior of clay mineral mixtures, which are more process and applications relevant. Tape casting is a shaping process allowing preparation of thin ceramic layers ranging from 25 µm to 1500 µm. These layers can be stacked, thermocompressed, cut, and sintered to make multilayer ceramics. Such products can allow preparing capacitors, filtration membranes or fuel cells.

Two clays were used namely: BIP kaolin from Kaolins de Beauvoir in France and NZCC halloysite from New Zealand. A dispersant, a plasticizer and a binder were also used namely: dolaflux B, polyethylene glycol 300 and polyvinyl-alcohol 22000. The first part is aimed at optimizing the milling step and dispersion of the different aqueous clay suspensions by considering the rheological behavior, particle size distribution, specific surface area, ionic conductivity and viscosity.

In a second part, the sintering conditions were determined using thermal analyses (thermogravimetric, differential thermal and dilatometric analyses). The structural characteristics of the manufactured green tapes and sintered tapes were performed using scanning electron microscopy, interferometric microscopy, X-ray diffraction, mercury porosimetry. Mechanical properties were also determined through biaxial bending tests.

Results (for kaolin/ halloysite mixture) indicated that dolaflux was the most suitable dispersant for the studied clay suspensions. The optimal dolaflux amount was 0.2 mass% regardless of the clay type. Concerning the shaping process, the binder/plasticizer ratio equal to 1 allowed to reach the required viscosity and to improve the quality of the tapes. The texturation within the tapes, due to the shape of clay particle (platelets) as well as the organic phase distribution, leads to structural anisotropy between the upper surface and the basal surface of clay tapes. This anisotropy was maintained after sintering at the optimized temperature of 1150°C, determined by dilatometriy measurements. Furthermore, the mechanical biaxial bending strength was increased from 80 to 150 MPa after sintering.

Keywords: kaolin, halloysite, illite, tape-casting, green tape, sintering, microstructure, porosity, mechanical properties.

Thermochemical study of clinochlore from Korshunovskoe deposit (Siberia, Russia)

Ogorodova L[1], Krupskaya V[2], Melchakova L[1], Kiseleva I[1], Vigasina M[1], Bryzgalov I[1], Lalomov A[3*]

1 - M.V. Lomonosov Moscow State University, Russia 2 - Institute of Ore Geology, Mineralogy, Petrography and Geochemistry, RAS 3 - Institute of Geology of Ore Deposits, Petrography, Mineralogy and Geochemistry of Russian Academy of Science IGEM RAS *lalomov@mail.ru

Chlorite - widespread in nature a group of layered minerals that occur in a variety of natural associations from magmatic to metamorphic sedimentary rocks. The sample of chlorite from Korshunovskoe deposit (Siberia, Russia) was studied using different methods of physicochemical investigations of mineral substance. The chemical formula was calculated on the basis of electron microprobe analysis ("Camebax SX-50", France) data and had the formula $(Mg_{4.9}Fe^{2+}_{0.3}Al_{0.8})[Si_{3.2}Al_{0.8}O_{10}](OH)_8$; according to recommendations of the IMA Nomenclature Committee (2006) the studied sample belonged to clinochlore. Results of X-ray study (D/Max-2200 Rigaku, Japan) confirmed the monomineral composition of the clinochlore sample. IR absorption spectrum (Fourier spectrometer FSM-1201, Russian) was obtained at room temperature in air on a powder suspension in vaseline oil and also showed the absence of impurities in the examined clinochlore. Thermal and thermogravimetric studies in the range from room temperature to 1000°C (Derivatograph Q-1500D, Hungary) showed the characteristic behavior of clinochlore, the total mass loss (removal of constitutional water) was about 13%. Thus, the sample of the chlorite from Korshunovskoe deposit being clinochlore - the main member of magnesium chlorite group - was the object of the present thermochemical study. The investigations were performed on a Calvet microcalorimeter "Setaram" (France) by high-temperature melt solution calorimetry method and allowed to determine the enthalpy of formation from the elements for studied clinochlore (-8811 ± 11 kJ/mol) and to estimate the enthalpy of formation of clinochlore of theoretical composition $(Mg_5Al)[Si_3AlO_{10}](OH)_8$: -8904 ±11 kJ/mol.

Tetrahedrally coordinated cobalt in synthetic mica solid solutions with excess protons

Robert J-L

CNRS-UPMC, Paris IMPMC (UMR 7590), Université Pierre et Marie Curie, CNRS, IRD, MNHN, Paris jean-louis.robert@impmc.upmc.fr

In the low-Al part of the K_2O-CoO-Al_2O_3-SiO_2-H_2O system, partial mica solid solution are observed between three end-members: Co-phlogopite (Co-Phl) $KCo_3(Si_3Al)O_{10}(OH)_2$, and two virtual end-members $K(Co_{2.5v0.5})Si_4O_{10}(OH)_2$ [A] , where v represents an octahedral vacancy and $KCo_3(Si_{3.5}Co_{0.5})O_{10}(OH)_2$ [B]. The [A] phase is a triocta-dioctahedral mica. At the [B] end-member, Co^{2+} is present in both 6-fold and 4-fold coordinations, which is an uncommon situation, considering the ionic radius of $^{[4]}Co^{2+}$ (0.58 Å). In the Co-Phl - [A] - [B] triangle, the mica color reflects the evolution composition, from pink for the Co-Phl end-member with only $^{[6]}Co^{2+}$, to purple, then deep blue as mica compositions come close to that of the [B] end-member.

Both UV-vis and FTIR spectroscopies confirm the presence of $^{[4]}Co^{2+}$ besides $^{[6]}Co^{2+}$. In UV-vis, micas with only $^{[6]}Co^{2+}$ exhibit two main transitions: a main band corresponding to the $^4T_{1g}(F) \rightarrow {}^4T_{1g}(P)$ transition, centered at 18800 cm^{-1} and a weaker band at 8150 cm^{-1}, due to $^4T_{1g}(F) \rightarrow {}^4T_{2g}(F)$. In $^{[4]}Co^{2+}$-bearing micas, two high-intensity bands are observed, one main band at 15430 cm^{-1} with two shoulders at 16730 and 15453 cm^{-1}, due to the $^4A_2(F) \rightarrow {}^4T_1(P)$ transitions and a low-intensity band at 8000 cm^{-1}, assigned to the transition $^4A_2(F) \rightarrow {}^4T_1(F)$. FTIR spectroscopy in the antisymmetric T-O-T region, also demonstrates the presence of $^{[4]}Co^{2+}$. Close to the [A] end-member composition, the FTIR spectrum consists of a doublet with a high-intensity band at 970 cm^{-1}, due to the antisymmetric Si-O-Si_{as} motion, and a low intensity one, at 1120 cm^{-1}, assigned to the Si-O perpendicular vibration. Close to [B], an inner doublet appears, at 1020 and 1080 cm^{-1}, also assigned to T-O-T_{as} and Si-O perpendicular vibrations but involving SiO_4 tetrahedra adjacent to CoO_4 tetrahedra.

In the Co-Phl - [A] - [B] triangle both octahedral vacancies and $^{[4]}Co^{2+}$ generate local charge imbalances. These two defects, which are expected to be as far as possible from each other, to minimize local charge imbalances, are actually associated. The resulting charge imbalance on apical oxygens of CoO_4 tetrahedra adjacent to an octahedral vacancy is compensated by the incorporation of an additional proton. A perfect 1:1 correlation is observed between excess protons and $^{[4]}Co^{2+}$. FTIR spectroscopy in the OH stretching region confirms the presence of $^{[4]}Co^{2+}$ and excess protons, with a complicated system of bands in the 3675-3540 cm^{-1} range, corresponding to the different octahedral environments, to the different local tetrahedral compositions (second neighbour effect) with and without $^{[4]}Co^{2+}$, and to additional protons.

Geochronology of the lithospheric mantle underneath the Gibeon kimberlite field, Namibia

Brey G P[1*], Hoefer C E[2], Shu Q[3], Gerdes A[1], Hoefer H E[1]

1 - Goethe-University Frankfurt *brey@em.uni-frankfurt.de 2 - ETH, Zuerich

3 - University of Alberta

The ~70 Ma old Gibeon Kimberlite Province is located within the Rehoboth Terrane in Namibia with crustal ages between 0.9-1.2 and 1.8-2.1 Ga. It consists of more than 75 non-diamondiferous kimberlite and carbonatite diatremes. Three major localities with garnet peridotite xenoliths are known: Hanaus, Gibeon Townlands and Louwrensia. Recent comparative work on xenoliths has shown differences and similarities between the mantle underneath the Archean Kaapvaal craton and the attached Proterozoic terranes (Bell *et al.*, 2003). Differences e.g. are higher average Fo-contents in olivines from the craton, Re depletion ages mostly older than 2.5 Ga and a thicker lithosphere. Similarities are similar geothermal gradients and an overabundance of orthopyroxene in part of the mantle samples. Luchs *et al.* (2013) determined the trace elements and Lu/Hf and Sm/Nd isotope ratios in garnets and clinopyroxenes from garnet peridotites for Hanaus and Gibeon Townlands by LA- and MC- ICPMS. They distinguished two peridotite types by their garnet REE patterns: i) peridotites with flat middle to heavy REE and ii) a minor proportion with sinusoidal REE patterns as they are common from the Kaapvaal craton. Bulk rock trace element contents and isotope compositions were calculated from the mineral modal abundances. A Lu-Hf isochron for the peridotites with the sinusoidal grt REE patterns yielded an age of 1852 Ma which was interpreted as the time of enrichment of a previously strongly depleted mantle (eHf(i) = +29). The garnet peridotites with the flat middle to heavy REE patterns yielded a Lu-Hf enrichment age of 810 Ma with eHf(i) = +3.3. These two ages lie within the range of crustal ages of the Rehoboth Terrane.

The same two garnet peridotite types as in Hanaus and Gibeon Townlands can be found in the Louwrensia kimberlite pipe and, in addition, a further type (four samples) with LREE depleted grt patterns and positively sloping middle and heavy REE up to 10x chondritic. These peridotites appear to be almost non-metasomatized restites of partial melting with garnet as a residual phase. Calculated bulk rock Lu-Hf isotope ratios align along an isochron with an age of 1064 ± 83 Ma and an initial eHf = +3.3. This time overlaps with the beginning of the Grenville orogeny in the adjoining Namaqua-Natal belt.

It appears that the mantle underneath the Rehoboth province consists of different portions with different ages of partial melting at various depths. Partial melting for the residues with sinusoidal and with flat grt REE pattern must have occurred prior to 1.9 respectively 0.9 Ga (the ages of metasomatism, see above) at shallow depth in the spinel stability field as indicated by low and variable HREE abundances. These ages correlate with the age of Kheis-Magondi respectively the Namaqua Natal belt and with the ages of the crustal components within the Rehoboth terrane. The onset of the Namaqua-Natal orogeny must have been connected with deep partial melting of a slightly depleted mantle in the garnet stability field.

Evolution of diamond resorption morphology from the mantle source to the emplacement of kimberlite at the surface: review of experimental data

Fedortchouk Y[1*], Zhang Z[2]

1 - Dalhousie University *yana@dal.ca 2 – Department of Earth Sciences, Dalhousie University, Halifax, NS

Fascinating complexity and diversity of morphologies and surface relief of natural diamond crystals reflect variety of conditions in diamond-forming and diamond-hosting environments such as different domains of subcratonic mantle and deep-seated magmas (kimberlite, lamproites, etc). Most of the surface features on diamonds are a result of dissolution in mantle or kimberlitic fluid by oxidation of carbon into CO_2. The most common resorption features, trigonal pits, occur on any natural gem diamond but their shape and abundance is extremely variable. Other features, such as circular pits, cavities, striation, hillocks, are present on some diamonds, or limited to a very small diamond population or to a particular kimberlite locality. Can we use the dimensions of trigonal etch pits and the presence of less common features on diamond crystals from a particular kimberlite pipe to infer crystallization conditions, volatiles, as well as conditions in the contributing mantle source? Which resorption features are the product of dissolution in the mantle and which are the product of kimberlite-induced resorption? Finding answers to these questions was a motivation for our experimental work on diamond dissolution. We explored the individual effect of various parameters on diamond morphology in attempt to reproduce and explain the features observed on natural diamond crystals.

Our experiments examined three environments of diamond resorption: mantle, ascent in kimberlite magma, and near-surface conditions in kimberlite pipe. Resorption in kimberlite magma was studied using piston-cylinder apparatus at 1-3 GPa and 1150-1400^{o}C. We examined the individual effects of melt composition (silicate vs. carbonate), fluid composition (H_2O:CO_2 ratio), temperature, and pressure. In order to quantitatively study the relationship of resorption morphology with the parameters of the system we employ Atomic Force Microscope (AFM), which produces three-dimensional models of individual etch features and allows measuring their geometry. We identify resorption morphologies characteristic of kimberlite magma with plentiful CHO fluid and of volatile-poor magma. We further show that AFM-derived parameters of trigonal etch pits can be used to quantify the proportion of H_2O to CO_2 in the fluid and to assess the emplacement temperatures for different kimberlite phases. We show that presence of hexagonal pits on diamond is an indicator of CO_2-rich fluid, whereas occurrence of circular pits indicates almost pure H_2O fluid at shallow levels. Pressure causes faster rounding of diamonds at lower weight loss and suppresses the rate of dissolution. Mantle resorption of diamond was examined in multi-anvil apparatus at 6 GPa and 1200-1500^{o}C using synthetic system $(Ca,Mg)SiO_3$ - $(Ca,Mg)CO_3$ - H_2O - CO_2. We show that silicate-rich aqueous fluid with various proportion of CO_2 produces a multi-corner stepped face morphological types common for natural diamonds. The second mantle-derived resorption type with deep hexagonal cavities requires carbonatitic melt. Natural diamonds with both resorption types differ in their thermal history recorded in nitrogen aggregation. Our study creates a framework for resorption-based diamond classification.

X-ray tomography pseudo thin-section textural analysis of diamondiferous mantle eclogites

Howarth G[1*], Sobolev N[2], Pernet-Fisher J[3], Barry P[3], Taylor L[1]

1 - University of Tennessee *ghhowarth@gmail.com 2 - Institute of Geology and Mineralogy, Siberian Branch of Russian Academy of Sciences 3 - Dept. of Earth and Planetary Sciences, The University of Tennessee

High-resolution (20-30 µm) X-ray computed tomography (HRXCT) of a suite of diamondiferous mantle eclogites, from the Udachnaya pipe, has successfully produced ~850 sequential two-dimensional slices for each sample. Each of these slices represents a "pseudo thin-section", allowing for detailed petrographic textural analysis of the entire eclogite xenolith. In particular, the relationships of diamonds and sulfides to the hosting silicates (garnet and clinopyroxene) are clearly observable.

Diamonds are always surrounded by secondary minerals, never observed in direct contact with garnet or clinopyroxene, and associated with metasomatic pathways. Sulfide abundances range from 0.1 to 1.5 vol.%, and four distinct textural associations are identified, which can be temporally constrained: 1) enclosed within silicates and diamonds, 2) enclosed within metasomatic pathways, 3) associated with cracks/fractures cross-cutting the xenoliths, and 4) blebs within marginal alteration zones.

Sulfides are the major carrier of highly siderophile elements (HSEs) in mantle eclogites, and as such, are used to date both the formation of eclogites and diamonds using Re-Os systematics. Therefore, understanding the timing of sulfide formation is crucial in interpreting sulfide-age-dates for diamonds and eclogites. The occurrence of multiple sulfide generations within individual eclogites suggests that sulfides are mobilized during several separate temporal events. Furthermore, the common association of sulfides as inclusions within diamonds, along diamond grain boundaries, and within cracks cross-cutting the xenoliths, implies several sulfide precipitation events pre- and post-dating diamond precipitation. Therefore, we suggest that sulfides and diamonds form from multiple metasomatic events; however, these processes may be entirely unrelated to one another. Furthermore, sulfide-diamond inclusions may commonly be proto-genetic, forming prior to diamonds, which has implications for the use of sulfides in dating diamonds and eclogite xenoliths.

Geochemistry and noble metal enrichment of the margin of the North Atlantic Craton: implications for Ni-Cu-PGE mineralisation in western Scotland

Hughes H[1*], McDonald I[1], Faithfull J[2], Upton B[3], Kerr A[1]

1 - Cardiff University *hughesh6@cf.ac.uk 2 - Huntarian Museum, University of Glasgow 3 - University of Edinburgh

The role of the lithospheric mantle as a metal source for certain types of mineralisation, particularly orthomagmatic Ni-Cu-PGE sulphide deposits, is contentious [1, 2]. Its role in metal sourcing may be physical and/or chemical, and the age and stability of the lithosphere may be critical. Mantle xenoliths reveal the mineralogy and bulk geochemistry of the lithospheric mantle. We use 6 suites of peridotitic mantle xenoliths obtained from a north-south transect of W Scotland, UK, to ascertain the major, trace element, and noble metal geochemistry of the lithospheric mantle keel below Scotland. This area straddles the margin of part of the North Atlantic Craton (NAC) including the marginal cratonic lithospheric keel and non-cratonic lithosphere.

Powdered whole-rock xenolith samples were subjected to ICP-OES and ICP-MS analysis for major and trace elements, and NiS fire assay with ICP-MS to determine PGE and Au abundances. The whole-rock data is evaluated in relation to the observed mineralogy and mineral chemistry of the xenoliths, as analysed by SEM and LA-ICPMS. This allows a rounded interpretation of the geologic history and major "enrichment" events that this portion of the NAC margin, and its surrounding terranes, experienced.

Most Scottish mantle xenoliths are spinel lherzolites, with rare wehrlites and dunites. Garnet-bearing peridotite xenoliths are entirely absent in this region. Where possible, xenolith suites were selected to be "fresh" with well-preserved pristine silicate mineralogy. Samples from within the Archaean craton at Loch Roag are haloed by a 3-5mm wide green-orange coloured alteration zone bearing Fe-oxide veinlets and vugs of baryte. In other xenolith suites, millimetre-scale flame-like veins of clinopyroxene, Cr-spinel and plagioclase have been preserved, representing frozen-in gabbroic partial melts (e.g., Hillhouse). Additionally, sub-millimetre anastomosing veinlets of chlorite ± ulvöspinel ± Ca-carbonate suggest interaction of a volatile-rich metasomatic agent (e.g., Streap). Abundant rounded sulphides (up to 150 µm diameter) occur interstitial to the main silicate mineral phases in all xenolith suites. These comprise intergrowths of Ni-Fe-Cu sulphides. Chalcopyrite can be absent from the sulphide assemblage. At Loch Roag, rare Pt-sulphide and Pt-arsenide grains up to 3 µm in length occur at a Cu-Fe sulphide margin.

Whole-rock trace element analyses demonstrate enrichment in LILE and LREE (10 - 100 x primitive mantle, PM) with corresponding depletion of Nb, Ta, Ti and Zr, Hf, indicating the geochemical influence of one/multiple subduction-like event(s). Overall the enrichment/depletion patterns are variable across W Scotland, but consistent within each xenolith suite, hinting at terrane-scale zoning across the Archaean craton margin into the neighbouring Proterozoic and Phanerozoic terranes to the south. Cu, Pt, Pd and Au concentrations are highly variable but always enriched above PM levels, and exceed concentrations in Greenlandic NAC and Kaapvaal cratonic peridotite xenoliths [3, 4]. PGE+Au PM-normalised spidergrams display flat "fertile" patterns, suggesting little or no Pd-group PGE depletion took place prior to xenolith entrainment.

The trace element geochemical fingerprint of "subduction" and "metasomatism" is observed in all samples included in this study, and appears to be integrally linked to the Cu, Au and noble metal fertility of this lithospheric mantle region.

[1] Begg G. *et al*. (2010). *Economic Geology* Vol. 105, 1057-1070.

[2] Arndt N. (2013). *Economic Geology* Vol. 108, 1953-1970.

[3] Wittig *et al*. (2010). *Chemical Geology* Vol. 276, 166-187.

[4] Maier *et al*. (2012). *Chemical Geology* Vol. 303, 119-135.

Radiogenic isotope constraints on lithospheric assimilation by sublithospheric melts in the generation of southern African kimberlite megacrysts: a comparison of on- and off-craton megacryst suites

Janney P

University of Cape Town. phil.janney@uct.ac.za

Megacrysts from Group 1 kimberlites likely formed as the result of sublithospheric melts infiltrating into and crystallizing within the deep continental lithospheric mantle to form veins or pods of large (typically >1 cm) crystals and mineral intergrowths. Although the Cr-poor megacryst suite is best known due to its relative abundance and the fact that its compositional variation tends to be well-explained by simple fractional crystallization, megacryst suites also often include Mg- and Cr-rich compositions (e.g., the Granny Smith suite), which could be the result of significant assimilation of lithospheric peridotite. The Sr-Nd-Hf-Pb isotope ratios of clinopyroxene (cpx) megacrysts from several Cretaceous southern African kimberlites, located both on the Archean Kaapvaal craton (most notably Monastery and Frank Smith) and on adjacent Proterozoic lithosphere (Pofadder and Gibeon) have been analyzed. Cpx megacrysts, selected to lie at regular intervals along the Cr-poor megacryst fractionation trend, show a transition from HIMU OIB-like compositions (e.g., high 206Pb/204Pb and 143Nd/144Nd, low 87Sr/86Sr) at the primitive end, toward more "enriched mantle" type compositions (i.e., higher 87Sr/86Sr and lower 206Pb/204Pb and 143Nd/144Nd) with increasing fractionation. This variation continues in an unbroken fashion well past the point where the evolution trend is deflected toward Mg- and Cr-rich compositions, strongly suggesting that Cr-poor and Cr-rich megacrysts are related through an assimilation-fractional crystallization process. Although this pattern is seen in cpx megacryst suites from both on- and off-craton kimberlites, two significant differences are observed: (1) the HIMU-like end-member expressed in megacrysts from cratonic kimberlites has higher initial 206Pb/204Pb and lower initial 143Nd/144Nd (i.e., more similar to St. Helena/Tubuaii/ Mangaia OIB) than that expressed in the off-craton suites, and (2) the extent of Pb isotopic variation for a given change in Ca# or Mg# along the Cr-poor evolution trend is two to four times higher for the off-craton as compared to the on-craton cpx megacryst suites. Both of these findings suggest a significantly higher degree of interaction between lithospheric peridotite and the magmas parental to the megacrysts in the off-craton as compared to the cratonic mantle environment. It remains to be determined whether these differences are attributable to the more refractory nature of cratonic mantle, a difference in the extent of metasomatism of cratonic and off-craton mantle lithosphere prior to megacryst magma infiltration, differences in the depth at which the megacryst parental magmas intersected the lithospheric mantle, or some other factor.

Mineralogy and geochemistry of megacrystalline pyrope peridotites from the Udachnaya pipe, Siberian Craton

Malkovets V[1*], Pokhilenko L[2], Pokhilenko N[3], Ota T[1], Nakamura E[1], Griffin W[4]

1 - Pheasant Memorial Laboratory, ISEI, Okayama University *vladimir.malkovets@gmail.com 2 - VS Sobolev Institute of Geology and Mineralogy, RAS 3 - VS Sobolev Institute of geology and mineralogy 4 - CCFS/GEMOC, Macquarie University

The Udachnaya kimberlite pipe brought to the surface a very wide range of uniquely fresh mantle xenoliths. One of the most interesting group of xenoliths is comprised of megacrystalline pyrope harzburgite-dunites, which consist primarily of ultracoarse olivine (up to 10 cm), orthopyroxene and subcalcic Cr-pyrope. Some of them may also contain diamond and chromite. The chemical compositions of their constituent minerals are very similar to the diamond-inclusion minerals found in Udachnaya kimberlite. Based on this argument it was proposed that harzburgite-dunite xenoliths with high-chromium subcalcic pyrope represent fragments of the host rocks of Siberian diamonds [1-3].

Pyrope composition varies over a wide range on Cr2O3 - CaO plot: Cr2O3 1.5-15.1 wt.% and CaO 0.86-7.58 wt.% [4]. Based on a study of more than 500 peridotitic pyrope inclusions in kimberlites worldwide Stachel and Harris defined a low-Ti (<0.04 wt.% TiO2) group which is least affected by mantle metasomatism [5]. Harzburgite-dunitic and lherzolitic pyropes from Udachnaya megacrystalline peridotites show a large range in TiO2 content, up to 0.4 and 1.24 wt.%, respectively. Among them 37 of the harzburgite-dunite pyropes belong to the low-Ti (<0.04 wt.% TiO2) group [4].

Trace elements have been determined in pyropes from 25 samples. Most of the studied pyropes have sinusoidal REEN patterns. They vary from strongly sinusoidal, typical for harzburgite-dunite pyropes, to mildly sinusoidal or "normal" patterns (positive slope from LREEN to MREEN and almost flat from MREEN to HREEN) typical for lherzolitic pyropes.

The core-to-rim variation of the REE, Sr, Zr and Hf have been studied for fifteen pyrope grains using CAMECA SIMS ims5f. All the grains display marked heterogeneity in Sr, Zr, Hf and LREEN. There are three major zoning patterns: 1) LREE and Sr enrichment of the pyrope rims; 2) LREE and Sr depletion of the pyrope rims; 3) MREE-HREE enrichment of the pyrope rims without concomitant LREE and Sr enrichment. The presence of the Sr, Zr, Hf and REE heterogeneities indicates relatively young multiple metasomatic events, probably several millions years before the formation of the Udachnaya kimberlite pipe. The heterogeneous distribution of Sr has been also reported for a sub-calcic pyrope inclusion in peridotitic diamond from the Mir kimberlite pipe, Yakutia [6].

Our new data on the geochemistry of sub-calcic pyropes from xenoliths of megacrystalline harzburgite-dunites shows significant heterogeneity in the trace element composition of all studied pyrope grains. This implies that these rocks experienced several relatively recent metasomatic events. The observed mineralogical and geochemical heterogeneities require very careful consideration of any isotopic data on these unique samples.

Acknowledgements: This work was supported by a Grant from the Russian Foundation for Basic Research (No 12-05-00487, 12-05-33035, 13-05-01051).

[1] Pokhilenko N.P., Sobolev N.V. and Lavrent'ev Yu.G. (1977). In: Extended Abstracts of the 2nd Intern. Kimberlite Conf. Santa Fe, USA. Ext. Abstr. № 71.

[2] Sobolev N.V., Pokhilenko N.P. and Efimova E.S. (1984). *Geologiya i Geofizika*, 25, 63-80.

[3] Pokhilenko N.P., Pearson D.G., Boyd F.R. and Sobolev N.V. (1991). Annual Report Dir. Geophys. Lab. Carn. Inst. Washington, USA, 1-18.

[4] Pokhilenko L.N., Malkovets V.G., Pokhilenko N.P., Korolyuk V.N. and Kuzmin D.V. (2014). *Doklady Earth Sciences*. 454 (2), 179-184.

[5] Stachel T. and Harris J.W. (2008). *Ore Geology Reviews*, 34, 5-32.

[6] Shimizu N. and Sobolev N.V. (1995). *Nature*, 375, 394-397.

Classification peculiarities of mantle eclogites from Udachnaya-East pipe (Yakutia)

Pokhilenko L*, Agashev A

VS Sobolev Institute of geology and mineralogy *blingoreluiy@ya.ru

The 54 eclogites (including 2 diamondiferous) from Udachnaya kimberlite pipe were investigated. The 22 of them were studied using SEM. The wide variety of compositions of the rock-forming minerals (garnet and pyroxene) was established in scale of the same sample. According to conventional classification [1] the eclogites can be divided into three groups (ABC), mainly by MgO-content in rock-forming garnet and pyroxene. It is a view that the grading by garnet and pyroxene coincide. But it is happened not any time. The detailed study shows that garnet or/and pyroxene can demonstrate more than one composition within the limits of the section. It makes difficult the determination of group for given rock. Primary pyroxene (normally omphacite) is represented by relicts of greenish grains, so its identification is not hard. Secondary pyroxene (usually diopside) can be present either as small grains in the cracks of primary pyroxene or simplectites with feldspar in the rims around primary pyroxene [1]. Moreover, high-Al pyroxenes are often situated in the rims around Gt. In some samples the pyroxene with high-Fe content was met additionally. So, we will have the discrepancy between "garnet" and "pyroxene" group grading if the primary pyroxene is completely replaced by one of the secondary.

It is not simple sometimes to establish the primary garnet. We investigated two relicts of garnet grains (Gt-A and Gt-C) located on either side of the elongate kyanite grain. They have close size, morphology, wide rims around. The same place we have analyzed the big grain of phlogopite with diopside (group A) inclusion in it. It is secondary pyroxene (in equilibrium with Gt-A) because the Gt-C inclusion was found in kyanite grain definitely proving the equilibrium between two last minerals.

The whole rock composition was defined for 17 studied samples. Division into 3 groups (ABC) in this case does not always coincide with the garnet-pyroxene classification due to a significant contribution of accessory minerals. Group C included the compositions of rocks in which garnet or pyroxene belongs to this group. There was a positive correlation between MgO and Fe_2O_3+CaO. A and B groups have the negative correlation between MgO and Fe_2O_3+CaO.

So, the classification of eclogites supposes first of all the identification of primary rock-forming garnet and pyroxene from the late similarly named minerals which were forming during the post-crystallization period of the rock origin under the influence of methasomatic fluids/melts.

[1] Taylor L.A. and Neal C.R. (1989). Eclogites with oceanic crustal and mantle signatures from the Bellsbank kimberlite, South Africa, part I: Mineralogy, Petrography, and whole rock chemistry. *J. Geol.*, 97, 551-567.

[2] Misra K.C., Anand M, Taylor L.A. and Sobolev N.V. (2004). Multi-stage metasomatism of diamondiferous eclogite xenoliths from the Udachnaya kimberlite pipe, Yakutia, Siberia. *Contrib Mineral Petrol*, 146, 696-714.

Peridotites of the diamond stability field of the ancient craton lithospheric mantle: relationship with evolution of lithosphere roots and kimberlite melts generation

Pokhilenko N[1*], Agashev A[2], Pokhilenko L[2]

1 - VS Sobolev Institute of geology and mineralogy *chief@igm.nsc.ru
2 - VS Sobolev Institute of geology and mineralogy

We present results of complex study of the rare finds of the diamondiferous peridotite xenoliths. These results show absence of any significant differences in the P-T conditions of both diamondiferous and diamond barren Cr-pyrope harzburgites and dunites formation: practically all of them were formed inside the diamond stability field at pressure over 45 kb and temperature over 900˚C. Very rare finds of majorite-bearing high-Cr subcalcic pyropes inclusions in diamonds having significant contents of majorite component definitely belonging to the extremely depleted peridotites of harzburgite-dunite paragenesis of extremely thick (>300km) lithospheric mantle.

Comparative analysis of the geochemical peculiarities of Cr-pyropes of the diamondiferous and diamond-free xenoliths shows a definite distinction in character and intensity of secondary metasomatic enrichment of diamondiferous and diamond barren harzburgite-dunites. A geochemical characteristics of metasomatic agents for the first type of rocks were close to those for carbonatitic melts, and the metasomatic treatment intensity was relatively low; for the metasomatic agents in the second case there were significantly higher roles of Ti, Na, Zr, heavy REE, and higher intensity of the secondary enrichment of initial rocks by carbonatitic components especially in Ca, reflected in increase of Ca-component in garnet and at its lherzolitic amount - up to appearance of Cr-diopside in harzburgite (enstatite + Ca diopside) - prohibited phase in initial ultra-depleted peridotites.

Of special interest is information related to the processes of the kimberlite formation. The character of such a relationship can be both genetically directly related to the kimberlite melts generation and evolution and indirectly related to the processes which occurred at the same time and related to the general activation of cratonic and subcratonic upper mantle. Of special importance are results of studies of extremely fresh xenoliths of sheared pyrope lherzolites of Udachnaya pipe representing zone of lithosphere-asthenosphere interaction and unique xenoliths of polymict breccias representing initial most deep-seated stages of kimberlite formation. A combination of compositional, geochemical, isotopic and petrographic features shows that the sheared pyrope lherzolites representing the most deep-seated rocks of the lithospheric mantle were intensely deformed under conditions of significant stress pressure in the base of lithosphere, and have a complex evolution of their chemical composition, including a stage of partial melting and at least two stages of metasomatic enrichment. A partial melting of the most enriched sheared pyrope lherzolites can be related with the primitive kimberlite melt formation as well as formation of the kimberlite megacrysts suite. Petrological and geochemical features of polymict breccias provide us with valuable information about conditions and character of the protokimberlitic melt generation and initial stages of its evolution.

The orthopyroxene interaction with the Na-Carbonate melt: a challenge of the assimilation-fueled buoyancy mechanism

Safonov O

Institute of Experimental Mineralogy. oleg@iem.ac.ru

J. K. Russell *et al*. [1] experimentally showed that interaction of orthopyroxene with a Na-carbonate melts provoked voluminous decarbonation, and this process was invoked as a major mechanism for the rapid ascent of kimberlite melts toward the surface. The more orthopyroxene reacts, the more active is the decarbonation. The "open-air" experiments were performed at 1 atm., although the rapid ascent of the kimberlite melts is well known to begin in the sub-lithospheric mantle. In order to testify the J.K. Russell's *et al*. hypothesis, the experiments on interaction of natural orthopyroxene with Na_2CO_3 at 2 GPa and 1000, 1050, 1100 and 1200^{O}C were carried out in sealed platinum capsules using the piston-cylinder apparatus. Weight ratio Opx:Na_2CO_3 in the experiments was kept 80:20. According to Russell *et al*. (2012), all carbonate melts must be decarbonated at these Opx:Na_2CO_3 ratio. However, the experiments demonstrated that the carbonate melt was stable at the above temperatures. The Na-Mg carbonate melt appeared at 1000^{O}C via a Opx-Na_2CO_3 reaction with formation of a silicate $Na_4Mg_8Si_{15}O_{40}$ (NMS) and forsterite: 5Opx + Na_2CO_3 = 1/4NMS + 5/4Fo + 1/2$Na_2Mg(CO_3)_2$. This reaction shows that the process was not accompanied by the CO_2 exsolution (at least, voluminous). As the NMS melted, a silicate melt appeared along with the carbonate melt at 1050^{O}C. This silicate melt contained 42.18 wt. % SiO_2, 6.27 wt. % Al_2O_3, 8.61 wt. % MgO, 17.21 wt. % Na_2O at oxide total 75.38 wt. %, which pointed to the notable concentration of the carbonate components. This conclusion was supported by the Raman analysis of the glasses. An increase of temperature did not change the situation: amount of the silicate melt increased, whereas the carbonate melts was still preserved as rounded globules in the silicate glass matrix. The composition of the silicate melts changed insignificantly: 40.27 wt. % SiO_2, 4.22 wt. % Al_2O_3, 9.00 wt. % MgO, 18.11 wt. % Na_2O, total 73.39 wt. %. Similar SiO_2 contents and the oxide totals indicated that the CO_2 loss was negligible within the temperature interval 1050-1200^{O}C. The present experimental data put in doubt the correctness of the Russell's *et al*. conclusion about the fair role of orthopyroxene in the decarbonation of the Na-carbonate melt, at least, for pressure 2 GPa. The mechanism suggested by these authors is valid just for sub-surface conditions and has no relation to the behavior of the carbonate melts in the upper mantle. This mechanism can be further challenged by the experiments in the complex carbonate systems, which are more realistic as kimberlite parental melts.

[1] Russell J.K. *et al*. (2012). *Nature*, 481, 352-357.

Micro-FTIR investigation of gem quality cubic diamonds from Siberian placers

Shiryaev A[1*], Titkov S[2], Zudina N[3], Zudin N[4]

1 - Institute of physical chemistry and electrochemistry RAS; IGEM RAS
*a_shiryaev@mail.ru 2 - IGEM RAS 3 - RSGPU 4 - Rony Carob Ltd.

Gem quality natural diamonds with low degree of nitrogen aggregation (type Ib-IaA) are rarely encountered and their properties are poorly studied. These diamonds often possess highly attractive yellow and orange coloration, but the responsible defect(s) are not fully understood. In recent years amount of such diamonds available for research increased and new exciting advances were made. In particular, a new important optical center significantly influencing the one-phonon IR absorption - the Y-defect, presumably a new form of single substitutional nitrogen in diamond lattice - was discovered [1]. These diamonds may also show numerous weak absorption lines, possibly related to H- and N-impurities.

In the present work six gem quality greenish-yellow, yellow, yellow-orange and orange diamonds of cubic habit, 0.92-1.38 ct in weight, from the placers in the North-East of the Central Siberian platform, were studied using μ-FTIR spectroscopy. These crystals were previously investigated with photoluminescence [2] and EPR spectroscopy [3]. Investigation of spatial distribution of IR-active defects and impurities with 100 or 50 microns steps was performed on plates cut from the crystals along profiles directed across crystallographic zoning using SpectrumOne spectrometer equipped with AutoImage microscope.

In the studied plates nitrogen in growth center is present exclusively in the A-form with concentration up to 990 at. ppm. Small amount of the B defects may also be present. Nitrogen content gradually decreases to very low values towards crystal periphery with simultaneous disappearance of the A-defects. In the outer part the one-phonon spectral region is very unusual: nitrogen is present as C-, X- (N^+) and Y-defects; weak bands in 1350-1380 cm^{-1} range typical for natural Ib diamonds are also observed. High spatial resolution of our study suggests that only the 1359 cm^{-1} peak is related to the Y-defect; whereas the 1374 cm^{-1} feature is independent of all the others. Note that investigation of the same crystals prior to cutting using diffuse reflectance IR-attachment strongly enhanced contribution of peripheral N-poor part.

In one sample a narrow zone with abundant A-defects is observed half-way from the center to the edge. The position of this zone and characteristics of defects may indicate that in some cases nitrogen might be incorporated into a growing diamond as pair if oxygen fugacity of the growth medium allows presence of N_2 molecules with low solubility in melt [4]. In this diamond the intensity of the H-related absorption at 3107 cm^{-1} positively correlates with the A-defect distribution, which may serve as a support for annealing-related origin of H-related IR absorption features [5].

Bands of microscopic inclusions mostly comprising carbonates and compressed quartz are observed in some samples. Apparently, in some cases the number density of the inclusions depends not only on growth zone, but also on crystallographic sector.

Whereas zones with variable N content are relatively frequently observed in natural diamonds, the gradual decrease is rarely observed. Such distribution of the impurity may indicate growth in a closed system with Rayleigh distillation process governing the N incorporation and/or at gradual change of T-fO_2 conditions favouring increased nitrogen solubility in growth medium. The diamonds were annealed for a short time only which permitted to preserve the C- and especially the Y-defects.

[1] Hainschwang T. *et al*. (2012). *Diam. Relat. Mater*. 21, 120-126.

[2] Zudina N.N. *et al*. (2013). *Zapiski RMO*, 142(4), 57-72.

[3] Mineeva R.M. *et al*. (2013). *Dokl. Earth Sci*., 448(6), 695-699.

[4] Shiryaev A.A. *et al*. (2005). *Dokl. Earth Sci*., 403A(6), 908-911.

[5] Kiflawi I. *et al*. (1996). *Diam. Relat. Mater*., 5, 1516-1518.

Partial melting, metasomatism and growth of diamonds in the Kaapvaal subcratonic mantle in relation to tectonomagmatic events in the crust

Shu Q[1*], Brey G[2], Gerdes A[2], Hoefer H[2]

1 - University of Alberta *qshu1@ualberta.ca 2 - Goethe University, Frankfurt

The origin, growth and amalgamation of Archean continental nuclei, and the temporal relationships between processes in the crust and mantle are fundamental questions concerning the stabilization of long-lived cratonic blocks by buoyant underlying lithospheric mantle keels. They have been addressed in a number of review papers. The main sources of information are zircons for tectonomagmatic processes in the crust (U-Pb ages and Hf isotope compositions) and peridotites and their sulfides (Re-Os and subordinate Sm-Nd isotope system model ages) for mantle melting. The main outcome is that the major periods of growth and reworking of the crust coincide with maxima in the frequency distribution curves of Re depletion (TRD) and Re model ages (TMA) from mantle xenoliths. The most prominent maximum lies between 2.7 and 2.9 Ga which is generally interpreted as reflecting the main period of depletion of the subcratonic mantle.

In our work, we applied two further isotope systems, Lu-Hf and Sm-Nd, to subcalcic garnets from cpx-free harzburgites and obtained a series of isochrons and errorchrons from garnet concentrates from various diamond mines on the Kaapvaal craton. They date metasomatic events, which overprinted a previously depleted mantle mainly between 2.6 and 3.3 Ga. This time span coincides with the time of supposed mantle depletion as it is interpreted from Re-Os TRD and T_{MA} ages. However, metasomatism must have added Re to the residue even though in small amounts. In consequence we interpret the majority of Re-Os T_{RD} ages to be affected by metasomatism, yielding minimum estimates of the formation of the peridotites. The major period of depletion of the Kaapvaal subcratonic mantle must have occurred earlier than 3.3 Ga (indicated by oldest Lu-Hf metasomatic age) which agrees with the oldest T_{RD} age at 3.5 Ga of Pearson *et al*. in 1995, at low pressures and in the absence of garnet. The latter is indicated e.g. by high to very high Cr# and very low HREE contents in the peridotites. The residues were subducted underneath the continental nuclei and metasomatized in the garnet stability field by small amounts of carbonatitic melts. These melts imposed high Zr/Hf and low Ti/Eu ratios onto the subcalcic garnets. These ratios are similar to those found in garnet inclusions in diamonds. Mantle metasomatism by carbonatitic melts and the growth of diamonds by redox reactions therefore appear to be co-genetic and contemporaneous.

The most important implication from the Lu-Hf and Sm-Nd isotope studies of garnet xenocrysts is that the depletion of the Kaapvaal mantle occurred before it was emplaced in the early Archean underneath its present day crust and that mantle metasomatism, formation of diamonds and tectonomagmatic events in the crust are contemporaneous processes.

Diamond formation at Attawapiskat (Craton) postdating the 1.1 Ga Rift

Smit K*, Stachel T, Stern R

University of Alberta *kvsmit@ualberta.net

Kimberlites in the Attawapiskat area of the western Superior – the first diamond-producing area on the Superior craton (De Beers' Victor Mine) - sampled the lithospheric mantle at two time periods: i) during the Mesoproterozoic, concurrent to the 1.1 Ga Midcontinent Rift and ii) during the Jurassic. Diamonds from Mesoproterozoic (T1) and Jurassic (U2) kimberlites have distinct nitrogen aggregation characteristics and carbon isotopic compositions.

Diamonds from the T1 kimberlite have a narrow range in $\delta^{13}C$ (mode of -3.4 ‰), with compositions that overlap other diamond localities on the Superior craton. Thinning of the lithosphere and diamond destruction occurred during the Mesoproterozoic in response to the thermal impact of the Midcontinent Rift. The associated elevated geotherm caused a narrow diamond window (< 30 km) close to the base of the lithosphere, compared to a wide diamond window of ~ 85 km following thermal relaxation (sampled by Jurassic kimberlites, such as U2). T1 diamonds have highly aggregated nitrogen, possibly due to the thermal effect of the Rift.

Cooling of the lithosphere since the Mesoproterozoic re-established diamond favourable conditions. The poorly aggregated nature of nitrogen in U2 diamonds - compared to highly aggregated nitrogen in diamonds from T1 - indicates that renewed diamond formation must have occurred only after the thermal impact of the Midcontinent Rift had subsided. The overall $\delta^{13}C$ distribution for U2 diamonds is distinct to T1 and other Superior diamonds, further suggesting that diamonds sampled by the Jurassic U2 kimberlite are not related to the older pre-rift diamonds.

The implied age of <1.1 Ga for the U2 diamonds is much younger than the majority of inclusion-bearing diamonds that have been dated worldwide and indicate that significant diamond-forming events in the lithospheric mantle extend into the Neoproterozoic and perhaps the Phanerozoic.

Metasomatic diamonds in eclogite xenoliths from Yakutian kimberlites: implications for diamond-grade estimation

Spetsius Z[1*], Griffin W[2], O'Reilly S[3], Bogush I[4]

1 - Scientific Investigation Geology Enterprise, ALROSA OjSC *spetsiuszv@gmail.com 2 - CCFS/GEMOC, Macquarie University 3 - GEMOC ARC National Key Centre, Macquarie University, Australia 4 - Scientific Investigation Geology Enterprise, ALROSA, Russia

Eclogites comprise most of the diamondiferous xenoliths in the pipes of Yakutia, South Africa and Canada. In addition, ≥30% of mineral inclusions in diamonds have compositions comparable with the minerals of eclogitic xenoliths and in the Botuobinskaya and Nurbinskaya pipes in the Nakynsky field of Yakutia, this reaches about 50%. Here we summarize published data and present additional results relevant to the metasomatic growth of diamonds, and explore their practical implications.

There are several lines of evidence pointing to the metasomatic origin of diamonds in mantle eclogites: (1) sharp boundaries between zones with different N contents and aggregation states; (2) large variations in C- and N-isotope composition between inner and outer parts of the same crystal; (3) abundance of sulfide inclusions and heterogeneity of sulfur isotopes; (4) inclusions of eclogitic and peridotitic parageneses within a single crystal; (5) large range in the Pb-isotope compositions of sulfides within a single diamond.

Particularly strong indications that some diamonds grew after the major eclogitic minerals are: (a) a correlation between the abundance of diamonds and the intensity of features interpreted as due to partial melting; (b) concentrations of diamond in deformation zones in the host eclogite; (c) distribution of diamonds around large grains of garnet and in metasomatised clinopyroxenes; (d) the presence of two diamond generations in one xenolith, differing in color, morphology and chemical properties.

Additional evidence comes from mapping the distribution of N and H impurities in about 100 diamond plates from eclogites from the Udachnaya and Nyurbinskaya pipes. More than 50% of eclogitic diamonds show obvious zonation, in many cases with multistage or interrupted growth. FTIR analyses show N abundances and aggregation state vary from the center to periphery of the crystal from 1400 to 370 at. ppm and from 45 to 28% IaB respectively. The hydrogen absorption line at 3107 cm^{-1} may change stepwise from 6.0 cm^{-1} to 0.1 cm^{-1}. It would appear that several episodes of diamond crystallisation are required to produce the full range of FTIR mapping data. These rapid and alternating changes are not likely during any magmatic process but are consistent with changes in the migrating metasomatic fluids that deposited the diamonds. The nature of these fluids is not known quantitatively at present. However, they are probably super-critical watery fluid K-rich fluids that carried carbon, perhaps akin to the low-temperature melting fraction of portions of the mantle. Very likely those fluids are enriched in sulfur as well, giving the well-known abundance of sulfide inclusions in diamonds. We may conclude that diamond growth in eclogite xenoliths does not depend on the conditions of formation of the primary eclogite.

Possible models for the different grades of kimberlite pipes can be based on these concepts about diamond growth. For this aim all deposits are divided into high-, middle-, low-grade and barren kimberlites. On the basis of well-known petrologic reconstructions, and summarizing data on SCLM composition in cratonic regions, we present four preliminary models for the controls on diamond grade in the kimberlites across Yakutia province, which may apply to other provinces as well.

The mantle source of Argyle diamonds

Stachel T[1*], Harris J[2], Hunt L[1], Muehlenbachs K[1], Kobussen A[3], EIMF T[4]

1 - University of Alberta *tstachel@ualberta.ca 2 - University of Glasgow 3 - Rio Tinto Exploration 4 - University of Edinburgh

Diamonds from the Argyle Mine, Western Australia, contain primarily (~90%) eclogitic inclusions, which cover a large compositional range and show in part unusually high concentrations of mantle incompatible elements (P, Ti, Na and K). Coherent trends in major elements (e.g., Ti or Na versus Mg-number) suggest that the eclogitic diamond source was created by a single process: igneous fractionation. Calculated bulk rock REE_N patterns match a section of oceanic crust reaching from lavas and sheeted dykes to upper gabbros. Positive Eu anomalies for garnet and clinopyroxene, with calculated bulk rock REE_N patterns similar to upper gabbros, are strong evidence for plagioclase accumulation, which is characteristic for the gabbroic portions of oceanic crust. For eclogitic garnet inclusions a correlation between $\delta^{18}O$ (mean of +7.2‰) and Na content is observed, consistent with coupled ^{18}O and Na enrichment during low temperature alteration of oceanic crust. The carbon isotopic composition of Argyle eclogitic diamonds forms a normal distribution around a $\delta^{13}C$ value of -11‰, indicative of mixing and homogenization of mantle and crustal (organic matter) derived carbon prior to diamond precipitation. Inclusion and nitrogen-in-diamond based thermometry reflect an unusually hot origin of the eclogitic diamond suite, indicative of derivation from the lowermost 25 km (about 180-205 km depth) of the local lithospheric mantle. This is consistent with emplacement of an oceanic protolith during subduction along the Kimberley Craton margin, likely during the Halls Creek Orogeny (about 1.85 Ga). Ubiquitous platelet degradation and plastic deformation of Argyle diamonds are consistent with derivation from a high temperature environment (softening the diamond lattice) close to the lithosphere-asthenosphere boundary (inducing strain). In combination, the Argyle data set represents a uniquely strong case for a subduction origin of an eclogitic diamond source followed by mixing of mantle and crustal components during diamond formation.

Some lherzolitic inclusions show a similarity in incompatible element enrichments (elevated P, Na and K) to the eclogitic suite. The presence of a mildly majoritic lherzolitic garnet further supports a link to eclogitic diamond formation, as very similar majoritic components were found in two eclogitic garnet inclusions. The carbon isotopic composition of peridotitic diamonds shows a mode between -5 to -4 ‰ and a tail extending towards the eclogitic mode (-11 ‰). This suggests the presence of multiple generations of peridotitic diamonds, with indications for an origin linked to the eclogitic suite being restricted to diamonds of lherzolitic paragenesis.

Carbon fluxes beneath cratons: insights from Greenland kimberlites, carbonatites, and diamonds

Tappe S[1*], Smart K[2], Stracke A[3], Romer R[4], Steenfelt A[5], Muehlenbachs K[6]

1 - De Beers Exploration *sebastian.tappe@debeersgroup.com 2 - University of the Witwatersrand
3 - Muenster University 4 - GFZ Potsdam 5 - GEUS Copenhagen 6 - University of Alberta

Kimberlite and carbonatite magmas intruding cratonic lithosphere are considered the deepest probes into Earth's mantle. In this setting their co-existence is commonly interpreted to represent a primary melting sequence of carbonated peridotite at >150 km depths, possibly as deep as the transition zone. The carbon involved in this magmatism is thought to be either of primordial origin or derived from recycled subduced oceanic crust, and it may play an important role in diamond forming processes.

To better understand carbon fluxes beneath cratons and their role in the deep carbon cycle, we have studied kimberlite dyke swarms and associated carbonatite intrusions of the North Atlantic craton in West Greenland. Our new Nd-Hf-Pb isotope data suggest that both magma types were derived from a common convective upper mantle source. Moreover, the absence of hallmark recycled oceanic crust signatures such as highly radiogenic Pb and decoupled Nd-Hf isotope systematics are indicative of a primordial mantle origin of the carbon involved in Greenland kimberlite and carbonatite magmatism. Based on phase relationships and geochemistry, including carbon isotopes, we identify Greenland kimberlites as near-primary melts (-6 to -4‰ $\delta^{13}C$). The intrusive carbonatites (-4 to -2‰ $\delta^{13}C$), however, represent mixtures of cumulus crystals and liquid. The kimberlites and carbonatites appear to be linked by a two-stage fractionation process that commenced at uppermost mantle depths. First, liquidus olivine+phlogopite were removed from kimberlitic carbonate-silicate melts at high-T, leading to residual carbonate-rich melt fractions. Second, upon continued ascent into the cratonic crust and cooling, these carbonate-rich melts precipitated calcite+dolomite along with minor olivine+magnetite. Rayleigh carbon isotope fractionation modelling suggests that 70-to-90 vol% of mantle-derived carbonate involved in this deep magmatism is now captured in the intrusive carbonatite bodies. Thus, it appears that CO_2 outgassing associated with kimberlite and carbonatite magmatic activity is volumetrically insignificant compared to global basaltic magmatism, and that carbonatite intrusions represent a major cache of primordial mantle carbon.

Subduction related diamond-forming fluids: evidence from micro inclusion-bearing diamonds from Ekati, central Slave Craton

Weiss Y[1*], McNeill J[2], Pearson G[3], Nowell G[2], Ottley C[2]

1 - Columbia University *yweiss@ldeo.columbia.edu 2 - University of Durham 3 - University of Alberta

Pristine C-H-O fluids trapped as micro-inclusions in fibrous diamonds vary between four end-members: saline high-density fluids (HDFs) which carry mostly K, Na and Cl and are depleted in carbonates and silicates; high-Mg carbonatitic HDFs characterized by high MgO and carbonate contents and low silica and alumina; low-Mg carbonatitic and silicic HDFs with varying amounts of carbonates, silicates and water. These HDFs induce metasomatism in the subcontinental lithospheric mantle (SCLM) and represent the medium from which their host diamonds grew. Fibrous diamonds originating from the Diavik and Ekati mines, Lac De Gras kimberlite field, central Slave craton, mostly carry saline microinclusion compositions.

We report here the HDF compositions of a suite of eleven diamonds from the Fox kimberlite, Ekati; nine diamonds trapped saline fluid microinclusions while two carry silicic fluids. Olivine and chromite (±orthopyroxenes and clinopyroxenes) microinclusions in the saline diamonds constrain their peridotitic paragenesis, while omphacite microinclusions found in one of the silicic diamonds suggest eclogitic origin. The overall trace-element pattern of the HDFs show "Ribbed" characteristics (Weiss *et al*., 2013), elevated Ba, U, Th and LREE, depleted Nb and Ta and in most cases, highly depleted alkalis (K, Rb and Cs), with some discrepancies between saline and silicic compositions. The REE patterns of the saline HDFs are steeper, with $(La/Gd)_{PM}$ ratios of 450 on average, and are characterized by positive Eu* anomalies compared to the silicic fluid, having $(La/Gd)_{PM}$=40 and Eu*=1.1. Furthermore, varying positive anomalies of Sr, higher levels of Ba and Th and fractionated Th/U ratios are observed for the saline HDFs; the silicic compositions are characterized by negative Sr anomalies. Sr isotopic composition in the saline HDFs vary between $^{87}Sr/^{86}Sr_{initial}$=0.7039-0.7090 (±0.0001) and correlate positively with La/(Pr,Nb), Th/(U,Nb), Eu*, Sr* and TiO_2 content; the silicic HDFs, although found in only two diamonds, seems to deviate from these correlations, except in the case of TiO_2 where the silicic compositions continue the trend of the saline fluids.

Fibrous diamonds from the Panda kimberlite (Ekati), from the Diavik mine and from the Wawa metaconglomerate (Superior craton) all carry HDFs of saline compositions and display similar characteristics to those from the Fox kimberlite (Ekati). It has been suggested that metasomatism and diamond formation beneath the Slave and Superior cratons were induced by subduction related processes, possibly related to the Wopmay origin in the case of the Slave craton. The Eu and Sr positive anomalies in diamond-bearing saline HDFs from these localities are consistent with their derivation from a subducting oceanic crust. The peridotitic paragenesis of these diamonds, however, suggest that the C-H-O fluids penetrated the SCLM, induced metasomatism and led to the on the other hand, we suggest that the subducted however, suggest implies that further investigation is needed to constrain the full characteristics of these HDFs and their relation to other HDF compositions.

Diamonds and highly reduced minerals in ophiolitic mantle rocks and chromitites

Yang J S[1*,4], Xu X Z[1], Zhang Zh M[1], Huang Zh[1], Robinson P T[1], Dilek Y[2], Griffin W L[3]

1 CARMA, State Key Laboratory of Continental Tectonics and Dynamics, Institute of Geology, Chinese Academy of Geological Sciences, Beijing, 100037,China
*yangjsui@163.com

2 Dept of Geol &Env Earth Science, Miami University, Oxford, OH 45056, USA

3 CCFS/GEMOC, Earth and Planetary Sciences, Macquarie University, NSW 2109 Australia

4. China University of Geosciences, Wuhan, 430074, China

Ophiolitic mantle rocks and chromitites are generally thought to have formed near the top of the upper mantle. However, our discovery of diamonds and highly reduced minerals in ophiolitic chromitites significantly challenges this model. Some new progresses are summarized as below:

1. A very significant milestone is that the diamonds have now been shown to occur in situ within chromite grains from the Luobusa and Polar Ural chromitites. This discovery has ended all doubts about the diamonds being the result of contamination during samples processing. Previously such contamination could not be conclusively ruled out because all the diamonds had been obtained from mineral separates.

2. The C isotope compositions and mineral inclusions of the diamonds from Luobusa and the Polar Urals are very similar, and are characterized by their light C isotopes (δ13C -18 to -28) and typical Mn-bearing mineral inclusions, such as Mn-olivine, Mn-garnet, Mn-spinel and Co-Mn-Ni alloy. These features, along with their typical occurrence in oceanic mantle rocks, clearly distinguish them from kimberlite diamonds within cratons and UHP metamorphic diamonds at plate margins. Thus, we propose a new occurrence of diamond on Earth, termed ophiolite-hosted diamond.

3. We have greatly expanded the number of ophiolites known to contain diamonds. Diamonds and highly reduced minerals have now been confirmed in mantle peridotites or chromitites from 11 ophiolites in 5 orogenic belts in different parts of the world. These include the Luobusa, Zedang, Xigaze, Dangqiong, Parang and Dongbo massifs in the Yarlung Zangbo suture and the Dingqing massif in the Bangong-Nujiang suture of Tibet, the Myitkyina massif in Myanmar, the chromitites in the Sartohai and Hegenshan massifs of the Central Asia Orogenic Belt, and the Ray-Iz massif in the Polar Urals. Thus, we propose that diamonds and their associated unusual minerals may be common within oceanic mantle, although not present in great abundance. If this can be proven with future studies, it will provide a previously unrecognized feature of the mantle and will lead to a better understanding of ophiolite and chromitite formation.

4. We discovered a new UHP mineral, named Qingsongite, which has been approved by the International Mineralogical Association (IMA2013-30). Experimental studies indicate that Qingsongite, which occurs as inclusions in coesite in the Luobusa chromitite, formed at 10-15GPa and 1300℃. The discovery of Qingsongite and stishovite pseudomorphs in the Luobusa chromitite, has lead us to propose a model for the deep formation of ophiolite-hosted diamonds and chromitite. In this model, UHP minerals and chromite grains crystallized simultaneously at a depth near the mantle transition zone, and were later brought to shallow levels by upwelling mantle and emplaced in ophiolites.

Olivine composition and craton evolution

Hatton C

Council for Geoscience. chatton@geoscience.org.za

The ubiquitous presence of highly forsteritic olivines (Fo93) in cratonic peridotite is usually ascribed to very high degree melting in mantle plumes, but even the Ontong Java - Manihiki- Hikurangi plume, the largest known, shows no evidence of exceptionally high temperature. Giant impacts are a more likely source of the enormous amounts of energy required to melt the mantle beyond the point of orthopyroxene exhaustion. A model in which the mass of giant impacts decreases exponentially in mass during the accretion of the earth provides the context in which the composition of olivine in cratonic peridotite can be explained. The first giant impact has mass of 24% of the present earth. When this accretes to the protoearth, the entire earth melts. After this impact the earth is 88% of its present mass. This impact leads to the formation of the core. For temperatures of core-mantle equilibrium between 3500 and 4000 K and core composition of 6 wt% Si, 6 wt% O, the magnesium number (100Mg/(Mg+Fe)) of Mg-silicate perovskite at the core-mantle boundary ranges between 99 and 99.9. Olivines formed during this event would be nearly pure forsterite, so the first giant impact cannot explain the existence of the Fo93 olivines in cratons. In the second giant impact an object with a mass 9% of the present earth accretes. This impact melts the outer layers of the mantle. Importantly, the inner layers of the mantle separate the iron and silicate melts generated during the second impact from the core, and these melts do not equilibrate with the core. Initially, iron rich melt sinks into the inner layers of the mantle. Forsteritic olivine (Fo93) then crystallises from the silicate melt, leaving a pyroxenitic residue. Remelting of the pyroxenite produces iron-rich basaltic crust which, on cooling, sinks into the outer mantle. Rising plumes entrain this basalt which then remelts. When impervious dunitic rafts halt the ascent of remelted basalt, siliceous melt rises from the basalt, metasomatising the dunitic rafts. The Greenland, Tanzanian, Slave, Wyoming, Kaapvaal and Siberian cratons are the products of this process. The third giant impact delivers the final 3% of Earth's mass. The silicate raft left after this impact is harzburgitic, rather than dunitic, and the olivine has a forsterite content of Fo92 and lower. Jordan's isopycnic hypothesis requires that the magnesium -poor, hence iron-rich harzburgite rafts are thinner than dunitic rafts. The thinner harzburgite rafts provide less of an impedent to the ascent of remelted basalt, which metasomatises the harzburgite directly. The end result of basalt metasomatism of harzburgite is 'primitive mantle' with Mg# 89.

The very high viscosity of Mg-silicate perovskite plays a central role in separating the products of the first giant impact from the products of later impacts. Despite the fact that the physical and chemical properties of Mg-silicate perovskite are very well known, this important mineral, the most abundant on earth, does not have a name of its own. Only the IMA can decide whether this unsatisfactory situation should persist.

Pink colour in Type I diamonds: is deformation twinning the cause?

Howell D[1*], Fisher D[2], Piazolo S[1], Griffin W[1], Sibley S[2]

1 - CCFS &GEMOC, Macquarie University *daniel.howell@mq.edu.au 2 - De Beers Technologies UK

Natural Type-I pink diamonds have been classified into 2 groups [1]. Group 1 pinks have only been found in the Argyle lamproite pipe (Australia) and Santa Elena alluvial deposits (Venezuela); they have low nitrogen concentrations that are quite highly aggregated. Group 2 pinks have much higher nitrogen concentrations with much lower levels of aggregation, and have been reported from deposits in southern Africa, Canada and Russia. In both groups the pink colour is intimately associated with deformation lamellae on the <111> crystal planes (known as colour graining). In Group 2 pinks, these <111> lamellae have been characterized as deformation microtwins [1, 2]. Subsequently the <111> lamellae in Group 1 pinks have been assumed to also be deformation microtwins. In this study we utilize electron backscatter diffraction (EBSD) to show that Group 1 pinks do not contain microtwins, and that orientation contrast imaging is a very quick and simple technique (compared to X-ray diffraction or TEM) for confirming their presence. We will also report infrared data providing evidence that a primary source of Group 1 pinks is still waiting to be identified in southern Africa.

[1] Gaillou E. *et al*. (2010). *Diamond &Related Materials*, 19, 1207-1220.

[2] Titkov S.V. *et al*. (2012). *Mineralogical Magazine*, 76, 143-149.

Kimberlite indicator minerals in terrigene sediments of Arctic regions of Siberian and North American ancient platforms: evidences of new cratons with thick lithosphere

Pokhilenko N[1*], Afanasyev V[2], Agashev A[1], Malkovets V[3], McDonald J[4], Kuligin S[1], Pokhilenko L[1], Vavilov M[1]

1 - VS Sobolev Institute of geology and mineralogy *chief@igm.nsc.ru 2 - Sobolev Institute of geology and mineralogy, Siberian branch 3 - Pheasant Memorial Laboratory, ISEI, Okayama University 4 - Diamondex Res. Ltd.

Alluvial sediments and some terrigene secondary collectors of large areas of arctic regions of the Siberian Platform (SP, ~120,000 km^2, area between Anabar River and lower part of Lena River), and North American Platform (NAP,~150,000 km^2, areas to N, NW from the Slave Craton and to W from Great Bear Lake) were sampled for kimberlite indicator minerals (KIM) during the diamond exploration programs (field seasons of 2002-2013). Cr-pyropes , magnesian ilmenites and chromites were found in many hundreds of samples, and over 70,000 of KIM grains from these samples were studied and analyzed using optical microscopes, SEM and EMP methods at Analytical Center of V.S. Sobolev Institute of Geology and Mineralogy, SB RAS, Novosibirsk, Russia.

A comparative analysis of composition features of KIM from the sampled area showed that: 1) there are variable and often high proportions of Cr-rich varieties of pyropes (>7 wt.% of Cr_2O_3) among the most of pyrope bearing samples; 2) several hundreds of samples contain high-Cr subcalcic knorringite-rich ($Mg_3Cr_2Si_3O_{12}$ up to 32 mol. %), and in several tens of these samples together with significant number of G10 garnets were found diamond crystals up to 2 ct in weight of kimberlitic morphological types; 2) magnesian ilmenites have all the compositional features of typical kimberlite ilmenites (MgO - 5,2-15,8 wt.%; Cr_2O_3 - 0.1-10,1 wt. %; hematite - Fe_2O_3 - 3-29 mol.%); 3) chromites also have all the compositional features typical for kimberlite chromites (Cr_2O_3 - 14-67 wt.%; MgO - 9.8 - 29.4 wt.%; TiO_2 - 0.01-8.5 wt.%).

KIM were found both in samples taken from modern alluvial sediments of many hundreds of rivers inside sampled areas and in samples taken from terrigene secondary collectors of the basal horizons of Paleozoic and Mesozoic ages. Very high concentrations of KIM were found in Cretaceous secondary collector of Blue Fish River, Canada, and in Triassic and Lower Carboniferous secondary collectors developed inside NE part of SP. Some of analyzed metamorphic zircons from samples taken from terrigene rocks (North of SP and NAP) and kimberlites of Mesozoic age (North of SP) have Archean U-Pb ages. It is especially important for large Birektinsky Terrain (SP) proposed earlier as terrain of Proterozoic age of stabilization.

So, all the obtained data both mineralogical and geological suggest that it is very likely that there are some new craton-sized blocks of the Archean age inside arctic parts both SP and NAP. A presence of diamonds and high pressure varieties of KIM (high-Cr subcalcic pyropes and high-Cr chromites) is a robust and reliable evidence of thick lithosphere (> 200 km) for this block and of presence inside them multiple kimberlite bodies including diamond-bearing ones. These results improve and support significance of both studied areas for successful diamond exploration.

Diamonds and accompanying minerals in the north Yakutia placers, Russia

Posukhova T[*], Sokolova M

Lomonosov Moscow State University *tposukhova@mail.ru

Nowadays we have different hypotheses about formation of the diamondiferous sediments at the North of the Siberia platform [1]: this is tuffisitic rock - unusual new hosts of the diamonds; this is a square intermediate collector; this is a halo of unknown kimberlitic bodies. Unusual diamond crystals of the "Ebalyakh types" were found in these rocks (V and VII types according to Yu. L. Orlov, 1985).

We examined morphology and physical properties of diamonds from different placers of Northern Yakutia [2]. The proportions of external forms vary for diamond crystals from different sources. The rhombododecahedra dominate (35.5-70 %) and aggregates are abundant (25.5-35.5 %). Degree of resorption is high. Colorless crystals of the Ia type predominate. Their spectra have characteristic series of lines corresponded to the A and B nitrogen defects. Brownish color of crystals is connected with plastic deformation of crystals and existence of C-defects.

We examined minerals accompanying diamonds from Triassic sediments of the river Bulkur at the mouth of the Lena River. They are characterized by high content of pyropes, very high content of diamonds, anomalous content of the anatase, absence of quartz in the light fraction. Garnet-chromite association with leucoxene and chlorite is typical for the heavy fraction. Minerals were investigated with different methods: IR-spectroscopy, SEM, X-ray structural and micro-beam analysis.

Our investigation shows, that the rocks are composed of oval and clastic grains of quartz, rutile, feldspars, pyrite, chlorites. These grains are cemented by cryptocrystalline aggregates of phyllosilicates (chlorite, montmorillonite, illite, and others). Whole grains have traces of mechanical wear; the remains of diatoms are revealed.

According to investigating data we can conclude that studied sediments were formed as polymictic conglomerates and haven't the volcanogenic materials. These complex rocks contain rounded and fragmented mineral grains, most of which bear the traces of mechanical processing which are typical for coastal marine sediments.

The composition of the garnet was investigated and their distribution on different chemical-genetic groups was established. High quantity of garnets from ilmenite-bearing and eclogitic rocks was established. Such almandine garnets are not typical for lamproites and group II kimberlites, and they are not stable in the supergene processes.

As a result we can conclude that the studied Carnian deposits are the collectors of xenogeneic kimberlitic minerals. The minerals with low chemical and mechanical stability were established in collector and this is not typical for ancient haloes with long supergene history. It is suggested that the Triassic placers could be formed by direct erosion of the close indigenous sources.

[1] Garanin V.K., Posukhova T.V. and Degtyareva A.V. (1994). Morphological features of the placer diamonds from alluvial deposit of the Anabar river // *Bulletin of the Russian Mineralogical society*, N1, pp. 71-80.

[2] Kudryavtseva G.P., Garanin V.K. and Posukhova T.V. (1996). *Morphology of diamonds from Russian deposits: Arkhangelsk Province, North Yakutia, Timan, Ural* // IMA-abstract, Toronto.

The origin and significance of crustal minerals in ophiolitic mantle rocks

Robinson P[1*], Yang J[2], Trumbull R[3], Schmitt A[4], Li J[5]

1 - Chinese Academy of Geological Sciences *paulrobinson94@hotmail.com 2 - Chinese Academy of Geological Sciences, Beijing, China 3 - Helmholtz Centre Potsdam, Germany 4 - University of Southern California, USA 5 - China University of Geosciences, Wuhan, China

Various combinations of crustal minerals, such as zircon, almandine garnet, corundum, kyanite, andalusite, rutile, titanite, and feldspar have been recovered from chromitites and peridotites of the Luobusa and Dongqiao ophiolites of Tibet, the Semail ophiolite of Oman and the Ray-Iz ophiolite of the Polar Urals, Russia. In all of the ophiolites these minerals are accompanied by highly reduced phases, such as native Fe, Ni, Ti, Si and Al, base-metal alloys and moissanite, as well as ultrahigh pressure minerals, including coesite and/or diamonds in the ophiolites of Tibet and the Polar Urals. Some of these crustal minerals occur in-situ or are attached to chromite grains, metallic alloys or rutile. Rounded grains of zircon, 50-300 µm in diameter, with very complex internal textures, are common in all of the ophiolites. U/Pb SIMS dates for the Luobusa zircons range from 549 to 1657 Ma, those from Dongqiao from 484 to 2515 Ma, and those from Semail from 84 to 1386 Ma, typically much older than the host ophiolites. Most of the zircons contain low-pressure mineral inclusions, including quartz, rutile, orthoclase, mica, ilmenite and apatite. All of the zircons have REE and trace element compositions compatible with a crustal origin. The crustal minerals, combined with the morphology and age of the zircon, indicate derivation from crustal rocks subducted into the mantle where they were mixed with UHP and highly reduced phases. Preservation of these minerals may be due to their encapsulation in chromite and olivine grains. We suggest that subducted crustal material is widespread in the upper mantle and that it may account for some of the observed mantle heterogeneity.

A composite garnet pyroxenite xenolith yields a minimum age of 2.4 Ga for eclogitisation in the Kaapvaal subcratonic mantle

Sieber M[1*], Brey G[1], Qiao S, Gerdes A[1], Heidi H[2]

*melanie-sieber@stud.uni-frankfurt.de 1 - Goethe-University Frankfurt 2 - DMG

We have studied a composite, 16x11x5 cm sized garnet pyroxenite xenolith with three petrographically and compositionally distinct layers (Type II after MacGregor and Carter, 1970) from the Roberts Victor diamond mine in South Africa.

The sample was thermally last equilibrated at 910 °C which corresponds to 4.2 GPa along a 38 mW/m^2 conductive geothermal gradient. The temperature was derived from neighbouring garnets and clinopyroxenes with the Fe-Mg grt-cpx exchange thermometer of Krogh (1988) in all three parts.

The aim was to find a model for the origin of the various layers from major and trace elements and to establish age constraints by the analysis of the Lu-Hf and Sm-Nd isotope ratios in the compositionally differing garnets.

Part I is a ~1 cm thick layer with approximately 20% Cr-rich garnets (up to 6 wt% Cr_2O_3) and 80% Cr-diopside. The Cr-diopside has 1-120 µm wide exsolution lamellae of presumably former opx (which is now replaced by calcite) and of subordinate, small patches (< 2 mm) of primary phlogopite. The rock changes compositionally and modally into a garnet-pyroxenite (part II; group A after Coleman *et al.*, 1965) perpendicular to the Cr-diopside layer with a gradient of the grt and cpx compositions which appears like a diffusion gradient. The individual mineral grains (mostly ~ 4 mm), however, are homogeneous. Cr_2O_3 in grts decreases from 4 to practically zero wt%, their Mg-# increase from 73 to 75 and cpx compositions change complementary. The REE, Zr and Hf follow the compositional trend of Cr.

In part III (a group A garnet-pyroxenite as well) no exsolution lamellae occur in the primary parts of the cpxs. Most of these, however, are replaced by secondary cpxs and primary compositions can only be obtained in places.

In part III Cr in grt is evenly low whereas Mg-# decreases again over 4 cm from 75 to 72. Zr and Hf also follow such a parabolic trend, whereas HREE, HFSE, Sc and V behave irregularly.

The grt/cpx partition coefficients in the various parts are parallel to the experimentally derived partition coefficients of Green *et al.* (2000) but are shifted parallel as a function of composition (Cr and Mg in grt). This indicates equilibrium on a local scale in major and trace elements over the whole xenolith.

We separate garnets from the different parts and obtained a Lu-Hf errorchron with an age of 2375±210 Ma with an initial $^{176}Hf/^{177}Hf$=0.2817±0.0012. This could be a minimum age for eclogitisation or metasomatism. We tentatively explain the origin of the Cr-diopside layer (part I) as a reaction front of a fluid or melt in a contact zone between a peridotite and a garnet-pyroxenite. Primary phlogopite reflects water in the fluid/melt. The apparent diffusional profile might be a 'thinning' effect of that process.

Iron containing surfaces of contact of diamond with kimberlite

Skvortsova V[1*], Samoylovich M[2], Belyanin A[2]

1 - Lomonosov Moscow State University, Russia *valskvor@yahoo.com
2 - Central Research Technological Institute "Technomash", Russia

It is known that diamond crystals embedded in kimberlites are separated from kimberlite rocks by polymineral thin layer with a large variety of local textural and geochemical features. The study of such a contact layer (in the literature it is called a rim, an imprint, a shell) gives some information on particular aspects of diamond genesis. Numerous experiments showed that metallic melts, in particular iron containing ones, form suitable media for synthesis of monocrystalline diamond. The theory of crystal growth implies that such melts act as diffusion boundary layers.

The present work is concerned with a study of phase compositions of iron containing contact layers as possible rudiments of diamond growth system. 13 kimberlite samples with imprints (from Rudenko collection, Udachnaya pipe, Yakutia) were selected by magnetic separation as being magnetic because of the presence of iron containing phases. Morphology and composition of contact layer surface were studied by SEM, without application of the diverter charge layer (CARL ZEISS LEO 1430 VP, equipped with an energy dispersive spectrometer). Identification of various phases was carried out by Raman spectroscopy using a micro-Raman spectrometer LabRAM HR800 (HORIBA Jobin-Yvon, 632.8 nm, He-Ne)).

Analysis of the results showed the presence in contact layers the following iron containing oxide phases: magnetite, maghemite, hematite, wustite; and also non-magnetic phases such as siderite, Mg-calcite and dolomite. Contents of amorphous and crystalline phases varied within wide limits. A significant result is the detection of a well-preserved fragment of imprint reflecting surface of the diamond crystal with the structure of linearly-stepped zoning and steps synchronously corrugated with diamond crystal. Corrugating of iron containing imprints can be probably explained by parallel topochemical interaction of diamond surface, both with Fe-rich metallic melts and with iron oxides in various oxidation states.

The data obtained allow consideration of the peculiarities of diamond monocrystal formation in nature with regard to the role of thin layers of metal melts

Understanding δ15N variations in the mantle using internal variabilities in natural diamonds

Southworth R[1*], Mikhail S[2], Howell D[3], Verchovsky A[4], Brenker F[5], Jones A[1]

1 - University College London *rebecca.southworth.11@ucl.ac.uk 2 - University of Edinburgh 3 - CCFS &GEMOC, Macquarie University 4 - Open University 5 - Goethe University

The average for both $\delta^{15}N$ and $\delta^{13}C$ values of mantle-derived diamonds is -5 ‰ [1, 2]. However, some individual mantle diamonds can show a very large range in $\delta^{15}N$ value with very narrow ranges for their corresponding $\delta^{13}C$ values [1]. These data can be explained by either (a) nitrogen isotope heterogeneity in the mantle (subduction induced or primordial) or (b) N-isotope fractionation during diamond growth. The former is the subject of this contribution.

To further investigate the possibility of mantle heterogeneity, we will have determined the internal C-N stable isotope variability for 10 monocrystalline diamonds from Juina, Brazil. Bulk stable isotope data show diamonds from Juina have a narrow range of $\delta^{13}C$ values for upper and lower mantle-derived diamonds (4 ‰), with a corresponding range of *ca*.10 ‰ for their $\delta^{15}N$ values [2]. These narrow ranges for both upper and lower mantle peridotitc diamonds were used to propose a heterogeneous mantle source beneath the Amazonian craton (Brazil) produced by whole mantle convection [2]. However, it was shown in [1] that $\delta^{15}N$ within an individual monocrystalline diamond from Juina can vary by up to +20 ‰ (one eclogitic and one unknown), while the corresponding range of $\delta^{13}C$ values vary by <3.4 ‰ [1]. The data in [1] cast doubts on whether or not the mantle is well-mixed with respect to nitrogen and further suggests that carbon and nitrogen are de-coupled during eclogitic diamond formation.

We have used stepwise combustion gas-sourced mass spectrometry to determine the carbon and nitrogen isotope values and nitrogen concentrations within 10 diamonds from Juina, Brazil. We will interrogate the $\delta^{13}C$-$\delta^{15}N$-[N] data from these samples to investigate the stable isotope systematics that are recorded in diamond growth beneath the Amazonian craton.

[1] Mikhail *et al.* (2014). *Chem. Geol.*, 366, 14-23.

[2] Palot *et al.* (2012). *EPSL*, 357-358, 179-193.

The cutting edge of fluid inclusion re-equilibration research

Bakker R

University of Leoben. bakker@unileoben.ac.at

The possible change in physical and chemical properties of fluid inclusions after their entrapment in minerals has been considered since the beginning of the 20th century. This research is of major importance to the interpretation of inclusion properties in the context of rock-forming conditions. The difficulty of assigning fluid properties to a specific geological environment is mainly a result of unknown re-equilibration processes, or insufficient characterization of fluid-trapping events. Recent experimental studies with synthetic and natural fluid inclusions in quartz have revealed a variety of re-equilibration processes that can be classified as diffusion and deformation. The most obvious process is brittle deformation (formation of micro-cracks adjoining inclusions) due to internal overpressure (i.e. decrepitation). The expression "stretched inclusion" is not an appropriate label for inclusions that have changed their morphology. Per definition, stretching is a one-dimensional lengthening, and it is erroneously used for a volume increase of fluid inclusions. It must be noted that a volume increase of inclusions cannot occur without micro-cracking and diffusion of host-mineral components. Experimental techniques to examine re-equilibration processes are not able to separate completely diffusion and deformation processes, but they can be minimized by the selection of specific experimental conditions. Diffusion of H_2O through the host mineral is induced by a fugacity gradient between inclusions and pore fluid at constant pressure and temperature. The diffusion is locally enhanced by deformation of the quartz around inclusions, due to pressure differences. These processes may change the salinity, composition and density of fluid inclusions without morphological alterations. Experiments with D_2O, a trace molecule for H_2O, illustrate the mobility of water through quartz crystals at temperature above 450 ˚C. The alpha-beta quartz phase transition affects the fluid properties of inclusions. This is mainly observed at relative low hydrothermal pressures, below 200 MPa. Experiments with natural H_2O-CO_2-NaCl-KCl-rich fluid inclusions have illustrated the mobility of H_2O and CO_2 at high temperatures (600 ˚C), and a change in the cation ratio, which implies the mobility of Na cations. The identification of individual processes that may affect fluid inclusion properties, and the efficiency at variable temperature, pressure, and pore fluid conditions is the main source of reliability of the interpretation of fluid inclusions for the conditions of geological events.

Ore-forming fluid of tungsten deposits in south Jiangxi province, China: evidence from infrared microthermometric study of fluid inclusions in coexisting quartz and wolframite

Ni P* Wang X, Huang J, Wang G, Wang T

Nanjing University *peini@nju.edu.cn

China ranks number one in the world in terms of tungsten resources and production. The Southern Jiangxi tungsten metallogenic belt, containing Chong-Yu-You, Jiulianshan, and Yushan ore cluster areas, hosts a lot of world-class wolframite-quartz vein type tungsten deposits. Most of previous research works have been done on the features and evolution of Mesozoic granite and it relation to tungsten mineralization. However, few works involved the studies of fluid inclusions from quartz and wolframite formed during ore deposition stage. Beginning in the 1980s, the use of infrared microscopes made it possible to study fluid inclusions in opaque ore minerals, such as wolframite, cassiterite, and rutile. In this paper, fluid inclusions in both quartz and coexisting wolframite from the three ore clusters were studied, in order to constrain the feature and evolution process of tungsten-forming fluids.

Liquid-rich two phase aqueous inclusions (type I) and two/three phase CO_2-bearing inclusions (type II) can be recognized in quartz. Only liquid-rich two phase aqueous inclusions (type I) can be identified in wolframite. Type I fluid inclusions from quartz in the Chong-Yu-You area show that fluid mixing was probably the dominant ore-forming process. The assemblage of type I and coexisting type II primary inclusions from quartz are common in the Jiulianshan and Yushan area, which indicates a process of fluid immiscibility. Type I inclusions in wolframite in all these three ore clusters show clearly temperature decreasing trend, which imply that temperature decreasing control ore deposition.

The composition, homogenization temperature, and salinity of fluid inclusions from wolframite and coexisting quartz show distinct characteristics, suggesting different physical and chemical conditions they formed. Thus, direct observation and microthermometric of the fluid inclusions trapped in ore mineral is the most ideal and the most reliable method for identifying the process of mineralization.

The role of highly saline fluids in shear related U-mineralization in Closepet granitoids, Dharwar Craton, India

Srikantappa C

Department of Earth Science, University of Mysore, India. srikantappac@gmail.com

Closepet granitoid (~ 2.5 Ga) is a conspicuous, arcuate igneous body emplaced within the Peninsular gneiss in the Dharwar Craton.The granitoids are classified into root-zone, transfer zone and intrusion zone. The northern part of the Closepet granitoid in highly potassic, strongly differentiated and contain higher amounts of uranium (up to 20 ppm U). The granitoid show significant zonation in fluid composition from the immiscible H_2O-NaCl and CO_2 fluids in the deeper parts, mixed CO_2-H_2O in the middle part to predominantly H_2O-NaCl in the upper levels. U-bearing primary minerals like zircon, monazite, allanite and sphene occur in granitoids.

The Clospet granitoid towards northern part show evidence of ductile and ductile-brittle deformation, along a major E-W shear zone. Petrographic of sheared granitoids show highly deformed nature with ribbon quartz grains (Qtz-I), recrystallisation of quartz (Qtz-II), biotite show retrograde alteration to chlorite and quartz. Highly resorbed U-bearing minerals like monazite, zircon and allanite occur in shear zones. The U-ore mineral pitchblende is the common associated with sulfide minerals.

Four type of fluid inclusions viz., 1. Halite (NaCl) bearing highly salinity fluids (26 to 35 wt.% NaCl eqv.) and Sylvite (KCl), 2. Low salinity aqueous fluids 3. Low density CO_2 inclusions and 4. Empty inclusions are recorded in sheared granitoids. Fluid inclusion chronological data show presence of both primary and pseudosecondary low salinity and Halite bearing fluids in Qtz-I. Presence of only primary halite bearing fluids as well as few CO_2-fluids occur in Qtz-II. U-ore (mainly pitchblende) occur associated with Qtz-II. Backscattered EPMA studies in monazite show strong chemical zonation with depletion of U and enrichment of Th, suggesting leaching and deposition of U by alkaline fluids along shear, suggesting channelised fluid flow process. Th data of fluids combined with chrlorite+quartz thermometry suggest mobility of saline fluids at T ranging from 425 to 185^{o}C at depths of 10 to 12 km (2.5 to 3.5 Kb). *In situ*, U-Pb isotopic study of zoned monazite show protracted timing of mineralization from ~ 1.5 to 0.8 Ma.

It is interpreted that along ductile, ductile-brittle shear zones, the early magmatic paleo-fluids were released during shear deformation in granitoids. As a result of Pf >Pl during shearing, the released fluids traversed the rock resulting in channelized fluid flow. The saline fluids reacted with the U-bearing primary minerals causing considerable leaching of U. The leached U was transported to higher crustal levels in alkaline solutions and deposited in favourable sites within the shear zone to form ore deposits.

Alkaline fluids in Precambrian deep-crustal metamorphism and their role in the origin of granulites and granites in Dharwar Craton, India

Srikantappa C

Department of Earth Science, University of Mysore, India. srikantappac@gmail.com

Granulites, termed as charnockitic-enderbitic granulites of Precambrian age (3.3 to 2.5 Ga), are well exposed in southern Peninsular India. They have been classified into 1) Massive / Banded charnockites (MBC) and 2) Incipient charnockite (IC). The MBC show regional granulite facies metamorphism with P-T (M1): 700 - 730^{o}C, 6 - 11 kbar. They show IBC P-T-t trajectories. The IC localities, occur on a local scale, occupying low-land areas, confined to shear zones with mineral P-T ~ 650 - 700^{o}C, ~ 6 kbar. Linear, N-S trending Closepet granites (~ 2.5 Ga) occur spatially associated with granulites.

Deep-crustal fluids like H_2O-NaCl, CO_2 and CO_2-H_2O have been recorded in both granulites and granites. For the first time occurrence of halite bearing, highly saline fluids (up to 42 wt.% NaCl eqv.) coeval with CO_2-rich fluids have been identified in both granulites and granites from the Dharwar Craton (Figure 1).

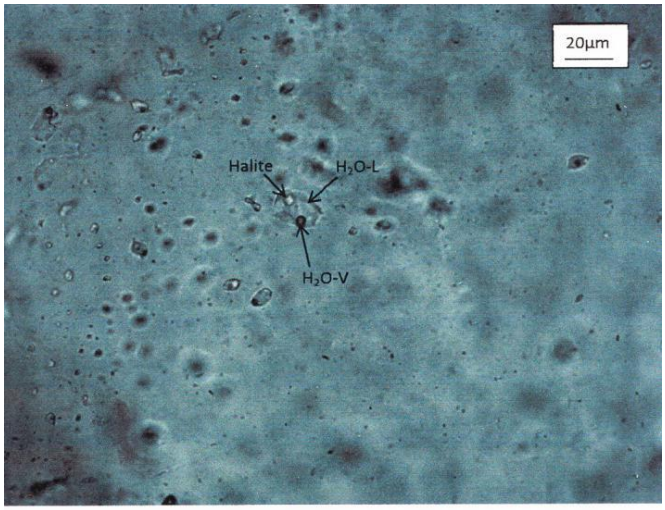

Figure 1: Trail bound halite bearing fluids in granulite.

A combined micro-textural, mineral P-T, fluid density and fluid evolution based on the chronology of entrapment of fluids in granulites show a synmetamorphic nature of alkaline and CO_2-rich fluids.

The present record of highly saline fluids in the granulites in the DC suggest that these salt solutions, immiscible with CO_2 are the fluids responsible for deep-crustal metamorphism in the craton in contrast to the earlier hypothesis of "Carbonic metamorphism".

Fluid inclusion study in the Closepet granite shows significant zonation from the immiscible H_2O-NaCl and CO_2 fluids in the deeper parts, mixed CO_2-H_2O in the middle part to predominantly H_2O-NaCl in the upper levels of the granites.

The source for these fluids appears to be the underplated alkali basaltic magmas, suggesting addition of mantle derived fluids into lower crust, implying growth of the continental crust vertically.

Ore genesis of the Neoproterozoic Jinshan orogenic gold deposit in the Dexing area, South China: evidence from fluid inclusions and isotopes

Wang G*, Ni P, Zhao C, Ding J

Nanjing University *ggwang@nju.edu.cn

The Jinshan gold deposit is located in the Neoproterozoic Jiangnan orogen between the Yangtze and Cathaysia Blocks. Ore genesis of the Jinshan gold deposit is hotly debated. Some researchers proposed that it was a typical Neoproterozoic orogenic gold deposit, but others pointed out that it belonged to Jurassic Dexing porphyry-epithermal ore system. In this paper, we would like to conduct detailed fluid inclusion and H-O-S-Pb isotopes to identify the ore genetic type and to constrain the origin of this deposit. Fluid inclusion studies were conducted on the auriferous quartz veins. Three types of fluid inclusions can be identified: H_2O-CO_2 inclusions (type I), CO_2-rich inclusions (type II), and aqueous inclusions (type III). The pre-ore stage, quartz-pyrite veins primarily contain type I inclusions with constant CO_2 bubble volumetric proportions. The main gold mineralization stage veins have all three types of inclusions with variable gas-phase ratios and CO_2 contents. The post-ore stage carbonate±chlorite veinlets only contain type III inclusions. Type I inclusions in the pre-ore stage display homogenization temperatures (Th) of 285-340°C, with salinities of 1.4-6.1 wt.% NaCl equivalent. In the main gold mineralization stage, type II and III inclusions show similar Th at 208-277°C, but contrasting salinity values with 0.6-3.6 and 3.5-8.9 wt.% NaCl equivalent, and type I inclusions show variable CO_2 phase proportions and have Th of 241-292°C and salinities of 1.0-7.0 wt.% NaCl equivalent. In the post-ore stage, type III inclusions yield Th of 109-201°C and salinities of 1.1-6.4 wt.% NaCl equivalent. Petrological observations and microthermometric results show that fluid immiscibility primarily occurred during the gold mineralization stages. The oxygen and hydrogen isotope compositions (δ^{18} O = +6.9‰ to +11.2‰, δD = −71‰ to −46‰) of inclusion water in quartz grains imply that ore fluids were principally metamorphic in origin. The sulfur and lead values of sulfide from the ores are analogous to those from the basement strata, suggesting a predominantly crustal source of the ore sulfides. Our research shows that the Jinshan deposit is a typical orogenic gold deposit.

Quartz mineralization during hydrothermal fluid flow and repeated fragmentation: fluidization, grain growth, deformation and recrystallization structures in the Rusey fault zone (Cornwall/UK)

Yilmaz T*, Kruhl J H

Technical University Munich. *tim.yilmaz@tum.de

Based on field and microstructural data, the spatial-temporal connection between fluid flow, quartz crystallization and deformation along the Rusey fault zone in Cornwall (UK) has been investigated. Various fragmentation and fluid-flow processes and their interaction lead to complex-structured quartz units such as early quartz veins, spheroidal coated and partly silicified wall rock fragments (Figure 1), microcrystalline quartz masses, mm-dm wide shear zones and late crosscutting quartz veins. Relicts of ameboid banding structures as well as feathery quartz textures indicate that quartz crystallized from chalcedony and originally precipitated from a silica gel. Material transport along the brittle shear zone is at least partly governed by flow of fluid-quartz-particle suspensions [1]. The complex meso- to microstructures are generated by repeated processes of fragmentation, quartz precipitation and grain growth. In general, the brittle Rusey fault zone represents a zone of multiple fragmentation, fluid flow, recrystallization and quartz dissolution and precipitation and is regarded as key example of large-scale cyclic interaction of these processes.

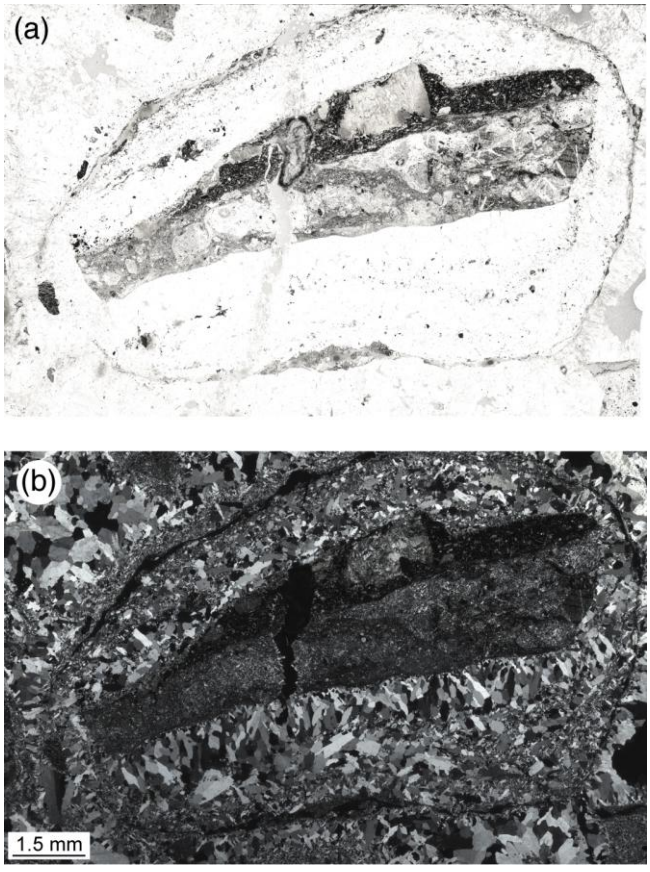

Figure 1: Photomicrograph of a Rusey Fault wall-rock fragment mantled by quartz; ll pol and X pol. (a) The dark fragment contains numerous small fragments of quartz. (b) The mantle is composed of at least two layers of quartz, an inner one of up to mm-sized palisade crystals and an outer one of µm-sized anhedral grains.

[1] Yilmaz T.I., Prosser G., Liotta D., Kruhl J.H. and Gilg H.A. (2014). *J. Struct. Geol.* submitted.

Raman spectroscopic study on Cu complexation in hydrothermal fluids at 300-600 °C, to 2.1 GPa

Schmidt C[1*], Watenphul A[2], Scholten L[3], Jahn S[1]

1 - GFZ German Research Centre for Geosciences *christian.schmidt@gfz-potsdam.de 2 - Earth, Planetary, and Space Sciences Department, UCLA 3 - Institut für Geowissenschaften, CAU Kiel

Knowledge of the abundant Cu species in aqueous fluids over a wide range of fluid compositions, pressure and temperature is important to understand copper mobility in the crust and subduction zones. Here, we applied Raman spectroscopy to study the Cu complexation in sulfur- and chlorine-bearing fluids to 600 °C and 2.1 GPa. Synthetic CuS crystals or a piece of Cu foil were reacted with aqueous HCl ± NaCl solutions using a hydrothermal diamond-anvil cell [1] in which the sample was contained by an Ir gasket. SEM analyses of the run products showed reaction of CuS to Cu_2S, formation of a Cu-Ir-sulfide, and a high sulfur content in an about 10 µm thick zone in the gasket where it was in contact with fluid. The Raman spectra of fluids in which CuS was equilibrated indicated high concentrations of HS^- and H_2S. Raman bands from S_3^- [2] were recorded only in one experiment at 18.2 mass% NaCl + 0.7 mass% HCl at 500 and 600 °C using a 532 nm laser, and were not observed at very similar conditions if the excitation wavelength was 473 nm.

Both sulfur-bearing and sulfur-free fluids showed Raman bands from Cu complexes between 200 and 400 cm^{-1}. The band at ~290 cm^{-1}, which is assigned to $CuCl_2^-$ [3], was usually the most intense. Further bands occurred at ~350 cm^{-1} (very weak, if present, and assigned to $CuCl(H_2O)^0$ [3]) and ~270 cm^{-1} and, at high HCl concentrations, at ~250 cm^{-1} (perhaps from $CuCl_3^{2-}$ [3]). Sulfur-bearing fluids showed a lower intensity of the bands from Cu-Cl vibrations compared to sulfur-free fluids at similar conditions, and a weak but significant Raman band at ~330 cm^{-1}, which differs from positions expected for Cu-Cl complexes [3]. Tentatively, we assign this band to a mixed Cu-Cl-HS^-/H_2S species, which still requires verification by *ab initio* molecular dynamics simulations with quasi-normal mode analysis. Generally, there was an increase in the sum of the integrated intensities of the bands assigned to Cu complexes with increasing HCl concentration. At all fluid compositions, the intensity of these Raman bands increased with decreasing pressure at constant temperature for single-phase fluids, which indicated a higher Cu solubility at low pressures. However, formation of additional bands was not evident in the Raman spectra.

In summary, Raman spectroscopy indicates Cu transport in reducing and acidic hydrothermal fluids via complexes with Cl^- and HS^-/H_2S and an insignificant role of S_3^-.

[1] Bassett *et al.* (1993). R*ev. Sci. Instr.*, 64, 2340.

[2] Pokrovski and Dubrovinsky (2011). *Science*, 331, 1052.

[3] Applegarth *et al.* (2014). *J. Phys. Chem. B*, 118, 204.

The effect of carbonate solid solution on the elasticity of natural fluorapatites

Cámara F[1*], Curetti N[2], Benna P[1], Ferraris C[3]

1 - University of Torino - CrisDi, Italy *fernando.camaraartigas@unito.it
2 - University of Turin 3 - Muséum National d'Histoire Naturelle, Paris

Apatite is an important mineral and knowledge of its stability at the Earth's interior is essential to understand its role as potential repository of phosphorous at the mantle depth. In biomedical field its mechanical properties are also important as apatite is a dental enamel constituent. Changes in the chemical and physical properties of apatite are observed when carbonate is incorporated into the apatite structure. Incorporation of carbonate can occur by substitution for both the channel anion and the phosphate ion with different effects on unit-cell parameters. Substitution of hydroxyl (OH) by type A carbonate results in progressive increase in *a* and decrease in *c*, whereas substitution of phosphate by type B carbonate results in progressive decrease in *a* and increase in *c*. So far several compression experiments have been carried out to investigate the compressibility of synthetic samples of fluorapatite, hydroxylapatite, and chlorapatite. A study of natural fluorapatite was performed by [1], who found a lower value of K_T than previous work (using a BM2, K_T = 91.6(1.0) GPa by [1] versus 97.9(1.9) GPa [2] and 97.8(1.0) GPa by [3]). Recently [4] have studied the effect of carbonate substitution on the compressibility of hydroxylapatite: the substitution of carbonate (both type A and B) lowers the value of K_T. However, it is difficult to assess if the softening is due to type-A or type-B or both types of substitution. Among the available data, only [3] have performed a single crystal diffraction study.

In order to clarify such discrepancies, we have performed a single crystal diffraction study of two natural fluorapatite and type-B carbonate fluorapatite ("francolite") samples coming from Muséum National d'Histoire Naturelle, Paris. Two crystals were mounted together in a DAC using quartz as pressure calibrant and a 16:3:1 mixture of methanol:ethanol:water as pressure-transmitting medium. We used SINGLE program [5] to collect data on a Siemens P4 four-circle diffractometer and EosFit7c [6] to fit the data.

Our data (16 pressure points up to 5.8 GPa), fit to a 3rd order Birch-Murnaghan Equation of State (BM3-EoS) show that type-B carbonate substitution effectively decreases the bulk modulus from K_T = 88.41(1.9) GPa [with K_T' = 5.8(0.8)] to K_T = 85.3(1.4) GPa [with a K_T' of 5.6(0.6)]. However, careful inspection of the F-*f* plot shows that two different elastic regimes (low-P <3.25GPa and high-P ≥3.25GPa) should be actually taken into account for fluorapatite. Moreover, collecting more data during decompression will allow to better constrain both pressure ranges. So far we have used a BM2 EoS for both the low-P and the high-P regimes obtaining K_T of 91.94(99) and 98.9(1.6) GPa for the low-P and the high-P regimes respectively. This preliminary result agrees well with previous findings for fluorapatite as the value obtained by [2] were probably biased by high pressure regime (although high pressure data >9 GPa was probably not hydrostatic) while the value obtained by [1] did not have enough observations at high pressure. In both cases the authors fitted the whole observed pressure range as a unique pressure regime.

[1] Matsukage K.N., Ono S., Kawamoto T. and Kikegawa T. (2004). *Phys Chem Minerals* 31, 580-584.

[2] Brunet F., Allan D.R., Redfern S.A.T., Angel R.J., Miletich R., Reichmann H.J., Sergent J. and Hanfland M. (1999). *Eur J Mineral* 11, 1023-1035.

[3] Comodi P., Liu Y., Zanazzi P.F. and Montagnoli M. (2001). *Phys Chem Minerals* 28, 219-224.

[4] Liu X., Shieh S.R., Fleet M.E., Zhang L. and He Q. (2011). *Am Mineral* 96, 74-80.

[5] Angel R.J. and Finger L.W. (2011). *J Appl Crystallogr* 44, 247-251.

[6] Angel R.J., Gonzalez-Platas J. and Alvaro M. (2014). *Zeit Kristallogr*, in press (DOI: 10.1515/zkri-2013-1711).

Unraveling the structural complexity of high-pressure orthorhombic iron oxides

Lavina B[1*], Meng Y[2]

1 - University of Nevada, Las Vegas *lavina@physics.unlv.edu 2 - HPCAT, Carnegie Institution of Washington

Occurring as accessory minerals in most rocks and forming large deposits of considerable economical importance, iron oxides have a key petrological importance. Their role as oxygen buffers, in differentiation processes and as magnetic phases summarizes the iron oxides critical importance in most geological contexts, independently of their abundance.

The recent discovery of a new compound in the Fe-O system, Fe_4O_5 [1], reshaped our assumptions on the behavior of iron oxides in the Earth's deep interior, where phases of FeO and Fe_3O_4 were considered the sole plausible players. Fe_4O_5 is stable at pressures greater than about 10 GPa and, with an iron average valence state of 2.5+, is a plausible accessory mineral of the deep Earth. Other studies found that Fe_4O_5 may be stable in a wide stoichiometry range [2] and can accept a wide extent of isomorphic substitutions [3]. Finding a new compound in one of the most investigated binary systems and in a pressure and temperature range that is experimentally accessible for decades is surprising. The discovery of Fe_4O_5 relies on high resolution high pressure microdiffraction mapping using highly focused high energy x-ray only available at synchrotron sources. We will present the procedures that led to the discovery of Fe_4O_5 [4], in particular how powder, single crystal and multigrain diffraction strategies may be combined within samples that are yet only about 100 µm large and less than 10 µm thick. This strategy can provide more robust identification and characterization of phases synthesized at high P-T and a characterization of samples heterogeneity.

We will present some of the latest results revealing an Fe-O system that shows at high pressure an unexpected complexity including important degrees of disorder, as evidenced by diffuse scattering effects.

[1] Lavina B. *et al.* (2011). Discovery of the recover- able high-pressure iron oxide Fe_4O_5. *Proc Natl Acad Sci U S A* 108, 17281-5.

[2] Woodland A.B., Frost D.J., Trots D.M., Klimm K. and Mezouar M. (2012). In situ observation of the breakdown of magnetite (Fe_3O_4) to Fe_4O_5 and hematite at high pressures and temperatures. *Am Mineral* 97, 1808-1811.

[3] Woodland A.B. *et al.* (2013). Fe_4O_5 and its solid solutions in several simple systems. *Contr. Mineral. Petrol.*, 1677-1686.

[4] Lavina B., Dera P. and Meng Y. (2013). Synthesis and microdiffraction at extreme pressures and temperatures. JOVE, e50613.

Carbon isotope fractionation during carbonated silicate melting under upper mantle conditions

Madhusoodhan S[1*], Yoshino T[2], Mizutani S[3]

1 - Niigata University *satish@geo.sc.niigata-u.ac.jp 2 - Okayama University
3 - Shizuoka University

Subduction of crustal materials, mantle melting and upwelling of deep mantle, in addition to a potential source from the core, largely controls the Earth's deep carbon cycle. Large variations in carbon isotopic composition between different reservoirs have been used widely to differentiate the source of carbon and to understand the carbon inventories and its recycling. How far high temperature and pressure conditions can affect the carbon isotope distribution, is a question still unanswered to address the deep carbon cycle. Here we present results of carbon isotope fractionation between graphite and carbonated silicate melt at 5 GPa and in the temperature range between 1400 and 1900 ºC. High pressure experiments were carried out in the carbon-saturated model harzbergite system (Enstatite-Magnesite-Olivine-Graphite), where carbonated silicate melt and graphite were the two stable carbon-bearing phases in the run products. Carbonated silicate melting resulted in an isotopic fractionation between graphite and carbon in the silicate melt, where the carbon in the melt is ^{13}C enriched than co-existing graphite [1]. ^{13}C enrichment in carbonate melt were further confirmed in experiments where redox melting between olivine and graphite produced carbonate melt as well as carbonate reduction experiments to form graphite.

According to the results of carbon isotope fractionation obtained in this study between graphite and carbonated silicate melt, heavier carbon will be selectively partitioned to the melt and graphite will be lighter than the melt in the order of 1 to 2 permil. If locally oxidative or reductive domains are present or melt extraction and a Rayleigh fractionation process dominate in the upper mantle, then carbonate silicate melt-graphite fractionation will have larger effect on carbon isotopic composition of mantle derived melt/diamond. It is possible that carbonate melt will progressively enrich in carbon isotopes, which corresponds to the primary igneous carbonatite values (-5 to -8 permil) and even rare carbonatites having the more enriched ^{13}C (-2 to -5 permil) may be explainable in terms of the existence of more reductive melting environment. Conversely, the graphite coexisting with such melts will have delta^{13}C values corresponding to main mantle carbon reservoir. Recent experiments have shown that carbonate melts can be a medium for the efficient crystallization of diamonds in Earth's mantle [2]. In addition, the experimental results on the Fe-C melt-carbon fractionation further support the presence of isotopic heterogeneity in mantle derived diamonds [3]. Therefore, redox reaction at different levels of mantle is likely to yield the range of carbon isotope variation of mantle derived diamond. Moreover, carbonated mantle melting according to redox melting in an upwelling mantle can be an alternative explanation for the formation of ^{12}C enriched diamonds in the deep mantle.

[1] Mizutani S., Satish-Kumar M. and Yoshino T. (2014). Experimental determination of carbon isotope fractionation between graphite and carbonated silicate melt under upper mantle conditions, *EPSL*, 392, 86-93.

[2] Palyanov *et al*. (2013). Mantle-slab interaction and redox mechanism of diamond formation. *PNAS*, 110, 20408-20413.

[3] Satish-Kumar *et al*., (2011). Experimental determination of carbon isotope fractionation between iron carbide melt and carbon: ^{12}C-enriched carbon in the Earth's core? *EPSL*, 310, 340-348.

Compressional velocity of hcp-Fe to 163 GPa and 3000 K, and constraints for the inner core composition

Ohtani E[1*], Sakamaki T[1], Fukui H[2], Kamada S[1], Mibe K[3], Tsutsui S[4], Baron A[5]

1 – Tohoku University *ohtani@mail.tains.tohoku.ac.jp 2 – University of Hyogo
3 - University of Tokyo 4 - JASRI 5 – RIKEN

Sound velocity of iron alloys can provide important clues on structure and composition of the core. We measured the compressional velocity of hcp-iron and other iron-light element alloys by the inelastic X-ray scattering (IXS) method using DAC at high pressure and temperature. We made successful measurements of the compressional velocity of hcp-iron up to 174 GPa at room temperature [1] and up to 164 GPa and 3000 K by inelastic X-ray scattering using both external heating and double sided laser heating DACs. We also measured the compressional velocity of non-magnetic Fe_3S and FeH at high pressure and room temperature.

Our experiments indicate that hcp-Fe has almost no temperature effect on Birch's law to 1000 K, but it has a clear temperature effect at higher temperatures of 2300 K and 3000 K consistent with recent theoretical works [2, 3]and shock compression experiments [3]. The present results suggest that compressional velocity of hcp-Fe at the inner core boundary (330 GPa and 5500 K) is higher than that of Earth's inner core. Thus, we can conclude that the light elements or combination of the light elements and nickel in the inner core decreases both density and compressional velocity of hcp-Fe simultaneously under the inner core conditions.

[1] Ohtani *et al*. (2013). *Geophys. Res. Lett*., 40, 5089-5094, doi:10.1002/grl.50992.
[3] Sha X. and Cohen R.E. (2010). *Geophys. Res. Lett*., 37, L10302.
[2] Vočadlo L. *et al*. (2009). *Earth Planet. Sci. Lett*., 288, 534.
[4] Brown and McQueen (1986). *J. Geophys. Res*., 91, 7485.

Olivine composition as a clue to mantle source composition and temperature

Sobolev A[1*, 2], Batanova V[1, 2], Krasheninnikov S[2], Borisov A[3], Arndt N[4], Kuzmin D[5]

1 - ISTerre, Grenoble. France; 2 - Vernadsky Institute, Moscow, Russia *alexander.sobolev@ujf-grenoble.fr 3 - IGEM RAS, Moscow, Russia 4 - ISTerre, Université de Grenoble 5 - V.S.Sobolev Institute, Novosibirsk, Russia

The composition of early olivine phenocrysts in mantle-derived melts critically depends on the phase composition and temperatures of their sources. Such elements as Ni, Mn, Co, Zn, Sc, Fe and their ratios in high Mg olivine were used to decipher the contribution of olivine-free sources in the mantle-derived primary melts [1-5]. This approach has been challenged for Ni contents in olivine considering compositional effect of the temperature difference between melt separation deep in the mantle and its crystallization near the surface [6]. The partition of Al between olivine and spinel was used to establish temperature of primary melts [7, 8]. In this paper we present new data on the composition of high-Mg olivine from mantle-derived melts, which confirm our approach in deciphering source composition [1, 2], and develop and use the new version of olivine-spinel Al thermometer to constrain temperatures of the mantle.

In order to decipher influence of compositional variation of coexisting olivine and spinel on the temperature estimates we performed several experiments at high temperatures (1450-1300 degree C), atmospheric pressure and controlled oxygen fugacity. In addition to known temperature effect of Al /Cr ratio of spinel [7, 8], we found considerable effects of Ti concentrations in spinel and Fo content of olivine.

Using new high precision electron microprobe and LA-ICP MS data on high Mg olivines and coexisting spinels from mid-ocean ridges, Hawaii, Reunion, Iceland, W. Greenland, Gorgona and Archean komatiites and new formulation of olivine-spinel Al thermometer we have found the following principal results.

1. The detectible contribution of melt from olivine-free lithologies is recoded in olivine composition of most investigated samples. The minimal proportions of such melts are characteristic for typical MORBs and komatiites. The maximal for OIBs and LIPs emplaced on thick lithosphere. It is especially shown that the high-Ni contents of Hawaiian olivine could not be explained by the proposed effect of the temperature difference between melt separation and its crystallization near the surface [6] but rather confirm melting of olivine-free lithologies from recycled crust in the mantle source under Hawaii [1, 2].

2. The results of olivine-spinel alumina geothermometry show contrasting crystallization temperatures of Mg-rich olivine of the same Fo content from different types of mantle-derived magmas, from the lowest (down to 1220 degree C) for MORB to the highest (up to over 1500 degree C) for komatiites and Siberian meimechites. These results match predictions from Fe-Mg olivine-melt equilibrium and confirm the relatively low temperature of the convecting mantle source of MORB and higher temperatures in the mantle plumes that produce the OIBs of Iceland, Hawaii, Gorgona, Archean komatiites and several LIPs (e.g Siberian and NAMP).

[1] Sobolev *et al*. (2005). *Nature* 434, 590-597.

[2] Sobolev *et al*. (2007). *Science*, 316, 412-417.

[3] Le Roux *et al*. (2011). *EPSL* 307, 395-408.

[4] Herzberg (2011). *J. Petrology* 52, 113-146.

[5] Davis *et al*. (2013). *GCA* 104, 232-260.

[6] Matzen *et al*. (2013). *J.Petrology* 54, 2521-2545.

[7] Wan *et al*. (2008). *Am. Mineral.* 93, 1142-1147.

[8] Coogan *et al*. (2014). *Chem. Geology* 368, 1-10.

Quasicrystals at HP-HT: implications for the stability of icosahedrite

Stagno V[1], Bindi L[2*], Shibazaki Y[1], Tange Y[3], Higo Y[4], Mao H[1], Steinhardt P[5], Fei Y[1]

1 - Carnegie Institution of Washington, USA 2 - University of Florence *luca.bindi@unifi.it 3 - Ehime University, Matsuyama, Japan 4 - Japan Synchrotron Radiation Research Institute, Japan 5 - Princeton University, USA

Icosahedrite, $Al_{63}Cu_{24}Fe_{13}$, the first natural-occurring quasicrystal, has been recently discovered in the Khatyrka meteorite, a new CV3 carbonaceous chondrite. Its finding has raised fundamental questions regarding the effects that pressure and temperature might have on its stability. Although several studies showed the stability at ambient temperature of synthetic icosahedral AlCuFe up to ~35 GPa, the simultaneous effect of temperature and pressure has been never investigated so far.

We carried out high-pressure *in situ* energy-dispersive X-ray diffraction experiments using multianvil device at beamline BL04B1 (Spring-8) on synthetic icosahedral AlCuFe to explore possible temperature-induced phase transformations at pressures of ~5 GPa and temperature up to ~1700 K. Additional quench experiments were also performed to investigate decomposition and/or melting of $Al_{63}Cu_{24}Fe_{13}$ between 3 and 21 GPa and in the temperature range 1300-2000K.

Results show the stability of i-AlCuFe phase with a negligible effect of pressure on the thermal expansion properties. In addition, an accurate structural analysis by single crystal X-ray diffraction of the recovered samples would exclude the transformation of icosahedral AlCuFe quasicrystalline phase to possible approximant crystalline phases. In addition, preliminary results from quench experiments would suggest that the increasing pressure acts to stabilize the i-AlCuFe at higher temperatures.

Results from this study extend our knowledge on the stability of icosahedral AlCuFe at higher temperature and pressure than previously examined, and provide a first constraint on the stability of icosahedrite in natural systems.

Experimental determination of the phase relations of $MgFe_2O_4$ at conditions of the deep upper mantle and transition zone: first results

Uenver-Thiele L[1], Woodland A[1*], Boffa Ballaran T[2], Frost D[2]

1 - Universitaet Frankfurt *woodland@em.uni-frankfurt.de 2 - Bayerisches Geoinstitut, Universitaet Bayreuth

Spinel-structured phases are common in the upper mantle and transition zone and have the ability to incorporate Fe^{3+} and Fe^{2+} into their structure. Information about phase stabilities, as well as the behaviour of Fe^{3+} at high-P-T conditions is available for some endmember compositions. For example, the high-P stability limit of magnetite was recently demonstrated to lie at about 10 GPa, where it breaks down to the assemblage Fe_4O5 + Fe_2O_3 rather than transforming into a post-spinel structure [1]. Other spinel-structured phases like $FeAl_2O_4$ break down to their constituent oxides [2]. Based upon P-V-T data on $MgFe_2O_4$ and available thermodynamic data, [3] proposed a phase diagram for the $MgFe_2O_4$ composition that includes a large stability field of MgO + Fe_2O_3 at intermediate P and T, and assumed the stability of a h-$MgFe_2O_4$ phase at higher P >17 GPa. However, [3] never produced the h-$MgFe_2O_4$ phase and reported no direct evidence for the existence of a MgO + Fe_2O_3 stability field in their room T experiments even up to 35 GPa.

Here we report the first results of an experimental study to determine the phase diagram for $MgFe_2O_4$ at conditions relevant to the deep upper mantle and transition zone. Multi-anvil experiments were carried out at 8-18 GPa and mostly at 1300°C using either stoichiometric mixtures of MgO + Fe_2O_3 or pre-synthesised $MgFe_2O_4$. PtO_2 powder was added to the capsule to maintain a high partial pressure of oxygen. Run products were analysed by microprobe and powder XRD. Preliminary results confirm the breakdown of $MgFe_2O_4$ to MgO+ Fe_2O_3, but at somewhat lower pressure (ca. 8-9 GPa at 1300°C) than proposed by [3]. The newly produced hematite incorporated Mg (1-3 wt % MgO), the amount of which appears to be a function of pressure. Within the stability field of MgO+Fe_2O_3 predicted by [3], a new phase, $Mg_2Fe_2O_5$ was also detected at 18GPa, which is isostructural with Fe_4O_5. This indicates that the phase relations in the $MgFe_2O_4$ system are more complicated than originally thought and further experiments are underway to address this. In addition, it appears that solid solution may be complete across the Fe_4O_5 - $Mg_2Fe_2O_5$ binary join.

[1] Woodland *et al.* (2012). *Am Mineral*, 97, 1808-1811.

[2] Schollenbruch *et al*. (2010). *Phys Chem Mineral*, 37, 137-143.

[3] Levy *et al*. (2004*). Phys Chem Mineral*, 31, 122-129.

Palladium alloy based redox sensors in high-pressure experiments

Vasilyev P*, Yaxley G, O'Neill H

Research School of Earth Sciences, Australian National University

*prokopiy.vasilyev@anu.edu.au

Oxygen fugacity is one of the key parameters along with temperature and pressure, which controls geochemical processes in the Earth's mantle. Thus investigation of those parameters in deep Earth mantle processes using high-pressure experiments is the prime importance. Experimental temperatures and pressures are usually imposed externally, but the control and the estimation of oxygen fugacity in experiments using various mantle lithologies (e.g. peridotite, eclogites) is frequently more difficult. The use of redox sensors based on noble metal alloys enable the determination of the oxygen fugacity for a given bulk composition at given pressure and temperature.

Palladium metal was employed in experiments as a redox sensor due to the presence of only one stable phase (γFe,Pd) over a large temperature range (900-1300°C) [1] and higher solubility of iron relative to iridium, thus facilitating precise measurement of post-run Fe content [2]. Hydrothermal experiments were performed in the piston-cylinder apparatus at various redox conditions (Co-CoO, W-WO_2, Fe-TiO_2-$FeTiO_3$ buffer systems) and T=850-900°C, P=10-30 kbar. The inner platinum capsule was filled by iron oxide (Fe_2O_3 or FeO) and two types of Pd alloy sensors ($Fe_{90}Pd_{10}$ and Pd). The use of thick-walled (1 mm) Ag outer capsules maintained the required high fH_2 during the experiments for 20-24 hours. The presence of equilibrium in the inner capsule between iron-bearing phases and Fe-Pd alloy redox sensors was checked by double alloy reverse technique.

The effect of pressure on the Gibbs free energy of Fe-Pd alloy in experiments at P=10,20,30 kbar was estimated as negligible. The accurate determination of activity coefficient of iron in Fe-Pd alloy after series of experiments at various fO_2 allows estimation of oxygen fugacity in any Fe-bearing experimental assembly at equilibrium due to reaction:

$$-\Delta G^o = RTln\left[\frac{a_{(Fe)}a_{(\Omega O)}}{a_{FeO_{\frac{x}{2}}(\Omega O)}}\right] + x/2RTlnf_{O_2}$$

where x is the valence state of iron, and (ΩO) refers to silicates [3].

The Pd alloy- based redox sensor was employed to estimate the redox state in the carbonate-bearing eclogite assembly at T=900-1200°C and P=35 kbar. The results of fO_2 measurments in these experiments were cross-checked using quantitative *in situ* XANES measurements of $Fe^{3+}/\Sigma Fe$ [4] in the experimental garnets.

[1] Kubaschewski (1982). *Iron-Binary Phase Diagrams*, Springer, 91-93.

[2] Borisov and Palme (2000). *Amer.Miner*. 85, 1665-1673.

[3] Woodland and O'Neill (1997). *GCA*. 61(20), 4359-4366.

[4] Berry *et al*. (2010). *Chem.Geol*. 278, 31-37.

Crystal chemistry of Ca-eskola-bearing eclogitic clinopyroxene in the system NCMAS

Woodland A*, Uenver-Thiele L, Klimm K, Knapp N

Universitaet Frankfurt *woodland@em.uni-frankfurt.de

Non-stoichiometric clinopyroxene (cpx) is known to be an important phase in mantle-derived eclogites. The non-stoichiometry arises from the incorporation of a Ca-eskola (CaEs, $Ca_{0.5}AlSi_2O_6$) component, which contains vacancies and leads to compositions relatively enriched in SiO_2. During tectonic uplift of eclogite bodies, coesite can be exsolved from such CaEs-bearing cpx. Thus understanding how this component behaves as a function of P, T and composition is of petrologic importance.

We have performed a series of experiments with model cpx compositions between 4 and 10 GPa and 1000-1350°C in order to determine the compositional controls on the extent of CaEs incorporation and to derive the molar volume of this component. Although the starting bulk compositions had a cpx stoichiometry with 50 mol % diopside (Di) and different Ca-Tschermak (CaTs), Ca-eskola and jadeite (Jd) contents, the run products always had an eclogitic assemblage of cpx+garnet+SiO_2. Higher temperatures favor the incorporation of CaEs and CaTs at the expense of Jd. As cpx is the only Na-bearing phase in the assemblage, these systematics lead to a shift in the modal amount of cpx relative to garnet and SiO_2. For starting compositions with equal fractions of CaTs and CaEs, coexisting garnet controls the cpx composition and both of these components decrease with increasing Jd content. This is similar to results in the CMAS system [1]. In starting compositions with a CaEs fraction higher than CaTs, cpx controls the garnet composition, which varies according to the availability of Ca. Saturation in CaEs at ~15 mol % is reached independent of Jd content at 6 GPa. This indicates CaTs and CaEs fractions cannot be varied independently of each other, consistent with the internal equilibrium in the presence of coesite of 2 CaEs = CaTs + 3 SiO_2.

Molar volumes have been determined by XRD for 13 cpx with compositions in the CMAS and NCMAS systems. Taking endmember volumes for Di, CaTs and Jd from [2] and assuming ideal mixing between Di and Jd [3], but accounting for non-ideality in Di-CaTs solid solutions [4], we obtain an average molar volume for the CaEs endmember of 60.96(74) cm^3. This value agrees within our uncertainties with the estimated value proposed by [5].

[1] Knapp N., Woodland A.B. and Klimm K. (2013). *Eur J Mineral*, 25, 579-596. DOI: 10.1127/0935.1221/2013/0025-2326.

[2] Holland T.J.B. and Powell R. (1998). *J Metamorphic Geol* 16, 309-343.

[3] Wood B.J., Holland T.J.B., Newton R.C. and Kleppa O.J. (1980). *Geochim Cosmochim Acta* 44, 1363-1371.

[4] Gasparik T. (1986). *Am Mineral* 71, 686-693.

[5] McCormick T.C. (1986). *Am Mineral* 71, 1434-1440.

Elasticity of single-crystal Phase D across the spin transitions of ferrous and ferric iron in the lower mantle

Wu X[1*], Lin J[2], Liu J[2], Mao Z[3], Guo X[4], Takashi Y[4], McCammon C[5], Xiao Y[6], Prakapenka V[7]

1 - Peking University *xiang.wu@pku.edu.cn 2 - The University of Texas at Austin

3 - University of Science and Technology of China 4 - Okayama University

5 - Universitaet Bayreuth 6 - Carnegie Institution of Washington 7 - University of Chicago

Phase D, the densest hydrous magnesium silicate synthesized at the Earth's mantle P-T conditions thus far, has been proposed to be a potential candidate for transportation of H_2O into the lower mantle by subduction of the hydrated oceanic lithosphere. A certain amount of iron, the most abundant transition metal element in the Earth's interior, is expected to be incorporated into the phase D. Here we synthesized high-quality single-crystal Fe,Al-bearing Phase D ($Mg_{0.89}Fe_{0.11}Al_{0.37}Si_{1.55}H_{2.65}O_6$, ~13.3wt% H_2O) with grain sizes of ~200 micron using the Kawai multianvil apparatus at 21 GPa and 1200 °C at the Institute for Study of the Earth's Interior, University of Oakayama, Japan. Conventional Mössbauer results indicate that the sample contains both ferrous and ferric iron that occupy the octahedral sites of the hexagonal structure. In situ high-pressure single crystal XRD and NFS experiments were performed up to megabar pressures at 13IDD beamline (GSECARS) and 16IDD beamline (HPCAT) of the Advanced Photon Source, respectively. Both experimental results clearly show that both Fe^{2+} and Fe^{3+} undergo a HS-LS transition at high pressures. High-resolution XRD results further indicate an abnormal compression behavior at approximately 37 GPa that can be linked with the previously proposed hydrogen bond symmetrization. Elasticity of phase D has a marked influence by the two-step spin transitions of both Fe^{2+} and Fe^{3+} and the hydrogen bond symmetrization, presenting in the seismic wave model, which is of implication for our understanding of the deep-Earth geophysics and geochemistry especially along the subducted slabs.

Multistage mantle metasomatism beneath the Sangilen Highland

Gibsher A[1*], Malkovets V[2], Kuzmin D[1]

1 - V.S. Sobolev Institute of Geology and Mineralogy SB RAS, Novosibirsk *n.gibsher@gmail.com 2 - Pheasant Memorial Laboratory, ISEI, Okayama University

Migration of magmas though the subcontinental lithospheric mantle is one of the key processes driving in the evolution of its modal composition. Late Ordovician lamprophyric dykes of the Agardag alkaline basaltic complex of West Sangilen carried up numerous large and unaltered xenoliths of spinel facies peridotites [1, 2] with several composite xenoliths - veins of volatile-bearing minerals in spinel peridotites. Here we report the results of detailed mineralogical investigations of four samples of contact xenoliths.

The studied samples are represented by CPx-Phlog, Amp-Phlog, and Amp veins crossing peridotites of the spinel facies. Detailed study of veined mantle xenoliths shows significant differences in the distribution of major- and trace elements at the contacts with veins of different compositions. Peridotites at the contact with Phlog-bearing veins are modified to wehrlites and characterized by profiles of metasomatic enrichment [3]; peridotitic minerals are characterized by trends with enrichment in Fe, Ca, Al, Ti and HREE in the rather narrow zone - 16 mm away from the contact [3]. Peridotitic minerals at the contact with Amp veins show practically no compositional variations with distance from the veins but have high Fe# (in comparison with those from xenoliths without magmatic veins [1]).

Detailed mineralogical and geochemical studies of composite xenoliths revealed the presence of at least two stages of metasomatic enrichment of the lithospheric mantle beneath the West Sangilen [4]. The last stage was related to the formation of the Phlog-bearing vein network. The time of their formation was closely preceded the camptonite intrusion that is evidenced from the surviving of the metasomatic enrichment profiles at the contact with Phlog-bearing veins. Parental melts of such veins are the alkaline silica-undersaturated melts, enriched in Ti and K, and volatiles such as H_2O, Cl, F, CO_2 and P_2O_5, incompatible elements, and probably related to the host camptonites. The earlier stage of the peridotite metasomatic enrichment was related to the formation of the amphibole veins, which crystallized from mildly alkaline transitional basaltic melts (iron reach, with lower titanium and potassium contents), and probably have older age in comparison with the Phlog-bearing veins [3]. The iron enrichment of peridotites at the contact with Amph-bearing veins could be formed by reaction of host refractory peridotites with evolved (Mg numbers 0.6-0.7) silicate melts at high melt/rock ratios, which replace olivine with orthopyroxene and decrease Mg numbers.

[1] Gibsher A.A., Malkovets V.G., Litasov K.D. *et al.* (2010). *Doklady Earth Sciences*, 433, 957-961.
[2] Gibsher A.A., Malkovets V.G., Travin A.V. *et al.* (2012). *Russian Geology and Geophysics*, 53, 763-775.
[3] Gibsher A.A., Malkovets V.G., Kuzmin D.V. *et al.* (2013). *Doklady Earth Sciences*, 448, 138-142.
[4] Gibsher A.A., Malkovets V.G., Kuzmin D.V. and Pokhilenko N.P. (2014). *Doklady Earth Sciences*, 454, 199-203.

Acknowledgements: This study was supported by the Foundation of the President of the Russian Federation (grant MK 2689.2013.5) and by the RFBR (projects No 12-05-00487, 12-05-33035, 13-05-01051)

A structural study of Cr-spinels from mantle xenoliths of Cameroon, Libya and Morocco

Lenaz D[1*], Musco M[1], Caldeira R[2], De Min A[1], Marzoli A[3], Mata J[4], Princivalle F[1], Youbi N[5]

1 - University of Trieste, Italy *lenaz@units.it 2 - National Laboratory for Energy and Geology, Amadora, Portugal 3 - University of Padua, Italy 4 - University of Lisbon, Portugal 5 - Cadi Ayyad University, Marrakech, Morocco

Cr-spinels of mantle xenoliths from Cameroon (CAM), Libya (LB) and Morocco (MOR) have been analysed by X-ray single crystal diffraction.

The cell edges of LB show the largest variability spanning between 8.1219 (1) and 8.2458 (2) Å, while, for MOR spinels, they are in the range 8.1334 (4) - 8.2021 (2) Å, and for CAM they vary between 8.1268 (1) to 8.1485 (2). For MOR and CAM, the oxygen positional parameter is very similar ranging between 0.2625 (1) and 0.26285 (9). However, for LB samples we noticed two distinct oxygen positional parameters, allowing their subdivision in two groups: Group I has an average value of about 0.2626 (1), lower than that determined for Group II with an average value of 0.26335 (7), that, till now, is the highest recorded for mantle xenoliths worldwide.

LB samples show a Cr/(Cr+Al) [Cr#] ratio in the range 0.07-0.50 and a Mg/(Mg+Fe^{2+}) [Mg#] ratio between 0.69-0.82, while those from MOR show a narrower distribution with Cr# 0.10 - 0.40 and Mg# 0.74 - 0.82. CAM has Cr# between 0.09 and 0.17, whereas Mg# range from 0.79 to 0.83.

In LB, TiO_2 is usually below 0.15%, MnO below 0.25 % and NiO between 0.1 and 0.4 %. In CAM samples, TiO_2 is on average higher than in LB samples but lower than 0.2 %, except for one sample which presents contents approaching 0.5 %, MnO below 0.15 % and NiO between 0.3 and 0.5 %. MOR samples show TiO_2 below 0.2%, MnO below 0.15 %, NiO between 0.3 and 0.4 %. It is interesting to notice that the content of MnO is somehow positively correlated with Cr# while NiO is negatively related with it.

Calculated intracrystalline closure temperatures (T*c*) are in the range 550-750°C (MOR), 480-650°C (LB I), 680-950°C (LB II), 630-760°C for CAM, suggesting different cooling histories for each of the studied suites. The effects of cooling preserved in mantle xenolith spinels have been usually related to the cooling rate of the lava hosting the xenoliths, to the size of the xenoliths and to the position of the crystal within the xenoliths. This is because large xenoliths are expected to cool more slowly than small ones and crystals close to the rim will close at a higher temperature than those located in the core of the xenolith. Alternatively, it was suggested that low T*c* for Antarctica spinels could be related to their higher Fe^{3+} content.

Unpublished data on Cr-diopside from the same xenoliths show that the equilibrature pressure is close to the spinel - garnet peridotite transition for all of them. Considering that the size of the xenoliths is similar, they all are from the core of the xenoliths and that Fe^{3+} content seems to be not very relevant for the here studied spinels, we propose that LB II spinels equilibrated deeper in the mantle and have been brought to the surface from that depth, while CAM, MOR and LB I spinels, probably re-equilibrated at a shallower depth before being disrupted and brought to the surface.

Acknowledgement: Funding was provided by FRA 2013 project of the Trieste University.

Elastic properties of iron-bearing carbonates and implications for the deep Earth

McCammon C[1*], Dubrovinsky L[1], Cerantola V[1], Kupenko I[2], Sinmyo R[1], Petitgirard S[1], Ismailova L[1], Kantor A[1], Chumakov A[2]

1 - Universitaet Bayreuth *catherine.mccammon@uni-bayreuth.de 2 – ESRF

Current models predict the occurrence of carbonates in subducting slabs, yet their presence may be challenging to detect using geophysical methods due to their low abundance relative to other phases. One of the important parameters in deciphering seismic data is the elastic properties of iron-bearing carbonates at high pressure and temperature, particularly the effect of the high-spin to low-spin transition reported in the literature to occur in Fe^{2+} around 50 GPa. Up to now, however, elastic wave velocities of iron-bearing carbonates have only been measured at ambient conditions. To address this problem, we undertook a diamond anvil cell study of iron-bearing carbonates (starting with high-pressure measurements of $FeCO_3$) on the nuclear resonance beamline (ID18) at the European Synchrotron Radiation Facility in Grenoble, France. Elastic wave velocities were derived from nuclear inelastic scattering data, and preliminary results show a substantial increase in shear wave velocity through the spin transition. We will present our latest results and discuss implications for the detectability of carbonate in the deep Earth.

High-pressure single-crystal X-ray synchrotron diffraction of kainite and pentahydrite

Nazzareni S[1*], Comodi P[2], Hanfland M[3]

1 - University of Perugia *sabrina.nazzareni@unipg.it 2 - Dipartimento di Fisica e Geologia, Università di Perugia, Italy 3 - ESRF

Sulphates are typical minerals in evaporitic environments and many terms of this family present a variable degree of hydration or enclose halogen (i.e. Cl). Often these hydrated sulphates have both OH groups and water molecules in their structures and thus they are intriguing to study the hydrogen bonds behaviour in minerals.

Kainite ($KMg(SO_4)$ Cl $3H_2O$) is monoclinic (sp. gr. *C*2/*m*), its structure is characterised by Mg- and K-octahedra and S-tetrahedra to form sheets that are linked together by Mg(3) octahedra, producing a perfect {100} cleavage. Nevertheless the sheet-like structure is only apparent. Chlorine are linked to K1 and K2 in 8-fold coordination and to K3 in 9-fold coordination.

Pentahydrite ($Mg(SO_4)$ $5H_2O$) is triclinic (sp. gr. *P*-1), its structure is characterised by Mg-octahedra and S-tetrahedra to form $Mg(OH_2)_4SO_4$ chains extending parallel to [110]. The chains are connected to each other by hydrogen bonds, formed by the water oxygen atoms in the chain and by the fifth water molecule, which is not coordinated to a Mg atom.

We studied the H*P* behaviour of kainite and pentahydrite by high-pressure single-crystal X-ray synchrotron diffraction. Crystals were loaded in DAC with ruby chips as pressure calibrant, and He as pressure transmitting media. The experiments were performed at ID09 (ESRF, Grenoble) up to 12 GPa.

Kainite remains stable up to 12GPa without phase transitions. Fitting the *P*-volume data by a 2nd-order Birch-Murnaghan EoS the bulk modulus is K_0=31.8(3) GPa V0=3045(4)$Å^{-3}$. The lattice parameters fitted by a BM2-EoS yield to: K_{0a}=38(5)GPa, a_0=19.731(4)Å; K_{0b}=38(1)GPa, b_0=16.217(3)Å, K_{0c}=23.3(2)GPa, c_0=9.532(2)Å. The axial compressibility is $ß_a$= -8.8 10^{-3}GPa, $ß_b$= -8.8 10^{-3}GPa and $ß_c$= -14.1 10^{-3}GPa, with a lattice anisotropy of $ß_{0a}$:$ß_{0b}$:$ß_{0c}$ =1:1:1.6.

Structure refinements showed a strong compression of the K1 and K3 polyhedra with a decrease in bond distances of 13% for K1-Cl2, 10% for K1-Cl1, 9% for K3-Ow6 and K3-O8B. S-tetrahedra are almost incompressible and the Mg-octahedra M1, M2 and M4 have similar behaviour decreasing of 2-4% the bond distances. Mg3-O7 and Mg3-Ow6 bond distances decrease of the same amount whereas Mg3-Ow3 is unchanged. Mg3-octahedron links together the T-O sheets with the Mg3-Ow3 bond pointing toward the cavity where K2 is located. The complex structural configuration explains the axial compressibility anisotropy.

Pentahydrite preliminary results show a structural stability up to 12GPa but a change in the compressional style at 5GPa with a discontinuity in the lattice parameters: lattice *c* and ß angle strongly decrease and alpha angle increases.

Fitting the *P*-volume data up to 5GPa with a 2nd-order Birch-Murnaghan EoS the bulk modulus is K_0=32.6(1)GPa V0=365.3(8)$Å^{-3}$. The 0-5 GPa lattice parameters fitted by a BM2 EoS yield to: K_{0a}=39(4)GPa, a_0=6.275(2)Å; K_{0b} =21(1)GPa, b_0=10.547(3)Å, K_{0c}=26(2)GPa, c_0=6.080(5)Å. The axial compressibility is $ß_a$= -8.5 10^{-3}GPa, $ß_b$= -15.8 10^{-3}GPa and $ß_c$= -12.8 10^{-3}GPa, with a lattice anisotropy of $ß_{0a}$:$ß_{0b}$:$ß_{0c}$ = 0.54:1:0.81.

Compressibility of carbonophosphate bradleyite $Na_3Mg(CO_3)(PO_4)$ by X-ray diffraction and Raman spectroscopy

Qin S[1*], Gao J[1], Huang W[2], Wu X[1], Fan D[3], Wu Z[2], Xia D[1]

1 - Peking University *sqin@pku.edu.cn 2 - University of Science and Technology of China 3 - Institute of Geochemistry, Chinese Academy of Sciences

Bradleyite $Na_3Mg(CO_3)(PO_4)$ is one typical carbonophosphate, representing dual properties of both carbonates and phosphates. Compressibility of bradleyite has been investigated using synchrotron radiation X-ray diffraction and Raman spectroscopy combined with diamond anvil cells up to 41 GPa at room temperature. Experimental results clearly demonstrate that bradleyite is stable in the investigated pressure conditions. Isothermal pressure-volume relationship has been fitted to the third-order Birch-Murnaghan equation of state with B_0=65.9(9) GPa, B_0'=3.08(3) and V_0=301.4(4) Å^3. All axes exhibit considerable compressibility but an unexpected stiffness of *b-axis* occurs at ~16 GPa. Insight into the behaviors of $[PO_4]^{3-}$ and $[CO_3]^{2-}$ groups has been obtained using Raman spectroscopy, with the symmetrical stretching bands being observed at 970.8 cm^{-1} and 1078.7 cm^{-1}, respectively. Both modes shift to higher frequencies on compression. The pressure coefficient of Raman shifts in C-O is $3.18(2)\times10^{-3}$ cm^{-1}/GPa, and the value of Grüneisen parameters (g) is ~0.22. $[PO_4]^{3-}$ groups in bradleyite exhibit a mode hardening, with a slope of $3.54(6)\times10^{-3}$ cm^{-1}/GPa, g=~0.24 below ~16 GPa, and of $2.37(1)\times10^{-3}$ cm^{-1}/GPa, g=~0.16 thereafter. These low g values are compatible with the rigidness of $[CO_3]^{2-}$ and $[PO_4]^{3-}$ in bradleyite, which have respectively been documented in carbonates and phosphates. Our present study may open new perspectives on carbonophosphate minerals, and shed light on other $[CO_3]^{2-}$ and $[PO_4]^{3-}$ coexistent phases.

Texture and strain analyses of polycrystalline materials using two-dimensional X-ray diffraction patterns under DAC experiments

Seto Y[1*], Nishihara Y[2], Tsujino N[3]

1 - Sci., Kobe University, Japan *seto@crystal.kobe-u.ac.jp 2 - GRC, Ehime University, Japan 3 - ISEI, Okayama University, Japan

Angle dispersive X-ray diffraction experiments using area detectors (CCD and CMOS cameras and image-plate recorders) give us wide opportunity for the determination of lattice preferred orientation (LPO) and lattice strain under stress condition of polycrystalline materials. LPO is reflected in circumferential oscillations along Debye rings, while the effect of lattice strain appears in elliptic distortions of the each ring and/or a deviation of the original crystallographic geometry among rings. These are substantial factors of bulk physical properties in polycrystalline materials, including seismic velocity, thermal/electric conductivity and so on. Diamond anvil cell (DAC) is the only technique that can create extreme pressures corresponding to the Earth's core, and it simultaneously involves non-hydrostatic, uniaxial stress for samples. Although such non-hydrostatic effects under DAC experiments have been reported in many previous studies, in many cases, the quantitative treatments have not yet been developed into a standard technique.

In order to examine quantitative LPO and stress conditions under DAC experiments, high pressure experiments were carried out in a symmetrical DAC in the present study. Two stating materials, Al_2O_3 (~1μm in diameter) and MgO (<0.1 μm), were used as stating materials, and no pressure media were loaded. Each runs were performed at the pressures from 0 GPa to 70 GPa by 10 GPa step under room temperatures, and synchrotron X-ray diffraction patterns were collected using a flat imag-plate at BL10XU at SPring-8. A software code was also developed by the author, which simulates a two-dimensional diffraction pattern based on given experimental parameters and (poly)crystalline properties. A fitting procedure was also incorporated into the code, where the orientation distribution and stress condition were iteratively modified according to a residual value of the simulated/observed patterns.

In runs of Al_2O_3 experiments, the diffraction peaks became distinctly broad and asymmetric shapes with increasing pressures, whereas the scattering angles (2θ) were apparently almost constant. This means that lattice compression involved by pressures was cancelled out by deviatoric stress. Nonetheless, the stress conditions could be derived mainly from the shapes of the peaks using the fitting procedure; e.g. at the highest pressure condition in the present study, maximum and minimum principal stresses could be estimated as 73GPa (parallel to compression axis) and 25 GPa, respectively, corresponding to the deviatoric stress of 50 GPa. The maximum principal stress was consistent with the estimated pressure by the diamond Raman pressure scale. On the other hand, MgO experiments maintained pseudo-hydrostatic conditions with small deviatoric stress only up to ~1GPa under all performed pressures. A whole pattern fitting method such as the code developed in the present study may help us understand the stress conditions under DAC experiments.

Applications of the Density Functional Theory in the study of the interior of the Earth

Caracas R

CNRS. razvan.caracas@ens-lyon.fr

The thermodynamic conditions ranging in the big planetary bodies, like Earth and beyond, quickly exceed the current limits attainable in experiments. Here we focus on some of the most recent exciting applications of first-principles calculations based on density-functional theory and density-functional perturbation theory to the study the major minerals building the telluric and icy planets.

We overview advances in the phase diagram of perovskite: the lattice instabilities, the magnetic spin transition, the partitioning of Al and Fe, the occurrence of post-perovskite, and the influence of these factors on the physical properties relevant to Earth sciences. We show how modeling the electrical conductivity of solid iron allows us to better understand the thermal history of our planet and the core evolution. We finish with a discussion of the chemical composition of the core in view of recent first-principles calculations.

Disclinations and grain boundary migration: evidence for a new deformation mechanism in olivine-rich rocks

Cordier P[1*], Demouchy S[2], Beausir B[3], Taupin V[3], Fressengeas C[3]

1 - University of Lille *patrick.cordier@univ-lille1.fr 2 - Geosciences Montpellier

3 - LE3M, Université de Lorraine

The rheology of olivine-rich rocks remains poorly constrained. In particular, the ability of orthorhombic olivine to bear large strains represents an apparent violation of the von Mises criterion due to a lack of slip systems.

In this study we show that a more general description of the deformation process including the motion of rotational defects referred to as disclinations can solve the olivine deformation paradox. Disclinations were proposed together with dislocations by [1] to account for elastic distorsions (distorzione) in solids. They have recently been evidenced in several deformed metallic alloys [2].

Using high-resolution EBSD maps we show that disclinations decorate grain boundaries in olivine samples deformed experimentally and in nature. We present a disclination-based model of a high-angle tilt boundary in olivine, which demonstrates that an applied shear induces grain boundary migration through disclination motion. This new approach allows further understanding of grain boundary-mediated plasticity in polycrystalline aggregates. By providing the missing mechanism for describing plastic flow in olivine, the present work allows multiscale modelling of the rheology of the upper mantle, from the atomic scale to the scale of the flow.

[1] Volterra V. (1907). Sur l'équilibre des corps élastiques multiplement connexes. Annales Scientifiques de l'École Normale Supérieure 24, 401-517.

[2] Beausir B. and Fressengeas C. (2013). Disclination densities from EBSD orientation mapping. *International Journal of Solids and Structures* 50 (1), 137-146.

First principles simulations of grain boundaries in mantle minerals at high pressure

Karki B*

Louisiana State University. *karki@csc.lsu.edu

Grain boundaries (GBs) are known to dramatically influence many physical properties of a material as they can serve as effective sinks for point defects including impurities and as nucleation sites. In recent years, we have simulated tilt grain boundaries in mantle minerals within density functional theory. Our first principles simulations of GBs in periclase and forsterite suggest that the interfacial regions separating the component crystal grains contain structural distortions (distorted bonds, over/under coordinated atoms), and void spaces (~10^{-10} m^3/m^2). Also, the interface induces splitting of electronic states from the conduction band and kinks at the top of the valence band. The simulated S5{310}/[001] (symmetric) tilt grain boundary in MgO stable at the zero pressure can be viewed as a series of dislocation pipes forming a well-defined channel structure. Such open structure is less pronounced and becomes denser in the asymmetric tilt GBs stable at 50 and 100 GPa. Simulations of different types of tilt grain boundaries, (0*l*1)/[100], (1*l*0)/[001] and (012)/[100] modeled with stepped and non-stepped surfaces in forsterite suggest that several configurations arising from Mg terminated planes with tilt angles ranging from 16° - 67° are energetically competitive at pressures up to 17 GPa.

We have also demonstrated high defect activity of MgO grain boundaries at all pressures. Like native defects, three types of impurities Ca, Al, and proton favorably segregate to the boundary, with the segregation considerably increasing with pressure. Also, the grain boundary diffusion is much easier, and more anisotropic and complex than bulk diffusion; the calculated migration enthalpies being as low as ~1.5 eV at 100 GPa compared to the bulk values of ~ 4 eV. Grain boundaries as predicted here are likely to serve as sinks and provide rapid diffusion pathways for point defects in MgO are thus crucial to mantle rheology and geo-chemical distribution.

Carbon isotope fractionation between diamond and iron carbide: experimental data and geochemical significance

Reutsky V*, Borzdov Y

V.S.Sobolev Institute of geology and mineralogy SB RAS *reutsky@igm.nsc.ru

Isotope fractionation of carbon among mantle minerals becomes popular for theoretical and experimental investigation during last decade. In particular, calculations of carbon isotope fractionation between iron carbide and diamond predict about 10‰ equilibrium fractionation at 1000°C [1]. A possibility of this scale carbon isotope fractionation at mantle temperatures can have significant impact for our vision and understanding of deep carbon cycle and carbon cosmochemistry.

We have experimentally investigating distribution of carbon isotopes during Fe-C melt crystallization at 6.3GPa and 1600-1400°C. In these experiments Fe_3C always show $d^{13}C$ values 2‰ higher in comparison with quenched Fe-C melt. Carbon isotope analysis was done using sampes taken directly from Fe_3C/Melt interface. When carbon abundance in iron is higher than 5.7%, a diamond was crystallized first from the Fe-C melt. $D^{13}C_{Dm\text{-}Melt}$ value for this PT-condition is known to be 4.5‰ [2]. At temperatures corresponding to crystallization of Fe_3C, diamond dissolves and returns heavy carbon isotope back to the melt. When crystallization of diamond follows by crystallization of iron carbide within peritectic region, calculation of mean $D^{13}C_{Dm\text{-}Fe3C}$ value in all experiments return 5.0+/-0.1‰.

It is known from phase diagram of Fe-C system [3] that diamond and Fe_3C are mutually exclusive in equilibrium with liquid at high temperatures. This is confirmed in our experiments. Our carbon isotope data have few important consequences. First, diamond crystallization in carbon-rich Fe-C melts leads to significant depletion of the melt by heavy carbon isotope. Considering natural systems, this process is equal to magma degasing at shallower depth and can provide localization of isotopically contrast pools of carbon in the mantle. Second, the fact that crystalline Fe_3C is isotopically-heavier than Fe-C melt means that crystallized from the same Fe-C melt a diamond and a Fe_3C never can be in isotope equilibrium. If equilibrium carbon isotope fractionation between diamond and Fe_3C equal to 10‰ and between diamond and Fe-C melt equal to 4.5‰, value of $D_{Fe3C\text{-}Melt}$ must be equal to -5.5‰. It means Fe_3C must be isotopically-lighter than the Fe-C melt ($D_{Dm\text{-}Fe3C}=D_{Dm\text{-}Melt}-D_{Fe3C\text{-}Melt}$). Accounting carbon isotope diffusion rates in diamond even at mantle temperatures [4], diffusion-controled isotope equilibration of macro-quantities of Fe_3C and diamond takes time exceeding of the Earth's age.

Acknowledgements: This work is supported by Russian foundation of basic research grant number 12-05-00846a.

[1] Schauble E.A. (2009). Equilibrium carbon and hydrogen isotope fractionation in iron. EOS, Transaction AGU, Fall Meeting 90, V11C-1967.

[2] Reutsky V.N., Borzdov Yu.M., Palyanov Yu.N. (2012). Effect of diamond growth rate on carbon isotope fractionation in Fe-Ni-C system. *Diam. Relat. Mater*. 21, 7-10.

[3] Lord O.T., Walter M.J., Dasgupta R., Walker D. and Clark S.M. (2009). Melting in the Fe-C system to 70 GPa. *EPSL*, 284, 157-167.

[4] Koga K.T., Van Orman J.A. and Walter M.J. (2003). Diffusive relaxation of carbon and nitrogen isotope heterogeneity in diamond: a new thermochronometer. *PEPI*, 139, 35-43.

Thermal property modeling of the core-mantle boundary

Tsuchiya T*, Dekura H

Ehime University *tsuchiya.taku.mg@ehime-u.ac.jp

Lattice thermal conductivity of minerals under pressure and temperature is a key property to understanding dynamics and evolution of the Earth's interior. We recently established an efficient ab initio technique for calculating the thermal conductivity of silicate minerals with complex structure and chemistry (Dekura, Tsuchiya, Tsuchiya, PRL, 2013). Calculated lattice thermal conductivity of MgSiO3 perovskite agreed satisfactorily with experimental values at room temperature, and post-perovskite was found to have thermal conductivity quite different from perovskite's, indicating that the D" discontinuity is not only the phase transition boundary but also the conductivity boundary. Using the obtained results, we determine the effective conductivity of the lower mantle and estimate the energy flow across the core-mantle boundary (CMB). Our results demonstrate that the CMB heat flux could change significantly from place to place by reflecting temperature heterogeneity located atop the core. A large CMB heat flow recently suggested from the outer core side can be reconciled only by considering polycrystalline assemblages yielding high-thermal conductivity.

First principles investigation of the stability of phase H in the lower mantle

Tsuchiya J*, Tsuchiya T

Geodynamics Research Center, Ehime University *junt@sci.ehime-u.ac.jp

The global circulation of water in the earth is important to investigate the evolution history and dynamics of the earth. It has been known that water is carried into the deep Earth's interior by hydrous minerals such as the dense hydrous magnesium silicates (DHMSs) in the descending cold plate. Recently, we have theoretically predicted the existence of new DHMS at the lower mantle pressure conditions by first principles calculation. This is experimentally confirmed and named as phase H. This phase has $MgSiO_4H_2$ chemical composition and is the highest pressure phase among known DHMSs so far. Here we discuss the effect of impurities such as aluminum on the stability of phase H in the lower mantle conditions.

High pressure study of dolomite and phase transition to dolomite II

Zucchini A[1], Belmonte D[2], Prencipe M[3], Comodi P[1*]

1 - Dipartimento di Fisica e Geologia, Università di Perugia, Italy. *paola.comodi@unipg.it 2 - DISTAV, University of Genoa, Italy. DISTAV, University of Genoa, Italy 3 - Dipartimento di Scienze della Terra, Università di Torino, Italy.

Dolomite and other carbonates have been claimed as possible carbon carrier minerals into the deep upper mantle.

Dolomite is a double carbonate with R-3 symmetry. The layered structure consists of alternated calcium and magnesium octahedral sites separated by nearly planar and parallel carbonate groups. At high-pressure (HP) dolomite has been observed to undergo phase transitions to dolomiteII (~17GPa) and dolomiteIII (~35GPa) polymorphs [1].

The behaviour of pure stoichiometric dolomite up to lower mantle conditions was studied by means of first principle calculations. CRYSTAL09 program [2] was used at the hybrid Hartree-Fock/Density Functional Theory level [3, 4]. The WC1LYP Hamiltonian, which includes a non local exact Hartree-Fock exchange contribution, was chosen.

Compressibility of dolomite was analysed together with crystal structure evolution with P in order to understand how dolomite approaches the phase transitions. Ordered and disordered geometries [5] were optimized at different pressures up to approximately 26GPa. Results do not account for any discontinuity on the P-V path. On the contrary, discontinuities on the compressional behaviour of cation polyhedra are observed. The regularity of Ca and Mg polyhedra increases with P as it can be seen from O-Ca-O and O-Mg-O angles which tend to 90°. As regards the ordered dolomite, 90° is the angle limit reached at approximately 13GPa. A further increase of P reflects in a loose of regularity, that is, O-Ca-O and O-Mg-O angles move back to the starting values. Therefore, ordered dolomite seems to approach the phase transition to dolomiteII at lower pressure than Fe-dolomite [1] by an increase in polyhedra regularity [6]. As regards the disordered dolomite, no discontinuities are observed in the compressional behaviour of polyhedra. After reaching 90°, angles keep on to spread out from their starting value. That is, disordered dolomite does not seem to undergo phase transition in the analysed P range. Compressibility analysis of ordered and disordered dolomite was performed up to approximately 13 GPa and gives K_0 = 88.4(8) GPa and K' = 5.5(2) for ordered dolomite and K_0 = 87.5(7) GPa and K' = 5.3(2) for disordered dolomite.

DolomiteII crystal structure was optimized in the P-1 space group at approximately 35GPa and the increase in the coordination number of Ca atoms from 6 to 8 [1] is confirmed. Calculations on the thermodynamic behaviour of dolomite I (oredered and disordered) and dolomiteII are still running to get new insights into their relative P-T stability and phase relations.

[1] Merlini M. *et al*. (2012). *PNAS*, 109, 34, 13509-13514.

[2] Dovesi R. *et al*. (2005). *Z. Kristallogr.*, 220, 571-573.

[3] Hohenberg P. and Kohn W. (1964). *Phys. Rev. B: Condens. Matter*, 136, 864-871.

[4] Kohn W. and Sham L.J. (1965). *Phys. Rev. A: At. Mol. Opt. Phys*., 140, 1133-1138.

[5] Zucchini A. *et al*. (2012). *Calphad*, 38, 177-184.

[6] Zucchini A. *et al*. (2014). submitted to *Phys Chem Miner*.

Reassessment of the importance of Ti for the incorporation of H into mantle olivine

Gaetani G[1*], O'Leary J[1], Koga K[2], Hauri E[3], Rose-Koga E[2], Monteleone B[1]

1 - Woods Hole Oceanographic Institution *ggaetani@whoi.edu 2 - Université Blaise Pascal 3 - Carnegie Institution for Science

Olivine comprises ~70% of the mode of typical fertile peridotite and is known to incorporate substantial amounts of H at upper mantle conditions. Incorporation of H into olivine is known to be influenced by a number of thermodynamic variables, including pressure, SiO_2 activity, olivine composition and the fugacities of H_2O and O_2, but their relative importance remains a matter of debate. Berry *et al.* (2005) concluded, on the basis of Fourier transform infrared (FTIR) spectra from experimentally crystallized forsterite, that OH^- stretching bands at 3572 and 3525 cm^{-1} reflect H incorporated as Ti-clinohumite-like defects, and that this is the most important mechanism for H incorporation into olivine in the shallow upper mantle. Results from new hydration experiments show no correlation between the concentrations of Ti and H in olivine, and in all but one of our experimentally hydrated olivines the concentration of Ti is too low for H to be incorporated dominantly as a Ti-clinohumite-like defect. Intense absorption bands at 3572 and 3525 cm^{-1} in our experimentally hydrated olivines correlate with the fugacity of H_2O, while the peak at 3525 cm^{-1} is also weakly influenced by the fugacity of O_2.

Fifteen hydration experiments were conducted at 1 to 2 GPa and 1200 ºC, using a piston-cylinder device, to determine the solubility of H in San Carlos olivine as a function of pressure, SiO_2 activity, olivine composition and the fugacities of H_2O and O_2. The fugacity of O_2 was controlled at the Fe-FeO, FeO-Fe_3O_4 or Ni-NiO buffer. The influences of pressure and H_2O fugacity were resolved using mixed H_2O-CO_2 experiments. Variable duration experiments indicate that equilibration is achieved within 6 h. Hydrogen contents of the experimental products were measured by secondary ion mass spectrometry, and relative changes to the point defect populations were investigated using FTIR.

Results from our experiments demonstrate that H solubility in San Carlos olivine is sensitive to pressure, the activity of SiO_2, and the fugacities of H_2O and O_2. Of these variables, the fugacity of H_2O has the strongest influence. The solubility of H in olivine increases with increasing SiO_2 activity, indicating incorporation in vacancies on octahedral lattice sites. The forsterite content of the olivine has no discernible effect on hydroxyl solubility between 88.17 and 91.41 Our experimentally hydrated olivines are characterized by strong infrared absorption peaks at wavenumbers of 3330, 3356, 3525, and 3572 cm^{-1}. The heights of peaks at 3330 and 3356 cm^{-1} correlate positively with O_2 fugacity, while those at 3525 and 3572 cm^{-1} correlate with H_2O fugacity.

Our data show that the concentration of Ti in our experimentally hydrated olivine is too low to account for the majority of the structurally bound H. Our FTIR spectra place additional constraints on the importance of Ti for H incorporation into olivine by allowing us to look specifically at H associated with Group I absorption bands. There is a weak positive correlation (r^2 = 0.3578) between the concentrations of Ti and H associated with the Group I bands of Bai and Kohlstedt (1993), but our data indicate that only 3 out of the 4 experiments analyzed by FTIR have Ti concentrations high enough for the H to be incorporated in the form of a Ti-clinohumite-like defect. If it is assumed that the absorption coefficient does not vary as a function of wavenumber, on average less than ~50% of the total H in these olivine is associated with Group I bands. Therefore, while some H may be incorporated into olivine in association with Ti, this does not appear to be the dominant mechanism.

Effect of water activity on reaction kinetics and intergranular transport at high-pressure: insight from the $Ca(OH)_2 + MgCO_3 \rightarrow CaCO_3 + Mg(OH)_2$ reaction

Gasc J[1], Brunet F[2*], Brantut N[3]

1 - CARS, University of Chicago, Argonne, USA 2 - ISTERRE, CNRS, Univ. Grenoble, France *fabrice.brunet@ujf-grenoble.fr 3 - Earth Sciences Department, University College London, UK

The kinetics of metamorphic reactions is strongly dependent on temperature, grain size and water availability. The latter parameter is probably the most difficult to quantify, especially in the course of a whole metamorphic cycle. Beyond the notion of water availability which describes the intermittent presence of water in the course of the metamorphic reaction process, the effect of water content on the kinetics of the reaction process is another issue. In fact, among the large experimental dataset of mineral reaction kinetics available in the literature (phase relationship, dissolution, etc …), most of experiments were performed under hydrothermal conditions, with large water/rock ratios. Consequently, when extrapolated to nature, assuming full water availability, this type of experimental data predicts that metamorphic reaction rates are fast and, that the preservation of metastable mineral assemblages (reaction overstepping) is short upon metamorphism timescales. Here, we propose to address the effect of water content on the intergranular transport in the course of the $Ca(OH)_2 + MgCO_3 \rightarrow CaCO_3 + Mg(OH)_2$ reaction at 1.8 GPa. The reaction kinetics was investigated at two different scales; bulk reaction progress was derived by in-situ synchrotron diffraction data on powders and, in addition, growth rate of $CaCO_3 + Mg(OH)_2$ rim around coarse magnetite grains was determined using SEM data on the corresponding quenched samples. Basically, three levels of hydration were achieved: water saturated, intermediate (grain boundary water only) and dry, *i.e.*, water fugacity was buffered by the $CaO + H_2O = Ca(OH)_2$ reaction. Both reaction and rim growth kinetics showed a strong positive dependency with water content. At the microscopic scale, Ca and CO_2 were found to be the diffusing (i.e., mobile) species. Between dry and intermediate hydration conditions, two different grain-boundary diffusion regimes were clearly identified with contrasted activation energies which decrease with increasing hydration level. Variations of less than 1 wt.% in water content have a tremendous effect on reaction kinetics (and GB diffusion coefficients), by several orders of magnitude. This confirms for Ca-bearing systems, the prominent role of water on chemical transport properties, comparable in magnitude to that of temperature. Considering previous work on Al [1] and Mg [2] grain boundary diffusion, it seems that a general scheme arises with a set of diffusivity regimes controlled by water content. The question whether, depending on the mineral system, there is a continuum between these diffusivity regimes or whether they are discrete mechanisms remains an open question.

[1] Carlson W. (2010). *J. Metamorphic. Geol*., 28, 735-752.

[2] Gardés E., Wunder B., Marquardt K. and Heinrich W. (2012). *Contrib. Mineral. Petrol*, 164, 1-16.

Water contents of Roberts Victor eclogites: primary *vs.* metasomatic controls

Huang J[1*], Griffin W[1], Xia Q[2], Li P[2], Greau Y[1], Pearson N[1], O'Reilly S[1]

1 - CCFS/GEMOC, Macquarie University *jinxiang.huang@mq.edu.au
2 - University of Science and Technology of China

The water content of the mantle affects many of Earth's properties and geological processes. Water contents are well studied in mantle peridotites, but not in xenolithic eclogites, a minor but important component of the subcontinental lithospheric mantle (SCLM). This information can constrain the formation and evolution of the SCLM.

A suite of eclogites from the Roberts Victor kimberlite has been extensively studied in terms of petrology and geochemical compositions. They were originally classified into Type I and Type II on the basis of mineral compositions and microstructures. It is now documented [1] that Type II (IIA and IIB) eclogites were heavily metasomatized by carbonatitic-kimberlitic melts/fluids to form Type IA and IB eclogites.

The water content of eclogitic garnet and omphacite (omp) was analysed by Fourier transform infrared spectrometry. Garnet does not contain measureable OH in any sample. The water content of Type IA, IB, IIA and IIB omp ranges from 211-1337 (mean 623), 416-1001 (mean 689), 342-764 (mean 491) and 675-1496 (mean 1073) ppm respectively.

The OH content of the omp was not disturbed by interaction with the host magma. No amphibole contributes to the OH measurement in omphacite. Some sheet silicates (e.g. clinochlore and amesite) may affect one small OH band of omphacite; even if they do, the results do not change significantly.

The crystal chemistry and structure of omp, and principally the vacancies on the M2 site, control the OH content of Type I eclogites. The OH content of Type II samples might be sensitive to the primary equilibrium temperature/pressure and local fugacities of H_2O, and O_2.

Metasomatism has reset the water content of the xenolithic eclogites; the calculated water content in the metasomatic melts/fluids is similar to that of the carbonatitic-kimberlitic melts/fluids. Type IIA and IIB may have different origins and/or have been affected by different secondary processes. Eclogites are an important water reservoir in the lithospheric mantle as the omphacite contains more water than do the pyroxenes in peridotites (typically 40-400 ppm).

[1] Huang J.-X., Greau Y. and Griffin W.L. (2012). Multi-stage origin of Roberts Victor eclogites: progressive metasomatism and its isotopic effects. *Lithos* 71(2-4), 337-351.

Identification of hydrogen defects linked to boron substitution in forsterite and olivine

Ingrin J[1*], Kovacs I[2], Deloule E[3], Balan E[4], Kohn S[5], Hermann J[6]

1 - University Lille1 *jannick.ingrin@univ-lille1.fr 2 - GGIH 3 - CRPG-CNRS, BP20, 54501 Vandoeuvre les Nancy, France 4 - IMPMC, UMR CNRS 7590, UMR IRD 206, Université Paris VI 5 - Department of Earth Sciences, University of Bristol, Queens Rd. 6 - Research School of Earth Sciences, ANU

Occurrence of a OH broad band at 3600 cm^{-1} in synthetic zoned forsterite [1] is correlated to the presence of bands at 1301, 1256, 1207 and 1170 cm^{-1} in the range of the B-O_x vibrations. Boron concentration in the forsterite crystal measured by ion probe matches the zoning of the 3600 cm^{-1} OH band within the crystal; it confirms that the hydrogen defect is linked to the substitution of Si by B. This is the first evidence of H defect coupled with B in forsterite.

A careful look at the infrared spectra of natural Pakistan olivine shows that the OH bands at 3597 and 3579 cm^{-1} are due to the same type of defect with respective B-O vibrations at 1299, 1254, 1205 and 1167 cm^{-1}. It is now possible to recognize OH bands linked to boron substitution in natural and synthetic samples and isolate their specific contribution. It is an important step toward a complete identification of H-defects in olivine. Accidentally, the occurrence of the $B(OH)Si_{-1}O_{-1}$ substitution in some synthetic forsterites is very probably linked to unwanted diffusion of boron from pieces of the high-pressure assemblages (BN, pyrex glass).

[1] Ingrin *et al*. (2013). *Phys. Chem. Minerals*, 40, 499-510.

Al incorporation in dense hydrous magnesium silicates

Inoue T[1*], Hayashi K[1], Yurimoto H[2]

1 - Ehime University *inoue@sci.ehime-u.ac.jp 2 - Hokkaido University

Subducting slabs are supplying water into the deep mantle, and some hydrous minerals may be present in the mantle transition zone and even in the uppermost lower mantle. The water storage capacities of mantle minerals are supposed to be significantly coupled with Al by a substitution with Mg^{2+}, Si^{4+} or Mg^{2+} + Si^{4+}, because Al^{3+} is the trivalent cation, and H^{+} is the monovalent cation. So in this study, we have examined the effect of Al for the water content and the stability of some hydrous phases in the system MgO - Al_2O_3 - SiO_2 - H_2O in the mantle transition zone and the uppermost lower mantle conditions. The experiments were conducted at 20 - 25 GPa and 1873 - 2273 K by MA8-type (KAWAI-type) high pressure apparatus. We succeeded to synthesize Al-bearing dense hydrous magnesium silicates (Al-bearing phase D, Al-bearing phase B, Al-bearing superhydrous phase B, Mg-Si bearing δ-AlOOH etc.), and found that the significant coupling of H and Al were occurred in these minerals. The chemical compositions and the lattice parameters are examined by SEM-EDS, SIMS and microfocus-XRD, and discussed about the difference between the pure chemical forms. Still more, the substitution mechanisms were considered basically by the chemical compositions and the information of the crystal structures. Our study strongly suggests that water can be stored in the mantle transition zone and the uppermost lower mantle in the form of Al-bearing hydrous minerals or nominally anhydrous minerals.

A review on the incorporation of "water" in the lithosphere beneath the Carpathian-Pannonian region: geodynamic and geophysical implications in a young extensional basin

Kovacs I[1*], Falus G[1], Szabó C[2], Pintér Z[3], Liptai N[2], Patkó L[2], Fancsik T[1], Mihály J[4], Németh C[4], Sándorné Kovács J[5]

1 - GGIH *kovacs.istvan.janos@mfgi.hu 2 Eötvös University 3 - Bayeriches Geoinstitut 4 - Hungarian Academy of Sciences 5 - Hungarian Institute for Forensic Sciences

The Carpathian-Pannonian region (CPR) is a Miocene extensional basin surrounded by the Alps, Carpathians and the Dinarides. The lithosphere beneath the region was sampled by alkaline basalts following the extension. Xenoliths entrained in alkaline basalts are direct samples of the lithosphere which was presumably subject to deformation, melt extraction and/or metasomatism during the Miocene extension. Thus, the CPR offers a unique natural laboratory to investigate the effect of extension on the "water" incorporation into the mantle lithosphere.

"Water" content of NAMs (olivine, pyroxenes) in more than 50 mantle xenoliths representing three different sectors of the CPR will be reported. Xenoliths from the "central" part originate from a very thin mantle lithosphere suffering considerable degree of extension during the Miocene. Another locality is in a "transitional" setting where the thickness of the mantle lithosphere changes rapidly under the volcanic field. The third area is in the immediate vicinity of the subduction along the East Carpathians providing xenoliths from a "supra subduction" setting which, in addition, was only indirectly affected by the Miocene extension.

In general the "water" content of NAMs appears to indicate near equilibrium conditions in the CPR, which is reflected in that the "water" content of coexisting pyroxenes changes mostly proportionally in each locality. In the "central" and "transitional" settings, however, the clinopyroxene/orthopyroxene partitioning ratio is usually near or higher than 3, whereas it is ~ 2 in the "supra subduction" setting. The "water" content varies considerably within each locality, nevertheless, there is marginally more water in NAMs of the "supra subduction" setting. In general xenoliths from the "transitional" setting have the lowest concentration of "water" in NAMs. The central area shows the most considerable variation in "water" contents. In addition, "water" contents in NAMs sometimes seem to show various degree of correlation with texture, chemistry and deformation patterns of xenoliths within each locality.

We will demonstrate how the changing concentration of "water" in NAMs from the different settings of the CPR may contribute to: 1) our understanding on the geodynamics of the CPR and 2) improvement on the interpretations of geophysical soundings (i.e. magnetotellurics, seismology).

A new water reservoir, hydrous phase H and phase delta solid solution $MgSiO_2(OH)_2$-AlOOH in the lower mantle

Ohtani E[1*], Amaike Y[1], Ohira I[1], Kamada S[1], Sakamaki T[1], Hirao N[2]

1 - Tohoku University *ohtani@mail.tains.tohoku.ac.jp 2 - JASRI

Several hydrous minerals such as phase D and superhydrous phase B have been reported to be stable up to the top of the lower mantle. It has been reported that hydrous phase delta (AlOOH) is formed as a breakdown product of phase Egg, $AlSiO_3(OH)$, and is stable up to the bottom of the lower mantle. Tsuchiya (2013) predicted that phase H, ($MgSiO_2(OH)_2$), which is the same structure as phase delta (AlOOH), is stable in a pressure range from 45 GPa to 55 GPa based on the ab-initio calculation. This phase was experimentally confirmed at around 50 GPa by Nishi *et al*. in 2014. Here, we present our recent results on synthesis experiments of hydrous phase H and a solid solution of phase H and phase delta up to the base of the lower mantle along the normal mantle geotherm. The high pressure and temperature in situ X-ray diffraction experiments were performed by using a double-sided laser heated diamond anvil cell at BL10XU, SPring-8. We observed that the stability field of this new hydrous phase H in the MgO-SiO_2-H_2O system expands at least up to 75 GPa and 2000 K, although the previous studies by Tsuchiya (2013) claimed that phase H is broken down at pressures above 55 GPa. Thus, hydrous phase H is a host phase of water in the lower mantle at least up to the depth of 2000 km along both slab and normal mantle geotherms. Our experiments also revealed that the solid solution of phase H and phase delta, AlOOH-$MgSiO_2(OH)_2$, containing 15 mol % of $MgSiO_2(OH)_2$ can coexist with Mg-perovskite and Mg-post perovskite up to 135 GPa and 2000 K. Thus, phase H-phase delta solid solution can be an important water reservoir at the bottom of the lower mantle.

A hydrous mantle transition zone indicated by ringwoodite included within diamond

Pearson G[1]*, Brenker F[2], Nestola F[3], McNeill J[4], Nasdala L[5], Hutchison M[6], Matveev S[7], Mather K[4], Silversmit G[8], Schmitz S[2], Vekemans B[8], Vincze L[8]

1 - University of Alberta *gdpearso@ualberta.ca 2 - Goethe University, Frankfurt, Germany 3 - University of Padua, Italy 4 - University of Durham, UK 5 - University of Vienna, Austria 6 - Trigon GeoServices Ltd, Las Vegas, USA 7 - University of Alberta, Edmonton, Canada 8 - Ghent University, Belgium

The ultimate origin of water in the Earth's hydrosphere is from the deep Earth - the mantle. Theory and experiments have shown that wheras the water storage capacity of olivine-dominated shallow mantle is limited, the Earth's Transition Zone (TZ) could be a major repository for water, due to the ability of the higher-pressure polymorphs of olivine - wadsleyite and ringwoodite - to host up to ~2.5wt. % H_2O. A hydrous TZ may play a key role in terrestrial magmatism and plate tectonics yet despite experimental demonstration of the water-bearing capacity of these phases, geophysical probes such as electrical conductivity have provided conflicting results, and the issue of whether the TZ contains abundant water remains highly controversial. In this study we report X-ray diffraction, Raman and infra-red spectroscopic evidence for the first terrestrial occurrence of any higher pressure polymorph of olivine: ringwoodite, included in a diamond from Juína, Brazil. The ringwoodite has a Mg# of ~ 75, suggesting that it may be mantle hybrised with a more fertile component such as subducted oceanic crust. The water-rich nature of this inclusion (~1.5 wt%), along with the preservation of ringwoodite, is the first direct evidence that, at least locally, the TZ is hydrous, to about 1 wt%. As well as being in agreement with recent magnetotelluric estimates of the TZ water content, this amount of water helps to reconcile measured TZ seismic velocities with those predicted from lab experiments. The finding also indicates that some kimberlites must have their primary sources in this deep mantle region.

Water incorporation in omphacite: concentrations and compositional relations in UHP eclogite samples from Pohorje, Eastern Alps

Skogby H[1*], Janák M[2], Broska I[2]

1 - Swedish Museum of Natural History *henrik.skogby@nrm.se 2 - Geological Institute, Slovak Academy of Sciences

Omphacite is one of the nominally anhydrous minerals that frequently accommodate relatively high concentrations of OH. The reasons for this are probably related to external factors, such as equilibration under high P_{H2O} conditions, as well as to intrinsic ones, such as sample composition and defect chemistry. In particular, vacancy formation via the Ca-Eskola component $Ca_{0.5}$ $[]_{0.5}AlSi_2O_6$ appear to be important for OH incorporation in omphacite. In order to increase the understanding of OH incorporation in omphacite and the role of the Ca-Eskola component, we have investigated a series of omphacites from UHP eclogites by FTIR- and Mössbauer spectroscopy, and microprobe analysis. The investigated eclogites come from the Pohorje Mts. in Slovenia, the south-eastern margin of the Alps. The UHP metamorphism in the Pohorje area was related to subduction of the continental crust during the Late Cretaceous (c.100-90 Ma) time [1]. Eclogites contain the peak metamorphic assemblage garnet-kyanite-omphacite-phengite, with polycrystalline quartz inclusions indicating former coesite. Omphacite occurs as large anhedral grains in the matrix, or as inclusions in garnet and kyanite. The most striking feature of matrix omphacite is tiny needles and rods of quartz. They display a parallel orientation with the c-axis, indicating exsolution from a pre-existing, more silicic clinopyroxene. The composition of primary omphacite estimated from modal content of quartz in omphacite using BSE image and integral analysis of omphacite together with SiO_2 precipitates under a defocused electron beam (25-30 µm) yields up to 10 mol% of the Ca-Eskola component. Geothermobarometry on the mineral assemblage garnet + omphacite + kyanite + phengite + quartz/coesite yields peak pressure and temperature conditions of 3.6 GPa and 834 °C, within the stability field of coesite [2]. Polarized FTIR spectra of oriented omphacite crystals show intense absorption bands around 3470 and 3520 cm^{-1}, strongly polarized in the gamma direction. For some samples, additional weak but sharp bands occur around 3670 cm^{-1}, indicative of amphibole, as well as weak but broader bands around 3620 cm^{-1}, possibly related to sheet silicates. Using a molar absorptivity of 65 000 $L \cdot mol^{-1} \cdot cm^{-2}$, the recorded spectra correspond to water concentrations in the range 530 - 840 ppm H_2O. These concentrations are among the higher reported for omphacite, and in line with equilibration under UHP conditions. Mössbauer spectra obtained by a point-source method reveal Fe^{3+}/Fe_{tot} ratios between 14 - 29 %. Constrained by the Fe^{3+}/Fe_{tot} ratios, the omphacite structural formulae show total cation deficiency and excess Al at the tetrahedral site, indicative of a Ca-Eskola component of 0.5 - 2.5 %. The Ca-Eskola component, and hence the amount of vacancies on the structural M(2) site, display a positive correlation with the OH concentration.

[1] Janák M., Froitzheim N., Lupták B., Vrabec M. and Krogh Ravna E.J. (2004). First evidence for ultrahigh-pressure metamorphism of eclogites in Pohorje, Slovenia: Tracing deep continental subduction in the Eastern Alps, *Tectonics*, 23, TC5014, doi:10.1029/2004TC001641.

[2] Vrabec M., Janák M., Froitzheim N. and de Hoog C.J. (2012). Phase relations during peak metamorphism and decompression of the UHP kyanite eclogites, Pohorje Mountains (Eastern Alps, Slovenia). *Lithos*, 144, 40-55.

OH-defects in orthopyroxene in multiple doped systems

Stalder R*, Karimova A

University Innsbruck. *roland.stalder@uibk.ac.at

Orthopyroxene single crystals were synthesized at 1150 °C between 4 and 8 GPa in the system $MgO\text{-}Al_2O_3\text{-}SiO_2\text{-}H_2O\text{-}CaO\text{-}Cr_2O_3\text{-}Na_2O$ as model system for the Earth's mantle. Experimental charges contained in all cases orthopyroxene and olivine. Depending on starting composition, pressure and temperature, clinopyroxene and/or garnet occurred as additional phase acting as buffer for the defect chemistry in orthopyroxene. Single crystals were manually aligned and measured by FTIR spectroscopy in order to characterise and quantify hydrous defects. Based on the OH-stretching modes two groups of absorption bands were observed, where group 1 is polarised parallel to n_{beta} and occurs at wavenumbers above 3570 cm^{-1} and group 2 is polarised parallel n_{gamma} and occurs below 3570 cm^{-1}. Compared to results from the more simple system $MgO\text{-}Al_2O_3\text{-}SiO_2\text{-}H_2O\text{-}Cr_2O_3$ (Prechtel &Stalder 2012) the pressure dependence of the hydrous defect composition shows that (1) the presence or absence of diopside is negligible, (2) in the presence of garnet, the ratio of Al-specific and Cr-specific absorption bands in enstatite is not sensitive to pressure, and (3) the ratio of group 1/group 2 bands is not sensitive to the CaO and Na_2O content of the starting composition. Similar to the more simple system the intensity ratio of group 2 and group 1 is dependent on Al/Cr, but for Al(Al+Cr) >0.6 - typical for orthopyroxenes from the Earth's mantle - a constant value is reached. The pressure trend for the integral absorbance (ratio of group 2 to group 1) as observed in natural mantle samples is therefore not explained by the content of Ca and Na. The empirically established geobarometer for OH-defects from IR spectra recorded on orthopyroxene single crystals [1] may still be applicable, but the crystal chemical background remains unsolved.

[1] Prechtel F. and Stalder R. (2012). *Eur J Mineral* 24, 471-481.

Reconstruction of water contents of clinopyroxenes of the Canary Archipelago, Spain

Weis F[1*], Skogby H[1], Troll V[2], Deegan F[2], Zaczek-Pedroza K[2]

1 - Swedish Museum of Natural History, SE-114 18 Stockholm, Sweden
*franz.weis@nrm.se 2 - Uppsala University, SE-75236 Uppsala, Sweden

Water plays a vital role in magma genesis, evolution and eruption, and its abundance in volcanic samples is usually measured in melt inclusions hosted in minerals such as olivine [1]. This approach, however, may be hampered by the lack of melt inclusions of suitable size for analysis, the absence of minerals containing them, or extensive degassing of some volcanic samples. Another way to reconstruct the water content of magmas is to use nominally anhydrous minerals (NAMs) such as pyroxenes [2]. NAMs include hydrogen in structural defects (e.g. charge deficiencies) and interstitial spaces during their growth from a hydrous magma. Depending on eruption style, clinopyroxenes are expected to lose parts of their hydrous contents according to the redox-reaction $OH^- + Fe^{2+} \leftrightarrow O^{2-} + Fe^{3+} + ½\ H_2$ [3]. However, hydrogen-associated defects in the crystal structure are considerably more stable, being linked to cation and vacancy diffusion with kinetics two orders of magnitude slower than the redox-reactions, and may thereby keep a "memory" of the initial hydrogen contents. In our study, we measured the water content of naturally erupted and degassed crystals of clinopyroxene (n=36) from different locations and eruptions in the Spanish Canary Archipelago (La Palma, Tenerife and El Hierro) using Fourier Transform Infrared spectroscopy (FTIR). The results vary, with some crystals showing almost complete degassing with water contents below the detection limit, while others reveal substantial amounts of water with contents as high as 870 ppm. Yet, most clinopyroxenes have water contents between 60 and 100 ppm (Figure1). We attempted to reconstruct the original water content at formation of the clinopyroxenes by heating the crystals in hydrogen gas at temperatures around 700°C for several hours, thus refilling the structural defects and interstitials from which hydrogen had been lost from the samples. FTIR analysis of the heated crystals revealed water contents between 200 and 500 ppm with most samples yielding contents between 240 and 390 ppm H_2O (Figure1). The reconstructed water contents of clinopyroxene, in combination with previously determined partition coefficients between a hydrous magma and the minerals (cf. Wade *et al*. 2008 [2]), will now be used to calculate primary water contents of magmas underneath the Canary archipelago. This, in turn, will give a better understanding of volcanic processes in the region.

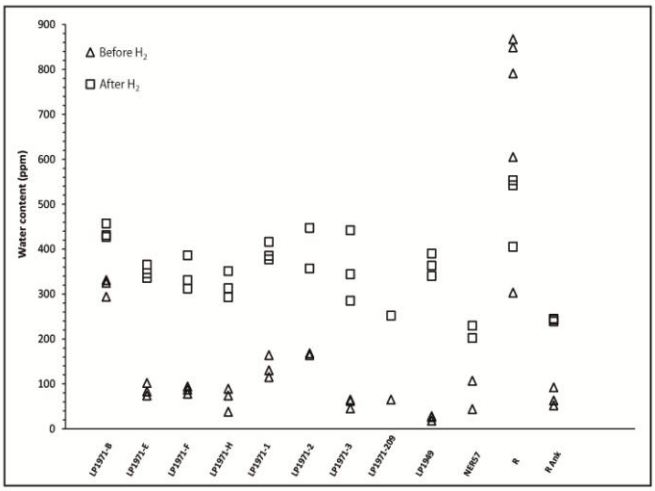

Figure 1: The measured water contents of the Canary Island clinopyroxenes before and after the treatment with hydrogen gas.

[1] Walker J.A., Roggensack K., Patino L.C., Cameron B. I. and Matías O. (2003). The water and trace element contents of melt inclusions across an active subduction zone. *Contributions to Mineralogy and Petrology*, 146,62-77.

[2] Wade J.A., Plank T., Hauri E.H., Kelley K.A., Roggensack K. and Zimmer M. (2008). Prediction of magmatic water contents via measurement of H_2O in clinopyroxene phenocrysts. *Geology*, 36, 799-802.

[3] Sundvall R., Skogby H. and Stalder R. (2009). Dehydration-hydration mechanisms in synthetic Fe-poor diopside. *European Journal of Mineralogy*, 21, 17-26.

Very low "water" content in NAMs from the lower crust beneath the central part of the Carpathian-Pannonian region

Kovacs I[1*], Németh B[1], Török K[1], Mihaly J[2], Német C[2], Fancsik T[1]

1 - GGIH *kovacs.istvan.janos@mfgi.hu 2 - Hungarian Academy of Sciences

"Water" content of nominally anhydrous minerals (NAMs) in lower crustal granulite xenoliths from the central part of the Carpathian-Pannonian region (CPR) is reported. The internal part of the CPR is a young extensional basin, which was formed during the Miocene. The central part of the area went through considerable thinning during this extension, when the crust was thinned from its original 50-60 km thickness to the present 25-30 km. The thinning was coupled with a significant increase in the temperature.

The lower crust was sampled by alkaline basaltic volcanoes after the Miocene extension. The granulite xenoliths entrained in these basalts may bear imprints of this preceding extension event.

The studied lower crustal xenoliths are metapelites and metabasic rocks having most commonly granoblastic texture. All the rock-forming minerals (garnet, pyroxenes, feldspar, silimanite, rutile) were analysed by micro-FTIR spectrometry to determine their "water" content. The studied xenoliths usually have NAMs with very low "water" content with buk water contents typically below 100 ppm. In particular garnet is absolutely dry in all but two xenoliths. Felsdspar and orthopyroxene show water contents usually below 100 ppm. The most "water" rich mineral is clinopyroxene containing from 75 to 440 ppm H_2O. These concentrations are much less than those have been reported from other lower crustal granulites worldwide so far.

The very low "water" content of NAM sin lower crustal granulite xenoliths from the central part of the CPR may be the consequence of the Miocene thinning and the accompanying temperature increase. The increasing temperature may have resulted in significant melting and melt extraction from the lower crust having left behind a very dry residue characterised by high equilibrium temperature. There are only a very few xenoliths which show evidence for subsequent enrichment by melt infiltration. In summary the studied granulite xenoliths highlight that the lower crust in young extensional settings may be very depleted in "water".

Multiple application of FTIR spectroscopy for nominally anhydrous mantle minerals and their fluid inclusions in mantle xenoliths from the Cameroon Volcanic Line, Cameroon

Pintér Z[1], Kovacs I[2*], Konc Z[3], Berkesi M[4], Szabó C[4], Perucchi A[5], Mihály J[6], Németh C[6], Patkó L[4]

1 - Bayerisches Geoinstitut 2 - GGIH *kovacs.istvan.janos@mfgi.hu 3 - Laboratoire Magmas et Volcans, UBP-CNRS-IRD, Clemont- Ferrand 4 - Eötvös University, Budapest 5 - Elettra Syncrotrone Trieste, Trieste 6 - Hungarian Academy of Sciences, Budapest

We have carried out detailed petrographic, petrophysical (EBSD), geochemical and fluid inclusion study (e.g. Raman, FTIR coupled synchrotron radiation, FIB) on spinel lherzolite xenoliths from Barombi Mbo (BM) and Nyos Lake (from Cameroon Volcanic Line) coupled with study of the water content of their nominally anhydrous minerals (NAMs).

Results indicate that the BM protogranular xenoliths provide a characteristic of a juvenile subcontinental lithospheric mantle suffered low degree partial melting and record deformation regime governed by combination of simple and pure shear. The porphyroclastic Nyos xenoliths preserve a transpressional deformation regime and metasomatism indicated by the presence of pargasite.

The fluid inclusions from both localities show the same fluid components, as CO_2 (96-99 mol%), H_2O (1-3 mol%) and some cases H_2S (0-1 mol%). FTIR measurements were used for the nominally anhydrous minerals and their fluid inclusions to identify the water content of the two mantle regions and to identify and map the solid phases inside the fluid inclusions. The water content of nominally anhydrous silicates in Nyos xenoliths (olivine: 1.4 - 2.0 ppm, orthopyroxene: 58 - 90 ppm, clinopyroxene: 261 - 334 ppm) are lower than in Barombi xenoliths (olivine: 5.0 - 9.1 ppm, orthopyroxene: 105 - 300 ppm, clinopyroxene: 368 - 513 ppm). The NAMs in Barombi xenoliths show moderate concentrations (total=100-130 ppm), whereas Nyos xenoliths show slightly lower concentrations (total=10-60 ppm). With infrared spectroscopy using synchrotron radiation we can detect and map the fluid inclusions' composition, their solid phases and H_2O content. Solid phases were detectable inside the fluid inclusion, the absorbance characteristics of which correspond to phlogopite, serpentine, and sometimes the combination of both pargasite and phlogopite in the OH-stretching range.

The Barombi xenoliths have high water contents and their fluid inclusions contain phlogopite (and serpentine), whereas Nyos xenoliths have lower water contents and their fluid inclusions contain both phlogopite and pargasite.

Pulsed neutron diffraction study of dense hydrous magnesium silicate phase E

Tomioka N*, Okuchi T, Purevjav N

Institute for Study of the Earth's Interior, Okayama University
*nao@misasa.okayama-u.ac.jp

Hydrogen plays important roles in chemical and physical properties of minerals. Dense hydrous magnesium silicates (DHMS) are thought to be major hosts of hydrogen in subducting lithospheres [1]. Therefore, their crystal structures are of particular interest to understand hydrogen behavior in the deep Earth. Phase E, which has an ideal stoichiometry of $Mg_2SiO_2(OH)_4$, is stable at the P-T conditions of the upper mantle and the transition zone [1]. This phase was first synthesized by Kanzaki (1989) [2] and its basic crystal structure has been refined by single crystal X-ray diffractometry [3]. The crystal structure of phase E contains brucite-like layers and the layers are crosslinked by SiO_4 tetrahedra and MgO_6 octahedra. A reconnaissance study on hydrogen position in the (Fe,Al)-bearing hydrogenated phase E has been carried out by single crystal X-ray diffraction and the 6c position was suggested as the hydrogen site [4]. Recent development of pulsed neutron diffraction technique would provide further insights into hydrogen in minerals, because neutron diffraction is more sensitive to hydrogen positions due to high-scattering efficiency of neutron for hydrogen than X-ray. The goal of the present study is precise determination of hydrogen position and its site occupancy in deuterated phase E based on powder neutron diffraction.

In the present study, deuterated phase E was synthesized by Kawai-type apparatus using mixture of synthetic $Mg(OD)_2$ and SiO_2 glass with 2:1 molar ratio. The mixture in a gold capsule with 5 mm in outer diameter was kept at 15 GPa and 1100 °C for 15 minutes. A large amount (50 mg) of homogeneous phase E was successfully recovered. The sample powder was enclosed into a TiZr sample container that has high transparency to neutron beam and does not show neutron coherent scattering. A powder neutron diffraction pattern was obtained with exposure time of 6.5 hours at the BL19 (TAKUMI) at J-PARC. By normalization of the intensities using an incoherent scattering pattern of vanadium, a diffraction profile with low and flat background was obtained. The Rietveld refinement using the Z-Rietveld code clarified that the 18h Wyckoff position is more preferable deuterium site than the 6c position. In the 18h model, hydroxyl bond in the phase E structure is tilted away from the direction normal to octahedral layers. The tilting of OD dipole is caused by the presence of hydrogen bond. The effect of hydrogen content on hydrogen positions in the phase E structure is under investigation to understand its hydration mechanism.

[1] Ohtani E. *et al.* (2004). *Phys. Earth Planet. Inter.*, 143-144, 255-269.

[2] Kanzaki M. (1989). *EOS*, 70, 508.

[3] Kudoh Y. *et al.* (1993). *Phys. Chem. Minerals.*, 19, 357-360.

[4] Uchiyama *et al.* (2011). *Photon Fact. Act. Rep.*, 28, 197.

A response of physicochemical and structural properties of clays on a 100 km overburden stress

Valter M, Ploetze M*, Ulmer P

ETH Zurich *ploetzel@ethz.ch

Clays as a part of sediments yield to compaction and burial diagenesis. Presented project is focused on changes of the physicochemical properties of clay as well as structural parameters of clay minerals induced by elevated pressures for different time periods. Three clays were studied: kaolin, sodium bentonite and illite. Pressures of 1.5 and 3.0 GPa were applied on air dry clays within a piston cylinder apparatus for 24 and 96 hours. The analyzed clay parameters include the cation exchange capacity (CEC) and the porosity, particularly the distribution of micropores (<15 Å). Furthermore, "crystallinity" indices and the dehydration/de-hydroxy-lation behavior were investigated with XRD and with thermal analysis (TG) resp.

The microporosity of the kaolin was almost completely diminished after each compression state. The same is true for illite but only after 97 hours of compression (Figure 1).

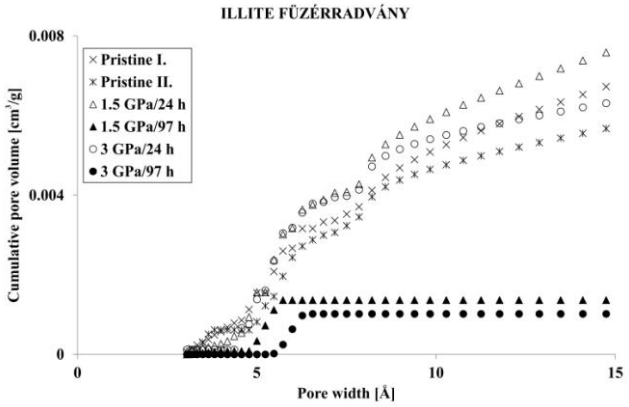

Figure 1: Response of the illite microporosity on experimental high pressure compression: Results of CO_2 adsorption measurements.

The microporosity of bentonite up to 15 Å, however, showed a weak decrease only. Which means, the interlayer of the smectite which forms part of the micropores in bentonite could be compacted if, then only slightly. Nevertheless, the CEC of bentonite decreased up to 10% probably because of a lowered accessibility.

The different "crystallinity" indices (Hinckley and Lietard indices of kaolinite, Weaver's sharpness ratio of illite) as well as the crystallite size in b-direction (060) decreased. Also, the thermal reactions of the compressed clays showed some changes. After compression, the clays were macroscopically wet. A more pronounced de-hydration could be observed. Additionally, the dehydroxylation temperature decreased. All these are signs for alteration in the octahedral sheet of the clay minerals.

Process mineralogical characteristics of REE-bearing carbonatite from the Songwe Hill deposit, Malawi

Al-Ali S[1*], Wall F[1], Pascoe R[1], Rollinson G[1], Dawes W[2], Brady A[2]

1 - Camborne School of Mines, University of Exeter *shaa201@exeter.ac.uk

2 - Mkango Resources Ltd.

Carbonatite-related rocks host many of the world's most important rare earth element (REE) deposits. The REE in carbonatites can occur in a wide variety of minerals and therefore it is essential to thoroughly understand the mineralogy of the deposit in order to be able to design efficient beneficiation techniques and thus optimise the grade and recovery of ore minerals.

The aim of this work is to characterise the modal mineralogy of drill core samples of the Songwe Hill carbonatite REE deposit, Malawi. The indicated resource of these deposits is 13.2 million tonnes with a grade of 1.62% of total rare earth oxides (TREO) [1].

The characterisation includes factors such as: modal mineralogy, mineral abundance, crystal size and shape, liberation and mineral association characteristics. The characterisations have been carried out using scanning electron microscopy (more than 100 backscattered electron images and 8 False-coloured digital images), X-ray diffraction profiles of 8 samples and automated mineralogy (QEMSCAN™).

All samples consist of calcite, ankerite, feldspar, iron oxides, Fe-Mn oxides, strontianite and barite as gangue minerals, while synchysite-(Ce), apatite and florencite-(Ce) are the most important rare earth and rare earth-bearing minerals. Synchysite-(Ce) mainly appears as accumulations of needle-shaped crystals and, less commonly, as lath-shaped crystals; apatite commonly occurs as veins and stringers but may also be well liberated, while florencite-(Ce), the least abundant RE-mineral, occurs as patches associated with other gangue minerals.

[1] Swinden S. and Hall M. (2012). NI 43-101, Technical Report and Mineral Resource Estimate for the Songwe Hill Rare Earth Element (REE) Project, Phalombe District, Republic of Malawi, Mkango Resources Ltd.

Late stage apatite: a potential heavy REE-enriched co-product of light REE minerals in carbonatites

Broom-Fendley S[1*], Wall F[1], Gunn G[2], Andersen J[1], Brady A[3], Dawes W[3]

1 - Camborne School of Mines, University of Exeter *s.broom-fendley@ex.ac.uk

2 - British Geological Survey 3 - Mkango Resources Ltd.

It is well established that carbonatites are excellent rare-earth element resources. They are typically high grade and can have large tonnages of the REE, but are usually enriched in the lower atomic number 'light' members of the REE series (LREE) [1]. The price of the LREE has been decreasing since the peak of 2011, and so carbonatites have become less attractive to exploration companies. Heavy REE (HREE) prices have also dropped since 2011 but they are still two orders of magnitude more expensive than the LREE. Thus, any mechanism to increase the percentage of extractable HREE from carbonatite deposits would greatly increase the value of an already important REE resource.

The Songwe Hill carbonatite, Malawi, is being used as a case study to explore potential HREE-enrichment in carbonatites. Exploration work by Mkango Resources Ltd. has established a mineral resource estimate, comprising an in-situ indicated and inferred component, of 13.2 million tonnes, grading 1.62% total rare earth oxides [2]. The main REE-bearing mineral is synchysite-(Ce) but apatite is a potential co-product.

At Songwe, apatite is found in all stages of the carbonatite emplacement. LA-ICP-MS analysis of the apatite has demonstrated that it typically is mid- to heavy-REE enriched [3]. It makes up to 5 % of the modal mineralogy of the carbonatite and thus could be a potential HREE-rich co-product of LREE extraction. Three stages of apatite formation have been identified and textural, geochemical and fluid inclusion evidence suggests that HREE-enrichment took place during the later stages of the intrusion.

Early apatite typically forms an ovoid habit, co-crystallising with calcite and zircon. It is interpreted as magmatic, is LREE-enriched and is uncommon at Songwe.

Later, second stage, overprinting apatite is prevalent. It is associated with ferroan calcite, florencite and appears to overprint synchysite. It forms stringers and small veins in the carbonatite and has lower La/Yb and Sm/Dy ratios. Increases in HREE concentration correlate with increased concentration of Th, Na and Sr. Preliminary fluid-inclusion analyses indicate minimum formation temperatures of around 300˚C.

Third-stage apatite, which has the most extreme HREE enrichment, is found in apatite-fluorite veins in contact breccia around the carbonatite, associated with fluorite, barite, calcite and quartz. It forms stringers, similar to late-stage apatite in the main carbonatite, and is similarly enriched in HREE, U, Sr and Na. The Th concentration in the apatite is low, but higher Th occurs in associated xenotime overgrowths. Fluid inclusions in the fluorite, paragenetically established as crystallising after the apatite, homogenise at 160˚C and constrain the lower limits of the crystallisation temperature of the HREE-enriched apatite.

The HREE enrichment may be the result of either (1) preferential mobility of the HREE into hydrothermal fluids during alteration of the carbonatite, or (2) early crystallisation of synchysite leading to relative enrichment of the HREE in the remaining fluid which crystallises later, at lower temperatures, and overprints earlier stages of the carbonatite. These two hypotheses are dependent on whether the enrichment took place in an open system or a closed system. Stable isotope analyses of the apatite (O) and carbonate (O and C) minerals are in progress to help distinguish this.

[1] Wall F. (2014). Rare Earth Elements. In: Gunn, A.G. (Ed) *Critical Metals Handbook*, John Wiley &Sons, Oxford. doi: 10.1002/9781118755341.

[2] Swinden S. and Hall M. (2012). NI 43-101 Technical report and mineral resource estimate for the Songwe Hill rare earth element (REE) project, Phalombe District, Republic of Malawi. MSA Group, South Africa.

[3] Broom-Fendley *et al.* (2013). Carbonatite-hosted late-stage apatite as a potential source of the heavy rare earth elements. SGA Conference abstracts, volume 4, pp. 1694.

Process mineralogy of rare earth element ores

Chetty D, Clark W, Gryffenberg L*

Mineralogy Division, Mintek, Randburg, South Africa *lelanieg@mintek.co.za

With the increased demand in rare earth element consumption, fuelled by cuts in Chinese exports, the economic exploitation of rare earth element (REE) deposits outside China has become more significant in recent years. Mintek is involved in various testwork programmes aimed at successful REE extraction from different ores, with carbonatite ores most tested for recovery of REE.

The typical processing route for extraction of REE will include aspects of comminution, gravity or other physical separation methods, flotation, chemical cracking and/or leaching, or even high temperature methods. At all stages, mineralogical examination is a vital part of the testwork programme. The techniques used for such studies of REE ores and metallurgical products include quantitative XRD, optical and scanning electron microscopy (SEM), electron probe microanalysis, and quantitative mineralogy by automated SEM.

Many of the carbonatite-hosted REE ores are light REE (La - Sm) enriched, with Ce and La most evident. Typical REE minerals include bastnaesite and synchysite, often found in syntaxial/acicular intergrowths intimately associated with carbonate and silicate gangue. This poses a challenge for physical upgrading, as extremely fine liberation sizes are required to separate the minerals. Additionally, high carbonate content poses problems for direct leaching, owing to acid, hence reagent, consumption. Quantitative XRD has been successfully applied as a rapid alternative to autoSEM analysis for an upfront answer on carbonate and other gangue mineral content in the ores. More detailed autoSEM applications provide quantitative information on REE mineral type, relative abundance, grain size distribution, liberation and association with other minerals. Complementary mineral chemical data aid in assessing REE deportment and potential for recovery. Chemical cracking and leaching are applied to concentrates, from which residues are usually examined by SEM to assess reasons for poor recovery.

Carbonatitic ores richer in apatite and xenotime represent heavy REE enriched resources. Where textural associations of these minerals are more conducive to upgrading, flotation is used, prior to chemical cracking to break the more refractory phosphate structures of the REE host minerals.

Calcining and smelting have been attempted to redistribute REE prior to re-upgrading and leaching of more difficult ores. Here, SEM studies provide useful chemical mapping for determining REE distribution in neoformed phases to guide further processing for their recovery.

Process mineralogical studies show that the nature of the REE minerals and associated gangue play important roles in determining whether considered process routes will be effective, but also for refining unit operational performance for the successful extraction of REE.

Strategic minerals in the Colombian Amazonas and Orinoco region – characteristics and possible impacts of their mining

Cramer T[1*], Amaya-Perea Z[1], Bonilla-Pérez A[1], Franco Victoria J[1], Alvarado Ávila A[1], Beltrán G[1], Castañeda Gómez A[1], Diaz J[2], Ochoa Gutierrez L[1], Horn H[3], Brooks W[4], Melcher F[5], Lehmann B[6], Sitnikova M[7]

1 - Universidad Nacional de Colombia, Geoscience Department, Bogotá *thcramer@unal.edu.co 2 - UNAL Bogotá 3 - Geological Institute of the Federal University of Minas Gerais 4 - Independent 5 - Montanuniversitaet Leoben 6 - Technical University of Clausthal, Germany 7 - Bundesanstalt für Geowissenschaften und Rohstoffe

Since 2009, information on coltan occurrences in eastern Colombia has indicated the need for field research in this large but little studied area adjacent to Brazil and Venezuela. A research project was thus prepared at the end of 2011 and finally started in December 2013 in four of Colombia's eastern departments: Vaupes, Vichada, Guainía and Guaviare. The project was called, "*An initial evaluation of strategic and industrial minerals (Ta, Nb, Sn, W, Ti, Fe, Mn, Al, Zr, Hf, U, Au, REE), gems and construction materials, their use and the possible environmental and social impact of mining them for the Llanos region's sustainable development*," and has involved some twenty geologists, biologists and sociologists visiting 18 study-areas during 9 fieldtrips spread over a 1-year period to obtain geological-mineralogical data and samples, as well as plant specimens and socio-demographic information.

Samples taken during field-trips to the Guainía and Vichada departments were processed and characterised by sieving, magnetic separation, density- and grain-analysis, transmitted light and ore microscopy, SEM, XRD and XRF. This revealed that many Ta-Nb-occurrences in alluvial black sand are accompanied by Fe- and Ti-oxide and that their chemical composition varies (<50% Ta, <20% Nb with mainly Fe, Ti and few Mn). Nb-rich rutile and pyrochlore inclusions occurred in ilmenite from the Guainía department, as well as some Ta-rich cassiterite. Later on, samples from illegally mined wolframite deposits were also analysed. Although pegmatites and acid magmatic rocks are the major primary sources of Ta-, Nb-, Sn-, W- and REE-minerals, abundant Ti-minerals which partly originate from gabbro intrusions indicate more complex geological settings.

Normally, the heavy minerals are mined from secondary alluvial or eluvial deposits. Scarce knowledge concerning the real economically exploitable content of coltan and other valuable minerals often leads to the speculative devastation of just Fe- and Ti-oxide bearing rain-forest areas by informal mining, which is sometimes linked to criminal activity.

The Amazonas department also wished to join the project following a first visit and presentation in the Vichada department. One of the project's important aspects concerns communication with both Indigenous communities and local actors (i.e. the people involved in the aforementioned illegal mining), in the latter case, aimed at teaching more sustainable exploitation practices in areas where mining is legally and environmentally suitable and agreed upon. A fundamental mid-term objective of the project concerns establishing permanent links between the Geosciences Institute in Bogota and local multipliers and future researchers from the target region. Something which started out some years ago, aimed at identifying so-called coltan, has thereby become a serious attempt at studying and increasingly understanding a very complex geo-environmental tropical system in a 1,2-1,6 Ga old geological terrain which is as large as Germany.

REE distribution, speciation and fractionation in a lateritic profile from Madagascar

Janots E[1*], Bernier F[2], Brunet F[2], Munoz M[2], Berger A[3], Trcera N[4], Lanson M[2]

1 - University of Grenoble *janotse@ujf-grenoble.fr 2 - ISTerre, University of Grenoble 3 - University of Bern 4 - Synchrotron Soleil

Despite containing relatively low REE concentrations, laterites are attractive as REE ion-adsorption deposits because REE are adsorbed on mineral surfaces (readily leached) and HREE are enriched in comparison to LREE. However, in laterites, the REE distribution is difficult to assess due to the small size of the host phases and their low REE concentrations. We present here an innovative approach to determine the microscale REE distribution, speciation and fractionation by combining geochemical data (whole-rock elementary and isotopic composition) with *in-situ* high-resolution characterization techniques including FE-SEM, EMP and spectrometric measurements using synchrotron radiation (µXANES and µXRF; LUCIA beamline at SOLEIL, France). The lateritic profile (Madagascar) develops over a tonalite and can be simply decomposed from bottom to top: (1) a saprolite (C-horizon) with no significant REE mass transfer, (2) an accumulation zone (B-horizon) where REE and particularly Ce are enriched compared to the bedrock and (3) the top of the profile (A-horizon) where REE are leached out . Highest REE concentrations are found in REE-minerals. While REE-phosphates of the rhabdophane group occur in the saprolite, they correspond to minerals of the alunite supergroup in the soil (B- and A-horizons). Cerianite only occurs in the B-horizon. *In-situ* spectrometric measurements using synchrotron radiation reveals the heterogeneous Ce distribution in the soft polymineral nodules of the B-horizon, where maximum Ce concentrations are systematically found in porous Mn-rich domains. XANES spectra in the L_{III} edge of Ce reveal unexpected results concerning Ce oxidation state in lateritic minerals. Remarkably, the Ce^{III}/Ce^{IV} ratio of secondary rhabdophane minerals in pores and cracks of the saprolite, is identical to that of the parent rock, indicating for no significant Ce^{III}/Ce^{IV} fractionation during alteration of primary minerals, transport in altering fluid and secondary mineral precipitation. In clayey material (A- and B-horizons), Ce^{III}/Ce^{IV} value (around 100%) indicates that primary Ce^{IV} was reduced during leaching and partly redistributed in its trivalent form in the clayey groundmass, with no Ce^{III}/Ce^{IV} fractionation. Subsequent water run off (during the dry season) caused water evaporation and oxidation and precipitation of redox sensitive elements in pores. This scenario accounts for the oxidation/scavenging of Ce^{III} in Ce^{IV} and consequent Ce enrichment in the pores associated with Mn-oxides of the accumulation horizon.

Interrogating the ultimate source of Proterozoic critical metal deposits in the Phalaborwa, Mount Weld and Mountain Pass carbonatites

Kavecsanszki D*, Moore K, Wall F

Camborne School of Mines, University of Exeter *kavecsdorii@gmail.com

It is noticeable that the magmatic systems that host the world's largest ore deposits of critical metals such as the REE and niobium were formed by melting in a carbon-enriched Proterozoic mantle. We have investigated the relationships between the thermal evolution of the mantle (using extant models), conditions of melt formation in a carbonated mantle, the frequency of carbonatite magmatism through time, and the potential of carbonatite magmas to flux the critical metals from the mantle to the crust. We deduce that two carbonatite-generating processes were likely to operate in the Proterozoic. (1) Large scale mantle overturns that formed as a result of high heat flow could have generated primary silicocarbonatites that evolved in the crust to become carbonatites. (2) Metasomatised mantle could melt directly to primary mantle carbonatites in between mantle overturns due to lowering of the solidus. Three case studies are being used to interrogate this hypothesis: the Phalaborwa (~2060 Ma) carbonatite in South Africa, Mount Weld (~2020 Ma) carbonatite in Australia and Mountain Pass (~1375Ma) carbonatite in the USA.

All of the three case studies coincide with the numerically-predicted timing of large scale mantle overturns. Phalaborwa and Mountain Pass have close temporal and spatial associations with large scale magmatic events (Bushveld complex in South Africa, Kaweenawan LIP in North America). The Mount Weld and Mountain Pass carbonatites appear to be more closely associated with melting of metasomatised mantle, although Mount Weld has trace element characteristics suggesting some input from a plume source. The Mount Weld and Mountain Pass carbonatites are associated with ultrapotassic rocks from different tectonic regimes, suggesting that metasomes can be re-melted by a variety of mechanisms. Our findings suggest that mantle overturns induced extensive metasomatism peripheral to large mantle-scale melting events, the evidence for which has not always been preserved, and that metasomatism occurred between mantle overturns as stated previously. The lack of evidence for a large scale melting event in proximity to Mount Weld (if preservation bias can be ruled out) implies melting of a metasome in between mantle overturns. If a mantle overturn with high heat flow is the mechanism that triggered production of carbonated magmas, then the parental magma that transported critical metals from the mantle is more likely to have been silicocarbonatite than carbonatite. We will attempt to reconstruct the parental magmas and their evolution in order to understand if large-scale mantle overturns are the reason that the largest and most economic critical metals deposits are restricted to the Proterozoic.

The geological controls on the heavy rare earth element (HREE)-enriched alteration zone of Area 4, Lofdal, Namibia

Loye E[1*], Swinden S[2], Wall F[3]

1 - University of Exeter *edloye@hotmail.com 2 - Swinden Geoscience

3 - Camborne School of Mines, University of Exeter

The Lofdal Alkaline Carbonatite Complex, Khorixas, Namibia has a proven CIM NI 43-101 compliant indicated and inferred resource and a particularly high potential monetary value for its combined REE (i.e. high 'REE basket price', TMR, 2014). This is because of its high proportion of the less abundant and more valuable "heavy" rare earths (HREEs). Most carbonatite deposits are highly LREE-enriched but Lofdal contains xenotime-(Y) in carbonatite dykes [1] and also within late hydrothermal zones. These zones, such as "Area 4", which is the subject of this study, are generally spatially controlled by older basement structures. Drill core textural features have been combined with major and trace element data (ICP-MS) and 41 samples, representing a range of xenotime mineralised intercepts, have been analysed using optical microscopy, cathodoluminescence, SEM/EDS and wavelength-dispersive electron microprobe.

The HREE mineralisation in Area 4 followed carbonatite-induced fenitisation and then brecciation, thought to be caused by later carbo-hydrothermal fluids. This timing is similar to that noted in fenites at the Kangankunde and Chilwa Island carbonatite complexes in Malawi [2]. Ninety per cent of the HREE deportment in Area 4 is in the mineral xenotime-(Y), which is commonly associated with rutile (+/-Nb), apatite, zircon, aeschynite-(Ce), synchysite-(Ce), and thorite. Variations of this assemblage contain albite and calcite, dolomite or ankerite, with or without phlogopite-biotite, and magnetite/hematite.

Subtle variations in the REE content of xenotime-(Y) may provide valuable clues to its formation environment. Gadolinium is in a unique position, marking the change from unpaired to paired electrons in the 4*f* orbitals and its behaviour is temperature dependent [3, 4, 5]. Loss of middle REE content in xenotime here eludes to hydrothermal modification of earlier REE bearing phases and is consistent with previous experimental studies [6, 7], in which lower temperature xenotime-(Y) has a higher HREE content, lower Th, but smaller grain size. Corrosion and re-precipitation of xenotime-(Y) leads to Th forming its own phase as thorite, leaving less Th in the xenotime lattice. The different stages of hydrothermal activity thus have economic implications for targeting ore and for mineral processing.

REE transporting ligands may have been a combination of bicarbonate and phosphate, for example, at >300°C, and chloride at <300°C. Decompression and fluid/rock interaction with albite, and especially dolomite, are effective factors in depositing xenotime from solution.

[1] Wall F. *et al*. (2008). *Can. Min*., 46, 1251-1267.

[2] Dowman E. (2014). Unpublished PhD thesis, Kingston University.

[3] Ni Y., Hughes J.M., and Mariano A.N. (1995). *Am. Mineral*.80**,** 21-26.

[4] Grantz R. and Heinrich W. (1997). *Am. Mineral*., 82, 772-780.

[5] Irber, W. (1999). *Geochim. Cosmochim. Acta* 63, 489-508.

[6] Kositcin N. and McNaughton N.J. (2003). *Geochim. Cosmochim. Acta*, 67, 709-731.

[7] Cook *et al*. (2013). Lithos Vols. 172-173, 192-213.

Simultaneous cathodoluminescence imaging and Raman and cathodoluminescence spectroscopies: applied mineralogy of the REE (Sn, Ta, Zr, F) ore from Pitinga, Brazilian Amazon

Neumann R[1*], de Souza Gonçalves Vasques F[2], da Fonseca Martins Gomes O[2]

1 - Centre for Mineral Technology - CETEM, Division for Technological Characterisation *reiner.neumann@gmail.com 2 - Centre for Mineral Technology - CETEM

Pitinga used to be the world's largest cassiterite mine, and still is one of the major tin and tantalum/niobium suppliers. It also hosts the largest reserves for heavy rare earth elements worldwide, with an estimate of over 70 kt of contained Y, and highly above average HREE/Y. The most important HREE carrier is xenotime, but gagarinite-(Y) and HREE-rich varieties, fluocerite-(Ce) and waimirite-(Y) and its HREE-rich correspondents have been described. The identification of these minerals and their varieties is not straightforward by SEM-EDS or transmitted/reflected microscopy, due mostly to the large compositional variations and elements difficult to assay by EDS, such as F and C. Mineral identification based on cathodoluminescence images, where most of the minerals can be targeted by their CL colour, is an alternative technique. The large mineralogical variety (including the non-REE minerals) however requires a previous study to link CL-colour to mineral. Here we present an instrumental setup the cathodoluminescence stage is mounted on a microRaman spectrometer, allowing for conventional Raman spectroscopy and cathodoluminescence spectroscopy (using the Raman's high-resolution spectrometer with the lasers switched off) to identify the minerals separated by its CL-colour. The proposed setup allowed for the quantification of the relevant phases, and for the precise identification of several compositional varieties of the minerals.

Geochemical and mineralogical characteristics of ion-adsorption type REE ores in South China and Southeast Asia

Sanematsu K[1*], Kon Y[1], Manaka T[2], Zaw K[2], Watanabe Y[1]

1 - Geological Survey of Japan, AIST *k-sanematsu@aist.go.jp 2 - CODES, University of Tasmania

Ion-adsorption type REE deposits are currently the predominant source of HREE and Y in the world, and the economic mines have been confined almost exclusively to South China. However, similar ore bodies can be found in the other countries of temperate and tropical areas. These ore bodies consist of weathered granitic rocks called ion-adsorption ores [1], characterized by significant amounts of ion-exchangeable REE and Y using an electrolyte solution. The ores are more or less enriched in HREE although REE grades are lower than those of other deposit types (e.g., carbonatites, alkaline rocks). In this study, we discuss geochemical and mineralogical characteristics of parent granites and weathered granites collected in South China and Southeast Asia, in order to elucidate the genesis of ion-adsorption type REE ores and enrichment of HREE.

Studied parent rocks of the ion-adsorption ores are ilmenite-series calc-alkaline granites, characterized mostly by metaluminous to weakly peraluminous (alumina saturation index <1.1) compositions and low P_2O_5 contents (< ~0.1 %). The granites contain allanite, titanite and/or REE fluorocarbonates (e.g., synchysite) as source minerals for ion-exchange and are poor in insoluble REE phosphates (monazite and xenotime). Strongly fractionated granites (SiO_2 >~74 %) can be enriched in HREE and contain a variety of fine-grained REE-bearing minerals such as REE fluorocarbonates, allanite-(Y), monazite and xenotime which crystallized in a deuteric alteration stage. These minerals commonly coexist with fluorite and chlorite, an alteration product of biotite. The occurrences of the alteration minerals and elevated F contents in HREE-rich granites suggest that REE are transported as fluoride complexes in hydrothermal fluids. Relative abundances of the REE-bearing minerals and their weathering resistances constrain the ion-adsorption ore formation and fractionation of LREE/HREE.

Since some REE-bearing minerals (e.g., REE fluorocarbonates, allanite, titanite) are less resistant to chemical weathering, they are degraded by low-pH soil water and release REE^{3+} during weathering. REE^{3+} are transported downward in a weathering profile and are immobilized by adsorption and/or incorporation into secondary minerals due to pH increase resulting from the contact of soil water with rock-forming minerals or higher-pH ground water. Ce is mostly immobilized as CeO_2 by oxidizing from Ce^{3+} to Ce^{4+} near the surface. The other REE^{3+} are most likely to be adsorbed on the surfaces of clays (e.g., kaolin) and/or to be contained in secondary phosphates. As a result, the weathering profile can be divided into a REE-leached zone of the upper part of the profile with positive Ce anomaly and a REE-accumulation zone (ion-adsorption ores) in the lower part with negative Ce anomaly and significant amounts of ion-exchangeable REE. Because the degree of negative Ce anomaly is positively correlated with ion-exchangeable REE concentrations, the depletion of Ce is a helpful geochemical indicator in exploration of ion-adsorption type ores [2]. HREE-rich ion-adsorption ores are sourced from strongly fractionated granites containing HREE minerals such as synchysite-(Y).

[1] Bao Z. and Zhao Z. (2008). Geochemistry of mineralization with exchangeable REY in the weathering crusts of granitic rocks in South China. *Ore Geology Reviews*, 33, 519-535.
[2] Sanematsu K. *et al*. (2013). Geochemical and mineralogical characteristics of ion-adsorption type REE mineralization in Phuket, Thailand. *Mineralium Deposita*, 48, 437-451.

A comparison of the mineralogy, processing and environmental characteristics of rare earth element deposits

Wall F

Camborne School of Mines, University of Exeter f.wall@exeter.ac.uk

There are many different types of rare earth element (REE) deposit [1] and many currently under active exploration [2]. They range from mineral sands, one of the original sources of rare earth element ores and still the subject of expanding and active mining in India, to fresh and weathered carbonatites, alkaline rocks, and granites, various other hydrothermal deposits and by products of large volume mining of commodities such as aluminium and phosphate. These deposits vary greatly in their mineralogy, rock type, concentration of REE, proportions of the various members of the REE series (i.e. ratio of light to heavy REE), and size. These characteristics influence the ease of processing and also the environmental characteristics of the deposit.

A key challenge facing companies developing REE deposits is the efficient beneficiation of the REE minerals and extraction and separation of the REE. The main REE ore minerals in active mines are bastnäsite-(Ce) and monazite-(Ce). Xenotime-(Y) has been produced, especially from mineral sands for many years, and loparite-(Ce) is mined as an ore of Nb and REE from the Lovozero complex, Kola Peninsula, Russia. Other minerals, such as ancylite-(Ce) and eudialyte are the main minerals in deposits under exploration, and require new methods to be developed. The most common means of beneficiation of REE minerals is flotation but physical methods are used for mineral sands. Ion adsorption clays have the advantage that the REE can be leached straight into solution, bypassing the mineral concentration stage.

Deposits types vary greatly in size and grade [3]. The economic levels of REE are very variable depending on whether the deposit contains the less expensive light REE or the more expensive heavy REE. The highest grade is Steenkampskraal, South Africa (14 wt% REO). Carbonatite deposits, such as Mountain Pass and the weathered carbonatite at Mount Weld also tend to be reasonably high grade. The largest deposits are the alkaline rocks, with lower grades but generally higher proportions of heavy REE. The smallest and lowest grade deposits are the ion adsorption clays mined for heavy REE in China, with less than 0.35 wt% REE.

Equally variable along with these deposit characteristics are the environmental characteristics of the deposits, such as energy use and carbon footprint, the potential for environmental pollution and disturbance, and the potential for resource efficient mines producing multiple commodities. The issue that has caused most public concern so far is radioactivity, relating to the Th content of the REE or associated minerals but most of the environmental damage caused by Chinese REE mines and factories could have been avoided by improved performance of companies involved. The issues are complex and it is difficult to weigh up the various factors. However responsible sourcing of commodities used in environmental technologies is likely to become increasingly higher profile.

[1] Orris G.J. and Grauch R.I. (2002). *Rare Earth Element Mines Deposits and Occurrences*, United States Geological Survey Open-File Report, 02-189.
[2] TMR (2014). Advanced Rare-Earth Projects Index, http://www.techmetalsresearch.com/metrics-indices/tmr-advanced-rare-earth-projects-index/ (accessed March, 2014).
[3] Wall F. (2014). Rare earth elements. p. 312-339 in Critical Metals Handbook (editor, Gunn G.), John Wiley &Sons, Ltd, UK.

Acknowledgement: NERC catalyst award NE/L002280/1, Geology to Metallurgy of Critical Rare Earths.

Jabal Tawlah, a heavy REE-rich prospect in northwest Saudi Arabia

Watanabe Y[1*], Hoshino M[1], Moriyama T[2]
1 - Geological Survey of Japan *y-watanabe@gipc.akita-u.ac.jp
2 - Toyota Tsusho Co. Ltd

Jabal Tawlah microgranite in northwest Saudi Arabia occurs in Proterozoic metamorphosed sedimentary rocks. This is one of the granite bodies heavily fractionated possibly from the Jabal az Zuhd alkaline granite located 5 km northwest of Jabal Tawlah. The microgranite is 310 m long, 110-120 m wide and 110-40 m thick in size. This intrusive body is partly covered by a thin layer of host sedimentary rocks that form a roof pendant for the granite, and the boundary zone consists of hybrid rocks of granite and sedimentary rocks.

The microgranite is composed of quartz, biotite, muscovite, albite, microcline with accessory minerals such as zircon, thorite, columbite, xenotime, samarskite-(Y), aeschynite-(Y), fergusonite and euxenite-(Y). Detailed mineralogical study detected the presence of Ca-Y-F and YF_3 minerals in the microgranite. Based on the observation of mineral paragenesis, the formation of these rare earth minerals is divided into a magmatic stage (xenotime, samarskite-(Y), YF_3 mineral) and a subsequent hydrothermal stage (Ca-Y-F mineral, euxenite-(Y), fergusonite). The microgranite is mineralized with high field strength elements such as REE (1.0 wt.%), Zr (2.57 wt.%), Nb (5628 ppm), Ta (283 ppm) and Th (1034 ppm) with elevated amounts of dysprosium (870pm), and is regarded as a potential source of heavy rare earth elements.

Be-Nb-W-Sn-Ti-Li-U-Mn-mineralization in the metarhyolite of Bükkszentkereszt, NE-Hungary

Zajzon N[1*], Németh N[1], Szakáll S[1], Kristály F[1], Gál P[1], Fehér B[2]
1 - Institute of Mineralogy and Geology, University of Miskolc, Miskolc, Hungary
*nzajzon@uni-miskolc.hu 2 - Herman Otto Museum, Miskolc, Hungary

The Ladinian-Carnian metarhyolite sequence of the East Bükk Mts. at Bükkszentkereszt became a target in a critical element prospecting project because of its previously known Be enrichment [1] in a Mn-U-fluorapatite layer. The stratovolcanic complex suffered prehnite-pumpellyite facies metamorphism ca. 80-90 Ma ago and it was folded and faulted in multiple phases, so syngenetic fabric and structures are strongly overprinted. The chemical composition is acidic and peraluminous (ASI = 1.2-2). Most abundant rock forming minerals are quartz, sericite, K-feldspar and chlorite, but the formation contains silicified, and albitized and silicified K-metasomatite bodies with peculiar parageneses.

The Mn-U-apatite-F layer contains up to 22 wt% P_2O_5, 23 wt% MnO, 320 ppm Be, 600 ppm U, 320 ppm W, 40 ppm Sn, 53 ppm Tl in bulk samples. The layer is built up of dominantly zoned apatite-F, quartz, smectite 15Å, cryptomelane, pyrolusite, todorokite, illite, nontronite, halloysite 10Å, phlogopite-F? and albite. Minor amounts of barite, cassiterite and rutile were found by SEM. The apatite-F contains ca. 12.5 m/m% carbonate CO_3^{2-} substitution in the PO_4 anionic site, and the $n_3PO_4^{3-}$ vibration shifts towards lower values, which can be the effect of distorted crystal structure caused by Be substitution according to IR investigations. LA-ICP-MS measurements of this assemblage proved that apatite-F, high F-phlogopite, clay minerals and Mn-oxides usually contain varying amount of Be (up to ca. 2500 ppm) and sometimes associated Li (up to ca. 2500 ppm).

The K-metasomatite bodies and quartz-feldspar veins contain quartz, orthoclase, albite, rutile with high W and Nb content (Figure 1), anatase, ilmenite, adularia, xenotime, monazite, cacoxenite, Nb-oxides, columbite-Fe-Mn solution, several sulfides, native gold and silver. The rare minerals typically occur in veins. Ti, Nb, W, Sn, Li and REE are enriched in this material. Both mineralogical and trace element compositions resemble a REE pegmatite. Possible genetic models are 1. intrusion (aplite) or pegmatitic impregnation from a highly evolved magma in the final phase of the rhyolite volcanism or 2. K-metasomatism from a subsequent peralkaline volcanism (Carnian metabasalt formation).

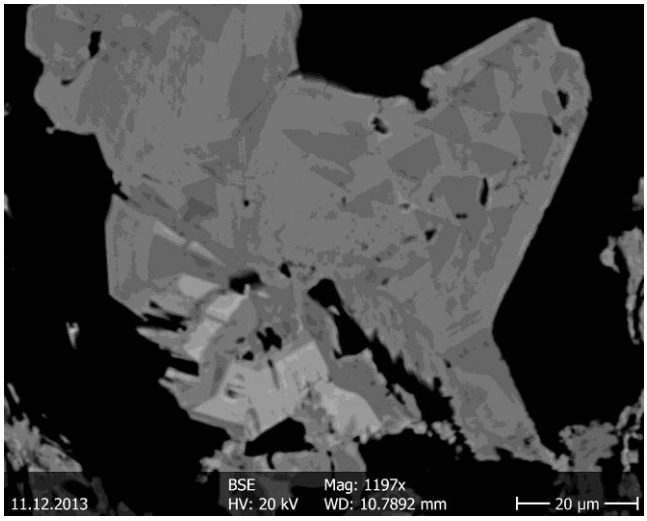

Figure 1: W and Nb zoned rutile, BSE image.

Acknowledgement: The research was carried out with the financial support of the "CriticEl" project, TÁMOP-4.2.2.A-11/1/KONV -2012-0005.

[1] Csáki F. and Csáki F.-né (1973). Összefoglaló jelentés a bükkszentkereszti kutatási területen 1969-1973 között végzett kutatómunkáról [Summary report on the prospecting at the Bükkszentkereszt area between 1969 and 1973]. Mecseki Érckutató Vállalat. Handwritten report. Mecsekérc Zrt. Adattár, Kővágószőlős, 289 pp.

Assessment on the rare metal ore mineralization of the selected areas in central Africa (Republic of Burundi)

Baibatsha A*, Dyussembayeva K, Kassenova A

1 - Kazakh National Technical University named after K.I. Satpayev
*baibatsha48@mail.ru

Tantalum and niobium rare metal ore mineralization (Burenge, Nyanza, Majuri, Santa Maria, Perimeter Ammg) is located in the territory of the Republic of Burundi (Central Africa). Placer samples have been selected and studied in a preliminary assessment of the ores. The selected areas on the tantalum-niobium ore mineralization are confined to the north-western slope of the Kibaransky Folded Belt.

To obtain objective results the placer samples have been studied for all grain-size classes, with the most informative class +0.1-0.25 mm. The results of spectral analysis of placer samples and data on the distribution of minerals of Ta and Nb in all classes showed that in all areas intermediate members of minerals of Ta and Nb (tantalite-columbite, columbite-tantalite) were prevalent but that end member tantalite and columbite were also present. Variations of minerals of Ta and Nb fluctuate within areas but there is sometimes a predominance of either tantalum or niobium end members: the tantalum component predominates in Majuri and Burenge, while niobium predominates in Burenge 7, Burenge Santa Maria and Santa Maria. The concentration of the minerals of Ta and Nb by approximate calculations is the highest in Burenge 7. Their quantity approximately halved in areas Majuri, Burenge 5, Burenge Santa Maria, with a more significant reduction in the rest. The content of Ta and Nb in the separately selected minerals is distributed as follows: Nb is expectedly in higher concentrations than Ta in columbite and tantalite-columbite, and there are equal concentrations of Ta and Nb in tantalite. The high contents of Ta and Nb in cassiterite are caused by inclusions of tantalite or columbite or their intermediate members in the mass of cassiterite. In other minerals and rocks (ilmenite, magnetite, kaolinite, pegmatite) the content of Ta and Nb is less. However, Ta and Nb are enriched in weathered greisens.

Plumbotantalite has been initially identified using the results of microprobe analysis. It contains significant concentrations of Pb - 25-29%, and Ta predominates over Nb. This contrasts with the literature, where plumboniobite ($(Ca, Pb, Fe, Y, U)_2 Nb_2O_7$) contains 8% Pb. Plumboniobite is a variety of the mineral samarskite $(Fe,Y,U)_2 (Nb, Ti, Ta)_2O_7$.

Geology of the heavy rare earth element-rich Lofdal Alkaline Carbonatite Complex, north west Namibia

Do Cabo V[1*], Wall F[2], Swinden S[3], Loye E[2], Ellmies R[4]

1 - Geological Survey of Namibia, Ministry of Mines and Energy
*vdocabo@mme.gov.na 2 - Camborne School of Mines, University of Exeter 3 - Swinden Geoscience 4 - Kunene Resources Limited

The Lofdal Alkaline Carbonatite Complex (LACC) is rare amongst carbonatites in that it contains the mineral xenotime-(Y) and is a potential economic deposit of heavy rare earths.

Carbonatites are the world's main source of the rare earth elements (REE) required for many digital and clean technologies but they are almost always strongly enriched in the low atomic number 'light REE' (LREE), La- Nd, compared to the higher atomic number members of the series that are classed as mid (Sm, Eu, Gd) and heavy REE (Tb - Lu). It is deposits of these mid and heavy REE that are currently the most sought after of the REE in order to provide diversity of supply from the ion adsorption clay deposits in southern China. Lofdal is thus more than a curiosity, it is an important new deposit, from which lessons may be applied to other carbonatite and alkaline complexes in order to improve exploration success for HREE. At the time of writing, it is the only HREE-enriched carbonatite under exploration, and the most HREE-enriched carbonatite described so far.

The swarm of carbonatite and phonolite dykes at Lofdal and the nearby syenite and nepheline syenite plugs called Oas were first noted during early regional mapping . Preliminary exploration was done, plus various geochronology studies and work on the petrogenesis of the syenites. Wall *et al.* [1] published the first detailed account of the xenotime-(Y) at Lofdal. A recent PhD study [2] together with exploration by Namibia Rare Earths Inc. has now identified additional carbonatite and phonolite dykes (total now over 1000 in an area of up to 200km^2, many LREE and HREE-enriched) and two larger carbonatite plugs, plus HREE mineralised zones, metasomatised rocks, breccias, nepheline syenite plugs, breccias and mafic rocks including a lamprophyre.

This paper describes the geology of the Lofdal Alkaline Carbonatite Complex, including its geochemistry and major mineralogy. It then discusses how Lofdal compares to other carbonatites, including other REE deposits, in order to understand better why the HREE are concentrated at Lofdal.

[1] Wall F. *et al*. (2008). *Canadian Mineralogist*, 46, 861-877.

[2] Do Cabo V.N. (2013). Unpublished PhD thesis, University of Exeter, UK.

An initial study on geochemical behavior of scandium associated with laterization in INFANTA nickel mine, Palawan, Philippine

Noda K[1*], Yonezu K[2], Gabo J[3], Santos R[4]

1 - Kyushu University, Japan *noda.cos@gmail.com 2 - Department of Earth Resources Engineering, Kyushu University 3 - Research Institute of Environment for Sustainability, Kyushu University 4 - MacroAsiaMiningCorporation

Nowadays high technology industries demand REE (Rare Earth Elements) including scandium and yttrium. However, price instability, substitution of alternative materials and development of technologies that use lower amounts of REE led to a decrease in demand and prices from the latter half of 2011 and is one of the problems for companies trying to open new REE mines. Thus, in terms of the economic aspect, recovering REE as a by-product from operating mines is a possible way to supply additional REE. The fact that most heavy REE are supplied from weathered granite deposits was the motivation for us to study REE including Sc related to the formation of Ni laterite. In addition, Sumitomo Metal Mine released news of its plan to build a pilot plant to recover scandium from nickel laterite at the Coral Bay Project, Rio Tuba, Palawan during 2014. Therefore, this study aims to understand the geochemical behavior of REE including Sc in Ni laterite working towards the possibility of REE and/or Sc production as by-product at MacroAsia's Infanta nickel area. The Southern Palawan study area has Ni laterite derived from ultramafic rocks, mainly harzburgite, related to ophiolite. The Sc content of the host rock is 6 ppm while the laterite shows 45 - 71 ppm, giving a very high concentration coefficient of around 10. There is positive correlation between Sc and Fe contents but not Ni. As Ni extreme enrichment is the result of the presence of garnierite, at least, garnierite formation is not related to concentration of Sc. The mineralogy of Sc is still ambiguous, however our preliminary extraction experiment suggests that coprecipitation of iron secondary minerals may have an important role in the concentration of Sc.The other REE show a different geochemical behavior. Total REE (except for Sc) contents of the host rock and laterite are 1.39 and 1.38 - 56.6 ppm, respectively. However, total REE contents have no clear correlation with iron oxide or laterization index (SiO_2 / (SiO_2+Al_2O_3+FeO)). Instead, concentrations of REE normalized to Th, which is immobile under the acidic geochemical conditions, showed a clear trend down the vertical profile of laterite. This result implies that that REE are leached out and transported to the deeper portion, then concentrated at the base of the laterite profile.

Petrology, geochemistry and petrogenesis of northern Palawan granites: implications on the rare-earth element mineralization

Padrones J[1*], Ujihara H[1], Imai A[1], Takahashi R[1], Tani K[2]

1 - Akita University *jenpadrones@gmail.com 2 - National Museum of Nature and Science, Tokyo

Significant exploration for rare metals brought about by increasing demand and diminishing supply are currently underway in the global scenario. Areas with felsic igneous complexes are revisited in order to find significant rare earth element (REE) concentration during magmatic differentiation processes. In the Philippines, the granitic intrusions are spatially distributed in northern Palawan, a rifted fragment of the southeastern Eurasian margin during the opening of the South China Sea basin. The granitic intrusives being investigated in this study are the recently recognized Cretaceous El Nido granitoids and the Middle Miocene Kapoas granitoids located in San Vicente. The El Nido granitoids include granodiorites and granites with minor biotite while the Kapoas granitoids include granites and granodiorites. The latter is composed of metaluminous, high-K calc-alkaline, I-type and ilmenite-series type granitoids. The rocks were mostly biotite-rich and contain xenoliths of schists and diorite, quartz xenocrysts, and mafic enclaves. Both granitic bodies and their weathered crust show LREE enrichment. The LREE concentration is higher in San Vicente than that of El Nido granitoids. Also, heavy mineral analysis of stream and beach sediments shows that REE-bearing minerals are only present in the San Vicente area. The REE-bearing minerals identified in San Vicente are allanite $(Ca,Ce,La)_2(Al,Fe)_3O(OH)SiO_4Si_2O_7$) and yellow igneous monazite $(Ce,La,Th)PO_4$). Both are enriched in LREE's such as Ce, La, and Nd associated with the radioactive element Th. The beach sediments concentrated in heavy minerals along the beach in Erawan and Ombo area contain up to >10,000 ppm of La, Ce, Nd and Sm.

Hydrothermal alteration and base metal-REE mineralization in granitoids at Panyabungan and its surroundings of North Sumatra, Indonesia

Setiawan I*, Takahashi R, Imai A

Akita University * bungafatharani@yahoo.com

Granitoids with REE and base metal mineralization are recognized in the Panyabungan area and its surroundings at the western part of North Sumatra, Indonesia. In the study area, at least two periods of granitoid formation are recognized in Permian-Triassic and Miocene ages. In the eastern part of Sumatra, granitoids have been considered as source rocks of tin and REE resources, whereas at the western part, granitoids are related to gold and base metal mineralization. However, detailed study of granitoids on the western area has not been done yet, especially for REE mineralization. The aim of this paper is to describe geological features of the hydrothermal alteration, and base metals-REE mineralization on the basis of the mineralogical and geochemical study. Most of granitoids in the study area are hydrothermally altered and mineralized. They have formed within Volcanic Arc Granite (VAG), indicating both magnetite and ilmenite series characteristics, except Sibolga Granitoids that were formed as within plate granite (WPG) indicating ilmenite series characteristics. Furthermore, the Sibolga Granitoids are associated with uranium, thorium and molybdenum mineralization, as represented by the occurrence of umohoite. Granitoids in the study area consist of granite, diorite, and granodiorite, which are composed of potassium feldspar, quartz, biotite, muscovite, and hornblende and accessory minerals such as zircon, allanite, monazite, sphene and apatite. Prophylitic alteration is present in the granitoids with mineral assemblages of chlorite, epidote, calcite, sericite-muscovite, silica, adularia, clay minerals and +/- tremolite. Ore minerals of magnetite, ilmenite, hematite, galena, pyrite, chalcopyrite and sphalerite occur as disseminations. The Sibolga granitoids show the highest LREE enrichment followed by Panyabungan, Kotanopan and Muarasipongi granitoids.

The lorandite experiment (LOREX): lorandite age and erosion rates at Allchar ore deposit

Amthauer G[1*], Anicin I[2], Boev B[3], Bosch F[4], Cvetkovic V[5], Henning W[6], Niedermann S[7], Pavicevic M[1], Pejovic V[2]

1 - University of Salzburg *georg.amthauer@sbg.ac.at 2 - Institute of physics Belgrade 3 - University of Stip 4 - GSI Darmstadt 5 - University of Belgrade 6 - TU Munich 7 - GFZ Potsdam

LOREX, the acronym for LORandite EXperiment, attempts the determination of the solar neutrino flux by measuring the ^{205}Pb content in the thallium-bearing mineral lorandite, $TlAsS_2$, from the mine of Allchar, FYR Macedonia, which is there formed via the neutrino-capture reaction $^{205}Tl + \nu_e \rightarrow {}^{205}Pb + e^-$. This geochemical detector offers the lowest threshold among all the detectors of only 52 keV for solar pp-neutrinos. The final step of LOREX, which is now underway, is the extraction of lorandite, while the ensuing quantitative determination of the ratio of ^{205}Pb / ^{205}Tl atoms would provide the product of solar neutrino flux and neutrino-capture cross section, integrated over the age of lorandite of 4.31×10^6 yr. The cosmogenic ^{205}Pb produced by fast muons, which constitutes the main component of background, is strongly depth-dependent and very sensitive to the long-term erosion history of the field area. It is estimated that, depending on palaeo-depth, 10 kg of lorandite contains about (3.5 -11.6) x 10^5 atoms of ^{205}Pb. This report presents new data on the accurate geological age of the minerals at Allchar, as well as the recent results for erosion rates at two lorandite rich locations. These are based on the accelerator mass spectrometry determination of ^{10}Be and ^{26}Al in characteristic samples as well as on the independent geo-morphological studies. Provided that the thus determined high values of erosion rates are corroborated by remaining measurements of additional samples, the experiment is expected to reach an acceptable signal-to-background ratio.

The light absorption characteristic of pyrite

Huang F*, Liu J, Meng L, Dan S, Gao W, Gao S, Yang D, Liu R

Northeastern University. *huangfei@mail.neu.edu.cn

Pyrite is a sulfide mineral widely found in nature. A previous study found that pyrite is a potential solar cell material, which not only has a suitable band gap (Eg = 0.95eV) and a high optical absorption coefficient (when $\lambda<750$ nm, $\alpha>6\times10^5$ cm^{-1}), but is also non-toxic, environmentally friendly and inexpensive. High quality pyrite was obtained through a series of refinements in the preparation of crystal and thin films. The morphology, composition, structure and photo electricity of pyrite have been researched, but not deeply enough. To study the optical absorption property of nano-micron pyrite systematically, our research group carried out research on both natural pyrite and hydrothermal experiment products.

The research group collected specimens from different ore deposits and selected well crystallized ones for further research. The studies found that pyrite formed under different geological conditions was also different in particle size, morphology, crystallization degree, trace element content, inclusions and defects. Furthermore, electronic conductivity variation between types of pyrite caused differences in light absorption and resulted in unstable performance of the pyrite solar cell, which is hardly usable.

The morphology, composition and structure of nano-micron granular pyrite synthesized from hydrothermal experiments were measured by using SEM, XRD and TEM methods. The results show that the products are mainly combination forms of cube and pentagonal dodecahedron, and a small amount of cubic and octahedral crystals. The product diameters are about 2~5 μm, and some are nanoscale. Most of the products are pyrite and contain a little orthorhombic pyrrhotite. The Cary 500 UV-Vis-NIR spectrophotometer showed an absorption peak at about 1879 nm in the 200-2000 nm test range, and the absorption spectrum is small. The band gap of the product is 0.6578 eV, calculated from the band gap formula.

Due to variety in particle size and morphology of products, the surface-exposed atoms and the light absorption of surface atomic structure are different. So, the band gap and the optical absorption coefficient are different from the theoretical values. The presence of sulfur vacancy defects and impurities (pyrrhotite) can also affect the band gap of pyrite.

In summary, the morphology, particle size, sulfur vacancy defects, and impurity phase of pyrite formed under different conditions are the important factors affecting the optical absorption properties of pyrite.

Polymer-derived ceramics; microstructure and high-temperature stability - a TEM study

Kleebe H-J

Technische Universität Darmstadt. kleebe@geo.tu-darmstadt.de

Hf-doped silicon oxycarbide and carbonitride ceramics were studied by transmission electron microscopy (TEM) upon isothermal annealing at 1300 °C for 1 to 200 hours. TEM investigations in conjunction with energy-dispersive X-ray spectroscopy (EDS) analysis revealed a pronounced reduction of the local carbon content in close proximity to internal surfaces. Such small microcracks are a consequence of the polymer-to-ceramic transition and, hence, are commonly formed upon thermal annealing. A systematic study of the degradation of SiCO and SiCN was performed, in particular, with focus on the carbon (and nitrogen) depletion in the vicinity of internal surfaces. The profiles of the carbon content between surface and bulk were analyzed employing error functions to yield carbon diffusivities. Apart from the lowering of the carbon content, surface crystallization of cristobalite was also observed after an incubation period of approximately 5 hours. The presented results clearly imply that the frequently- reported high thermal stability of such polymer-derived ceramics is rather limited, especially when thin film applications are anticipated.

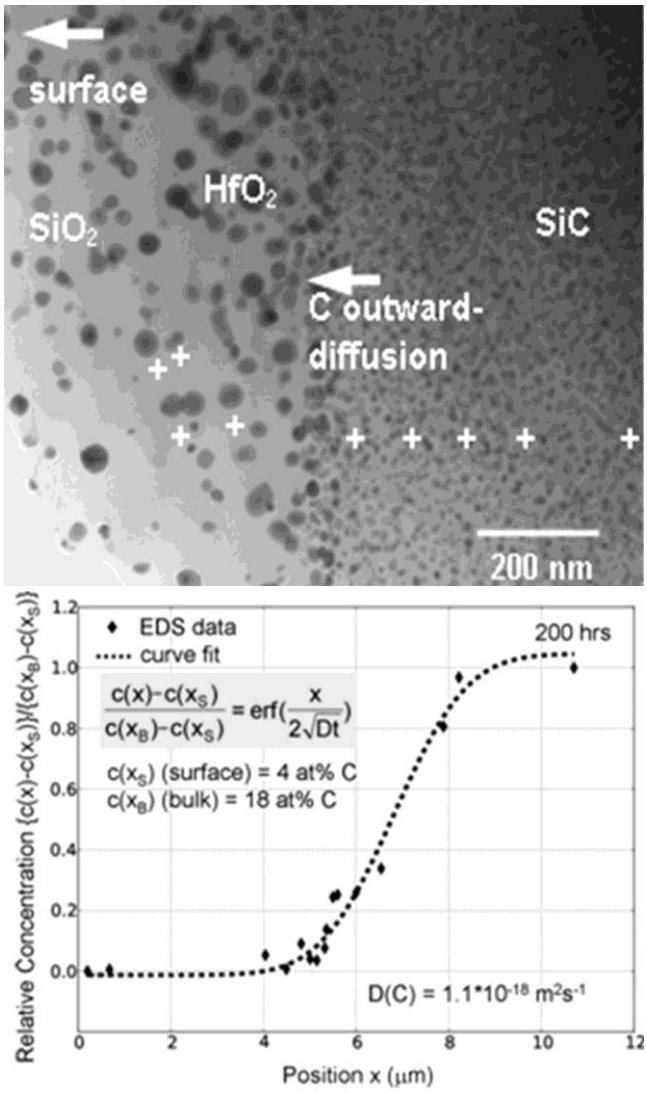

Figure 1: TEM bright-field image of the SiOC-Hf sample annealed at 1300 °C for 200 hrs. Electron beam positions for the EDS measurements are indicated. The carbon concentration depends on the proximity to the surface. The HfO_2 particle size distribution is correlated with the C concentration profile [1].

[1] Nonnenmacher, K. *et al*. (2013). *J. Am. Ceram. Soc.* 96(7) 2058-2060.

Recycling of waste plastics into cokemaking

Melegy A[1*], Sýkorová I[2], Havelocova M[2]

1 - National Research Centre *amelegy@yahoo.com 2 - Institute of Rock Structure and Mechanics, Prague

Recently, there has been an increase in interest in the pyrolysis of waste plastics as a route to waste minimization. Metallurgical coke manufacture is a valuable alternative to the use of mixed plastic wastes for feedstock recycling. Processing of the plastic wastes and co-processing with other organic raw materials by means of pyrolysis under a controlled atmosphere were used for the production of liquid fuels and carbon materials. Mixtures of coal and waste plastics were pyrolyzed using a coke oven (IRSM) with the addition of 0, 5, 20 % of plastic waste.

The distribution of organogenic elements (C, H, N, S, O) into the final products of pyrolysis was ascertained. Coke prepared from original coal presents as a relatively hard and porous material. It's matrix consists of isotropic, partly fused matter with pores and fewer desiccation cracks. An increase in addition of waste plastic causes a higher proportion of fused coke matrix and random reflectance values which vary between 5.80 % and 5.95 %. The optimal resistance and microscopic texture of coke were found in the sample produced from a blend of coal and 5 % waste plastic. The results demonstrated that co-processing with 5 % of waste plastics is promising for coke, tar and gas production.

Nucleation and grain growth in LiF-doped Mg-Al-spinel

Mueller M[1*], Rubat du Merac M[1], Stricker K[1], Kleebe H[1], Reimanis I[2]

1 - Technische Universität Darmstadt *mueller@geo.tu-darmstadt.de 2 - Colorado School of Mines

$MgAl_2O_4$ is considered a promising material for optical applications and hence has been researched for more than 40 years worldwide [1]. The densification mechanism of $MgAl_2O_4$ doped with lithium fluoride (LiF) as a transparent ceramic has been intensively studied.

Optical transparency requires densification to a value near the theoretical density since residual porosity, which acts as scattering source, has to be eliminated. In addition, impurities and secondary phases have to be removed to avoid scattering or absorption of the transmitted radiation (visible or IR light).

LiF greatly reduces the sintering temperature and facilitates densification at lower temperatures. However, the basic mechanisms behind the sintering process are still not fully understood, as neither LiF nor an additional secondary phase is detectable in the final product.

Based on individual studies [2-4], Reimanis, Kleebe and Rozenburg postulated three major processes during sintering of spinel with LiF including (i) enhanced volume diffusion by incorporation of O-vacancies, (ii) dissolution – reprecipitation, and (iii) wetting – dewetting. In a recent work it was shown that these mechanisms occur simultaneously interacting with each other [5].

Since conventional sinter regimes for this material system are pressure-supported the geometry of sintered devices is limited. Therefore, the overall aims of the present study are (i) to verify the postulated mechanisms, and (ii) to transfer this knowledge to a pressure less sinter process.

Based on dedicated model experiments and a characterization using *e.g.* electron microscopy it was shown for the first time that (a) a dissolution-reprecipation process occurs at significantly lower temperatures by the formation of a variety of transient phases (Figure 1), (b) a vapour transport mechanism leads to a notable mass transport involving the magnesium, and (c) an exaggerated grain growth of a second generation of spinel hinders the densification process.

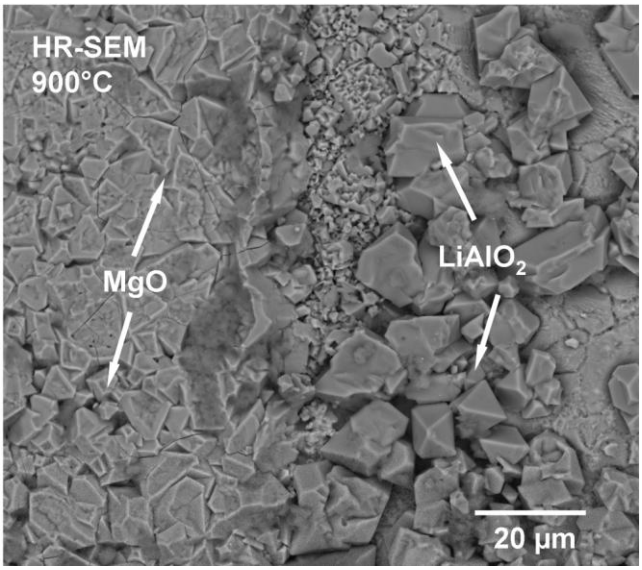

Figure 1: HR-SEM micrograph of MgO and $LiAlO_2$ as transient phases observed in a model experiment at a sintering temperature of 900° C.

[1] Rubat du Merac M. *et al.* (2013) *J. Am. Ceram. Soc.*, 96 (11), 3341-3365.
[2] Reimanis I. E. *et al.* (2007). *J. Am. Ceram. Soc.*, 98 (12), 1273-78.
[3] Rozenburg K. *et al.* (2007) *J. Am. Ceram. Soc.*, 90 (7) 2038-2042.
[4] Rubat du Merac M. *et al.* (2013). *Int. J. App. Ceram, Tech.*, 10 (SI) E33-E48.
[5] Müller M.M. and Kleebe H-J. (2013). *J. Am. Ceram. Soc.*, 95 (10) 3022-3024.

Mineralogical study of natural oxygen carriers for chemical looping combustion and subsequent CO_2 storage

Schopf A[1*], Mayer F[2], Massonne H[1]

1 - Inst. für Mineralogie und Kristallchemie, Universität Stuttgart *alexander.schopf@mineralogie.uni-stuttgart.de 2 - IFK, Universität Stuttgart

Chemical looping combustion (CLC) is a new technology for burning solid, liquid and gaseous fuels in power plants. The exhaust gas of this technique is pure CO_2 which can be collected and stored. Another benefit is the avoidance of NO_x. CLC requires an oxygen carrier (OC) for the combustion process. The OC is reduced in the fuel reactor, transported to the air reactor, and oxidized by air. Afterwards, the OC can be used again for the next combustion cycle.

The target of this study was to identify environmentally-friendly, natural OCs with the following characteristics: high abrasion resistance, high reactivity with the combustion gases (CO, H_2 and CH_4), high oxygen carriage capacity, good price-performance ratio, and thermal stability up to 1000 °C. For this purpose, commercially available Fe, Mn, and Cr ore concentrates were selected. These concentrates consisted either mainly of magnetite (provenance: South Africa, Norway, Brazil, Vietnam), hematite (Austria, Mauritania, Germany), ilmenite (Australia), hausmannite (South Africa) or chromite (South Africa). These potential OCs were studied by thermal gravimetric analysis (TGA) to simulate the conditions in a CLC power plant. The applied TGA was therefore enhanced by a gas mixture facility for safe and fast switching from combustion gas to air. Thus, the selected oxides could be heated to 900 °C in presence of a combustion gas or air. Afterwards, this cycle was repeated several times. Before the TGA study, the oxides were crushed and sieved to particle sizes between 125 and 250 µm to ensure comparable test conditions. Before and after the treatment in the TGA, we analyzed the OCs using a polarizing microscope, a C-H-analyzer, an X-ray powder diffractometer, an X-ray fluorescence spectrometer, and an electron microprobe.

For example, granular ilmenite and a platy hematite (MIOX® ME 400 from the Kärntner Montanindustrie) endured more than 12 oxidation-reduction-loops. The ilmenite grains continuously accumulated TiO_2 at their rims and in many cases a layer of iron oxide on top, whereas the hematite developed holes inside the grains. Both materials were still functional as OC. After testing the suitability of potential OCs in the TGA, large-scale experiments were also performed in an electrically heated 10 kW_{th} test power plant at IFK (Institute of Combustion and Power Plant Technology), Universität Stuttgart. It could be demonstrated that the studied natural OCs are capable of being used in CLC power plants.

Nanocomposite assembly based on delamination of montmorillonite and layered double hydroxide

Wang L*, Xie X

Guilin University of Technology. *wlinjiang@163.com

Delamination of layered solids followed by restacking the exfoliated layers in the presence of guest species is a good method for the preparation of well dispersed layered nanocomposites. In this work, montmorillonite (MMT) and layered double hydroxide (LDH) were used as starter materials to study nanosheet delamination and assembly because they are typical cation and anion clay minerals, respectively. The delamination of clay minerals was achieved by dispersing the modified MMT and LDH in formamide and ethyl alcohol during heating, stirring and ultrasonic treatment to obtain nanosheet delamination colloidal dispersion. Solvothemal treatment and electrostatic adsorption methods were used to study the assembly behaviour of MMT and LDHs and prepare assembly composites. The results show that the thickness of clays changed from pristine 250 nm to several stagger lamellas, and finally about 7 nm which corresponds to several monolayers. The assembly composites show higher thermal stability and poor spinel formation, and hence better structure reconstruction as compared to the pristine clays.

Stability of kimberlite garnets exposed to chemical weathering: relationship with Cr content

Afanasyev V*, Pokhilenko N, Snegirev O, Tychkov N

Sobolev Institute of geology and mineralogy, Siberian branch. *avp-diamond@mail.ru

Garnets from kimberlites, mainly pyropes, exposed to chemical (lateritic) weathering are unstable and dissolve to produce distinct corroded surface patterns, the orange low-Cr garnets being less stable than violet Cr-rich varieties. As a result, the placer assemblages that underwent alteration in laterite weathering profiles consist mostly of violet pyropes, with few orange ones, and have generally higher bulk Cr_2O_3 contents. This fact has important practical implications as it imposes limitations on direct chemical comparison between placer and primary kimberlite-hosted garnets as a way of identifying trains of kimberlite indicator minerals.

The objective of this study was to estimate the relative dissolution stability of garnets of different paragenesis and that differ in Cr_2O_3 contents. The relative chemical stability of garnets from kimberlites has been studied in HF etching experiments which are a good model of natural lateritic weathering. Etching was applied to a large collection of pyrope grains which represented the whole paragenetic diversity of kimberlite garnets. The experiment lasted 42 days and included weight loss monitoring and EMPA of the residue.

Natural garnets of different paragenesis were studied in the pairs "kimberlite-placer" ("Mir kimberlite - Vodorazdelnye Galechniki (*Watershed Pebble*) placer"), the placer known to be derived from the Mir kimberlite and to have undergone laterite weathering (dissolution) in the Middle Paleozoic. Additionally, we analyzed garnets from unweathered dense kimberlite and related eluvium at the XXIII CPSU Congress pipe. Each grain from the representative natural collection was likewise studied by EMPA and identified in terms of its paragenesis.

Comparison of the pairs "kimberlite - placer" and "fresh - weathered kimberlite" (XXIII CPSU Congress pipe) reveals greater Cr_2O_3 contents in weathered kimberlite than in fresh garnet assemblages.

The data on natural garnets agree with the experimental evidence. The weight loss curves for pyrope grains grouped according to their parageneses show greater weight loss in low-Cr pyropes, *i.e.*, dissolution stability is proportional to Cr_2O_3 contents.

Nanoanatase as accessory mineral of clay cover from lateritic profile

Costa M[1*], Pöllmann H[2], Figueira B[1], Kaden R[3], Goeske J[4]

1 - UFPA *marcondeslc@gmail.com 2 - MLU 3 - University of Halle 4 - ZWL Lauf

Anatase is a virtually ubiquitous accessory mineral found in Cenozoic lateritic formations, especially those containing bauxite deposits. In older formations anatase is rarer, and seems to have been transformed by diagenesis and even metamorphism of rutile. In lateritic formations and tropical soils the anatase has only been identified by X-ray diffraction and has not yet appeared in publications showing images, crystals size and chemical composition from bauxite formations. On the other hand, in sedimentary and metamorphic rocks and some veinlets and pockets, anatase occurs as a sub millimetre to centimetre crystals, when its crystalline structure including its possible applicability to radiometric dating is described. In Amazon lateritic formations the anatase is always present, but only recognized by XRD and its abundance inferred from TiO_2 bulk contents, when other Ti minerals are absent according to XRD analysis. As part of a major project this work aims to demonstrate that anatase is a typical accessory mineral of the lateritic clay cover formation (Belterra Clay). In laterite profiles anatase is a neoformed nanomineral, litho dependent in concentration and maybe one of the key minerals to understand the lateritisation and laterite alteration. To study it in the clay cover it was extracted and concentrated by chemical methods. Anatase in these formations occurs mainly as crystals of 20 to 200 nanometers along the main axis. Crystallites (SEM images) normally present a tetragonal shape with a short prism, diffuse edges, though prismatic bipyramidal crystals occur. Its XRD pattern is characteristic, with high crystalline order and, among several analyzed samples, no variation of unit cell dimensions was observed along the cover. The smaller crystallites show diffuse shape and size of kaolinite crystallites. Nanoanatase and nanokaolinite in the clay cover are, thus, intimately linked and physical separation was not possible. Anatase crystallites seem to be formed early on the clay saprolite horizon of the laterite profile from primary silicate decomposition and then remain stable along the whole profile except in the clay cover, where it has been concentrated. So nanoanatase is a natural mineral typical from clayey cover (Belterra Clay) from laterite-bauxite formations.

Thermal diagenesis in the phosphate-sulfate sequence from Gura Dobrogei Cave, Dobrogea, Romania

Dumitras D[1*], Marincea S[1], Diaconu G[2]

1 - Geological Institute of Romania *d_deliaro@yahoo.com 2 - Emil Racoviţă Speleological Institute

Gura Dobrogei Cave is located in Constanta County, Dobrogea Region, Romania, about 3 km west of the homonymous locality, and about 40 km NNW from Constanta, the major city in the area. The cave is also known as the "Bat Cave" (Pestera Liliecilor) of Gura Dobrogei. It seems to represent an upper (fossil) level of a karstic system that developed on Visterna Brook, affluent of Casimcea Valley, and is developed in Upper Jurassic limestone of the Casimcea Syncline. A rich deposit of fossil bat guano is hosted by two of the galleries of the cave: the E-W oriented "Gallery with Ceramics" and the N-S oriented "Gallery with Fossils". Two primary mineral associations developed as a result of the guano-derived phosphate and sulfate assimilation by the bedrock: (1) taranakite with relics of illite, kaolinite quartz and minor gypsum, and hydroxylapatite on the clay-rich, innings bedrock, and (2) hydroxylapatite, brushite, ardealite, and gypsum on the carbonate bedrock or in fallen carbonate blocks in the guano mass. Thermal diagenesis affected both mineral associations locally, resulting in the following documented evolutions: (A) taranakite [*a* = 8.694(2) Å, *c* = 94.98(4) Å] was partially replaced by francoanellite [*a* = 8.695(2) Å, *c* = 82.438(23) Å]; (B) gypsum [*a* = 5.679(4) Å, *b* = 15.202(9) Å, *c* = 6.523(5) Å and *beta* = 118.46(2)°] was partially replaced by bassanite [*a* = 12.099(3) Å, *b* = 6.919(1) Å, *c* = 12.689(4) Å and *beta* = 90.46(2)º]; (C) brushite [*a* = 5.797(2) Å, *b* = 15.163(7) Å, *c* = 6.228(3) Å and *beta* = 116.28(2)°] was partially replaced by monetite [*a* = 6.919(7) Å, *b* = 6.667(9) Å, *c* = 6.919(7) Å, *alpha* = 94.17(3)º, *beta* = 104.06(6)º, *gamma* = 87.25(8)º], and (D) ardealite [*a* = 5.724(3) Å, *b* = 30.977(13) Å, *c* = 6.261(4) Å, *beta* = 117.25(3)°] was partially replaced by monetite [*a* = 6.912(4) Å, *b* = 6.680(5) Å, *c* = 6.963(4) Å, *alpha* = 96.35(8)º, *beta* = 103.90(3)º, *gamma* = 88.73(7)º] and bassanite [*a* = 12.046(11) Å, *b* = 6.921(8) Å, *c* = 12.749(13) Å, *beta* = 90.05(6)º]. Topotactic substitutions were observed in the cases of francoanellite on taranakite, bassanite on gypsum and monetite on brushite, respectively. Francoanellite, bassanite and monetite formed during a later diagenetic stage affecting guano, typical for the "dry" karst systems, and were found in the driest part of the cave. This stage of diagenesis was characterized by temperatures of up to 80 ºC, and critically depends on the exothermal reactions in the the guano mass. These reactions prompted the oxidation of organic matter in the guano itself and of allogenous pyrite and may be correlated with the presence of $(SO_4)^{2-}$ in the late solutions that leached the guano mass.

Superposed parageneses in the gehlenite-bearing, high-temperature skarns from Oraviţa (Banat, Romania)

Marincea S[1*], Dumitras D[1], Ghinet C[1], Bilal E[2]

1 - Geological Institute of Romania *marincea@igr.ro 2 - Ecole Nationale Supérieure des Mines de Saint-Etienne, France

A shallow-level dioritic pluton of Upper Cretaceous age caused extensive contact metamorphism of a Callovian - Aptian calcareous sequence at Oraviţa - Ciclova (Banat, Romania), at about 35 km SSW of Reşita, the major city in the area. The resulting high-temperature skarn can be better observed on Crişenilor Brook, where it crops out at about 200 m upstream from its confluence with the Oraviţa Valley. The skarn from Crişenilor Brook is clearly zoned, the zones being individualized by the massive presence of one distinct mineral species. This zoning is, from the outer to the inner part of the metasomatic area: calcite (marble) / vesuvianite (+ wollastonite 2M) / gehlenite / plagioclase + diopside + calcic garnet / diorite. The inner endoskarn is largely dominated by the abundant development of calcic garnet (Grs 33.78 - 82.07 mol.%, Adr 13.45 - 64.36 mol.% with up to 9.47 mol.% morimotoite in the solid solution), titanite and diopside, in a mass conserving albite-substituted plagioclase (An 14 - 42 mol.%) and orthoclase (Or 95-97 Ab 5-3). The outer endoskarn is practically monomineralic, consisting of a gehlenite groundmass (åkermanite 34.10 - 51.18 mol.%, Na-melilite up to 3.60 mol.%) with minor monticellite (with 8.53 to 11.66 mol.% kirschsteinite and from 0.91 to 2.52 mol.% glaucochroite in solid solution), grossular-andradite (Grs 34.05 - 86.27 mol.%, Adr 10.23 - 64.41 mol.% with up to 3.80 mol.% morimotoite in the solid solution), wollastonite (the 2M polytype), hydroxylellestadite, vesuvianite, pyrrhotite, scarce magnetite and fukalite and secondary minerals such as hibschite, thomsonite, tobermorite, calcite and allophane. The exoskarn is also monomineralic, consisting of a mass of vesuvianite, with minor wollastonite, clintonite, aluminian diopside, hydroxylellestadite, scarce andradite, and secondary clinochlore, talc and scolecite. Based on the reciprocal relationships of the main mineral species we identified four different mineral assemblages that correspond to different stages of the metasomatic evolution. The peak metamorphic assemblages (stage I) include wollastonite, gehlenite, diopside, grossular-andradite, perovskite, pyrrhotite. A second, subsequent paragenesis (stage II) is partly retrograde and includes magnetite, monticellite, titanian garnet, vesuvianite, aluminian diopside, hydroxylellestadite, clintonite and occasional fukalite. A late hydrothermal stage (stage III) produced retrogression of the first two stages and a paragenesis including hibschite, clinochlore, talc, scolecite and thomsonite. A weathering paragenesis, corresponding to the late stage of evolution, is also present, and prompted the formation of aragonite (probably on portlandite), calcite, tobermorite and allophane. The compositional data combined with experimentally established and calculated equilibria accounts for a peak temperature of ~750 °C that perfectly agrees with the temperature estimated for the dioritic magma.

Changes of mineral composition and microstructure of silica refractory raw materials during firing

Všianský D[1*], Lang K[2], Kotouček M[2]

1 - Department of Geological Sciences, Masaryk University *dalibor@sci.muni.cz
2 - P-D Refractories

Silica refractory serves as a lining of coke furnaces, hot blast stoves, and glass furnaces. It is produced by firing with the maximum temperature about 1430 °C and 12 hours soaking. Silicic rocks containing more than 93 wt % of SiO_2 are the basic raw materials of silica refractories. The final mineralogical composition of the silica depends on firing and the action of mineralizers. It mostly consists of two polymorphs of tridymite, cristobalite, unmodified quartz, very low contents of calcium and magnesium-iron silicates such as pseudowollastonite,pyroxenes (enstatite, ferrosilite), and an amorphous phase. Tridymite is the most desirable form of silica, due to its low volume changes during heating and cooling. Contents of unmodified quartz are required to be as low as possible.

To judge the suitability of various silicic rocks for silica manufacturing based on their potential for quartz transformation and tridymite formation during firing without the presence of mineralizers, samples of orthoquartzite, quartzite, and chert were subjected to firing experiments in an industrial furnace. Mineralogical composition and microstructure before and after firing was examined by means of x-ray diffraction and polarizing light microscopy. The chemical composition of the rocks before firing was determined by energy-dispersive x-ray spectroscopy. Although both chemical and mineralogical compositions of raw samples were comparable, the rate of quartz transformation and cristobalite/tridymite ratio significantly differed after firing. Hence the role of microstructure is crucial. In fired quartzite samples, mullite was also identified. Mullite has not previously been found in refractory silica bricks.

Of the three groups of silicic rocks tested, the properties of fired cherts are the most favourable with respect to refractory production. Thin section photomicrographs of chert (spongolite) from Mirna, Slovenia, before and after firing are shown in Figure 1.

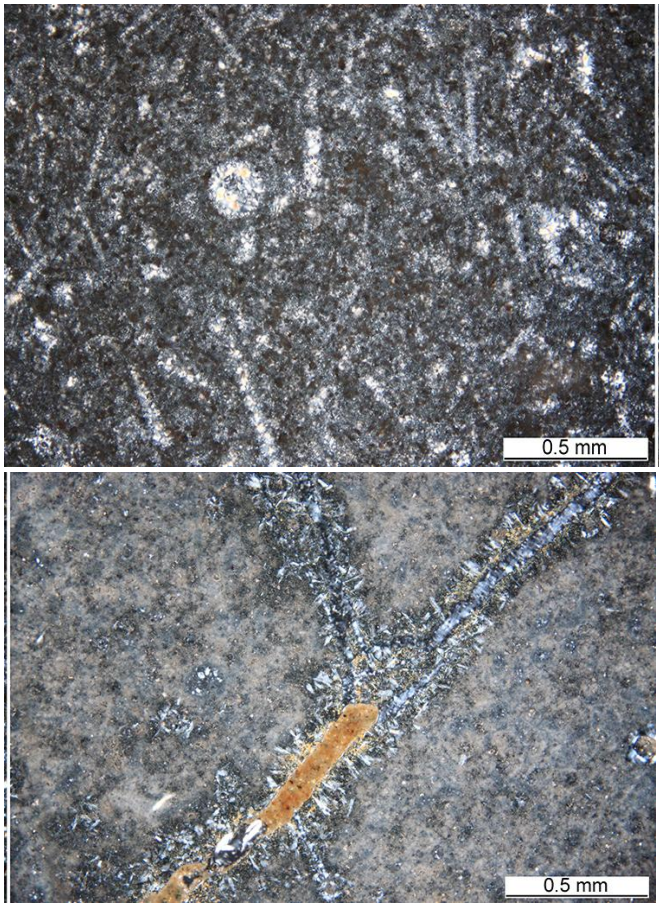

Figure 1: Photomicrographs of raw spongolite with chalcedony and quartz pseudomorphs after sponges (top) and the same sample after firing in an industrial furnace with arrow-like tridymite crystals mostly situated perpendicular to cracks (bottom); both in crossed polarized light. The majority of the fired sample is formed by cristobalite.

The magmatic evolution of the Fir carbonatite system and implications for Ta enrichment in carbonatites

Chudy T[1*], Groat L[1], Cempírek J[2]

1 - The University of British Columbia *tchudy@eos.ubc.ca 2 - Department of Earth, Ocean and Atmospheric Sciences, The University of British Columbia

The Fir carbonatite system is located in the Monashee Mountains of east-central British Columbia in the Canadian Cordillera. It is composed of sill-like bodies of dolomite carbonatite with subordinate calcite carbonatite that are surrounded by a selvage of phlogopite fenite. The Fir carbonatite contains an indicated plus inferred resource of approximately 60 Mt grading 190 ppm Ta_2O_5 and 1500 ppm Nb_2O_5. The consistently elevated Ta contents are highly unusual for carbonatites, as is the absence of any significant amounts of associated silica-undersaturated rocks. The dolomite and calcite carbonatites also contain fluorapatite, calcium and sodium-calcium amphiboles, pyrrhotite, ilmenite, magnetite, ferrocolumbite and pyrochlore. Accessory phases are monazite, thorite, microlite, fersmite and aeschynite.

The dolomite carbonatite shows two mineralogical facies based on the distribution of amphiboles and the Nb-Ta oxide minerals that developed from the margin to the center. The margins are characterized by low-sodium amphiboles such as tremolite and winchite and by the presence of ferrocolumbite. Towards the centre, the amphiboles become enriched in sodium (katophorite and richterite) and ferrocolumbite is replaced by pyrochlore-group minerals. The amphiboles have in general low Al and Ti contents and very high F contents of up to 3.44 wt.%. Within their respective facies both primary ferrocolumbite and pyrochlore show an increase in Ta content towards the centre of the carbonatite. The compositional evolution of primary ferrocolumbite is similar to columbite-group minerals in rare metal pegmatites, although much more restricted (XTa up to 0.05). The pyrochlore composition evolves from the Nb-end-member (Nb/Ta = 5-8) towards Ta-Ti-rich compositions (Nb/Ta = 3-4) in the same direction. Secondary metasomatic alteration of the ferrocolumbite is characterized by higher XTa (up to 0.12) and the precipitation of high-Ta pyrochlore (Nb/Ta from 0.9 to 1.8) as is typical for many rare metal pegmatites.

The documented increase in alkalinity from the margins towards the centre of the carbonatite sills can be explained by in-situ internal differentiation during crystallization of the carbonatite, as opposed to simple fractional crystallization during magma ascend. The change in alkalinity also controlled the stability of columbite and pyrochlore, where the former is stabilized under acidic and the later under alkaline conditions.

The elevated Ta contents in the Fir carbonatite system can be explained by a combination of high F contents (as evidenced by the amphibole composition), relatively high intrusion temperatures of 700°C (Cal-Dol geothermometry), and a primary carbonatitic parental melt (as evidenced by the absence of genetically related igneous silicate rocks). The first two factors contribute to the high solubility of Ta in the melt, preventing fractional crystallization of liquidus Nb-Ta oxide minerals, which otherwise would effectively remove Ta at an early stage in the magmatic evolution. The primarily carbonatitic composition of the parental melt prevented partitioning of Ta into the silicate phase and its depletion in the carbonatite during liquid immiscibility at crustal levels.

Trace elements in Fe-oxides as mineralogical vectors for exploration of Ni-Cu-PGE deposits

Dare S A S[1*], Barnes S-J[2], Beaudoin G[3], Ames D E[4], Lightfoot P C[5]

1 - L'Université du Québec à Chicoutimi, now at University of Ottawa *sasdare@hotmail.com 2 - L'Université du Québec à Chicoutimi 3 - Université Laval 4 - Geological Survey of Canada 5 - Laurentian University

There is growing interest in using detrital magnetite, from sediments and/or glacial till, as an indicator mineral in the exploration of ore deposits because magnetites from different ore-forming environments have distinct trace elements signatures [1, 2]. For Ni-Cu-PGE deposits, magnetite is commonly present in massive sulfide ore, having crystallized at high temperature from large pools of sulfide liquid. However, magnetite together with ilmenite is also present in the upper parts of mafic-ultramafic igneous complexes that in some cases the complex may host Ni-Cu-PGE deposits in their base. Using examples from two of Canada's largest Ni-deposits (1.85 Ga Sudbury Igneous Complex, Ontario and 1.34 Ga Voisey's Bay, Newfoundland), we demonstrate that trace elements in Fe-oxides, analyzed by laser ablation ICP-MS from both ore and the host igneous complex, can be used as mineralogical vectors for the exploration of Ni-Cu-PGE deposits. Trace elements in Fe-oxides are also useful petrogenetic indicators of fractionation of silicate and sulfide melts [2, 3].

The trace element signature of magnetite from massive sulfide ore can be distinguished from magnetite in all other settings, by their high Ni+Cr values, and from magnetite in host mafic intrusions by their low Mg and, in most cases, low Ti contents [1, 3, 4]. The content of lithophile elements (Cr, V and Ti) in magnetite is controlled by fractionation of the sulfide melt and is inversely proportional to the Pt+Pd/(Os+Ir+Ru+Rh) ratio of the whole rock [3, 4]. Thus the Cr content of magnetite could be used to indicate the type of mineralization (Cu-Pt-Pd-rich or Fe-rich, Pt-Pd poor sulfides) represented in grains from till samples.

An efficient tool in the exploration of Ni-Cu-PGE deposits is the depletion of highly chalcophile metals in host intrusions, as recorded by whole rock ratios (e.g., Cu/Zr, Cu/Pd, Ni/Ni*) and Ni depletion in olivine. This is because Ni, Cu and PGE strongly partition into sulphide liquid. We demonstrate that sulfide saturation is also recorded by magnetite and ilmenite, which show relative depletions in Cu and Ni in igneous complexes that host Ni-deposits (i.e., fertile) compared to those in layered intrusions barren of Ni-deposits, such as Bushveld (South Africa), Sept Iles (Canada) and Newark Island (Canada). Thus, chalcophile element depletion in Fe-oxides has the potential to identify fertile intrusions with buried Ni-sulfide mineralization. The advantages of using Fe-oxides include their resistance to post-magmatic processes such as alteration, their preservation and good recovery in surficial sediments.

[1] Dupuis &Beaudoin (2011). *Miner Deposita*, 46, 319-335.

[2] Dare *et al.* (2013). *12th SGA Biannual Meeting*, 1, 256-259.

[3] Dare *et al.* (2012). *Geochim. Cosmochim. Acta*, 88, 20-57.

[4] Boutroy *et al.* (submitted) *J. Geochem. Explo.*

Mn-ilmenites associated with standard KIMs, Lena West, NWT, Canada

Davies R*, Davies A

Talmora Diamond Inc. *rayal.davies@sympatico.ca

Numerous kimberlite indicator minerals (KIMs) including 18 diamonds are widely distributed (400 x 400 km) over the Lena West diamond region of the Northwest Territories. Within the limits of the Cretaceous basin that covers much of the area the KIMs show very little variation as if they are from a restricted source area. There is evidence that the source of these KIMs is pre-Cretaceous kimberlite located to the east and that the KIMs within the basin are derived from concentrations at the base of the Cretaceous sediments.

The Darnley Bay kimberlite cluster, outside and NE of the basin, has very different mineral chemistry. The Dharma kimberlite, outside and SE of the basin, has mineral chemistry that could have contributed to that of KIMs within the basin but does not cover the full range of that mineral chemistry. The Talmora area, outside the basin on the west side of the unglaciated Melville Hills, has matching mineral chemistry but is deficient in numbers of silicate KIMs. There is evidence that many of Talmora's silicate KIMs were destroyed by paleo-lateritic weathering (55 Ma) and subsequent glacial erosion was weak and only partly removed the weathered zone.

Mn-ilmenite is not a standard KIM used in exploration. However, Tompkins and Haggerty (1985) and Kaminsky *et al.* (2001) recommend that it be included in the list of diamond indicator minerals. Mn-ilmenites are found in samples of till taken within the Lena West Cretaceous basin and from the Darnley Bay, Talmora and Dharma areas outside the basin. Those in the Darnley Bay area differ from those of the Lena West, Dharma and Talmora areas. The Mn-ilmenites from all parts of Lena West have similar compositions and are similar to Mn-ilmenites in kimberlites from Guanaimo, Venezuela but differ from more Ti-rich Mn-ilmenites in kimberlites from Juina, Brazil. Some grains in the Lena West tills have compositions that match those of diamond inclusions from both Guanaimo and Juina.

In the Darnley Bay and Talmora areas the Mn-ilmenites are accompanied by diagenetically altered grains. However, the altered grains diminish in number down-ice from Talmora across the Darnley Bay area and are apparently related to the paleo-lateritic weathering. Cuttings from a drill hole that sampled the weathered zone above a magnetic kimberlite target on the Talmora property contained 4 unaltered and 9 altered Mn-ilmenites together with 14 spinels and 1 picro-ilmenite. The absence of altered grains within the basin is presumably because they, like the silicate KIMs, were deposited in the basin prior to lateritic weathering and were sheltered from weathering by covering Cretaceous sediments.

The identical relation of Mn-ilmenites and standard KIMs to an area of lateritic weathering outside the basin suggests they have a common source and the absence of any other source is strong evidence that the Mn-ilmenites are kimberlitic. The association of altered and unaltered Mn-ilmenites indicates that the source of both is the area of weathering and in this area altered Mn-ilmenite can be considered a KIM.

Late-stage magmatic-hydrothermal mineral associations in the Ni-Cu-PGE sulphide-bearing (ultra-) basic Uitkomst Complex, South Africa

Gauert C[1*], Trubač J[2], Ackerman L[3]

1 - University of the Free State *gauertcdk@ufs.ac.za 2 - Czech Geological Survey, Praha, Czech Republic 3 - Institute of Geology v.v.i., Acad. of Sc. of the Czech Republic

With the recent availability of drill core material on Little Mamre 538JT the first complete intersection of the downdip extension of the complex was generated. Interesting research questions comprise the lithological and mineralogical continuity of the rock units.

Petrographic and SEM-WDS studies of the Basal Gabbro chilled margin and parts of the Upper Gabbro unit reveal titanite, apatite and previously undescribed zircon associated with large biotite porphyroblasts, and green amphibole, and occasional carbonate veins. The gabbro chills represents the composition of the early magma on emplacement, possibly contaminated by chert-rich carbonatic floor and quartzitic roof rocks. Carbonatic fluids contributed to the formation of titanite from the Ti-bearing melt and magmatic ilmenite.

Titanite, ilmenite, apatite, amphibole, biotite and albite are common accessory minerals in pegmatite 'pockets' within the Main Peridotite unit and in the dioritic part of the Upper Gabbro and represent the evolved, H_2O-rich late-stage melt as part of the differentiation sequence. The mineral assemblage is indicative of pegmatitic to hydrothermal formations in the late stage magma under medium grade metamorphic conditions.

The trace element chemistry of titanite in evolved amphibole-bearing gabbroic rocks and their metasomatised equivalents constitutes a tool for understanding late-stage igneous and metasomatic processes. The Uitkomst titanites contain Al, K, Fe, Ta and some REE, some crystals contain Mn, F, Mg, Na, Zr, and V; zircons contain more than 3 wt.% of P_2O_5, 1.5 wt.% of CaO, 1.9 wt.% of ThO_2, and traces of Na, Al, Ti, Mn, Fe and REE. According to Colwell *et al.* ([1], the understanding of titanite chemistry allows constraints on conditions of crystallization, metasomatic reactions, and the nature of hydrothermal fluids. Zr-in-titanite temperatures will be compared to Ti-in-zircon temperatures from coexisting zircons.

Late stage apatite is commonly associated with interstitial quartz both in the lower as well as upper gabbro. A chemical characterization shows constant P_2O_5 and CaO compositions, however variable minor F, Cl, and Nb_2O_3 contents, as well as traces of K, Si, Na, Al, Fe and Ba. Apatite compositional heterogeneity within samples and internally in crystals may reveal a complex history of late-stage magma evolution at Uitkomst possibly within short timescales.

PGE contents in base metal sulphides of the lower three rock units (Basal gabbro, lower pyroxenite and chromitiferous peridotite) analysed by LA-ICP-MS are two magnitudes lower than comparable sulphides from the Bushveld. Pentlandite PGE contents are highest (0.8 ppm on avg.), Pd-dominated and Rh-bearing, pyrrhotite (0.21 ppm) is Ru-dominated and Os-bearing, and chalcopyrite (0.15 ppm) is Ru- and Au-dominated. PGEs in BMS are strongly depleted (Ir and Pt more than a 100 times, in the sequence Cpyr>Po>Pe) compared to chondrite, except for Pd in pentlandite. Overall, there is a negative correlation of PPGE and IPGE in the sulphides whereas the two groups among each other correlate positively. The observed PGE distribution within the disseminated BMS supports Theart and de Nooy's findings [2] that most of the PGM phases in the massive sulphides are hosted as inclusions or along grain boundaries by pyrrhotite, and to a lesser extent by chalcopyrite and pentlandite. They suggest that the igneous immiscible sulphide phase forming the BM and PGE-enriched massive sulphides at the base of the complex, attained hydrothermal characteristics.

[1] Colwell L.E., John B.E., Cheadle M.J. and Wooden J.L. (2011). Chemistry of titanite (sphene) in ocean crust: A tool for understanding late-stage igneous and metasomatic processes at mid-ocean ridges. Am. Geophys. Union, Fall Meeting 2011, abstract #V11A-2493.

[2] Theart H.F.J. and de Nooy C.D. (2001). The Platinum Group Minerals in two parts of the Massive Sulphide Body of the Uitkomst Complex, Mpumalanga, South Africa. *S. Afr. J. Geology*, 104, 287-300.

Uranium ore heterogeneity in vein deposits of the Southwest UK

Keatley A* Scott T

University of Bristol. *a.keatley@bristol.ac.uk

Over the past 20 years there have been a number of studies which have successfully traced uranium ores and uranium ore concentrates (UOCs) back to specific mining areas via nuclear forensic fingerprinting. However more recent studies have identified that heterogeneity within a single deposit can be greater than the variation between different mines [1-4]. These arising heterogeneity issues bring into question the reliability of any reference database consisting of small sample masses and samples representing entire mining regions.

The current project addresses this heterogeneity issue by examining the degree of heterogeneity within single mines, mining sites and mine regions. The project is also examining how heterogeneity is carried through the first stages of uranium ore processing, with the aim of informing the use of appropriate sample databases. In the past year work has been undertaken on the hydrothermal uranium mineral veins of South-west England, in order to test the hypothesis that Uranium ore bodies can exhibit significant in-body heterogeneity for mineralogy, elemental and isotopic composition.

A large sample library has been established with sample suites collected from individual mineral veins across the region. After initial gamma spectrometry and sample preparation, the samples have been analysed by SEM (Scanning Electron Microscopy) to determine differences in texture, EDX (Energy-dispersive X-ray spectroscopy) mapping has been used to determine the major phase composition and association. EPMA (Electron microprobe analyser) has been used to determine the minor element composition of the major uranium phases. Initial results show large textural and compositional variations on a centimetre scale. For example EMPA analysis has shown variations of up to 1.8 mass % in certain REE's along a single 3m mineral vein (Figure 1). Other accessory elements such as Pb, Fe, As, P and S have been found to vary by up to 20 mass % along the same body. These findings could greatly influence future forensic fingerprinting approaches as REE trends have previously been used as a key tool in origin location studies.

We present data from numerous mineral vein sample sets, associated with different granite intrusions across the South-West of England. Ore variation is compared on a regional scale to identify any general trends that might be used as a characteristic forensic fingerprint.

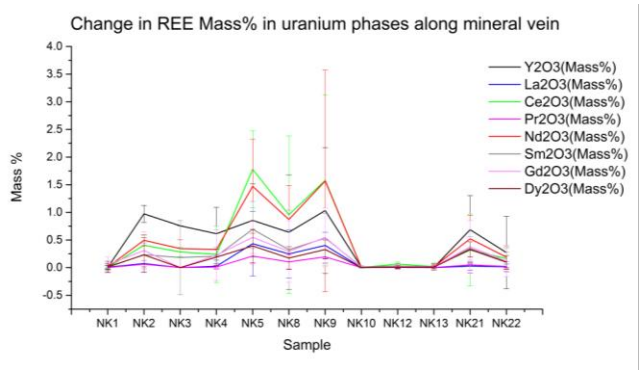

Figure 1: Change in mean mass % of REE along a 3 meter uranium mineral vein (error bars ± 1sd)

[1] Bopp C. *et al.* (2009). *Geology* 37, 611.

[2] Varga Z. *et al.* (2009). *Analytical chemistry* 81, 8327.

[3] Brennecka G. *et al.* (2010). *Earth and Planetary Science Letters* 291, 228-233.

[4] Keegan E. *et al.* (2008). *Applied Geochemistry* 23, 777.

Metal exploration in historical ore processing residues in the Harz mountains, Germany

Kuhn K*, Meima J, Rammlmair D, Martin T, Knieß R, Noell U

Federal Institute for Geosciences and Natural Resources (BGR). *kerstin.kuhn@bgr.de

From over 1,000 years of metal mining in Germany there are many dump sites of mine waste left. According to their origin, they derive from mining, processing, and metallurgy. Whereas these residues were previously considered only with respect to their environmental risk potential, they are nowadays also regarded as a possible metal source. Within the research project ROBEHA (BMBF, 033R105), we investigate the economic potential of historical mining dumps in the Harz Mountains as a source of non-ferrous metals, high-tech metals, and construction aggregates.

In the Harz Mountains, ore processing wastes are most interesting for economic recovery. Residues older than 1930 were density separated. These residues are characterised by high metal concentrations but medium quantities. Ore processing wastes younger than 1930 descend from flotation with lower metal concentrations but larger quantities compared to older material. The ore processing waste generally has small grain sizes, which will keep milling costs for further processing low.

Within this study, a resource evaluation is developed for a 100-year old mining dump containing residues from density-separated Ag- and Sb-rich Pb-(Zn)-gangue ores. According to most mining disposals, the investigated dump is heterogeneously structured and therefore needs a large amount of samples for characterisation. In order to limit the amount of samples and to avoid the generation of many pathways for water flow by extensive sampling, we use a combination of different scaled exploration methods.

First of all, geophysical exploration was applied to reveal different zones within the dump body and to provide a basis for an estimation of the waste material volume. Electrical resistivity tomography (ERT) indicated that the ore processing residues differ from the bedrock by higher resistivities with values of more than 400 Ωm compared to 200 Ωm or less. Other geophysical techniques like RADAR and Spectral Induced Polarisation (SIP) are currently being tested to minimize uncertainties in the ERT-model and to distinguish between different sulphides and sulphide concentrations.

Based on the geophysical model, 19 ramming drill cores were taken. The split cores were analysed with a LIBS Core Scanner (Laser-Induced Breakdown Spectroscopy) to generate 2D-element distribution images for major and minor elements (Figure 1). These images were used to identify zones of metal enrichment, allowing selective sub-sampling for further chemical and mineralogical analysis (XRF, ICP-MS, SEM+MLA, Microprobe, LA-ICP-MS). Additionally, LIBS emission intensities are calibrated to estimate average metal concentrations as a basis for the resource estimation.

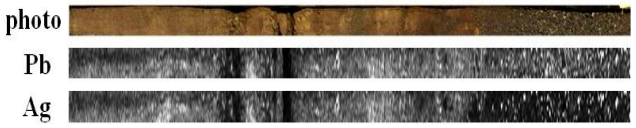

Figure1: Relative element distribution of Pb and Ag measured with the LIBS Core Scanner for one drill core meter. Bright colours reveal high element concentrations.

The investigated Pb-Ag-Sb-rich ore processing wastes consist of a mixture of sand to pebble-sized material with minor contents of silt and some fine-grained layers of silt- to clay-sized material. The bedrock as well as some blocky debris within the mining dump consist of greywacke and argillaceous shale. Average Pb concentrations are 4.4 % for the sandy material and 7.5 % for the silty material. In contrast to the sandy material with galena (PbS) and cerussite ($PbCO_3$) as the major Pb-containing minerals, the silty material is characterised by an almost complete alteration of galena to cerussite. Silver and Sb are bound to the galena mineral lattice as well as to some Ag-Sb-Cu-Fe-S-compounds with varying compositions, probably freibergite (>20 wt-% Ag), argentian tetrahedrite (<20 wt-% Ag), as well as bournonite and pyrargyrite. These phases occur as separate minerals or inclusions within the galena. Further sulphides include pyrite as well as minor chalcopyrite and sphalerite.

The analytical fingerprint of "conflict minerals"

Ndikumana A*, Nziza L, Kabeya F

BGR/ICGLR - International Conference on the Great Lakes Region/Federal Institute for Geosciences and Natural Resources - ICGLR/BGR, Bujumbura, Burundi

*arndikumana@yahoo.fr

Tin (cassiterite), tungsten (wolframite) and tantalum (coltan) ore has been mined in the Great Lakes Region for many years, both by artisanal and semi-industrial means. Since the 1990's, mining and trading of these minerals has partly contributed to catalyze the conflict in eastern Democratic Republic of Congo (DRC) thus the term "conflict minerals" was formed.

The artisanal "conflict mineral" mining sector in the Great Lakes Region represents an important livelihood base for the local population. There is a need for a sustainable development of this sector to improve the livelihood base. Thus responsible companies facing international supply chain due diligence demands require confidence in mineral traceability measures in order to continue mineral sourcing in the Great Lakes Region. An independent mechanism is required to support the credibility of standard mineral traceability procedures in a larger due diligence framework.

The Analytical Fingerprint method (AFP) is a scientific and optional tool developed since 2006 by the Federal Institute for Geosciences and Natural Resources (BGR) to verify the documented origin of the three minerals produced in the Great Lakes Region.

This method intends to support the certification mechanism of the International Conference on the Great Lakes Region (ICGLR) by producing an independent line of evidence on the origin of the three minerals. In fact, it uses intrinsic data of the minerals generated by laboratory analyses like "DNA" tests.

AFP may be applied proactively by mining companies or their customers wishing to demonstrate a conflict-free origin of their minerals, or as a forensic tool in the frame of chain of custody risk assessments and supply chain due diligence audits as part of a mineral certification scheme.

The main objective of AFP is to provide independent evidence with regards to the link between a sample of a given mineral shipment and its claimed origin, the latter representing a mineral deposit or mine site integrated into the AFP reference database.

To transfer the full ownership of the method and ensure its proper application in the Great Lakes Region, a management unit has been established in Bujumbura, Burundi since May 2013. This unit has the responsibility of coordinating and facilitating the collection of reference samples and preparation of polished sections in AFP preparation laboratories in three pilot countries (Burundi, DRC and Rwanda), evaluating and interpreting quantitative analytical data (mineralogical and geochemical) produced by analytical laboratories and reporting.

The reference database is extended continuously. In January 2014 it comprises about 400 reference samples from about 250 individual production sites from Rwanda, DRC, and Burundi.

Perspectives:

Integrate main productive sites of coltan, cassiterite and wolframite located in Burundi, DRC and Rwanda in our reference database.

Increase our analytical capacity as the number of reference samples taken is increasing now.

Further development of parameters indicating similarity which will be used when comparing a given sample to samples of known origin stored in our database.

Mineral chemistry of scheelite as an indicator of hydrothermal fluid evolution of the Riviera W-Mo-REE endoskarn deposit, Western Cape, South Africa

Pieterse L*, Rozendaal A

University of Stellenbosch *15737217@sun.ac.za

The Riviera deposit has a resource of 46 million tons at a grade of 0.216 % WO_3 and 0.02 % Mo. Mineralization is hosted by zones of endoskarn in the cupola of late stage, A-type granitoids of the Neoproterozoic Cape Granite Suite. The principal ore minerals are scheelite ($CaWO_4$), molybdenite (MoS_2) and allanite, a light rare earth element enriched member of the epidote group. This study focused on the chemistry of the economically most significant ore mineral scheelite. Spot analyses (~30µm) by means of LA-ICP-MS supported by cathodoluminescence (CL) images and UV fluorescence provided high resolution geochemical data. UV lamping indicated two groups of scheelite with distinct blue and yellow fluorescence respectively. CL images showed that the entire scheelite population was strongly zoned. Spot analyses provided detailed multi-element geochemical data that explained the observed characteristic features. The UV fluorescent colour was a function of the molybdenum content of the grains, where yellow fluorescence indicated molybdenum enrichment and the blue colour molybdenum depletion. Observed zonation of scheelite was mainly produced by variation of molybdenum and total light rare earth element content. The cores of the grains were Mo-enriched and LREE depleted whereas the rims displayed the inverse relationship. The observed features indicate that the tungsten-enriched hydrothermal fluids responsible for the mineralizing process were molybdenum-rich at the outset and evolved to LREE-rich in the waning stages. This indicates that fluid evolution was controlled by Eh conditions changing from mildly reducing to oxidizing with time. Geometallurgical implications of the results of this study indicate that it will be challenging to separate the unwanted molybdenum-rich cores from the high demand low molybdenum scheelite because of their zonal interrelationship.

Allanite chemistry as an indicator of fluid evolution and genesis of the Neoproterozoic Riviera W-REE-Mo skarn deposit, Western Cape, South Africa

Santana M*, Rozendaal A

University of Stellenbosch *monicas@sun.ac.za

The Riviera W-REE-Mo deposit is associated with granitoids of the Neoproterozoic Cape Granite Suite that are intrusive into the meta-volcano-sedimentary Malmesbury Group of the Saldania Belt. Scheelite, allanite and molybdenite are the principal ore minerals and are hosted by hydrothermally altered granite and quartz monzonite. Zones of potassic alteration and endoskarn in the cupola of the essentially phyllic altered pluton, display high grade mineralization.

The significant concentrations of allanite, a light rare earth-enriched mineral of the epidote group, could constitute an economically important by-product, although seldom recovered as a principle LREE-ore. As a result it requires a detailed spatial, textural and mineral chemistry investigation. In addition the rare earth element characteristics could be a good indicator of hydrothermal fluid evolution and genesis of the deposit. Allanite concentration is closely associated with zones of endoskarn, but spatially correlates poorly with tungsten and molybdenum mineralization indicating possible late stage crystallization. It is a complex mineral showing poikilitic and metamict textures, variable chemistry, irregular zonation and variable, but generally coarse grain size. The two most common types are allanite (Ce) and ferriallanite (Ce). Chondrite normalized REE patterns for the whole rock analyses are similar to those of the single grains and suggests that most of the rare earth elements are hosted by allanite. The steep slope of the pattern demonstrates significant LREE enrichment and Eu-anomalies vary from slightly negative, neutral to slightly positive. A high ∑LREE content of allanite correlates with a negative Eu-anomaly whereas the positive anomalies are associated with low concentrations. This suggests that the partitioning of REE in allanite is redox sensitive and that the hydrothermal fluids evolved from initial reduced, rare earth element depleted to oxidized and rare earth element enriched. Similar studies of zoned scheelite from this deposit support these observations and indicate that changing redox conditions of the fluid controlled sequential precipitation of rare earth elements associated with genetically early scheelite and late stage allanite.

VMS-type mineralization in the Barberton Greenstone Belt

Schwarz-Schampera U

BGR. u.schwarz-schampera@bgr.de

The 3.57 to 3.08 Ga Barberton greenstone belt is situated on the eastern margin of the Archean Kaapvaal Craton in the Republic of South Africa. It belongs to a group of Archean greenstone belts in the craton including the Murchison, Pietersburg and Gyiani belts, all trending subparallel to the Limpopo orogenic belt. It is shown that intermediate to felsic volcanic units of the greenstone belts in the craton (e.g., Upper Onverwacht Group and Lower Fig Tree Group of the Barberton belt; Rubbervale Formation of the Murchison belt; Ysterberg Formation of the Pietersburg belt) are suitable exploration targets for volcanic-hosted massive sulfide deposits. This study aims at distinct exhalite horizons within the 3.26 Ga Lower Fig Tree Group of the Barberton greenstone belt. These horizons host several volcanic- and sediment-hosted base metal sulfide prospects and hydrothermal iron formations delineating a zone of rift-related hydrothermal activity. The ore prospects include the 3.256 Mt Zn-Pb-Cu-Ag Bien Venue deposit, the M`hlati zinc and iron formation exhalite prospect, and a massive iron formation at Spago. Massive sulfide ores, mineralized rocks, and associated wall rocks from the Bien Venue and the M`hlati VMS deposits have been studied in greater detail. The mineralogical, geochemical and isotopic composition has been investigated to reconstruct the processes that controlled the formation conditions and to better understand the geological evolution of the 3.45 to 3.22 Ga Fig Tree Group of the Barberton Swaziland Supergroup. The mineralized calc-alkaline volcaniclastic units are hosted by epicontinental sedimentary sequences. There is strong evidence for explosive volcanism at shallow water depths with the deposition of pyroclastic products. The volcanic rocks share many geochemical similarities with felsic volcanic arc magmas as evidenced by Ta-Yb, rare-earth and spider diagrams. The LREE and Eu show characteristic mobility in the seawater-dominated hydrothermal fluids and predominate over HREE. Eu enrichments in sediments indicate a strong influence of high-temperature hydrothermal fluids. The hydrothermal alteration trends in the wall-rocks follow the characteristic pattern of many VMS-type ore deposits and approach the ideal quartz-muscovite alteration assemblage of the immediate ore zone. The sulfides at Bien Venue and M`hlati are characterized by a high-sulfidation mineralogy with a distinct trace metal enrichment. The Bien Venue VMS deposit is characterized by a pyritic Zn-Ag-Au-(-Cu-Pb-Sb-As-Ba) mineralization and shows an unusual Ag-Cu-Sn enrichment. The M'hlati sulfide ores are partly banded and are mainly composed of pyrite, sphalerite, pyrrhotite, chalcopyrite, magnetite, with traces of pentlandite, galena, covellite and chalcocite. The ores are rich in Ag-As-Te-Se-Bi. The associated sulphur isotope variation deviates from typical juvenile sources around 0‰ δ34S and this is in agreement with significant variations in the barite sulphur isotope signatures. The isotope fractionation may be influenced by sulphur disproportionation, induced by boiling processes in a rather shallow marine environment. The mineralogical and geochemical characteristics of the prospects and mineralized horizons share many similarities with a number of other VMS deposits and Proterozoic to Phanerozoic iron formations above significant VHMS deposits, as well as with seafloor hydrothermal systems at modern oceanic island arcs.

Exploring the ridges in the Indian Ocean: structural and petrological constraints for the occurrences of polymetallic sulfides

Schwarz-Schampera U[1*], Freitag R[1], Franke H[1], Lehrmann B[1], Bartsch C[1], Heeschen K[2]

1 - BGR *u.schwarz-schampera@bgr.de 2 – GFZ

The Central and Southeast Indian ridges were studied for sulfide prospecting and exploration during the cruises INDEX 2011, 2012 and 2013. The major emphases were to examine the bathymetry, structural geology, magnetic and gravimetric signatures, and the crustal development of the area as well as the petrogenesis and indicators for hydrothermal activity. The central Indian ridge (CIR) marks the spreading of the African and Australian plates between the Carlsberg Ridge to the North and the Rodriguez Triple Junction (RTJ) to the South. In the area north of the RTJ the CIR is considered a slow to intermediate spreading centre with rates between about 42 and 55 mm per year. The bathymetry is typically characterized by features common for slow to intermediate spreading centres including a strong segmentation of a deep central rift valley. The regional structural pattern of seafloor spreading is highly variable. The axial valley is 5 - 35 km wide and 500-1800 m deep hosting a large number of neovolcanic ridges and single cone shaped volcanoes, which are the focus of present day volcanism in the central valley or at its flanks. The outline of the rift valley is usually asymmetrical with steeper slopes on the eastern part. Common structural features within the rift valley include overlapping and bending as well as updoming. The formation of regional detachment faults have led to the exhumation of deep proportions of the oceanic lithosphere (gabbros, harzburgites) and the formation of oceanic core complexes (OCCs). A shallowing of the central rift valley to the north is likely caused by a thickening of the crust that was assigned to the nearby occurrence of the Reunion Plume at roughly 19°S. The CIR is characterized by anomalous Sr, Nd and Pb isotope ratios which have been addressed to the so-called DUPAL anomaly. The explanations for this regional mantle heterogeneity along the Indian Ocean ridges include influences of major mantle plumes related to the breakup of Gondwana, subducted continental lithosphere and/or oceanic crust and sediments. The impregnation of the mantle does alter the composition of the newly formed ocean crust. Apart from modified isotopic signatures, the occurrence of E-MORBs is a common feature along the ridges. It can be concluded that the enrichment of incompatible elements compared to normal MORB may have an influence of the occurrence and composition of polymetallic sulfides. It is also suggested that the occurrence of large scale detachment faults has an influence on the onset, the longevity and the life-cycle of hydrothermal processes. The CIR shows a number of active (EDMOND, KAIREI) and inactive (SONNE, GAUSS, SCORE) polymetallic sulfide sites. It can be concluded that structural and petrogenetic constraints and long-term sustained heat flow along the ridges make the Indian Ocean ridge system a prime target in the exploration for marine polymetallic sulfides.

Analytical fingerprint of 'conflict minerals': sampling, variability, statistics

Sitnikova M*, Gäbler H, Goldmann S, Oberthür T

Bundesanstalt für Geowissenschaften und Rohstoffe, Germany

*mariaalexandrovna.sitnikova@bgr.de

The Analytical Fingerprint method (AFP) is a scientific tool to verify the documented origin of cassiterite, coltan, and wolframite ore concentrates. AFP is based on analytical data from ore concentrates which are compared to data from samples of known origin stored in a reference database. Cassiterite, coltan, and wolframite plus gold are termed 'conflict minerals' as trading and illegal taxation are used to fund armed conflicts (e.g., in the eastern Provinces of the Democratic Republic of the Congo).

The critical parameters for the AFP are major and trace element composition of individual ore mineral grains from ore concentrates and a geochronological U-Pb age estimate. The chemical composition and U-Pb isotopes of single grains are measured in-situ by LA-ICP-MS. Scanning electron microscopy with automated mineralogy is used to define the targets for laser ablation.

Mineral grains from one mine site exhibit chemical compositions which are highly variable and show nonparametric statistical distributions. The range of the variability is characteristic for a particular ore body. So, the distribution functions of major and trace element concentrations in different mineral concentrates from the same mine site are similar to each other. This similarity can be used for the development of an analytical fingerprint.

Data variability will be presented and sampling requirements are deduced. Statistical approaches will be proposed to meet the requirements of an analytical fingerprint as an optional tool in mineral certification.

Mineralogical characteristics of Fe-Ti oxides from Xinjie mafic-ultramafic layered intrusion and their indicative significance for metallogenic conditions

Tan W*, Wang C, He H, Liang X, Zhong Y

Guangzhou Institute of Geochemistry, Chinese Academy of Sciences
*tanwei@gig.ac.cn

Fe-Ti oxides are ubiquitous in igneous and metamorphic rocks, and are of great significance in palaeomagnetic studies, as well as in paragenetic studies as geothermometers and oxygen geobarometers. Fe-Ti oxides crystallize as three major solid-solution series depend on the Ti/(Ti+Fe) rate and oxygen fugacity, including: 1) the cubic spinel (titanomagnetite) series (M_3O_4) between magnetite ($Fe^{2+}Fe^{3+}{}_2O_4$) and ulvöspinel ($Fe^{2+}{}_2TiO_4$); 2) the rhombohedral "α-oxide" series (M_2O_3) between hematite (Fe_2O_3) and ilmenite ($Fe^{2+}{}_2TiO_4$) ; and 3) the orthorhombic series (M_3O_5), between pseudobrookite ($Fe^{3+}{}_2TiO_5$) and ferro-pseudobrookite ($Fe^{2+}Ti_2O_5$). Fe-Ti oxides in plutonic rocks are complex intergrowth of stable Fe-Ti oxides, such as magnetie, ilmenite and rutile due to extensive sub-solidus re-equilibration during cooling process. The intergrowth textures comprehensively reflect the original components of Fe-Ti oxides and subsolidus conditions (e.g., temperature, oxygen fugacity and cooling rate) prevalent during crystallization and subsequent cooling process, which have been employed to probe the magma component and evolution of mafic/ultramafic magma.

The Xinjie mafic-ultramafic intrusion comprises a marginal zone and three cyclic zones, from the base upward. The Fe-Ti oxides are disseminated throughout the intrusion and (or) form several Fe-Ti oxide-rich layers, including a thick oxide mineralization in the upper parts of the sequence. These Fe-Ti oxides hosted by different layers of Xinjie intrusion exhibit distinct paragenesis and intergrowth textures. This research employed several micro-scale in-situ characterization methods, e.g., EMPA, micro-Raman spectra and micro-XRD, to conduct systematic characterizations on Fe-Ti oxides of Xinjie intrusion and their micro intergrowth textures, including several typical exsolution textures, and two symplectite textures. From the base upward, Fe-Ti oxides occur repeatedly in the sequence: ilmenite+rutile symplectite (with or without titanite)→ilmenite→intergrowth of textured titanomagnetite and ilmenite. This multi-cycle reflects the fluctuation of Ti/(Ti+Fe) and Fe^{3+}/ Fe^{2+} ratios of magma. The fluctuation of Ti/(Ti+Fe) and Fe^{3+}/ Fe^{2+} ratios of different layes from Xinjie intrusion indicate the physical-chemical conditions of magam, such as fluctuation of oxygen fugacity, component of volatile, temperature and pressure, which is helpful to reveal the mineralization condition and build a genesis model of vanadium titano-magnetite deposits occurring in the layered intrusions.

Mineralogy of Ni-phyllosilicates in the Falcondo Ni-laterite deposit (Dominican Republic): a multiscale approach

Villanova-de-Benavent C[1*], Proenza J[1], Galí S[2], Nieto F[3], García-Casco A[4], Roqué-Rosell J[5], Tauler E[1], Lewis J[6]

1 - Dept. Cristal., Miner. i Dipòsits Minerals; Fac. Geologia; UB *cvillanovadb@ub.edu 2 - Dept. Cristal., Miner. i Dipòsits Minerals; Fac. Geologia; UBa 3 - Depto. Mineralogía y Petrología; UGr 4 - Depto. Mineralogía y Petrología; UGr; IACT 5 - Advanced Light Source, Lawrence Berkeley National Laboratory 6 - The George Washington University

Ni-bearing Mg-phyllosilicates are significant ore minerals in Ni-laterite deposits of the hydrous silicate-type [1]. However, the characterisation of these mineral phases is complex, as well as their classification and nomenclature, due to their fine-grained nature, poor crystallinity and frequent occurrence as mixtures [2]. The aim of this study is to shed some light to the nature of the Ni-phyllosilicates occurring at the Falcondo Ni-laterites. In this deposit, these minerals are found within the saprolite horizon mainly as fracture-fillings, coatings on joints and as breccias. The Falcondo Ni-phyllosilicates display easily distinguishable different shades of green and characteristic textures, which correspond to different mineral phases. These phases were defined by X-ray diffraction (XRD), optical and electron microscopy, and electron microprobe (EMP) analyses: a) talc-like (10 Å-type), b) serpentine-like (7 Å-type), c) mixtures of talc- and serpentine-like, and d) sepiolite-like types. Further information was obtained by differential thermal analysis and thermogravimetry (DTA-TG), transmission electron microscopy (TEM), and Raman spectroscopy, in order to achieve a more detailed characterisation of these mineral phases.

EMP oxide totals and DTA-TG indicate that talc-like contain higher H_2O than talc *sensu stricto* (about 4.5% mass loss at 200ºC, and up to 5% at 650ºC), and thus the names kerolite-pimelite $[(Mg,Ni)_3Si_4O_{10}(OH)_2{\cdot}nH_2O]$ should be used instead of talc-willemseite $[(Mg,Ni)_3Si_4O_{10}(OH)_2]$. Compositional data showed continuous Mg-Ni solid solution along the joins lizardite-népouite (serpentine-like), kerolite-pimelite (talc-like) and sepiolite-falcondoite (sepiolite-like). Talc-like and the mixed phases displayed the highest Ni contents (up to 2.2 apfu both). Also, EMP analyses of the mixed phases showed deviations from the stoichiometric Mg-Ni solid solutions of serpentine and talc. This is best explained by mixing at the nanoscale, which was confirmed by XRD and high resolution TEM imaging. HRTEM enabled to measure the characteristic basal spacings of these phyllosilicates (7.2 Å for serpentine-like, 9.5 Å for talc-like, 11.5 Å for sepiolite-like). Also, these images showed the wide variety of nanotextures in which these phases occur: 15-sectored polygonal serpentine, chrysotile tubes, and talc- and sepiolite-like fibres. In addition, a detailed textural study by means of EMP quantified X-ray element imaging was used to explain the relationships between textural position, sequence of crystallization and mineral composition of the studied Ni-phyllosilicates. These results indicate several stages of growth with variable Ni content, pointing to recurrent changes in the physical-chemical conditions during the precipitation of the different Ni-phyllosilicates. Characteristic Raman bands were observed for serpentine- (228, 385, 688 cm^{-1}), talc- (188, 362, 385, 640, 675, 735, 822 cm^{-1}) and sepiolite-like phases (196, 386, 640, 673, 705, 823 cm^{-1}). In particular, the bands of both serpentine- and talc-like were identified in the mixed phases spectra (184, 368, 680 are of talc-like, and 210 is of serpentine-like). In summary, the various analytical techniques applied to the Ni-phyllosilicates of this study provide an accurate outlook of their complex mineralogy, structures, textures and chemistry at different scales.

[1] Freyssinet Ph, Butt C.R.M., Morris R.C. (2005). *Econ. Geol. 100th Anniv. Vol.*, 681-722.

[2] Brindley G.W., Hang P.T. (1973). Clay. *Clay Miner*. 21, 27-40.

Beach sand mineral composition of the UAE eastern coast, an indicator for mineral prospects of the Fujairah Mountains

Alaabed S*, Mahmoud B, Hadher A

Department of Geology, UAE University. *s.alaabed@uaeu.ac.ae

The northeastern part of the UAE is bordered by the northern extension of the Indian Ocean (Eastern Coast) and dominated by the northern section of the Oman Mountains. These geographic and geological features have made Fujairah Emirate distinct from the other parts of the UAE. Its beach narrow plain consists of various types of mineral grains mainly representing the rock composition of the mountainous hinterland.

Fujairah Mountains may cause a surface area limitation for population. In contrast, they appear to be a sustainable resource. They have become the main local source for building material and dimension stones. The abundant hard rocks such as gabbro and peridotite will probably secure the future needs. In addition, occurrences of some importance industrial minerals are well recorded at the coastal sands. Pyroxene, olivine, chromite, magnetite, hematite, rutile, calcite and others are found in a reasonable amount for consideration, as some like chromite is already minded.

Because a concentration of any mineral at the beach may represent the relative volume of the minerals at the mountains; the beach mineral composition of the UAE Eastern Coast is a good indicator for ores or mineral deposits.

Mineralogy and geochemistry of Taurides' Pb-Zn mineralization (Southern Turkey)

Ciftci E[1*], Lermi A[2]

1 - Istanbul Technical University *eciftci@itu.edu.tr 2 - Nigde University

The Tauride belt is one of the major tectonic units forming Anatolia within the Alpine-Himalian Orogenic Belt. This belt is host to great number of various types of mineralization with different size and content. The Taurides can be divided into 4 subdistricts with regards to ore deposit occurrences: (I) Western Taurides, (II) Bolkarlar, (III) Aladaglar-West Zamanti, and (IV) East Zamanti.

Carbonate-hosted lead and zinc mineralization is basically epigenetic emplacements and their formation can be considered as structurally controlled in many occurrences. These occur essentially as oxides-carbonates with relics of sulfides. Ore mineralogy throughout the belt for the subject deposits is fairly simple and comparable: galena-sphalerite - cerussite - smithsonite - Fe-oxihydroxides. In most of the deposits, galena is the only sulfide mineral which has survived.

However, gangue mineralogy shows considerable differences from district to district. In the western part of the belt, fluorite and barite are common. In Bolkarlar, plumbojarosite and quartz with subordinate calcite and dolomite dominate. In Aladaglar-West Zamanti, calcite and dolomite are widespread. In East Zamantı, although quartz locally becomes significant, dolomite and calcite are prevalent. Host rocks are mostly limestones, however dolomites, calcschists and marbles are also important in some deposits. These deposits are and were mined for lead and zinc, however, barite, copper, silver, gold, gallium are significant in some of the districts.

Distribution of trace elements in the sulfide minerals from Roşia Poieni porphyry Cu deposit, Romania

Cioaca M[1], Munteanu M[1], Walle M[2], Costin G[3], Marincea S[1*], Dumitras D[1]

1 - Geological Institute of Romania *smarincea@yahoo.com 2 - ETH Zurich, Institute of Geochemistry and Petrology, Switzerland 3 - Rhodes University, Department of Geology, Grahamstown, South Africa

Roşia Poieni (9.42 ± 0.14 Ma) is the largest porphyry Cu deposit in Romania, located in the Golden Quadrilateral from the Metaliferi Mountains and is hosted in a microdioritic subvolcanic body. The mineralization is developed in the central-deep potassic alteration zone and includes chalcopyrite, magnetite, bornite, and subordinate pyrite and molybdenite. Phyllic alteration overprinted the margins of the potassic zone and advanced argillic alteration affects the upper part of the volcanic structure. Pyrite is the main metallic mineral associated with the phyllic and argillic facies and occurs as disseminated grains and veinlets. The cm-thick epithermal veins that crosscut porphyry mineralization contain tetrahedrite-tennantite, enargite, sphalerite, galena, chalcopyrite and pyrite, as well as tellurides and germanium minerals.

Whole rock samples show trace elements concentrations of 0.2-1 ppm Au, 0.7-2 ppm Ag, 4-324 ppm Mo and 5-104 ppm Te.

Preliminary electron microprobe analyses on pyrite (9 grains) and bornite (6 grains) showed that the trace elements have an inhomogeneous distribution, reflected in a wide range of contents. In pyrite, Au has contents in the range <60-120 ppm, while Ag is concentrated in bornite (970-1910 ppm). Tellurium varies from <20 to 40 ppm in pyrite, and from <200 ppm to 1,000 ppm in bornite.

LA-ICP-MS data indicate mean values of Au is <0.18 ppm in chalcopyrite (2 spot analyses) and <0.50 ppm in bornite (5 spot analyses). In chalcopyrite, Ag is 24 pm and Te is 4 ppm, while in bornite, Ag and Te are more than one order of magnitude higher than in chalcopyrite (268 ppm Ag and 60 ppm Te). Both chalcopyrite and bornite are enriched in Se (362 and 785 ppm, respectively), Bi (6.5 and 1445 ppm, respectively) and Ge (6 ppm and 3 ppm, respectively). LA-ICP-MS profiles suggest the presence of galena and Bi minerals as fine inclusions in chalcopyrite, and sphalerite and discrete Au and Ag minerals as fine inclusions in bornite. The role of bornite as main carrier of Ag and Bi is confirmed by our investigation. The porphyry copper mineralization from Roşia Poieni is Te-rich, similar to the epithermal mineralization in the Metaliferi Mountains.

The broad ranges of electron microprobe results for each element suggest the presence of nanoparticles of Au, Ag and probably Ag-Te compounds in the host minerals. Analyses for gold taking into account the matrix effect are going to be done through high-energy X-ray fluorescence imaging in the on-going MAXI ERA-MIN project.

Reactive transport simulation of the formation of Ni-laterite profiles (Punta Gorda, Moa Bay, Cuba)

Domenech C, Galí S*, Proenza J, Villanova-de-Benavent C

Dept. Cristal., Miner. i Dipòsits Minerals; Fac. Geologia; UB. *gali@ub.edu

The Punta Gorda Ni laterite deposit is part of a larger province of nickel laterites in northeast Cuba (Moa Bay district). This laterite profile is composed of four principal horizons from bottom to top: (1) serpentinized peridotite, (2) saprolite, (3) limonite and (4) ferricrete. Based on the mineralogy of the principal ore-bearing phases, the Punta Gorda deposit is classified as an oxide-type deposit. In this case, the upper part (limonite zone) is the main ore horizon. This limonitic horizon is mainly composed of goethite (>50 wt.%), and minor amounts of hematite, maghemite, gibbsite and Mn-Ni-Co oxyhydroxides (lithiophorite and "asbolane-lithiophorite intermediates"). The nickel content in goethite varies from 0.3 to 4.5 wt.% (average value = 1.4 wt.%). However, the exact location of nickel in goethite is still unclear, either adsorbed onto the surface or forming a solid solution within goethite.

In this study a 1D reactive transport model is applied to simulate the formation of this deposit. The weathering of a column of partially serpentinized peridotite is simulated by assuming the dissolution of primary minerals and the precipitation of secondary phases due to flow of meteoric water. This peridotite parent rock is basically composed of Ni-bearing forsterite (~0.4 wt.% Ni), enstatite, oceanic (primary) serpentine (~0.4 wt.% Ni) and magnetite. The dissolution of the forsterite and enstatite is assumed to be kinetically controlled, whereas that of primary serpentine and magnetite is considered to occur according to local equilibrium. As a consequence of the dissolution of these minerals, goethite (chosen as representative of Fe-bearing oxides) and a secondary Ni-rich serpentine (>1 wt.% Ni) are allowed to precipitate if oversaturated, following local equilibrium. Once released from primary minerals, Ni is considered to sorb onto the surface of goethite and/or to precipitate with the secondary serpentine.

Calculations have been done at 25ºC. The reactive transport model is performed with the geochemical code Phreeqc vs.3. Thermodynamic data used in calculations are from wateq4f.dat database although some changes were applied to the Ni-bearing minerals.

Modelling results show that both the observed mineral succession and the Ni content can be reproduced by considering the proposed conceptual model, showing that sorption of Ni onto goethite surface can account for the concentration of Ni in this horizon. This kind of studies is thus to be considered as a useful tool to improve the understanding of the different factors governing the process of lateritization of ultrabasic serpentinized rocks.

Characterisation and oxidation of seafloor massive sulphides, a study of the potential environmental impact of deep sea mining

Fallon E

University of Bristol. e.fallon@bristol.ac.uk

As the demand for metals continues to grow due to advances in technology, so does the price of metals. With the majority of economically viable terrestrial resources already exploited and fewer being discovered, previously discounted sources of metals are beginning to be more seriously considered. With beneficial advances in technology arising from the offshore hydrocarbon industry, the era for deep sea mining may soon arise. In order to support this future economic prospect, our knowledge and understanding of such deposits requires improvement with an associated need for study of the environmental impact that any future endeavours may have.

Sediment plumes have the potential to be created in both the exploration and extraction phase of deep sea mining. These plumes and their dispersal have largely been focussed in regards to nodule mining and their impacts on benthic ecosystems [1, 2]. There is however, limited study on the impact of the dissolution of these suspended particles in the water column and their subsequent dispersal or accumulation in the wider oceanic environment. Whilst dissolution studies of specific minerals have been undertaken [3], the majority are within the context of acid mine drainage arising from terrestrial mines [4, 5]. No dissolution studies exist that emulate the true composition of the sediments that will be thrown into aqueous suspension as a result of deep sea mining in a colder, more saline context. This material will include a variety of minerals, and it is the interaction of these minerals and inclusions in regards to galvanic interactions, that have the ability to substantially increase the dissolution of metals into the water column [6]. Of course, there a multitude of factors to consider in regards to the plume, such as its size, mineralogy, bulk chemistry, grain size distribution and surface area of the sediments, settling rate, temperature, pressure, salinity, dissolved oxygen and ocean currents. Whilst it has been suggested that mining will have no major environmental impact due to the high density of sulphides and thus their immediate re-deposition upon disturbance [7]; there is no real evidence to support this. Furthermore, even if settling does occur rapidly, the mining process ultimately exposes a high surface area of fresh sulphide minerals to the corrosive effects of seawater, allowing for oxidation and dissolution.

In order to identify the trace elements and potential toxins that will be contributed to the water column, a review of a multitude of sulphides from various tectonic settings with a range of mineralogy and geochemistry will be produced. This database will provide an accurate assessment of grain size distribution, mineralogy and bulk rock chemistry across samples prior to experiments. A variety of analytical techniques will be utilised including SEM: EDX and EBSD, XRD, and EPMA. Samples include those from a sediment hosted environment (Atlantis II Deep), volcanic hosted environment (TAG), back arc rift (Pacmanus), ultramafic hosted (Logatchev) and high temperature vent (Turtle Pits).

Subsequent experiments have begun to examine dissolution of different suspended sulphide materials at a range of temperatures, pH, dissolved oxygen contents and salinities - representing the variation in the plume environment. These experiments will seek to determine both the dissolution and settling rates of sulphides during active mining conditions and to better understand the variables that control this process.

[1] Bluhm H. (1994). *Aquatic Conservation: Marine and Freshwater Ecosystems*, 4, 187-201.
[2] Sharma R. *et al.* (2001). *Deep Sea Research Part II*, 48, 3363-3380.
[3] Feely R. *et al.* (1987). *J. Geophys. Res.*, 92, 11347-11363.
[4] Acero P. *et al.* (2013). *Applied Geochemistry*, 22, 659-666.
[5] Constantin C. *et al.* (2013). *J. Appl. Electrochem*., 43, 659-666.
[6] Abraitis P.K. *et al.* (2004). *Mineral. Mag.*, 68, 343-351.
[7] Halfar J. *et al.* (2002). *Mar. Policy*, 26, 103-106.

Fluid inclusion studies of the Boccassuolo VMS deposit (northern Apennines, Italy) – preliminary results

Kiss G[1], Garuti G[2], Zaccarini F[2*]

1 - Eötvös Loránd University 2 - University of Leoben
*federica.zaccarini@unileoben.ac.at

Numerous volcanogenic massive sulphide (VMS) deposits, classified as Cyprus-type Cu-(Pb-Zn), and formed in the Jurassic Ligurian Ocean occur in the ophiolites of the Italian Northern Apennines. One of these deposits, Boccassuolo, is found in the vicinity of the city of Modena. It consists of sulphide mineralized quartz veins cutting across pillow-basalt and basalt breccia. Mining activity was remarkable at Boccassuolo, thus several levels of this stockwork mineralisation can be studied. This unique situation allows the modeling of vertical changes in the hydrothermal system. Thus, the aim of the present study was to describe more precisely the characteristics of this hydrothermal process, especially because no fluid inclusion study was performed in the area before.

The stockwork mineralisation can be interpreted as the feeder zone of submarine hydrothermal vents. Pyrite, chalcopyrite and in the upper levels, sphalerite and galena also are the most common ore minerals, which occur together with quartz and calcite. As the sphalerite was not transparent in IR light, fluid inclusion study was performed only on the gangue minerals. Three different generations of quartz were distinguished; the earliest generation is characterised with coarse grained, eu- and subhedral crystals, the second generation contains medium grained, subhedral crystals, while the crystals of the last generation are fine grained and anhedral. The calcite fills up the remaining space, thus can be interpreted as the last mineral precipitated from the solution. The ore minerals occur syngenetically with the first and more commonly with the second quartz generation.

Primary fluid inclusions in the quartz and calcite contain vapour (V) and liquid (L) phases, and occur commonly along the growth zones of the crystals. The phase ratios are constant; 10-15% V and 90-85% L are typical in the generally 4-10 µm sized inclusions. One of the upper levels of the mineralisation is characterised with decreasing homogenisation temperatures from 233±38°C through 163±30°C to 111±2°C (from coarse through medium to fine grained quartz) and to 81±13°C (late calcite), while a locality representing one of the lower levels is characterised with decreasing homogenisation temperatures from 288±25°C to 239±31°C (from coarse to medium grained quartz) and to 80±6°C (late calcite). The inclusions found both in the quartz and in the calcite contain methane gas, thus chlathrate formation occurs upon cooling. Calculation of the salinities was done based on the Raman spectra of the inclusion fluid, as the small size did not allow observing the differences between the ice and chlathrate melting phenomena. A rather highly saline fluid of 12.6±2.8 NaCl equiv. wt% was found in every studied quartz samples.

Based on these results, a slight decrease in the temperature of the hydrothermal fluid can be interpreted, leading to the top of the system, which explains well the found mineralogical changes, too. The possible contribution of a magmatic fluid (gas) and the development of a rather dense brine zone can be also presumed.

Skarn minerals and scheelite in the Xintianling scheelite skarn deposit, southern Hunan province, China

Lu J*, Wang R, Zhang R

Nanjing University. *lujj@nju.edu.cn

The large-scale Xintianling scheelite skarn deposit in Nanling Range is located in southern Hunan province, China, and is genetically related to the biotite granite with high oxidation state. The granite has higher normal magnetite (~0.86 wt%) and low normal ilmenite content (~0.33 wt%) and high magnetic susceptibility with an average of 827×10^{-6} emu/g (n=14). Several distinct stages of skarnization and mineralization are inferred from paragenetic relationships based on observations of field and thin section. They can be divided into five broad stages in chronological order: grossularite + andradite + diopside (I), hornblende + actinolite + Fe-rich andradite + scheelite (II), vein type scheelite mineralization (III), molybdenite mineralization (IV), and calcite+pyrite+sphalerite+galena vein stage (V). Scheelite mineralization occurred dominantly in the Stage II as disseminated and less in stage III as vein type. Disseminated scheelite is closely associated with hornblende+actinolite assemblage. In terms of mineral assemblage, three kinds of scheelite-bearing vein can be identified: quartz + scheelite, epidote + fluorite + sphalerite + scheelite and tourmaline + chlorite + scheelite vein. Mineral assemblages in stage I indicate oxidized skarn. From stage I to stage II, compositions of garnet change from $And_{31-60}Gr_{38-63}Sp_{3-10}$ (And I) to $And_{58-81}Gr_{10-37}Sp_{1-10}$ (And II), indicating an increasing trend of Fe-end member mineral and oxygen fugacity. After replacement by hornblende and actinolite, And II was usually formed around And I. The occurrence of late stage molybdenite mineralization (stage IV) and calcite + pyrite + sphalerite + galena assemblage (stage V) suggests oxygen fugacity decreased in post-scheelite mineralization. A small amount of Spessartine ($Sp_{72-85}Alm_{6-17}Gr_{7-12}$) associated with sulfides is observed as spessartine-calcite vein in stage I skarn, corroborating further low oxygen fugacity in the late stage. The formation of spessartine is possibly related to the involvement of Mn from the wallrocks. The characteristics of garnet compositions and mineral assemblages in the different stages indicate that scheelite mineralization took place under higher oxygen fugacity condition. The compositions of pyroxene are $Di_{46-69}Hd_{20-52}Jo_{2-11}$. Hornblende and actinolite exhibit narrow Fe-rich and F-poor edges. Chlorite formed by replacing hornblende and actinolite is chiefly brunsvigite with $Fe^{2+}/(Fe^{2+}+Mg+Mn)$ ratios of 0.26 to 0.4, whereas chlorite in the late stage scheelite veins is mostly ripidolite with $Fe^{2+}/(Fe^{2+}+Mg+Mn)$ ratios ranging from 0.65 to 0.8. Tourmaline is mainly feruvite with a thin edge of uvite. The skarn minerals in the different stages contain extremely low W and no Sn. Mo contents in scheelite is less than 0.3 wt% and lower than those in oxidized scheelite skarn of other mines. Scheelite has higher Ce contents (1~2 wt%). Re contents of molybdenite range from 44 ppm to 110 ppm and are higher than those in molybdenite of other scheelite skarn and wolframite-quartz type deposits associated with S-type granite in Nanling Range, illustrating that Re content in molybdenite is probably influenced by oxygen fugacity of magma.

Mineral chemistry of skarn deposits in the north west of Iran

Mollai H

Department of geology Mashhad branch Islamic Azad University.
hamollai@yahoo.com

Skarn deposits in the northwestern Iran are the result of extensive I-type calc-alkaline and alkaline magmatic activity of Late Eocene-Oligocene and Oligo-Miocene age. This magmatic activity was responsible for the contact metasomatic mineralization as well as the porphyry-type copper occurrences in NW Iran. The important skarn deposits in these areas are Mazraeh skarn, Sungun skarn porphyry and Anjered skarn deposits. Skarn deposits in the northwest Iran formed at or near the contact of Oligo-Miocene magmatic bodies with Cretaceous impure limestone. Both endoskarn and exoskarn are developed along the contact and ore skarn in between as discontinuous belt. In general the dominant calc silicate (skarn) minerals in the area are garnet, pyroxene, actinolite and epidote, which are accompanied by quartz, feldspar, minor vesuvianite and hornblende. Based on EPMA data the andradite mole fraction in the garnet ranges from 30-99 %, followed by grossularite (0-57 %), and pyralspite (0-13 %). The composition of garnet appears to be controlled by the chemistry of the replaced mineral: garnet replacing plagioclase is richer in grossularite and that replacing pyroxene and calcite is richer in andradite. Within the ugrandite area, the pyralspite content increases with increasing substitution of Mg and Mn for Ca and the grossular content increase with increasing substitution of $A1^{+3}$ for Fe^{+3}. In the veins the andradite component predominates (>99%). Epidote is one of the important products of hydrothermal fluid that was rich in Al. This Al-rich fluid may have played important role in carrying sulfide ore solution. Fe^{+3} replacing Al ranges from 71-95 mol%. The Mn^{+3} in the epidote ranges between 0.7 and 5.35 mol% piemontite. Pyroxene belongs to the diopside-hedenbergite series, with 38 mole % Hd/(Hd+Di) and minor amount of Mn.

Keywords: mineral chemistry, garnet, epidote, skarn, North West of Iran.

Uncommon telluride compositions from Musariu, Apuseni Mts., Romania

Săbău G[1], Berbeleac I[2], Negulescu E[1], Costin G[3*]

1 - Geological Institute of Romania 2 - Institute of Geodynamics Bucharest 3 - Rhodes University *g.costin@ru.ac.za

The Musariu native tellurium and telluride vein assemblages are dominated by a stage of profuse tellurium and sylvanite deposition. In two depositional stages bracketing this main episode we identified apparently new phase compositions (Table 1). Localized areas within the Te masses contain engulfed and partly digested clusters of pyrite, altaite and quartz with minor Bi tellurides. Pyrite-quartz swarms contain rucklidgeite grains overgrowing pyrite (Figure 1a), occasionally associated with frohbergite and magnetite. Altaite-rich inclusion clusters associate instead with Bi tellurides (Figure 1b and c). Antimonian tellurobismuthite is accompanied by phase $SbBi_4Te_7$, corresponding to the tellurobismuthite derivative $(Bi,Sb)_{2.14}Te_3$, equivalent to $Bi_2{\cdot}14(Bi,Sb)_2Te_3$ or $12(Bi,Sb)_2Te_3{\cdot}2Bi_3Te_3$.

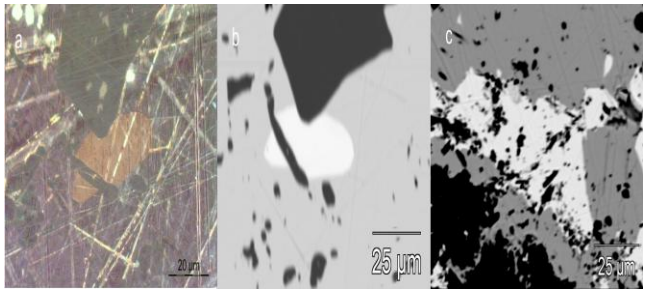

Figure 1: (a) Rucklidgeite including pyrite relics in tellurium host (reflected light, crossed polarizers); (b) BSE image of (a); (c) Bi-telluride blebs around altaite also included in tellurium, BSE image.

Other uncommon compositions appear in the stage postdating sylvanite deposition, namely Ag-tellurides (Figure 2) which mantle and corrode sylvanite, also insinuating along a network of interconnecting veinlets. Very often the Ag-telluride crystals are pervaded by worm-shaped cavities propagating inside from the grain boundaries. The compositions partly correspond to empressite (compact grains), while excess Te compositions are habitually recorded in spongy crystals. Ag-telluride compositions with excess Te straddle the AgTe-Te join, where no stable phases are known so far from nature and experiments. The spongy crystals suggest crystallization of metastable Ag-Te phases from which excess Te is unmixed and levigated, leaving the vermicular voids behind.

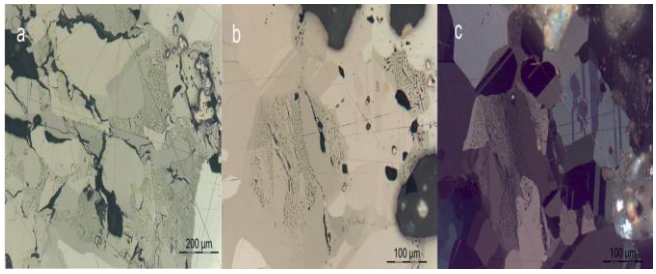

Figure 2: (a) Ag-tellurides with worm-like channels corroding tellurium, altaite and sylvanite; (b, c) indifferent relationship between crystal boundaries and channel swarms in Ag-telluride infiltrating in a sylvanite aggregate - photomicrographs, reflected light

Table 1. Composition of the phases referred to in text

Mineral	*S*	*Te*	*Se*	*Sb*	*Bi*	*Ag*	*Pb*	*Fe*	*Total*
Rucklidgeite	0.01	44.79	0.85	2.34	37.41	1.16	13.2	0.13	99.89
$SbBi_4Te_7$	0.01	48.27	0.15	7.26	42.28	0.5	2.06		100.53
Ag_4Te_5	0.03	60.39	0.07	0.09		41.1		0.05	101.73
Ag_2Te_3	0.01	63.26	0.1	0.04		37.15			100.56
$AgTe_2$	0.02	70.98	0.13	0.14		30.06			101.33

Determination of mercury in the Allchar Mine

Soufek M[1*], Spasevski L[2], Bermanec V[3]

1 - Croatian Natural History Museum *marin.soufek@hpm.hr 2 - Department of Chemistry of Faculty of Science and Mathematics, University of Zagreb 3 - University of Zagreb

The Allchar deposit, in the Republic of Macedonia, is unique in the world because of the economic concentrations of thallium and the consequent assemblage of thallium minerals. A number of thallium minerals have been found for a first time in Allchar. It is the type locality for ten thallium minerals, many of them found nowhere else.

In addition to the presence of mercury into vrbaite, it has not been registered in any other mineral present in this location. This work found that there is more generation of lorandite and realgar on which were conducted morphological and chemical determinations. The later generation of lorandite and realgar show the presence of mercury. For the earlier generation, in both minerals, the presence of mercury is not even recorded.

A total of 11 samples of lorandite ($TlAsS_2$) and 10 realgar (AsS) samples of later generation were investigated in this study. The concentration of mercury in lorandite and realgar samples was studied by Electron Microprobe analysis and Energy-dispersive X-ray spectroscopy (EDS), while distribution of mercury was determined by EDS and SEM technique. Studies indicate that these samples have constant contents of mercury, of 0.29-0.34 wt.%Hg in lorandite and 0.39-0.64 wt.%Hg in realgar.

During this investigation cinnabar (HgS) was asserted very rarely and for a first time it occurs in crystals up to 2 mm.

Keywords: Allchar, mercury, thallium, lorandite, realgar, cinnabar, Electron Microprobe analysis, EDS chemical analysis

Abstract Number : 684

Micrometer scale mineralogical and textural study of multiphase manganese oxide ores in the Úrkút Manganese Deposit, Hungary

Topa B[1*], Leskó M[1], Váczi T[1], Vigh T[2], Weiszburg T[1]

1 - Department of Mineralogy, Eötvös Loránd University *topabogi@gmail.com
2 - Manganese Mining and Processing Ltd., Úrkút

In the Úrkút Manganese Deposit (Bakony Mountains, Transdanubian Range, Hungary) related to the Toarcian oceanic anoxic event, both oxidic and carbonate manganese ores occur. Our goal was to trace the connection between the two ore types. We sampled geological sections in the mine containing both ore types in an undisturbed, intimate, layered texture as well as transition zones between the ore body and the limestone footwall. In the current work we focus on the oxidic layers and their relationship to the surrounding formations (laminated carbonate ore or the limestone footwall). The formation of these compact black ("oxidic") layers has been assumed to be in connection with the postdiagenetic oxidation of the carbonate ore related to sulphuric acid formation and the remobilization of manganese. However, details of that process have not been worked out, neither mineralogically, nor geochemically.

The manganese-oxide(-hydroxide) minerals determined by bulk phase analytical methods are of too small grain size for proper optical identification, thus previously only speculations could be set up for the relationship between the observed textures and the mineral phases.

Our aim was to map, down to the micrometer size range, the texture-related mineralogical features in order to separate the pre-diagenetic, diagenetic and post-diagenetic processes. In our study we combined X-ray powder diffraction (XRD), scanning electron microscopy (SEM-BSE, SEM-SE), X-ray microanalysis (SEM+EDX) and Raman spectroscopy for the qualitative phase analysis in textural context.

In our geological profile the lowermost manganese-bearing layers, right on the top of the footwall, are oxidic followed by several m thick lamellar carbonate ore sequence in which oxidic layers/lamellae are also present. The measurements show that manganite and cryptomelane are the dominant minerals, while other Mn-bearing phases (e.g., hollandite) are present in subordinate amount.

Raman spectroscopic fingerprinting was very effective in separating the different manganese oxide(-hydroxide) mineral phases at the micrometer scale. The direct identification of these phases by using Raman databases was simple for manganite, however we needed to set up a collection of Raman reference samples in order to overcome the limited coverage of Raman data published for other minerals in the system.

Our combined method allowed us, for the first time, to connect oxidic manganese mineral phases, known before from bulk phase analyses only, directly to microtextural features.

The observed textural characteristics of the investigated oxidic layers show fully preserved normal diagenetic instead of postgenetic sedimentological features. The complex manganese oxide mineralogy within that special texture indicates that a more complicated genetic expla-nation is needed for the formation of these oxidic layers than the earlier theories expected.

A unique gold mega-event in the Mesoarchaean: possible sources for Witwatersrand-type gold mineralization

Frimmel H

University of Würzburg hartwig.frimmel@uni-wuerzburg.de

A holistic approach to, and comparison of, Witwatersrand-type gold deposits/ occurrences worldwide revealed that this style of conglomerate-hosted mineralization is by no means unique to the Kaapvaal but common to most Archaean/Palaeoproterozoic cratons. The age of the variably mineralized fluvial to fluvio-deltaic conglomerates ranges from 3.1 to 1.9 Ga, its tectonic setting from continental rifts to passive margins and syn-orogenic foreland basins. For each example a case can be made for a paleoplacer model. Although several of the examples show evidence of post-depositional hydrothermal overprint and local mobilization of ore components, purely epigenetic hydrothermal models fail to explain the geometry of the ore bodies as well as available lithogeochemical, mineral chemical and isotope data. Conglomerates older than 2.4 Ga are characterized by the abundance of detrital (and secondary) pyrite, and in most cases also detrital uraninite, whereas younger examples (<2.2 Ga) contain Fe-oxides instead. A common denominator of all Witwatersrand-type deposits/ occurrences is the stratigraphic position on top of erosional unconformities and an Archaean to Palaeoproterozoic hinterland.

The Witwatersrand deposits differ from all other examples by a Au endowment that is two to three orders of magnitude greater, a lack of point sources (such as orogenic-type auriferous quartz veins), an abundance of gold-rich kerogenous seams that reflect former microbial, probably cyanobacterial mats, a scarcity of typical gold nuggets, and orders of magnitude higher Os contents in the gold. These systematic differences help to explain the most likely source for Witwatersrand gold. A genetic model is proposed that involves extraction of Au into juvenile crust from an anomalous (i.e. highly siderophile elements-enriched) mantle domain by high degrees of partial melting in the Mesoarchaean when mantle temperature reached its maximum. The cause for the postulated mantle heterogeneity could have been exogeneous addition during intense meteorite bombardment of the Palaeo-to Mesoarchean Earth or endogeneous, i.e. plume-like ascent of left-overs from inefficient core formation or plumes from the core-mantle boundary. Mesoarchaean crust thus enriched in Au became subject to intense weathering under an aggressive, reducing atmosphere. This, combined with very high erosion rates due to the lack of land vegetation and high solubility of Au in Archaean river water, led to a Au-flux from the Archaean land into the oceans about four orders of magnitude greater than today. En-route and in shallow marine coastal environments, local presence of oxygen from early aerobic microbial (cyanobacterial) mats acted as effective trap for the Au dissolved in river water. Low resistance to erosion caused most of these microbial mats to be re-worked during regressive events, thus providing the source for the majority of detrital gold particles in the Witwatersrand conglomerates. Post-depositional hydrothermal/metamorphic overprints explain why today much of the gold is found in texturally late positions but had little significance on the macro-scale distribution of the gold.

Elsewhere, a less fertile hinterland and/or less reworking of older sediments led to correspondingly lower Au endowment. Most of the Archaean sediments were affected by crustal reworking in the course of later tectonic overprints. The multitude of fluids and melts involved in these reworking processes gave rise to the great variety of gold deposit types known in post-Archaean rock crustal sections.

Magmatic salt melt and vapor – extreme fluids and Cl-rich minerals in the Biely Vrch shallow porphyry gold deposit (Western Carpathians, Slovakia)

Kodera P[1*], Heinrich C[2], Lexa J[3], Bačík P[4], Uher P[4], Wälle M[2]

1 - Dept of Mineral Deposits, Comenius University, Slovakia

* peter.kodera@gmail.com 2 - Department of Earth Sciences, ETH Zürich, Switzerland 3 - Geological Institute, Slovak Academy of Sciences, Slovakia 4 - Dept. of Mineralogy and Petrology, Comenius University, Slovakia

The recently discovered Biely Vrch deposit in the Western Carpathian magmatic arc is the most extreme example of a porphyry gold deposit, with an exceptionally low Cu/Au ratio (0.018 wt% Cu / ppm Au) and with a lack of sulfide minerals. The deposit is located in the central zone of the Neogene Javorie andesite stratovolcano in Central Slovakia, centered on a diorite to andesite porphyry stock. Alteration is dominated by intermediate argillic type that variably overprints earlier K-silicate at shallow and Ca-Na silicate alteration at deeper levels. Ledges of advanced argillic alteration are the youngest type. Stockwork of quartz veinlets, including characteristic banded quartz veinlets, is coincident with the area of economic Au mineralization (34 t Au @ 0.8 g/t Au; Hanes *et al*., 2010). As indicated by the paleovolcanic reconstruction, the intrusion was emplaced at a very shallow depth (~500 m), similar to porphyry gold deposits in the Maricunga belt of N Chile, which had important consequences for fluid properties of associated fluids and some alteration minerals.

Four types of fluid inclusions have been recognized in quartz veinlets: ubiquitous vapor inclusions coexisting with unusual but widespread salt melt inclusions; rare brine inclusions restricted to the deepest parts of the porphyry; and minor secondary aqueous inclusions of variable salinity, associated with argillic alteration. The salt melt inclusions contain several salt crystals, but no visible liquid at room temperature, while based on Raman spectroscopy most of the solid phases are water-free. Based on CL imaging and Ti-in-quartz thermometry, they are hosted by early veins formed between near-magmatic temperatures and at least ~590°C, but also in banded veinlets, formed at temperatures down to 380°C. LA ICP MS microanalyses showed near-constant composition of the salt melts (~50 wt% $FeCl_2$, ~30 wt% KCl and ~20 wt% NaCl), with a compositional trend consistent with precipitation of K-bearing halite from fluids that cooled from high temperature. The fluids contained about 10 ppm Au, and their Au/Cu ratio was similar to or even higher than the bulk metal ratio in the Biely Vrch deposit. This exceptional fluid required an Fe-rich dioritic magmatic source that was emplaced at shallow subvolcanic depth (<3.5 km), directly exsolving a hypersaline liquid and magmatic vapor at high temperature (~850°C). During ascent to the level of the porphyry intrusion (0.5 to 1 km), fluid expansion at high temperature but low pressure led to halite precipitation and further water loss to the vapor, generating an increasingly Fe-K-rich salt melt with high concentrations of Au but negligible Cu. The low sulfur fugacity resulting from fluid expansion, suppressed precipitation of sulfides, explaining the gold-only enrichment of ore. Our data indicate that the subsolidus evolution of magmatic fluids towards Fe- and Au-rich salt melts is favored by relatively mafic and alkalic source magmas, probably generated from a mantle enriched in Au by preceeding subduction metasomatism and re-melted in an extensional setting.

Unusually high concentration of Cl in fluids resulted in high concentration of Cl in some silicate minerals in altered diorite porphyry, especially in hydrothermal biotite and amphibole from the early K-silicate and Ca-Na silicate alteration, and in tourmaline probably associated with some later alteration. Some of the biotites (chlorine-dominant annite) contain here up to 7.5 wt% Cl, while some of the amphiboles (potassic-chlorohastingsite) contain up to 5.0 wt% Cl. Tourmaline attains here up to 0.45 wt% Cl (X-site vacant Al-rich oxy-tourmaline). In the case of biotite and tourmaline, Cl content is significantly higher than ever published in these minerals worldwide.

Acknowledgement: Support by APVV grant 0537-10 is acknowledged.

Nuggets to nanoscale: the distribution of Au in adularia-sericite epithermal deposits

Mauk J[1*], Koenig A[1], Menzies A[2], Fyfe S[3], Newton A[3], Lowers H[1]

1 - US Geological Survey *jmaum@usgs.gov 2 - Universidad Católica del Norte

3 - The University of Auckland

New petrographic, SEM, EMPA, LA-ICP-MS, and QEMSCAN analyses, combined with published studies, provide insight into the distribution of Au in adularia-sericite epithermal deposits. The majority of the Au in these deposits resides in relatively fine-grained electrum that is commonly 1 to 5 microns, and is typically recoverable by conventional cyanidation techniques. The electrum normally resides in banded veins, in bands that are enriched in other ore minerals such as acanthite, naumannite aguilarite, or telluride minerals.

Electrum grains that are greater than one mm in diameter occur in some deposits, mostly in zones that contain bonanza-grades (>30 g/t Au). The coarse grain size of this electrum can cause a nugget effect that may inhibit effective recovery by conventional cyanidation, and the addition of a gravity circuit to extract this coarse-grained electrum may significantly improve recoveries.

In some deposits a portion of the Au appears to be in solid solution in arsenian pyrite, where arsenic occurs as As^{-1}, which substitutes for S, and as As^{+3}, which undergoes coupled substitution with monovalent cations such as Au^{+1}, for Fe^{+2} in the pyrite structure. The As^{-1} is common in reduced deposits, such as Carlin type and adularia-sericite epithermal deposits, whereas the As^{+3} occurs in more oxidized deposits such as high sulfidation epithermal deposits. The As causes distortion of the pyrite lattice, which allows Au to enter the pyrite structure. Significantly, this Au is refractory, and cannot be recovered by cyanidation. For most adularia-sericite epithermal deposits, the amount of Au that resides in solid solution in arsenian pyrite is relatively minor, but in some places, such as the Golden Eagle deposit, USA, Au in arsenian pyrite appears to be the predominant form of Au.

In addition, there is increasing recognition that nanoparticles less than 1 µm across play an important role in hosting Au in adularia-sericite epithermal deposits. This Au appears to mostly occur as electrum nanoparticles in deposits hosted by calc-alkaline rocks, but in deposits hosted by alkaline volcanic rocks, Au telluride minerals may form a significant fraction or even the majority of the Au nanoparticles.

In summary, the distribution of Au in adularia-sericite epithermal deposits may be more varied and complex than commonly accepted. Furthermore, defining Au distribution at individual deposits may provide opportunities for increasing Au recovery, and for deeper knowledge of the mechanisms that control this distribution.

Association of bonanza grade gold with pyrobitumen in the Rompas Au-U prospect, Peräpohja Schist Belt, Northern Finland

Molnár F[1*], Pohjolainen E[1], Johanson B[1], Pakkanen L[1], Takács Á[2], Váczi T[2], Cook N[3], Vanhanen E[3], Hudson M[3]

1 - Geological Survey of Finland *ferenc.molnar@gtk.fi 2 - Eötvös Loránd University, Hungary 3 - Mawson Resources Ltd., Australia

The Rompas prospect is one of the most important recent ore discoveries in Northern Finland, with numerous occurrences of bonanza grade gold (e.g. an average of 0.59m@203.6 g/t Au in 80 channel samples). It is located in the northern part of the Peräpohja Schist Belt, a Paleoproterozoic (2.5-1.9 Ga), continental platform to rift related sedimentary-volcanic sequence metamorphosed and deformed during the Svecofennian Orogeny (1.9-1.8 Ga; [1]).

The high grade ore at Rompas is spatially associated with a swarm of 0.5-20 cm thick calc-silicate veins hosted by ca. 6 km strike length metabasalt units. These mafic units are intercalated with quartzite, mica schist and graphitic schist, but calc-silicate veins in the other rock types do not host ore. Metamorphism resulted in recrystallization of the originally quartz-carbonate- veins to a ferroan dolomite - ankerite - diopside (± graphite ± residual quartz) composition with coarse grained uraninite grains, which are partially replaced by the carbonate groundmass and minor coffinite. Mineralogy and Raman spectra of graphite imply >500°C, amphibolite facies conditions. Multiple deformation resulted in complex folded vein structures and formation of actinolite, chlorite and calcite during retrogression.

Gold occurs in fractures of coarse grained uraninite in the calc-silicate veins and in fractures or on the surface of undeformed pyrobitumen nodules. These nodules contain round or fragmented, few tens of microns sized grains of uraninite in thin (0.1-10 cm) undeformed calcite veins that cut the calc-silicate veins. Pyrobitumen also rim coarse grained uraninite, occasionally-the pyrobitumen nodule textures are comparable with radiolitic polymerization of hydrocarbons on uraninite grains.

The coarse grained uraninite in calc-silicate veins contains less than 2.5 wt % ThO_2 and around 0.5 wt.% Y_2O_3, whereas uraninite have ThO_2 and Y_2O_3 contents up to 15 wt. % and 2.5 wt. %, respectively, in the pyrobitumen nodules. Pb contents are highly variable depending on the alteration of uraninite. The composition of gold is identical in the different types of ore with 1.2 ± 0.95 wt.% Ag, 1.97 ± 0.54 wt.% Cu and 1.55 ± 0.32 wt.% Pb. The pyrobitumen contains around 1 wt.% sulphur. Gold is associated with galena, altaite, nickeline, cobaltite and rare Pb-bearing maldonite, hunchunite and auricupride in the porphyroblastic uraninite. Pyrite, pyrrhotite, chalcopyrite, galena, altaite, molybdenite, Bi-tellurides and titanite associate with gold in pyrobitumen-related occurrences.

Raman spectra show differences between the well-ordered graphite structure of carbonaceous material in the calc-silicate veins and the disordered structure of undeformed pyrobitumen nodules. Mean random reflectance data for pyrobitumen recalculated to vitrinite are between 2.48 and 4.40 % suggesting a 270-340°C maximum temperature for thermal maturation.

The formation of the high grade gold zones post-dated metamorphism and even a hydrocarbon mobilization event. The high Th-content of uraninite associated with pyrobitumen and the relatively high temperature for maturation of the pyrobitumen indicate a potential role of the late orogenic granite magmatism (Central Lapland Granite Complex, ca. 1.810-1.76 Ga [2]). Highly concentrated precipitation of gold was probably driven by local de-sulphurization processes and other chemical changes triggered by formation of galena and altaite from the radiogenic lead content of uraninite and by the taking up of sulphur by pyrobitumen. Mineralogy of gold enrichment suggests a source rock role for black schists in the region.

[1] Laajoki K. (2005). Karelian supracrustal rocks. In: Lehtinen, M., Nurmi, P., Rämö, O.T. (eds.), *Precambrian geology of Finland - Key to evolution of the Fennoscandian Shield*. Elsevier B.V., 281-341.

[2] Lauri L. (2012). Temporal and Hf isotope geochemical evolution of southern Finnish Lapland from 2.77 Ga to 1.76 Ga. Bulletin of the Geological Society of Finland, 84, 121-140.

Gold in the epithermal ores of Kamchatka

Okrugin V[1*], Andreeva E[2], Etschmann B[3], Brugger J[3]

1 - Institute of Volcanology and Seismology FED RAS, Vitus Bering Kamchatka State University *okrugin74@gmail.com 2 - Russian Academy of Science &Vitus Bering Kamchatka State University 3 - Monash University

Kamchatka is one of the most prospective mining regions of Northeastern Russia. Kamchatka covers an area of 464 300 km2 and features an active continental margin, resulting in high seismicity, magmatic (32 active volcanoes) and hydrothermal activity (more than 264 hydrothermal systems). Exploration of and research into mineral deposits began only in the middle of the last century.

In Kamchatka, gold epithermal deposits are an important resource containing up to 1,000 ton of gold and 10,000 ton of silver. There are three main types of gold deposits: (i) polymetallic veins (Amethystovoe, Kumroch, Oganchinsky, Mutnovsky); (ii) low-sulfidation Au-Ag type (Sergeevsky, Aginskoe, Kungurtsevskoye, Rodnikovoye, Asachinskoye), and (iii) high-sulfidation type (Maletyvayam, Ozernovskoye).

The ages of these deposits correspond to the age of the volcano-plutonic belts with which they are spatially and genetically connected. It varies from 90-75 Ma (Sergeevskoye) to 0.05 Ma-present (Mutnovsky). The majority of veins can be described as multi-phase and polygenic. Ore formation occurs actively at the Mutnovsky ore field.

Gold minerals include native gold, Au-Ag alloys, uytenbogaardtite, and Au-Ag tellurides. Native gold occurs mainly in small particles - from 2 to 1000 µm with complex morphologies. There are signs that microorganisms participated in the formation of native gold. There are oxidation zones in which both primary and secondary gold can be found. Mustard gold, formed via the transformation of Au-tellurides, is widespread in some deposits [1].

[1] Okrugin V.M., Andreeva E., Etschmann B., Pring A., Li K., Zhao J., Griffins G., Lumpkin G.R., Triani G. and Brugger J. (2014). Microporous Au: comparison of textures from Nature and experiments. *American Mineralogist*. DOI: 10.2138/am.2014.4792.

Metallogenic models and gold exploration – a focus on Africa

Robb L

Department of Earth Sciences, University of Oxford. laurence.robb@earth.ox.ac.uk

More gold has been produced from the African continent than from any other. Numerous orogenic gold deposits of Archaean age are found on several stable cratonic blocks, as well as in the Palaeoproterozoic Birimian orogeny of West Africa, although gold production on the continent is still dominated by the Witwatersrand basin on the Kaapvaal Craton. The search for new gold deposits in Africa continues unabated, with exploration activity catalyzed by companies who acquire licences on the basis of (i) the availability of tenements that occur within geological/tectonic provinces with known gold endowment; and (ii) metallogenic models that fit the characteristics of other deposits in the region and can be used to guide exploration.

A number of examples illustrate the importance of developing better constrained metallogenic models:-

1. Although it is generally accepted that the modified placer model best explains the origin of gold in Witwatersrand conglomerates, the nature and timing of gold remobilization is poorly understood and there has been little or no application of this paradigm to the search for additional gold resources either within the basin, or adjacent to it;

2. The "continuum model" is apt for explaining the formation of many orogenic gold deposits but is less applicable to gold deposits where exhumation and extension have focused auriferous fluids in structures that are neither steep nor compressional, such as at Damang in Ghana;

3. There is now compelling evidence that a significant proportion of orogenic gold occurrences is associated spatially and temporally with granitoid emplacement. The origin of fertile granitoid intrusions, however, remains uncertain and a variety of settings is implicated, including porphyry Cu-Au look-alikes (Gaoua), IOCG analogues (Guelb Moghrein) and the reduced intrusion related (RIRG) Au-Bi deposits of the Kibaran orogeny;

4. Although the nature and composition of auriferous hydrothermal fluids is well studied, the role of fluid - rock interaction and the controls of gold precipitation is less well understood. Alteration parageneses play a critical role in determining the controls on gold concentration and new techniques, such as the application of portable infrared spectroscopy, will play an important role in future exploration strategies;

5. Obtaining accurate ages of host rocks is now routine, but determining well constrained ages of mineralization is more challenging. Knowing the relationship between host rock, metamorphism/tectonism and ore precipitation may reveal unexpected nuances, such as in the Murchison greenstone belt of South Africa where gold mineralization is now known to form part of a broader system at 2.97 Ga that also resulted in VMS style Cu-Zn mineralization.

Explorers of the future will look increasingly to non-conventional tectonic settings as conventional and more mature provinces are depleted. Previously overlooked terranes, such as the rifts of Ethiopia, the poly-orogenic Birimian-Panafrican terranes of Western Nigeria and the Mesoproterozoic Kibaran orogenic belt, are now beginning to attract attention.

Investigation of mineralisation characteristics of the Kago low-sulfidation epithermal deposit, Nansastu District, Japan

Tindell T[1*], Imai A[2], Takahashi R[2], Yonezu K[1], Boyce A[3], Schersten A[4], Ogata T[2], Watanabe K[1]

1 - Kyushu University *tindell-tom@mine.kyushu-u.ac.jp 2 - Akita University

3 - Glasgow University 4 - Lund University

The Nansatsu District, located in the southern part of the Satsuma peninsula, hosts numerous Au-Cu high-sulfidation mineralisations. About 2 km north of these classic Nansatsu-type mineralisations lies the Kago low-sulfidation Au-Ag deposit. The proximity of these differing epithermal styles suggests that there is an intimate relationship in the shallow hydrothermal system. The dominant structural trend in southern Kyushu is orientated NE-SW, which is mirrored in the breccias and fractures of all Nansatsu high-sulfidation deposits. Similarly, hydrothermal veining and breccias of the Kago deposit exhibits the same structural trends. The deposit is hosted in the Shimanto Supergroup, which is composed of Cretaceous mudstone and sandstone interstratifications. Conversely, the high-sulfidation deposits are hosted in the Miocene Nansatsu-Group volcanics (approx. 7 to 4.5 Ma). The linear NE-SW trend aligns the Kasuga, Sonomi, Kurigano silicified bodies and the Kago deposit, which make up the western extent of mineralisation. Precious metals present in colloform and crustiform banded quartz ore include; electrum, polybasite and Ag-tetrahedrite. The highest-grade ores are present in hydrothermal quartz breccias. EPMA analysis of electrum from high-grade breccias shows that gold composition has a narrow range from 52-56 at%. Colloform and crustiform banded ore and hydrothermal breccias host significant adularia to enable accurate Ar/Ar age dating, which suggests that the principal age range for all vein groups is from 3.98 to 4.23 Ma. The principle deposits of the Nansatsu-type mineralisations range from 5.5 to 4.15 Ma. This would indicate that mineralisation of the Kago deposit was co-eval with that of the neighbouring deposits. Quartz oxygen isotopic data suggest that fluids of the Kago deposit are composed of meteoric waters ranging from -4.7‰ to -0.3‰ based on a fluid inclusion temperature range of 220-240°C, with late stage chalcedony forming at 170-190°C. This suggests that it may have been generated by recirculated ground waters, heated by the magmatic hydrothermal system of the principal Nansatsu high-sulfidation deposits. However, the pyrite sulfur isotopic composition suggests that sulfur was derived from outside the Shimanto Supergroup host, ranging from -1.7 to +2.7‰. Although this result is similar to sulfur isotopic results from the Kasuga high-sulfidation deposit, much of the sulfur is present as sulphate, which is not mirrored in the Kago deposit.

Structural setting and styles of gold-bearing shear zones in the Bissa mining district, Goren Greenstone Belt, Burkina Faso

Tourigny G[1*], Houssou N[1], Putro S[2], and Cameron D[3]

1 SEMS Exploration, Ouagadougou, Burkina Faso.
*ghislain.tourigny@sems-exploration.com

2 Bissa Gold SA, Burkina Faso. 3 Goldrush Resources Ltd., Canada

The Goren Greenstone Belt (GGB) forms part of the Paleoproterozoic Baoulé-Mossi domain of the West African Craton and hosts several structurally-controlled gold deposits including the Bissa mine and satellite prospects including the Ronguen gold deposit in Northern Burkina Faso. These two deposits contain total reserves and resources exceeding 1.8 million ounces. Gold mineralization consists of pervasive sulfide disseminations and fracture related sulfides with auriferous quartz-vein systems that are associated with brittle-ductile shear zones.

Well-foliated and lineated greenschist facies tectonites recorded evidence of two principal phases of deformation and faulting. The early phase D1 is responsible for the development of gently inclined thrust faults and of a bedding-parallel foliation which is coplanar with the axial plane of an early NW- to ENE-trending fold set. F1 folds range from sub-horizontal to upright and involve a thin-skinned tectonic event characterized by recumbent folds developed on the hanging wall of bedding-parallel thrust faults that propagated along weak layers. The D2 deformation is responsible for the development of a penetrative NE-trending regional foliation, upright or slightly overturned F2 folds and associated NE-trending steep sinistral-reverse faults well-developed at the Bissa mine.

Greenschist facies volcano-sedimentary rocks of the Bissa district are heterogeneously deformed and obliquely cut by two types of gold-bearing shear zones chronologically associated with D1 and D2 respectively. Fault-controlled D1 mineralization is composed of a typical orogenic quartz-carbonate vein system occupying the central part of gently south-dipping and north-verging bedding-parallel thrust faults identified at the Ronguen deposit. This early mineralization developed mostly on the limbs of recumbent F1 folds along graphitic argillite layers and at the contact between competent diorite dykes and surrounding softer metasediments.

Fault-controlled D2 mineralization is best observed at the Bissa mine and is associated with pyritic disseminations and pyrite veinlets and to a minor extent with quartz-carbonate-pyrite veins and veinlets. The principal vein set is composed of shear veins and breccia veins found in NE-trending sinistral-reverse shear zones developed along a major volcano-sedimentary contact as well as within a complexly folded turbiditic sequence. In addition to fault-controlled ore, some orebodies lie along the culminations of NE-trending fold axes. The Bissa Southwest gold deposit is on the hinge zone and limbs of a major F2 anticline where fractures associated with fold hinges and parasitic folds may have played an important role in localizing mineralization.

The results of the study show that gold deposits of the Bissa district formed during a protracted inhomogeneous progressive deformation involving an early thin skin thrust tectonism (D1) followed by a major regional transcurrent shearing event (D2). The metallogenic implication of this study is of particular interest because it suggests that gold mineralization is polyphased and linked to both D1 thrusting (Tangean, 2100-2130 Ma) and D2 transpression (Eburnean, 2130 to 1980 Ma) events.

West African orogenic gold deposits: do they fit the global paradigm?

Treloar P[1*], Lambert-Smith J[1], Lawrence D[2], Wiedenbeck M[3], Boyce A[4]

1 - Kingston University *p.treloar@kingston.ac.uk 2 - Randgold Resources
3 - GFZ-Potsdam 4 - Glasgow University

The current paradigm with respect to orogenic gold deposits is that they are dominantly sourced from metamorphic fluids. In this model metals are leached during metamorphism and transported in low salinity, CO_2 rich alkaline fluids largely as S complexes. This is in complete contrast to epithermal gold deposits. Evidence for the metamorphic model is maybe tenuous and is largely built around S isotope signatures and the nature of the low salinity, CO_2 rich fluids. There has long been a debate in the literature as to how valid this paradigm actually is. Recently, Lawrence *et al.* [1, 2] used mineralogical and fluid inclusion data to argue for a magmatic input into the Loulo gold deposits in West Mali, although accepting a dominant metamorphic signature.

The Loulo mining camp of West Mali hosts gold mines with a combined resource of over 17 Moz, making this one of West Africa's most important Au regions. Here, both the Gara and Gounkoto deposits feature two distinct hydrothermal fluids: 1) A high temperature, hypersaline, Na-Fe-Cl-B bearing fluid of uncertain origin and 2) a lower temperature, low salinity, CO_2-N_2-H_2S rich metamorphic fluid. Lawrence *et al*. [1, 2] argued that the former fluid had a magmatic source, potentially linked to Fe skarn bodies associated with quartz diorite plutons. Tourmaline is a key component of the Loulo deposits. New Boron isotope data suggest that the tourmalines have a sedimentary rather than magmatic source suggesting that the hypersaline fluids probably also have a metamorphic source. This would be consistent with the $\delta^{34}S$ isotope data of >10 reported by Lawrence *et al.* [1, 2].

However, other orogenic gold deposits from the region are less clearly sourced from metamorphic fluids. Deposits from Massawa (Eastern Senegal) and Morila (South Mali), for both of which mineralisation can be demonstrated to be synchronous with felsic magmatism, as well as Tongon (Northern Cote d'Ivoire) where gold mineralisation may be linked to exo-skarn mineralisation have $\delta^{34}S$ signatures close to 0, which would be consistent with a magmatic fluid.

In this presentation mineral paragenetic data together with fluid inclusion and stable isotope chemistries will be used to suggest that the role of magmatic fluids in the development of world-class orogenic gold deposits may have been underestimated.

[1] Lawrence *et al.* (2013). *Econ. Geol.* 108, 199-227.

[2] Lawrence *et al.* (2013). *Econ. Geol.* 108, 229-257.

Gold nuggets and associated minerals from the Murcielago placer deposit, Lepaguare valley (Honduras)

Alunno S[1], Nazzareni S[2*], Zaccarini F[3], Mattioli M[4], Renzulli A[4]

1 - Goldlake 2 - University of Perugia *sabrina.nazzareni@unipg.it 3 - University of Leoben 4 - University of Urbino

The presence of lode and placer gold deposits has been reported from several countries in Central America [1]. However, little is known about gold mineralization in Honduras and only lode deposits have been described [2-4]. According to these authors, the Honduras gold deposits occur in quartz veins and in Au-Cu skarns. One ot these deposits is located in the valley of Lepaguare (Olancho district, central Honduras) and consists of gold mineralization in quartz veins hosted by low-grade metamorphic rocks comprising graphitic schists and quartzites of the pre-Mesozoic metamorphic basement [4]. Recently, Eucantera company (Goldlake) started a gold mining project in this area based on "green" environmentallly friendly extraction. The processing of gold-bearing sand and gravels does not use cyanide or other harmful chemicals but it's based on piloting gravimetric technology. The material is washed and gravimetrically concentrated with a full reprocessing of mining waste (gravel and clay). In this contribution we present a mineralogical investigation based on electron microprobe analyses and X-ray diffraction of gold nuggets and associated minerals extracted from the alluvial placer deposit of the Murcielago mine (Eucantera Co.), located in the Lepaguare valley. In the investigated area, the Lepaguare River cuts across a sequence, about 4 meters thick, composed of fine to coarse grained sandstones and conglomerates. The placer deposit contains abundant quartz accompanied by andradite, augite and Ca-amphiboles. Epidote, dravite-schorl, zircon, Ce-monazite and xenotime are also present. Magnetite, hematite, ilmenite and rutile are the most common oxides in the placer. Gold nuggets have three morphologies: i) rounded grains, ii) sheet and ii) wire varying in size from few micrometers up to 2 mm. Gold grains intergrown with quartz are also present. The composition of the nuggets, as at%, varies almost continuously from Au88-Ag12. Therefore, the analysed nuggets can be classified as electrum. Most of them are characterized by a homogeneous composition and only a few grains were found to be zoned, showing a pure gold rim developed over a core composed of electrum. Concentrations, as ppm, of the following trace elements have been detected in the gold nuggets: Hg up to 15000, As up to 1500, Zn and Fe up to 1000, Se, Sb, Ni and Co up to 450 and S up to 400. Cu was not present. Based on their chemical composition, zoning, morphology and associated minerals, we can argue that the studied nuggets have suffered limited transport and were affected by negligible post-depositional processes. Therefore, their primary source was, probably, the lode gold deposit described by Mattioli *et al.* [4] that occurs in the same valley and not far from the investigated placer.

[1] Nelson C. (2007). Bundschuh J, Alvarado GE Eds Central America: geology, resources and hazard.
[2] Svandholm J. (1975). *World mining*, 28, 30-31.
[3] Drobe J. and Cann R.M. (2000). *Explor Mining Geol*, 9, 51-63.
[4] Mattioli M. *et al.* (2013). *Int J Earth Sci*, DOI10.1007/s00531-013-0987-0.

Mineralogy and formation conditions of a Ag-Au epithermal deposit Nová Baňa (Slovakia)

Berkh K[1*], Majzlan J[2], Kodera P[3], Chovan M[4], Bakos F[5]

1 - Friedrich-Schiller University Jena, Germany *khulan.berkh@uni-jena.de 2 - Jena University 3 - Dept of Mineral Deposits, Comenius University, Slovakia 4 - Dept of Mineralogy and Petrology, Comenius University, Slovakia 5 - EMED Slovakia, Banská Štiavnica, Slovakia

The historical Nová Baňa epithermal Ag-Au deposit is located in the peripheral zone of a large Miocene andesite stratovolcano within the Central Slovakian volcanic field. This epithermal system spans an area of about 4 km^2 and contains more than 20 veins with a length of up to 1 km, thickness up to 2 m, and a vertical extent of around 300 m. Veins are accompanied by stockwork zones tens of metres thick.

According to bulk chemical analysis, the Au content reaches up to 116 g/t and Ag up to 1110 g/t. The mineralization occurs in extensional or stockwork-like veins, and as disseminations in partly brecciated rhyolite and andesite or their pyroclastics. Hydrothermal alteration comprises extensive silicification, argillic alteration (illite-smectite, kaolinite), adularization, hematitization, and propylitic alteration. Some parts (Althandel) were also affected by strong pyritisation.

The base-metal sulfide association consists of pyrite (up to 4.9 wt.% As), marcasite, stibnite, arsenopyrite, realgar, chalcopyrite, sphalerite (with up to 1.5 wt.% Cd), galena, plagionite (with up to 0.8 wt.% Ag) and tetrahedrite-tennantite. The Ag carriers are dominated by polybasite-pearceite (with up to 5.8 wt.% Au), freibergite (with up to 18.1 wt.% Hg) and miargyrite. Minor Ag bearing phases are acanthite, andorite, argentotetrahedrite-argentotennantite, diaphorite, and proustite-pyrargyrite. Gold occurs as Au-Ag alloy (electrum), which tends to contain either 65 wt.% or 80 wt. % Au (presumably formed in two generations).

Analyses of fluid inclusions indicate fluids with low salinity (0-3 wt% NaCl eq.), which is typical for low sulfidation epithermal systems. Homogenisation temperatures varied mostly between 190 and 240 °C, depending on the part of the vein system. Abundant co-existence of liquid- and vapor-rich inclusions in several samples indicates boiling of fluids, which was the likely reason for precipitation of gold. Assuming hydrostatic pressures, boiling occurred from 12 to 35 bars, corresponding to a paleodepth of boiling 130 to 400 m, reflecting variable erosion levels in individual parts of the vein system.

Isotopic composition of vein quartz ranged from 4.5 to 10.3 ‰ $\delta^{18}O$ (mostly 5.3 to 5.8 ‰), while illite-smectite from wall-rock alteration had 1.9 to 6.9 ‰ $\delta^{18}O$ and -66 to -98 ‰ δD. Composition of fluids in equilibrium with quartz (-5.9 to -3.0 ‰ $\delta^{18}O$) and illite-smectite (-5.5 to -0.6 ‰ $\delta^{18}O$; -80 to -46 ‰ δD) indicate a mostly meteoric origin for fluids affected by isotopic reequilibration with country rocks.

Tellurides, sulfides and sulfosalts in the mineral paragenesis of the Corcoesto orogenic gold deposit, NW Spain

Cepedal A[1*], Fuertes-Fuente M[1], Martin-Izard A[1], Boixet L[2]

1 - Oviedo University *mcepedal@geol.uniovi.es 2 - Mineira do Corcoesto

The Corcoesto gold deposit (A Coruña, NW Spain) currently constitutes one of the biggest gold resources in the Iberian Peninsula (24.2 Mt at 1.32 g/t, over 1Moz, www.edgewaterx.com, 2013). The deposit lies in the Malpica Gold Belt [1], a N30ºE-trending dextral shear band, about 2 km wide. This belt is located in the Galicia-Tras Os Montes Zone, which represents the inner part of the NW sector of the Iberian Variscan Massif. The outcropping lithologies are mainly metasediments, which are affected by variable intensity of migmatization, and highly deformed biotitic and leucocratic granitic rocks. Gold mineralization is related to extensional zones trending N70ºE which represent second order dextral shear bands that have formed in brittle-ductile conditions. Most of the gold occurs in quartz-arsenopyrite veins within these shear bands. These veins exhibit sheeted-vein systems in the most competent lithologies, especially in the leucocratic orthogneiss. Locally, mylonites and breccias are also mineralized [2]. Felsic dykes were intruded along previous structures such as foliation and fractures (N70ºE, N70ºW). The aim of this work is to present a preliminary description of the ore mineralization with special emphasis placed on ore petrography and the associated types of veins and hydrothermal alterations.

Mineralized samples from Corcoesto exhibit different types of veins. The earliest ones are quartz-arsenopyrite or K-feldspar-quartz-arsenopyrite veins, often including scheelite. These veins produced silicification, potassic and minor phyllic alteration, and appear deformed. They are crosscut by veins, infilled by quartz, adularia, carbonate, chlorite, rutile and fluorite, which also produced K-feldspatization and chloritization of the host rocks. The main sulfides related to these veins are pyrite, pyrrhotite and chalcopyrite, and to a lesser degree sphalerite and stannite. Other minerals are Sb-bearing bismuthinite, native-Bi, Bi-Pb-Sb sulfosalts (cosalite and probable ustarasite) and in less proportion Ag-bearing sulfosalts (lillianite-gustavite). Native gold occurs isolated, as aggregates with the above mentioned minerals, as inclusions within the arsenopyrite grains or gangue minerals, or as disseminations in host-rocks associated with chloritization. Moreover, gold occurs along with Bi-Te-S minerals (maldonite, hedleyite and/or joséite) as composite grains showing triple junctions between phases, indicating equilibrium crystallization from a melt [3].

In the NW Iberian Variscides, Au-bearing quartz-arsenopyrite veins hosted by Hercyniangranites their host rocks are widespread, e.g. Corcoesto and Santa Comba-Fervenza in the Malpica Gold Belt [1, 4, 5] or Três Minas and Limarinho in the northern of Portugal [6, 7]. According to these authors, in all these ores a direct relationship exists between mineralization and later brittle deformation with hydrothermal filling. This preliminary study from Corcoesto has shown some differences in the gold paragenesis with respect to the above mentioned deposits, especially in the content of Ag and Pb. A detailed study of the metallic association in these gold deposits could shed light on their genesis.

[1] Spiering E.D., Pevida L.R., Maldonado C., González S., García J., Varela A., Arias D. and Martín-Izard A. (2000). The gold belts of Western Asturias and Galicia (NW Spain). *J Geochem. Explor*., 71, 89-101.

[2] Boixet Ll., Gleeson C.F. and García-Nieto J. (2007). In: 23rd Intern. Applied Geochem. Symp., p. 85.

[3] Ciobanu C.L., Cook N.J., Damian F. and Damian G. (2006). *Mineral. Petrol*., 87, 351-384.

[4] Garcia del Amo D., Lunar R., Sierra J., Oyarzun R. and Doblas M. (1992). *Bol. Geol. Minero*, 103-1, 109-119.

[5] Castroviejo R. (1990). *Mineral. Deposita*, 25, 42-52.

[6] Noronha F., Cathelineau M., Boiron M.C., Banks D., Doria A., Ribeiro M.A., Nogueira P., Guedes A. (2000). *J Geochem Explor*., 71(2), 209-224.

[7]Fuertes-Fuente M., Cepedal A., Martin-Izard A., Campos de Lima A., Dória M.A., Ribeiro M.A. and Guedes, A. (2011). In: Let´s Talk Ore Deposits, 11th SGA Meeting, Chile, Proceedings, 2, 539-541.

Gold-bismuth-bearing ore mineral association of Piilola occurrence (Kuhmo Greenstone Belt, Eastern Finland)

Ermolina O*, Belogub E, Novoselov K

Institute of mineralogy, UB RAS, Russia. *ocoetzee@srk.co.uk

Archaean greenstone belts are interesting because of their gold potential within mesothermal (orogenic) type of deposits.

The object of this study is the Piilola ore occurrence, located in the central part of the Archaean greenstone belt Kuhmo (Eastern Finland). The aim is to characterize ore mineralization of the central part of the Kuhmo greenstone belt. Objectives are to characterize host rocks, to define mineral association, to define the morphology of gold, and to study the chemical composition of gold and associated minerals. The Archaean greenstone belt Kuhmo, whose age is estimated at 2800-2750 Ma, is characterized by the meridional strike [1]. There are 15 ore occurrences including Piilola within the Kuhmo greenstone belt [1, 2]. Increased gold grades are associated with sulphide mineralization. On the basis of textural and mineralogical features the following types of ores have been indicated: 1) disseminated pyrrhotite, pyrite-pyrrhotite; 2) disseminated arsenopyrite-pyrrhotite; 3) brecciated ore with pyrrhotite cement; 4) sulphide inclusions in quartz veins.

Disseminated pyrrhotite, pyrite-pyrrhotite ores are widespread along the whole section. The predominant sulphide mineral is pyrrhotite, with accessory pyrite, chalcopyrite and pentlandite.

Disseminated arsenopyrite-pyrrhotite ore is most interesting due to the presence of gold-bismuth mineralization. Native gold has been described as inclusions in arsenopyrite and rarely in silicate matrix where it occurs as single grains and intergrowths with native bismuth and Bi minerals. Chemically, the gold contains traces of silver and copper. For the first time in the Piilola ore, occurrences of native bismuth, bismuthine (Bi_2S_3), maldonite (Au_2Bi) and intermetallic compounds of Te-Bi were described (Table 1). Bismuth minerals occur as intergrowths with native gold within arsenopyrite crystals and a silicate matrix. Intermetallic compounds of Te-Bi are characterized by a different ratio between Te and Bi with a stable predominance of Bi. Thus, the gold-bismuth-bearing ore mineral association of the Piilola occurrence is marked by arsenopyrite, pyrrhotite, chalcopyrite, pyrite, sphalerite, native gold, native bismuth, maldonite, bismuthine and intermetallic compounds of Te-Bi. The association of native gold and native bismuth reflects a relatively low-temperature of crystallization in a reduced environment. Crystallisation of the gold-bismuth association took place in a regressive metamorphism phase under greenschist facies. Native gold and bismuth trapped in arsenopyrite may be interpreted as melt inclusions [3, 4]. Mineralogical features associated with the gold can be explained using the Liquid Bismuth Collector Model [5]. The supposed source of gold is dispersed sulphides from volcanogenic wall rocks.

Table 1. Chemical composition of intermetallic compounds of Te-Bi (wt %)

Position	Bi	Te	Pb	Sum	Formula
Bi_3Te					
1962c	82.84	16.73	0	99.57	$Bi_{1.00}Te_{0.33}$
1962d	82.24	17	0.06	99.3	$Bi_{1.00}Te_{0.34}$
1963j	82.18	17.16	0.64	99.98	$Bi_{1.00}Te_{0.34}$
1963m	81.34	18.07	0.31	99.71	$Bi_{1.00}Te_{0.36}$
Bi_2Te					
1963g	78.17	21.63	0	99.79	$Bi_{2.00}Te_{0.91}$
1963n	76.63	21.76	1.34	99.73	$Bi_{2.00}Te_{0.93}$
1961e	76.3	22.98	0	99.28	$Bi_{2.00}Te_{0.99}$
1963e	74.81	22.89	2.29	99.98	$Bi_{2.00}Te_{1.00}$
1963h	73.64	23.04	2.55	99.22	$Bi_{2.00}Te_{1.02}$
1961d	75.2	24.23	0.28	99.71	$Bi_{2.00}Te_{1.06}$
Bi_3Te_2					
1961f	70.72	29.18	0.08	99.98	$Bi_{3.00}Te_{2.03}$
1961g	69.64	29.7	0.07	99.41	$Bi_{3.00}Te_{2.10}$
1961h	67.57	31.73	0.13	99.43	$Bi_{3.00}Te_{2.31}$
BiTe?					
1961i	66.62	32.59	0	99.21	$Bi_{1.00}Te_{0.80}$
1961c	66	32.74	0.58	99.32	$Bi_{1.00}Te_{0.81}$

[1] http://en.gtk.fi/index.html

[2] Papunen H. *et al*. (2009). Archaean evolution of the Tipasjarvi-Kuhmo-Suomussalmi greenstone complex, Finland. Geological Survey of Finland, Bulletin 403. Espoo: GTK. 68 p.

[3] Belogub E.V. *et al*. (2010). Native bismuth, tsumoite and lead-bearing variety of tsumoite from Tarnierskoye copper-zinc massive sulfide deposit (The North Urals). Zapiski RMO, N6, 108 - 119.

[4] Tomkins A. *et al*. (2007). On the initiation of metamorphic sulfide anatexis.Journal of Petrology, 48(3), 511-535.

[5] Douglas N., *et al*. (2000). The liquid bismuth collector model: an alternative gold deposition mechanism. AGC Abstr., vol 59, p.135.

LA-ICP-MS analyses of Au-bearing pyrite ores from NW Iberian Variscan Belt: preliminary results

Fuertes-Fuente M*, Cepedal A, Martin-Izard A

Oviedo University *mercedf@geol.uniovi.es

Gold deposits are abundant in the Variscan belt of the NW Iberian Peninsula, and comprise a variety of gold deposit models: skarns, e.g. [1, 2, 3], intrusion related and intrusion-hosted gold deposits, e.g. [4, 5, 6], orogenic gold deposits, e.g. [7, 8, 9] and low temperature gold mineralizations that share strong analogies with the Carlin-type model, e.g. [10, 11]. In some of these occurrences a certain proportion of gold appears as "invisible gold" in sulfides. Hence, the goals of our research are to evaluate the possibility of economically exploitable gold concentrations in sulfides and to improve the understanding of how gold is accommodated within specific sulfides. Both aspects are important for the development of gold exploration strategies and for successful processing of such ores.

The analyzed samples were Au-bearing As-rich pyrites from the El Valle deposit (Asturias, NW Spain). These pyrites showed Au contents by EMPA from below 250ppm (lower detection limit) to 800ppm, and traces of Tl, Hg and Sb [11]. In this study, the pyrite samples showing no detectable gold by EMPA were analyzed using a LA-ICP-MS to provide insight into the occurrence and distribution pattern of gold, and other trace elements, at lower concentrations. LA-ICP-MS analyses were performed at the Oviedo University (Spain). Every sample analysed was followed by one analysis of NIST SRM 612 and MASS-1 in order to correct the time-dependent drift of sensitivity and mass discrimination. The analyzed elements were $^{197}Au^{202}Hg^{205}Tl^{75}As^{121}Sb$. ^{57}Fe was also monitored and used as internal standard for quantitative calibration. The results are reported as original signal intensity (counts per second). Data were acquired from both single-spot and line raster (up to 250µm in length) analyses. The analyses were obtained with a spot diameter of 40µm, a laser-repetition rate of 10 Hz and 7 mJ/pulse and for laser in line-raster mode operation with a raster speed of 4 µm/s.

All time-resolved LA-ICP-MS profiles obtained from the studied pyrite grains show the presence of As, Sb, Hg and Tl, however gold detection is variable. The profiles can be gathered into two groups: (1) relatively smooth profiles with an extremely low Au-signal and (2) more spiky profiles with a distinctive Au-signal intensity. In the last group of profiles, Au peaks in line-rasters sometimes correspond to peaks in As, whereas Sb, Hg and Tl signals are, in general, more homogeneous. A tentative quantitative calibration was made using MASS-1 as a calibration standard and, for internal standardization, the iron content of these pyrites was calculated from EMPA. Au concentrations obtained were up to 20ppm. However, these values should be treated with caution because of the lack of a world-wide recognized calibration standard appropriate for quantitative analysis of trace elements in sulfides by LA-ICP-MS.

From this study, we conclude that the As-bearing pyrites of this deposit have widely variable gold contents. Smooth profiles of As, Sb, Hg and Tl can be interpreted as these elements are chemically bound and homogeneously distributed in pyrites that do not contain gold (extremely low gold signals above background). Spike profiles, with arsenic variations often parallel to those of gold, may be interpreted as compositional zoning of the crystals. Furthermore, the latter supports the proposal that the highest Au-contents are in As- rich zones previously as proposed by Cepedal *et al.* [11].

[1] Martín-Izard *et al.* (2000). *J Geochem. Explor*., 71, 153-175.

[2] Fuertes-Fuente *et al.* (2000). *J Geochem. Explor*., 71, 177-190.

[3] Cepedal *et al.* (2000). *J Geochem. Explor*. 71, 119-151.

[4] Martin-Izard *et al.* (2009). In: Williams, *et al.* (Ed.), Smart Science for Exploration and Mining, 725-727.

[5] Martínez-Abad *et al.* (2011). In: Let´s Talk Ore Deposits, 11th SGA Meeting Proceedings, 2, 548-550.

[6] Cepedal *et al.* (2013). *J Geochem. Explor*., 124, 101-126.

[7] Noronha *et al.* (2000). *J Geochem. Explor*., 71, 209-224.

[8] Boiron *et al.* (2003). *Chem. Geol*., 194, 119-141.

[9] Fuertes-Fuente *et al.* (2011). In: Let´s Talk Ore Deposits, 11th SGA Meeting Proceedings, 2, 539-541.

[10] Crespo *et al.* (2000). *J Geochem. Explor*., 71, 191-208.

[11] Cepedal, *et al.* (2008). *Can. Mineral.* 46, 233-247.

Geology and mineralization characteristics of the epithermal gold deposits in the Zamboanga Peninsula, Philippines

Gabo J*, Imai A[2], Ishihara Y[2], Hagiwara A[2], Watanabe K[3]

1 - Research Institute of Environment for Sustainability, Kyushu University *jillian-g@mine.kyushu-u.ac.jp 2 - Akita University 3 - Kyushu University

The Zamboanga Peninsula in the western portion of Mindanao Island, southern Philippines is characterized by an abundance of epithermal gold deposits scattered throughout the peninsula, many of which have yet to be characterized in detail (Figure 1). The study focuses on the geology, host rock geochemistry, ore mineralogy and ore-forming fluid characteristics of three major gold deposits being explored in the area: Sibutad, Balabag, and Sirawai.

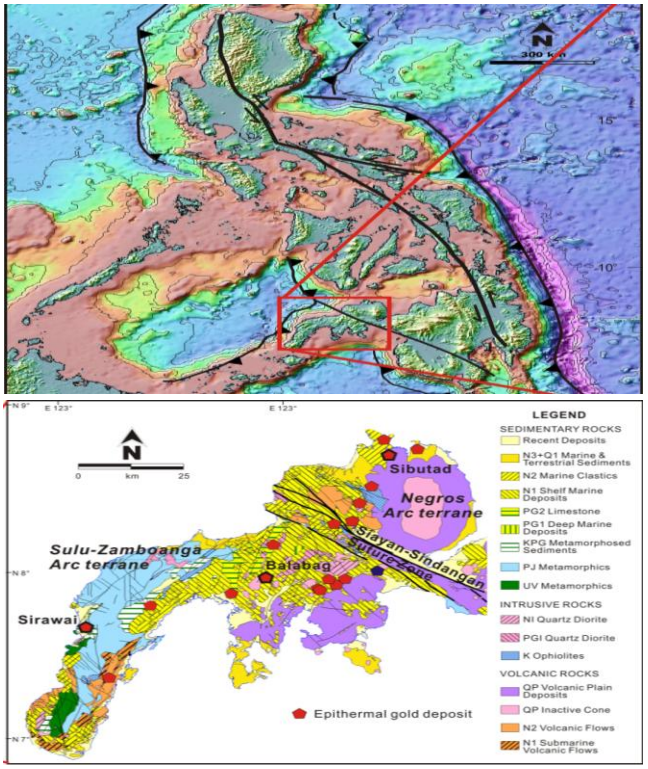

Figure 1: Location of epithermal gold deposits in the Zamboanga Peninsula, with emphasis on the three deposits investigated: Sibutad, Balabag, and Sirawai.

The Zamboanga Peninsula consists of two distinct terranes: the Negros Arc terrane of island arc affinity and the Sulu-Zamboanga Arc terrane of continental origin. The terranes are separated by the northwest-trending Siayan-Sindangan Suture Zone, a northwest-trending left-lateral strike slip fault produced from the docking of the Philippine Mobile Belt during the late Miocene to early Pliocene. The epithermal gold deposits in the study area share common characteristics. They are hosted in Middle to Late Miocene calc-alkaline andesitic volcanic rocks, which are cut by multiple stages of Late Miocene andesite porphyry and diorite intrusions. The host rocks are altered by silicification and argillic alteration in the main ore zones, and by propylitic alteration in the distal portions. Mineralization is related to quartz veining and brecciation, with the structures dominantly trending northwest and minor structures oriented northeast. Typical ore minerals include pyrite, chalcopyrite, sphalerite, galena and electrum. Two-phased fluid inclusions from quartz and barite indicate homogenization temperatures of 150-315°C with salinities of 2 - 5 wt% NaCl. The deposits investigated reveal either sulfide stockwork veins or potassic alteration in the deeper or distal portions of the main orebodies.

The Miocene subduction of the proto-Sulu trench resulted in arc magmatism that formed the igneous host rocks in the Zamboanga Peninsula. This was followed by multiple intrusion events in the Late Miocene, as well as the formation of the northwest-trending Siayan-Sindangan suture zone after the suturing of the two terranes in the Zamboanga Peninsula. These events could have triggered the formation and circulation of hydrothermal fluids that precipitated the epithermal gold mineralization. Continuous suturing and uplift might have caused the exposure of the epithermal gold deposits in the Zamboanga Peninsula.

Ore-bearing characteristics at the Purnama high sulfidation deposit, Martabe, North Sumatra, Indonesia

Saing S[1*], Takahashi R[2]

1 - Akita University *stephanie@ymail.com 2 - Akita Univeristy, Japan

The Martabe mine is a gold-silver high and low sulfidation type deposit located in the Batang Toru district, North Sumatra, Indonesia. The Purnama Au-Ag deposit of Martabe mine is located in the Sunda-Banda arc, which is hosted by a Late Tertiary dacitic dome-diatreme complex that was emplaced into a volcanic-sedimentary sequence. N-S trending quartz veins in the Purnama deposit are hosted by multiphase breccia and andesite of the Miocene to Pliocene Angkola Formation. Quartz veins show banding, vuggy, crustiform-colloform, lattice and massive textures. Ore minerals recognized at Purnama are native gold, tetrahedrite-tennantite, enargite and pyrite. Pyrite occurs as disseminated and banded textural varieties in the mineralized zone at a depth of 238-273 m . From assay analysis, there is no clear correlation between Au, Ag and Cu. Hydrothermal alteration in Purnama is characterized by quartz-kaolinite-dickite ± alunite ± illite ± pyrophyllite. Alunite includes K-Alunite, Ca-Alunite and Na-Alunite on the basis of the mineral spectrometer data. Fluid inclusions are bi-phase (liquid + vapor) H_2O-NaCl type with vapor rich inclusions. Fluid inclusion microthermometry of quartz indicates a temperature range of 190 - 403^{0}C (average 230^{0}C) and a salinity range of 2.7 - 8.6 wt% NaCl eq. (average 5.3 wt% NaCl eq.).

Gold mineralization in the Neale area: an extension of the Tropicana-Havana gold system at the cratonic boundary of the Yilgarn Craton and the Albany-Fraser Orogen, Western Australia, with atypical geochemical affinities?

Sweetapple M, Gonzalez-Alvarez I*

CSIRO, CESRE, Minerals Down Under Flagship, Western Australia
*i.gonzalez.alvarez@gmail.com

A single major gold deposit is located in the Yilgarn Craton-Albany-Fraser Orogen (AFO) margin: the Tropicana-Havana gold system with a Mineral resource of 6.41 Moz Au, discovered in 2005.

Tropicana-Havana is located 330 km Northeast of Kalgoorlie, Western Australia. Based on the initial Tropicana deposit, and the proximity of Yilgarn-like greenstone outcrops, the area was considered prospective for deposits with Yilgarn lode-gold style affinities. Subsequent work on the Tropicana deposit has proven that this mineralization is not a counterpart of Yilgarn style gold deposits, but was formed by hydrothermal activity in the AFO as the result of metamorphism of a pre-existing Archaean gold deposit. Gold is concentrated in quartzofeldspathic gneiss. Higher gold grades (up to 6.6 g/t) are associated with anastomosing biotite-sericite fracture infill and crackle breccia zones. Quartz veining and pervasive carbonate alteration is absent. The Tropicana Project area lies adjacent to a NE-trending magnetic feature, which extends over 550 km in length. This feature is interpreted as the major tectonic suture between the Yilgarn Craton and the Proterozoic AFO. The Atlantis and Hercules gold prospects are located on the same magnetic structure and, therefore, could be expressions of the Tropicana-Havana gold system further to the northeast.

Anomalous auriferous samples from diamond drillholes from the Hercules and Atlantis prospects (~5 kilometres apart) are located within basement lithologies of the Neoarchaean to Palaeoproterozoic felsic gneiss. This host unit is weakly foliated to mylonitic, and is mingled with metagabbro, and minor hybrid units of metagranodiorite and metadiorite composition. Mineralization could be related to later Mesoproterozoic granites (1345-1260 Ma/1215-1140 Ma) at least ~45 km away to the southwest. Alternatively, gold could represent redistributed or reworked relicts of earlier events.

The higher silver content of the northern area (Hercules) points towards this mineralization being an atypical lode gold deposit. Additionally, this style of mineralization is associated with a wide range of anomalous elements, including Cu-Pb-Zn-Bi-Te-W-Mo-LREE that may indicate a component of hydrothermal-magmatic fluid derived from a felsic intrusive source. Copper mineralization associated with a quartz-'sericite' vein in a phyllosilicate altered metagranitoid was also identified at Hercules. The presence of widespread gold with ubiquitous copper minerals in the southern area (Atlantis) together with phyllosilicate altered felsic metagranitoids supports the possibility of a disseminated mineralization type. In contrast with the northern area, silver was not detected with gold particles. Furthermore, the mylonites themselves are potential hosts for mineralization, where mylonite zones were subjected to later fracturing, alteration and introduction of auriferous fluids.

The combinations of elemental signatures from accessory mineral chemistry, veining and associated alteration mineralogy, and gold intersections on the same apparent magnetic lineament as the Tropicana-Havana gold system, suggest that the gold prospects at Hercules-Atlantis are related to the Tropicana-Havana system.

Geochemical characteristics of epithermal Au-Ag and porphyry Cu-Mo mineralization in the Chatree mining district, Thailand

Takahashi R*, Imai A, Chida Y, Charusiri P, Blamey N

Akita University, Japan *ryohei@gpic.akita-u.ac.jp

The Chatree gold deposit is located in the Loei-Phetchabun volcanic belt, north central region of Thailand. The mining is on-going for epithermal Au-Ag ore bodies, where the A-pit represents one of several pits at the Chatree mine that contains a significant portion of the remaining gold and silver reserves. In addition, the N-prospect targets porphyry Cu-Mo mineralization which is located 2 km south of the epithermal ore bodies. Formation ages have been reported as 250 Ma for adularia-quartz veins of the epithermal Au-Ag mineralization, and 244 Ma for granodiorite of the porphyry Cu-Mo mineralization. Fluid inclusion gas analysis was conducted on quartz and vein calcite from the A-pit and N-prospect. The analyses reveal relatively high CO_2 and H_2S contents in the fluid inclusions for quartz veins of the N-prospect. On the basis of the N_2/Ar vs. Ar/He discrimination diagram, both the A-pit and the N-prospect indicate a magmatic fluid component, with the N-prospect showing highly elevated Ar/He ratios due to fluid boiling. Oxygen isotope analysis and fluid inclusion microthermometry indicate that the ore fluids in the N-prospect have the characteristics of magmatic water. On the other hand, oxygen isotope compositions of fluids based on assumed temperatures for the A-pit are concordant with the characteristics of meteoric water.

CO_2-rich inclusions in various depths of the Dongchuang and Dongtongyu gold deposits, Xiaoqinling Mt area, China

Xu J*, Lin L, Wu X, Wei H

Univ. Sci. Tech. Beijing *jiuhuaxu@ces.ustb.edu.cn

The Dongchuang and Dongtongyu gold deposits, located on the border between Shaanxi and Henan provinces, are large scale deposits in the Xiaoqingling gold district and are operated underground. The gold-bearing quartz veins occur in a series of east-west shear zones within the Archaean Taihua Group (Figure 1), which extend in an east-west trending folded structure and mainly consist of amphibolite, plagioclase gneiss and migmatites. The gold-bearing vein systems are also related to late Yanshanian (Cretaceous) granite. Principal alterations around shear zones are sericitization, silicification, pyritization and carbonization. Four structural stages of mineralization can be distinguished: I) pyrite-quartz stage; II) gold-bearing quartz-pyrite stage; III) gold-carbonate-polymetallic sulphide stage; and IV) quartz-calcite stage.

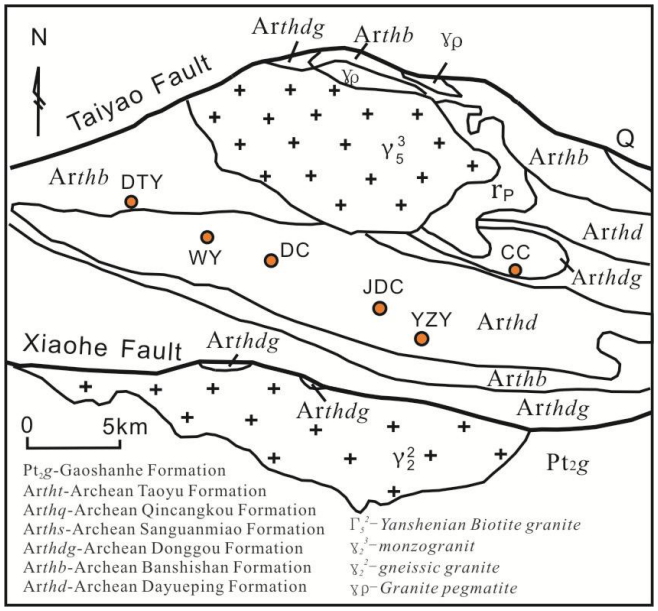

Figure 1: Sketch map of the Dongchuang (DC) and Dongtongyu (DTY) gold deposits (modified from [1])

Fluid inclusions are abundant in various stages of vein quartz in the Dongtongyu and Dongchuang gold deposits. Three types of primary fluid inclusions can be observed at room temperatures: CO_2-H_2O inclusions, carbonic inclusions, and aqueous inclusions. CO_2-H_2O inclusions are commonly seen in stages I, II, and III, which are composed of an aqueous phase and a liquid CO_2 phase (20 to 90 vol.%), with size of 5 to 20 mm.

The temperatures of CO_2 triple points ($Tm_{,CO2}$) of CO_2-H_2O inclusions from the 2110m level of vein V507 in the Dongchuang deposit are -58.5~-58.3℃(QI), and -57.3~-56.8℃(QII), corresponding to 0.02~0.07 of X_{CH4}; the CO_2 partial temperatures ($Th_{,CO2}$, homogenized to liquid CO_2) are 9.0~14.5℃(QI), and 18.5~26.5℃(QII), corresponding to 0.80~0.75g/cm^3(QI) and 0.78~0.71g/cm^3(QII) of CO_2 densities. The melting temperatures of CO_2 clathrates are 4.8~9.3℃, corresponding to 9.3~1.4wt%NaCleqv of salinities. The final homogenization temperatures ($Th_{,TOT}$, homogenized to H_2O) of CO_2-H_2O inclusions are 251 to 298℃ for stage I, and 205 to 350℃ for stage II. The CO_2-H_2O inclusions (QI) from 1300m level of vein V531 in the Dongtongyu deposit have $Tm_{,CO2}$=-58.8~-59℃, $Th_{,CO2}$= 18.0~ 25.9℃, and $Th_{,TOT}$ =299~335℃. Those (QIII) from 600m level of vein Q2051 have $Tm_{,CO2}$=-59.3~-60.3℃, $Th_{,CO2}$= 8.7~ 22.3℃, and $Th_{,TOT}$ =299~335℃; and those from 550m level of veins Q14 and Q8 have $Tm_{,CO2}$=-57.8~ -60.1℃, $Th_{,CO2}$= 14.1~28.4℃, and $Th_{,TOT}$ =265～348℃. It is indicated that no obvious changes are seen for $Th_{,CO2}$ and $Th_{,TOT}$, from shallow to deep, but X_{CH4} might increase because of $Tm_{,CO2}$ lowering.

Acknowledgements: Funded by National Nature Science Foundation of China (41372096)

[1] Jiang N. *et al*. (1999). *Mineralium Deposita*, 34, 150-162.

Mineralogy of ores from the Ganeevskoe gold deposit associated with berisites and listvenites (Republic of Bashkortostan, Russia)

Zabotina M[1*], Belogub E[1], Novoselov K[1], Palenova E[1], Martesheva A[2], Blinov I[1]

1 - Institute of Mineralogy, UB RAS *mary_7-88@mail.ru 2 - Ilmen State Reserve UB RAS

The Uchaly region in the Republic of Bashkortostan is a classical ore district with numerous VMS and gold-sulfide deposits, which are hosted in volcanosedimentary rocks mostly of the Middle Devonian Karamalytash Formation [1]. At the same time, the gold-quartz deposits are related to the volcanosedimentary complexes, which were transformed during collision. These deposits are confined to the tectonic zones and their formation is attributed to dynamometamorphic and metasomatic processes typical of gold deposits of greenstone belts [2]. Our research is focused on the mineralogy and geochemistry of ores and altered rocks from the Ganeevskoe gold deposit (Uchaly region), which is localized in berisites and listvenites of the longitudinal tectonic zone. A band of altered rocks has a tectonic contact with basalts and tuffs of the Karamalytash Formation in the west, and metabasalts of the Early Silurian Polyakovka Formation in the east [3]. No granites are found in the region around the deposit. The host rocks (metabasalts and quartz-chlorite schists) are foliated and contain tectonic lenses of talc-bearing serpentinites. The ore zone includes listvenites, berisites and quartz veins. Listvenites consist of quartz, albite, magnesite, dolomite, fuchsite, and rare talc and paragonite and are characterized by a low content (wt.%) of SiO_2 (24.02-30.02), Al_2O_3 (0.52-0.68), and TiO_2 (<0.5-0.12) and high content of MgO (8.7-30) and CO_2 (13.46-18.98). The high content of Cr (503-740 ppm) and Ni (1336-1545 ppm) indicate the formation of listvenites after ultramafic rocks. Berisites are composed of sericite, dolomite, ankerite, albite, pyrite and quartz and have increased contents (wt.%) of SiO_2 (46.3-46.86), Al_2O_3 (12.04-13.23), and TiO_2 (1.00-0.92) and decreased contents of MgO (4.7-5.9) and CO_2 (9.44-10.46) relative to listvenites. Berisites are characterized by an elevated Cu content (up to 241 ppm) that is typical of basalts from this district. The chemical composition of berisites is similar to the composition of metabasalts and quartz-chlorite schists, which were formed after volcanosedimentary rocks in this region. The influx of Na and CO_2 and loss of SiO_2 resulted in the formation of berisites, listvenites and quartz veins that is typical of the potassium-sodium metasomatic processes. The quartz veins occur at the contacts of listvenites and quartz-chlorite rocks and also contain dolomite. The Au contents reach 18, 10 and 3 gramm per ton in berisites, listvenites, and quartz veins, respectively. The major ore minerals of listvenites and berisites are pyrite and goethite. Chalcopyrite is abundant. Rare minerals are gold, galena, sphalerite, pyrrhotite, fahlore, magnetite and hematite. Gold occurs as inclusions in pyrite and goethite. The composition of gold in listvenites and berisites is similar and is characterized by an Ag content of up to 11 wt.%. The quartz veins contain major galena, widespread chalcopyrite and rare tennantite, aikinite, polydymite, millerite, petzite, hessite, and native gold. Gold occurs as inclusions in quartz, galena and tellurides and contains up to 17 wt.% Ag. Thus, two types of gold in the Ganeevskoe deposit may be distinguished: 1) the high-fineness gold associated with pyrite in berisites and listvenites and 2) low fineness gold associated with galena and minerals of Bi, Te and Ag in the quartz veins. The composition and mineral association of gold at the Ganeevskoe deposit are similar to classical gold deposits associated with berisites and listvenites and are distinct in composition from altered rocks (the presence of albite) and the absence of granites.

[1] Prokin V.A. and Bushlaev F.P. (1999). Massive copper-zinc sulfide deposits in the Urals. *Ore Geology Reviews*, 14, C. 1-69.

[2] Dube B. and Gosselin P. (2007). Greenstone-hosted quartz-carbonate vein deposits In: Mineral Deposits of Canada: A Synthesis of Major Deposit-Types, District Metallogeny, the Evolution of Geological Provinces, and Exploration Methods. Geological Association of Canada, Mineral Deposits Division, Special Publication. No. 5, 49-73.

[3] Galiullin I.B. (2010). Geochemical zonality of the Ganeevskoe gold deposit in the Buyda area (Uchaly region, Republic of the Bashkortostan). In: Metallogeny of ancient and modern oceans-2010. Miass: Imin UB RAS, 163-166. [in Russian].

Supergene nonsulfide zinc ores: state of the art

Boni M

University Napoli. boni@unina.it

Nonsulfide zinc deposits (NSZ) are a relatively uncommon ore type. They were the earliest source of mined zinc, and in recent years have enjoyed a renewed interest due to new processing technologies. Two types of deposit are indicated: hypogene and supergene [1], which can be distinguished according to their geological setting and mineralogical characteristics.

Hypogene ores are derived from high temperature fluids in hydrothermal and/or metamorphic environments (e.g. Vazante-Brazil, Beltana-Australia and Franklin-USA). Hypogene NSZ mainly consist of anhydrous zinc silicates and oxides. They are less abundant and economically less significant (with the exception of Vazante) than supergene types. Supergene NSZ are derived from the weathering of primary sulfide deposits: a combination of conditions is needed for the development of economically significant deposits of this type. Key conditions include: (1) pre-existing zinc concentrations, (2) efficient oxidation promoted by tectonic uplift and/or prolonged deep weathering; (3) permeable wall rock to allow for ground-water movement; (4) effective trap sites; (5) hydrogeological environments that do not promote dispersion and loss of Zn-bearing fluids.

These deposits contain hydrated zinc silicates and carbonates such as hemimorphite ($Zn_4Si_2O_7(OH)_2 \cdot H_2O$) and hydrozincite ($Zn_5(CO_3)_2(OH)_6$), or the most common carbonate smithsonite ($ZnCO_3$). The best example of a supergene nonsulfide Zn deposit is the Skorpion operation in Namibia [2]. There are other examples: e.g. Accha [3] and Yanque [4] in Peru, or Hakkari [5] in Turkey. Other deposits, which have been long considered supergene, are instead related to the circulation of low temperature hydrothermal fluids (as Angouran in Iran [6], and -partly- the well-known "La Calamine" deposit in Belgium).

Recent developments in processing technologies for the treatment of NSZ zinc deposits (acid-leaching, AmmLeach®, pyrometallurgy, electrowinning) have increased the commercial interest for NSZ ores with a revival in exploration throughout the world, blossoming at the beginning of the twenty-first century. Nevertheless, at several mines the hydro-metallurgical plants are underperforming relative to initial expectations, which has resulted in delays in the development of NSZ deposit exploitation. Capital and operating costs, acid consumption and metal recoveries have not completely met the feasibility study expectation, and other oxide resources (Mehdiabad-Iran, Sierra Mojada-Mexico, Torlon Hill-Guatemala, Jabali-Yemen) are still battling with technical and/or political issues. However, many technical problems can be mitigated by a better identification of the mineralogical association of the metallic and nonmetallic minerals. This should be a fundamental step in the exploration of nonsulfide mineral deposits, because the extraction process is highly sensitive to mineralogy. Therefore, before metallurgical processing methods are chosen, it is necessary to take into account both the physical and chemical properties of the ores and their gangue minerals.

[1] Hitzman *et al*. (2003). *Economic Geology*, 98, 685-714.

[2] Borg *et al*. (2003). *Economic Geology*, 98, 749-771.

[3] Boni *et al*. (2009). *Economic Geology*, 104, 267-289.

[4] Mondillo *et al*. (in press) *Economic Geology*.

[5] Santoro *et al*. (2013). *Ore Geology Reviews*, 53, 244-260.

[6] Boni *et al*. (2007). *Mineralium Deposita*, 42, 799-820.

Non-sulfide zinc deposits of Morocco: from mineralogy to age characterization

Choulet F[1*], Charles N[2], Barbanson L[3], Branquet Y[3], Sizaret S[3], Chen Y[3], Aomar E[4], Badra L[5]

1 - Chrono-Environnement UMR6249, Université de Franche-Comté/CNRS *flavien.choulet@univ-fcomte.fr 2 - BRGM Orléans 3 - ISTO - UMR7327, Université d'Orléans/CNRS 4 - Groupe Managem, Morocco 5 - Université Moulay Ismaïl, Meknès

In Northern Africa, Zn-Pb ore deposits are numerous, and Zn ores of supergene origin have been long extracted for local use using calcination to smelt the metals. While the renewal of interest in non-sulfide ores coincides with improvements in mineral processing, the recent opening of a Zn-oxides production plant in Morocco attests to the multipartite will to revive interest in the non-sulfide ores disseminated throughout the Atlas Mountains, as it represents a direct source of employment and an opportunity to create infrastructure in remote places.

Six non-sulfide Zn-Pb ore deposits, namely Toulal, Aït Labbès, Tadaghast, Beni Tajite, Bou Arhous, Tizi n'Firest, (representing an overall production of ca. 1Mt at 24% Zn) hosted in the Lower Jurassic reef to para-reef limestone have been investigated in the Moroccan High Atlas, to understand processes and timing of their formation. Ore occurs either in veins associated with a faulted anticline, or in orthogonal fractures or stratabound horizons in tilted strata. A vertical zoning from deep Zn-Pb sulfide stratabound lenses to shallow non-sulfide deposits has been reported. Zn (Pb) carbonates, Zn silicates and hydrated associated minerals directly replace the sulfide ore bodies or filled cavities along fractures related to the Atlasic events.

Field observation has been complemented by a multidisciplinary approach (Raman, SEM, EPMA) for mineralogical characterization, revealing a similar paragenetic evolution for all deposits, as follows: 1) formation of the protore sulfides, 2) early supergene weathering with formation of Zn-Pb-bearing carbonates and iron oxi-hydroxides replacing protore sulfides or in the form of karst-related internal sediment and 3) late supergene weathering with deposition of Zn-carbonates, Zn-silicates and hydrated phases. Direct replacement of Zn-Pb sulfides strongly controlled by pyrite oxidation is accompanied by precipitation of zinc non-sulfide minerals in cavities or karst-related internal sediment filling.

A complementary rock magnetism study from the Toulal and Aït Labbes ore deposits have been carried out. It shows that magnetite and minor hematite and goethite are the magnetic carriers. Measurement of the anisotropy of the magnetic susceptibility (AMS) from both ore and karstic internal sediments has revealed consistent directions and horizontal magnetic fabrics, with the magnetic lineation usually paralleling the direction of the calamine veins. The attitude of the AMS parameters (P_J and T) suggests an absence of significant deformation supporting the theory that the magnetic fabric originates from sedimentary dynamics within the veins. High temperature components of primary origin have been isolated from the localities. The reverse and normal directions of this component are antipodal and similar within error for both calamines and karst-related internal sediments, suggesting that non-sulfide ore deposits and karst-related internal sediments are contemporaneous. We therefore calculated an average paleomagnetic direction for each locality. The corresponding poles are consistent with the last 30 Ma of the Apparent Polar Wander Path (APWP) of Africa. These promising results pave the way for an efficient method to constrain the age of Zn supergene deposits.

The proposed three-step scenario can be placed within the tectonic evolution of the Moroccan High Atlas belt. Deposition of primary sulfides is contemporaneous with opening of the Tethyan and Atlantic oceans. During the Tertiary, intracontinental deformation has given rise to the High Atlas fold-and- thrust belt and to regional uplift. As a result, Zn-Pb sulfides, hosted in carbonates experienced oxidation under an arid climate (with short intermediate humid episodes facilitating karst development) to form karst-related Zn-Pb non-sulfide ore bodies.

Zn-rich clay minerals in nonsulfide ores (Cuzco area, Peru): a TEM study, with inferences for genesis and processing

Mondillo N[1*], Nieto F[2], Balassone G[3], Boni M[4]

1 - Dipartimento Scienze della Terra, dell'Ambiente e delle Risorse - Università di Napoli *nicola.mondillo@unina.it 2 - Dpto. Mineralogia y Petrologia, Universidad de Granada 3 - DiSTAR, Università di Napoli Federico II 4 - University Napoli

Zn-bearing clay minerals occur in several nonsulfide zinc ores, where they can represent an important metal source [1]. They are also common in some mining wastes [2]. Among the trioctahedral smectites, the Zn-bearing variety sauconite [3, 4] occurs in several ore districts worldwide. At Skorpion (Namibia), Zn-smectite predominates over the other Zn-nonsulfide minerals [5]. The Yanque nonsulfide Zn prospect in Peru (inferred resources 26,491 kt @ 2.37% Zn and @ 2.18% Pb) is similar to Skorpion, due to its prevailing sauconite content. Sauconite also occurs in the Peruvian Accha deposit (res. 5.1 Mt @ 8.2% Zn and 0.9% Pb) [6]. At Yanque, the Zn-smectite occurs as replacement of detrital feldspars and/or hydrothermal muscovite/illite and kaolinite. At Accha, the Zn-smectite replaces hemimorphite and smithsonite, and fills small karst cavities.

In spite of decades of researches on the various dioctahedral/trioctahedral members of the smectite group, the chemical and structural properties of Zn-bearing smectites are still poorly understood. Structure refinement and interlayer composition of these natural smectites have to be clarified. Here we report preliminary data on Zn-clay minerals from the Yanque and Accha prospects (Peru), obtained by transmission electron microscopy (TEM-HRTEM), following XRD, SEM-EDS, WDS and petrography. TEM is an invaluable tool for the characterization of crystalline materials at nano- and sub-nanometre scale [7]. It allows a wide range of imaging and diffraction techniques, together with analytical tools (AEM) that provide information on elemental composition and atomic structure down to a single atom.

Based on the TEM-AEM analyses, the clay fractions of the Accha and Yanque samples are a mixture of trioctahedral Zn-smectite (sauconite), Zn-bearing beidellite, Fe oxides and amorphous material with Si+Al composition. In the octahedral layer of sauconite, Zn (contents ranging from 1.49 to 2.60 afu) is associated with Mg, Al, Fe and Mn, which, in the analyzed clays, occur in highly variable proportions. In some samples, Mg is completely absent whereas Mn occurs in significant amounts. The interlayer cations population is highly variable: K and Ca have been found as major interlayer cations, whereas Na could not be determined due to the interference of a L line of Zn. Sauconite usually forms grains constituted by aggregates of curved thin clay layers, which, from the electron diffraction patterns, seems to have a *turbostratic* arrangement. Beidellites present their normal compositions and morphologies except for the Zn content, which ranges from 0.05 to 0.54 afu.

[1] Mondillo N., Boni M., Balassone G., Villa I.M. (2014). *Econ Geol*, in press.

[2] Helios-Rybicka E. and Wójcik R. (2012). *Appl Clay Sci*, 65-66, 6-13.

[3] Ross C.S. (1946). *Amer Mineralogist*, 31, 411-424.

[4] Newman A.C.D. and Brown G. (1987). *Chemistry of Clays and Clay Minerals*, *Mineralogical Society Monograph*, n. 6: New York, Wiley Interscience, 1-128.

[5] Borg G., Kärner K., Buxton M., Armstrong R. and Van Der Merwe S.W. (2003). *Econ Geol*, 98, 749-771.

[6] Boni M., Balassone G., Arseneau V. and Schmidt P. (2009). *Econ Geol*, 104, 267-289.

[7] Nieto F. and Livi K.J.T. (2013). Minerals at the nanoscale. *EMU Notes in Mineralogy*, vol.14, 440 p.

The Vazante and northern extension hypogene zinc silicate deposits: evidence for fluid mixing during mineralization

Olivo G[1*], Percy E[1], Kyser K[1], Oliveira G[2], McGladrey A[1], Slezak P[1], Neto B[3]

1 - Queen's University *olivo@geol.queensu.ca 2 - Votorantim Metais 3 - Votoratim Metais

The Vazante and northern extension deposits (18 Mt at 19% Zn and 850Kt at 16% Zn, respectively) comprise the largest structurally controlled, hypogene, nonsulfide zinc orebodies in the world. They are hosted in the dolomitized carbonate rocks of the Serra do Poço Verde Formation, deposited in an intertidal to supratidal environment. This Formation is part of the Neoproterozoic Vazante Group, which is located in the Brasília Fold Belt along the western margin of the São Francisco Craton. The hypogene orebodies occur within major tectonic-hydrothermal breccias controlled by a NE-trending fault zone. The faults and the ore breccias are interpreted as having formed during the D_2 deformation event of the Late Proterozoic Brasiliano Orogeny [1, 2]. The faults were reactivated during their evolution and are cut by later NW-trending structures, which host supergene ore (mainly hemimorphite).

The Vazante and northern extension hypogene ore consists mainly of willemite, which occurs in breccias containing variable proportions of hematite, quartz, Fe-dolomite, dolomite, as well as minor franklinite, magnetite and/or sphalerite. Fe-carbonate started to precipitate early, followed by various generations of hematite and willemite with minor franklinite and late dolomite. The Vazante mine contains higher proportions of sphalerite than the northern extension orebodies, but the latter is enriched in hematite. Franklinite and magnetite concentrations increase near the basic dikes that cut the sedimentary units at Vazante. The orebodies are strongly enriched in Ag, Cd, Fe, Pb and Zn, and are anomalous in As, Ba, Be, Bi, Cu, Ge, Hg, In, Mo, Ni, Sb, Se, Si, U, V, and W. Isolated veins containing sphalerite, pyrite, dolomite, quartz and bitumen also cut the host rocks. These veins and the main ore stage zinc silicate breccias are cut by a late dolomite generation and by Pb, Cu and Ag-rich sulfide veinlets.

The Fe-bearing dolomite formed in the early stages of silicate zinc mineralization yielded $\delta^{18}O_{SMOW}$ of 20.2 to 20.8 per mil and $\delta^{13}C_{PDB}$ of 0.7 to 1.8‰. However the late generations of dolomite have lighter $\delta^{18}O_{SMOW}$ (15.8-17.1 ‰) and $\delta^{13}C_{PDB}$ (0.1 to 1.3‰) compositions. These values are distinct from the dolomite from the veins with sulfide and bitumen, in which $\delta^{13}C_{PDB}$ values range from 0.1 to -2.3 and $\delta^{18}O_{SMOW}$ values range from 21.9 to 22.0. These various stages of hydrothermal dolomite and Fe-bearing dolomite are depleted in $\delta^{18}O$ when compared with the unaltered host dolomite ($\delta^{18}O_{SMOW}$ = 24-27 ‰), but show a similar range of $\delta^{13}C_{PDB}$ (0.6-3.26 ‰ in the host). Ore stage hematite $\delta^{18}O_{SMOW}$ values vary from +3.6 to -0.2 ‰, from the early to the latest generation, respectively. The various generations of willemite yielded $\delta^{18}O_{SMOW}$ values ranging from 11.2 to 13.6 ‰.

The paragenetic and isotopic results for the hypogene silicate zinc ore are consistent with a hydrothermal system formed at temperatures around 200°C by mixing of hot metalliferous brines with either cooler evolved meteoric water or sea water. As for the pyrite- sphalerite- bearing veins, the stronger depletion in the $\delta^{13}C_{PDB}$ in the associated dolomite is interpreted as being due to the interaction of hot brines with organic matter and/or hydrocarbons.

[1] Slezak P., Olivo G.R., Diniz-Oliveira G., Dardenne M.A. (2014). *Ore Geology Reviews*, 56, 234-257.

[2] Monteiro L.V.S., Bettencourt J.S., Juliani C. and Oliveira T.F. (2007). *Gondwana Research*, 11, 362-381.

Carbonate-hosted nonsulphide Zn-Pb mineralization, an unusual base metal deposit type in the Canadian Cordillera

Paradis S

Geological Survey of Canada. suzanne.paradis@nrcan-rncan.gc.ca

Many carbonate-hosted Zn-Pb sulphide deposits in the Canadian Cordillera have near-surface Zn- and Pb-bearing iron oxide-rich gossans. These gossans formed when carbonate-hosted, base-metal sulphide mineralization was subjected to intense weathering. The iron oxide-rich gossans consist of a mixture of hydrated zinc and lead silicates and carbonates, iron oxyhydroxides, and iron oxides. Two types of supergene carbonate-hosted nonsulphide deposits, direct replacement ("red ores") and wallrock replacement ("white ores"), are present in the Cordillera; however, most of the nonsulphide deposits are of direct replacement-type.

The direct replacement deposits formed by the direct oxidation of the primary sulphides; the base metals passed into solution and were redistributed and trapped within space occupied by the oxidized portion of sulphide protore. The nonsulphides usually cap the protore. Depending on the extent of replacement of the sulphides by Zn-, Pb- and Fe- bearing oxides, silicates, carbonates and phosphates, the resulting ore can be called "mixed" (sulphides and nonsulphides) or "nonsulphide".

The wallrock replacement-type deposits formed when the base metals liberated by the oxidation of sulphide ore were not trapped locally, and were transported by circulating supergene solutions down and/or away from the sulphide ore to form wallrock replacement deposits. Only one deposit in the southern Canadian Cordillera (i.e., Oxide, Salmo area, SE British Columbia) was identified as a possible wallrock replacement nonsulphide deposit.

In southern British Columbia, the direct replacement zones consist of iron-rich gossans over carbonate-hosted zinc-lead sulphides in which they replace (pseudomorph) the sulphide aggregates, forming large irregular replacement masses, encrustations, and open-space fillings. They consist predominantly of Fe-oxyhydroxides, goethite, hematite, hemimorphite, and minor smithsonite, hydrozincite and cerussite.

In central and northern British Columbia and in the Northwest Territories, nonsulphides variably replaced base metal sulphides. The deposits consist of pervasive fine-grained sulphide and nonsulphide disseminations and aggregates forming pods and masses, sulphide- and nonsulphide-bearing quartz (±calcite) veins, and crackle breccias. Sphalerite and galena are the most abundant sulphides. They are accompanied by trace concentrations of pyrite and tetrahedrite-tennantite. Smithsonite is the dominant nonsulphide. Lesser amounts of hemimorphite, cerussite, hydrozincite, and possibly anglesite are present locally.

The Reef Ridge supergene nonsulphide zinc mineralization, Alaska

Santoro L[1*], Boni M[2], Woodman J[3]

1 - Universita Federico II, Napoli *shiva4386@hotmail.it 2 - University Napoli

3 - Doyon Ltd.

The Reef Ridge (RR) deposit is a typical supergene "Nonsulphide" zinc prospect, located in the McGrath area in the Yukon-Koyukuk region of west central Alaska (USA). The area has been intensively oxidized, with both goethite and hematite occurring in surface gossans and in core specimens. The potentially economic mineralization is in the oxidation zone; it consists mainly of Zn carbonates mixed with Fe-(hydr)oxides. The deposit was discovered in 1975. Since then, several exploration activities (Doyon Ltd. and other companies such as Patino Inc. and Pasminco Exploration Ltd.) have been carried out around Reef Ridge; this led to the discovery of a larger area with similar showings of ore similar to Reef Ridge (i.e. Saddle, Midway, Beaver Pass, Soda Creek etc.) [1]. The RR deposit has been the only one further investigated for its high Zn grade 460 Mt at 17.4% Zn.

RR is located in sedimentary rocks of the Farewell Terrane (FT), which represents, according to recent studies, a micro-continent between the Siberian and Laurentian (North American) cratons [2]. The mineralization is hosted in Lower-Middle Devonian shallow water brecciated dolomite of a Paleozoic carbonate platform sequence belonging to the Nixon Fork subterrane (NFST) [3]. The mineralization consists of oxidized minerals (mainly Fe-hydroxides and zinc-nonsulphides), associated with minor remnant sulphides. Locally, the cores of the breccias are cemented by sphalerite, with minor amounts of pyrite and/or marcasite concretions. The zinc sulphides, hosted in silicified lithotypes and detected in two minor drill intercepts, are not considered economic. A complete petrographic and mineralogical characterization of both surface specimens and core samples has been conducted in collaboration with Doyon Ltd. The samples were analyzed by XRD, chemical analysis (ICP-ES and ICP-MS), and SEM-EDS. Preliminary investigation with QEMSCAN has also been carried out at the Camborne School of Mines. The results indicate that most of the assayed zinc in the nonsulphide ore occurs as smithsonite (with up to 75 weight % in a few samples). Smithsonite replaces sphalerite and dolomite precipitates as cement in the macro- and microporosity of the carbonates and occurs as veinlets of various sizes. Small amounts of zinc have also been identified in Fe-(hydr)oxides, which are abundant both in drill core and surface samples (especially in the gossanous specimens). Zinc traces have been identified in clay minerals (illite/muscovite and kaolinite). In order to detect the nature of the fluids that deposited the nonsulphide ores, we have carried out stable isotope analyses on smithsonite and carbonate host rocks. The data suggest that C originated from the Devonian carbonates, while the O precipitated from local meteoric waters at very low temperatures.

To further enlarge the prospecting area, new geochemical data (soil sampling) were collected by Doyon during the summer 2012 around three magnetic anomalies SE of RR. The survey detected anomalous concentrations of Cu and As in the soil samples, that could suggest a link to a polymetallic, skarn-related mineralization similar to the Au-Cu Nixon Fork deposit.

[1] Doyon Ltd report 1981.

[2] Blodgett *et al*. (2002). Geological Society of America, Boulder, Co, Special Paper, 360, 273-280.

[3] Decker *et al*. (1994). Geological Society of America, Boulder, Co, The geology of North America, G1:285-310.

Characterization and origin of clays in the Bou Arhous (Morocco) non-sulfide Zn ore deposit

Choulet F[1*], Buatier M[2], Barbanson L[3], Guégan R[3], Ennaciri A[4]

1 - Chrono-Environnement UMR6249, Université de Franche-Comté/CNRS
*flavien.choulet@univ-fcomte.fr 2 - ChronoEnvironnement, UFC Besançon 3 - ISTO UMR7327, Université d'Orléans/CNRS 4 - Groupe Managem, Morocco

Supergene non-sulfide Zn deposits offer high mineralogical diversity including clay minerals that can incorporate significant amounts of Zn like sauconite. Although clayey material is commonly observed in such ore deposits, its nature and origin have been rarely studied, especially in carbonate-hosting environments. However the role of clay minerals is essential for mineral processing because they usually have a negative impact on zinc recovery.

In this work, we focus on the Bou Arhous Zn-Pb ore deposit in Eastern High Atlas, Morocco. This deposit is located in an anticline formed by Lower Jurassic limestone and marl, with Upper Triassic shale in the core of the anticline. Zn-rich clayey material fills karstic cavities and two types of clay rich deposits have been identified field: 1) white to ochre granular clay (kaolinite/smectite (K/S) irregular mixed layers, smectite and illite) and 2) red smooth clay (kaolinite, chlorite, illite). The white to ochre granular clays are closely associated with supergene willemite (zinc silicate), one of the main Zn bearing mineral phases of the Bou Arhous deposit. The red smooth clays fill karst-related cavities cutting across the non-sulfide mineralized bodies. The red smooth clays present evidence of stratification that reflects internal sedimentation processes during karst evolution. Bulk chemical analyses reveal that the Zn content is highly variable in all clayey samples and even can reach several percent. This enrichment may be due to fine inclusions of zinc silicate or carbonate in the clayey material, or to the occurrence of Zn clay minerals (i.e. sauconite).

The mineralogy of clays and associated minerals in bulk powders and separated <2µm oriented fractions from the two types of clay deposits and from surrounding Triassic to Lower Jurassic rocks has been investigated. X-ray diffraction (XRD) analyses complemented by Scanning Electron Microscope (SEM) observations, have allowed us to identify the nature of the clay minerals and to characterize the textural relationships between clays and other zinc-bearing minerals like willemite. In a few samples with high zinc content (5%), bulk XRD analyses do not reveal the occurrence of zinc sulphides, carbonates or silicates, suggesting that zinc is associated with clay minerals. Preliminary XRD results indicate that white and ochre clays are composed of kaolinite/smectite (K/S) irregular mixed layers with up to 20% of smectite in some samples; smectite, illite and chlorite are also present. On the other hand, the red clays contain kaolinite, chlorite, illite, and illite/smectite mixed layers (goethite is commonly present in these samples). SEM observations demonstrated that willemite crystals are partially dissolved and are surrounded by authigenic clay minerals. Microprobe analyses and cation-exchange capacity on clay mineral fractions are currently performed to highlight the localization of zinc within the structure of clay minerals, and to provide crucial information on Zn recovery potential of the studied deposit. All these new results will enable characterizing Zn speciation in these supergene deposits to check the following hypotheses for clay origin: 1) interactions between Zn-rich solution due to supergene oxidation and residual clays originated from dissolution of limestone-dominated host rocks, 2) secondary alteration of Zn minerals like willemite into clay minerals, and 3) reaction between detrital clays and Zn-rich solutions.

Low sulfide high-grade sperrylite-epidote-quartz zone, Sudbury Canada: implications for hydrothermal-magmatic processes

Ames D[1*], Hanley J[2], Jackson S[1]

1 - Geological Survey of Canada *doreen.ames@nrcan-rncan.gc.ca

2 - Saint Mary's University

High grade, low sulfide (S) platinum group element (PGE) mineralization is a minor component of the Sudbury Ni-Cu-PGE-PGE-Au ore system yet, clearly identifies significant hydrothermal activity in the footwall that has also affected the magmatic Ni-Cu mineral deposits. Well studied [1] magmatic, high S, Cu-PGE veins, that are hosted by footwall breccia zones below the igneous complex, are commonly associated with low S PGE-rich mineralization that can be overlooked.

A spectacular sperrylite (<13 mm) - epidote-quartz zone (Figure 1) in the Broken Hammer open pit has PGE/S ratios 5 orders of magnitude higher than the associated high S sharp-walled veins.

Figure 1: Quartz-epidote-sperrylite (9mm) assemblage in low sulfide zone, Broken Hammer. Wallbridge specimen. M. Bainbridge photo.

The hydrothermal assemblage of coarse sperrylite -epidote - quartz contains minor chlorite-Kspar-merenskyite, and trace michenerite. Inclusions of gold, petzite, galena and aleskite occur in coarse sperrylite crystals, whereas complex intergrowths of Pd-, Bi- and Ag- tellurides are found locally with cassiterite and specular hematite-gold or fine sulphides and may reflect rapidly fluctuating reducing and oxidizing conditions. Late chalcopyrite-millerite occupies the core of the silicate-dominant vein.

In-situ analysis of minerals and fluid inclusions along growth zones in quartz, imaging and line of spots laser ablation ICP-MS mapping of pyrite, pyrrhotite, chalcopyrite, pentlandite from different ore environments and mineralization types tracks the magmatic-hydrothermal history of the mining district. Fluid inclusions occur in immiscible assemblages of hydrocarbon (CH_4-dominated)-brine (high Ca-Sr-Ba-Zn-Mn) that have bulk and stable isotope compositions consistent with mixing of Archaean groundwater and an exotic (primitive) fluid possibly released by contact metamorphism/melting/degassing of lower crust or Nipissing diabase during impact.

[1] Dare *et al*. (2014). *Econ Geol*, 109, 343-366.

Palladium transport in aqueous fluids

Brugger J[1*], Mei Y[1], Reith F[2], Etschmann B[1], Fiorentini M[3], Barnes S[4]

1 - Monash University *joel.brugger@monash.edu 2 - University of Adelaide 3 - University of Western Australia 4 – CSIRO

Characterising the speciation and solubility of platinum group elements (PGE) in aqueous fluids is useful in understanding the formation of PGE deposits and the dispersion of PGE around deposits during weathering or metamorphism. Palladium has the highest mobility of all PGEs in aqueous fluids. At the type locality (Bom Sucesso Creek, Minas Gerais, Brazil), secondary palladium is forming via biologically mediated processes. A number of experimental studies have investigated Pd speciation and solubility in hydrothermal chloride solutions, with reasonable agreement over the nature and stability of Pd(II) chlorocomplexes [1]. In contrast, there are significant discrepancies among the available thermodynamic properties for the predominant Pd bisulfide species. This uncertainty severely hinders numerical modelling of PGE mobility in hydrothermal fluids.

Ab-initio molecular dynamics (MD) simulations and synchrotron-based X-ray Absorption Spectroscopy (XAS) experiments were performed to investigate the stability of Pd-Cl and Pd-HS complexes in hydrothermal fluids. Both simulations and experiments revealed the preference of four-fold square planar structures of both chloride and bisulfide complexes at high P,T. The stability constants for the formation of Pd-Cl and Pd-HS complexes in hydrothermal fluids at 300 ˚C, 500 bar were calculated via thermodynamic integration (see Figure 1 [2]). We obtained very good agreement (better than ½ a logK unit) for the stability constant of Pd(II)-Cl complexes. For Pd(II) bisulphide complexes, our MD simulations indicate higher stability than the Pd-Cl complexes, which allow to solve the large discrepancy among existing experimental studies, and support the models that predict limited Pd(II) mobility in sulphur-rich fluids [1].

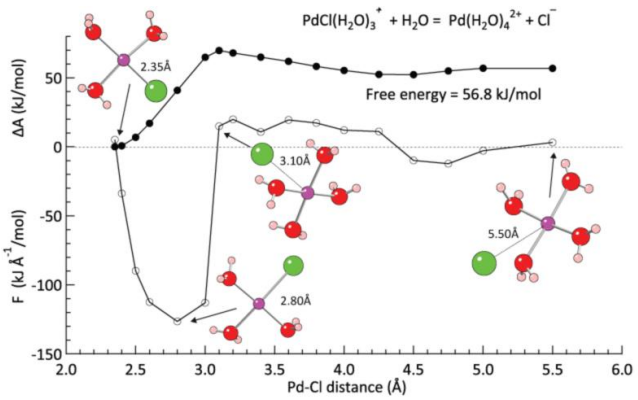

Figure 1: Calculating the free energy of a ligand exchange reaction.

[1]Barnes and Liu (2012). *Ore Geol. Rev.*, 44, 49-58.

[2]Mei *et al*. (2013) *Geochim. Cosmochim. Acta.*, 102, 45-64.

Platinum minerals from the Fazendão hematite-ore mine, Quadrilátero Ferrífero of Minas Gerais, Brazil

Cabral A[1*], Galbiatti H[2]

1 - Mineral Deposits, Technische Universität Clausthal
*alexandre.cabral@tu-clausthal.de 2 - Vale S.A.

Platinum minerals were found in a gold-rich, heavy-mineral concentrate from jacutinga-style auriferous mineralisation at Fazendão, an itabirite-hosted hematite-ore deposit in the eastern part of the Quadrilátero Ferrífero of Minas Gerais, Brazil. The Fazendão jacutinga occurs as a vein-type overprint on the contact between itabirite and manganiferous hematite ore.

Silvery grains, a few mm across, have been characterised as hongshiite (PtCu, massive, no cleavage) with patches of platiniferous tetra-auricupride (AuCu, with 28.1 wt.% Pt, 3.4.wt% Pd and 0.8 wt.% Hg). The hongshiite aggregates have marginal, Cu-depleted domains of prominent cleavage, which are enriched in Pt and, subordinately, Hg (11.4 - 18.9 wt.% Cu; 77.8 - 83.8 wt.% Pt; 1.1 - 3.5 wt.% Hg).

The finding of hongshiite is relevant - it links Fazendão to the hongshiite of Itabira (Kwitko *et al*., 2002, Can. Mineral., 40, 711-723), some 60 km NNE of Fazendão - in the context of the ~0.6-Ga-Brasiliano-controlled distribution of Au-Pd-Pt deposits that delineates the platiniferous Au-Pd belt of Minas Gerais [1].

[1] Cabral *et al*. (2009). *Econ. Geol*, 104, 1265-1276.

Formation of the chromitite layers of the Merensky Unit, Bushveld Complex

Cawthorn G[1*], Wansbury N[2]

1 - University of the Witwatersrand *grant.cawthorn@wits.ac.za 2 - Lonmin Platinum

The PGE mineralization of the Merensky Unit is concentrated in or close to chromitite layers. Hence, understanding the genesis of the chromitites is of vital importance to understanding the mechanism of PGE concentration. There may be one, two or three chromitite layers in the Merensky Unit. Typical vertical successions for these three facies are: (i) anorthosite - chromitite - pyroxenite (normal grain size); (ii) anorthosite - chromitite - pegmatitic pyroxenite - chromitite - pyroxenite; (iii) anorthosite - chromitite - pyroxenite - chromitite - pegmatitic (sometimes) pyroxenite - chromitite - pyroxenite. In order to construct the evolution of this package it is necessary to correlate laterally and to determine to which chromitite in a three-chromitite or two-chromitite facies does the single chromitite facies equate. Such lateral variations require regions of either non-deposition or erosion. These issues are addressed by analysis of chromitites from numerous sections from Lonplats mines. Ten grains were analysed (core and rim) in vertical sections through 34 chromitite layers, and the data from 13 layers from previous other publications are also included for interpretation. Grains in a single layer have constant composition regardless of footwall and hangingwall to each layer, and nature of enclosing host mineral (plagioclase and pyroxene) within the layer. Either the compositions obtained represent the primary compositions, or all grains have reacted and equilibrated with a considerable volume of surroundings (order of cm^3), not with immediate host grain (mm^3). The proportion of chromite in the different layers ranges from 26 to 70% by mode in this study. There is no correlation between proportion of chromite and composition, and so the observed compositional variations are not due to post-cumulus processes.

The average compositions of each of these chromitite layers show considerable variations. The mg# ranges from 0.44 to 0.22 (excluding 2 very low values) and Cr# ranges from 0.81 to 0.58, and there is a strong inverse correlation between these two parameters. No systematic lateral variation exists across Lonplats mines (12 km) for these parameters, but lower layers tend to have higher mg# and lower Cr# than the respective overlying layers. We interpret these variations as reflecting inhomogeneity of the magma (due to incomplete mixing) along strike. High mg# chromitites reflect formation from magma with a greater proportion of more primitive, new magma, whereas lower mg# values reflect a greater contribution from the residual, more evolved magma.

Five samples were taken from an exposure where a one-chromitite layer facies changes laterally into a two-chromitite layer facies with intervening pegmatitic pyroxenite. The chromite compositions show that the composition of the single chromitite layer facies corresponded with the upper of the two in the two-chromitite facies. There was no chemical evidence for the continuation of the lower layer of the two-chromitite facies at the base of the one chromitite facies. Hence, it is concluded that it had been eroded, as has the overlying pegmatitic pyroxenite, prior to the formation of the layer comprising the single chromitite facies.

It is suggested that crystallization of chromite grains is not a function purely of a specific magma composition, but may have been triggered by earthquake-generated shock waves that initiated nucleation of chromite grains.

Magmatic origin of platinum-group minerals from an evolving sulfide liquid at Sudbury, Canada

Dare S A S[1*], Barnes S-J[2], Prichard H M[3], Fisher P C[3]

1 - L'Université du Québec à Chicoutimi, now at University of Ottawa*sasdare@hotmail.com 2 - L'Université du Québec à Chicoutimi

3 - Cardiff University

Chalcophile and platinum-group elements (PGE) are collected by a magmatic sulfide liquid and form PGE (± Ni-Cu) deposits. The PGE are distributed among platinum-group minerals (PGM) and base metal sulfides by a number of processes: crystallization from the sulfide liquid, subsolidus exsolution and remobilization during metamorphism or by hydrothermal fluids. It is important to determine the host phases of the PGE in order to understand the petrogenesis of the deposit and to improve PGE extraction.

We have investigated the origin of PGM from Sudbury Ni-Cu-PGE deposits by combining a PGM study with whole-rock data and a laser ablation-ICP-MS study of the sulfides [1-4]. Samples of Fe-rich sulfides represent early-crystallizing Fe-rich monosulfide solid solution (MSS), enriched in Os, Ir, Ru and Rh (IPGE). Samples of Cu-rich sulfides represent the end-stage of crystallization of intermediate solid solution (ISS) from the residual liquid, which was enriched in Pt, Pd, Ag, As, Bi, Te and Sn. At subsolidus temperatures, Fe-rich MSS exsolves to pyrrhotite and pentlandite and Cu-rich ISS exsolves to chalcopyrite and cubanite. In contrast to much of the previous work at Sudbury, which has invoked the role of late-magmatic and/or hydrothermal fluids in the collection of precious metals, we show that many PGM formed originally by magmatic processes over a wide range of temperatures.

In the rocks rich in pyrrhotite and pentlandite (MSS cumulates) up to 50% of the whole rock palladium is hosted in pentlandite. The balance is in laths of $(PtPd)(BiTe)_2$ and PdBiTe which exsolved from MSS during cooling. The behaviour of Ir, Rh and Pt depends on the amount of As initially present in the sulfide liquid, which depends on the type of country rock assimilated. In As-poor liquids, Ir and Rh are hosted in solid solution in MSS. In As-rich liquids, As-PGM (IrAsS, RhAsS ± $PtAs_{-2}$) crystallized early (1200-900°C) from the sulfide liquid, thus depleting co-crystallizing MSS (now pyrrhotite and pentlandite) in these elements.

However, in the Cu-rich ores, Pt and Pd are hosted almost entirely by PGM dominated by Bi-Te-phases ($PdBi_2$ and (Pt,Pd)BiTe) with minor As- and Sn-phases ($PtAs_{-2}$, Pd_2Sn and PtSn). From this we infer that during the crystallization of ISS from the Cu-rich residual melt, Pt, Pd, Bi and Te behave incompatibly and were thus enriched in small volumes of late-stage melt trapped between ISS. A sequence of PGM crystallized from this late-stage melt and formed composite grains with a core of Sn- or As-bearing PGM (stable at higher temperatures) hosted in Bi-Te-PGM (lower temperatures) and commonly surrounded by accessory tellurides (Ag-, Bi-, Pb-bearing) and sulfides (galena, sphalerite). At the very end of crystallization, at low temperatures (< 500°C), the small amount of Cl that was soluble in the sulfide liquid crystallized as primary chloride minerals (e.g., $PbCl_2$) either from the late-stage melt or from an exsolved Cl-rich late-magmatic fluid. Many PGM also show evidence of partial corrosion and dissolution most likely by late-magmatic/hydrothermal fluids that probably remobilized and deposited PGE in the surrounding footwall.

[1] Dare *et al*. (2010). *Econ Geol*, 105, 1071-1096.

[2] Dare *et al*. (2010). *Miner Deposita*, 45, 765-793.

[3] Dare *et al*. (2011). *Miner Deposita*, 46, 381-407.

[4] Dare *et al*. (2014). *Econ Geol*, 109, 343-366.

Peculiarities of phase formation in the system Pd-Bi-Te

Evstigneeva T[1*], Boeva N[1], Vymazalová A[2], Trubkin N[1]

1 - IGEM RAS, Moscow, Russia *evst@igem.ru 2 - Czech Geological Survey, Prague, Czech Republic

The kotulskite-sobolevskite ss series was studied previously. According to published data there are two polymorph modifications of PdBi: monocl.α and orthorh.β, α↔β ~210 ^{0} C. Two minerals with the composition "PdBi" are known in nature: polarite and sobolevskite. It is interesting that sometimes both minerals form joint intergrowths. Polarite corresponds to orthorhombic β-PdBi. The position of thehexagonal phase (sobolevskite) in the system remains unclear. And the co-existence of orthorhombic and hexagonal minerals with the same composition requires explanation. We can only assume that the hexagonal modification is stabilized by a minor impurity (i.e.Te?).

In order to refine properties and conditions of phase formation in the series PdBi-PdTe, a detailed study of Pd(Te,Bi) compounds was performed using SEM + EDD (JCM 5600LV) and STA (NETZSCH STA 449 F3 Jupiter ®). Thermal characteristics of PdBi-PdTe compounds were determined using Simultaneous Thermal Analysis (STA) [TGA + DSC].

Mixtures of samples with the same starting composition synthesized at 200, 400, 600^0 C were used as charges for STA. All samples were generally homogeneous but with small variations in Te and Bi content. Bi5 is composed of two phases- PdBi (1,5 Wt.%Te) and ~$Pd(Bi_{0.75}Te_{0.25})$. XRD data of all samples produced almost the same set of d_α higher for Te-rich. Intensities and peak shape suggests some structural distortion.

Table 1: PdTe-PdBi phase melting temperatures

Samples	Te:Bi	T of melt.,? C (expected)	Te:Bi	T of melting,? C (measured)
Bi12	0:100	618	0:100	580,1
Bi5	20:80	640	3:96 17:82 26:73	540,4
Bi2	33:67	650	37:63 26:74	556,0
Bi1	34:66	660	35:65 40:60 29:71	558,7
Bi6	40:60	670	40:60	552,3
Bi7	61:39	710	65:35	560,6
Bi8	80:20	736	80:20	574,6
PdTe	100:0	746	100:0	

Melting T^0 of the series PdBi-PdTe ss must increase gradually from 610^0 C to 736 ^{0} C. But TG curves show the melting effect at lower T^0 than expected (Table). Some weak peaks at ~ 204-209 ^{0}C on Bi-rich samples TG could correspond to α ↔ β PdBi phase transition. Other very weak TG effects may be associated with reactions between Pd-Bi-Te compounds during heating.

The Waterberg Extension to the Bushveld Complex

Kinnaird J[1*], Yudovskaya M[1], Botha T[2]

1 - University of the Witwatersrand *judith.kinnaird@wits.ac.za 2 - PTM, Platinum House, Johannesburg

In 2011 Platinum Group Metals (PTM) announced the discovery of PGE mineralisation in Main Zone rocks beneath Proterozoic Waterberg red bed sedimentary rocks, north of the surface outcrop of the northern limb of the Bushveld Complex. Since the discovery, extensive drilling of more than 130 boreholes, has confirmed the presence of PGE mineralisation within the first 17 km strike of a 35 km long northeast lobate arc defined by airborne geophysics. The exposed northern limb forms the eastern part of what appears to be a much larger 'basin', 100 x 130 km in size based on geophysical data [1]. Until the discovery of buried Bushveld rocks, it had been assumed that the exposed northern limb linked in a westward arcuate form with the Villa Nora segment of exposed Upper Zone. However, the confirmation of buried Bushveld rocks 20 km north of the exposed northern limb refutes these earlier correlations. The Bushveld succession in the PTM cores comprises a Main Zone (MZ) and Upper Zone (UZ). The contact between the Bushveld rocks and the Waterberg sedimentary cover is often mylonitised with a weathered reddened Bushveld gabbro below the contact, characterised by gibbsite with hematised and chloritised silicates. Commonly a granofels or agmatite forms the footwall to the Bushveld succession, which is interpreted to be re-mobilised footwall gneiss interfingered with pyroxenite. The UZ of ferrogabbro, ferronorite and gabbronorite varies between 10 and 500 m in thickness. Although cumulus magnetite occurs in UZ of the Waterberg project as observed in core samples and identified based on magnetic susceptibility, typical magnetitite layers are lacking, except in one of the early cores in the south of the project area. The MZ rocks are characterised by gabbronorites with thick troctolite layers and minor harzburgites, locally pegmatoidal, towards the base that are atypical of MZ rocks elsewhere in the Bushveld Complex. This package of olivine-rich rocks is at least 50 m thick. Commonly, a pyrrhotite-bearing pyroxenite, generally lacking any PGE grade occurs below the troctolites. There are at least two "reefs" or 'mineralized zones', an upper T reef and a lower F reef. The T reef is restricted to the southern portion of the project area, whereas the F reef has been intersected with drilling for a 17 km strike to date. Further exploration drilling is in progress. The Bushveld succession thickens northwards from the discovery hole with greater separation between the two reefs. There is a correlation between visible chalcopyrite and pentlandite abundance and grade of PGE. In the discovery hole the T reef is ~30 m thick but northwards thickens to <50 m thick. It comprises an upper T1 and a lower T2 unit with a middling between the two zones that varies in thickness from ~20 cm to 20 m of olivine-bearing feldspathic pyroxenite, pegmatitic gabbro or a vari-textured feldspathic-rich zone. T1 is associated with varied rock types that include a feldspar-rich pegmatoid, feldspathic pyroxenites, troctolite /harzburgite and gabbronorite and is ~20 m thick in the most northerly hole in which it occurs. T2 is mainly in a gabbronorite. Grade in both T1 and T2 is typically 3.4 g/t 3E, although locally with <14 g/t in more northerly cores. Both zones have a consistent and unusual metal ratio of ~50% Pd, ~30% Pt and anomalous 20% Au with 0.1% Ni and 0.17% Cu. The F reef which is hosted in serpentinised troctolite/harzburgite, is at a minimum depth of 180 m from the surface. The olivine-rich zone is 200 m thick in Hole WB99, although more typically it is 100 m in thickness. However, only part of this unit is mineralised. In the southern portion, the mineralised F zone is typically <10 m thick but in the central portion, the "Super F reef" thickens to 60 m in true thickness, with grades of 3 g/t over this interval. A typical prill split has 65% Pd, 30% Pt and 5% Au with 0.07% Ni and 0.17% Cu. Both T and F units remain open at depths below 1000 m which for initial purposes was taken as an economic depth cutoff. PGE enrichments in the Main Zone of the northern limb are also known on Moordrift, Aurora, Drenthe but none of these localities had troctolites associated with the PGE enrichment. The mineralized olivine-rich layers have more similarities to parts of the composite Platreef that resulted from multiple influxes [1].

Acknowledgments: We would like to acknowledge the support of R. Michael Jones, Rob van Egmond, Gordon Chunnett, geologists at the project site and postgrads at the University of the Witwatersrand.

[1] Kinnaird J. *et al.* (2005). *Mineral. Deposita*, 40, 576-597.

An unusual Se-bearing moncheite and Te-bearing palladseite, Miessi River, Inari, Finland

Kojonen K[1*], McDonald A[2], Stanley C[3], Johanson B[1], Tranberg J[1]

1 - Geological Survey of Finland *kari.kojonen@gtk.fi 2 - Department of Earth Sciences, Laurentian University 3 - Natural History Museum, London, UK

A grain mount of a black, heavy-mineral concentrate from a Miessi River gold concession, Inari, Finland was analyzed by a SEM-EDS and Feature image analysis. 1109 features were calculated following (# of the features, vol.%): sperrylite (391, 47.13), isomertieite (11, 1.46), braggite (5, 0.62), cooperite (11, 0.24), vysotskite (1, 0.13), moncheite (21, 0.23), Pt (2, 0.24), Au (14, 0.52), (Pb,Sb) (64, 3.54), Bi (44, 4.02), arsenopyrite (39, 0.06), Fe-sulfides (21, 0.11), monazite (46, 3.46), wolframite (1, 0), cassiterite (66, 7.02), zircon (8, 0.14), rutile (8, 0.11), ilmenite (6, 0.11), titanomagnetite (4, 0.01) hematite (37, 37, 1.29), chromite (17, 1.84), Nb-Ta minerals (14, 1.94) and Th-U-oxide (278, 24.13). Two grains of unknown chemical composition were found. The first mineral showed EDS composition (average wt.%) 10.65 Se, 44.82 Te and 44.53 Pt and the second Se 41.40, Te 3.22 and Pd 55.32 f. The WDS results were (in wt.%): 10.05 Se, 45.38 Te, 0.02 Sb, 0.66 Pd, 0.02 Ag and 43.92 Pt for the first phase corresponding to $(Pt_{0.95}Pd_{0.03})\sum 0.98(Te_{1.49}Se_{0.53})\sum 2.02$ and 35.11 Se, 0.04 Sb, 4.02 Te, 1.14 Cu, 0.39 Os, 0.24 Au, 0.96 Pt, 57.13 Pd with a formulae $(Pd_{15.84}Cu_{1.17}Os_{0.12}Pt_{0.03}Au_{0.02})\sum 17.18\ (Se_{12.03}Te_{1.81}S_{0.51}Sb_{0.02})\sum 14.37$ for the second. The PXRD indicate a powder pattern of moncheite for the first phase and palladseite for the second, but the chemical data are previously unreported for both minerals.

The Se-rich moncheite appears yellowish white in plane-polarized and is isotropic. Moncheite crystallizes in the space group P m1, and unit-cell refinement based on 18 reflections (20-125º2Θ) gives a 3.994(2) Å, c 5.233(3) Å, V 70.49 Å3, Z = 1, class m, c:a=1.310, density 9.590 g/cm3(calc). It is macroscopically metallic steel gray. The VHN25 values are 83-116 with average 101(3, df-cv) corresponding to a Mohs hardness of ca. 3 which is higher than that of moncheite [1]. The reflectance measured for the in the COM standard wavelengths are 58.7 (470 nm), 59.3 (546 nm), 59.6 (589 nm) and 60.0 (650 nm) higher than those reported by Cabri [1]. Se replacing Te in the lattice of moncheite decreases the unit cell size but increases the VHN and reflectance values.

Palladseite crystallizes in the space group Pm3m. The refined unit-cell edge for the calculated Te-bearing palladseite (based on 28 reflections for 32-123º2Θ) is: a 10.653(2) Å, V 1208.97 Å3, Z 2, space group Pm3m, class m3m, density 7.958 g/cm3(calc.). It is macroscopically a dark metallic steel gray, and in polished section, a creamy white. The reflectance (%) is 46.5 (470 nm), 48.3 (546 nm), 48.4 (589), 48.3 (650 nm), The VHN25 values are 459-484, average 472 (5, p-sf) corresponding to Mohs hardness ca. 5. The VHN and the reflectance reported by Cabri [1] are lower than in Te-bearing palladseite. Te replacing Se in palladseite increases the cell size,

The PGM paragenesis is rather poor in sulphur. Se and Te are replacing each other in moncheite and palladseite in the Miessi River. Both elements belong to group 16 of the periodic system and have a similar charge and less than 15 % differing ionic radius (Se2- 1.98Å and Te2- 2.21Å) [2]. Similar replacement of Te and Se has been reported [3] in miessiite isostructural with isomertieite.

[1] Cabri L.J. (2002). The Platinum Group Minerals. In: The Geology, Geochemistry, Mineralogy and Mineral Beneficiation of Platinum-Group Elements. Ed. by Louis J. Cabri, Ottawa, Ontario. *Can. Inst. of Mining, Metallurgy and Petroleum*, Spec. Vol. 54, 13-129.

[2] Vaughan D.J. and Craig J.R. (1978). *Mineral chemistry of metal sulfides*. Cambridge University Press, 493 p.

[3] Kojonen K., Tarkian M., Roberts A.C. and Heidrich S. (2007). Miessiite, $Pd_{11}Te_2Se_2$, a new mineral species from Miessijoki, Finnish Lapland, Finland. *Can. Mineralogist*, 45, 1221-1227.

PGE-bearing minerals in chromitites of the Critical Zone (LG-6 TO UG-3A) on Winterveld 293KT, Eastern Bushveld Complex

Kotzé E*, Gauert C

University of the Free State *2007005974@ufs4life.ac.za

The distribution of PGE in abundantly occurring base metal sulphides of the LG-6, MG-4, MG-5, UG-2, and UG-3 &-3A chromitite layers of the Critical Zone of the Bushveld Complex north of the Steelpoort Fault Zone was determined by electron microprobe analysis. The data allows us to infer possible mechanisms/ conditions of PGM formation in chromitites. The analyses, however, allow no distinction to be made between PGE present in solid solution in base metal sulphides, and PGE present as discrete inclusions.

By far the most abundant PGE present in base metal sulphide is rhodium, ranging up to over 1wt-% in pentlandite. Palladium is also abundant, but platinum occurs mostly below detection limits. In some samples, the high amount of Pt reported is inferred to be due to inclusions of braggite or cooperite. Ruthenium is also generally below detection limits, but was found in pentlandite and pyrite. Osmium and iridium report concentrations of a few hundred ppm each.

Of the minerals analysed, pentlandite consistently reported the highest values, with relatively high Rh in all samples, high Pd in many samples, and occasional high values of Pt, Ru and Ir. The total PGE content for pyrrhotite and chalcopyrite was below 100 ppm, with chalcopyrite showing approximately equal proportions of the IPGE and PPGE. The PGE values in pyrite are surprisingly high, with some layers reporting Rh and Pd values similar to that of pentlandite (Figure 1).

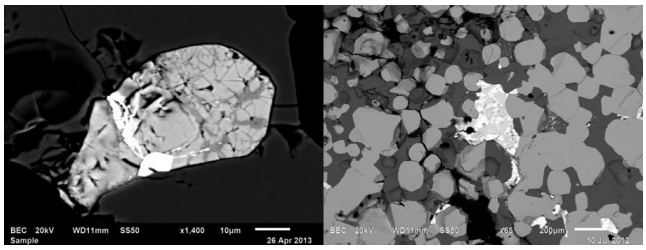

Figure 1: Left: Pt-Pd phase (brightest) in Rh-bearing pentlandite (UG-2). Right: Pyrite-pentlandite-chalcopyrite intergrowth (UG-2).

A search for discrete PGMs revealed that the most common minerals are braggite/ cooperite (Figure 1), along with Pt-Fe alloy. Tellurides and arsenides were found only in the UG-2 layer. After the Pt-Pd minerals, laurite with Os and Ir in solid solution with Ru was the most common mineral. This typically occurs as inclusions in chromite, but could also be associated with other sulphides. Rh does not appear as a measurable Rh-mineral, and also does not substitute for Pd and Pt.

Along with the sulphides found in the chromitites, PGE analyses were carried out on pentlandite, chalcopyrite, and pyrrhotite associated with an intrusive pegmatoid and vein formation using LA_ICP-MS. The intrusive pegmatoidal pyroxenite was found to contain sulphides with up to about 50 ppm total PGE, while sulphides in a vein contained much lower PGE concentrations (<1 ppm).

In general, the PPGE content in chromitite layers increases upwards in the stratigraphy relative to the IPGE content due to laurite inclusions in chromite crystals co-crystallizing with chromite from a PGE-saturated melt at an early stage. Os and Ir were partially scavenged by this early-forming phase, depleting the magma in IPGEs relative to PPGEs. Repeated chromitite formation enriched the magma higher up in the chamber in PPGEs.

Pyrite occurs in the UG-2, MG-5, MG-4 and MG-1, containing significant concentrations of different PGEs. This pyrite may have been the legacy of a late-stage sulphur-enriched fluid which migrated upwards through the sequence during PGM crystallization. Redistribution of PGEs in pyrite causes pyrite to inherit PGE signatures of the original magmatic BMS assemblage, which was dissolved by the fluid. A late-magmatic fluid bearing S could be formed by desulphurization of pyrrhotite in the chromitites.

(Bio-) Leaching of oxidized PGE ores (Great Dyke): enhanced platinum and palladium mobilization with biogenic and conventional leaches

Kraemer D[1*], Bau M[1], Oberthür T[2], Junge M[2]

1 - Jacobs University Bremen *d.kraemer@jacobs-university.de 2 - Federal Institute for Geosciences and Natural Resources (BGR) Germany

We present data on the mobilization of platinum and palladium from oxidized Main Sulphide Zone (MSZ) ores of the Great Dyke, Zimbabwe.

The *pristine* material mined at those sites is treated following conventional metallurgical practice by - inter alia- froth flotation and subsequent matte smelting, and recovery rates for Pt and Pd of more than 85% are commonly achieved.

The Great Dyke in Zimbabwe hosts about 160-250 Mt of *oxidized* MSZ material with average grades of 3 to 5 ppm Pt+Pd. The resources of oxidized material available in the Bushveld may even exceed those of the Great Dyke oxidized ores. The complex mineralogical composition of the oxidized PGE ores is challenging, as processing of the surficial, intensely weathered ('oxidized') ores is uneconomic at present (recoveries mostly <<50%) and no metallurgical technology is available that yields sufficiently high (hence economic) recovery rates for oxidized PGE ores. Therefore, in spite of the considerably large resources available, oxidized PGE ores are currently not mined.

In order to tackle the processing issue, leaching experiments with organic and inorganic reagents were conducted and two organic leaches that selectively mobilize either Pt or Pd from the bulk oxidized ore material with only minimal amounts of Ni co-mobilized were developed. One of the tested reagents is easily produced by a wide range of organisms and plants, enabling the option of potential bioleaching efforts, whilst the other is a non-toxic organic food additive, easily available and rather inexpensive. Additionally, leaches based on inorganic chemical reagents were tested and it was found that these mobilize almost all of the Pt and Pd in one leaching step whilst base metal liberation including Ni is restricted.

Our work shows that leaching with either inorganic or organic chemical reagents is a highly efficient option in making these extremely valuable PGE deposits profitable for the mining industry. Bioleaching and heap leaching of vast amounts of easily accessible, and in some areas stockpiled ore, represent two promising techniques in the processing chain of (oxidized) PGE deposit in the future

Our research also indicates that Pt and Pd can be extracted from bulk oxidized ore separately using two subsequent leaching stages. Currently, our studies aim at the optimization of the leaching stages, potential up-scaling, simulation of heap leaching situations, and the recovery of platinum-group metals from multi-element solutions containing inorganic and/or organic reagents.

Acknowledgements: Thanks to Andrew du Toit and his team from Zimplats for providing sample material of oxidized MSZ from the Great Dyke.

.

Role of magma and fluid flow processes in distribution of copper, nickel and PGE in the Duluth Complex, Minnesota

Mogessie A[1*], Benko Z[1], Molnar F[2], Hauck S[3], Severson M[3], Raic S[1]

1 - Institute of Earth Sciences, University of Graz, Austria
*aberra.mogessie@uni-graz.at 2 - Geological Survey of Finland, Espoo, Finland
3 - NRRI, University of Minnesota, USA

Cu-Ni-PGE mineralization in the ~1.1 Ga age Duluth Complex is largely confined to the basal portions of the Partridge River (PRI) and South Kawishiwi (SKI) intrusions. Although the style of mineralization in all of the deposits is dominated by disseminated Cu-Ni sulfides, differences occur between the deposits in igneous stratigraphy, sulfide mineralogy, Cu-Ni and PGE grade, mineralization thickness, and contained tonnages. This variation is suggested to be due to the importance of various aspects of sulfide deposition. Previous geological research recognized enrichments of Cu, Pt, Pd and Au which are difficult to model using orthomagmatic processes. These enrichments can be related to zones where interaction of fluids of different origin (magma, footwall, footwall inclusions in the magmatic rocks) with the host lithologies is evident. Based on detailed microscopic (both transmitted and reflected light) investigations of selected drill core samples, we have documented different types of Cu-Ni-PGE mineralizations in the Archean charnockitic footwall of the SKI, as well as in the basal zone of the SKI and PRI. The mineral assemblage includes chalcopyrite, cubanite, pentlandite and bornite. In the intensively metamorphosed and molten charnockitic rock, one finds net-textured sulfide droplets of pyrrhotite + pentlandite + chalcopyrite. Towards the external zones, bornite-chalcopyrite with a symplectite intergrowth texture occurs. Precious (PGM, Au, Ag) and base (Cd, Ni, Bi, Te, Se) metals associated with the bornite-chalcopyrite assemblage point towards the increasing role of fluids in metal transport. Millerite, galena and other low temperature sulfide minerals in association with the bornite-chalcopyrite assemblage and hydrous silicates like actinolite, chlorite, prehnite, support a continuous transition from a metamorphic to hydrothermal conditions of mineralization.

Acknowledgement: We acknowledge financial support by the Austrian Research Fund (P23157-N21) to A. Mogessie

Mineral chemistry of PGE-bismuthotellurides in the Platreef, Akanani Prospect, Lonmin plc

Ramakoloi N*, Viljoen F

Department of Geology, University of Johannesburg *ramakoloi@gmail.com

Platinum group minerals occurring in the P2 horison at the Lonmin Akanani Prospect on the Platreef of the Bushveld Complex in South Africa comprise Pt-Pd alloys, PGE-bismuthotellurides, PGE- arsenides Ferroplatinum and PGE- Sulfides. The PGE-bismuthotellurides, namely; michenerite, moncheite, merenskyite, kotulskite and maslovite are the most abundant. An investigation into the mineral chemistry of the PGE- bismuthotellurides was conducted using the Mineral Liberation Analyzer and an Electron Microprobe. PGE- bismuthotellurides typically occur surrounded by primary silicates (such as feldspar, pyroxene and olivine), secondary silicates (such as serpentine, chlorite, and grossular), oxides (magnetite), sulfides (pyrrhotite, pyrite, pentlandite and chalcopyrite), and alloys (altaite and hessite). Other minor platinum group minerals present in contact with PGE- bismuthotellurides include PGE- arsenides (sperrylite and hollingworthite), isoferroplatinum, Pt-Pd alloys (plumbopalladinite, zvyagintsevite and altaite) and PGE- sulfides (cooperite). Based on microprobe analyses Te is more abundant than Bi in all Pt- bismuthotellurides, and the opposite is true for Pd- bismuthotellurides. A variety of other elements such as Ni, Cu, Zn, As, Rh, Sb are also encountered. Up to 3wt% of Fe and Pb occur in some of the PGE-bismuthotellurides. Most of the Pt- bismuthotellurides analysed belong in the maslovite (PtBiTe) - moncheite ($PtTe_2$) series, in a form of solid solution. Pd- bismuthotellurides mostly correspond to michenerite (PdBiTe) with limited solid solution towards e.g. polarite, froodite, merenskyite and kotulskite.

Metallic-Fe deposits in basalts: Siberia, Greenland, and Germany

Taylor L[1*], Day J[2], Goodrich C[3], Howarth G[1], Pernet-Fisher J[1], Barry P[1], Ryabov V[4], Pokhilenko N[4]

1 - University of Tennessee *lataylor@utk.edu 2 - Univ. of California, San Diego

3 - Planetary Science Institute 4 - V.S. Sobolev Institute of Geology and Mineralogy

Metallic-Fe is a common feature in certain extra-terrestrial rocks, including lunar basalts [1], as well as chondritic and iron meteorites [2], due to highly-reducing conditions during their formation. However, occurrences of metallic-Fe in terrestrial crustal rocks are extremely rare, forming only when magma interacts with carbonaceous layers within the upper-crust (e.g., coal, oil-shale), which effectively reduces the magma to fO_2 conditions equivalent to below the IW buffer. There are three known terrestrial occurrences of primary metallic-Fe, which are associated with basaltic magmas: Disko Island (West Greenland), Bühl (Kassel, Germany), and the Siberian flood basalt extrusions (NW Siberian Platform, Russia). Furthermore, some deposits contain extremely-high, highly siderophile element (HSE) abundances [Ru, Rh, Pd, Os, Ir, Pt, Re, and Au] within the metallic-Fe (Figure 1), due to enrichment in a plumbing-system prior to intrusion into the upper-crust.

Metallic-Fe basalts are enriched (>>1 ppm), relative to continental crust and intra-plate basaltic lavas (~10 ppb) [3], with Siberian samples displaying the highest HSE contents (>10 ppm; up to 50 ppm) versus Disko Island (~2 ppm), and Bühl (<1 ppm; Figure 1). Variations in the extent of HSE enrichment are probably function of metal/silicate partitioning of the total-HSE contribution in staging chambers.

We focus on the Siberian localities that possess abundant metallic-Fe and anomalously high HSEs [4], reporting new mineral major- and trace-element data for these samples. We use the Siberian flood-basalt trap occurrences to illustrate the unique nature of HSE enrichment in terrestrial systems. We surmise that the magma must have come in contact with highly reducing lithologies (e.g., coal, oil shale) during ascent, however, the mechanism for these HSE enrichments remains enigmatic. Hypotheses include: 1) an early stage of HSE enrichment in lower-crustal staging chambers, associated with sulfide-liquid immiscibility [5] and 2) enrichment in upper-crustal ore-hosting intrusions [6]. The former hypotheses is preferred; however, both require a period of HSE enrichment in the parent magma, prior to further intrusion and eventual crystallization, in order to produce such rare HSE-rich ore deposits.

[1] Taylor L.A. *et al*. (2004). *Amer. Mineral*., 89, 1617-1624.

[2] Treiman A.H. *et al*. (2002). *Meteor. Planet. Sci.*, 37, B13-B22.

[3] Day J.M.D. (2013). *Chem. Geol.*, 341, 50-74.

[4] Ryabov V.V. and Lapkovsky A.A. (2010). *Aust. J. Earth. Sci*., 57, 707-736.

[5] Li C. *et al*. (2009). *Econ. Geol.*, 104(2), 291-301.

[6] Arndt N. T. *et al*. (2003). *Econ. Geol.*, 98(3), 495-515.

Figure 1. Total PGE concentrations (ppm) for Siberian metallic-Fe rocks versus other occurrences [3-5].

Mineral textures in the central zone of the Bon Accord Ni-oxide body, Barberton region, South Africa: indications of a remnant of the Earth's core formation event?

Tredoux M*, Miller D

University of the Free State *mtredoux@ufs.ac.za

The first major differentiation event in the history of a planet is the separation of Fe-Ni alloy from the silicates to form a core; this process permanently influences the concentrations of the highly siderophile elements (HSE), such as Au and the PGE, in the material which eventually forms the mantle and crust of the planet. While iron meteorites can be used as analogies of planetary cores, the exact state of the residual mantle is less easily accessible, especially in the case of a tectonically active planet such as the Earth: both mantle convection and the possible addition of chondritic material after core formation will obscure the original post-core HSE geochemistry of the upper mantle.

We believe that the Bon Accord Ni-rich oxide (BANO) body, found in the northern part of the Barberton greenstone belt, may offer a sample of the deep mantle shortly after core segregation. The BANO is comprised of a massive central portion surrounded by a schistose envelope, and was originally modelled as an altered Archaean iron meteorite [1]); however, investigation of its Cr isotopic ratios [2] has demonstrated convincingly that the material is from a terrestrial source. Considering possible precursors, the BANO has been interpreted as an olivine-spinel mantle xenolith (Wildau, [3] worked on a suite of 12 samples spanning both of the zones) and as an oxidised remnant of an Archaean massive NiS deposit (O'Driscoll *et al*., [4] who worked on a single sample from the schistose rim).

We are inclined to agree with the mantle origin inferred by Wildau [3], but we do not accept that the BANO represents a metamorphic rock, as her model implies. The textures in the undeformed central part of the body are extremely similar to those observed in slags associated with pre-industrial iron smelting [5]: large olivine crystals, which are surrounded by grain boundary oxides and contain dendritic exsolution of oxides within them. In the archaeological samples the minerals are Fe-rich, while the BANO olivine crystals are liebenbergite (the Ni end member) and the oxides are the Ni-rich spinels trevorite, nichromite and cochromite. We suggest that the BANO can be interpreted as a Ni-rich end member of a similar igneous segregation process to the one forming archaeological slags. If this model is correct, then the PGE concentrations of the BANO inner zone, which indicate that the group members from the sixth row of the periodic table (Os, Ir and Pt) are depleted relative to the fifth row members (Ru, Rh and Pd), may reflect a fundamental geochemical feature of the Earth's mantle.

[1] De Waal (1979). *Trans. Geol. Soc. S. Af.* 82, 335-342.

[2] Tredoux *et al*. (2014). *Min. Mag*. (under review).

[3] Wildau (2012). *Unpubl. M.Sc*., Univ. of the Free State, S. Af.

[4] O'Driscoll *et al*. (2014). *Min. Mag*. 78, 145-163.

[5] Miller and O'Killick (2004). *J. Afr. Archaeol*., 2, 23-47.

Morphology and microstructures of chromite crystals from the Merensky Reef: implications for inclusion entrapment

Vukmanovic Z[1*], Barnes S[2], Reddy S[1], Godel B[2], Fiorentini M[3]

1 - Curtin University, Perth, Australia *zoja.vukmanovic@curtin.edu.au 2 - CSIRO, Perth, Australia 3 - University of Western Australia, Perth Australia

Two chromitite layers from the Merensky Reef have been studied with different techniques such as electron backscatter diffraction analysis (EBSD), high-resolution X-ray microtomography, crystal-size distribution (CSD) analysis and electron microprobe analyser (EMPA). The two Merensky layers show very distinctive chromite morphologies. The lower chomitite layer contains large anhedral "ameoboidal" grains and small euhedral grains whereas the upper chromitite layer is characterised by only fine euhedral grains.

Both upper and lower chromitite layers show the absence of preferred crystallographic orientation but the two chromite populations show different internal microstructures. In the two layers, small euhedral grains remained undeformed, while "amoeboidal" grains develop subgrain boundaries at the protruding parts of grains. Crystal-size distribution analyses show two different CSD curves for the two layers. While CSD curve for the upper layer reveals an almost steady-state crystallization, the CSD curve for the lower chromitite layer shows multiple changes in slope implying complex crystallisation [2]. In terms of chemistry, the lower chromitite layer shows a lower Cr number, higher Mg number and lower TiO_2 and Fe_2O_3 [1].

A variety of models have been proposed for an inclusion entrapment mechanism for chromite crystals. A sintering model [1] involves amalgamation of multiple euhedral grains along triple junctions due to high local stresses in the presence of reactive liquid. However, EBSD data showed that "amoeboidal" inclusion bearing chromites are single crystals. Such observations do not rule out the possibility of a sintering process, however, it also requires other conditions. There are two possible scenarios for the formation of "ameoboidal" inclusion bearing grains: 1) sintering of grains with initially the same crystallographic orientation (e.g. epitaxial growth) and 2) sintering of crystals with different crystallographic orientations that is subsequently followed by recrystallization. The first scenario is not supported by the EBSD data, as there is no crystallographic preferred orientation. A scenario that requires recystallisation is unlikely due to the presence of preserved crystal aggregates in the upper layer with different crystallographic orientation in the upper layer and hence there is no evidence that recrystallization occurred in the Merensky reef chromtites.

In the absence of microstructural evidence in support of sintering, we propose another model. We interpret the final "ameboidal" inclusion bearing morphology of the chromite crystals to be the product of two-stage growth. Following the model of Cawthorn and Boerst [3] we suggest that initially dendrite chromites formed as a result of an influx of hot magma over a relatively cold underlying anorthosite layer. Such a model is supported by a more enriched composition for lower chromite grains. Chromite saturation of Merensky reef magmas can be caused by mixing with resident magma or by contamination with partial melts derived from the underlying anorthosite [4]. Saturation in chromite gave rise to a population of small euhedral grains (represented by the linear CSD) with a small number of dendritic grains arising from rapid cooling against the anorthosite. Periods of rapid growth form a small number of nuclei resulting in dendritic crystal growth and this is supported by a kinked CSD curve for the lower chromitite layer. During subsequent crystallisation, these dendrites experienced modification of their morphology in an attempt to attain lower surface areas and greater textural equilibrium.

The addition of a second pulse of magma [3], from which the upper chromitite layer crystallised, resulted in textural re-equilibration of the lower chromite which gave rise to the kinked crystal size distribution curve for the lower chromitite grains. During prolonged cooling of the crystal pile, following the magma influx event, modification of initially dendritic chromites occurred through a ripening process whereby those parts of the grains with the highest surface area dissolved while the more energetically stable surfaces grew. The highly evolved nature of the polymineralic silicate inclusions requires final entrapment close to the solidus. The evolution of the amoeboidal chromite grains therefore spans the temperature range from liquidus to solidus, consistent with our model for textural modification of original dendrites.

[1] Hulbert L.J. and Von Gruenewaldt G. (1985). *Econ Geol*, 80(4), 872-895.

[2] Vukmanovic Z. *et al*. (2013). *Contrib Mineral Petrol*, 165, 1031-1050.

[3] Cawthorn R.G. and Boerst K. (2006). *J Petrol*, 47(8), 1509-1530.

[4] Ballhaus C. (1998). *Earth Planet Sci Lett*, 156(3-4), 185-193.

PGE geochemistry and mineralogy of chromitite dykes from the Sopcheozero deposit, Monchegorsk layered intrusion, Russia

Chistyakova S[1*], Latypov R[1], Zaccarini F[2]

1 - School of Geosciences, University of the Witwatersrand*sofia.chistyakova@wits.ac.za 2 - University of Leoben

We present the results of an investigation of PGE geochemistry and mineralogy of chromitite dykes recently discovered in the Sopcheozero deposit. The deposit is located in the south-western part of a dunite block that represents the lower part of the Monchegorsk layered intrusion, Kola Peninsula, Russia. The ore body of the Sopcheozero deposit consists of disseminated to massive chromitite layers hosted by dunite and peridotite. The recently discovered chromitite dykes are exposed in a quarry in the north-western part of the ore body where they cut the layered sequence of dunite and stratiform chromitite layers. The dykes represent almost monomineralic massive chromitite ore with a cumulate texture (<5% interstitial silicate). Approximately 700 microprobe analyzes of chromite were performed on 27 samples from four chromitite dykes (1.5, 3.5, 11 and 18 cm thick).

Chromite contains 12-14 wt% of Al_2O_3 and 49-53% of Cr_2O_3. In all dykes chromite showed significant compositional variation in terms of MgO and FeO. From the margins inwards, MgO and Mg number (Mg number = $Mg^{2+}/(Mg^{2+}+Fe^{2+})$) systematically increase whereas FeO decreases. Other major oxides such as Al_2O_3, TiO_2 and Cr_2O_3 do not show any compositional variation across the chromitite dykes. The concentration of total PGE in 27 chromitite samples ranges from 405 to 736 ppb. There is no obvious correlation between PGE abundance and chromite composition. All samples display enrichment in Ru (186-368ppb), Ir (81-141ppb) and Os (115-194 ppb). Rh, Pd and Pt contents range from 19 to 30 ppb, 3 to 9 ppb and 5 to 24 ppb respectively. Chondrite-normalized PGE patterns for chromitite dykes show high (Os+Ir+Ru)/(Rh+Pt+Pd) ratios and are characterized by a consistent, positive anomaly in Ru, and a negative anomaly in Pt and Pd.

A mineralogical study of 11 polished sections resulted in finding 35 grains of platinum group minerals (PGM). The mineralogy is consistent with chemical data and shows a relative abundance of Ru, Ir and Os minerals, and an absence of separate Rh, Pt and Pd phases. The most abundant PGM are sulfide of the laurite-erlichmanite series (RuS_2-OsS_2), accompanied by minor iridium, osmium and an unnamed sulfide of Ir and Rh. All the PGM encountered are less than 10 microns in size. They occur as single phase or poly-phase grains associated with rutile, millerite and silicates, and are included in fresh chromite. A few grains of laurite were found in the silicate matrix that fills interstices in the massive chromitite, and one grain of iridium was found associated with pentlandite occurring interstitial to chromite. It is probable that PGM inclusions in chromite are either pre-chromite or syn-chromite, primary magmatic minerals. They crystallized under increasing sulfur fugacity and decreasing temperature, up to the stability of erlichmanite. Iridium associated with pentlandite probably represents a low temperature exsolution product.

Distribution of platinum-group elements and the presence of nanometer-sized platinum-group minerals in sulfides from the Bushveld Complex

Junge M[1*], Oberthür T[1], Wirth R[2], Melcher F[4]

1 - Federal Institute for Geosciences and Natural Resources (BGR) *malte.junge@bgr.de 2 - GFZ German Research Centre for Geosciences, Germany 4 - Montanuniversitaet Leoben

The Bushveld Complex in South Africa hosts the world's largest resources of platinum-group elements (PGE), which occur both as discrete platinum-group minerals (PGM), and hosted by sulfides e.g. [1, 2, 3]. It is generally thought that the PGE are present in solid solution in sulfides, however, recently nanometer-sized PGM (nPGM) were described in sulfides from the Merensky Reef [4].

In the present study, high resolution maps were prepared using a transmission electron microscope (TEM) in order to reveal the distribution of PGE in sulfides. For this investigation electron transparent foils (5 x 10 x 0.15 µm) were prepared using the FIB technique, sputtering material from the sample with Ga-ions accelerated to 30 keV [5]. The foils were prepared from pentlandite of the UG-2 chromitite (Karee Mine) and of the Platreef (Sandsloot).

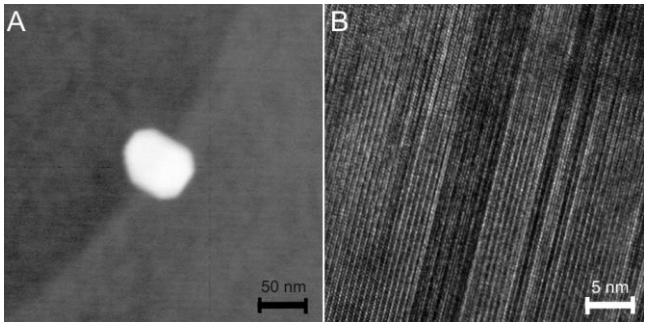

Figure 1: TEM-photomicrographs. A: Nanometer sized PGM (PtSn) in pentlandite of the Platreef. B: High-resolution images of Rh- and Ir-rich lamellae in pentlandite of the UG-2.

In both cases, discrete PGM (e.g. cooperite/braggite, Pt-Fe alloys, laurite, tellurides with grain sizes from ~1 to 100 µm) were detected by ore microscopy and subsequently analyzed by EPMA.

The TEM study confirmed the presence of µm-sized PGM. However, in addition PGE occur in pentlandite (i) as nano-inclusions of PGM (Figure 1A), and (ii) within the pentlandite lattice substituting for Ni and/or Fe.

(i) nPGM (e.g. Pt-tellurides, Pt-bismuthides, (Pt,Pd)Sn Pt-Fe-Cu alloy), are ~50 nm in size and do not show any obvious orientation relationship with the host sulfide mineral.

(ii) PGE (Rh, Pd, Ir) within the pentlandite lattice substitute for Ni and/or Fe. In pentlandite grains with elevated concentrations of PGE (up to 0.5 wt% Pd and Rh) found in the UG-2 and the Platreef, PGE are randomly and patchily distributed within the crystal lattice.

In pentlandite, grains from the UG-2 with unusually high concentrations of Rh (up to 12.5 wt%) and Pd (up to 0.05 wt%), Rh and also Ir form an ordered arrangement within the crystal lattice in the form of orientated nanometer-thick lamellae (Figure 1B). EDX analyses demonstrate that these structures represent alternating Rh-/Ir-rich lamellae and relatively Ni- and Fe-poor zones. These periodic structures form a superlattice, i.e. an ordered arrangement within a crystal.

It is concluded that PGE in the UG-2 and in the Platreef are present as a continuum of discrete PGM to nPGM, substituting for Ni and/or Fe in the crystal lattice of pentlandite, and at extremely high concentrations, PGE may form superlattice structures.

[1] Godel B. *et al.* (2007). *J. Petrol.*, 48, 1569-1604.

[2] Junge M. (2014). *Econ. Geol.* 109, 795-810.

[3] Osbahr I. (2013). *Miner. Deposita*, 48, 211-232.

[4] Wirth R. *et al.* (2013). *Can. Mineral.*, 51, 143-155.

[5] Wirth R. (2004). *Eur. J. Mineral.*, 16, 863-876.

Platinum group elements within the Merensky Reef: preliminary results of a high resolution mineralogical and geochemical study

Magson J[1*], Tredoux M[1], Roelofse F[2]

1 - Department of Geology, University of the Free State *markramj1@ufs.ac.za

A study of the Merensky Reef was undertaken in the south-western portion of the Western Limb of the Bushveld complex, where it occurs either as a pegmatoidal or a non-pegmatoidal reef. The mineralogy and geochemistry were described on core sections across both reef types from the area.

The cores were analysed in 2 cm intervals. Samples were analysed by optical microscopy. Quantitative analysis was done using scanning electron microprobe and electron microprobe analysis. Major elements were determined by using x-ray fluorescence and trace elements by using ICP-MS (inductively coupled plasma mass spectrometry). Platinum-group elements (PGE) were determined by Ni-S fire assay with an ICP-MS finish and sulphur by an Eltra Infrared Analyser.

Microscope analysis showed sulphide inclusions visible in chromite grains (Figure 1). These inclusions display negative crystal shapes imposed by the crystal structure of the host chromite. Similar trapped sulphide inclusions have been described from chromites in the Platreef by [1].

Results indicated that there is a close relationship between chromium and PGE enrichment (Figure 2). Chondrite normalized patterns showed a relative increase in Pd in the footwall with a significant decrease in the hangingwall. The opposite can be seen for Pt. REE plots suggest a small amount of local differentiation with respect to La.

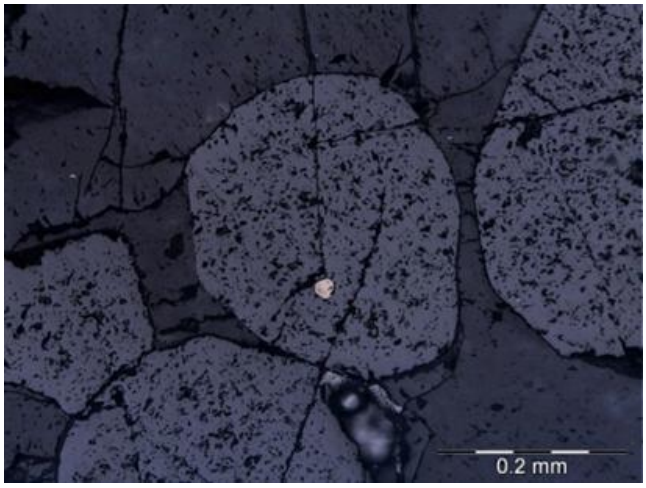

Figure 1: Microscope analysis of non-pegmatoidal Merensky Reef, sulphide inclusion visible in chromite grain.

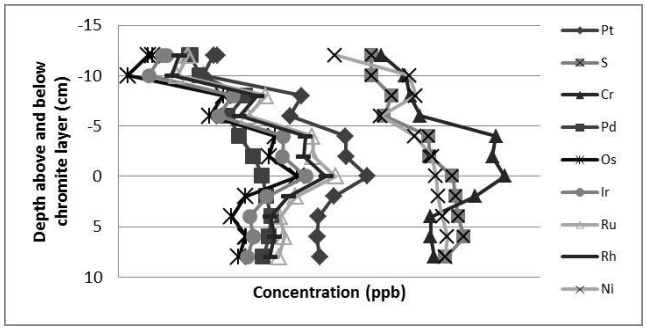

Figure 2: PGE, Cr, S and Ni concentrations vs. depth. The PGE concentrations, except for Pd, correlate with the chromite enrichment with depth, whereas Pd tends to show a better correlation with S enrichment.

[1] McDonald I. and Holwell D.A. (2011). Geology of the Northern Bushveld Complex and the Setting and Genesis of the Platreef Ni-Cu-PGE Deposit. *Reviews in Economic Geology*, 17, 297–327.

An unusual assemblage of platinum group minerals (PGM) and other accessory phases in the Cedrolina chromitite, Goiás State, Brazil

Portella Y[1], Zaccarini F[2*], Garuti G[2], Angeli N[1], Thalhammer O[2]

1 - UNESP - São Paulo State University 2 - University of Leoben
*federica.zaccarini@unileoben.ac.at

The Cedrolina chromitite is located about 300 km northwest of Brasília, in the State of Goiás (Brazil). It consists of a tabular, elliptical body up to 2.4 m thick, covering an area of 230 x 100 meters and striking NE-SW, with a NW plunge of about 20°. The chromitite body is emplaced concordantly within mica-talc-chlorite schists representing the poly-metamorphic product of ultramafic rocks. The chromite ore displays a peculiar nodular texture, consisting of rounded and ellipsoidal nodules (up to 1.5 cm in size) sometimes strongly deformed and fractured, immersed in a matrix of altered silicates (mainly chlorite and talc) and minute chromite fragments. Chromite is characterized by high Cr# (0.80-0.86), high Fe^{2+}# (0.70-0.94), and low TiO_2 (av. = 0.18 wt%) consistent with variation trends in spinels from metamorphic rocks. The chromitite contains a suite of accessory minerals which include platinum group mineral (PGM), accompanied by monazite-Ce, rutile, uraninite, thorianite, zircon, Au-Cu-Ni/Au-Pd alloys and tiemanite (HgSe). These minerals occur as minute particles, usually less than 10 µm, disseminated in the altered silicate matrix. Only monazite may form grains up to 200 µm. The PGM consist of irarsite (IrAsS) and an Au_3Pd alloy. Gold, argentite, a Ag-Cu-As-Sb sulfide and an alloy characterized by the composition Au_3Cu_3Ni have also been encountered. Electron microprobe analyses indicate that monazite has a high Ce/La ratio and rutile an unusually high Cr_2O_3 content (up to 5,7 wt%). Uraninite, thorianite and zircon were only identified qualitatively. Paragenetic considerations suggest that only irarsite could be a relict of the original igneous assemblage, whereas the Au-Pd and Au-Cu-Ni compounds are more likely to represent products of low-temperature reworking of primary igneous phases. Rutile probably formed by ex-solution of Ti from chromite, during alteration. Other accessory minerals containing elements which are normally incompatible with an ultramafic system (Ce, Th, P, U, Zr, Ag, Hg), are believed to have been introduced by metasomatic hydrothermal fluids emanating from the felsic intrusions that affected the area during the long history of metamorphic events.

A 3D study of the Middle Group chromitites, Bushveld Complex, South Africa

Purchase M*, Tredoux M, Duvenhage M

Department of Geology, University of the Free State. *purchasemd@ufs.ac.za

The PGE have been classified as chalcophile elements, being mostly associated with sulphur. The PGMs occur associated with base-metal sulphides, chromite and with gangue minerals (e.g. within and along the boundaries of chromites). Intensive studies have been carried out on the PGM-sulphide associations but less is known about the correlation between PGE and chromium. This was the motivation to initiate a project investigating PGE within chromitite layers in the Bushveld complex. This study involves the borehole, HEX 10 (Figure 1) drilled in the Eastern lobe of the Bushveld complex. A feature of this borehole is that it contains all four of the Middle Group chromitite layers, i.e. MG1, MG2, MG3 and MG4. ToF-SIMS (time of flight-secondary ion mass spectroscopy) analysis was used to analyse individual chromites of the MG1 chromitite. In this method, atoms are released from the first or second crystal layers by bombardment with Bi^{3++} ions and then analysed when they travel through the "time of flight" portion of the machine. Depth profiling involves two ion beams, where the first (O^-) is used to sputter a few layers from the sample surface and the second beam (Bi^{3++}) is used to analyse the newly exposed surface. Alternating between the beams creates a depth profile, allowing for a three dimensional investigation of the chromites.

Figure 2 shows a 30x30µm area that was analysed by compiling a depth profile within the boundaries of a chromite grain. Results show that individual Rh atoms or clusters of atoms can be found randomly distributed within the crystal lattice of the chromite.

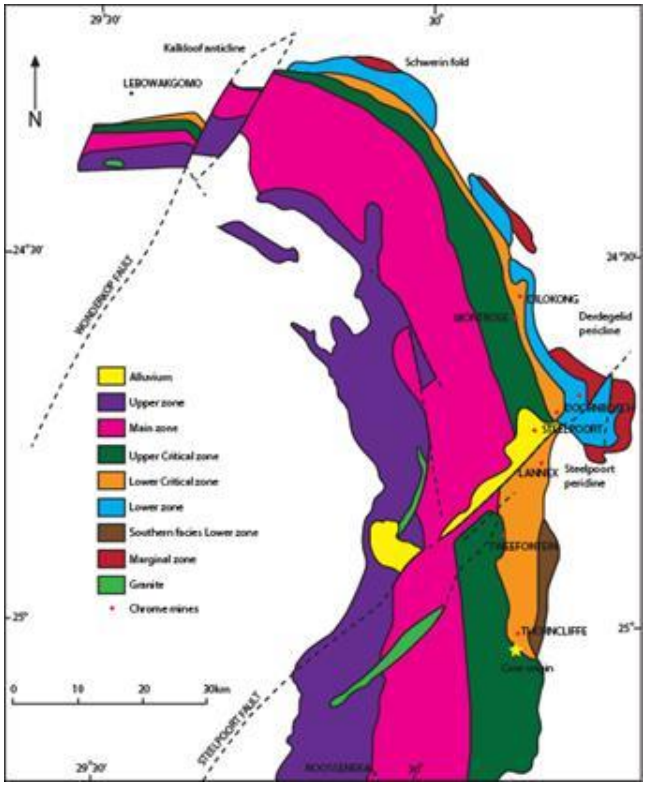

Figure 1: Modified map of the eastern Bushveld complex. The star indicates the approximate origin of the core HEX10.

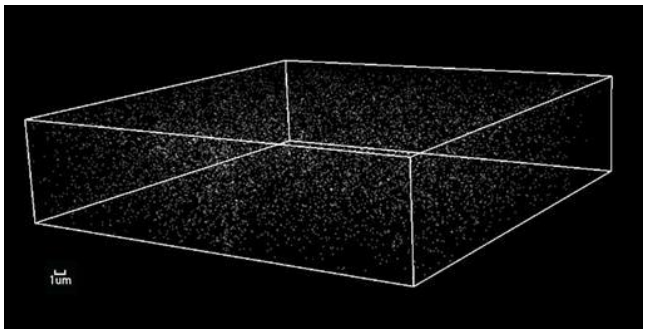

Figure 2: 3D depth profile of rhodium.

PGE mineralization in a chrome ore occurrence Egart (Polar Urals)

Shaybekov R

Institute of Geology Komi SC UB RAS. shaybekov@geo.komisc.ru

A new chrome ore occurrence, called «Egart», was discovered in 2010 on the eastern slope of the Voykar-Syninsky massif (Polar Urals). It is hosted by a dunite-harzburgite-pyroxenite complex that forms an aureole at the top of the chrome ore occurrence. These rocks consist of a congruous folded sill body. Harzburgite is represented by strongly tectonized serpentinites. Dunites in the supine wing are completely re-crystallized, forming coarse-crystalline and pegmatoidal dunite. Chromite concentration varies from 8 to 43.6 modal % and consists of high Cr-chromite and ferrian chromite. It was found in the apical part of the dunite congruous sill body.

Chromite contains gold minerals which are sometimes accompanied by small amounts of silver and occurs in cracks, cavities and in intergrowths with isometric chromite crystals (grains size about one micron). The gold composition varies from 98.36 up to 100 Au (wt %), and Ag - up to 1.64.

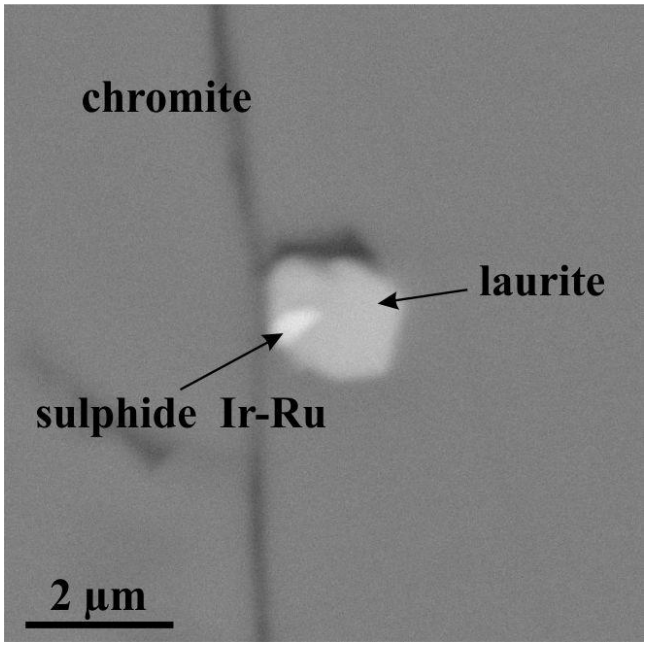

Figure 1: Laurite and Ir-Ru sulphide inclusion in chromite.

Laurite occurs as isometric inclusion in chromite (grain size up to 2 µm) and has the following composition (wt%): Ru - 36.17, Os - 19.51, Ir - 11.47, S - 32.85, with a formula $(Ru_{0.70}Os_{0.20}Ir_{0.12})_{1.02}S_2$. An Ir-Ru-Cu sulfide was found associated with laurite. The chemical content of mineral (wt%): Ir - 71.70, Ru - 9.87, Cu - 5.77, Os - 2.08, S - 10.58. Due to its small size, it was impossible to calculate a precise chemical composition, but probably it is a cuproiridsite.

Irarsite forms isometric inclusions in heazlewoodite up to several microns in size. It is characterized by the following composition (wt%): Ir - 47.98, Rh - 6.01, Ni - 5.89, Pt - 2.88, Fe - 0.56, As - 23.39, S - 13.29, crystal-chemical formula $(Ir_{0.60}Ni_{0.24}Rh_{0.14}Pt_{0.04}Fe_{0.02})_{1.04}As_{0.75}S$.

This study of the noble elements minerals associated with the chrome ore occurrence Egart varies insignificantly and is consists mainly of gold and Ir-Ru sulphides and sulphoarsenides. The obtained data on noble metal mineralization are new and at this stage of research there is a specification toward gold-silver mineralization, rather than to the platinum group minerals.

Acknowledgement: The work was made under support of grant RFBR and Government of the Komi Republic r_north_a № 13-05-98819, of the program of the project Ural and Far East Branch number 12-C-5-1006 and SC-4795.2014.5.

Initial geochemical study on platinum associated with laterite of Macroasia's Infanta Nickel Area, Palawan, Philippines

Yonezu K[1*], Noda K[1], Gabo J[2], Juanerio J[3], Laguerta E[3], Santos R[3], Santos R[3]

1 - Department of Earth Resources Engineering, Kyushu University
*yone@mine.kyushu-u.ac.jp 2 - Research Institute of Environment for Sustainability, Kyushu University 3 - MacroAsia Corporation

The nickel laterite of MacroAsia's Infanta nickel area in Southern Palawan, Philippines was examined in order to understand the geochemical and mineralogical association of platinum and palladium with nickel laterite. Magmatic mafic and ultramafic rocks containing nickel and copper are some of the possible platinum resources, especially after they have been exposed to weathering. This research included geochemical analysis, with emphasis on platinum and palladium concentrations in the weathering profiles of the ultramafic rocks from the bedrock through saprolite to top soil (the limonite section). In addition, soil pH and Eh measurements on site, and mineralogical research using petrography and X-ray diffraction were also conducted.

Most of the nickel laterite areas considered in this study are weathering profiles that developed from harzburgite bodies belonging to the Beaufort ultramafic complex of the Palawan Ophiolite. The bedrock consists of olivine, orthopyroxene and spinel. The nickel content of the bedrock averaged around 2700 ppm. However, the laterite profiles of test pit 2 (TP 2: 8 m depth) and test pit 3 (TP 3: 10 m depth) have concentrations of up to 2.3% and 1.8% nickel, respectively. Nickel concentration can be divided into two groups depending on the presence of garnierite. Garnierite tends to develop in deeper parts of the profile after serpentinization. In contrast, platinum is likely to be associated with the upper zone (up to 100 ppb platinum). There is a good positive correlation between iron and platinum in bulk but no correlation with nickel. The soil pH and Eh ranged from 5 to 7 and 500 to 650 mV, respectively. Relatively low pH (lower than about 5.5) is associated with a relatively high platinum concentration (more than 50 ppb). As the platinum is mobilized during the weathering process, enrichment by precipitation or coprecipitation with goethite or amorphous iron hydroxide may play an important role in the concentration of platinum. However, the mode of occurrence of platinum in both bedrock and laterite profiles is still being investigated by microprobe analysis. In addition, palladium has a good positive correlation with platinum and occurred in concentrations of up to 80 ppb.

Mineralogy of platinum furnace slags: optimising base metal and PGE recovery

Andrews L[1]*, Scharneck Y[2]

1 - Private *lesley.andrews52@gmail.com 2 - Anglo American Technical Solutions

Platinum-bearing sulphide concentrates are smelted in South Africa by Anglo American's Platinum business [1, 2]. Slags from the primary melting furnaces and slag cleaning furnace (SCF) are tapped then granulated in high-pressure streams of water. The quenched slags consist of amorphous Mg-Fe-Al silicate glass and trace amounts of entrained Fe-Ni-Co matte as sulphide inclusions. Since the quenched slags reflect the phases present in the molten slags, slag mineralogy studies can provide information on matte-slag equilibria [3]. This can assist with optimisation of the compositional and physical smelting parameters in the furnaces.

Recovery of the PGE as well as nickel, copper and cobalt from the quenched slags is of economic importance; the slag is milled and floated to recover entrained matte. Electron probe microanalysis of the silicate slag glass has shown the presence of small amounts of nickel, copper and cobalt. Although these metals partition preferentially into the entrained matte sulphide phases, the relatively small modal percentage of the matte (as determined by auto-SEM) allows the prediction of low base metal flotation recoveries, and this is borne out in practice [4]. PGE, however, partition almost exclusively into entrained matte phases, and recoveries are much higher.

Entrained matte phases in slag flotation feed differ between melting furnace slag and SCF slag [5]. There are variations in phase size, modal percentages, in the type and amount of sulphide and alloy phases present, and in the PGE distribution. Such information can be used to optimise mill and float recovery processes.

[1] Jacobs M. (2006). In: Jones R.T. (ed.), *Southern African Pyrometallurgy* 2006, *Southern African Institute of Mining and Metallurgy*, Johannesburg, South Africa, 17-28.
[2] Hundermark R.J. *et al*. (2011). In: Jones R.T. and den Hoed P. (eds*), Southern African Pyrometallurgy* 2011, *Southern African Institute of Mining and Metallurgy*, Johannesburg, South Africa, 295-307.
[3] Andrews L. and Pistorius P.C. (2010). *Trans. Inst. Min. Metall. C*, 2010, 119(2), 52-59.
[4] Andrews L. (2005). Trans. Inst. Min. Metall. C, 2005, 114(3), 130-134.
[5] Scharneck Y. and Andrews L. (2012). *Proc. 9th Int. Conf. on Molten Slags, Fluxes and Salts, Beijing, China, 2012.*

Automated robotic chemical and mineralogical analysis of heavy mineral sands

Bornefeld M[1*], Spicer E[2], Rakgalakane B[2]

1 - ThyssenKrupp Industrial Solutions *marc.bornefeld@thyssenkrupp.com

2 - Richards Bay Minerals

Ilmenite, rutile and zircon are present in economic concentrations in heavy mineral sands as important sources of Fe, Ti and Zr for various industrial uses. The beach sands of northern KwaZulu-Natal, along the Zululand Indian Ocean coastline in South Africa, are mined for these minerals. During 2013 a replacement automated robotic laboratory was commissioned. The design of the automated system centered around the provision of chemical and mineralogical information for metallurgists during a continuous 24 hourly shift basis operation, enabling fast reaction times to produce high quality final products.

A number of pre-feasibility tests were performed to ensure quality data are provided, free of interferences and contamination, during the automated preparation and analysis of various final products in one robotic circle. Grinding time, grinding speed and pressing force of the automated mills and presses were optimized with special emphasis placed on the reduction of cross-contamination between final products. Cross-contamination is of particular importance as a wide range of different final products and grades, such as rutile, zircon and titanium slag is produced.

Throughout the beneficiation process ilmenite, rutile and zircon are separated in varying degrees of cleanliness from the heavy mineral sands to produce the final products and grades of each mineral. Ilmenite is reduced in a high-temperature smelter environment to titanium slag. Every step in the beneficiation process is monitored through sampling methods every hour or two-hourly, depending on the specific product stream. Automated sample preparation, X-Ray Fluorescence and - Diffraction analysis is performed on these samples by the robotic laboratory to ensure a high level of quality product is produced throughout the value chain.

The newly designed laboratory and equipment are flexible, user-friendly, programmable, produce short turnaround times between sample dispatch and analysis and provide support to maintain critical process control parameters from raw materials to final products.

Process mineralogical characterization of copper ores from Kansanshi Mine, Zambia

Jacobs T*, Becker M, Kalichini M, Greyling L, Reid D

University of Cape Town *jcbtam004@gmail.com

Kansanshi is a major operating copper mine in Africa, which exploits a geological sequence that has experienced a complex geological history comprising hypogene sulphide mineralization and subsequent supergene enrichment processes, leading to a highly complex copper mineralogy and associated textures. At Kansanshi the run of mine is processed in three different circuits: sulphide ore, mixed ore and oxide ore. This study entails a thorough process mineralogical characterization of the different ores using modern analytical techniques and approaches.

The principal copper-bearing minerals within the sulphide ore include chalcopyrite (which dominates), chalcocite, and bornite. Within the mixed and oxide ores, the principal copper-bearing minerals are malachite, chrysocolla, chalcopyrite, chalcocite, tenorite, and bornite. Chrysocolla dominates in the mixed ore but malachite assumes this role in the oxide ore. The gangue mineralogy of the ores shows considerable variation depending on the degree of alteration of the primary hypogene ore, with pyrite, quartz, calcite, plagioclase and limonite occurring as the major minerals. Unlike some Copperbelt deposits, the Kansanshi ores show no enrichment in cobalt bearing minerals.

In the sulphide ore, chalcopyrite occurs as disseminated grains and as a secondary infill within quartz veins forming a distinctive stock-work texture. The oxide ore shows textures diagnostic of open-space deposition with malachite and chrysocolla occurring predominantly in vugs. The textural association within the mixed ore is highly variable with the most commonly occurring textures being a cellular box-work texture defined by chalcopyrite and chalcocite, and open-space deposition of malachite and chrysocolla.

A comparison of chalcopyrite grain sizes between the sulphide and mixed ores at equivalent grinds (80% passing 150 µm) shows the former has a much broader grain size distribution with more than 10% of the chalcopyrite coarser than 100 µm, leading to >95% liberation. In contrast, the mixed ore has a narrower grain size distribution with less than 5% of the chalcopyrite coarser than 100µm, leading to only 65% liberation. Batch flotation tests of the sulphide ore show greater than ~98 % copper recovery, characteristic of the close relationship between chalcopyrite liberation and floatability. Use of the selective *AERO MX5149* collector ensured the recovery of chalcopyrite whilst limiting pyrite to less than 8 %.

This information will be used as a bench mark for comparison of the process mineralogical behaviour of the nearby Sentinel copper project, which is currently under construction.

Modelling of comminution geometallurgy at the La Colosa project, Colombia

Linton P[1*], Jahoda R[1], Montoya P[1], Harris P[2], Pendock N[2]

1 - AngloGold Ashanti *plinton@anglogoldashanti.com 2 - Geospectral Imaging

This paper describes the use of hyperspectral core imaging, ICP geochemistry and core logging for geometallurgical mapping and modelling at AngloGold Ashanti's La Colosa project in Colombia. La Colosa is a large porphyry gold deposit, with a resource of 1 billion tons at an average grade of 1g/t containing ~25Moz of gold. Early metallurgical testwork showed the ore to be hard, both in terms of impact breakage (A*b 25-35) and grindability (BMWi 16-18) and that comminution would be a major driver of project economics. The first phase of geometallurgical work therefore focused on relating the core logging, spectral data, and ICP geochemistry to measured A*b, SPI and BMWi data as a means of mapping the distribution of these across the entire orebody, and so to spatially model comminution variability. Using the plant design, the modelled comminution parameters have been used to produce a block model of throughput for input into financial modelling.

The significance of geometallurgy to continuously improve mineral resource utilisation at the Namakwa Sands heavy minerals mine, west coast of South Africa

Philander C*, Rozendaal A

1 - Stellenbosch University *carlo.philander@za.tronox.com

Namakwa Sands is a heavy minerals mining and beneficiation business operating along the west coast of South Africa. The primary ore body, which boasts pre-mining mineral resources in excess of 1.1 billion tons at a grade of approximately 10% total heavy minerals was discovered in 1986 and production commenced in 1994. Today, Namakwa Sands is a leading supplier of titania slag, pig iron, premium ceramics grade zircon and rutile concentrates to several export markets.

The bulk of the economic mineralisation, which includes zircon, rutile, ilmenite and leucoxene, is hosted by a late Cainozoic aeolian succession overlying remnant palaeo-strandline sediments. Relatively younger duricrust layers cement a significant part of the generally unconsolidated ore. In sharp contrast to this mineral wealth is a challenging ore extraction and beneficiation character resulting from the complexity and particularly the intrinsic heterogeneity of the mineral assemblage.

In response, Namakwa Sands has turned to the cross-over discipline of geometallurgy, which provides an ideal means to define and quantify all key mineralogical and geotechnical properties of the Namakwa Sands mineral resource. This may impact on the mining and processing of the ore over the life of the mine. Augmenting the mineral resource model with key geometallurgical data is envisaged to ultimately aid the improved beneficiation of the present mineral suite and increase mineral resource utilisation.

The Namakwa Sands geometallurgical study was designed to integrate with the current mineral resource management processes and rests on two tenets or pillars, namely process mineralogy and ore characterisation. Ore characterisation refers to the determination of an ore's bulk physical and chemical properties, quantitative mineralogy as well as its processing, or metallurgical character. Process mineralogy, also referred to as applied mineralogy describes the characterisation of ore and minerals according their behaviour during treatment and aims to establish relationships between these mineral characteristics and typical process performance indicators such as throughput, grade, recovery and quality.

The presentation demonstrates the geometallurgy of the Namakwa Sands deposit by defining the constituent ore types in terms of bulk geochemistry and mineralogy, including the mineral characteristics that could possibly affect recovery. A representative suite of ore and process samples have been systematically studied with the help of optical microscopy, XRF, XRD, SEM, QEMSCAN, LA-ICP-MS and electron micro-probe. A novel geometallurgical template model was developed to study and quantify the penalties that deleterious mineral characteristics could potentially impose on the recovery of the ore minerals.

Poor mineral liberation, an anomalously high abundance of garnet and pyroxene and variation in particle chemistry are recognized as the key recovery penalties. The gangue content proved the most significant constraint to ilmenite recovery, whereas zircon chemistry is the most important negative factor in the production of premium quality zircon concentrate. In addition to enhanced mineral resource definition, this geometallurgical template model allows mineral resource scoring and ranking based on potential mineral recoveries

Mineralogical factors affecting the dense medium separation of nickel ores

Pillay K[1*2], Becker M[2], Mainza A[2], Chetty D[1]

1 - Mineralogy Division, Mintek *keshreep@mintek.co.za 2 - University of Cape Town

Dense medium separation (DMS) is a pre-concentration method used to upgrade ores before their main processing stage, such as flotation. It has been applied to base metal sulfide (BMS) ores with varying results. The aim of DMS is to reject a large portion of gangue material upfront in order to create cost, energy and time savings during processing. As lower grade ores with complex mineralogy are being increasingly exploited, the properties of the gangue minerals begin to play a more important role in the upgrading of the ore. It is therefore important to understand these mineralogical factors to be able to select suitable processing routes for a specific ore.

Two nickel deposits were chosen as case studies in order to understand differences in DMS efficiency for different ores: the Main Mineralised Zone (MMZ) of the Nkomati deposit, South Africa, and the Phoenix deposit of the Tati greenstone belt, Botswana. Pilot plant testwork on both ores showed their amenability to DMS, with successful nickel upgrades to the underflow. Both deposits show similar sulfide mineralogy, with pentlandite as the main host of nickel, and pyrrhotite and chalcopyrite as dominant sulfide minerals. The pentlandite occurs mainly as small flame-like lamellae within pyrrhotite in the low grade zones. The study includes the description of the DMS products of each ore, in terms of bulk mineralogy, mineral chemistry, textural relationships and particle properties such as size and shape. Mineralogical data were derived using petrography, X-ray diffraction, electron probe microanalysis and QEMSCAN analysis.

Sulfide texture is the main controlling factor shown to affect the individual particle recovery by DMS, with massive and net-textured sulfides having larger grain sizes and therefore higher liberation than disseminated sulfides. In addition to the DMS concentration of sulfide minerals, primary and secondary silicate minerals are separated by their density differences, which can affect the recovery of finely disseminated sulfides associated with them. Secondary silicates such as chlorite and talc report preferentially to the overflow, with denser silicates such as pyroxene being more abundant in the underflow. A higher degree of alteration of the ore is linked to increased silicate-hosted nickel, which results in nickel losses to the overflow. Particle size is also important in DMS, with near-density material separating on size rather than density. Dense material with small particle size is also generally misplaced to the overflow.

Based on differences in ore composition and texture, the understanding of the mineralogical properties affecting DMS can then be used to aid in the prediction of the suitability of DMS pre-concentration for different ore types.

From geometallurgy to ecometallurgy: building mines for the future

Pirard E

University of Liège. eric.pirard@ulg.ac.be

Geologists, when looking at the complexity in thin sections of a rock or ore specimen, too often tend to look backwards, trying to find out which natural processes caused the heterogeneity and variability. Geometallurgy, instead, requires geologists to look forward and inform the engineers how this heterogeneity will impact mining and downstream processing, thus establishing a dialogue and bridging the gaps between the disciplines. With the increasing complexity of ores and an ever widening range of possible processing routes, geometallurgy will become the central pivot of a successful mining operation.

Recently, Europe has awakened from a long period of lethargy in the raw materials sector. A series of important initiatives inspired by the European Innovation Partnership (EIP) have paved the way for more intense cooperation between industry, research centres and universities. Among these, the establishment of a Knowledge Innovation Community (KIC) in 2015 will definitely boost innovation and education in the sector. Interestingly, EIP addresses the whole value chain and considers mining, recycling and substitution as essential pillars of the raw materials policy.

This vision strengthens the role of geometallurgy but also brings up the need for a close dialogue between mineralogists, metallurgists and product designers. Microelectronics and nanotechnologies are ubiquitous in our technologies and have greatly improved their functionality, but they have also made recycling and efficient recovery of metals a tough technical challenge. Our urban mines formed by the accumulation of end-of-life products should be scrutinized from now on using an ecometallurgical approach whereby important questions should be addressed such as:

1. Metal concentrations: Is the metal grade high enough to pay for recycling? Does the manufacturer help to maintain grades above a technological cut-off?
2. Metal speciation: Under which form (alloy, salt, organic compound, etc.) is the metal present? Is there a processing technology available to separate these species?
3. Metal paragenesis: What are the metal assemblages found in the product? Will it be feasible to separate those metals and at what costs? Are there penalty or contaminating elements associated?
4. Textural assemblage: How will the product behave during dismantling? Is it realistic to liberate a given component? What comminution strategy will be needed to achieve phase liberation?
5. Reserve estimation: What are the tonnages expected for this kind of product? Can selective collection be organised?
6. Homogeneity: What will the next generation of products look like? Should one expect strong differences in concentration, speciation, paragenesis, etc.? Will this kind of product be blended with others during collection? How will this impact on downstream recycling?

Ecometallurgy, as introduced here, is essentially about establishing a dialogue with product designers and material scientists to make sure that, once unearthed, metals will remain easily and sustainably available for the future generations. Geologists and mineralogists, even though generally kept away from the synthetic materials, could greatly contribute to this progress by bringing their expertise in dealing with complex and variable orebodies of the future.

Characterisation of New Vaal coal using automated mineralogy with a view on liberation

Pretorius D*, Viljoen F, Cairncross B

University of Johannesburg *don.j.pretorius@gmail.com

The depletion of good quality coal in South Africa for energy production and exporting purposes will demand a shift in focus toward poorer quality coal that contains a higher amount of both mineral matter and potentially hazardous trace elements. Coal from the Sasolburg-Vereeniging coalfield contains a high abundance of gangue minerals such as clays, carbonates and other silicates, and along with the Waterberg coal represents some of the poorest quality coal currently being burned in South Africa (i.e. coal with a low calorific value and high ash content). Coal samples from the New Vaal Colliery were used to evaluate the application of Mineral Liberation Analyser technology to the measurement of mineral liberation upon crushing, of this low quality coal. The extent of liberation upon crushing of the coal determines the ease/difficulty with which the gangue constituents may be removed and thus impacts on the beneficiation processes.

The liberation of the coal is compared with the liberation of gangue minerals (expressed through the parameter of liberation by particle composition or liberation by free surface) for the three liberation classes: locked (0-25%), middlings (25-75%) and liberated (75-100%). Coal samples were crushed into three sieve size classes: -1mm, -212µm and -75µm. During the investigation of liberation by particle composition, most of the coal (>64 wt%) and minerals (>76 wt%) are liberated in the liberated liberation class. Logically it should be expected that an increase in crushing, should increase the liberation (liberation by particle composition parameter) of both coal and gangue minerals, but physical results revealed that an increase in crushing has increased the liberation of coal, while that of gangue minerals decreased. With the increase in coal liberation with increase crushing (based on the liberation of coal by particle composition parameter), density separation will be used as the preferred metallurgical beneficiation method if further processing of the liberated coal was desired. Results indicated that gangue minerals are more liberated (even if liberation of gangue minerals decreases with increase in crushing) in the liberated class than coal; hence changing the density medium to favour the liberated class will liberate gangue mineral and not the desired coal.

Furthermore, the investigation of coal liberation by free surface parameter indicates that coal (>72 wt%) is more liberated than gangue minerals (>52 wt%) in the liberated class. Similarly to the liberation of coal by particle composition parameter, liberation of coal by free surface parameter also indicated that an increase in crushing to finer sizes enhanced the liberation of coal while that of minerals decreased. Further coal processing by means of coal liberation by free surface will entail the usage of froth flotation technologies. Conveniently coal is the most liberated by free surface in the liberated class (over gangue minerals), hence froth flotation will be favourable (i.e. producing higher coal yields). Based on the results and comparing dense medium separation with froth flotation technologies, -1mm crushed coal material should rather be beneficiated by froth flotation than dense medium separation.

High-speed PIXE: automated mineralogy using a color X-ray camera

Renno A[1*], Buchriegler J[2], Hanf D[2], Munnik F[2], Nowak S[3], Scharf O[3], Ziegenrücker R[1]

1 - Helmholtz-Institute Freiberg for Resource Technology *a.renno@hzdr.de

2 - HZDR; Institute of Ion-Beam Physics and Materials Research 3 - IfG Institute for Scientific Instruments GmbH

Methods of automated mineralogy form the analytical backbone of geometallurgy. Most of them exploit the combined imaging and analytical capabilities of optical and scanning electron microscopes. Typical results are "phase maps" either derived from the distribution of major elements or determined directly (Figure 1). The effective application of such methods for strategic metals which are won as by-products from other metal ores is handicapped by the restricted possibilities to determine the spatial distribution of such trace elements like In, Ga, Ge or the rare earth elements (REE).

The recently commissioned High-Speed PIXE (Particle Induced X-Ray Emission) setup at the Helmholtz-Institute Freiberg for Resource Technologies will overcome these limitations.

We use the SLcam® X-ray Color Camera - a novel pnCCD Pixel detector (264 x 264 = 69696 Pixel) combined with a polycapillary X-ray optic [1] as the detector for the element specific X-ray radiation. This design allows us the simultaneous determination of the trace element distribution on a 12 * 12 mm^2 area with a lateral resolution of about 50 µm. First results of geometallurgical applications of this method are presented.

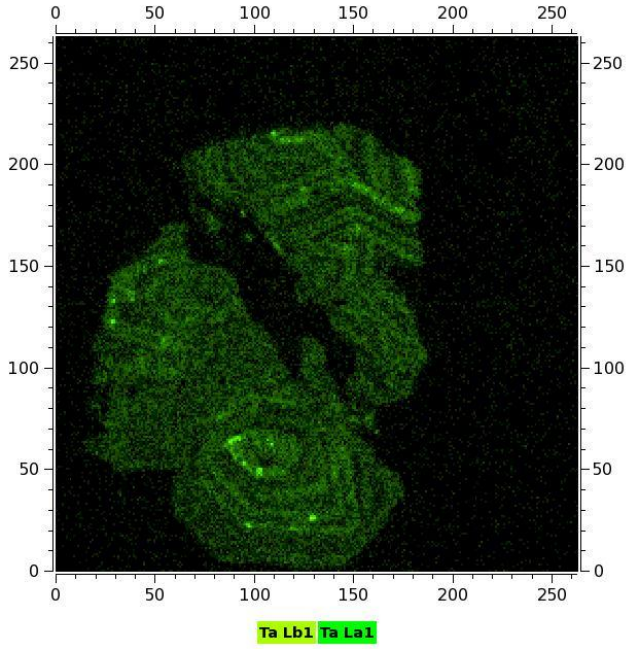

Figure 1: X-ray elemental distribution map of Ta (L-lines) in a zoned cassiterite crystal. Image width: 12 * 12 mm.

[1] Scharf O., *et al.* (2011). Compact pnCCD-Based X-ray Camera with High Spatial and Energy Resolution: A Color X-ray Camera. *Analytical Chemistry*, 83, 2532-2538.

Cluster analysis of XRD data and some applications to metallurgy and geometallurgy

Richards J*, Walliser A, Theron S

Exxaro Resources *jill.richards@exxaro.com

One of the powerful tools of modern X-ray diffraction (XRD) analytical software has been development of full pattern cluster analysis to group closely similar patterns. While this can be very useful for reducing the amount of work and therefore time taken to analyse large numbers of patterns from related samples, it can sometimes also be used to assist metallurgists to design test programs and reach conclusions by reducing the numbers of samples that need to be tested. In addition, interpretation of the resultant clusters can also often be incorporated into geometallurgical databases.

At Exxaro we found that cluster analysis of XRD patterns provided insight into the grouping of samples, which could not otherwise be distinguished from each other and especially not when using chemical analysis. This was particularly so with heavy mineral deposits where it is frequently the case that bulk chemical analysis is of limited assistance in compositing samples with similar characteristics, whereas XRD is very good for determining which Ti and Fe minerals are actually present. Composite samples are frequently used in metallurgical testwork especially when insufficient material of individual samples is available. Therefore, any technique that can group samples with similar mineralogical compositions can be extremely useful in that it can reduce the number of samples to be tested and the time that it takes to reach meaningful conclusions. Examples will be shown of instances where this occurred and the impact on metallurgical testing. Other types of samples where the technique has either proved to be of benefit or has shown promise include the interpretation of slags produced by an experimental ferromanganese furnace, of clays in an ore deposit and mineral matter in a coal deposit.

There are various advantages to using cluster analysis, namely a reduction in the number of samples which might have to be analysed or quantified by XRD, a statistical identification of the most representative and the two most divergent samples in a cluster and, with interpretation, an indication of the minerals influencing the clustering or grouping of samples. This can lead to an 'intelligent 'or 'knowledge-based' compositing of samples prior to metallurgical testwork in situations where this type of information did not previously exist.

As a relatively cheap and rapid means of analysing large numbers of samples, it has the potential to reduce the time and cost of testwork when used in conjunction with metallurgy.

A mineralogical characterisation of Eastern Bushveld Merensky and UG2 ore processed through an MF2 circuit

Rose D*, Viljoen F, Mouri H

University of Johannesburg *derekr@student.uj.ac.za

An MF2 (mill-float-mill-float) circuit situated at the Two Rivers Platinum Mine concentrator plant, on the Eastern limb of the Bushveld Complex, was sampled over two campaigns with the primary and secondary rougher circuits being the focus of interest. By convention, UG2 ore is processed through an MF2 circuit while Merensky Reef ore is processed through an MF1 circuit. In the current study both UG2 and Merensky Reef ores were processed through the MF2 circuit at the concentrator plant.

For the Merensky Reef sample, seven samples were collected and these were: primary rougher feed (PRF), primary rougher concentrate 1 (PRC1), primary rougher concentrate 2 (PRC2), primary rougher tails (PRT), secondary rougher concentrate 1 (SRC1), secondary rougher concentrate 2 (SRC2) and secondary rougher tails (SRT). The UG2 reef sample set consisted of eight samples, as described for the Merensky Reef with the eighth sample being the secondary rougher feed (SRF).

The aims of this study were not to perform a full-scale plant survey but rather to identify the modal mineralogy of the different plant streams as well as the platinum-group mineral (PGM) occurrences and abundances across the different streams. Other aspects of interest were the mineral associations, the grain sizes and mineral liberations of the platinum-group minerals as well as that of the base-metal sulfides. Although such studies are not too uncommon for both the Merensky and UG2 reefs, most of the previous studies in this regard focused mostly on the Western Bushveld. There is a dearth of such studies, more so for both the Merensky and UG2 reefs to be processed through a concentrator plant optimized for UG2 ore. Results for the two ore types will be compared and discussed.

Geometallurgy – not a quick fix

Schouwstra R[1*], de Vaux D[2], Muzondo T[3], Prins C[1], Snyman Q[4], Mohanlal K[5]

1 - Anglo American *robert.schouwstra@angloamerican.com 2 - Anglo American Technical Solution's Research 3 - Mogalakwena Mine, Anglo American Platinum 4 - Geosciences and Exploration, Anglo American Platinum 5 - Resources, Anglo American Platinum

Geometallurgy is not a new concept and has been used by mining companies in various guises and to various extents for many years.

It is understood that from a change management perspective one of the most difficult aspects is to improve communication and collaboration between the various disciplines involved in the mining and extraction of the value metal or mineral from the ore.

However, another vital question revolves around the technical knowledge required to successfully implement a geometallurgical program. This presentation will focus on this question and cite examples from a program currently undertaken at the Anglo American Platinum Limited's Mogalakwena operation. The discussion will not only focus on the technical aspects, but will also address some of the problems experienced in terms of introducing the concept of geometallurgy and the progress made in improving collaboration between the various disciplines via the technical program.

It will be demonstrated that a better understanding of the various ore types from a geological, mineralogical and chemical perspective makes it possible to develop a proxy/proxies for the metallurgical characteristics of the ores. With a better understanding of the behaviour of these ore types in the concentrator the geometallurgical principles should, at least, improve production forecasts and, with full implementation of the principles and subsequent optimisation in metallurgical treatment, add value to the bottom line.

A quantitative mineralogical investigation of variable flotation performance produced by different Merensky Reef facies types at Bafokeng Rasimone Platinum Mine, South Africa

Smith B[1*] Viljoen F[1], Schouwstra R[2], Roberts J[3], Gutzmer J[4]

1 - University of Johannesburg *bertuss@uj.ac.za 2 - Anglo American 3 - Anglo American Technical Solutions - Research 4 - Helmholtz Institute for Resource Technology Freiberg, Germany

The Merensky Reef, which occurs in the Bushveld Complex of South Africa, is one of the largest known resources of platinum group elements (PGE) in the world. Lateral and vertical variations in the geology, grade distribution and mineralogy of the Merensky Reef are well known [1, 2]. At Bafokeng Rasimone Platinum Mine (BPRM), situated on the western limb of the Bushveld Complex, south of the Pilanesberg Complex, eleven distinct Merensky Reef types or facies have been identified based on differences in reef and footwall geology, stratigraphy and PGE grade distribution [3]. The manner in which these facies variations influence flotation response has been documented from quantitative mineralogical work on the flotation feeds [4]. Three of these facies were sampled at BRPM South and D Shafts and subjected to bench-scale single cell flotation to generate five concentrates at pre-determined intervals for each feed. The geochemistry and mineralogy of the feeds and concentrates were quantified to establish the impact of facies differences on flotation.

Differences between facies in overall Pt and Pd recovery are slight, but more pronounced for the enrichment (concentrate to head grade) ratios. Cu and total Ni grades and recoveries are more variable and dissimilar to Pt, Pd and total S. Pentlandite, chalcopyrite and PGE-sulphide recovery is enhanced in the early concentrates. Alteration silicates also have enhanced recoveries in early concentrates due to a strong association with base metal sulphides (BMS). Following decreased recoveries in second and third concentrates, alteration silicate recoveries improve in the final concentrates due to entrainment of liberated grains. Pyrrhotite, pyroxene, PGE-telluride and PGE-alloy recovery improves with flotation residence time. Pyroxene is the predominant silicate diluent in all the concentrates. The recovery of the BMS and platinum group mineral (PGM) types is related to differences in their kinetic response and liberation, association and size in the milled flotation feed.

The data highlight the importance of grade distribution and mining cut in flotation performance. Flotation feeds produced by facies with common footwall mineralization contain less pyroxene and yield higher grade concentrates due to lower pyroxene dilution. The opposite is true for facies in which most of the PGE grade is hosted by pyroxenite. However, mineralisation of the feldspar-rich footwall can be much finer than the pyroxene-rich reef, and may result in poorer BMS and PGM liberation and recovery.

[1] Wagner (1929). *Platinum deposits and mines of South Africa*. Struik, Cape Town.

[2] Viljoen (1994). *Proceedings of the 15th CMMI Congress, SAIMM,* 183-194.

[3] Moodley (2008). *Third International Platinum Conference, SAIMM,* 87-95.

[4] Smith *et al.* (2013). *Min Eng*, 52, 155-168.

A mineralogical investigation of nickel reporting to tailings, Nkomati Mine, South Africa

Steenkamp N C

University of Pretoria. steenkamp.nc@gmail.com

The Uitkomst Complex hosts a Ni-Cu-PGE deposit and South Africa's only primary nickel mine, Nkomati. The disseminated sulphide mineralisation is hosted in two mineable horizons, namely the Main Mineralised Zone (MMZ) and the Peridotite Chromitiferous Mineralised Zone (PCMZ). The ore from these two mineralised zones differs so significantly that it is treated by two separate plants. After commissioning of the MMZ plant it was noted that a significant percentage of nickel was reporting to the tailings. A mineralogical study was undertaken to determine the source of the nickel. Petrographic descriptions of host rock were taken from core samples and feed material that was sourced in the same general area. The sulphide mineralisation in the MMZ is generally comprised of grains consisting of a pyrrhotite centre, surrounded by coarse grained pentlandite and chalcopyrite. The host rock is an olivine-pyrite assemblage that has been subjected to retrograde hydrothermal alteration. The result is that the precursor primary mineralogy has been replaced to a large extent by amphibolite-talc-chlorite assemblages and minor serpentine. The dominant amphibole is actinolite-tremolite that has surrounded and partially replaced the coarse grained sulphide minerals, resulting in a slight reduction of the sulphide grain size. Slight alteration of the sulphide grains was also observed with the development of secondary magnetite and minor violarite. The feed material and tailings were collected and polished sections were prepared for six intervals of size fractions. In the feed the sulphide grains in the range +150µm down to 38µm were observed to be the coarse grained sulphide assemblages of pyrrhotite-pentlandite-chalcopyrite with actinolite-tremolite intergrowths. In the range 38µm down to -20µm the grains were ground to such an extent the suphide grains had been broken into single mineral type fragments. A petrographic inspection of the tailings revealed that all of the coarse grained pentlandite and chalcopyrite had been recovered and that most of the pyrrhotite had reported to the tailings. Exsolution pentlandite flames were clear in these pyrrhotite grains and are cited as the source of the nickel reporting to the tailings.

Visilog: efficient image processing software for metallurgical process design and control

Blancher S, Orberger B*, Goguelin A, Bellver Baca M

1 - Eramet Group *beate.orberger@erametgroup.com

The VISILOG software is applied to image processing and commonly used in the automobile industry for production control. An innovative easy-to-use application is the estimation of surficial proportions (%) of mineral groups, shapes and grain sizes. These data are crucial for developing metallurgical designs for ore processing. VISILOG also allows verifying the efficiency of a metallurgical process, e.g. after magnetic separation or flotation.

Prior to image processing complete high resolution SEM-BSE photo-micrographs were obtained on polished surfaces. Minerals and organic matter were defined through Energy Dispersive Spectroscopy (EDS) and Wavelength Dispersive Spectroscopy (WDS). SEM-BSE images show various grey scales of minerals which reflect an average atomic number of the mineral. Minerals with similar atomic numbers are thus difficult to differentiate, but minerals, mineral groups or phases with contrasting atomic numbers can be discriminated.

Several examples illustrate the efficiency of SEM-BSE image processing by VISILOG through quantitative estimations on surfaces. (1) In Mn-carbonate rich shales, rhodochrosite, quartz, muscovite and organic matter portions, and entities of texturally intergrown minerals, were quantified; (2) In lateritic ores, the portions of REE, Nb, Ta carriers could be estimated against Fe-oxides, and Fe-Al oxyhydroxides and silicates. (3) In Ni-carbonate pellets, after processing and compaction, porosity and inhomogeneity were evaluated. VISILOG is a rapid method, but needs to be operated by a skilled mineralogist experienced with the VISILOG software.

Assessment of geometallurgical responses of Merensky Reef facies and the UG2 at the Lonmin Marikana Mine, Bushveld Complex, South Africa

Dzvinamurungu T*, Viljoen F, Knoper M

University of Johannesburg *tdzvina@yahoo.com

We report on a study of the influence of mineralogy on the comminution and flotation performance (for recovery of Au, PGE, Co, Cr, Ni, and S) of the Merensky Reef facies (BK, RPM, and WP facies types) and UG2 ore at the Marikana mine. Quantitative mineralogical and geochemical information were obtained using a Mineral Liberation Analyser (MLA) and chemical analysis respectively. Approximately 20 individual 10cm channel samples were collected from each facies type and coarsely crushed for modal mineral abundances determination by MLA, and analysis for Au, Co, Cr, Cu, Ni, S, and PGE by chemical analysis. The mineral assemblages of the three Merensky Reef facies and UG2 at this locality consists of, in varying quantities, orthopyroxene, clinopyroxene, plagioclase, olivine, talc, serpentine, chlorite, chromite, magnetite and sulphides (mainly chalcopyrite, pentlandite and pyrrhotite).

High sulphide abundances and the base metals, PGE and S concentrations correlate positively with chromitite stringers in all the Merensky Reef facies types. UG2 has less sulphide abundance than Merensky Reef facies; PGE are concentrated at the base and Cr, Cu and Ni in the middle. Pt, Pd and Ru are the most abundant in UG2, in that order.

The samples show variable milling times required to produce a grind of 60% passing 75µm. This milling behaviour is controlled by the abundance of plagioclase, orthopyroxene and chromite. Size distribution of the base metal sulphides is similar for the Merensky Reef samples, but coarser for the UG2 ore. BMS are best liberated in BK facies relative to RPM and WP; with the least in UG2.

WP has the highest cumulative mass pull during flotation due to its higher abundance of orthopyroxene relative to the other samples. A high flotation recovery of PGE, Cu and S is observed in all the samples; however BK has the highest recovery among the Merensky Reef ores. Ni recoveries are generally poor suggesting that Ni is hosted in both gangue and pentlandite. BK facies is the best ore quality of the three facies types of Merensky Reef and it is characterized by high PGE grade, low abundance of enstatite, a high abundance of BMS and a higher degree of BMS liberation upon milling of the ore.

Determining iron impurities in calcined kaolin clays.An approach using short and long wavelength infrared spectroscopy

Guatame-Garcia A[1*], Buxton M[2]

1 - Resource Engineering, Geoscience & Engineering, Delft University of Technology *l.a.guatame-garcia@tudelft.nl 2 - Resource Engineering, Delft University of Technology

Short and long wavelength infrared reflectance spectroscopy is used to determine the presence of iron impurities in calcined kaolin. For industrial applications, primary kaolin is calcined by roasting at temperatures of greater than 1100 °C. The resulting calcined kaolin clays are widely used in the manufacture of pigments and coatings. For such applications the key parameters determining calcined product quality are colour and brightness. The presence of iron impurities in the primary kaolin prior to calcination affects these properties in the processed calcined clay. Excess iron yields lower brightness and increasing yellow colouration. Knowledge of the quantity and type of iron impurity in kaolin is therefore essential for successful industrial processing to achieve required product specifications. Iron is present as oxide or hydroxide in the form of hematite or goethite, respectively. However, it is also sometimes hosted in the kaolinite crystal structure. Commonly used techniques for clay analysis examine chemistry or mineralogy, but generally not both. Therefore, a comprehensive and complete determination of iron impurities is not possible simultaneously. Traditional analytical methods are also constrained by other parameters such as particle size, or require extensive preparatory work. As a result there is strong industrial interest in the development of new or complementary methods for chemical and mineralogical iron characterization.

Three samples of kaolin with different iron content were analysed with short and long wavelength infrared reflectance spectroscopy. The samples were calcined at various temperatures using a muffle furnace. Each feed was sequentially calcined at temperatures from 500 to 1200 °C at 100 °C intervals. Spectral analysis focused on the identification of Fe_2O_3 and FeOOH absorption features. Characteristic kaolinite features were also taken into account. Spectral parameters including absorption wavelength position, depth and shape were correlated with calcination temperature, chemical composition (given by XRF data), and colour/brightness (measured with standard ISO laboratory analyses). Additional work also suggests that RAMAN spectroscopy might support infrared reflectance spectra mineralogical observations.

The preliminary results of the spectral analysis are presented in this poster. The results show that variation in colour is expressed by the shortest wavelengths. Spectral features between 0.5 and 1.2 µm are directly correlated with the amount of iron present in the samples and with the colour expressed as "yellowness". Mineralogical changes are detectable from the variations of M-OH (M=metal) absorptions in the short as well as in the long wavelength ranges (Figure 1). Al-OH features illustrate the transformation from kaolinite to metakaolin with caused by increasing temperature during calcination. The Fe-related features can be used to indicate if Fe is hosted in the kaolinite crystal lattice or present as a secondary mineral. An integrated analysis of these spectral parameters may lead to a model to determine kaolin iron impurities and able to predict related optical properties. This could be applied before and after calcination to enable more precise control of calcined kaolin properties and help to optimise the calcination process.

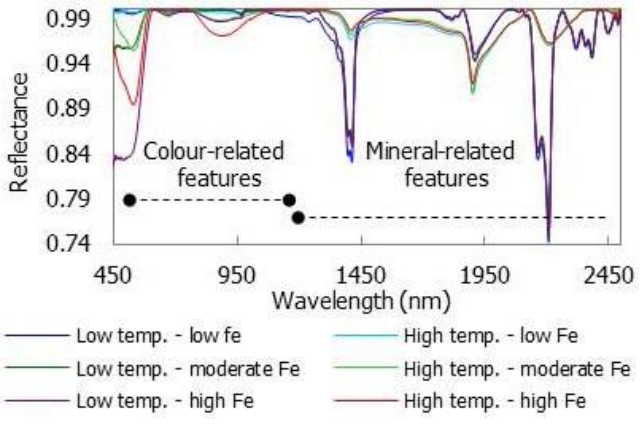

Figure 1: Short wavelength infrared spectra of kaolin with different iron quantities, calcined at extreme temperatures (low 500°C, high 1200°C).

Acknowledgements: This work was facilitated by Imerys Minerals Ltd &the STOICISM research project. It has been supported by the European Commission under the 7th Framework Programme through the grant number 310645.

Optimisations of X-ray computed tomography for the spatial resolution, particle size analysis and simple phase discrimination of Bushveld Complex ore

Jardine M[1*], Miller J[2], Becker M[1], du Plessis A[2]

1 - Centre for Minerals Research, Department of Chemical Engineering, University of Cape Town, South Africa. *jrdmit001@myuct.ac.za 2 - Stellenbosch University

Process mineralogy is becoming increasingly important in minerals processing as the mining industry moves towards the processing of more mineralogically complex, low grade ores. Well established analytical techniques such as auto-SEM technology (eg. QEMSCAN, MLA) are generally accepted analytical methods for ore mineral characterisation providing detailed, quantitative information on bulk mineralogy, grain shape, size, liberation and association in two dimensions. However, use of these techniques is limited by the need for extensive sample preparation, slow turnaround time, and high cost.

The use of X-ray computed tomography (XCT) for mineral characterisation presents an alternative ore characterisation method. This method reduces turnaround time to a few hours with the need for only minor sample preparation, making this a potentially viable technique for process mineralogy. The discrimination of mineralogy is limited however, since XCT cannot determine mineral composition on its own. Mineral X-ray attenuation is the only property used in mineral identification in XCT. In this study, a UG2 ore from the Bushveld Complex in South Africa was investigated. A sample preparation method was developed enabling a voxel resolution of 2 microns on a General Electric Phoenix V|Tome|X L240 X-Ray scanner. A UG2 ore flotation feed sample that had been milled to 40% passing 75µm was split and loaded into plastic drinking straws. Geometrically, the straw allowed for optimum X-ray optics and the imaging of this ore. Defect analysis results suggest that there is a relationship between particle size, sphericity, surface area and density: sphericity increases with decreasing particle size and surface area, and average grey values decrease with decreasing particle size. Imagery reveals complex density variations within some minerals and displays grain size as a function of colour. Grey scale densities have been extracted for the proposed different mineral phases for easy study. Beam hardening artefacts create false dense cores in larger particle size fractions; here small dense particles have the same grey scale a core of a larger lower density particle. Therefore, for optimal imaging, the ore feed should be split into particle size classes before analysis.

Further investigations using complementary autoSEM data will focus on developing XCT techniques and methodologies that will allow for the extraction of more specific process mineralogy information. This will include mineral phase differentiation using X-ray attenuation properties of high density particles to determine quantitative bulk mineralogy, and calculations of 3D grain size distribution coupled with phase information to quantitatively determine texture and liberation.

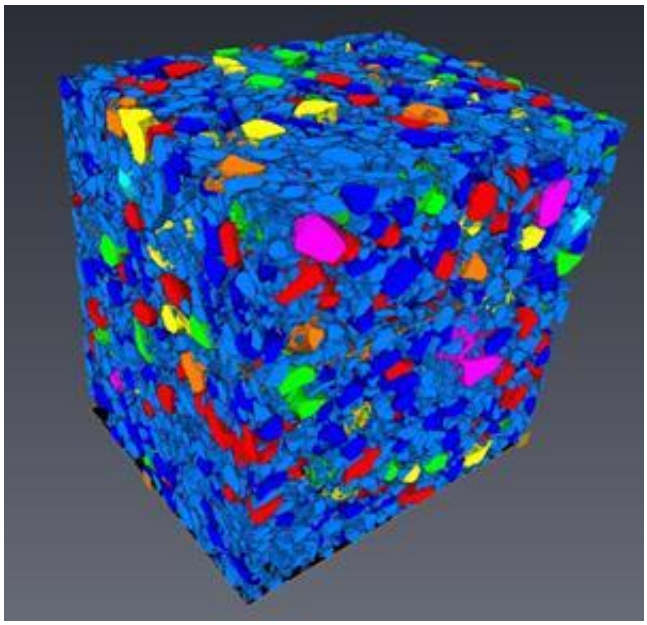

Figure 1: A 3D model produced in Avizo Fire of UG2 ore feed prepared into a straw mount. The dimensions of which are 4×4×4 mm. This volume has been cropped out of an initial cylindrical model. The grains have been coloured according to size. Pink displays the largest grains and blue the smallest grains.

Keywords: X-ray Computed Tomography, process mineralogy, liberation.

Laser modification of mineral surface properties

Kotova O[1*], Leonenko N[2], Gazaleeva G[3]

1 - Institute of geology Komi SC UB RAS *kotova@geo.komisc.ru

2 - Institute of Mining of Far-Eastern Branch of RAS 3 - Uralmekhanobr OJSC, Russia

Ores with complex material composition and low contrast of physical-chemical and technological properties of valuable components are the basis of the raw minerals base of Russia. Energy influences are considered as an efficient method of intensification of raw mineral processing and applied to increase the contrast of mineral properties and efficient disintegration of fine mineral complexes.

The aim of the present work is an experimental study of mechanisms of laser influence on the phase composition, structural, chemical and technological properties of materials for the development of processing technologies of bauxite ores, red muds and gold-containing tailings.

Electron microscopy was the basic investigation method. X-ray methods were used for the analysis of the phase composition.

New experimental data on the laser influence on the phase composition, geometrical and technological properties of bauxite minerals, red muds and gold-containing tailings are presented. The mechanisms of formation of micro- and nanophases on mineral surfaces are influenced by the energy. The change of surface atom state, concentration of metals, agglomeration of titanium minerals and formation of new phases occurred under the laser influence on bauxite and red mud. The mechanism of agglomeration of gold is also presented.

Acknowledgements: The work was supported by the projects of RAS Programs: 12-M-35-2055; 12-III-A-08-020 &RFBR: 13-05-00586

A geometallurgical examination of gold, uranium and thorium in the Black Reef quartzite formation

McLoughlin A*, Blignaut L, Viljoen F

Geology Department, University of Johannesburg *mcloughlinandrew49@gmail.com

The Black Reef quartzite formation forms part of the Transvaal Supergroup. It has significant concentrations of gold and uranium. This mineralization occurs predominantly in the BSPL (buck shot pyrite leader) reef of the Black Reef formation. In the present study we examine for the first time ever, the nature of the gold and uranium mineralization in the reef using Mineral Liberation Analyzer (MLA) technology. Samples were taken from Gold One International's operation at Modder East in Johannesburg's gold rich East Rand region. The size distribution and mineral association of gold and uranium are critical during metallurgical processing of the ore. Thin sections of the samples were analyzed to determine the size distribution and mineral association of gold and uranium within the reef. Gold is primarily associated with quartz, pyrite, muscovite and chlorite, and lower levels of association are also observed in the case of pyrophyllite, uraninite and kerogen. The association of the gold is very similar to that found within the Witwatersrand reefs as the same strong association between quartz and pyrite is also observed. The size distribution for gold found in these samples varies with position above, within and below the BSPL reef, with smaller grains of gold encountered above the reef (2-90 µm in size). Gold within buckshot pyrite reef is much larger, varying in size from 2 micron to 200 micron. Gold from below the reef can vary in size up to 180 micron. This pattern is repeated for uraninite, with similar size distribution curves observed although the uraninite is much finer than the gold. The uraninite is markedly associated with kerogen globules but also does occur in association with quartz, muscovite, pyrophyllite, sphalerite and chalcopyrite on a much lesser scale. The characteristics of the uranium are similar to those found in the carbon seams of the Witwatersrand reefs.

Geometallurgical assessment of Pit 3 ore Nkomati Mine, South Africa

Mishra G*, Viljoen F, Mouri H

University of Johannesburg *gargigeo@gmail.com

The Nkomati Ni-Cu-Co-PGE deposit is located in the Uitkomst Complex, which is a layered mafic to ultramafic tabular intrusion situated approximately 50 km east of the eastern limb of the Bushveld Complex. Sulfide is hosted within the lower pyroxenite and peridotite rock types. The bulk flotation of sulfide is the main process involved in the concentration of ore.

A comprehensive understanding of the ore mineralogy is the key to understanding the flotation response of various minerals in an ore body. This study aims to evaluate the influence of gangue mineralogy in flotation of pentlandite by detailed characterisation of the ore and flotation products. For this, 29 samples were selected from Pit 3 at the Nkomati mine.

The quantitative information on modal mineral abundances, grain size distribution, mineral liberation, and mineral association assisted in determining the drivers for metallurgical response of the ore. Upon detailed mineralogical characterisation, it was observed that textural variations of sulfide mineralisation in the studied samples depend on host rock types, grain size, and the availability of the sulfides. The main textural variants include net texture, bleb texture, disseminated texture, semi-massive texture, and massive texture.

Once mineralogical characterisation was completed, each sample was subjected to the standard rougher flotation test for metallurgical characterisation. Geochemical assays were obtained on flotation products and feed. These assayed values were used in the calculation of Ni grade, recovery, and mass pull percentage and flotation kinetics. Based on these values, mainly three flotation trends were recognised: fast flotation response, intermediate flotation response, and slow flotation response.

It was observed that fast flotation samples usually have high quantities of sulfides in their original feed, are relatively coarse-grained in comparison to intermediate, and slow flotation samples.

Mineralogical assessment of the Aggeneys-Gamsberg district and the implications thereof for the mineral processing behaviour

Nkomo T*, Viljoen F, Mouri H

University of Johannesburg *nkomothobeka@gmail.com

The major Cu-Pb-Zn base metal deposits of the Northern Cape occur in the Aggeneys Ore Formation of the Bushmanland Group within the Namaqua-Natal Metamorphic Province. Four significant deposits, (Black Mountain, Broken Hill, Gamsberg and Big Syncline) are known. The geology of the terrain consists of alternating layers of quartzite and schists and is perceived to be a metamorphosed sedimentary exhalative deposit. The deposits have been subjected to dynamic metamorphism ranging from greenschist to granulite facies metamorphic grade, accompanied by polyphase deformation, which results in complex mineralogical, textural and geochemical variations in the various ore types. These variations may have significant impact on mineral processing and are expected to result in different metallurgical responses for each ore type. A composite ore sample of each of Broken Hill, Gamsberg, and Black Mountain was investigated through the acquisition of mineralogical data in conjunction with chemical assays as well as laboratory-scale milling and flotation testing. Base metal sulphides present include sphalerite, galena, chalcopyrite, acanthite, alabandite, barite, pyrite, pyrrhotite, cobaltite, and arsenopyrite. Major silicate minerals observed includes quartz, micas, feldspars, garnet, amphiboles, chlorite, and pyroxmangite. The sphalerite minerals have complex chemistry consisting of trace quantities of Fe, Mn, Ag, Ti, Cu, Co, Cd, and In. Geometallurgical test results are consistent with a complex mineralogy in the ores.

The processing of Namibian granite-hosted uranium under the microscope

Youlton B[1*], Kinnaird J[2]

1 - SGS South Africa *brandon.jayyoulton@sgs.com 2 - University of the Witwatersrand

The economic processing of Namibian granite-hosted uranium is influenced by a wide range of factors, including the hardness of the rock, a shortage of inherent iron, refractory uranium and gangue acid consumption. Each of these factors is controlled by the mineralogy of the rock. A link between the mineralogy of the ore, and its performance during processing, has been established by comparing the results of mineralogical analyses and bench-scale metallurgical tests.

Paleoenvironmental controls on formation of giant early Paleoproterozoic BIF and associated iron and manganese deposits in southern Africa

Beukes N

University of Johannesburg. nbeukes@uj.ac.za

The 2.64 - 2.06 Ga Transvaal Supergroup on the Kaapvaal Craton of southern Africa hosts the largest and best-preserved single deposits of banded iron formation (BIF) and manganese formation (MnF) in the world. The largest BIF, namely the 2,5-2,45 Ga Kuruman-Griquatown succession, holds important clues as to paleoenvironmental conditions on earth prior to the rise of atmospheric oxygen at ~2.32 Ga with the MnF, namely the 2,2 Ga Kalahari Manganese Deposit (KMD), indicating conditions in its immediate aftermath. A reappraisal of the depositional setting of the giant BIF indicates that oceans along the Archean-Paleoproterozoic boundary were not permanently density stratified as commonly envisaged. Rather they were dynamic with good circulation and contained a flux of free oxygen, derived from photosynthesis, down into deep water where it interacted with iron dissolved in hydrothermally-enriched deep water to form hematite facies BIF.

The stratigraphic interval between 2,45 and 2,32 Ga in which the rise atmospheric oxygen took place, is characterized by glacial diamictites, ^{13}C -enriched carbonates and oolitic ironstone. After the rise ocean water contained sufficient oxygen for precipitation of manganese oxides from a deep water hydrothermal plume to form the KMD hosting 78% of the world's land-based Mn ore resources. Although deposition of the manganese at ~ 2.2 Ga required higher levels of free oxygen in the environment, it was not directly linked to the rise of atmospheric oxygen which took place 120 Ma earlier.

The low-grade (35 - 38 wt. % Mn) primary Mamatwan-type sedimentary manganese ore in the KMD is composed of microcrystalline braunite and kutnahorite with abundant tiny diagenetic Mn-carbonate concretions. The ore displays negative Ce anomalies whilst the Mn-carbonates are depleted in $d^{13}C$ suggesting original deposition as Mn^{4+}oxyhydroxides with Mn-respiration in presence of organic matter leading to formation of early diagenetic braunite and Mn-carbonates. The Mamatwan-type ores have locally been upgraded to high-grade (42 - 50 wt. % Mn) Wessels-type ore by hydrothermal fluids along a conduit system of normal faults in late Mesoproterozoic times at ~ 1,1 Ga. The hydrothermal alteration resulted in roasting of Mn-carbonates to form hausmannite and bixbyite with loss of silica from braunite to form braunite-II.

Deposition of the giant KMD was followed by uplift and erosion with development of an extensive lateritic weathering profile shortly after intrusion of the Bushveld Complex at 2,054 Ga. The profile hosts large Sishen-type high-grade hematite iron ores in supergene-enriched BIF.

Paleogeographic reconstructions, based on paleomagnetism in combination with stratigraphic correlations, indicate that the Transvaal Supergroup was deposited in a basin that was directly linked to that of the time-equivalent Mount Bruce Supergroup on the Pilbara Craton in Australia. This finding has obvious exploration applications and impacts on reconstructions of global conditions on earth in Late Neoarchean - Early Paleoproterozoic times.

A geochemical and geometallurgical analysis of the Kalahari Manganese Deposit, Northern Cape

Blignaut L[1*], Viljoen F[1], Tsikos H[2]

1 - University of Johannesburg *ljolly@uj.ac.za 2 - Department of Geology, Rhodes University, Grahamstown

The largest and most important deposit of the ± 2220 Ma Kalahari Manganese Field (KMF) is the 320 km^2 Kalahari Manganese Deposit (KMD). The manganese (Mn) is exploited from three beds that are interbedded with hematite lutite and banded iron formation [1]. The northern KMD ores were affected by hydrothermal alteration, involving carbonate dissolution, removal of CO_2 and the introduction of alkali elements, base metals and iron into the system [2]. Normal and thrust faults were important in localising the alteration system, as they acted as conduits for hydrothermal fluids [3]. They, however, were not the only factor that contributed to the alteration of the ores. Another possibility for this enrichment involved the flow of isotopically light fluid throughout large parts of the KMF which was related to the Hotazel/Olifantshoek unconformity [4]. The Mn is divided into the low-grade Mamatwan and the high-grade Wessels-type ores, with the latter being constrained to the northern part of the KMD [5]. The lowermost Mn bed is the thickest and most Mn-rich and, thus, most favourable for mining [1]. A thorough understanding of the ore (through detailed analysis of the genesis and alteration of the ore, as well as the fluid-rock interactions) is essential in order to optimize exploitation and maintain the high quality and quantity output of the ore. Mineralogy includes braunite, hematite, hausmannite, jacobsite, bixbyite, kutnahorite, and carbonates. Major and trace element analyses indicate an inverse relationship between Mn_3O_4, MgO and LOI with Al_2O_3, Fe_2O_3, SiO_2 and CaO, with Mn_3O_4 concentrations generally increasing with depth and increasing grade. Trace elements, Cu, Pb, Co and Y display a decrease in abundance with depth and increasing grade, which correlates with Al_2O_3, Fe_2O_3, SiO_2 and CaO, whereas Zn, Sr, Ba and Ga correlate with Mn_3O_4 and MgO in terms of exhibiting an increase in concentration with depth and increasing grade. These characteristics can be correlated to mineralogical variations within the ore and also indicate a depletion of SiO_2, CaO and Al_2O_3 or a leaching of carbonates from the upper to the lower Mn bed and from the low to high-grade ore and thus, resulting in an enrichment of the Mn ore. ICP-OES analyses show that boron (B) concentrations, increase with depth to a maximum of 4500 ppm in the lower Mn bed. Mn_3O_4 and B concentrations are directly comparable in terms of an increase in the abundance with depth. This is problematic, as the higher the Mn grade, the better the steel quality, however, concentrations of B above 400 ppm, are highly undesirable and detrimental to the steel quality. Rare earth element (REE) analysis indicates enrichment in heavy REE over light REE and an overall increase in REE with an increase in alteration. The REE signature is similar to that of present day shallow level seawater. The Mn ore was upgraded through either residual enrichment or lateral introduction of Mn.

[1] Beukes N.J. (1983). *Developments in Precambrian Geology*, 6, 131-209.

[2] Evans D.A.D. *et al*. (2001). *Economic Geology*, 96, 621-631.

[3] Kleyenstüber A.S.E. (1993). *Resource Geology*, 17, 2-11.

[4] Tsikos H. (2003). *Economic Geology*, 98, 1449-1462.

[5] Kleyenstüber A.S.E. (1984). *Transvaal Geological Society of Southern Africa*, 87, 257-272.

Transformation of native gold in hypergene conditions and sources of placer gold in Sukhoi Log gold-bearing field

Lalomov A

1 - Institute of Geology of Ore Deposits, Petrography, Mineralogy and Geochemistry of Russian Academy of Science IGEM RAS. lalomov@mail.ru

Processes of transformation of native gold in hypergene conditions in the sedimentary system "primary source - weathering crusts - fluvial channels" have significant influence on both estimation of placer deposits potential of gold-bearing fields and reconstruction of primary sources of gold placers. The study of native gold from Sukhoi Log gold-bearing field (Bodaibo area of Trans-Baikal Siberia) reveals that disseminated gold from pyritic black shales consolidates in hypergenic conditions of linear weathering crusts and during subsequent slope and fluvial transportation. In result, primary, very small gold transform into gravity concentratibility size classes that constitute a significant part in the formation of placer gold deposits.

Bodaibo goldfield area has 150-years of mining history and provided about 2000 tons of mainly placer gold, but primary placer-forming gold ores of gold-quartz formation are not revealing hitherto. On the other hand, giant sulfide gold deposit Sukhoi Log is not considered as placer-forming because it contains mainly dispersive gold of size fraction 10-50 μm. A variety of typomorphism of placer gold indicates the presence of several sources of placer gold.

Current research reveals at least one more possible source of placer gold. A system of minor northeast-orientated faults is often accompanied by linear weathering crusts developed along carbonaceous shales and siltstones. In the case of superposition of the linear weathering crusts onto zones of dispersive sulfide ore mineralization it contains gold of larger size (up to 100-200 μm) which can form alluvial placer deposits.

The study of the typomorphic characteristics of the native gold from different levels of sedimentary systems (unaltered sulfide gold ore - weathering crusts *in situ* - displaced weathering crusts - alluvial valleys) reveals an increase of the gold grains with increasing roundness. In the weathering crust the gold grains have a finer surface zone in comparison with inner zones due to lower contents of silver and arsenic. Also, the grains are coated by iron oxides. In displaced crusts the oxide coating disappears and the fine border becames wider and more pronounced. In alluvium of middle order valleys the amount of admixtures in gold decreases and the distribution of admixtures becomes more uniform. Hypergene transformed gold close to weathering cores forms up to 40% of placer gold deposits.

Increase in the grain size can be a result of both low temperature hydrothermal activity confined to northeast-orientated faults, as well as hypergene redistribution of gold. Where hydrothermal gold is usually accompanied by mercury, hypergene processes rise hallmark of gold. Typomorphic characteristics of the studied gold indicate that hypergene processes prevailed.

The study of the transformation processes of native gold in hypergene conditions allows the development of a rational technological mining scheme and the estimation of placer potential of sulfide-gold mineralization that had been considered unpromising for gold placer deposits.

Acknowledgement: The work was supported by grant of Russian Foundation for Basic Researches (RFBR) # 13-05-00449-a.

Unusual manganese enrichment associated with the Mesoarchean sedimentary rocks of the Mozaan Group, Pongola Supergroup, South Africa

Ossa Ossa F[1*] Hofmann A[1], Vidal O[2], Kramers J[1], Belyanin G[1]

1 - Department of Geology, University of Johannesburg, South Africa. *frantz.ossaossa@gmail.com

2 - LGCA, UMR 5025, Université Joseph Fourier, Grenoble Cedex 09, France.

Carbonate-rich banded iron formations and ferruginous shale of the Sinqeni and Ntombe formations within the c. 2.9 Ga Mozaan Group, from the White Mfolozi Inlier (KwaZulu Natal, South Africa), are associated with abnormally high manganese contents. Rocks were studied in drill core not affected by any supergene processes, and where observed MnO contents may reach 7 wt.% in well preserved samples showing minor evidence of fluid circulations. Manganese enrichment in this type of samples is associated with early diagenetic carbonate nodules and shale intraclasts. The latter represent Mn-rich mud-drapes reworked in an intertidal environment. This suggests that Mn precipitation took place in a shallow marine environment during sedimentation and early diagenesis. New geochemical data indicating the evidence of oxygenated shallow marine water, probably related to oxygen photosynthesis, would have played a first-order control during manganese precipitation. Therefore, these well preserved carbonate-rich banded iron formations and ferruginous shale may be considered as Mn parent rocks where primary MnO contents would have been as high as 7 wt.%. Values higher than that, reaching 15 wt.%, are interpreted to have resulted from the thermal alteration of the above carbonate-rich parent rocks. A detailed mineralogical and petrographic study shows that the parent rocks are mainly characterized by a Mn-rich carbonate phase situated in the theoretical solid solution field between manganoan siderite and ferroan rhodochrosite. This phase is associated with other Mn- and Fe-rich mineral phases, such as magnetite, ferroan chlorite, kutnahorite and pyrite. In the absence of recent weathering, their thermal alteration allowed a diversification of mineral assemblages where ferroan tephroite, hematite, calcian rhodochrosite, rhodochrosite, pyrochroite, jacobsite, manganite, pyrophanite, cronstedtite-like mineral phase, manganoan Fe-rich chlorite, manganoan phlogopite and pyrite replaced partially or totally the previous mineral assemblage. Thermodynamic modeling performed on chlorite phases associated with the described mineral paragenesis illustrate a decrease of average crystallization temperatures from ca. 310 ± 54 °C in early metamorphic phases to ca. 244 ± 41 °C in mineral phases associated with late fluid circulations. This suggests that an event of retrograde greenschist metamorphism involving fluid circulation and hydrothermal alteration post-dating metamorphism controlled the mineral transformation processes in carbonate-rich banded iron formations and ferruginous shale of the above Mesoarchean formations. $^{40}Ar/^{39}Ar$ dating performed on K-rich phyllosilicate phases affected by fluid circulations shows step dates ranging between 1300 and 1500 Ma, with near-plateau ages between 1420 and 1440 Ma. This indicates that the thermal event controlling mineral transformation processes was a late, separate event not related to diagenesis and probably also not to regional metamorphism. Mineral transformation would have been accompanied by local metal remobilization allowing a progressive Mn enrichment from unaltered parent to altered rocks, probably during the Mesoproterozoic.

Proterozoic Broken Hill-type base metal sulphide deposits are (not?) metamorphosed sedimentary exhalative deposits: evidence from South African and Australian examples

Rozendaal A

University of Stellenbosch. ar@sun.ac.za

Classification of ore deposits is generally based on a number of common denominators which collectively define a specific deposit-type. This may be related to similar stratigraphy, mineralogy, age, tenor, tectonic setting and may result in a shared genetic model. In most examples, however, there are a number of characteristics that are unique to an individual deposit. These differences may radically influence the definition of a deposit-specific exploration model. The classification of stratiform-stratabound base metal sulphide deposits is no exception and it is the aim of this paper to contrast world class deposits classified as BH-t and (meta)-SEDEX type in metamorphic terranes with the focus on South African and Australian examples.

The fact that Cannington and Broken Hill (Australia) and deposits of the Aggeneys-Gamsberg Ore District (South Africa) have been metamorphosed to medium-high grade, display various degrees of metasomatism, have been polyphase deformed, are Pb-Zn-sulphide-rich with world class resources, are of Proterozoic age, stratabound but also stratiform, have skarnoid silicate mineralogy and are mainly sediment hosted allowed them to be classified as a special group referred to as BH-t deposits. Within this group, however, a sheath fold preserved, mega-deposit such as Gamsberg displays the features typical of a SEDEX affiliation. These include a stratiform graphitic meta-pelite host, high iron sulphide content, redox facies controlled zonal distribution of iron and manganese and a barite association that extends for kilometres beyond the lateral and vertical periphery of the sulphide deposit.

Although BH-t deposits have much in common as a group there are distinct differences between individual deposits suggesting that a common genesis and exploration model is not obvious.

Controls on regional gaps in sediment-hosted stratiform copper mineralization: evidence from the Midcontinent Rift System, USA

Woodruff L, Mauk J*

US Geological Survey *jmauk@usgs.gov

Sediment-hosted stratiform copper deposits account for approximately 23 percent of Earth's Cu production and resources. These deposits typically form in sedimentary basins where metalliferous saline aqueous fluids encountered environments that led to precipitation of cupriferous sulfide minerals. Copper mineralization is not uniform in favorable host units; instead some areas have greater Cu endowments than others. Here, we explore possible controls on this variability, based on regional work in the Midcontinent Rift System, USA.

The Mesoproterozoic Midcontinent Rift extends more than 2,000 km in an arc across the central North American craton and is one of the world's major continental rifts. It formed at 1.1 Ga from a mantle plume that created voluminous outpourings of basalt up to 20 km thick. Following volcanism, subsidence along the central rift axis created basins filled by clastic sedimentary rocks up to 10 km thick. The post-volcanic sedimentary units in the Lake Superior region include a conglomeratic sandstone/siltstone (Copper Harbor Conglomerate), an overlying gray siltstone/shale (Nonesuch Formation), and an overlying brown sandstone (Freda Formation). The western Lake Superior portion of the rift in northern Michigan contains the White Pine deposit, which is the largest sediment-hosted stratiform Cu deposit in North America, and the nearby Copperwood deposit. These deposits occur in the basal portion of the Nonesuch Formation and together contain more than 2.5 Mt Cu, primarily as chalcocite.

In contrast to northern Michigan, the Nonesuch Formation in the Ashland syncline, a continuation of the Midcontinent Rift in northern Wisconsin and only 150 km southwest of the White Pine-Copperwood mineralization, is barren to only weakly mineralized. The Nonesuch Formation in the White Pine, Copperwood, and Ashland syncline areas contains similar S and C contents, suggesting that its geochemistry was broadly favorable for Cu precipitation in all three localities. Furthermore, all three areas contain similar types of sedimentary rocks in the favorable horizons of the lower Nonesuch, predominantly siltstones, with local sandstone and shale. Detailed comparison shows remarkable continuity of the lithostratigraphy in the White Pine-Copperwood area, but the marker horizons that define the fine-scale stratigraphy in that region show only intermittent continuity into the Ashland syncline area. These results are consistent with previous interpretations that the area that is now the Ashland syncline formed a sub-basin within the Midcontinent Rift that was either partially or completely separated from the larger main rift basin hosting the White Pine and Copperwood deposits.

Taken together, these results suggest that one major constraint on the Cu endowment of favorable strata in the Nonesuch may have been the size of the available mineralizing diagenetic fluid source. The White Pine-Copperwood deposits are on the margin of the large main rift basin that would have been able to contribute significant quantities of mineralizing fluid. In contrast, the smaller size and restricted connectivity of the rift sub-basin in the Ashland syncline area would have had a smaller fluid source thereby limiting the potential metal endowment in that area. In addition, factors such as fluid focusing, local redox changes, and variable lithogeochemical changes that affect fluid chemistry and permeability undoubtedly also played important roles. These and other factors may be preeminent in controlling Cu mineralization in other basins worldwide.

Diagenetic/low-temperature hydrothermal gangue leaching and hematite mineralisation in the Neoproterozoic Santa Cruz iron ore deposit, Corumbá region, Brazil

Angerer T[1], Hagemann S[1], Walde D[2*], Mendonça A[3]

1 - University of Western Australia 2 - UnB, Brasilia *walde.detlef@gmail.com 3 - Vetria Mineraçao S.A., Sao Paulo

Banded iron formations (BIF, 25 to 68 wt% Fe) are the major source of iron for the global economy. Common in the Archean and Paleoproterozoic, significant BIF of the Rapitan-type also appeared in Neoproterozoic times. The latter are interpreted to be glaciogenic and associated with Snowball Earth events. Recent investigations on the Jacadigo BIF in the Corumbá (Urucum) region in Brazil revealed deposit-scale diagenetic/low-temperature hydrothermal and supergene Fe-upgrade processes superimposed on glaciogenic iron oxide BIF. The following sequence of geological events led to an economic, low-aluminium, medium-grade iron ore deposit (average 55 wt% Fe).

During Cryogenian or Early Ediacaran (between ca 635 and 580 Ma) time the Jacadigo Group with mainly siliciclastic sediments and BIF was deposited. The approximately 450 m thick lower dolomite-chert-hematite and upper chert-hematite BIF (interpreted 30-40 wt% Fe), with intercalated diamictites, which defines the Santa Cruz Formation, was deposited. Sedimentation was in response to a glacial transgression-regression cycle interacting with a CO_2-charged snowball earth marine basin (fjord or shelf setting) fertilized with Fe^{2+} and Mn^{2+} ions sourced from low-temperature hydrothermal alteration of oceanic crust.

Burial diagenesis and metamorphism (~175° C, 4 to 7 km depth) in an extensional structural setting resulted in deformation and associated hydrothermal alteration of BIF (between ca 580 and 545 Ma). Processes included early diagenetic ptygmatic veins, which are interpreted as buoyancy-driven 'escape' structures of silica gel, followed by late diagenetic vertical shortening under differential stress ($s_1 > s_2 \geq s_3$). The compaction led to volume reduction accommodated by dissolution-mobilization and podding of SiO_2 mesobands and lepidoblastic (orthogonal to s_1) to anhedral growth of hematite. Dissolution-mobilization of SiO_2 is facilitated by infiltration of high volumes of a Si-undersaturated, heated, alkaline fluid. The diagenetic/low-T-hydrothermal process resulted in an upgrade of Fe to 40-50 wt%.

Minor brittle thrusting and gentle folding at ca 545-500 Ma took place in the region and enhanced the fracture density, thus permeability, within the BIF deposit. However, only minor changes in the oxide mineralogy, such as isolated magnetite and specular hematite in hydrothermal quartz-carbonate veins and faults, were related to this event.

Modern exhumation led to significant supergene leaching and goethite replacement of dolomite in the upper 150 m below surface. Only minor chert was leached. These supergene processes resulted in an average of 55 wt% Fe in the BIF. Locally, particularly in colluvial deposits, a maximum of 64 wt% Fe is reached.

The diagenetic/low-temperature hydrothermal Fe upgrade for the Rapitan-style Santa Cruz Formation BIF, described here the first time, is a unique example of iron ore mineralisation in the diagenetic stages, which was accommodated by the early influx of Si-undersaturated fluids that were probably derived from overlying carbonate rocks.

Crystallographic control of trace element (Cu-Ga-Ge-Fe-Cd) distribution in MVT sphalerites, Tennessee, USA

Bonnet J[1*], Mösser-Ruck R[1], Cauzid J[1], Bailly L[2], André A[1]

1 - Université de Lorraine, UMR 7359 GeoRessources *julien.bonnet@univ-lorraine.fr
2 - BRGM, Bureau de Recherches Géologiques et Minières

Mississippi Valley Type (MVT) sphalerites from Tennessee (two districts: Middle Tennessee Mine (MTM) and East Tennessee Mine (ETM)) were analyzed for the first time; (i) to determine their trace element contents and (ii) to decipher the substitution mechanisms that control their distributions.

Analysis by Electronic Microprobe (EMPA) and by Laser Ablation ICP-MS has revealed two main geochemical associations of trace elements: a first group with correlation between Fe and Cd and a second one with Cu, Ga and Ge. Sphalerites from MTM have both high grade of Cu/Ga/Ge and high grade of Fe/Cd while ETM have only high grade of Fe/Cd. Data have revealed respectively correlations between Cu and Ga + Ge (ratio close to 1), and between Fe and Cd (with two Fe/Cd ratios: one close to 1 and one close to 50 (only in ETM)). These results lead to propose the following substitutions mechanisms: (1) $Cu^{+} + Ga^{3+} \leftrightarrow 2Zn^{2+}$; (2) $2Cu^{+} + Fe^{2+} + Ge^{4+} \leftrightarrow 4Zn^{2+}$ and (3) $Fe^{2+} + Cd^{2+} \leftrightarrow 2Zn^{2+}$.

These correlations have been also evidenced by mapping with EMPA and XRF with a preferential incorporation of Fe and Cd following the (010) faces and a preferential incorporation of Cu, Ga and Ge following the (011) faces (Figure 1).

XANES/EXAFS spectroscopy at K-edge of germanium has also revealed three germanium configurations in sphalerite from Tennessee Mines: a Ge^{2+} form surrounded by sulfur atoms in tetrahedral coordination; a Ge^{4+} form surrounded by sulfur atoms in tetrahedral coordination and a Ge^{4+} form surrounded by oxygen atoms in tetrahedral coordination. A fourth substitution mechanism will probably occur in sphalerite: (4) $Ge^{2+} \leftrightarrow Zn^{2+}$. The presence of Ge^{4+} surrounded by oxygen atoms implies a sphalerite-argutite (GeO_2) association in some samples.

Raman spectroscopy has also revealed the presence of two "crystallographic" forms of ZnS: cubic (sphalerite) and hexagonal (wurtzite) but none of these two forms have been yet connected to one group of trace elements or substitution mechanism.

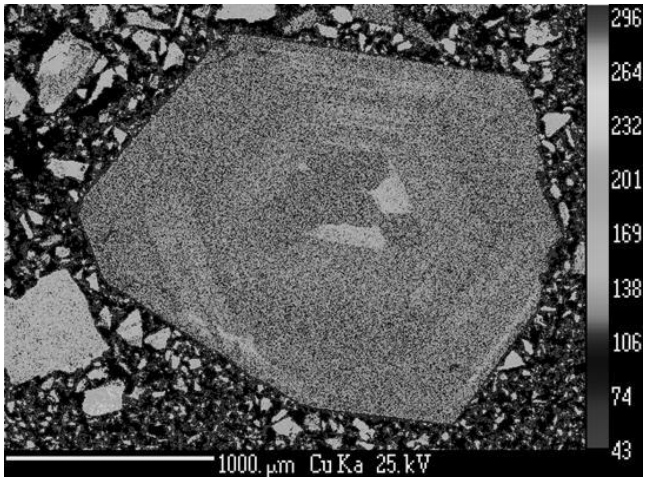

Figure 1: Map distribution of copper in euhedral sphalerite crystal cut perpendicular to the axis 3 (111).

Keywords: Sphalerite, wurtzite, traces elements, XANES/EXAFS spectroscopy

Plastic deformation, strain-assisted transformation, and fracture-related mineralization in pyrrhotite from a metamorphosed massive sulfide deposit

Chen C[*], Huang K, Jiang W

Department of Earth Sciences, National Cheng Kung University, Tainan, Taiwan
**cjchen67@hotmail.com

Complex deformation, replacement, and crystallization microstructures of pyrrhotite from a cupriferous iron-sulfide deposit, Tung-Ao, eastern Taiwan were investigated utilizing electron backscatter diffraction and X-ray energy dispersive spectrometry techniques. The sulfide deposit metamorphosed under greenschist-facies conditions contains a primary assemblage of pyrrhotite, sphalerite, and chalcopyrite with laminated microstructures. The pyrrhotite crystals are dominantly with Fe/S molar ratios (~0.91) that closely approximate to the composition of a "hexagonal" pyrrhotite and exhibit a high degree of lattice preferred orientation with their *c* axes (based on a hexagonal lattice) largely perpendicular to the lamination.

Inverse-pole-figure and misorientation analyses suggest that the primary pyrrhotite crystals display numerous deformation bands that are roughly normal to the lamination and associated with mutually perpendicular primary and subordinate dislocation walls. The deformation mode is dominated by the basal slip system {0001}<10-10> and includes the less abundant prism slip system {11-20}<10-10>. Notably high misorientation gradients are present in the border region of some large pyrrhotite grains. Such high-strain domains and partially recrystallized pyrrhotite grains near iron-bearing sphalerite crystals are associated with compositions close to Fe_7S_8 characteristic of a monoclinic pyrrhotite. In addition, many submicrometer-sized transgranular linear fractures filled with pyrite occur in parallel with the deformation bands, locally associated with elongated dissolution pits loaded with euhedral pyrite crystals. Furthermore, partial replacement of pyrrhotite by marcasite propagates along the pyrrhotite {0001} slip planes (roughly normal to the transgranular linear fractures), having an epitaxial relationship of $\{100\}_{Mrc} \parallel \{0001\}_{Po}$, $\{010\}_{Mrc} \parallel \{10\text{-}10\}_{Po}$, and $\{001\}_{Mrc} \parallel \{1\text{-}210\}_{Po}$. Micrometer-sized intergranular fractures are numerous as well, occurring along subgrain and grain boundaries in pyrrhotite. The subgrain boundaries are accompanied with parallel elongated dissolution pits. Mineralization of siderite and minor chlorite occurs in the intergranular fractures and oriented dissolution pits.

The high abundance of various types of oriented microstructures suggests that the Tung-Ao pyrrhotite has been strongly affected by ductile deformation. The deformation led to strain-assisted phase transformation, elemental mobilization, and recrystallization in the plastically deformed pyrrhotite. Subsequent mineralizations or mineral replacements were defect- and structure-controlled and primarily occurred at the subgrain and grain boundaries and slip planes in pyrrhotite. The result demonstrates potential influences of structural defects in pyrrhotite undergoing intense ductile deformation on mineral crystallization and transformation and element transport and redistribution in pyrrhotite-bearing sulfide deposits.

Gold enrichment at mineral reaction fronts in bismuth sulphosalt assemblages

Ciobanu C*, Cook N, Wade B

University of Adelaide *cristiana.ciobanu@adelaide.edu.au

Gold enrichment in ores is often a matter of local reactions between pre-existing sulphides and superimposed fluids. This is highly predicable when the sulphides themselves are Au-carriers (pyrite, arsenopyrite and bismuth-chalcogenides). Here we show an assemblage of Pb-Cu-Bi-sulphosalts (Ag-bearing lillianite homologues, aikinite and minor emplectite), and sulphides (galena, minor chalcopyrite and alabandite) from a polymetallic skarn where native gold and hessite are present as micron-scale inclusions. Mapping by Laser-Ablation Inductively-Coupled-Plasma Mass-Spectrometry (LA-ICP-MS) (Figure 1a) shows Au-richer domains overlap with subtle compositional changes in the lillianite homologues, i.e., increase in Cu and Ag, decrease in Cd. Using the Focussed Ion Beam-SEM (FIB-SEM) technique, we track coarser particles of gold nucleating along fluid pathways marked by porosity at the site of reaction (Figure 1b). Imaging by Transmission Electron Microscopy (TEM) shows this area also features sub-solidus chemical diffusion leading to nanoscale mineral nucleation (Figure 1c, d). The results thus are evidence for nanoscale mineral reaction and gold trapping during crystal-chemical changes in the sulphosalts.

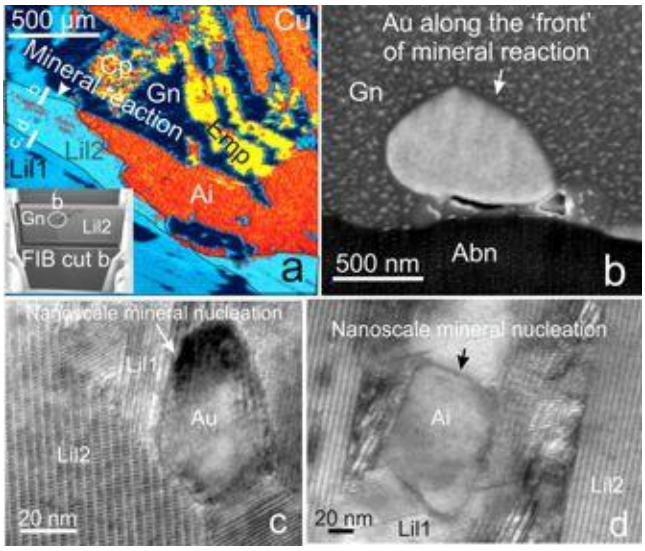

Figure 1: a) LA-ICP-MS map for Cu, where the lowest concentrations are shown in dark blue and the highest levels in yellow. FIB cross-section (b) and TEM images (c, d) showing details along the mineral reaction front in (a). Abn - alabandite; Ai - aikinite; Au - native gold; Cp - chalcopyrite; Emp - emplectite; Gn - galena; Lil 1 and 2 - lillianite homologues.

Trace element concentrations in base metal sulphides

Cook N*, Ciobanu C, George L, Lockington J, Wade B

University of Adelaide *nigel.cook@adelaide.edu.au

Laser-Ablation Inductively-Coupled Plasma Mass Spectrometry allows accurate quantification of trace element concentrations in common sulphides with excellent precision, sub-ppm detection limits and good spatial resolution. Concentration data and element maps for samples from different ore deposits are used to identify statistically valid trends that elude to underlying correlations between trace element concentrations and ore type, conditions of ore formation, and partitioning among co-existing sulphide species. Here we present new data for metamorphic sphalerite, and galena from a broad variety of ore systems.

We show that sphalerite is a good host for Cd, Mn, In, Ge and Hg. Concentrations of other elements, believed to only occur in sphalerite as micro- to nano-scale inclusions, notably Pb and Bi, diminish with increasing metamorphic grade. This is interpreted as due to recrystallization and remobilisation of these elements from sphalerite to form discrete minerals elsewhere. The concentrations of lattice-bound elements (Mn, Fe, Cd, In, Hg) show no correlation between concentration and metamorphic grade. Source and physico-chemical conditions of primary crystallisation are dominant in defining the concentrations of these elements, and they appear to be readily re-incorporated into recrystallised sphalerite. In sphalerite free of chalcopyrite disease, a moderately strong positive correlation between Cu and In concentrations is observed, confirming the coupled substitution $2Zn^{2+} \leftrightarrow Cu^{+} + In^{3+}$.

Trace element analyses of galena by LA-ICP-MS from 36 samples from 24 mineral deposits of different types shows that Ag, Bi and Sb are the most common trace elements present in galena. Concentrations of each can, in some samples, exceed 1 wt.%. Copper, Tl and Cd are also present at detectable concentrations in all samples. We observe that the good correlation coefficient between Ag and (Bi+Sb) is improved if Cu and Tl are also assumed to be monovalent and are included with Ag, giving the generalised coupled substitution $2Pb^{2+} \leftrightarrow (Ag,Cu,Tl)^{+} + (Sb,Bi)^{3+}$. We observe extensive solid solution of Se in galena, and much more limited solid solution of Te. Although concentrations of Sn are generally low, galena maybe an important Sn-host in some deposits. Gold and mercury are present at concentrations of, at most, a couple of ppm. Chromium, Mn, Fe, Co, Ni, Zn, Ga, As, Mo or W are not present at concentrations above 1 ppm in galena from any sample analyzed. We also present element maps for low-temperature epithermal galena which show that the mineral can spectacular display oscillatory and sectorial zoning with respect to trace element concentrations.

Lastly, we examine trace element concentrations in sphalerite-galena-chalcopyrite assemblages, with and without coexisting pyrite. The partitioning behaviour of some elements, notably Tl and Sn, changes from assemblage to assemblage suggesting that the ability of these elements to be incorporated into specific minerals may be strongly influenced by the conditions of crystallization. In turn, this raises the prospect of trace element concentrations in co-existing sulphides being of value as petrogenetic indicators.

Textural complexity in sulfide and telluride minerals resulting from mineral replacement reactions

Etschmann B[1], Brugger J[1*], Pring A[2], Zhao J[3], Li K[3], Ngothai Y[3], Altree-Williams A[3]

1 - Monash University *joel.brugger@monash.edu 2 - Flinders University

3 - University of Adelaide

Over the past decade, many mineral replacement reactions have been recognized to occur via the coupled dissolution re-precipitation (CDR) mechanism, *i.e.* they proceed via dissolution of the parent phase into a fluid, coupled with the precipitation of the product(s). The product is porous, enabling the reaction to run to completion. Recent research has dramatically improved our understanding of the mechanisms and kinetics of CDR reactions, with applications to understanding mineral formation processes in nature, but also in materials synthesis. We review existing studies relevant to mineral processing and ore petrology, with a particular emphasis on the diversity of textures resulting from CDR reactions, and the role of CRD reactions in controlling the scavenging of minor ore components.

Pentlandite ($(Fe,Ni)_9S_8$) and violarite ($(NiFe)_3S_4$) are the main Ni ores in massive sulfide deposits; the nature of these phases is important for flotation and smelting. Violarite pseudomorphs after pentlandite are common in the cementation zone; however, solid-state transformation of pentlandite to violarite is sluggish and results in multi-phase assemblages. In contrast, using CRD reactions, pentlandite can be quickly transformed to violarite under mild hydrothermal conditions. The replacement is pseudomorphic and preserves the crystallographic orientation of the parent pentlandite (epitaxial nucleation); the scale of the replacement depends upon the relative rates of the dissolution and precipitation steps, with nm-scale preservation when the precipitation rate is much faster than the dissolution rate.

Refractory Au-Ag-tellurides are replaced by gold in ~24h via CRD under hydrothermal conditions (200 °C), providing an alternative to roasting. The gold textures are similar to those observed in natural 'mustard gold'. Depending on the nature of the Au-Ag-telluride, the replacement can lead to remarkably complex textures that belie the simple reaction conditions. These textures evolve because of the interaction between CRD and solid-state driven reactions.

Experimental studies of the sulphidation of hematite in the presence of Cu(I) provide insights into the formation of chalcopyrite and bornite. In uranium-bearing experiments, uranium scavenging was coupled with the mineral replacement reactions. This process could be important for explaining U distribution in IOCG deposits.

Experimental sulphidation of magnetite and pyrrhotite reveal that reaction textures and the nature of the reaction products are controlled primarily by non-equilibrium processes (e.g., kinetics of dissolution and reprecipitation). In systems containing Bi(III) and Au(I) in solution together with pyrrhotite, pyrrhotite did not scavenge Au at temperatures lower than the Au(s)-Bi(s) eutectic, but a Au-rich metallic Bi melt precipitated at higher temperatures. The Bi-melt precipitation was coupled with the topotactic replacement of pyrrhotite by magnetite.

These new experimental results reveal a wealth of complexity in fluid-mediated mineral replacement textures, which are governed by a complex interplay between processes such as mineral dissolution, nucleation and growth of new phases, evolving reaction-generated porosity and/or fracturing, or competition with solid-state diffusion.

Occurrence of tellurides in the Stavelot Massif, Belgium

Hatert F*, Baijot M, Dal Bo F

University of Liège, Belgium *fhatert@ulg.ac.be

The Stavelot Massif, Belgium, is a large massif of Cambro-Ordovician metasediments (ca. 100 x 40 km), surrounded by discordant Lower Devonian conglomerates. Tellurides were reported in two localities: (i) in sulphide-bearing quartz veins cross-cutting chloritoid-bearing schists of Ordovician age in the Salm syncline, and (ii) in quartz veins cross-cutting a granodiorite mineralised in molybdenite, chalcopyrite, marcasite and pyrrhotite, outcropping at Herzogenhügel, close to the Helle valley.

Copper sulphides, occurring in the quartz veins from the Salm syncline, show petrographic textures which were investigated in detail by Hatert [1, 2, 3]. Primary assemblages mainly contain bornite, chalcopyrite, and chalcocite, whereas secondary sulphides are djurleite, digenite, anilite, spionkopite, yarrowite, and covellite. Tellurides occur as minute inclusions in bornite and chalcocite, frequently showing myrmekitic textures indicating a syncrystallization of tellurides and primary sulphides. Identified tellurides are native tellurium, altaite, melonite, and tellurobismuthite. Inclusions of galena, cobaltite, and wittichenite were also observed in bornite.

In the quartz veins from the Helle valley, tellurides occur in close association with galena, marcasite, chalcopyrite, molybdenite, and pyrrhotite. These minerals form tiny black metallic grains reaching 2-3 mm in diameter, included in the quartz veins. Under the ore microscope, beautiful myrmekitic textures were observed. Identified tellurides are joséite-B, aleksite, benjaminite, hessite, as well as an unidentified telluride.

All tellurides were examined under the ore microscope, to observe their petrographic textures. They were analysed with an electron-microprobe, to determine their chemical compositions. These compositions fit very well with the ideal formulae of these tellurides, except for the unidentified telluride from the Helle valley, which shows a composition between those of pilsenite and tsumoite. This mineral certainly corresponds to a new species.

In the Helle valley, tellurides are of magmatic origin, and crystallized during the formation of the quartz veins cross-cutting the schists hosting the granodiorite intrusion. In the Salm valley, tellurides formed during the crystallization of primary sulphides, shortly after the peak of Variscan metamorphism that reached 360-420°C / 2 kbar in this area. The occurrence of tellurium-bearing minerals in the Salm valley is due to the presence of coticule and pseudocoticule in these rocks, for which a hydrothermal origin is now clearly established [4].

[1] Hatert F. (1996). *Etude minéralogique préliminaire de quelques sulfures du Massif de Stavelot*. Unpublished Master thesis, University of Liège.

[2] Hatert F. (2003). Occurrence of sulphides on the bornite-idaite join from Vielsalm, Stavelot Massif, Belgium. *European Journal of Mineralogy*, 15, 1063-1068.

[3] Hatert F. (2005). Transformation sequences of the copper sulfides from Vielsalm, Stavelot Massif, Belgium. *Canadian Mineralogist*, 43, 623-635.

[4] Baijot M., Hatert F. and Philippo S. (2012). Mineralogy and geochemistry of phosphates and silicates in the Sapucaia pegmatite, Minas Gerais, Brazil: genetical implications. *Canadian Mineralogist*, 50, 1531-1554.

Formation of micrometer-sized stoichiometric mackinawite in cold-seep sediments offshore south western Taiwan

Huang K[1*], Chen C[1], Horng C[2], Wong Y[3], Huang A[1], Jiang W[1]

1 - Department of Earth Sciences, National Cheng Kung University, Tainan, Taiwan *kochunh@hotmail.com 2 - Institute of Earth Sciences, Academia Sinica, Taipei, Taiwan 3 - Central Geological Survey, MOEA, New Taipei City, Taiwan

Mackinawite is a widespread iron-monosulfide mineral in low-temperature aqueous systems and often occurs as one of the principal constituents of acid volatile sulfides (AVS) in marine sediments. However, direct observations and compositional analyses of the mineral from marine sediments are scarce due to its nanoparticulate nature. A rare occurrence of micrometer-sized mackinawite crystals in marine sediments was discovered in millimeter-sized iron-sulfide nodules from a cold-seep site (MD178-10-3292) at the southeastern end of Good Weather Ridge offshore southwestern Taiwan.

The mackinawite as characterized with field-emission scanning electron microscopy, X-ray energy-dispersive spectroscopy (EDS), and electron backscatter diffraction techniques, has a Fe/S molar ratio of 0.98 ± 0.01 based on 23 EDS analyses with totals in the range of 98.03 to 99.44 wt%. It occurs within iron-sulfide nodules as disseminated bipyramid crystals in pore spaces among detrital silicate grains or as chain-like aggregates of bipyramid crystals that intervene between or enclose phyllosilicate layers. The mackinawite crystals have sizes ranging from sub-micrometers to *ca.* 2 µm. Other constituents of the iron sulfide-rich nodules include oxidized AVS phases and pyrrhotite which has a Fe/S molar ratio of 0.88 ± 0.01 approximate to the ideal Fe_7S_8 composition of a monoclinic pyrrhotite. The pyrrhotite forms platy crystals sub-micrometers to several micrometers in thickness and exhibits complex and intimate growth relationships with mackinawite including complete or partial inclusion of mackinawite crystals and overgrowth or cross-cutting by mackinawite crystals. Interstratification of pyrrhotite crystals and phyllosilicate layers are common. Crystallization of pyrrhotite on the surface or in the cavities of iron-sulfide nodules was identified as well.

The Good Weather Ridge mackinawite forms the largest crystals ever reported for mackinawite formed in diagenetic marine environments or from low-temperature synthetic experiments and appears to be stoichiometric FeS with no other metals detected. Mackinawite is thermodynamically metastable and has often been considered transitional in dynamically changing marine sediments. The iron-sulfide (AVS) nodules remained in anoxic sediments under the influence of high methane fluids could have provided microenvironments with relatively stable supplies of high dissolved iron and sulfide concentrations kinetically favorable for the growth of "large" and stoichiometric mackinawite crystals and for the formation of authigenic pyrrhotite which has also been rarely reported to occur in normal marine sediments.

LA-ICPMS investigation of base and precious metal contents in rock-bearing sulfides from the Troodos Ophiolite, Cyprus: implications for the cycle of metals during hydrothermal alteration of oceanic crust

Jégo S[*], Pichavant M, Coelho G, Ramboz C, Sizaret S, Arbaret L, Branquet Y

ISTO-Université d'Orléans-BRGM *sebastien.jego@univ-orleans.fr

The Troodos ophiolite in Cyprus, formed in a Cretaceous (92 Ma) supra-subduction zone setting, is considered to be one of the best-preserved ophiolite complexes in the world. This ophiolite hosts several dozen Volcanogenic Massive Sulfide (VMS) deposits that are up to ~20 Mt in size and were exploited for both sulfur and base metals. VMS deposits have been shown to originate through leaching of metals during hydrothermal alteration of the sheeted dike complex. A recent study [1], has performed mass balance calculations by considering the protolith composition and the secondary mineral assemblages, and thus was able to quantitatively constrain the release of base metals from the altered sheeted dikes. These authors report bulk metal contents of basaltic andesite glass protoliths and variably altered facies rocks from the epidosite zone of the Troodos ophiolite, and suggest that Cu was totally lost during the early stages of alteration owing to complete breakdown of igneous sulfides originally present in the protoliths, whereas the release of other base metals (Ni, Zn, Mn, Co) towards mineralizing fluids was controlled by the secondary mineral assemblage, i.e., the relative abundance of epidote and chlorite ± amphibole. This interpretation stresses the role of silicate minerals in the redistribution of metals during hydrothermal alteration of the sheeted dike complex, and contrasts with the common assumption that accessory phases, such as sulfides, control base metal concentrations within mineralizing fluids in VMS systems.

Here we propose to test this hypothesis by providing measurements of the metal contents of sulfide minerals contained in various lithologies from the Troodos ophiolite. We report laser-ablation ICPMS analyses of 14 base and precious metals (Ti, Cr, Mn, Co, Ni, Cu, Zn, Zr, Mo, Ag, W, Pt, Au, and Pb) in sulfides present in samples representative of different stratigraphic levels and chronological stages of the hydrothermal alteration within the ophiolite complex. Preliminary results show a large variability of metal concentration and behavior depending on the lithology. Igneous sulfides present in least-altered metabasalts from the upper part of the crust are notably enriched in Co, Ti, Cu, Pb, Mn and Ag. They likely contain most of the bulk metal budget of the primary lavas. Importantly, numerous sulfides are still preserved in the epidotized sheeted dike complex, and remain enriched in Co, Ti, Pb, Mn (while Cu and Ag appear to have been remobilized). The sulfide-bearing quartz veins corresponding to the discharge upwelling of hydrothermal fluids show very low metal concentrations, with the exception of Ni, Pb and Cu. Finally, the massive sulfide deposits are made of Cu-, Zn-, and Co-rich pyrite and Pb-, Mo-, Zn- (and Ti-) rich chalcopyrite. These observations suggest that sulfides may have a significant role in controlling the progressive release of some metals during the different steps of hydrothermal alteration, and need to be considered in conjunction with the secondary silicate minerals.

[1] Jowitt S.M. *et al.* (2012). *J. Geochem. Explor.*, 118, 47-59.

Mineralogical and geochemical significance of fahlerz in late Cretaceous volcanogenic massive sulfide (VMS) deposits of eastern Pontides (NE Turkey)

Ciftci E

Istanbul Technical University. eciftci@itu.edu.tr

The Eastern Pontide Tectonic Belt (Notheastern Turkey), a paleoarc environment analogous to the Green Tuff Belt of Japan, is host to a significant number of volcanogenic massive sulfide deposits of Kuroko-type in broad sense. Due mainly to similarities in major characteristics including geological settings, host-rock lithology, ore mineral paragenesis, element contents, sulfur and lead isotope characteristics, VMS deposits of the region are considered as sister deposits. Sulfosalts occur mainly in the form of tetrahedrite and tennantite occur in Stage-II mineral assemblage following sphalerite and galena formation replacing earlier phases. Extensive ore microscopy and electron microprobe analyses (EPMA) indicated that tetrahedrite occurs mainly with black and/or semi-black ore dominating deposits whereas tennantite occurs in yellow ore dominating deposits. Tennantite is part of the ore paragenesis in the major deposits including Irsahan, Kuvarshan, Murgul, Cayeli, Lahanos, and Kankoy. Koprubasi, İstala and Harköy are the deposits where tetrahedrite prevails in the mineral paragenesis. Tetrahedrites contain significant amounts of silver, whereas bornite is the major host of silver in tennantite dominating deposits. Bismuth, mercury, and tellurium may reach significant levels in both tennantite and tetrahedrite.

Paragenetic studies at Bou-Azzer district: the key for understanding mineralizing processes

Fanlo I[1*], Subias I[1], Gervilla F[2], Colás V[1], Lázaro M[1], Lasobras E[1]

1 - Dept. Earth Sciences, University of Zaragoza *fanlo@unizar.es 2 - Dept. of Mineralogy and Petrology. University of Granada

The Bou Azzer mining district, worked since 1928, generates 4-8% of the annual world cobalt output. The district comprises more than 60 orebodies, all of which are spatially associated with serpentinites of a Neoproterozoic ophiolite sequence. The orebodies vary in morphology and size depending on their position relative to serpentinite massif [1]: lodes, veins and stocks along subvertical faults, which constitute the contacts between serpentinite and adjacent rocks or flat lenses and complex shells along subhorizontal tops of serpentinite massifs directly covered by the Ediacaran ignimbrites. From west to east, the deposits being studied represent different types of mineralization: the Aghbar deposit is a complex shell, the Tamdrost deposit is a flat lens, and the Aït-Ahmane deposit occurs as stocks located on small offsets of the serpentinite-gabbro contacts. The mineral assemblages display noticeable variations depending on the deposit and the type of mineralization. At the Aghbar deposit, three different ore types formed along a three-stage depositional history: Ni ore, Co-Fe ore and a late Cu-sulfides ore. The Tamdrost deposit is characterized by a four-stage depositional history with an early crystallization of Co-triarsenides and diarsenides, followed by Ni-arsenides and diarsenides and Co-diarsenides and triarsenides. The third stage consisted of Ni-Co sulfarsenides and, finally, Cu-sulfides. The Aït-Ahmane deposit is also marked by a four-stage depositional history, although somewhat different to that recognized at the Tamdrost deposit. Co-triarsenides and calcite during stage I, followed by Ni-diarsenides, Ni-Co-Fe- diarsenides, Ni- arsenides and sulfarsenides (stage II). Stage III was characterized by the precipitation of Co-Ni triarsenides and during stage IV Co-Fe diarsenides, sulfarsenides, Co-Fe triarsenides and diarsenides were formed. As a whole, there are significant differences in the proportion of Ni ore minerals, which increase eastward, coeval with an increase in sulfur fugacity and abundance of sulfarsenides. Moreover, the eastern deposit (Aït-Ahmane) contains the highest proportion of gold (grains up to 20 mm) related with sulfarsenides. The aforementioned paragenesis allows the constraint of the formation conditions using the compositional field of arsenides determined by Hem and Makovicky [2] and Hem [3]. Thus, the first triarsenides from the three deposits reveals temperature formations fitting well the experimental field at 650ºC for the first stage, and between 500-400ºC for the latest one.

[1] Leblanc M. (1986). Co-Ni arsenide deposits, with accessory gold, in ultramafic rocks from Morocco. *Can. J. Earth Sci*., 23, 1592-1602.

[2] Hem S.R. and Makovicky E. (2004). The system Fe-co-Ni-As-S. II. Phase relation in the (Fe,Co,Ni)$As_{1.5}S_{0.5}$ section at 650ºC and 500ºC. *Can. Mineral*., 42, 63-86.

[3] Hem S.R. (2006). Solid solution in the Fe-Co-Ni-As-S system. *Chem. Geol.*, 225, 291-303.

Characterisation of Main Mineralized Zone open pit and underground nickel bearing materials

Madingoana I*, Mulaba A

University of Johannesburg *ike.madingoana@gmail.com

A South African nickel ore mine has installed a Blue Cube MQi in-line real-time mineral analyser in the flotation final concentrate line, in order to provide grade data in real time. The unit applies the concept of diffuse reflectance spectroscopy (DFS) and is calibrated by linking optical data with the material grades.

Knowledge of the plant feed and concentrate material composition is of fundamental importance in understanding and monitoring the performance of the unit. The characterisation of the open pit, underground and the flotation concentrate will be established by assessing the mineralogical, chemical and physical properties of the materials. A combination of X-ray Diffraction (XRD), X-ray fluorescence (XRF) and Mossbauer spectroscopy will be used in addition to inductively coupled plasma optical emission spectrometer (ICP-EOS) for characterisation.

Mineralogy and chemical composition of the Ag-Pb-Zn-Cu-Sb metallic association at the distal-disseminated gold deposit of Arcos (NW Spain)

Martínez Abad I*, Cepedal A, Arias D

University of Oviedo *iker@geol.uniovi.es

The Arcos deposit is located in the NW of Spain, within the West Asturian Leonese Zone [1] of the Iberian Massif. The deposit is included in the Vilalba Gold District and has been classified as a Au-As (Ag-Pb-Zn-Cu-Sb) distal-disseminated deposit [2]. The sedimentary rocks at Arcos consist of quartzites, green, black and calcareous slates and impure limestone (Lower Cambrian) that were folded, thrusted, faulted and metamorphosed during the Variscan Orogeny [3]. During the Late-Variscan, the area was affected by subvertical N-S trending fault systems through which several rhyolitic dikes intruded. The mineralization at Arcos, which is spatially related to the rhyolites, took place in two stages: 1) Au-As; 2) Ag-Pb-Zn-Cu-Sb. The first Au-As stage consists of fine-grained gold-bearing pyrite and arsenopyrite, forming disseminations in phyllic altered, dolomitized and silicified rocks, as well as filling veins together with quartz and calcite [4]. The aim of this work is to describe the mineralogy of the Ag-Pb-Zn-Cu-Sb second stage of mineralization of Arcos, as well as the chemical composition of their most representative ore minerals.

The second mineralization stage consists of base-metal sulfides, sulfosalts and gangue minerals. These minerals form a second stage of vein filling, as well as the infilling of cavities or cracks affecting the minerals of the first stage, often replacing them. Moreover, they form individual veinlets that crosscut hydrothermally altered host-rocks and rhyolite dykes and unaltered rocks located just beside them. The veinlets are normally irregular in shape and rarely exceed 5 mm in thickness.

The second-stage gangue minerals consist of Ca-Mg-Fe carbonates (calcite, dolomite, ankerite and siderite) and quartz, with locally abundant fluorite and chlorite. The metallic assemblage includes sphalerite, tetrahedrite, bournonite, boulangerite, chalcopyrite and galena with jamesonite, pyrrhotite, Ni-Co-Fe sulfides (ulmanite, gersdorfite, cobaltite), electrum, izoklakeite and arsenopyrite as accessory minerals. Two different sphalerites were found: an Fe-poor sphalerite (2.2 to 2.7 wt.% in Fe) as subhedral grains, sometimes coarse (up to 1mm), filling individual veinlets that crosscut the hydrothermally altered host-rocks and rhyolite dykes, and an Fe-rich sphalerite (5.9 to 6.7 wt.% in Fe) that occurs as a later infill, often replacing Fe-rich carbonates, along with chalcopyrite, pyrrhotite and galena. The tetrahedrite shows variable Zn contents (from 3 to 8 wt.%), and up to 4.3 wt% of Ag. Other Ag-bearing minerals are electrum with contents ranging from 25.8 to 27.7 wt% Ag, while galena only shows traces (up to 0.3 wt%). Fluorite, when it occurs, shows needles of boulangerite as inclusions. Low-salinity aqueous carbonic fluid inclusions measured in these crystals show minimum conditions of T from 210 to 242 ºC, at pressures up to 600 bar, this representing the lower temperature limit of the Arcos deposit formation.

[1] Julivert M., Fontboté J. M., Ribeiro A. and Conde L.N. (1972). Mapa Tectónico de la Península Ibérica y Baleares. Inst. Geol. Min. Esp.

[2] Martínez-Abad I., Cepedal A., Arias D. and Martín-Izard A. (2011). The Villalba gold district (Lugo, NW of Spain) In: Let's Talk Ore Deposits. (E. Barra, M. Reich, E. Campos and F. Tornos, eds.). Ediciones Universidad Católica del Norte, Antofagasta, Chile, 550-552.

[3] Martínez Catalán J.R., Pérez Estaún A., Bastida F., Pulgar J.A., Marcos A. (1990). West Asturian-Leonese Zone. Structure. In: Dallmeyer, R.D. and Martínez García, E. (eds.). Pre-Mesozoic Geology of Iberia. Springer-Verlag, 103-114.

[4] Martínez-Abad I., Cepedal A., Arias D., Martín-Izard A., Roberts S. (2011). Invisible gold at the Arcos Deposit (Lugo, NW of Spain) In: Let's Talk Ore Deposits. (E. Barra, M. Reich, E. Campos and F. Tornos, Eds.). Ediciones Universidad Católica del Norte, Antofagasta, Chile, 553-555.

Pyrites in modern and paleohydrothermal systems of Kamchatka

Okrugin V[1*], Yablokova D[2], Etschmann B[3], Brugger J[3]

1 - Institute of Volcanology and Seismology FED RAS, Vitus Bering Kamchatka State University *okrugin74@gmail.com 2 - FED RAS, Vitus Bering Kamchatka State University 3 - Monash University

Kamchatka is an area of modern (MHS) and paleohydrothermal (PHS) ore-forming activity. It contains more than 75% of Russian thermal reserves and mineral waters. There are more than 264 modern hydrothermal systems (MHS), and hot springs are localized in volcanic belts of various ages. Hydrothermal activity began 80-90 million years ago and continues today. As a result of paleohydrothermal activity (PHS) numerous volcanic hydrothermal mineral deposits were created. In terms of economic significance, MHS are used for producing geothermal electricity and for heating, while the ore deposits associated with PHS have recently started to be mined, with two new mines having just produced the first 10,000 kg of gold. Pyrites are widespread in many of the modern hydrothermal systems, and in different types of ores and associated alteration.

Analytical scanning electron microscopy coupled with energy-dispersive X-ray spectral analyses were applied to studying the micro-morphology and chemical composition of pyrites. 12 PHS and 12 MHS samples were studied. PHS and MHS pyrites have various forms from idiomorphic crystals to framboides and spherolites. They contain impurities including As, Se, Te, Sb, Cu, Pb, Bi, Mn, Zn, with concentrations varying from 0.5-1.0 to 5-10 wt%.

The Kireunsky and Dvukhjyurtochny MHS deposits (Northern Kamchatka) contain sulphidic spherolites ranging in size from hundreds of µm to 5 000 of µm, with a characteristically heterogeneous distribution of As, Hg and Sb. The pyrites from Vilyuchinsky and Mutnovsky MHS (the Southern Kamchatka) contain a heterogeneous distribution of As, Mn, Au, Hg.

PHS pyrites (epithermal gold-silver and gold-base metal ore deposits) have the greatest variety of textures, mineral associations and chemical compositions. Pyrites from most of the gold-silver deposits have elevated concentrations of As. In pyrites of base metall ores there are the microzones enriched with Pb, Bi, Zn, Mn, Zn (0.5-2.5 wt%). Pyrites from the Te- and Se-containing ores commonly display zones enriched in Te and Se (3-5 wt%). In pyrites from the Aginskoe Au-Te-deposit there are microzones with up to 2-3% enrichment of copper.

Pyrites play a role as indicators of mineral-forming hydrothermal processes. Kamchatka offers outstanding opportunities to study the formation of sulphide minerals in both modern hydrothermal environments and in recent ore deposits evolving in these systems.

Sulphur isotopic signature at the Bou-Azzer mining district, Morocco – preliminary report on the origin of sulphur

Subias I[1*], Fanlo I[1], Gervilla F[2]

1 - Dept. Earth Sciences, University of Zaragoza *isubias@unizar.es
2 - Dept. Mineralogy and Petrology, University of Granada

The Bou Azzer mining district, one of the larger cobalt districts in the world, is located in the central part of the Anti-Atlas Mountains of southern Morocco. The deposits are located in the Bou Azzer inlier, a Proterozoic block occurring between the South Atlas Fault and the Central Atlas Fault, and probably representing an accretionary mélange sutured to the northern edge of the West African Craton. Sulphur isotope compositions were determined for di-, tri-arsenide, sulfarsenide and sulfide minerals from different depositional stages, and encompassing all morphological types. Analyses were performed at the University of Salamanca, Spain. Sulfur isotopic ratios were obtained by pyrolysis on an Elemental Analyzer (EurovectorEA3000) coupled on line with an ISOPRIME (Micromass) continuous flow mass spectrometer and by SO_2 liberated by standard stable isotopic extraction techniques [1], which was analyzed using a dedicated SIRA-II (VGIsogas) dual inlet mass-spectrometer. Due to the small SO_2 quantities produced, we included V_2O_5 to favor combustion in both methods. Results are reported in the standard delta per mil notation relative to Canyon Diablo Troilite (CDT). Replicate analyses of reference standards gave an average reproducibility of ±0.3. The heaviest δ34S values were obtained in ores from the westernmost deposit (Aghbar) where δ34S ranges from -16.0 to +9.5‰ (mean +2.0‰). The lightest δ34S values were found in ores of the easternmost deposit (Aït-Ahmane) where δ34S varies from -22.5 to -3.3‰ (mean -9.2‰). The Tamdrost deposit, located in the center of the district, show intermediate values with δ34S ranging between -1.8 and +3.6‰ (mean +0.7‰). There is thus a systematic decrease in sulfur isotope values eastwards.

Although determination of the composition of local sulfur reservoirs is currently underway, the origin of sulfur can be interpreted with reference to known regional reservoirs [2] as the result of mixing between heavy and a light δ34S components. Light sulfur could be leached from the surrounding black shale basement rocks (δ34S=-38‰) while heavy sulfur could be leached from rhyolitic domes (δ34S=-7 to -2‰). The heavy source had a stronger contribution in the western part of the district (Aghbar) and the lighter source in the eastern part (Aït-Ahmane). The central part of the district, typified by Tamdrost, reflects an intermediate situation.

[1] Coleman, M.L., Moore, M.P., 1978. Direct reduction of sulfates to sulfur dioxide for isotopic analysis. *Anal. Chem*., 50, 1594-1595.
[2] Levresse, G., Cheilletz, A., Gasquet, D., Reisberg, L., Deloule, E., Narty, B., Kyser, K. (2007). Osmium, sulphur, and helium isotopic results from the giant Neoproterozoic epithermal Imiter silver deposit, Morocco: evidence for a mantle source. *Chemical Geology*, 207, 59-79.

ESR, ^{226}Ra-^{210}Pb, and ^{228}Ra-^{228}Th dating of barite in sea-floor hydrothermal sulfide deposits in the Okinawa Trough

Toyoda S[1*], Fujiwara T[1], Uchida A[1], Ishibashi J[2], Nakai S[3], Takamasa A[4]

1 - Okayama University of Science *toyoda@dap.ous.ac.jp 2 - Kyusyu University, Fukuoka 3 - University of Tokyo 4 - National Institute of Radiological Sciences

The evolution of sea-floor hydrothermal fields is one of the important scientific issues as they accommodate ores and also biological communities sustained by the chemicals supplied by the hydrothermal activity. Dating methods have been employed for hydrothermal sulfide deposits, such as the U-Th disequilibrium method and ^{226}Ra-^{210}Pb and ^{228}Ra-^{228}Th method.

In the present paper, ESR (electron spin resonance) dating method for barite is developed and applied to those crystals extracted from hydrothermal sulfide deposits taken at sea-floor hydrothermal fields in the Okinawa Trough in comparison with ^{226}Ra-^{210}Pb, and ^{228}Ra-^{228}Th methods.

The obtained ESR ages range from 4.1 to 16000 years. It was found that Yoron Hole field is the youngest, then, Daiyon-Yonaguni Knoll field, Hatoma Knoll field, being nearly equal to Iheya North Knoll field.

For the youngest group of samples of several years, ^{226}Ra-^{210}Pb, and ^{228}Ra-^{228}Th ages are consistent with ESR ages. However, for those in the range of several tens to one hundred years, the ESR ages are largest and the ^{228}Ra-^{228}Th ages are smallest while the ^{226}Ra-^{210}Pb ages are in-between. This would be due to several hydrothermal activities to form the sulfide deposits where the dating method using the radioactive parent nuclei with shorter half-lives will give younger ages as they decay while ESR ages will give "averaged" ages.

Pb-Bi-(Ag)-sulphosalts from Nagybörzsöny, Hungary

Zajzon N[1*], Szakáll S[1], Kristály F[1], Hartai É[1], Fehér B[2]

1 - Institute of Mineralogy and Geology, University of Miskolc, Miskolc, Hungary *nzajzon@uni-miskolc.hu 2 - Herman Otto Museum, Miskolc, Hungary

The Nagybörzsöny mineralized area is located about 50 km NNW of Budapest, Hungary, in the central part of the Börzsöny Mountains. Mining of silver and gold at Nagybörzsöny started in the 14th Century. Although the production was not high, mining activity in the area lasted - with stoppages and restarts - for about 600 years. The Börzsöny Mts. is basically built up by a Middle Miocene andesitic stratovolcanic sequence. In the Nagybörzsöny ore deposit bismuth, lead, zinc, arsenic, with less tungsten, gold, silver and tellurium are found. Minerals are bismuthinite, arsenopyrite, bismuth, ikunolite, gold, ferberite/hübnerite, Pb-Bi-(Ag)-sulphosalts and Bi-chalcogenides (joséite-A, ingodite). The Rózsa Hill mineralization occurs in a breccia pipe structure. The location was re-investigated by us as part of an ongoing project.

Cosalite and lillianite with up to 5 wt% Ag and 1 wt% Se are the most common sulphosalts in the mineralization (Figure 1). The lillianite homologue eskimoite has lath-like crystals closely intergrown with pavonite. There is a wide range of Bi-for-Pb substitution in the pavonite, the Pb content varies between 7-9 wt% and additional selenium (average 1.07 wt%). The cannizzarite has curvy-banded lath like crystals, 0.5-1.5 mm in size. It commonly contains selenium between 0.06-1.28 wt%, and sometimes tellurium (up to 0.33 wt%). This sulphosalt association includes cannizzarite, bismuthinite, bismuth, cosalite, lillianite, ikunolite and ingodite.

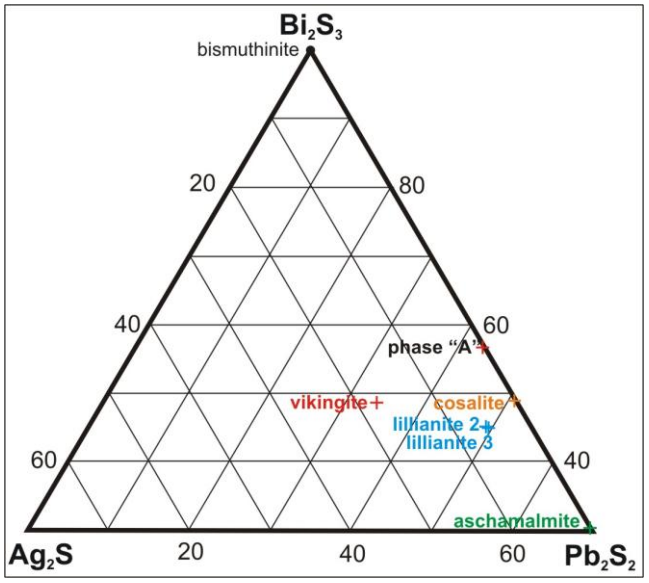

Figure 1: EPMA analyses of some sulphosalts with Ag content.

Acknowledgement: Research was carried out as part of the TÁMOP-4.2.2.A-11/1/ KONV -2012-0005 project as a work of Center of Excellence of Sustainable Resource Management, in the framework of the New Széchenyi Plan. The realization of this project is supported by the European Union, co-financed by the European Social Fund.

Aikinite-bismuthinite series sulphosalts from Pátka, Velence Hills, Hungary

Zajzon N*, Szakáll S, Kristály F, Mádai F

1 - Institute of Mineralogy and Geology, University of Miskolc, Miskolc, Hungary
*nzajzon@uni-miskolc.hu

At Pátka, Szűzvár-mine, a fluorite-quartz-polymetallic hydrothermal mineralization is located, which was exploited for fluorite and galena-sphalerite between 1949 and 1973. The deposit is vein type with major quartz gangue, and relates to intrusion of the 291-271 Ma Velence Granite. The mineralization was recently reinvestigated, as part of a new ongoing project on critical elements/minerals. The dominant sulphides are galena and sphalerite with subordinate chalcopyrite and tetrahedrite-tennantite. Digenite and covelline were formed from chalcopyrite in the cementation zone. The mineralization is strongly tectonised and affected by oxidation processes which altered the sulphides to various secondary minerals as the dominant pyromorphite and cerussite, some APS-minerals, also some malachite, cuprite, azurite, rosasite, smithsonite and oxyplumboroméite. The sulphosalts are the rarest minerals in the paragenesis. A large number of Bi-Pb-Cu-sulphosalts were identified by EPMA bismuthinite-pekoite, gladite, paarite, krupkaite, lindströmite, emilite, hammarite and friedrichite were found in quartz with scattered chalcopyrite. The sulphosalts have 10-100 µm grain size and max 10x30 µm crystal size enclosed in quartz. They are inhomogenous, built up from different Bi-Pb-Cu-sulphosalts, which were formed as exsolution members. Some of the larger grains were subjected to powder XRD and the mixtures of the above species were also identified. Ore microscopy was applied to observe the appearence of the different assemblages.

The shift from the ideal compositions (Figure 1) towards Pb (visible among compositions with higher Pb-Cu content) is interpreted in terms of galena exsolution lamellae with size below the resolution of the microprobe used.

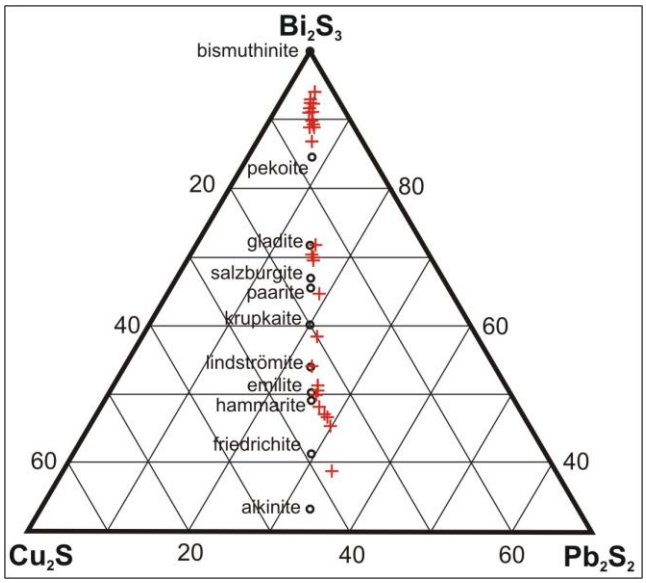

Figure 1: EPMA analyses of Bi-Pb-Cu-sulphosalts

Acknowledgement: The described work was carried out as part of the TÁMOP-4.2.2.A-11/1/KONV -2012-0005 project as a work of Center of Excellence of Sustainable Resource Management, in the framework of the New Széchenyi Plan. The realization of this project is supported by the European Union, co-financed by the European Social Fund.

Pressure-induced intrusion and supra-molecular organization of guest molecules in FER-type zeolites: a combined experimental and theoretical study

Arletti R[1*], Quartieri S[2], Vezzalini M[3], Fois E[4], Tabacchi G[4]

1 - University of Torino - NIS Torino *rossella.arletti@unito.it 2 - University of Messina, Italy, Department of Physics and Earth Sciences 3 - University of Modena and Reggio Emilia, Italy 4 - University of Insubria

The response to pressure of a synthetic all-silica ferrierite (Si-FER) and of a natural ferrierite from Monastir (Sardinia, Italy) (Mon-FER, $Na_{0.56}K_{1.19}Mg_{2.02}Ca_{0.52}Sr_{0.14}$)($Al_{6.89}Si_{29.04}$)$O_{72}$•17.86$H_2O$) is here investigated combining HP synchrotron XRPD experiments and molecular dynamics simulations. The experiments were carried out by using penetrating (methanol:ethanol:water 16:3:1, m.e.w.; ethanol:water 1:3, e.w.) and non-penetrating (silicone oil, s.o.) pressure transmitting media (PTM). In Si-FER compressed in e.w., both water (w.) and ethanol molecules (e.) enter the pore system even at 0.2 GPa. The structural refinement of the data collected at 0.8 GPa reveals 8 w. and 4 e. molecules in the 10- and 6-membered ring channels, in tight agreement with the results of MD simulations. In Si-FER compressed at 0.2 GPa in m.e.w., only water molecules penetrate the 10-membered ring channels (15 per u.c.), organized in chains running along the channel axis. The interactions among the guest species and the framework oxygen atoms are very weak, due to the hydrophobicity of the framework. Upon decompression, the intruded extra-molecules are not completely released, so giving rise to new materials with different extra-framework contents. The results obtained for Si-FER compressed in m.e.w. and s.o. were compared to those obtained for Mon-FER, demonstrating that the zeolite composition and the PTM strongly influence the overall elastic parameters of the investigated samples. Specifically, Mon-FER shows a much higher rigidy than Si-FER in both media, due to the stiffening effect of the numerous extraframework species present in the natural sample. The higher rigidity of Si-FER in m.e.w. with respect to s.o. can be explained by the penetration, in the former case, of the PTM molecules, which contribute to stiffen the framework.

Dehydration behavior and pressure-induced structural modifications of zeolite-like cavansite and pentagonite

Danisi R

University of Bern. rosamicaela.danisi@libero.it

Cavansite and pentagonite, dimorphs of $Ca(VO)(Si_4O_{10})\cdot 4H_2O$, are the only natural known examples of microporous vanadosilicates. These vanadosilicate frameworks have similar properties and applications as traditional zeolite structures. However, the structural changes of these microporous materials under non-ambient conditions are not well known. In this light, the investigation of the thermo-elastic stability of vanadosilicates is crucial in the characterization of their functionality for technical applications.

The dehydration behavior of cavansite (space group *Pnma*, a = 9.6329(2), b = 13.6606(2), c = 9.7949(2) Å, V = 1288.92(4) Å^3]) and pentagonite (space group $Ccm2_1$, a = 10.3708(2), b = 14.0643(2), c = 8.97810(10) Å, V = 1309.53(3) Å^3) was studied by means of temperature-dependent single crystal X-ray diffraction using an in-house designed nitrogen stream heater. The cavansite framework appears to be rather stiff, while pentagonite undergoes phase transitions to a monoclinic structure at 175 °C (*Pn*, 1 H_2O pfu) and to an orthorhombic structure at 225 °C ($Pna2_1$, 0 H_2O pfu). Between ambient conditions (4 H_2O pfu) and 225 °C (0 H_2O pfu) the normalized unit-cell volume of pentagonite decreased by 21% whereas in cavansite the volume change between room temperature (4 H_2O pfu) and 350 °C (1 H_2O pfu) was only 10%. After removal of the last H_2O molecule at 400 °C, the cavansite structure collapsed and became amorphous. In contrast, anhydrous pentagonite was stable at least up to 600 °C. A new bond between Ca and O at the opposite channel wall prevents collapse ofthe pentagonite structure. This is possible due to the higher flexibility of the pentagonite framework compared to cavansite, allowing compression of the channels. Thus, the limiting Ca coordination coupled with the different flexibility of the two frameworks seems to be responsible for either phase transitions or structural collapse in pentagonite and cavansite, respectively.

The different flexibility of the two frameworks is also evident tracking the pressure-induced structural modifications up to ~ 8 GPa by means of *in-situ* synchrotron X-ray powder diffraction analysis with a diamond anvil cell under hydrostatic conditions in the presence of penetrating (methanol:ethanol:water 16:3:1, m.e.w.) and non-penetrating (silicone oil, s.o.) pressure transmitting mediums. The volume contraction in cavansite is 1.75% GPa^{-1} in m.e.w. and 1.68% GPa^{-1} in s.o. The compression is stronger along **b** perpendicular to the tetrahedral layers. The response to pressure of pentagonite strongly depends on the size of molecules in the pressure-transmitting medium. The volume contraction in m.e.w. is 0.60% GPa^{-1} and 1.30% GPa^{-1} in s.o. We assume that the unusual low compressibility in m.e.w. is due to pressure induced hydration (PIH). Pentagonite undergoes phase transitions at 2.96(6) GPa in m.e.w. and to 1.71(3) GPa in s.o, while no symmetry change is observed as a function of pressure in cavansite.

A new type of water in natural mayenites – a spectroscopic research

Dulski M[1*], Gfeller F[2], Marzec K[3], Kusz J[1], Armbruster T[2], Galuskina I[1], Bailau R[1], Galuskin E[1]

1 - University of Silesia *mdulski@us.edu.pl 2 - University of Bern 3 - Jagiellonian University

Synthetic mayenite with the crystal chemical formula $Ca_{12}Al_{14}O_{33}$ may be used as a high-temperature air water vapour sensor [1, 2]. The water bonding capabilities are realized according to the scheme: $\{Ca_{12}Al_{14}O_{32}\}^{2+}{}_{framework}[O^{2-}[]\square_5]_{cage} + H_2O = \{Ca_{12}Al_{14}O_{32}\}^{2+}[(OH)_2\square[]_4]$ where ~1.4 wt% H_2O may be incorporated into mayenite. The hydroxylation process changes the electric properties of mayenite and the hydroxylated phase is stable up to 1100 °C. The Raman spectrum, where the OH group occupies the central position in structural cage of mayenite, is characterized by band located at 3570 cm^{-1}.

Raman and XRD single crystal studies of mayenite group minerals from pyrometamorphic rocks showed that there are two other mechanisms of water incorporation into the mayenite structure.

The first mechanism is due to a lack of OH groups at the central position in the structural cage in partially hydrated mayenite from the Eifel, Germany. The composition of this phase is expressed by the empirical formula $\{Ca_{12}Al_{14}O_{31.25}(OH)_{2.25}\}[Cl_{1.25}[]\square_{4.75}]$ where the hydroxylation process is according to the scheme: $[Cl] + \{O^{2-}\} \rightarrow [\square]_{vac} + \{3(OH)^-\}$ changing part of the Al coordination from tetrahedral to octahedral. As a result of hydroxylation, 38% of the end member $Ca_{12}Al_{14}O_{30}(OH)_6$ is observed in the composition of mayenite from Eifel. This corresponds to 1.4 wt% H_2O [3]. This type of OH group is represented by a Raman band with a maximum at 3670 cm^{-1}. The temperature-dependent experiments showed that hydrated mayenite loses a part of water at temperature higher than 350 °C according to the scheme $Ca_{12}Al_{14}O_{31.25}(OH)_{2.25}[Cl_{1.25}\square_{4.75}] \rightarrow Ca_{12}Al_{14}O_{32}[Cl_{1.25}(OH)_{0.75}\square_4] + 0.75H_2O$. The dehydroxylation leads to structural phase transition where aluminium octahedral → tetrahedral coordination takes place with reorganization of some of the OH groups to the central position in the mayenite structural cage.

The second mechanism is connected with the incorporation of a H_2O molecule of unusual geometry into the empty structural cages of F-mayenite or Cl-mayenite according to the scheme $Ca_{12}Al_{14}O_{32}[(F,Cl,OH)_2\square_4] + 4H_2O \rightarrow Ca_{12}Al_{14}O_{32}[(F,Cl,OH)_2(H_2O)_4]$. This type of water incorporation was found in two new minerals, kyuygenite $Ca_{12}Al_{14}O_{32}[Cl_2(H_2O)_4]$ and fluorkyuygenite $Ca_{12}Al_{14}O_{32}[F_2(H_2O)_4]$, described form pyrometamorphic rock from the Caucasus and Israel. The Raman spectra of these phases are characterized by broad band in the 3000-3500 cm^{-1} range which disappears above 400 °C.

[1] Nurse W. (1960). Fourth International Symposium of the Chemistry of Cement, 39.

[2] Roy D.M. and Roy R. (1960). Fourth International Symposium of the Chemistry of Cement, 307.

[3] Galuskin E.V. *et al.* (2012). *Mineralogical Magazine*, 76(3), 707-716.

Microporous mayenite $Ca_{12}Al_{14}O_{32}$ $[x^{2-}]$ and isostructural minerals

Gfeller F[1*], Galuskin E[2], Galuskina I[2], Bailau R[2], Armbruster T[1], Sharygin V[3]

1 - University of Bern *frank.gfeller@krist.unibe.ch 2 - University of Silesia 3 - Siberian Branch of the RAS

Mayenite is a mineral name as well as the hypernym of isostructural microporous synthetic Ca-aluminates which are used as catalysts, ion-conductors or clinker-phase in high-alumina cements. The mineral mayenite was first found and reported from volcanic rocks of the Ettringer Bellerberg Volcano near Mayen, Germany. The mineral was described as the natural analogue of the previously- known microporous compound $Ca_{12}Al_{14}O_{32}[O\ \#_5]$ with 32 framework oxygen and one "free" 33rd oxygen distributed statistically over six structural cages. A second occurrence has been reported from the pyro-metamorphic rocks of the Hatrurim formation, Israel. Mayenite with 2 Cl^- in the structural cages instead of O^{2-} has been described as the new mineral brearleyite from the NWA 1934 meteorite.

Re-investigation of the known natural occurrences of mayenite revealed that naturally grown mayenites do not incorporate O^{2-} as extra-framework anions but usually Cl^-, F^- and OH-groups. The true formula of mayenites from the type locality is reported as $Ca_{12}Al_{14}O_{31.24}OH_{2.28}[\#_{4.76}Cl_{1.24}]$. Thus mayenite from the type locality are in fact Cl-mayenites. Mayenites from the Hatrurim formation are fluorine bearing and have been defined as the new mineral fluormayenite $Ca_{12}Al_6Al_8O_{32}[\ \#_4F_2]$ (IMA2013-019). An analogous redefinition of mayenite from the type locality to "chlormayenite" demands discrediting the mineral brearleyite, which is identical with the material from the type locality of mayenite. The name mayenite is well established in different branches of science and should be kept for a potential mineral with the formula $Ca_{12}Al_{14}O_{32}[O\ \#_5]$ to avoid misunderstandings. As several minerals and potential new minerals isostructural with mayenite exist, we propose the mayenite supergroup. The new supergroup comprises two groups of minerals isostructural with mayenite (space group No. 220, *I*-43*d*, $a \approx 12$ Å) with the general formula $X_{12}T_{14}O_{32-X}(OH)_{3x}[W_{6-3x}]$: mayenite (oxides) and wadalite (silicates), for which the anionic charge over 6 *W* sites is -2 and -6, respectively. Currently, only minerals dominated by end-members with x = 0 and simplified formula $X_{12}T_{14}O_{32}[W_6]$, have been reported. The mayenite group includes four minerals: (1) brearleyite = "chlormayenite" $Ca_{12}Al_{14}O_{32}[Cl_2\ \#_4]$, (2) chlorkyuygenite $Ca_{12}Al_{14}O_{32}[(H_2O)_4Cl_2]$, (3) fluormayenite $Ca_{12}Al_{14}O_{32}[F_2\ \#_4]$ and (4) fluorkyuygenite $Ca_{12}Al_{14}O_{32}[(H_2O)_4F_2]$. The wadalite group comprises two mineral species, wadalite with end-member formula $Ca_{12}Al_{10}Si_4O_{32}[Cl_6]$, and eltyubyuite with end-member formula $Ca_{12}Fe^{3+}{}_{10}Si_4O_{32}[Cl_6]$.Current research on minerals and synthetic compounds indicates that minerals close to the composition of ideal end-members, such as $Ca_{12}Fe^{3+}{}_{10}Si_4O_{32}[F_6]$, $Ca_{12}Si_9Mg_5O_{32}[Cl_6]$ and $Ca_{12}Al_{14}O_{30}(OH)_6[\#_6]$, could be found in nature.

Topological and structural complexity of zeolites: quantitative evaluation

Krivovichev S

St. Petersburg State University. skrivovi@mail.ru

Zeolites are among the most complex minerals and inorganic materials. Their structural and topological complexity can be quantitatively evaluated using Shannon Information Theory [1]. Within this approach, the content of the reduced unit cell volume is considered as a message with atoms as symbols. Two atoms are considered equivalent if they belong to the same crystallographic orbit. The framework complexity is characterized by its total topological information content, $I_{G,total}$. Topological complexity parameters are calculated for the 201 zeolite structure types listed in the International Zeolite Association Zeolite Structure Database. On the basis of the proposed complexity measures, zeolite frameworks can be classified into very simple, simple, intermediate, complex, and very complex. The six most complex zeolite frameworks are [$I_{G,total}$ in bits]: SFV [19557.629], ITV [2825.097], IMF [2614.111], CLO [2413.449], and LTN [2285.985]. The six simplest zeolite frameworks are: SOD [16.529], BCT [19.020], ABW [23.020], NPO [28.529], EDI and NAB [32.603]. The sodalite-cancrinite group of zeolite frameworks can be used to investigate evolution of complexity within modular series of structurally related zeolites. The topological complexity measurements can be also be useful to investigate the evolution of complexity during crystallization and transformation of zeolites.

[1] Krivovichev S.V. (2013). *Micropor. Mesopor. Mater*., 171, 223-229.

Structural intergrowth merlinoite/phillipsite and its temperature dependent dehydration behavior: a single crystal X-ray study

Danisi R[1*], Armbruster T[1], Nagashima M[2]

1 - University of Bern *rosamicaela.danisi@libero.it 2 - Yamaguchi University

Supposed "merlinoite" crystals, $CaK_7[Al_9Si_{23}O_{64}]\cdot x\ H_2O$ from Monte Somma, Vesuvius (Italy) and $Ca_2Na_1K_5[Al_{10}Si_{22}O_{64}]$ 20 H_2O from Fosso Attici, north of Rome (Italy), represent highly twinned coherent intergrowths between merlinoite and phillipsite on a submicroscopic level. The MER and PHI frameworks of similar composition are assembled from identical tetrahedral units, though with a different connectivity. Coherent intergrowth and twinning of the two frameworks leads to $P4_2/mnm$ pseudosymmetry, which is diagnostic of the intergrowth. Under ambient conditions merlinoite has *Immm* symmetry or *I*4/*mmm* if twinned. A low symmetry model of space group $P12_1/m1$ ($a \approx 14.2$, $b \approx 14.2$, $c \approx 10$ Å, $\beta = 90°$) allows refinement and quantification of the two frameworks. Samples from Monte Somma converged to a merlinoite/phillipsite ratio of about 1/1, varying between 0.6/0.4 and 0.4/0.6 in the three studied crystals. The sample from Fosso Attici consisted of 67% merlinoite and 33% phillipsite.

Upon *in situ* dehydration to 250 °C the unit-cell volume of Monte Somma merlinoite/phillipsite displays an intermediate trend between previously studied pure merlinoite from the Khibiny massif (Russia) $NaK_{11}[Al_{12}Si_{20}O_{64}]\cdot 15H_2O$ and Ba-rich phillipsite. At 250 °C the framework of Monte Somma merlinoite shows the same characteristics of framework distortion as merlinoite from the Khibiny massif, which is in contrast with the high temperature distortion of a synthetic sample of similar composition.

The Monte Somma crystal studied by temperature dependent single crystal X-ray methods also contained a subordinate chabazite inclusion without defined structural coherency relation to the merlinoite/phillipsite framework. Thus chabazite dehydration could also be studied. Our results also emphasize how powerful area detectors are for the investigation of composite mineral aggregates by single-crystal X-ray diffraction.

European LIFE+2010 project "Zeolife – water pollution reduction and water saving using a natural zeolitite cycle". Results after the first year of experimental cultivation

Faccini B[1], Di Giuseppe D[2], Coltorti M[2], Abbondanzi F[3], Campisi T[3], Laurora A[4], Passaglia E[4], Malferrari D[4], Vezzalini M G[4*]

1 - Department of Physics and Earth Sciences, Italy 2 - University of Ferrara, Italy 3 - CRSA Med Ingegneria srl, Italy 4 - University of Modena and Reggio Emilia, Italy *mariagiovanna.vezzalini@unimore.it

The ZeoLIFE project (LIFE+10 ENV/IT/000321) was conceived to test an integrated use of zeolititic tuffs (zeolitite), aimed at: i) reducing pollutant content in livestock effluent, ii) correcting agricultural soils, and iii) economizing both irrigation water and fertilizers. Zeolites are capable of the uptake NH_4 from solutions (*e.g.*, manure) and release it gradually in cultivated soils through cationic exchange induced by humic acids of plant roots, according to the real needs of the cultures. An open-field experimentation of the integrated zeolitite cycle, for 2 year cultivation, is currently being carried out.

Chabazite-rich zeolitite from Sorano (Grosseto, Italy) was mechanically mixed with swine manure in a prototype tank. In a time span of 12-18 hours, natural zeolitite attained cationic equilibrium by subtracting a considerable amount of NH_4^+ from the swine manure by selective cationic exchange (ranging from 0.4 to 0.8 mmol of NH4/g zeolitite). NH_4-charged zeolitite was thus ready to be spread on the experimental field.

During the first year of cultivation, the experimental field was divided into 6 parcels, on average 1 hectare wide. One parcel was treated with 7 kg/m^2 of NH_4-charged zeolitite; two parcels were treated with 5 and 15 kg/m^2 of natural zeolitite respectively, and the three remaining were used as controls, *i.e.* cultivated in a traditional way. In the parcel treated with NH_4-charged zeolitite, synthetic fertilizers were reduced by 50%, whereas in the two parcels treated with natural zeolitite, synthetic fertilizers were reduced by 30%. All parcels were sown with sorghum.

The first agronomic measures carried out in July 2013 indicated that in the parcel treated with NH_4-charged zeolitite, plants had a higher number of flowers and a more homogeneous distribution of plant highs with respect to the control parcels. In September 2013, just before harvest, 3 plants per parcel were sampled and dimensional and weight analyses were carried out on both whole plants and their parts (leaves, stems, flowers). Plants of the control parcels were heavier than those cultivated in the treated parcels. Despite this fact, the most relevant outcome is that in the two parcels treated with natural zeolitite and in the parcel amended with NH_4-charged zeolitite, the yield was respectively 4.9% and 15.1% higher than in the control parcels.

Critical issues to be taken into account when assessing the feasibility of the ZeoLIFE project are: 1) the payback period for field amendment with zeolitite (either natural or NH_4-charged), which varies between 5 and 10 years, 2) difficulties related to zeolitite spreading in the field, and 3) the time needed for zeolitite NH_4-charged zeolitite production in the prototype.

Influence of co-absorbed water on the spectroscopic properties of dye-zeolite L composites

Gigli L[1], Arletti R[2], Vitillo J[3], Martra G[4], Calzaferri G[5], Devaux A[6], Belser P[6], Quartieri S[7], Vezzalini M G[8*]

1 - Department of Earth Sciences, Turin, Italy 2 - University of Torino - NIS Torino

3 - Department of Science and High Technology, Como, Italy 4 - Department of Chemistry, Turin, Italy 5 - Department of Chemistry and Biochemistry, Bern, Switzerland 6 - Department of Chemistry, Fribourg, Switzerland 7 - Department of Physics and Earth Sciences, Messina, Italy 8 - University of Modena and Reggio Emilia, Italy *mariagiovanna.vezzalini@unimore.it

Zeolite L (ZL) [1, 2] is an ideal host matrix for supramolecular organization of photoactive species and for the realization of hierarchically organized multifunctional composite materials. As is well known, supramolecular organization inside the ZL nanochannels depends on the shape and size of the dye, which affects its orientation due to geometric constrains of ZL, and on extraframework content (e.g. cations, H_2O molecules). Fois and co-workers [3] demonstrated the effect of the presence of water on the absorption and emission properties of ZL/dye composites. In this study the influence of water was investigated in a new host−guest composite, named ZL/tB-DXP [2] through an integrated approach based on IR spectroscopy and SR-XRPD structural refinement. The ATR-IR spectra were collected on the pure dye, the hydrated and dehydrated form of the ZL/tB-DXP composite. In both the composites all IR peaks of the dye are strongly shifted with respect to the pure dye. It is noteworthy that in the hydrated form the shift is significantly higher than in the dehydrated form, a clear indication that the water molecules present in the channels strongly affect the molecular structure of the dye and its interactions with the hosting framework. This fact was also evidenced in the diffuse reflectance UV-Vis spectrum, where the blue shift of the whole spectrum is observed upon the water removal.

The SR-XRPD structural refinement of the hydrated ZL/tB-DXP composite revealed the presence of about 0.25 tB-DXP molecules per unit cell –aligned along the main 12MR channel of ZL (Figure 1) –and of two dye-ZL interactions : 1) CH---framework oxygen hydrogen bond; 2) K-O_2H---O=C.

The results of the IR measurements and structural refinement highlight the effective influence of the water molecules on the optical properties of ZL/tB-DXP composite.

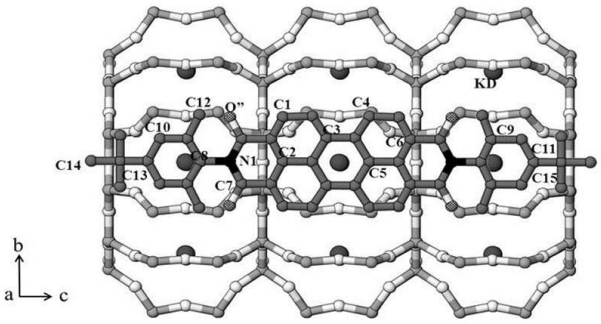

Figure 1: One tB-DXP molecule along the main 12MR channel of ZL as obtained by the structural refinement.

[1] Calzaferri G. *et al*. (2012). *Langmuir*, 28, 6216-6231.

[2] Devaux A. *et al*. (2013). *J. Phys. Chem. C*, 117, 23034-23047.

[3] Fois E. *et al*. (2013). *Langmuir*, 29, 9188- 9198.

Pressure-induced amorphization and guest-molecule penetration in high-Si mordenite

Quartieri S[1*], Leardini L[1], Arletti R[2], Vezzalini M G[3]

1 - University of Messina, Italy, Department of Physics and Earth Sciences *squartieri@unime.it 2 - University of Torino - NIS Torino 3 - University of Modena and Reggio Emilia, Italy

The high-pressure (HP) behaviour of a high-silica mordenite (HS-MOR, $SiO_2 \cdot 5\ H_2O$, SiO_2/Al_2O_3 ~ 200, s.g. *Cmcm*) in its protonated form was investigated by in-situ synchrotron X-ray powder diffraction (XRPD) using silicone oil (s.o.) as a non-penetrating pressure transmitting medium (PTM), and the following penetrating PTM: (16:3:1) methanol:ethanol:water (m.e.w), (3:1) water:ethanol (w.e), ethylene glycol (e.g.) and resorcinol (res). The HP synchrotron XRPD experiments were performed in DAC at SNBL1 (ESRF, Grenoble). The powder patterns were collected on an image plate in the P ranges reported in Table 1. Other patterns were measured upon decompression. The evolution of the structural features was followed by full profile Rietveld refinements.

In the P_{amb}-1.2 GPa range, the volume contraction of HS-MOR compressed in s.o. (Table 1) is the highest found among the high silica zeolites studied up to now in the same P range [1-2]. Above this P value, a rapid and irreversible loss of long range order is observed in the diffraction patterns. These results indicate an irreversible P-induced amorphization.

The main results obtained in penetrating PTM are the following,
i) no complete X-ray amorphization achieved up to the highest investigated P,
ii) no phase transitions observed in the studied P range,
iii) penetration of additional guest species into the channels, even at very low P,
iv) lower cell volume contraction with respect to that found in s.o. in the same P range (Table 1 and Fig.1),
v) partial reversibility of the P-induced effects upon decompression.
The lower compressibility of HS-MOR in penetrating PTM with respect to s.o. (Figure 1 and Table 1) is justified by the entrapping of additional guest molecules, which contributes to substaining the framework and stiffening the material.

Table 1. Experimental details and cell-volume variations of HS-MOR compressed in different PTM

PTM	*P range*	*ΔV (P_{amb}-1.2 GPa)*
silicone oil	P_{amb} - 8 GPa	-6.40 %
m.e.w	0.1 - 11.8 GPa	-0.96 %
w.e	0.3 - 2 GPa	-0.86 %
e.g.	P_{amb} - 8.8 GPa	-1.47 %
res	P_{amb} - 8.5 GPa	-1.02 %

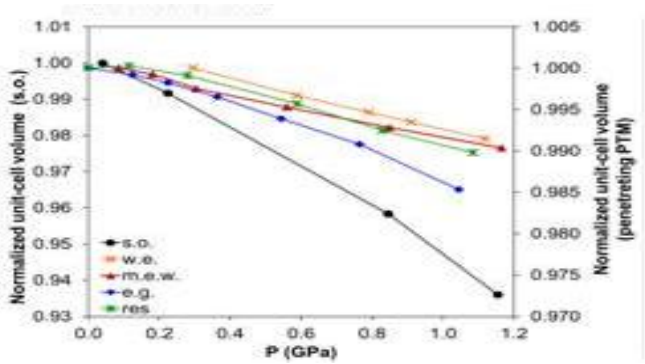

Figure 1: Unit-cell V vs. P of HS-MOR compressed in different PTM

[1] Quartieri S. *et al.* (2012). *J. Solid State Chem.*, 191, 201-212.

[2] Colligan M. *et al.* (2004). *J. Am. Chem. Soc.*, 126(38), 12015-12022.

Remediation of high acidity mine drainage

Ayora C[1*], Macías F[2], Caraballo M[3], Nieto J[2]

1 - CSIC *cayora1@gmail.com 2 - University of Huelva, Spain 3 - Dept. of Mining Engineering, Universidad de Chile

The Iberian Pyrite Belt (SW Spain and Portugal) contains one of the largest reserves of pyrite in the world, with mining activities dating back to prehistoric times. About one hundred abandoned mine waste dumps and galleries release a huge acid and metal load to the Tinto and Odiel rivers. Once the mining activity is over, polluting discharges can persist for decades or even centuries with no specific responsible entity. In-situ passive remediation technologies are especially suitable for these orphan sites. The concept is to insert a reactive porous material in the natural flow path of contaminated surface and ground waters, and it is implemented through infiltration ponds and reactive barriers, respectively. Calcium carbonate pea-size gravel is the common alkalinity supplier to neutralize acidity and precipitate metals. These remediation systems have been traditionally implemented in coal mines. However, the acid drainages from the Iberian Pyrite Belt contain metal concentrations one to two orders of magnitude higher than those from coal mines and require special designs to avoid quick clogging or passivation (coating) of the grains of reactive material. To overcome these problems, a Dispersed Alkaline Substrate (DAS) mixed from fine-grained limestone sand and a coarse inert matrix (e.g. wood chips) was developed. The small grains provide a large reactive surface and dissolve almost completely before the growing layer of precipitates passivates the substrate. The high porosity and the dispersion of nuclei for precipitation on the inert surfaces retard clogging. However, limestone dissolution only raises pH to values around 6.5, which is sufficient to precipitate the hydroxides of trivalent metals (Al, Fe), but it is not alkaline enough to remove divalent metals. Magnesium oxide, which hydrates to Mg hydroxide upon contact with water, buffers the solution pH between 8.5 and 10. A DAS system replacing limestone with caustic magnesium oxide has been tested to be very efficient to remove divalent metals (Zn, Cd, Mn, Cu, Co, Ni, Pb) from drainage previously treated with limestone.

The role of aluminum sulfate nanoparticles in the natural mitigation of mine water pollution in alpine rivers (Paradise Portal, CO, USA)

Caraballo M[1,2,3*], Hochella Jr. M[2], Wanty R[4], Verplanck P[4], Ayora C[5]

1 - Dept. of Mining Engineering, Universidad de Chile *mcaraballo@ing.uchile.cl

2 - Geoscience Department, Virginia Tech 3 - Geology Dept., University of Huelva, Spain 4 - US Geological Survey 5 - Institute of Environmental Assessment and Water Research, Spain

Water chemistry and suspended particle mineralogy were studied along a one kilometer transect of the Paradise Portal creek (San Juan County, Colorado, USA). Four different samples were obtained: adit outflow (PP1), Al-cascades foot (PP2), 0.5 km from the adit (PP3), and 1km from the adit (PP4). Two different processes were assigned for the natural attenuation of the metal pollution observed in these waters: a) dilution with pristine alpine waters, and b) precipitation of colloidal hydrobasaluminite ($Al_4(SO_4)OH_{10}$•12-36 H_2O). A detailed transmission and scanning electron microscopy (TEM and SEM) study revealed that hydrobasaluminite colloids were comprised by a network of nano-spheres ranging from a mean diameter of 100 nm (samples PP1 and PP2) to 50 nm (sample PP3). The existence of a Si-rich matrix agglomerating the hydrobasaluminite nanoparticles was also observed. The sequence of specific geochemical and mineralogical processes generating the nanoparticle-based hydrobasaluminite colloids is yet to be unravelled. Notwithstanding, these results will undoubtedly serve as a natural proxy to facilitate and stimulate our current knowledge in nano-geosciences and water metal pollution remediation.

The reduction of Cr(VI) using pilot-scale bioreactors

Diedericks V*, Castillo J, van Heerden E

University of the Free State *diedericksv@ufs.ac.za

Chromium has been used extensively in industrial processes such as leather tanning, electroplating and many other industrial uses, which generate large amount of chromium, as Cr(VI), that is discharged into the environment. Cr(VI) is a severe contaminant with high solubility and mobility in aquatic systems. The mine in this study (referred to as the study area) stored industrial waste containing a high concentration of chromium in regions rich in dolomite. However, over the past decades leaching of Cr(VI) on site has occurred. For this reason this study focussed on the remediation efforts for the removal of Cr(VI).

In this study four different field experiments were demonstrated using bioreactors with different characteristics, to demonstrate the efficacy of biological treatment systems using naturally occurring communities of metal-reducing bacteria. The concentration of Cr(VI) in the influent water was between 3 and 5 mg/L. The aim was to reduce the Cr(VI) to potable water quality, with additional benefits by lowering the nitrates and sulphates in the water.

Bioreactor A was a flatbed bioreactor with a porosity of 40% (~18 000 L) containing dolomite, fed with gravitational flow and varied residence time. The system, once optimized, can show Cr(VI) reduction of up to 80%, with a correlation between ORP, Cr(VI) reduction and NO_3 reduction. This design introduced oxygen which increased the ORP and therefor decreased Cr(VI) reduction efficacy. Bioreactor B was another flatbed bioreactor (~11 000 L) with a smaller depth to surface area ratio and set-up as described in Reactor A. Unexpectedly, the design did not decrease the O_2 intrusion, and therefore the efficacy could only be improved when this system was operated in batch mode (~15% in continuous mode to ~90% in batch mode). Bioreactor C was an upflow bioreactor compsisting of four tanks (~1800 L per tank) but flow controlled by pumping. The results varied over a period of 6 months obtaining Cr(VI) reduction of up to 99%. There was a correlation between the residence time and Cr(VI) reduction in the system. An additional effect was demonstrated by initiating a partial chemical step in addition to the reactors. This step consisted of 250 l drums containing a combination of sulphur, charcoal and activated carbon and was used as a secondary step treating a small amount of the effluent water. This additional step yielded effective results, deducing Cr(VI) up to 100%.

The combination of a chemical and biological system is currently the most effective treatment showcased and can be considered for sustainable on-site treatment of Cr(VI) where the concentrations are lower than 5 mg/l.

Mineralogical aspects of metal removal by nanoscale secondary phases emerging from advanced water treatment technologies (iron nanoparticles/ferrates IV,V,VI)

Filip J[1*], Tuček J[1], Prucek R[1], Kolařík J[1], Hušková I[1], Kašlík J[1], Sharma V[2], Zbořil R[1]

1 – RCPTM, Palacký University, Olomouc, Czech Republic *jan.filip@upol.cz

2 - School of Rural Public Health, Texas A&M University, USA

Nowadays, some advanced remediation technologies applied for (heavy) metal removal from polluted waters and soils are based on utilization of zero-valent iron nanoparticles (nZVI) or iron(IV)/(V)/(VI) ferrates. Zero-valent iron nanoparticles act as an efficient reducing agent, while iron(IV)/(V)/(VI) ferrates are used as oxidizing agents. In both cases, the reaction products (i.e., after nZVI oxidation or ferrate reduction) are nanocrystalline, frequently nearly-amorphous iron(III) oxides/oxyhydroxides co-precipitating with targeted inorganic pollutants and/or further acting as sorbents. Based on experiments aimed at removal of various metals under controlled laboratory conditions (namely metals like Al, Cr, Co, Ni, Cu, Zn, Cd and As), and detailed characterization of iron-based reaction products (i.e., employing instrumental methods like X-ray powder diffraction, Mössbauer spectroscopy, X-ray photoelectron spectroscopy, transmission electron microscopy), we have defined the mechanisms and efficiencies of metal removal, as well as the manner of metal incorporation into iron-based solid phases. The identified secondary phases are mainly represented by nanocrystalline maghemite, nearly-amorphous ferric oxyhydroxides, ferrous hydroxide, green rust or magnetite. The experimental results were compared with adsorptions of respective metals onto preformed sorbents. Evidently, the different structural forms of iron oxide/oxyhydroxide can incorporate different amount/types of metals into their crystal structure. Finally, the results of laboratory experiments on model solutions were compared with attenuation of metals from real contaminated waters (i.e., in laboratory-scale experiments) and also with results from localities treated by nZVI/ferrates in pilot scale. The effects of particular remediation technology on physico-chemical parameters of the treated waters will be discussed as well.

Evidence for effective treatment of alkaline mine drainage using a matrix of $BaCO_3$ and wood chips: solution for in-situ passive treatment

Gomez- Arias A*, Castillo J, Posthumus J, van Heerden E

1 - University of the Free State *albita.anortita@gmail.com

Passive remediation reactor treatment functions as a permeable barrier that enables the water to pass through while removing metals by biogeochemical reactions. Conventional passive treatments are based on calcite dissolution; this system increases the pH to values between 5 and 6, which are not sufficiently high to precipitate divalent metals. Also, the calcite is not dissolved at these high pH values, therefore it cannot be used to treat alkaline mine drainage. Alternative treatments are based on sulphate-reducing bacterial process that precipitate metals as metallic sulphides. These redox reactions are too slow to treat large volumes of contaminated water flow. A passive treatment reactor, with a reactive matrix of $BaCO_3$ and wood chips (B-DAS), has been developed based on the hydrogeochemical characteristics of most of mining leachates from South Africa, that generally are moderate acid or alkaline, with high concentrations of sulphates, TDS (total dissolve solid), salinity and heavy metals (mainly Cr, Fe and Al) as well as radionuclides (U and Ra).

The treatment is demonstrated in column experiments with a reactive matrix in different proportions; 1:2 (20 g wood chips: 40 g $BaCO_3$), 1:3 (20 g wood chips: 60 g $BaCO_3$), 1:4 (20 g wood chips: 80g $BaCO_3$) with a residence time of 24 hours. This allows one to assess the best ratio for the permeability and reactivity of each column. Moreover, the dissolution of $BaCO_3$ in contact with water release Ba^{2+} and HCO_3^-, which react with the sulphates, Ca^{2+} and Mg^{2+} contained in the AMD, which would precipitate as $BaSO_4$, $CaCO_3$ and $MgCO_3$, respectively. The pH could be increased up to values 8 or 9, which is important because allows removal divalent metals, that need high pH values to precipitate as carbonates like the Zn^{2+} and Mn^{2+}. The columns were maintained for 6 months and the results in 3 columns demonstrate the reactivity, since it showed a total removal (100%) of sulphates (1400 to 0 mg/L) as well as 50% hardness (Ca, Mg, Na and Cl) without saturation or clogging of the columns. The porosity was increased in the 3 columns from approx. 66.7% to 70% after 6 months, that means the $BaCO_3$ is used as suggested. The metal removal (Fe, Al, Cu, Zn and Mn, at moderate concentration) also was 100% effective in all of them. Therefore, parameters such as salinity, TDS (total dissolved solids) and conductivity decreased throughout the experiments. Worth mentioning that the Eh values were around -200 mV, due to the dissolution of barium carbonate, which could promote the activity of sulphate-reducing bacteria (SRB). Therefore, a bioreactor based on SRB and $BaCO_3$ could be effective and should be consider as this would decrease the volume of barium carbonate used and therefore its cost.

Optimization of a bioremediation system of U(VI) based on the biostimulation of an indigenous bacterial community

Maleke M[1*], Castillo Hernandez J[1], Williams P[1], Ojo A[1], DeFlaun M[2], van Heerden E[1]

1 - University of the Free State *malekemm@ufs.ac.za 2 - Geosyntec Consultants

High concentrations of Uranium(VI) in the Witwatersrand Basin, South Africa, a result of gold mining, is a serious health concern, thus it is important to minimize its spread in the environment [1]. Based on hydrochemical characteristics of this mining leachate, treatment systems have been created. However, the treatment systems are both costly and ineffective. Therefore, optimization of a bioremedial system of U(VI) based on biostimulation of an indigenous bacterial community can be considered as a sustainable, low maintenance alternative to address this problem. The present study describes the results of two bioreactors composed of inert support and sediment sludge (20% w/v) as a natural inoculum. The upflow bioreactors had a residence time of 24 hours that was maintained for 82 and 79 days, an efficiency porosity of the columns were 41 and 39 % and flow allowed for the on-site water to supply donor at a selected rate. The main objective of this study was to promote tolerance of indigenous bacterial community to increasing concentrations of uranium and stoichiometrically balance the donor demand for optimal U(VI) removal. The results show that the current contamination of U(VI) (37ppb) in the catchment, but more interestingly increased concentrations up to 10 ppm, can be effectively reduced to below the South African National Standard for drinking water (15 ppb). The second bioreactor was able to successfully adapt and effectively deal with increasing levels of U(VI) (10 ppm) provided that enough electron donor was supplied to balance this ratio (24 ppm). This study shows that U(VI) could be reduced to U(IV) and immobilized especially under sulphate-reducing conditions. The molecular biology analysis, which identified a diverse but novel population of bacterial species, including *Desulfovibrio sp.* and *Geobacter sp.* that have been shown to be able to reduce U(VI) and other metals, emphasized the selective nature/biostimulation of the population. The mineralogical analysis determined that part of the uranium precipitated intracellularly (TEM), which means that the remaining U(VI) was precipitated as U(IV) oxide. This was predicted with the geochemical modelling, that demonstrates that the treated drainage is supersaturated with uraninite, U_4O_9 and amorphous UO_2. From the results obtained it can be concluded that the tolerance of the indigenous bacterial community could be optimized to remediate higher environmental contamination and the system can be up scaled and employed for remediation of U(VI) impacted sites.

[1] Winde F. (2010). *Water SA*, 36(4), 257-278.

Speciation of polysulfides generated by lepidocrocite reduction in the presence of sulfate-reducing bacteria

Moloantoa K[1*], Castillo J[1], Wan M[2], Peiffer S[2], van Heerden E[1]

1 - University of the Free State *moloantoakm@ufs.ac.za 2 - University of Bayreuth

Polysulfides are the most interesting compounds of the zerovalent sulfur species, since they represent the most reactive form of elementary sulfur. These species are responsible for intermediate compound generation as well as pyrite formation. Furthermore, polysulfides are responsible for keeping high concentrations of trace metals sequestrated in anoxic sediments [1]; therefore, the polysulfides play an important role in numerous environmental processes due to their high reductive and nucleophilic reactivity [2]. However, the nature and behaviour of polysufides generated indirectly by the SRB activity is not clear, but it is suggested that the interaction of biogenic H_2S reduces the iron oxyhydroxide (lepidocrocite) that in turn facilitates the formation of polysulfides. Two experiments were conducted with different lepidocrocite concentrations (0.2 g [A] and 2 g [B]), with pH kept between 7-7.2. Experiment [A] showed an oversaturation of dissolved sulfides with almost complete reduction of Fe^{3+} to Fe^{2+}, whereas in experiment [B], this oversaturation was marked by higher concentrations of Fe^{2+} due to the initial concentration of Fe^{3+}, which was reduced by the action of the reduced sulfur species generated in the experiment. Magnetite is probably formed as a transitory mineral phase according to the PHREEC modelling. S^0 was also generated by the reaction between lepidocrocite and HS^- in both experiments. The polysufides produced are probably generated by two ways: indirectly -where S^0 reacts with HS^- or directly - where HS^- in excess reacts with Fe^{3+} of lepidocrocite and generates polysulfides which are the key reactants in nucleation process of pyrite.

The evolution of polysulfides was similar in both experiments, although some species were present in abundance where the lepidocrocite concentration was increased (experiment A (0.2 g) to B (2 g)). The most stable polysulfides were $S_7^{2-} \geq$, $S_6^{2-} \geq$, $S_8^{2-} \geq$, S_4^{2-} although not the most reactive in the order. The most reactive polysulfides were $S_2^{2-} \geq$, $S_3^{2-} \geq$ and S_4^{2-}. These species are probably the promoters in the formation of pyrite and intermediate phase in these experiments. However, the lack of reactivity of most stable polysulfides could be attributed to the lack of other metals present with those could react more easily such as Cu^+, As^+ or Cr^+.

This study verified and identified polysulfide species which can be generated by the interaction of HS^- generated by sulfate reducing bacteria and Fe^{3+} from lepidocrocite. The production of the iron monosulfides, elemental sulfur and polysulfides generated in these experiments was also determined. These experiments raised different questions about toxic metal retention (As, Cr, Cd) and their stability in Fe and Al oxyhydroxides, especially under bacterial sulfate-reducing conditions as well as the role and importance of the polysulfide in this process.

[1] Brooks R.R. *et al.* (1968). *Geochimica et Cosmochimica Acta*, 32, 397-414.
[2] Kamyshny A.Jr. *et al.* (2006). *Analytical Chemistry*, 78, 2631-2639.

Accelerated weathering of steel slag using organic amendments

Oty U[1*], Rogerson M[2], Greenway G[3], Mayes W[1]

1 - Centre for environmental and marine sciences, University of Hull, UK. *u.v.oty@2010.hull.ac.uk 2 - Geography, earth and environmental sciences University of Hull 3 - Department of chemistry, University of Hull.

The leaching of oxyanionic metals such as V, Mo and Cr from steel slag at high pH can pose environmental problems at disposal sites and in slag used as aggregate. This study presents a novel biologically-mediated approach that both (1) accelerates the rates of slag weathering so the timescales over which environmental impacts are apparent is reduced, and (2) provides an opportunity for the recovery of valuable e-tech metals such as V and Li from leachates. A series of column and batch experiments were set up to investigate the effect of organic amendment of steel slags using municipal solid waste (MSW) compost. The impact of the physical structure of the treatments and the effect of microbial or redox controls versus the leaching rate of V and Li were also studied. Results showed that capping of steel slag with municipal compost accelerated the release of V and Li from initial concentrations of 250 ppb and 12 ppb to a four-fold and three-fold increase respectively within the equilibration period of 50 days. The leaching rate of various elements were found to be dependent on the structural arrangement of the compost within the slag, with high pH (10-11.5) water in contact with organic layers crucial for the solubilisation of V and Li. This is likely explicable by organic complexation of metals. Batch experiments highlighted that with and without organic amendment, under aerobic conditions, V concentrations in leachate from slag reached 1000 ppb a full order of magnitude faster than under anaerobic conditions. The effect of microbial processes on the leaching process however remains uncertain, even though the V concentration in sterilised aerobic flasks was lower compared to the unsterilised ones. In addition to the potential value recovery of materials from these by-products, the compost amendment holds the promise to reduce the lifetimes over which polluting waters are released from the slag and minimise the hazard of fugitive dusts.

Metal fluxes across the water-sediment interface in a reservoir affected by acid mine drainage: reactive transport modeling

Torres E[1*], Ayora C[2], Couture R[3], Shafei B[4], Nardi A[5], Van Cappellen P[6]

1 - Hydrosciences *ester.torres@univ-montp2.fr 2 - CSIC 3 - Norwegian Institute for Water Research-NIVA, Oslo, Norway 4 - School of Earth and Atmospheric Sciences, GATech, Georgia, USA 5 - Amphos 21 Consulting S.L 6 - Ecohydrology group, University of Waterloo, Waterloo, Canada

The Sancho water reservoir has been impacted by acid mine drainage (AMD) since the Tharsis mine stopped activity in 1998. As a result, the water reservoir nowadays has a pH around 3.5, as well as high concentrations of sulfate, aluminum, iron and trace metals. Thus far, the expected removal of contaminants by sediment burial has not been as effective as expected in improving water quality within the reservoir. To better design remediation strategies, new tools capable of quantifying metal and acidity transfers across the water-sediment interface (WSI) are needed. A 1-D, non-steady-state biogeochemical reactive transport model with a comprehensive set of equilibrium and kinetic biogeochemical reactions was adapted [1] to simulate the fate and transport of trace metal and acidity in sediments affected by AMD. Two submodels account for the spatial heterogeneity of the oxygen concentration of the bottom water. The "permanently oxic" submodel represents the sediments in areas shallower than the thermocline, while the "holomictic" submodel represents the deeper sediments where bottom water oxygen levels are affected by turnover events (which cause the bottom waters to oscillate between completely anoxic and oxic conditions). The model was calibrated with measured depth distributions of pore water and solid phase chemistry. Model results imply that under permanently oxic conditions the sediments act as a sink for acidity (H^+), as well as aqueous Al, Zn, Cu, Co and Ni, but as a source of aqueous Mn, Fe and As. The latter are released to the overlying water as a result of Mn and Fe (hydr)oxide reduction. In the holomictic submodel, when bottom waters turn anoxic, metal sulfides precipitate in the sediment. When the bottom waters subsequently switch to oxic, the metal sulfides are oxidized (along the oxygen front) and the associated metals are released to the overlying water. About 30% of the sediment pools of ZnS, CuS, CoS and NiS, and around 45% of FeS is reoxidized. However, overall, the sediments act as a net sink of the pollutants considered in the model. Around 10% of S, Al, Zn and Cu that enter the reservoir accumulate in the sediment; for Co and Ni this is around 2%. For Fe, As and Mn sediment accumulation efficiencies are 80%, 98% and 70%, respectively. The model was used to predict how the sediment would react if AMD input to the reservoir would completely cease. According to the simulations, within ten years after cessation of AMD the sediment would reach a new steady state with negligible release of aqueous contaminants from the sediments to the reservoir.

[1] Couture R.M. *et al*. (2010). *Environ. Sci. Technol*. 44(1), 197-203.

Geochemical study of the interaction of acid and alkaline mine drainage (AMD) with $BaCO_3$: optimization of the biological and chemical processes for AMD treatment

Castillo J*, Posthumus J, Gomez- Arias A, van Heerden E
University of the Free State *castillohernandezj@ufs.ac.za

In this study the geochemical behaviour of $BaCO_3$ was investigated and the optimization of its use in acid (pH 2.93) and alkaline (pH 8.2) mine drainage with high concentrations of sulphate (> 1400 mg/L) and moderate concentrations of metals (mainly Fe^{2+}>, Mn^{2+}>, Al^{2+}>, Zn^{2+}>, Cu^{2+}) was determined. In addition, the use of $BaCO_3$ later to promote growth of sulphate-reducing bacteria (SRB) used in bioreactors was also investigated. Batch experiments were conducted using a series of four interactions with $BaCO_3$:AMD ratios of 1:400 (0.1g:40mL), 1:57 (0.7g:40mL) and 1:160 (0.25g:40mL), 1:80 (0.5g:40mL) with $AMD_{alkaline}$ and AMD_{acid}, respectively. Each series of experiments were composed of 12 sub-samples in which the reactions were stopped at different time intervals (0 to 168 h). The biological experiments were conducted similar to the chemical experiments with the addition of using a SRB inoculum under anaerobic conditions. In all the experiments, reactions achieved steady state conditions in approx. 6 h. The neutralization process increased the pH (between 8.3 and 9.98) through alkaline additive dissolution (attributed to the release of HCO_3^- and OH^-), as well as decreased the metal solubility and precipitate formation of $BaSO_4$ and divalent metals (Mn and Zn) as carbonates and poorly crystallized Fe-Al oxy-hydroxides, which acted as a sink for trace elements to the extent that solutions reached the pre-potability requirements of water for human consumption. The results showed 98% removal of SO_4^{2-} in AMD with an initial concentration of 1400 mg/L, with the treatment with 2500 mg/L $BaCO_3$ and a residence time of 6 hours. In addition, the treatment of alkaline or acidic AMD with $BaCO_3$ removes up to 50% TDS, salinity and conductivity. Furthermore, the Eh reached (around -62.5 and -132.5 mV) at the end of the experiments were suitable for developing a combined continuous system with $BaCO_3$ and sulphate-reducing bacteria (SRB) for treating AMD with high sulphate concentrations. In the batch experiments with SRB, bacterial growth was observed with 60% of $BaCO_3$ after 3 days, therefore improving the conditions for the SRB and reducing the acclimation time of the bioreactors. The use of SRB could lower the cost of the treatment system since the SRB has additional 30% efficiency for removing sulphates when conditions have been adapted. The final products are $BaSO_4$ and BaS sludge with low metal concentrations, especially in alkaline drainage of coal mines, could even be used by other industries.

Mineralogical characterization of selected South African mine tailings for the purpose of mineral carbonation

Amponsah-Dacosta M*, Reid D, Muedi R, Khalo M, Lekgau S

Department of Geological Sciences, University of Cape Town
*ampmax001@myuct.ac.za

Increasing atmospheric CO_2 concentration is rising to unacceptable levels causing major climate change predicaments. Fossil fuel combustion is responsible for a significant component of the total amount of CO_2 annually released in South Africa. Various technologies for CO_2 storage have been evaluated to reduce the ever-increasing rate of emission, including the storage in bottles at sites like the syn-fuels industry at Sasolburg and Secunda. This source of 95% pure gas provides the opportunity to permanently store the CO_2 through the carbonation of minerals.

Ultramafic/mafic mine tailings produced in vast tonnages by South African base- and precious-metal companies have the potential to be recycled in a variety of innovative schemes designed to reduce their footprint. Tailings samples were collected from seven different mining operations across four South African provinces, with the main objective to evaluate their suitability for mineral carbonation. Important features under characterization include mineral species, mineral proportions, mineral structures, mineral composition, morphology, particle size distribution and surface area. Quantification of these parameters is being carried out using a spectrum of laboratory based analytical techniques in order to rank the different tailings sites in terms of their carbonation potential. Mine tailings containing higher levels of olivine and pyroxene, rather than plagioclase and chromite, have greater stoichiometric capacity for CO_2 absorption. However, their reactivity is strongly influenced by surface area and average particle size. Other factors such as reaction kinetics, energy accounting, and the logistics of transporting the CO_2 and/or the tailings need to be incorporated into the ranking exercise.

Current results have indicated that tailings from Mogalakwena Platinum Mine have the largest surface area (5.2 m^2/g) with 83% of material reporting below 25 µm per 100 g of sample screened. These results are outstanding when compared to other tailings facilities within this study and could be essential in the ranking exercise. The targeted outcome is an improved ranking scheme for several mining operations in South Africa in order to identify a suitable mine tailings facility for the purpose of mineral CO_2 carbonation.

Keywords: Mineral CO_2 sequestration, ultramafic, tailings.

Dynamic pore-scale monitoring of wollastonite carbonation

Boone M[1*], Nielsen P[2], De Kock T[1], Masschaele B[3], Quaghebeur M[2], Cnudde V[1]

1 - UGCT - Dept. Geology and Soil Science, Ghent University
*marijn.boone@ugent.be 2 - Unit Sustainable Materials Management, VITO, Belgium 3 - X-Ray Engineering (XRE) - UGCT, Belgium

Accelerated mineral carbonation is considered a safe and permanent method to store anthropogenic CO_2 emissions. Most studies, especially in the field of ex-situ carbonation, focus on carbonation in slurry phases with liquid to solid ratios (L/S) above 2. Direct carbonation in the pore space of rocks occurs at L/S ratios well below 1, especially due to the displacement of water by CO_2 in the pore space. In this research, carbonation of wollastonite grains in low L/S ratio is monitored in 3D using X-ray computed microtomography (micro-CT) in combination with a specially designed X-ray-transparent reactor cell. Wollastonite was chosen as a model mineral for silicate carbonation due to its high reactivity. A reactive pore network was generated by packing granulates of wollastonite in the reactor cell. Water was added to the grain pack and subsequently scanned using micro-CT, enabling mapping of the distribution of the water in the pores. Afterwards, dynamic scanning using the Environmental micro-CT (EMCT) setup at the Centre for X-ray Tomography of the Ghent University (UGCT - www.ugct.ugent.be), was applied while injecting CO_2 at a pressure of 20 bar into the reactor cell. Dynamic scanning with the EMCT permits to obtain full 3D images of the grain pack with a temporal resolution of 1 minute. This allows (1) analysis of the change in the distribution of water in the pore space while injecting CO_2, (2) visualization and localization of the carbonate precipitation during the carbonation process and (3) analysis of the influence of the carbonate precipitation on the porosity in the grain pack. The results (Figure 1) show a close link between the location of the residual water films after CO_2 injection and the precipitation of carbonates, indicating the importance of the pore network properties on the mineral carbonation process and subsequently on the porosity and permeability after carbonate precipitation.

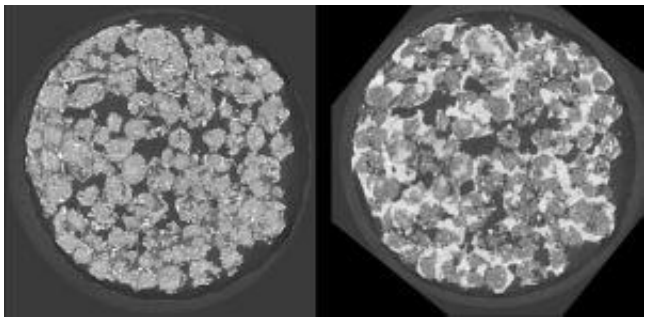

Figure 1: 2D slice through 3D microCT volume of a wollastonite grain pack before (left) and after (right) carbonation with the precipitated carbonate phases in white.

MgO carbonation in the context of CO_2 geological sequestration

Davila G[1*], Cama J[1], Soler J[1], Galí S[2]

1 - IDAEA-CSIC *gaba1983@hotmail.com 2 - Barcelona University

Introduction

MgO is proposed as an alternative for Portland cement in CO_2 injection wells. Injection of CO_2 at depth will cause the acidification of groundwater, causing MgO carbonation (its dissolution and production of Mg carbonates). Autoclaved experiments where MgO reacted with CO_2-rich water under 10, 50 and 74 bar of pCO_2 and 25, 70 and 90°C were performed to gain insights into the overall MgO carbonation process.

Experimental Methodology

Stirring batch experiments were performed under 10, 50 and 74 bar of pCO_2 and 25, 70 and 90 °C. MgO with a grain size between 60 and 150 mm reacted with Milli-Q water equilibrated with respect to calcite with a solid/solution ratio of 5.3 g/47.7 ml. Experimental time spans varied from one experiment to another: 5, 10, 20, 43 and 67 h, Once solid and solution were placed in the autoclave, the desired pCO_2 and temperature were applied and maintained constant during the whole experimental run. At the end of the experiment, 10 ml of solution was sampled, immediately filtered and acidified. The output Ca and Mg concentrations were analyzed by ICP-AES and the retrieved solid samples were analyzed by XRD. The experimental variation of Mg and Ca concentrations and pH with time at the different temperature and pCO_2 was simulated using the reactive transport codes Cheproo-Traconf and CrunchFlow.

Results

MgO reacts with CO_2-rich water previously equilibrated with respect to calcite and forms brucite ($Mg(OH)_2$) which dissolves producing magnesium carbonate phases. Precipitation of these secondary phases (magnesite and/or metastable $MgCO_3$ phases, such as nesquehonite ($MgCO_3 4(H_2O)$) or hydromagnesite ($Mg_5(CO_3)_4(OH)_2 3(H_2O)$) depends on pCO_2 and temperature. Precipitation of the non-hydrated Mg-carbonates is favoured by increasing temperature and pCO_2.

Simulations reproduce the experimental evolution of the aqueous concentrations and indicate that the initial porosity of the MgO cement diminishes by increasing temperature and pCO_2. This fact suggests that the process of MgO carbonation in conditions of geological CO_2 sequestration is beneficial for the performance of the cement as a seal.

CO_2-water-rock interactions experimentally investigated under elevated temperature hydrothermal conditions

Ferretti M[1*], Gaggero L[2], Sanguineti E[1], Caratto V[1], Belfortini C[1]

1 - University of Genoa, DCCI *ferretti@chimica.unige.it 2 - University of Genoa, DISTAV

The increase of anthropogenic CO_2 concentration in the Earth's atmosphere has been linked to global warming which in turn has driven international efforts to explore mitigation strategies to CO_2 emissions. Carbon sequestration by mineral carbonation appears to be a realistic option for the capture and storage of CO_2. In particular, mafic rocks which primarily consists of Ca, Mg silicate minerals, have a high acid neutralization capacity by providing alkaline earth elements that form stable carbonate minerals. These reactions are part of a natural alteration process that concurred in regulating atmospheric CO_2 levels across geological times.

In this study, we investigated the mineralogical changes of serpentinite, basalt and syenite bulk rock compositions subjected to CO_2 exposure in hydrothermal conditions for a period between 25 and 250 hours. The experiments were carried out at laboratory scale on powders with grain size far below the value of natural rocks, in order to provide comparable rate of reactions among the three investigated systems and increase the reactivity of the samples for potential industrial ex-situ storage. All tests were carried out in a stainless steel vessel filled up to 50% volume by a slurry of finely powdered sample (grain size <63 µm) and distilled water (1:1).

The CO_2 was injected to a pressure of 4 MPa and then the sealed vessel was heated and kept at constant temperature of 100°C and 150°C respectively.

At the end of the experiment the pH of the solution was measured and then the slurry was separated by centrifugation, dried and characterized by XRPD, SEM-EDS, and calcimetry.

The most significant results arose for serpentinite composition, in particular: i) the number of minerals in the slurry increased with time, in particular after 250 h exposure, with the appearance of magnesite, as shown in XRPD patterns (Figure 1); a differential increase of olivine and other non-reacting minerals occur by transformation of pristine lizardite; ii) in very fine grained (pelite) powder high resolution FE-SEM shows neat euhedral lens-shaped polycrystalline aggregates of magnesite overgrown upon lizardite at micron to mm scale (Figure 2). These preliminary results match in-situ natural process observed in Alpine serpentinite [1].

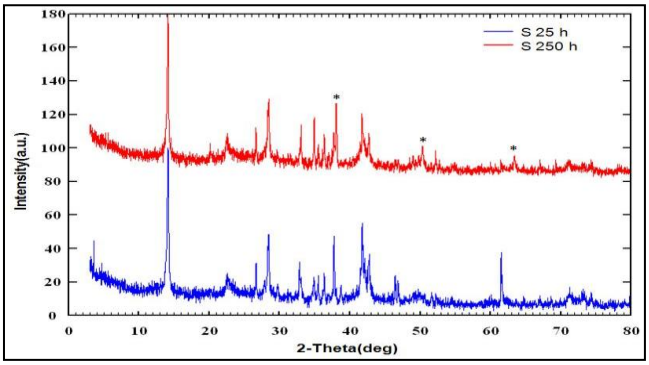

Figure 1: XRPD patterns of serpentinite samples after 25 and 250 h treatment at 150°C, 40 MPa CO_2. * indicates magnesite peaks.

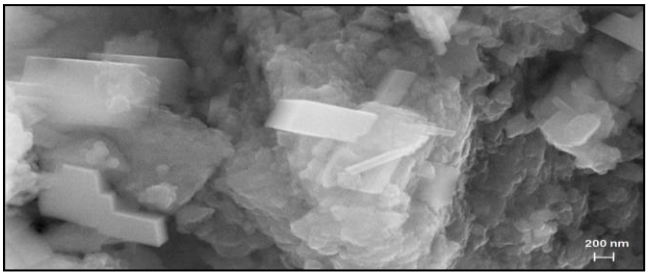

Figure 2: FE-SEM photomicrograph (EHT=20.00 KV) of magnesite overgrowing lizardite in serpentinite sample after 250 h treatment at 150°C, 40 MPa CO_2.

[1] Schwarzenbach E.M. *et al.* (2013). *Lithos*, 177, 226-244.

Limestone dissolution and gypsum precipitation in supercritical CO_2 conditions

Garcia-Rios M, Cama J*, Luquot L, Soler J M

Institute of Environmental Assessment and Water Research (IDAEA), CSIC, Barcelona, Catalonia, Spain *jordi.cama@idaea.csic.es

Introduction

A technology demonstration plant for geological storage of CO_2 in a deep saline aquifer is currently run at Hontomín (Burgos, northern Spain). CO_2 will be injected in the reservoir rock which is mainly composed of limestone. After CO_2 injection, the resulting CO_2-rich acid solution will likely promote the dissolution of carbonate minerals and, since the reservoir resident solution contains sulfate, gypsum (or anhydrite at depth) may precipitate.

Interaction between sulfate-CO_2-rich solutions and limestone under P = 150 bar and T = 60 ºC was studied using (i) columns filled with ground limestone (pCO_2 = 34 bar) and (ii) mechanically fractured limestone cores (pCO_2 = 62). We evaluate the effect of the coupled reactions of calcite dissolution and gypsum precipitation on porosity and fracture permeability.

Experimental methodology

In the column experiments, approximately 1 g of ground sample (grain size of 250-500 µm) was placed in a Teflon cell of 0.7 cm in diameter and 1.7 cm in length. Initial porosity was calculated to be around 55 %. In the fractured cylindrical cores (0.8 cm in diameter and 1.8 cm in length), the fracture apertures ranged from 4 to 12 µm. A sulfate-rich solution equilibrated with respect to gypsum, pH of ca. 3.2 and I of 0.6 M circulated through the column at 0.01 mL h^{-1} (residence time = 0.6 h) and through the fractured cores at rates that ranged from 0.2 mL h^{-1} to 60 mL h^{-1} (residence time = 0.1-15 s).

Results and discussion

In both types of experiments, the output Ca and S concentration was respectively higher and lower than the input one. The PhreeqC simulated output pH rapidly increased up to 4.9 ± 0.4. In the range of P-pCO_2 and T of this study only gypsum precipitation took place (no anhydrite was detected).The significant calcite dissolution at the experimental pCO_2 is related to the weak character of the H_2CO_3 acid, acting as a pH buffer.

In the column experiment, in terms of volume of dissolved limestone and precipitated gypsum, the percentage of dissolved limestone with respect to the initial sample volume was 4.95 % (after 100 pore volumes). The volume of precipitated gypsum was smaller than the volume of dissolved carbonate minerals which led to an increase in porosity (approximately 4 %).

In the fractured cores, the evolution of the fracture morphology determined the variation of fracture permeability. At the lowest flow rate (Q = 0.2 mL h^{-1}) no preferential flow paths were created and permeability change was negligible. At Q = 1 mL h^{-1}, a single dominant wormhole formed with significant increase in permeability. At Q of 5 and 60 mL h^{-1} wormhole formation and uniform dissolution were observed together with a significant increase in permeability. The final fracture volumes were always higher than the initial ones by a factor of approximately 15 % even when gypsum precipitated.

Characterization of structural and hydrodynamic parameter changes due to dissolution and precipitation processes in limestone samples

Luquot L[1*], Roetting T[2], Carrera J[1]

1 - Consejo Superior de Investigaciones Cientificas, Barcelona *linda.luquot@idaea.csic.es 2 - CIMNE, UPC, Barcelona

CO_2 sequestration in deep geological formation is considered an option to reduce CO_2 emissions in the atmosphere. After injection the CO_2 will slowly dissolve into the pore water producing low pH fluids with a high capacity for dissolving carbonates. Limestone rock dissolution induces geometrical parameter changes such as porosity, pore size distribution, or tortuosity, which may consequently modify transport properties (permeability, diffusion coefficient). Characterizing these changes is essential for modelling flow and CO_2 transport during and after the CO_2 injection. Indeed, these changes can affect the storage capacity and injectivity of the formation.

Very few published studies evaluate the transport property changes (porosity, permeability, pore size distribution, diffusion coefficient) due to fluid-rock interactions.

Some in situ brine solution contains some sulfates and the dissolution of calcite can favor gypsum precipitation and modify the local pore geometry and consequently the flow parameters.

Here we report experimental results from the injection of acidic fluids (some of them equilibrated with gypsum) into limestone core samples of 25.4 mm diameter and around 25 mm length. We studied two different limestone samples: one composed of 73% calcite and 27% quartz, and the second one of dolomite. Experiments were performed at room temperature. Before and after each acidic rock treatment, we measured the sample porosity, the diffusion coefficient and the pore size distribution. We also imaged the 3D pore network by X-ray microtomography. During percolation experiments, the permeability changes were recorded and chemical samples taken to evaluate calcite dissolution and gypsum precipitation. Several dissolution/precipitation-characterization cycles were performed on each sample in order to study the evolution and relation of the different parameters.

These experiments show different dissolution regimes depending of the fluid acidity and of the limestone sample. Wormhole formation is the dominant dissolution regime.

An investigation into the dissolution of pyroxene group minerals

Meyer N[1], Becker M[2*], Broadhurst J[1], Reid D[2], Franzidis J[1]

1 - Minerals to Metals Initiative, University of Cape Town 2 - University of Cape Town
*megan.becker@uct.ac.za

With the growing need for atmospheric CO_2 sequestration and the increased awareness of the opportunities provided by mineral carbonation, the focus has turned to investigating the potential of various industrial wastes as CCS feedstock. The Bushveld PGM tailings in South Africa may provide such an opportunity given the large volumes of tailings produced annually, fine particle size distribution, high divalent cation content (18 to 22 wt.%) and close proximity to a readily available source of >95 % pure sequestered CO_2 produced by the SA synfuels industry.

The tailings, however, are dominated by the mineral orthopyroxene which hosts more than 80 % of the total Mg; and given its alleged low reactivity, potentially limits the overall conversion of tailings to carbonates. We report here the results of a study that investigated the dissolution behaviour of the pyroxene group minerals that occur in the SA tailings, together with other local examples that extend the range in composition: enstatite, augite, diopside, and wollastonite.

The extraction of cations within each pyroxene was: Ca >Fe >Mg >Si, which resulted in the order of reactivity being: wollastonite >diopside = augite >enstatite. The degree of extraction increases with temperature from ambient to 70 °C and also with a decrease in particle size from +75/-106 µm to -38 µm for the pyroxene samples investigated. The relative increase in cation extraction with an increase in temperature had the greatest effect on the +75/-106 µm size fraction. On the particle-scale, SEM imaging on the surface of reacted grains showed distinctive 'stepped' features (terraces) but no indication of etch pits. Precipitation of Ca-Si on the surface of wollastonite was present, but not secondary precipitates were imaged for enstatite, augite, and diopside. Elemental distribution of the leachate and residue surface indicates almost-congruent dissolution reaction for enstatite and diopside, and incongruent reaction for augite and wollastonite when compared to the stoichiometric ratio of the individual minerals.

The dissolution of silicate minerals follows the surface protonation model. In the case of pyroxene, the reaction front exploits the high-energy sites created by the cleavage. Cleavage planes expose the M2 cation site in pyroxenes, allowing for faster removal of the metal cation. However, the orientation of the silicate chain with respect to the cleaved surface results in an overall congruent reaction. In the pyroxene reactivity series, the incorporation of a larger cation (e.g. Ca) in the silicate structure of clinopyroxenes and pyroxenoids distorts the chain structure by lengthening the metal-oxygen bond. The increased metal-oxygen bond length reduces the energy needed to remove the metal cation. Therefore the order of reactivity is pyroxenoid > clinopyroxene > orthopyroxene. Furthermore, particle-size reduction changed the kinetics of pyroxene dissolution. The calculated apparent activation energy of the -38 µm and +75/-106 µm enstatite samples showed that the smaller size fraction had intermediate to diffusion-controlled kinetics (Ea = 27 kJ), whereas the larger size fraction showed reaction-controlled kinetics (Ea = 66 kJ). This means that the advantage of size reduction by grinding is not only limited to particle size reduction, but it also improves the kinetics of the reaction by increasing the number of high-energy sites created during grinding.

The generally low extraction of Mg from enstatite under all experimental conditions investigated (Mg extraction of between 0.13 and 4 %) indicates that the potential CO_2 storage from Bushveld PGM tailings is much lower than previously calculated. However, the viability of CO_2 storage via mineral carbonation of Bushveld PGM tailings can be improved.

Olivine source rocks of South Africa

Senzani F*, Mulaba-Bafubiandi A

University of Johannesburg *freeman_senzani@hotmail.com

Review and map capture of olivine-bearing rocks in South Africa reveals that they are present in nearly all the components of the country's stratigraphic column. The rocks are spread throughout the country. This should promote their exploitation for use in carbon sequestration.

In Palaeo-Archaean and Meso-Archaean (3500Ma to 3360Ma) rocks, the olivine is hosted, firstly, in coarse-grained layered peridotites, which consist of various combinations of dunite, harzburgite, lherzolite and wehrlite. These are found as part of the layered Archaean greenstone belts. Secondly, they are present, also in the greenstone belt setting, as fine-grained, also layered rocks, comprising komatiites, komatiitic basalt, picrite and picritic basalt. The layered Archaean coarse and fine-grained rocks are deduced to be from the same igneous events and magmas, with the coarser portions having cooled and crystallised over longer periods. The phaneritic varieties also occur as intrusions into the layers of the greenstone belts and the closely associated granite-gneiss masses. Both the coarse and fine varieties also are also reported where fragments of the greenstone belts have been preserved outside the main bodies. High-grade equivalents of both are located in the Southern Marginal Zone of the Limpopo Metamorphic mobile Complex. All the above rocks are altered to different extents to produce mainly serpentinite.

Ventersdorp Supergroup (3000Ma to 2100Ma) lavas also host komatiitic basalt and picrite in the lower parts of the Allanridge Formation and the Loraine and Edenville formations. The Lower Zone of the Rustenburg Layered Suite, which constitutes a section of the lower part of the Bushveld Igneous Complex (2050Ma), hosts coarse peridotites as extensive tabular bodies. Satellite intrusions associated with the complex also host similar rocks. Olivine-rich rocks also occur as pipes which cut across the layered portions in the Lower and Critical zones of the suite. These tend to be composed of a core of dunite which, in places, hosts economic platiniferous and nickeliferous deposits. The dunite is enveloped by pyroxenites with variable contents of olivine.

The Tugela Rand Suite, as well as the Mambulu and Sithilo complexes, both being parts of the Tugela Terrane, also host peridotite, as do the Sithilo Complex and the Equeefa Suite in the Mzumbe Terrane. These rocks were formed in the Late Proterozoic at around 1120Ma. Falling almost on the border with Mozambique, between the Shingwedzi and Crocodile rivers, is the Umkondo Igneous Province (1112Ma-1106Ma). Its lithologies include komatiites. Picrite is also observed in the Grootderm Formation of the Late Proterozoic to Early Palaeozoic (900Ma-450Ma) Gariep Belt.

Karoo (250Ma to 150Ma) basic volcanic rocks are also host to ultramafic, phaneritic and peridotitic components. Rift-related tholeiitic picrites are recorded in volcanic sequences along the Libombo-Mwenezi-Save monoclinal flexures.

Olivine is also an essential mineral in kimberlite pipes and dykes. In South Africa, they occur in ten main clusters and range in age from the Late Proterozoic to the Cretaceous. Some are economically diamondiferous but most are not.

Key words and phrases: carbon sequestration, olivine, stratigraphic column, dunite, harzburgite, lherzolite, basalt, wehrlite, peridotite, basalt, picrite, komatiite, melilitite, nephelinite, serpentine, kimberlite, pyroxenite

The suitability of the onshore Zululand Basin for geological CO_2 storage in South Africa: sedimentology, mineralogy and borehole correlations

Tibane V[1*], Landman B[1], Ndongani F[1], Harris P[2], Altermann W[1]

1 – Department of Geology, University of Pretoria, South Africa
*victor.tibane@up.ac.za 2 - GeoSpectral Imaging

A geological CO_2 storage project in South Africa aims at injection of CO_2 into underground formations, starting a test injection phase in 2017 [1]. One of the proposed injection test sites is the Cretaceous onshore Zululand Basin, KwaZulu-Natal. During the 1960s, ten boreholes were drilled on the onshore Zululand Basin by SOEKOR for exploration of hydrocarbons. The barren and dry drills were, however, soon abandoned. The cores ZA, ZB and NZA, stored at the National Core Library of the Council for Geosciences, Pretoria, were logged and spectrally scanned using a sisuRock Mobile hyperspectral imaging instrument, and studied for lithofacies, mineralogy and geochemistry, to investigate the vertical lithological distribution and lateral facies correlations. Thin sections prepared from 100 rock samples from the cores were studied as to the morphological and mineralogical properties of these rocks. The same 100 samples were investigated using XRF and XRD.

The onshore Zululand Basin covers an area of 1000-5000 km² with sedimentary rocks reaching 3500 m depth, dipping north-eastwards, and extending into Mozambique. The offshore part of the Zululand Basin covers an area of *c*. 13,500 km^2 in more than 200 m water depths.

The stratigraphy of the Zululand Basin comprises three formations: the Makatini Fm. of probably 125-115 Ma (Barremian to Aptian), unconformably overlies the Lebombo Group volcanic rocks of the Karoo Igneous Province [2]. It comprises small-pebble conglomerates, sandstone, silts/siltstones and limestones and is 80 m thick. The Mzinene Fm. consists of glauconitic siltstones and cross-bedded sandstones which contain a rich invertebrate fauna including bivalves, gastropods, ammonites, nautiloids and echinoids and is up to c. 650 m thick, as indicated by the borehole data. In places, the Mzinene Fm. rests unconformably on the Lebombo lavas and is separated by a hard ground from the Makatini Fm. This hard ground has however not been identified in the cores. The St Lucia Fm. (reaching probably into Maastrichian) exposes a similar lithology to the Mzinene Fm. It is separated from the latter by a slight angular unconformity interpreted from seismic profiles, but not traceable in the borehole. The thickness of St Lucia Fm. is c. 900 m, as indicated by the borehole data.

The clastic rocks of the three formations consist of silty sandstones at the bottom covered by igneous rocks which are in turn overlain by intercalation of sandstone with siltstone, silty mudstones and calcareous sedimentary rocks, with limestones at the top of the sequence. The mineralogy comprises quartz, plagioclase, mica, clay minerals and accessory hematite in places, cemented by calcite. The carbonate cement content decreases significantly moving down the stratigraphy. The lithofacies of ZA core correlate well with those of ZB. Correlation to NZA borehole is less good. In general, the silty sandstones of the basin are overlain by mudstones and siltstones, making the Zululand basin a potential laboratory for experimentation of CO_2 storage. ZA and ZB contain silty sandstones at the depth greater than 800 m. The sandstones are of mineralogical compositions that can react with $scCO_2$. They are bounded by mudstones intercalating with siltstones. The overlying mudstones contain the suitable mineralogy for trapping of CO_2 after injection.

[1] Cloete M. (2010). *Atlas on geological storage of carbon dioxide in South Africa*. Council for Geoscience, Pretoria, p. 59.
[2] Shone R.W. (2006). Onshore post-Karoo Mesozoic deposits. Chapter 26 In: Johnson M.R. *et al*. (Editors): *The Geology of South Africa*. Geol. Society of South Africa. 541-552.

Environmental mineralogy for soil contamination by radioactive Cs due to 2011 Fukushima NPP accident

Akai J[1*], Kudo H[2], Fukuhara H[3]

1 - Department of Geology, Fac.Science, Niigata University *akai@geo.sc.niigata-u.ac.jp 2 - Dep.Chem., Fac.Sci., Niigata Univ. 3 - Dep.Bio. Fac. Ed. Niigata University

The Fukushima Daiichi Nuclear Power Plant accident has caused as wide soil contamination by radioactive Cs as the Chernobyl accident did. It is well known that sorption of radioactive Cs in soil does not go so deep: most of the Cs is less than 10 cm deep. This is due to strong sorption of Cs by soil. Soil is fundamentally composed of minerals containing clay minerals and organic matters, and various organisms living in it. Absorption and desorption experiments of Cs were conducted for several phyllosilicates (kaolinite, sericite, montmorillonite, vermiculite, chrysotile and biotite), zeolite and solid organic matter (dead and green leaves). The results confirmed the characteristic sorption and desorption of Cs by these materials. The relative capacity and strength of different materials for sorption of Cs followed the order: zeolite (clinoptilolite) >2:1 type clay mineral >1:1 type clay mineral >dead and green leaves.

Culture experiments using bacteria of both naturally living on dead leaves in Iitate village, Fukushima Pref., and bacterial strains of *Bacillus subtilis*, *Rhodococcus erythropolis*, *Streptomyces aomiensis* and *Actinomycetospora chlora* were carried out. Non-radioactive 1% Cs solution (CsCl) was added to the culture media. Two types of strong or considerable bacterial uptakes of Cs were found in bacterial cells. One is that Cs was contained mainly as globules inside bacteria (Figure1) and the other is that Cs was absorbed in the whole bacterial cells. The globules consisted mainly of Cs and P. Thus, characteristics of important factors of phyllosilicates, organic matter containing dead leaves, bacteria and microorganisms, and plants, in recirculation of Cs were clarified in more detail.

The future diffusion and recirculation behaviour of Cs in the environment is discussed using a schematic model figure (Figure 2). The concrete process of 'hot spot' formation depends on each situation of every environment.

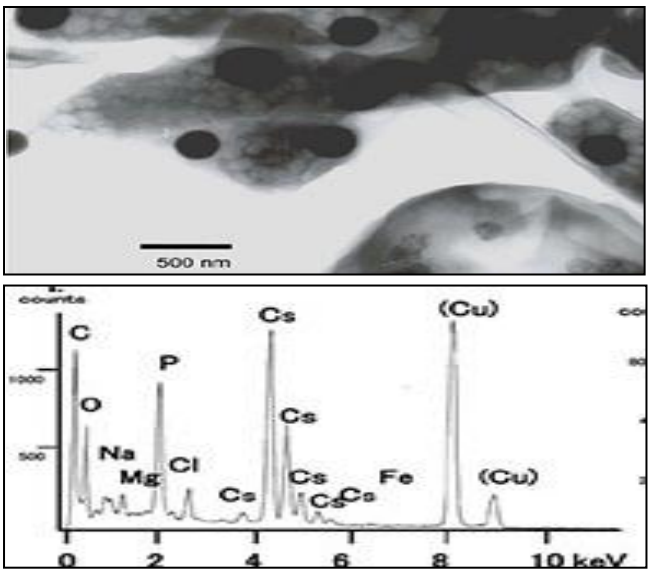

Figure 1: TEM image of bacteria containing Cs-rich granules (top) and its EDS analysis result (bottom)

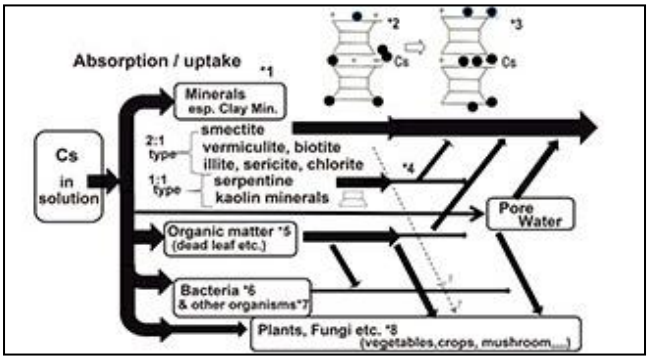

Figure 2: Possible recirculation of radioactive Cs in the surface environment for the case of Fukushima Daiichi NPP accident.

Mineralogy and microbial diversity in As-rich waste dumps

Amoako F[1*], Majzlan J[2], Kothe E[1]

1 - Friedrich-Schiller-University *yeboco@gmail.com 2 - Jena University

Weathered sulphides are a rich source of secondary minerals, including ferric-arsenates. The geochemistry and chemical stability of the arsenates is the subject of many research fields, due to the severe impact of arsenic on the environment. The microbial impact on such habitats is of great interest as well. Here, we study biogeochemical changes upon microbial impact on arsenate minerals from the medieval waste dumps in the Kaňk deposit, Kutná Hora (Czech Republic), and two historical mines from Rotgülden-Salzburger Land (Austria) and Chyžné (Slovakia).

The minerals occur as olive-green, yellow or brown nodules or crust precipitates. Optical microscopy shows anhedral, fine-grained, nanocrystalline or amorphous phases trapped in the interstices of subhedral quartz and feldspars gangue minerals, indicating a strongly altered environment. In X-ray diffraction, scorodite ($FeAsO_4{\cdot}2H_2O$), with sulphates; gypsum ($CaSO_4{\cdot}2H_2O$) and hydroniumjarosite [$(H_3O)Fe^{3+}{}_3(SO_4)_2(OH)_6$], are common in all three localities. The ferric arsenates comprise zýkaite [$Fe_4(AsO_4)_3(SO_4)(OH){\cdot}15H_2O$], bukovskýite [$Fe_2(AsO_4)(SO_4)(OH){\cdot}9H_2O$] and kaňkite ($FeAsO_4{\cdot}3.5H_2O$). The scanning electron microscope images show the arsenate morphology as prismatic, acicular or botryoidal crystals in the fine-grained clay-rich matrices. The arsenic is highly mobile, distributed widely in other mineral phases, and is enriched in the gel phases. The amorphous gels predict the paragenesis of the Fe-rich secondary minerals, through element partitioning in the inhomogeneous mass.

The microbial diversity was assessed by cultivation to study the microbial community functions and ecological relevance, and to obtain strains for study of physiological features. The samples show low microbial prevalence (cfu $<2*10^5$), and are dominated by coccoidal, Gram-positive strains (90 %). More microbial diversity was obtained from standard agar media while the wild-type microbes thrived on modified minimal agar media. The majority of the isolated strains is aerobic or facultative anaerobic, and are able to excrete siderophores, while tolerating 5 mM to 1000 mM arsenate. Only a few nitrate reducers were found. The 16S PCR rDNA sequences were dominated by actinobacterial (*Bacillus sp.* and *Afipia sp.*) and proteobacterial (*Advenella sp.*) strains. The most prevalent fungi were identified to be ascomycetes, with low counts for basidiomecytes or zygomycetes, most likely because of mould ascomycetes producing high amounts of asexual spores able to survive detrimental conditions.

Transformations, immobilization and mineralization of toxic metals by microbes

Cheng Y*, Xu X, Han R, Lin W

College of Environment and Resources, Fuzhou University, Fujian, 350108, China
*yjcheng@fzu.edu.cn

Anthropogenic sources of the toxic metals chromium and uranium have contaminated the ecosystem and become major public and political concerns. Bioremediation, a process by which microorganisms transform aqueous metal ions into amorphous or crystalline precipitates, is regarded as a promising and cost-effective strategy for remediating chromium and uranium contamination. In this report, we describe the potential and limitations of bioremediation for these two toxic metals and highlight the important mechanisms of biologically mediated transformations, immobilization and mineralization of toxic metals during the course of remediation. The results are as follows:

Firstly, experiments were designed to explore the factors that affect the immobilization of Cr(III) in a bacterial system. We focused our study on the cell debris of *Ochrobactrum anthropi*, which was proven to be the active component for both Cr(VI) reduction and Cr(III) immobilization. X-ray absorption fine structure (XAFS) analysis and the selective modifications of cell debris clearly verified that the coordination of Cr(III) occurs on the *Ochrobactrum anthropi* cell surface via the chelating coordination with carboxyl- and amido-functional groups. Competitive coordination experiments of Cr(III) revealed that the most active coordination molecules for Cr(III) are the ones with conformation of carboxyl and amido functional groups or two carboxyl functional groups or mercapto, carboxyl and amido functional groups. We believe that it is the preferential coordination of Cr(III) to the soluble organic molecules such as amino acids and their ramifications, or molecules containing multi-carboxyl groups in the bacterial culture medium, that inhibits an effective immobilization of Cr(III) on the cell. Based on this understanding, a strategy with two-step control of the medium was proposed, and this achieved the full immobilization of Cr(VI) as Cr(III) by *O. anthropi* in 50 l pilot-scale experiments.

Secondly, microbial communities of the Shihongtan uranium deposit, Xinjiang, China, were investigated by molecular biological techniques and traditional cultivation techniques. PCR-DGGE and PCR-RFLP analyses suggested that there were a number of bacteria and archaea in Shihongtan uranium deposit. Phylogenetic analysis indicated that the bacterial communities were homologous with *Firmicutes*, *γ-Proteobacteria* and *Actinobacteria*, while most of archaea showed close evolutionary relationship with *Halobacteriaceae*. Furthermore, a total of 36 bacterial strains were isolated from the uranium deposit and two pollution sites. A selection of three kinds of native bacteria and two kinds of genetically engineered bacteria were grown in a pure culture, and then interaction mechanisms were investigated between these five kinds of bacteria and uranium by AFM, electron microscopy and XAFS.

Primary and secondary minerals in the South African coal mine environment and their role in acid-mine drainage

Fourie J

Geostratum Groundwater and Geochemistry Consulting. johan@geostratum.co.za

A summary is given on geochemical test results performed as part of acid-mine drainage (AMD) studies at collieries in South Africa from the Witbank, Highveld, Free State, Ellisras and Springbok Flats coal fields. The acid-base accounting and X-ray diffraction (XRD) test results of 547 coal and clastic rock samples were assessed. X-ray fluorescence (XRF) and Scanning Electron Microscope (SEM) were performed on some samples.

Coal minerals are typically dominated by quartz and kaolinite, with some accessory to minor muscovite, plagioclase (typically oligoclase composition), K-feldspar and traces of pyrite, calcite, dolomite, siderite and rutile. In clastic rocks quartz is more dominant with respect to the other minerals above. In sandstone K-feldspar and traces of rutile are often higher, and pyrite and carbonate minerals often lower, with respect to coal and shale. Shale in the roof and floor often has higher siderite content than coal which in turn has a higher pyrite content which indicates a 1) higher sulphur activity and 2) more reducing conditions in the coal during deposition. Smectite clays are present as a result of weathering whereas chlorite (as a minor to major mineral) is often associated with recrystallisation of clays under contact metamorphism (with dolerite dykes) or higher geothermal gradient during diagenesis, e.g. in the Kwazulu-Natal Coalfield.

Disseminated euhedral pyrite is recognized as the dominant sulphide in coal although exceptions exist on local scale. Marcasite has been identified where pyrite recrystallization under neutral - slightly alkaline conditions took place. Cu and Pb were often assumed to be present in pyrite but Scanning Electron Microscope (SEM) studies at two mine sites rather found them present as chalcopyrite and galena respectively.

Calcite and dolomite are frequently present as traces in the sedimentary rocks but are usually not high enough to neutralize acid drainage from coal and shale in contact with atmosphere.

Sulphate is the major anion in coal mine drainage. The secondary mineralogy in AMD often controls actual measured sulphate and metal concentrations of mine decant. As most of central South Africa is semi-arid, efflorescences of secondary minerals are especially abundant during the drier months. Sulphate salts of Ca, Mg, Na, K, Al and Fe are typically present and gypsum, halotrichite, hexahydrite, bloedite, thenardite and jarosite are just some minerals identified by XRD at 3 mine sites. The challenge for geochemical modelling is that limited thermodynamic data is available on several important secondary minerals that control AMD.

In acidic drainage Al, Fe and Mn are often elevated to between 10 - 100 ppm, but much higher values up to 500 ppm are possible, especially for Al and Fe. Mn is often present as Mn-oxides in sedimentary rocks or as a trace in especially siderite as identified by SEM. Mn is often elevated in mine drainage as a very persistent contaminant as it is stable even under neutral conditions.

Ni and Co are present as traces in pyrite and therefore also abundant in acidic drainage. At one site it was found that Ni and Co (at 500 - 1000 ppb) did not initially adsorb to ferrihydrate in acid drainage (pH 2-3) but were transported until more neutral conditions are encountered in the drainage course.

Characterization of a metal-contaminated waste rock dump using field portable X-ray fluorescence (FPXRF) spectrometry

Marescotti P[1*], Solimano M[1], Mazzei F[2], Panetta D[2], Brancucci M[3], Marin V[4], Salmona P[4], Lucchetti G[1]

1 - DISTAV - University of Genova *marescot@dipteris.unige.it 2 - TQ s.r.l., Genova, Italy 3 - Geospectra s.r.l. Genova, Italy 4 - DSA - University of Genova

Waste rocks dumps are chemically heterogeneous deposits piled up during mining exploitation over tens of years. They contain non-mineralized rocks and low-grade mineralization and are typically characterized by significant vertical and lateral heterogeneities in grain size, lithology, mineralogy and chemistry. Waste rock dumps are often sites of environmental concern because they commonly contain high levels of metals and metalloids which may be released to the circulating waters during weathering. Moreover, the metal leaching may be exacerbated, in sulphide-bearing waste rocks, by Acid Mine Drainage (AMD) processes.

With this work we investigated the chemical composition and the metal distribution within a sulphide bearing waste rock dump using a field-portable energy dispersive X-ray fluorescence (FPXRF) spectrometer (X-MET7500, Oxford Instruments) with a FP (Fundamental Parameter) calibration built-in by the factory. Confirmatory analyses were performed by means of ICP-OES and ICP-MS (AcmeLabs®, Canada).

The site chosen for this study is a small-sized dump (about 3500 m^2) from an abandoned Cu-sulphide mine (Rio Bansigo mine, eastern Liguria, Italy), which was extensively exploited from 1877 to 1935. We performed a superficial sampling (20 cm from topographic surface) by applying statistical methods based on a 15 m^2 sampling grid designed using the open source GIS software GrassGis 6.4. Moreover, four samples from the uncontaminated soils surrounding the waste rock dump were analyzed to determine the natural background of the studied area. The results, obtained with these different techniques, showed a good correlation for most of the detected elements. Regression analysis shows a near 1:1 correspondence between FPXRF and ICP for Cu and Zn and a good correlation for Ni, Mn, Cr, V and Pb. The only elements with significant statistical differences are those occurring in concentrations very close to the minimum detection limits of the FPXRF (Ba, Cd, Sn).

The analytical data were processed in GIS for spatial analysis in order to recognize the spatial relationships among the different variables. Thanks to the possibility of analyzing a large number of samples by means of FPXRF, very detailed contour maps were then drawn for each metals, which allowed to evaluate the metal distribution in the entire mine dump area and to recognize the presence of several hot spots.

Our results evidenced the feasibility of a detailed evaluation of the metal hazard within waste rock dumps using a field-portable XRF device, thus providing a powerful tool for quick decision-making in the field and reducing the need of off-site laboratory analyses. Moreover, the possibility to perform a large number of *in situ* analyses, in a cost-efficient and timely manner, allows the production of geo-environmental models and detailed mapping of metal distribution based on a geostatistical approach as well as the recognition of pollution hot spots.

Assessing environmental risks associated with sulfidic mine waste: a gold case study

Opitz A[1*], Becker M[2], Broadhurst J[2], Harrison S[1], Franzidis J[2]

1 - Centre for Bioprocess Engineering Research (CeBER), University of Cape Town *optale001@myuct.ac.za 2 - Minerals to Metals Initiative, University of Cape Town

Acid rock drainage (ARD) poses one of the most serious environmental challenges associated with the mining industry. Formed through the oxidation of sulfide minerals in the presence of oxygen and water, ARD generation is further exacerbated by the regeneration of lixiviates by naturally occurring, iron- and sulphur-oxidising micro-organisms. In South Africa, ARD is most commonly associated with the coal and gold mining industries. Of particular concern is the number of historical and abandoned mines and the quantities of mining waste posing potential environmental hazards.

Management and prevention of this issue relies on accurate characterisation of the ARD generation potentials of waste samples. Classification of the ARD potential is achieved through the quantification of acid-generating and acid-consuming components present within a sample. This quantification is often completed sequentially from laboratory-scale screening tests through to kinetic field studies. In addition, mineralogical sample analysis is used to assist in the screening process and interpretation of experimental results. Initial laboratory-scale static ARD tests, however, are focused on primary oxidation of sulfide minerals within the sample and often fail to account for potential environmental impacts due to leaching of non-sulfidic constituents. In addition, the toxicity and concentrations of trace elements within samples is not included in the screening tests. This study aimed to assess the environmental risks associated with a sample of gold gravity tailings from a historical dump using mineralogical analysis and standard laboratory ARD screening tests.

Results from the static ARD characterisation tests indicated no net acid generation would result from sulfidic oxidation of the tailings sample. Biokinetic accelerated weathering tests and ARD potentials calculated based on mineralogy confirmed this result. Trace metal analysis of the leach liquors, however, showed a significant environmental risk associated with the release of As, Pb and U during laboratory tests. Other elements of potential environmental significance included Al, Cu, Zn and Ni. Mineralogical test work indicated uraninite and brannerite as the sources of soluble U, while metal sulfides accounted for the presence of Pb, As and base metals. In conjunction with these results, sequential chemical extraction experiments were performed to provide information on the distribution and potential availability of elements within the tailings sample. The findings from this study will be used to aid in the development of a more robust protocol for the characterisation of environmental risks associated with sulfidic mining wastes.

Mineral formation processes at the burning dump of the Anna coal mine, Alsdorf, Germany

Witzke T[1*], Kolitsch U[2], de Wit F[3]

1 - PANalytical *thomas.witzke@panalytical.com 2 - NHM Wien, Austria
3 - Maastricht, The Netherlands

The Anna coal mine at Alsdorf near Aachen, North Rhine-Westphalia, Germany, produced bituminous coal from 1854 to 1983. On the Anna I dump material was deposited from 1850 to 1964. Self-ignition of the dump started in the 1950s, and the burning process is still active in 2014. Detailed mineralogical studies resulted in the identification of around 60 phases (some new to science) formed as products of the dump fire [1].

The geochemical system of the Anna I coal mine dump includes, beside the original rocks (sedimentary rocks, coal, etc.), the endogenic and exogenic processes. Rocks and minerals are altered by self-ignition and the continuing combustion of the residual coal. Pyrometamorphism leads to changes in mineralogy and chemistry of the rocks. Several minerals, mainly sulfates and chlorides, are newly formed from gaseous species or from the action of acidic solutions on the rocks. Exogenic influences include rainwater, snow, and the oxygen supply by wind pressure. Gaseous species originated directly from the coal combustion or the interaction with sedimentary rocks comprise H_2O, CO_2, NH_3, HCl, HF, H_2S, H_2Se, SO_2, SO_3, $C_{14}H_{10}$, SiF_4, and Fe_2Cl_6 / $FeCl_3$. Most of these species are directly involved in the mineral formation processes. Additional elements like Al, Mg, Ca, Na, K, Ni, Zn, Mn and B are transported via acidic solutions near the surface of the dump.

Mineral formation processes in the burning coal mine dump can be in some cases very simple and in others very complex. Generally, as formation processes can be established:

1) phase transitions including sublimation, condensation, solidification and solid-state phase transformations (sulfur, selenium, ravatite - $C_{14}H_{10}$),
2) chemical reactions of gases, like the reaction of NH_3 and HCl, the oxidation of H_2S or H_2Se, and the reaction of gaseous Fe_2Cl_6 with H_2O (salammoniac, sulfur, selenium, cryptohalite, hematite),
3) pyrometamorphism, high-temperature metamorphism of sedimentary rocks to low-grade dehydration reactions (indialite, mullite, bassanite),
4) metasomatism (no example from the Anna mine), and
5) nucleation from solutions (kremersite, most of the sulfates like tschermigite, boussingaultite, alunogen, thermessaite-(NH_4), adranosite-(Fe) and -(Al) and many others).
The mineralogy of the burning Anna I mine dump is comparable to that of volcanic fumarolic systems, especially to the La Fossa crater, Vulcano, Italy.

[1] Witzke T. *et al.* (2014). Mineralogy of the Burning Anna I Coal-Mine Dump, Alsdorf, Germany. Chapter 7 in: Stracher, G. B., Prakash, A. and Sokol, E. V.: *Coal and Peat Fires: A Global Perspective*, Volume 3. Elsevier.

Distribution patterns of contaminants in the Mogale gold tailing dam: a case study from South Africa

Abegunde O*, Wu I C, Okujeni C, Siad A

University of the Western Cape *3207599@uwc.ac.za

This study evaluated the magnitude of possibly leachable metals and predicted the AMD discharge over time, from the Mogale tailings dam into the environs in Randfontein area, Witwatersrand Basin, South Africa. Drill core samples were analysed for multi-elements and evaluated using multivariate statistical and geochemical mass balance techniques.

The tailings dam lithology was grouped into four distinct layers. The uppermost oxidized layer is siliceous and contains the highest SiO_2 (87.32%) contents, which is accompanied by the lowest contents in U, As, Zn, Ni, Co, and Cu. A decrease in SiO_2 (76.39%) content occurs, coupled by an increase in U, As, Zn, Ni, Co, and Cu, reaching maximum contents in layer 3. Layer 4 is the least weathered horizon.

The cluster analysis grouped the samples into four sub-clusters based on the variation in SiO_2 and Al_2O_3 contents. Factor analysis, which explained 83.542% of the total data variance, related the seven controlling factors of element distribution to the occurrence in ore elements (sulphides), silicates, mining additives and refractory minerals. The geochemical mass balance showed variable gain and loss of oxides and trace elements within each layer. Based on the variation patterns of the total sulphur contents and other mobile elements, about 0.164kg/tonne/yr. (±0.02) of the tailings materials are leached yearly. Layer 1 is the most altered.

Keywords: Acid Mine Drainage; Assessment; Prediction; Weathering; Geochemical data; Geochemical mass balance; Multivariate statistics; Contamination

Identification of silica impurities in bentonite by SEM-EDX analysis

Bai J, Yuan G, Jia Y, Han Z, Zhao Z, Zhang B, Su H*

School of Chemistry and Chemical Engineering, Inner Mongolia University.
haiquansu@yahoo.com

Bentonites usually contain quartz, α-cristobalite and opal as associated silica impurities that are difficult to identify and remove. The silica impurities must be removed due to the carcinogenicity of silica dust. Therefore, it is more important to identify effectively the silica impurities in bentonites.

This work exploits the use of the SEM-EDX to provide a non-destructive method for the determination of the associated silica impurities in the bentonites. The mineral composition of the sample is as follows: montmorillonite, 65.1%; cristobalite, 34.9%; quartz, 1.9%. As seen from SEM images and EDX maps of the selected section (Figure 1) and line (Figure 2), the abnormal enrichment of silicon and oxygen elements relative to other elements indicates silica grains were easily distinguished.

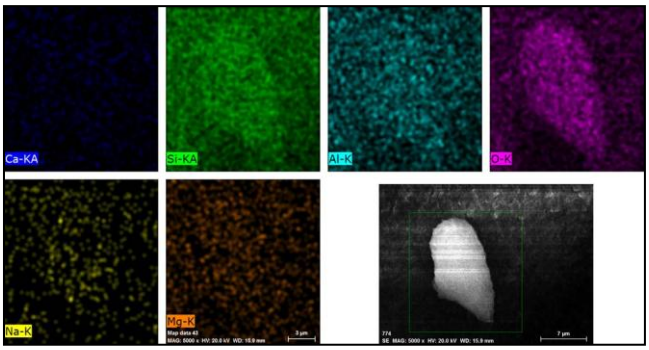

Figure 1: SEM image and EDX maps of elements Ca, Si, Al, O, Na, and Mg for section across silica impurities in bentonite.

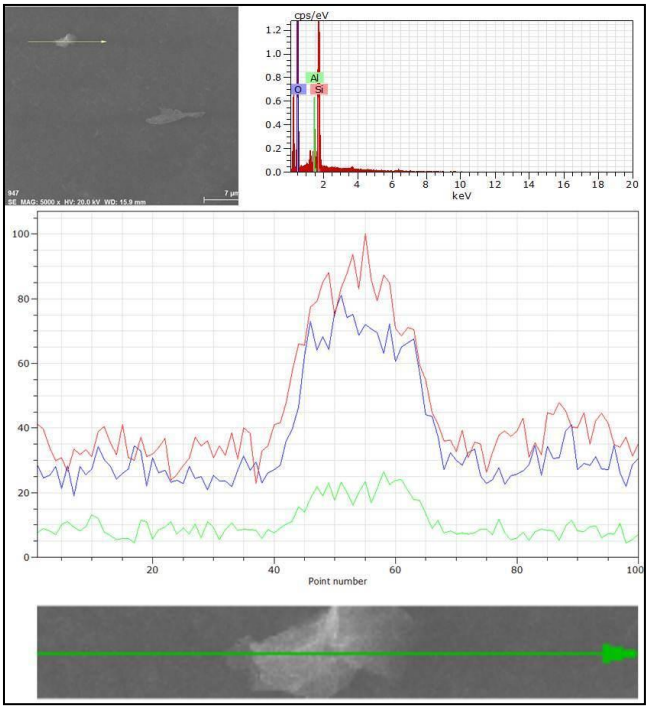

Figure 2: SEM image and line scanning EDX maps for sections across the silica impurities in bentonite.

Acknowledgement: Project supported by the science and technology innovation team of high efficiency and clean conversion technology for superior resources in Inner Mongolia (grant no. 21020101) and the Inner Mongolia University high-level scientific research foundation for the introduction of talent (grant no. 135128).

A geochemical characterization of sediments of the Mt. Amiata Hg district and a preliminary estimation of mercury background

Di Benedetto F[1*], Rimondi V[1], Benvenuti M[1], Benvenuti M M[1], Buccianti A[1], Costagliola P[1], Lattanzi P[2]

1 - Univ. Firenze - Dip. di Scienze della Terra, Italy *francesco.dibenedetto@unifi.it
2 - Univ. Cagliari - Dip. di Scienze Chimiche e Geologiche, Italy

The Mt. Amiata region (southern Tuscany, Italy) hosts one of the most important Hg districts in the world, determining a widespread Hg (and associated As) geochemical anomaly. Mercury ores have been exploited for Hg production up to the end of 1970s, resulting in the widespread occurrence of Hg-contaminated discarded materials next to the mine centres. As a result, extensive Hg contamination affects the Pagliola Creek ecosystem, which drains the most important Hg mine of Abbadia San Salvatore. Stream sediments of different age were sampled along the Pagliola Creek in order to reconstruct the history of Hg(As) diffusion in this region. Moreover, a paleo-hydrographic reconstruction of the Pagliola Creek was attempted, and four different typologies of sediment sampled. Multivariate analysis was applied to observe if the operational subdivision of sediments by stratigraphy corresponded to remarkable differences in main geochemistry. Analysis showed that sediments can be clustered in two main groups, *i.e.* pre- and post-mining sediments, on the base of the Al_2O_3/CaO ratio. Accordingly, Al_2O_3/CaO >1 and Al_2O_3/CaO ≈1 characterized pre- and post-mining sediments, respectively, suggesting a progressive enrichment in CaO as sediments become younger in age (post-mining). According to our study, Hg in the Mt. Amiata sediments is not randomly distributed: Hg, in fact, is inversely correlated to Al_2O_3/CaO ratios (R^2 = 0.87) and directly to the CaO content, increasing up to two orders of magnitude between pre- and post-mining sediments. Common to most of Hg mines worldwide, calcination was carried out at the Abbadia San Salvatore mine, which consisted in the addition of lime to a first roasted material to recover residues of metallic Hg. Final discarded wastes are then termed calcines, and are enriched in CaO and Hg, due to the inefficiency of the extraction process. Natural weathering of these materials caused CaO and Hg enrichment of recent and present-day (post-mining) stream sediments of Pagliola, which are still directly impacted by runoff from the Abbadia San Salvatore mine site. Accordingly to the results of our study, CaO likely represents a geochemical marker of such a weathering of calcines, and can act as a proxy for Hg in the Pagliola Creek watershed.

A preliminary Hg regional background of 2-6 µg/g was set up for the Mt. Amiata area, which largely exceeds the Hg established contamination level of Italy. As a result of this study, a new reliable regulation for Hg should be defined for this region, taking into account the natural Hg presence in the environment.

Micro-XANES investigations on oxidation crusts from mine-waste rocks affected by AMD process

Carbone C[1], Consani S[1], Giuli G[2], Marescotti P[1*], Lucchetti G[1]

1 - DISTAV - University of Genova *marescot@dipteris.unige.it 2 - Scuola di Scienze e Tecnologie - University of Camerino

In this work we studied the mineralogical and chemical variations of representative mine-waste rock samples from the Fe-Cu sulphide Libiola Mine (Eastern Liguria, Italy), by means of combined synchrotron-based µ-XRD, µ-XRF, and µ-XANES analyses performed at ESRF beamlines (Grenoble). The waste-rocks of this site are acid generating and are characterized by high amounts of completely to partially altered sulphide-rich mineralization. Moreover, another major environmental problem is the potential mobilization of PTE (Potential Toxic Elements, such as transition and heavy metals and other harmful elements), which can be concentrated in circulating waters, thus polluting soils as well as aquatic and subaerial ecosystems. The aim of this work was to study Fe-oxides and -oxyhydroxides occurring in different types of sulphide-rich rocks representative of the Libiola mine wastes, in order to monitor the alteration mechanisms during AMD processes. The studied samples are composed by: a) stratified crust formed by the ageing of ochreous muds precipitating from acid mine waters discharged at mine adits, b) partially altered massive pyrite-rich mineralization; c) recrystallized pyrite-rich stockwork mineralization. In this study, we demonstrated that the combined use of micro-synchrotron-based techniques can be succesfully applied to the study of complex mineralogical systems, since these techniques are more sensitive than "routine" ones. Moreover, the coupled use of synchrotron-based µ-XRD and µ-XRF enables to obtain a picture of the mineralogical and chemical evolution of the alteration process; in fact, µ-XRD and µ-XRF analyze with great detail the mineralogy and the mineral chemistry of primary and secondary minerals allowing to investigate the chemical behaviour of PTE and their distribution among primary and secondary phases. In particular, the combined use of µ-XRD and µ-XRF highlighted a different behaviour of some PTE, such as Zn and As, during the evolution of the alteration process. The µ-XANES analyses, performed at S k-edge and Fe k-edge, proved to be even more sensitive with respect to the alteration process than the other synchrotron-based techniques. In fact, µ-XANES at S k-edge analyses showed the presence of sulphates phases even when present concentrations too low to be detected by the other techniques (XRD). Fe k-edge µ-XANES data allowed to detect Fe redox variation, due to alteration processes of sulphides, across selected transects. A quantitative analysis of the sulfide/sulphate ratio was performed using the µ-XANES S k-edge spectra, while the Fe k-edge spectra were used in order to obtain the distribution of Fe^{3+} between primary and secondary phases.

Metal accumulation in plants and its toxic effects on cells in the upper part of ore deposits

Song C A[1*], Song W[2], Yang Z[3], Jang C[4]

1 - College of Earth Science, Guilin University of Technology, China *gldysca@126.com 2 - Guangdong University of Technology, Guangzhou, China 3 - Guilin Research Institute of Geology for Mineral Resources 4 - Guilin University of Technology

We conducted a study on characteristics of vegetation geochemical anomalies and the cell in plants (*Cunninghamia lanceolata*, *Pinus massoniana* and *Dicranopteris pedata*) at the Xinglu Sn-Pb, the Dachang Sn-Pb-Sb-Zn, the Lingchuan Pb-Zn and the Longshui Au-Cu ore deposits in Guangxi Province, P. R. China. This study shows that the content of metal elements in the soil and plants growing in the ore deposits exceeds those in background area, and produced obvious geochemical anomalies. Elements are categorized into two types according to their plant absorbed-rate. One is the non-obstacle type whose absorbed-rate is greater than or equals 1, such as Au, Ag. The other is the obstacle type whose absorbed-rate is smaller than 1, such as Cu,Pb,Zn,Sn,As and Sb. Under a transmission electron microscope (TEM), the excess metal elements in the ore deposit-grown plants are presented as high electron-density substances (HEDS) **(Table 1)**. HEDS are precipitated in the plant leaf cell walls, chloroplasts and vacuoles in irregular pellets and in a radial pattern. HEDS can result in phytotoxic effects, deforming and injuring cellular tissue. For example, the directional sheet-phyllo structures in chloroplast have suffered significant damage.

#	K	Na	P	S	Ca	Si	Al	Ti	Fe	Cr	Cu	Pb	Au	Ag	Sn
XL01	6.70	4.43	-	0.72	12.6	-	0.57	3.31	-	17.0	53.0	-	-	-	1.71
LC01	2.54	-	-	-	4.40	8.30	-	-	2.04	-	40.7	42.0	-	-	-
LS02	-	-	-	29.9	9.49	-	-	-	-	-	23.3	-	37.3	-	-

Table 1. Analytical results (10^{-2}) of centralized high-electron density substances in the cells of plants grown in mining polluted soil by energy dispersive spectrometry. XL01 the leaf of *Dicranopteris pedata* grown in Xinglu Sn-Pb ore deposit soil; LC01 the leaf of *Dicranopteris pedata* grown in Lingchuan Pb-Zn ore deposit soil; LS02 the leaf of *Pinus massoniana* grown in Longshui Au-Cu ore deposit soil; "-" not detected.

Acknowledgment: This study is supported by the National Natural Science Foundation, P. R. China (41363003); the PhD Start-up Fund of Guangdong Natural Science Foundation (No. S2012040007439).

Protective effects of minerals on organic matter

Blattmann T[1], Ploetze M[1*], McIntyre C[1], Wessels M[2], Eglinton T[1]

1 - ETH Zurich *ploetzel@ethz.ch 2 - ISF Langenargen

Environmental matrices including soils and fluvial and lacustrine sediments from the Lake Constance catchment and basin were investigated to assess controls of mineralogy and mineral surface area on organic carbon contents. Provenance of organic carbon was quantitatively evaluated by natural abundance stable and radiocarbon isotopic compositions using a ternary mixing model distinguishing between rock, soil, and lacustrine-derived organic matter. Overarching trends between mineral surface area and organic carbon contents were found for soil and sedimentary material strongly suggesting associations between organic matter and mineral surfaces. Large amounts of oxidation-resistant organic carbon fractions were found in phyllosilicate-rich (especially smectite and illite), high surface area soil and sediment mesodensity fractions supporting the notion that phyllosilicates intensely participate in the stabilization of organic matter. From coupled organic radiocarbon and quantitative mineralogical information, organic carbon turnover and type appears linked with mineralogy. There is evidence for an association between petrogenic organic carbon and quartz in modern soils and sediments inherited from eroding parent sedimentary rocks. Environmental matrices with phyllosilicate fractions high in smectite content exhibit rapid organic carbon turnover.

Binding of amino acids on mineral surfaces: results from X-ray scattering, optical spectroscopy and AIMD simulations

Waychunas G[1*], Stubbs J[2], Eng P[2]

1 - Lawrence Berkeley National Laboratory *gawaychunas@lbl.gov 2 - University of Chicago

The interaction and binding of organic species and amino acids with mineral surfaces is a large frontier in geochemistry. It is well known that mineral surfaces may sequester, sort, or contribute to breakdown (or conversely, condensation) reactions of organic molecules, but the details of these processes are very poorly informed. As opposed to inorganic sorbates, which interact with a surface by forming covalent and hydrogen bonds, and also couple strongly to surface water molecules; organic structures may have partial or dominant hydrophobic interactions and reduced interaction with waters, multiple charges on a single molecule such as a zwitterion, and very complex multi-site interactions with surface functional groups. In addition, a range of molecular conformations are possible, which may differ markedly from the solvated water-borne entity. These considerations have limited both the scope and utility of many studies in the past, with the vast majority involving measurement of uptake concentrations without information on the actual binding geometry or mechanisms. Yet the topic remains one of profound interest given enormous numbers of industrial organic pollutants, natural biological agents, and pharmaceutical breakdown products in the environment. Other questions, such as involving enantioselective processes in separating important bioactive molecules from racemates, have yet to be answered satisfactorily.

We are developing a program to couple sum-frequency vibrational spectroscopy (SFVS), surface X-ray scattering methods, and computer simulations to characterize organic species topologic interactions with well-known mineral surfaces. Initial investigations examined ethanol as a single monolayer, and as a bulk liquid, on the corundum R-plane (1-102) surface using SFVS. Subsequent studies have examined selenomethionine and other heavy atom-substituted amino acids sorbed on corundum and hematite surfaces. Such heavy atom substituted species enable both X-ray surface scattering and anomalous scattering measurements to be correlated. Ideally, X-ray scattering can reveal any surface atomic relaxations responding to the organic binding, and these can then be combined with moiety orientation and polarization from the SFVS data to reveal molecular binding and conformation. Anomalous scattering using the heavy atom also can reveal its ordered positioning and act as a convenient check point for structural modelling. The complexities and advantages of this approach will be described, as well as most recent results.

Crystal morphology of natural and synthetic colloids

Wieczorek A*, Händel M, Totsche K
Friedrich-Schiller University Jena *arkadiusz-krzysztof.wieczorek@uni-jena.de

The formation of colloids from natural aqueous solutions is influenced by a multitude of biogeochemical and physicochemical processes and the presence of a large diversity of geogenic and biogenic, inorganic and organic solution components. A frequently neglected class of components, when analyzing their influence on natural colloid creation, is dissolved organic matter (DOM) and physical constraints of pore space geometry. As DOM will interact with other phase components of solution and pore boundaries, what will influence the colloid creation processes in ground water? Therefore, we hypothesize that nanosized and colloidal particles formed in DOM bearing solutions and within confined space may differ from synthetic precipitates either by size, shape, crystallinity, composition or combinations of these elements. To investigate this, we analyzed natural colloidal particles collected from a limestone aquifer of the Upper Muschelkalk formation at Hainich National Park, Thuringia, Germany. Major components of this groundwater are Ca^{2+}, Mg^{2+}, Na^{+}, SO_4^{2-}, Cl^{-}, HCO_3^{-}, and about 1 ppm of total organic carbon (TOC) in dissolved and colloidal form. Synthetic nanoparticles were precipitated from a series of oversaturated solutions containing one or more of the following salts $CaSO_4$, $MgSO_4$, $Ca(HCO_3)_2$ and NaCl, typical for limestone environments. The solutions were produced using natural groundwater and pure water (milli-Q). Additionally, mixtures of organic solutions of acetate, citrate and pyruvate with above salts were created, as a control samples to the DOM solution. Droplets of such produced colloidal suspension were pipetted on silicon wafers and subject to air drying. For pore boundary representation we used physical constraints in the form of different types of metal grids with few to a few hundred micrometer-sized enclosed regions. The wafers were then analyzed by scanning electron microscopy (SEM) with energy-dispersive X-ray spectroscopy (EDX) and atomic force microscopy (AFM) to observe differences in shape, size, crystallinity and nanomechanical surface properties between natural colloidal nanoparticles and our synthetic counterparts.

Effects of surface heterogeneity in adsorption on silica polymorphs quartz and cristobalite

Zhu J*, Tang C, Zhou Q, Wei J, He H
Guangzhou Institute of Geochemistry, Chinese Academy of Sciences
*zhujx@gig.ac.cn

Silica minerals, any of the forms of SiO_2 including quartz, tridymite, cristobalite, coesite, stishovite and several others, make up approximately 12 percent of the Earth's crust and are the second in mineral abundance. The silica minerals are also important mineral composition of the soil, sediment, and air dust. As a kind of environmental mineral, the silica minerals play an important role in environment-related interface reaction process. Their surface chemistry properties, which are restricted by the structural characteristics, affect many physico-chemical processes which react on the surface of minerals or interface between minerals and waters.

Surface properties of silica are greatly affected by the surface silanols. There are two main types of silanol on the silica surface: the single and the germinal. Their distribution and density differ depending on the type of silica polymorphs and crystal surfaces. As a result, their performance in the adsorption of molecules will be different.

Surface properties of the most common crystalline silica, α-quartz, have been investigated experimentally and computationally. However, the differences between silica polymorphs are not yet clarified, and there is still a lack of enough experimental data and appropriate action mechanisms to interpret the heterogeneity of silica polymorphs. In our research work, two common silica polymorphs, α-quartz and α-cristobalite, were chosen to study the surface heterogeneity. Traditional acid-caustic titration method was used to measure the density of surface hydroxyl groups. Batch methylene blue adsorption experiments results reveal there is a slight but significant difference in the saturated adsorption amount of α-quartz and α-cristobalite. This difference is positively correlated with the difference of total surface silanols. The adsorption isotherm shows the adsorption is monolayer and the proportion of single and germinal silanols determines the affinity. X-ray photoelectron spectroscopy (XPS) results indicate the adsorption mechanism is electrostatic attraction. Combined with adsorption isotherms and XPS results, a novel model of dye molecules adsorption on the silica surface can be put forward.

Computational simulations have been performed to study the phenol adsorption on different surfaces of α-quartz and α-cristobalite and the influence of the surface silanol sites. The different adsorption energies of phenol on the surface of α-quartz and α-cristobalite have been discovered, corresponding to experimental data. The results also show that the surfaces with germinal silanols but lower silanol density have stronger interactions with the phenol molecule, indicating that for a single surface, the type of surface silanols has greater impact to organic adsorption than the density of silanols.

An XAS and EPR study of industrial quartz-resin composites: preliminary results and health survey in Tuscany

Di Benedetto F[1*], Bartoli D[2], Banchi B[3], d'Acapito F[4], Farina G[2], Iaia T[2], Innocenti M[5], Montegrossi G[6], Poli C[2], Romanelli M[1], Scancarello G[3], Tarchi M[2], Zoleo A[7], Capacci F[8]

1 - Univ. Firenze - Dip. di Scienze della Terra, Italy *francesco.dibenedetto@unifi.it 2 - AUSL 77 Empoli, Italy 3 - Lab. Sanità Pubblica, AV Toscana Sud Est, Italy 4 - CNR - OGG/IOM c/o ESRF, France 5 - Univ. Firenze - Dip. di Chimica, Italy 6 - CNR - IGG, Firenze, Italy 7 - Dip. Scienze Chimiche, Univ. Padova, Italy 8 - ASF, Italy

In the Empoli area of Tuscany, 8 companies are active in working stone and quartz-resin composite materials. Workers' exposure during finishing of artificial stones is associated with severe cases of silicosis arising in young subjects with relatively short seniority, often leading to lung transplantation.

The fate of respirable dust produced by this unhealthy activity (mechanical finishing of the artificial stone) is investigated through continuous-wave EPR, pulsed EPR and XAS spectroscopy, together with SEM-EDS microanalysis, and X-ray diffraction. The preliminary results show that that artificial stones, in spite of consisting almost exclusively of quartz and amorphous silica, are variably tinged with minute amounts of different mineral species. A variable speciation of numerous transition metal ions is also observed, coupled with the presence of a drastic change in the inorganic radical population. In contrast, no evidence of the presence of organic radical species was observed. Radical species consist of the Al defects in quartz in the raw samples, and frequent association with Si species is evidenced in manufactured materials. Moreover, the Fe speciation is completely changed from the raw to the manufactured materials, indicating the rare presence of metallic Fe contamination. Correlations with the manufacturing process, in particular comparing the dry and wet finishing steps, are proposed.

Potential risk of COx poisoning for casual workers at a South African brick manufacturing plant

Diko Makia L

University of Limpopo. dikom73@gmail.com

The South African Clay Brick Industry (CBI) is a sector that contributes towards job creation in the country, accounting for about 16921 direct employees. It is unclear if this estimate includes casual workers (CW). The latter refers to persons employed mostly during busy periods, and usually paid for results rather than time. In the production of bricks, the CBI mainly employs clamp kiln technology (accounting for 69% of total production). Despite their cost effectiveness, clamp kilns are associated with significant COx emissions. Exposure through incomplete combustion of scintles may lead to COx poisoning. In some instances (due to economic drivers of demand and supply), the kiln is not allowed to cool down completely prior to unloading of bricks. This may predispose CW to incidental exposures of COx through inadvertent inhalation. This study ascertains the extent to which such exposures may pose health threats to the CW. It further interrogates the legal framework and related ethical issues. The study concludes with recommendations for best practice.

Recent studies of biomolecular adsorption by minerals: cooperative and competitive effects

Hazen R[1*], Feuillie C[1], Foustoukos D[1], Cody G[1], Estrada C[2], Sverjensky D[2], Lee N[2]

1 - Carnegie Institution *rhazen@ciw.edu 2 - Johns Hopkins University

Experimental investigation of the adsorption of amino acids, pentose sugars, nucleosides, and nucleotides onto crystalline surfaces of rutile (TiO_2), brucite [$Mg(OH)_2$], diopside ($CaMgSi_2O_6$), alumina (Al_2O_3), zeolites, and clay minerals reveal both cooperative and competitive effects. We employ batch adsorption and proton titration, surface-enhanced Raman (SERS) and infrared (ATR-FTIR) spectroscopies, atomic force microscopy (AFM), sum-frequency generation (SFG) non-linear spectroscopy, and neutron scattering, as well as theoretical modelling. Recent experiments confirm earlier findings that molecules often adopt two competing adsorption conformations (e.g., standing up vs. lying down), depending on pH, ionic strength, and solute concentration. We observe cooperative adsorption effects, for example in amino acid adsorption on rutile or brucite surfaces. Ca^{2+} enhances glutamate adsorption, whereas it suppresses lysine adsorption onto rutile - effects that point to cooperative adsorption between Glu and Ca^{2+} and competitive adsorption between Lys and Ca^{2+}. We see similar effects for aspartate adsorption onto brucite, which is up to 5 times greater in the presence of Ca^{2+} (Figure 1). We find significant enhancement of aspartate (Asp) adsorption on brucite in the presence of 4 other amino acids and Ca^{2+} ions. Under all conditions Asp adsorbs more strongly than glycine, leucine, lysine, or phenylalanine. However, adsorption increases fivefold in a 4 mM Ca^{2+} solution compared to Ca-absent solutions (Figure 2), suggesting formation of a Ca-Asp complex.

These results have implications for origins-of-life models. Mineral surfaces represent plausible templates for the selection, concentration, and organization of biomolecules. In this regard, cooperative and competitive effects must have played significant roles in the emergence of life. Future experimental studies will describe the role of mineral substrates and redox on the stability of amino acids under hydrothermal conditions.

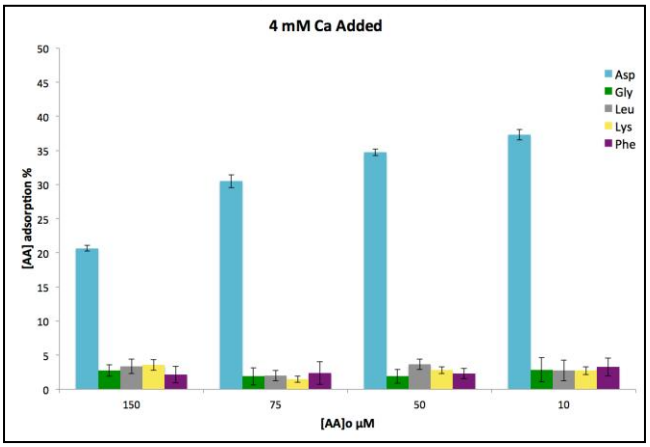

Figure 1: Adsorption of amino acids onto brucite, no Ca^{2+}.

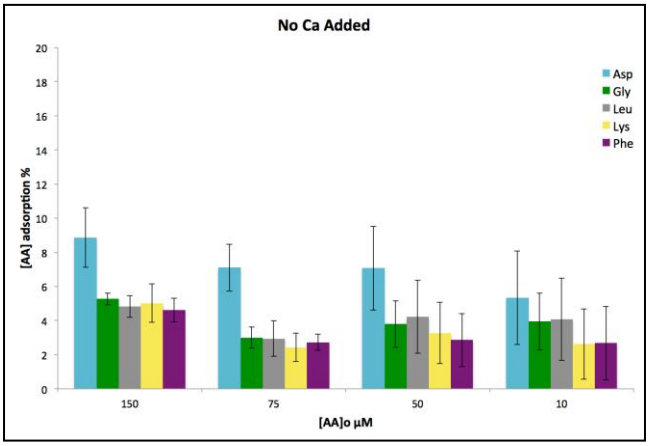

Figure 2: Adsorption of amino acids onto brucite, 4 mm Ca^{2+}.

Vibrational spectroscopic study of pyromorphite-vanadinite solid solution series

Janicka U[1*], Bajda T[2], Topolska J[2], Manecki M[2]

1 - AGH University of Science and Technology, Faculty of Geology, Geophysics and Environment Protection *ujanicka@agh.edu.pl 2 - AGH University of Science and Technology

Pyromorphite $Pb_5(PO_4)_3Cl$ and vanadinite $Pb_5(VO_4)_3Cl$ are members of the apatite supergroup of minerals. They are ubiquitous secondary lead minerals in oxidation zones forming on lead-bearing ores. The crystal structure of these minerals allows the accommodation of numerous cationic and anionic substitutions. Furthermore, they are very stable in the earth-surface environments.

In natural and drinking waters, vanadium dominantly exists in either the +4 or +5 oxidation state as the aquatic species vanadyl (VO_3^{2-}) or vanadate (VO_4^{3-}) [1]. In the paper on "Identification and Distribution of Vanadinite ($Pb_5(V^{5+}O_4)_3Cl$) in Lead Pipe Corrosion By-Products" [2], vanadinite was identified as the mineral occurring in the layers of the studied water distribution systems in the USA. Due to high flexibility of structures of the lead apatites, and phosphate presence in natural waters, the occurrence of the minerals in the form of the pyromorphite-vanadinite solid solution series in layers of lead pipes is possible. Knowledge about the pyromorphite-vanadinite solid solution series is sparse. Therefore, to fill this gap we synthesized these minerals and performed their spectroscopic characterization.

Pyromorphite, vanadinite and their solid solutions were synthesized from aqueous solutions. Solutions of $Pb(NO_3)_2$, Na_3VO_4, $(NH_4)_2HPO_4$ and NaCl were dropwise mixed at 25 ^{0}C and pH = 3.5. The products of these syntheses were analyzed by X-Ray diffraction (XRD), infrared absorption spectroscopy (FTIR) and Raman spectroscopy methods.

Synthetic precipitates were identified by XRD as pyromorphite, vanadinite and their solid solutions. The analyses did not yield any impurities within the detection limit of XRD. Certain diffraction peaks of pyromorphite-vanadinite solid solution series were shifted due to replacement of PO_4 by VO_4.

Mid-IR spectra of pyromorphite-vanadinite solid solutions series were of mixed profile. The bands ν_1, ν_3 and ν_4, attributed to vibrations in the PO_4 tetrahedra, appeared at 1100-900 cm^{-1} and 600-500 cm^{-1}. Stretching vibrations ν_3 in the VO_4 tetrahedra occurred in the range 900-700 cm^{-1}. In the Raman spectra of the pyromorphite-vanadinite solid solutions series, the bands which are characteristic for vibrations in the PO_4 and VO_4 tetrahedra were also observed. The bands attributed to vibrations in the PO_4 tetrahedra appeared at 1600-900 cm^{-1}, 580-520 cm^{-1}, 430-380 cm^{-1} and 250-100 cm^{-1}. One intense band attributed to vibrations in the VO_4 tetrahedra appeared in the range 830-820 cm^{-1}. Other bands were observed in the range 380-280 cm^{-1}. Analysis of Mid-IR spectra and Raman spectra showed shifts of the bands caused by substitutions. The positions of certain peaks of the Raman and IR spectra of the minerals from pyromorphite-vanadinite series vary primarily as a function of the P/(P+V) ratio in the solid solutions.

Acknowledgement: The project was financed with resources of the National Science Centre of Poland, granted based on decision no. DEC-2013/09/N/ST10/00677.

[1] Minelli L. *et al*. (2000). Vanadium in Italian waters: monitoring and speciation of V(IV) and V(V). *Microchemical Journal*, 67, 83-90.

[2] Gerke T.L. *et al*. (2009). Identification and Distribution of Vanadinite ($Pb_5(V^{5+}O_4)_3Cl$) in Lead Pipe Corrosion By-Products. *Environmental Science &Technology*, 43, 4412-4418.

Major occurrence of As-sulfides and para-alumohydrocalcite at Sarul Dornei (East Carpathians, Romania)

Kristály F*, Szakáll S, Zajzon N

University of Miskolc, Institute of Mineralogy and Geology *askkf@uni-miskolc.hu

Para-alumohydrocalcite is a mineral with rare occurrences and rather poorly defined crystallography/properties. It may be observed in the oxidation zone of sulphide ore deposits, among halloysite, allophane or other hydrate carbonate species. Due to its fine grained nature, it might be easily mistaken for more common species. According to our current knowledge, it has only a few documented occurrences in the Carpathians, and usually appears as minor part of assemblages.

In the Şarul Dornei As-sulphide occurrence large amounts of white alteration crusts are observed together with As-sulphides. The earliest studies showed the presence of realgar and orpiment [1]. The host rock is rich in muscovite and illite-group clay minerals, situated between neogene volcanic field and metamorphic series with sedimentary formations also. The crusts are made up mainly by calcite and para-alumohydrocalcite, but it was also observed in the cracks of realgar veins [2]. Alumohydrocalcite is also present in the samples, but XRD patterns suggest also the presence of partly dehydrated phases. However, it is difficult to obtain unambiguous data for hydration, since the sub-micrometric fibers are themselves mixtures of these phases, in different hydration state. For a detailed reconnaissance of the species, samples of below milligram quantity were subjected to XRD. Thermal analysis and FTIR investigations were also performed on the samples. As-sulphides occur mostly as realgar and para-realgar, with minor orpiment, the latter two being probably formed on the expense of realgar.

Results indicate, that para-alumohydrocalcite was formed similarly to oxidation zone products. The effect of acidic environment on phyllosilicate alteration produced available Al, while Ca and carbonate were transported by infiltrating solutions. The As-sulphide assemblage also has a layered, vein like texture, probably formed by the circulation of solutions rich in S and/or As. A source of As may also be the hosting rock, a flysch type sedimentary material. Similar As-sulphide occurrences are known in the larger area [3], and were formed by post volcanic activity interacting with flysch deposits. The proximity of Călimani-caldera could also be a trigger for the Şarul Dornei occurrence.

[1] Ghergari L. *et al*. (1992). *Rom. J. Mineral*., 75/1 (abstr.), pp.12-13.

[2] Kristály F. and Szakáll S. (2009). Mitteilungen der Österreichischen Mineralogischen Gesellschaft, 155, pp. 94.

[3] Kristály F. *et al*. (2006). *Rom. J. Mineral Deposits and Rom. J. Mineral*., joint vol. 82, pp 192-195.

The distinct effects of Mn substitution on the reactivity of magnetite in heterogeneous Fenton reaction and Pb(II) adsorption

Liang X*, He H, He Z, Liu P

Guangzhou Institute of Geochemistry, Chinese Academy of Sciences

*liangxl@gig.ac.cn

The spread of organic pollutants and heavy metals in surface water and groundwater has become a critical issue worldwide. Thus, it is imperative to develop novel, efficient and friendly materials and technologies to remove these contaminants. A number of iron oxides including goethite, hematite, magnetite, ferrihydrite and lepidocrocite, were efficiently applied to adsorb heavy metal species and initiate the advanced oxidation processes (AOPs) as heterogeneous catalysts for organic degradation. In most natural magnetites, iron cations are usually isomorphously substituted by divalent (Co, Ni, Zn, Cu, Mn, etc.), trivalent (Al, V, Cr, etc.) and tetravalent (Ti) cations. These substitutions vary the structure and physicochemical properties of magnetite, and would accordingly affect its surface reactivity in heavy metal adsorption and catalyzing AOPs. In this study, a series of Mn substituted magnetites were used as catalysts in the heterogeneous Fenton degradation of acid orange II and adsorbents for Pb(II) removal, in order to investigate the effect of Mn substitution on the reactivity of magnetite. The valence and local environment of both Fe and Mn in the spinel structure of magnetite were investigated by powder X-ray diffraction (PXRD) and X-ray absorption fine structure (XAFS) spectroscopy. The incorporation of Mn did not change the valence and local structure of Fe in the synthetic magnetite, while Mn was in the valences of +2 and +3. The distribution of Mn on the octahedral sites of magnetite surface increased with increase of Mn content. A new phase of feitknechtite was found in the samples with high Mn content. The Mn introduction led to an improvement of catalytic activity and adsorption property of magnetite. The sample with minimum Mn content displayed the best efficiency in $^{\bullet}OH$ production and the degradation of acid orange II, while the other substituted samples did not show obvious difference in their catalytic performance. The adsorption capacity of magnetite samples toward Pb(II) was gradually increased with the increase of Mn content. These results illustrate the remarkable effect of Mn substitution on the catalytic activity and adsorption properties of magnetite and would be beneficial for the application of magnetite-group minerals in environmental protection.

Size effect on biotic and abiotic reduction of hematite nanoparticles

Liu J[1*], Pearce C[2], Shi L[3], Wang Z[3], Shi Z[3], Arenholz E[4], Rosso K[3]

1 - Peking University *juan.liu@pku.edu.cn 2 - The University of Manchester

3 - Pacific Northwest National Laboratory 4 - Lawrence Berkeley National Laboratory

In natural environments, hematite is ubiquitous and involved in a wide variety of abiotic and biotic redox processes, which influence the transformation and transport of redox-active metals and contaminants. This study presents the size-dependent reduction of hematite particles with OmcA, an outer membrane cytochrome of *Shewanella oneidensis* MR-1, and ascorbic acid, respectively. In microbial reduction of hematite with MR-1, OmcA, as the important terminal reductase, plays a key role in transferring electrons across the outer membrane to mineral surface. Ascorbic acid, as an analog reducing agent for bio- and geochemical reactions in nature, was selected to compare with OmcA. Reduction kinetics of hematite particles with mean primary particle sizes of 15, 30, 55, and 173 nm were systematically studied in reactions with OmcA and ascorbic acid, respectively. The changes of hematite particles before and after reaction with OmcA were investigated using XRD, TEM, and XMCD. The different size effect in reactions with OmcA and ascorbic acid was discussed in terms of factors, such as primary particle size, size of reductase, and aggregation. This study suggested that the effect of particle size or aggregation might be more substantial in biotic reactions. It can be contributed to the relatively larger size of biomacromolecule and bacteria than dissolved ions. The accessible reactive surface area is much less than the measured BET surface area in biotic reactions. It implies that new methods are needed to quantify the amount of surface area accessible for biomacromolecule and bacteria in biotic reactions with aggregated mineral particle suspensions.

The use of mineralogical techniques in the identification of asbestos in brake linings

Lombard A, Mosinyi D

SGS South Africa *annegret.lombard@sgs.com

Asbestos has been used in friction products such as brake linings since the early 1900s. Asbestos is a generic term used to describe a number of hydrated Mg silicates that are needle shaped or fibrous in habit, including some amphiboles and serpentines. Their specific properties with regards to insulation, incombustibility, flexibility and tensile strength, makes them ideal for this application. The use of asbestos in brake lining does however pose a health risk to mechanics servicing brakes on vehicles, as well as an environmental hazard with regards to the disposal of the brake linings. Worldwide the mining and trade of asbestos is strictly regulated and monitored. The use of some asbestos products is even banned in some countries. South Africa has no legislation prohibiting the use of asbestos in brake linings, but brake lining manufacturers, as well as importers are increasingly leaning towards the safer and environmentally friendly asbestos-free alternatives. This case study will illustrate how a combination of X-ray diffraction (XRD), scanning electron microscopy (SEM) and image analysis is used to identify phases present in brake lining to assess the mineral phases present, their semi-quantitative compositions, as well as their aspect ratios, as evaluation criteria.

Mineralogical studies, ^{40}Ar-^{39}Ar and U-Th-He dating of peloids from the fossil-bearing cave deposits of the Malapa site at the Cradle of Humankind, South Africa

Makhubela T*, Kramers J, Belyanin G

University of Johannesburg *vkhubz@gmail.com

An unusual class of peloids was studied in fossil-bearing cave deposits of the Malapa site, notable for hosting fossils of *Australopithecus sediba*. Such peloids are present in all the cave deposits at the Cradle of Humankind and they show characteristics of microbial-assisted in-situ formation such as a concentric shell internal structure, with a quartz grain in their centre. We have studied their chemistry, mineralogy and textures, and carried out ^{40}Ar/^{39}Ar as well as U-Th-He dating.

The concentric coatings of peloids consist of an aggregate mixture of nano-sized silicate minerals and poorly crystallized iron- and manganese-hydroxides and oxides (Figure 1). From electron microprobe analysis and scanning electron microscope EDS mapping, they were found to contain ~1 wt. % potassium. This is in part located in the iron-manganese oxide/hydroxide matrix, but a portion of it is associated with discrete grains in the 5-20 µm size range, showing enhanced aluminium and (to a lesser extent) silicon content, indicating illite or fine-grained sericite.

Dating by ^{40}Ar/^{39}Ar yielded apparent ages ranging from 500 to 2000 Ma, with the oldest one appearing as a near-plateau, and the younger ones showing staircase-type age spectra. Thus either the peloids as such, or the potassium-bearing components, were probably derived from the Malmani Dolomite host rock. In the second case the peloids themselves might still have been formed in the cave environment. However, U-Th-He dating yielded dates ranging from 3 to 80 Ma. The path length of α-particles in mineral is about 15 µm on average, much in excess of the grain size of peloid components. Therefore these results document variable helium loss from the objects, which obviously predated both the cave sediment and soil processes on the African land surface. The combined results render it plausible that peloids of this class stem from the Malmani Dolomite itself, and the search for mineral proxies to date clastic cave sediments directly is continuing.

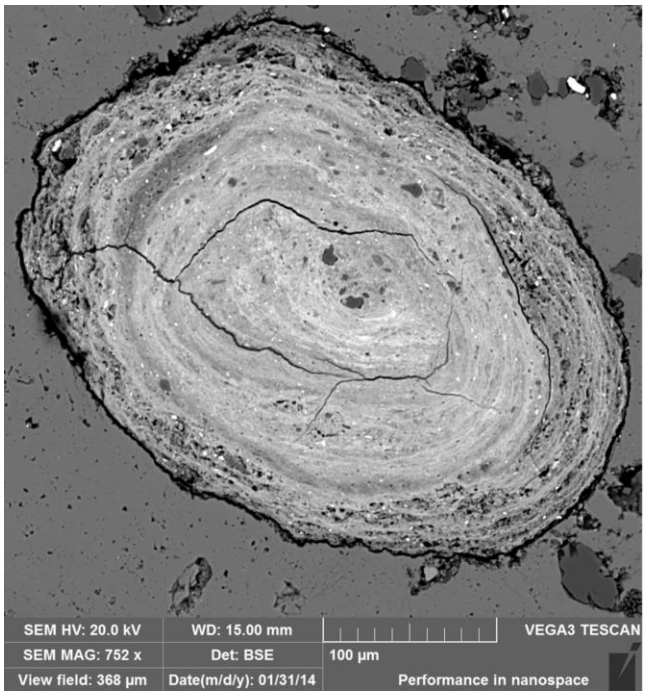

Figure 1: Scanning electron microscope backscattered electron image of a peloid found in fossil-bearing cave deposits of the Malapa site. Here the quartz centre is completely covered by the concentric coating composed of an aggregate mixture of nano-sized silicate minerals and poorly crystallized iron- and manganese-hydroxides and oxides.

Incorporation of zinc into human pathological calcification

Meng F[1], Wang C[2*], Li Y[2], Lu A[2], Mei F[3], Liu J[3]

1 - School of Earth and Space Sciences, Peking University

2 - Peking University *cqwang@pku.edu.cn 3 - Health Science Center of Peking University

Zinc is an essential trace element in human bodies. It has a close relationship with the occurrence and development of diseases. Up to now, the distributing characteristics and incorporating mechanisms of zinc in inorganic calcification of human bodies, such as in pathological mineralization, is still unclear. This study carried mineralogical measurements on 28 cases of various pathological mineralizations, including breast cancer, fibroadenoma of the breast, breast hyperplasia, breast inflammation, ovarian serous cancer, aortic calcification and coronary artery calcification, seeking to provide a new insight into the incorporation mechanism of zinc in inorganic pathological calcifications.

After mineral separation processes, the elemental content was measured by micro-area synchrotron radiation X-ray fluorescence (µ-SRXRF). The results revealed that zinc existed in the mineralizations of all diseases studied. The Ca/Zn (mM concentration) value in breast cancer (approximately 165) is significantly lower than that in breast benign lesions (about 860 in breast hyperplasia and breast inflammation, and approximately 650 in breast fibrodenoma) ($P<0.01$), presumably due to the fact that concentration of zinc in tissues of breast cancer is higher than that of breast benign lesions.

µ-SRXRF mapping was also performed on tissue sections to determine the distribution of zinc and calcium. The distribution patterns of zinc in most cases are consistent with those of calcium. It is therefore probable that zinc takes place of calcium in the crystal lattices of (carbonate) hydroxyapatite (HAP).

To confirm the chemical state of zinc in the mineralization, X-ray absorption fine structure (XAFS) was conducted on separated samples. Data of synthetic zinc-doped HAP were also collected for normalization and comparison. According to [1], the peak splitting between peaks A (9662 eV) and B (9665 eV) and the position of peak C (9674 eV) can be utilized for distinguishing Zn-doped HAP with Ca1 site substitution from Zn-doped HAP with Ca2 site substitution. After normalization, our results showed reasonable agreement with the reported spectrum of Zn-doped HAP with Ca2 site substitution (Figure 1). This suggested Zn2+ took up Ca2 sites on the screw axis (Figure 2).

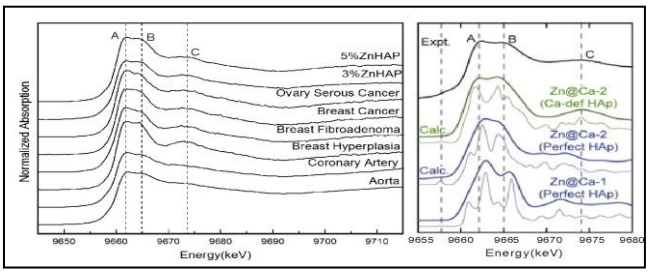

Figure 1: Experimental XAFS results of mineralization (left) in our study compared with calculated (Calc.) and experimental (Expt.) data (right) of Zn-doped HAP in ref. [1]. For each disease type, measurements of two or three samples were averaged.

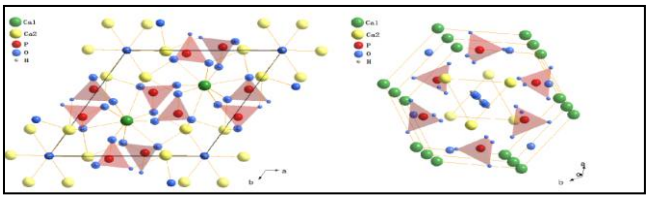

Figure 2: Crystalline structure of hydroxyapatite. In pathological calcifications, Zn^{2+} took up Ca2 sites (yellow balls).

In conclusion, the present study showed that zinc distributed in various gynaecological neoplasm and cardiovascular calcification, but the concentrations vary in different disease cases, especially when concerning breast lesions. According to XAFS, Zn^{2+} incorporates into inorganic pathological calcifications by taking up Ca2 site in (carbonate) hydroxyapatite.

Acknowledgement: This work was supported by the National Natural Science Foundation of China (No. 41272048, 40872196). We thank staff at BL15U, SSRF for providing beam time and help.

[1] Matsunaga K., Murata H., Mizoguchi T., Nakahira A. (2010) Mechanism of incorporation of zinc into hydroxyapatite[J]. Acta Biomaterialia, 6, 2289-2293.

Mineral and chemical composition of wood ash from a medium-sized boiler

Michalik M[*], Wilczynska-Michalik W[2]

1 - Jagiellonian University, Institute of Geological Sciences, Krakow, Poland *mjmichalik@post.pl 2 - Pedagogical University, Institute of Geography, Krakow, Poland

It is commonly considered that biomass combustion does not contribute to the greenhouse effect because of CO_2 neutrality. Other advantages are also important (e.g. reduction in SO_x and NO_x emissions, conservation of fossil fuel resources, utilization of agricultural and forest residues, recultivation of non-utilized farming areas, reduction of biomass-containing waste). Increasing production of energy from biomass combustion results in a large amount of ash. Due to the great variability of mineral and chemical composition of biomass ash it is possible to discuss its innovative utilization or safe disposal.

We studied six samples of wood ash obtained from a 8 MW boiler used for heat production (temperature of combustion between 800 and 1100°C). Ash was obtained during combustion of wood mixtures (e.g. pine, poplar, oak, acacia, birch) of wood chips obtained from single species or dominated by single species. Ash samples are grey or brownish-grey and contain different proportions of slag-like vesicular fragments, fine-grained loose aggregates and char particles.

Chemical composition of ash varies significantly (SiO_2 from 21 to 76 wt%; Al_2O_3 from 1.1 to 2.9 wt%; MgO from 1.2 to 3.2 wt%; CaO from 8.2 to 30.8 wt%; K_2O from 3.4 to 7.4 wt%; Na_2O from 0.2 to 0.4 wt%; P_2O_5 from 1.1 to 5.72 wt%; loss of ignition value from 3.9 to 48.7 wt %). Slagging index based on $(Fe_2O_3+CaO+Na_2O+K_2O+MgO)/(SiO_2+Al_2O_3+TiO_2)$ is between 0.19 and 1.13.

Mineral composition of ash with an SiO_2 content above 60 wt% is strongly dominated by quartz accompanied by subordinate cristobalite, feldspars, wollastonite, portlandite, larnite, calcite, Ca, Ca-K, Ca-Mg phosphates, and other minor compounds. In samples with SiO_2 content around 36 and 21 wt% (and highest values of slagging index) quartz is also present but it occurs along with calcite, portlandite, lime?, and phosphate minerals (Ca, Ca-K, Ca-Mg phosphates) in sample with P_2O_5 content above 5 wt%. Ca silicates occur within glassy matrix composed mainly of Si, Ca, K with minor amount of P.

Mineral composition of the ash is related to the chemical composition of wood (influenced partly by soil composition and contamination or fertilizers used), but mineral compounds from soil or aeolian dust captured during cultivation, harvesting, transportation and storage are important.

Ash contains primary minerals (e.g. quartz, feldspar, zircon, monazite) present in fuel and secondary minerals formed during combustion and/or storage (e.g. wollastonite, larnite, lime, portlandite, calcite, numerous phosphates).

Composition of studied ash samples indicates that it is possible to consider wide range of utilizations (e.g. soil amendments and fertilisation, building materials, CO_2 storage by mineral carbonation) but, on the other hand, variation of the composition of ash related to biomass type makes utilization of these combustion by-products more difficult.

Mineralogy and As-distribution in geogenically As-rich soil from the Swiss Jura Mountains

Petrikis J[1*], Voegelin A[2], Majzlan J[1]

1 - University Jena *julia.petrikis@uni-jena.de 2 - EAWAG

Soils contaminated by toxic elements, like arsenic or thallium, present a health risk for humans, animals, and plants. In order to assess the risks, natural immobilization mechanisms in soils, such as inorganic fixation of toxic elements by secondary minerals, has to be taken into account. In this work, we investigated the mineralogy and distribution of a geogenic As- and Tl-contaminated, barren soil from the Swiss Jura mountain range [1]. The soil at this site has been naturally formed on dolomitic limestone [2], hosting a small, intensively weathered ore deposit, which was locally mined and smelted in Medieval times [3] and thus can be considered as a long-term analogue for sites contaminated by mining operations and other anthropogenic activities.

Transmitted and reflected light microscopy on petrographic thin sections revealed minute fragments of primary galena PbS, sphalerite ZnS, molybdenite MoS_2, magnetite $FeFe_2O_4$, and native copper and indicated intense weathering of the ore body. In some samples, As-bearing primary ore minerals like pyrite FeS_2 and arsenopyrite FeAsS could also be identified by X-ray diffraction (XRD) and wave-dispersive electron microscopy (WD-EMP). Bulk analyses by energy-dispersive X-ray fluorescence spectrometry (ED-XRF) indicated that the average arsenic concentration in the soil is 3700 mg/kg. The topsoil As content ranges from 100-1000 mg/kg, and reaches up to several 1000 mg/kg in the subsoil horizons. Strongly weathered ore fragments can reach up to 4 wt% As. Intriguingly, the soil is also enriched in Tl, with concentrations ranging from a few 100 to a few 1000 mg/kg. The average Tl concentration in the bulk soil was determined to 857 mg Tl/kg. A maximum of 5700 mg Tl/kg is reached in yellowish ore fragments found in a depth of 65 cm.

Arsenic accumulates dominantly in secondary iron arsenate minerals like pharmacosiderite, scorodite $Fe^{3+}[AsO_4]\cdot 2H_2O$, and arseniosiderite $Ca_2(Fe, Mn)_3^{3+}[O_2|(As_{2.78}P_{0.22})O_{12}]\cdot 2H_2O$, but also in hydrous ferric oxides like goethite α-FeOOH. Electron microprobe (EMP) analyses of pharmacosiderite crystals show that the incorporation of arsenic and thallium in pharmacosiderite is a viable explanation of the location of the toxic elements.

The chemical formula for the investigated authigenic pharmacosiderite, obtained from WDS-EMP analyses, is $(Ba_{0.42}K_{0.09}Na_{0.05}Tl_{0.02}\ddot{y}_{0.42})^{+}(Fe_{3.87}Al_{0.13})[(OH)_4|(As_{2.85}P_{0.15})O_{12}]\cdot 6.41H_2O$. Considering the large excess of K over Ba in the soil matrix, this composition points to a high selectivity of natural pharmacosiderite towards Ba over K. Furthermore, EMP revealed that pharmacosiderite may not only be a major secondary host mineral for As attenuation, but may also accommodate minor amounts of Tl in its structure.

[1] Truninger E. (1922). Arsen als natürliches Bodengift in einem schweizerischen Kulturboden - Der Boden der Erzmatt bei Buus (Baselland). Landwirtschaftliches Jahrbuch der Schweiz, 35, Mitteilung aus der schweizerischen agrikulturchemischen Anstalt, Bern. S. 1015-1030.

[2] Suter R. (1915). Geologie der Umgebung von Maisprach (Schweizerischer Tafeljura). Inaugural-Dissertation, Basel. Buchdruckerei Birkhäuser, 58 S.

[3] Hänger H. (2011). Erzenberg, Erzloch, Erzmatt, Erzweid. Jahresbericht 2010 der Stiftung für Orts- und Flurnamen-Forschung Baselland Ischlag, 3.

Health impact of the alkaline Pilanesberg Complex on communities in the semi-arid region of the North West Province, South Africa

Shelembe R[1*], Mouri H[2], Kramers J[2]

1 - Council for Geoscience *rshelembe@geoscience.org.za 2 - University of Johannesburg

South Africa, like many other African countries, has naturally occurring geological problems that can have direct or indirect effects on human and animal health. However, data of such problems are very few or do not exist for some localities. Therefore, rigorous studies are needed to examine the possible links between the geology of a specific area and its health problems.

The study area is semi-arid and is situated at the southern edge of the Kalahari Desert about 60 km northwest of Rustenburg, North West Province. In this study, particular focus is given to the possible association between the geology of the alkaline Pilanesberg Complex and the mafic Rustenburg Layered Suite in the area and the health of communities living there. In this locality, almost all communities depend on groundwater for domestic use. Data from previous reports as well as preliminary results from some groundwater samples indicate high concentrations in F, Ca, U and total dissolved solids (TDS). The concentrations of these elements in previous reports are about 10 times more than the allowable limits published by the Department of Water Affairs (South Africa) and the World Health Organisation. According to the Mortality profile report of the North West Province, skeletal fluorosis, cardiovascular related diseases, renal diseases and diarrhoea are prevalent. In addition to this, local health data from the study area show a prevalence of hypertension (which may be coupled with musculoskeletal and mental disorders), diarrhoea and irregular menstrual cycles. Providing holistic-approach solutions to help communities with preventative measures to healthier living conditions is also important for this investigation.

Mineralogy of the psammoma bodies in papillary thyroid carcinoma

Wang C[1*], Li Y[1], Zhao W[1], Lu A[1], Liu J[2], Mei F[2]

1 - Peking University *cqwang@pku.edu.cn 2 - Peking University Health Science Center

As one of the most common cancers around the world, thyroid carcinoma has affected an increasing number of patients, especially in the past 10 years. Microcalcifications observed in imaging examinations play important roles in clinical diagnosis of thyroid cancer due to its high specificity, even 100% in diagnosing papillary thyroid carcinoma (PTC). Microcalcification in PTC usually has a concentric lamellate structure, named psammoma bodies (PBs). However, the mineralogical characteristics of PBs are unclear. In this study, 16 cases of PTC with PBs were investigated by mineralogical measurements and the mechanism of PB formation in PTC was discussed.

Under optical microscope, 10 to 30 μm dark-stained calcified bodies with dense concentric lamellated structure were observed after HE staining (Figure 1).

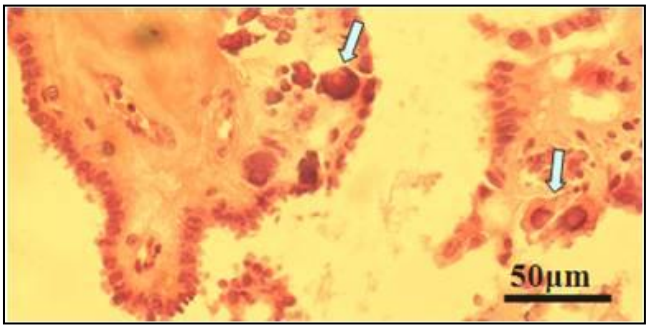

Figure 1: Photomicrograph of the papillary thyroid with PBs (HE)

Under environmental scanning electron microscope (ESEM), 0.1 to 2 μm wide gaps between the concentric layers of PBs were observed. Some PBs have only one concentric layered structural centre (Fig. 2a), but others have multiple centres with varying sizes (Fig. 2b). The fracture surfaces of the PBs were grainy, while the surface showed typical oolitic appearance, intertwined with many filamentous collagen fibers.

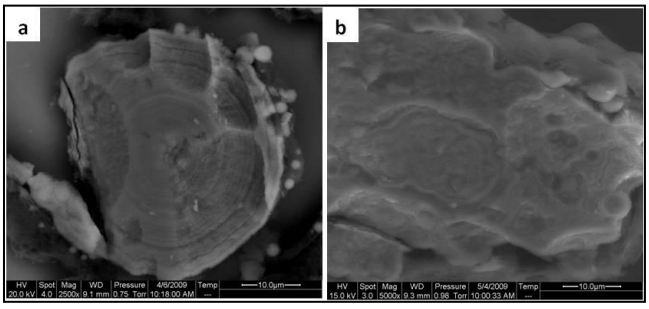

Figure 2: ESEM images of the PBs in papillary thyroid carcinoma

Energy dispersive X-ray analysis (EDAX) showed PBs contained C, O, P and Ca, as well as trace elements Na and Mg. The Ca/P atomic ratios (from 1.335 to 1.701) of different regions are within the scope of calcium phosphate series minerals. Since most of the tested Ca/P (At %) ratios were lower than that of theoretical carbon-hydroxyapatite (CHAP), it can be inferred that the PBs are combination of calcium phosphate series minerals with different Ca/P ratios. From the periphery to the centre of the PBs, the Ca contents and Ca/P ratios showed an increasing trend.

Morphological observations under high resolution transmission electron microscopy (HRTEM) revealed the PBs consisted of large granules, which are 5 to 10 nm long. The electron diffraction patterns demonstrated they are amorphous calcium phosphates as indicated by some continuous and wide diffraction ring. The square ratio of diffraction rings' diameter was approximately 3:4:7:9:12:16, which followed the law of hexagonal system. Moreover, the *d* values were similar to that of CHAP (ICDD, 15-0100).

In conclusion, the PBs in PTC consisted of crystalline CHAP and amorphous calcium phosphates. As the Ca contents and Ca/P ratios of PBs increased inwards, high content of Ca should be a crucial factor of PB nucleation at initial stage. Proposed formation mechanism of PBs in PTC is that the changes of microenvironment and abnormally high levels of Ca^{2+} in thyroid tissue fluid caused the deposition of Ca^{2+} and PO_4^{3-} around the core in colloid system after nucleation induced by interstitial.

Acknowledgement: This work was supported by the National Natural Science Foundation of China (No. 41272048, 40872196).

Bismuth dispersion in the supergene environment

Williams P*, Leverett P, Murphy T, Roper A
University of Western Sydney *p.williams@uws.edu.au

The chemical dispersion of Bi in oxidised ores is buffered by secondary minerals and associated processes may be evaluated by "reverse solubility" modelling based on thermochemical data. For common anions, important phases are bismoclite, BiOCl, and bismutite, $Bi_2O_2CO_3$. Both are known to be present in hundreds of deposits. Sulfates such as cannonite, $Bi_2(SO_4)O(OH)_2$, and riomarinaite, $BiSO_4(OH)\cdot H_2O$, are too soluble to exert any significant effect on Bi mobility. For bismoclite and bismutite assemblages at 25°C, total dissolved Bi never exceeds *ca* 10^{-6} *M* with $1 \leq pH \leq 9$ and with $a(Cl^-)$ and $p(CO_2)$ ranging from 0 to 10^{-1} and $10^{-2.5}$, respectively. Between pH 3 and 6, total dissolved Bi never exceeds *ca* 5 x 10^{-9} *M*. Thus it may be concluded that chemical dispersion of Bi is quite limited in the supergene zone. When Mo or W is present, as is the case for a large number of deposits in eastern Australia, other mineralogical controls on dispersion become more important. Koechlinite, Bi_2MoO_6, and russellite, Bi_2WO_6, are very common minerals in the supergene zones of such deposits and they significantly reduce the solubility of Bi. With more complex assemblages containing As sulfosalts, rooseveltite, $BiAsO_4$, preisingerite, $Bi_3(AsO_4)_2O(OH)$, and atelestite, $Bi_2(AsO_4)O(OH)$, also play a key role in the immobilisation of Bi. Recently derived thermochemical data are presented for all of the abovementioned phases (and others that are related). We conclude that Bi is a very chemically immobile element in the oxidised zone. Implications for the use of Bi in exploration geochemistry applications will be addressed, particularly with respect to granite-hosted Bi-Mo-W deposits that are endemic to eastern Australia.

Performance of tubular halloysite and platy kaolinite as carriers for the loading and release of the herbicide Amitrole

Yuan P[1*], Tan D[1], Annabi-Bergaya F[2], Liu D[1], He H[1]
1 - Guangzhou Institute of Geochemistry, CAS *yuanpeng@gig.ac.cn
2 - CNRS-Université d'Orléans

Pesticides, mainly including insecticides, herbicides, and fungicides, are used worldwide in agriculture. However, the excessive use of pesticide has created serious health problems and environmental contaminations. Developing controlled-release formulations of pesticides attracts increasing interest because such formulations provide safer use of pesticides and minimize the potential environmental contaminants by simultaneously reducing the amount of pesticide and increasing the efficiency of the pesticide. Tubular halloysite is a hydrated polymorph of platy kaolinite. Both tubular halloysite and platy kaolinite are 1:1 layered aluminosilicate. In comparison with the platy kaolinite, the unique tubular structure of halloysite makes it a promising carrier for loading and controlled-release of various guests, e.g., drugs, enzymes, and anticorrosives. In most cases, the lumen of halloysite is the main loading space for guests, and the interlayer space of halloysite is unavailable for guest loading.

In this work, both tubular halloysite and platy kaolinite were used as carriers for the loading and release of the herbicide Amitrole (AMT) for the first time. The interlayer methoxy-modification of halloysite and kaolinite was adopted to increase the loading and release performances of AMT on halloysite and kaolinite. In addition, the effects of the microstructures and morphologies of halloysite and kaolinite on the loading and release of AMT were investigated in detail.

The AMT loading content in the halloysite was 17.5 mass%, 69.9% greater than that in kaolinite; and this result is attributed to the significant loading of AMT in the lumen of the halloysite. The methoxy modification of the halloysite and kaolinite made their interlayer spaces available for the intercalation of AMT. The intercalated AMT was of amorphous state, and presented as a horizontal monolayer arrangement in the interlayer spaces of clay minerals. The AMT loading content in methoxy-modified halloysite reached as high as 30.5 mass%, corresponding to 27.9% intercalated AMT and 72.1% non-intercalated AMT. The AMT loading content in methoxy-modified kaolinite was 20.8 mass%, corresponding to 47.6% intercalated AMT and 52.4% non-intercalated AMT. This substantial promotion of AMT loading was ascribed to that the methoxy modification permitted the intercalation of AMT into the interlayer spaces of the halloysite/kaolinite.

The release profiles of the AMT fit with the modified Korsmeyer-Peppas model. The release of AMT from the modified kaolinite was much slower than from the modified halloysite. This arose because the different microstructures and morphologies of halloysite and kaolinite. In the case of the AMT-loaded modified kaolinite, there was higher proportion of intercalated AMT, of which the diffusion was strongly restricted by the lamellar structure of clay minerals. In addition, the diffusion of the intercalated AMT from the kaolinite had a longer diffusional path than from the halloysite. This longer diffusional path arose because the greater size of the kaolinite particles and the all-horizontal diffusion direction of the AMT in the interlayer space of the kaolinite, whereas the diffusional direction of the intercalated AMT in the halloysite was only longitudinally parallel to the halloysite nanotube.

These above results demonstrate that methoxy-modified halloysite and kaolinite are promising for applications in the pharmaceutical, agrochemical, and coating industries.

Keywords: Clay Minerals; Methoxy Modification; Intercalation; High Loading Capacity; Controlled Release.

Acknowledgements: This study was financially supported by the Team Project of Natural Science Foundation of Guangdong Province, China (S2013030014241) and the National Natural Science Foundation of China (Grant No. 41072032).

Geogenic arsenic enrichment in Upper Permian and Lower Triassic sedimentary rocks of Thuringia, Germany

Abratis M[1*], Viereck L[1], Majzlan J[2]

1 - Friedrich-Schiller University Jena, Germany *michael.abratis@uni-jena.de 2 - Jena University

The average concentration of the trace element arsenic in the Phanerozoic rocks in Germany ranges from 5 to 12 μg/g for different lithologies [1]. However, arsenic concentrations can be several times elevated in certain sedimentary lithologies such as pelites and even more so in coal beds and their seams.

In the present study, we investigated all sequences of the Lower Triassic and Upper Permian formations with their different lithologies (sandstones, mudstones, evaporites, volcanic ash layers, coal beds) in order to identify relevant sedimentary carriers of arsenic. Motivation for this study is the fact that the aquifer systems of the Lower Triassic formation are locally important sources of drinking water and affected by elevated arsenic concentrations. Data from the water wells in north-western Thuringia show arsenic concentrations above the WHO limit value for drinking water (10 μg/l).

The regional distribution as well as lack of secondary vein mineralization or anthropogenic sources within this area point to a geogenic, strata-bound source of arsenic.

Geochemical analyses on sedimentary rock samples from selected drill cores and outcrops in Thuringia show elevated arsenic contents of >50 μg/g, especially in the carbonaceous sediment sections as well as in the gray-green claystones. Mineral phases that incorporate arsenic in the Upper Permian coal beds seem to be sulfides, whereas arsenic seems to be bound to clay minerals in the Lower Triassic sedimentary rocks of lacustrine origin. Further aim of the study is to identify the processes and conditions under which arsenic is mobilized from the relevant mineral phases and transferred into the groundwater.

[1] Viereck-Götte L. *et al*. (1997). Natürliche Grundgehalte bodenrelevanter Metalle in Festgesteinen in NRW. Literaturstudie im Schwerpunkt Digitale Bodenbelastungskarten. Im Auftrag des Landesumweltamtes Nordrhein-Westfalen, p 39 + appendix p 25.

Arsenic drainage in some former gold mines located in the Central Iberian Zone, Portugal

Carvalho P*, M. R. Neiva A, Silva M, Santos A

University of Coimbra *paulacscarvalho@gmail.com

The old Au-Ag mine of Escádia Grande is located about 11 km south of Góis, Coimbra district, and belongs to the tin-tungsten province of central Portugal. The mineralized quartz veins fill N30ºW,45ºSW faults that cut a Neoproterozoic-Cambrian, low-metamorphism, flysch sequence of phyllites and metagreywackes with some marble intercalations, known as the Schist-Greywacke Complex (SGC). The mine was active between 1939 and 1952, during which about 42,878 tonnes of material was exploited. At the Valongo anticline, several Sb-Au quartz veins (in the old Montalto and Tapada mines) cut the SGC that crops out in the core, whereas the As-Au mine of Banjas cuts the Ordovician black slates at the eastern limb. The Sb-Au and As-Au mines were closed down at the end of nineteen century. Between 1864 and 1888, 27,500 tonnes of material was exploited in Montalto, containing 0.58 tonnes of gold and 732 tonnes of antimony. Between 1880 and 1890, at Tapada-Ribeiro da Serra, 360,000 tonnes of material was exploited, containing 14,400 tonnes of antimony [1]. In the Banjas mine 23,787 tonnes of material with 0.083 g/t of Au was produced. In the three old mining areas there are mine dumps and tailings deposited close to the streams. Moreover, nowadays the mine galleries drain to the streams. The surface waters close to the Au-Ag mining area have the highest arsenic content (252.46 µg/L) when compared to those close to the old Sb-Au (23.50 µg/L) and As-Au (63.70 µg/L) mining areas. Stream sediments around the old Au-Ag mining area also have the highest arsenic content (434 mg/kg) when compared to those of Sb-Au (235 mg/kg) and As-Au (225 mg/kg) mining areas. The pH values of the stream sediments in the Au-Ag mining area are slightly higher (5.12-5.97) than those from Sb-Au (4.18-6.11) and As-Au (4.24-5.03) mining areas. Similarly, pH values of surface waters from the Ag-Au area (5.33-7.77) are higher than those from Sb-Au (3.50-6.60) and As-Au (3.80-5.50) mining areas. The arsenic adsorption at pH higher than 5.0 significantly decreases [2], explaining the high As contents in waters. Moreover, sulphide minerals were detected in the stream sediments close to the Au-Ag mine, explaining their high arsenic contents. Most surface waters are contaminated because arsenic concentrations exceed the human consumption and irrigation limits, 10 µg/L and 100 µg/L, respectively, of the Portuguese law. However, in the three mining areas the arsenic mainly occurs as the pentavalent species in the surface water, the less toxic arsenic species. The Au-Ag mine was active more recently than the Sb-Au and As-Au mines, suggesting a greater arsenic release from mine dumps and tailings in the former mine.

[1] Parra A., *et al*. (2002). Sistema de Informação de Ocorrência e Recursos Minerais Portugueses - SIORMINP. Instituto Geológico Mineiro, Lisboa.

[2] Kim M.J. (2010). Effects of pH, adsorbate/adsorbent ratio, temperature and ionic strength on the adsorption of arsenate onto soil. *Geochem Explor Environ Anal*, 10, 407-412.

Stability of selenides under near-surface environments

Charykova M[1*], Krivovichev V[2], Depmeier W[3]

1 - St.-Petersburg University, Russia *m-char@yandex.ru 2 - Sankt-Petersburg State University 3 - Institute of Geosciences, University of Kiel, Germany

Since the discovery that acute and chronic livestock poisoning was caused by Se assimilated by forage crops from soil, there has been continued study of the geologic occurrence and geochemistry of Se in oxygenated aqueous environments. Drainage mined areas may have high dissolved Se concentrations, and are of major interest as the natural sources of Se in waters, soils and plants likely to be the low-temperature oxidizing environments in the vicinity of ore bodies which contain Se-bearing sulfides, and selenides [1]. The understanding of mechanisms of the Se`s behavior under near-surface conditions is one of the actual problems of modern mineralogy and geochemistry, and is very important for solving of some environmental problems.

Most selenides are formed by chemical weathering of ores by oxygenated water establishing conditions of increased Eh and low pH. An estimation of the activity of the components in natural waters which are formed outside of zones with pollution by Se ($a_{\Sigma Se}=10^{-9}$, $a_{\Sigma Fe}=10^{-5}$, $a_{\Sigma Cu}=10^{-7}$, $a_{\Sigma Zn}=5\cdot10^{-7}$, $a_{\Sigma Co}=a_{\Sigma Pb}=10^{-8}$, $a_{\Sigma Ni}=6\cdot10^{-8}$), and waters which are formed in an oxidation zone ($a_{\Sigma Se}=10^{-5}$-10^{-4}, $a_{\Sigma Fe}=a_{\Sigma Cu}=a_{\Sigma Ni}=a_{\Sigma Zn}=10^{-2}$, $a_{\Sigma Co}=10^{-3}$, $a_{\Sigma Pb}=10^{-4}$) was done. The interpretations are summarized in Eh-pH diagrams, synthesized from equilibrium calculations, and reported geological occurrences. Most recent thermodynamic data available were used for the construction of diagrams from reactions which are balanced equations of Eh-pH relationships among selenides which are thermodynamically stable within the ranges of oxidation potential and pH considered for each reaction. Eh-pH diagrams of systems Me-Se-H_2O (Me=Co, Ni, Fe, Cu, Zn, Pb) have been constructed by means of the software (GMB 9.0) for the average content of these elements in underground waters and for their contents in acidic waters of the oxidation zones of sulphide deposits [2]. The formation of selenides of Co, Ni, Fe, Cu, Zn, Pb under near-surface conditions are discussed.

The aim of the works [3, 4] were to synthesize analogs of ahlfeldite and cobaltomenite and to study their solubility in water, as well as their enthalpies of formation and low-temperature heat capacity. The formation and stability areas of chalcomenite [5, 6], ahlfeldite and cobaltomenite [3, 4], selenite of Zn [7] under near-surface conditions are discussed.

Acknowledgement: The work was supported by grants of St-Petersburg State University (#3.38.83.2012).

[1] Plant J.A. *et al.* (2014). Arsenic and Selenium / In Treatise on Geochemistry. 11, 13.

[2] Krivovichev V.G. *et al.* (2011). IV. Eh-pH diagrams of the systems Me-Se-H_2O (Me=Co, Ni, Fe, Cu, Zn, Pb) at 298 K. *Geology of Ore Deposits*., 53(7), 514.

[3] Charykova M.V. *et al.* (2012) VI. Solubility of synthetic analogues of ahlfeldite and cobaltomenite at 25^0C. *Geology of Ore Deposits*., 54(8), 638.

[4]. Charykova M.V. *et al.* (2014). A calorimetric and thermodynamic investigation of the synthetic analogues of cobaltomenite, $CoSeO_3{\cdot}2H_2O$, and ahlfeldite, $NiSeO_3{\cdot}2H_2O$. *Am. Miner*., 99 (in press).

[5] Krivovichev V.G. *et al.* (2012). V. Chalcomenite and its synthetic analogue, properties and conditions of formation. *Geology of Ore Deposits*., 54(7), 498.

[6] Fokina E.V. *et al.* (2014). Thermal stability of synthetic analog of cobaltomenite and features of its dehydration and dissociation. *Geology of Ore Deposits*., 56 (in press).

[7] Charykova M.V. *et al.* (2014). Physicochemical conditions of formation and thermal stability of selenide of zinc. *Geology of Ore Deposits*., 56 (in press).

Mount Etna fine ash: first data from investigation on surface area, reactivity and medical hazard

Di Benedetto F[1*], Barone G[2], Cannas C[3], Costagliola P[1], De Giudici G[3], Giuffrida A[2], Mazzoleni P[2], Medas D[3], Podda F[3]

1 - Univ. Firenze - Dip. di Scienze della Terra, Italy *francesco.dibenedetto@unifi.it

2 - University of Catania, Department of Biological, Geological and Environmental Sciences 3 - Univ. Cagliari - Dip. di Scienze Chimiche e Geologiche (Italy)

Mount Etna is the most active and largest volcano in Mediterranean area and is located on eastern Sicily (Italy). The recent activity of the volcano is characterized by paroxysmal events from the South-East Crater [1] consisting in lava fountains associated with flow emission and the formation of ash-plumes. We studied the possible respiratory health effects of the fine ashes erupted during the 2013 activity using leaching experiments with Gamble solution [2]. Etna volcanic ashes are mainly made of volcanic glass and subordinately by plagioclases and pyroxenes; cristobalite occasionally occurs due to the presence of quartz-rich xenoliths. However, the chemical characterization of the amorphous phases evidenced that surfaces of ash particles are widely modified by their interaction with the gas/aerosol of the plume [3].

The surface area of the sampled volcanic ashes was investigated by BET analysis finding values in the range 0.09 - 0.8 m^2/g. Such values indicate low porosity of the ash particles. To investigate the effect of lung exposure to fine volcanic ash particles (<38 micron), leaching experiments in simulated lung fluid (Gamble solution) were carried out. The adopted ratio of ash to leaching solution was 1:100, and extraction time was 24 H. S, Si, Li, Ni, Cu and Tl were found in the leachates above detection limit only for grain size <38 micron. Zn, Ba, Fe and Al were found in meaningful amounts in all samples. As was found only in one sample. Leached amount of elements was normalized by BET surface area. Normalized leached elements were not found always dependent on BET surface area. Accordingly, the variability of BET total surface area and chemistry of leachate solutions are conceivably indicating an intrinsic dependence of sample properties and reactivity on location, actual wind, elapsed time from eruption. In further experiments, the leachate solutions will be used for cellular toxicity testing.

[1] Andronico *et al.* (2011). *Bull. Volcanol.*, 73, 1165-1178.

[2] Stewart *et al.* (2013). (http://www.ivhhn.org/images/pdf/volcanic_ash_leachate_protocols.pdf).

[3] Barone *et al.* (2014). *Surf. Interface Anal.*, DOI 10.1002/sia.5395.

KOH activation and etching to prepare diatomite-templated carbons with high porosity and zeolite by-product

Liu D*, Yuan W, Yu W, Tan D, Yuan P

1 - Guangzhou Institute of Geochemistry, CAS *liudong@gig.ac.cn

Hierarchically porous carbons are attracting attention because the macropores or mesopores of carbons can improve the transport of adsorbed molecules through the porous framework of carbons. Recently, hierarchically porous carbons with unique macroporous carbons have been prepared using diatomite as the template. However, the obtained carbons lacked microporosity and showed the ordinary adsorption capacity for the small-sized molecules. Moreover, recycling and further utilization of silicon-containing waste solutions from the diatomite template etching have not been investigated.

In this study, KOH was used as the etchant and activation agent to prepare the highly porous diatomite-templated carbon with the inherent solid acid sites as the catalyst, and a zeolite K-H by-product was simultaneously obtained via utilization of the silicon- and potassium-containing solutions as a source of silicon and potassium.

The obtained diatomite-based carbons were composed of macroporous carbon pillars and tubes, which were derived from the replication of diatomite templates and were well preserved after KOH activation. Abundant micropores and mesopores were also formed by KOH activation. Compared with the original diatomite-templated carbons and CO_2-activated carbons, the KOH-activated carbon possessed much higher specific surface areas (988 m^2/g), pore volumes (0.675 cm^3/g) and high methylene blue adsorption capacity (645.2 mg/g). The zeolite K-H by-product showed the stick-like morphology and possessed nanosized particles with mesopore-predominant porous structure, as observed by TEM for the first time.

These fundamental results demonstrate that the preparation of hierarchically porous diatomite-templated carbons and diatomite-based zeolite using KOH as the activation agent and etchant is both facile and economically viable.

Keywords: Diatomite-templated carbon; KOH activation; High porosity; Zeolite K-H

Acknowledgments: The financial supports from the National Natural Scientific Foundation of China (Grant No. 41202024), National Key Technology Research and Development Program of the Ministry of Science and Technology of China (Grant No. 2013BAC01B02) and Key Laboratory of Mineralogy and Metallogeny, Chinese Academy of Sciences (No. KLMM20110201) are gratefully acknowledged.

Sunlight exposure as ageing process of modern and fossil resins; physico-chemical data

Neacsu A[1], Cioaca M E[2], Dumitras D[2*]

1 - University of Bucharest 2 - Geological Institute of Romania *d_deliaro@yahoo.com

Ageing studies are important for gemmology, allowing the distinction between amber and fakes, and also for understanding the degradation mechanisms in the environment where resins, subfossil resins and amber have been exposed during the geological ages. A special look is accorded to conservation measures of amber materials from archaeological sites and old collections, in order to prevent degradation. There are several factors which cause amber degradation, *e.g.* temperature, light, oxygen, relative humidity, pH, air pollutants, chemical substances, *etc*. The aim of this study was to establish if, from the physical and chemical point of view, a relatively short period of time of external atmospheric exposure could deteriorate the surface of amber and modern tree resins. Our experiment was made in the temperate-continental climate of Bucharest, Romania. Several prisms of approximately 16x7.5x3 mm of Baltic and Romanian amber, and also of angiosperm resins, weighting 700±10 mg were directly exposed to external atmosphere for three consecutive months (April, May and June)y. Samples were checked regularly to ensure the exposure of every surface of prisms for equal periods of time. Some control prisms (blind samples) were used for comparing analyses before and after air ageing. After three months, no change in colour and surface of prisms were macroscopically observed. The microscopic study in transmitted light (Panphot Leitzer, NII, N+) of the surfaces of ageing prisms did not show the presence of new cracks, any modification of isotropy of Baltic amber or of the weak anisotropy of Romanian amber. No supplementary re-distribution and also no significant modification in the amount of air bubbles were observed before and after ageing experiment in the amber and resin thin sections. From every ageing prism one small piece was removed from the external surface and was compared with similar pieces of blind prisms using FT-IR spectroscopy (JASCO FT-IR microscope system, FT-IR 4100 spectrometer and Irtronμ (IRT-1000) microscope). The measurements were made on pellet-shaped samples (KBr) and showed changes in chemical groups due to air ageing. FT-IR absorbance spectra (FT-IRA) were recorded for this study. Our own spectral database offered the possibility to compare spectra of angiosperm resins before and after ageing. The peaks at ca. 888 ±1 cm^{-1} and ca. 3098 cm-1 are obvious in fresh angiosperm resins and less visible in ageing samples, meaning that the increase of temperature and oxidation could affect the strengths of the $=CH_2$ vibrations. Modern resins and amber samples present a slight increase in absorbance of >C=O (of esters and acids) between 1740 and 1712 cm^{-1}, due to the photo-oxidative activity. *The fingerprints area* of ageing Baltic amber presented a decrease of absorbance intensity at 888±1 cm^{-1}, and also an increase in slope of the Baltic shoulder (1235-1175 cm^{-1}, -CO-O of succinate) due to oxidation. A decrease of intensity band at 1650-1600 cm^{-1} related to >C=C< (non-conjugated) after ageing was detected in Baltic amber and modern resins. This band is not characteristic for romanite (fossil resin), probably as a consequence of its geological origin. The loss in C=C groups is an effect of maturation or ageing of amber. The IR analyses demonstrate that romanite has more carboxylic groups than Baltic amber, so romanite is strongly oxidized. In summary, an older hypothesis that romanite could be 'ageing' Baltic amber is revealed. The results of the ageing experiment show that visible light, atmospheric oxygen and the increase of air temperature give spectroscopic changes after three months of external atmospheric exposure of amber and angiosperm resins.

Dissolution reaction and surface iron speciation of tremolite asbestos in buffered solution at pH 7.4: a combined ICP-OES, XPS and TEM investigation

Andreozzi G[1*], Pacella A[1], Fantauzzi M[2], Turci F[3], Cremisini C[4], Atzei D[2], Rossi A[2]

1 - Sapienza University of Rome *gianni.andreozzi@uniroma1.it 2 - University of Cagliari 3 - University of Torino - Dip. Chimica 4 - ENEA, C.R. Casaccia

Results of the study on dissolution reactions and surface modification of two fibrous samples of tremolite asbestos incubated for 0.5, 1, 24, 48, 168 and 1440 h in a phosphate buffered solution at pH 7.4 with H_2O_2 are presented. The samples come from southern Italy (Castelluccio Superiore, Basilicata) and eastern USA (Montgomery County, Maryland), and are Fe-poor and Fe-rich, respectively. Inductively Coupled Plasma Optical Emission Spectrometry (ICP-OES) was used to monitor the ion release into solution, X-Ray Photoelectron Spectroscopy (XPS) was performed to unveil the chemistry of the leached surface, and High Resolution Transmission Electron Microscopy (HR-TEM) was carried out to monitor the structural modifications of the fibres. Results obtained are compared with those previously obtained in the same conditions on UICC crocidolite.

A congruent cation mobilization is only observed for the Maryland tremolite and not in the case of Castelluccio: this because of the presence of small amount of chrysotile in the Castelluccio sample. For both samples Fe mobilization is not detected at any incubation time. In the under-saturated conditions (0-48 h), dissolution rate of the Maryland tremolite fibres has been estimated to be $d(Si)/dt = 0.014$ µmol h^{-1}. Notably, tremolite lifetime is shown to be roughly twice that for UICC crocidolite in the same experimental conditions. XPS results evidence a depletion of Mg and Ca after 0.5 h of incubation for the Maryland sample, and Fe(II) oxidation to Fe(III) in the first 0.5 h for the Castelluccio sample. For the UICC crocidolite the oxidative environment promoted increasing Fe(II) oxidation only after 1h. HR-TEM results show that the buffered H_2O_2 solution does not significantly alter tremolite fibres even after 168 h, as fibrous habit and high aspect ratio are largely preserved for both samples. Amorphous connective material and degraded fibres are observed for the Maryland tremolite, but nanoparticles (likely amorphous and Fe-bearing) are clearly observed at higher magnifications on top of the fibres of the Castelluccio tremolite. Similar iron armouring was previously observed on the UICC crocidolite.

Asbestos deposits, work environments, and "deposits" in the lungs of workers: where and why they differ

Case B

McGill University. bruce.case@mcgill.ca

For decades, scientists have studied mineral fibre exposures and their relation to health hazard and risk assessment using the lungs of workers. Tissue from those exposed offered interdisciplinary researchers opportunities to measure long-term fibre accumulation and to relate it to exposure parameters and disease outcome. Methodology and interpretation of fibre recovery has been technically difficult and at times controversial. Results have been considered at least representative of exposure and internal dose. Recently even these parameters have come into question due to complexity of issues around where the minerals in lung in some situations actually "come from". Examples are discussed from the author's own research at the Jeffrey Mine in Asbestos, Quebec and from the United States.

THE JEFFREY MINE, QUEBEC: Lung chrysotile, without accompanying tremolite or other minerals, was found in excess vs. age and sex-matched controls in a single-hospital autopsy series of those living within 40 km of this asbestos mine, the second largest on earth. None had worked in or lived with persons who worked in the mine itself. In epidemiological studies none showed increased risk for any asbestos-related diseases. The situation was quite different in a birth cohort of workers themselves. These men born 1891-1920 showed excesses of lung cancer, mesothelioma, asbestosis and other diseases. Analysis of their lungs was surprisingly different from community residents and from other Quebec mines. Tremolite, present in low concentration in dykes surrounding and intersecting the ore body, was commonly found but well below levels seen elsewhere. More surprisingly, fibrous riebeckite ("crocidolite") was found in the lungs of three quarters of workers, having particularly high concentrations (geometric mean 2.5 million fibres longer than 5 micrometres) in six of seven workers who developed mesothelioma. Suggestions that crocidolite might be present in the deposit were proven false by mineralogical mapping. Answers came from finding out more about jobs for the miners/millers and factory workers with mesothelioma who had autopsy lung analysed for fiber content by TEM. Miners and millers' median dust exposure was an order of magnitude higher than that of factory workers (373 vs. 42 million particles per cubic foot-years, $p < .05$). Nonetheless the factory workers were five times more likely to die from mesothelioma: 1.08 per cent of all deaths compared with one in 500 among miners/ millers. Crocidolite was used in the factory to make military gas masks during the period those who developed disease worked. One man worked only three years before going to war in 1939, but died of mesothelioma in 1985; lung analysis showed only crocidolite. Of the eight mesothelioma cases who worked only in the mine or mills, five worked in the latter. These "chrysotile" mills did mill crocidolite during some periods, and elevated crocidolite was present in their lungs as well. By comparison, for 15 workers with mesothelioma for whom tissue was available at asbestos mines and mills elsewhere in Quebec, no crocidolite was present ($p < .01$ vs. Jeffrey workers). However, geometric mean tremolite elsewhere was 105 million fibres/ gram dry lung compared to 3.4 million for the Jeffrey workers ($p < .01$).

DISSONANT FINDINGS IN AMERICAN COUNTIES: For some years, mesothelioma rates among workers in Minnesota taconite mines have been higher than expected; county rates are the highest in the USA. Miners are exposed to non-asbestiform cummingtonite-grunerite, some of which is indistinguishable from amosite asbestos by TEM alone. To date, investigators have found only that some victims may have had occupations in which imported commercial amphibole use was likely. Jefferson Parish, Louisiana, presents an even more complex situation in which environmental, domestic, and shipyard or factory occupational exposures overlap producing America's greatest mesothelioma epidemic. Lung content and historic details helps separate the exposures. In situations like these, detailed work involving mineralogists, medical specialists, epidemiologists, hygienists and others can untangle the facts. These are not "academic" questions, having public health relevance beyond the situations themselves, particularly for natural and industrial legacy occurrences of fibrous minerals.

Breakdown of asbestos-containing waste by self-propagating high temperature synthesis (SHS)

Gaggero L[1*], Ferretti M[2], Sanguineti E[2], Caratto V[2], Belfortini C[2], Musi L[2]

1 - University of Genoa, DISTAV *gaggero@dipteris.unige.it 2 - University of Genoa, DCCI

Following the dismissal of asbestos, increasing amounts of fibre-bearing wastes represent a priority in environmental alert. In the perspective of reducing the environmental issue and to explore recycling of the breakdown products, we experimented with the use of self-propagating high temperature synthesis (SHS), exploiting the highly exothermic and fast self-propagating high temperature combustion synthesis (SHS) reactions [1].

The starting reactant was a natural chrysotile from a veined serpentinite, previously characterized by optical microscopy, SEM-EDS and XRPD analysis. Experimental procedures typically referred to the SHS method were adopted, taking advantage of the energy release of the highly exothermic reactions ignited by a relative low heat source.

Reactants were selected between different oxide - metal couples (Hem+Mg; Mgt+Mg; Hem+Al) liable to activate the aluminothermic reaction and to break down the chrysotile. The successful experiments are based on the couples Fe_2O_3 + Mg and Fe_3O_4 + Mg. The reaction chamber is made by a heated base made of a metallic support to the sealed glass bell, and a refractory heated element (T_{max} = 800°C) to pre-heat or cool down the sample. On the whole, at constant pellet pressing (1,5 t/m^2), varying parameters are:

- Aluminothermic (Magnesio-thermic) reactants: Hem + Mg; Mgt + Mg; Hem + Al;
- Chrysotile abundance: Ctl45%, Ctl50%, Ctl_std, Ctl60%, Ctl65%;
- Size of the pellet: diameter (10 mm - 13 mm); height ($h_{average}$ = 7-8 mm; h_{max} = 13 mm)
- Homogeneous and layered texture of the pellet (alternating layers of chrysotile with layers of reactants).

After ignition, the average loss of weight of the sample resulted c. 4% that normalized to the percentage of chrysotile in the pellet corresponds to a variable weight loss between 10 and 12 %, likely corresponding to the dehydroxylation of chrysotile.

As the toxic action of asbestos resides in habit, composition and size, inertization requires the structural change of mineral fibre. Following the combustive reaction, all experiments demonstrated effective in destructing the fibrous habit of chrysotile, turning its composition to stubby olivine grains (Figure 1).

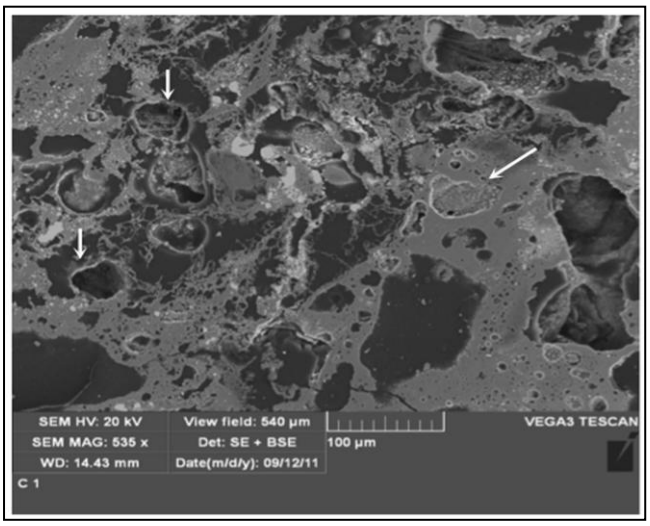

Figure 1: SEM photomicrograph of SHS treated pellets. The sample was stratified. Spongy texture defined by wustite shells enclosed in forsterite (light grey, arrow on the right side)

The asbestos inertization is particularly advantaged by the SHS process in comparison with conventional thermal treatments, due to fast reaction time, low activation energy and simple instruments, that positively reflect into time and costs of the process. Finally, the product of this transformation is liable to be re-used as second material.

[1] Munir Z.A. (1988). Synthesis of high temperature materials by Self-Propagating Combustion methods, *Amer. Ceram. Soc. Bull.*, 67, 342 - 349.

Thermal analysis characterization of hazardous mineral fibres

Bloise A[1], Catalano M[1], Barrese E[1], Gualtieri A[2*], Capella S[3], Belluso E[3]

1 - Università della Calabria 2 - Università di Modena e Reggio Emilia

* alessandro.gualtieri@unimore.it 3 - Università di Torino

For many years mineral fibres, like serpentine asbestos (chrysotile) and grunerite asbestos (amosite), due to their good physical and mechanical properties, have been used in many applications and to construct various types of artifacts (asbestos cement, tubing, reinforcing agents, fire retardants, etc.). Other fibrous minerals, like erionite zeolite and tremolite asbestos, have been indirectly used because they were present in rocks or soils that were processed. Unfortunately, if breathed in high doses, they may cause several respiratory diseases in both humans and animals and therefore their use is banned or avoided in many countries. Several authors suggest that different factors may be involved in the fibres' toxicity such as their morphology and size, chemical-physical characteristics, surface reactivity and biopersistence, but which mechanisms provoke the damage of cells remains still a crucial unanswered question. In this scenario, the first step of the interdisciplinary project called: "Mineralogical and physico-chemical characteristics of mineral fibres, reactivity and impact on human health" will be an in-depth mineralogical characterization of the fibres before their interactions with the cell lines (bio-toxicity *in vitro* test). In this contribution we present the results of a complete set of thermal analyses of the following monominerallic fibrous samples: (1) UICC chrysotile from Canada; (2) chrysotile from Val Malenco (Italy); (3) chrysotile from Balangero (Italy); (4) UICC crocidolite from South Africa; (5) erionite from Jersey Nevada (USA); (6) tremolite from Val d'Ala (Italy); (7) UICC anthophyllite from Paakkila (Finland); (8) UICC amosite from Penge (S. Africa). Thermogravimetric and differential scanning calorimetry (TG-DSC) were performed in an alumina crucible under a constant nitrogen flow of 30 cm^{3}min^{-1} with a Netzsch STA 449 C Jupiter in a 25 - 1200 °C temperature range, with a heating rate of 10 °C/min. The resulting thermal data allowed us to establish a relationship between the chemical composition and the dehydroxylation temperatures of thermal decomposition of mineral fibres above listed.

The Zeta potential of mineral fibres

Gualtieri A*, Pollastri S

University of Modena and R.E. Italy *alex@unimore.it

The Zeta potentials of eight relevant mineral fibres (chrysotiles, amphiboles and erionite) were systematically investigated to understand the relationship between the surface reactivity and fibre pathogenicity. A revised model explaining the Zeta potential of chrysotile, amphiboles and erionite was postulated. In double distilled water, chrysotiles show positive values of the Zeta potential, while crocidolite and erionite show negative values. In contact with organic solutions, all fibres tend to assume negative values of Zeta potential, demonstrating that this parameter is not discriminating when fibres are in contact with the surfactant mimicking the surface environment of alveolar cells and resident macrophages. The Zeta potential of the fibres displayed at pH = 4.5 and 7.0 is invariably negative, with values approximately in the range -10 to -26 mV. The decrease of the Zeta potential of the fibres is a known effect of the defensive chemical macrophage response, aimed at minimizing haemolytic damage and negatively charged reactive surfaces favour the binding of collagen and redox activated Fe-rich proteins, to form the so-called asbestos bodies. The negative Zeta potential at the fibre surface prompts the formation of $HO^{\cdot}$ via the reaction with peroxide that is associated with increased fibre-induced carcinogenicity. An additional mechanism accounting for higher carcinogenicity is related to the possible Ca^{2+} sequestration by fibres with the surface negative Zeta potential, impairing the mitochondrial apoptotic pathway. Finally, with a negative Zeta potential, the attractive forces prevail over repulsions and favour processes such as agglomeration, known to induce a tumorigenic chronic inflammation, as observed in the case of agglomerated silica that induced more potent inflammatory responses than non-agglomerated particles.

Mineralogical and crystal chemical characterization of hazardous mineral fibres of social and economic importance

Gualtieri A[1*], Pollastri S[1], Barrese E[2], Bloise A[3], Belluso E[4], Belpoggi F[5], Cavallo A[6], Croce A[7], Lezzerini M[8], Perchiazzi N[9], Pugnaloni A[9], Rimoldi B[10], Caterina R[11]

1 - University of Modena and R.E. Italy *alex@unimore.it 2 - Dipartimento di Scienze della Terra, Università della Calabria 3 - Università della Calabria 4 - University of Torino 5 - Istituto Ramazzini, Bentivoglio Bologna Italy 6 - Università di Milano-Bicocca Milan Italy 7 - Università del Piemonte Orientale Alessandria Italy 8 - Dipartimento di Scienze della Terra, Università di Pisa Italy 9 - Università Politecnica delle Marche Italy 10 - CONTARP INAIL Lombardia, Milano (Italy) 11 - University of Piemonte Orientale

Mineral fibres are ubiquitous on Earth. Because many of them possess outstanding technological properties, they have been used since ancient times for a huge number of applications. They are considered now one of the most interesting and complex examples of inorganic to organic sphere interaction with direct consequences for human health. The most important mineral fibres are serpentine asbestos (chrysotile), amphibole asbestos species and the zeolite erionite. If inhaled, because of their peculiar fibrous-asbestiform crystal habit and chemical-physical surface reactivity, these mineral fibres may induce, after a long latency period, fatal lung diseases. All amphibole asbestos minerals are banned worldwide whereas chrysotile is banned only in the countries strictly following the indication of the International Agency for Research on Cancer (IARC) which includes chrysotile in Group 1 "substance carcinogenic to humans". No ban has been proposed for the zeolite erionite so far. Explaining human toxicity of mineral fibres is not straightforward at all. The difficulties stem from the fact that mineral fibres possess a variety of chemical compositions, atomic structural arrangements, morphologies that affect biogeochemical reactions in the body. Due to the interplay of all these factors, the mechanisms by which mineral fibres induces cyto- and geno-toxic damage remain unclear.

Our research group is actually involved in the study of the bio-interaction and toxicity of the mineral fibres from the well pondered assemblage of chemical-physical, mineralogical-structural, and biological information.

In this work, we present the results of the mineralogical and chemical physical characterization of mineral fibres belonging to the major classes of mineral fibres of economic and social importance: three chrysotile species including the UICC standard, Balangero and Valmalenco (Italy), crocidolite UICC standard, amosite from Penge (South Africa), anthophyllite UICC standard, tremolite from Val d'Ala (Italy) and the zeolite erionite from Jersey valley (Nevada USA). Data are discussed in the frame of the existing contradictory literature data.

Hazard of airborne and waterborne naturally occurring asbestos from asbestos-polluted areas in the Italian Western Alps

Turci F[1*], Aldieri E[2], Daghino S[3], Favero-Longo S[3], Tomatis M[1], Fubini B[1]

1 - University of Torino - Dip. Chimica *francesco.turci@unito.it 2 - University of Torino - Dip. Oncologia 3 - University of Torino - Dip. di Scienze Vita Biologia Sistemi

In many countries, including EU, USA, and South Africa, the use, manufacture and processing of asbestos is prohibited due to the large number of deaths that occupational exposure to asbestos is still causing today. In those counties, the main exposure settings were asbestos mines and industries manufacturing asbestos. Asbestos-polluted areas represent now the legacy of asbestos industry and the researchers from the "G. Scansetti" Center are investigating the risk posed by these areas in the Italian Western Alps. Naturally occurring asbestos (NOA) is mostly associated to serpentinite rocks, where the fibers occur within different generations of metamorphic veins. Natural sources primarily comprise areas where fibers can be released in the environment following the weathering of asbestos-bearing rocks and/or human activities on asbestos-rich soil. We observed that physical and chemical agents and biota may actively favor the release of airborne and waterborne fibers and high concentration of asbestos is commonly observed. Biotic and abiotic weathering was reported to alter the toxicity-relevant properties of asbestos fibers, including the presence of iron ions, which role in asbestos toxicity has been confirmed at the molecular level with a synthetic chrysotile fiber. We modelled agricultural activity in an asbestos-polluted field and measured a significant increase of the airborne level of fibers. In those settings, we also studied waterborne fibers, for which a worldwide-accepted threshold level is still missing. Waterborne asbestos is characterized by the occurrence of nanometric fibers, with an unknown toxicity profile. A correlation between nanometric fiber diameter and cellular toxicity was found in an in vitro study. Both ad hoc hazard evaluation and unconventional remediation strategies are proposed for NOA in the environment.

Environmental exposure to asbestos and asbestiform minerals. Identification, hazard and inactivation routes: a multidisciplinary approach

Turci F[1*], Aldieri E[2], Belluso E[3], Capella S[4], Compagnoni R[4], Daghino S[5], Gazzano E[2], Ghigo D[2], Groppo C[6], Favero-Longo S[5], Perotto S[5], Piervittori R[5], Tomatis M[1], Fubini B[1]

1 - University of Torino - Dip. Chimica *francesco.turci@unito.it 2 - University of Torino - Dip. Oncologia 3 - University of Torino 4 - University of Torino - Dip. Scienze della Terra 5 - University of Torino - Dip. Scienze Vita Sistemi Complessi 6 - Dip. Scienze della Terra

While strict regulations in Europe have banned the use of asbestos, there is a lack of information and regulations on naturally occurring asbestos (NOA) in the environment. Safety protocols for tunnelling and excavation in asbestos bearing rocks are urgently needed. The toxicity of weathered asbestos fibers exposed for long periods of time to abiotic and biotic agents should be assessed. Waterborne asbestos fibers are not regulated by the current legislations. Analytical methods are often inadequate to deal with NOA, where altered asbestos minerals have to be unambiguously identified and quantified in the presence of polymorphs or other fibrous minerals. These are just few of the main open issues that require urgent answers when NOA are involved. The Piedmont region in the Italian Western Alps is rich in natural asbestos and the area has one of the highest numbers of deaths in Europe among people exposed to asbestos in a non-occupational setting. In Italy, NOA are mostly associated to serpentinite rocks, where the fibres occur within different generations of metamorphic veins. The fibers can be released in the environment following weathering of asbestos-bearing rocks and/or human activities on asbestos-rich soil. Since asbestos-polluted areas represent the legacy of the asbestos industry, and the risk posed by these areas largely undefined, a multidisciplinary project has been carried out by the researchers from the "G. Scansetti" Center with the aim to: i) localize asbestos mineralisation in serpentinites, characterize and identify both conventional and non regulated asbestos; ii) measure fiber dispersion in air following agricultural activity in asbestos-polluted fields and evaluate waterborne fibers, for which a worldwide-accepted threshold level is still missing; iii) evaluate the presence of asbestos fibers in the organs of nearby animals and in the exposed population; iii) investigate the toxicity of the new asbestiform minerals whose interaction with animal tissues and impact on human health have never been studied; iv) investigate the toxicity of nanometric fibers, abundant in natural waters, that still have an unknown toxicity profile and v) evaluate the effect of weathering and of growth of fungi or lichens on the fiber composition and reactivity to propose unconventional remediation strategies for NOA.

"Rinse & trickle": the fine art of TEM sample preparation for extracting inorganic matter from biological samples through gentle bleaching

Vigliaturo R[1*], Capella S[1], Rinaudo, C[2], Gualtieri A[3], Bloise A[4], Belluso E[1]

1 - University of Torino *vigliaturo_ruggero@libero.it 2 - University of Piemonte Orientale 3 - University of Modena and Reggio Emilia 4 - Università della Calabria

The target of this work is to present a different sample preparation approach that allows the characterization by TEM-EDS of inorganic fibers and particulate matters from a morphological, crystallographic, and chemical point of view. The method used has to avoid any damage to the inorganic material extracted from a biological sample. Moreover, it should not generate artefacts through chemical attacks or mechanical stress. Attention has been paid to ensure that residues of used ingredients wouldn't influence the analysis.

In this study, different techniques of preparation have been evaluated and tested; selecting the most rapid and simple one, working on a limited number of steps, to transfer the withdrawn inorganic matter onto the TEM grid.

The developed and tuned preparation method includes as a main step the digestion of the biological component of the sample by sodium hypochlorite (NaClO 14%) in an oven at 60 °C for 6-24 hours. After this, it is a priority to remove the salt from the suspension, since it could damage the coating carbon film when it's trickled on the TEM grid (usually more than one drop, from this comes the term "trickle"). The removal is carried out with a series of centrifugation steps and rinse cycles in deionised water, reducing drastically the digestive power of the NaClO. Furthermore the centrifugation steps allow the concentration of inorganic fibres and particulate matter to the bottom of the tube.

A simple preparation allows for an appreciable flexibility of applications, with the possibility to modify and adapt the steps for the different kinds of possible biological samples (e.g. urine, intestine tissues etc).

This technique allows to make TEM-EDS detailed investigation to fully characterize exogenous inorganic materials that enter the organism and the transformations that occur during bio-interactions. The extrapolated data can be used in an interdisciplinary study (by mineralogists, chemists, biologists, pathologists) to better understand the pathological effects caused by the inorganic materials penetrated into human body.

Keywords: TEM sample preparation, inorganic material, biological samples.

A permeable reactive barrier to retain Cs-137: from laboratory to a field scale experiment

Ayora C[1*], De Pourcq K[2], Carrera J[2], Missana T[3], Garcia-Gutierrez M[3]

1 - CSIC *cayora1@gmail.com 2 - IDAEA-CSIC Barcelona 3 - CIEMAT, Madrid

A Permeable Reactive Barrier has been designed to treat Cs-137 polluted groundwater. In order to check both reactivity and permeability, laboratory batch and column tests combined with reactive transport modelling have been performed. The trapping mechanism is based on the sorption of cesium on illite-containing clays. Batch experiments were conducted to obtain the partition coefficients (Kd) of different clay samples in solutions with different potassium concentration. The results were modelled with a cation-exchange model.

The permeability of the reactive material is provided by the dispersion of the clay on a matrix of wooden shavings. Constant head tests allowed obtaining permeability values. The mixture of wooden shavings and clay (2:1 by weight) is a material that has a hydraulic conductivity (10^{-4} m/s) high enough to ensure an adequate hydraulic performance for an eventual PRB excavated in many aquifers.

Several column experiments with different flow rates were conducted to confirm the Cs retention under different conditions. A blind 1D reactive transport model based on the cation-exchange model was able to predict reasonably well the results of column experiments.

The reactive transport model, validated with the column experiments, was used to investigate the performance and duration of 1m thick barrier under different scenarios (flow, clay proportion, Cs-137 and K concentration). As expected, the sensitivity tests proved that the retention capacity of dissolved Cs-137 in groundwater depends linearly on the amount of clay used in the filling material. Also, the operation time increases linearly when decreasing the flow rate. Finally, the concentration of potassium in inflow water has a remarkable and non-linear influence in the retention of Cs-137. Very high concentrations of potassium are the greatest threat and can lead to the infeasibility of the permeable reactive barrier. Due to the Cs-K competition, the barrier is comparatively more efficient to treat high concentrations of Cs-137.

The impact of nanoscale metal oxide clusters on mineral aqueous solubility

Burns P[*], Qiu J, Balboni E

University of Notre Dame *pburns@nd.edu

Focusing on nanoscale cage clusters of uranium oxide polyhedra, we explore the impact of such clusters on the aqueous solubility of uranyl minerals. We have developed a family of more than 80 uranyl peroxide cage clusters that form spontaneously in aqueous solution, and that may be important for transport of uranium in geochemical systems, in nuclear waste repositories, and in nuclear accident scenarios where damaged fuel interacts with water. These anionic cage clusters are stable in solution, and often are much more soluble than simple uranyl ions or their complexes in solution. As such, the conventional concept of mineral solubility as a competition between the simple aqueous species and the solid phase is not applicable. Our experiments have shown that much more uranium is typically in the aqueous phase when nanoclusters are present. We will explore hypothesis that relate the total uranium content in solution to its distribution in the solution, including factors that control mineral solubility in such systems. These will include studies of the solubility of uraninite, uranophane, and autunite.

Leachability of uranium from sedimentary mine waste rocks and ore from the Karoo Supergroup

Fourie J

Geostratum Groundwater and Geochemistry Consulting. johan@geostratum.co.za

An assessment was made on the leachability of uranium from sedimentary rocks from the upper Northern Rukuru Formation, Karoo Supergroup, Malawi. Scanning Electron Microsocopy (SEM) performed in this study identified coffinite as the principal ore mineral with minor uraninite.

Leach testing were performed on 'clean' waste rock (nom. <100 ppm U), marginal ore (nom. 200 - 400 ppm U), low-grade ore (nom. 400 - 600 ppm U) and high grade ore (nom. >2 000 ppm U). Uranium leached at high initial concentrations during the first few weeks of column leach tests. It was observed that these elevated concentrations could directly be correlated with bicarbonate in the solution which was the most prominent in leachate of the low and high grade ore. These samples also have high calcite content. After about 10-20 weeks the uranium leached at a more constant concentration from the different columns. Speciation numerical modelling showed that $(UO)_2CO_3(OH)_3^-$, and to a lesser degree $UO_2(CO_3)_2^{2-}$ and $UO_2(CO_3)_3^{3-}$, are the prominent uranium species in the near-neutral leachate.

Kinetic numerical modelling was performed in order to simulate the column test results. The high uranium and carbonate during the initial weeks could be explained by the dissolution of traces of secondary uranium minerals in the samples. The presences of uranophane and meta-autunite have been confirmed in XRD but various other hydrated and carbonate uranyl species may be present. Dissolution of primary ore minerals is responsible for the more constant uranium concentration after the initial few weeks.

For extrapolation to field conditions assumptions had to be made on the water:rock ratio and the differences in particle size. Sensitivity analyses were performed and some useful predictions were made to the long-term leaching potential of uranium from the residue wastes.

Retention of selenium oxyanions at the water-mineral interface in the context of nuclear waste repositories

Franzen C[1*], Hering D[2], Jordan N[1], Weiss S[1]

1 - Helmholtz-Zentrum Dresden Rossendorf; Institute of Resource Ecology
*c.franzen@hzdr.de 2 - University of Applied Sciences, Zittau-Görlitz

The radioactive isotope Selenium-79 is a fission product found in nuclear waste. Due to its long half-life of $3.27 \cdot 10^5$ years and its high mobility, it is expected to be one of the isotopes contributing significantly to the potential radiation dose according to safety assessments of nuclear waste underground repositories. A detailed knowledge of the mobility and bioavailability of selenium in its different oxidation states is therefore of great importance for a safe disposal of radioactive waste.

Adsorption onto mineral surfaces of both the engineered and geological barrier is a major process controlling the retention of the water-soluble selenium oxyanions, selenate ($Se^{VI}O_4^{2-}$) and selenite ($Se^{IV}O_3^{2-}$). In this context, it is important to understand to what extent this sorption is influenced particularly by characteristic parameters as expected in deep underground repositories for high level radioactive waste. These parameters include *inter alia* the presence of different background salts and elevated temperatures.

In this study, a combination of macroscopic sorption experiments, electrophoretic mobility measurements and *in-situ* ATR FT-IR spectroscopy was used to study the interaction of $Se^{VI}O_4^{2-}$ and $Se^{IV}O_3^{2-}$ with aged γ-Al_2O_3 in the presence of NaCl and $MgCl_2$ and at elevated temperatures up to 60 °C. In this context, γ-Al_2O_3 can be considered as model mineral phase for more complex rock and backfill materials associated with a nuclear waste repository.

It could be shown that the retention of both Se(VI) and Se(IV) is affected by all three investigated factors – pH, ionic strengths of the solution, and temperature. The increase of each parameter results in a decrease of sorption, with the retention of Se(IV) generally being higher than the one of Se(VI). *In-situ* ATR FT-IR spectroscopy and electrophoretic mobility measurements evidenced the formation of an outer-sphere surface complex of Se(VI) on γ-Al_2O_3. Concerning Se(IV), a mixture of inner-sphere and outer-sphere surface complexes could be derived.

Any sorption on mineral surfaces is dominated by the surface charge of the mineral. The impact of salinity and temperature on the variable surface charge of γ−Al_2O_3 was evaluated by zeta potential measurements using laser Doppler electrophoresis. The isoelectric point (pH_{IEP}) of γ-Al_2O_3 is located at pH 9.6 with a positively charged surface at lower pH values and a negatively charged surface for higher pH values. Increasing the amount of NaCl in the solution (up to I = 1 M) reduces the zeta potential for both the acidic and alkaline pH range. However, in the alkaline range the decrease of the zeta potential is more pronounced. In the presence of 0.1 M $MgCl_2$, the surface charge of γ-Al_2O_3 becomes positive throughout the studied pH range (3-11). Above pH 10, a sharp potential decrease occurs due to $Mg(OH)_2$ precipitation. The increase of temperature shifts the pH_{IEP} to lower values and decreases the zeta potential in the acidic range.

These changes in the surface properties of the γ-Al_2O_3 are consistent with the changes in the sorption behaviour of selenate and selenite.

These results indicate that for geochemical modelling and long-term safety assessments concerning selenium-containing waste it is crucial to include the impact of temperature and ionic strengths effects.

Scientific issues and role of mineralogists in treatment and disposal of the radioactive waste produced by accident at Fukushima Daiichi NPP

Sato T

Faculty of Engineering, Hokkaido University. tomsato@eng.hokudai.ac.jp

The Fukushima Daiichi nuclear disaster was a series of equipment failures, nuclear fuel meltdowns, and releases of the fission products and feasible neutron activated nuclides to the environment at the Fukushima Daiichi Nuclear Power Plant (NPP), following the 9.0 magnitude east-Japan earthquake and the ensuing tsunami on 11 March 2011. As the result of radionuclide releases, the soils, water, foods, building wall and road in Fukushima were widely contaminated with the radionuclides, especially ^{134}Cs and ^{137}Cs. Although it is urgent to figure out how radioactive materials were spread not only in the area close to the nuclear reactors but also over surrounding, rather wide district, decontamination methods of the radionuclides should be considered to reduce the public health impact and to regain their daily life. While the public health impact appears to have been low, the economic and nearby environmental consequences are severe. There is no doubt that land restoration will take over a decade and perhaps much longer. However, we have to work on the decontamination of radioactive caesium without further delay to take back daily life to the inhabitants in Fukushima. For the efficient decontamination, we have to understand the followings concerning the radioactive caesium in the environment: 1) distribution by environmental monitoring, 2) state (water extractable, cation exchangeable, passive states, and so on). During the operation of decontamination, huge amount of the waste with radioactivity will be produced. Therefore, the method of decontamination should be connected with how to dispose of the waste.

On the contrary, in the site of Fukushima Daiichi NPP, there is also huge volume of radioactive waste such as cut-down trees, debris produced at hydrogen explosion, adsorbents used in the decontamination system for water using in "feed and bleed" cooling of the reactor core. For the timber and concrete debris, the reduction of their volume will be a required action. Development of technology therefore will be necessary for safety and reasonable combustion and surface decontamination. Various kinds of adsorbents such as synthetic zeolites and ferrocyanide compounds have been used in the Cs decontamination system for the cooling water. Multi-nuclide Removal Equipment (ALPS) will be operated so that the radioactivity of the 62 nuclides in the cooling water want to be reduced to below the limit specified by the reactor regulation. In the ALPS system, various kinds of adsorbents such as ferric hydroxides, carbonates, active carbon, titanate, and resin will be used. After using those materials, we have to hold huge volumes of the waste contaminated with various kinds of radionuclides. These wastes are more complicated to treat and dispose than adsorbents from Cs decontamination system for the cooling water because more complicated radionuclides should be contained in the wastes. For the present, however, it is still ambiguous for the treatment and disposal because there is no information about the containment of the radioactive nuclides and their concentration. Consequently, we have to go ahead for treatment and disposal of the waste without sufficient information about contamination.

In this presentation, the present status of the actions and inherent issues in decontamination of the radionuclides and safety waste disposal during the decontamination would be presented and discussed. The author will alert mineralogists to the need for research and development in safe geological disposal of the different kinds of waste materials.

Simultaneous incorporation of REEs and selenite into the secondary mineral phases formed in HLW repositories

Wu S*, Chen F

Guangzhou Institute of Geochemistry, Chinese Academy of Sciences *wus@gig.ac.cn

The corrosion of nuclear waste compounds will release radionuclides into the groundwater along with the precipitation of secondary mineral phases. However, some of the released radionuclides can be incorporated into the secondary phases, resulting in re-immobilization. Usually, the incorporation of radionuclides into minerals is investigated in isolation, which is different to the real situation in environment/nuclear waste repositories. This study aims to figure out the interaction of both cationic and anionic radionuclides and common secondary minerals (calcite, hydrotalcite and saponite). Therefore, calcite, hydrotalcite and saponite adopted with both REEs (as surrogate of Am^{3+} and Cm^{3+}) and selenite were synthesized using co-precipitation method. The samples were characterized with XRD, SEM, TEM and XPS while the concentration of REEs and selenite was measured using ICP-AES and ICP-MS.

The results showed that Eu^{3+} and SeO_3^{2-} can be incorporated into calcite simultaneously. However, the interaction of Eu^{3+} and SeO_3^{2-} incorporated into calcite appears to vary and depends on the concentration of Eu^{3+} and SeO_3^{2-} in the solution in which calcite is precipitated. When the concentration of Eu^{3+} was lower than 50 ppm, incorporated Eu^{3+} could be enhanced while SeO_3^{2-} was present. Nevertheless, when the concentration of Eu^{3+} was higher than 50 ppm, Eu^{3+} incorporation was inhibited by SeO_3^{2-} obviously. Furthermore, the morphology of calcite changed with incorporation of Eu^{3+} and SeO_3^{2-}. TEM observation demonstrated that the incorporation of Ce^{3+} and SeO_3^{2-} gradually changed the morphology of hydrotalcite from flat to needle shaped, while the size of saponite became smaller. The results showed that interaction of cationic and anionic radionuclides changed with different minerals.

Uranium behavior in the systems relevant to nuclear waste glasses

Wu S[1*], Depmeier W[2], Alekssev E[3], Albrecht-Schmitt T[4]

1 - Guangzhou Institute of Geochemistry, Chinese Academy of Sciences *wus@gig.ac.cn 2 - Institute of Geosciences, University of Kiel, Germany 3 - Forschungszentrum Jülich GmbH 4 - Florida State University

Glasses, both borosilicate and borophosphate, are currently used or proposed to be used to immobilize high-level nuclear wastes (HLW). Currently, it is well known that various alteration phases will form together with the release of radionuclides during the corrosion of nuclear glasses. There are minor actinides (U, Np, Pu, Am, Cm) within the glass matrix, though the main composition of glass is SiO_2 and B_2O_3 for borosilicate, and P_2O_5 and B_2O_3 for borophosphate. On the one hand, uranyl silicates and uranyl phosphates are known as minerals while actinide borates can be synthesized in laboratory. On the other hand, there are around one hundred borosilicate minerals and several borophosphate minerals found naturally. It will be interesting for the prediction of long-term behavior of nuclear glasses and the fundamental chemistry science and crystallography to know whether actinide containing borosilicate / borophosphate may form. Therefore, we used uranium as a model of actinide to study its crystallographic behavior in systems relevant to borosilicate and borophosphate glasses.

Using solid state reaction, flux method and high temperature / high pressure method, we successfully obtained the first uranyl borosilicate $K_5(UO_2)_8(BO_3)_3(BSiO_5OH)O_4{\cdot}3H_2O$ (KBSiU-1), uranyl borate-phosphate $Ba_5[(UO_2)(PO_4)_3(B_5O_9)]{\cdot}0.125H_2O$ (BaBPU-1) and uranyl borophosphates $Ag_2(NH_4)_3[(UO_2)_2\{B_3O(PO_4)_4(PO_4H)_2\}]H_2O$ (AgNBPU-1), $Ag_{(2-x)}(NH_4)_3[(UO2)_2\{B_2P_5O_{(20-x)}(OH)_x\}]$ (x=1.26) (AgNBPU-2) and $Ag_{(2-x)}(NH_4)_3[(UO_2)_2\{B_2P_{(5-y)}As_yO_{(20-x)}(OH)_x\}]$ (x=1.43, y=2.24) (AgNBPU-3). KBSiU-1 is a layered structure with an anionic layer composed by uranyl pentagonal bipyramids, borate triangle and disorded silicate tetrahedron. BaBPU-1 is a complex structure based on borate nanotubes which is connected to uranyl phosphate subfragment. According to the classification of borophosphate, BaBPU-1 belongs to uranyl borate-phosphate since the borate group is isolated with phosphate groups. However, AgNBPU-1,2,3 are uranyl borophosphate because the borate group is directly connected to the phosphate group. The structure of AgNBPU-1 is based on layers constructed from complex borophosphate finite clusters linked by uranyl pentagonal bipyramids. There is an unprecedented fundamental building block (FBB) in AgNBPU-1, composed of three BO4 and six PO4 tetrahedra which can be written as 9□:[ϕ] □‹3□›□|□‹3□›□|□‹3□›□|. AgNBPU-2 and AnNBPU-3 are isostructural while some As substituted P in AgNBPU-2 resulting in AgNBPU-3. The structure of AgNBPU-2,3 is a 3D framework based on 1D borophosphate chains with complex geometry linked by uranyl pentagonal bipyramids. The borophosphate chains in AgNBPU-2, 3 provide a new FBB based on two BO4 and five PO4 groups. This FBB is based on seven tetrahedra and can be represented by 7□:□‹4□›□|□. It is noteworthy that only two thirds P position in AgNBPU-2 is substituted by As atoms resulting in AgNBPU-3. The formation of the specific solid solution of AgNBPU-3 is probably due to the different coordination environment of phosphate group in AgNBPU-2.

In summary, the behavior of uranium in systems relevant to borosilicate and borophosphate glasses is complex and unpredictable currently since it is affected by the experimental condition and the reagent ratio. The results indicate that it is possible to form crystalline actinide borosilicate and borophosphate during the long-term disposal of nuclear waste glasses.

Indigenous iron-sulfur-oxidizing bacteria capable of bioleaching nickel from laterite mineral ores and their application in nickel laterite bioleaching

Chaerun S K[1*], Hung S[1], Mubarok M Z[2], Sanwani E[2], Kadarusman A[3], Djafar A[4]

1 - School of Life Sciences and Technology, Institut Teknologi Bandung, Indonesia *skchaerun@gmail.com 2 - FTTM - Institut Teknologi Bandung, Indonesia 3 - PT. ANTAM Tbk - Unit Geomin, Jakarta, Indonesia 4 - PT. Vale Indonesia Tbk, South Sulawesi, Indonesia

Biohydrometallurgical extraction (microbial leaching) is a microbiological process that involves an interaction between minerals and microbes. The interactions are of some significance for the development of biohydrometallurgy technology, in particular for metal extraction from low-grade ores and mineral concentrates. Since worldwide reserves of high-grade ores are diminishing, the development of metal recovery from low-grade, lower value mineral ores based on the activity of microbes is highly needed. Hence, the present study describes the isolation and identification of indigenous iron-sulfur-oxidizing bacteria capable of bioleaching nickel from laterite mineral ores at a nickel laterite mine area in Sorowako, South Sulawesi Province, Indonesia. Seven indigenous bacteria were able to be isolated (strains SKC/S-1 to SKC/S-7) from the lateritic ores and 16S rRNA gene sequence analysis identified the bacteria as *Pseudomonas putida* (98.7% similarity), *Bacillus vallismortis* (99.6% similarity), *Paenibacillus pasadanensis* (97.8% and 98.4% similarities), *Bacillus mucillaginosus* (99.7% similarity), *Bacillus subtilis* (99.7% similarity) and *Bacillus altitudinis* (99.6% similarity). A consortium of these bacteria was subsequently employed to recover nickel from saprolite and limonite ores in bioleaching experiments using a mixture of tofu and tempeh wastes and molasses as culture media supplemented with two types of sulfur (i.e., elemental sulfur and thiosulfate). Bioleaching experimental results revealed the ability of the bacterial consortia to recover nickel from limonite and saprolite ores. X-ray diffraction (XRD) and scanning electron microscope-energy dispersive X-ray spectroscopy (SEM-EDX) analyses were also used to determine the change of mineral compositions in mineral ore samples before and after bioleaching and the feature of mineral-bacteria interaction. These results may contribute to our understanding of the potential interactions of lateritic minerals with iron-sulfur-oxidizing bacteria that may have the potential for developing the nickel bioleaching processes from low-grade lateritic mineral ores.

Keywords: Nickel, Bioleaching, Saprolite, Limonite, 16S rRNA gene sequencing, XRD, SEM-EDX

A method for the extraction of valuable metals from Jinchuan copper-nickel sulfide tailings

Cui X*, Lu A

Peking University *cxl-cxl0521@163.com

During exploitation of mineral resources, large quantities of tailings will be produced. Jinchuan Ni-Cu deposit, the world's third-largest currently exploited magmatic sulfide Ni-Cu deposit, is the largest manufacturing base of Ni and Cu in China. The method of bioleaching combined with sulfuric acid leaching was used to recover the valuable metals Ni, Cu and Co from Jinchuan Ni-Cu sulfide flotation tailings, which can generate revenue for the enterprise, cut down the tailings greatly, and solve the bottle neck problem of the large stock of sulfuric acid and waste acid in the enterprise.

Jinchuan Ni-Cu sulfide flotation tailings were investigated by X-ray diffraction. Mineralogical investigation indicates that the flotation tailings of Jinchuan mine contain lots of silicate minerals, as well as minor carbonate, metal oxide and metal sulfide minerals. The major elements present in Jinchuan copper and nickel sulfide flotation tailings are Si, Mg and Fe. Additionally, the tailings contain significant Cu, Ni and Co, which can be the second resources. The occurrence modes of Ni, Cu and Co are complicated, as these elements occur not only in the sulfide minerals, but also occur within the lattice of silicate, carbonate and oxide minerals. It is difficult to recycle efficiently by conventional methods of mineral processing.

A.f. was studied to reveal the effect of the microbial extraction of valuable metals. Jinchuan tailings samples were selected to interact with *A.f.* for different periods and then perform the sulfuric acid chemical effects. The concentrations of Cu, Ni and Co were tested by Inductively Coupled Plasma Atomic Emission Spectrometry to characterize the capability of microbial extraction of valuable metals. The optimum leaching conditions of the valuable metals Ni, Cu and Co from the tailings are microbial leaching time of 10 days, liquid-solid ratio of 50:2, inoculation volume ratio of 5:50, sulfuric acid concentration of 4 mol/L, liquid-solid ratio of 6, temperature of 90˚C, and leaching time of 6h. Under the optimum conditions, the leaching ratios of Cu, Ni and Co in the tailings are increased by a large margin, compared with sulfuric acid leaching.

Key words: Jinchuan; tailings; A.f.; acid leaching; valuable metal

Mineral-microbe interactions and implications for heavy metal remediation

Dong H

Miami University. dongh@miamioh.edu

Mineral-microbe interactions indirectly affect the geochemical fluxes and biogeochemical cycling of a large number of toxic heavy metals and radionuclides. Heavy metals and radionuclides enter the environment from various sources such as mining activity, nuclear weapons production, metallurgical and chemical industries. Other metals, such as lead, arsenic, antimony, and cadmium, are enriched in certain environments by either natural or anthropogenic processes. Because many of these metals and radionuclides are carcinogens, their release into the environment and their fate cause intense public concern and are the subject of substantial research.

There are several mechanisms for the remediation of heavy metals and radionuclides by clay minerals. One classical strategy is adsorption and absorption, which take advantage of the high external and internal surface area of clay minerals. Although this strategy may be effective in the initial removal of heavy metals, it may not be permanent because these contaminants can be remobilized if the environmental conditions change. Other strategies involve the co-precipitation of metals and radionuclides into clay mineral structures. This strategy may be more "permanent" as clay minerals are fairly stable under a wide range of conditions.

A more recent approach is redox manipulation facilitated by microbes. It is assumed that Fe(II) in smectite, possibly produced via biological reduction of structural Fe(III), can reduce oxidized forms of heavy metals, such as Tc(VII), Cr(VI), and U(VI), to reduced form as a way of immobilization. A number of studies have examined the interactions of clay-associated Fe(II) with heavy metals and radionuclides, including Tc, U, and Cr. Even when excess Fe(II) is available, not all Fe(II) is reactive. Fe(II) reactivity depends on the crystal chemical environment of Fe(II) in clay minerals. For Tc(VII) reduction, Fe(II) in smectite is the most reactive, and Fe(II) in illite the least. Surface area, surface charge, layer expandability, and layer charge between smectite and illite are important factors in accounting for this difference. For this reason, any transformation of smectite to illite has an adverse effect on metal reduction and immobilization. Conversely, any method to reverse the S-I reaction would be of benefit. Not only does smectite reduce and immobilize Tc(VII), but the reduced Tc(IV) resides inside the clay mineral matrix, minimizing the potential for remobilization. Reduced structural Fe(II) in smectite is an effective reductant for Cr(VI) as well. Sorption of Cr(VI) onto a clay mineral surface appears to be a prerequisite for subsequent reduction. Unlike Tc(VII) and Cr(VI), U(VI) reduction by clay-associated Fe(II) is kinetically slow. For some clay minerals, such as nontronite, redox chemistry may favor the oxidation of U(IV) by structural Fe(III) in clay minerals, which is opposite to the direction of the Tc(VII) reduction reaction. Because of the rapid oxidation of U(IV) by structural Fe(III) in nontronite, uranium can serve as an electron shuttle for microbial reduction of structural Fe(III) in chlorite, with the implication that Fe(II) in nontronite may not reduce and immobilize U(VI).

Microbe-mineral interactions and impacts on geochemical behavior of arsenic in sulfide tailings of Shizhishan Cu-Au Mine, Tongling, Eastern China

Lu X*, Lu J, Wang R, Li J, Zhu T, Ouyang B

Nanjing University *xcljun@nju.edu.cn

Mining activities have created great wealth, but they have also discharged large quantities of tailings. In sulfide tailings, thought as important sources of heavy metal contamination, various microbe-mineral interactions greatly influence the release/precipitation of heavy metals and secondary mineralization. The mineralogical composition and contents of heavy metals in closed tailing impoundments in Shizishan Cu-Au mine, Tongling, eastern China, were analyzed by using multiple laboratory techniques. In the shallow part (less than 25 cm below the surface) of the tailings is the active oxidation zone, where secondary minerals (e.g. goethite, jarosite, and gypsum) form. The heavy metals bound in sulfides may be either released into pore water or sequestered by secondary minerals via adsorption on iron oxides/hydroxides or co-precipitation in sulfates. In this zone, the pore water is acidic (pH 2.5~4.2), and autotrophic (i.e. capable of fixing inorganic carbon to organic carbon), oxidizing bacteria prevail in its microbial community. In contrast, in the reduction zone in the deep part, where the pore water becomes slightly alkaline due to alkalinity-producing reduction reactions, dissimilatory iron-reducing bacteria and sulfate-reducing bacteria become dominant. Microbial reduction of sulfate and Fe^{3+} is the main geochemical process, and thus sulfides as well as calcite and siderite are found here.

For clarifying the mechanism of microbe-mineral interactions and influences on activities of arsenic in tailings, oxidation of arsenopyrite by *Acidithiobacillus ferrooxidans* and microbial reduction of jarosite by *Shewanella oneidensis* have been experimentally studied. Based on high resolution X-ray photoelectron spectroscopic depth profiles of biotically and abiotically oxidized arsenopyrite surfaces, a conceptual model for microbial oxidation of arsenopyrite, integrating surface etching and electron transferring in the alternated surface layer is proposed. Accompanying the anaerobic reduction of jarosite by *Shewanella oneidensis*, bicarbonate, acetate and ferrous ions in experimental solution as well as both ferric and ferrous iron minerals were disclosed. Green rust and goethite, as well as some amorphous iron containing precipitations, occurred as intermediate products, and further release of ferrous ion stimulated the transformation of intermediate phases to end minerals as magnetite and siderite. In both processes, the chemical state of arsenic changes greatly through mobilization/remobilization and fixation mediated by bacteria.

Acknowledgement: This research was supported by the National Basic Research Program of China (973 program, 2014CB846004) and National Science Foundation of China (40930742, 41272056).

Activities in Muschelkalk – biologically induced calcification

Weist A[1*], Singh M[1], Kastner A[1], Gleixner G[2], Gaupp R[3], Büchel G[4], Kothe E[1]

1 - FSU Jena, Institute of Microbiology - Microbial Communication *aileen.weist@uni-jena.de 2 - Max Planck Institute, Biogeochemical cycles 3 - FSU Jena, Institute of Earth Sciences, General and Historical G 4 - FSU Jena, Institute of Earth Sciences, Applied Geology

The carbon cycle is an important natural process which involves the exchange of carbon between different reservoirs such as atmosphere and biosphere. The metabolic activity of organisms and the cycle of organic carbon affect the flux of atmospheric CO_2 in the form of carbonates. The precipitation and weathering of carbonates are influenced by changes of the milieu. These mechanisms are both controlled by geogenic processes and bacterial activity.

In this study, bacteria isolated from limestone, were analyzed for their ability to form carbonates. Therefore, samples were taken in the Thuringian Basin, which is surrounded by layers of Muschelkalk. The bacteria were isolated from groundwater, rock samples, as well as soil formed on Middle and the Lower Muschelkalk.

The bacterial strains were cultivated on calcium containing media to study their ability to form carbonates. Most bacterial strains were able to from crystals through calcification. By applying SEM, surface structures as well as the microbial impact on the crystals were observed. Crystal morphologies varied broadly, and microbial cells were visualized on the crystals. The present minerals were identified to be carbonates using EDX and XRD. Additionally, the biomineralization was dependent on water content, calcium salts supplied and temperature. Thus, we can provide evidence for environmental and microbial impact on the naturally occurring processes effecting the formation of carbonate mineral phases.

Structural change in montmorillonite mediated by a *Bacillus mucilaginosus* strain

Yang X[1*], Li Y[1], Lu A[1], Zhu Y[2], Wang H[1], Ding H[1]

1 - Peking University *yxx1101@pku.edu.cn 2 - National Research Centre for Geoanalysis

The occurrence of mixed-layer clay minerals is often used to mark essential stages in pedogenic or diagenetic processes,and the mechanisms of structure and phase transition of smectite have long been a research focus. Many reports have concluded that the transformation of smectite requires years of time through burial and thermal histories, or at least a few months in hydrothermal simulation systems. However, research in the last few years proposed a comparatively rapid transformation of smectite mediated by microbes. For example, many researchers have demonstrated that when catalyzed by certain microbes under anoxic atmosphere, illitization of nontronite could take place in two weeks at room temperature and normal pressure. Notably, nontronite is rich in Fe, and is not the most common type of smectite in nature. Fe-poor montmorillonite, however, is ubiquitous in natural sediments and soils,but few research studies to date have referred to the interactions between Fe-poor smectite and bacteria under aerobic conditions. Therefore, it is believed this subject should be more meaningful and interesting.

In our study, bentonite containing about 90% montmorillonite and 10% cristobalite from the Jianping District of Liaoning Province, China, was selected as the mineral sample. The aerobic bacterium was *Bacillus mucilaginosus* 3017A, kindly donated by the Chinese Academy of Agricultural Science. The bacteria were inoculated into suspension of sterilized bentonite powder and cultured for 25 days. Abiotic controls with only sterilized bentonite were conducted simultaneously. The culture media contained 5 mg/L of $FeCl_3 \cdot 6H_2O$, 10 mg/L of $CaCl_2$, 0.5 g/L of $MgSO_4 \cdot 7H_2O$, 0.2 g/L of K_2HPO_4, 1.0 g/L of yeast extract, and 5.0 g/L of sucrose. All experiments were conducted under aerobic atmosphere at 35°C and 1 atm. During the period, 3.5 mL solutions were extracted regularly for pH, Si and Al concentration analysis. After the experiments, minerals were separated and characterized by FTIR, XANES, SR-XRD and SEM.

Initially, the pH of biotic solutions decreased, probably caused by acidic metabolites produced by bacteria. Meanwhile, Si concentration in the solutions increased and then slightly decreased, suggesting the release of Si from the tetrahedral sheets of solid mineral. These might later trigger a local structure distortion in montmorillonite, as indicated by the FTIR spectrum. As inferred from the broadened edge crest in the Fe k-edge XANES, altered symmetry of coordinate octahedral geometry also occurred. More importantly, newly formed silica was detected by SR-XRD. Furthermore, layer collapse and edge curling were observed by SEM. It is highly possible that the crystal structure of montmorillonite was distorted locally in the first place, mainly by the complexation of targeted sites on the mineral surface with acidic metabolites, and the contact between bacteria and mineral particles. This local structural change might later diffuse to a wider scale, triggering release of Si atoms and their later aggregation to silica. The structural change of montmorillonite represents an important initial stage of smectite transformation, and this aerobically microbe-mediated reaction may help explain Si release and mineral transformation in Fe-poor smectite bearing soils and sediments.

Biogenesis of Mn nodules and Co-rich manganese crusts in the Pacific Ocean

Akai J[1*], Akiyama S[2], Tsuchiyama A[3], Akai K[4]

1 - Department of Geology, Fac.Science, Niigata University *akai@geo.sc.niigata-u.ac.jp 2 - Tsukuba University. 3 - Kyoto University. 4 - Niitsu T. High School

Deep-sea Mn nodules and Co-rich manganese crusts have been examined variously [1, 2, 3], but were problematic in their genetic interpretation. Recently, Akai *et al*. [4] proposed a hypothesis for Mn nodule genesis as deep sea stromatolite. In this study, more detailed mineralogy of Co-rich manganese crusts and Mn nodules was comparatively examined. Several samples from the the Pacific Ocean, were collected. Some of these samples were closely examined by optical microscopy, XRD, TEM, SEM, X-ray CT and mathematical simulation for morphological characteristics.

Co-rich manganese crust samples were also examined mineralogically. Thin sections of these samples showed columnar stromatolite-like structures with rhythmic bands. XRD data indicated two types of Mn oxides: 10 Å phyllomanganate and/or a 2.5 Å vernadite-like mineral.

Mn-nodules: the fractal characteristics of spherical to dome-like forms were fundamentally composed of at least four ranks. The 4th order form corresponds to the stromatolite dome top shapes. Similar granular domain units and porous characteristics in Mn nodules were also observed by X-ray CT sections. Mathematical simulation based on fractal models reproduced similar morphologies.

Co-rich manganese crust: the forms are not nodular but sometimes similar in morphologies of botryoidal characteristics to Mn-nodules. Stromatolite-like structures were also found (Figure 1). SEM and TEM observations showed that mineralized bacteria were found on the surface of Mn-nodules and Co-rich manganese crusts (Figures 2 and 3). So, the samples could be said to be stromatolite themselves. An HRTEM image of the ion-thinned samples of Mn nodule showed slightly irregular layer structure of the Mn oxides (Figure 4). Layered Mn oxide minerals are playing an important role as accumulators of useful metals such as cobalt, copper, nickel and so on, in the sea water environments. So, finally it could be said that Mn nodules are deep sea aggregated stromatolite sometimes with fractal signatures and Co-rich manganese crusts have also fundamentally similar characteristics as Mn nodules, that is, biogenic. Differences between Mn-nodules and Co-rich manganese crusts may depend on the surrounding environments of the ocean bottom (locality in the ocean, depth, geomorphology, environments for bacterial growth etc.).

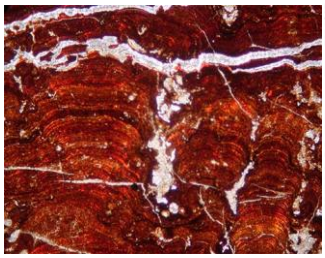

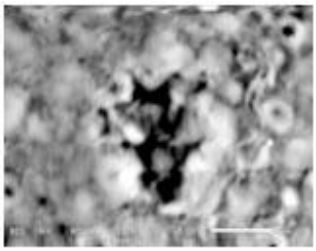

Figure 1 (left) Thin section image of Co-rich Manganese crust, suggesting stromatolite structure: lateral width= 1mm; Figure 2 (right) SEM image of biomineralization products on the surface of Co-rich manganese crust

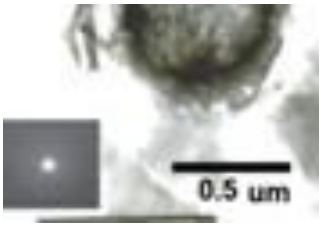

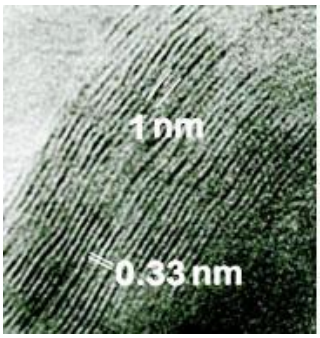

Figure 3 (left) TEM image of bacterial fossil on the surface of Mn nodule; Figure 4 (right) HRTEM image of 10 Å phyllomanganate layer structure with irregularities

[1] Ehrlich H.L. (2002). Geomicrobiology. 4th ed. Marcel. Dekker Inc, NY.

[2] Han X. *et al.* (2003). *Earth and Planet. Sci. Lett*., 211, 143-157.

[3] Feng X.H.*et al*. (2005). *Acta Petrolog. Mineralog*., 6, 135-233.

[4] Akai J.*et al*. (2013). *Physics and Chemistry of the Earth*., 58-60, 42-48

A spectroscopic study of Mn(II)-bearing calcites: comparison between inorganic calcite and biocalcite, obtained by the bacterium *Bacillus subtilis*

Di Benedetto F[1*], Perito B[2], Montegrossi G[3], Passaponti M[4], Pardi L A[5], Romanelli M[1]

1 - Università Firenze - Dip. di Scienze della Terra, Italy *francesco.dibenedetto@unifi.it 2 - Università Firenze - Dip. Biologia, Italy 3 - CNR-ICCOM, Italy 4 - Università Firenze - Dip. Chimica, Italy 5 - CNR-IPCF, Italy

The first multi-analytical characterisation of a biogenic calcite, produced from bacterial activity, is reported in this study. Microcrystalline calcite powders were obtained from the model bacterium *Bacillus subtilis* grown on a suitable precipitation medium. The powders were analysed, without further manipulation, by means of X-ray powder diffraction (XRPD), and by Electron Paramagnetic Resonance (EPR) spectroscopy. Both techniques reveal unusual spectral parameters, attributed to the effects of the bioprecipitation of the mineral.

In particular, XRPD pointed out an anomalous c0/a0 ratio, which was noticed before only in microcrystalline calcite samples grown by biomineralisation of seashells. The usual ratio for inorganic calcite is recovered by opportune thermal treatments.

The specific anomalies in the parameters of the EPR spectroscopy mainly consists in an anomalously large distribution of the zero-field splitting interaction, which allows to clearly distinguish bacterial and inorganic calcite. These values, coupled to the data concerning the fine, hyperfine and Zeeman interactions, confirm the clear spectroscopic fingerprint of bacterial biocalcite.

As a consequence, this study fosters the coupled use of XRPD and EPR for identifying the traces of bacterial activity in fossil carbonate deposits, with particular reference to the reconstruction of palaeoclimate and in geochemical cycles of pollutants.

Microfungi in a Cu-rich waste rock dump from an abandoned Fe-Cu sulphide mine (Libiola Mine, Eastern Liguria, Italy)

Marescotti P*, Zotti M, Di Piazza S, Roccotiello E, Mariotti M G, Lucchetti G

DISTAV - University of Genova *marescot@dipteris.unige.it

A multidisciplinary study has been performed in order to evaluate the mycoflora in a Cu-rich waste rock dump from the derelict Fe-Cu sulphide mine (Libiola Mine, Eastern Liguria, Italy). The goals of this research were to test the growth responses of isolated strains in copper enriched media and to evaluate their potential use in mycoremediation.

The study area is a flat part of the dump (covering a surface of about 60 m^2) which is characterized by a barren substrate composed of gravely-sandy sediments with relatively low silty- and clayey-fractions (≤ 25%). The pH of soils is acid and generally homogeneous among the studied samples (3.5 to 4.2). Also the mineralogical and lithological composition of the studied waste rock soils is quite homogeneous, being mainly composed of fragments of goethite-rich oxidation crusts (65-70%), polycrystalline rock fragments (serpentinites, basalts; 20-25%), and strongly altered sulphide (pyrite and minor chalcopyrite) mineralization (10%). From the chemical point of view, the studied soils evidence significant enrichments of several metals with very high copper concentrations (up to 2700 ppm) and bioavailability.

The isolation of fungal strains and fungal Morphological Taxonomic Units (MTUs) count were carried out in the laboratory by the dilution plate method using different media (Rose Bengal and Malt Extract Agar with cloramphenicol).

More than 90 Petri dishes were inoculated and a total amount of 301 MTUs were counted. On the whole 23 strains belonging to 11 different taxa were isolated. The species most recurrent are filamentous microfungi: *Trichoderma harzianum*, *Clonostachys rosea* and *Aspergillus alliaceus*. We hypothesized that these fungi are particularly tolerant/resistant to copper.

The Cu tolerance level of *Trichoderma harzianum* and *Clonostachys rosea* were tested in vitro at increasing Cu (II) concentrations. The tests have shown a Cu (II)-tolerance capability ranging from 100 to 400 mg L^{-1}.

These preliminary analyses prove that several fungal species are able to grow in Cu-contaminated media, underlying the importance to select new tolerant strains and test their potential metal uptake capability for application in mycoremediation protocols.

Moreover, our study outlines the importance of a multidisciplinary approach for a better understanding of the fate of ecotoxic metals in highly contaminated soils and of the relationships between accumulation of these metals by fungi and soil mineralogy, bulk metal concentrations, and chemical speciation.

Research on *Cronobacter sakazakii* bio-reduction on goethite

Wang H*, Yang X, Ding H, Lu A

Peking University *whrpku@163.com

Iron occurs in many oxide and hydroxide minerals. Under hypoxia and anaerobic conditions, some microbes can use Fe(Ⅲ) in iron-bearing minerals as an electron acceptor for the metabolism. Such microorganisms are known as dissimilatory Fe(Ⅲ) reduction bacteria, which are common in anaerobic environments like underground water, bay sediments, lake sediments and so on. A dissimilatory Fe(Ⅲ) reducing bacterial strain, *Cronobacter sakazakii*, was isolated from oil production water, in Daqing Oilfield, northeastern China. For the purpose of understanding the physiological feature of this bacterium and its reduction on iron-bearing minerals, we measured total protein, Fe(Ⅱ) concentration and mineral phase after bioreduction on synthetic goethite under anaerobic cultivation. Under anaerobic conditions, using sodium acetate as the electron donor and Fe(Ⅲ) in goethite as electron acceptor, *Cronobacter sakazakii* can reduce Fe(Ⅲ) for its metabolism. We recorded total protein and Fe(Ⅱ) concentration of the suspension (Figure 1). The graph shows there are three periods through the cultivation. In the proliferation period, from beginning to the 4th day, the bacteria reduce the goethite rapidly and the Fe(Ⅱ) is accumulated; in stable growth period, the 4th day to the 8th day, the bacteria go on reducing the goethite to a peak point 29.9 mg/L; in the decline period, the generation of Fe(Ⅱ) is slowed down; when the activities of bacteria stop, Fe(Ⅱ) is no longer accumulated and ultimately keeps stable at the amount of 31.24mg/L.

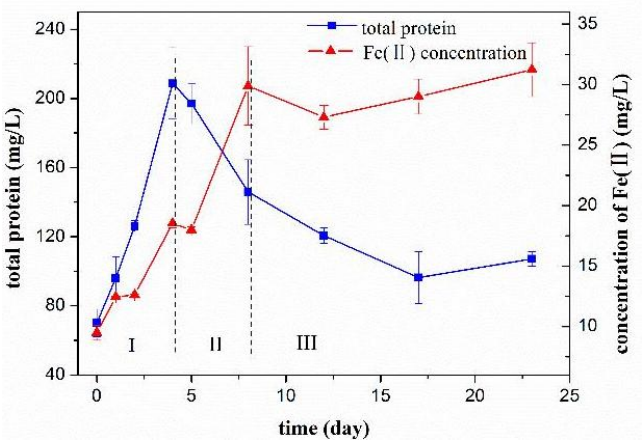

Figure 1: Total protein and Fe(Ⅱ) concentration of the microbe-mineral interaction suspension.

In further research, synchrotron radiation XRD (Figure 2) of the bio-reduction products shows a series of new peaks: 4.8, 6.03, 6.13, 6.84, 7.7 and 11.4Å, which might be referred to green rust with layer structure.

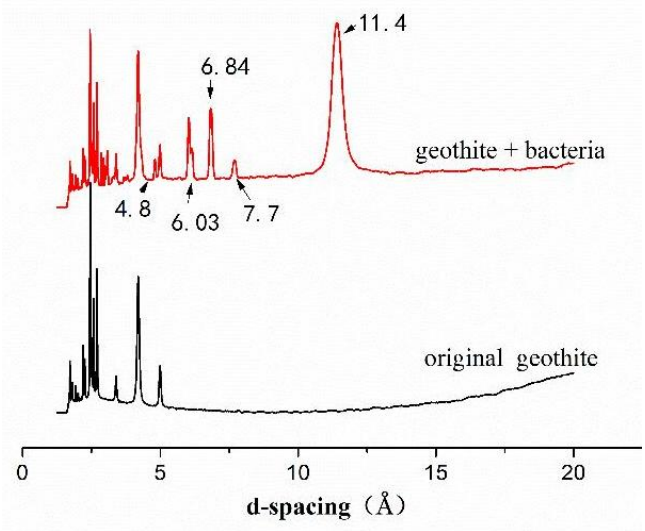

Figure 2: The phase change after bio-reduction. The results indicated *Cronobacter sakazakii* can use sodium acetate as the electron donor and Fe(Ⅲ) in goethite as electron acceptor for metabolism.

Kinetic analysis of the setting reaction of magnesium-potassium phosphate ceramics: influence of MgO reactivity

Gualtieri A[1*], Viani A[2], Peréz Estébanez M[2], Pollastri S[1]

1 - University of Modena and R.E. Italy *alex@unimore.it 2 - Centrum of Excelence Telč, Telč, Czech Republic

Mg-K chemically bonded phosphate ceramics, like most MgO-based binding materials, show high early age and long-term strength, good water resistance, high adhesive properties and affinity for cellulose materials; these properties make them attractive for many applications such as fast repairing of damaged structures, waste encapsulation, bone repair, natural fibre composites and products for bioengineering applications. Setting occurs through reaction of MgO with KH_2PO_4 (KDP) and water to produce magnesium potassium phosphate (MKP). The mechanism of the reaction has been long debated. No quantitative data on reaction kinetics of MgO-KDP system are available to date. In this work, the role of the reactivity of MgO powder in affecting reaction kinetics has been investigated. MgO powders were calcined at 1400 °C, 1500 °C, and 1600 °C. For each annealing temperature 3 samples, each one with a different grain size distribution, have been produced by milling. In order to derive quantitative kinetic parameters and validate plausible kinetic models, the reaction with KDP and water was followed *in situ* with synchrotron X-ray powder diffraction. Hydration has been conducted using deionized water and a water:solid weight ratio of 0.3. Preliminary data treatment confirmed the influence of both temperature and grain size distribution on reaction kinetics.

Figure 1 reports a-time plots of samples obtained from MgO calcined at 1400 and 1500 °C with coarser (black symbols) and finer (gray symbols) grain size. The ln(1-a)-time plots for MKP for samples annealed at 1500 °C suggest that the reaction can be described as a first order reaction, but the same doesn't apply to other samples. Derivation of quantitative kinetic parameters and the evaluation of plausible models for the reaction will be presented.

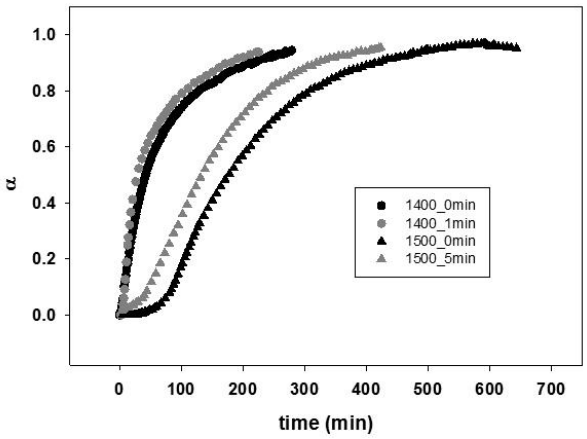

Figure 1: a-time plots of samples obtained from MgO calcined at 1400 and 1500 °C with coarser (black symbols) and finer (gray symbols) grain size.

Mineralogical study of the pozzolanic properties of calcined clays

Hollanders S, Elsen J*

Katholieke Universiteit Leuven *jan.elsen@ees.kuleuven.be

Portland cement-based materials are the most widely produced construction materials. The expansion of the cement industry might be a cause for concern, since the production process is very energy-intensive and because of the large amount of carbon dioxide emitted. Sustainable low-energy and low-carbon binders have become of great importance in the search for alternatives to clinker cement. The addition of supplementary cementitious materials (SCMs) is considered to be one of the most effective ways of reducing the environmental impact of the cement industry. SCMs chemically react at ambient temperature with calcium hydroxide in the presence of water to form compounds that possess cementing properties. One of the most promising alternative sources of SCMs are calcined clays. The main objective of this study is to investigate the potential use of calcined clays from a mineralogical point of view by linking the characteristics of the untreated clays to the pozzolanic activity of the calcined clays and to the reaction products formed after hydration. Since it is of key importance to understand the origin and determine the main parameters that influence the pozzolanic activity, pure reference clays have been calcined as a first step of the research project. The raw materials and the calcined clays have been fully characterised by the determination of the mineralogical (XRD) and chemical (ICP-OES) composition, physical characteristics like grain size (laser diffraction) and specific surface area (BET), and spectroscopic characteristics (FTIR). Four reference clays, high grade kaolinite (KGA-1), low grade kaolinite (KGA-2), Na-montmorillonite (SWy-1) and Ca-montmorillonite (SAz-1), were purified and thermally treated in order to estimate their pozzolanic potential and their optimal firing temperature. The clays were calcined in a fixed-bed electrical furnace at temperatures ranging between 500°C and 900°C. Their pozzolanic activity is evaluated by Chapelle test and thermogravimetry (TGA) on calcined clay-lime mixtures after 3, 7, 14 and 28 days. The results indicate that both high grade and low grade kaolinites are highly active at a broad range of firing temperatures. There are no main differences in the activity between kaolinites fired at 500, 700 or 900°C. The crystallinity of the raw kaolinite only influences the short-term activity of the calcined clay-lime reaction. After 28 days high- and low- grade kaolinite mixtures show the same activity. The montmorillonite samples possess a clear optimal firing temperature at 800°C. Ca-montmorillonite is proven to be somewhat more reactive than Na-montmorillonite, although, even at 800°C, its activity is low compared to that of kaolinite

Production of self-healing blast furnace slag concrete immune to carbonation

Kempl J*, Copuroglu O

Technical University of Delft *j.kempl@tudelft.nl

Blast Furnace Slag (BFS) is a waste product of industrial steel production and a very common additive in the cement industry in Northern European countries. However, pastes, mortars and concrete made from BFS cement, particularly CEM III/B, are very susceptible to carbonation and consequently to frost-salt-scaling.

Recent investigations [e.g. 1, 2] have shown that the surface application of Na_2FPO_3 on BFS cement products can improve the surface durability of BFS concrete, mortars and pastes. This makes BFS cement a very attractive cement component to be used in concrete manufacturing, especially with regard to industrial waste disposal and environmental aspects.

On the basis of previous studies [e.g. 3, 4] we are investigating the self-healing mechanism of BFS cement with Na_2FPO_3 as self-healing agent from a mineralogical point of view in order to obtain a sustainable and strong building material with a long lifetime. In this experimental study we impregnate blast furnace slag cement mortars with varying concentrations of Na_2FPO_3 in aqueous solution under vacuum. The sample aliquots are exposed to a 3% CO_2 atmosphere before and after Na_2FPO_3 treatment. Between each chemical treatment, samples are analyzed by various state-of-the art techniques (SEM, powder X-ray diffraction, Rietveld Refinement, and FTIR). Above all, we are aiming to study the pH-changes of the pore water after [5] to gain a better understanding of the chemical processes in BFS cement products.

[1] Copuroglu *et al*. (2006). *Cem. Concr. Res*. 36, 1475-1482.
[2] Sisomphon *et al*. (2010). *Cem. Concr. Comp.* 32, 1475-1482.
[3] Sisomphon *et al.* (2010). *Sci. Asia* 36, 223-230.
[4] Sisomphon *et al*. (2011). *Heron* 56, 13-32.
[5] Barneyback and Diamond (1981). *Cem. Concr. Res.*, 11, 279-285.

Production of sustainable conglomeratic materials made with aggregates recycled from returned concrete

Secco M[1], Artioli G[2], Dalconi M[1], Valentini L[1*], Ferrari G[3]

1 - University of Padua *luca.valentini@unipd.it 2 - Università di Padova

3 - MAPEI S.p.A.

Nowadays, one of the main waste materials produced by ready-mix concrete plants is returned concrete, the residual amount of fresh concrete not poured at the building site and returned to the production plant by the truck mixer. Recently, a new technology has been developed to convert such waste into sustainable concrete aggregates, based on the utilization of two types of additives - a super-absorbing polymer (SAP) and a set accelerator - that transform fresh concrete into a solid, granular material consisting of a core of original coarse aggregate surrounded by a composite shell of sand and hydrated cement. In the present contribution, the results of a series of characterization studies based on both experimental and modelling approaches are reported, to investigate the properties of such materials at the fresh and hardened state.

One of the key technological issues related to the treatment of returned concrete with this procedure is related to the definition of an appropriate period of curing, with the aim of obtaining a material with both granular characteristics and proper mechanical properties. For this purpose, a series of numerical simulations were performed using the VCCTL microstructural model, with the aim of defining the appropriate curing intervals, depending on temperature, composition and water/cement ratio.

Furthermore, experimental measurements have been performed to investigate the chemical, physical and microstructural properties of the obtained granular materials. The standard characterization tests (density and absorption measurements, abrasion and freeze/thaw resistance determination, soluble chlorides and sulfates quantification) confirmed that such materials are suitable for use as concrete aggregates. Furthermore, micro-analyses by X-ray micro-tomography and scanning electron microscopy (SEM-EDS) revealed extremely good interfacial properties between the aggregate core and the surrounding composite shell.

Finally, the effects of recycled aggregates addition into conglomeratic materials of different strengths have been investigated by means of uniaxial compression tests, absorption tests and SEM-EDS micro-analyses. For the purpose, two types of granular materials have been produced, from original low strength and high strength concretes, respectively. Then, the resulting aggregates have been used with a 30% by weight degree of substitution to produce three concretes characterized by different compressive strength classes (low, medium and high, respectively). The properties and the nominal strength class of the concretes did not deteriorate as a result of the aggregate substitution in any of the tested cases. Furthermore, the water permeability properties of the final concretes are always significantly improved by the addition of the recycled aggregates. Such improvements in the technological properties of concretes are explained by a substantial absence of interfacial transition zones (ITZ) between recycled aggregates and surrounding cementitious matrices.

Commercial implications of phase evolution in alkali-activated concrete

Van Deventer J

University of Melbourne. jannie@zeobond.com

The global construction industry is worth annually about USD 8 trillion, which is 10% of global GDP. World annual cement production exceeds 4 billion tonnes, making the concrete produced from it (by adding sand, aggregate and water) the highest-volume commodity in the world, behind water. Ordinary Portland Cement (OPC) production has a significant environmental penalty of almost one tonne CO_2 per tonne cement, and contributes at least 5% of global CO_2 emissions. If formulated optimally, alkali-activated cement (AAC) made from fly ash, metallurgical slags and natural pozzolans could reduce by at least 80% the CO_2 emissions associated with the manufacturing of OPC. This paper will review recent research on the microstructure and gel evolution in these systems and explain how such insight enhances the commercial adoption of these new construction materials.

Significant progress has been made in developing an understanding of the colloid and interface science, gel chemistry, phase formation, reaction kinetics and transport phenomena underlying alkali-activation of calcium aluminosilicates, especially using synchrotron-based analysis in conjunction with advanced computational techniques. Recent thermodynamic modelling has confirmed the existence of stable phases like Al-tobermorite (found in Roman concrete), hydrotalcite and strätlingite in AAC. By using X-ray pair distribution function (PDF) analysis it has been shown that the ordering of calcium aluminium silicate hydrate (C-A-S-H) binding phase in alkali-activated slag can be short compared with the higher extent of ordering in C-A-S-H formed in hydrated OPC-slag blends.

Tests for the durability of OPC concrete have been validated against its long track record and may not be applicable to AAC. AAC concrete usually has high resistance to acid, fire, freeze-thaw, chloride diffusion and sulphate, but shows higher porosity in tests that require boiling of the concrete. Standard accelerated carbonation tests are not appropriate for AAC concrete, which displays satisfactory carbonation rates in-service in contrast to poor laboratory testing. It has been shown that the mode of drying has a major effect on the microcracking of AAC gels, which explains why some tests are inappropriate for AAC. It has also been shown that a higher MgO content in slag enhances reactions and reduces Al incorporation into the C-A-S-H due to the formation of hydrotalcite which reduces carbonation.

In the absence of a long in-service track record, research is required to validate durability testing methods and improve AAC technology. The fact that all concrete standards are based on OPC remains a major obstacle to the commercial adoption of AAC. Even when asset owners and specifiers such as government, architects and design engineers accept the results of durability testing of AAC, the main barrier to entry of these new materials into an established market is access to a suitable supply of source materials including fly ash, granulated blast furnace slag and alkaline activators. These issues are seldom appreciated by researchers, governments or the ultimate users of concrete.

Demand pull by a carbon conscious market continues to be the main driver for the short term uptake of AAC in Australia. There are indications that regulatory pressure to add value to waste fly ash and slag in some countries will become an additional driver for adoption of AAC. The scale-up from the laboratory to the real-world is technically challenging but achievable, leaving the core challenge as the scale-up of industry participation and acceptance of AAC. High profile application projects in Australia have demonstrated the vast regulatory, asset management, liability and industry stakeholder engagement process required to commercialise AAC. It is important for commercial producers of AAC binders and concretes to work closely with research partners to develop testing methods for accelerated durability, especially as longer term in-service testing data become available. Substantial progress has been made in Australia, where the local road authority has recognised AAC as equivalent to OPC.

The use of secondary resources to produce special cements

Costa M[1], Angelica R[2], Pöllmann H[3*]

1 - UFPA 2 - Univ Belem 3 - MLU *herbert.poellmann@geo.uni-halle.de

Large kaolin and bauxite deposits showing layers of topsoils, which are very interesting as secondary resources for cement production, occur in the Amazon region. In this study some of these secondary resources are used as starting materials for the production of low-CO_2 cement. The following cementitious materials were investigated in this study:

1. Portland cement based systems - composite cement- Pozzolanic cement
2. Sulfoaluminate cement-based systems
3. Sulfoaluminate-Ferrite cement based systems
4. Ferrite cements

All the different materials are available in large quantities and can be used as sources to produce low CO_2 cement. However, many aspects must be taken into account, as still a source of CaO must be available for the production of these types of cementitious materials. The Amazon region is a preferential area capable to provide many of these high quality industrial by-products for application in the building materials industry. Additional materials can be found in the Al-rich topsoils (Belterra Clay) in the same region. The calcium sulfate source is available from the Maranhão state. The use of such industrial waste as secondary cementing materials would reduce the environmental impact of mining in this region.

RieCalc: a tool for the quantitative analysis of hydrating cement pastes based on in-situ XRD

Valentini L[1*], Dalconi M[1], Artioli G[2], Ferrari G[3]

1 - University of Padua *luca.valentini@unipd.it 2 - Università di Padova 3 - Mapei S.p.A.

The study of cement hydration by in-situ X-ray diffraction, combined with Rietveld analysis, provides fundamental details on the phase composition of the hydrating cement paste. The time evolution of the concentration of the crystalline phases present in hydrating cement pastes, characterized by significantly different rates of reaction, can be successfully monitored by this method. However, the XRD amorphous nature of the main hydration product (C-S-H) and capillary water poses a serious issue in the interpretation of the data. Methods based on the use of standards can provide the total amount of amorphous matter present in the system, however they cannot discriminate between C-S-H and capillary water.

Here, a method for calculating the amount of both C-S-H and capillary water, based on mass balance, is presented.

This method is implemented in a MATLAB® tool named RieCalc. By using Rietveld refined XRD data as input and an intuitive graphical user interface, RieCalc calculates rescaled phase fractions present in a hydrating cement paste (including C-S-H and capillary water). Furthermore, based on the recalculated phase fractions and on the enthalpy of dissolution of the cement phases present in its database, RieCalc calculates theoretical curves of the heat released during the hydration process.

Stand-alone executable for Windows and Linux operating systems are freely distributed.

Rare minerals and extreme differentiation in peralkaline nephelinite at Nyiragongo, East African Rift

Andersen T[1*], Elburg M[2], Erambert M[1]

1 - University of Oslo *tom.andersen@geo.uio.no 2 - University of Johannesburg

Nyiragongo in the Virunga volcanic province (D.R. Congo) is an active stratovolcano, built up by lavas and pyroclastic rocks ranging in composition from (rare) alkali olivine basalt to nephelinite, leucite nephelinite, melilite nephelinite, and melilitite. Highly peralkaline nephelinites have provided type material for rare minerals such as götzenite and combeite which have proved important for the understanding of the petrology of peralkaline magmas. In order to understand the paragenetic relationships of these and associated rare minerals and their importance for the crystallization history of highly peralkaline nephelinite, we have carried out an electron microprobe study of leucite and melilite-bearing nephelinite ejecta collected by Th.G. Sahama and collaborators during 1950s expeditions to the volcano, and now kept in the Royal Museum of Central Africa, Tervuren, Belgium.

The eruptive temperature of the lava was ca. 980 ^{o}C. Early magmatic assemblages with nepheline, melilite, titaniferous magnetite, olivine, leucite ± kalsilite define a cooling trend at highly reducing conditions (log fO_2< QFM-2). Götzenite, kirschsteinite, delhayelite (all of which were first described from Nyiragongo), umbrianite, nepheline, kalsilite and leucite form a late-magmatic assemblage coexisting with iron- and volatile-rich silicate glass with (Na+K)/Al up to 18. Rare barium-bearing minerals are members of the same assemblage, including the one-locality mineral andremeyerite, fresnoite, unnamed alkali barium and barium-iron silicate minerals and an unnamed alkali barium phosphate mineral. The crystallization temperature for this assemblage is estimated to 650-700 ^{o}C. Combeite appeared as a (near-)solidus mineral (ca. 600 ^{o}C) that remained stable through sub-solidus recrystallization down to 500 ^{o}C.

The presence of a semi-permanent lava lake in the summit crater has caused the cooling rate of the upper part of the volcanic cone to be slow enough for silicate liquid to coexist with minerals over an extended temperature range rather than quench to glass upon eruption. The late magmatic mineral assemblages with götzenite, delhayelite and other F- and Cl-bearing minerals have formed a result of the highly peralkaline residual melt composition and infiltration of halogen-bearing fluids from the lava lake during this slow cooling process.

The götzenite-delhayelite-combeite -bearing nephelinite has mineralogical features in common both with agpaitic nepheline syenites and the peralkaline nephelinites of Oldoinyo Lengai. In contrast to Oldoinyo Lengai, there is no evidence of the presence of carbonatite liquid at Nyiragongo. The reason for this may be that the presence of the lava lake has allowed continuous degassing of CO_2 to the atmosphere, preventing buildup of sufficient CO_2 pressure to stabilize carbonatite magma.

Olivine in kimberlites: lithospheric versus shallow processes

Arndt N[1*], Cordier C[2], Sauzeat L[2], Boullier A[2]

1 - ISTerre, Université de Grenoble *nicholas.arndt@ujf-grenoble.fr 2 - Univ Grenoble

Most kimberlites contain abundant mantle nodules, i.e. centimetre-sized, rounded, commonly multi-grained ellipsoids commonly referred to as "macrocrysts". A striking feature of nodules in many kimberlites is their multigranular but monomineralic dunitic lithology, associated with a wide range of olivine composition. From nodule to nodule in a single kimberlite sample, the composition varies from Fo83 to Fo94, while within a single nodule the composition is constant. Fine outer margins that crystallized from the kimberlite magma mantle many nodules. These rims have roughly constant Fo contents (ca. Fo88 in Type-I, and Fo91 in Type- II kimberlites), but highly variable minor element contents (e.g., 500 to 2500 ppm of Ni). In this study, we combine chemical and microstructural data on olivine xenocrysts and rims in well-preserved kimberlites from Greenland and African cratons. We attribute the olivine chemical variability to two processes at two levels, the first in the lithospheric mantle and the second during magma transit toward the surface. The composition of the rims can be reproduced by crystallization during kimberlite ascent of olivine only: there is no need to invoke orthopyroxene dissolution at this stage. Conversely, a metasomatic event involving CO_2-rich fluids within the lithospheric mantle explains the formation of dunitic lithologies from initial peridotite by removal of orthopyroxene and garnet, and synchronous development of the wide range of olivine composition. The olivine composition records the position of the mantle sample relative to fluid-rich zones.

In situ trace-element geochemistry and U-Pb dating on perovskite from kimberlites of the Lundas Norte province (NE Angola): petrogenetic and tectonic implications

Castillo-Oliver M[1*], Galí S[1], Melgarejo J C[1], Zinchenko V[2], Belusova E[3], Griffin W[3]

1 - Facultat de Geologia, Universitat de Barcelona, Catalonia, Spain *montgarricastillo@ub.edu 2 - ENDIAMA, Major Kanhangulo, 100, Luanda, Angola 3 - CCFS/GEMOC, Macquarie University, Australia

Perovskite ($CaTiO_3$) is a typical groundmass mineral in kimberlite rocks; it has recently become a prime target to date kimberlite and carbonatite eruptions. Major- and trace-element and Sr-Nd isotope analysis of perovskite can provide additional invaluable information about the compositional evolution of the kimberlitic magma and its source. Despite the undeniable potential of such an approach, up to now no similar study has been done on Angolan kimberlites and the subcratonic lithospheric mantle (SCLM) of the Congo-Angola craton remains poorly understood. In the present work, perovskite grains in seven kimberlite intrusions from the Lundas province (NE Angola) have been texturally and chemically characterised by means of SEM, EMPA and LA-ICP-MS techniques, and their emplacement ages determined using U-Pb dating. Sr-Nd isotopes are currently being analyzed and the results will be presented in the conference.

Three main textural types were recognised in the studied kimberlites: i) anhedral, inclusion-free, groundmass perovskite; ii) reaction-induced rims of perovskite on ilmenite and iii) euhedral groundmass perovskite, usually with strong oscillatory zoning and multiple micro-inclusions. Type-I perovskite commonly shows evidence of late alteration producing crystallisation of spongy TiO_2 and locally, titanite rims.

Type-I and Type-II perovskites have similar compositions, characterised by low average contents of REE (~2.5 REE wt%), Nb (~1 Nb_2O_5 wt%), Th (<10-5150 ppm), Zr (65-2280ppm) and Na (up to 1.66 Na_2O wt%). In contrast, euhedral groundmass perovskite shows significant enrichment in La, Ce and Nd (up to 25.6 wt% ΣLREE), Nb (0.9-8.8 wt% Nb_2O_5) and Na (0.37-2.49 wt% Na_2O). Perovskite from both compositional groups shows higher structural affinity for Th, Ta, Hf, Ho and LREE relative to U, Nb, Zr, Y and HREE. Niobium+Fe-rich perovskite mantles grains of groundmass perovskite, suggesting late interaction with an evolved kimberlitic melt.

With the exception of the Calonda kimberlite (90.2±2.5 Ma), all U-Pb dating yielded Early-Cretaceous ages (115-130 ± 4.6 Ma). Therefore Angolan kimberlite magmatism is related to the Gondwana break-up, with the main eruptive peak (120 Ma) coinciding with the onset spreading of the South Atlantic Ocean. This is in very good agreement with other kimberlite eruptive episodes documented in Africa, also related to NE-SW fault systems [1]. The Calonda intrusion could be associated with a reactivation of a pre-existing fault system during the separation of India from Madagascar. Alternatively it can also reflect strain accommodation along the lithospheric faults, as it has been proposed for other African kimberlites [2].

[1] Jelsma H.A., de Wit M., Thiart C., Dirks P.H.G.M., Viola G., Basson I.J. and Anckar E. (2004). Preferential distribution along transcontinental corridors of kimberlites and related rocks of Southern Africa. *South African Journal of Geology*, 107, 301-324.

[2] Jelsma H., Barnett W., Richards S. and Lister G. (2009). Tectonic setting of kimberlites. *Lithos*, 112S, 155-165.

Linking together the dissolution and reaction features of kimberlite-hosted diamond and Fe-Ti oxides with magmatic fluid and its role in kimberlite emplacement

Fedortchouk Y[1*], Chinn I[2], Kressall R[3], Milligan R[3], Li Z[3]

1 - Dalhousie University *yana@dal.ca 2 - De Beers Exploration, Johannesburg, South Africa 3 - Department of Earth Sciences, Dalhousie University

Kimberlite magmas quickly ascend through >150km of continental lithosphere collecting fragments of the surrounding rocks including diamond and other mantle minerals. These minerals react with the hot volatile-rich kimberlite magma and develop surface dissolution features, compositional zoning, and reaction rims. Experiments show that the morphology of diamond dissolution features greatly depends on the presence and composition of magmatic fluid during kimberlite emplacement, e.g. the proportion of the two main volatiles H_2O and CO_2.

Fe-Ti oxides (chromian spinel and ilmenite) occur in kimberlites as xenocrysts and phenocrysts; their abundance, relative proportions, and composition show a great diversity and often correlate with diamond potential. However, these empirical correlations are still not well explained. Dissolution features, complex or simple zoning, and reaction rims on chromites and ilmenites could provide an independent estimate of the behavior of kimberlitic fluid and therefore could be used for predicting diamond preservation and quality in kimberlites. In this study we make an attempt to understand how different types of reaction features on diamond, chromite, and ilmenite are related to the crystallization conditions and composition of kimberlite magma.

The study uses micro-diamond parcels and separates of chromite and ilmenite macrocrysts from three kimberlite localities that represent different cratons and geologically different kimberlite types: 1) a single-and a multi-phase kimberlite from the Orapa cluster (Botswana) filled with coherent kimberlite facies; 2) Snap Lake kimberlite dyke (Canada); 3) six predominantly volcaniclastic facies kimberlite pipes from Ekati Mine (Canada). Dissolution features on oxides and diamond were examined using a scanning electron microscope (SEM), and diamond surfaces were further studied using Atomic Force Microscope (AFM) to obtain precise quantitative measurements of the geometry of trigonal etch pits (trigons). Comparison of AFM parameters of trigonal pits on natural diamonds to those on diamond crystals from experiments allowed evaluation of H_2O:CO_2 ratio in the reacting fluid. The effect of internal diamond properties was assessed using Fourier transform infrared spectroscopy (FTIR) to obtain nitrogen content and aggregation for selected diamonds. Compositional zoning and reaction products on oxide grains were studied using back-scatter-electron images (BSE) and electron microprobe analyses (EMP). Observation of reaction products on natural mineral grains was compared to the products of dissolution of diamond, chromite, and ilmenite in experiments with silicate and carbonate melt and variable H_2O:CO_2 content conducted at 1-2 GPa and 1150-1400°C in piston-cylinder apparatus at Dalhousie University. Each kimberlite locality in this study reveals a unique style of reaction between kimberlite magma and the three studied minerals (diamond and two oxides). We integrate these data to constrain the composition of volatiles, behavior of kimberlitic fluid, and its role in kimberlite emplacement.

Paleogene phonolites of the Aris, Staalhart and Klinghardt groups, central and south Namibia, Africa

Koller F[1*], Skoda R[2], Palfi A[3], Popp F[1], Jost B[4]

1 - University of Vienna *friedrich.koller@univie.ac.at 2 - Masaryk University Brno
3 - Eximus Technologica Corporation Ltd. 4 - Institute of Geochemistry and Petrology

Within the Aris area, situated ~27 km south of Windhoek, a cluster of alkaline volcanic rocks intrude the Paleoproterozoic basement of polymictic gneisses. They are composed of variable phonolites, formed as either sheetflows or extrusive plugs. At least three individual phonolite types, intruded by a few dikes of nepheline trachyte, and commonly pyroclastic accumulations of trachytic composition are the main rock types. Moreover one trachybasaltic sill was found in the vicinity of the phonolites.

In the Rehoboth area, situated ~80 km south of Windhoek, a different group of individual plugs comprising phonolites and trachytes and one mafic dike are exposed.

About 150 km south of Lüderitz, in the restricted "Sperrgebiet" area, a large number of individual plugs, few sills and pyroclastic rocks of phonolitic to trachytic composition form the Klinghardt Group.

The main mineralogy of all phonolites is composed of nepheline, sodalite, sanidine, albite and aegirine. Blue amphiboles, mainly arfvedsonite, are extremely rare and were found only locally so far. Nepheline and sodalite may be altered to natrolite and other zeolites. The alkali pyroxenes can be zoned with a Di+He rich core (acmite >30%) and a Na-rich rim (acmite >90%). The nepheline minerals can be defined by X_{Ks} of 0.15-0.19, sodalite minerals with X_{Cl} values of 0.80-0.85. Feldspar is commonly homogeneous and rather close to its end member with $Or_{0.90-0.95}Ab_{0.10-0.05}$ and $Ab_{0.97}Or_{0.03}$.

Typical accessory minerals in the Aris group are Mn-pectolite, rosenbuschite and/or götzenite, eudialyte, villiaumite or fluorite and an unidentified secondary mineral belonging to the britholite group. Further phases are Mn-neptunite, baddeleyite, catapleiite, pyrochlore, pyrophanite, different REE carbonates and numerous Na-Zr-silicates, besides various other unidentified phases.

The Rehoboth Group phonolites contain locally up to 2 cm large crystals of nosean combined with sanidine and nepheline. Some of the phonolites contain an older biotite. As accessory phases, Mn-pectolite, fluorite, pyrochlore and various Zr- (possible labuntsovite group) and Nb-silicates are common. A few samples include also kalsilite/kaliophyllite minerals.

In the Klinghardt Group aenigmatite is a common mafic phase beside clinopyroxene/aegirine. Accessory phases are titanomagnetite, titanite, apatite, and minerals belonging to the eudialyte and rosenbuschite group.

The bulk geochemistry of all sampled phonolites is rather uniform featuring a Na/K ratio of ~3, some of the Staalhart Group are K enriched. In contrast to their rather homogeneous bulk composition, a strong variation of F (200-12000 ppm) and Cl (50-6200 ppm) content is apparent, further an even wider variation exists in trace elemental compositions. Zr content ranges from 500-3000 ppm for Aris, from 400-1000 ppm for Staalhart and from 400-3700 ppm for Klinghardt samples. Zr/Nb ratios are close to 4 for Aris and Klinghardt samples, about 1 for Staalhart. Staalhart samples further show the highest Nb/Y ratios. The REE-patterns show enriched LREE with La_N/Lu_N ratios varying in the range of 25-50 and moderately negative Eu anomalies.

A record of structural and chemical processes in the mantle preserved in a suite of deformed garnet megacrysts from Monteleo kimberlite, South Africa

Perritt S[1*], Preston R[2], Viljoen F[1], van der Linde G[2]

1 - University of Johannesburg *sperritt@uj.ac.za 2 - De Beers Group Services

Micro-structural studies indicate that the unusually flattened and elongated morphology of garnet megacrysts from the Monteleo Group II kimberlite, South Africa, developed as a consequence of plastic deformation. The deformation resulted in intracrystalline development of shear-related plastic mismatch microcracks and also imparted a preferred orientation to the numerous rod-like sulphide inclusions present within the garnets. The deformation occurred prior to entrainment of the garnets in the host kimberlite and is attributed to the development of localized transpression within the upper mantle, associated with shearing parallel to the Agulhas-Falkland Fracture Zone during Gondwana breakup. A simple fractional crystallization origin is suggested for the garnet megacrysts by the results of both major and trace element analysis. Pressure-temperature modelling indicates that they crystallized from a >1334^{o}C melt at a depth of ~180 km, within a zone of extensive metasomatism within the lithospheric mantle. A similarity in chemical composition between the megacrysts and garnets from associated lherzolitic lithologies suggests that percolation of the megacryst parental melt through the lithospheric mantle was responsible for the metasomatism.

Mineral chemistry of pyrochlore from the Bonga Carbonatite (Huila, Angola)

Amores Casals S[1*], Bambi A C J M[1], Gonçalves A O[2], Melgarejo J C[1]

1 - Universitat de Barcelona *sandra.amores@ub.edu 2 - Universidade Agostinho Neto

The Bonga Carbonatite complex (Huila, Angola) is emplaced at the SW domain of the Cretaceous Lucapa structure which cuts the Congo, Kasai and Angola cratons [1]. The Bonga Carbonatite is a subvolcanic structure with a concentric shape two kilometres in diameter hosted by strongly fenitized Precambrian granite. It comprises a central plug of massive calcite carbonatite replaced by ankerite carbonatite surrounded by a ring of carbonatite breccias and several concentric carbonatite ring dykes. Some trachytic dikes crosscut the ensemble [2]. A mine tunnel opened few months ago allowed a detailed sampling of fresh rocks.

Primary pyrochlore ($A_{2-m}B_2X_{6-w}Y_{1-n}\cdot pH_2O$) from the Bonga Carbonatite tends to be euhedral and most commonly intergrown with calcite, fluorapatite, and magnetite as well as minor amounts of pyrite, chalcopyrite, sphalerite, galena, ilmenite and chromite. It commonlt exhibits oscillatory concentric zoning under the microscope and it may be replaced by ankerite and dolomite veins. By contrast, hydrothermal pyrochlore forms irregular replacement veins or patches, associated with secondary fluorapatite, dolomite, ankerite, strontianite, barite and REE-bearing minerals (synchysite, monazite and britholite).

The primary U-, Ta-pyrochlore crystal cores mantled by Ca-pyrochlore crystallized early. The B site is occupied by elevated proportions of Ta and Ti (up to 0.31 and 0.32 apfu respectively) (Figure 1). Also, a remarkable content of U (up to 0.09 apfu) fills the A site together with a predominant number of vacancies. Primary Na-rich pyrochlore shows a wide range of Na and Ca contents in the A site; variation in F proportions causes the common oscillatory zoning. Ca-rich pyrochlore shows total loss of Na and F content with concurrent increase in number of vacancies in A and Y sites (up to 1.50 apfu) formed after a Na leaching process. Th and Ce enrichment (up to 0.05 and 0.06 apfu respectively) may be notable.

Hydrothermal pyrochlore presents high Sr proportions (between 0.18 and 0.58 apfu) in the A site with high Th (up to 0.06 apfu) and Ce content (up to 0.05 apfu) and vacancies while the B site is fully occupied by Nb. Furthermore, secondary Ca pyrochlore is distributed along magnetite crystals as fine anhedral grains intimately associated with synchysite, dolomite and baddeleyite and displaying similar compositions to primary pyrochlore. Late U-, Ta-rich pyrochlore forms anhedral crystals that are strongly fractured and interstitially distributed among dolomite, ankerite and fluorapatite grains, intergrown with niobian rutile, or filling geodes. In comparison to Ta-U primary phase, it is U-rich (up to 0.21) and records slightly high Pb, Ba and Th contents in the A site. In the B site, Ta and Ti enrichment reaches up to 0.25 apfu and 0.44 apfu respectively, nearer to the microlite end-member (Figure 1). High Fe (up to 0.51 apfu) and Si (up to 0.23 apfu) contents have also been recorded.

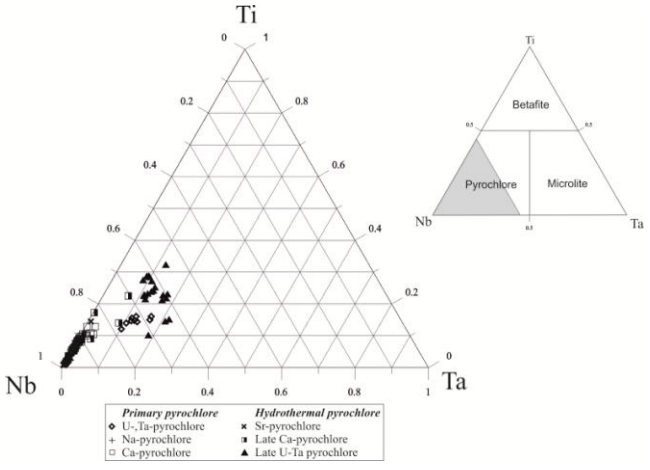

Figure 1: Chemical composition of pyrochlore from Bonga Carbonatite in the Ti-Nb-Ta classification diagram.

[1] Issa Fillho *et al*. (1991). *J. Geochem. Explor.*, 40, 205-226.

[2] Bambi *et al*. (2012). *Mineral. Mag.*, 76, 377- 392.

The Songwe-Hill Carbonatite, Malawi: new mapping, geochemistry and U-Pb dating

Broom-Fendley S[1*], Brady A[2], Horstwood M[3], Wall F[1], Gunn G[4], Dawes W[2], Andersen J[1]

1 - Camborne School of Mines, University of Exeter *s.broom-fendley@ex.ac.uk 2 - Mkango Resources Ltd. 3 - NERC isotope geoscience laboratory (NIGL) 4 - British Geological Survey

The Chilwa Alkaline Province (CAP), in Malawi, has been considered a carbonatite 'Mecca' since the discovery of carbonatites in Africa. Many of the carbonatite complexes of Malawi have been extensively studied and documented, resulting in excellent memoirs such as those on Chilwa Island, Tundulu, and Kangankunde. The Songwe Hill carbonatite, however, was not subject to the same extensive surveying and mapping as the nearby complexes and only short summaries exist in the literature. New mapping, geochemistry and dating are presented to remedy this dearth of information, as well as to extend our knowledge on the petrogenesis of the CAP and the formation of REE-deposits. These data are the result of extensive REE-exploration by Mkango Resources, utilising 6 850 m of drill core and resulting in a NI 43-101 compliant mineral resource estimate of 13.2 mt grading 1.62 % total rare earth oxides.

The Songwe carbonatite is intruded into the northern rim of Mauze Mountain: a large nepheline-syenite intrusion on the Malawi-Mozambique border. New mapping of the carbonatite shows that it is not a simple small sovite ring-structure, as previously documented, but it is a complex multi-phase intrusion characterised by diverse carbonatites and breccias exhibiting a range of alteration. The carbonatite is subdivided into earlier calcite-carbonatite, later ankerite-carbonatite and latest subordinate ferrocarbonatite. Breccia is common at Songwe, with many of the carbonatite types incorporating clasts of fenite.

The calcite carbonatite is formed of irregular, massive bodies which have been emplaced in several stages. White-grey calcite-carbonatite is probably the closest to the original carbonatite magma. It is composed of euhedral to subhedral calcite, with minor ovoid apatite and subhedral zircon. Later phases of calcite carbonatite consist of Fe- and Mn-rich calcite with ankerite, subhedral apatite, Fe- and Mn-oxides, pyrite, fluorite and K-feldspar. Typically, this stage of the intrusion is less REE-rich than the later stages; concentrations of the total rare earths (TREE) are between 5 000 and 20 000 ppm.

Ankerite-carbonatite forms extensive veins, breccias and thin dykes. It is formed of ankerite, with large bands of apatite and REE-fluorcarbonates as well as pyrite, calcite and rare quartz. This carbonatite is commonly rich in REE, with concentrations typically between 20 000 and 50 000 ppm total REE. These ankerite-rich bands are followed by Fe- and Mn-rich oxide-rich veins which may represent the same unit after supergene alteration.

U-Pb dating of zircon from Songwe and Mauze was carried out by LA-ICP-MS at NIGL. Magmatic zircons were selected from primary carbonatite and nepheline-syenite. These zircons were pre-screened for zoning using cold-cathodoluminescence and back-scattered electron imagery. The results show discordant ages for Songwe and Mauze, of ~140 and ~130 Ma respectively.

The new data show that Mauze was among the first intrusions in the CAP, suggesting that igneous activity in the CAP may have commenced in the south-east of the region. There was a substantial hiatus, up to 10 Ma, between emplacement of Mauze nepheline-syenite and Songwe carbonatite. This suggests the carbonatite is unlikely to have been derived from the neighbouring nepheline-syenite. The carbonatite is interpreted to have been intruded as a volcanic/sub-volcanic vent, composed of multiple stages of emplacement. Potentially economic REE concentrations, as well as interesting HREE-rich apatite, formed during the later stages of the intrusion carbonatite-derived from carbo-hydrothermal fluids.

Insights into the mantle structure beneath the Lunda Norte kimberlitic province (NE Angola): petrography and palaeothermobarometry of fresh mantle xenoliths

Castillo-Oliver M[1*], Galí S[1], Melgarejo J C[1], Pervov V[2], Griffin W L[3]

1 - Facultat de Geologia, Universitat de Barcelona, Catalonia, Spain *montgarricastillo@ub.edu 2 - ENDIAMA, Major Kanhangulo, 100, Luanda, Angola 3 - GEMOC/CCFS, Macquarie University (Australia)

In addition to their high economic interest, kimberlites are usually regarded as a window into Earth's mantle, providing priceless information for the understanding of the structure, the composition and the dynamics of the subcratonic lithospheric mantle (SCLM). At present the Catoca kimberlite (Angola) is the sixth ranked diamond producer worldwide but, due to the particular historical context, Angolan kimberlites and the mantle structure of the SW edge of the Congo craton are still poorly studied. The aim of this work is to shed light on the petrography and the structure of the underlying mantle using a suite of fresh mantle-derived xenoliths sampled by kimberlites of the Lunda Norte province.

Grt-peridotites are the dominant xenolith type (50%), followed by eclogites (24%), megacrystalline clinopyroxenites (18%), sp-peridotites (4%) and grt-ilmenite wherlites (4%). A combination of petrography and two-mineral thermobarometry defines a layering of the SCLM beneath the Lundas province. Two grt-peridotite suites can be distinguished, differing in texture, mineral composition and PT equilibrium conditions. The low-temperature suite (850-1080ºC; 38-53 kbar) is characterised by coarse-grained peridotites, whereas the high-temperature grt-peridotites (1280-1330ºC; 63-70 kbar) systematically show sheared microstructures, defined by olivine and clinopyroxene neoblasts. #Mg decreases with depth, with olivine and garnet from coarse grt-peridotites the richest in MgO. In contrast, the whole assemblage of sheared grt-peridotites is significantly richer in Cr, Ti and Ni. These textures and compositions are common features of the SCLM worldwide. The gap between the two textural types of grt-peridotite corresponds to a layer rich in Type II eclogites, ranging from 950 to 1250ºC at 44 to 58 kbar. The origin of these eclogites is still being tested, and, because there is a lack of geophysical data, further geochemical studies are currently being carried out. These eclogites could either have crystallised from deep-seated mafic melts (cumulate origin) or represent a remnant of a subducted slab between two compositionally and texturally different grt-peridotite layers.

A 4-layer model is used to define the geotherm constrained by the mantle xenoliths, which yields 30-34mW/m^2. This value implies slightly cooler mantle conditions compared to the SW Angola and South African kimberlitic clusters. A maximum lithospheric thickness of 240 km in the Mesozoic is defined by the intersection of the cooler geotherm with the 1300ºC adiabat.

Evolution of silicocarbonatite parental magmas to form the Phalaborwa igneous complex: a complex history of melting of multiple mantle sources, magma mingling, differentiation and magmatic exsolution

Kavecsanszki D*, Moore K, Wall F

1 - Camborne School of Mines, University of Exeter *kavecsdorii@gmail.com

The Phalaborwa Igneous complex is dominated by pyroxenites but its economic significance lies in the high copper enrichment of the carbonatite deposit situated at Loolekop. Valuable by-products include platinum group elements, gold, silver, magnetite, sulphuric acid, zirconium, nickel sulphate vermiculite and apatite. The most important rock is the transgressive carbonatite with the highest (>0.9%) copper content. Isotope studies of Eriksson [1] showed that the pyroxenite and carbonatite have a different mantle source. However, Wu *et al.* [2] obtained similar mantle isotopic signatures for transgressive carbonatite and pyroxenite at Loolekop.

Our studies on transgressive carbonatite samples using the QEMSCAN® technique revealed magma mingling textures between an oxidised carbonatite magma and a copper-bearing reduced sulphide magma indicating a magmatic origin for the copper. Considering that the two magmas have such different oxidation states we hypothesise that open system processes acted between magmas from different mantle sources. We suggest a model for the Phalaborwa complex which encompasses an ultramafic silicate magma with a deep mantle source that exsolved an immiscible sulphide magma, which subsequently mingled with a fractionated carbonatite magma from a shallower metasomatised mantle source, possibly in the subcontinental lithospheric mantle.

We have adapted Proterozoic mantle evolution models to try and understand the formation of large economic carbonatite deposits. Initial results predict that Phalaborwa formed during a mantle-scale magmatic event and that silicocarbonatite was likely to be the parental magma composition. We have used QEMSCAN® analysis of mineral abundances in Loolekop rocks to assess the validity of various hypothetical fractionation paths from a silicocarbonatite parent, to generate a range of intermediate differentiated magmas and end-member cumulate compositions. This research-in-progress indicates that the Loolekop lithologies are unlikely to have been generated by one single fractionation trend, which accounts for lithological diversity and the apparent dichotomy between rock composition and commonly cited source magma compositions.

[1] Eriksson S.C. (1989). Phalaborwa: a saga of magmatism, metasomatism and miscibility. In: Bell K. (ed) Carbonatite: genesis and evolution. Unwin Hyman, London, 221-254.

[2] Wu F.J., Yang Y.H., Li Q.L., Mitchell R.H., Dawson J.B., Brandl G. and Yuhara M. (2011). In situ determination of U-Pb ages and Sr-Nd-Hf isotopic constraints on the petrogenesis of the Phalaborwa carbonatite Complex, South Africa, *Lithos*, 127, 209-327.

Sb-As-Au-Hg mineralization in listvenites of the Murchison Greenstone Belt (MGB), South Africa

Blaauwbroek N[1*], Bach W[1], Schwarz-Schampera U[2], Klügel A[1]

1 - Universität Bremen *nikki.blaauwbroek@uni-bremen.de 2 - Bundesanstalt für Geowissenschaften und Rohstoffe (BGR)

The 3.09 to 2.97 Ga Murchison Greenstone Belt (MGB) represents one of a number of Archaean volcano-sedimentary belts within the Kaapvaal Craton, South Africa. The MGB is well known for its numerous precious and base metal deposits, including Sb and Au mineralization along a central structural lineament, the Antimony Line (AL). The AL hosts a set of Archean Sb-Au-As-Hg deposits, located in a quartz-carbonate altered listvenite with a complex deformation history.

This study will attempt to provide a geochemical perspective on the Sb-As-Au-Hg mineralization, to examine what caused the mobilization, deposition and remobilization of the Sb in the AL.

Field observations strongly indicate that the Sb mineralization in quartz-carbonate veins is located primarily in the fuchsite-rich listvenites, near the contact between a chlorite-rich schist and a talc-rich schist. These field relations are interpreted as typical 'blackwall' metasomatism under greenschist facies conditions between komatiite and granodiorite, which has been overprinted by later deformation and fluid-induced metasomatism (listvenitization).

First results of $\delta^{18}O$ measurements of the quartz-carbonate (dolomite and magnesite) alteration veins indicate temperatures of 140 to 200°C and mantle carbon $\delta^{13}C$ signatures. Two distinct groups of dolomite have been recognized, based on their chondrite-normalized REE quantity and their significant differences in LREE and HREE contents. The magnesite contains the lowest concentration of REE and the depleted LREE and enriched HREE suggests an ultramafic origin.

The listvenite is also characterized by relative high Cr-contents in chlorite and dravite. EMPA measurements reveal that dravite, additionally found near the quartz-carbonate veins, contains up to 5 wt.% Cr_2O_3.

These results provide an input for geochemical reaction path modeling aimed at assessing whether the primary mineralization of the stibnite is tied to the event causing the blackwall metasomatism. The modeling has been performed for different temperatures and a constant pressure of 1 kbar. The model works on the assumption that Sb is hosted primarily in the granodiorite, which may have formed in an ancient volcanic arc. The fluids interacting with the granodiorite are expected to have high O_2 and S_2 fugacities, and Sb is highly soluble even at temperatures around 200°C. When percolating into the komatiite, these fluids cause serpentinization, which lowers the O_2 and S_2 fugacities and decreases the Sb solubility by two orders of magnitude. These initial models are very robust in predicting greatly increased solubility of Sb in felsic sulfide-bearing rocks over a range of temperatures (150-300°C). In this temperature range, precipitation of Sb species from such a fluid is expected to occur immediately behind the metasomatic front.

We hypothesize that deformation and fluid migration during later stages caused the recrystallization of Sb to stibnite (and berthierite) within the quartz-carbonate alteration veins.

Ongoing modeling studies address this remobilization of Sb during the overprinting quartz-carbonate alteration and also the behavior of Au and the relation between the mineralization of Sb, As, and Au.

Listvenite: hosts for precious metal deposits and hope for mineral carbon sequestration

Falk E[1*], Kelemen P[2], Goldstein S[2], Eiler J[3]

1 - Woods Hole Oceanographic Institution *efalk@whoi.edu 2 - Lamont-Doherty Earth Observatory 3 - California Institute of Technology

Listvenite is a silica-carbonate rock formed by CO_2 metasomatism of ultramafic rocks. Listvenite in the strictest definition is characterized by a mineral assemblage consisting of Mg-bearing carbonates, quartz, and Cr-mica (fuchsite/mariposite), but not all listvenite-like rocks contain Cr-mica, and the term has also been broadly applied to describe many other carbonate-rich alteration products of ultramafic rocks. Listvenites have long attracted attention due to their association with ore deposits, particularly gold. Gold deposits associated with listvenite have been of major economic and historical importance. However, not all listvenites contain economic levels of gold or other metals. In recent years, listvenites have been highlighted as a natural analog for mineral carbon sequestration. The conversion of olivine or serpentine to solid carbonate has been proposed as a method of permanent CO_2 storage. As an example of fully carbonated peridotite, with all Mg in carbonate minerals and all Si in quartz, the presence extensive listvenite bodies in nature demonstrates that complete carbonation of peridotite is attainable *in situ*, and constraining the conditions under which listvenites can help guide engineered carbon capture and storage schemes involving mineral carbonation of peridotite.

However, the conditions of listvenite formation are not fully understood. It is generally agreed that listvenite forms during hydrothermal alteration of ophiolitic ultramafic rocks at moderate temperatures, with temperature estimates for most listvenites between ~200-250°C, though temperatures as low as 65°C or as high as 350°C have been suggested for some locations. The sources of hydrothermal fluids, CO_2, and gold are subject to more debate, and it is likely that no single model universally accounts for all listvenites. Proposed fluids responsible for listvenite formation include seawater-derived fluids formed during late stages of ophiolite emplacement, magmatic fluids released by granitic intrusions, metamorphic fluids released by crustal devolatilization, mantle degassing, and deep circulation of meteoric waters.

Listvenite from the base of the Oman ophiolite supports a model of carbonation via fluids derived from underlying sediments during emplacement of the ophiolite. Rb-Sr dating produces an internal isochron age of 97 ± 29 Ma, consistent with the timing of emplacement of the ophiolite. Initial $^{87}Sr/^{86}Sr$ values in the listvenite are mostly significantly higher than seawater values and consistent with values measured in the underlying metasediments, suggesting mass transfer from these sediments during alteration. In transitional zones along the margins of the listvenite, coexistence of antigorite, talc, and quartz correspond to a phase boundary at a temperature of ~80-110°C, and clumped isotope thermometry in carbonates from the listvenite yields peak temperatures of ~100°C. During emplacement of the ophiolite over allochthonous and autochthonous sediments, these temperatures were probably reached at depths of ~10-25km. Although favored by elevated CO_2 concentrations, the magnesite-quartz listvenite assemblage would be thermodynamically stable at these PT conditions even for a fluid only slightly enriched in CO_2 relative to seawater, making release of carbonate-saturated pore-water due to compaction of subducted sediment or low-pressure phase transitions of hydrous minerals probable sources of the CO_2-bearing fluid. By analogy, carbonate dissolution from subducted sediments and transfer of CO_2 to the mantle wedge via listvenite formation may be an important process in forearc hydrothermal systems worldwide.

Hydrothermal recrystallization of dunitic olivine: peridot from Pyaung-Gaung, Myanmar and other examples

Harlow G[1*], Thu K[2]

1 - American Museum of Natural History *gharlow@amnh.org 2 - Macle Gem Trade Laboratory

Large well-formed olivine crystals (peridot) form in cavities in peridotite at Zabargad, Egypt, Sagat, Pakistan, and Pyaung-gaung, Mogok Tract, Myanmar and are important for fashioning large gems. Study of the geology and origin of peridot from the former two deposits generally supports a hydrothermal process, however, relatively little is known about the Myanmar deposit. Recent reconnaissance of the Pyaung-gaung deposit supports hydrothermal crystallization of cavity peridot.

Peridot from the Bernardmyo/Pyaung-gaung/Zalataung region occurs in fault slices of partially to highly serpentinized ultramafics (peridotite and dunite) adjacent to the Momeik fault at the northern extent of the Mogok Stone Tract (Themelis 2007). Harzburgite consists of comminuted olivine (Fo_{92-93}), brown orthopyroxene (En_{92-93}), chromian magnetite ($Mgt_{61}Pcm_{18}Cm_{10}Sp_9$) and minor phlogopite with lizardite coating all grain boundaries. Dunite samples consist of olivine (Fo_{92-93}) and spinel ($Mgt_{65-70}Cm_{20-22}Pcm_8Sp_4$), again, with an intergranular coating of lizardite. Both rock types are cut by shear zones of shiny lizardite and veins of magnetite-rich spinel or snow-flake talc ± lizardite.

Peridot is found in cavities generally associated with dunite in which olivine crystals grow from the walls into cavities now filled with a mixture of talc, fine-grained carbonate (mostly calcite but also dolomite and pyroaurite-$Mg_6(Fe^{3+})_2CO_3(OH)_{16}{\bullet}4H_2O$), lizardite and possibly brucite. Cavity peridot is very homogeneous-Fo_{92-93} with NiO = 0.4-0.5 wt%. Peridot near the walls of the cavities contains white inclusions (~<500 µm diameter) that are filled with antigorite, brucite, magnetite and vapor(?). Healed fractures in peridot are decorated with small (~≤ 10 µm) inclusions of what appears to be the same phase assemblage as the larger inclusions. Near the cavities in the host ultramafic are fractures along which grow large brown enstatite crystals ($En_{90}Fs_8CaTs_2$) and/or phlogopite; this assemblage is used as an exploration guide in finding peridot cavities ([1]; information from miners).

Although Takla *et al*. [2] have argued for an igneous origin for Zabargad pocket peridot, evidence here strongly supports the role of a hydrous fluid in their formation. At Pyaung-gaung, the compositions in the assemblage Ol+Opx+Spinel yield an estimated equilibrium T of 730 ºC ± 40 (OFM 2012; PTEXL2-2), rather than >950 ºC (e.g., magnetite rather than chromite). This argues for exhumation of peridotite and dunite from a mantle source, consistent with the tectonic setting for Pyaung-gaung (and other cavity peridot sources). Inclusions in cavity peridot are most readily interpreted as a hydrous fluid, trapped at temperatures above the $Ol+H_2O \rightarrow Atg + Brc$ reaction, probably between 370 and 500 ºC, or higher above 2 kbar. This fluid later reacted with the host peridot to produce the observed solid phases. A high-T hydrous fluid entering tension gashes within dunite would facilitate the crystallization of large well-formed peridot crystals, much like the interpretation for Sapat, Pakistan [3] and Zarbagad, Egypt [4]. While further research is required to understand the detailed fluid - ultramafic interaction, Pyaung-gaung is another demonstration of its mineralogical and commercial significance.

[1] Themelis T. (2007). Gem and Mines of Mogôk, 352p. A&T Press, Bangkok.

[2] Takla, M.A. *et al*. (1997) *Ann. Geol. Surv. Egypt* 20, 451-478.

[3] Bouilhol P. *et al*. (2012). *Can. Mineral.*, 50, 1291-1304.

[4] Kurat G. *et al*. (1993). *Mineral. Petrol.*, 48, 309-341.

A comprehensive ion microprobe study on zircon from jadeitites and related rocks from the Rio San Juan Complex, Dominican Republic

Hertwig A[1*], McClelland W[2], Kitajima K[3], Schertl H[1], Maresch W[1], Valley J[3]

1 - Institute of Geology, Mineralogy and Geophysics, Ruhr-University Bochum *andreas.hertwig@rub.de 2 - Dept. Earth and Env. Sci., University of Iowa, Iowa City 3 - WiscSIMS, Dept. Geoscience, University of Wisconsin, Madison

The Rio San Juan Complex consists of subduction-related schists and serpentinite mélanges that host different types of metamorphic blocks (e.g. blueschist, eclogite, orthogneiss) and a variety of quartz-free and quartz-bearing jadeitites and related jadeite-rich rocks. Most of these rocks occur as loose blocks; however, quartz-bearing jadeitites may also form concordant layers or veins in lawsonite blueschist, a rare association worldwide that allows direct study of jadeitite-blueschist relationships. Proposed mechanisms for jadeitite formation include crystallization of jadeitite from a HP fluid and metasomatic replacement of a suitable protolith. To evaluate these concepts, we conducted a study on the geochronology, geochemistry and oxygen isotopes of zircon in two settings; (1) from a jadeitite and also an albite-rich jadeite rock found as loose blocks within the mélange, and (2) from a quartz-bearing jadeitite layer and its host blueschist.

Loose blocks: Zircons from both the jadeitite and albite-rich jadeite rock show faint to pronounced oscillatory zoning and are often rimmed by irregularly shaped CL-bright domains of variable thickness. Although distinguishable by CL, these zircon rims are almost identical to the core domains in age (SHRIMP U/Pb: jadeitite, 115.0 ±0.9Ma; jadeite-albite rock, 113.4 ±1.3Ma), with respect to the $\delta^{18}O$ values (IMS-1280: jadeitite, $\delta^{18}O$(Zrn) = 5.1 ±0.6‰; 2 SD, VSMOW; albite-jadeite rock, $\delta^{18}O$(Zrn) = 4.7 ±0.8‰) and REE patterns.

Blueschist-hosted jadeitite layer: Zircon grains separated from the jadeitite layer show either an irregular to pronounced oscillatory zoning pattern or no obvious zoning at all. CL-dark zircon domains can be differentiated from CL-bright domains, are in general oscillatory zoned and exhibit an age of 117.1 ±0.9 Ma and a $\delta^{18}O$ value of 5.4 ±0.4‰. In contrast to the loose-block samples above, in the jadeitite layer the CL-bright zircon domains differ significantly from the CL-dark zircon domains in terms of age (77.6 ±1.3Ma), $\delta^{18}O$ value (6.3 ±0.8‰) and REE patterns. Zircon grains from the jadeitite-hosting blueschist form a texturally homogeneous population of oscillatory and patchy zoned grains. These zircons are slightly younger (113.6 ±1.1Ma) than the CL-dark zircon domains of the jadeitite layer, but show, within error, an identical value of $\delta^{18}O$ (5.6 ±0.6‰).

The measured $\delta^{18}O$ values and other geochemical characteristics of zircon from the loose jadeitite and albite-jadeite rocks, the blueschist zircons and the CL-dark zircon domains from the jadeitite layer are all similar to values and patterns obtained from igneous zircon of the oceanic crust ($\delta^{18}O$(Zrn) = 5.2 ±0.5‰; [1]). Thus, these zircons are best interpreted to be igneous in origin, either as remnants of a metasomatically altered protolith or as xenocrysts. The CL-bright zircon domains from the jadeitite layer show geochemical features of metamorphic overgrowth and/or replacement and might either have formed contemporaneously with the jadeite in the layer or represent a different metamorphic event.

[1] Grimes *et al*. (2011). *Contrib Mineral Petr*, 161(1), 13-33.

Mantle wedge infiltrated with saline fluids from dehydration and decarbonation of subducting slab

Kawamoto T[1*], Yoshikawa M[2], Kumagai Y[2], Mirabueno M[3], Okuno M[4], Kobayashi T[5]

1 - Institute for Geothermal Sciences, Graduate School of Science, Kyoto University *kawamoto@bep.vgs.kyoto-u.ac.jp 2 - Institute for Geothermal Sciences, Kyoto University 3 - Philippine Institute of Volcanology and Seismology, University of the Philippines 4 - Dept of Earth System Science, Fukuoka University, Japan 5 - Dept of Earth and Environmental Sciences, Kagoshima University, Japan

Slab-derived fluids play an important role in heat and material transfer in subduction zones. Dehydration and decarbonation reactions of minerals in the subducting slab have been investigated using phase equilibria and modeling of fluid flow. Nevertheless, direct observations of the fluid chemistry and pressure-temperature conditions of fluids are few. This report describes CO_2-bearing saline fluid inclusions in spinel-harzburgite xenoliths collected from the 1991 Pinatubo pumice deposits. The fluid inclusions are filled with saline solutions with 5.1 ± 1.0% (wt) NaCl equivalent, magnesite crystals, CO_2-bearing vapour bubbles, and a talc and/or chrysotile layer on the walls. The xenoliths contain tremolite amphibole, which is stable at temperatures lower than 830°C in the uppermost mantle. The Pinatubo volcano is located at the volcanic front of the Luzon arc associated with subduction of warm oceanic plate. The present observation is the first report suggesting hydration of forearc mantle and the uppermost mantle by slab-derived CO_2-bearing saline fluids. Dehydration and decarbonation take place and seawater-like saline fluids migrate from the subducting slab to the mantle wedge. The presence of saline fluids is important because they can dissolve more metals than pure H_2O and affect the chemical evolution of mantle wedge (Figure 1).

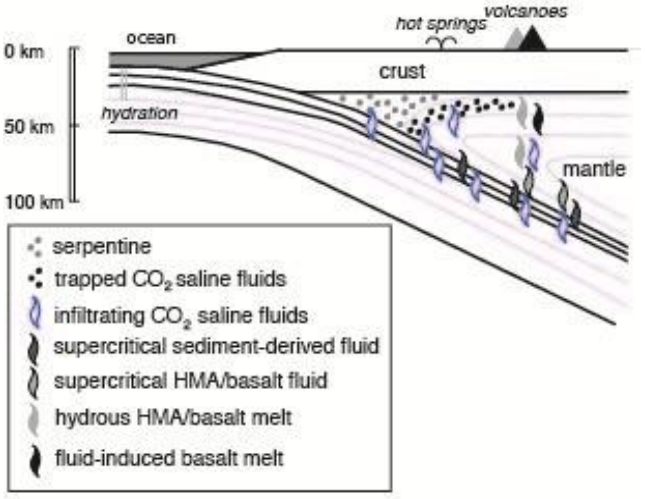

Figure Schematic illustration of fluid migration in subduction zone

[1] Kawamoto T. *et al.* (2012). *Proc Natl Acad Sci USA*, 109, 18695 http://www.pnas.org/content/109/46/18695.full.

[2] Kawamoto T. *et al.* (2013). *Proc Natl Acad Sci USA*, 110, 9663 http://www.pnas.org/content/110/24/9663.full.

Rodingites from the Ricaze ophiolites, Southern Tibet – new insights into the process of sea floor rodingitization

Li X*, Kong F, Chen H

Shandong University of Science and Technology, Qingdao, China *lixuping@sdust.edu.cn

The Ricaze ophiolite represents one of the most pronounced occurrences of Neo-Tethyan ocean remnants in the central part of the Yarlung-Zangbo suture zone in southern Tibet, formed by the collision of the India and Asia Plates during the Jurassic and Cretaceous. It was proposed to have formed in a marginal intraoceanic transtensional basin that developed by subduction of the Tethys ocean in response to the convergence of India and Eurasia [1]. More studies, however, considered the formation of the Ricaze ophiolite at a midoceanic ridge [2, 3, 4].

Abundant veins and bands of rodingite were found in the Ricaze ophiolites, extending from Bailiang to Jiding along the Yarlung-Zangbo suture zone. They occur spatially together with diabase and gabbro. The rodingites represent former fluids which intruded ultramafic rock sequences and are thus found essentially within the serpentinized mantle part, while diabase and gabbro dykes are more abundant in the upper part of the ophiolite sequence [5]. Crust and mantle at Jinlu massif of the Ricaze ophiolite region are in fault contact [6], which means although rodingites and diabase/gabbro are intermingled with mantle serpentinite, they may have undergone a different geological evolution [7].

Rodingitization is basically seen as a Ca-metasomatic process genetically linked to serpentinization. Rodingites are Ca-rich, Si-undersaturated rocks consisting of various proportions of Ca and Ca-Mg silicates. The mineral assemblages of rodingites from the Ricaze area are highly variable and form (1) hydrogrossular-diopside-chlorite-calcite-, (2) amphibole-clinozoisite-diopside-chlorite-titanite-, (3) amphibole-diopside-prehnite-calcite-ilmenite-titanite-, (4) hydro- grossular-amphibole-prehnite-chlorite-ilmenite-titanite-, and (5) hydro-grossular-vesuvianite-diopside-chlorite-parageneses. The formation conditions of the South Tibet rodingites studied here are similar to those of rodingites in ophiolites from Northwestern China such as Tianshan, however also similar to those from Zermatt/Switzerland, Dun Mountain/New Zealand and even from IODP hole along the Mid-Atlantic Ridge.

Geochemical studies document that the rodingite samples as well as other mafic rocks (diabase and gabbro) from the Ricaze ophiolite all have nearly identical flat LREE patterns, with $[La/Yb]_{CN}$=0.6−1.1 and 0.5-1.6, respectively; in addition they are characterized by slightly negative Ta, Nb and Ti anomalies. Trace elements plotted in a chondrite-normalized multielement diagram show a depletion of highly incompatible elements (LILE and LREE), compared to the less incompatible elements (HREE). Patterns are relatively flat from HFSE to HREE. Chemical characteristics show a back-arc basin affinity for these rocks. In respect to possible genetic interrelations it is important to know that rodingite and diabase/gabbro have the same crystallization age of about 130 Ma.

This study shows that the formation conditions of rodingites and associated diabase/gabbro dykes from the Ricaze ophiolite have the same geochemical and geochronological characteristics and that all the lithologies derive from oceanic lithosphere.

Acknowledgement: The current study was supported by the SGSTSP of the Chinese Academy of Sciences XDB03010201, the Chinese Geological Survey Project, grants 1212011221116, 1212011221117

[1] Dubois-Coté V. *et al.* (2005). Petrological and geochemical evidence for the origin of the Yarlung Zangbo ophiolites, southern Tibet. *Chemical Geology*, 214, 265–286.

[2] Nicolas A. *et al.* (1981). The Xigaze ophiolite (Tibet): a peculiar oceanic lithosphere. *Nature*, 294, 414–417.

[3] Xiao X. (1984). Les ophiolites de Xigaze au Tibet méridional et quelques problèmes tectoniques les concernant. In: J.L. Mercier and Li Guancen (Editors), Mission Franco-Chinoise au Tibet 1980. C.N.R.S. (Cent. Natl. Rech. Sci.), Paris, No. 11, pp. 167-188.

[4] Agrinier P. *et al.* (1988). Hydrothermal activity in a peculiar ocean ridge – oxygen and hydrogen isotope evidence in the Xigaze ophiolite (Tibe, China). *Chemical Geology*, 71, 313-335.

[5] Girardeau J. and Mercier J.-C.C. (1988). Petrology and texture of the ultramafic rocks of the Xigaze ophiolite (Tibet): constraints for mantle structure beneath slow-spreading ridges. *Tectonophysics*, 147, 33– 58.

[6] McDermid I.R.C. *et al.* (2002). The Zedong terrane: a Late Jurassic intraoceanic magmatic arc within the Yarlung-Tsangpo suture zone, southeastern Tibet. *Chem. Geol.*, 187, 267–277.

[7] Göpel C. *et al.* (1984). Lead isotopic study of the Xigaze ophiolite (Tibet): The problem of the relationship between magmatites (gabbros, dolerites, lavas) and tectonites (harzburgites). *Earth and Planetary Science Letters*, 69, 301-310.

Mechanism and rate of blackwall formation revealed from extreme magnesium isotope fractionation at outcrop scale

Marschall H[1*], Pogge von Strandmann P[2], Dohmen R[3], Elliott T[4]

1 - Woods Hole Oceanographic Institution *hmarschall@whoi.edu 2 - University of London 3 - Ruhr-Universität Bochum 4 - University of Bristol

Blackwalls are cm to m thick zones of hybrid rock that form at the contact between two different precursor rocks of strongly contrasting chemical and mineralogical composition, typically ultramafic and crustal rocks, respectively. They are typically rich in OH-bearing minerals, such as chlorite, talc, biotite or amphibole, commonly forming sequential layers of mono- or bimineralic assemblages. Blackwall formation generally proceeds through tectonic mixing or mechanical juxtaposition of crustal and mantle rocks followed by metasomatic transfer of material. The term 'metasomatism' in this context has been used rather loosely, lumping together processes of advective transport aided by flux of externally derived fluids parallel to the initial contact with diffusive flux across the lithologic contact driven by the stark chemical gradients between the juxtaposed rocks.

Bulk diffusion can occur on many different scales within silicate rocks. Major elements, such as Mg and Fe, have repeatedly been shown to diffusively exchange in silicate minerals, and Mg may also diffuse on larger scales in bulk rock processes. However, advective metasomatism must also be considered as an additional operating mechanism, and some geochemical studies on blackwall rocks have altogether neglected the effects of diffusion and interpreted their formation as solely controlled by advection with far-reaching consequences for their geochemical interpretation.

How can we identify a contribution of diffusion to blackwall formation? Experimental and natural studies have shown that the diffusion of species along a chemical potential gradient can be accompanied by isotopic fractionation, because the lighter isotopes will diffuse faster than the heavier ones. Of all the major elements, Mg isotopes are ideally suited to reveal the effects of diffusion, because of their large relative mass differences and the strong chemical potential gradient at the contact between crustal and mantle rocks. Hence, Mg isotope fractionation during diffusive transport provides novel means of constraining the style and timing of metamorphic transformations in general and blackwall formation in particular.

Our study demonstrates how length scale and shape of measured diffusion profiles can be used to extract information on the mechanisms and timescales involved in the growth of blackwalls. We document a major (~1 ‰) decrease in the Mg isotopic composition of the reaction front of an exhumed contact between rocks of subducted crust and serpentinite, in a mélange zone on Syros island (Greece). This isotopic perturbation extends over a notable length-scale (~1 m), implicating diffusion of Mg through an intergranular fluid network over a period of ~100 kyr. These novel observations confirm models of diffusion-controlled growth of reaction zones formed between rocks of contrasting compositions, such as found at the slab-mantle interface in subduction zones. The results also demonstrate that diffusive processes can result in exotic stable isotope compositions of major elements with implications for fluid veins, mantle xenoliths and complex intrusions.

Jadeitite from Itoigawa, Niigata Prefecture, central Japan

Miyajima H

Fossa Magna Museum. mac314@mac.com

Itoigawa city meets the Sea of Japan in the north, where the mountains of the Japan Alps sink into the Sea. Itoigawa is the biggest jadeitite-bearing region in Japan. This jadeitite is found as tectonic blocks in serpentinite mélange.

Jadeitite from Itoigawa is closely connected with human history, being the site of the oldest known jade working culture in the world. The hammer of jadeitite discovered from the Ogakuchi archeological site in Itoigawa was used about 7000 years ago. The suspended jadeitite decorations discovered in the Odake Shell Mound in Toyama Prefecture, 70 km west-southwest of Itoigawa, were used about 5500 years ago. Processed jadeitite produced in Itoigawa spread throughout Japan, and some even reached the Korean Peninsula. Use of precious stones in Itoigawa is among the oldest examples in the world comparable to use in Egyptian culture. However jadeitite production ceased for unknown reasons during the Nara period about 1200 years ago. Knowledge about Itoigawa's jadeitite was lost completely after this time. The jadeitite was rediscovered in the Kotakigawa River in Itoigawa in 1938.

A petrological and mineralogical study of the origin of jadeitite from Itoigawa was carried out by Kawano (1939) and Omori (1939).

Although jadeitite originates in serpentinite mélange, in Itoigawa, the jadeitite in serpentinite cannot be observed; rather jadeitite is seen as rolling stones and boulders in the riverbed or along the seashore. The largest of these jadeitite boulders exceeds 100t and the site where they are found is protected as one of the natural monuments of Japan.

The relationships between the colour of jade and mineral species contained within jadeitite are as follows: white jade, nearly pure jadeite; green jade, omphacite and jadeite; lavender jade, Ti-bearing jadeite; blue jade, Ti-rich omphacite and jadeite; and black jade, jadeite and tiny graphite. The cause of green colouration of jade from Itoigawa is not chromium but iron.

Itoigawa's jadeitite does not contain quartz. Therefore, it is possible that the jadeitite from Itoigawa did not form by decomposition of albite to jadeite and quartz.

It's been observed that there are veinlets of jadeitite and idiomorphic crystals of jadeite in natrolite matrix. It is thought that jadeitite from Itoigawa formed by precipitation from hydrothermal solution.

The most striking feature of jadeitite from Itoigawa is its richness in Sr- and Ba-dominant minerals as follows: Sr-dominant minerals: itoigawaite, rengeite, matsubaraite, tausonite, strontianite, stronadelphite, lamprophyllite, slawsonite, stronalsite, and thomsonite-(Sr). Ba-dominat minerals: cersian, hyalophane, and banalsite.

These minerals closely coexist with jadeite. The origin of Sr-dominant minerals results from the difference in the ionic radius of Ca and Sr. That is, Ca is compatible in jadeite, but Sr is incompatible. Although the hydrothermal solution was initially enriched in Ca over Sr, progressive crystallization of jadeite enriched the hydrothermal solution in Sr, and Sr minerals crystallized in the late stage of jadeitite formation. The cause of crystallization of Ba-dominant minerals is the same as Sr-dominant minerals.

The Sr- and Ba-dominant minerals are also found in rodingite, albitite and corundum rocks in Itoigawa as follows: "Niigataite" = clinozoisite-(Sr), epidote-(Sr), stronalsite, ohmilite, strontio-orthojoaquinite, stronitiojoaquinite, benitoite, leucosphenite, stronadelphite and Sr-analogue of margarite. No such minerals are found in crystalline schist in the serpentinite mélange. The existence of Sr- and Ba-dominant minerals reflects the difference between the generation age and the mechanism of formation.

[1] Kawano Y. (1939). A new occurrence of jade (jadeite) in Japan and its chemical properties. *Journal of Japanese Association of Mineralogy and Petrology, and Economic Geology*, 22, 195-201. (in Japanese)

[2] Omori K. (1939). Optical properties of Japanese jade. *Journal of Japanese Association of Mineralogy and Petrology, and Economic Geology*, 22, 201-212. (in Japanese)

High-pressure metamorphic rocks in serpentinite-hosted mélanges of the Dominican Republic: the role of jadeitites

Schertl H[1*], Maresch W[1], Hertwig A[1]

1 - Institute of Geology, Mineralogy and Geophysics, Ruhr-University Bochum

*hans-peter.schertl@rub.de

New occurrences of jadeitite, jadeite quartzites, and jadeite-lawsonite quartzites have been recently discovered in the Rio San Juan Complex (RSJC) of the northern Dominican Republic. These rocks are found in serpentinite mélanges associated with a former intra-oceanic subduction zone. The mélanges contain blocks of various high-pressure (HP) metamorphic rock types such as blueschist, eclogite, jadeitite, orthogneiss, rare cymrite-bearing rocks, marble and metapelite. Comprehensive petrological studies on different types of eclogite and blueschist reveal a broad diversity of PTt-paths which are closely interrelated. In the early stages of the evolution of the subduction zone, PT-paths are both clockwise and anticlockwise with low ("hot") P/T-gradients; maximum PT-conditions derived from eclogites are about 800°C/2.5 GPa (a Lu-Hf-age on eclogite is 103.9 Ma). Omphacite-bearing blueschists document a continuous cooling and steepening of the PT-gradient; their recorded peak metamorphic conditions are 500-550°C/1.6-1.8 GPa at 80.3 Ma (Rb-Sr on Phe-Amp-WR). Very steep ("cold") P/T-gradients are derived from jadeite blueschists; Rb-Sr-ages (Phe-Amp-WR) of 62.1 Ma and Ar-Ar ages of 71.9 Ma date the peak metamorphic conditions of 360-380°C at about 17 kbar.

Jadeitites are known from only about 20 localities worldwide. They are thought to either crystallize directly from HP aqueous fluids or to form by metasomatic replacement of a suitable protolith such, for example, tonalite, trondhjemite or plagiogranite. A very unusual feature of the jadeitites of the RSJC compared to other jadeitites worldwide is their occurrence as layers and veins in jadeite-lawsonite blueschist and omphacite-garnet blueschist country rocks. The principal types of jadeite-bearing rocks observed in the RSJC can be categorized as (1) jadeitites *s.str*. (quartz-free, albite-bearing, >90 vol% jadeite), which have so far been found only as loose blocks/boulders in the mélange, and (2) jadeitites *s.str*. (quartz-bearing) and jadeite quartzites (JQ) which grade into jadeite-lawsonite quartzites (JLQ); while also occurring as loose blocks/boulders, these can also form concordant layers and discordant veins within blueschists. In addition, monomineralic omphacitite veins have also been found in such blueschists.

The unusual diversity of jadeite-bearing rocks in the RSJC, in context with their observed contact relationships with different blueschist country rocks, reflects their formation at different PT-conditions (350-500°C at minimum pressures of about 1.5 GPa and 500-600°C at ca. 1.1-1.5 GPa) over an extended time span of tens of millions of years in a continuously evolving subduction-zone environment. In addition, evidence for both crystallization directly from a HP aqueous fluid as well as formation by metasomatic replacement is found.

Lithium isotope zoning in prograde-zoned garnets in HP-LT metabasaltic rocks: a new tracer of fluid heterogeneity in a subduction channel

Tsujimori T[1*], Ota T[1], Shimaki Y[1], Kunihiro T[1], Nakamura E[1]

1 - Okayama University Misasa *tatsukix@misasa.okayama-u.ac.jp

In this contribution, we present a first demonstration of lithium (Li) isotope zoning in garnet (Grt) produced during prograde H*P*-L*T* metamorphism of basaltic rocks. We extracted euhedral Grt, with a rhombic dodecahedron morphology, from type I and II lawsonite eclogites from the South Motagua Serpentinite Mélange, Guatemala [1] and cut these Grts into halves in efforts to sample the growth centers of the grains and thus obtain complete growth records. Based on over 1200 trace element and 400 isotope analyses by SIMS, combined with major element profiles and inclusion mineralogy, we have identified some systematic behavior of Li and its isotopes during the Grt growth.

All of the Grt (4 to 8 mm in size) in these samples is almandine-rich and exhibits zoning in which Mg/(Mg+Fe) atomic ratio increases continuously from core to rim, X_{Mn} decreases rimward and shows oscillatory spikes at the rims, and X_{Ca} decreases subtly at the rim. Grts from type I eclogite contain texturally pre-eclogite facies omphacite (Omp) and jadeite; HREE-enriched patterns of Omp inclusions indicate that the pyroxene formed prior to Grt growth. HREE, Y and Li decrease from core to rim. Values of δ^7Li range from -10 to +4‰ and show oscillatory changes; the heaviest value is found in a titanite (Ttn)-bearing small seed at the nucleation center, and the light values (< -7‰) occur in the inner rims. The δ^7Li profile of the Grt is somewhat asymmetric and shows no obvious correlation with zoning in Li concentrations. Values of δ^7Li are similar for Omp inclusions in Grt and in the matrix. Grts from type II eclogite are characterized by the presence of inter core (Omp-free), outer core with very small inclusions (Omp + Ttn), and rim with trails of coarser-grained inclusions (Omp + rutile). HREE, Y and Li show a distinct 'M-shape (with a central peak)' profile; the two shoulders on the profile are same positions to the textural core-rim boundary, *i.e.*, the Ttn-out isograd within the Grt. Omp inclusions show a HREE-depleted pattern suggesting crystallization to be coeval with Grt formation. In a single Grt crystal, changes in δ^7Li are about 5-8‰, but the range varies among crystals; for example, -3 to +5‰, -6 to 0‰. Except for one sample, the δ^7Li zoning does not correlate with Li zoning. Values of δ^7Li decrease in the core, but show oscillatory changes in the rims.

Our observation are thus that (1) early stage growth was characterized as having heavy δ^7Li, (2) the 'M-shaped' Li (and HREE and Y) zoning is controlled by the formation of rutile at the expense of Ttn, and (3) δ^7Li values oscillate significantly during the growth stage in which rutile was stable and are mostly decoupled from Li concentrations. We suggest that δ^7Li zoning of Grt in L*T* eclogites reflects the nature of aqueous fluids present during Grt growth rather than changes in *P-T*. At the blueschist-to-eclogite transition, Li concentrations in Grt might be buffered by Omp (the major sink of Li) but δ^7Li in Grt could reflect heterogeneity in the Li delivered to the Grts in subduction channel fluids. In a subduction channel, the fluid heterogeneity most likely reflects change in aqueous interactions of various mélange rocks (ultramafic rocks, metabasalt, sediments, etc). Deciphering the growth history of garnet by assessment of Li isotope zoning has a great potential as a new tracer of the fluids process in subduction zone mélange.

[1] Tsujimori *et al*. (2006). doi:10.1130/2006.2403(09)

Jade artefacts from the Playa Grande site, Dominican Republic: mineralogical characterization and archeological implications

Schertl H-P[1*], Hertwig A[1], Knippenberg S[2], Maresch W[1], Speich L[3], Lopez A[4], Hofmann C[2], Rodríguez Ramos R[5]

1 - Institute of Geology, Mineralogy and Geophysics, Ruhr-University Bochum *hans-peter.schertl@rub.de 2 - Faculteit Archeologie, Caribbean and Amazonia, Leiden 3 - Ruhr-University Bochum 4 - CAST, Fantino Falco No. 47, Santo Domingo, Dominican Republic 5 - University of Puerto Rico, Utuado, Puerto Rico

Jadeitite (or jadeite jade), a rare hard and tough rock type composed mainly of the mineral jadeite, is now known from Ceramic Age sites on many islands in the Caribbean. It represents a prized lithic raw material for the manufacture of axes and adzes. Although initial provenance work in the early 2000's pointed to Guatemala as its likely source, new discoveries in Cuba and the Rio San Juan Complex (RSJC) in the northern Dominican Republic (DR) have made sourcing more equivocal. Jadeitite characterization is complex, and considerable mineralogical and geochemical intra-site variations are recognized, e.g., [1]. The known potential sources are serpentinite mélanges with a similarly variable inventory of metamorphic blocks.

Very recent work in the northern DR has revealed the first evidence of local celt manufacture at the multi-component Late Ceramic Age coastal site of Playa Grande (AD 750 - 1600), from where the material appears to have been exchanged and distributed. The Playa Grande (PG) site is located only 20-30 km from the RSJC jadeitite source region recently described by Schertl *et al*. [2]. At PG, an unusually high percentage of the artefacts are celts, adzes and related tools, 35% of which appear to be jadeitite. Eleven celts and one adze were chosen for an on-going petrographical, mineralogical and geochemical analysis for direct comparison with the potential RSJC source material, where [2] recognized: (1) a quartz-free jadeitite suite and (2) a heterogeneous quartz-bearing suite in which jadeitites can grade into jadeite, jadeite-lawsonite, and lawsonite quartzite. Suite (2) is particularly common in mélanges near the coast, whereas the quartz-free suite is found mainly 20-30 km inland in rugged hills representing the catchment area of the San Juan River. Nine of the twelve artefacts are jadeite-rich rocks. Seven of these are identical to or extremely similar in both mineralogy and petrography to jadeitites from the RSJC, with all but two corresponding best to the quartz-free suite of [2]. Two artefacts, composed essentially of jadeitite+lawsonite but lacking quartz, are rocks so far not known from the RSJC. One artefact is a silicified greenschist commonly associated with the jadeitite-bearing mélanges, while the other two are glaucophane-rich blueschists. Although the latter are common in the mélanges, the artefacts in detail contain an unusual omphacite+garnet+lawsonite association not yet described from the RSJC. These results show that most of the artefacts at PG most likely originated locally from the RSJC. Rather than exploiting easily accessible coastal outcrops, the PG inhabitants followed the San Juan River toward its source area and collected river cobble blanks. Jadeitites from the RSJC and the PG artefacts lack paragonite, a characteristic feature that may help in future provenance studies.

[1] García-Casco *et al*. (2013). *J. Arch. Science*, v. 40, 3153-3169.

[2] Schertl *et al.* (2012). *Eur. J. Mineralogy*, 24, 199-216.

Why is jadeitite so rare? Quick exhumation?

Shi G

School of Gemology. shiguanghai@263.net.cn

Jadeitite always occurs in subduction zones in association with serpentinite mélange bearing HP/LT metamorphic rocks like blueschist and eclogite [1]. However, jadeitite occurrences are very rare, with only 19 localities reported worldwide [2], which are far fewer than those of serpentinite mélange, blueschist, and even rarer than coesite- and/or diamond-bearing eclogite [3]. In jadeitite-containing HP/LT metamorphic belts, jadeitite outcrops represent only a tiny proportion, very much less than 1% of the entire belt.

Evidence increasingly demonstrates that jadeitite-forming components are derived from the subducted oceanic crust. The requisite aqueous fluid rich in Na, Al, and Si is therefore expected to be common in subduction zones, so formation of jadeitite should be as well. That metasomatic albitite appears to be more common [4] may hold a clue to the rarity of jadeitite. Preservation requires a rapid change of P-T conditions during exhumation; otherwise jadeite would either react with residual fluid or otherwise convert to a lower-P assemblage if pressure decreased too slowly.

A review of the geological settings of jadeitite occurrences reveals that strike-slip faults, thrust faults or underplating structures commonly occur with or adjacent to almost all jadeitite deposits, and for serpentinite mélanges as well. For example, Guatemala jadeitite occurs in serpentinite mélange in distinct settings on both sides of the Motagua fault, the current North American-Caribbean plate boundary [5]. Likewise, jadeitite from Sierra del Convento, eastern Cuba [6] is located close to the Oriente fault zone, a left lateral strike slip fault [7]. Myanmar jadeitite straddles the Sagaing Fault, which is inferred as a key factor responsible for rapid exhumation of the Myanmar jadeitite [8]. Other examples related to thrust faults include jadeitite from the Itoigawa-Omi District and the Osayama jadeitite-bearing serpentinite mélange [9]. The Syum-Keu ultramafic complex containing the Polar Urals jadeitite is distributed along the Polar Urals thrust-and-fold belt [10]. Essentially, available data show that all the subduction-related jadeitites are exclusively and spatially correlated with these tectonic settings. Subduction characterized by low geothermal gradients, especially in an intra-oceanic setting [11], would keep the jadeitite cool for a period [8]. Although not directly related to jadeitite formation, these faults enabled rapid exhumation and preservation of high-pressure lithologies [12-14].

[1] Harlow G.E. and Sorensen S.S. (2005). *Inter. Geol. Rev.*, 47, 113-146.

[2] Tsujimori T. and Harlow G.E. (2012). *Euro J. Mineral.*, 24, 371-390.

[3] Liou J.G. *et al*. (2009). *J. Asian Earth Sci.*, 35,191-198.

[4] Wang J. *et al*. (2013). *Acta Petrol. Sinica*, 29, 1450-1460.

[5] Harlow G.E. *et al*. (2007). *Mineral. Ass. Canada*, 207-254.

[6] Garcia-Casco A. *et al*. (2009). *Contr. Mineral. Petrol.*, 158, 1-16.

[7] Rodriguez M.O.C. and Córdoba D. (2010). *Geotectonics*, 44(2), 176-202.

[8] Shi G.H. (2014). *Gondwana Res*. doi.org/10.1016/j.gr.2013.08.007.

[9] Tsujimori T. (1997). *Mineral. Mag.*, 61, 845-852.

[10] Meng F.C. (2011). *J. Asian Earth Sci.*, 42, 596-606.

[11] Shi G.H. *et al*. (2009). *Lithos*, 112, 342-350.

[12] Agard P. *et al*. (2009). *Earth-Sci. Rev.*, 92, 53-79.

[13] Michard A. *et al*. (1993). *Tectonophysics*, 221, 173-193.

[14] Platt J.P. (1993). *Terra Nova*, 5, 119-133.

Formation of Fengtien Nephrite, Taiwan: inference from low-temperature hydrothermal thin (< 20 micrometer) zircon rim dating by nanoSIMS

Yui T[1*], Usuki T[1], Chen C[1], Ishida A[2], Sano Y[2]

1 - Institute of Earth Sciences, Academia Sinica, Taipei, Taiwan *tfyui@earth.sinica.edu.tw 2 - Atmosphere and Ocean Research Institute, The University of Tokyo

Nephrite in the Fengtien area occurs in association with serpentinites within the subduction-accretionary complex, the so-called Yuli belt, in the eastern part of the Central Mountain Range, Taiwan. In addition to nephrite, other metasomatic rocks, such as diopsidite and epidotite, might also be present between serpentinites and metasedimentary rocks. All these metasomatic rocks may or may not occur together. When all these rocks are present at one outcrop, the common lithologic sequence is serpentinite-nephrite-diopsidite-epidotite-metasedimentary rocks. Nephrite, diopsidite and epidotite are interpreted as resulting from Ca-Si-rich fluid-rock (serpentinite+country rocks) interactions under convergent tectonic environments. Field evidence and petrographic observations clearly show that while nephrite and diopsidite are mainly metasomatic products after serpentinite, epidotite is after metasedimentary rocks. The formation temperature has been estimated to be 300 - 400^{o}C based on regional geology and thermodynamic calculations by previous studies. Timing of these metasomatic processes, however, has not been constrained, although the hosting subduction-accretionary complex was thought to be of late Cretaceous in age due to paleo-Pacific subduction beneath the Eurasia continent and to be correlated with the Sambagawa belt in Japan. Zircons were separated from one epidotite sample in this study. Most of these detrital zircons were shown to have a thin zircon rim, which is less than 15 - 20 micrometer in thickness. These zircon rims are considered to be newly formed during metasomatic reactions between serpentinite and country rocks, leading to nephrite/diopsidite/epidotite formation. Occasionally, newly-formed zircon was also observed along zircon fractures. The CAMECA NanoSIMS NS50 at AORI of the University of Tokyo was employed to date these low-temperature thin zircon rims with a ~ 5 nA O^{-} primary beam confined to a ~ 15 micrometer diameter spot on zircon surfaces, which was pre-ablated for 5 minutes to remove the surface Au coating and any possible surface contaminants. Subsequent data acquisition time was 500 seconds. The resulting $^{238}U/^{206}Pb$-$^{204}Pb/^{206}Pb$ inverse isochron gave a young age of 3.3±1.7 Ma (MSWD = 2.1, n = 5). Following the regional geological background, the collision of the Eurasian plate and the Luzon arc began at 5.0 - 6.5 Ma in the Taiwan area. The present date clearly shows that the fluid-rock interaction leading to the formation of Fengtien nephrite would have taken place during the exhumation of the Yuli belt, which should be late Cenozoic subduction-accretionary complex related to subduction of the South China Sea plate beneath the Luzon arc. The Ca source and the process that triggered the infiltration of the inferred Ca-Si-rich fluid during rock exhumation, however, remain to be explored.

Dating of Proterozoic orogenic events around the Tanzania Craton: new insights from in-situ zircon and monazite geochronology

Boniface N[1*], Tsujimori T[2]

1 - University Of Dar es Salaam *nelson.boniface@udsm.ac.tz 2 - Okayama University Misasa

The western and southern margins of the Tanzania Craton border the Ubendian-Usagaran Orogenic Belts (UUOB) thought to have acquired their current configuration by collision, subduction, and magmatism in Paleoproterozoic times. The accumulation of *in-situ* zircon and monazite geochronology, including our own data, reveals the poly-orogenic nature of the Ubendian-Usagaran Belt. EPMA Th-U-Pb chemical dating of monazite and SIMS and LA-ICPMS U-Pb dating of zircon shows three clear Proterozoic metamorphic events. The Paleoproterozoic tectono-thermal magmatic events reveal a prolonged nature and are dated between 2.0 Ga and 1.86 Ga. During the Paleoproterozoic times the UUOB experienced orogenic processes that were coupled with subduction of oceanic lithosphere manifested by relics of eclogites. Eclogite-granulite transitional-facies metabasalts with a MORB-affinity yield U-Pb zircon ages of 1.89-1.87 Ga as a subduction event that was followed by a possible collisional event at 1.83-1.82 [1]. Preliminary U-Pb dating of zoned metamorphic zircon from a Ubendian eclogite with granulite-facies overprinting yields an upper-intercept age of 1.96 Ga for a possible eclogite-facies stage core and 605 Ma for granulite-facies rim. The Mesoproterozoic tectonic events occurred between 1.4 Ga and 1.0 Ga; these events overprinted the earlier events and do not show any evidence of subduction-related high-pressure metamorphism. In contrast, the Neoproterozoic times saw the subduction of an oceanic lithosphere in the Ubendian Belt between 590 Ma and 540 Ma [2]. U-Pb zircon geochronology for relict eclogites of mafic granulite blocks within migmatitic gneiss shows a Pan-African metamorphic event. The Neoproterozoic orogenic event is associated with the closing of small ocean basins between the Archean cratons of Tanzania and Bangweulu.

Reconstruction of a multiple tectono-metamorphic history based on reconnaissance of *in-situ* dating has just begun. Particularly, further understanding of a series of long-living orogenic processes surrounding the Tanzania Craton requires more comprehensive petrochemical studies and systematic *in-situ* geochronology. In this contribution, new insights, including our on-going project, into the metamorphic evolution of the UUOB are presented.

[1] Boniface N. *et al.* (2012). *Precambrian Research*, 192-195, 16-33.

[2] Boniface N. and Schenk V. (2012). *Precambrian Research*, 208-211, 72-89.

On the interpretation of Lu-Hf geochronology for prograde garnet

Cheng H

Tongji University. oahgnehc@gmail.com

The element-partitioning behavior of garnet generally favors a high parent/daughter ratio of Lu-Hf, making it a useful mineral for chronology. The assumption that the Lu-Hf age of prograde zoning-preserved garnet-bearing metamorphic rocks skews towards the early stage of prograde garnet growth, however, needs to be evaluated in specific samples. The most frequently reported garnet Lu-Hf ages are from bulk multigrain garnet fragments for which no attempt has been made to separate different garnet growth zones or generations. Because the growth of garnet may span over millions of years, such bulk-garnet-grains dates fall somewhere within the garnet growth interval. Linking the zoned-garnet Lu-Hf geochronology to a specific P-T segment or any related tectonic process is crucial to the age interpretation. We have summarize our recent garnet Lu-Hf dates for high-pressure eclogites from various orogenic belts in China and showed that interpretation of the Lu-Hf geochronology for prograde garnet could be rather diverse, such as skewing to the early garnet growth, an average of the whole growth span and reflecting later overgrowth of garnet. Ultimately, higher spatial resolution by means of separating concentric growth shells of chemical zoning within a single garnet, such as micro-drill sampling and laser ablation, is urgently required in order to unravel the vast amount of geochronologic information stored in the zoned garnet.

Geological evidence of "excess-argon wave" in K-Ar and Ar-Ar mica geochronology of metamorphic rocks

Itaya T[1*], Tsujimori T[2]

1 - Okayama University of Science *itaya@rins.ous.ac.jp 2 - Okayama University Misasa

The accumulation of data and knowledge on K-Ar (Ar-Ar) mica geochronology from HP-UHP metamorphic rocks reveals that the release of inherited argon from mica during dynamic recrystallization results in a "concordant" age. In other words, the high-ductility deformation is more significant to reset the K-Ar system in mica rather than thermally activated diffusion. However, anomalously old K-Ar (Ar-Ar) mica ages have been known from various localities of regional MP-HP-UHP metamorphic terranes, e.g., Dora Maira, Sesia, and Gran Paradiso (Italy), Sulu, Dabieshan, and Longmenshan (China), Kaghan valley (Pakistan), Tso Morari (India), Gourma (Mali), Tavsanli Zone (Turkey) and Betic Cordillera (Spain). The presence of these "discordant" ages suggests that a temperature-induced resetting of the Ar isotopic system of mica (muscovite and biotite) in polymetamorphic rocks is higher than generally thought. Although the K-Ar (Ar/Ar) "discordant" ages are generally attributed to the presence of excess argon, inherited from the precursor rocks during polyphase metamorphic events, the spatial distribution and amount of inherited argon are not always consistent; in fact, mica grains with a normal "concordant" age are ubiquitous in such polymetamorphic rocks.

In contrast, another process besides inherited argon to yield the extremely old "discordant" ages for micas is the 'Excess-Argon Wave' (EAW), which was first discovered in 1993. In a Barrovian-type metamorphic complex of the Longmenshan orogen, eastern Tibet, the upper kyanite-grade metapelite yields Ar-Ar biotite ages 4 to 5 times older than those in the sillimanite-grade. The kyanite-grade metapelite represents geological evidence of the fossilized EAW; we interpret that muscovite with a significant amount of radiogenic argon has decomposed to make the EAW. A discovery of detrital kyanite with extremely high excess argon (1-170 x 10^{-5} ccSTP/g, giving apparent ages of 14 to 16 Ga) from the Abukuma Mountains (NE Japan) also supports the presence of EAW in a middle crustal depth. More recently, we found another example of EAW in an eclogite-facies metagreywacke (quartz-rich kyanite eclogite) associated with a meta-peridotite body from Sanbagawa metamorphic belt (SW Japan). In this example, the EAW may have formed by an interaction between the metagreywacke and the meta-peridotite at eclogite-facies depth. We interpret that the mantle-derived noble gas (including extremely high radiogenic argon) diffused from mantle material into sediments during fluid exchange between deep-subducted sediments and mantle material.

Considering the above geological evidence, the EAW is a common geological phenomenon in nature. A high argon pressure environment at mid-crustal depth may occasionally trap large amount of excess argon into micas. Decomposition of minerals containing significant amounts of radiogenic argon can cause the EAW throughout fluid infiltration. Although dynamic recrystallization of phengitic mica is likely to reset the Ar isotope system, the limited-argon-depletion due to lower deformation prevents release of the trapped argon.

Garnet chronology in metamorphic systems

Lapen T

Earth and Atmospheric Sciences, University of Houston. tjlapen@uh.edu

Garnet is a common mineral in many types of medium- to high-grade metamorphic rocks. Texturally and chemically, garnet can record multiple discreet metamorphic events and continuous processes such as growth during prograde metamorphism. Analytically, garnet chronology has advanced in recent years such that the uncertainty of a Sm-Nd or Lu-Hf isochron age can be smaller than the duration of the process being dated. In order to strengthen linkages between the measured ages and segments of the metamorphic cycle they correspond to, advancements have been made in garnet growth modeling and microsampling techniques. Even with these advancements, samples have to be treated individually with analytical protocols tailored to the petrology of each sample being dated. This is particularly true for garnets with inclusion assemblages that dilute their typically high Sm/Nd and Lu/Hf ratios and/or inherited (unequilibrated) phases from the protolith or from an earlier metamorphic cycle.

Issues with inherited grains and troublesome inclusion assemblages are illustrated by ultra-high pressure (UHP) pyrope white schists from the Dora Maira nappe, western Alps, Italy. Lu-Hf garnet-whole rock geochronology applied to metamorphic rocks that contain old and unequilibrated zircon can effect both the isochron age and calculated initial Hf isotope composition. Preservation of old U-Pb zircon ages in the sample suggests that Hf within the zircons may have only partially equilibrated with the UHP metamorphic assemblage, producing two reservoirs of Hf: one in old zircon and another in UHP-equilibrated phases that crystallized at ~35 Ma. The Lu-Hf age and initial 176Hf/177Hf ratio for samples that included the inherited zircon in the garnet dissolution is 35.74±0.71 Ma (2σ) and 0.282580±7, respectively; this compares with 34.1±1.2 Ma and 0.282661±16 obtained for samples that only included minimal inherited zircon in the dissolution. Based on the present data, roughly 30-40% of the protolith zircon (by volume) equilibrated during UHP metamorphism. This partial equilibration preserves significant differences in Hf isotope compositions between the two reservoirs and is coupled with a systematic, but subtle difference in the measured Lu-Hf ages which are within error of one another. Because some zircon will be dissolved during sample digestion regardless of technique employed, any liberated Hf that did not isotopically equilibrate during metamorphism will result in the rotation of an isochron. In order to obtain accurate Lu-Hf ages of rocks such as the Dora Maira, the difference in age between protolith zircon and metamorphism must be less than a few tens of Ma or nearly all of the zircon must have equilibrated with its co-existing phases during metamorphism.

Samarium-neodymium chronology of the pyrope white schists is promising because the 147Sm/144Nd ratio of the pyrope garnet is determined by laser ablation ICPMS to average 4-5, relatively high compared to other garnet data published in the literature. Unfortunately, the low overall Nd concentration in garnet (~50 ppb) and abundant light rare earth element-rich phosphate mineral inclusions have so far precluded its application to this sample. Additional tests with aggressive dissolution methods that target the phosphate minerals are underway.

Timing of prograde and retrograde stages of an anticlockwise P-T path, Mary Kathleen fold belt, NE Australia: constraints from in-situ monazite, xenotime and rutile dating

Reinhardt J[1*], Zeh A[2], Rubenach M[3]

1 - University of KwaZulu-Natal *reinhardtj@ukzn.ac.za 2 - Goethe University Frankfurt 3 - James Cook University, Townsville

The Mary Kathleen Fold Belt in the central Mount Isa Inlier, NE Australia, is a classic low-pressure, high-temperature metamorphic terrain which experienced an anticlockwise P-T evolution [1]. The prograde P-T path passes through the andalusite into the sillimanite stability field where peak P-T conditions had been reached at 550-650 °C (from lowest- to highest-grade zones) at about 4 kbar. Retrograde metamorphism is recorded in cordierite schists by incipient, and locally pervasive, breakdown of cordierite due to H_2O infiltration, resulting in aluminosilicate + chlorite + quartz assemblages. The anticlockwise P-T evolution is well constrained by the successive formation of sillimanite, kyanite, and andalusite, as observed in the strongly re-hydrated rocks [1, 2]. Prograde metamorphism correlates with major compressive deformation resulting in the formation of a subvertical axial-planar foliation (S_2) in which the peak minerals are aligned. Retrograde overprinting produced random mineral orientations which, in case of pervasive retrogression, eliminated all signs of S_2.

In order to constrain the timing of the anticlockwise P-T evolution, accessory monazite, xenotime and rutile from prograde and retrograde rocks have been dated *in situ* by means of electron microprobe (*cf.* [3]) and LA-SF-ICP-MS. Using a large set of non-retrograde samples, monazites present in the schist matrix and as inclusions in andalusite and cordierite have been analysed by electron microprobe, which resulted in a unimodal age peak with a mean value of 1581±5 Ma (based on nearly 400 analysis points). *In-situ* dating by LA-SF-ICP-MS on monazite grains, including S_2-aligned monazite, from samples lacking evidence for hydrous retrogression yielded a concordant U-Pb age of 1580±4 Ma, which is practically identical to the microprobe result. Monazite and xenotime in strongly retrogressed samples show features that suggest they have grown during hydration and are not inherited from the prograde assemblages. They tend to form large, randomly oriented euhedral crystals, and monazite may show distinct concentric birefringence zoning. Xenotime appears to be confined to retrograde samples. Compared to prograde monazite, LA-SF-ICP-MS dating of monazite and xenotime from two retrograde kyanite-chlorite-rich samples gave slightly younger U-Pb ages of 1572±5 and 1573±4 Ma, respectively.

Prograde and retrograde rutile yielded identical U-Pb ages of *ca.* 1570 Ma, most likely dating the cooling of the respective rocks to below 500°C. The new results from monazite, xenotime and rutile confirm that the anticlockwise P-T path of the Mary Kathleen Fold Belt is monocyclic. In combination with thermobarometric constraints the age data indicate that the initial cooling from peak temperatures to 500 °C was relatively rapid, in the order of 10-15 °C per million years.

[1] Reinhardt J. (1992). *Geological Magazine*, 129, 41-57.

[2] Reinhardt J. (2011). *European Journal of Mineralogy*, 23, 795-803.

[3] Montel J.-M. *et al*. (1996).*Chemical Geology*, 131, 37-53.

Dating UHT metamorphism in the Brasília Belt: further evidence from zircon $\delta^{18}O$ signature

Della Giustina M[1*], Martins Pimentel M[1], Whitehouse M[2], Ferreira Filho C[1], Flores V[1]

1 - Universidade de Brasília *maria_emilia@unb.br 2 - NORDSIM

In the Brasilia Belt, high-grade rocks are exposed in the Anápolis-Itauçu Complex, which consists of ortho- and paragranulites, as well as granites and layered mafic-ultramafic complexes. Previous investigations on M-UM bodies have shown that they represent a voluminous magmatic event dated at 680-670 Ma and, due to spatial relationship to the UHT occurrences, they are interpreted as the additional heat source necessary for the development of such special mineral assemblages on contiguous paragranulites. In these layered complexes, zircon grains exhibit internal textures typical of a coupled dissolution-reprecipitation process, which have affected the U-Pb signature and the trace element content. Zircon fluid inclusions are more abundant in altered rims and are mainly aqueous in composition. Conversely, $\delta^{18}O$ SIMS analyses reveal homogeneous values even in totally recrystallized sections, thus preserving the original, primary igneous signature. This data suggests that the magma, originally with a mantelic signature, has interacted with a heavier $\delta^{18}O$ fluid during emplacement and crystallization. Nd isotopes have already proposed a variable but consistent crustal contamination of these layered complexes. Thus, zircon oxygen isotopic signature indicates that fluids/melt from metamorphic reactions ongoing in adjacent rocks may have contributed to the higher $\delta^{18}O$ values obtained in the M-UM complexes. Also, the conservation of the primary oxygen isotopic signature, even in the recrystallized domains, reveals that the system has remained closed to O during high-grade metamorphism and, hence, the fluids responsible for the coupled dissolution-reprecipitation process in zircon grains did not have any external contribution. These data, therefore, provide further evidence that peak metamorphic conditions were attained at *ca*. 680 Ma in the Brasilia Belt.

Myrmekites from the Weinsberg granite, Moldanubian zone: underlying processes and thermodynamic model

Abart R[1*], Heuser D[1], Habler G[1]

1 - Department of Lithospheric Research, University of Vienna

*rainer.abart@univie.ac.at

Myrmekites have attracted the attention of petrographers for more than a century. Several genetic models have been proposed, which are still discussed controversially. We report on myrmekites from the Weinsberg granite of the Moldanubian zone of upper Austria. There, myrmekites replace large crystals of perthitic alkali feldspar along former contacts with primary magmatic plagioclase. The myrmekites are comprised of an intimate intergrowth of quartz lamellae or rods enclosed in a matrix of plagioclase, where the grain size decreases towards the replacement front. The myrmekite plagioclase has XAn = 0.25 and is somewhat more sodic than the primary magmatic plagioclase (XAn = 0.32). Crystal orientation imaging using EBSD reveals grain internal deformation in the quartz, whereas the plagioclase is largely undeformed. The presumed original contact between primary alkali feldspar and the neighbouring plagioclase is marked by a continuous layer of quartz suggesting that the reaction initially produced a corona microstructure and only later switched over to form the symplectic microstructure. In the fine-grained domains of the myrmkite the anorthite content of the plagioclase increases systematically towards the interfaces with the quartz rods or lamellae. Based on this evidence we infer fluid mediated replacement of alkali feldspar by the myrmekite. The replacement was metasomatic on the scale of the myrmekite domains requiring addition of sodium and calcium and removal of potassium from the reaction site. In contrast, silica and aluminum appear to have been conserved across the replacement front. Phase relations suggest formation temperatures around 500°C. Myrmekite formation involves two potentially rate-limiting processes: On the one hand, the precursor alkali feldspar must be dissolved and the quartz and plagioclase of the myrmekite must be precipitated at the replacement front. The bulk of the microscopic processes involved in this step determine the kinetics of the respective interface reaction. On the other hand, aluminum and silicon must be re-distributed across the replacement front, as the Al/Si proportions are different in the precursor alkali feldspar and in the newly formed quartz and plagioclase requiring diffusion of Al- and Si-bearing species along the replacement front. A thermodynamic model is presented that employs the principle of maximum free energy dissipation as a criterion for selecting the most favourable micro-structural type. Parabolic growth is predicted for a corona microstructure, which is more favourable during incipient reaction than the linear growth that is predicted for the symplectic microstructure. In addition, the composition zoning of matrix plagioclase is predicted for the case, when component re-distribution along the replacement front becomes rate-limiting and the kinetics of the interface reaction is comparatively fast. The grain-internal deformation of myrmekite quartz is interpreted as a growth feature related to variations of the transformation strain along the myrmekite replacement front, which is, in turn, controlled by the relative mobilities of the Al- and Si-bearing species in the replacement front.

Processes governing garnet growth during prograde metamorphism of lawsonite eclogite from south of the Motagua Fault Zone, Guatemala

Bradley D*, Sisson V, Lapen T

Department of Earth and Atmospheric Sciences, University of Houston

*drbradley@uh.edu

Garnet nucleation and growth rates have been attributed to two different mechanisms: diffusion controlled, and interface controlled. In order to identify which mechanism drives garnet growth in a particular system, chemical zonation, crystal size distribution, and textural analysis must be performed. This analysis, when applied to garnets in lawsonite eclogites from south of the Motagua Fault Zone, has revealed a complex growth history that has neither been fully explained in prior literature, nor can it be explained fully through use of one growth model.

The major and trace element concentration profiles from garnet core to rim follow typical prograde element zoning patterns within the interior of the garnets. However, the garnet rims exhibit an increase in concentration of Mn as well as the heavy rare earth elements (HREE) which is at odds with expected prograde element zoning patterns. Fe and Ca concentrations are relatively constant from core to rim in all garnet samples, but at approximately the same distance from the rim that the Mn concentration begins to increase, Fe decreases and Ca increases by a few percent towards the rim. REE profiles also display similarly complex zonation patterns; a roughly bell-shaped core-to-rim depletion profile typical of the HREE is interrupted near the rim by a subsequent enrichment. These data, along with crystal size distribution and textural analysis serves as evidence for the identification of multiple mechanisms of garnet growth and suggests the possibility of either multiple stages of garnet growth or changes in growth rate which must be constrained and defined before geochronological analysis of these samples can be conducted.

Geochemistry of the Hlagothi Complex, Kwazulu-Natal, South Africa

Dunlevey J[1*], Misra S[2]

1 - University of Limpopo *john.dunlevey@ul.ac.za 2 - University of KwaZulu-Natal

The ~2.98 to 3.05 Ga Hlagothi Igneous Complex (HIC) was intruded as multiple sills into the Mesoarchaean Pongola Supergroup overlying the granitoid basement of the Kaapvaal Craton in the eastern KwaZulu-Natal, South Africa.

The aggregated maximum thickness of sills is ~500 m, and individual sills are <200 m thick. Although the HIC sills are somewhat altered to an actinolite-tremolite-serpentine-chlorite assemblage, identification of relict textures and mineral remnants indicates a three-fold subdivision. The base of each intrusion consists of an olivine-bearing wehrlite, olivine websterite or lherzolite zone, followed by two-pyroxene bearing layer overlain by a gabbro unit. This sequence is indicative of gravity-driven in-situ fractionation of the whole body. The whole-rock geochemistry of the HIC is minimally altered, when compared with CNKM-Al_2O_3-FeO^T diagram, and can thus be used to evaluate the original magmatic composition and evolution. The HIC represents an Al-undepleted komatiite sequence whose parent magma [Al_2O_3/TiO_2 ~25, Magnesium number (Mg#) ~0.81] appears to have been derived by ~50% partial melting of a garnet peridotite in the upper mantle at ~1770^{o}C and 3 to 7 GPa, at a depth of ~200 km below the continental crust. The parent magma experienced complex two-stage fractionation; in the first stage the komatiite parent fractionated to a komatiitic basalt (with a minor change of Mg# from ~0.83 to 0.77) leaving olivine and orthopyroxene as cumulates. The komatiitic basalt further evolved through clinopyroxene and plagioclase crystallization (resulting in a large decrease of Mg# from ~0.77 to 0.50), to produce a gabbroic magma that solidified at ~1360^{o}C and 0.7 GPa. The HIC (Al_2O_3/TiO_2 ~20) is close in composition to the Abitibi Greenstone Belt komatiites, Canada, and represents a sequence where an Al-undepleted komatiite magma fractionated to form a Ti-depleted komatiite.

Unlike the widely accepted mantle plume model, the HIC magma was apparently generated by partial melting of an enriched upper mantle source, followed by a complex two-stage fractionation.

Integrating mineralogy, geochemistry and airborne electromagnetics for greenfields mineral exploration in the regolith-dominated Albany-Fraser Orogen, Western Australia terrain: understanding surface geochemistry

Gonzalez-Alvarez I*, Ley-Cooper Y, Salama W

CSIRO, CESRE Division, Minerals Down Under Flagship, Western Australia
*i.gonzalez.alvarez@gmail.com

The Albany-Fraser Orogen (AFO) in the south of Western Australia is a regolith-dominated terrain with very limited outcrop. Field observations, drilling, mineralogy and airborne electromagnetics (AEM) data show that the regolith ranges in thickness from ~5 m to a maximum of ~60 m and comprises 2-25 m of transported cover an *in situ* ranges between overlying 22 to 70 m saprolite. There are four principal regolith units: a ferruginous sediments package, silcrete (4-20 m thick), an upper kaolinitic saprolite and a lower ferruginous saprolite unit (combined 18-50 m thick), developed on a granitic/gneiss and gabbro/basalt basement. These units are laterally continuous throughout the area surveyed.

The interpreted AEM conductivity-depth sections in the area were superimposed with drilling information and field observations on the regolith stratigraphy. The thickness of the transported cover (2-25m) fits the AEM interpretation of the less conductive unit at the top of the profiles. The transported cover corresponds mainly with aeolian sands at the surface, and cemented sands and gravels at depth, which are poor electrical conductors. The upper kaolinitic saprolite is clearly defined in the drill core/cuttings, whereas the AEM shows a weak conductive response with transitional upper, lower and lateral boundaries. The lateral variability is interpreted to be due to patchy cementation of the silcrete. Where the silcrete is weakly cemented, it is more permeable to fluid flow and appears to be associated with more intense vertical weathering so that the upper kaolinitic saprolite appears as a more conductive in the AEM profiles. However, the as the silcrete becomes more cemented, the underlying units are more sheltered from vertical weathering, reducing the kaolinite content and, therefore, behaving as a more resistive unit with a lower EM response.

The lateral variability in weathering of the upper saprolite does not reflect any change in basement lithology, and possibly has significant implications for exploration. The zones of poorly cemented silcrete potentially represent "windows" through which trace elements derived from the basement or residual regolith might be dispersed vertically into surficial regolith units to produce a reliable geochemical signal. In contrast, where the silcrete is a more strongly cemented dispersed elements will be prevented from reaching the surface.

Excess fluorine in vacancy-rich mica solid solutions

Robert J

IMPMC (UMR 7590), Université Pierre et Marie Curie, CNRS, IRD, MNHM, France
*jean-louis.robert@impmc.upmc.fr

In the K_2O-MgO-SiO_2-H_2O-HF system, an extended solid solution exists between two end-members the tetrasilicic mica $K(Mg_{2.5v0.5})Si_4O_{10}(OH,F)_2$ where v represents an octahedral vacancy, and the virtual $^{[4]}Mg^{2+}$ end-member $KMg_3(Si_{3.5}Mg_{0.5})O_{10}(OH,F)_2$, at temperatures below 600°C and 0,1 GPa water pressure. Along the Si_4 - $Si_{3.5}Mg_{0.5}$ join, the solid solution range is limited to $0 < {}^{[4]}Mg^{2+} < 0.35$. High $^{[4]}Mg^{2+}$ contents, >0.35 pfu, yield an assemblage $^{[4]}Mg^{2+}$-mica and forsterite. In the F-free system, several kinds of OH groups are identified along the join: trioctahedral, bonded to $3Mg^{2+}$, at about 3735 cm^{-1} and dioctahedral, bonded to $2Mg^{2+}$ and adjacent to vacant octahedral site close to 3695 cm^{-1}. These two types of hydroxyls are sensitive to local fluctuations of the tetrahedral composition (second neighbour effect). The presence of $^{[4]}Mg^{2+}$ generates additional OH bands, at lower wavenumbers, corresponding to the associations $^{[6]}Mg_3$-OH → $^{[4]}(Si_5Mg)$, for trioctahedral environments, and to $^{[6]}(Mg_2v)$ → $^{[4]}$(Si, Mg) for dioctahedral ones. The intensities of these new bands increase with the $^{[4]}Mg^{2+}$ content. Along the join, $^{[4]}Mg^{2+}$ and $^{[6]}v$ induces local charge imbalances in tetrahedral and octahedral layers respectively. Surprisingly, these two "defects" are associated in the structure, which provokes a strong charge imbalance on the apical oxygens of (MgO_4) tetrahedra adjacent and a vacant octahedron. Therefore, these apical oxygens trap an additional hydroxyl groups, whose amount strictly follows the $^{[4]}Mg^{2+}$ content. The structural formula of the mica with the highest $^{[4]}Mg^{2+}$ content is $K(Mg_{2.75}v_{0.25})(Si_{3.5}Mg_{0.5})O_{9.5}$ $(OH)_{2.5}$.Fluorine can quantitatively replace all hydroxyl groups with a partition coefficient between sites which is correlated with the intensity of hydrogen bonding between the hydroxyl proton and surrounding oxygens. F favours sites with low H-bonding. Thus, the new, interstitial hydroxyls can also be replaced by fluorine, which gives the structural formula $K(Mg_{2.75v0.25})(Si_{3.5}Mg_{0.5})O_{9.5}F_{2.5}$. This leads to consider that positives F anomalies sometimes observed in phyllosilicates, and usually rejected as faulty, can be due to the presence of additional fluorine, which can reach 25% excess.

Keywords : micas, vacancy, tetrahedral Mg, protons, fluorine

Geochemistry of the late Neoproterozoic post-collisional volcanic rocks in the Meknas area, SE Sinai, Egypt

Sadek Ghabrial D

National Research Centre. dghabrial@yahoo.com

The geochemical features of the Neoproterozoic Meknas volcanic rocks in southeastern Sinai, Egypt, have been studied. These rocks belong to the northernmost segment of the Arabian-Nubian Shield (ANS) and are present as successive sheets ranging in composition from andesite to rhyolite. Geochemically, they display medium- to dominantly high-K calc-alkaline affinity and are characterized by relatively high silica contents, clear LILE- and LREE-enriched patterns with clear Nb depletion, being consistent with the nature of Dokhan volcanics from other areas in Egypt. These geochemical features are shown by the rocks originated in a post-orogenic setting that has been previously modified by metasomatic melts/fluids released from subducted slab or sediments and could not be the result of crustal contamination. They were mainly generated through fractional crystallization process, whereas the crustal contamination or assimilation played a limited role in their evolution. The model of orogenic collapse and extensional thinning of the lithosphere after continental collision can be suggested for the generation of this Ediacaran magmatism. In this model, lithosphere delamination and/or slab break-off are the main mechanisms proposed to explain the magma generation.

OH-defect content in detrital quartz grains as archive for crystallization conditions and information source for crustal sampling

Stalder R

University Innsbruck. roland.stalder@uibk.ac.at

Infrared spectra of 433 oriented detrital quartz grains from different large sedimentary reservoirs worldwide were recorded and evaluated with respect to their OH-defect concentration (expressed as wt ppm water), reaching from 0 - 160 wt ppm for individual grains. Two of the most OH-defect rich grains from our data set were observed in oldest and the most strongly cemented sandstone investigated (1400 Ma old Jotnian sandstone from Dalarna/Sweden), suggesting that the defects are barely affected during diagenesis conditions even over extended geological time scales. OH-defect contents averaged over each individual sample range between 5 and 20 wt ppm defect water, with a mean value around 10 wt ppm. Sand samples tend to have lower average OH-defect contents than sandstones deposited earlier from a similar source region. Furthermore, the average OH-defect content of each sample is well correlated to its chemical maturity and mainly reflects the fraction of water-poor (< 5 wt ppm defect water) quartz grains. Combined with results from high-pressure experiments in different model systems, the new results may provide an indirect method to estimate the source rock inventory of the upper crust (igneous versus metamorphic or depth of the sampled crustal section). Results further suggest that provenance analyses of mature sediments and sedimentary rocks could benefit from the analysis of OH-defect content in quartz, as quartz grains from distant sources are by far less under-represented than unstable minerals from the same source.

Magmatic olivine trace element variations as a mirror of mantle source heterogeneity

Sushchevskaya N[1], Belyatsky B[2], Krymsky R[3], Migdisova N[1], Sobolev A[1]

1 - Vernadsky Institute of Geochemistry RAS, Moscow, Russia *sobolev@geokhi.ru

2 - VSEGEI CIR 3 - VSEGEI CIR, S.Petersburg, Russia

Oceanic magmatism evolution within rift zones framing northeastward of Antarctica occurred due to spreading propagation from 160 to 2 m.y. ago and tholeiite magmas identified mainly pointed to an enriched source. The main reason of E-MORB-type melts formation is determined by source heterogeneity specified by: recycling of old oceanic crust, hotspots within immediate proximity to rift zone, formation of metasomatised mantle at the early stage of ocean opening which is involved in melting process later on.

We have studied olivine composition as olivine is a main liquidus phase of tholeiite and plume magmas of Antarctic continent (Schirmacher and Jetty oasises) and East Antarctic flanking spreading zones (Powell, Bransfield, Southwestern Indian Ridge within Bouvet Triple Junction - BTJ). Minor elements such as Ni, Mn, Ca and Cr in olivine can be tracers of the melting source. Ni excess over Mg, and Mn deficiency over Fe in olivine phenocrysts suggest the presence of olivine-free pyroxenite lithologies in the source of primary melts. Peridotite-derived and pyroxenite-derived melts are mixing in the mantle. Following crystallization of these hybrid magmas produces olivine phenocrysts with definite enrichment in Ni and depletion in Mn.

Our estimations of pyroxenite component share in the mantle source for the Mesozoic Karoo-Maud plume based on the olivine compositions of Schirmacher Oasis dolerites show 20-30% and increase up to 60-80% for later Jetty alkaline basalts and enriched basalts of the early Powell spreading zone. Pyroxenite component varies in general within 20-30% for single outcrop sampled but in some cases olivine phenocryst compositions are characterized by extremely variations within single sample and pyroxenite share changes from 0 to 90% reflecting inhomogeneity intermediate chamber melts.

There is some correlation between amounts of suggested pyroxenite component and Pb isotope composition of the East Antarctica magmas. Basic lavas of the studied region originated under Karoo-Maud plume influence and riftogenic as well (from Powell, Bransfield and BTJ) fall on a single trend within Pb isotope diagram between depleted source (MORB-like) and enriched one which was formed during long-lasted geodynamic and geochemical evolution of the eastern margin of Antarctica. Development of Karoo-Maud plume caused the formation of considerable mantle heterogeneity and contributed of disintegrated continental blocks within the forming South Ocean. Magmatism of the Powell old spreading basin is characterized by greater range of enrichment and evidence to possible melting of pyroxenites which represented the fragments of low parts of continental lithosphere involved into the melting process due to asthenospheric mantle upwelling in spreading zones.

Ni-Mg-phyllosilicates from Bon Accord, Barberton, South Africa: new data on willemseite and nimite

Villanova-de-Benavent C[1*], Tredoux M[2], Aiglsperger T[1], Proenza J[1]

1 - Dept. Cristal., Miner. i Dipòsits Minerals; Fac. Geologia; UB
*cvillanovadb@ub.edu 2 - University of the Free State

Willemseite and nimite are Ni-Mg-phyllosilicates first reported in a small deposit near the Scotia Talc mine, in the Bon Accord area, Barberton District, South Africa [1, 2]. The Bon Accord deposit was completely mined out, and its original structure may only be inferred from early descriptions and a few small hand specimens. The orebody was possibly composed of an undeformed Ni-oxide-dominant core, containing trevorite (Ni-Fe spinel), bunsenite (Ni-oxide), liebenbergite (Ni-olivine), Ni-Co-Cr spinels and minor hydrated silicates, enclosed in a Ni-phyllosilicate-dominant foliated envelope of nepouite (Ni-lizardite), willemseite (Ni-talc), nimite (Ni-chlorite), bonaccordite (Ni-borate) and minor trevorite [3].

The samples used are from the Bon Accord collection of the University of the Free State. The two phases were separated by hand-picking from the fraction >150 µm of crushed and sieved material. Powder X-ray diffraction (XRD) and electron microprobe (EMP) analyses were performed for a first mineral identification. In addition, micro-Raman spectroscopy was used to complete the characterisation of these minerals. In the literature, very little mineralogical information on willemseite and nimite exists, and to the knowledge of the authors, available mineral databases of micro-Raman spectra do not show references of these minerals, or they are unreliable. In this work, micro-Raman results of these rare Ni-phyllosilicates are complemented by an accurate mineral identification and a chemical characterisation.

According to the XRD data, characteristic basal spacings have been observed at 9.4 and 3.1 Å for willemseite; and 14.4, 7.1, 4.7, 3.6 and 2.8 Å for nimite. The mean structural formula of willemseite is $(Ni_{1.7}Mg_{1.1}Fe^{3+}_{0.2})(Si_{3.9}Al_{0.04})O_{10}(OH)_2$, and the formula of nimite is $(Ni_{4.5}\ Mg_{4.0}Al_{2.0}Fe^{2+}_{1.3}Fe^{3+}_{0.1})(Si_{6.2}Al_{1.8})O_{10}(OH)_8$, which do not differ significantly from the ones published by de Waal [1, 2].

Raman spectra were obtained with a HORIBA Jobin Yvon LabRam HR 800 dispersive spectrometer, equipped with an Olympus BXFM optical microscope. Non polarized Raman spectra were obtained by applying a 532 nm laser (beam size around 2 µm) at 0.5 mW, with 4 measurement repetitions for 20 seconds each.

The Raman results for willemseite and nimite show distinctive characteristic features. In general, bands in willemseite are well defined and have higher intensities, whereas bands in nimite are wider and less intense. In willemseite, very strong bands were observed at 185, 296, 383, 671, 3622, 3645 and 3660 cm^{-1}, and weaker bands were at 109, 410, 789 and 1043 cm^{-1}. According to [4], 185 and 671 are typical bands for talc, and are also associated with willemseite (RRUFF database). In nimite, the bands are 196, 279, 547, 678 and 3645 cm^{-1} and show similar low intensities. Those at 196, 279 and 548 are also found in clinochlore and chamosite (Mg and Fe analogues, respectively; RRUFF database), and bands at 369 and 678 are slightly shifted.

[1] de Waal (1970). *Am Miner*., 55, 18-30.
[2] de Waal (1970). *Am Miner*., 55, 31-42.
[3] Tredoux *et al.* (1989). *J Geophys Res*, 94(B1), 795-813.
[4] Holtz *et al.* (1993). *Phys Rev B* 48, 13312-13317.

CO_3-bearing apatite-ellestadite series mineral from Japan

Banno Y[1*], Miyawaki R[2], Momma K[2], Bunno M[3]

1 - Geological Survey of Japan, AIST *y-banno@aist.go.jp 2 - National Museum of Nature and Science 3 - The University Museum, The University of Tokyo

A CO_3-bearing apatite-ellestadite series mineral was found in a specimen of skarn xenolith in two-pyroxene andesite at a quarry in Tadano, Fukushima Prefecture, Japan. The skarn xenolith consists mainly of wollastonite, grossular, andradite, gehlenite, apatite supergroup mineral and vesuvianite. The apatite supergroup mineral occurs as subhedral to anhedral crystals, up to 0.6 mm long. Backscattered electron images of the mineral indicate that it is composed of dark and light parts that correspond to P-rich and P-poor parts, respectively. The P-rich core is surrounded by the P-poor rim. The other P-poor part cuts the P-rich host to form veins. This texture indicates that the P-rich parts formed earlier than the P-poor parts. Chemical analyses were performed on an electron microprobe. The P-rich part is F-rich hydroxylapatite. Qualitative analyses by a microprobe confirmed that F, Cl, Si and S were present in the P-poor part. The IR spectrum of the P-poor part exhibited the ν_3 mode of the carbonate group. It was observed at 1417 and 1454 cm^{-1}, demonstrating a partial replacement of PO_4 by CO_3. Chemical formula for the P-poor part was calculated on the basis of Ca = 5 apfu. CO_2 contents were calculated on the assumption of P + Si + S + C = 3 apfu. H_2O calculation was based on the assumption F + Cl + OH = 1 apfu. Representative analysis of the P-poor part gave; SiO_2 9.60, CaO 56.89, SO_3 5.05, P_2O_5 20.90, F 0.54, Cl 1.30, H_2O(calc.) 1.24, CO_2(calc.) 4.02, O = F+Cl -0.52, total 99.02 wt.%, corresponding to $Ca_{5.000}[(PO_4)_{1.452}(SiO_4)_{0.787}(SO_4)_{0.311}(CO_{2.971})_{0.450}]_{\Sigma 3.000}(OH_{0.679}F_{0.140}Cl_{0.181})_{\Sigma 1.000}$. The P-poor part has a wide range of varying composition; Si = 0.31-0.92, S = 0.09-0.46, C (calc.) = 0.15-0.54, P = 1.13-2.40, F = 0.05-0.34, and Cl = 0.04-0.35 apfu. There is a remarkable inverse correlation between Si and P in the P-poor part as shown in Figure 1.

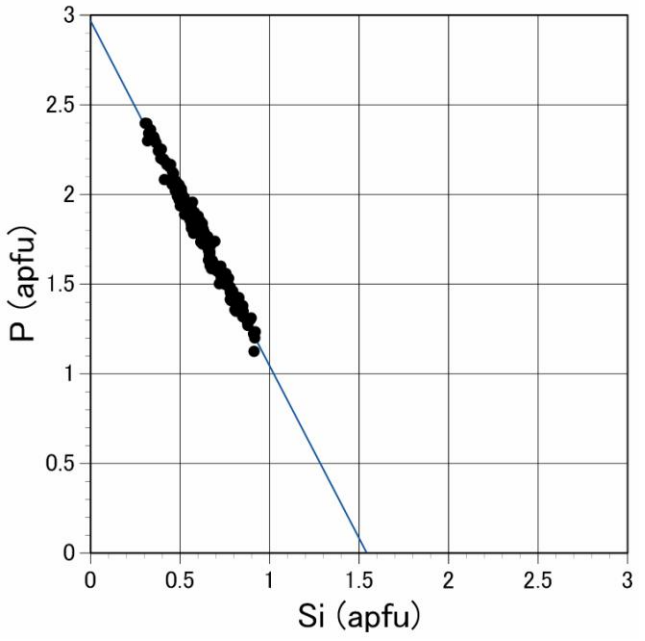

Figure 1: Si-P plots of the P-poor part in the apatite supergroup mineral.

The regression equation is P = -1.92Si + 2.97 (r^2 = 0.98). This fact indicates that the substitution mechanism $(SO_4,CO_3)^{2-} + (SiO_4)^{4-} = 2(PO_4)^{3-}$ is most likely present for the P-poor part. Therefore, it was concluded that the P-poor part corresponds to a CO_3-bearing apatite-ellestadite series mineral. The unit cell parameters of CO_3-bearing apatite with P = 1.81, Si = 0.57 and S = 0.22 apfu are; hexagonal *a* = 9.459(1) and *c* = 6.913(2) Å.

Formation conditions of quartz recorded by OH-point defects – experimental and analytical approach

Baron M[1], Stalder R[2*], Konzett J[2]

1 - University of Oslo 2 - University of Innsbruck *roland.stalder@uibk.ac.at

Quartz is a common nominally anhydrous mineral of the Earth's crust. It occurs in many different geodynamical environments both as a primary or secondary phase. Trace amounts of water structurally incorporated as OH-point defects, commonly act as charge compensators in substitution reactions such as Si^{4+} by Al^{3+}, with charge balance maintained by monovalent cations (H^+, Li^+ and Na^+), trivalent (Fe^{3+}, B^{3+}) or pentavalent cations (P^{5+}). The systematic study of the OH-point defect generation can possibly give us powerful insights about the quartz formation conditions especially in pegmaitic bodies.

The geochemical behavior of OH incorporation in quartz in Al-, B- and Li-bearing systems (granite-tourmaline-water and granite-spodumene-water) was studied in order to determine the effect of pressure and temperature on OH-defect generation. Piston-cylinder experiments were carried at pressures between 2.5 and 25 kbar and temperatures between 800 and 1050°C. Oriented and polished single quartz crystals were characterized with FTIR spectroscopy and water contents were calculated using mineral-specific and general wavelength-specific calibrations. The observed OH absorption features were assigned to Al^{3+}- substitution (Al-H defect, band-triplet at 3320, 3383 and 3434 cm^{-1}), B^{3+}-substitution (sharp absorption band at 3597 cm^{-1}), Li^+ -incorporation (weak absorption band at 3475 cm^{-1}) and hydrogarnet $(4H)_{Si}$ defect (absorption at 3585 cm^{-1}). Experimental results were also compared with spectra obtained from natural quartzes from both Li- and B- bearing pegmatites.

As a result, synthesized quartz crystals from both chemical systems indicate a negative correlation of incorporated OH content versus pressure. In the B-bearing system, OH-defects cause OH concentrations (expressed as wt ppm water) of about 450-750 ppm H_2O at 5 kbar and 72-106 ppm H_2O at 25 kbar. In Li-bearing system virtually OH-free quartzes were observed from high pressure (10-15 kbar) runs, but 360-549 ppm H_2O were measured on crystals equilibrated at lower pressures (5 kbar). Therefore, our results imply that IR spectra of quartzes can be used as a tracer of petrological formation conditions. Moreover, quantifying charge balancing B^{3+}- and Li^+- content from IR spectra is a novel and indirect analytical tool to detect traces of light elements in quartzes.

Early Paleozoic HiBaSr diorites from the Tatra mountains, Poland: consequences for plate tectonic evolution of Gondwana

Gawęda A[1*], Burda J[1], Golonka J[2]

1 - University of Silesia *aleksandra.gaweda@us.edu.pl 2 - University of Mining and Metallurgy

So-called HiBaSr granites were identified by Tarney and Jones [1] on the basis of trace elements characteristics: high content of Ba, Sr and LREE and low content of Nb, Ta and HREE. They are interpreted as a result of interaction of mantle and crustal material. In most cases the subducted plate delamination, upwelling the asthenosphere and further partial melting of the lower crust is suggested as a plausible model for the HiBaSr granite-diorite formation [2]. Four investigated samples of orthogneisses from Western Tatra Mountains represent two petrographically different types: biotite orthogneisses and amphibole-biotite orthogneisses.

Analysed samples could be classified as high-K - calc-alkaline diorite-monzodiorite, enriched in phosphorus (P_2O_5 = 0.43-0.62). Meta-diorites show very low Rb/Sr ratios (0.092-0.094), anomalous Ba and Sr enrichment, moderate LREE enrichment (Ce/Yb = 17-19) and very low Ta and Nb content. All these features suggest their HiBaSr character [1].

U-Pb LA-MC-ICP-MS analyses of the oscillatory-zoned zircon crystals yield a concordia age of 510 ± 4 Ma (MSWD= 3.2), interpreted here as the age of crystallization of igneous protholith. Initial I_{Sr}^{510} ratio equals = 0.70368, while e_{Nd}^{510} = 4.067, suggesting mantle origin of primary magma. Calculated T_{DM} at 0.864 Ga is comparable with T_{DM} age of mafic precursors for Tatra granite. Geochemical characteristics and U-Pb age data suggest the presence of post-Cadomian magmatic event at c. 510 Ma, connected with subducted plate delamination and mantle upwelling at the northern margin of Gondwana. Taking into account the plate-tectonic model for 510 Ma, these data suggest the continuum between the Cadomian orogenesis and opening of the Rheic Ocean.

[1] Tarney J. and Jones C.E. (1994). Trace element geochemistry of orogenic igneous rocks and crustal growth models. *J. Geol. Soc. London*, 151, 855-868.

[2] Fowler M.B., Kocks H., Darbyshire D.P.F. and Greenwood P.B. (2001). Petrogenesis of high Ba-Sr plutons from Northern Highlands Terrane of the British Caledonian province. *Lithos*, 105, 129-148.

Characterization and evaluation of basalt rocks from Egypt for possible applications

Hassan M

Central Metallurgical R&D Institute hassan_mervat@yahoo.com

Mineralogy, chemistry and petrography of basalt rocks from four areas; Gebel Abu Terrify (Cairo-Suez Road), El Arish, Sinai, Baharia Oasis and Fayium were carried out using X-ray diffraction (XRD), X-ray Fluorescence (XRF), optical and scanning electron microscopy. The results from XRD analysis of fresh basalt samples show plagioclase as the most abundant mineral in addition to forsterite and fayalite. Clinopyroxene; auguite and enstatite are recognized. Iron oxide and oxyhydroxide represented by hematite, magnetite and goethite. However, the XRD pattern of altered basalt revealed the abundance of phyllosilicate minerals such as kaolinite, smectite, celadonite and chlorite in addition to carbonate and zeolite.

The mineralogical composition of basalt samples of Gebel Abu Terrify showed that, the clinopyroxene (Augite), feldspar (albite) and olivine (forestrite) are pyrogenic crystals, as remnant of basalt. Trioctahedral smectite is the principal clay minerals phase present in these samples. Calcite and zeolite are recognized in the samples as main non-clay minerals in variable concentrations. These authogenic minerals formed in joints, fractures, and interstices, although most occur in central cavities of basalt pillows. Overall alteration of the G. Abu Terrify basalts ranges from 50% to ~100% based on petrographic observations of thin sections, SEM as well as XRD patterns. One characteristic of this alteration is the replacement of olivine phenocrysts by iddingsite. In general, the basaltic samples are highly enriched in MgO, Ca_2O_3 and Fe_2O_3 in addition to traces of TiO_2 (1-2 %), total alkali (2-3%), Zn (0.014%), Mn (0.13-2.68%) and P (0.15-0.30%). However, loss in weight is dependent on the degree of basalt alteration.

The basalt samples from different localities were evaluated as soil conditioners to provide the plants with the major and minor nutrient as well as, the samples were evaluated as adsorbent to remove lead from synthetic solution. The results will be presented later.

Mineralogy and petrography of xenoliths from Neogene volcanics, Tokaj Mts. (NE-Hungary)

Horváth A, Kristály F*, Zajzon N

Institute of –Mineralogy and Geology, University of Miskolc, Miskolc, Hungary
*askkf@uni-miskolc.hu

The igneous rocks of the Tokaj Mts., NE Hungary (Carpathian Basin) are situated in a half graben, formed during the large-scale strike-slip movements between the ALCAPA and Tisza-Dacia megaterranes. The Tokaj Mts. belong to the Inner Carpathian Volcanic Belt which was formed in a back-arc basin setting, during the Miocene closure of the Tethys Ocean remnants. The igneous sequence of the Tokaj Mts. is built up by Badenian and Sarmatian volcanic formations and can reach a thickness as much as 2.5 km. The chemical composition of the magmas followed a differentiation path in both cycles, which produced increasingly more basic rock types. The basement of these volcanic formations is not well-known, therefore we can obtain additional information by investigating xenoliths.

Former researches showed that basement rocks crop out at the NE part of the mountains (Vilyvitány Block) and belong to the Zemplinicum. The block is made up of metamorphic micashists and gneisses, which are overlain by Carboniferous-Permian terrestrial sediments. S from Vilyvitány Block there are numerous xenoliths that also derive from this block in a relatively large area. At Sátoraljaújhely and Sárospatak the basement consists of Zempinicum and Dachstein type limestones. Szendrő type C_{org}-bearing slate xenoliths are abundant in the SW part of the mountains. Gneiss xenoliths from a supposed Gemeric type basement occur at the NW part of the mountains.

Our investigations mostly support the former findings. However some new results were obtained. Some enclosures have a unique mineral paragenesis, which was formed during xenolith-magma interaction or by earlier high temperature processes.

The authigenic enclosures often carry hercynite which is frequently associated with biotite as an alteration product. Hercynite was not mentioned by former researchers. It can appear in two forms. Single hipidiomorphic crystals formed probably before igneous activity. In the other fabric type the simplectitic hercynite-magnetite (together with anorthite) may be the result of solid-state exsolution. The Fe and Al to form hercynite may derive from the contamination of pelitic sediments. Another possible explanation is that hercynite is an ultrabasic cumulate mineral from the magma.

One xenolith from the NE part of the mountains (South from the outcropping metamorphic rocks) has a mineral assemblage typical for high grade metamorphic rocks (amphibolite facies). This xenolith consists mainly of cordierite, plagioclase, hercynite and of corundum, magnetite, anorthite in small amount. Hercynite is replacing corundum as indicated by their fabric. Cordierite and corundum may have formed before magmatic activity during high temperature metamorphism of pelitic protolith. Hercynite and magnetite sometimes forms simplectitic structures as observed in several authigenic enclosures. This latter feature is perhaps the result of magma-xenolith thermal interaction. Based on the abovementioned facts the xenolith is a torn-up fragment from the metamorphic basement.

Acknowledgements: The research was carried out in the framework of the Sustainable Resource Management Center of Excellence at the University of Miskolc, as part of the TÁMOP-4.2.2/A-11/1-KONV-2012-0049 "WELL aHEAD" project in the framework of the New Széchenyi Plan, funded by the European Union, co-financed by the European Social Fund.

Structural state and chemical composition of zones in zircon from Variscan granitoids

Kis A[1*], Weiszburg T[1], Gadas P[2], Váczi T[1], Buda G[1]

1 - Department of Mineralogy, Eötvös Loránd University *annamari.kis@gmail.com
2 - Department of Geological Sciences, Masaryk University

The chemical composition [1] and the structural state [2] of zircon zones carry important information about the geological processes, therefore the knowledge of these are necessary for the reliable age interpretation when using local (e.g. SHRIMP or LA-ICP-MS based) U-Pb or Th-Pb geochronology of zircon.

Our zircon samples were separated from granitoid bodies (Mórágy, Hungary and Rastenberg, Austria) at the easternmost margin of the Western-Central-European Variscan collision zone, characterized by lamprophyre-derived mafic enclaves within the granitoids, and a late/postmagmatic overprinting effect, connected possibly to the potassium enrichment of both rock types. Our goal is to conduct systematic U-Pb, Th-Pb dating on zircon to clarify the restitic vs. in situ unmixing origin of mafic enclaves and the age of the overprinting effect for a better paleotectonic reconstruction of the Variscan plutonic rocks in Europe.

Three morphological types [3] of zircon crystals were present: normal prismatic zircon (S_{24}, S_{25}), flat prismatic zircon (AB_5), elongated prismatic zircon (P_5). Zircons show both primary (growth/sector zoning ± xenocryst core) and secondary (convolute) zoning features on SEM-CL and SEM-BSE images.

SEM-CL/SEM-BSE imaging and Raman spectroscopy (FWHM) were used for determining the structural state of the zircon zones. Normal and flat zircon crystals show zones of all structural states (well crystallized, intermediate, metamict), while the latter state is not present in elongated zircons. Chemical composition of the zones was measured by EMPA.

The data confirm that very low electron back-scatter intensities can be found at zones of elevated U, Y, P and REE concentrations but damaged structural state [4], but in many crystals there is only limited structural state variation in the zones and the SEM-BSE contrast depends mainly on changes in chemical composition. The border between core and rim may need special interpretation.

Based on these measurements about 190 well characterized, undisturbed measuring areas of 96 crystals have been selected for future SHRIMP and LA-ICP-MS studies. These areas cover all the three expected geological processes and give chance for determining the 1) age of inherited zircon of crustal origin (xenocrystic core), 2) crystallization age of rock (growth zoning), 3) the age of the overprinting effect (convolute zoning).

[1] Finch J.R. and Hanchar J.M. (2003). Structure and chemistry of zircon and zircon-group minerals. In: Hanchar J.M. and Hoskin, P.W.O. (Eds.), Zircon. *Rev. Mineral. Geochem.*, 53, 1-25.

[2] Nasdala L. *et al.* (2006). Effects of natural radiation damage on back-scattered electron images of single-crystals of minerals. *Am. Mineral.*, 91, 1738-1746.

[3] Pupin J.P. (1980). Zircon and granite petrology. *Contrib. Mineral. Petr.*, 73, 207-220.

[4] Nasdala L. *et al.* (2009). The phenomenon of deficient electron microprobe totals in radiation-damaged and altered zircon. *Geochim. Cosmochim.Acta*, 73, 1637-1650.

Polymetamorphism of siliceous dolomitic marbles and calcsilicate rocks from the Cretaceous high pressure wedge of the Austroalpine Basement, Eastern Alps, Austria

Puhr B[1], Hoinkes G[2*], Schuster R[3], Proyer A[4]

1 - Institute of Earth sciences, University of Graz, Austria 2 - University of Graz *georg.hoinkes@uni-graz.at 3 - Geological Survey of Austria, Vienna, Austria 4 - University of Botswana

The Koralpe-Wölz nappe system of the Eastern Alps consisting mainly of metapelites, metabasites and metacarbonate rocks represents a high pressure wedge caused by collision of the European and Adriatic plate in the Cretaceous. This collision was preceded by a crustal extension in the Permian causing a low P - high T metamorphic overprint of the pre-Austroalpine basement. The distribution of the diagnostic mineral assemblages of the siliceous dolomitic marbles of the CM(A)SCH-system is consistent with increasing metamorphic conditions from N to S and fits to the well-known eo-Alpine field gradient from ~500°C/10kbar to ~700°C/20kbar derived from metapelites and metabasites. The sequence of diagnostic mineral assemblages A1 to A4 from N to S along a cross section in the central Eastern Alps from the Wölzer Tauern to the Koralpe Mountains represents increasing temperatures which were calculated using calcite - dolomite solvus thermometry based on corrected Mg-contents in calcite due to reintegration of dolomite exsolutions:

A1: Dol + Qz + Cal (437 - 480°C); A2: Tr + Qz + Cal ± Dol (540 - 562°C);

A3: Di ± Tr + Cal + Dol (660 - 691°C); A4: Di + Fo + Cal + Dol ± Chu ± Chl (680 - 740°C)

These assemblages represent a prograde sequence along geothermal gradients from ~16°C/km in the N towards ~10°C/km in the S and are characterized by a H_2O-rich fluid. Specifically the occurrence of Fo in A4 as well as Di-coronas around Tr in A3 can only be explained by high H_2O-contents.

Assemblage A5: Fo + Spl + Cal + Dol (750 - 830°C) occurs further to the east at the eastern end of the Eastern Alps near the village of Sieggraben. Widespread Dol-exsolution shows different generations with lamellar to patchy shapes. Reintegration of coarse dolomite lamellae in Cal results in Cal-Dol temperatures of 850°C which is compatible with the stability of Fo even at raised X_{CO2}-values but anyway at lower pressures. Reaction coronas of Di-Dol around Fo were formed at temperatures below about 750°C according to reintegration of fine-grained bleb-like or patchy Dol-exsolutions which represent a later stage of exsolution.

Calcsilicate rocks representing the CASCH-system from the Koralpe mountains rarely contain Scp of meionitic composition which is accompanied by Cpx, Czo, Cal, Qz, Amp, Pl and Afs. Activity corrected T-X_{CO2} calculations of the stability of Scp result in minimum temperatures of about 670°C and a CO_2 - rich fluid. Scp is typically replaced by complex An-Czo-Grs - coronas which are stable at significantly higher H_2O-contents at temperatures below 650°C.

In conclusion, the metacarbonates of the Austroalpine high pressure wedge mainly reflect the eo-Alpine metamorphic imprint but there are clear indications for a multistage metamorphic history. They may either be interpreted as due to a retrogressive PT-evolution in the presence of a H_2O-rich fluid after eo-Alpine metamorphic peak conditions as possibly documented in the Scp-bearing calcsilicate rocks or as a two stage metamorphic evolution due to different metamorphic events as most probably documented by two generations of exsolutions in calcite and by Fo-Di - replacement textures at Sieggraben. Calculated high T conditions of granulite facies for the older generation are in contradiction to eo-Alpine subduction and fit better to a high T event like the Permian extensional event. Therefore in this case Fo replacement by Di-bearing coronas may reflect the two stage Permian - Cretaceous metamorphic history.

Forearc basaltic magmatism in middle Miocene SW Japan

Shinjoe H[1*], Orihashi Y[2]

1 - Tokyo Keizai University *shinjoe@tku.ac.jp 2 - ERI, the University of Tokyo

In the forearc region of SW Japan, middle Miocene voluminous felsic to intermediate igneous rocks were widely distributed intruding the Cretaceous to Neogene accretionary complex. These igneous bodies were formed immediately after the opening of the Japan Sea and clockwise rotation of SW Japan with the subduction of young hence hot Shikoku Basin of the Philippine Sea plate. Almost coeval basaltic igneous rocks were distributed in the region closer to the Nankai trench than felsic to intermediate igneous bodies. We present geochemical and geochronological data of these igneous bodies to discuss origin of magmas and implication for the tectonic setting of the forearc magmatism of middle Miocene SW Japan.

Basaltic igneous rocks in the region close to the trench of SW Japan were classified to tholeiitic basalt/gabbro (Shionomisaki and Muroto igneous bodies) and Alkali dolerite/gabbro (Ashizuri and Tanegashima igneous bodies).

Previous studies on the origin of tholeiitic basaltic rocks proposed that tholeiitic basaltic magmas had been supplied from subducting Shikoku Basin at the ceasing stage of the spreading. Indeed basaltic igneous bodies with tholeiitic chemical signature were distributed relatively close to the fossil spreading ridge of the Shikoku Basin. Our geochemical data also basically supports the interpretation. For example, Sr-Nd isotopic compositions of the most depleted toleiitic basalt samples are within the range of the Shikoku-Parece Vela Basin basalts, although slight contamination of sediment is suggested by Pb isotopic compositions.

Alkali basaltic rocks of Ashizuri and Tanegashima bodies have OIB-like LILE enriched trace element composition. Pb isotopic composition of dolerite from Tanegashima is close to those of terrigenous sediments. Dolerite from Ashiruri is with lower $^{206}Pb/^{204}Pb$ and $^{207}Pb/^{204}Pb$ ratios than those of Tanegashima. On the other hand, Tanegashima dolerite has more depleted Nd isotopic composition than those of Ashizuri dolerite. Zircon U-Pb age of the Ashizuri body is ca. 13 Ma, clearly after the initiation of subduction of Shikoku Basin. On the other hand, previously reported radiometric age of Tanegashima bodies ranges 16-18 Ma, so its intrusion may predate the subduction of the Shikoku Basin. Difference of the isotopic compositions may reflect the change of the mantle composition beneath the forearc region of SW Japan.

Doleritic enclaves with bulk rock composition close to those of the tholeiitic basaltic rocks are observed in the Kumano Acidic Rocks, a voluminous S-type felsic igneous complex near the Shionomisaki body. This fact may suggest that melting of the sediments by intrusion of tholeiitic basalt magma derived from subducting Shikoku Basin formed the S-type felsic magma within the accretionary complex in the forearc region.

Geochemical effects of hausmannite on Raman spectrometry

Vafeas N*, Beukes N, Blignaut L, Smith B

University of Johannesburg *nickvafeas@gmail.com

The RAMAN spectrometer can be extensively useful in the study of minerals and their associated chemically derived differences. Despite this however, it is relatively poorly understood, and its applications are not utilised as much as those of traditional analytical apparatuses, such as the Scanning Electron Microscope (SEM) and X-ray Diffractometer (XRD). Using molecular and crystal lattice variations, the vibrational spectra distinct to each individual mineral is created. As such, the vibrational spectra generated is specifically sensitive to changes in the mineral compositions and bonds, the variations in phases, the crystallographic phases and the chemical environment of samples in any form, be it solids, liquids or gasses [1]. The manganese (Mn) ore of the Kalahari Manganese Field (KMF) is well documented to contain ovoids (layered, calcium carbonate-based, primary structures measuring <0.5-2 mm in length, that have been partially flattened due to tectonics). These ovoids are particularly susceptible to alteration even under the slightest changes in conditions, with Mn-bearing hausmannite being the main alteration product replacing $CaCO_3$. A RAMAN analysis of hausmannite from the high-grade northern and low-grade southern regions of the Kalahari Manganese Deposit (KMD) yields distinctly different spectra. The chemical variation in hausmannite specimens has an effect on the vibrational spectra generated by the RAMAN, specifically the variation between the Fe, Mn and Si concentrations within the low grade and high grade ore. This difference in chemistry generates RAMAN spectra in the low grade ore that are positioned at lesser wave number values in comparison to that of the standard RRUFF spectrum for hausmannite. Conversely, the higher Mn and lower Fe and Si concentrations in the high grade ore generate RAMAN spectra that are positioned at higher wave number values when compared to that of the standard RRUFF spectrum for hausmannite.

[1] Schreiner M., Strlie M. and Salimbeni R., (2008). *Handbook on the Use of Lasers in Conservation and Conservation Science.* COST office, Brussels.

Oriented inclusions in apatite and fluid-mediated regime of carbonate-rich UHP rocks from the Tromsø Nappe (N. Norway)

Broska I[1*], Ravna E[2], Janák M[1], Kullerud K[2], Vojtko P[1], Bačík P[5]

1 - Geological Institute, Slovak Academy of Sciences, Bratislava *igor.broska@savba.sk 2 - Department of Geology, University of Tromsø, Norway 3 - Comenius University, Faculty of Natural Sciences, Bratislava

Many observations indicate that accessory apatite is stable also under high- to ultrahigh-pressure metamorphic (UHPM) conditions. The retrogressive regime following the progressive metamorphic phase may have triggered exsolution processes that resulted in the precipitation of new minerals within the apatite crystals (e.g. formation of monazite). On the other hand, phases that seemingly exsolved from the apatite structure may be a product of fluid-aided activities that resulted in precipitation of some inclusions. An example of formation of inclusions in apatite is the presence of long tiny pyrrhotite rods found in fluorapatite from silicate bearing carbonate rocks associated with UHP eclogites in the Tromsø Nappe (Scandinavian Caledonides). The evidence for ultrahigh-pressure (UHP) metamorphism in this area (3.5 GPa; 750-800 ºC) is obtained from eclogites and by the presence of metamorphic diamond in the associated gneisses. The host rock in which the apatite occurs is composed of a Mg-rich calcite matrix (30 vol. %) with dense trellis of tiny dolomite exsolutions, almandine-grossular garnet, low jadeite clinopyroxene, magnesiohornblende and phlogopite. The modal abundance of fluorapatite is up to 10 vol. %. Other accessory minerals are mainly zircon, Fe-Ti oxides and allanite-(Ce). Euhedral fluorapatite occurs in the carbonate matrix and less often in garnet and clinopyroxene. The fluorapatite is rich in a hydroxylapatite component (up to 40 vol. %) with minor ellestadite and britholite, traces of CO_3^{2-}, and CN^- and also contains oriented pyrrhotite needles. Precipitation of pyrrhotite in the hydroxyl-rich fluorapatite was probably facilitated by a sulphur volatile phase such as H_2S_{aq}, which migrated through the apatite nano-channels and interacted with the octahedral Fe of apatite. The hydrogen sulphide was liberated during alteration of primary pyrrhotite into the host rock. On the other hand, the anhydrite rods found in apatite along with pyrrhotite and dolomite, could be derived from tetrahedral sulphur in apatite. Crystallisation of anhydrite and probably also associated pyrrhotite in apatite occurred at 550-650 ºC according to calcite-dolomite thermometry. In such circumstances, precipitation of pyrrhotite resulted from post-UHP retrogression at amphibolite facies conditions. Relaxation of the fluorapatite structure during retrogression/decompression played a more significant role in the a-axis direction. This is true because the *a*/*c* ratio is negatively correlated to pressure and compression which is likely a result of the greater compressibility of nanochannels in the fluorapatite. A fluid-mediated regime implies rapid pyrrhotite precipitation in the apatite nanochanels during retrogression of HP/UHP rocks.

Water splitting through the oxidation of Fe^{2+}-bearing minerals (olivine and siderite): experimental study of an abiogenic H_2 forming process

Brunet F[1*], Milesi V[2], Malvoisin B[3], Recham N[4], Dairou J[5], Crouzet C[1], Guyot F[6]

1 - ISTERRE, CNRS, Univ. Grenoble, France *fabrice.brunet@ujf-grenoble.fr 2 - IPGP, Univ. Paris Diderot, France 3 - ISTE, Geopolis, Lausanne, Switzerland 4 - LRCS, Univ. Picardie, Amiens, France 5 - BFA, Univ. Paris Diderot, France 6 - MNHN, Paris, France

It is now well established that serpentinization of oceanic peridotites generates reducing conditions which promote the formation of abiogenic dihydrogen (and indirectly hydrocarbons) through the water splitting reaction: H_2O => H_2 + ½ O_2 with O_2 being incorporated into minerals. Recently, water - siderite interactions have also been proposed to promote the unconventional generation of hydrocarbons through CO_2 reduction by H_2-rich fluids [1]. In these two types of occurrences, oxygen fugacity below the classical $C + O_2 = CO_2$ buffer is achieved thanks to the oxidation of Fe^{2+} contained in mineral phases. Basically, oxidation of ferrous iron is driven by the formation of magnetite, $Fe^{2+}Fe^{3+}{}_2O_4$, which is stable over a wide range of P-T-fO_2 conditions. The hydrothermal decomposition of olivine, $(Mg,Fe)_2SiO_4$, into serpentine + magnetite + brucite and, the Fe_3O_4-producing dissolution of siderite, $FeCO_3$, are two examples of abiogenic H_2-forming reactions related to the oxidation of iron from ferrous (olivine, siderite) to ferric (magnetite).

In order to investigate hydrogen production by water splitting under geologically relevant conditions, San Carlos olivine - water and siderite - water experiments were conducted in gold sealed container using externally heated pressure vessels (50 MPa argon pressure). In such closed chemical systems, the aqueous fluid composition changes as the reaction proceeds (reaction path) and the fH_2 in the solution cannot be simply derived by considering buffering reactions as it is the case when, for instance, excess carbonaceous matter is present. It is therefore important to be capable of monitoring these reactions on a time-resolved basis. Serpentinization of San Carlos olivine has been monitored directly on the encapsulated samples taking advantage of the magnetic properties of magnetite. The time-resolved production of magnetite was determined by measuring the saturation remnant magnetization (Jrs) and the saturation magnetization (Js), collected at the end of the run. Hydrogen production kinetics was then indirectly derived from additional thermochemical modelling.

Siderite dissolution, which can be summarized by the simplified $3FeCO_3 + H_2O = Fe_3O_4 + H_2 + 3CO_2$ reaction, has also been investigated at 200 and 300°C (50 MPa). The sealed gold container which contained siderite + water was pierced at the end of the run to collect the produced gases. The evolution of H_2 and CO_2 concentrations was found to be controlled by siderite equilibrium dissolution in a first stage. In a second stage, however, H_2 concentration decreased while CO_2 concentration increased. This unexpected trend can potentially be accounted for by two processes: 1) hydrogen loss through the capsule wall with CO_2 being buffered by residual siderite and 2) carbonaceous matter formation through CO_2 reduction, i.e. $CO_2 + 2H_2 = C + 2H_2O$. The results of both long-term experiments and TEM investigation on the solid products are consistent with the second process. Further analyses of dissolved organic compounds using GC-MS is in progress.

The overall consistency between thermochemical models and experimental results shows that the experimental tools developed here are suitable to the study of low-temperature abiogenic H_2 formation. The next experimental target will be the formation of unconventional hydrocarbons in H_2-rich CO_2-bearing aqueous fluids.

[1] Milesi V., Prinzhofer A., Guyot F., Brunet F., Richard L., Dairou J. and Benedetti M. (2013). Goldschmidt Conf. Abstr., 1259.

The permeability of the impermeable lower crust

Connolly J

IGP-ETHZ. james.connolly@erdw.ethz.ch

Metamorphic devolatilization in the lower crust generates both fluid and grain-scale porosity at the expense of the solid volume. Evidence for high fluid pressure requires that devolatilization must occur under poorly drained conditions. Under such conditions that the rocks overlying a metamorphic reaction front must act like a permeable piston, whose weight drives fluid expulsion at a rate limited by either the capacity of the reacted rocks to resist compaction or the permeability of the overlying rocks. In the former case the time scale for compaction must be much greater than the metamorphic time scale, thus fluid flow patterns are entirely by details of the hydraulic permeability. The alternative scenario is that compaction processes are fast relative to metamorphism. In this case permeability is dynamic and fluid flow is compaction driven and accomplished by waves of fluid filled porosity. The waves are propagated by a front of anomalously high fluid pressure that is responsible for dilating the porosity in the upper portion of the wave, and trailed by a wake of low fluid pressure that causes the porosity to compact in the lower portions of the wave. Depending on rock rheology, the waves may cause pervasive, but temporally variable, fluid flow or patterns in which fluid flow is channelized. In contrast to the flow patterns that develop in rigid rocks, which are controlled by the permeability of the least permeable lithology, in ductile rocks flow patterns are dictated by the weakest lithology.

Possible occurrence of silicate melt, carbonate-rich melt and fluid during anatexis at medium pressure: a melt and fluid inclusion study in stromatic migmatites from eastern Bavaria

Ferrero S[1*], O'Brien P[2], Wunder B[3], Hecht L[4], Ziemann M[2]

1 - Universität Potsdam Institut für Erd- und Umweltwissenschaften *sferrero@geo.uni-potsdam.de 2 - Universität Potsdam 3 - Helmholtz-Zentrum Potsdam, GFZ 4 - Museum fuer Naturkunde Berlin

The recent finding of anatectic melt inclusions within enclaves and high-grade terrains opened up the possibility to directly analyse unadultered anatectic melt [1]. Primary crystallized MI (Figure 1A, black arrows), or "nanogranites", and FI (Figure 1B; white arrows) occur as clusters in garnet from stromatic migmatites from Eastern Bavaria (Moldanubian Zone). During the Carboniferous, these Grt+Bt+Sill+Crd+Spl metapelitic gneisses underwent HT/MP metamorphism, followed by a HT/LP event. Nanogranites, ≤20 µm in size, consist of Qtz+Bt+Wm+Ab±Ap, and show abundant nanoporosity. FI are smaller, generally ≤10 µm, and contain CO_2+N_2+CH_4 plus siderite, pyrophillite and cristobalite, mineral phases not observed in the surrounding rock or as mineral inclusion in garnet. Their coexistence in the same cluster of the MI suggests that a COH fluid was present during anatexis [2]. Polycrystalline inclusions containing Cc+Wm+Chl±Qz, commonly ≤10 µm in diameter, occur in the same cluster with MI and FI (Figure 1C). Microstructural features, negative-crystal shape and the well-developed crystalline faces of calcite within inclusions suggest that they may be the result of the crystallization of a carbonate-rich melt. This would suggest the occurrence of a silicate melt and a carbonate-rich melt during anatexis at relatively shallow crustal levels.

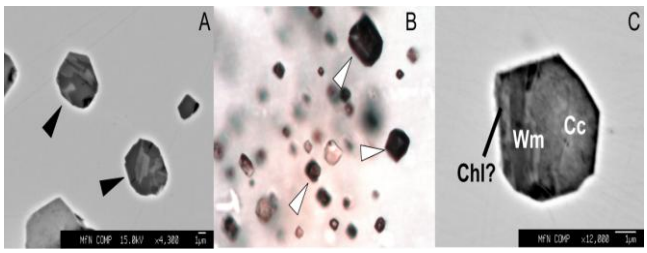

Figure 1: (A) Nanogranites *(black arrows)*; (B) Fluid inclusions *(white arrows);* (C) Cc-bearing inclusion.

[1] Ferrero S., Bartoli O., Cesare B., Salvioli Mariani E., Acosta-Vigil A., Cavallo A., Groppo C. and Battiston S. (2012). Microstructures of melt inclusions in anatectic metasedimentary rocks. *Journal of Metamorphic Geology*, 30, 303-322.
[2] Ferrero S., Braga R., Berkesi M., Cesare B. and Laridhi Ouazaa N. (2014). Production of Metaluminous melt during fluid-present anatexis: an example from the Maghrebian basement, La Galite Archipelago, central Mediterranean. *Journal of Metamorphic Geology*, 32, 209-225.

Fluid induced dehydration of the mafic lower crust from amphibolite to granulite facies: nature and experiment

Harlov D

GeoForschungsZentrum. dharlov@gfz-potsdam.de

Natural evidence for the role of low H_2O activity fluids (CO_2 or concentrated brines) in the dehydration of H_2O-rich, mafic amphibolite-facies rocks to H_2O-poor, Opx-bearing granulite-facies rocks (700-900 °C and 500-1000 MPa) for both highly localised dehydration zones (CO_2; cm's) as well as regional terranes (brines; km's) [1] include the presence of Kfs micro-veins along Qtz-Plg grain boundaries; Plg grains metasomatised in a K-rich fluid; Mnz and/or Xn inclusions in the FAp grains; Bt enriched in Ti, F, and Cl; and FAp enriched in Cl and F. These features are not seen in the "source" amphibolite facies terrane along the same traverse. When log(fHF/fH_2O) for either Bt or FAp is plotted as a function of the distance from the fluid/heat source, a uniform decrease in log(fHF/fH_2O) is observed across the granulite to amphibolite facies traverse suggesting the presence of a uniform low H_2O activity uniform fluid front. Dehydration experiments (900 °C; 1000 MPa; 3 weeks; Au capsule; quenched) involving a cylinder of natural tonalitic Bt gneiss (Plg, Qtz, Bt) (220 mg) and a concentrated KCl brine (20-30 % H_2O; 70-80 % KCl) (8 mg) placed at the base of the cylinder have been conducted in the piston cylinder apparatus (CaF_2 setup). Micro-veins primarily of Kfs, with some evidence of partial melting, formed along Qtz/Plg grain boundaries, though only where Bt and Qtz were in contact. Here the Bt reacted with Qtz to form numerous small Opx and Cpx grains as well as minor Ilm from the 2-3 wt % of TiO_2 present in the Bt. The two principle reactions responsible for both the formation of the Kfs micro-veins as well as the pyroxenes include: (1) An (in Plg) + Qtz + KCl (in fluid) = Kfs + $CaCl_2$ (in fluid) and (2) Bt + Qtz = Opx + Kfs + H_2O. The same experiment performed under the same P-T conditions involving either a concentrated NaCl brine (20-30 % H_2O; 70-80 % NaCl) or a CO_2-rich fluid (80 % CO_2, 20 % H_2O) or a fluid absent dry melt resulted in micro-veins approximating a granitic composition that formed along Qtz/Plg grain boundaries. This is accompanied by numerous small Opx grains and minor Ilm forming along biotite grain boundaries, again only when the Bt and Qtz were in contact. Due to an absence of KCl in these three cases, only reaction (2) was relevant.

[1] Harlov and Förster (2002). J. Petrol, 43, 769

Slab-fluids contain chlorine: fluid inclusions in sub-arc mantle peridotites and partitioning experiments between aqueous fluids and magmas

Kawamoto T[1*], Mibe K[2]

1 - Institute for Geothermal Sciences, Graduate School of Science, Kyoto University *kawamoto@bep.vgs.kyoto-u.ac.jp 2 - Earthquake Research Institute, University of Tokyo

Chemical fractionation of slab-derived supercritical fluids can play an important role in elemental transfer from subducting slab to the mantle wedge and arc magmatism [1]. A recent finding of saline fluids from sub-arc mantle peridotite indicates that aqueous fluids in mantle wedge can contain 5 wt% NaCl [2]. It is, therefore, important to determine the effect of Cl on the trace element partitioning between fluids and melts.

Synchrotron radiation X-ray fluorescence (XRF) analysis was conducted to know elemental partitioning between aqueous fluids and high magnesian andesite melt using radiography technique [3] at BL04B1, SPring-8, Japan. A series of experiments has been carried out to obtain partition coefficients between fluids and melt at 1000-1200 °C and 0.5 - 2.2 GPa. There is a positive correlation between partition coefficients and pressure, as well as salinity. The results suggest that (Na, K)Cl in aqueous fluids have large effects on the partitioning as have been suggested by previous studies using quench experiments [4].

Two slab-derived components, namely a melt and a fluid component, are suggested to explain trace element characteristics of basalts and basaltic andesites in the Mariana arc [5]. The fluid component is characterized by enrichment of alkali and alkali earth elements. In addition to these, the melt component has immobile elements such as REE [5]. Such features can be explained if the fluid component is a Cl-rich aqueous fluid, because alkali earth elements and Pb are much less mobile with Cl-free fluids than Cl-rich fluids [4]. We suggest that slab-derived components have compositional features consistent with a Cl-rich aqueous fluid and a melt, which can be formed through a separation of a slab-derived supercritical fluid [1]. Slab-derived supercritical fluids contain Cl, and aqueous fluids inherit much of the Cl and some of the large ion lithophile elements.

[1] Kawamoto T. *et al.* (2012). *Proc. Nat. Acad. Sci. USA*, 109, 18695.

[2] Kawamoto T. *et al.* (2013). *Proc. Nat. Acad. Sci. USA*, 110, 9663.

[3] Mibe K. *et al*. (2004). *Geochim. Cosmochim. Acta*, 68, 5189.

[4] Keppler (1996). *Nature*, 380, 237.

[5] Pearce J.A. *et al.* (2005). *Geochem. Geophys. Geosys*., 6, Q07006.

Towards the definition of a petrological Low Velocity Zone (LVZ)

Massuyeau M[1*], Morizet Y[2], Gaillard F[1]

1 - ISTO-CNRS/Université Orléans/BRGM *malcolm.massuyeau@cnrs-orleans.fr

2 - LPGN-CNRS/Université Nantes

Carbon and others volatiles that are present in the Earth's mantle at ppm concentration levels, induce partial melting. CO_2-H_2O-rich melts are stable under the P-T-fO_2 conditions of the Low Velocity Zone (LVZ). Recent experimental studies about the Earth mantle conductivity have shown the primordial importance of small amounts of hydrated CO_2-rich melts in the geophysical signature of the LVZ. Nevertheless, the chemical composition of these melts is difficult to capture as it depends on T-P and redox state.

Using Margules formalisms, we established a multi-component model describing the Gibbs free energy of melt produced by mantle melting in presence of CO_2-H_2O that are carbonatite-carbonated melt-nephilinite-basanite and basalt with increasing degree of partial melting. This parameterization is calibrated on crystal-liquid, redox, fluid-liquid and liquid-liquid equilibria obtained by experimental studies in the P-T range 1-10 GPa and 900-1800°C.

We propose a calculation of the composition of melts produced in the oceanic LVZ as a function of age. At about 80 km depth, we show that the composition of the melts is >30 wt% SiO_2 for ages <20 Ma, and comes closer to the carbonatitic terms for older lithosphere. Besides lateral chemical variations, our model calculates the melt composition along an oceanic ridge adiabat, predicting an abrupt compositional transition between a H_2O-rich carbonatitic melt and a carbonated silicate melt, between 140 km and 160 km. With the distance to the ridge, this transition is shifted to lower depths between 70 and 90 km. We propose a chemical mapping of the melt composition (and of the degree of partial melting) as a function of the distance to the ridge and of the depth. The chemical variations between carbonated and silicated melts may be related to the geophysical observations.

Fluid inclusion characteristics of regional high grade granulite terrain of Biligirirangana Hill, southern Karnataka, India

Mayachar G[1*], Ghosh S[2]

1 - Geological Survery of India. *girishgeosu@gmail.com 2 - Fluid Inclusion lab, PPOD, Division, RSAS, SRO, Geological Survey of India, K. S. Layout, Bangalore

Biligirirangana Hill charnockite massif consists of massive to banded/foliated charnockite with enclaves of basic granulites and metasediments (banded magnetite quartzite, quartzite and pelite). All these lithologies show a prominent N-S structural trend, which is a major trend prevalent during the Archean period. Based on the field and petrographic studies the Biligirirangan Hill terrain has revealed evidence of strong deformation and high-grade metamorphic events. The banded/foliated charnockites are medium- to coarse-grained, consisting of orthopyroxene, clinopyroxene, hornblende, feldspars, biotite and quartz with zircon, rutile and opaques as accessories. The development of symplectites of clinopyroxene-plagioclase after early formed hornblende, hornblende-plagioclase after orthopyroxene, and the formation of boudin structures characterize these stages of metamorphism. The geochemical signatures of Biligirirangana Hill charnockite indicate a trondhjemitic composition and are of low Mg number. Rb and Sr data reveal that their magmatic protoliths originated from the mantle to lower crust.

PT conditions of Biligirirangana Hill charnockite were estimated using orthopyroxene-clinopyroxene and orthopyroxene-biotite Fe-Mg exchange thermometry, and orthopyroxene-plagioclase-hornblende barometry. It reveals temperatures of 750-850ºC and pressures of 7.7-8.5 Kb at near-peak metamorphism. Two types of fluid inclusions were observed in the charnockite, namely carbonic (CO_2) inclusions and aqueous carbonic (H_2O+ NaCl+CO_2(L)+ CO_2(V) ±CH4) inclusions. All the inclusions show melting temperatures in the range of -59.2 to -56.6ºC, suggesting dominantly pure CO_2 with minor traces of CH_4 and other gases. The carbonic inclusions show high densities (1.162 to 1.021 g/cm^3; Th_{CO2} = -51.9 to -17.8ºC). This is confirmed by the shift in the CO_2 peak to 1281 cm^{-1} in Raman spectroscopy studies, while the aqueous carbonic inclusions indicate salinities of 1.15 to 3.2 wt% NaCl equivalent.

Field, petrographic, geochemical and fluid inclusion data indicate that the high density CO_2 fluids imply a synmetamorphic origin of mantle-derived fluids that pervasively influxed from the lower continental crust. These fluids were present during the peak metamorphism. It is concluded that these fluids were the dominant agents for granulite facies transformation on a regional scale, and might also be responsible for the formation of regional charnockites.

Chemical compositions of coexisting aqueous fluid and silicate melt in the vicinity of second critical endpoint in the system peridotite-H_2O and their bearing on the possible origin of komatiite and boninite by liquid-fluid immiscibility

Mibe K[1*], Kawamoto T[2]

1 - Earthquake Research Institute, University of Tokyo *mibe@eri.u-tokyo.ac.jp 2 - Institute for Geothermal Sciences, Graduate School of Science, Kyoto University

In order to understand the petrogenesis in the hydrous upper mantle, we have been investigating the stability fields and chemical compositions of aqueous fluid, silicate melt, and supercritical fluid magma in the peridotite-H_2O system. Mibe *et al*. [1] reported that the second critical endpoint occurred at around 3.8 GPa in the system peridotite-H_2O. Using the quenched recovered samples obtained by Mibe *et al*. [1], chemical compositions of coexisting aqueous fluid and silicate melt and supercritical fluid in the vicinity of the second critical endpoint were determined using electron probe micro analyzer. A 10- to 30-micrometer diameter electron beam was used to obtain the composition of quenched materials from aqueous fluid and silicate melt.

In the run at 3.6 GPa, aqueous fluid and silicate melt were coexisting with olivine. The composition of aqueous fluid in this run was high-Mg andesitic (i.e., boninitic), whereas the composition of silicate melt was komatiitic. At 4 GPa (i.e., above the second critical endpoint), the composition of supercritical fluid magma was peridotitic and was the same as the starting material within the experimental uncertainties.

In some Archean greenstone belts, the co-occurrence of komatiites and boninites are reported [2, 3]. Our experimental results suggest that komatiite and boninite can be generated at the same time as a result of liquid-fluid immiscibility in the hydrous upper mantle.

[1] Mibe K. *et al*. (2007). *J Geophys Res*, 112, B03201.

[2] Kerrich R. *et al*. (1998*). Earth Planet. Sci. Lett*, 164, 303.

[3] Poidevin J-L. *et al*. (1994). *Precambrian Res*, 68, 97.

Fluid-melt-rock interaction at slab/mantle interface in subduction zones: results of experimental modelling under UHP conditions

Perchuk A, Shur M, Yupaskurt V

Geological Faculty, Moscow State University, Russia *alp@geo.msu.ru

The slab/mantle interface represents an intriguing geological environment in which thermal and oxygen fugacity gradients are superposed on contrasting lithologies. Although it is widely accepted that metamorphic fluids released from the slabs play a crucial role in subduction zones, processes at slab/mantle interface remain so far poorly studied. In this contribution, we report results of sandwich experiments with analogues of oceanic crust and mantle rocks carried out in a piston-cylinder apparatus at 750-850^{o}C and 2.9 GPa, i.e. under P-T conditions of the "hot" modern or ancient subduction zone. Powders of carbonate-bearing blueschist or garnet amphibolite in the lower part of the capsules served as a source for COH fluid that migrated with dissolved components (and dacitic melt in the HT runs) upward and reacted with the olivine or clinpyroxene + orthopyroxene powders.

Experiments reveal contrasting behavior of alkalis in different mantle analogues. Pervasive fluid (melt) flux into the olivine layer produced a Na-free reaction zone consisting predominantly of orthopyroxene with some magnesite±phologopite at the metabasite-olivine interface. Local growth of orthopyroxene + garnet ± magnesite ± chlorite ± phlogopite occurs in the olivine layer above the reaction zone. Similar fluid (melt) flux into the two-pyroxene layer leads to the formation of an orthopyroxene- and K-free reaction layer consisting of omphacite+coesite+magnesite with local development of garnet and omphacite above it. Thus, subduction zone fluids (melts) in peridotites are likely enriched in sodium in contrast to K-rich fluids migrating through pyroxenites. We also propose that fluid controlled replacement of orthopyroxene by omphacite+coesite (quartz) assemblage might take place not only in pyroxenites but also in mature orthopyroxene-rich reaction zones at the metabasite-peridotite (i.e. slab-mantle) interface.

Acknowledgement: Financial support by RFBR grants #12-05-01093.

Interaction of peraluminous metapelites with fluidized trondhjemitic magma in the Petronella shear-zone, Limpopo Complex, South Africa

Safonov O[1*], Tatarinova D[2], van Reenen D[3], Golunova M[1], Yapaskurt V[2]

1 - Institute of Experimental Mineralogy, Russia *oleg@iem.ac.ru 2 - Moscow State University 3 - University of Johannesburg

In addition to the pervasive and localized fluid fluxes, the interaction of Precambrian granulite complexes with granite-greenstone cratons might also be expressed in formation of granitic, trondhjemitic and granodioritic magmas. We present results of a petrological, fluid inclusion and thermobarometric study of interaction between fluidized trondhjemitic magma and orthopyroxene-cordierite granulites within the regional high-grade Petronella shear zone located in the Southern Marginal Zone (SMZ) of the Limpopo Granulite Complex (South Africa). The hot (T ~ 1000^{o}C) trondhjemitic magma, which, presumably, originated from partial melting of amphibolite material at the base of the granulite complex or at the top of the under-thrusted greenstone blocks, intruded granulites at P ~ 7.5-8.5 kbar (23-25 km depth) at 2.667±0.9 Ga during the exhumation of the SMZ. The magma heated and assimilated metapelites and dragged them to a depth of 18-20 km (6.3-6.5 kbar). The heterogeneous saturation of the trondhjemitic melt in MgO, FeO, Al_2O_3 by the dissolved metapelites provoked crystallization of several garnet generations. Various mineral assemblages included in the garnet allowed application of the TWQ method combined with PERPLE_X pseudo sections to trace sub-isobaric cooling of the magma from T ~ 900^{O}C to ~600^{O}C at 6.3 - 6.5kbar. The isobaric cooling also affected the associated metapelite heated by the magma. Fluid inclusions trapped in garnet and quartz in the trondhjemite show that the magma transported CO_2 fluid coexisting with aqueous-salt fluid (preserved as inclusions with salinity up to 20.58 wt. % NaCl eq.). These fluids with a_{H2O} <0.3 bearing Na, K and Ca salts, being exsolved from the magma on cooling and solidification, provoked formation of complex Na-gedrite + biotite + sillimanite (kyanite) + quartz ± staurolite ± plagioclase-bearing assemblages after cordierite in trapped metapelites at 630-570^{O}C and 6.3-6.5 kbar. These data show that hot trondhjemitic melts played a critical role in the exhumation of granulites onto the adjacent granite-greenstone craton. The melts transferred heat from the lower to the middle crust and also transported large volumes of external H_2O-CO_2-salt fluids that subsequently participated in the rehydration of a significant portion of the SMZ.

Acknowledgements: The study is supported by Russian Foundation for Basic Research (projects 13-05-00353 to OGS), by the RFBR-NRF South Africa grant 14-05-93962 (to OGS and DDvR), by grants from the National Science Foundation of South Africa (GUN: 2053192) and the University of Johannesburg as part of the Russian-South African scientific collaboration

Ti-in-zircon thermometry and the role of coupled dissolution-reprecipitation process: constraints from high-grade rocks from Central Brazil

Della Giustina M*, Pimentel M, Ferreira Filho

1 - Universidade de Brasília *maria_emilia@unb.br

Ti-in-zircon thermometry is widely used to investigate high-grade terranes aiming at constraining the nature of metamorphic reactions involving zircon growth and/or recrystallization. In Central Brazil, zircon grains from the Serra da Malacacheta (SMC) - Barro Alto (BAC) layered mafic ultramafic complex were investigated. In the studied samples, the textural, isotopic and chemical characteristics of zircon grains indicate that the primary signature is only partially preserved due to a coupled dissolution-reprecipitation process operating during high-grade metamorphism. Ti-in-zircon analyses reveal homogeneous temperatures for all samples, with a mean value of 700±40°C. There is no correlation between Ti concentrations and U-Pb ages or Hf isotopic signature and identical temperatures were observed on both cores and recrystallized rims. Similar behavior is also observed for REE and other trace elements. Thus, the homogeneous Ti-in-zircon data reproduces neither igneous crystallization temperatures for mafic-ultramafic magmas nor metamorphic conditions. The recrystallization process seems to have operated until a "lower boundary" was reached, rendering a Ti concentration compatible with temperatures between ~650-700°C. Therefore, it is suggested that Ti-in-zircon temperatures on recrystallized grains from high-grade terranes, comparable to the SMC and BAC, should be evaluated with caution when applied in investigations of peak metamorphic conditions.

Oxygen isotope systematics of high-grade rocks and associated leucogranite from the South Marginal Zone of the Limpopo Complex, South Africa

Dubinina E[1*], Aranovich L[2], van Reenen D[3], Avdeenko A[2]

1 - IGEM RAS *elenadelta@gmail.com 2 - Russian Academy of Sciences 3 - University of Johannesburg

We present oxygen isotope data obtained by laser fluorination technique for three outcrops from the South Marginal Zone (SMZ) of the Limpopo granulite complex, South Africa. These outcrops are respectively located within the granulite zone (Bandelierkop quarry locality), on the retrograde (orthopyroxene-out) isograd (Manamead locality), and within the zone of rehydrated granulite south of the retrograde isograd (Klipbank locality). The studied localities represent two main lithological types of SMZ rocks, namely Baviaanskloof tonalite-trondhjemite gneisses (Klipbank), and metapelites of the Bandelierkop Formation at Manamead and Bandelierkop quarry. In addition to these host lithologies, all studied localities also include felsic (leucogranite) rocks that occur as intrusive veins and veinlets in the host tonalite gneisses or the metapelite. Oxygen isotope thermometry has been applied in combination with conventional mineral thermometry (the TWQ method) to estimate T-P conditions of formation of the rocks at the different localities. Isotopic data also allowed the estimation of the role of fluids and the degree of open system behavior of the oxygen isotope systems in the rocks at both the metamorphic peak (Bandelierkop) and during the retrograde stage (Manamead and Klipbank), as well as tracing the genetic relations of the felsic (leucogranite) rocks with the associated SMZ lithologies. Based on similarities in the $\delta^{18}O$ (BR) values, the leucogranite rocks at the Klipbank locality (south of the orthopyroxene isograd) involved material of the host tonalitic gneisses and were formed under the influence of a fluid with X_{CO2} >0.24. These data contradict a model of *in situ* dehydration melting and support the influx of external fluids (i.e. rehydration melting). Oxygen isotope closure temperatures of the leucogranite rocks and host tonalitic gneisses are strongly different (540 and 740°C, respectively).

Evidence for pervasive fluid flux was also inferred for metapelites located on the retrograde isograd (Manamead) and in the granulite terrane at Bandelierkop quarry. At Manamead, the oxygen isotope closure temperature occurred within the narrow range of 630-650°C that corresponds closely with published data obtained for the retrograde stage of metamorphism. At Bandelierkop quarry in the granulite zone, the thermal history of the host metapelite has been clearly disturbed by a contact metamorphic event caused by intrusions and injections of large volumes of leucogranite. Oxygen isotope closure temperatures of leucogranites and host metapelite near the contact zone vary from 680 to 720°C, while other metapelites show that internal oxygen isotope equilibrium was absent.

Isotopic and geochemical features of the leucogranite thus unambiguously indicate the role of fluids and the genetic relation to the tonalitic Baviaanskloof gneisses at Manamead, but strongly deny the formation of leucogranite via in situ partial melting of metapelites at Bandelierkop quarry, a process favored by other workers.

Evolution of subduction in the Precambrian and consequences on the formation of continental crust

Fischer R*, Gerya T

ETH Zurich, Institute of Geophysics *ria.fischer@erdw.ethz.ch

Phanerozoic plate tectonics with its typical subduction and orogeny is relatively well understood and can be traced back in the geological records of the continents. Interpretations of geological, petrological and geochemical observations from Proterozoic and Archean orogenic belts e.g., [1], however, suggest a different tectonic regime in the Precambrian. Due to higher radioactive heat production the Precambrian lithosphere shows lower internal strength and was strongly weakened by percolating melts. The fundamental difference between Precambrian and Phanerozoic tectonics is therefore the mantle potential temperature, which determines the strength of the upper mantle [2] and further tectonic history.

3D petrological-thermomechanical numerical modelling experiments of oceanic subduction at an active plate margin with varying mantle potential temperatures show different subduction regimes. For temperatures <175 K above the present day value a subduction style appears which is close to present day subduction but with more frequent slab break-off. At temperatures 175 - 250 K above present day values steep subduction continues but the plates are weakened enough to allow buckling and also lithospheric delamination and drip-offs. For temperatures >250 K above the present day value no subduction occurs any more. The whole lithosphere is delaminating and due to strong volcanism and formation of a thicker crust subduction is inhibited.

This stage of 200-250 K higher temperature which corresponds roughly to the early Archean [3] is marked by strong volcanism due to sublithospheric decompression melting and increased crustal growth. The new formed crust is mainly of dacitic composition but preferentially at its rim also granitic. The strong crustal growth leads to an equal thickness of both oceanic and continental plates and as a consequence subduction is inhibited. However, a compressional setup instead will lead to orogeny between a continental or felsic terrain and an oceanic or mafic terrain as well as internal crustal convection. Small-scale convection with plume shaped cold downwellings also in the upper mantle is of increased importance compared to the large-scale subduction cycle observed for present temperature conditions.

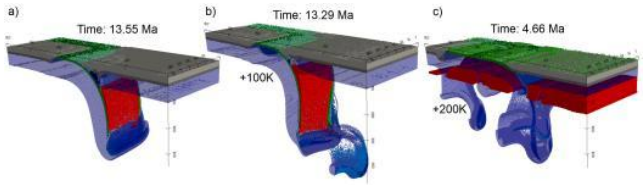

Figure 1: Subduction depends strongly on mantle potential temperature. (a) Modern subduction with present day temperature (b) Increase of temperature by 100 K leads to melting and drip-off of the of the slab-tip. (c) A temperature increase of 200 K leads to buckling of the subducting slab and Rayleigh-Taylor instabilities not only at the slab-tip but the whole lithosphere-asthenosphere boundary. At this stage subduction is no longer possible as the slab melts before it can be subducted into the mantle.

[1] Brown M. (2006). Duality of thermal regimes is the distinctive characteristic of plate tectonics since the neoarchean. *Geology*, 34, 961-964.

[2] Brun J.P. (2002). Deformation of the continental lithosphere: Insights from brittle-ductile models. Geological Society, London, Special Publications 200, 355-370.

[3] Abbott D., Drury R., Smith W.H.F. (1994). Flat to steep transition in subduction style. *Geology*, 22, 937-940.

Rare element sources for chambers of diamond-and-inclusions parental carbonatite magma: experimental and geochemical evidence

Kuzyura A[1*], Litvin Y[1], Jeffries T[2]

1 - Institute of Experimental Mineralogy, Russia *shushkanova@iem.ac.ru 2 - Department of Mineralogy, Natural History Museum

Interphase mineral-carbonatite melt partition coefficients (K_D^{RE}) of representative rare elements Li, Rb, Cs, Ba, Th, U, Ta, Nb, La, Ce, Pb, Pr, Sr, Nd, Zr, Hf, Sm, Eu, Gd, Tb, Dy, Y, Ho, Er, Tm, Yb, Lu, Sc and Zn have been experimentally determined in a partially melted diamond-forming peridotite-eclogite-carbonatite system at 7.0 - 8.5 GPa. The coefficients for olivine, clinopyroxene and garnet demonstrate that the heavy rare earth elements are predominantly concentrated in garnets. Based on (i) the experimental partition coefficients K_D^{RE}, and (ii) the rare element contents in diamond-hosted minerals of peridotite and eclogite paragenesis as well as minerals of diamondiferous xenoliths in kimberlites, the plausible rare element concentrations in natural diamond-forming completely miscible carbonate-silicate (carbonatite) melts were calculated. A spidergram showing both model melts and natural carbonatite melts from diamond inclusion was constructed (Figure 1).

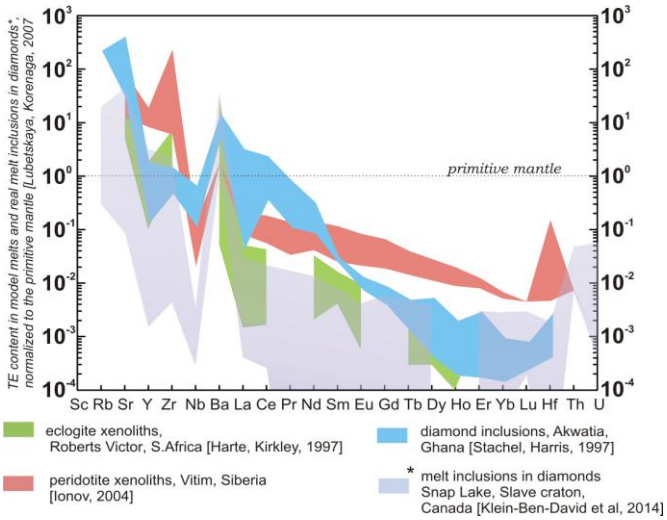

Figure 1: Spidergram showing model melts and natural carbonatite melts from diamond inclusions

It was found that upper mantle components mainly contributed rare elements into the parental melts. The parental melts are depleted by medium (Sm, Eu, Gd) and heavy (Tb, Dy, Ho, Er, Yb, Lu, Hf) rare elements in comparison to the primitive peridotite. The elevated contents of Sc, Rb, Sr, Y, Zr, Nb, Ba indicate another source of rare elements involved in the diamond-and-inclusions parental melts. The "metasomatic agent" is the most probable source of this group of rare elements. The chambers of the diamond-and-inclusions parental melts could thus have formed during interaction of the upper mantle garnet lherzolite with a chemically active alkali- and CO_2-bearing "metasomatic agent". As a result, the carbonate-silicate parental melts originally included components of both mantle peridotite and of the "metasomatic agent".

Acknowledgement: Grant of the President of RF #MK-1386.2013.5, RFBR grants: 12-05-33044, 13-05-00835, 14-05-00537.

The role of volatiles (H_2O, CO_2) in the mantle incipient melting captured by a multi-component model

Massuyeau M[1*], Morizet Y[2], Gaillard F[1]

1 - ISTO-CNRS/Université Orléans/BRGM *malcolm.massuyeau@cnrs-orleans.fr 2 - LPGN-CNRS/Université Nantes

The link between volatiles and mantle melting has so far been illuminated by experiments revealing punctually, at a given P-T condition and under a specific chemical system, properties such as solubility laws, redox equilibria, and phase equilibria. Our aim is to establish a multi-component model describing the Gibbs free energy of melt produced by mantle melting in presence of CO_2-H_2O: that are carbonatite-carbonated melt-nephilinite-basanite and basalt with increasing degree of partial melting.

Near solidus melts are dominated by carbonate-rich compositions, evolving towards basaltic compositions at higher temperatures. However, this carbonate-silicate transition is complex, abrupt, and dependent on temperature, pressure and the chemical composition of the system. In order to simulate partial melting in a variety of mantle conditions, we established a parameterization of the mixing properties allowing the complex activity-composition relationships for multi-component hydrated carbonated melts to be accounted for. Using the Margules formalism, this parameterization is calibrated on crystal-liquid, graphite-liquid, fluid-liquid and liquid-liquid equilibria obtained by experimental studies in the P-T range 1-10 GPa and 900-1800°C. We so far adjusted the activity of the SiO_2 and CO_2 melt components, which constitutes the main part of the silicated and carbonated frameworks. The SiO_2-CO_2 interaction reveals a strong non-ideality requiring a strongly asymetric Margules formulation. We also determined the standard thermodynamic properties for the CO_2 melt component and we have refined the standard volume properties for liquid SiO_2.

Major and trace element mineral chemistry of a suite of mantle-derived eclogites from the Balmoral kimberlite in South Africa

Mxinwa T*, Viljoen F, Mouri H

University of Johannesburg *tmxinwa@gmail.com

Eclogites form a minor component of the Earth's mantle. However, they play a vital role in our understanding of geodynamic processes such as the subduction of oceanic crust and the crystallization of diamond within the sub-cratonic lithosphere. These high pressure eclogite xenoliths are commonly encountered in kimberlite pipes on the Kaapvaal craton, and may be diamond-bearing. The current study presents the first comprehensive investigation into the petrology, mineralogy and whole-rock geochemistry of a mantle-derived eclogite xenolith suite from the Balmoral kimberlite.

A large portion of eclogites from the Balmoral kimberlite pipe is comprised of bimineralic (garnet and clinopyroxene) rocks with the rest being corundum-bearing (between 1 and 6 vol% corundum). Textures of Balmoral eclogites are ambiguous and chemical criteria are thus used to classify all Balmoral eclogites into Group II. Garnet from bimineralic rocks shows a trend from pyrope-rich towards grossular-rich compositions, whereas garnet from corundum-bearing eclogites are mainly comprised of the grossular component. Clinopyroxenes are omphacitic in composition.

The Balmoral major bulk compositions exhibit variations in MgO and CaO contents. Calculated garnet-clinopyroxene equilibration temperatures in Balmoral eclogites ranges between 1085 to 1350°C. Corundum-bearing eclogites exhibit relatively high equilibration temperatures (ca. 1200 to 1350°C) whereas bimineralic rocks occur at cooler temperature conditions (ca. 1000 to 1200°C). There is a strong positive correlation between CaO content in garnets and equilibration temperatures of Balmoral eclogites. Thus eclogites with high CaO content in garnet tend to have comparatively higher temperatures of equilibration than their low CaO counterparts.

Protolith comparisons of Balmoral eclogites show that MgO-rich bimineralic xenoliths have compositions similar to tholeiitic basalts whereas MgO-poor assemblages mirror MORBs. However, corundum-bearing eclogites have compositions that are broadly comparable to oceanic gabbros. Similarly, trace element evidence in Balmoral eclogites points towards an oceanic crustal rock protolith. Although trace elements are depleted in these rocks, incompatible trace elements are slightly enriched, which is believed to be due to a late stage metasomatic event. The protoliths for Balmoral xenoliths is a subducted oceanic crustal section comprising tholeiite, MORB and gabbro.

Fluid-assisted interaction of the carbonate and chloride-rich metabasalt with fertile peridotite under conditions of "hot" subduction

Safonov O[1*], Kiseeva K[2]

1 - Institute of Experimental Mineralogy *oleg@iem.ac.ru 2 - Department of Earth Sciences, Oxford University

Altered oceanic basalts subducted into the upper mantle transport more than 2.5 wt. % H_2O, about the same amounts of CO_2 and significant amount of chlorides. Their metamorphism in the subduction zones, thus, can serve as a strong source for aqueous-carbonic-salt fluids and melts that might metasomatize the mantle wedge. The chemical transport between the subducted basaltic crust and the peridotite mantle has been studied in the experiments on interaction of H_2O, carbonate and chloride-bearing metabasalt with pyrolite that were performed at 4 GPa/1000^{O}C, 3 GPa/900^{O}C and 2 GPa/750^{O}C. These P-T conditions represent the average temperatures at different levels of the subducting slabs in the hot subduction zones. The synthetic "eclogitic" starting material contained (in wt. %) SiO_2 46.91, TiO_2 1.59; Al_2O_3 17.68; FeO 10.52; MnO 0.17; MgO 8.49; CaO 10.27; Na_2O 3.73; K_2O 0.47. It was mixed with 20 wt. % of the $CaCO_3$+KCl+NaCl mixture and oxalic acid accounting for 3 wt. % H_2O in the system. The "peridotitic" portion was represented by the synthetic mixture MPY90. Zoning, which appeared between the eclogitic and peridotitic portions, reflects an active influence of the "eclogitic" volatile components on the peridotite. Influence of peridotite on the eclogitic portion at 4 GPa and 1000^{O}C is expressed in the increase of the MgO content in the eclogitic portion (up to 20 мас. % in contrast to the starting 6.8 wt. %). At 4 GPa/1000^{O}C, K, Na, Ca and Cl are accumulated in the contact zone between the eclogitic and peridotitic portions. The inner zone of the eclogitic portion loses these components and is composed of Grt, Rut and a melt containing 38-45 wt. % SiO_2, 9-12 wt. % CaO, 2.5-4 wt. % Na_2O and 11-18 wt. % MgO, but strongly poor in K and Cl. Concomitant enrichment of the peridotitic portion in K, Na and Cl results in crystallization of Cl-bearing Phl. Opx is a predominant phase in the peridotitic portion at 4 GPa/1000^{O}C, which additionally contains Cpx, Grt and magnesite (Ms), but does not contain Ol. Such assemblage results from reactions Ol + CO_2 = Opx + Ms and 3/2Ol + 1/2Grt + 1/2K_2O + H_2O + 3/2CO_2 = Phl + 3/2Ms with the aqueous carbonate-chloride melt uprising from the eclogitic portion. Distribution of components between the eclogitic and peridotitic portions is very different at 2 GPa/750^{O}C. Although major components are distributed stepwise in accordance with the starting distribution, K and Cl are equally distributed along the profile. An assemblage of Pl, Amph, Cpx, Rut and Ca-Mg carbonate forms in the eclogitic portion, while the contacting peridotitic portion does not contain Ol and is composed of Opx, Ms, Phl and, possibly, norbergite. The experiments demonstrate different ways of chemical transport between the carbonate, chloride and water-rich metabasalt and fertile peridotite in dependence on P-T conditions. The chloride-carbonate melt accumulating at the contact zone at 3 GPa/900^{O}C and 4 GPa/1000^{O}C removes both K and Na, as well as Cl, from eclogite and causes formation of Opx+Ms+Phl in the peridotite after Grt and Ol. Fixation of Na by crystalline phases in the eclogite at 2 GPa/750^{O}C "immobilizes" it at these conditions. K and Cl tend to concentrate in the brine fluid, which provokes "potassic" metasomatism in the peridotite.

Multiple hydration processes of retrogressed pelitic granulite from the Southern Marginal Zone of the Neoarchean Limpopo Complex, South Africa

Koizumi T[1], Tsunogae T[1*], van Reenen D[2]

1 - University of Tsukuba *tsunogae@geol.tsukuba.ac.jp 2 - University of Johannesburg

Fluids in the lower crust are thought to have played a critical role in the evolution of high-grade metamorphic rocks. Particularly, during granulite formation, it is generally accepted that fluid composition must have been of low H_2O activity to stabilize anhydrous orthopyroxene-bearing assemblages. In contrast, during the exhumation (retrograde) stage, influx of H_2O-bearing fluid from an external source appears to be a common phenomenon, because granulite-facies rocks often show evidence for retrograde hydration reactions, during which anhydrous high-grade minerals are partly or completely replaced by secondary hydrous minerals. Therefore, hydration of granulites and formation of amphibolite-facies mineral assemblages characterize high-grade metamorphic terranes worldwide. However, the quantity of water in such retrograde fluids necessary to drive the hydration reactions is unknown. Here, we report new petrological data for a partially hydrated pelitic granulite from the retrograde (orthopyroxene-out) isograd developed in the Southern Marginal Zone (SMZ) of the Neoarchean Limpopo Complex in South Africa, and discuss the *P-T*-fluid evolution based on mineral equilibrium modelling in the NCKFMASH system. The results demonstrate the stability of the peak M1 assemblage (garnet + biotite + orthopyroxene + K-feldspar + plagioclase + quartz) at 750-900°C and 8-9 kbar, and relatively dry condition of $a$$H_2O$ [H_2O activity] = 0.40-0.55. M1 was followed by near-isothermal decompression to M2 (ca. 800°C, 7.7-8.0 kbar, M(H_2O) [mole H_2O % of the rock] = 0.5-2.5 mol.%, $a$$H_2O$ = 0.4-0.5) as inferred from garnet + biotite + orthopyroxene + cordierite + K-feldspar + plagioclase + quartz assemblage in the sample. The formation of anthophyllite corona around orthopyroxene and kyanite + orthoamphibole + quartz intergrowth after cordierite suggest significant interaction with an aqueous fluid during retrograde metamorphism. The *T*-M(H_2O) pseudosection constrains the first hydration event (M3a), during which anthophyllite replaced orthopyroxene at 630-730°C and M(H_2O) = 3.0-3.5 mol.%, to have occurred after the M2 event. Further increase in M(H_2O) condition (4.5-6.0 mol.%) and cooling to <630°C triggered the progress of the second hydration event (M3b) and M4 event, during which kyanite/sillimanite + orthoamphibole + quartz and garnet + kyanite/sillimanite + quartz replaced cordierite. A consistent $a$$H_2O$ condition of 0.2-0.3 during M3 and M4 events suggests that $a$$H_2O$ was buffered to lower levels by progress of the hydration reactions. Such an increase in mole H_2O content in the rock with the formation of hydrous mineral assemblages after anhydrous assemblages estabished a retrograde isograd and zone of hydrated granulite in the SMZ. This event might be related to influx of H_2O-bearing fluid along the Hout River Shear Zone (HRSZ) that marks the major crustal break between the SMZ and the adjacent Kaapvaal Craton. The aqueous fluid was probably derived from devolatilization of low-grade underthrusted greenschists in the footwall section of the HRSZ by the overriding granulites during the thrust-controlled spreading of the SMZ onto the Kaapvaal craton.

Fluid-rock interaction and high- to ultrahigh-temperature metasomatism related to brine infiltration in the Neoarchean Limpopo Complex, South Africa

Tsunogae T[1*], van Reenen D[2]

1 - University of Tsukuba *tsunogae@geol.tsukuba.ac.jp 2 - University of Johannesburg

It is generally known that interaction of the lower crust with fluids of magmatic or metamorphic origin controls various granulite-forming processes, including dehydration/hydration reactions, partial melting, material circulation, and high-temperature metasomatism. Although many arguments in favor of fluid-absent metamorphism related to dehydration melting are offered as a possible mechanism to form granulites, the widespread occurrences of metamorphic fluids trapped as primary inclusions in various high-grade minerals suggest that at least some fluids must have been present during high-grade metamorphism. In this contribution, we report new petrological data obtained from metamorphic enderbite and its metasomatized equivalents from the Southern Marginal Zone (SMZ) of the Neoarchean Limpopo Complex, South Africa, and evaluate the alteration process caused by infiltration of high-salinity aqueous fluids during granulite-facies metamorphism. At the study area on the farm Commissiedraai, enderbite (Pl + Qtz + Kfs + Opx) is partly metasomatized with the formation of continuous alteration zones comprising Pl + Qtz + Kfs + Opx + Grt, Pl + Qtz + Kfs + Grt, and finally antiperthite + Qtz + Grt + Sil. Bulk K_2O increases, and CaO, MgO, FeO, and TiO_2 decreases continuously from enderbite to the most intensely metasomatized rock. The occurrence of aqueous fluid inclusions with final melting temperatures of -29.2°C to -21.6°C trapped as a primary phase within quartz in the highly-altered sample indicates that a high-salinity brine (probably NaCl rich) with additional components such as $MgCl_2$ and $CaCl_2$ controlled metasomatism. We employed a phase equilibrium modelling technique to evaluate the metasomatic process in the system NCKFMASH using THERMOCALC 3.3, and discovered that addition of K to and removal of Ca and Fe from the precursor enderbite gave rise to the metasomatized mineral assemblages. Modelling also indicated that metasomatic alteration occurred at ca. 900°C, which is consistent with peak metamorphic conditions reached in the SMZ, and with temperature calculations based on ternary-feldspar geothermometry of antiperthite in the highly-metasomatized sample. The brine fluid that accompanied metasomatism infiltrated along the high-temperature Petronella Shear Zone, and was probably derived from devolatilization of metavolcanic rocks of the Kaapvaal Craton as the result of thrusting hot granulite over cool greenstones. Our results therefore suggest that metasomatism at this locality occurred during or closely after peak metamorphism having been reached in the root zone of the Limpopo orogeny at ~2.72Ga.

Lateral variations in plagioclase compositions, Main Zone, Bushveld Complex, South Africa: evidence for slow mixing of magmas in basinal structures

Cawthorn G[1*], Lundgaard K[2], Tegner C[2], Wilson R[2]

1 - University of the Witwatersrand *grant.cawthorn@wits.ac.za 2 - Aarhus University

The nature of magma recharge through the interval including the Pyroxenite Marker (PM) in the Main Zone of the eastern Bushveld Complex, South Africa, is examined. The plagioclase compositions (An) in five previously published and three new profiles (each at least 600 m vertically) along a strike length of 110 km are compiled to emphasize lateral as well as vertical variations. Lateral variations show a range in: (i) the minimum An value reached in each profile prior to the onset of magma recharge (An_{51} to An_{59}), (ii) the depth below the PM at which the minimum value is observed (50 to 575 m), (iii) the An value close to the PM (An_{54} to An_{75}), (iv) the maximum value recorded above the PM (An_{63} to An_{76}), (v) the height above the PM at which this maximum value is reached (0 to 300 m). In all cases highest values of An occur in the north. It is also important to note that the PM terminates toward the south, and the footwall rocks change from gabbronorite in the north to magnetite gabbronorite in the south. A vertical cross-section through these profiles defines a major basin shape with an upfold toward the south, and a second southern basin (that contains one of these profiles). These results show that initially added magmas ponded at the bottom of the basin and did not homogenise the entire chamber. The added magma was more magnesian than the extant magma, but was lower in SiO_2 content and so was more dense. Addition of this magma was not a single event, but was continuous or intermittent while a few hundred metres of the Main Zone accumulated taking several thousands of years. There is more variability in the profiles showing the mg# of the pyroxenes than of the An content of plagioclase, which results from the trapped liquid shift effect that is most pronounced where there is a low abundance of mafic phases.

Melting conditions and sources of 3.5 Ga komatiites from ICDP drilling in the Barberton Greenstone Belt, South Africa

Coetze G[1], Arndt N[2*], Blichert-Toft J[3], Wilson A[1]

1 - University of the Witwatersrand 2 - ISTerre, Universite de Grenoble *nicholas.arndt@ujf-grenoble.fr 3 - ENS Lyon

We analysed major and trace elements and Nd-Hf isotopes in 18 samples of komatiites from the core recovered from the ICDP drilling project in the Barberton Greenstone Belt, South Africa. Two fractions of magmatic clinopyroxene from a surface sample were also analysed. All samples are of the Al-depleted Barberton-type komatiite and all show the geochemical signature of residual garnet in the source (low Al/Ti, depleted HREE). One sequence, however, is unusual in that it contains petrographic and geochemical evidence that orthopyroxene as well as olivine crystallized during solidification of the lavas. The whole-rock data and the clinopyroxene separates define linear arrays in the Sm-Nd and Lu-Hf systems that correspond, within error, with the accepted age of the rocks (3.48 Ga). Initial isotopic values for the clinopyroxene separates provide high-precision results, with epsilon Nd(T) = -1.1 and -1.5 and epsilon Hf(T) = +3.3 and +4.1. The positive Hf values are in line with other results from komatiites from the Barberton Belt but the negative Nd value is surprising in that it indicates an enriched source with low Sm-Nd. The peculiar characteristics of this source - low Sm/Nd and high Lu/Hf - is found in the trace element compositions of some of the komatiite lavas, which are moderately enriched in LREE and have negative Hf anomalies. The enriched LREE are consistent with that of a liquid extracted after deep melting but the origin of Hf deficit remains uncertain.

The orthopyroxene-phyric komatiites are isotopically indistinguishable from the other komatiites indicating that the Si-rich character probably was acquired during melting rather than being derived from an older source. All these komatiites were produced by about 30% batch melting, at about 300 km depth, under conditions in which garnet remained in the residue during the melting process.

Apatite and olivine characteristics in the Upper Zone of the Bushveld Complex Northern Limb, South Africa: insights into late-stage processes in layered intrusions

Honour V C[1], Longridge L[2*], Humphreys M C S[3], Robb L J[1], Stock M J[1]

1 - Department of Earth Sciences, University of Oxford 2 - Bushveld Minerals Limited *lukelongridge@gmail.com 3 - Department of Earth Sciences, Durham University

The presence of cumulus apatite and magnetite in the topmost portions of the Upper Zone of the Bushveld Complex, South Africa, has been attributed to either large-scale liquid immiscibility (e.g. [1]) or to the final stages of closed-system fractional crystallization (e.g. [2]). Assay results from boreholes intersecting the apatite-bearing Upper Zone (recently drilled by Bushveld Minerals Limited on the Northern Limb of the Bushveld Complex) reveal geochemical heterogeneity, with fluctuations in Fe, V, Ti and P reflecting variations in the concentrations of magnetite, ilmenite and apatite through the core. Fe_2O_3 contents range from 10% to 70%, related to variations in the magnetite content.

Two major spikes in P_2O_5 (apatite) are observed within the core samples. The lower apatite-bearing zone starts abruptly over 10 m, is accompanied by a significant decrease in Fe and Ti, and is preceded by a drop to low V, Cu and Ni contents. The upper apatite-bearing zone is of a similar magnitude but is not accompanied by a decrease in transition metal contents.

Reaction microtextures between olivine, Fe-Ti oxides and pyroxene are observed in these rocks and have been ascribed to open-system behaviour in other layered complexes [3]. Together with petrologic observations of apatite grain size distribution, these textures may support a model of liquid immiscibility in the upper portions of the Bushveld Complex.

[1] VanTongeren J.A. and Mathez E.A. (2012). Large-scale liquid immiscibility at the top of the Bushveld Complex, South Africa. *Geology*, 40 (6), 491-494.

[2] Cawthorn R. (2013). Rare earth element abundances in apatite in the Bushveld Complex—A consequence of the trapped liquid shift effect. *Geology*, 41 (5), 603-606.

[3] Holness M.B., Stripp G., Humphreys M.C.S., Veksler I.V., Nielsen T.F.D., and Tegner C. (2011). Silicate Liquid Immiscibility within the Crystal Mush: Late-stage Magmatic Microstructures in the Skaergaard Intrusion, East Greenland. *Journal of Petrology*, 52 (1), 175-222.

In situ origin of the Merensky Reef, Bushveld Complex?

Latypov R[1*], Chistyakova S[2], Page A[3]

1 - School of Geosciences, University of the Witwatersrand *rais.latypov@wits.ac.za

2 - University of the Witwatersrand 3 - SRK Consulting

The current debate on the origin of platinum group element (PGE)-reefs in layered intrusions centres mostly on gravity settling of sulphide liquid from the overlying magma ("downers" model) versus its introduction together with interstitial melt/fluids migrating upward from the underlying cumulate pile ("uppers" model). We have recently developed a model that suggests the formation of PGE deposits may not require a long-range gravitational settling of chromite crystals and sulphide droplets from the overlying magma and/or large-scale upward migration of interstitial liquid/fluid from the underlying crystal mush. In essence, these two mechanisms may not be absolutely crucial for the formation of PGE deposits in layered intrusions. As an alternative, we have proposed an *in situ* origin for PGE reefs in the Rum Layered Suite (NW Scotland), in which sulphide droplets form directly at the crystal-liquid interface and extract noble metals from fresh magma delivered towards the base by flow/convection in the magma chamber [1]. In this presentation, we would like to discuss two geological features of the Merensky Reef of the Bushveld Complex that appear to provide confirmatory evidence for the above idea. First, many sections of Merensky Unit with extensive development of regional 'potholes' show 1-2 cm thick chromitite seams of the Merensky Reef that occur along the vertical to overhanging sidewalls of these potholes (e.g. [1, 2, 3, 4]). Clearly, gravity settling cannot produce such chromite seams on overhanging sidewalls of depressions, suggesting instead that the Merensky Reef is likely a result of magma crystallization *in situ*, i.e., directly at the crystal-liquid interface. Second, there are examples of sulphide-bearing dykes of the Merensky Reef that cross-cut the footwall stratigraphy and occur 10-25 m below the normal Merensky Reef elevation on the margins of large potholes (e.g. [5, 6]). The dykes often show 1-2 cm thick chromitite seams along both margins and are commonly enveloped by anorthosite rims that are formed by reconstitution of adjacent noritic rocks. The existence of the Merensky Reef dykes is hard to reconcile with gravity-driven crystal settling from 'above' onto the magma chamber floor. In a similar manner, the textural and compositional features of the dykes are not compatible with late-stage remobilization of the semi-consolidated crystal mush of the Merensky Reef and are better explained by in *situ* sidewall crystallization from through-flowing magma in a conduit. We believe that these two geological observations are indicative of the formation of the Merensky Reef from a basally-emplaced layer of new magma, in which nucleation and crystallization of chromite and sulphides and concomitant scavenging of PGE from the magma took place essentially *in situ*, i.e., directly at crystal-liquid interface. The inferred *in situ* origin of the Merensky reef of the Bushveld Complex therefore appears to be a logical conclusion in light of the current consensus on layered intrusions as magma chambers that gradually lose heat and crystallize in situ from margins inwards.

[1] Latypov R.M., O'Driscoll B. and Lavrenchuk A. (2013). Towards a model for in situ origin of PGE reefs in layered intrusions: insights from chromitite seams of the Rum Eastern Intrusion, Scotland. *Contributions to Mineralogy and Petrology*, 166, 309-327.

[2] Ballhaus C. (1988). Potholes of the Merensky reef at Brakspruit shaft, R.P.M. - primary disturbances in the magmatic stratigraphy. *Econ. Geol*. 83, 1140-1158.

[3] Ballhaus C.G. and Ryan C.G. (1995). Platinum-group elements in the Merensky Reef. I. PGE in solid solution in base metal sulfides and the down-temperature equilibration history of Merensky ores. *Contrib. Miner. Petrol*, 122, 241-251.

[4] Ballhaus C. and Sylvester P. (2000). Noble metal enrichment processes in the Merensky reef, Bushveld Complex. *J Petrol* 44, 545-561

[5] Carr H.W., Groves D.I. and Cawthorn R.G. (1994). A GIS based spatial analysis of controls on the distribution of Merensky reef potholes at the Western Platinum Mine, Bushveld Complex, South Africa. *S Afr J Geol*, 97, 431-441.

[6] Carr H.W., Kruger F.J., Groves D.I. and Cawthorn R.G. (1999). The petrogenesis of Merensky Reef potholes at the Western Platinum Mine, Bushveld Complex: Sr-isotopic evidence for synmagmatic deformation. *Mineralium Deposita*, 34, 335-347.

The role of magma advection and regional thermal evolution in prolonging fractionation in spatially and temporally associated magmatic systems: examining conditions for extreme differentiation and formation of granophile ore deposits

Lentz D

University of New Brunswick. dlentz@unb.ca

It is well known in magmatic ore deposits that various types of fractionation of metallic components is an important process. In felsic magmatic systems, the formation of a wide variety of granophile ores is also related to some type of fractionation, although problematic for several reasons. Some reasons are relatively simple, i.e., melt diffusivities and viscosities make the approach to interpolating equilibrium thermodynamics more problematic. Bulk D values for the Niobium Tuff (Western Australia) or Macusani Tuff (Peru) better represent end-members of extremely fractionated systems from which we can estimate mineral distribution coefficients or bulk distribution coefficients as they represent their greatest degree of fractionation (lowest T). In all magmatic systems, D is a function of T and as T decreases D changes and bulk compositions change markedly therefore experimentally or empirically calculated D values tend to be underestimated. For extremely incompatible elements, with actual D values <0.01 then issues of determining these values is highly problematic due to the kinetic limitations in these felsic systems in which incompatible element-enriched ore systems are formed, i.e., melt boundary layers etc. limit our ability to determine these values accurately, and extrapolation to actual D values is virtually impossible. Furthermore the rheology of these systems is much more limiting than in mafic systems, so the energetics of the overall system, become more critical during fractionation. Boundary layer crystallization, solidification fronts, etc. have been invoked to explain fractionation in felsic magmatic systems that are "rheologically challenged" such that convection-enhanced separation of crystals and crystal setting are not limiting features of fractional crystallization. However, these processes all still inhibit extreme fractional crystallization in low T, evolving felsic magmatic systems; typically we turn to fluxes (F, B, etc) to explain lower T's and observed extreme fractionation, which are relevant and critical; lowering liquidi and solidi allow these systems to evolve to lower T (changing D as well), but time becomes a greater and greater factor, as diffusivities affecting crystal-melt partitioning become exponentially lower. More energy in a system allows a magma to evolve towards lower T's (very slowly) enhances ideal fractionation and promotes extreme differentiation. The combination of problems of determining D values in extremely fractionated systems and of calculating them through a range of low T's appropriate for ore deposit formation, and of achieving near-perfect fractionation given the crystal boundary layer effects and crystal-melt separation in very high viscosity low T environments makes the energetics (heat budget) of these systems one of the most critical factors in enhancing extreme fractionation. The thermal gradient in a system (inside &out) controls the efficiency of these reactions and separation processes, i.e., crystal fractionation and even settling are significantly enhanced if thermally limited, evolved felsic magmatic systems are considered. Although this should be considered for Li-Cs-Ta pegmatites and related Sn-rich and U-rich magmatic systems, within anomalous geothermal gradients that have protracted magmatic input and (or) slow uplift, Nb-Y-F pegmatites and high-level Nb-Y-HREE magmas also have these same complex considerations. The size of the felsic magmatic systems and timing of emplacement in the upper crustal environment relative to other mafic magmas advecting heat into the crust are important to enhancing protracted fractional crystallization to extremes, such that enrichment of ore-forming granophile elements is possible, i.e., in LIP and SLIP settings. Volcanic products of these and their hypabyssal equivalents, as noted earlier, show that these are magmatic processes and not (only) hydrothermal enrichments of moderately fractionated systems. Rather there are numerous examples of extreme fractionation/differentiation (granophile elements) in felsic peraluminous, peralkalic and related silica-undersaturated felsic systems including related pegmatites that have formed world class ore deposits

The origin of the Troctolite Unit near the top of the Main Zone, Northern Limb of the Bushveld Complex, South Africa

Longridge L[1*], Davey J[2], McDonald I[2]

1 - Bushveld Minerals Limited *lukelongridge@gmail.com 2 - Cardiff University School of Earth &Ocean Sciences

A troctolite marker horizon, comprising a number of cyclic harzburgite-troctolite-anorthosite units, is found near the top of the Main Zone in the Northern Limb of the Bushveld Complex, South Africa and was first recognized by Van der Merwe [1]. The unit marks the re-appearance of Mg-rich olivine in the crystallization sequence following the development of gabbronorites that characterize the lower Main Zone. Although previously suggested to be a sliver of Critical Zone [2], REE patterns and incompatible trace element ratios suggest a Main Zone signature. The observed crystallization sequence cannot be modelled using published Main Zone (B3) parental magma compositions, regardless of pressure conditions used. The ultramafic units are unusually Cr-poor (Cr/MgO from 2-64) which precludes any origin via mixing with a new pulse of mafic magma. Instead, assimilation of a highly Mg-rich dolomite is required to shift the liquidus order to that observed. Such a contamination scenario is consistent with petrographic observations of carbonate assimilation and serpentinization. It is suggested that the first stage of contamination may have occurred in a staging chamber, forming a Mg-rich magma which crystallized olivine first. Subsequent injection of olivine-rich melt/mush into a Main Zone plagioclase crystal mush may have formed the troctolite marker unit, with olivine diffusion zones above and below into the 'typical' Main Zone gabbronorites. PGE mineralization is known to be associated with the troctolite, but the origin of this mineralization is less clear. PGEs are found within anorthosites at the top of each troctolite cycle and correlate closely with incompatible trace elements (Zr, Hf etc.) implying they may be associated with interstitial liquid.

[1] Van der Merwe M.J. (1976). *Economic Geology*, 71, 1337-1351.

[2] Ashwal L.D., Webb S.J. and Knoper M.W. (2005). *South African Journal of Geology*, 108, 199-232.

Small scale magma heterogeneity as evidenced by chromium and vanadium in magnetitite layers of the Bushveld Complex, South Africa

Maila P*, Cawthorn G

School of Geosciences, University of the Witwatersrand *rapmphelane.p@gmail.co.za

Magnetitite layers are an important feature of the Upper Zone of the Bushveld Complex, South Africa. The vanadiferous, 2 m-thick Main Magnetitite Layer (MML) has an extremely sharp basal contact with anorthosite and an intermediate zone about 10 cm thick where a minor proportion of cumulus plagioclase occurs, referred to as the "feldspar parting". The top contact is gradational into an anorthosite over a vertical distance of about 30 cm. 3 m and 6 m above this layer are two further layers (layers 1 and 2), which are about 20 cm thick. In an attempt to understand the genesis of such layers we have undertaken a study of the Cr and V content of pure magnetite mineral separates from a number of settings, namely: 4 detailed vertical sections (26 samples in each profile) through the MML; 32 samples along the basal contact at 10 m and a shorter section at 2 m intervals; 7 profiles (42 samples) through the feldspar parting; 11 and 7 (10 samples in each profile) detailed profiles through layers 1 and 2 respectively. These results extend studies made by Cawthorn and McCarthy [1], Klemm *et al*. [2], Kruger and Smart [3], Cawthorn [4].

Vertical profiles through the MML typically show an upward decrease in Cr (12 000 to 580 ppm) with 3 of the 4 profiles showing reversals in Cr. The V concentration through the MML appears to be constant (avg. 0.76 wt%) with one high concentration (0.92 wt%) at the top. Small reversals in Cr occur in four of the 7 profiles across the "feldspar parting", however, V shows no discernible trend or correlation with Cr. There is lateral variation in Cr in the feldspar parting profiles as reversals and absolute abundances are erratic. The 10 m and 2 m spaced basal profiles show lateral variation characterised by peak and low Cr and V contents. The 10 m profile shows an erratic trend in Cr ranging from 10 000 ppm to 16 000 with one high (28 000 ppm) Cr. Average V is 1.0 wt% excluding one peak (1.09 wt%) and three low (avg. 0.85 wt%) values, however, V shows no correlation with Cr. The 2 m profile shows an average Cr of 12 300 ppm excluding one peak (17 000 ppm) and one low (9 200 ppm) value. V, however, appears to be constant (avg. 0.84 wt%) showing no variation across the base. Profiles through layers 1 and 2 typically show an upward decrease in Cr (3300 to 1000 ppm). All profiles except two profiles, show several reversals but reversals cannot be correlated. However, V shows no discernible trend.

Previously proposed mechanisms for the genesis of magnetitite layers include double diffusive layer breakdown, magma addition, liquid immiscibility and sudden changes in either oxygen fugacity or pressure. Supporting or eliminating any of these possibilities with the current data set is difficult. However, it appears the magma must have been slightly inhomogeneous.

[1] Cawthorn R.G. and McCarthy T.S. (1981). *Transactions Geological Society of South Africa*, 81, 45-50.

[2] Klemm D.D., Henkel J., Dhem R. and Von Gruenewaldt G. (1985). *Economic Geology*, 80, 1075-1088.

[3] Kruger F.J. and Smart R. (1987). *Journal of Volcanology and Geothermal Research*, 34, 133-142.

[4] Cawthorn R.G. (1994). *South African Journal of Geology*, 97, 455-461.

Isotopically heterogeneous plagioclase populations in the Bushveld Complex suggest mush intrusion

Roelofse F[1*], Romer R[2], Ashwal L[3]

1 - Department of Geology, University of the Free State *roelofsef@ufs.ac.za 2 - GFZ German Research Centre for Geosciences 3 - School of Geosciences, University of the Witwatersrand

Recent work on the Bushveld Complex and other layered intrusions has shown the presence of locally significant isotopic heterogeneity, both between and within co-existing cumulate minerals. Various processes have been proposed to account for this, including the intrusion of variably contaminated crystal mushes from deeper staging chambers, the mixing of semi-consolidated crystal mushes as a result of subsidence during cooling, the infiltration of contaminants into a partially solidified crystal mush, the density-driven mixing of minerals from isotopically distinct magma pulses, contamination of crystals at the roof of an intrusion and mechanical incorporation of such contaminated crystals into the lower crystallisation front as a result of gravitational instability at the upper crystallisation front, and late-stage metasomatic processes. Here we present precise Sr-isotopic compositions for rim and core domains of plagioclase from the Main and Upper zones of the Bushveld Complex, which show the presence of multiple, isotopically heterogenous populations of feldspars occurring within the same rocks. We propose that the data are best explained through the intrusion of variably contaminated crystal mushes derived from a sub-compartmentalized, sub-Bushveld staging chamber that underwent different degrees of contamination with crustal rocks of the Kaapvaal craton. The presence of intracrystalline isotopic disequilibrium and multiple isotopic populations of the same mineral suggest the inadequacy of studying mineral separates (even using sequential leaching experiments) in deciphering the petrogenesis of layered mafic intrusions.

Variation in plagioclase chemical and isotopic composition in the UCZ of the Eastern Bushveld Complex, South Africa

Schannor M[1,2*], Hecht L[2,1], Veksler I V[3], Manyeruke T D[4], Romer R[3]

1 - Institut für Geologische Wissenschaften FU Berlin, Germany *mathias.schannor@fu-berlin.de 2 - Museum für Naturkunde (MfN) Berlin, Germany 3 - GFZ German Research Centre for Geosciences, Potsdam, Germany 4 - Nkwe Platinum (SA) (Pty) Ltd, Sandton, Republic of South Africa

The layering of the ~2050 Ma old Bushveld Complex and especially the petrogenesis of chromitite layers remains a matter of debate until today. This study aims to examine the inferences on chromitite formation that can be drawn from chromitite associated plagioclase chemistry. We analysed mineral chemistry and Sr isotopes of cumulus and intercumulus plagioclase associated with Upper Group 2 chromitite (UG2) in the Upper Critical Zone (UCZ) of the Eastern Bushveld Complex, South Africa.

In contrast to the adjacent silicate host rocks, potassium and rubidium are clearly depleted in chromitite-hosted plagioclase regardless of whether it is a massive chromitite layer or a thin chromite seam. Iron contents of plagioclase in chromitites are lower than in neighbouring silicate rocks suggesting a gradient of redox potential.

Initial $^{87}Sr/^{86}Sr$ isotope ratios of interstitial plagioclase at the base of chromitite layers tend to be more radiogenic (0.707-0.708) than those of plagioclases in the neighbouring silicate rocks (0.705-0.706). Observed isotopic variations are consistent with a model of a new influx of magma intruding the residual magma and interacting with the overlying felsitic Rooiberg roof melt to reach chromite saturation [1]. The observed variation in Sr isotopic composition can be obtained by contamination with 10 % Rooiberg melt ($^{87}Sr/^{86}Sr_i$ ~0.713 [2]). The crystallising chromites then move to the floor of the chamber entraining a small amount of magma within the mush, which crystallises interstitial plagioclase with higher Sr isotope ratios. With ceasing chromite saturation, mixing with the residual magma occurs, which leads to magmas that precipitate plagioclase with typical $^{87}Sr/^{86}Sr$ of the UCZ (0.7050-0.7065).

A positive correlation of the Sr isotopic composition with PGE content within UG2 chromitite layer indicates noble metal enrichment by magma mixing and contamination. The process invokes chromite crystallisation accompanied by formation of immiscible sulfide melts that scavenge PGE when settling through the residual magma towards the floor of the chamber.

Postcumulus processes could explain the depletion of alkali elements: Migration of alkali metals in conductive intercumulus melts along gradients of redox potentials from chromitite layers to the underlying silicate rocks and overlying main liquid layer may have caused potassium and rubidium depletion of the studied chromitites [2].

[1] Schönberg *et al*. (1999). *EPSL*, 172, 49-64.

[2] Buchanan *et al*. (2004). *Lithos*, 75, 373-388.

Partial melting and X-ray computer tomography of Skaergaard cumulates

Veksler I[1*], Hess K-U[2], Ertel-Ingrisch W[2], Wiesmaier S[2], Nielsen T F D[3], Dingwell D B[2]

1 - GFZ Potsdam *veksler@gfz-potsdam.de 2 - LMU Munich 3 - GEUS, Copenhagen

Intercumulus crystallisation and material transport at the final stages of solidification of cumulus rocks in mafic intrusions remain poorly understood despite a potentially significant role, which the processes may play in the formation of magmatic layering and related mineralization. The objectives of this study are to reproduce the distribution and chemical composition of the last portions of intercumulus melt by partial melting experiments on classical gabbro cumulates of the Skaergaard intrusion in East Greenland. We study four samples from the Skaergaard mineralisation in the upper Middle Zone of the Layered Series. They range from leucocratic gabbro to melanocratic ferrogabbro with high modes of pyroxene and Fe-Ti oxide minerals. Cumulus phases comprise plagioclase, augite, pigeonite and FeTi-oxides dominated by ilmenite. Olivine and Ti-magnetite are intercumulus phases. Experiments were performed on cores, 15 mm in diameter and 20 mm in length. The samples placed in alumina crucibles are heated for 5 days at 1100-1200 °C and atmospheric pressure in CO-CO_2 gas mixture at redox conditions corresponding to those of the QFM buffer. Each sample is scanned in 3D by X-Ray computer tomography (XRCT) before and after heating runs to document structural changes, and the distribution and volumes of intercumulus melt. At 1200 °C the degree of partial melting reached 23-25 vol.% . Melting is seen at the interfaces between pyroxene and plagioclase crystals. Most of the melt drained out of the sample during the experiment leaving behind a network of interconnected empty channels. Partial melt appears to have low viscosity and a high pyroxene norm. The preliminary results imply high permeability of gabbroic cumuluates even at relatively low melt fractions.

Zonal PGM and PGE distribution in the platinum reefs at the base of cyclic units in the layered intrusions

Yudovskaya M[1*], Kinnaird J[1], Grobler D[2]

1 - University of the Witwatersrand *marina.yudovskaya@wits.ac.za 2 - Ivanplats Ltd., South Africa

Bushveld reef-style mineralisation generally shows coeval variations in PGE, Au and base metals with the highest concentrations closely associated with chromitite seams and changes in rock types at the base of cyclic units. This persistent pattern was explained by continued sulfide segregation as a result of a magma mixing event whereas the offset profile, which is typical for the Great Dyke Main Sulfide Zone, requires the involvement of a more complicated mechanism. Here we describe the zonal distribution of platinum group minerals (PGM) in a vertical section through the PGE reef at Turfspruit (the northern limb of the Bushveld Complex). The Turfspruit PGE reef is a mineralized zone more than 8 m thick hosted in olivine-bearing plagioclase orthopyroxenite within the Platreef sequence. The highest grade is confined to two top chromitite seams 1-2 cm thick. This chromite-bearing interval contains predominantly Pt-Pd sulfides (up to 90 vol. % of total PGM); PGMs in the adjacent underlying interval are represented mostly by Pt-Fe alloy (up to 90 vol. %) that shows a transition to assemblages of predominantly Pt-Pd bismuthtellurides and, finally, sperrylite. We suggest that the zonal PGM distribution is formed in situ as a result of directional crystallization under thermal gradient. It is interlinked with chromitite that was deposited as a reaction phase in the zone of mixing. An eutectic mix of Pt-Pd sulfides, Pt-Fe alloy and pyrrhotite crystallizes first from sulfide liquid with Bi, Te, As -enriched remnants migrating downwards.

Previously, lateral variations of PGM mineralogy were reported for the Merensky Reef and Platreef platinum horizons. The changes in mineralogy were ascribed to the influence of superimposed process such as pothole formation and fluid activity. We have now noted a vertical zonation in the Platreef on Turfspruit with the Pt alloy zone being a constituent of primary magmatic vertical zoning. To check the influence of fluid activity on mineralization we analysed phlogopite through the Platreef sequence and underlying Lower Zone cumulates. The elevated F and Cl contents in phlogopite were found both in the PGE-rich horizons and in the evolved portions of the Platreef, Lower and Marginal zones. We conclude that postmagmatic fluids were exsolved at the top of the magmatic fractionating columns and the higher abundance of volatiles is an accompanying but not an essential factor of mineralization.

Plagioclase composition in the Panzhihua layered intrusion, SW China: possible evidence for intercumulus silicate liquid immiscibility

Hou T[1], Veksler I[2*]

1 - China University of Geosciences, Beijing 2 - GFZ Potsdam
*veksler@gfz-potsdam.de

Silicate liquid immiscibility has been proposed as an important process in the origin of the economic stratiform Ti-magnetite deposits in the lower part of the Panzhihua intrusion, China [1]. Previous studies of the Skaergaard intrusion in east Greenland [2] showed that plagioclase composition can be used as a sensitive indicator of the magma evolution, especially when the magma starts to unmix. Here we present an electron microprobe study of cumulus and intercumulus plagioclase in the Fe-rich lower gabbroic horizons of the Lower (LZ) and Middle (MZ) Zones of the Panzhihua intrusion. At two stratigraphic levels in the MZ we observed reversals in plagioclase composition back to higher An contents, which were accompanied by simultaneous reversals of clinopyroxene and olivine compositions to higher Mg#. The reversals are probably due to chamber-scale recharge with a hotter and more primitive magma. Most Ca-rich plagioclase compositions (An68-79) were found in the two major Fe-Ti oxide ore bodies. In the ore bodies and in melanocratic gabbros plagioclase crystals are zoned with more calcic, Fe-rich and Ti-poor compositions at rims. Such zoning is similar to the one that was previously described at Skaergaard and interpreted as a result of intercumulus crystallization from a late-stage Fe-rich immiscible liquid [2]. Thus, plagioclase chemistry at Panzhihua implies that intercumulus liquid immiscibility and subsequent loss of interstitial Si-rich immiscible liquids from the cumulus mush may have taken place during the formation of the stratiform Ti-magnetite ore deposits.

[1] Zhou M.F. *et al*. (2005). *J Petrol* 46: 2253-2280.

[2] Humphreys M.C.S. (2011). *J Petrol* 52: 147-174.

Variation in mineral chemistry across the UG2 chromitite layer, eastern Bushveld Complex

Kaufmann F[1], Bethke M[2], Schannor M[2], Manyeruke T[3], Hecht L[4*]

1 - Fachgebiet Mineralogie-Petrologie, Technische Universität Berlin 2 - Institut für Geologische Wissenschaften, FU Berlin 3 - Nkwe Platinum (SA) (Pty) Ltd 4 - Museum fuer Naturkunde Berlin *lutz.hecht@mfn-berlin.de

The Upper Group 2 (UG2) chromitite layer of the so-called Critical Zone of the Bushveld Layered Intrusion hosts the largest known resources of PGE on Earth. The origin of massive chromitite layer formation is still a matter of debate and existing models involve processes like magma mixing, assimilation, mechanical sorting and injection of crystal slurries (e.g. [1] and references therein). This study is aimed at giving some insights into the petrogenesis of chromitite layers by means of detailed mineral chemical investigations. Samples supplied by Nkwe Platinum (Pty) Ltd. were taken from diamond drill core material of HPK 016 that was drilled ~ 12 km NW of Steelpoort on Hoepakrantz 291KT farm in the Eastern Bushveld Complex. A 2 m profile covering the UG2 (~ 60 cm), hanging wall and footwall pyroxenites, and anorthosite was studied in detail. The major and/or trace element composition of chromite, pyroxenes and plagioclase of the UG2 chromitite layer differs from those in the silicate rocks in the UG2 footwall and hanging wall. The UG2 chromite has lower Fe and higher Mg contents, resulting in significantly higher #Mg compared to the silicate rock layers. The scatter in chemical composition of chromite (e.g. Cr# and Mg#) in pyroxenites is much higher than in the chromitite. The UG2 chromite shows fluctuating variation in composition with depth in cm scale. In this case Cr# shows a negative correlation with Mg#. Similar rhythmic chemical variation of chromites in UG2 has recently been demonstrated for the Western Bushveld [2] and was interpreted to result from continuous fractionation repeatedly interrupted by the influx of more primitive magma. The orthopyroxenes (opx) and clinopyroxenes (cpx) show on average higher Mg#, Cr, and Ni content in the chromitite layer compared to adjacent pyroxenites. The Ni content of opx and cpx increases from bottom to top of UG2. This is likely the result of intercumulus melt differentiation probably caused by continuous crystallization in the vertical direction of UG2. Fe and K content in intercumulus plagioclase of UG2 is drastically lower compared to the hanging and footwall rocks. This suggests more reducing conditions in UG2 that prevented incorporation of Fe^{3+} into plagioclase. K contents in UG2 plagioclases are by far too low to be explained by normal partition coefficients, possibly implying that K has been removed from UG2 via diffusion. All our observations are consistent with a model of multiple magma replenishment involving assimilation of siliceous country rocks followed by fractionation (e.g. [3]). Intercumulus melt in UG2 developed (differentiated) as a more or less closed system although some outward migration of mobile elements (alkalis) likely occurred before complete solidification.

[1] Maier *et al*. (2013) *Min. Dep.* 48, 1-56.

[2] Junge *et al*. (2014). *Econ. Geo.* 109, 795-810.

[3] Schönberg *et al*. (1999). *EPSL* 172, 49-64.

Primary and secondary mineral assemblages in monazite-bearing peridotites from Yangtiangou, Sichuan, China: late magmatic alteration of ultramafic cumulates derived from an alkaline magma

Munteanu M[1], Yao Y[2], Costin G[2*], Wilson A[3], Malatji T[2]

1 - Geological Institute of Romania, Bucharest, Romania 2 - Department of Geology, Rhodes University, Grahamstown, RSA *g.costin@ru.ac.za 3 - University of the Witwatersrand

Yangtiangou is an ultramafic intrusion (peridotite to olivine pyroxenite) related to the Permian Emeishan large igneous province in SW China that includes tholeiitic flood basalts, tephrites, trachytes, rhyolites and corresponding intrusive rocks. The Yangtiangou intrusion is dike-like and hosts magmatic sulfide mineralization (Ni-Cu-PGE). Most rocks in the intrusion exhibit cumulate textures, with a primary mineral assemblage consisting of cumulus olivine (Fo_{84-87}), Cr-spinel and clinopyroxene, with Ti-rich biotite (6-7% TiO_2) and ilmenite as the main interstitial phases. The chilled facies of the intrusion contains olivine and clinopyroxene phenocrysts in a groundmass of potassium feldspar ± albite, Fe-Ti oxides, pyroxene and biotite. This assemblage is reflected in the chemical compositions of the rocks, with the peridotites containing up to 1.38% K_2O, 0.64% Na_2O and 2.3% TiO_2, while the rocks of the chilled facies, classified as trachybasalts, contain ca. 4% K_2O, 3% Na_2O and 4.2% TiO_2. The Ti-rich compositions of bulk rock samples and minerals support the formation of the intrusion from a high-Ti magma.

Detailed petrological, mineralogical and geochemical studies indicate that the peridotite underwent partial alteration, which induced chloritization of some of the intercumulus biotite, but the olivine and pyroxene remained unaltered. In local zones of biotite decomposition, apatite, monazite and Na-rich amphibole occur within a chlorite matrix. The primary sulfide assemblage (pyrrhotite-chalcopyrite-pentlandite) has been altered to pyrite-chalcopyrite-millerite. Galena micro-inclusions occur in the pyrite and chalcopyrite. Sperrylite crystals are contained within pyrite. EPMA dating on monazite indicates that the alteration stage took place within the time interval 215-265 Ma, which includes the eruption stage of the Emeishan basalts.

The Yangtiangou intrusion most likely represents the wide zone of a magmatic conduit, where olivine and clinopyroxene accumulated in a situation of reduced magma flow. During the cooling of the intrusion, a late circulation of fluids determined biotite decomposition and mobilization of phosporus and rare earth elements to form monazite. Considering that the chilled facies is chemically similar to the magma that generated the intrusion, Yangtiangou is an unusual case whereby a magmatic Ni-Cu-PGE deposit is related to alkaline magmas of the Emeishan large igneous province.

Apatite-hosted melt inclusions in the Upper Zone of the Bushveld Complex

Wang M[1], Veksler I[2*], Cawthorn G[3]

1 - China University of Geosciences 2 - GFZ Potsdam *veksler@gfz-potsdam.de 3 - University of the Witwatersrand

Occurrences of Fe- and Si-rich melt inclusions in apatite have provided the best evidence for silicate liquid immiscibility in the Skaergaard and Sept Iles layered intrusions [1, 2]. In the Bushveld, large-scale immiscibility has been proposed at the top of the Upper Zone [3]. However, an alternative interpretation of their data exists [4] and no supporting melt inclusion evidence has been presented so far. We have found that apatite crystals in the Upper Zone nelsonites and gabbro contain numerous crystallized melt inclusions. The inclusions fall in two distinct compositional groups but the compositions significantly differ from those of the typical immiscible melts previously described at Skaergaard and Sept Iles. The average composition of the most common type of the inclusions (SiO_2 30.8; TiO_2 0.81; $Al_2O_3$12.7; FeOt 35.8; MgO 7.7; CaO 1.6; K_2O 0.66, all in wt. %) has FeO and SiO_2 contents similar to those of the immiscible Fe-rich melt, but very low CaO and TiO_2, and too high Al_2O_3 arguably are inconsistent with the immiscible origin. Chlorite is a major daughter mineral of the inclusions, implying strong hydrothermal alteration. Crystallized melt inclusions of the second type are composed of quartz, biotite, Ca-amphibole, albite, orthoclase and chlorite, and have the bulk average composition (SiO_2 50.6; TiO_2 0.72; $Al_2O_3$10.4; FeOt 22.9; MgO 1.54; CaO 6.6; K_2O 1.52) similar to that of ferrodiorite. Although the origin of the hydrated Fe-rich inclusions at the moment remains unclear, large scale liquid immiscibility in the Upper Zone of the Bushveld Complex appears to be unlikely. Our preliminary interpretation of the melt inclusion data is that apatite formed from a ferrodioritic, volatile-rich magma, possibly in the presence of a separate hydrothermal fluid phase.

[1] Jakobsen J.K., Veksler I.V., Tegner C. and Brooks C.K. (2005). *Geology*, 33, 885-888.

[2] Namur O., Charlier B., Toplis M.J., Higgins M.D., Liégeois J.-P., and Vander Auwera J. (2010). *J. Petrol*., 51, 1203-1236.

[3] VanTongeren J.A. and Mathez E.A. (2012). *Geology*, 40,491-494.

[4] Cawthorn R.G. (2013). *Geology*, 41,603-606.

Magma mixing and mingling at the 15 Ma Heldburg Phonolite, Germany

Abratis M[1*], Pfänder J[2], Hentschel R[1], Viereck L[1]

1 - Friedrich-Schiller University Jena, Germany *michael.abratis@uni-jena.de 2 - Technische Universität - Bergakadamie Freiberg, Germany

With the exception of the East Eifel and the Rhön volcanic fields, magmatic differentiates such as trachyte and phonolite are volumetrically subordinate to mafic volcanics within the Cenozoic Central European Volcanic Province. The phonolite of the Heldburg Castle Mountain represents the only known occurrence of differentiated magmatic rocks within the so called Heldburg or Grabfeld dyke swarm area. However, the Heldburg phonolite is famous foremost for containing spinel lherzolite xenoliths [1, 2]. Former studies proposing a cogenetic relationship between the phonolite and the peridotites concluded that the phonolite magma must have evolved under upper mantle conditions [3].

In the current study we present clear petrographic and geochemical evidence for magma mixing and mingling in the Heldburg phonolite melt due to the intrusion of mantle derived basanitic magma which is exposed today as a dyke at the foot of the Heldburg Castle Mountain. During this process, the mantle xenoliths were introduced into the phonolite melt as they all contain a rim of basanitic magma. During detailed field investigations in the Heldburg Castle Mountain area and subsequent lab work we identified three major lithologic units, ranging in composition from basanite to tephrite to phonolite. Extensive mingling features (e.g., schlieren layers, load casts, flame structures, mafic enclaves) are developed between these units, indicating that all of them were melts at the time of mixing. These petrographic and geochemical indications of two coeval melts of different composition were substantiated by Ar-Ar dating of the two mixing end members to the same age of 15 Ma.

[1] Irving A.J. and Price R.C. (1981). Geochemistry and evolution of Iherzolite-bearing phonolitic lavas from Nigeria, Australia, East Germany and New Zealand. *Geochim Cosmochim Acta*, 45(8),1309-1320.

[2] Grant T.B., Milke R., Pandey S. and Jahnke H. (2013). The Heldburg Phonolite, Central Germany: Reactions between phonolite and xenocrysts from the upper mantle and lower crust. *Lithos*, 182-183, 86-101.

[3] Kunzmann T. (1996). *Der Phonolith von der Heldburg (Thüringen); Ein Fraktionierungsprodukt alkalibasaltischer Magmen unter den Bedingungen des Oberen Mantels*. Habilitation thesis, Ludwig-Maximilians-Universität München, p 149.

Why microgranitoid enclaves resemble their granitic host

Elburg M[1*], Bons P[2]

1 - University of Johannesburg *marlinae@uj.ac.za 2 - University of Tuebingen

Mafic magmatic (or 'microgranular') enclaves within granitoids have been interpreted as fragments of restite, accumulations of early-crystallised minerals or globules of more mafic magma that mingled with and chilled against the cooler magma of the host granitoid. Although the shapes of many enclaves point towards an origin of magma mingling, the similarity of the mafic minerals in enclaves and their host rocks has been used as an argument against this interpretation; in this case an interpretation as "chill-cumulates" has been preferred (e.g. Donaire *et al.* [1]).

Although diffusional equilibration has long been recognised as a mechanism for erasing geochemical distinctions between enclaves and host granitoid, enclaves are often richer in incompatible trace elements than their hosts, which could be interpreted as necessitating the process of uphill diffusion to have taken place. Another problem is the time-scale during which diffusion needs to have operated. Diffusion has been measured as being rapid for the alkalis, but, in the case of mingling between mafic mantle-derived magma and peraluminous granites, aluminium and silicon with measured diffusivities that are orders of magnitude lower [2], also need to equilibrate to form the observed mineral phases in the enclave.

In order to assess these problems, we developed a simplified 1D computer model to simulate diffusional exchange between partially solidified enclaves and host magma, focussing on 1.) the behaviour of trace elements, with variable compatibilities in the (inferred) original mafic minerals in the enclaves (clinopyroxene) and the equilibrated minerals (biotite); 2.) the time-frame involved in enclave equilibration. For the latter point, we adjusted existing diffusion coefficients based on the 'relaxation of concentration' values based on mixing experiments [3].

First results suggest that the enrichment of some trace elements (e.g. Rb) can be explained by the 'sink effect' of reacting clinopyroxene to biotite, but for others (e.g. Zr) more complicated models may need to be invoked, whereby diffusivities vary as a function of melt composition.

[1] Donaire T., Pascual E., Pin C. and Duthou J.-L. (2005). *Contributions to Mineralogy and Petrology*, 149, 247-265.

[2] Baker D.R. (1990). *Contributions to Mineralogy and Petrology*, 104, 407-423.

[3] Perugini D., De Campos C.P., Dingwell D.B. and Dorfman A. (2013). *Chemical Geology*, 335, 8-23.

Magma mixing and episodic construction of granitoid intrusion – a case of the Tatra granitoid pluton, Central Western Carpathians

Gawęda A[1*], Burda J[1], Klötzli U[2], Crowley Q[3]

1 - University of Silesia *aleksandra.gaweda@us.edu.pl 2 - University of Vienna 3 - Trinity College Dublin

Mixing of the mafic and felsic magmas is one of the most important processes, explaining compositional variability in the granitoid group [1]. The long-living, regional scale shear zones are thought to be the best place for the migration of felsic and mafic magmas, assembling incrementally. The Tatra granite is an example of such a case, with pronounced magmatic layering.

Geochemical and isotopic data from the polygenetic Tatra granite point out the presence of two separate magma pulses (X and Y). Pulse X is characterized by lower $I_{345}Sr$ values (0.705-0.706) and higher $e_{345}Nd$ (+0.90 - -2.28), T_{DM} = 0.98-1.2, Rb/Sr = 0.13-0.64 and high K-calc-alkaline to shoshonitic characteristic, while pulse Y shows slightly higher $I_{345}Sr$ values (0.7062-0.7072), lower $e_{345}Nd$ (-1.9 - -3.63),T_{DM} = 1.2-1.4, Rb/Sr = 0.05-0.35 and calc-alkaline- to high K - calc-alkaline characteristics. The Pb isotopic composition of granites from both pulses is typical of the lower crust.

In both pulses the presence of textural assemblage typical of magma mixing was found: quartz-titanite ocella, calcic spikes in plagioclases, K-feldspar porphyrocrysts with inclusion zones, underlying normal, reversed, and irregular chemical zonation, poikilitic feldspars, blade-shape "hydrogenic" biotite, all in the contact zones of mafic microgranular enclaves of different size and shape and host granite. Cumulates developed as a consequence of layering at the bottom of layers.

Geochemical modelling suggests 61% of the felsic component for pulse X and 74% of the felsic component for pulse Y. LA-ICP-MS U-Pb zircon dating showed that the X granitoid magmas intruded at 350-340 Ma, while Y granitoids are older and cover the span 371-360 Ma. Probably the Tatra intrusion developed as discrete magma pulses in the regional-scale shear zone. The continuous shearing, magma mixing/mingling and magmatic erosion of former layers enabled the instability inside the following magmatic sheets and led to the formation of magmatic layering and other sedimentary-like structures.

[1] Perugini D. and Poli G. (2012). The mixing of magmas in plutonic and volcanic environments: Analogies and differences. *Lithos*, 153, 261-277.

Multiple source components and magma mixing involved in the genesis of high-K calc-alkaline granitoids, as recorded by in situ trace element and Sr-Nd-Hf isotope data

Laurent O[*], Zeh A, Gerdes A

1 - J.W. Goethe University, Institute of Geosciences, Frankfurt am Main, Germany *oscarlaurent86@gmail.com

The so-called "I-type", high-K calc-alkaline granitoids are often considered as "hybrid" in origin, i.e. involving both mantle and crustal components in their petrogenesis. However, it is not clear if the interactions between both components systematically take place (1) at mantle levels (i.e. enriched mantle source); (2) at emplacement levels (i.e. crustal contamination and/or magma mixing with crustal melts) or (3) both. This mainly arises from the fact that these mechanisms can be distinguished neither on the basis of whole-rock elemental and isotope geochemistry, nor numerical modelling. In contrast, investigating the elemental and isotope chemistry of the magmatic minerals which crystallized from such "I-type" granitoid magmas allows a much greater spatial resolution, and therefore has a better potential, to unravel the different components involved in their genesis and how they interacted with each other in the course of magma evolution.

To this end , this study investigates the petrogenesis of a suite of late-Archaean (2.69 Ga-old) high-K, calc-alkaline granitoids from the Pietersburg block, northern Kaapvaal Craton (South Africa), using LA-(MC-)ICPMS *in* situ analyses of trace elements and Sr-Nd-Hf isotopes in magmatic minerals (plagioclase, zircon, apatite, titanite, epidote), coupled to field data, whole-rock geochemistry and micro-textural information (CL images). The Mashashane, Matlala, Matok and Moletsi granitoids range from diorites to monzogranites, emplaced at different crustal levels but all within a relatively short time span and show compelling evidence for interactions between each other, both at the outcrop scale (mingling relationships, hybrid phases, magmatic enclaves...) and the mineral scale (oscillatory zoning in accessory minerals such as apatite, zircon and titanite). Some samples also show clear evidence of interaction with a fluid phase of unknown origin and composition

Hf isotope data on zircon confirm that all rocks are cogenetic (identical $\varepsilon_{Hf}(t)$), but trace element and Sr-Nd isotopes on plagioclase and apatite point to the involvement of several components in their petrogenesis, at different stages of the magma evolution. The most mafic rocks (diorites) derive from interaction, at mantle levels, between depleted peridotite and a sedimentary component of quartzofeldspathic nature (arkose or greywacke with moderate Rb/Sr ratio). Only 10 to 20% of the latter is required to explain the isotope systematics in the diorites, which makes them a significant contributor to juvenile crust formation. The mineral chemistry of other granitoid rocks (granodiorites, monzogranites, leucogranites) can be explained by a combination of two different mechanisms, namely (1) differentiation from the diorite magmas by fractional crystallization; and (2) interactions with magmas derived from melting of local crust, either tonalite-trondhjemite-granodiorite (TTG) rocks, metasediments and meta-mafic rocks. Of importance is the association of the latter interactions with magma mixing processes, which are recorded solely by trace element zoning and Sr-Nd isotope heterogeneity in apatite. As this mineral crystallized early in the magmatic sequence, it implies that magma mixing can only take place early in evolution of the magma, close to the liquidus, and relatively deep in the crust. Finally, some samples were affected by interactions with an externally derived fluid, presumably associated with devolatilization of metapelitic rocks in the lower crust, as revealed by extreme radiogenic Sr contents in epidote.

Our results indicate that the "hybrid" character of "I-type", high-K calc-alkaline granitoids is both inherited from the (mantle) source, and acquired during magma evolution at emplacement levels, through magma mixing and mingling with melts derived from local crust. It also highlights that *in situ* trace element and Sr-Nd-Hf isotope analyses in magmatic minerals from granitoids

Geochemistry and mineralogy of calc-alkaline lamprophyres in the east Kunlun orogenic belt, Northern Tibet Plateau: implications for magmatic history

Ma C[1*], Xiong F[1], Yang J[2]

1 - China University of Geosciences *cqma@cug.edu.cn 2 - China University of Geosciences and CARMA

The East Kunlun orogenic belt (EKOB), located on the northern margin of the Tibetan Plateau, is a composite orogenic belt resulted from the subduction of the Proto- and Paleo-Tethys, and terrain collisions from early Paleozoic to early Mesozoic. The orogenic history of EKOB during the early Mesozoic is of considerable importance in the reconstruction of the eastern Paleo-tethys because it occupies a central place on the boundary between the Gondwana and Eurasia domains. Mid-Ocean Ridge Basalt (308 Ma) and island arc volcanic rocks (260 Ma) were distinguished in EKOB, respectively, which may constrain the time of Paleo-Tethyan ocean opening and subduction. Recently, syn-collisional granites (240-231 Ma) and post-collisional granitoid rocks (226-208 Ma) were identified in EKOB, which could constrain the time of the continents collision and accompanying extension. However, mantle chemistry and magmatic evolution during orogenic processes are less well constrained.

Recently, we have identified lamprophyre dyke swarms in EKOB, which are spessartites with euhedral amphibole phenocrysts, and have zircon U-Pb geochronology of 253.0 ± 2.5 Ma. These dykes are enriched in large-ion lithophile elements (e.g., K, Rb, Sr, Ba) and light rare-earth elements, but depleted in high-field-strength elements (e.g., Ta, Nb, P and Ti), and have enriched Sr-Nd-Hf isotopic compositions ($(^{87}Sr/^{86}Sr)_i$ = 0.70883 ~ 0.71045, $\varepsilon_{Nd}(t)$ = -5.51 ~ -5.72, εHf(t) = -4.42 ~ -0.38). Geochemical studies show that the dykes were derived from enriched lithospheric mantle that has been metasomatized by subduction-related fluid.

Amphiboles are present as phenocrysts and in the groundmass of lamprophyres. The core of phenocrysts has a much higher content of MgO, CaO and Na_2O and lower content of FeO than the rim. Most of the cores can be classified as magnesiohastingsite with Mg# [(Mg# = atomic ratios Mg/(Mg+Fe)] varying from 62 to 68 (Leake *et al*. 1997), while most rims of phenocrysts are ferropargasite with Mg#<50. This change is recorded as chemical zoning indicating that a Fe-rich, Si-rich, Mg-poor and Ca-poor magma appeared later. The amphiboles in the groundmass have compositions similar to those in the rims of phenocrysts, with variable Mg# from 29 to 69. Two types of plagioclase are identified, i.e., zoned plagioclase and unzoned plagioclase. The cores of zoned plagioclase are compositionally identical to the unzoned plagioclase (~An_{68-83} and An_{66-89}, respectively), which is in equilibrium with their parental magma, indicating their mantle origin. However, the composition of the rim in zoned plagioclase varies from An_{43} to An_{65}, which is much lower than that of the core. Furthermore, because the crystal composition in a magma mainly depends on crystallization conditions, such crystals provide us with a record of magma conditions (pressure and temperature) in the magma chamber. "Normal" zoning in plagioclase is a continual change from a high-temperature Ca-rich composition in the core to a lower-temperature Na-rich composition at the rim (decreasing from 1150 to 950℃). This compositional change suggests cooling and chemical differentiation of the lamprophye magma. The Al content in hornblende is a useful geobarometer for appropriate plutonic and volcanic rocks, since a positive correlation exists between total pressure and the Al content of hornblende in certain assemblages of minerals and silicate melt. The "Normal" zoning of amphibole phenocrysts shows a decrease in aluminum from core to rim, indicating that decompression during magma ascent further promoted the crystallization of phenocrysts, with pressure decreasing from 9.2~11.4 kbar to 7.8~8.2 kbar. This study shows that porphyritic rocks can actually contain two types of mineral with the core of phenocrysts in chemical equilibrium with their primary magma, and the matrix and rims of phenocrysts just reflecting an evolved magmatic system.

Cathodoluminescence response from feldspars to multistage crystallization-recrystallization processes in composite plutons

Slaby E*, Moszumańska I

Institute of Geological Sciences Polish Aacademy of Sciences *e.slaby@twarda.pan.pl

Composite plutons are commonly considered as magmatic bodies showing extreme geochemical and textural heterogeneities on both macro and micro scale. These heterogeneities can be more accurately analyzed in minerals than in whole rocks hosting them. The underlying processes are complex, their signatures overlapping. To reconstruct properly the whole path of crystal formation/transformation, a selection of appropriate, but also simple and reliable tools is becoming an important challenge.

Induced by mixing, crystal growth progresses in an environment where the dispersion of magmas proceeds by chaotic stretching and folding. As a result, magma domains with differing characteristics may occur simultaneously and/or sequentially, close to the growing mineral surface, therefore elements from all domains are incorporated due to advection and diffusive fractionation. The migration of the crystals is associated with frequent deviation from equilibrium resulting in dissolution. Re-establishing the equilibrium restores crystallization. The process of growth and re-growth is reflected in crystal morphology and chemistry. The crystallization process is usually obscured by interaction with post-magmatic fluids. This interaction leads to partial re-equilibration, which again results in recrystallization of some feldspar domains.

The most powerful tool for recognition of all of these processes is cathodoluminescence. Several facts confirm that. The luminescence of feldspars, both plagioclase and alkali feldspar, strongly correlates with their geochemistry and order-disorder of their structure. The dynamics of feldspars crystallization in mixed magmas is also reflected in the arrangement of their structure and chemistry [1]. Some trace elements introduced into the feldspar structure during such processes can cause local structural distortions and affect the appearance of increased density of structural defects [2]. The appearance of structural defects increases luminescence. Also, the interaction of fluids and feldspar can result in increasing order in the structure and a decreasing defect density [3]. Some trace elements act as activators.

Thus, even a subtle change in the environment of feldspar crystallization and recrystallization can result in every reaction being registered as a change in feldspar luminescence. Most of these changes are invisible or hardly recognizable under the microscope.

In this presentation we wish to show a full reconstruction of the feldspar crystallization process as it proceeds in very dynamically stirred magma with subsequent overprinting by post-magmatic recrystallization. The advantage of cathodoluminescence over other methods is demonstrated.

Acknowledgement: The work has been funded by IGS PAS project "Lotny".

[1] Marfunin A.S. and Bershov L.V. (1970). *Doklady Akademii Nauk*, 193, 412-414.

[2] Słaby *et al*. (2008). *Lithos*, 105, 85-97.

[3] Finch A.A. and Klein J. (1999). *CMP*, 135, 234-243.

From basalt to rhyolite: uniform components and mixing regimes in magma systems of the Central Andes

Wörner G[1*], Banaszak M[2,3], Brandmeier M[2], Heistek R[2]

1 - Geowissenschaftliches Zentrum Göttingen, GZG *gwoerner@gwdg.de 2 - Universität Göttingen 3 - TU Berlin

Major element compositions of mafic Quaternary to Miocene magmas in the Andean Central Volcanic Zone encompass high-K to medium-K calc-alkaline basaltic andesites (52-55 SiO_2 wt%) and have large ranges in major (3.6-9.4 wt% MgO, 4-7 wt% Na_2O+K_2O, 0.8-1.8 wt% TiO_2) and trace element concentrations (9-197 ppm Ni, 501-1944 ppm Sr, 95-257 ppm Zr). Trace element ratios are also highly variable (LILE/HFSE: 93>Sr/Y>24; LREE/HREE: 8>La/Yb>63). Such a remarkable variability and the absence of truly primitive lavas in the CVZ since the onset of crustal thickening >20 Ma ago reflect distinct sources in the mantle wedge and variable petrogenetic processes during ascent through exceptionally thick continental crust (70 km).

Our statistical analysis (Polytopic Vector Analysis, PVA) on a subset of our large data base of Andean magmas (>1000 samples) which have complete major- and trace element data and isotope compositions shows that the entire compositional space of Central Andean magmas can be described by the same three endmembers: (1) a low-Mg high-Al calc-alkaline basaltic andesite (BA), (2) an incompatible trace element enriched basalt (EB), and 3) a high-K calc-alkaline rhyodacite (RD). The first mixing stage produces a range of hybrid baseline magmas consisting of EB and BA. These represent typical recharge magmas into more evolved magma chambers at shallower crustal levels. There, a second mixing stage occurs with mixing between the already mixed, mafic (BA+EB) and the silicic RD component, which typically is crystal rich. Mixing proportions between these endmembers vary widely and magma compositions of endmembers and/or hybrids are overprinted by different degrees of magmatic differentiation and crustal assimilation.

These three endmember magmas enclose nearly all Quaternary CVZ lavas in a mixing triangle and account for the entire compositional variability of the Quaternary volcanic rocks in the CVZ. A first mixing stage produces hybrid baseline magmas consisting of EB and BA. The second mixing stage represents shallow crustal magma mixing between already mixed, mafic (BA+EB) and the silicic RD components. Mixing proportions between these endmembers vary widely and magma compositions of endmembers and/or hybrids are overprinted by different degrees of magmatic differentiation and up to 20% crustal assimilation.

A particular setting is required for andesite lava fields that occur throughout the Central Andes (Huambo, Andagua, Negrillar). These Quaternary lava fields are unrelated to stratovolcanoes and probably reflect direct differentiation of the mafic hybrids towards phenocryst poor pyroxene-andesites without interaction with crystal-rich shallow crustal magmas.

A survey of our data base for older (Pliocene and Miocene) andesites and dacites shows a surprisingly similar compositional pattern and compositional variance.

The BA, EB, and RD magma mixing endmembers represent distinct sources: the mantle wedge, enriched (lithospheric?) mantle, and the continental crust, respectively. These endmembers are thus ubiquitous in the Central Andes and only their mixing proportions appear to change in space and time.

These same mixed magmas give rise to, and are genetically associated with large volume ignimbrite eruptions (ignimbrite "flare-ups", >3000km^3 magma erupted in 1 Ma) that are hybrids between a crustal melting endmember (20% - 50%) and a mantle-derived component. Further, evolution of these silicic magmas towards the thermal minimum, results in rather uniform major element compositions and smoothing out of compositional diversity in the constituent magmas. Minor differences remain in trace element patterns. A rigorous statistical analysis on the compositional data of >800 ignimbrites throughout the Central Andes identifies four groups that reflect the assembly of large magma volumes from slightly different source components at different P-T-X conditions.

Evidence of peculiar iron speciation in natural glasses by variable temperature optical spectrophotometry

Chassé M[1*], Galoisy L[1], Métrich N[2], Calas G[1], Lelong G[1]

1 - Institut de minéralogie, de physique des matériaux et de cosmochimie (IMPMC) - Université Pierre et Marie Curie (UPMC) *mathieu.chasse@impmc.upmc.fr

2 - IPGP

Fe has long been known to play an important role in determining the properties of natural magmatic liquids and glasses [1]. The determination of the sites occupied by ferrous and ferric cations in volcanic glasses may provide information on the physico-chemical conditions prevailing at the magmatic stage as well as on the cooling conditions during the emplacement of the magma. We will present an overview of a spectroscopic investigation of Fe speciation in various natural glasses (e.g. obsidians, pantellerites, tektites and basalts) and in glass inclusions in minerals. Optical absorption spectroscopy (OAS) is used to investigate these glasses because of the sensitivity of the method to the speciation of transition elements [2].

In order to investigate micrometer-sized glass inclusions, a Cassegrain microscope has been especially designed and adapted on a spectrophotometer. The first optical absorption spectra obtained on glass inclusions (about 100 µm diameter) allow a unique comparison of Fe speciation between the magmatic melt (frozen in glass inclusion) and the corresponding erupted glass sampled on the volcano.

By coupling the microspectrophotometer with a cooling/heating stage and combining the results with previous low temperature data, we show, in obsidians, the presence of specific absorption bands characterized by a dramatic intensity dependence as a function of temperature over the range 1000K-10K. This unique property may be assigned to Fe-Fe intervalence charge transfers (IVCT) transitions [3]. By contrast, tektites, and Fe-bearing glasses with similar Fe content do not show such a contribution. The presence of Fe-oxide nano-clusters, suspected for a long time from previous EPR studies [4], is confirmed by this IVCT process. These clusters, showing a local rearrangement around Fe, are related to the cooling history of the glass, as they are not found in the medium range structure of the fast-quenched tektites. The unexpected shape of the ferrous iron absorption band in obsidians suggests that most Fe^{2+} occurs in these clusters, a major difference with the surrounding of Fe^{2+} in synthetic glasses [5].

[1] Galoisy L. *et al.* (2001). *Chem. Geol.*, 174(1-3), 307-319.

[2] Burns R.G. (1993). *Mineralogical Applications of Crystal Field Theory*, Cambridge University Press.

[3] Mattson S. and Rossman G.R. (1987). *Phys. Chem. Minerals*, 14(1), 94-99.

[4] Calas G. and Petiau J. (1983). *Bull. Minéral.*, 106(1-2), 33-55.

[5] Weigel C. *et al.* (2008). *Phys. Rev. B*, 78(6), 064202.

Structure of calcium and magnesium silicate glasses and melts: diffraction results

Cormier L

IMPMC, CNRS - UPMC, France. cormier@impmc.upmc.fr

Liquids between olivine and pyroxene compositions are a good starting point in modelling the mantles of terrestrial planets. Most information about the structure of silicate liquids comes from the structural study of the corresponding glasses that represent the liquid structure frozen-in at the glass-transition temperature. The structure of silicate glasses and melts and its composition dependency exerts a fundamental control on the dynamical and physical properties of silicate magmas (density, energy, entropy, crystal-melt element partitioning, and transport properties including viscosity and diffusivity).

Alkali and alkaline earth cations act as network modifiers in silicate melts and glasses and their surrounding is a long standing problem to obtain a complete picture of these amorphous structures. Neutron diffraction can be successfully applied to Ca and Mg to obtain chemically selective information by using isotopic substitution. We have recently successfully used the isotopic substitution technique $^{25}Mg/^{nat}Mg$ to determine accurately the Mg environment in a simple enstatite glass with the composition, $MgSiO_3$ [1].

In this contribution, we illustrate the possibility of using the neutron diffraction technique on several silicate glasses, mainly in the $MgO\text{-}CaO\text{-}SiO_2$ ternary [2]. The Ca and Mg end-members have the composition of wollastonite ($CaSiO_3$) and enstatite ($MgSiO_3$) minerals, while $CaMgSi_2O_6$ corresponds to the diopside composition. Examples of the structural description of cationic environments such as Ca and Mg will be given. The experimental data are coupled with numerical simulations (Molecular Dynamics and Reverse Monte Carlo). In this investigation, we focus on understanding the evolution of important structural parameters with the composition and the temperature, the structural differences between the glass and the mineral counterparts and the evolution with temperature.

[1] Cormier *et al*. (2011). *Phys. Rev*., B 83, 224204.

[2] Cormier *et al*. (2013). *Geochim. Cosmochim. Acta*, 122, 498.

An EPR, HFEPR and XAS study of volcanic ashes from Mt. Etna, Catania (Italy)

Di Benedetto F[1*], Mazzoleni P[2], Barone G[2], Benvenuti M[1], Costagliola P[1], Montegrossi G[3], Rimondi V[1], Romanelli M[1], d'Acapito F[4]

1 - Univ. Firenze - Dip. di Scienze della Terra, Italy *francesco.dibenedetto@unifi.it
2 - University of Catania - Department of Biological, Geological and Environmental Sciences 3 - CNR-IGG, Italy 4 - CNR-IOM-OGG @ESRF, France

The surfaces of the volcanic ashes are widely modified during explosive eruption by the interaction with the gas/areosol occurring in the plume. The mineralogical and compositional changes have important consequences for the impact on the environment and human health. In this context, the behaviour of the iron is largely unpublished. In particular, the oxidation state and the formations of new phases due to the S, Cl and F present in the plume are key points for the analysis of the consequences that these products may have on human health. In this study, we report the data collected on volcanic tefra of the Mt. Etna eruptions occurred in numerous explosive episodes which occurred during 2013.

The tefra samples were investigated by a wide multianalytical study, which included conventional EPR, HFEPR and XAS, this latter performed at the Fe K edge. The three techniques were chosen in order to get the closest information onto the Fe valence state and coordination, as being highly element selective. The preliminary results, presented here, highlight, from the pre-edge and the XANES regions, the coexistence of Fe(II) and Fe(III) species in an almost constant ratio. Fe(III), in turn, is distributed over at least two different phases, most of it being included in the volcanic glass, and the remaining hosted in an own, magnetic, phase, probably an Fe oxide. The two phases were clearly isolated by means of the coupled study through EPR and HFEPR. Moreover, information on the spectral behavior of samples differing in granulometric distribution or as a function of progressive leaching under laboratory conditions is discussed.

Sulfide solubility in silicate liquids under extremely low oxygen fugacity (ΔIW-5 to -8): implications for magmatism on the planet Mercury

McCubbin F[*], Vander Kaaden K

University of New Mexico *fmccubbi@unm.edu

On January 14, 2008, the Mercury Surface, Space Environment, Geochemistry and Ranging (MESSENGER) spacecraft had its first encounter with the planet Mercury and has since been collecting data on the structure, chemical makeup, and density of the planet among other important characteristics. One of the most interesting features on the surface of the planet is the relatively high amount of S as well as the relatively low amounts of FeO, up to ~4 wt% and 2 wt% respectively [1-3]. Much of our geochemical understanding of elements in natural systems comes from empirical observations of rocks on Earth and from other planetary bodies; however Mercury's enigmatic surface chemistry may deviate from what has typically been observed elsewhere, so any broad geochemical interpretations that are rooted in these empirical observations may be misguided. In the present study, we have sought out to determine the origin of elevated sulfur on Mercury's surface, which is associated in many cases with volcanic terrains [3]. To do this we have experimentally investigated sulfide solubility at sulfide saturation in silicate liquids as a function of pressure, temperature, and oxygen fugacity using a synthetic composition that is equivalent to the Northern Volcanic Plains lavas on Mercury. Previous studies have shown that sulfide solubility increases greatly with decreasing oxygen fugacity below about ΔIW-2 [4, Figure 1]. Preliminary estimates of Mercury's oxygen fugacity from Fe and S abundances at the surface range from ΔIW-2.6 to -7.3 [4-5]. In our experiments we controlled oxygen fugacity by adding Si metal, and the Si-SiO_2 buffer is at approximately ΔIW-5 at 1200° C. Our experiments were run over a range of pressures and temperatures (0.5-5 GPa and 1300-1850 °C), and the oxygen fugacity for each run was calculated relative to the IW and Si-SiO_2 buffers assuming ideal behavior. The f_{O2} calculations typically agreed within about 1 log unit, and our experiments were typically between ΔIW-5 to -8. All experimental charges were analyzed by EPMA. Our experiments indicate that the NVP melt compositions can hold between 1.2 and 5.8 wt% sulfide (Figure 1), which compares to the global average on Mercury of roughly 2 wt.% [1]. From our experiments, S solubility at sulfide saturation increases with increasing pressure and temperature, although additional work is needed to understand which has a stronger effect. The extreme f_{O2} conditions of Mercury's interior have contributed to its enigmatic chemistry, and are at least in part responsible for many of the unique characteristics that have been observed, including very low FeO abundances and elevated S abundances. Further studies are needed to determine how other elements may have been affected and distributed within Mercury's interior during its thermal and magmatic evolution.

[1] Nittler L.R. *et al.* (2011). *Science, 333*, 1847-1850.

[2] Peplowski P.N. *et al.* (2012). *JGR*, E00L04.

[3] Weider S.Z. *et al.* (2012). *JGR, 117*, E00L05.

[4] McCubbin F.M. *et al.* (2012). *GRL, 39*, L09202.

[5] Zolotov M.Y., *et al.* (2013). *JGR*, 118, 138-146.

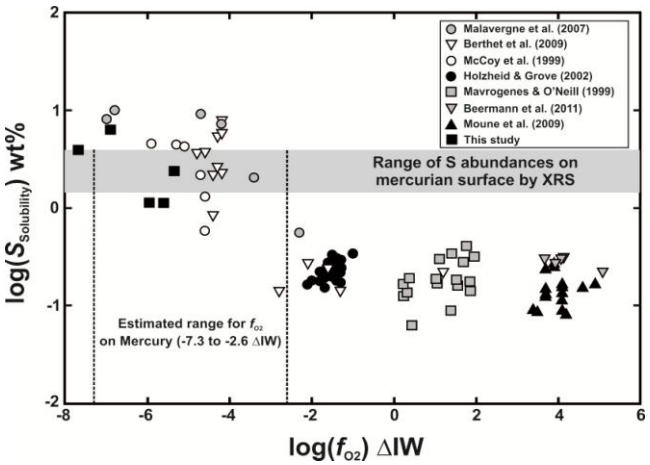

Figure 1: Sulfide solubility and oxygen fugacity relationships

In-situ structural changes of amorphous diopside ($CaMgSi_2O_6$) up to 20 GPa: an O K-edge X-ray Raman spectroscopy study

Moulton B[1], Henderson G[1*], Fukui H[2], Hiraoka N[3], Kanzaki M[4]

1 - University of Toronto *granth@es.utoronto.ca 2 - University of Hyogo 3 - SPring-8 / Harima Institute 4 - Institute for Study of the Earth's Interior

The O K-edge of $CaMgSi_2O_6$ glass has been investigated up to 21 GPa using X-ray Raman spectroscopy. We combine x-ray absorption near edge structure spectroscopy with XRS results to interpret the O *K*-edge at high-pressure. The results show four distinct structural transitions. At low pressure, Ca coordination appears to increase along with deformation of the SiO_4 tetrahedron. At moderate pressures both Mg and Ca coordination appear to increase while the contribution from tetrahedral Si decreases. This is interpreted as reflecting an increase in average Si coordination. At 16 GPa increasing Mg coordination remains important while an intensity increase observed around ~544 eV may indicate the presence of $^{[6]}$Si. At the highest pressure, 21 GPa, we observe dramatic changes in the spectra including the formation of π^* anti-bonding orbitals. These structural changes may explain known anomalies in transport properties of diopside melts.

Structure and properties of glasses and melts in the $SrO\text{-}Al_2O_3\text{-}SiO_2$ system

Neuville D*, Latapie L

IPGP-CNRS *neuville@ipgp.fr

The chemical and structural role of strontium in silicate and aluminosilicates glasses and melts is of interest with regard to the vitrification of high-level radioactive waste, glass ceramic and ceramic material. The configurational properties of melts and glasses provide fundamental information needed to characterize industrial processes. A main difficulty is to link the "macroscopic" configurational entropy with the structure of melts. This has been done by combining viscometry with Raman and X-ray absorption/diffraction spectroscopic studies. From the viscosity measurements, we have obtained the configurational entropy, *Sconf* (*log h = Ae + Be/TSconf*, were *h* is the viscosity, *T* the temperature and *Ae*, *Be* two constants). Raman spectra and X-ray diffraction give structural information on the middle range order and on the connected rings and X-ray absorption spectroscopy give structural information on the short range order. The structural information, which is related to the aluminosilicate network, can be affected by the presence and nature of non-network former cations. Indeed, strontium can play a different structural role: either as a modifier that participates to the network depolymerization, or as a charge compensator at the proximity of $(AlO_4)^-$ tetrahedra.

We have studied several Sr- aluminosilicate glasses, using viscosity measurements, Raman spectroscopy, and XANES at the Sr K-edges in order to investigate the substitution of Si by Al at SrO constant.

The viscosity measurements show a decrease of viscosity with decreasing SiO_2 content. When replacing Al by Si with SrO constant, a rapid decrease of the high frequency region (1100 cm^{-1}) is observed. These decreases can be attributed to the substitution of Si by Al. The anionic units determined by Raman spectroscopy are Q^4, Q^3 and Q^2, where tetrahedrally coordinated Al^{3+} is probably partitioned between these units. The abundance of these units and Al^{3+} partitioning are functions of chemical composition and temperature. The structural information can be related to the configurational entropy determined from the viscosity measurements.

Vibrational and X-ray absorption spectroscopy of chloride-carbonate-silicate glasses quenched at 5 GPa

Safonov O[1*], Shiryaev A[2]

1 - Institute of Experimental Mineralogy *oleg@iem.ac.ru 2 - Institute of physical chemistry and electrochemistry RAS; IGEM RAS

Alkali-rich carbonate-silicate melts in the upper mantle are considered as products of low-degree partial melting of carbonated peridotites and eclogites. Their ability to concentrate trace elements and dissolve large amounts of volatiles along with the ability for rapid migration and segregation because of low viscosity and density make them a a leading metasomatic agent ,s both in the upper mantle and in the lower crust, responsible for the formation of kimberlite, carbonatite and alkalic magmas. The unique properties of the carbonate-silicate melts are a consequence of their structure which combines structural features of both silicate and carbonate melts, and which can be deciphered using vibrational and X-ray absorption spectroscopies.

The paper reports results of the combined application of IR, Raman and X-ray absorption spectroscopies on the carbonate-silicate glasses quenched at 5 GPa and 1500 and 1600°C from the melts in the system $CaMgSi_2O_6$-Na_2CO_3(±$CaCO_3$)-KCl [1]. Special attention is paid to Cl on the structure of the glasses, since this volatile causes immiscibility in the carbonate-silicate melts with the formation of coexisting Cl-bearing carbonate-silicate melts and Si-bearing chloride-carbonate melts [1, 2]. Modifications of the glass (and, probably, corresponding melts) structure correlates with an increase in the $CaMgSi_2O_6$ content and decrease in the carbonate/silicate ratio. The enrichment of the melt with $CaMgSi_2O_6$ results in a general increase in intensity of the silicate bands with respect to the CO_3^{2-} bands in the Raman spectra of glasses. This is expressed in gradual polymerization from single units SiO_4^{4-} (Q^0) and dimers $Si_2O_7^{6-}$ (Q^1) to $Si_2O_6^{2-}$chains (Q^2) and, subsequently, $Si_2O_5^{2-}$ sheets (Q^3). Similar to silicate glasses, the silicate units in the carbonate-silicate glasses can coexist and transform in accordance with the equilibria $Q^1 = Q^0 + Q^2$ and $3Q^2 = Q^0 + Q^3$. The polymerization is accompanied by destruction of Ca-bound carbonate groups and stabilization of Na-bound carbonate groups in the following sequence: $Ca_2Na_2(CO_3)_3 \rightarrow Na_2Ca(CO_3)_2 \rightarrow Na_2CO_3$, showing a strong affinity of Ca to silicate units and Na to carbonate units.

Addition of KCl into the carbonate-silicate melts results in the increase of intensities of silicate bands with respect to the carbonate bands in quench glasses and promotion of polymerization. X-ray absorption data reveal that the Cl is bonded mostly or exclusively to K and/or Na as KCl and NaCl groups. Thus, the increase in polymerization occurs due to the formation of chloride-rich clusters extracting carbonate. The growth of these clusters finally results in immiscibility. The K/Cl ratio in the carbonate-silicate melts coexisting with the immiscible chloride-carbonate liquids positively correlates with the degree of melt polymerization suggesting a strong affinity of K with the silicate units in the glass (melts).

[1] Safonov O.G. *et al.* (2007). *EPSL*, 253. 112-128.

[2] Safonov O.G. *et al.* (2009). *Lithos*, 12S, 260-273.

Mineral reactions and deformation of solid-phase inclusions and their host crystals

Abart R*, Griffiths T, Kuleci H, Kovaleva E, Habler G

Department of Lithospheric Research, University of Vienna *rainer.abart@univie.ac.at

Solid-phase inclusions in rock-forming minerals are an essential tool for reconstructing complex geological histories. Deformation may be an important process for post formation modification of mineral inclusions. We present three examples illustrating the coupling between deformation and mineral reactions.

The first example is taken from the Koralpe crystalline complex of the Austroalpine basement, where Permian metapegmatites contain garnet with abundant submicron-sized mineral inclusions of rutile, xenotime, zircon, corundum, ilmenite, and Fe-Mn phosphate. The inclusions were probably formed during or after magmatic crystallization. Eclogite facies metamorphism and associated deformation during the Cretaceous produced brittle cracks in the garnet, which are now healed. Along the cracks the micro-inclusions have coarsened producing inclusion trails with grain sizes of several micrometers. The submicron-sized inclusions are missing in a 50 to 100 µm wide bleaching zone along the inclusion trails. Mineral chemical analysis revealed that the coarsening can occur isochemically. Using the cross correlation EBSD method a zone of garnet lattice rotation of up to 0.45° was detected, which correlates spatially with the bleaching zones. TEM investigations confirm increased dislocation density in this zone. We conclude that material re-distribution was enhanced in a plastically deformed zone along former brittle cracks, which probably formed at the propagating crack tip.

In a second example we focus on zircon grains of up to several tens of microns size, which are present as inclusions in plagioclase and in biotite from amphibolite facies rocks of the Tauern Window (Eastern Alps) and from granulite facies rocks of the Ivrea-Verbano Zone (Southern Alps). Crystal orientation imaging by EBSD revealed internal grain deformation, with the activation of various slip systems. In the granulite facies rocks the strain is spatially distributed leading to continuous orientation variation; in the amphibolite facies rocks it takes the form of low-angle grain boundaries. FE-EMPA analyses showed that chemical alteration may be associated with these low angle grain boundaries where Uranium and Yttrium have been removed. We infer that plastic deformation of micrometer sized zircon grains is a viable mechanism for modifying its trace element and radiogenic isotope content.

In a third example we address the mechanical effects associated with swelling particles in a rock matrix. We study the interplay between hydration and rock deformation by choosing the hydration of periclase to brucite in a calcite matrix. Dense calcite-periclase aggregates with periclase present at 10 vol. % and with less than 5 vol. % porosity were produced by hot isostatic pressing. The aggregates were then exposed to an aqueous fluid at 200 MPa and 400 to 600 °C in the stability field of brucite. Despite the low porosity of the aggregate, the periclase to brucite transformation turned out to be so rapid that the calcite matrix reacted by brittle failure enhancing the penetration of water and leading to a positive feedback. We infer that fracturing associated with the swelling of reactive inclusions my lead to a positive feedback enhancing further reaction.

Solid phase inclusions in garnet from UHP rocks with granulite facies overprint in the Moldanubian Zone (Bohemian Massif)

Faryad S[1*], Jedlicka R[2], Ettinger K[3]

1 - Institute of Petrology and Structural Geology, Charles University, Prague, Czech Republic. *faryad@natur.cuni.cz 2 - Institute of Geology and Paleontology, Charles University, Prague 3 - Institute of Geosciences, University of Graz, Austria

Eclogites and garnet pyroxenites hosted by garnet peridotite bodies are common within felsic granulites in the Moldanubian Zone of the Bohemian Massif. Mafic lenses and layers within mantle peridotites are interpreted as the result of melt infiltration into mantle rocks above the subduction zone. Garnet zoning in eclogites and pyroxenites indicates growth during cooling and pressure increase followed by decompression and heating under granulite facies conditions. Solid phase inclusions were studied in garnet with a compositional zoning that indicates a pressure increase and temperature decrease followed by decompression and heating. The inclusions are formed by one or more of minerals: amphiboles, micas (phlogopite, paragonite), alkali feldspars, carbonates, chlorite, apatite, clinopyroxene and spinel. The amphibole is alumino-pargasite with relatively high K and Cl+F contents. In addition to almost pure calcite, dolomite with dolomite-ankerite solid solution was found. Apatite has halogen contents between 2.7-3.7 wt. %. It contains exsolution lamellae of monazite or sulfide. In addition to monomineralic omphacite inclusions, diopside usually occurs together with one or more other minerals. Spinel associated with diopside is poor in Cr. Iron sulphides were observed in polyphase inclusions with amphibole + calcite and plagioclase + amphibole + diopside, respectively. It is almost pure FeS with no detectable amounts of Ni, Cu or As. Some inclusions have the negative shape of garnet crystals. In addition to one or more of the above minerals, there seem to be melt inclusions with total oxide content between 92.86 and 98.65 wt %.

These inclusions together with negative shapes following crystallographic planes in garnet indicate precipitation or crystallization from a fluid-bearing phase or from melt which was present during garnet formation. Mineral analyses and modal amounts of phases in the studied inclusions within garnet indicate that the composition of former melt varied from one inclusion to another, even in the same grain of host mineral. In addition to the monomineralic phases *e.g.* biotite, calcite, amphibole, *etc*., the reintegrated composition of poly-phase inclusions shows a large range of major oxide contents. This is in contrast to the *in situ* melt inclusions trapped during crystallization in the magmatic system, where equilibrium magma is enclosed by the host mineral. The presence of mineral inclusions with lithophile elements (Na, K, Ba) or volatiles (H_2O, F, Cl, CO_2 and SO_4) is interpreted as garnet crystallization during subduction when fluids formed by dehydration and melting of crustal material were available. As the rocks were subject to granulite facies metamorphism, some of hydrous minerals could melt, which resulted in the formation of negative shapes in garnet. Inclusions of omphacite signify eclogite facies conditions, diopsidic clinopyroxene, spinel and plagioclase, however, are representative of the granulite facies stage.

Diopside inclusions in anorthite and PT history of a coronitic gabbro from the Moldanubian Zone (Bohemian Massif)

Faryad S[1], Kachlík V[2], Hoinkes G[3*]

1 - Institute of Petrology and Structural Geology, Charles University, Prague, Czech Republic. 2 - Institute of Geology and Paleontology, Charles University, Prague 3 - University of Graz *georg.hoinkes@uni-graz.at

Coronitic gabbro from the Moldanubian Zone adjacent to the Brunovistulian Block is characterized by amphibole + spinel + sapphirine coronas around orthopyroxene that occurs in a medium-grained plagioclase matrix. Countless diopside inclusions (1-10 micrometer, maximum 20 micrometers in size) are present in plagioclase of anorthite composition. They are abundant mostly in large porphyric grains and less common in the medium-grained plagioclase of the matrix. The inclusions are monomineralic and form columnar crystals without shape-preferred orientation. There is no evidence for the presence of former melt or polyphase inclusions in the plagioclase. The frequency of inclusions depends on their size; the smaller the grain size, the larger number of inclusions in the plagioclase. Amphibole is found at triple junctions of the plagioclase grains in the matrix. The corona consist of orthopyroxene in the core with two or three zones; the first is represented by calcic amphibole, the second by symplectite of amphibole with spinel, sapphirine and accessory corundum and the third by garnet and amphibole with relics of spinel. The orthopyroxene forms a monomineralic aggregates that may contain a serpentine cluster in the core, suggesting its formation after olivine. Relics of clinopyroxene were observed within the amphibole zone.

Based on the mineral and geochemical composition, the rock corresponds to olivine gabbro with normative anorthite = 55 %, olivine = 33 %, orthoclase = 3 %, albite = 3 % and diopside = 6 %, where olivine is transformed into orthopyroxene, and possible clinopyroxene in the matrix into amphibole. Because of low normative clinopyroxene content in the rock, the amphibole present around the coronas and in the triple junctions of plagioclase could also form by the reaction between olivine (orthopyroxene) and plagioclase.

The presence of tiny diopside (X_{Mg} = 0.80) inclusions in plagioclase (An_{98}) suggests rapid cooling after melt crystallization reached the cotectic line between olivine and diopside and continued to the ternary eutectic point with plagioclase. The orthopyroxene in the core of corona has X_{Mg} = 0.78 and the surrounding amphibole corresponds to alumino-tschermakite with X_{Mg} = 0.76-0.85. Textural relations indicate that the amphibole corona around orthopyroxene was followed by formation of a symplectite of amphibole + spinel + sapphirine with corundum at granulite facies conditions, and finally garnet (Alm_{26-29}, Prp_{45-51}, Grs_{22}, Adr_2, Sps_1) was formed during rapid cooling but still at granulite facies conditions. It contains inclusions of spinel. In addition to availability of water, stabilization of calcic amphibole instead of clinopyroxene under granulite facies conditions was governed by the local mass balance of Na, K and Al in adjacent plagioclase. Small amounts of talc after orthopyroxene and the presence of muscovite within plagioclase and chlorite at contact with amphibole, are later-stage alteration products.

Immiscible sulfide and silicate melts in UHP gneisses from the Kokchetav Massif (Northern Kazakhstan)

Mikhno A*, Korsakov A

Institute of Geology and Mineralogy SB RAS. *mao14@list.ru

The ultrahigh pressure (UHP) metamorphic rocks from the Kokchetav massif (Northern Kazakhstan) record PT-conditions as high as P = 6-7 GPa, T = 1000 °C and provide a unique opportunity to study partial melting processes occurring at mantle depth. The Kokchetav Massif is considered as a *megamelange* zone (approximately 17 km wide and 80 km long) where slices of continental crust were exhumed from depths of at least 120 km.

It is claimed that metapelites (protholiths of gneisses) underwent melting near peak metamorphic conditions and hydrous melt was released. This melt migrated into the marbles and reaction lead to the formation of the K-cpx-bearing rocks. The finding of K-Cpx with prograde zonation allowed the last stage of prograde metamorphism to be constructed and also revealed that melting of metapelites started prior to peak metamorphic conditions. Herein, we present the results of 2D Raman imaging of primary fluid and melt inclusion porphyroblasts (garnet and kyanite) from gneisses along with data on the composition of different types of melt inclusions.

We focused on the UHP gneisses from the Barchi-Kol area (Kokchetav massif). These rocks are composed by Grt, Qtz, Mu, Ky, Bt. The accessory minerals of UHP gneisses are Ap, Ttn, Zrn, ±Dia, ±Gr, Po, ±Coe. Fluid, polyphase and sulfide inclusions occur in the cores of garnet and kyanite porphyroblasts, whereas rims of porphyroblasts are inclusion-free.

Sulfide and polyphase silicate inclusions were found coexisting in the cores of the garnet porphyroblasts. The polyphase silicate inclusion-associations for gneisses include apatite, calcite, phengite, vermiculite, phlogopite, coesite/quartz. Sulfide inclusions are composed of sphalerite, chalcopyrite, pyrrhotite and pentlandite. Fluid inclusions are extremely rare in gneisses. We found only one H_2O-fluid inclusion coexisting with the silicate inclusion in the core of garnet porphyroblast.

The silicate melt inclusions (of bulk composition SiO_2~63-64 wt%, Al_2O_3~15 wt%, FeO~6 wt%, MgO~6-8 wt%, CaO~3 wt%, Na_2O~0-1 wt%, K_2O~4-5 wt%) coexisted with sulfide inclusion in gneisses and show much lower K_2O than that previously reported as well as a very high content of MgO+FeO=12-14 wt%. The low K_2O-content in the silicate melts indicates that this melt was formed as the result of pervasive melting which decreased the amount of K_2O in the melt. This melting likely occurred during a retrograde stage due to phengite dehydration melting. This extensive melting also led to high contents of MgO+FeO, which in experimental studies of partial melting of the metapelites usually do not exceed 3 wt%. The occurrence of silicate and sulfide melt inclusions coexisting in garnet porphyroblast reveals that immiscible sulfide and silicate melts may coexist at high pressure and temperature conditions.

While experimental studies do not preclude the coexistence of silicate and sulfide melts, the presence of a fluid free phase remains highly debatable. Our finding of a single fluid inclusion raises the question of the possible mechanism of its formation: (i) initially it was trapped as a hydrous melt, but then necked down during the retrograde stage because of high water content in the UHP hydrous melt and (ii) the fluid inclusion was captured together with melt inclusions during a retrograde stage of metamorphism when PT-conditions were below the second critical endpoint for metapelitic systems.

Our findings imply that extensive melting of metapelite triggers the formation of coexisting silicate and sulfide melts during UHP metamorphism. The liberation of a H_2O-rich fluid phase likely occurs during a retrograde stage of metamorphism.

Apatite with sulphide exsolution lamellae in UHP eclogites from the Nové Dvory, Moldanubian Zone, Czech Republic

Perraki M[1], Faryad S[2*]

1 - Department of Geo-Sciences, School of Mining and Metallurgical Engineering, National Technical University of Athens 2 - Institute of Petrology and Structural Geology, Charles University, Prague, Czech Republic. *faryad@natur.cuni.cz

Eclogites from Nove Dvory are part of the high-grade rocks (the Gföhl Unit) which also comprise garnet peridotites, having experienced UHP conditions of 4-5 GPa and 1000-1200 °C as estimated by thermobarometry based on mineral compositions [1, 2, 3]. The Nove Dvory eclogites are medium- to coarse-grained with garnet porphyroblasts having sizes between 1 and 3 mm, locally up to 8 mm. The eclogite studied is weakly foliated and consists of garnet, omphacite, kyanite and quartz in a fine-grained matrix with clinopyroxene, plagioclase and amphibole. Minor amounts of rutile, apatite, sulphides and sulphates are also present. Apatite is common and it occurs in the matrix as intergranular grains and also as inclusions in garnet and omphacite. It is rich in fluorine (2-3 wt%) and has a maximum chlorine content of 1.1 wt%. It can reach up to 1 mm in length. It bears very fine crystallographically-oriented needle-like exsolution lamellae (Figure 1). SEM/EDS study and Raman microspectroscopy indicated that the lamellae are formed by copper-iron- and iron-bearing sulphide minerals, most probably chalcopyrite and pyrite, respectively. Minor iron oxides also occur. Similar features are frequent in eclogites as well as in ultramafic rocks in the Dabie-Sulu UHP metamorphic belt eclogites, China [4]. Experimental studies [5] showed that CuS_2 crystal can only be synthesized under high temperature and high pressure conditions (T = 700-1000 ^{0}C, at P = 4.5-5.0 GPa). Thus, sulphide-bearing exsolution-rich apatite has been interpreted as a pre-UHP phase in which UHP sulphides are preserved. In this case, no pure copper sulphide was identified. In non-metamorphic granites, pyrhhotite exsolutions in apatite have been interpreted as a result of simultaneous crystallization of apatite and pyrrhotite from a melt [6]. In the latter case, however, no copper-bearing sulphide was reported. It seems probable that the exsolution lamellae in apatite formed during decompression and cooling from UHP/HT conditions.

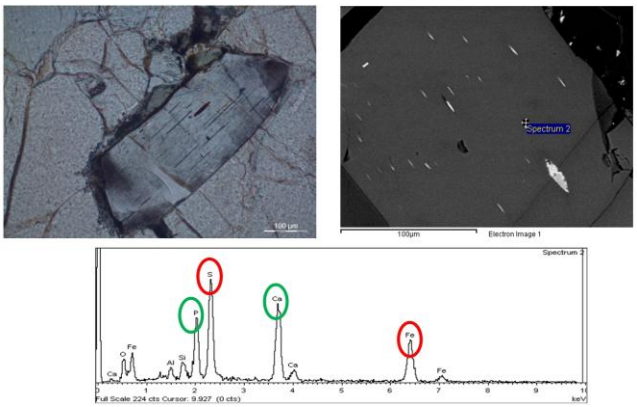

Figure 1: A photomicrograph (top left), a BSE image (top right) and an EDS spectrum (bottom centre) of sulphide lamellae in apatite from Nove Dvory eclogite.

[1] Medaris *et al.* (1990). *Lithos*, 25, 189-202.

[2] Nakamura *et al.* (2004). *J. Metamorph. Geol.*, 22, 593-603.

[3] Faryad *et al.* (2009). *J. Metamorph. Geol.*, 27, 601-845.

[4] Chen *et al.* (2006). *Acta Petrol. Sin.*, 22, 1921-1926.

[5] Bithert *et al.* (1966). *Solid State Commun.*, 4 , 533-535.

[6] Gottesmann and Wirth (1997). *Eur. J. Mineral.*, 9, 491-500.

Mineral inclusions - their genesis and fate

Proyer A

University of Botswana. alexander.proyer@uni-graz.at

Mineral inclusions are important because they recount a part of the evolution of a rock that is different from that recorded as the main equilibration stage in the rock matrix: it is generally an earlier history (proto- and syngenetic inclusions) or a later one (epigenetic inclusions). Proto- and syngenetic inclusions are hard to differentiate - perhaps only by geochronology. Epigenetic inclusions can be the result of re-equilibration or of exsolution. Shape preferred orientation (SPO) and crystallographically preferred orientation (CPO) have been invoked as criteria to differentiate exsolutions from primary inclusions (without SPO/CPO) but these criteria are ambiguous as epitaxial growth may produce similar features. Whereas exsolution has hitherto been considered an isochemical process, the recently discovered "open system precipitation" (OSP) adds an allochemical component [1, 2]. Many hitherto inexplicable oriented inclusions in minerals like clinopyroxene, garnet, titanite or apatite can be explained by OSP. Various forms of geochronology and geothermobarometry can be applied to inclusions, and a reintegration of exsolved material with the host is used to reconstruct "original compositions" of solid solution phases under extreme conditions of metamorphism (ultrahigh pressure or temperature). In the latter case a serious overestimate of P-T conditions may occur if only some, but not all, of the exsolved minerals are considered, *e.g.* pyroxenes exsolved from garnet while omitting exsolved ilmenite and/or rutile. Many inclusions record disequilibrium, like garnet within garnet or dolomite within dolomite, but also calcite replacing magnesite and others. Hence kinetics may play a pivotal role in inclusion formation, particularly of epigenetic ones. Sometimes not even primary inclusions are in compositional equilibrium with their overgrowing host, as proved by eclogite-facies coronitic metagabbros. One generally expects the oldest inclusions in the core of a porphyroblast and younger ones towards the rims, but in a few cases it may just be the other way round. Not only exchange reactions but even dehydration reactions may occur within an inclusion or between inclusion and host mineral, forming cracks and opening the system towards the matrix, as in the case of lawsonite inclusions within garnet. Lawsonite inclusions within quartz can be altered into zoisite/clinozoisite within an apparently closed system. These and more examples of "weird" inclusions will be presented to set the stage and discuss the sometimes miraculous world of mineral inclusions and their fate.

[1] Proyer A. *et al.* (2009). *Journal of Metamorphic Geology*, 27, 639-654.

[2] Proyer A. *et al.* (2013). *Contrib Mineral Petrol*, 166, 211-234.

What can mineral inclusions tell us about plate-scale processes?

Storey C[1*], Bruand E[1], Fowler M[1], Hart E[1], Schertl H[2]

1 - University of Portsmouth *craig.storey@port.ac.uk 2 - Institute of Geology, Mineralogy and Geophysics, Ruhr-University Bochum

Accessory minerals, which are dense and robust, are increasingly being used as repositories of geochemical data, which can be reliably analysed (usually by *in-situ* techniques) sometimes even after the host rock has undergone weathering, alteration and high-grade metamorphism. However, in some cases geochemistry (*e.g.* trace elements, stable and radiogenic isotopes) of the accessory phase may not allow all of the information related to the petrogenesis of the host rock to be gleaned. Mineral inclusions shielded within accessory phases offer an opportunity to obtain extra information, which could aid considerably in reconstructing the history of the host rock.

In this contribution, we have been focusing particularly on the trace element geochemistry of apatite inclusions within zircon and titanite. We are able to demonstrate that the inclusions do faithfully record the REE bulk composition of the host rock (recalculated using appropriate distribution coefficients) and to also investigate a method for fingerprinting different magma types from the apatite trace element geochemistry. This permits a method to analyse detrital zircon grains (for their U-Pb age, Lu-Hf and O isotopic compositions) and access information about the type of magma from which the zircons crystallised. Thus, the balance of magmas formed by different processes (*e.g.* TTG *vs.* Calc-alkaline) can be tracked through time as a function of changing geodynamics.

We have also been studying mineral inclusions within rutile, which have been extremely effective in helping to constrain pressure. The Zr-in-rutile geothermometer allows T to be constrained in rutile, but hitherto there has been no independent method of obtaining P, unless one uses a separate method within the host rock. By analyzing mineral inclusions within rutile, and calculating average PT (using Thermocalc) we have an opportunity to potentially be able to calculate PT for individual rutiles and even detrital rutiles. With U-Pb dating, O isotope composition and trace element geochemistry, we are potentially able now to reconstruct the thermobarometric and lithological evolution of high-pressure metamorphism in the past for where the whole rocks have been destroyed but where rutiles from these rocks have been preserved as detritus in younger sediments. Potentially, this could aid in circumventing the problem of high-pressure rocks being scarce in the Precambrian rock record, if that is mostly due to their being metastable and geographically restricted.

Oriented Fe-Ti oxide micro-inclusions in plagioclase from Mid Ocean Ridge gabbro

Ageeva O[1*], Habler G[2], Abart R[2], Pertsev A[1]

1 - Institute of Geology of Ore Deposits, Petrography, Mineralogy and Geochemistry *ageeva@igem.ru 2 - Department of Lithospheric Research, University of Vienna

Several micrometers long and less than a micrometer wide needles and plates of titano-magnetite, magnetite-ilmenite intergrowths and ilmenite were found as inclusions in plagioclase from dredged gabbro samples of the Mid Atlantic ridge at 13°30'-13°35'N. A first group of inclusions comprises needles of magnetite and magnetite-ilmenite lamellar intergrowths with strong shape- and lattice-preferred orientation. The plagioclase (An 34-65) host is twinned according to the albite twin law. One set of twin individuals hosts abundant inclusions with Mag{111} parallel to Pl(112) and rather free rotation by the common pole with two maxima at Mag[110] perpendicular to Pl(1-50) and at Mag[110] parallel to Pl[1-10] and less abundant inclusions with Mag(111) parallel to Pl(1-50) and free rotation of the magnetite around the common pole. In the second set of twin individuals the orientation relations are less regular. The most abundant group of inclusions is oriented with Mag(111) parallel to Pl(150), whereas a less abundant group is characterized by Mag(111) parallel to Pl(1-50).

When ilmenite forms lamellar intergrowths with magnetite, these phases show a crystallographic orientation relation with Ilm(001) parallel to Mag(111), Ilm(100) parallel to Mag(110) and Ilm(110) parallel to Mag(112). Ilmenite also forms independent plates, which show only weak crystallographic orientation relations with the plagioclase host having their (001) plane oriented approximately parallel to the main plagioclase crystallographic planes.

In the magmatic stage of gabbro formation the first group of titanomagnetite inclusions were probably exsolved from Fe,Ti-rich plagioclase at subsolidus conditions. Associated with plagioclase twinning during cooling, the second stage of inclusion formation corresponds to the intrusion of plagiogranites into the gabbro. At this stage fluid-mediated remobilization of Fe and Ti lead to the decomposition of the titanomagnetite inclusions producing ilmenite-magnetite lamellar intergrowths. In domains, where this process was pervasive, Fe-Ti oxide inclusions disappeared leading to inclusion-free domains in the plagioclase. Late stage hydrothermal alterations caused further remobilization of Ti and Fe leading to the dissolution of ilmenite-magnetite inclusions and crystallization of separate ilmenite plates.

The microstructural and textural evolution starting with the formation of titanomagnetite needles with strict lattice and shape preferred orientation in the plagioclase host to successively less strictly oriented precipitates correlates with the mineralogical change from titanomagnetite via magnetite-ilmenite lamellar intergrowths finally to ilmenite. This succession probably reflects a series of mineral reactions starting with the exsolution of Ti and Fe from plagioclase under supposedly water deficient conditions, followed by fluid-mediated redistribution, phase separation and recrystallization in association with plagiogranite intrusion and late hydrothermal alteration.

Natrocarbonatite composition of melt inclusions from Bailundo and Longonjo carbonatites (Angola)

Castellano Calvo A[1*], Melgarejo Draper J C[2], Kamenetsky V[3], Kamenetsky M[3]

1 - Departamento de Cristalografía, Mineralogía y Depósitos Minerales (University of Barcelona) *amaiacastellano@gmail.com 2 - Dep. Mineralogia, Yacimientos Minerales, University of Barcelona 3 - ARC CODES (UTAS) Tasmania

The Bailundo and Longonjo carbonatites are two of the largest carbonatite complexes of Angola, and their age is assumed to be Cretaceous. The primary mineralization largely consisted of carbonates, apatite, pyrochlore (I) and magnetite, with lesser amounts of sulphides (pyrite and galena). However, these carbonatites have been extremely affected by subsolidus and hydrothermal processes, and the result is a mixture of scarce restites of the primary associations with large volumes of secondary associations produced by replacement. The secondary alterations comprise extended silicification of the carbonatite, as well as development of secondary carbonates. During hydrothermal processes, new pyrochlore generations (II and III) and secondary apatite were produced, as well as large amounts of barite, strontianite, witherite, celestite, REE carbonates, silicates and phosphates, and minor amounts of baddeleyite and niobian rutile. Moreover, these rocks have been affected by intensive weathering, which replaced the carbonates by secondary iron oxides.

A large variety of magmatic and hydrothermal inclusions have been found in different minerals from the Bailundo and Longonjo carbonatites that provide an informative, though fragmentary, record of the original carbonatite melt and of late hydrothermal solutions. These inclusions were studied by optical and scanning electron microscopy (SEM-FESEM) and RAMAN spectroscopy.

Inclusions of nyerereite/shortite, bradleyite, ferrotychite and undetermined (F+K+Mg+Na+Ba+Cl+C) composition occur in pyrite from Bailundo, and are interpreted as melt inclusions, as are shortite/nyerereite and eitelite inclusions in magnetite. There are also gregoryite, shortite/nyerereite, halite and anhydrite triphasic inclusion in fluoroapatite as well as nyerereite and calcite biphasic inclusion in fluoroapatite from the Bailundo carbonatite. In addition, nyerereite/shortite, burbankite, eitelite and bradleyite inclusions occur in Sr-rich dolomite from the Longonjo carbonatite. All these types of Na-, K- rich melt inclusions are indicative of the existence of an alkali-enriched parental magma for the Bailundo and Longonjo carbonatites. Moreover, they are indicative of a natrocarbonatite component in the primary carbonatitic magmas. Also, the Na- and K- carbonatitic melt inclusions in dolomite minerals, and the occurrence of biphasic melt inclusions consisting of calcite and shortite/nyerereite suggest the occurrence of magma immiscibility processes during the crystallization of the Bailundo and Longonjo carbonatites.

This is the first report of alkaline melt inclusions in sulphides from carbonatites.

Cr-Mg-staurolite: highest Cr_2O_3 content in staurolite to date; example from quartz-free eclogites from Lezer Mountains, South Carpathians, Romania

Costin G[1*], Negulescu E[2], Săbău G[2], Luffi P[3], Ménot R[4]

1 - Rhodes University *g.costin@ru.ac.za 2 - Geological Institute of Romania, Bucharest 3 - Department of Mineralogy, University of Bucharest 4 - Lab. Magmas et Volcans, Université J. Monnet, Saint-Etienne

Cr-Mg-staurolite occurs together with other Cr-rich phases (Cr-kyanite, Cr-phengite) in fine aggregates as rare and dispersed mm-size, grass-green spots, within a fine grained eclogite near Leresti (Iezer Mountains, South Carpathians, Romania). The eclogitic bodies occur as flat lenses of 0.3-1 m, parallel with the foliation of host metapelitic schists. The eclogites are quartz-free and show lack of deformation, having a granoblastic texture, with small (2-3 mm) garnets ($Prp_{41-56}Alm_{24-36}Gross_{15-23}Spess_{0.5-1}$) floating in a mass of omphacite (Jd_{20-45}) and Ca-amphiboles. The Cr-aggregates developed as a fine greenish corona around a central ragged core represented by a relict chromite $(Fe^{2+}_{0.71}Mg_{0.16}Zn_{0.13})_{\sum=1}(Cr_{1.65}Al_{0.35})_{\sum=2}O_4$. In a few such aggregates, the BSE images show Cr-Mg-staurolite, Cr-kyanite (7-10.5% Cr_2O_3) and rutile as replacement textures after chromite. Both Cr-Mg-staurolite and Cr-kyanite develop on chromite, invading it, sometimes as distinct lamellae in spinel, suggesting preferential replacement along distinct crystallographic planes or along former exsolution lamellae of the magmatic spinel (Figure 1). Cr-phengite (5.75% Cr_2O_3) occurs in the external part of the Cr-rich aggregates. Within the Cr-aggregates and/or at the exterior of these, little grains of rutile are present. The amphibole and omphacite neighbours to Cr-rich aggregates are also anomalously rich in Cr. The Cr-Mg-staurolite studied here represents the staurolite with the highest Cr_2O_3 content reported to date. The composition of Cr-Mg-staurolite (average of 10 EPMA analyses) show (wt%): SiO_2=28.672, TiO_2=0.535, Al_2O_3=46.710, Cr_2O_3=10.259, FeO=5.598, MnO=0.016, MgO=4.895, ZnO=1.259, Total=97.928. The Cr_2O_3 range is 7.93-12.04 wt%. The structural formulae of Cr-Mg-staurolite, when normalized to 23.5 Oxygen is $(Mg_{1.034}Fe^{2+}_{0.663}Zn_{0.135}\square_{0.167})_{\sum=2.000}(Al_{7.802}Cr_{1.149}Ti_{0.057})_{\sum=9.008}Si_4O_{23}(OH)$. The X_{Mg}=(Mg/(Mg+Fe^{2+}) range from is 0.583-0.706 with an average of 0.61, showing that it represents a high-pressure Mg-staurolite. The Cr-Mg-staurolite, together with Cr-kyanite and Cr-phengite resulted from high pressure breakdown of magmatic chromite, during (Variscan?) high-pressure metamorphism of an ultramafic or picritic protolith.

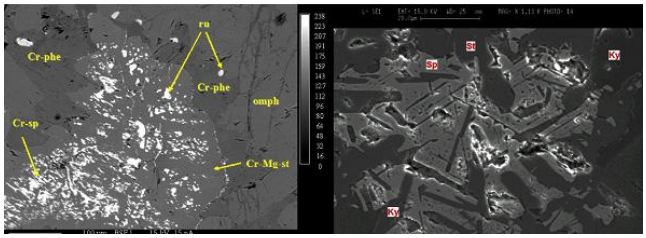

Figure 1: (left) Relict chromite (Cr-sp), transformed to Cr-Mg-staurolite (Cr-Mg-st), surrounded by Cr-phengite (Cr-phe) and rutile (ru); kyanite not visible at this scale. BSE image. (right) Chromite (sp) with kyanite (ky) lamellae; Cr-Mg staurolite (st) and kyanite grains surround the relict chromite. BSE Image.

Interaction between host mineral deformation and submicron inclusion re-equilibration

Griffiths T[1], Habler G[1], Abart R[1*], Rhede D[2], Wirth R[2]

1 - Department of Lithospheric Research, University of Vienna *rainer-abart@univie.ac.at 2 - GFZ Potsdam

Mineral inclusions are an essential tool in the interpretation of complex geological histories. Deformation can facilitate or drive inclusion re-equilibration, creating fast diffusion pathways in the host in the form of cracks (brittle) or dislocations and (sub)grain boundaries (ductile). This work aims to go beyond observation of inclusion re-equilibration *via* deformation and attempts to pin down the mechanisms by which it occurs.

Sampled Permian meta-pegmatite garnets (almandine-spessartine composition) from the Koralpe (Eastern Alps, Austria) contain abundant submicron-sized inclusions (1 µm - 2 nm Ø), which originated during or subsequent to magmatic garnet growth. The Permian magmatic assemblages were affected by eclogite facies metamorphism during the Cretaceous tectono-metamorphic event. The meta-pegmatite garnet deformed crystal-plastically at this metamorphic stage.

Trails of coarser inclusions (1-10µm Ø) crosscut the magmatic submicron inclusion density zoning in the garnet, defining curviplanar geometrical surfaces in 3D. In 10-100 µm broad 'bleaching zones' flanking inclusion trails, the ≤1 µm sized inclusions are absent in optical microscope and SEM images, though TEM observations show that inclusions <100 nm are unaffected. From their microstructural characteristics it is inferred that the trails formed at sites of healed brittle cracks.

FEG-microprobe data show that inclusion-trails and associated bleaching zones can be formed isochemically, although some trails show non-isochemical coarsening. In both cases no change in garnet major element composition is observed.

Bands of slightly misoriented garnet correlating spatially with bleaching zones were mapped using EBSD. Using the cross correlation EBSD method garnet lattice orientations were determined to a precision of better than ± 0.04°. Misorientation relative to undeformed garnet increases towards the centre of trails. Typical gradients in misorientation angle on the order of 0.01° per µm correspond to low dislocation densities, nonetheless higher than in unrotated garnet outside the bleaching zone. Maximum misorientation reaches 0.1-0.45°.

Targeted TEM foils confirm the presence of dispersed dislocations in bleaching zones at low densities without forming subgrain walls. A negligible amount of dislocations was found outside bleaching zones.

Localized enhanced transport at sites of former brittle cracks presumably caused inclusion coarsening and formation of inclusion trails. EBSD data show ductile deformation of garnet correlated with the microstructure. Dislocations could have originated in the plastic zone at the crack tip during crack propagation; enhanced transport by pipe diffusion with limited external input could explain the isochemical coarsening seen in some trails. In trails where a more varied phase assemblage and non-isochemical coarsening is observed, input of external components and fluid-enhanced diffusion are inferred to have played a greater role in facilitating coarsening. Alternatively, it is possible that dislocations signify strain localization in garnet domains with reduced nanoinclusion content. Both possibilities represent mechanisms of interaction between deformation and re-equilibration of host and inclusion at the nanoscale.

Rheological behavior of zircon in deformed rocks: crystal-plastic deformation and its consequences for trace element content

Kovaleva E[1], Habler G[1], Kloetzli U[1], Rhede D[2], Abart R[1*]

1 - Department of Lithospheric Research, University of Vienna *rainer.abart@univie.ac.at 2 - Helmholtzzentrum Potsdam, Detusches GeoForschungsZentrum

Zircon is one of the most abundant and wide-spread accessory minerals in many rock types. Due to its resistivity and incorporation and preservation of radioactive U and rare earth elements (REE), zircon is used for isotopic dating and as a geochemical monitor. In this study, zircon is investigated *in situ* as a mineral inclusion within high-temperature ductile shear zones in various rock types that formed under different metamorphic conditions. Several scanning electron microscopy (SEM) techniques, including secondary electron (SE), backscattered electron (BSE), forward scattered electron (FSE) and cathodoluminescence (CL) imaging as well as crystallographic orientation imaging by electron backscatter diffraction (EBSD) were used in combination with compositional data from field emission electron probe micro-analysis (FE-EPMA). Hosted by metamorphosed and strained rocks, zircon often shows evidence of crystal-plastic deformation and associated chemical alteration.

Zircon plastic behavior varies in rheologically different local host environments. Zircon, embedded and deformed within rheologically relatively weak material, activates the common and most energetically preferable slip systems. In this case, the misorientation axes cluster close to [001]. At these conditions, zircon sometimes develops a crystallographic preferred orientation (CPO) as a consequence of dynamic recrystallization by a subgrain rotation mechanism. Zircon deformation within a rheologically stronger medium is controlled by the host phase configuration activating uncommon slip systems and occasionally forming twist walls and cross slip.

Furthermore, zircon deformation behavior differs in rocks from different metamorphic grade investigated in this study. In the amphibolite-facies rocks, zircon develops well-defined subgrains with enclosed boundary walls and no internal orientation variations. In the rocks from granulite-facies units, zircon shows an undulatory strain pattern without subgrain boundary formation. In the second case, intragranular misorientation angles are much larger and concentrated at prominent tips or along the long side(s) of the grain. In some cases, the deformation affects the entire grain and causes gradual bending of the crystal.

Plastic deformation structures developed in zircons hosted by shear zones may cause enhanced intragranular diffusion of trace elements and/or re-equilibration of isotopic systems that are crucial for zircon geochronology and potential time constraints on deformation events. Element distribution maps together with CL images show evidence of local variations of trace-element composition across subgrain boundaries. Uranium and Yttrium compositional maps demonstrate linear features of element depletion in zircon that are spatially related to deformation structures. CL images often show bright domains associated with subgrain boundaries.

The combination of different analytical techniques shows the relationship of deformational structures and trace element compositional variations in natural strained zircons. Thus, plastic deformation mechanisms in zircon may be usable for zircon geochronology to accurately date deformation events.

Fracturing in a calcite matrix induced by hydration of periclase

Kuleci H[1], Abart R[1*], Rybacki E[2]

1 - Department of Lithospheric Research, University of Vienna *rainer.abart@univie.ac.at 2 - Helmholtzzentrum Potsdam Deutsches GeoForschugnsZentrum

Hydration of mantle minerals such as olivine and orthopyroxene is an important geological process leading to serpentinization and lowering bulk rock density. Hydration is accompanied by a substantial volume increase of the solids which generates stresses that may eventually cause fracturing or plastic flow depending on the rate of hydration and creep of the rock matrix. We investigate the effect of the volume increase associated with hydration of periclase immersed in a matrix of calcite as a model case. The formation of brucite by the hydration of periclase produces a 100% volume increase of the solids and, at the same time, calcite behaves as a non-reactive matrix phase. Periclase single crystals and Carrara marble were pulverized, to a grain size of 63 to 200 microns and less than 63 microns, respectively. The powders were homogenized and subsequently dried for more than 24 h at 120 °C. The mixture was cold-pressed into thin walled cylindrical steel sleeves of 10 mm diameter and 20 mm length. Dense calcite-periclase aggregates with a periclase to calcite proportion of 10/90 by volume were prepared by using hot isostatic pressing (HIP) technique in a Paterson type gas medium apparatus within the stability field of calcite and periclase at a temperature of 700 °C and a confining pressure of 300 MPa for 2 h The hipped samples have a largely equilibrated microstructure with abundant 120° triple junctions in the calcite matrix, a porosity of less than 5% and they are devoid of cracks. The calcite-periclase aggregate was then exposed to an aqueous fluid at 200 MPa and temperatures of 400 to 600 °C to induce periclase to brucite transformation. The hydration of periclase was so violent that the hot pressed aggregate reacted by intense fracturing leading to complete disintegration. Apparently periclase hydration was too fast to allow for accommodation of the associated volume increase by creep of the calcite matrix.

Stability of iron oxyhydroxide inclusions in micritic dolomite of carbonate hosted banded iron formations of the 2.4 Ga Cauê Formation (Quadrilátero Ferrífero, Brazil)

Orberger B[1*], Tudryn A[2], Wirth R[3], Morgan R[2]

1 - Eramet Group *beate.orberger1@orange.fr 2 - Université Paris Sud, France 3 - GFZ Potsdam, Germany

Iron oxyhydroxide inclusions in micritic dolomite from carbonated banded iron formations from the 2.4 Ga Caué Formation, Itabira Group, Brazil, were studied by FIB-TEM and Fourier-transform analyses. An HAADF overview of the dolomite FIB-foil shows that two dolomite crystals are joined at a low angle crystal boundary. Fast Fourier Transform (FFT) diffraction pattern of the inclusions, such as nanometric laths being part of clusters, indicate the probable presence of two minerals, ferrihydrite and goethite. Euhedral hematite is also present. These inclusions are often associated with voids, which resemble fluid inclusion spaces. EDX analyses on the ferrihydrite-goethite indicate the presence of Si traces. As the transformation of ferrihydrite to goethite most likely occurs through a dissolution-precipitation process, and ferrihydrite forms poorly crystalline phases, the euhedral shapes suggest goethite as the most likely inclusion. Whole rock Curie balance analyses show that at temperatures of ≥ 790 °C thermal decomposition of dolomite, goethite and hematite occurred, and magnesioferrite or Mg-rich maghemite were formed. The goethite inclusions are interpreted as having formed during early diagenesis and probably precipitated from Fe-(Si) bearing fluid inclusions.

Pseudo-inclusions in inherited zircons from Myanmar jadeitite

Yui T

Institute of Earth Sciences, Academia Sinica, Taipei, Taiwan.
tfyui@earth.sinica.edu.tw

Characteristic mineral inclusions in zircons have been used as an indicator for metamorphic conditions, under which the enclosing zircon domains grew/recrystallized and the characteristic minerals were entrapped concurrently. The geological meaning of the U-Pb ages retrieved from such zircon domains can thus be specified. The technique has been successfully applied to zircons from UHP and UHT metamorphic rocks. On the other hand, interpretation of mineral inclusions in zircons from lower grade metamorphic rocks may not be so straightforward because inclusion minerals and/or zircon itself may react with fluid infiltrating through zircon fractures to form new minerals. Such new phases included in zircons actually postdate the enclosing zircon domains, which may also not be completely recrystallized. This kind of "pseudo-inclusion", if not recognized, may lead to erroneous interpretations of U-Pb zircon ages.

The present study gives an example in this regard. Zircons from Myanmar jadeitite have been dated previously. Both studies reported that zircons contain jadeite/omphacite inclusions, indicating a non-igneous origin, and that the Myanmar jadeitite would have formed during the late Jurassic. However, detailed SEM/EPMA/Raman-spectroscopy work shows that zircons from Myanmar jadeitite contain feldspars (K-feldspar and albite), chlorite, jadeite, Na-amphiboles and less commonly, catapleiite as mineral inclusions. All these inclusions can be divided into two types: primary inclusions and pseudo-inclusions. The primary inclusions are feldspars and are mostly mono-phase in one inclusion. They are smaller than 10 microns in size and are usually round in shape. The pseudo-inclusions are quite often polyphase and comprise jadeite, omphacite, Na-amphibole and catapleiite. They are large in size, 10-100 microns, and generally have irregular/angular form with microfractures. Some small chlorite inclusions might be interpreted as alteration products of primary pyroxene or amphibole inclusions, although chlorite is also common in large pseudo-inclusions replaced by jadeite/omphacite. Zircon grains or domains without mineral inclusions or with primary inclusions generally exhibit oscillatory zoning patterns under cathodoluminescence (CL). These zircons usually display medium to dark, and occasionally light, CL. On the other hand, zircon grains or domains, which are fractured or contain pseudo-inclusions, mostly show a heterogeneous, patchy, cauliflower-like texture. It is concluded that the zircons in Myanmar jadeitite are inherited. Primary inclusions are most probably of igneous origin, while pseudo-inclusions formed concurrently with jadeitite formation. The reported late Jurassic age would be the age of the igneous protolith. Jadeitite should have formed later.

Mineral chemistry of Shigar Valley pegmatites, Skardu, Pakistan: evidence for source lithologies and origin

Agheem M H[1*], Shah M T[2], Khan T[3], Dars H[1]

1 - Centre for Pure and Applied Geology, University of Sindh, Jamshoro, Sindh, Pakistan *mhagheem@yahoo.com 2 - National Centre of Excellence in Geology, University of Peshawar, Peshawar, Pakistan 3 - Department of Earth and Environmental Sciences, Bahria University, Islamabad, Pakistan

Shigar Valley pegmatites are famous due to the occurrence of various types of gemstones. Based on field features, two types of pegmatites (i.e., simple and complex or zoned pegmatites) are recognized. The proper characterization of mineral constituents of any pegmatite is of utmost importance because on this criterion; the pegmatites are not only classified but it supports the determination of stages of differentiation and the source lithologies involved. So far, all of the mineral constituents of Shigar valley pegmatites are analyzed through electron probe microanalyzer (EPMA) and in the light of such data; the source lithologies, stages of evolution and origin of these pegmatite are investigated.

The common rock-forming minerals identified are: two feldspars, quartz, muscovite, biotite, garnet, tourmaline, zircon, chlorite along with gemstones such as aquamarine, goshenite, topaz, apatite, schorl and fluorite. The EPMA data indicate that the Shigar Valley pegmatites are mainly composed of albite along with quartz and alkali feldspar, which is an indication of miarolitic type of pegmatites. The miarolitic nature of pegmatites is also clear due to the association of albite with different gemstones at the core-margin zone. The FeO contents of orthoclase are 0.01 to 0.14 wt % and as a result, the biotite is generally absent in the zoned pegmatites (i.e., gemstone-bearing) while it is present in the simple pegmatites (i.e., gemstone-barren). Muscovite is the main accessory mineral of all the zones but its size continuously increases from border towards central zone, where it encloses gemstones in the cavities with its large sheets (books).The presence of muscovite and absence of lepidolite indicates that these pegmatites are of muscovite sub-type. The relative enrichment of fluorine into muscovites of core-margin zone also indicates progressive crystallization from border to core.The high % of Fe^{+2} in biotites show the high acidic and evolved character of these pegmatites. EPMA data indicates that the tourmalines are schorl; where Al_2O_3, FeO and Na_2O qualify for schorl. The absence of biotite in the zoned pegmatites can be justified due to the presence of schorl, where Fe^{+2} is incorporated by schorl rather than biotite. The garnet composition in pegmatites is almandine-spessartine while that of host rocks is almandine-grossular. This suggests that the garnets of pegmatites are of primary nature. The MnO contents of muscovite are generally less than 0.08 wt. %, which indicates that manganese apparently concentrated in the residual magma until the formation of almandine-spessartine. The spessartine contents range from 27-40 mole %, therefore, it is probable that the pegmatites could have been emplaced at a depth of 12 to 15 km.

Some of the minute crystals are identified as pure zircons having small input of Y, Yb and P. Small concentration of hafnon can be attributed to the absence of lithium and tantalum bearing minerals in these pegmatites. Apatite is mainly mangan-apatite and is noticed in the core-margin or central core zone. The green colored fluorites are also found from the core-margin or central core zone and EPMA analyses indicate that these are pure CaF_2.

The field features and radiometric ages of both the host rocks of Shigar Valley pegmatites and nearby plutonic units are not correlated. However, the minerals' characterization show that these pegmatites are separate magmatic pulses and are formed from partial melting of a sedimentary protolith, which was at least deficient in lithium content.

Tourmaline evolution in the granitic pegmatite of the Cruzeiro Mine, Minas Gerais, Brazil

Andreozzi G[1*], Bosi F[1], Hålenius U[2], Gori C[3]

1 - Sapienza University of Rome *gianni.andreozzi@uniroma1.it 2 - Swedish Museum of Natural History 3 - University of Parma

Crystal chemistry of a large color-zoned tourmaline crystal from the Cruzeiro pegmatite is described, and tourmaline evolution process is defined in terms of site population at the Y site (Al, Fe, Li etc.) and at the O1 site (O, OH, F). Four crystals were extracted from the color-zoned tourmaline and investigated by crystal-structure refinement, electron microprobe analysis, Mössbauer spectroscopy and optical absorption spectroscopy. Tourmaline evolution from schorl to fluor-elbaite, with minor contribution of fluor-schorl, oxy-schorl and elbaite, is proved to occur from core to rim. Comparison with previous studies [1, 2, 3] revealed that tourmaline composition regularly varies across the pegmatite zones. In particular, the blue-green fluor-elbaite only crystallizes in the Intermediate zone, immediately after the end of black schorl/fluor-schorl formation (in the Border and Wall zones) and before the beginning of multi-color elbaite formation (in the miarolitic cavities, shaped by fluid phase ex-solution).

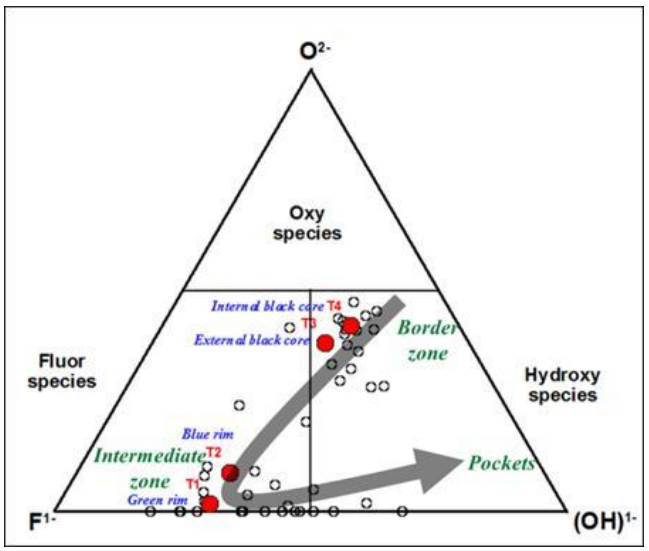

Figure 1: Tourmaline evolution in the Cruzeiro pegmatite

[1] Federico M., Andreozzi G.B., Lucchesi S., Graziani G. and César-Mendes J. (1998). Crystal chemistry of tourmalines. I. Chemistry, compositional variations and coupled substitutions in the pegmatite dikes of the Cruzeiro mine, Minas Gerais, Brazil. *Canadian Mineralogist*, 36, 415-431.

[2] Bosi F., Andreozzi G.B., Federico M., Graziani G. and Lucchesi S. (2005). Crystal chemistry of the elbaite-schorl series. *American Mineralogist*, 90, 1784-1792.

[3] Bosi F., Andreozzi G.B., Skogby H., Lussier A.J., Yassir A. and Hawthorne F.C. (2013). Fluor-elbaite, $Na(Li_{1.5}Al_{1.5})Al_6(Si_6O_{18})(BO_3)_3(OH)_3F$, a new mineral species of the tourmaline supergroup. *American Mineralogist*, 98, 297-303.

Mineralised pegmatites of the Damara Belt, Namibia: fluid inclusion and geochemical characteristics with implications for post-collisional mineralisation

Ashworth L[1*], Kinnaird J[2], Nex P[2], Harris C[3], Müller A[4]

1 - GeoSpectral Imaging *luisa@geospectral.co.za 2 - University of the Witwatersrand 3 - University of Cape Town 4 - Geological Survey of Norway

Namibia is renowned for its abundant mineral resources, a large proportion of which are hosted in the metasedimentary lithologies of the Damara Belt, the northeast-trending inland branch of the Neoproterozoic Pan-African Damara Orogen. Deposit types include late- to post-tectonic (~ 523 - 506 Ma) LCT (Li-Be, Sn-, and miarolitic gem-tourmaline-bearing) pegmatites, and uraniferous pegmatitic sheeted leucogranites (SLGs), which have an NYF affinity. Fluid inclusion studies reveal that although mineralization differs between the different types of pegmatites located at different geographic locations, and by extension, different stratigraphic levels, the fluid inclusion assemblages present in these pegmatites are similar; thus different types of pegmatites are indistinguishable from each other based on their fluid inclusion assemblages. Fluid inclusion petrography indicates that although fluid inclusions are abundant in the pegmatites, no primary fluid inclusions are present, and rather those studied are pseudosecondary and secondary. These are aqueo-carbonic (± NaCl), carbonic, and aqueous. It is proposed that all of the pegmatites studied share a similar late-stage evolution, with fluids becoming less carbonic and less saline with the progression of crystallisation. Oxygen isotope ratios allow the discrimination of different pegmatites into two groups, Group A (Sn-, Li-Sn-, and gem-tourmaline-bearing LCT pegmatites), and Group B (Li-Be-bearing LCT, and U-bearing NYF pegmatites). Group A pegmatites have O-isotope ratios ranging from 11 to 13 ‰ suggesting that they have an I-type affinity. These values are, however, elevated above those of typical I-type granites the derivation of these pegmatites from a non-pelitic/S-type metaigneous source. Group B pegmatites have higher $\delta^{18}O$ ratios ($\delta^{18}O$ = 15 - 16 ‰), indicative of their S-type affinity, and their derivation from metapelitic source rocks. Trends in the trace element concentrations of both Group A and Group B pegmatites are very similar to each other, making the two groups indistinguishable from each other on this basis. The Damaran pegmatites also share similar geochemical trends with their country rocks. There is, however, no direct field evidence to suggest that the pegmatites were derived from the *in situ* anatexis of the country rocks. It is more likely that anatexis occurred some distance away from where the pegmatites were ultimately emplaced, and that the melts migrated and were finally emplaced in pre-existing structures, possibly formed during Damaran deformation. O-isotope and Ti-in-quartz geothermometry indicate that Damaran pegmatites can be subdivided into two groups based on their crystallisation temperatures. LCT pegmatites crystallised at temperatures ranging from ~ 450 - 550 ºC, while the NYF pegmatites crystallised at higher temperatures, ranging from 630 - 670 ºC. It is important to note that the subdivision of pegmatites in Groups A and B based on their O-isotope systematics does not correspond with their subdivision into the LCT and NYF pegmatite families according to their crystallisation temperatures. In addition to clarifying aspects of the emplacement and evolution of the Damaran pegmatites, this study points out that there are several discrepancies in the current classification schemes of pegmatites. It shows that in addition to the problems encountered when trying to distinguish between LCT and NYF pegmatites based on their mineralogy, they also cannot truly be distinguished from each other using their geochemical and isotopic characteristics, or their tectonic settings. It is tentatively proposed that crystallisation temperature be considered as an alternative or additional characteristic in the classification of pegmatites, and that it be considered on a regional scale rather than only in the evaluation of the highly evolved end-members of a pegmatite swarm.

Petrographic textures of primary phosphates from pegmatites of the Conselheiro Pena district, Minas Gerais, Brazil: transformation sequence and genetic implications

Baijot M[1*], Hatert F[1], Dal Bo F[1], Simon P[2]

1 - University of Liège * mbaijot@ulg.ac.be 2 - Natural history museum of Luxembourg

In Brazil occurs one of the most important pegmatite provinces in the world, the Eastern Brazilian Pegmatite Province (EBPP), which is located at the eastern side of the São Francisco craton. The Conselheiro Pena pegmatitic district forms part of the EBPP where two intrusions crosscut the basement rocks and its cover: the Galiléia and Urucum magmatic suites which belong to the G1 and G2 supersuites, respectively. Pegmatites intrude the garnet-, biotite-, and sillimanite-bearing schists of the São Tomé Formation (Rio Doce group, Late Proterozoïc).

In 2008 and 2010, we visited several pegmatites located in the Conselheiro Pena district, between Galiléia and Mendes Pimentel, in order to investigate the petrography of phosphate minerals and their relationships with associated silicates. According to their macroscopic features and their mineralogy, three kinds of phosphate masses were found. The aims of the present paper are (i) to describe in detail the petrographic texture affecting these primary phosphate minerals in order to explain their crystallization sequence and the physico-chemical conditions prevailing during the magmatic stage of the pegmatite, and (ii) to better understand how the hydrothermal stages affected the phosphate masses throughout the chemical and petrological study of secondary species, which crystallize during these stages.

During the magmatic stage, phosphate associations developed three kinds of primary textures, which may occur in the same pegmatite: association I is constituted by dendritic triphylite, forming intergrowths with silicates (spessartine or albite); association II forms blocky nodules; and association III shows exsolution lamellae of triphylite in massive beusite. These primary textures and the Fe/Fe+Mn+Mg ratio of primary triphylite allow one to establish the crystallization sequence of the primary phases in pegmatites of Conselheiro Pena district. The relationships between primary intergrowths of association I, involving spessartine and triphylite, will also be discussed.

After these magmatic stages, the primary associations are affected by hydrothermal stages and form secondary phosphate minerals. Their petrographic relationships lead us to the crystallization sequence of these secondary phases. It clearly appears that the hydrothermal stages don't affect one whole pegmatite in the same way: in the same pegmatite, some masses may be completely oxidized while other masses remain almost unaltered. Moreover, the nodular phosphate masses evolved like a relatively closed system since secondary species, which crystallized during low temperature hydrothermal stage, strongly depend on the cations which are locally available in the sample zone.

Tourmaline geochemistry of the Erongo Granite, Namibia

Boudreaux A, Simmons W*, Falster A, Webber K

1 - University of New Orleans *wsimmons@uno.edu

The miarolitic NYF Erongo Granite in the Erongo Complex of Namibia is well-known for abundant tourmaline mineralization. Tourmaline from granite, tourmaline orbicules, and NYF-type miarolitic segregations and pegmatites was analyzed by EMP. All tourmalines belong to either the alkali or X-site vacant groups. The X-site alkali dominant tourmalines are Fe-rich and belong to the schorl subgroup. X-site vacant samples segregate into two clusters with respect to Fe versus Li+Al dominance. Samples that are X-site vacant and black in color plot in the foitite field, whereas the colored portions of color-zoned tourmalines plot in both the foitite and rossmanite fields. The F/(F+^{W}OH) apfu ratio for all samples ranges from 0.02 to 0.82. Fluor-schorl and -foitite are most abundant, and rossmanite is hydroxyl-dominant. Figure 1 shows the Na/(Na+Vac) *apfu* ratio *vs.* ^{Y}Al/(^{Y}Al+Fe) *apfu* ratio for all samples, colored to show the hosting lithology. Color-zoned tourmalines were sampled from miarolitic cavities but are displayed separately. Black tourmaline exhibits a compositional trend from schorl to foitite. Samples from the granite and tourmaline from orbicules plot exclusively in the schorl field, whereas miarolitic cavity samples range in composition from schorl to foitite but are dominantly schorl. The color-zoned tourmaline samples plot in the fields of schorl, foitite, and rossmanite. The backscattered electron image in Figure 2 shows the complex zoning pattern typical of the color-zoned samples. Within this single crystal, three species are present. The compositional trend of schorl to foitite displayed by the miarolitic cavity samples is interpreted to be the result of fractional crystallization within a heterogeneous magma. Fe and Na became increasingly scarce with progressive crystallization of biotite and albite, resulting in tourmaline compositions that trend toward rossmanite. In some locations, miarolitic cavities were found to be surrounded by haloes of K-spar and quartz, suggesting that the rate of schorl formation outpaced diffusion of Fe and Na to the crystallization front. If the local melt could not provide sufficient Fe and Na, tourmaline composition graded into foitite. In extreme and localized cases, late stage fluids partially dissolved schorl crystals and overgrew them as a mixture of fluor-foitite, schorl, and rossmanite.

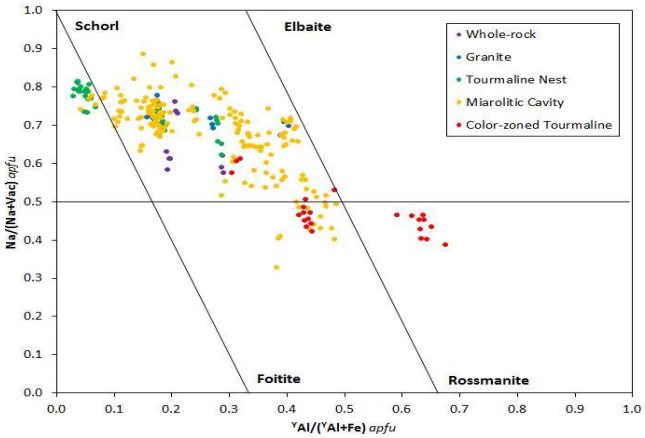

Figure 1: Na/(Na+Vac) *apfu* ratio versus ^{Y}Al/(^{Y}Al+Fe) *apfu* ratio for all samples.

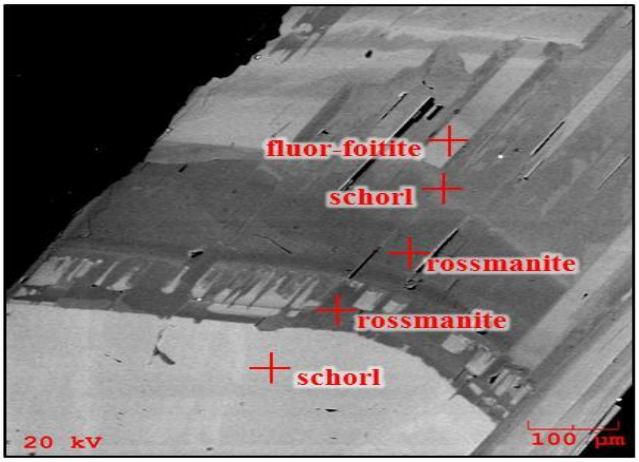

Figure 2: Backscattered electron image of a color-zoned tourmaline crystal hosting three species

Pegmatitic pods and insights into the final stages of Proterozoic anorthosite crystallization in the Mealy Mountains Intrusive Suite, Canada

Bybee G

School of Geosciences, University of the Witwatersrand. grant.bybee@wits.ac.za

The anorthositic members of the Mealy Mountains Intrusive Suite (MMIS), a typical Proterozoic anorthosite massif in the Grenville Province, are host to 0.5-5 m-diameter pegmatitic, pod-like segregations, originally described as graphic granite pods. U-Pb zircon geochronology confirms that the pods are coeval with the previously established 1650-1630 Ma emplacement age range for the MMIS. Petrographic and geochemical analysis of five pods from anorthositic rocks of the Mealy Mountains Intrusive Suite reveal that the pods are diverse, ranging from monzodiorite to granite, and varying from Fe-rich and Si-poor, to Fe-poor and Si-rich compositions. Each pod shows a range of noteworthy graphic, myrmekitic and symplectic textures, along with distinctive mineralogical assemblages and highly enriched trace-element geochemical compositions. Evolved mineralogy (e.g., apatite and zircon), high concentrations of Fe, Ti, P (and in some cases SiO_2) and 10-1000 X chondrite enrichment in LREE, U, Th, Rb indicate that many of the pods are highly fractionated. The array of textural intergrowths provides clues about the final stages of crystallization in the pods. Macroscopic quartz - K-feldspar graphic intergrowths demonstrate primary, end-stage cotectic crystallization of felsic phases, whereas microscopic myrmekitic (plagioclase-quartz) and symplectic (plagioclase-orthopyroxene) intergrowths on primary grain boundaries indicate replacement of phases in the presence of reactive fluids. In assessing the nature of these pegmatitic pods based on field, petrographic and geochemical evidence, I conclude that they represent the fluid-bearing, late-stage crystallization products of a residual liquid in the massif anorthosite system. The compositional variation amongst the pods in the MMIS is linked to mineralogical variations in the host anorthosite (leuconorite vs. leucotroctolite), suggesting that the diversity observed in proposed residual liquids in the Proterozoic anorthosite system may be caused by compositional variations in pulses of parental magma.

A review of the rare-element pegmatites of the Alto Ligonha Pegmatite Province, northern Mozambique

Cronwright M

The MSA Group. michaelc@msagroupservices.com

INTRODUCTION: The Pan African (PA) rare-element pegmatites of the Alto Ligonha Pegmatite Province (ALPP) of northern Mozambique are famous for their gemstones, rare and unique mineral specimens and as a source for a variety of rare element minerals such as beryllium, tantalum and niobium.

REGIONAL SETTING: The main concentration of economic pegmatites in N. Mozambique are in the ALPP in the Nampula Subprovince, mostly NNE-SSW orientated PA Namama Thrust Belt (NTB), which extends from the Mugeba Klippe in the SW to NE of Alto Ligonha in the north (Figure 1). The geology is dominated by Mesoproterozoic medium- to high-grade gneisses of the Nampula Complex that were reworked during the PA Orogeny and intruded by early Palaeozoic late-PA granitoids and pegmatites.

PEGMATITES OF THE ALTO LIGONHA PEGMATITE BELT: The economic pegmatites are characteristic of the LCT family, with some NYF (Niobium-Yttrium-Fluorine) family affinities, and can be subdivided into 4 main types - 1) Sodalithic; 2) Potassic with beryl and columbotantalite; 3) Potassic rich in metamict uranium, thorium and rare-earth bearing minerals; 4) Amazonite-bearing (found in the Nacaroa pegmatite field) and tourmaline-bearing pegmatite.These pegmatites can also be differentiated on the complexity of the internal structure or relative lack thereof. These pegmatites have been dated at between 481-440 Ma, thereby post-dating the intrusion of the late undeformed Pan African granites dated at ~521-495 Ma. The per- to sub-aluminous composition of the granites is also consistent with fertile granites related to late- to post-orogenic LCT (and NYF) pegmatite provinces. The sodalithic pegmatites have important concentrations of Nb-Ta, beryl and lithium and include large pegmatites, such as Muiane, Naipa, Marropino, Morrua and Moneia. Mineral and geochemical typomorphism show the potassic and RE-type have similar degrees of fractionation and possibly represent two sub-types of a single pegmatite type corresponding to the Beryl type of Cerný (1991). The amazonite-bearing and tourmaline-bearing pegmatites have similar degrees of fractionation to the sodalithic and potassic pegmatites respectively. There is a strong lithostratigraphic control on pegmatite distribution with >50% of all the pegmatites hosted in the paragneisses of the Molócuè Group (which is more pronounced for the sodalithic types with ~79%). Structurally ~73% of all pegmatites and 95% of the sodalithic pegmatites are within the broad limits of the NNE-SSW orientated NTB and are orientated parallel to the regional fabric within the NTB and the Mugeba Klippe. The potassic pegamtites tend to be more widely distributed through the region (Figure 1).

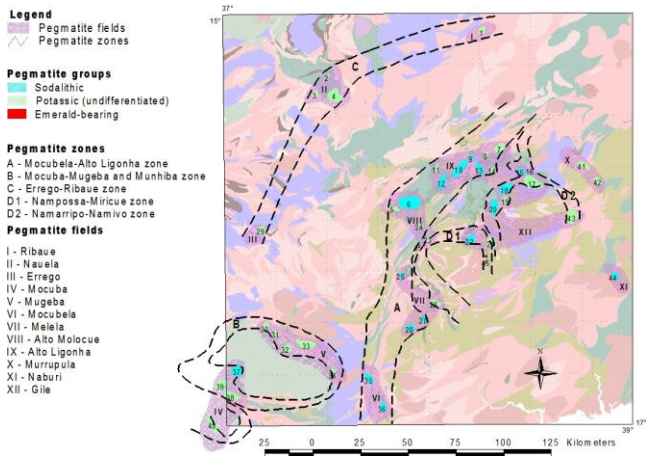

Figure 1: Pegmatite distribution in Northern Mozambique

Which parameters control the Variscan pegmatites field-scale organization ?

Deveaud S[1*], Silva D[2], Gumiaux C[3], Gloaguen E[4], Branquet Y[3], Lima A[5], Villaros A[3], Guillou-Frottier L[4], Melleton J[4]

1 – BRGM *s.deveaud@brgm.fr 2 - Department of Geology-FCUP, Porto, Portugal 3 - Université d'Orléans, ISTO, France 4 - BRGM, ISTO, France 5 - Centre of Geology-UP, Porto, Portugal

The emplacement of rare-element granitic pegmatites is subjected to a lively debate opposing mainly two genetic models with essential metallogenic consequences. In the first model an underlying parent granitic body releases residual enriched melt which, at the end of its crystallization, leads to the formation of pegmatites. The second model does not involve a granitic parent but rather a low melting rate of crustal material and successive injections of independent batches of melts which are favoured by regional shear-zones. The first model is commonly assumed for regional exploration; however few recent studies favour the second model. In particular, the emplacement of the LCT-type pegmatite field of Monts d'Ambazac (Massif Central, France) is first controlled by a NNE-SSW oriented faults-system rather than by the crystallization of its host granite. In order to strengthen these findings, we investigated through statistical spatial analysis two other Variscan (320-310 Ma) pegmatite fields which present similar mineralized objects (barren to petalite-spodumene and barren to petalite-lepidolite subtypes), but different spatial organizations and hosts: the Forcarei pegmatite field (FPF, NW Galicia, Spain) and the The Barroso-Alvão pegmatite field (BAPF, Northern Portugal, ~ 100 km southeast from FPF). Many data are available on these fields where granitic bodies, migmatites and shear-zones are present. The FPF is limited in its southern edge by the Celanova migmatitic dome, resulting from a low-temperature hydrated melting of crustal material. Moreover, some pegmatites occurred in a "reservoir zone" which give to the local migmatites a diatexite texture. These observations favor *a priori* the second model of direct crustal anatexis. Finally, spatial statistical analyses and syn-kinematic criteria as shear-bands and pulled-apart tourmaline, that are observed in pegmatites seem to suggest that the left-lateral Serra do Suido shear-zone near to the pegmatite field has a major role during pegmatite emplacement. Indeed, pegmatites are clustered and preferentially oriented in the same broad N-S direction as the associated shear-zone. The formation of the BAPF also matches the second model since it is located near to the southern edge of Celanova migmatic dome. The distribution of pegmatite bodies shows no preferred orientation and cross-cutting of pegmatite-subtypes. The lack of recognized regional shear zones in BAPF indicates the key role of such structures on the pegmatite field. These preliminary results favour the influence of shear zones as flow channels on i) the Variscan LCT-type pegmatite field emplacement and ii) pegmatites subtypes field-scale organization. As demonstrated recently by laboratory experiments, the fluxes enrichment of H_2O, Li and F drastically reduces the viscosity of pegmatitic melts favouring their ascent through crustal-scale permeable zones as confirmed by our preliminary numerical model where the role of low viscosity on magma ascent is especially investigated. Thus, we hypothesize that the spatial distribution of mineralized pegmatites could be partly controlled by surrounding tectonic structures, their fluxe content and the resulting pegmatitic melt rheology.

Rare phosphate assemblages in granite pegmatites from Mt Wills, northeast Victoria, Australia

Eagle R[1], Birch W[2*]

1 - Mandalay Resources 2 - Museum Victoria * bbirch@museum.vic.gov.au

Pegmatite dykes associated with the 430-Ma-old Mt Wills Granite in northeastern Victoria, Australia, are cassiterite-bearing and were briefly mined for tin in the 1890s. No mineralogical studies were undertaken at the time, but recent investigation of two pegmatites, here named the Blue Jacket and Knocker, has revealed an unusual suite of phosphate minerals hosted by coarse-grained quartz, albite, Li-bearing muscovite and tourmaline, with sporadic cassiterite grains. An assemblage of iron-rich phosphates forms isolated irregular patches which are complex mixtures of secondary/alteration phases, including wolfeite, 'ferrian alluaudite', a member of the arrojadite group, heterosite and whitmoreite; no primary Fe-dominant phosphate appears to have survived. Small etch cavities contain crystals of whitmoreite, rockbridgeite and so-far uncharacterised members of the jahnsite and/or whiteite groups. A more Al-rich phosphate assemblage includes montebrasite, scorzalite, brazilianite and bertossaite, while Mn-bearing fluorapatite is also present. Accessory minerals include columbite-tantalite, arsenopyrite, monazite, xenotime, microlite and zircon.

The Mt Wills pegmatite dykes belong to the LCT family of granite pegmatites, and the phosphate-bearing dykes are the most fractionated as well as the most distal and elevated from the Mt Wills Granite. CHIME Th/U/Pb dating for monazite crystals from the Knocker pegmatite yielded an age of 420 Ma, in keeping with a late-stage origin from the Mt Wills Granite. The complex phosphate pegmatite assemblages in the Mt Wills pegmatites bear a close similarity to those occurring within the Buranga pegmatite in central Rwanda.

A new find of complex Na-Zr silicates in the Stettin Complex, Marathon Co., Wisconsin

Falster A*, Buchholz T, Simmons W, Guidry J, Johnson C

University of New Orleans *afalster@uno.edu

The Stettin complex (SC) is a 1565 Ma (±3.5) alkalic complex which is part of the Wausau complex exposed in Marathon Co., Wisconsin. The complex measures approximately 6 by 8 km and is concentrically zoned. The eastern and southern margin consists of a complex series of altered volcanic rocks, pendants, enclave-rich syenites, and nepheline syenite .The outer zone of the SC is made up of a discontinuous ring of nepheline syenite and K-feldspar-rich syenite toward the interior. The intermediate zone consists of amphibole and pyroxene syenites. The core of the complex consists of 1.5 km mass of pyroxene syenite. The core is surrounded by a second ring of nepheline syenite. Most of the nepheline syenites of these two rings exhibit a miaskitic chemistry. Zircon and titanite are the typical high-field-strength-element-bearing minerals. Clinopyroxene in the SC shows one of the most pronounced agpaitic compositional trends observed in alkaline complexes worldwide.

In a few areas in the outer ring of the nepheline syenite, a previously undescribed agpaitic assemblage of the eudialyte-group species, catapleiite and baddeleyite has been discovered. The eudialyte group minerals occur in raspberry-red masses up to 1 cm in the nepheline syenite that are confirmed by EMPA to be Mn-rich kentbrooksite ($Na_{15}Ca_6Mn_3Zr_3Nb(Si_{25}O_{73})(O,OH,H_2O)(F,Cl)_2$ (Figure 1). The eudialite group minerals are associated with pale brown catapleiite and along altered zones of the eudialyte group species, baddelyite has been identified. Baddeleyite occurs as a late-stage replacement of kentbrooksite along fractures and along some part of the rims of the kentbrooksite masses. Zircon is absent in these nepheline syenites. Woehlerite and Bastnaesite-(Ce) occur associated with the Na-Zr-silicates in this assemblage. Several other unknown species are intergrown or in close proximity to the masses of kentbrooksite and catapleiite. It is remarkable that kentbrooksite occurs instead of the more typical association of eudialyte with nepheline syenite.

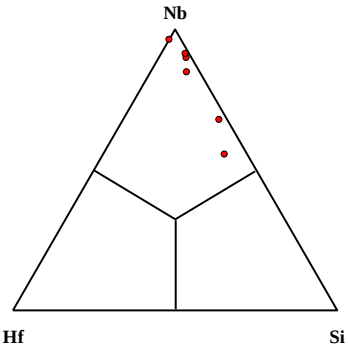

Figure 1: M_3 site occupancy in Stettin complex kentbrooksite

An unzoned rare element pegmatite in the Eastern Alps – the spodumene deposit 'Weinebene'/Koralpe, Austria – a summary

Goed R

University of Vienna, Center for Earth Sciences. richard.goed@univie.ac.at

An extensive exploration program carried out in the eighties led to the discovery of a significant lithium resource in the Eastern Alps [1]. The "Weinebene" spodumene deposit is located in Carinthia, the southernmost province of Austria, some 270 km southwest of Vienna. Previous results as well as results of recent exploration activities based on a total of 16000 m of core drilling and some 1400 m of drifting are summarized in this presentation.

The regional geology is characterized by an E-W striking, eastwards plunging anticline, separating the deposit into a northern and southern part respectively.

The spodumene bearing pegmatites form *strictly concordant* dykes within eclogitic amphibolites and kyanite bearing micaschists. The average thickness of the amphibolite hosted pegmatites (below referred to as AHP) and the micaschist hosted pegmatites (referred to as MHP) display an average thickness of 2 m (max. 5 m) and have been traced along strike to a maximum length of 1.5 km and to a maximum depth of 450 m downdip *continuously* consistent in their mineralogical and geochemical composition. Their late-orogenic emplacement is of Permian age. (U-Pb-zircon age: 240 my; [2]), followed by a later metamorphic overprint in context with the alpine orogeny.

However, AHP and MHP differ significantly in texture, spodumene content and geochemistry.

The emplacement of the AHP caused an alteration halo of several dm in the hosting amphibolites characterized by biotitization and the formation of holmquistite.

An aplitic spodumene-free seam of about 10 cm symmetrically borders the pegmatites.

AHP are coarse grained and display locally a primary magmatic texture. Spodumene, homogeneously distributed, is the only primary lithium bearing mineral. Its average content is ≈22 wt%, equivalent to ≈ 1.6 wt% Li_2O which corresponds to thermal minima in relevant experimental systems [3]

MHP are totally recrystallized giving rise to a cataclastic fabric. The grain size varies within the mm- range, the spodumene crystals are rarely recognizable by naked eye. This rock has therefore to be described as meta-pegmatite. The spodumene contributes to ≈15wt%, equivalent to ≈ 1.2 wt%.

The mineral chemistry of spodumene is the same in both pegmatite types displaying 7.4% Li_2O and 0.45% FeO likewise.

Tin and beryllium are the only trace elements of significance. The beryllium content is identical in AHP and MHP, averaging around 100 ppm whereas tin contents differ between AHP and MHP with average contents of 150 ppm and 60 ppm respectively. Niobium and tantalum concentrations are low.

These differences between AHP and MHP are interpreted as being caused by the different mechanical and geochemical properties of the amphibolite and micaschist host rocks.

The bulk composition, the trace element signature and an average K/Rb ratio of 20 support an igneous derivation of the pegmatites.

[1] Göd R. (1989). The spodumene deposit at "Weinebene", Koralpe, Austria; *Mineralium Deposita*, 24, 270-278.

[2] Heede H.-U. (1997). Isotopengeologische Untersuchungen an Gesteinen des ostalpinen Saualpenkristallins, Kärnten-Österreich; Münstersche Forschungen zur Geologie und Paläontologie, Heft 81, 168 pp.

[3] Stewart D.B. (1987). Petrogenesis of lithium rich pegmatites. *American Mineralogist*, 63, 970-980.

Geochemistry of tourmaline from the Usakos Pegmatite, Namibia

Grassi L, Simmons W*, Falster A, Webber K

1 - University of New Orleans *wsimmons@uno.edu

The LCT type Usakos Pegmatite in Usakos, west central Namibia, Africa, is a world class locality for gem quality tourmaline. The pegmatite is characterized by a greater abundance of muscovite than biotite, Sn, Ta>Nb and Li mineralization. It is a large, poorly zoned, miarolitic granitic pegmatite dike hosted by metasedimentary rocks of the Kuiseb formation. Tourmaline was sampled from the country-rock contact (CT), the outer zone, and areas around pockets in the interior portion of the pegmatite. In addition, a suite of gem-quality, polychrome tourmaline was obtained from the mine owner. Tourmaline was analyzed *via* EMP. Li, B, and H, were estimated based on stoichiometry. Tourmalines from the Usakos pegmatite are plotted according to their natural color. They belong to the alkali tourmaline group and range in composition from schorl to elbaite with virtually no Mg enrichment (Figure 1). Most tourmalines are F-dominant in the W-site (Figure 2). With the exception of CT samples, tourmaline shows a fractionation trend from Fe-rich schorl to Fe-depleted elbaite (Figure 3). The earliest stage of black Fe-rich elbaite crystallization at the contact is inferred to be enriched in Al as a result of the melt interacting with the Al-rich country rock (Figure 3: black circles). It appears that tourmaline crystallization underwent a hiatus until the melt achieved sufficient B and H_20 concentration to allow for schorl crystallization to commence (Figure 3: gray triangles). The final stage of elbaite crystallization in and around pockets displays a fractionation trend from higher Na and Fe to higher Al and X-site vacancy (Figure 3: diamonds). Color is strongly tied to composition, as Fe content is highest in the black tourmaline and virtually absent in pink and colorless tourmalines (Figures 1 and 3).

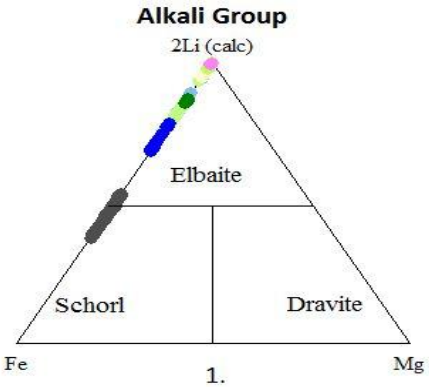

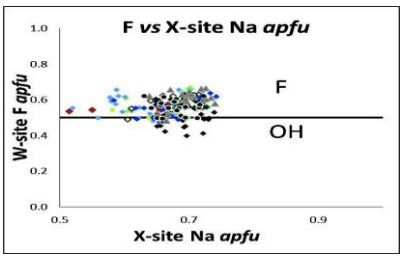

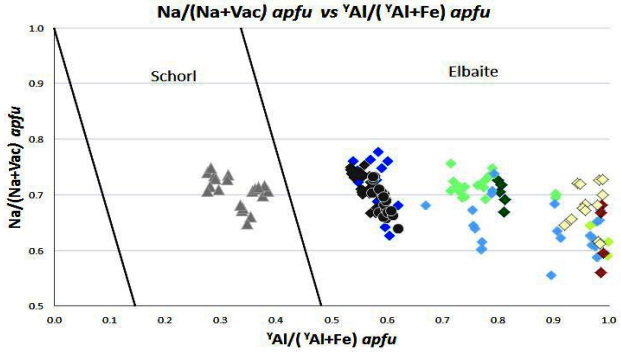

Figure 1: (top), Figure 2 (middle), and Figure 3 (bottom) showing geochemical plots of tourmalines from the Usakos Pegmatite

Granitic pegmatites: the larger the body, the more likely an acid-reflux overprint: economic ramifications

Martin R[1*], De Vito C[2]

1 - McGill University *robert.martin@mcgill.ca 2 - Scienze della Terra, Sapienzia Università di Roma

Bodies of granitic pegmatite, be they of NYF or LCT affiliation, crystallize from evolved felsic magmas. Those relatively enriched in niobium, yttrium and fluorine (NYF) either represent the end stage of fractionation of a syenitic parental magma, or a product of anatexis of alkali-metasomatized lower crust, emplaced in an anorogenic tectonic setting. Those relatively enriched in lithium, cesium and tantalum (LCT) crystallize from the products of fractionation of calc-alkaline magmas, typically containing a mixed crust and mantle signature. Both types of pegmatite are subject to postmagmatic cycles of hydrogen metasomatism by an acidic aqueous fluid interpreted to have become subalkaline by reactions proceeding in and beyond the exocontact. We envision paths of efficient postmagmatic metasomatic reactions (*i.e.*, at a T below the solidus) within the pegmatite along which microcline is consumed, to produce albite + muscovite ± fluorapatite in its place. These fluids cause an LCT-type overprint on the pegmatite body because they pick up elements in the enclosing envelope of diverse crustal rocks, possibly rocks that have been through a subduction cycle or much more ancient rocks of metasedimentary parentage. In this way, NYF pegmatites can display an overprinted enrichment not only in Li, Cs and Ta, but also Ca and Al, elements that were relatively depleted in NYF magma. However, chances of buildup of Li, Cs and Ta to an economically attractive level are much enhanced where the overprint of Li, Cs and Ta affects an LCT pegmatite, already relatively enriched in those elements. We contend that such examples of primary LCT + secondary LCT overprint make prime targets for exploration, especially in view of enhanced demand for Ta and Li. Furthermore, the larger the heat engine favouring the circulation of the aggressive late acidic fluid phase within the pegmatite, the longer these replacement reactions will last, and the greater the degree of enrichment in Ta and Li. It is obvious that a detailed assessment of the potential of a large body of granitic pegmatite will require recognition of what is primary (*i.e.*, magmatic) and what is secondary (*i.e.*, postmagmatic) in a granitic pegmatite. Microcline and albite of cleavelandite habit are secondary phases, pseudomorphic after the primary feldspar. Muscovite and fluorapatite may be primary or secondary; both are commonly present in an LCT pegmatite. Columbite is likely primary, whereas tantalite is largely secondary. Indeed, the selective leaching and mobilization of Ta can lead to the hydrothermal crystallization of tantalite-(Fe), tantalite-(Mn), microlite, rynersonite and fersmite, and can thus create economically attractive targets of mineralization.

Tantalum-(niobium-tin) mineralisation in African pegmatites and rare metal granites. Constraints from Ta-Nb oxide mineralogy, geochemistry and U-Pb geochronology

Melcher F[1*], Graupner T[2], Gäbler H[2], Sitnikova M[2], Henjes-Kunst F[2], Oberthür T[2], Gerdes A[3], Dewaele S[4]

1 - Montanuniversitaet Leoben * frank.melcher@unileoben.ac.at 2 - BGR 3 - Goethe-University Frankfurt 4 - Royal Museum for Central Africa

Tantalum, an important metal for high-technology applications, is recovered from oxide minerals that are present as minor constituents in rare-metal granites and granitic rare-element pegmatites. Columbite-group minerals (CGM) account for the majority of the current tantalum production; other Ta-Nb oxides (TNO) such as tapiolite, wodginite, ixiolite, rutile and pyrochlore-supergroup minerals may also be used.

For 13 rare-element granite and pegmatite districts in Africa, mineralogical and geochemical data with a focus on opaque minerals as well as age determinations on CGM using the U-Pb method are presented.

Each period of Ta-ore formation is characterised by peculiar mineralogical and geochemical features that assist in discriminating these provinces. Compositions of CGM are extremely variable: Fe-rich types predominate in the Man Shield (Sierra Leone), the Congo Craton (Democratic Republic of the Congo), the Kamativi Belt (Zimbabwe) and the Jos Plateau (Nigeria). Mn-rich columbite-tantalite is typical of the Alto Ligonha Province (Mozambique), the Arabian-Nubian Shield and the Tantalite Valley pegmatites (southern Namibia). Large compositional variations through Fe-Mn fractionation, followed by Nb-Ta fractionation are typical for pegmatites of the Kibara Belt of Central Africa, pegmatites associated with the Older Granites of Nigeria and some pegmatites in the Damara Belt of Namibia. CGM, tapiolite, wodginite and ixiolite accommodate minor and trace elements at the sub-ppm to weight-percent level. Trace elements are incorporated in TNO in a systematic fashion, e.g. wodginite and ixiolite carry higher Ti, Zr, Hf, Sn and Li concentrations than CGM and tapiolite. Compared to tapiolite, CGM have higher concentrations of all trace elements except Hf and occasionally Zr, Ti, Sn and Mg. The composition of TNO related to rare-element pegmatites is rather different from rare-metal granites: the latter have high REE and Th concentrations, and low Li and Mg. Pegmatite-hosted TNO are highly variable in composition, with types poor in REE, typical of LCT-family pegmatites, and types rich in REE - showing affinity for NYF-family or mixed LCT-NYF pegmatites. Major and trace elements show regional characteristics that are conspicuous in normalised trace element and REE diagrams. CGM from Ta-ore provinces are characterised by the predominance of one type of REE distribution pattern characterised by ratios between individual groups of REE (light, middle, heavy REE) and the presence and intensity of anomalies (e.g. Eu/Eu*).

Despite textural complexities such as complex zoning patterns and multiple mineralisation stages, the chemical compositions of CGM, tapiolite and wodginite-ixiolite from rare-metal granite and rare-element pegmatite provinces indicate that they are cogenetic and reflect specific source characteristics that may be used to discriminate among rocks of different origin.

In Africa, formation of rare element-bearing pegmatites and granites is related to syn- to late-orogenic (e.g., West African Craton, Zimbabwe Craton), post-orogenic (Kibara Belt, Damara Belt, Older Granites of Nigeria, Adola Belt of Ethiopia) and anorogenic (Younger Granites of Nigeria) tectonic and magmatic episodes. The late-orogenic TNO mineralisation associated with A-type granites in the Eastern Desert of Egypt shares geochemical features with the anorogenic Younger Granites of Nigeria.

The Northern Cape pegmatite belt

Minnaar H*, Lambert C

Council for Geoscience *hminnaar@geoscience.org.za

The Northern Cape pegmatite belt is defined by a concentration of pegmatite bodies extending over a distance of about 510 km and an average width of 50 km. Sizes of individual bodies within the belt vary from a few centimetres to about 5 km in diameter. Their shapes may be elongated, rounded or irregular or they may occur in the form of veins and dykes. The dykes may form swarms and the bodies may occur scattered or in pegmatite fields. Two distinct compositional types are recognized namely homogeneous and zoned.

Mineralogically, the homogeneous bodies consist of a matrix in which quartz, feldspar and mica are more or less evenly distributed and the grain size is limited to a few centimetres. Within the zoned bodies, quartz and feldspar are concentrated in the core while mica is mostly concentrated in the wall zone. Individual crystals may be up to a few metres in diameter and a variety of intergrowths occur. The zoned bodies also contain economically important accessory minerals including beryl, tantalite, RE minerals (e.g., gadolinite, euxenite, monazite), Li-minerals (e.g., spodumene, lepidolite) and crystals (any well-developed crystal of gem or precious quality). Historically, economic exploitation has been executed only of the compositionally zoned bodies.

There are a number of economically important bodies in the belt and exploitation dates back to 1925. Mining activities have historically been sporadic and mining methods involved selective mining, hand-picking and the sale of raw materials. Throughout the years, the targeted commodity depended on market demand. Beryl was a high priced commodity during the 1930's and 1950's. Mica was important during the early days of electronics. Tantalite became prominent when communication systems started utilizing rechargeable batteries. During recent years, mining operations have depended on feldspar as a stand-alone commodity to sustain the operations. The local glass industry currently presents the only sustainable market while the local ceramics industry provides sporadic opportunities. Until recently, rose quartz also contributed to revenue from pegmatite mining.

According to the prevailing ore deposit model, the zoned pegmatites represent late stage crystallization products after fractional crystallization of a calc alkaline granitic pluton with volatiles such as F, P and B playing a significant role as fluxes. The zoned character is explained by sequential crystallization from the wall inwards. The pegmatites of the Northern Cape can be classified as Rare Element pegmatites. They are associated with amphibolite facies metamorphic rocks of the Namaqualand Metamorphic Province and are especially enriched in incompatible elements like Li, REE, Cs, Be, Ta, Nb and Sn. The identification of their source is problematic due to significant migration from the source pluton. They are spatially associated with the ~1.9 Ga Vioolsdrif Suite in the west and ~1.1 Ga Keimoes Suite in the east. They are also associated with two distinct tectonic terranes namely the Richtersveld and Gordonia Subprovinces, occurring near and parallel to the bounding structures represented by the Southern Front-Namaqua Front and the Lower Fish River-Hartbees River thrusts. Radiometric crystallisation ages for the pegmatites fall into two groups namely 1 000 and 950 Ma. On a regional scale, the bodies strike mostly parallel to the foliation, which is predominantly northwest. However, they also cut across the foliation, especially in the west. On outcrop scale, sharp intrusive contacts are numerous, both cross-cutting and concordant. Gradational contacts are also observed, especially in syeno- and alkali feldspar granite bodies. The above evidence suggest that the pegmatites are the products of primary melts generated during partial melting of granitic plutons during the late stages of the Namaqua orogeny.

Initiative of a new classification of pegmatites – a review of initial thoughts

Müller A[1*], Simmons W[2], Wise M[3], Thomas R[4], Martin R[5], Beurlen H[6], Ihlen P[1]

1 - Geological Survey of Norway *axel.muller@ngu.no 2 - University of New Orleans 3 - Smithsonian Institution, Washington DC 4 - Helmholtz Centre Potsdam 5 - McGill University 6 - Universidade Federal de Pernambuco

Pegmatites are characterized by extreme variations in grain size and have as their major constituents minerals commonly found in "normal" igneous rocks. Pegmatites display a strong diversity with regard to composition, mineralogy, size, shape, structure, distribution of rock types, depth and temperature of formation, and age. They are associated with diverse rock types, including migmatites, metamorphic rocks ranging from granulites to greenschists, and igneous rocks. They commonly exhibit chemical interactions with the wallrocks. All these characteristics make it extremely difficult to establish a distinct and easily applicable classification that can be used for scientific purposes and also in evaluations of economic potential.

The first generally recognized classification was established by Fersman [1], who utilized the estimated temperature of crystallization of pegmatites for classification. Later, the depth-zone classification introduced by Ginsburg and Rodionov [2] has become widely applied even in the most recent classification by Černý and Ercit [3]. However, this latest classification mixes mineralogical, geochemical, and structural criteria with necessary knowledge of P-T conditions during pegmatite formation. Over the last decade, various studies have shown that some types of pegmatites do not fit into the available schemes of classification. In addition, these classifications use inferred criteria (crystallization depth) instead of measurable criteria (bulk composition, mineralogy, structure) for the first level of classification.

For these reasons, discussions for the establishment of a new classification were initiated recently. So far, the group agrees that the new classification should utilize simple measurable and objective criteria (bulk composition, mineralogy, modal content of type minerals, structure) for the first levels of the classification dendrogram. Genetic considerations, based on measurable attributes, should be second-order criteria. In addition to characteristic assemblages of minerals, the trace element content of major pegmatite-forming minerals, including feldspar, mica, and quartz, has potential for a chemical classification, even though these minerals commonly show a strong chemical zonation within one pegmatite body.

[1] Fersman A. (1930). A geochemical genetic classification of pegmatites. Monograph Akademiia Nauk SSSR. (in Russian).
[2] Ginsburg A.I. and Rodionov G.G. (1960). On the depths of the granitic pegmatite formation. *Geologiya Rudnykh Mestorozhdenyi, Izd. Nauka, Moskva*, l, 45-54.
[3] Černý P., Ercit T.S. (2005). The classification of granitic pegmatites revisited. *Canadian Mineralogist*, 43, 2005-2026.

Chemistry of pegmatite quartz – a possible classification criterion for granitic pegmatites?

Müller A

Geological Survey of Norway. axel.muller@ngu.no

The classifications of granitic pegmatites proposed by Černý [1] and Černý and Ercit [2] are the most widely applied classification schemes. Both are primarily depth-zone classifications that blend mineralogy, geochemistry, and structural features with necessary knowledge of the P-T conditions during pegmatite formation. These classifications have been criticized because they merge different categories of measurable and deduced criteria: alternative classification schemes are under discussion.

The chemistry of major pegmatite-forming minerals such as mica, feldspar and quartz could be possible classification criteria. In this pilot study, the trace element concentrations of quartz from 229 pegmatites worldwide have been determined by inductively coupled plasma mass spectrometry (LA-ICP-MS) in order to test if the trace element signature of pegmatite quartz can be used for classification of the pegmatites. The samples originate from pegmatites in Norway, Brazil, Germany, Argentina and Portugal. Sample traverses were taken across the pegmatite bodies in order to test the chemical variability of quartz within each pegmatite.

The investigated quartz samples show great variability in concentrations of Al, Li, Ti, Ge, and B. Abyssal and niobium-yttrium-fluorine (NYF)-type pegmatites have generally low Al <200 ppm, low Li <30 ppm, low Ge <3 ppm and partially high Ti, up to 60 ppm. Quartz of chemically more evolved lithium-cesium-tantalum (LCT)-type pegmatites has moderate to high Al (100 to 3000 ppm), low Ti <20 ppm, and partially high Ge (up to 25 ppm) and B (up to 30 ppm) and highly variable Li (10 to 300 ppm). Within the LCT group two chemical types of quartz can be distinguished: (1) a high Al-low Li type and (2) a high Al-high Li type. The preliminary data imply that (1) the chemistry of quartz has a great potential for use in pegmatite classification and (2) the variability of quartz chemistry is controlled by the initial source composition of the pegmatite magmas and, thus, by the tectonic setting rather than by intermediate magmatic fractionation processes. However, LA-ICP-MS analysis of quartz is an advanced method which is not easily to access and perform.

[1] Černý P. (1991). Fertile granites of Precambrian rare-element pegmatite fields: is geochemistry controlled by tectonic setting or source lithologies? *Precambrian Research*, 51, 429-468.
[2] Černý P. and Ercit T.S. (2005). The classification of granitic pegmatites. *Canadian Mineralogist*, 43, 2005-2026.

Zoned crystals of columbite-oxide group minerals and their inclusions and exsolution products from some Portuguese granitic aplite-pegmatite dikes and sills

M. R. Neiva A[1*], L. Gomes C[2], B. Silva P[3]

1 - University of Coimbra * neiva@dct.uc.pt 2 - University of Minho, Portugal 3 - LNEG National Laboratory of Energy and Geology, Portugal

Columbite-tantalite crystals occur in granitic aplite-pegmatite dikes and sills from the Gouveia area that intruded a late-D3 Variscan two-mica granite. Some aplite-pegmatites belong to the muscovite class and others to the rare-element class. Some of the latter belong to the beryl-columbite subtype and others to the lepidolite subtype. Textural and chemical studies of columbite-tantalite crystals were carried out combining backscattered-electron images and spot electron-microprobe analyses, showing different zoning patterns. Progressively zoned crystals and overgrowths occur in muscovite class and lepidolite subtype aplite-pegmatites, whereas oscillatory zoned crystals appear in the former and reversely zoned crystals occur in the latter. Complexly zoned crystals occur in beryl-columbite subtype and lepidolite subtype, but they are more complex in the latter. Chemical compositions are of columbite-(Fe) in muscovite class aplite-pegmatites and columbite-(Fe), columbite-(Mn) and tantalite-(Mn) in beryl-columbite subtype and lepidolite-subtype aplite-pegmatites. Progressively zoned crystals present gradational contacts between core and rim and show increase in Ta and Mn contents and Ta/(Ta+Nb) and Mn/(Mn+Fe) values and decrease in Nb, Ti and Fe contents from core to rim. This zoning pattern corresponds to fractionation trends. Oscillatory zoned columbite-(Fe) crystals show sharp contacts between a darker core, a lighter intermediate zone and a darker rim. The intermediate zone has higher Ta, Ti contents and Ta/(Ta+Nb) ratio and lower Nb content than core and rim, explained by the hypothesis of faster crystal growth rates than diffusion of these cations through liquid, but with a return to Nb-richer oxides due to depletion of components from the boundary liquid causing crystal growth stopping periodically and allowing the boundary layer to equilibrate by diffusion. Reversely zoned crystals show a sharp contact between a tantalite-(Mn) core and a columbite-(Mn) rim. The Nb, Ti contents increase and Ta, Sn contents and Ta/(Ta+Nb) decrease from core to rim, which are explained by the hypothesis of oscillations in the compositions of the melt from which they grew, alternating between a Ta-enriched boundary layer and a bulk melt that is less fractionated. Overgrowth occurs in crystals showing either irregular or sharp contacts between a core and a more evolved rim and with a chemical compositional gap between core and rim. Different complexly zoned crystals occur: a) a progressively zoned core has an overgrowth rim; b) a reversely zoned crystal has an overgrowth; c) a crystal has an overgrowth followed by progressive zoning; d) some crystals show a progressive evolution within the inner part followed by an overgrowth containing a progressive zoning.

Very small and rare accidental inclusions of simpsonite, without any preferred orientation, occur in the columbite-(Mn) core of two crystals from the lepidolite sub-type aplite-pegmatites. Columbite-(Mn) cores and tantalite-(Mn) cores of crystals from the lepidolite-subtype aplite-pegmatites exsolved orientated both columbite-(Mn) and tantalite-(Mn) blebs and only tantalite-(Mn) blebs, respectively. The exsolutions have higher Ta content, Ta/(Ta+Nb) ratio and lower Nb content than the host core. In some crystals, a progressive evolution occurs from the host core to exsolutions, but in others a chemical compositional gap occurs between them.

Exsolution patterns in alkali feldspar from pegmatites

Sánchez-Muñoz L[1*], del Campo A[2], Modreski P[3], Fernández J[2], de Moura O[4], Zagorsky V[5], Martin R[6], Frost B[7]

1 - ICV-CSIC *lsm@icv.csic.es 2 - Instituto de Ceramica y Vidrio, CSIC, Madrid, Spain 3 - USGS, Federal Center, Denver, CO, USA 4 - Vilas Breta, Gov. Valadares, MG, Brazil 5 - Vinogradov Inst. Geochem. SBRAS, Irkutsk, Russia 6 - McGill University 7 - Dept. Geol. Geophys. University of Wyoming, Laramie, WY, USA

Perthitic microtextures in alkali feldspar $(K,Na)AlSi_3O_8$ form mainly by solid-state exsolution at the subsolidus stage, but are partly modified by interactions with aqueous fluids as the host rocks cool. With such microtextures, one can infer geological information, but serious challenges arise because of widespread overprinting at the deuteric stage. We have sought "fresh samples" with minimal deuteric modifications, to establish correlations with the geological environment and genetic factors. These samples were obtained from selected outcrops at thirty-two pegmatite districts around the world, of Phanerozoic, Proterozoic and Archean ages, including the type locality in Perth, in other pegmatites of the Grenville province in Canada; Hercynian province in Spain; Minas Gerais and Borborema provinces in Brazil; Wyoming, North Carolina, Black Hills and Colorado provinces in USA; Kola Peninsula and Siberian provinces in Russia; San Luis Ranges in Argentina; Yilgarn, Pilbara and Curnamona provinces in Australia. Granitic, syenitic and nepheline syenitic pegmatites from subvolcanic to granulitic settings are compared, i.e., wet and dry magmatic systems at low and high pressures. Perthite data were obtained by means of X-ray diffraction, X-ray fluorescence, electron-probe micro-analysis, optical microscopy, transmission electron microscopy, atomic force microscopy, scanning electron microscopy, and elastic (Rayleigh) and inelastic (Raman) scattering spectroscopic microscopy techniques using a confocal laser configuration. Some features of perthite patterns are non-random and depend on the primary bulk composition (including the ratio K/Na, structurally bound H_2O as an internal catalyst, and impurities), as well as on the geological environment upon cooling, especially where tectonic stress and depth play major roles. Film perthite forms by nucleation and growth at high temperature (near-equilibrium conditions) as coherent pseudoperiodic lamellar patterns; it is later transformed into semicoherent lamellar patterns, with an extensive development of misfit-induced dislocations along phase boundaries. Coarsening occurs by diffusional and clustering mechanisms. Film perthite is strongly modified when the orthoclase-to-microcline recrystallization takes place, leading to vein perthite. Such vein perthite can be expected where the primary alkali feldspar has a bulk Na_2O content greater than about 1.5 wt.% i.e., ~12 mol.% of Na-feldspar in the original solid-solution, as a far-from-equilibrium phenomenon in complex systems. Here, unmixing takes place by nucleation from long-range chemical waves induced by tectonic stresses, with later growth by diffusion and clustering into larger veins. Hence, an alkali feldspar is a very sensitive and adaptive medium, in which the exsolution patterns record precious geological information. For instance, one can distinguish between distinct events of pegmatite formation in polygenetic provinces.

Crystal-chemical constraints of U-Pb dating in monazite and xenotime from Aust-Agder pegmatites, Norway

Tomasic N[1*], Bermanec V[1], Scholz R[2], Soufek M[3], Skoda R[4], Cobic A[1]

1 - University of Zagreb *ntomasic@geol.pmf.hr 2 - Federal University of Ouro Preto 3 - Croatian Natural History Museum 4 - Masaryk University

The pegmatites of the Aust-Agder province, Norway, have been widely recognized for their numerous occurrences as well as interesting and versatile mineralogy. They formed during Sveconorwegian orogeny (around 1 Ga ago). The samples of monazite and xenotime were collected at two different pegmatite fields: the Evje-Iveland field with the localities of Eptevann and Eikeråsen, and the Froland field with the Garta locality. The collected minerals were heated at 200, 500, 800 and 1000°C at 1 atm for 24 hours, and examined by XRD and SEM to investigate their crystal-chemical properties and thermal behaviour. The ages of the monazite samples were determined using U-Pb geochronology by quadrupole LA-ICP-MS technique.

The electron microprobe analysis gave a monazite-(Ce) composition for both monazite samples concerned, with Ce_2O_3 ranging from 22.69 to 24.86%, Y_2O_3 0.05 to 2.25%, ThO_2 9.18 to 9.92%, and UO_2 0.47 to 0.53%. The xenotime-(Y) sample contains 45.16% Y_2O_3, 0.31% ThO_2, 0.31% UO_2, and is significantly impoverished in LREE (below detection limits). The age of 868±20 Ma was obtained for the Evje-Iveland monazite from Eptevann, and 1023±27 Ma for the Kongsberg-Bamble monazite from Garta.

A thorough SEM analysis using back-scattered electrons and energy-dispersive detector revealed numerous inclusions therein. Inclusions of $ThSiO_4$ are found in the monazite samples, which are sometimes surrounded by Y-rich monazite/xenotime and apatite. The xenotime sample also contains $ThSiO_4$ inclusions with frequent uraninite inclusions. Zircon, mica and quartz are intimately intergrown with xenotime.

Annealing experiments induced a slight decrease of unit cell volume ranging 0.70-0.76% in monazite, and 0.72 % in xenotime. The unit cell decrease is greater in the monazite from Eptevann which is more enriched both in Y and Th. However, both monazite samples have unit cell volume very close to that of the pure $CePO_4$, and when heated up to 1000°C it is approaching to the one of pure huttonite. The reduction of the unit cell volume of the xenotime sample indicates reinforcement of the xenotime structure, since any additional incorporation of Th or U from the $ThSiO_4/UO_2$ inclusions into its structure would result in a unit cell increase. This is also supported by X-ray diffraction data, which showed occurrence of a monazite-type phase at temperatures above 800°C along with the pre-existing xenotime.

SEM examinations of the samples heated at 1000°C showed that the monazite, as well as the $ThSiO_4$ inclusions, is cracked. Sparse YPO_4 inclusions are still present, being positioned rather over than around $ThSiO_4$ inclusions as in the case of the unheated samples. The crackings also appeared in the case of xenotime both in the mineral matrix and the inclusions. Generally, the crackings divide the $ThSiO_4$ inclusions from the xenotime matrix. The idiomorphic inclusions of UO_2 in $ThSiO_4$, especially those situated close to the edges of the $ThSiO_4$ grains, separated from the $ThSiO_4$ by the crackings. The occurrence of the monazite-type phase in the XRD pattern of the annealed xenotime sample could be related to the $ThSiO_4$ inclusions that re-crystallized as huttonitic phase due to the heating treatment. Also, inclusions with cheralite-type composition seem to be present in the heated xenotime, and thus contribute to the monazite-structure peaks in the XRD pattern.

The thermal treatment of the monazite and xenotime samples showed their thermal stability as well as the one of the $ThSiO_4$ inclusions, which recrystallize as huttonite in the case of both minerals. In spite of numerous $ThSiO_4/UO_2$ inclusions, the dating for both monazite samples gave ages comparable to the previous zircon ages.

Evolution and decomposition of Zr-Hf-U-bearing columbite-group minerals in Koktokay no. 1 granitic pegmatite dyke, Altai, northwestern China

Wang R*, Yin R, Zhang A

1 – Nanjing University, State Key Laboratory for Mineral Deposits Research, School of Earth Sciences and Engineering *rcwang@nju.edu.cn

The Koktokay No.1 pegmatite dyke is a Li-Cs-Ta-rich granitic pegmatite in Altai, northwestern China, and is located 1.2 km southwest of the famous No.3 pegmatite. It inclines to the southwest and the average obliquity is about 25°. The Koktokay No.1 pegmatite is ~1400 m long and varies in thickness from 1 to 7 m. The dyke intruded into metagabbro. From the contact with the country rock, the pegmatite dyke is divided into aplite zone (I), quartz-muscovite zone (II), cleavelandite-quartz-spodumene zone (III), and blocky quartz, K-feldpar zone (IV-V). Extreme fractionation from zircon to hafnon has been demonstrated in this dyke.

Columbite-group minerals are observed from the contact zone to the inner zone (zone III) with extensive variation in Ta/(Nb+Ta) ratio (0.06-0.98) and moderate variation in the Mn/(Fe+Mn) ratio (0.58-0.99), thus consist of manganocolumbite in the contact zone to manganotantalite in zone III. They also contain various amounts of Zr, Hf, and U, which slightly increase from the contact zone to zone II, and elevates obviously in zone III, up to 1.68 wt% ZrO_2, 0.73 wt% HfO_2 and 1.25 wt% UO_2 in this zone. Moreover, tiny inclusions of Zr-wodginite, zircon, uraninite ± uranmicrolite are also found in some areas of manganotantalite crystals, where Zr, Hf, and U contents are below or near the detection limits.

Nb/Ta increases in columbite-group minerals reflect highly fractional crystallization of the Koktokay No. 1 pegmatite. Enrichments in Zr, Hf and U in tantalite are consistent with abundant occurrence of high-Hf zircon (even as hafnon) in zone III, likely owing to Zr, Hf, U-rich environment in the pegmatitic melt. Inclusions of Zr-U minerals probably resulted from dissolution-recrystallization of primary Zr-Hf-U-rich tantalite, enhanced by late fluids.

Zr-Hf-U-rich columbite-group minerals could be used as targets for columbite U-Pb geochronology, and possible Hf isotope geochemistry.

Allanite-(Ce) alterations in the Mukinbudin Feldspar Quarries pegmatite, Mukinbudin, Western Australia

Bermanec V[1*], Jacobson M I[2], Soufek M[3], Cobic A[1], Tomasic N[1]

1 - University of Zagreb *vberman@public.carnet.hr 2 - Private 3 - Croatian Natural History Museum

The Mukinbudin area, Western Australia, comprises a pegmatite field with pegmatite bodies classified as NYF-type [1]. Allanite-(Ce) has been found in Mukinbudin Feldspar Quarries in form of metamict masses. The allanite masses are round-shaped being up to tens of centimeters in diameter and show no distinct crystal faces. The mineral is black, brittle and glassy in appearance. It has distinctive ochre to brown coating with red tint which is up to few millimeters thick. Along with allanite, the mineral assemblage comprises albite, beryl, biotite, chalcopyrite, fergusonite-(Y), magnetite, microcline, monazite, pyrolusite, quartz, and zircon.

XRD pattern of the allanite sample showed that the mineral is heavily metamictized with just a dozen diffraction poor-resolved maxima yielding a unit cell a=8.99 (2), b = 5.76 (2), c = 10.28(3) Å, β = 115.1(2)°, V=482(2) Å^3. The volume of the unit cell exceeds the one of recrystallized allanite (V ~ 478 Å^3) due to metamictization. The coating around allanite masses is composed mainly of bastnäsite based on XRD pattern.

SEM analysis showed veinlets throughout the investigated allanite grain, whereby some of them could be observed macroscopically. Preliminary chemical analyses (EDS) showed a typical allanite-(Ce) content. The veinlets inside allanite are mostly composed of titanite. Throughout the grain there are lot of $ThSiO_4$ inclusions which are frequently aligned in almost straight-line clusters. In some cases, $ThSiO_4$ inclusions are surrounded by tiny grains of titanite and an Y-Ti-Fe oxide. The rim zone of the allanite masses is distinct from the rest of the grain showing a more complex composition. Generally, the rim is composed of altered allanite-(Ce) that is intersected by veins of bastnäsite-(Ce) and mica (Figure 1). ED spectra yielded fluorine in the composition of bastnäsite, but IR spectra showed also the presence of OH group, which in part could also originate from the altered allanite-(Ce) and mica.

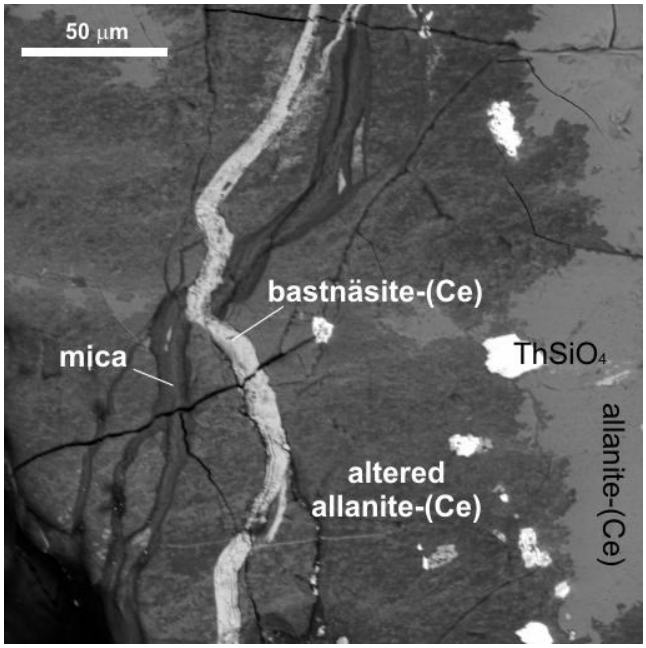

Figure 1: BSE image of the rim zone of allanite-(Ce) from Mukinbudin

[1] Jacobson M. I., Calderwood, M.A. and Grguric B.A. (2007). *Guidebook to the Pegmatites of Western Australia*, Hesperian Press, Carlisle, p. 356.

A possible new mineral species, "ferrogatehouseite" $(Fe,Mn)_5(PO_4)_2(OH)_4$ from Conţu Pegmatite, Romania

Calin N[1], Fransolet A[2], Baijot M[2], Marincea S[1], Dumitras D[1*], Hatert F[3], Anason M[1], Iancu A[1]

1 - Geological Institute of Romania *d_deliaro@yahoo.com
2 - University of Liège, Laboratory of Mineralogy, Belgium 3 - University of Liège

Gatehouseite, $Mn_5(PO_4)_2(OH)_4$, is a rare Mn-bearing phosphate, since this mineral is only reported in a sedimentary iron ore deposit in Australia [1]. Like in many Mn-bearing phosphates structures, Fe may replace Mn and a complete solid solution often exists between the Mn- and Fe-bearing end-members. One more time, our work leads us to consider the existence of a hypothetic new species, "ferrogatehouseite", which would be the iron dominant equivalent species of gatehouseite.

During the research on the Li-bearing pegmatites from Conţu (Cibin Mountains, South Carpathians, Romania) a rich phosphate association, including heterosite - purpurite, lithiophilite - triphylite, sicklerite - ferrisicklerite, fluorapatite, vivianite, monazite, wolfeite was identified. Other associated minerals include spodumene, quartz, muscovite, K-feldspar, plagioclase, beryl, cassiterite, columbite group minerals, lepidolite, rutile, scarce schorl, uraninite, topaz, spessartine, sillimanite, titanite. Pegmatites from Conţu are hosted by micaschists and gneisses related to the Sebeş - Lotru Series.

Phosphates belonging to the triphylite - lithiophilite series generally occur as nests in the spodumene and feldspar masses. They form granular masses of greenish gray color that turns locally into dark brown or black, due to the weathering. Both optical and scanning electron microscope studies show that triphylite abundantly contains inclusions of wolfeite and of a gatehouseite-like phase, the later occurring in the (001) perfect cleavage plane of triphylite.

X-ray powder data were obtained on a representative sample and indexed according to ICDD file 01-070-0516, belonging to gatehouseite. These data allow the refinement of the unit-cell parameters, in the space group $P2_12_12_1(19)$: a = 9.103(3) Å, b = 18.019(6) Å and c = 5.685(9) Å. The a and b parameters are slightly larger while c is slightly smaller compared to those of gatehouseite, given by Pring and Birch (1993), i.e., a = 9.097(2) Å, b = 18.002(3) Å and c = 5.693(2) Å.

Electron-microprobe analyses of this mineral, identified as iron-rich gatehouseite (sample 14/c4), yielded (in wt.% oxides): P_2O_5 = 26.76, FeO = 38.97, MnO = 27.15, MgO = 0.41, CaO = 0.05, H_2O (calculated for charge balance) = 6.79, total =100.13. But the empiric formula of this sample is $(Fe_{2.877}Mn_{2.030}Mg_{0.053}Ca_{0.004})(PO_4)_2(OH)_4$, which is related to the one of gatehouseite but with Fe >Mn. Chemical analyses on two other samples yielded similar empiric formulae, i.e., $(Fe_{3.083}Mn_{1.855}Mg_{0.021}Ca_{0.009})(PO_4)_2(OH)_4$ and $(Fe_{2.735}Mn_{1.717}Mg_{0.042}Ca_{0.003})(PO_4)_2(OH)_4$ (samples 13/c4 and 17/c4, respectively).

Further investigations by FTIR and micro-Raman are needed to acquire more details about the H_2O content of this potential ferrous homologue of gatehouseite. The petrographic texture indicates that "ferrogatehouseite" as well as wolfeite, partially replaced triphylite along its cleavage plane during the hydroxylation hydrothermal stage.

[1] Pring A., and Birch W.D. (1993). Gatehouseite, a new manganese hydroxy phosphate from Iron Monarch South Australia. *Mineralogical Magazine*, 57, 309-313.

Wyllieite reaction coronas on scorzalite in pegmatite dykes

Dias P[1], Leal Gomes C[1], Guimarães F[2], Hatert F[3*]

1 - CIG-R, Univ. Minho, Portugal 2 - LNEG, S. Mamede de Infesta, Portugal
3 - University of Liège *fhatert@ulg.ac.be

In the region of Serra de Arga (Northern Portugal) pegmatite dykes with approximately 50 cm thick and 2 m long, affected by Variscan deformation, contain scorzalite that is partially replaced by wyllieite reaction coronas. Mineral composition of the dykes consists of quartz, albite, K-feldspar and muscovite. Accessory minerals include andalusite, Mn-rich fluorapatite, columbite-(Fe), gahnite, uraninite, montebrasite and brazilianite [1].

Scorzalite occur as disseminated bluish to greenish single crystals up to 3 mm in size (Figure 1a). Inclusions of muscovite, gahnite and montebrasite (?) were identified. Scorzalite often displays complex alteration patterns corresponding to the development of brownish Al-Fe-Mn rich products (childrenite-eosphorite?). Other breakdown products include associations of crandallite-goyazite and variscite. Scorzalite electron-microprobe analysis showed the following average composition: $(Fe^{2+}_{0.90}Mg_{0.05\text{-}0.07}Mn_{0.02}Zn_{0.0\text{-}0.01})_{\Sigma 0.95\text{-}1.01}Al_{2.0\text{-}2.1}(PO_4)_2(OH)_2$.

Wyllieite forms light blue corona-like overgrowths around primary scorzalite and also penetrate along fracture fillings of the scorzalite crystals, as revealed by transmitted light microscopy (TLM) and EMP study (Figure 1b). Electron-microprobe analysis provided P_2O_5 = 45.5-47.2; Al_2O_3 = 8-8.6, MnO = 15.2-16.3, FeO = 23.5-24.6%, MgO = 0.44-0.54; Na_2O = 4.2-5.3 wt. %. The resulting formula, calculated on the basis of 12 O, is $(Na_{0.64\text{-}0.79}Ca_{0.02\text{-}0.03}Mn_{0.30\text{-}0.39})_{\Sigma 1.01\text{-}1.22}(Mn_{0.60\text{-}0.71}Fe^{2+}_{0.29\text{-}0.40})_{\Sigma 1}(Fe^{2+}_{0.27\text{-}0.61}Fe^{3+}_{0.34\text{-}0.67}Mg_{0.05\text{-}0.06})_{\Sigma 1}(Al_{0.72\text{-}0.77}Fe^{3+}_{0.23\text{-}0.28})_{\Sigma 1}(PO_4)_3$. Some of these compositions correspond to wyllieite, while oxidized grains correspond to rosemaryite [2].

Such unusual previously undescribed scorzalite breakdown was caused by post-magmatic, Na bearing fluids interacting with the pegmatite. Na could have become available by feldspar breakdown. Both albite and K-feldspar occur in the matrix and reflect distinct high phosphorous contents. K-feldspar contains up to 3.6 wt% of P_2O_5 and coexisting albite up to 1.98 wt%. Distribution of P between Fk and Ab ($P_{Fk/Ab}$) is 1.8. Textural relationships indicate albitization of the K-feldspar.

According to [2], wyllieite could have formed at temperatures lower than 400ºC, considering a pressure of 0.1Kbar. These estimates are within the considered field for scorzalite collapse (475-560ºC, 1-3Kbar) [3].

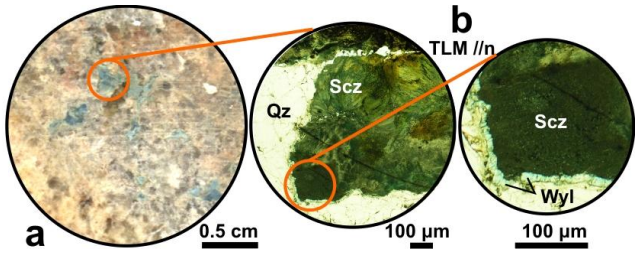

Figure 1: Scorzalite-wyllieite representative intergrowths.

[1] Dias (2012.) Ph.D Thesis, Univ. Minho, *464p*.

[2] Hatert F. *et al*. (2006). *Eur. J. Mineral*., 18, 775-785.

[3] Schmid-Beurmann *et al*. (2000). *Miner. Petrol*., 70, 55-7.

Fe, Mg and Mn distribution among tourmaline, micas and phosphates from the Tres Arroyos granitic pegmatites (Central Iberian Zone, Badajoz, Spain)

Garate-Olave I, Roda-Robles M E*, Gil-Crespo P, Pesquera A

UPV/EHU *encar.roda@ehu.es

The Tres Arroyos pegmatite field is located southeast from the Nisa-Alburquerque pluton (Central Iberian Zone, Badajoz, Spain). This is a late Variscan body composed of peraluminous monzogranites and leucogranites, with associated pegmatitic and aplitic dykes, which intrude into metamorphic rocks from the Schist-Greywacke Complex of Upper Precambrian to Lower Cambrian age. Pegmatites are classified into three different groups according to their texture, mineral association and spatial distribution. The bodies occurring closest to the pluton show the less evolved facies, with feldspars, quartz and muscovite as main constituents, and zinnwaldite, tourmaline, topaz and Fe-Mn phosphates as common accessories. In an intermediate area some albite-rich dikes occur, where K-feldspar, quartz and micas are also abundant, whereas fine-grained topaz and montebrasite crystals occur as accessory phases. The third group, in the furthest areas from the pluton, are Li-rich dikes, with albite, K-feldspar, quartz and lepidolite as the main constituents, and montebrasite, cassiterite, topaz and columbite-group minerals as minor phases.

Fe±Mg±Mn-bearing minerals have only been found in the first group of pegmatites. Zinnwaldite occurs as fine-grained flakes, with a slight pleochroism from colourless to light beige. Chemically, crystals are quite heterogeneous, with a broad range for FeO (5.96-12.66 wt%) and smaller for F (2.11-4.48 wt%). Muscovite shows negligible amounts of both Fe and Mg. Tourmaline appears as small black prismatic crystals that under the microscope show different shades of brown, frequently displaying a concentric colour zoning. However, all tourmaline crystals analyzed up to now correspond to quite homogeneous, Mg-poor schorl. The Fe-Mn phosphates identified are ferrisicklerite, eosphorite-childrenite, jahnsite, rockbridgeite and lipscombite. All of them occur as fine-grained crystals, scattered among the silicates. Jahnsite and lipscombite replace partly or completely the ferrisicklerite. Most of these phosphates belong to the Fe-rich term of their Fe-Mn series, with Fe/(Fe+Mn) ratios of 0.88-0.89 for ferrisicklerite, 0.67-0.82 for jahnsite, and 0.91-0.98 for lipscombite and rockbridgeite. Eosphorite is the only phosphate richer in Mn than in Fe, with ratios in the range 0.38-0.62. As it is expected in this pegmatitic environment, the studied minerals are Mg-poor, with the exception of the Mg-jahnsite (5.75-8.00 wt% MgO). The rest of the minerals show pretty low contents in Mg (<0.72, <0.29 and <0.14 wt% for phosphates, micas and tourmaline, respectively). In general, tourmaline is richer in Fe and poorer in Mg and Mn than zinnwaldite, whereas Mn preferentially partitions into the phosphates (up to 4.25wt% for lipscombite and rockbridgeite, up to 5.23wt% for ferrisicklerite, up to 1.80wt% for jahnsite, and up to 18.04wt% for eosphorite).

The pegmatites associated with the Fe±Mg±Mn-bearing minerals show moderate levels of fractionation, with a relative enrichment in F, Li and Na. The scarcity of Fe-Mg-Mn-bearing minerals indicates a very low content in Mg, Fe and Mn at the beginning of crystallization of the dykes of the first group. The lack of ferro-magnesian-(manganoan) phases in the other two groups of dykes in Tres Arroyos, suggests that these elements were mainly consumed during the crystallization of the dykes closest to the batholith. There, Mn partitions preferentially into the phosphates, whereas tourmaline is the Fe-richest phase and zinnwaldite shows, in general, the highest contents in Mg and higher values in Mn than the tourmaline.

Mineralogical and fluid inclusion characteristics of the spodumene-bearing Noumas I pegmatite, Northern Cape, South Africa

Gauert C[1*], MacDonald N[2], Roelofse F[1]

1 - Department of Geology, University of the Free State *gauertcdk@ufs.ac.za 2 - Inst. for Groundwater studies, UFS, South Africa

The Li-rich zoned Noumas I pegmatite of approximately 1 Ga age formed along fractures and tectonic planes of folded granodioritic host rocks of the Vioolsdrift suite, similar to other pegmatite occurrences in southern Africa. The residual magma, enriched in volatiles and rare elements, intruded along fissures into the surrounding rocks.

The economic minerals in the pegmatite are the Li-bearing spodumene, petalite, lepidolite, amblygonite as well as accessory beryl, columbite-tantalite, and bismuthinite. Mineral textures and microthermometric studies suggested a slow cooling rate of the source melts. The textural, crystal morphology and geochemistry supports a slow growth rate. The depth of emplacement for the pegmatite was estimated at 300 Mpa corresponding to 14 km depth, using the inferred pressure from the quartz-saturated phase relationship for Li-minerals related to approximate formation depth and metallogenic character of granites [1].

The compositionally peraluminous Noumas pegmatite shares similar geochemical trends with upper continental crustal rocks which were probably the source for the melts. During ascent through the crust the magma was depleted in Nb, Ta, Sr, and Zr, but enriched in Li, B, F, and P. The granodioritic host rock also played an important role in the minerals formation of the contact zone of the Noumas I pegmatite. Garnet and beryl were enriched in Fe and Mg by assimilation of these elements from the host rock. The mineralogy evolved during the crystallization period from spodumene, feldspar and garnet-rich to more quartz dominated assemblages. The presence of bismuthinite in the wall zone suggests more reducing conditions in the early magma composition, while a negative Ce anomaly determined from ICP-MS analyses, indicates that the intermediate and core zones were formed during a period of stronger oxidation of the magma.

Microthermometry, Raman and FTIR studies on quartz showed fluid inclusions to be H_2O-rich with low (6.5 to 7.4 % NaCl-equivalent in wall and core zones) to medium (12 % NaCl-equivalent in the intermediate zone) salinity, containing predominantly K/NaCl but also Mg_2+$CaCl_2$ in the inner zones. CO_2 was present in inclusions of the wall, intermediate and core zones, whereas small amounts of CH_4 were only found in the intermediate zone. It is concluded that the initial melt interacted with formation waters, which lowered the fluid salinity and homogenization temperature in the wall zone, followed by more saline magmatic fluids exsolving from the medium zone melt. A solute-poor low-salinity fluid in the melt finally formed the core zone.

The Noumas I pegmatite can be classified as a Li-columbite-tantalite (LCT) pegmatite, derived from peraluminous granites that concentrate Li, Rb, Cs, Be, Sn and Ta, Nb in the presence of B, P and F. An enrichment factor of approximately 6900% would be needed to produce the observed Li concentration in the Noumas I pegmatite from source granite with a concentration of 40 ppm Li. The mineral paragenesis indicates a definite change in chemistry and mineralization over the crystallization period of the pegmatite.

[1] Strong D.F. (1988). A Model for Granophile Mineral Deposits. In: Roberts, R.G. and Sheahan, P.A. (eds.) Ore deposit Models. *Geoscience Canada Reprint Series*, 3, The Geological Association of Canada. Dept. of Earth Sciences, Memorial University of Newfoundland, 59-66.

Spectroscopy behaviour of thermally treated pink and colorless elbaites from the Borborema Province of Brazil

Maria de Lima Correia A[1], de Brito Barreto S[1*], Guzzo P[2], Bermanec V[3]

1 - UFPE/Department of Geology *sandrabrito@smart.net.br 2 - UFPE/Department of Mine Engineering 3 - University of Zagreb

Tourmaline is a borosilicate mineral with structural formula $Y_3Z_6(T_6O_{18})(BO_3)_3V_3W$. In that case, each site is often occupied by ions (or vacancy) as X= Na^{1+}, Ca^{2+}, K^{1+}, and vacancy; Y=Fe^{2+}, Mg^{2+}, Al^{3+}, Li^{1+}, Fe^{3+} and Cr^{3+}; Z=Al^{3+}, Fe^{3+}, Mg^{2+} and Cr^{3+}; T=Si^{4+}, Al^{3+}, and B= B^{3+}; V=OH^{1-} and O^{2-}; and W= OH^{1-}, F^{1-} and O^{2-}. The nature, abundance and occurance of cations/anions in these sites result in the varied species. The tourmalines from Northeast Brazil (Borborema Pegmatite Province - BPP) have attracted the attention of mineralogists and gemologists for their extraordinary characteristics, especially their color. The most attractive are "electric" blue colored known as "Paraiba" tourmaline. The beauty of gemstones is influenced by two important features - color and transparency - which determine how attractive the gemstones are. The thermal treatment is a simple and accessible way of enhancing the color of minerals. This paper presents spectroscopy data of pink and colorless tourmalines from the same pegmatites that mineralized "Paraíba Tourmalines", in order to define parameters for enhancing color thus transforming them into more desirable and valuable gemstones. The Li-bearing tourmalines studied are elbaites coming from four pegmatite bodies ; Capoeiras, Quintos, Batalha and Bulandeira, which occur in the states of Rio Grande do Norte and Paraíba, Northeast Brazil. The samples were characterized by spectroscopy in the ultraviolet and visible (UV -Vis), and infrared (IR) before and after heat treatment. For measurements UV-Vis spectrometer Perkin Elmer and infrared FT-IR Spectrometer ABB Bomen FTLA 2000 were used. The heat treatment was performed in an air furnace (Mufla 1.1 - chamber 1,5l) using two experiments with different steps of heating. The optical absorption spectra of the colorless and pink tourmaline allowed identification of the chromophore elements responsible for the absorption bands. Some studies have been carried out and they propose that the pink color is attributed to mechanisms of ionic interactions involving ions of Mn^{2+}, Mn^{3+} and Fe3+. The spectra obtained in natural colorless tourmaline, showed bands at ~450 nm , ~704-718 nm and 914-922 nm, related to Mn^{2+}/Fe^{3+}, Fe^{2+}/Cu^{2+} and Cu^{2+}, respectively. The pink elbaites exhibited principal absorption at ~450 nm and ~520 nm associated with Mn^{2+} and Mn^{3+}, respectively. On mid-infrared region we identified bands: 3628-3701 cm^{-1} related to OH_1 , the band 3534-3541 cm^{-1} assigned to CH_3 group and the bands 2997-3022 cm^{-1}, 2293-2374 cm^{-1} and 2489-2519 cm^{-1} of H_2O. After heat treatment, the colorless elbaite becames pink and the pink elbaite became colorless. The IR spectra after heat treatment in the same samples showed that the colorless and pink elbaites have no significant changes in the mid-infrared region. On the other hand, in the visible and near infrared region, where the colorless elbaite transformed into pink, main absorption bands at ~450 nm (Mn^{2+}) and 520 nm (Mn^{3+}) appear, and already pinkish hues become colorless. No significant absorption bands in the visible region were observed. In conclusion, this study shows that the heat treatment of colorless elbaite from these pegmatites could add value to these gemstones, enhancing the color to pink elbaite which is more desirable in the gemstone trade.

Mineralogical zonation and rare metal (Ta-Sn-Li-Be) distribution in Precambrian pegmatites of Keffi area, Central Nigeria

Okunlola O

University of Ibadan. gbengaokunlola@yahoo.co.uk

Rare metal bearing pegmatites occur as vertically dipping and low lying pegmatite bodies around the Keffi area, central Nigeria have been studied with a view to elucidate their petrographic features and rare metal (Ta-Sn-Li-Be) distribution .

Geological mapping, first on a scale of 1:50,000, then on a larger scale of 1:5,000 reveal that these pegmatite bodies which intrude older lithologies of Schist and Older Granite have varied and distinct mineralogical zones. The vertically dipping type exhibit more mineralogical zonations with five distinct zones identified. These are Muscovite-Quartz- Microcline- Albite- Tourmaline (MQMAT), Lepidolite-Muscovite-Tourmaline (LMT), Microcline-Albite (MIA), Quartz-Muscovite-Albite (QMA) and Quartz-Beryl-Muscovite-Albite-Tourmaline (QBMAT) zones respectively. However, the low lying bodies exhibit less zonal complexity with only two distinct mineralogical zones, viz the Quartz- Microcline- Tourmaline zone (QMIT) and the Quartz- Albite-Microcline (QAM) zones.

Chemical analysis for rare metal Ta-Nb -Sn -Li-Be content of the pegmatite bodies using the inductively coupled plasma (ICP AES) instrumentation technique show that these rare metals have preference for specific mineralogical zones. For example, Ta has affinity for the albite and tourmaline rich zones while Li concentration is greater in zones of lepidolite and microcline enrichment. Sn, which has the highest values generally, shows preference mainly for the LMT zone. Generally however, the pegmatite bodies are more of a Sn-Li prospect with subordinate Ta-Nb enrichment. The distinct compositional preference of rare metal content for certain mineralogical zones is thus a useful exploration guide for rare metal exploration in the pegmatite bodies of the study area.

Keywords: Pegmatite, rare metal, mineralogical, analysis, zonations

Phosphates associated with the Li-F-Sn-bearing pegmatitic rocks from Castillejo de Dos Casas (Central Iberian zone, Salamanca, Spain): textural and chemical characterization

Roda-Robles M E*, Alfonso P, Pedro G, Garate-Olave I

UPV/EHU *encar.roda@ehu.es

The Castillejo de Dos Casas (C2C) pegmatitic bodies are located in the Central-Iberian-Zone (CIZ), where Variscan granitic rocks intruding into metasedimentary materials of the Schist Metagraywacke Complex (SMC) are common. The main pegmatitic body of C2C occurs in the upper part of one leucogranitic apophysis, the hanging wall being in direct contact to the metasediments of the SMC. The hosting granitic rocks are two-mica leucogranites, showing occasionally pegmatitic facies, with quartz, albite, K-feldspar and micas as main minerals, and apatite, tourmaline, topaz, lepidolite, montebrasite and cassiterite as accessory. The pegmatitic body is heterogeneous, including different mineral associations. The most common facies consists of a fine-grained matrix of quartz, plagioclase and Li-mica, where coarser crystals of K-feldspar grow perpendicularly to the contacts, and topaz, montebrasite, petalite, cassiterite and manganocolumbite are accessory. Another facies includes fine- to medium-sized layered textures, with lepidolite-rich bands alternating rhythmically with albite-rich ones. Close to the schists of the hanging wall, lepidolite is less common while fine crystals of Fe-rich tourmaline are relatively abundant. Phosphates occur in all these facies, including montebrasite, F-apatite, ferrisicklerite, sicklerite, varulite, triplite, and lipscombite. Lipscombite replaces ferrisicklerite from the outer facies, appearing as very dark rims around the orange ferrisicklerite crystals, whereas varulite replaces the sicklerite from the Li-rich inner facies, occurring as yellowish patches inside the orange sicklerite. Important compositional variations have been observed among phosphates of different facies. The Fe/(Fe+Mn) is higher for the Fe-Mn phosphates occurring in the facies in contact with the schists (ferrisicklerite: 0.63-0.72) than for the Li-rich inner facies (sicklerite: 0.31-0.56). The chemical composition of F-apatite also changes depending on the facies, with high values for FeO and MnO for the apatite associated with the outermost facies (0.6-3.6 and 2.25-6.72 wt% respectively), and lower values for the apatite occurring in the Li-rich inner zones (0-0.3 and 1.68-3.76 wt% respectively). The observed chemical variations suggest an inward fractional crystallization for this pegmatitic body, with a progressive enrichment in Mn parallel to a decrease in Fe, mainly consumed by the phosphates and tourmaline from the outer facies.

Trace-element geochemistry of Fe-Mn phosphates from the Cañada granitic pegmatite (Central Iberian Zone, Salamanca, Spain)

Roda-Robles M*, Pesquera-Perez A

UPV/EHU *encar.roda@ehu.es

The Cañada Li-P-(Sn-Nb-Ta)-bearing pegmatite, which intrudes partly into a gabbro and partly into a leucogranite, is localized in the Central Iberian Zone (Salamanca, Spain). Based on paragenesis, texture, and chemical composition three different phosphate associations are distinguished in this Li-P-(Sn-Nb-Ta)-bearing granitic pegmatite: 1) Border Zone, with Mg-rich ferrisicklerite, graftonite, wagnerite and johnsomervilleite, coexisting with Fe-Mg silicates; 2) Transition Zone, with ferrisicklerite, graftonite, Mn-apatite and xenotime-Y; and 3) Inner Zone, with triphylite, sarcopside and graftonite, also including minor montebrasite, ferrocolumbite, and cassiterite. The genetic model proposed for this pegmatite involves inward crystallization from the margins and contamination of fluids from wall rocks into pegmatite-forming melt. In order to better understand the behaviour of phosphates in pegmatitic systems, trace element geochemistry has been done by EMP and LA-ICP-MS techniques. There are important differences in the trace element contents for the different primary phosphates of the three associations. Zinc is the most abundant trace element in all them, with the highest proportions in graftonite (>2300 ppm) and the lowest in apatite (<114 ppm). Scandium is also common in these phases, with values up to 6000 ppm in johnsomervilleite, and values between 25 and 79 ppm for triphylite, sarcopside and graftonite. Other elements show high values just for some of the phosphates. The REE, Y, U and Pb are especially abundant in apatite, johnsomervilleite and, in lower contents, in graftonite; whereas the highest Zr contents are found in johnsomervilleite (average 2115 ppm), and the highest Nb values belong to wagnerite (average 311 ppm). Phosphates also show significant variations for some elements depending on the phosphate association. Primary ferrisicklerite from the border and transition zones is richer in Na, K, Sc, Rb, Sr and U than the secondary ferrisicklerite from the inner zone, which is richer in Zn. Trace element contents in this secondary ferrisicklerite and in the replaced triphylite are quite similar, except for the Zn, Sr and Rb, higher in the ferrisicklerite. Triphylite and sarcopside (exsolution lamellae inside triphylite) show quite similar contents too, except for Na, K, Zn and Rb, higher in the sarcopside. Petrogenetic, paragenetic and crystal-chemical constrains are considered to be the main factors to control the behaviour of trace elements in phosphates from pegmatites.

Montebrasite and amblygonite from Nagatare, Fukuoka Prefecture, Japan

Shirose Y*, Uehara S

Kyushu University *shirose@kyudai.jp

Minerals of montebrasite-amblygonite series, showing complete solid solution with $LiAlPO_4(OH)$ and $LiAlPO_4F$, generally occur as primary phosphates from LCT pegmatites and topaz-bearing granites. The montebrasite series mineral from the Nagatare pegmatite, Japan, is described by [1]. However, the detailed mineralogical study has not been reported. Therefore, we studied the montebrasite and amblygonite in an LCT pegmatite from Nagatare, Fukuoka Prefecture, Japan, with X-ray powder diffraction (XRD) experiments at room temperature and high temperatures, electron microprobe analyses (EPMA) and transmission electron microscope (TEM) observations. The montebrasite and amblygonite from the Nagatare pegmatite occur as large subhedral to euhedral crystals with lepidolite, Li tourmaline and petalite in quartz and albite. Small dendritic crystals are also contained in K-feldspar. The crystals are colorless, milky-white-colored and light-salmon-colored with vitreous luster, which show white veins parallel to cleavages in the cross sections. Under the polarizing microscope, montebrasite and amblygonite are mostly cloudy by very fine inclusion, and polysynthetic twins are observed. Fluorine contents for montebrasite-amblygonite series minerals were estimated from bulk powder X-ray diffracted patterns using Kallio's method [2]. The obtained values of F/(F + OH) in the bulk compositions are 0.40-0.59. However, EPMA analyses show they are partially replaced by low-F montebrasite, and they contained secondary vein phosphates such as crandallite, goyazite, fluorapatite, morinite, viitaniemiite and wardite [3]. Lacroixite is also contained in all specimens as scattered lamella embedded in montebrasite (Figure 1) and amblygonite. This texture is same as "natromontebrasite" discredited species: the mixture of an OH-rich amblygonite and lacroixite [4]. The micro texture and crystallography were also observed by TEM. Montebrasite-amblygonite series is topologically identical to the lacroixite structure, and Na could not substitute Li at low temperature in the montebrasite-amblygonite structure [5]. Thus, there is a possibility that lacroixite is exsoluted as Na-bearing phase with a temperature decrease and distributed within montebrasite and amblygonite. The high temperature XRD experiments showed decreases in α, β and γ angles with increases in V of a montebrasite-amblygonite, and these parameters are more closely to that of lacroixite.

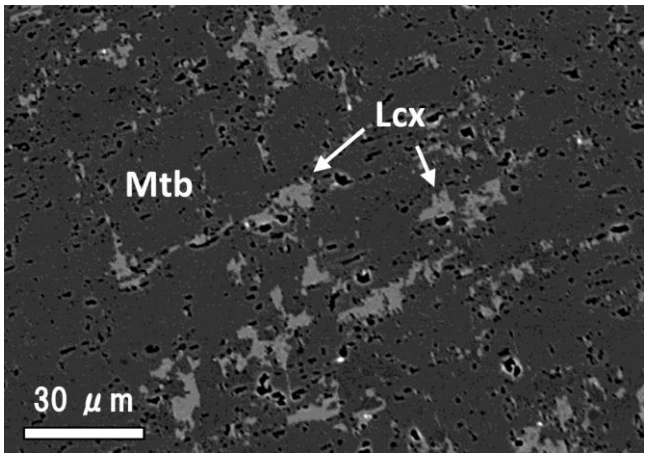

Figure 1: BSE image showing scattered lamella of lacroixite (Lcx) embedded in montebrasite (Mtb) [3].

[1] Shibata H. (1934). *J. Geol. Soc. Jpn.*, 41, 582-603.

[2] Kallio P. (1978). *Am. Min.*, 63, 1249-1251.

[3] Shirose Y. and Uehara S. (2014). *J. Mineral. Petrol. Sci* (in press).

[4] Fransolet A.-M., Fontan F. and de Parseval P. (2007). *Can. Min.*, 45, 391-396.

[5] Groat L.A., Raudsepp M., Hawthorne F.C., Ercit T.S., Sherriff B.L. and Hartman, J.S. (1990). *Am. Min.*, 75, 992-1008.

The tantalite-tapiolite gap revisited: experimental constraints from pegmatitic melts

Van Lichtervelde M[1*], Holtz F[2]

1 - Université de Toulouse *marieke.van-lichtervelde@get.obs-mip.fr
2 - Leibniz Universität Hannover

Manganotantalite $MnTa_2O_6$ and ferrotapiolite $FeTa_2O_6$ are common tantalum ores and are often associated in granitic pegmatites. The compositional gap that exists between the two minerals is well constrained from natural examples, and a few experimental studies have investigated the role of pressure and temperature on the gap extent. However, these experiments were run in conditions which are not representative of natural systems (dry conditions, high temperatures, atmospheric pressure). In the present study, the tantalite-tapiolite gap was investigated through crystallization experiments from a flux-rich, slightly peraluminous, nearly water-saturated pegmatitic melt, doped with different proportions of Ta/(Nb+Ta) (Ta*) and Mn/(Fe+Mn) (Mn*). The changing parameters are pressure (100 to 200 Mpa), temperature (700 to 1000°C), fO2 (NNO to MQF+4) and minor element composition (Nb,Ti). All experimental products consist of homogeneous glass and manganotantalite and/or ferrotapiolite crystals. The crystal size varies from 2 µm at 700°C up to 20 µm at 1000°C. Figure 1 shows the results of two sets of experiments, one with Ta*=1 and the other with Ta*~0.8, at 1000°C and 200MPa. When compared to natural systems (Figure 2), the resulting gap shows significant shift to higher Mn* ratios. Our preliminary results show that lower temperatures do not affect significantly the position of the gap, whereas lower pressure and the presence of Ti in the Ta-minerals shifts the gap to lower Mn* ratios. If this is verified by additional experiments, the tantalite-tapiolite gap could then be used as a geobarometer for Ta mineralization in granitic pegmatites.

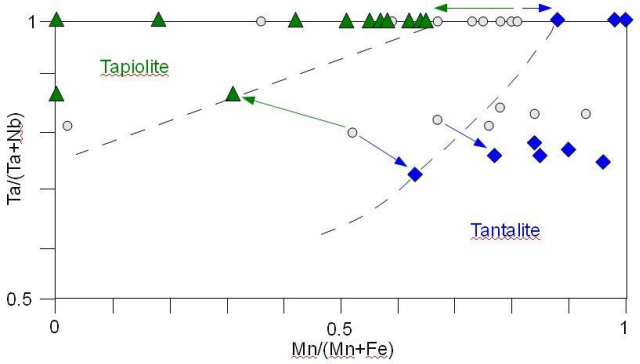

Figure 1: Compositional gap between tapiolite (triangles) and tantalite (diamonds) observed in experiments at 1000°C and 200MPa. The grey circles represent the starting glass compositions.

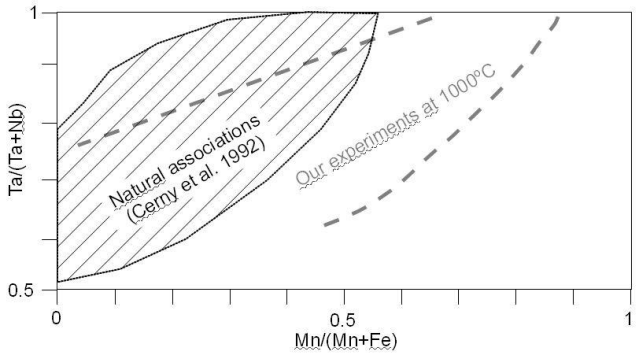

Figure 2: Comparison between the gap observed in natural systems and the gap obtained from our experiments at 1000°C and 200MPa.

U-Pb geochronology on zircon and columbite-group minerals of the Cap de Creus pegmatites, Spain

Van Lichtervelde M [1*], Gerdes A[2], Grand'Homme A[1], de Saint Blanquat M[1], Olivier P[1], Melgarejo J[3], Druguet E[4]

1 - Université de Toulouse *marieke.van-lichtervelde@get.obs-mip.fr
2 - Goethe-University Frankfurt 3 - Universitat de Barcelona 4 - Universitat Autònoma de Barcelona

The Cap de Creus peninsula, in Catalonia, northeastern Spain, hosts an important group of about 400 pegmatite bodies which are distributed along parallel zones of progressive fractionation degrees ranging from simple (muscovite class) to complex (rare-element class) pegmatites. The area represents the easternmost part of the Pyrenees affected by the Hercynian orogenesis, and the pegmatites intrude a Proterozoic series of metasediments and metavolcanics that were affected by several episodes of deformation and a low-pressure, high-temperature regional metamorphic event increasing from chlorite-muscovite zones in the south, to sillimanite-K-feldspar zones in the north of the peninsula. Type I (barren) and type II (beryl-columbite subtype) pegmatites occur in high-grade rocks of the migmatite and sillimanite-muscovite zones in the north, whereas type III (beryl-columbite-phosphate subtype) and type IV (albite subtype) pegmatites occur in medium-grade rocks of the cordierite-andalusite zone in the south. The area hence represents an excellent opportunity to study the relationships between magmatism, metamorphism and deformation during the Hercynian orogenesis.

The anatectic (melting of country rock) *versus* granitic (extreme fractionation of granitic melt) origin of pegmatites is still warmly debated especially in cases where no potential parent granite is observed and the pegmatites are associated with migmatites, which is the case in Cap de Creus. The distribution of the pegmatites and their fractionation trends indicate an origin by differentiation of a granitic melt originating from the north of the peninsula, whereas their spatial association with migmatites has been used to argue for an anatectic origin. Therefore, dating the Cap de Creus pegmatites is not only important to frame the magmatic history of the Pyrenees, but also to clarify their anatectic *versus* granitic origin.

In the present study, both zircon and columbite-group minerals from the different types of pegmatites where dated using U-Pb isotope systematics from LA-ICP-MS analyses. The results on both minerals display an age of 297 +/- 3 Ma, which is concomitant to the emplacement of the latest Pyrenean granites dated at 298.5 +/- 1.8 Ma in the Albera massif. Pegmatites therefore represent the latest magmatic event in the Hercynian orogenesis. Their anatectic *versus* granitic origin will be discussed in the light of field evidences and age constraints.

Mica crystallisation as a marker of pegmatite composition

Villaros A[1*], Deveaud S[2], Pichavant M[1]

1 - ISTO-CNRS-BRGM Orléans, France *arnaudvillaros@gmail.com 2 – BRGM

Micas are ubiquitous minerals within granitic and pegmatitic magmas. The presence and the composition of micas are believed to depend strongly on the magma they crystallised from. The Upper Carboniferous Variscan St Sylvestre Leucogranite Complex (SSLC), located in the western Massif Central (Limousin, France) is composed of five main granitic facies: a biotite-only facies (Brame), a two-mica facies (St Sylvestre); a coarse grained two-mica facies (St Goussaud); a fine grained two-mica facies (Châteauponsac) emplaced as sills within the Brame facies; finally a muscovite-only facies (Sagne). Pegmatitic bodies within the SSLC are enriched in rare-elements (e.g. Li, Be, Nb, Ta) and most of them are intrusive within the St-Sylvestre facies. Pegmatites in the SSLC can be divided in six groups depending on their chemistry, mineralogy and internal structuration. I.) No rare-element-rich phase (not sampled); II.) Be bearing phase only; III.) Be and Nb rich; IV.)Be, Nb and Ta rich phases; V.) Be, Nb, Ta-rich phases and Li-enrichment; VI.) Li-rich phase (lepidolite, petalite). From I to VI the volume ratio between aplitic and pegmatitic texture increases. Sampling of micas within the pegmatites have been realised accordingly to this classification.

We analysed major and trace elements using both electron microprobe and Laser Ablation ICP-MS, within primary micas (biotite, muscovite and lepidolite) from both granite and pegmatite within the St Sylvestre leucogranitic complex. Within the granite, biotite and muscovite do not vary significantly in composition in regard of granite facies. Interestingly, biotite within pegmatite records a considerable change in composition from biotite in granite towards lithium-rich biotite in regard of pegmatite facies, changing from annite-phlogopite composition to zinnwaldite (in type-V pegmatite). On the contrary, muscovite is very homogenous and its composition has only a slightly higher Li-mica content than granitic muscovite. Experimental studies of mica crystallisation from a pegmatitic magma suggest that compositional changes observed in biotite can be directly related to the differentiation of pegmatitic magmas.

Behind the apparent compositional homogeneity provided by major elements within muscovite, trace element contents reveal compositional changes. These changes are very similar to the variation of trace elements contents observed in biotite in agreement with the pegmatite type, yet with significantly lower concentration for most elements considered here. It appears that both biotite and muscovite record compositional variability within pegmatitic magmas. Both biotite and muscovite record a subsequent decrease of Ba, Sr and Sc during differentiation while contents of Li, Be, Nb, Rb, Ta, Cs and Zn increase significantly with differentiation degree within both biotite and muscovite.

Differences of trace element concentration between biotite and muscovite can either be the consequence of partition coefficient between biotite and muscovite or a diachronous crystallisation of muscovite and biotite. Additionally the reduced variability in muscovite structural formulae emphasizes a lack of sensitivity of muscovite in regard of magmatic differentiation.

Cathodoluminescence and trace element content of magmatic topaz from the Ary-Bulak massif, Russia

Agangi A*, Gucsik A, Hofmann A

University of Johannesburg, Johannesburg, South Africa, *aagangi@uj.ac.za

Despite recent studies [1, 2], the cathodoluminescence characteristics of natural topaz [$Al_2SiO_4(F,OH)_2$] are still poorly understood. In order to define the cathodoluminescence properties of magmatic topaz and its relations with trace element compositions, we studied topaz samples from the Ary-Bulak ongonite massif using different techniques including scanning electron microscope cathodoluminescence (SEM-CL), electron microprobe, laser ablation ICP-MS, and Micro-Raman spectroscopy. The Ary-Bulak massif includes F-rich felsic rocks containing phenocrysts of feldspar, quartz, Li-mica, and locally topaz [3]. Topaz forms euhedral, prismatic and locally splinter-shaped phenocrysts up to 1-2 mm long, and elongate prisms up to ~100 µm long, commonly forming aggregates of radially oriented crystals occurring in the groundmass. SEM-CL panchromatic images of topaz phenocrysts reveal strong, micrometer-scale variations, which define euhedral growth textures. Several truncations of these growth textures occur in single grains implying multiple growth and resorption events during topaz crystallisation. Electron microprobe analyses indicate high F concentrations with only minor OH replacement (average OH/(OH + F) = 0.04 calculated by difference, 100 wt.% - EPMA tot), consistent with what has been found in topaz-bearing granites [4]. The OH stretching vibration (~3653 cm^{-1}) was detected by Raman spectroscopy. Laser ablation ICP-MS traverses performed across the CL textures detected a large amount of trace elements at ppm to thousands of ppm levels, including Fe, Mn, Li, Be, B, P, Nb, Ta, W, Ti, Ga, light rare earth elements, Th, U. The lack of discrete peaks in time-resolved plots of ablation intensity suggests that these elements are incorporated in the mineral lattice rather than in inclusions. Gallium, Li, W, Nb and Ta appear to be correlated with CL intensity, suggesting a role for some of these elements as CL-activators in topaz. In contrast, no clear correlation was found between CL intensity and F contents, despite the fact that the replacement of OH for F is known to affect the lattice properties of topaz [5, 6]. These trace element traverses and related CL variations can be potentially used as a proxy for trace element fluctuations in the parent melt during topaz crystallisation. We also intend to extend this study into cathodoluminescence spectroscopy, including CL spectral measurements, to distinguish different wavelengths contributing to the total CL, and finally obtain more information about the relationship between the CL-bright as well as CL-dark zones and their dependence on trace element contents in topaz.

[1] Correcher *et al*. (2011). *Spectroscopy Letters*, 44, 486-489.
[2] Song and Yuan (2009). *Journal of Geography and Geology*, 1, 13-19.
[3] Kovalenko and Kovalenko (1976). *Nauka Press.*
[4] Breiter *et al*. (2013). *Mineralogical Magazine*, 77, 403-417.
[5] Alberico *et al*. (2003). *European Journal of Mineralogy*, 15, 875-881.
[6] Schott *et al*. (2003). *European Journal of Mineralogy*, 15, 701-706.

Pressure's control on K incorporation in tourmaline

Berryman E[1,2*], Wunder B[2], Wirth R[2], Heinrich W[2], Franz G[1]

1 - TU Berlin *berryman.eleanor@gmail.com 2 - GFZ Potsdam

Potassium is commonly considered incompatible in tourmaline [$XY_3Z_6(T_6O_{18})(BO_3)_3V_3W$] and typically found in trace concentrations at the [9]-coordinated X-site. However, K concentrations as high as 0.58 K pfu have been found in otherwise dravitic tourmaline from the (ultra) high-pressure rocks of the Kokchetav Massif, Kazakhstan [1], and recently we synthesized tourmaline with up to 0.71 K pfu at 4.0 GPa and 700°C [2], raising the question of the influence of pressure on tourmaline's ability to incorporate K into its structure.

To investigate the effect of pressure, fluid composition, and temperature on the relative incorporation of Na and K at the X-site, we synthesized tourmaline in the MgO-Al_2O_3-B_2O_3-SiO_2-KCl-$NaCl$-H_2O system from an oxide mixture and excess fluid at a range of conditions: 0.2 - 4.0 GPa, 500 - 700°C, and variable fluid composition. Analysis of the synthesized tourmaline by electron microprobe (EMP) and transmission electron microscopy (TEM) shows that the incorporation of K at the X-site increases with pressure and KCl concentration in the fluid (Figure 1); a maximum of 0.71 K pfu (leaving 0.29 X-sites pfu vacant) was incorporated in K-dravite synthesized at 4.0 GPa from a 4.67 *m* KCl, Na-free fluid. In contrast, Na incorporation depends predominately on fluid composition rather than pressure; dravite with the highest-measured Na content of 0.96 Na pfu was synthesized at the lowest pressure investigated (0.2 GPa) from a 4.11 *m* NaCl and 1.24 *m* KCl fluid. Reflecting the relatively large size of the ion, the unit cell volume of tourmaline as determined by Rietveld analysis of the X-ray diffraction spectra increases with K-incorporation, which in turn increases with pressure. Comparison of our results with K-dravite from the Kokchetav Massif suggests that the latter formed in a K-rich, Na-poor environment at ultrahigh pressure, in or near the diamond-stability field. These results have motivated the experimental investigation of the partitioning of K and Na between tourmaline and coexisting mica and fluid as a function of pressure, which may allow tourmaline to be used as a geobarometer.

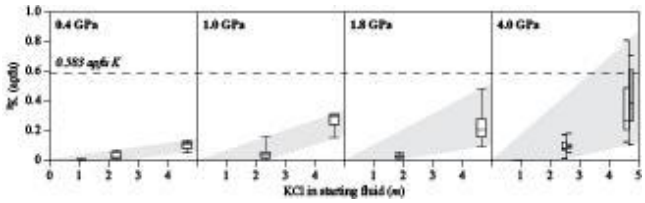

Figure 1: Amount of K incorporated at the X-site at different pressures as a function of concentration of KCl in the starting fluid. The dashed line indicates the maximum K content analysed in K-rich tourmaline from the Kokchetav Massif from [1].

[1] Shimizu R. and Ogasawara Y. (2013). *Journal of Asian Earth Sciences*, 63, 39-55.
[2] Berryman, E. *et al.* (2014). *American Mineralogist*, 99, 539-542.

Accessory mineral chemistry of high Ba-Sr granites from northern Scotland: constraints on petrogenesis and records of whole rock signature

Bruand E, Storey C*, Fowler M

University of Portsmouth, Portsmouth, U.K., *craig.storey@port.ac.uk

The Rogart and Strontian high Ba-Sr plutons (Northern Highlands, Scotland) comprise a range of lithologies from felsic to ultramafic rocks (so-called appinites). The latter rocks are mantle-derived and their differentiation to produce the felsic components is the result of fractional crystallisation and variable assimilation of the surrounding Moine metasediments. New results presented here demonstrate that accessory phase chemistry can give further insight into petrogenesis and highlight the petrological potential of apatite and titanite. Furthermore, in some cases, whole-rock trace element concentrations can be calculated by the use of accessory mineral chemistry.

Three of the main accessory phases (titanite, apatite and zircon), bearing most of the rare earth elements (REE) in the high Ba-Sr plutons, are studied here. Results on apatite and titanite show that careful imaging and in-situ trace element analyses give constraints on the petrogenetic history of the host rock. In both plutons, apatite and titanite record in-situ crystallisation and fractionation. In Strontian, apatite and titanite from the granitoids both record a mixing event with mafic magma in their rim compositions. Apatite and titanite chemistries are sensitive to the nature of their host rocks (felsic versus appinitic) and some elements (Sr, V) closely reflect whole rock chemistry and the degree of fractionation. Thus, trace elements in accessory phases can give direct access to the nature and the crystallisation history of plutonic rocks. This petrologic tool will allow further constraints in provenance studies using accessory phases, and since high Ba-Sr plutons have recently been equated with Archaean sanukitoids, might also be important in constraining the temporal distribution of this important magma type.

Tourmaline as a provenance indicator: using the complete chemical spectrum

Curry J[1], McMillan N[1], Dutrow B[2*], Henry D[2]

1 - New Mexico State University 2 - Louisiana State University *dutrow@lsu.edu

Provenance studies using the compositions of heavy minerals in modern and ancient sediments have changed the way we view earth's history. Archived in detrital grains found in clastic sediments and (meta)sedimentary rocks are signatures of the original source rocks that contributed the grains. Retracing this preserved signature to create the critical linkage to the protolith requires that the clastic minerals are chemically and mechanically stable throughout the weathering cycle. The 'big' three refractory minerals relied on for geologic provenance studies are zircon, tourmaline and rutile. Tourmaline supergroup minerals are extraordinary recorders of provenance because they are imprinted with and maintain chemical fingerprints of their complex geologic evolution; thus, they have been likened to a geologic DVD. This imprinted chemical fingerprint stems from their complex crystal chemistry permitting stability over a wide range of pressures (P), temperatures (T) and fluid compositions (X), the ability to form in widely varying rock and fluid compositions, and their recalcitrant behavior that minimizes diffusion such that they retain the original chemical signature. These features and their mechanical resistance combine to preserve records of the geochemical environment of formation. Consequently, tourmaline can be an insightful indicator of its provenance, i.e. the lithology in which the tourmaline crystallized. Initial provenance-based tourmaline determinations demonstrated that these minerals could be powerful provenance indicators. This study relied largely on major-element compositions of Al-Fe-Mg, easily measured with the electron microprobe. However, much more chemical information is embedded in the tourmalines that additional data can potentially provide new avenues for provenance determinations, if appropriate methods for interrogation are available.

Laser-Induced Breakdown Spectroscopy (LIBS) and chemometric analyses provide a new method to interrogate tourmaline chemistry for provenance studies. LIBS captures attributes of the entire chemical spectrum of the tourmaline and thus provides added constraints on tourmaline provenance. LIBS is preferable to electron microprobe analysis for three main reasons: (1) LIBS analysis is sensitive to and captures signatures of light elements such as Li, B and H; (2) each LIBS spectra contains 13,600 - 40,000 variables, depending on the resolution of the spectrometer, and contains information on the concentrations of all elements in the periodic table, isotopic ratios, ionic valences, matrix effects and interferences due to processes in the produced plasma that together provide a unique spectral fingerprint of each tourmaline; and (3) LIBS analysis is rapid and relatively inexpensive, with a minimum of sample preparation allowing analysis of many samples.

Tourmaline from a variety of world-wide localities were analyzed using an Ocean Optics © 2500+ LIBS instrument with a Nd-YAG laser that emits light at 1064 nm. Principal component analysis and partial least squares regression were used to determine the provenance of tourmaline by calibrating and validating the provenance model with crystals of known provenance. Our data indicate that tourmaline provenance can be easily discriminated and binned into seven categories: (1) Li-rich pegmatites; (2) hydrothermally altered aplites and diorites; (3) Li- and Al-rich pegmatites; (4) Ti-rich tourmalinites; (5) Na-rich leucocratic granites; (6) Cr- and V-rich sediments; and (7) F- and B-rich granites. Utilizing tourmalines from well-constrained igneous, metamorphic, and hydrothermal environments, underscore the potential of this new technique to facilitate provenance determination by this widespread, petrogenetically important mineral. In addition, the occurrence and LIBS spectra of tourmaline can help refine provenance of detrital mineral suites.

B-isotope study of hydrothermal tourmaline in silicified komatiites from the Barberton Greenstone Belt, South Africa

Farber K[1*], Dziggel A[1], Meyer FM[1], Trumbull R[2], Wiedenbeck M[2]

1 - Institute of Mineralogy and Economic Geology, RWTH Aachen
*farber@iml.rwth-aachen.de 2 - GFZ Potsdam

Many Mesoarchaean greenstone belts are pervasively silicified, yet the reason for the silicification is not well understood. In the Barberton Greenstone Belt, South Africa, the silicification process is generally attributed to fluid circulation in shallow subseafloor convection cells [1]. An unusual aspect of this hydrothermal system is the widespread presence of tourmaline. The B-isotope composition of tourmaline has the potential of discriminating seafloor alteration from other fluid sources. This study presents chemical and B-isotope composition of tourmaline from komatiite and chert rocks of the Mendon Formation to constrain the source and evolution of the alteration fluids.

Six samples were studied, comprising highly altered and silicified komatiites, of which some show spinifex textures, foliated fuchsite cherts, and chert breccias, and a finely laminated chert that has previously been interpreted as stromatolite. The samples mainly consist of quartz, fuchsite, and Cr-spinel and locally contain chlorite and/or carbonate. Tourmaline occurs mainly in mica-rich layers and often has Cr-spinel, rutile, or quartz inclusions. It is typically idiomorphic or fragmented, with grain sizes of up to 200 µm. The composition is dravitic, and many grains show patchy zoning, which is mainly defined by variations in Cr-content.

In-situ boron isotope analyses by SIMS revealed an extreme range of $\delta^{11}B$ values, from -22 to +7 ‰ (typical 1 sd uncertainty is 1‰). Three of the samples yielded narrow ranges of $\delta^{11}B$: two of them between -6 to -8 ‰ (stromatolite and altered komatiite), and a third (altered komatiite) between +4 to +7 ‰. The other samples showed unusually strong internal variations, with up to 18 ‰ contrast in individual samples and even 14 ‰ in single grains. The frequency distribution of $\delta^{11}B$ in the heterogeneous samples shows a peak between -6 to -8 ‰, and a large number of light $\delta^{11}B$ values from -10 to -22 ‰.

Our preliminary interpretation of this B-isotope diversity is based on mixed fluid sources. We interpret the positive $\delta^{11}B$ values to represent boron derived from serpentinites, with heavy boron reflecting interaction with seawater. The intermediate compositions of -6 to -8 ‰ is present in nearly all lithologies and may represent a metamorphic fluid whose B-source lies in the greenstone magmas (mantle-derived) and/or in the granitoids surrounding the greenstone belt. The highly negative $\delta^{11}B$ values are more difficult to explain, as mature continental crust has not been identified in this setting. Negative $\delta^{11}B$ values (-10 ‰) in tourmaline were found in an earlier study using bulk methods [2] and attributed to non-marine evaporites. Our in-situ data show a much larger range of $\delta^{11}B$, a patchy heterogeneity, and a correlation with low Cr-contents. It is significant that the largest isotopic diversity is found in the deformed and brecciated samples, but a full explanation for the large range of $\delta^{11}B$ remains open.

[1] Hofmann A. and Harris C. (2008). *Chemical Geology*, 257, 224-242.

[2] Byerly G.R. and Palmer M.R. (1991). *Contributions to Mineralogy and Petrology* 107, 387-402.

Using mineral inclusions in rutile to determine metamorphic conditions

Hart E, Storey C*, Bruand E

University of Portsmouth, Portsmouth, U.K., *craig.storey@port.ac.uk

Rutile (TiO_2) is a common mineral in high grade metamorphic rocks. It is a major host of HFSE, such as Nb, Ta and Cr, which can be useful in discriminating between source rock lithology. It can also be dated using U-Pb, and temperatures can be obtained using the Zr-in-rutile geothermometer. The robust nature of rutile during diagenetic processes therefore makes it a useful tool in sedimentary provenance studies as it retains geochemical information from the source rock.

At present, there are no petrological tools which allow the estimation of P-T conditions of rutile growth using single grain analysis. In this contribution, we have studied inclusions present within rutile to determine the P-T conditions of their growth and therefore develop a new petrologic tool.

For this study, rutiles from three localities (Dora Maira and Sesia-Lanzo, Western Alps and Syros, Greece) have been analysed. These samples have been chosen as they have different bulk compositions (metaquartzite in the Dora Maira, metapelite in Sesia Lanzo, and metabasalt in Syros) and differing metamorphic conditions within the rutile stability field. Inclusions within rutile, identified using reflected light microscopy (Figure 1), have been analysed using electron microscopy and Raman spectroscopy and the trace element concentrations of the host rutiles have been analysed using LA-ICP-MS.

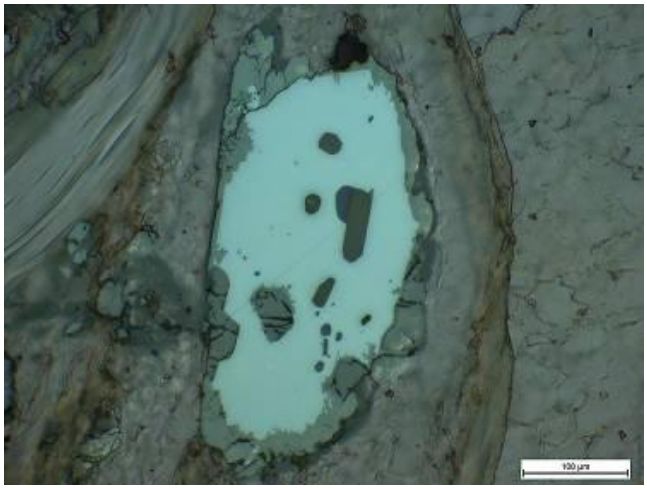

Figure 1: Reflected light image of a rutile grain with multiple inclusions

The systematic study of the mineral inclusions within rutile reveals important findings. Firstly, our study proves that the nature and the chemistry of the mineral inclusions match the minerals in the matrix of the respective samples. Secondly, P-T calculations using THERMOCALC v3.33 software allow us to obtain average P-T or average P which are consistent with P-T estimates in these localities The novel use of average P(-T) calculations with rutile inclusions can therefore help to place important constraints on the minimum pressure of rutile stability and, thus, facilitate the interpretation of detrital rutile. The use of Raman spectroscopy has also shown that rutile in UHP rocks can retain preserved coesite, meaning that it is a good repository to look for evidence for UHP metamorphism in otherwise retrogressed samples.

The petrologic potential of tourmaline: interaction between crystallography and local environment revisited

Henry D*, Dutrow B

Louisiana State University, USA, *glhenr@lsu.edu

The relationship between tourmaline's composition and the nature of the local environment of tourmaline formation has been explored for almost 30 years. With the improved understanding of the tourmaline crystallography has come a more robust interpretation of its petrologic significance. In a complementary way, a wider array of major and trace elements as well as isotopic investigations on tourmaline has opened up additional avenues of exploration. The co-evolution of these study areas has resulted in tremendous advances in the understanding of tourmaline's petrologic potential. Some noteworthy advances include the following:

Crystallographic framework of tourmaline. The general structural formula of tourmaline is now known to be: $XY_3\ Z_6(T_6O_{18})(BO_3)_3V_3W$ where the common ions at each site are X = Na^{1+}, Ca^{2+}, K^{1+} and vacancy: Y = Fe^{2+}, Mg^{2+}, Al^{3+}, Li^{1+}, Fe^{3+} and Cr^{3+}; Z = Al^{3+}, Fe^{3+}, Mg^{2+} and $Cr^{3+;}$ T = Si^{4+}, Al^{3+} and B^{3+}; B = B^{3+}; V = OH^{1-} and O^{2-}; and W = OH^{1-}, F^{1-} and O^{2-}. Several crystallographic and chemical issues influence its stability range and its interaction with the encasing petrologic environment. (1) Tourmaline exhibits a wide array of heterovalent and homovalent coupled substitutions. (2) Within the tourmaline structure F^{1-} occurs only in the W site, and (3) short-range bond-valence requirements and order-disorder reactions control the type and crystallographic positions of ions in the structure. With this knowledge a new nomenclature for the tourmaline supergroup minerals has been established, with over 30 IMA-approved species. The extremely low diffusion rate and wide stability range of tourmaline is likely related to these crystallographic features. In addition, chemical changes in tourmaline are a function of both crystallographic constraints and the petrologic environment, e.g., F^{1-} incorporation in the W site with different X-site occupancy.

T-P-fluid stability range of tourmaline. Tourmaline is known to be stable over most crustal PT conditions. Tourmaline has been found in diagenetic evaporitic and hydrothermal environments that record T < 150°C and P < 1 MPa. At the upper T extreme tourmaline is found to be stable at > 900°C in experiments and is locally found in granulite-facies rocks. The upper P stability is high - based on experiments, tourmaline is stable up to 7 GPa and it can be associated with high-P minerals such as coesite and diamond. Within the extensive PT stability range, tourmaline is unstable in environments that have fluids with high pH and selected aqueous species.

T-P-fluid determination using tourmaline. Tourmaline is a crystallographically asymmetric mineral that incorporates different concentrations of cations at opposite poles of the crystal as a function of temperature, commonly exhibiting sector zoning at lower T. This compositional asymmetry has been empirically calibrated as a thermometer that can be used to infer much of the thermal growth history of metamorphic tourmaline. Recent discoveries of tourmalines in ultra-high P environments suggest that high K contents in dravitic tourmalines indicate the possibility that K contents may be calibrated as a potential geobarometer. However, crystallographic factors can result in high-K tourmaline in other environments such as found in Fe^{3+}-rich povondraitic compositions at low P. Additionally, experiments show that the dissolved species in aqueous fluids associated with growing tourmaline can be related to the X-site Na and Ca in the tourmaline. Other compositional trends can also be related to fluid compositions. For example, the oxy-dravite-povondraite trend appears to be diagnostic of growth in low-T hypersaline environments. Finally, an increasing number of studies of trace elements and isotopes, commonly taking into account sector zoning, are revealing additional ways to establish PTX conditions in rocks and underscore the petrogenetic utility of tourmaline.

What can zircon hosted apatite from TTGs tell us about the bulk rock?

Sarafian A[1*], Marschall H[1], Meyer H[2], Zeh A[3]

1 - Woods Hole Oceanographic Institution, Woods Hole, MA, USA, *asarafian@whoi.edu 2 - Universität Heidelberg, Heidelberg, Germany 3 - Goethe University Frankfurt, Frankfurt, Germany

Sediments preserve records of vast areas of the continental crust. Detrital zircons are used in provenance studies because they are robust minerals, hold valuable geochemical information about their source rock, and can be accurately age dated.

Mineral inclusions in zircons are ubiquitous and can also provide insight into the petrogenesis of the host rock. Apatite, a common mineral inclusion, has been shown to record bulk rock information for a modern intrusive suite [1]. However, the Archean rock record is dominated by rocks of the tonalite-trondhjemite-granodiorite (TTG) intrusive suite. Classifications based on apatite chemistry cannot simply be transferred to the study of the TTG series rocks, due the characteristic chemical differences in the bulk rock compositions between modern and TTG intrusives. We have measured trace and major elements in apatite by electron microprobe on a suite of TTG gneisses from the Ancient Gneiss Complex, Swaziland, southern Africa.

We found that the initial calibration of apatite inclusion Y/Ce vs bulk rock SiO_2 remains valid for TTGs. The most robust indicator for bulk rock SiO_2 is the Y/Cl of apatite inclusion. Some apatite inclusions in zircon from TTG show Sr/Ce ratios that are distinctly higher than in apatites from modern granitoids, while other TTG apatites have no measurable Sr, but have elevated Na. The two populations of TTG apatite inclusions, Sr-rich/Na-poor and Sr-poor/Na-rich, are interpreted to represent a difference in crystallization sequence. The Sr-rich apatites likely crystallized closer to the liquidus, i.e., earlier in the crystallization sequence of their host magma, whereas the Sr-poor apatites crystallized later in the crystallization sequence after significant feldspar crystallization [2]. Hence, the Sr/Ce of a detrital zircon-hosted apatite can be used to determine whether the source rock was a modern K-rich granitoid or a rock of the TTG suite for Sr-rich apatites, but for late crystallizing, Sr-poor apatites we are unable to distinguish between TTG and modern granitoids. In addition, for Si-rich rocks (SiO_2>72 wt.%) the Mn content of apatite separates modern granitoids from the TTG suite.

These updated and improved trace-element tools for apatite inclusions in zircon provide additional information in provenance studies of detrital zircon. It can differentiate between source rocks of the TTG suite and modern intrusives, and provide estimates about their SiO_2 content.

[1] Jennings E. *et al.* (2011). *Geology*, 39, 863.

[2] Tollari N. *et al.* (2006). *Geochimica et Cosmochimica Acta*, 70, 1518.

Detrital rutile records the high-pressure history of orogenic belts

Storey C[1*], Marschall H[2], Enea F[1], Konrad-Schmolke M[3], Schertl H-P[4]

1 - University of Portsmouth, Portsmouth, U.K., *craig.storey@port.ac.uk 2 - Woods Hole Oceanographic Institution, Woods Hole, MA, USA 3 - University of Potsdam, Potsdam, Germany 4 - Institute of Geology, Mineralogy and Geophysics, Ruhr-University Bochum, Bochum, Germany

Laser Ablation Inductively-Coupled Mass Spectrometry has been used to analyse rutile grains from high-pressure metamorphic rocks and as detritus in river sediments draining their catchments. Associations based on the trace element signature of these rutiles have been made. Rutiles from high-pressure / low-temperature mica schists of the Sesia Lanzo Zone of the western Alps are strongly correlated with detrital grains from the main local catchment areas. Most of the detrital grains, based on Nb vs Cr concentrations, are from a meta-pelitic protolith, as expected. Using the Zr-in-rutile thermometer, a peak temperature at 541°C was obtained, which agrees well with the peak temperature calculated for the Sesia Lanzo Zone samples - 538 °C, and with previous published estimates (500-600 °C). This demonstrates the applicability of the Zr-in-rutile thermometer and the Nb vs. Cr discrimination diagram in blueschist-facies settings. The Dora Maira UH*P* metapelites show no overlap with sediments from the closest catchment areas (Varaita and Maira Rivers) on the Nb vs. Cr diagram. However, the Zr-in-Rutile thermometer clearly indicates the presence of a H*T* signature with a temperature peak of 728 °C in the Maira River that is close to the average value for the metamorphic rutiles - 694 °C. This might suggest that these rivers are not the catchment area of the UH*P* rocks from the Dora Maira Massif, or that the discrimination diagram has a limited applicability for the H*T* rocks. This study also examines the potential presence of H*T* granulite-facies metapelitic rutiles from the Ivrea-Verbano Zone in river sediments and of the Dora Maira gneisses and Monviso metapelites and metagabbros in order to provide better constraints on the main source rocks. Finally, detrital rutiles from the Po River, downstream from the confluence of all other examined streams, implies that blueschist-facies rutiles are predominant compared to (U)H*P*-H*T* grains. In turn, this may indicate that H*P*-L*T* metamorphic rocks have a lower preservation potential than their (U)H*P*-H*T* equivalents. In this case, records of H*P*-L*T* metamorphism in older orogens may best be sought in sediments eroded from that orogen and containing detrital rutile grains.

Broken Hill-type mineralisation in the Bushmanland region, South Africa

Theron S

Exxaro Resources, Pretoria, South Africa, salomon.theron@exxaro.com

The Aggeneys complex of Zn-Pb-Cu-deposits in the Northern Cape province of South Africa consists of a number of ore bodies and sub-economic mineral occurrences, including Black Mountain (Swartberg), Broken Hill, Gamsberg, and Big Syncline. Big Syncline is a sub-economic mineral occurrence, which is spatially very closely associated with the Broken Hill and Black Mountain deposits [1]. These Zn-Pb-Cu-deposits are all hosted by a metamorphosed banded iron formation (meta-BIF) horizon. Although this meta-BIF horizon is generally not more than one to two meters thick, it represents the main greenfield exploration target for other Broken Hill-type Zn-Pb-Cu-deposits throughout Bushmanland. The meta-BIF is easily recognisable within the larger siliciclastic sequence, but it is only part of a much thicker (up to 5 meters) metamorphosed exhalite horizon. This exhalite horizon is characterised by an enrichment in Fe, Mn, P, Ba, ±Ca-Mg, and where mineralised in Zn, Pb, Cu, Ag, ±Bi, ±Sb, ±Tl and ±Mo. This meta-exhalite horizon is, however, laterally and vertically inhomogeneous, and close to surface also overprinted by supergene weathering effects. The challenge is, thus, to distinguish the "fertile" metal-bearing parts of this horizon from the "barren" or "infertile" parts. A number of petrological tools, including geochemistry and mineralogy, have been developed to identify and target the more "fertile" parts of this laterally extensive meta-exhalite horizon.

The host sedimentary sequence has been metamorphosed to amphibolite-granulite facies, with minerals such as magnetite, Fe-Mn-Ca-garnet, Fe-Mn-amphibole, Fe-olivine, Fe-Mn-orthopyroxene, Fe-Mn-pyroxenoids, Fe-Mn-clinopyroxene, zincian spinels, zincian staurolites, barite, Ba-K-feldspars and Ba-micas characterising the meta-exhalite. The mineral chemistry of some of the resistate indicator minerals, such as garnet and spinel, is a powerful exploration tool. For example, the Mn-content of garnets increases in the ore horizon to 47 to 53 mol % spessartine. The garnet chemistry reflects the chemistry of the original host rocks, and it is known that the Mn/Fe ratio increases towards the ore body in many sedimentary hosted exhalative (SEDEX) deposits, e.g., McArthur-type [2].

Trace element chemistry, including rare earth element (REE) signatures, also proved to be very effective to distinguish between "fertile" and "barren" meta-exhalite horizons. The "fertile" meta-exhalite horizons are characterized by positive Eu anomalies, which reflect a hydrothermal signature, while the "barren" meta-exhalite horizons are characterized by positive Ce anomalies, which reflect a seawater signature [3]. Where mineralised, the "fertile" meta-exhalite horizons are also anomalous in other trace elements such as, Tl, Bi, As and Sb.

[1] Von Gehlen K. *et al.* (1983). *Mineralogical Magazine*, 47, 481-486.

[2] Large R.R. *et al.* (2005). Economic Geology 100th Anniversary Volume, 931-863.

[3] Thomson J. *et al.* (1984). *Geochim. Cosmochim. Acta*, 48, 1935-1948.

Current trends and future promise of rutile microgeochemistry

Zack T

University of Gothenburg, Gothenburg, Sweden. zack@gvc.gu.se

More than 50 years after the introduction of the ZTR index by Hubert [1], it is finally becoming apparent that not only zircon is an invaluable ultra-stable accessory mineral, but also the other siblings of this triplet. Concentrating on the capital letter R, a surprisingly large number of geochemical tools have been developed that are based on rutile, such as Zr-in-rutile thermobarometry, O isotope qtz-rt thermometry, Nb-Cr provenance indicators, and U/Pb thermochronology. In this review I would like to illustrate that most new applications were possible due to advances in analytical methods. For example, the somewhat surprising discovery that rutile is conductive, even under an intense O_2^+ beam [2] has opened up precise and accurate dating of low-U rutile, allowing dating now of mafic blueschist and rutile-bearing mineral deposits.

Given the fact that geochemistry-related instrument development is in full swing, one can be hopeful that this is an ongoing trend. In Gothenburg we have started to explore a new generation of collision-cell ICP-MS, which eliminates notorious interferences such as ^{204}Hg on ^{204}Pb, so that for rutile, common lead ^{208}Pb/^{204}Pb ratios can be measured simultaneously with radiogenic ^{207}Pb/^{206}Pb ratios. The relevance of such new analytical developments becomes apparent only after implementation and rigorous testing on a range of well-characterized rutiles.

Predicting the future of rutilology, it is safe to say that provenance studies will benefit significantly from U/Pb rutile dating, as rutile gives reliable information on the last metamorphic overprint of (a) source area(s). Furthermore, it is also safe to say that rutile in relation to mineral deposits has largely been neglected up-to-now, and promises a variety of information, considering that rutile can in some ore deposits clearly be linked to hydrothermal Ti-mobilization and in other mineralizations as originating from passive Ti-enrichment by leaching.

[1] Hubert (1962). *J. Sediment. Petrol*., 32, 440-450.

[2] Schmitt and Zack T. (2012). *Chem. Geol*., 332-333, 65-73.

Permeable sedimentary units as pipelines for basinal brine circulation in the Belt-Purcell Supergroup, Western North America: monazite, a mineral proxy for fluid characterization

Gonzalez-Alvarez I[1*], Kusiak M[2]

1 - CSIRO, CESRE, Minerals Down Under Flagship, Western Australia *i.gonzalez.alvarez@gmail.com 2 – Institute of Geological Sciences, Polish Academy of Science, Warsaw

Monazite has largely been used in geochronological studies of igneous and metamorphic rocks, and ore deposits, frequently linking diverse fluid-flow alteration history to a range of tectonothermal events. However, studies of the diversity of monazite chemical compositions associated with fluid-flow at low temperatures and basinal brine circulation are scarce, due to the difficulty of isolating single monazite grain generations as representative of distinct fluid events.

This study describes the chemical composition of monazite grains from permeable sandstone units in the Grinnell Formation of the Belt-Purcell Supergroup (BPS), Western North America, to evaluate their efficacy as a proxy for describing the characteristics of basinal brine circulation along these regional -scale pipelines.

The Mesoproterozoic Belt-Purcell Supergroup is a dominantly siliciclastic sedimentary succession of ca. 1.47-1.40 Ga that records ~70 Myr of depositional history, with a thickness of ~17 km. Samples for this study were collected from sandstone units of the Ravalli Group, dominantly composed of fine-grained siliciclastic facies, with interbedded units of medium to coarse sandstone, which become more abundant towards the upper part of the sequence. These facies are interpreted as prograding alluvial aprons.

Two monazite populations have been described in the BPS: the first has detrital textures, with ages >1.4 Ga, comparatively lower ΣLREE/ΣHREE, and higher ThO_2 and Y contents; whereas the second has euhedral textures, post-depositional ages up to ~1 Ga, and lower ThO_2 and Y, but higher ΣLREE/ΣHREE than their detrital counterparts. This second population is interpreted to be the result of post-depositional alteration due to episodic circulation of alkaline oxidizing basinal fluids, mainly circulated within the most permeable sandstone units of the basin.

In addition to the above, post-depositional monazite grains collected for this study from the most permeable sandstone units record significant fractionation as evident in La/Pr, Pr/Nd and La/Nd ratios (ranging from 1.2 to 3.6, 0.3 to 0.5 and from 0.35 to 0.55 respectively), enrichment of MREE with reference to their detrital counterparts, together with <1 wt% ThO_2. A sub-population of monazite-(Nd) grains displays an unusual Nd/La ratio > 3 and Nd/Ce of 0.8-1.6. EMPA chemical ages calculated for all sampled post-depositional monazite grains using a Th-Pb mean age cluster at ~0.9 Ga.

A lack of allanite in the permeable basinal units suggests a fluid with low Ca content - even if limestone units are present in the stratigraphy; whereas Nd/Ce ratios ranging from 0.8 to 1.6 support oxidizing conditions for the crystallization of monazite within. Fluid pH remains a challenge to be addressed from the data collected.

The chemical composition of the post-depositional monazite grains is consistent with oxidizing basinal brine conditions that are geochemically fingerprinted in the whole sedimentary sequence of the BPS. The age clustering at ~0.9 Ga suggests a major event that overprinted previous fluid flow events recorded by post-depositional monazites in other sedimentary units. A major tectonothermal event that reactivated the basinal brines and pumped the fluids through the Ravalli Group is inferred. However, the link of this event with regional tectonic events remains unclear.

NH_4-bearing tourmaline: experiments and natural occurrences

Wunder B[1], Berryman E[1,2*], Rhede D[1], Koch-Müller M[1], Plessen B[1], Heinrich W[1]

1 - GFZ Potsdam, Potsdam, Germany, *berryman.eleanor@gmail.com 2 - TU Berlin, Berlin, Germany

Experimental studies have shown that under UHP metamorphic conditions dravitic tourmaline is able to accommodate high concentrations of potassium of at least 0.7 K pfu [1] and therefore can potentially serve as a geobarometer. Indeed, dravite with up to 0.58 K pfu was recently reported in the UHP metamorphic rocks from the fossil subduction zone in the Kokchetav Massif, Kazakhstan [2]. In addition, it is well known that most K-bearing silicates can incorporate high amounts of nitrogen in the form of ammonium (NH_4^+) in their structures due to the similar ionic radius of K^+ and NH_4^+ [3] The association of K-dominant tourmaline with deep subduction raises the question if tourmaline may also represent a carrier of nitrogen (as NH_4^+) into the deep Earth.

To investigate tourmaline's ability to incorporate NH_4^+, we conducted piston-cylinder experiments in the system $(NH_4)_2$-MgO-SiO_2-Al_2O_3-B_2O_3-H_2O at 4.0 GPa, 700 °C, with 5-day run durations, producing an assemblage of tourmaline, phengite and coesite. The synthesized tourmaline crystals were up to 10 x 40 microns in size. Their compositions were determined by EMP and the average structural formula following normalization to 15 cations in the Y, Z and T sites is: $^{X}((NH_4)_{0.1(Vac)0.9})^{Y}(Mg_{2.3}Al_{0.7})^{Z}(Al_{5.9}Si_{0.1})^{T}(Si_6O_{18})(BO_3)_3(OH)_4$. The analysis of various characteristic stretching and bending bands in IR-spectra of hand-selected single-crystal tourmaline pressed into a thin film provides further evidence for the structural incorporation of NH_4 in tourmaline.

It is well established that in eclogite facies metasediments nitrogen in the form of NH_4 is mainly bound in micas, where concentrations reach up to a few thousand ppm [4, 5]. However, to the best of our knowledge, the occurrence of nitrogen in tourmaline is yet to be reported. We therefore investigated a NH_4-bearing (400 ppm NH_4, whole rock) mica schist from a high pressure and low temperature (> 1.2 GPa/550 °C) unit of the Erzgebirge, Germany, interpreted as metasediments that underwent deep subduction during the late Variscan orogeny [5]. In these rocks, tourmaline coexists with biotite, phengite, quartz, chloritoid, and garnet. Careful EMP analyses show that tourmaline, along with biotite and phengite, contains significant amounts of nitrogen. The NH_4 concentrations in the three main NH_4-bearing phases are: biotite (~1500 ppm) > phengite (~700 ppm) > tourmaline (~500 ppm). In the large-scale, long-term cycling of light elements between the crust and the deep Earth, tourmaline is an important carrier of nitrogen, as well as boron.

[1] Berryman *et al.* (2014). Synthesis of K-dominant tourmaline. *American Mineralogist*, 99, 539-542.

[2] Shimizu and Ogasawara (2013). Diversity of potassium-bearing tourmalines in diamondiferous Kokchetav UHP metamorphic rocks: A geochemical recorder from peak to retrograde metamorphic stages. *Journal of Asian Earth Sciences*, 63, 39-55.

[3] Watenphul *et al.* (2009). High-pressure ammonium-bearing silicates: Implications for nitrogen and hydrogen storage in the Earth´s mantle. *American Mineralogist*, 94, 283-292.

[4] Busigny *et al.* (2003). Ammonium quantification in muscovite by infrared spectroscopy. *Chemical Geology*, 198, 21-31.

[5] Mingram and Bräuer (2001). Ammonium concentration and nitrogen isotope composition in metasedimentary rocks from different tectonometamorphic units of the European Variscan Belt. *Geochimica et Cosmochimica Acta*, 65, 273-287.

X-ray diffraction topography images of Colombian trapiche emeralds

Agrosì G[1], Pignatelli I[2*], Giuliani G[2], Ohnenstetter D[2], Mathieu S[3]

1 - Università di Bari 2 - CRPG-CNRS *isabella.pignatelli@univ-lorraine.fr 3 - SCMEM Université de Lorraine

The trapiche texture of Colombian emeralds takes its name from a similarly shaped crushing gear used in sugar cane production [1]. Trapiche texture shows a central core surrounded by several trapezoidal or triangular growth sectors. Boundaries with complex composition separate the growth sectors and can intersect at a central point if the core is not developed. The dark appearance of these boundaries is due to the presence of organic matter [2] sourced from the Lower Cretaceous black shales in the western border of the Eastern Cordillera basin, where trapiche emeralds occur [3]. Variations in trapiche textures [3, 4] and formational mechanisms [5] are not well understood and still debated. In this study, three cross-sections cutting perpendicular to the *c* axis of trapiche emeralds from the Muzo mine were studied. For the first time, X-ray diffraction topography was used to analyse the distribution of structural defects and to characterise them to better understand trapiche emerald formation. The preliminary results reveal consistent crystallinity between arms and hexagonal core. The simultaneously diffraction contrast of the slices was interrupted only by fractures that misaligned different crystalline portions. The topographs obtained with diffraction vectors *hk*0 show bundles of dislocations that run perpendicularly to the prismatic growth fronts and nucleating from the surrounding boundary of the hexagonal core. The boundaries between the growth sectors and the hexagonal core are always out of contrast. The core becomes, instead, visible on topographs obtained with diffraction vectors inclined to the *c* axis. The implications of X-ray diffraction topography images in the formation of the trapiche emerald are discussed in the context of Colombian emerald deposits genesis [6]. The role of fluid chemical composition, the host-rock interaction, the compressive-tectonic style of the emerald-related veins, and breccia is discussed in terms of physico-chemical mechanisms responsible for the development of the trapiche texture.

[1] McKague (1964). *Gems and Gemmology*, 11, 210-213 and 223.
[2] Muñoz (1948). Emeralda di Colombia, Bank of the Republic of Colombia, Bogota, Colombia, p. 122-123.
[3] Ohnenstetter *et al*. (1998). in L'émeraude, Association Française de Gemmologie, Paris, p. 119-124.
[4] Nassau and Jackson (1970). *American Mineralogist*, 55, p. 416-427.
[5] Sunagawa *et al*. (1999). *Journal of crystal growth*, 206, p. 322-330.
[6] Branquet *et al*. (1999). in Fractures, fluid and mineralisation: Geological Society, London, Special Publication 155, p. 183-195.

Near-colorless CVD and HPHT synthetic gem diamonds – quality advances and identification methods

D'Haenens-Johansson U F S*, Breeding C M, Wang W

Gemological Institute of America *ujohansson@gia.edu

The majority of commercial laboratory grown diamond manufacturers focus their efforts on synthesizing diamond material solely for industrial applications. Nevertheless, limited numbers of synthetic diamonds grown using either the high pressure, high temperature (HPHT) or chemical vapor deposition (CVD) methods began to appear in the gem market in beginning of the 1990s. Unlike the natural diamond gem trade, which is dominated by D - Z colored products, the samples introduced to the early synthetic diamond trade were generally distinctly colored, with typical HPHT synthetics being either blue or yellow while CVD synthetics were usually brown. These colors arise from the presence of different impurities, which readily incorporate into the material during the growth process by dopants introduced intentionally or by contamination. The stringent restrictions placed on the impurity content for the production of near-colorless material meant that it was only in the most recent years, through technological advances coupled with an improved understanding of the chemical processes occurring during synthesis, that growers have been able to gain sufficient control to commercially synthesize colorless and near-colorless specimens with gemological properties comparable to top-quality natural diamonds in popular sizes up to about 2 ct. Additionally, post-growth treatment of CVD synthetics by HPHT annealing has been found to reduce the concentration of brown-color producing defects, further facilitating the fabrication of colorless diamond material. In order to protect the integrity of the diamond certification process it is imperative that the GIA characterize a varied and populous suite of synthetic diamonds and develop identification criteria to effectively distinguish them from their natural counterparts. In this study, colorless and near-colorless CVD synthetic diamonds provided by Gemesis Corp. and Scio Diamond Technology Corp. in addition to HPHT synthetics by the AOTC Group (totaling 16, 19, and 40 samples, respectively) have been investigated using a combination of gemological and spectroscopic testing techniques including FTIR absorption, photoluminescence, microscopy and DiamondView fluorescence imaging. Through the methods that will be outlined these synthetic diamond products can be unequivocally recognized as laboratory grown.

The Fiskenaesset gemstone district, SW Greenland – a new source of ruby and pink sapphire

Fagan A*, Groat L

1 - University of British Columbia *afagan@eos.ubc.ca

The gem corundum deposits of southwest Greenland have received little scientific attention to date. The main deposits lie within several lithologically similar trends adjacent to the coastline approximately 120 km south of the capital, Nuuk. Over 60 individual corundum showings have been recorded at surface by Government agencies and industry exploration programs since the 1960's. At present the Fiskenaesset Gemstone District's flagship Aappaluttoq deposit hosts over 400 million carats of corundum within 65 m of the surface; the project has received a 30-year mine licence from the Greenland Government and gemstone sales are expected in 2014.

The gem deposits are hosted in the Archean (2970 Ma) aged Fiskenaesset Anorthosite Complex. This layered igneous intrusion spans several hundred kilometres across southwest Greenland and forms part of the North Atlantic Craton. The Aappaluttoq deposit is hosted within the Middle Gabbro stratigraphic sequences and lies along the contact zone between a meta-leucogabbro and meta-melanogabbro. Each unit is distinctive in its mineralogy and structure, with the essential chromophore (Cr) probably mobilized from the nearby ultramafic units. Regional to local scale metamorphism and metasomatism appear to be at least partially responsible for the formation of the deposits. Regional prograde granulite facies metamorphism and the metasomatism connected to the amphibolite facies retrogressive cooling can be observed in mineral assemblages throughout the area.

This study will present new geological mapping, major and trace elemental geochemical and geochronological data, and oxygen isotope compositions from the corundum and the various unusual host assemblages. The host rocks, fluids and metamorphic/metasomatic conditions encountered are very different to the traditional gem corundum settings in other parts of the world, and few analogous deposits are known to exist. This makes the study of these deposits important from both an academic and an economic perspective. Further work is still required to evaluate and understand the link between the regional metamorphism and the formation of the gem corundum deposits.

Oxygen isotope and trace element evidence for the origin of sapphire and/or ruby in the Mbuyi-Mayi kimberlite (DRC) and the Changle alkali basalt (China)

Giuliani G[1,2*], Fallick A[3], Pivin M[4], Demaiffe D[4], Ohnenstetter D[2]

1 - GET/IRD 2 - CRPG/CNRS *giuliani@crpg.cnrs-nancy.fr 3 - SUERC

4 - Université Libre de Bruxelles

Xenocrysts of sapphire in Miocene basalts from Changle, Shandong peninsula, eastern China, and ruby and sapphire from the Upper Cretaceous Mbuyi-Mayi kimberlite in the Archean Congo-Kasai Craton, Democratic Republic of Congo, were studied to trace their primary sources. Blue, and yellowish to brown sapphires from Changle have $\delta^{18}O$ 4.5 to 5.65 ‰, mean 5.0 ± 0.3‰, n= 10, that falls within the worldwide range defined for BGY-magmatic sapphires related to basaltic fields (3 <$\delta^{18}O$ <8.2‰, n=150; mean 5.8 ± 1.2 ‰). It overlaps also the range defined for magmatic sapphires in syenite (4.4 <$\delta^{18}O$ <8.3‰, n=29; mean 6.8 ± 1.4 ‰). The inclusions of columbite-group minerals, Nb-bearing rutile, and the chemistry of the sapphires characterized by a lack of Cr, high Ga (>150 ppm), high Fe (8000 <Fe <14500 ppm), and low Mg (< 20 ppm), confirm their magmatic source with a clear mantle derivation. The sapphire-bearing syenite was intruded by the alkali basalt and the xenocrysts were transported to the surface.

The $\delta^{18}O$ of 13 corundum samples from the kimberlite spans 4.3 to 5.6‰. Pinkish to greyish sapphires have $\delta^{18}O$ 4.3 to 5.4‰ (mean $\delta^{18}O$ = 4.9 ± 0.4%, n= 10). They fit the $\delta^{18}O$ range of the sapphires from Changle but differ totally in their inclusions of the Mn ilmenite group, rutile and muscovite, and their low Fe content (< 6200 ppm) as well as the presence of Cr between 2500 and 6200 ppm. The Cr-sapphires indicate a source equivalent to that of the pink sapphires associated worldwide with mafic and ultramafic rocks (1.25 <$\delta^{18}O$ <6.8‰, n=21). The three Cr-rich rubies (up to 38400 ppm) with $\delta^{18}O$ 5.5 to 5.6‰ (n=3), mean 5.55 ± 0.0.5‰ indicate clearly the mantle-derivation with no substantial variation. The isotopic range corresponds to that of ruby carried by alkali-basalts (1.25 <$\delta^{18}O$ <5.9‰, n= 80). The ruby is the relic of a mafic lithology in the lowermost crust or upper mantle of cratons crosscut by the kimberlites.

Gemstones in Kenya: typology and geological setting

Ichangi D[1*], Giuliani G[2,3], Martelat J[4], Wamunyu A[5], Nyamai C[5]

1 - University of Nairobi *dwichangi@yahoo.com 2 - GET/IRD 3 - CRPG/CNRS

4 - University of Lyon 5 - University of Nairobi

Gemstones in Kenya belong to the East African gemstone province, which is now recognized as one of the richest gemstone-bearing areas in the world. The Kenyan gemstones represent a wide and varied typology whose geologic setting is similar to those of neighbouring Tanzania, and more distant Sri-Lanka and Brazil, which share similar geology and which were once part of the Supercontinent Gondwanaland which began its break-up during the Triassic-Jurassic times. Although the formation of gemstones in Kenya is closely related with collisional tectonics and metamorphism during the Proterozoic times, these gemstones in Kenya occur in two distinct environments. The first environment consists of lithologies of the high metamorphic grade Neoproterozoic (Pan-African) Mozambique Orogenic Belt with an array of characteristic gemstones. The second environment consists of Paleogene-Neogene basaltic volcanics in the Northern and Central Kenya Rift regions. More specifically, the occurrence of gemstones in Kenya is related mainly to four (4) geologic settings. The first setting involves desilication of granitic pegmatites or gneisses by adjacent ultramafic bodies leading to the formation of ruby and sapphire (corundum), spinel, alexandrite and tourmaline. The second setting involves high grade metamorphism of closely associated limestones, graphitic gneisses and schists, and calc-silicate gneisses leading to the formation of the characteristic tsavorite (green) garnet. The third setting involves the emplacement of typical coarse grained complex lithium and beryllium rich granitic pegmatites, which produce pegmatite-associated gemstones such as beryl, so far mainly aquamarine, and also amethyst. The fourth setting involves the relatively young basaltic volcanics, which are known to host sapphire and ruby. These basaltic lavas are associated with Rift related Paleogene-Neogene magmatism associated with the formation of the Kenya Dome and associated East African Rift System (EARS). These basaltic volcanic are interpreted to have transported the gemstones to the surface from the underlying Neoproterozoic Mozambique Mobile Belt Basement.

Emeralds from Itatiaia (Minas Gerais, Brazil)

Karampelas S[1*], Schnellrath J[2], Schwarz D[3], Scholz R[4], Gubelin S[1], Link K[1], Azzaro A[5]

1 - Gubelin Gem Lab *s.karampelas@gubelingemlab.ch 2 - Centro de Tecnologia Mineral, Rio de Janeiro, Brazil 3 - Asian Institute of Gemological Sciences, Bangkok, Thailand 4 - Universidade Federal de Ouro Preto 5 - Universidade Federal do Rio de Janeiro, Brazil

Brazil, Colombia and Zambia are today the three most important gem quality emerald producing countries. Emeralds were first discovered in Brazil at the start of the 20th century; however, gem quality occurrences were not identified until the middle of the century. Currently, most gem quality emeralds in Brazil are mined at Itabira in the Nova Era region of Minas Gerais. Recently, gem quality emeralds were also identified in Minas Gerais, in the Itatiaia mine in the southern part of the Conselheiro Pena pegmatite district (CPPD). The pegmatite body is hosted by a quartz-biotite-garnet schist with local intercalations of calc-silicate and ultramafic rocks. The emerald mineralization occurs near the contact between the phlogopite schist and the pegmatite. Locally emerald crystals also occur in a talc schist. Rough emeralds are usually less than a cm, but crystals up to 5.5 cm are present; most samples show a colourless core. Several stones >2 carats were faceted, varying from a light green to a bluish green colour. Microscopically, the samples present numerous fluid inclusions and growth structures. Mineral inclusions of phlogopite, chlorite, apatite, zircon, pyrite, uraninite, tourmaline, nickeline, gersdorffite and quartz were identified. The emeralds contain high concentrations of alkalis (Li: 1180 to 1450 ppm, Na: 12300 to 13500 ppm, K: 280 to 550 ppm, Rb: 80 to 130 ppm, Cs: 1460 to 3650 ppm) as well as other elements such as Mg (12000 to 17000 ppm), Ca (35 to 120 ppm), Sc (25 to 65 ppm), Ti (60 to 80 ppm), Mn (10 to 40 ppm), Co (1 to 2 ppm), Ni (5 to 10 ppm), Zn (30 to 50 ppm), Ga (10 to 14 ppm), Rb (90 to 120 ppm) and Sn (0.8 to 1.5 ppm). The colour is principally due to chromium (1130 to 3310 ppm) and iron (1395 to 3100 ppm) with only limited quantities of V (35 to 60 ppm) detected. Itatiaia emeralds are associated with highly evolved pegmatites, similarly to Zambian (Kafubu) emeralds and different from emerald at Itabira. Current work in the area is concentrating on delimiting the extent of this new emerald mineralization.

Amphibole related rubies from Mozambique: a revolution in the ruby trade

Pardieu V

GIA Laboratory. vpardieu@gia.edu

Historically, most of the gem quality rubies found in the trade before the end of the 20th century were mainly coming from two types of deposits, i.e., marble such as those from Myanmar and related to the Himalayan orogen, and Cenozoic alkali-basalts from East Asia and Africa. In November 2006 the discovery of a ruby deposit near Winza, in Tanzania, was a key event as, within few months, several very significant high quality rubies were mined from amphibolites. During summer 2007 some rubies from Northern Mozambique were presented to foreign gem merchants in Winza. The new high quality rubies were mined in amphibolites from a remote illegal site inside the Niassa National Reserve. In May 2009 the deposit of Montepuez was discovered. As the authorities closed the illegal mining site in Niassa during summer 2009, most of the miners moved to Montepuez. The area was soon stormed by thousands of illegal miners. Currently the deposit is exploited by the Gemfields Company on an area about 400 square kilometres. Mining in Montepuez was easy as rubies in amphibolites are found either in primary or secondary deposits just digging a few meters in soft ground or weathered rocks.

In Thailand, the world capital of the ruby trade, if before the discovery of Montepuez, most of the rubies available in the market were coming from Myanmar, within a year most of the rubies available were coming from Mozambique. The quality of the finest Mozambique stones is excellent. For the stones that are not naturally fine enough to be traded only after cutting and polishing, Thai ruby burners successfully developed efficient heat treatment techniques using heat only, flux healing and lead glass to bring to the mark*et al*l the stones. Nowadays rubies in amphibolites originating from Mozambique are supplying the worldwide market from commercial (treated) grade to fine untreated gems.

Geological setting, geochemistry, and genesis of tsavorite deposits associated with graphitic gneisses in the Davis Mine, Mwatate (Taita Taveta region, Kenya)

Wamunyu A[1], Ichangi D[1*], Nyamai C[1], Giuliani G[2,3], Martelat J[4]

1 - University of Nairobi *dwichangi@yahoo.com 2 - GET/IRD 3 - CRPG/CNRS 4 - University of Lyon

The Davis Tsavorite Mine is geologically located within the Neoproterozoic Metamorphic Mozambique Belt in the Mwatate area of the Taita Taveta region, South East Kenya. The Lualenyi Member in the Mgama-Kuranze area hosts open pit Lualenyi Tsavorite Mines, including the Davis Tsavorite Mine, itself located on Kide Hill in the Mgama Ridge. The Davis Mine has two active mine pits referred to as Pit 2 and Pit 3 which have two and five tsavorite mineralization horizons respectively, consisting of graphitic gneiss, graphitic schist and calc-silicates. Tsavorite occurs as nodules in boudins within the host horizons in both pits. Samples from the Mine show that it is on a continental margin (0.5-5.5 for Na_2O/Fe_2O_3 and 2-14.4 for K_2O/CaO) with turbidite sequences (0.1-0.4 for Na_2O/Fe_2O_3 and 0.5-1.5 for K_2O/CaO). Na_2O-Fe_2O_3 ratio with increasing SiO_2 content is low at 0.1. Chondrite-normalized REE patterns show La/Yb (3.3-17.1) ratios for host rock and La/Yb (8.9-12.3) ratios for tsavorite, with a negative steep Eu anomaly. La/Yb and Gd/Yb ratios are used simultaneously to determine sediment REE enrichment. The high chondrite-normalized La/Yb ratios and Gd/Yb (1.0-1.8 for host rock and 1.1 and 1.7 for tsavorite) indicate LREE sediment enrichment, which is consistent with active continental crust values in the post-Archean record. In mineralized nodules, tsavorite is composed of 0.6-2.4 wt% V_2O_3 and the V/Cr ratios range from 3.1-4.3. These V/Cr ratios are lower than worldwide deposits of Tanzania, Madagascar, and Pakistan (V/Cr ratio›5.8) but higher than the local Kenyan mines from the Mgama mining district (V/Cr ratio<1). The Davis Tsavorite Mine is interpreted to be in an active continental crust environment of sedimentary origin and the tsavorites were formed in metasedimentary facies.

Carbon isotope analysis of CVD synthetic gem diamonds

Wang W[1*], D'Haenens-Johansson U F S[1], Smit K[1], Breeding C M[1], Stern R[2]

1 - Gemological Institute of America *wwang@gia.edu 2 - University of Alberta

During the past decade, the quality of single-crystal synthetic diamond grown by Chemical Vapor Deposition (CVD) has improved significantly [1, 2]. In recent years, many CVD synthetic diamonds have been introduced to the diamond jewelry market, generating tremendous concern. The ability to confidently separate these synthetic diamonds from natural ones is critical for consumer confidence. Current identification methods focus on optical properties, including types and concentrations of impurities or combinations of impurities and their distribution in the diamond lattice. This approach has proven very successful for separating CVD synthetics from HPHT synthetics and natural diamonds. However, continuous improvement of CVD growth technology and, in particular, post-growth treatments introduces new identification challenges. In an effort to proactively confront these challenges, we present a preliminary evaluation of carbon isotope analysis as a tool for comparison of CVD synthetic diamonds with natural ones.

Nineteen CVD synthetic diamonds from three manufacturers (Gemesis=7; Scio=11; Element Six=1) were analyzed by SIMS using the Cameca IMS1280 Ion Probe in the Canadian Center for Isotope Microanalysis at the University of Alberta. All samples were carefully polished with a large flat surface, on which 5 to 10 spots were analyzed for each crystal. Unlike natural diamonds, which typically show heterogeneous carbon isotope distributions, the CVD synthetic diamonds exhibited very homogeneous isotope compositions (Figure 1). The standard deviation among multiple analyses on each sample was less than 0.6‰, which is close to the instrument analytical uncertainty. Carbon isotope compositions ($\delta^{13}C$) of CVD diamonds from Scio were in the range -35 to -45‰, whereas samples from Gemesis were -55 to -75‰. The single sample from Element Six was -63.7‰, consistent with the Gemesis range (Figure 1). These results strongly suggest that CVD synthetic diamonds are much lighter in carbon isotope composition than natural diamonds [3], which occur in the range $\delta^{13}C$ = -10 to 0‰ (peridotitic) or extend to values as low as -30‰ (eclogitic). Effectively, no overlap is observed in carbon isotope chemistry between natural and CVD diamonds. In combination with the homogenous distribution of carbon isotopes in CVD diamonds, this separation in $\delta^{13}C$ values could be a very useful feature for separating natural diamonds from CVD synthetics. In addition, very large differences were revealed between CVD diamonds from different manufacturers, as well as among CVD diamonds from the same manufacturer. Variations in the carbon-containing gas chemistry or growth conditions (pressure and temperature) may have contributed to the observed fractionation of carbon isotopes.

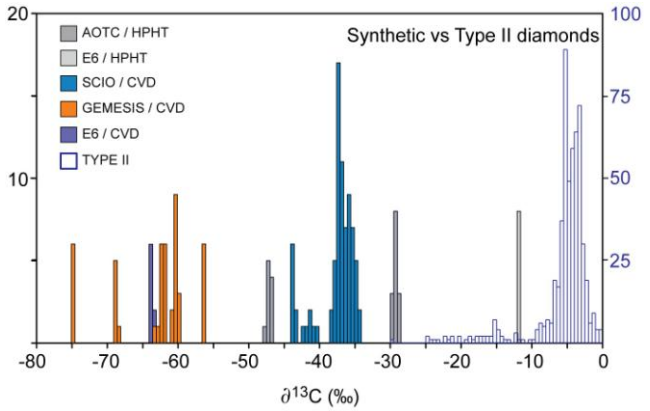

Figure 1: Distribution of carbon isotope measurements for synthetic and natural type II diamonds.

[1] Martineau P.M., Lawson S.C., Taylor A.J., Quinn S.J., Evans D.J.F. and Crowder M.J. (2004). Identification of synthetic diamond grown using chemical vapor deposition (CVD). *Gems &Gemology*, 40, 2-25.

[2] Wang W., D'Haenens-Johansson U.F.S., Johnson P., Moe K.S., Emerson E., Newton M.E. and Moses T.M. (2012). CVD synthetic diamonds from Gemesis Corp., *Gems &Gemology*, 48, 80-97.

[3] Stachel T., Harris J.W. and Muehlenbachs K. (2009). Sources of carbon in inclusion bearing diamonds. *Lithos*, 112S, 625-637.

Characterization of gem diamonds from Eastern Zimbabwe

Breeding C M*, Wang W

Gemological Institute of America *christopher.breeding@gia.edu

Since 2006, the Marange diamond fields in eastern Zimbabwe have produced large quantities of diamonds, many of which have entered the gem diamond markets. In 2013, the total production from the area was estimated to account for more than 10% of the global supply of rough diamonds. The diamonds recovered from the alluvial deposit are unique and interesting. In an effort to characterize them, we employed observational microscopy, absorption spectroscopy (IR, UV-Visible-NIR), luminescence spectroscopy (photoluminescence, Raman), and imaging techniques (UV fluorescence, crossed polarizing filters).

The rough stones are typically octahedral in shape and covered by dark brown staining. Upon cleaning, abundant green and brown colored spots cover the usually strongly etched and pitted surfaces of the diamond crystals. These spots are evidence of natural radiation damage to the diamond lattice, most likely caused by interaction with crustal fluids in the alluvial diamond deposit. The staining and spots lend distinctive green and brown color components to the otherwise near colorless to yellow body colors of most of the diamonds. Distinctive, patterned clouds of minute inclusions were also observed in most of the diamonds.

Infrared absorption spectroscopy revealed that the vast majority of diamonds from eastern Zimbabwe are type Ia with abundant aggregated nitrogen impurities. In addition, significant hydrogen impurities were detected in the diamonds. UV-Visible-NIR absorption spectroscopy indicated that the diamonds had undergone varying levels of radiation damage and natural annealing during residence in the alluvial environment. The observed combination of elevated hydrogen impurities and natural radiation damage features is somewhat characteristic of these diamonds, but is not quantifiable to the level of being useful as a reliable indicator of geographic origin. Additional spectroscopy features, including those revealed by photoluminescence analysis and fluorescence imaging are being investigated to evaluate their usefulness in identifying these natural diamonds. Once fully faceted to gemstones, many of the distinctive surface features of eastern Zimbabwe diamonds are removed, leaving only spectroscopy data for evaluation.

Petrology, geochemistry and genesis of tsavorite deposits associated with graphitic gneiss and calc-silicate rocks from Lemshuku and Namalulu, Tanzania

Feneyrol J[1], Giuliani G[1,2*], Ohnenstetter D[1], Fallick T[3], Demaiffe D[4], Monie P[5]

1 - CRPG/CNRS *Giuliani@crpg.cnrs-nancy.fr 2 - GET/IRD 3 - SUERC 4 - Université Libre de Bruxelles 5 - Géosciences Montpellier

Tsavorite, the gemmological trade name for the vanadian green grossular, is hosted by graphitic gneisses or calc-silicates, often associated with dolomitic marbles, and belonging to the Metamorphic Neoproterozoic Mozambique Belt (1000-540 Ma). The green grossular is today mined only in south-eastern Kenya, north-eastern and south-eastern Tanzania, and southern Madagascar. It has been sporadically exploited in the Swat Valley in Pakistan and is known from the Sør Rondane Mountains in East Antarctica [1]. Tsavorite is found either: (i) in primary deposits as nodules or within quartz veins crosscutting metasedimentary host-rocks; or (ii) in placers mined in Tanzania. In the primary deposits, tsavorite is always contained within graphitic gneiss and calc-silicates with intercalations of marble, which suggests a lithostratigraphic control over mineralization.

Study of the Lemshuku and Namalulu deposits in Tanzania has shown that the metamorphism of organic matter-rich and evaporite-rich sedimentary protoliths occurred at P = 7.0 ± 0.4 kbar and T = 677 ± 14°C, at 634 ± 22 Ma (U-Th-Pb dating on monazite). The metamorphic series cooled at around 500 Ma (^{40}Ar-^{39}Ar dating on muscovite). Two metasomatic stages are linked to formation of tsavorite: (i) diffusion metasomatism forming nodules at P = 5.0-7.4 kbar and T = 580-691°C; (ii) calcitic infiltration metasomatism forming quartz veins at P = 3.6-4.9 kbar and T = 505-587°C. The latter has been dated *in situ* by Sm-Nd at 606 ± 36 Ma. Continental evaporites, deposited in a coastal marine sabkha with (Si, Ca)-bearing sediments, transformed into tsavorite in the case of the nodules. The mineralisation is controlled by lithostratigraphy and structure. The mineralogical study of tsavorites suggests a new protocol to certify their geographical origin, based on the V/Cr ratio, Mn content and δ^{18}O.

[1] Feneyrol J., Giuliani G., Ohnenstetter D., Fallick A.E., Martelat J.M., Monié P., Dubessy C., Rollion-Bard Cl., Le Goff E., Malisa E., Rakotondrazafy A.F.M., Pardieu V., Kahn T., Ichang'i, D., Venance E., Voarintsoa N.R., Ranatsenho M., Simonet C., Omito E., Nyamai C. and Saul M. (2013). Worldwide tsavorite deposits: new aspects and perspectives. *Ore Geology Reviews*, 53, 1-25.

Emerald mineralization at the Anuri prospect, Nunavut, Canada

Groat L[1*], Brand A[1], Cempirek J[1], Kleespies P[2]

1 - University of British Columbia *groat@mail.ubc.ca 2 - North Country Gold Corp.

Emerald has been identified in seven intervals from three drill holes at the Anuri Au and Ag prospect, which is located ~410 km N of Rankin Inlet in Nunavut. The prospect is within the Committee Bay Greenstone Belt, which forms part of the Rae domain of the western Churchill province. The emerald occurs in rocks of the Neoarchean volcano-sedimentary Prince Albert Group, primarily in an altered komatiite with a texturally and mineralogically variable matrix of phlogopite, muscovite, actinolite, plagioclase (≤0.2 *pfu* Ca), pyrite and occasional quartz, calcite, and accessory minerals such as fluorapatite, titanite, rutile, chalcopyrite, molybdenite and rare tellurides. The emerald (and colorless beryl) can occur in quartz veins, at contacts, and potentially as a hydrothermal overprint. Electron probe microanalysis shows that the dominant chromophore is Cr (with essentially no V), with a maximum content of 2.62 wt% Cr_2O_3 or 0.20 Cr *pfu*. The emerald also contains unusually high concentrations of Na (maximum 2.66 wt.% Na_2O, or 0.49 Na *pfu*), Mg (to 3.41 wt.% MgO, or 0.48 Mg *pfu*), and Fe (up to 1.99 wt.% FeO, or 0.16 Fe *pfu*). Micas are represented by F-rich phlogopite and fluor-phlogopite (X_{Mg} ~ 0.8) and muscovite with elevated aluminoceladonite component (~30 mol%). Amphiboles range between tremolite and ferri-magnesiohornblende, and are enriched in F and Na (0.2-1.2 *pfu* F; ≤0.42 *pfu* Na). Titanite has elevated contents of F and Al (F ≤ 0.17 *pfu*, Al ≤ 0.14 *pfu*). The source of the Be, F, and Na-bearing fluids is likely a nearby 2718 Ma tonalite [1] which intrudes the komatiites.

We will also report on recent efforts to apply geochemical (e.g. Na/K >1) and structural criteria (e.g. tear faults) developed to explore for emerald in Colombia to similar rocks in northwestern Canada.

[1] Skulski *et al*. (2003). Geological Survey of Canada, Current Research C22.

Conditions for the formation of crystalline colored gemstones (CCGs)

Saul J M

ORYX. john.saul@wanadoo.fr

Transparent, crystalline colored gemstones (CCGs) exist as a naturally-occurring group. Approximately fifty mineral species with hardness H >6, from andalusite to zoisite, are included. The cut-off at H = 6 is arbitrary. Excluded from the definition of CCGs are transparent quartz, diamond, blue-green-yellow sapphires, gem beryl and topaz associated with Rapakivi granites, emerald and alexandrite associated with massive mica, and San Carlos type peridots, all of which are special cases [1].

The oldest known CCGs crystallized in Pan-African times, approximately 650 Ma ago. With few exceptions, deposits of CCGs are located somewhat inland of former continent-to-continent collision zones. These orogenic zones are characterized by nappes, and deposits of CCGs are confined to highest levels in uppermost nappes, where the pressure was locally lowest. The host rocks of primary CCG deposits commonly emit an "organic" smell when hammered or sawn, as do certain included gems when they are worked in the lapidary. The smell is attributable to accumulations of gases in localized low-pressure zones associated with folding and boudinage and other structural features, and in cases, also in association with the mobilization of evaporites.

The oblique collisions between continental plates may permit minerals to crystallize in a transparent "gemmy" manner [1]. In such collision zones, high pressure and high temperature are both produced at points along plate contacts. But whereas pressure decreases in a uniform manner, heat flows as a fluid. In consequence, small 3-D zones come into being with normal pressures but elevated temperatures. In such instances, crystallization occurs at higher than usual temperatures, hence, at lower than usual pressures. In places where lowered constraining pressure is combined with facilitating features such as folds and boudins, gem-quality crystallization may take place. The presence of fluxes from evaporite minerals may also facilitate high quality crystallization, and in cases may be essential. Low pressure causes concurrent accumulation of gases, whether from mobilized evaporites or from other sources.

The Earth's crust may have become loose as a consequence of the multiple episodes of oblique continent-to-continent collisions and the deep subduction events that characterize Pan-African times, thereby initiating modern-style plate tectonics [1].

[1] Saul J.M. (2014). *A Geologist Speculates*, Les 3 Colonnes, Paris, 160 pp.

Ruby and sapphire from Tajikistan, Central Asia: new geological and mineralogical data

Sorokina E[1*], Hofmeister W[2], Litvinenko A[3], Haeger T[2], Jacob D[4], Nasreddinov Z[5]

1 - Fersman Mineralogical Museum RAS, Moscow *elensorokina@mail.ru 2 - Johannes Gutenberg University Mainz, Germany 3 - GIA Moscow, Russia 4 - Macquarie University, Sydney, Australia 5 - Mining and Metallurgy University, Chkalovsk, Tajikistan

Discovered at the late 1970s by soviet geologist E.A. Dmitriev *et al*., the ruby and sapphire Snezhnoe deposit in Tajikistan continued its production until the collapse of the former Soviet Union in the early 1990's. However, recently, the interest in this occurrence was renewed due to insufficient study of its geological and mineralogical features. The Snezhnoe deposit is located geographically in the Murgab region of the Eastern Pamir, east of the Republic of Tajikistan. The ruby mineralization is found in marbles (Figure 1) of the Muzkol metamorphic series (PR_1), which is the central part of the Muzkol-Rangkulskiy anticlinorium, located in the eastern part of the Cimmerian folded zone of the Central Pamir. The ruby-bearing Sarydzhilginskaya suite, with other suites of the Muzkol series (total thickness exceeding 6 km), underwent at least two tectonic metamorphic cycles: *I cycle* - 1,8-1,6 Ga ago - high temperature metamorphism at amphibolite facies (T ≈ 700° C, P ≈ 8 kbar); *II cycle* - 0,1-0,02 Ga ago - is a zonal metamorphism from epidote-amphibolite up to greenschist facies (T ≈ 750 - 350°C, P ≈ 9 - 4 kbar).

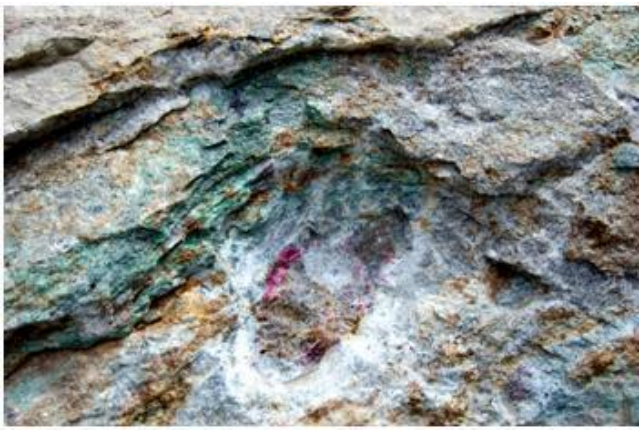

Figure 1: Fragments of ruby crystal within marbles surrounded by greed fuchsite, Snezhnoe deposit.

During the first cycle (I), corundum crystal habit, crystal chemistry and colour changes in the following order: violet colour *elongate-prismatic* crystals (~ 0,05 wt.% of Cr_2O_3) → pale-pink *flattened-prismatic* crystals (~0,25 wt.% of Cr_2O_3) → dark red *pinacoid* crystals (~0,25 wt.% of Cr_2O_3, 0,25 wt.% of Fe_2O_3). Besides, we have detected small contents (less than 100 ppm) of Ti, V and Ga within these samples by both LA-ICP-MS and EMPA analyses. All these crystals showed polysynthetic twinning and partings parallel to *c*, *a* and *r* cleavages. Additionally, we confirmed the presence of allanite inclusions in ruby according to literature. Other inclusions are zircon, Cr-rutile, Ca- and Na-margarite. In the second cycle (II), the recrystallization of primary corundum produced gem quality bright red colour *flattened-prismatic* and *irregularly shaped* ruby crystals (~0,5 wt.% Cr_2O_3). These crystals are free of any solid inclusions and morphological defects. The colour of Tajik rubies is very similar to Mogok ones in Myanmar but their quality is lower. Reflective indices (RI), birefringences, specific gravities, Vis- and UV-spectra of Tajik rubies are closely similar with those from South-East Asia marble-hosted occurrences. However, identified solid inclusions within Tajik gems such as allanite, Cr-rutile and Ca- to Na-margarite allowed to distinguish them from those of South-East Asian deposits.

Acknowledgements: To Colleagues, who assisted in carrying out of analyses and collecting of stone materials.

Dating and characterising fluid activity and diagenesis by in-situ LA-ICP-SFMS isotope analysis

Gerdes A

Goethe-University Frankfurt. gerdes@em.uni-frankfurt.de

The mobility of uranium in aqueous fluids opens the possibility that via U-bearing phases fluid activity in the past can be dated. Such secondary mineralisation can be formed under variable conditions, such as hydrothermal activity, subsurface weathering and diagenetic processes. The minerals of interest are either tiny, complexly grown, and rare or contain low U concentrations combined with low $^{238}U/^{204}Pb$ <200. Thus, suitable mineral phases have to be identified and their position documented by thorough SEM-based BSE and CL imaging prior to analysis using techniques with high spatial resolution.

This study will, documented by some interesting examples, highlight the advantage of laser ablation ICP sector-field mass spectrometry (LA-ICP-SFMS) for in-situ isotope analysis of various isotope systems and mineral phases. At Goethe University (GUF) spot sizes as small as 5-10µm (resolution with dual-volume S155 cell) can be applied to analyse for instance the isotope composition of B, Rb-Sr, Sm-Nd, Lu-Hf, and U-Th-Pb in single growth domains of individual minerals, providing elemental concentrations are sufficiently high.

The growth of secondary monazite related to hydrothermal fluids during retrograde metamorphic evolution, in shear zones, or during ore mineralisation is widely known. Despite analysing accessory minerals having a high µ ($^{238}U/^{204}Pb$: 10^3 to 10^7) it will be shown that the LA-ICP-SFMS method can be also used for dating Mesozoic-Cenozoic minerals with low µ of 20-100 and low U content (< 10 ppm). This opens the possibility of direct dating diagenesis, hydrothermal activity and even palaeosurfaces. To explore capabilities and limitations, the method has been tested on various sedimentary phosphorites, pedogene carbonates as well as Fe- and Ti-oxides of known and unknown age.

Furthermore, the combination with LA-MC-ICPMS analysis of B and Sr isotopes allows the distinction between a marine and non-marine origin of the fluid involved. Examples will be shown and discussed.

Constaints on Alpine hydrothermalism and deformation from Th-Pb dating of cleft monazite (Western Alps)

Grand'Homme A[1*], Janots E[1], Seydoux-Guillaume A-M[2], Bosse V[3], De Ascenção Guedes R[4]

1 - ISTerre *alexis.grandhomme@ujf-grenoble.fr 2 - GET 3 - LMV 4 - Le Règne Minéral

This study provides new constraints on fluid circulation and deformation in the Western Alps, through the elementary and isotopic analyses of alpine cleft monazite (LA-ICP-MS and EMP measurements). Alpine clefts are hydrothermal veins that formed during deformation under metamorphic conditions below the ductile/brittle transition (T <450°C). The studied veins are filled by hydrothermal crystals of quartz, chlorite (± epidote), albite and accessory minerals (monazite, apatite, xenotime, anatase, rutile). In these veins, large monazite crystals up to few millimeters can precipitate.

Prior to dating, the cleft monazite composition was thoroughly studied to reveal potential zoning and bring constraints on the behavior of REE+Y, Th, U and Pb in hydrothermal systems and during fluid/rock interaction. Cleft monazite crystals are commonly zoned in composition and age, indicating successive growth episodes that have been dated using in-situ isotopic techniques (LA-ICP-MS). Due to the low U concentrations (and possible ^{206}Pb excess) in Alpine clefts, $^{208}Pb/^{232}Th$ ages (no common Pb correction) are presented here.

In the Internal Alpine domains (Briançonnais) Th-Pb dating yields ages at 32.1±0.2 (Mesozoic cover, limit with Piedmont zone) and 23.3±0.2 Ma (Zone Houillère). The timing of cleft monazite precipitation is coeval with major deformation events well recorded by other chronometers (activity of the pennic front and thrusting of the Helvetic nappes).

In two External Crystalline Massifs (ECM, Belledonne and Mont-Blanc), seven veins have been dated (155 measurements), giving Th-Pb ages that are distinguished into two distinct populations at 12.6 - 11.2 Ma and 8.6 - 6.3 Ma. Intra-grain dating in different compositional domains can give different ages up to 1.5 Ma.

The cleft formation occurs in periods of increasing exhumation rates (zircon fission track data) in the ECM, suggesting for a prominent role of deformation on the Neogene exhumation of the western Alps.

In-situ Sr isotope LA-ICP-MS-analyses of scheelite, apatite and U-Pb isotope data of zircon from the Felbertal scheelite deposit (Eastern Alps, Austria): implications for timing and source of tungsten mineralization

Kozlik M[1*], Raith J[1], Gerdes A[3]

1 - Montanuniversitaet Leoben, Chair of Resource Mineralogy
*michael.kozlik@unileoben.ac.at 3 - Goethe-University Frankfurt

The scheelite deposit Felbertal in the Eastern Alps is a tungsten producer of global importance. The genesis of this strata-bound deposit is debated; sedimentary-exhalative as well as granitic magmatic-hydrothermal models (with later regional metamorphic overprint) were proposed.

Sr isotopes of two chemically distinct scheelite generations from different lithologies were measured *in-situ* by LA-MC-ICP-MS. Additionally, Sr isotope values of zoned apatite from a mineralized highly evolved leucogranite (K1-K3 orthogneiss), which occurs in a close spatial relationship to several ore bodies, are presented. These data are used to constrain the possible sources of the tungsten mineralization. Furthermore *in-situ* U-Pb dating on zircons of the K1-K3 orthogneiss and of its possible parental granitoid (Felbertauern augengneiss) were carried out to elucidate the age relationships and the magmatic evolution of these metagranitoids.

Initial $^{87}Sr/^{86}Sr$ ratios for the primary Mo-rich scheelite generation (Scheelite 2) show a remarkable cluster between 0.7243 and 0.7637. A later metamorphic remobilized Mo-free scheelite generation (Scheelite 3) displays even more radiogenic ratios scattering between 0.7679 and 0.8048. Zoned apatites from the K1-K3 orthogneisses have $^{87}Sr/^{86}Sr$ between 0.7204 and 0.7451 for the cores and 0.7454-0.7794 for metamorphic rims. The high ratios for the cores may indicate a magmatic-hydrothermal signature, though textural and mineral chemical data still point to an orthomagmatic growth of apatite. The scattered and highly radiogenic values suggest that mineralizing fluids, released during the magmatic-hydrothermal stage from the K1-K3 granitic melts, have interacted with ca. 200 Ma older Early Paleozoic host rocks. Scheelite precipitated from this fluid was enriched in ^{87}Sr. A considerable scatter of the Sr isotope ratios is also recorded on a small scale, within single scheelite porphyroblasts. This suggests either no equilibration of Sr isotopes even at a sub-cm scale during scheelite crystallization or multiphase growth during infiltration, continuously or in pulses, of isotopically heterogeneous hydrothermal fluids. Scheelite was remobilized during the subsequent regional metamorphism and interacted with even more radiogenic fluids to form the Mo-free scheelite generation. Preferential breakdown of Rb-rich mica relative to plagioclase in the host rocks is a likely explanation for the ^{87}Sr-enriched fluids.

Crystallization ages of zircons from four K1-K3 orthogneiss samples range between 336.6±2.1 Ma and 340.9±2.5 Ma. These ages correspond with the crystallization age of the Felbertauern augengneiss (337.8±2.0 Ma). The *in-situ* U-Pb zircon data support geochemical criteria, suggesting a cogenetic evolution of the highly fractionated K1-K3 orthogneiss found in the ore deposit and the regionally occurring Felbertauern augengneiss. Our new data confirm the importance of the Variscan orogenic event for formation of the Felbertal tungsten deposit.

U-Pb and Lu-Hf isotope systematics of Nb-Ta mineralization

Marko L[1*], Gerdes A[1], Melcher F[2], Van Lichtervelde M[3]

1 - Goethe University Frankfurt *lmarko@stud.uni-frankfurt.de

2 - Montanuniversitaet Leoben 3 - Université de Toulouse

Rare element pegmatites comprise a wide variety of accessory minerals and contain high concentrations of large ion lithophile (LIL) and high field strength elements (HFSE) such as Nb, Ta, W, Li and Sn. For many of these pegmatites the timing, origin, and processes involved in metal enrichment is not well understood. The combination of high-spatial resolution Sm-Nd and Lu-Hf isotope systematics with U-Pb geochronology could be used as a tool to characterize the origin and source of the parental magma and to identify a possible contribution from the mantle or the country rocks (leaching, assimilation) to the mineralization. It is even possible that each mineralizated system has its distinct isotopic signature, which can be used as a fingerprint to characterize a certain locality or even an entire pegmatite province.

We studied columbite-group minerals (CGM) from Tanco granitic pegmatites (LCT) in southeastern Manitoba in Canada and of Kibaran age from Central Africa. Their internal structure varied from oscillatory over progressive to patchy zoning. LA-SF-ICP-MS U-Pb ages from CGM from the Tanco pegmatites show quasi concordant ages between 2.67 - 2.50 Ga as well as strongly discordant analyses with $^{206}Pb/^{238}U$ ages of 0.35 to 1.6 Ga. While the older age range is consistent with a multiphase evolution of crystallisation and (hydrothermal) recrystallisation, the young ages are not yet understood. U-Pb ages of CGM samples from the Kibaran pegmatites vary between ~975 and ~930 Ma and are interpreted to be associated with the G4 Granite, which formed at 986 ±10 Ma [1]. As in the case of Tanco, Kibaran CGM show clear age variations as well as some discordance in their U-Pb systematics, pointing to a complex history.

Lu-Hf isotopes of specific domains in CGM were analysed by isotope dilution technique using a Neptune MC-ICP-MS after dissolution in acid and subsequent separation of the Lu and Hf fraction by ion exchange chromatography. Samples of 0.5 to 1.5 mg were collected from thick section guided by BSE images using a microdrill and Resolution Excimer Laser, respectively. The Hf concentration varied from 25 to 720 ppm with Lu/Hf of 0.001 - 0.99. The εHf from 0.7 to 2.2 shows rather small variation for Tanco CGM. In the case of Kibaran pegmatites our results show considerable variation with εHf ranging from -2.9 to -17.0. The heterogeneity within single mineralization and implications for the genesis will be discussed.

[1] Dewaele S., Henjes-Kunst F., Melcher F., Sitnikova M., Burgess R., Gerdes A., Alonso Fernandez M., De Clercq F., Muchez P. and Lehmann B. (2011). *J. African Earth Sci*. 61, 10-26.

Polyphased rare-element magmatism during late orogenic evolution: geochronological constraints from the NW Variscan Iberia

Melleton J[1], Gloaguen E[1], Frei D[2*]

1 - BRGM, Direction Géoressources, ISTO 2 - Stellenbosch University *dirk.frei@gmail.com

U-Pb geochronological data were collected on columbite-tantalite from rare-element pegmatites and granites (Li, Ta, Nb, Be, Sn) from the Iberian Variscan Massif in order to investigate timing of rare-element events during the late evolution of the Variscan belt and the connection with granitoid suites. Our data set emphasises three events: (i) The Argemela rare-element granite, from the Central Iberian Zone (CIZ), emplaced at 326±3 Ma and predates the three main late orogenic granitoid suites, (ii) most of the studied rare-element pegmatites of the LCT family from the Galicia-Trás-Os-Montes Zone (GTOMZ) gave an average age of 310±5 Ma, contemporaneous with an early syn-D3 granodiorite-monzogranite suite and the syn-D_3 two-micas granites suite; and (iii) The youngest event is dated at around 301±3 Ma and is marked by emplacements of rare-element pegmatites of the LCT family in both the CIZ and in the South of the GTOMZ. This event postdates the late to post-D_3 bt±crd-granodiorite-monzogranite suite emplacements, which are probably not genetically related to rare-element pegmatites. Several pegmatites dated during this study do not display contemporaneous ages with neighbouring supposed "parent" granites.

Contemporaneous rare-element pegmatites fields seem to be located along belts as it is observed for granitoids suites. Considering both GTOMZ and CIZ fields, emplacement ages look to decrease toward the South. This is in good agreement with the known propagation of deformation, metamorphism and magmatism between the different geotectonic zones of the Iberian Massif.

Lower crustal processes are not at the origin of rare-element granite genesis since in the Iberian Massif, RM magmatism is polyphased with at least three distinct events. Hypothetical sources of RM melts are supposed to be set in a middle to upper crust position, as it has been shown for granitoid magmatism.

Chronology of the B1 marginal sills, eastern Bushveld Complex, South Africa

Wabo H[1*], de Kock M[1], Klausen M[2], Soderlund U[3], Beukes N[1]

1 - University of Johannesburg *waboherve@yahoo.fr 2 - University of Stellenbosch 3 - Lund University

The Rustenburg Layered Suite (RLS) of the Bushveld Complex in South Africa consists of coarse-grained cumulative rocks that can be divided into the Lower, Critical, Main and the Upper zones. Along its base is a discontinuous zone of finer-grained rocks known as the Marginal Zone, representing the intrusion's early chilled margin against its cooler host rock. The RLS is associated with marginal sills that intrude into the Pretoria Group. These sills are in contact and share some geochemical similarities with different zones of RLS. They have also been classified in terms of chemical composition, which suggests their fractionation from distinct parental magma compositions (so-called B1, B2 and B3 parental magmas). Existing high-quality paleomagnetic constraints for the RLS originate from the top of the Critical to Upper zones, which are associated with B2 and B3 marginal sills. The geochemically verified B1 marginal intrusions are here used as a proxy for constraining the timing of the lower part of the RLS. Twenty-five intrusions were sampled near Belfast and between Dullstroom and Lydenburg. Demagnetization results of B1 intrusions revealed the existence of a dual polarity magnetic component, which we show to predate regional folding of Transvaal strata. The calculated pole for these intrusions is similar to established Bushveld Complex poles. We further report ~2058 Ma U-Pb baddeleyite ages from two B1 sills of opposite magnetic polarity (2058.4 ± 1.3 Ma and 2058.1 ± 6 Ma). Our ages are older than the 2054-2056 Ma ages from the upper layers of the RLS, but near identical to an age of the Marginal Zone and ages from the upper Critical Zone below the Merensky Reef. The current data thus suggest that the emplacement of the RLS was protracted, with bimodality in ages that could be interpreted as two episodes of magma emplacement. Petrological considerations, however, make the possibility of an extensive magmatic hiatus at the level immediately below the Merensky cyclic unit unlikely, even though this level in the RLS is characterized by a magmatic erosional unconformity and a sudden shift in initial $^{87}Sr/^{86}Sr$ that indicate a major influx of liquid. Here we do not come up with a solution for the age bimodality, which appears to require a rethink of models proposed for the Merensky cyclic unit. Instead we urge for all geochronology data to first be scrutinized. Ideally, a series of datings should be done throughout the RLS at the same laboratory, on the same mineral, and with the same technique to cancel out any systematic errors that could result in this discrepancy.

Emplacement processes and melt compositions for the Bushveld Lower Zone from in-situ Sr isotopic data

Wilson A[1*], Zeh A[2], Gerdes A[2]

1 - University of the Witwatersrand *allan.wilson@wits.ac.za 2 - Goethe University Frankfurt

Previous Sr-isotopic studies carried out on the Bushveld Complex have provided a powerful insight into initial magma compositions, mixing processes and mineralization. On this basis, and combined with distinct geochemical signatures, a variety of parental magmas have been identified relating to the different phases of the Bushveld Complex. However, the overall coverage of the Bushveld Complex, particularly for the Marginal and Lower Zones, remains limited. We have carried out precise *in-situ* Sr isotopic and trace element analyses on plagioclase using the LA-MC-ICPMS method on a continuous suite of rocks from the Marginal and Lower Zones and Basal Ultramafic Sequence in the eastern Bushveld Complex.

The LA *in-situ* method for the determination of Sr isotopes requires corrections for interferences arising from double charged REE (Er, Yb), Kr (mu 84, 86), Ca dimers, and Rb. Whereas the former three have only a negligible effect, the correction for isobaric interference of ^{87}Rb on ^{87}Sr can be critical for the accuracy and precision of $^{87}Sr/^{86}Sr_i$. In the case of the Bushveld rocks (2055 Ma) the growth of ^{87}Sr through time due to ^{87}Rb decay becomes additionally important. It is therefore crucial to know the correct Rb mass bias and Rb/Sr interelement fraction. Both are estimated through analyses on NIST-610 and verified by analyses of plagioclase with high and variable $^{87}Rb/^{86}Sr$. Although NIST 610 has a $^{87}Rb/^{86}Sr$ of 2.82, which relates to an isobaric interference of ^{87}Rb 4times ^{87}Sr, the obtained $^{87}Sr/^{86}Sr$ (0.7096 ±0.0010; n =12) is within uncertainty of the accepted value. Performance and accuracy were checked by multiple measurement of the feldspar standard (MIR), which yielded values of $^{87}Sr/^{86}Sr$ 0.703096 ± 0.000017 (n=22) in perfect agreement with conventional TIMS data of 0.703096.

The study of 66 rock samples with over 500 individual Sr isotope analyses reveals a wide-range and systematic changes in the $^{87}Sr/^{86}Sr_i$ (at 2.05 Ga) from 0.7049 to 0.7072 (± 0.0002). Systematic changes in $^{87}Sr/^{86}Sr_i$ are observed through the sequence and correspond to changes in fundamental compositional parameters such as Mg#. Dunite layers containing primitive olivine (Fo_{91} and higher) have higher $^{87}Sr/^{86}Sr_i$ suggesting greater degrees of crustal contamination in the hotter magmas. The chill zone investigated in detail by Wilson [1] has a more elevated crustal signature of 0.7068 whereas the dunite layer in the chill sequence has a more primitive $^{87}Sr/^{86}Sr_i$ of 0.7056.

The observed variations reflect variable degrees of crustal contamination, arising either through enrichment of the mantle source or from a staging chamber interacting with the crustal wall rocks.

[1] Wilson A.H. (2012). A chill sequence to the Bushveld Complex: Insight into the first stage of emplacement and implications for the parental magmas. *Journal of Petrology*., 53, 1123-1168.

Rutile alteration and formation in auriferous aqueous fluids: evidence from microstructures, trace-element compositions and U-Pb ages

Zeh A[1], Cabral A R[2*], Koglin N[3], Seabra Gome A A Jr.[4]

1 - Goethe University Frankfurt 2 - Mineral Deposits, Technische Universität Clausthal *alexandre.cabral@tu-clausthal.de 3 - University of Würzburg 4 – GEO T, Nova Lima

Uranium-Pb ages, rare earth element (REE) and trace-element data have been provided for rutile grains from quartzitic rocks of the Moeda Formation (Minas Supergroup, Quadrilátero Ferrífero of Minas Gerais, Brazil). The clastic succession is ≥2.65-Ga old [1] and has intercalations of Witwatersrand-like auriferous metaconglomerate. The rutile grains show unusually high contents of Th, REE and trace elements. Uranium-Pb ages are about 2.25 Ga, except for three grains with inherited ages of 2.72, 2.63 and 2.55 Ga. Considering shape, microstructures and trace-element contents, the rutile grains can be divided into two types. Type-1 rutile grains are generally rounded and highly porous (sponge-like), displaying large variations in their trace-element contents: e.g., Th (12-73 ppm), Zr (39-427 ppm), Cr (2959-15017 ppm), W (107-2043 ppm), Mo (0.06-0.58 ppm), Sb (8-58 ppm), ΣREE (1-132 ppm). The type-1 grains most likely formed by a pseudomorphic (coupled) dissolution-re-precipitation process, whereby pre-existing detrital rutile was incompletely transformed into metamorphic rutile. The type-2 grains are sub- to euhedral and contain inclusions of muscovite. Their trace-element contents are remarkably lower compared to the type-1 rutile: e.g., Th (1-21 ppm), Zr (31-72 ppm), Cr (1742-3266 ppm), W (947 ppm), Mo (0.04-0.14 ppm), Sb (3.5-9.1 ppm), ΣREE (3-80 ppm). The rutile grains of type 2 most likely formed by precipitation from an aqueous fluid, perhaps after dissolution of pre-existing detrital rutile grains, trace-element transport and homogenisation. Both rutile types contain Au in the range from 0.10 to 0.50 ppm.

The relative high contents of Th, REE and trace elements, which are atypical for rutile [2, 3], can be explained by accumulation of these elements in interstitial positions and/or in nanopores. Uranium-Pb ages, trace-element data and microstructures indicate that the rutile grains were formed and/or altered by distinct fluid-related dissolution-re-precipitation processes at ~2.25 Ga during the Transamazonian Orogeny [4, 5]. The fact that rutile grains of both types contain some hundred ppb of Au indicates hydrothermal overprint by fluids capable of carrying gold.

[1] Cabral *et al*. (2012). *Precam Res*, 204-205, 40-45.

[2] Mezger *et al*. (1989). *Earth Planet Sci Lett*, 96, 106-118.

[3] Zack *et al*. (2011). *Contrib Mineral Petrol*, 162, 515-530.

[4] Marshak *et al*. (1989). *Geology*, 25, 415-418.

[5] Alkmim and Marshak (1998). *Precam Res*, 90, 29-58.

The Rustenburg Layered Suite (Bushveld Complex) crystallised in less than 1.6 million years – constraints from CA-ID-TIMS dating, geothermometry, and inclusions in zircon

Zeh A[1*], Ovtcharova M[2], Wilson A[3], Schaltegger U[2]

1 - Goethe University Frankfurt *a.zeh@em.uni-frankfurt.de 2 - University of Geneva
3 - University of the Witwatersrand

The timing and period of crystallisation of the Rustenburg Layered Suite (RLS) is the subject of ongoing debate. We present new results of a detailed study on zircon grains, comprising high-precision U-Pb CA-ID-TIMS dating, Ti-in-zircon thermometry, and mineral inclusions. The zircon grains were separated from different rock units throughout the RLS, comprising a chilled sequence from the Marginal Zone, chromite-bearing rocks from the Lower and Upper Critical Zone, including the Merensky Reef, as well as anorthosite from the Main Zone, and a magnetite layer from the Upper Zone. The combined dataset reveals that zircon in all these rocks crystallised from highly fractionated, silica-saturated intercumulus melts at temperatures between 890 - 670°C, within a short time interval of 1.02 ± 0.63 Ma. The oldest age of 2055.91 ± 0.26 Ma is obtained from zircon grains of a chill sequence of the Marginal Zone, having a B1 magma composition. This age is considered to most closely represent the intrusion age of the RLS. The youngest age of 2054.89 ± 0.37 Ma is obtained from a pyroxenite directly below the Merensky Cyclic Unit. Zircon grains in all other cumulate rocks crystallised within the same time interval, as is reflected by weighted mean $^{207}Pb/^{206}Pb$ ages of 2055.68 ± 0.29 Ma (Marginal Zone), 2055.40 ± 0.30 and 2055.65 ± 0.38 Ma (Lower Critical Zone), 2055.32 ± 0.30 Ma (UG2 chromitite layer), 2055.16 ± 0.40 Ma (Merensky Reef), 2055.01 ± 0.44 Ma (lower Critical Zone), and 2055.81 ± 0.67 Ma (Upper Zone). The results of our study are in good agreement with field observations and petrological data which require a relatively fast and continuous crystallisation process, periodically interrupted by new magma replenishment [1]. However, they differ from previous high-precision U-Pb zircon dating that indicated periodic crystallisation over an interval of 5.2 ± 0.79 Ma [2].

[1] Cawthorn R.G. and Walraven F. (1998). Emplacement and crystallization time for the Bushveld Complex. *J. Petrol.* 39, 1669-1687.

[2] Scoates J.S., Wall C.J., Friedman R.M., VanTongeren J.A. and Mathez E. (2012). Age of the Bushveld Complex. Abstr. Goldschmidt Conference, Montreal, Canada.

Rb-Sr geochronology of sphalerite from fluorite-barite-sulfide veins of the Freiberg ore district, Erzgebirge (Germany)

Ostendorf J[1*], Henjes-Kunst F[2], Seifert T[1], Gutzmer J[3]

1 - Department of Mineralogy, TU Bergakademie Freiberg *joerg.ostendorf@mineral.tu-freiberg.de 2 - Federal Institute for Geosciences and Natural Resources 3 - Helmholtz Institute for Resource Technology Freiberg, Germany

Hydrothermal veins form as a result of hydrothermal fluids that are mobilized during tectonic or magmatic events. In order to constrain the relation between regional tectonic and/or magmatic events and vein formation, geochronological studies are of fundamental importance. This applies in particular as vein deposits are typically polyphase in origin, i.e., mineralization formed episodically and multiple reactivation of the same tectonic structures give rise to ore formation at distinct geological times (e.g. [1]). The Ag-Pb-Zn deposit district of Freiberg in the Erzgebirge of SE Germany is an excellent example of polyphase vein mineralization. Different styles of vein-type mineralization have been recognized, three of which were of particular importance in previous mining periods, namely (1) quartz bearing As(-Au)-Zn-Cu(-In-Cd)-Sn-Pb-Ag-Bi-Sb polymetallic sulfide association ("kb ore type"), (2) carbonate bearing Ag-Sb polymetallic sulfide association ("eb ore type"), and (3) barite-fluorite-sulfide association ("fba ore type") (e.g. [2]). The kb and eb ore types in the Erzgebirge have long been thought to be of late Variscan age (c.f. [3]), but precise ages are not known. The fba ore type has been regarded as being significantly younger (c.f. [3]), but again without precise age constraints. Here, we investigate the age of sphalerite of the fba ore type with the Rb-Sr method (e.g. [4]). Seven data points plot on a well-defined isochron yielding an age of 113 Ma ± 4 Ma (MSWD = 6.4). This age coincides with the opening of the North Atlantic and the break-up of Gondwana and, furthermore, widespread hydrothermal activity all over Europe (e.g. [1, 5, 6, 7]). It may thus be concluded that the Freiberg "fba ore veins" formed when older, deep seated structures were reactivated in response to the opening of the Atlantic Ocean.

[1] Pfaff K., Romer R.L. and Markl G. (2009). U-Pb ages of ferberite, chalcedony, agate, 'U-mica' and pitchblende: Constraints on the mineralization history of the Schwarzwald ore district. *European Journal of Mineralogy*, 21, 817-836.

[2] Seifert T. and Sandmann D. (2006). Mineralogy and geochemistry of indium-bearing polymetallic vein-type deposits: Implications for host minerals from the Freiberg district, eastern Erzgebirge, Germany. *Ore Geology Reviews*, 28, 1-31.

[3] Baumann L., Kuschka E., Seifert Th. (2000). Ore deposits of the Erzgebirge. Enke im Georg Thieme Verlag, Stuttgart, New York: 1-303 (in German).

[4] Nakai S.I., Halliday A.N., Kesler S.E., Jones H.D., Kyle J.R. and Lane T.E. (1993). Rb-Sr dating of sphalerites from Mississippi Valley-Type (MVT) ore deposits. *Geochimica et Cosmochimica Acta*, 57, 417-427.

[5] Galindo C., Tornos F., Darbyshire D.P.F. and Casquet C. (1994). The age and origin of the barite-fluorite (Pb-Zn) veins of the Sierra del Guadarrama (Spanish central system, Spain): A radiogenic (Nd, Sr) and stable isotope study. *Chemical Geology*, 112, 351-364.

[6] Munoz M., Premo W. and Courjault-Radé P. (2005). Sm-Nd dating of fluorite from the worldclass Montroc fluorite deposit, southern Massif Central, France. *Mineralium Deposita*, 39, 970-975.

[7] Piqué À., Canals À., Grandia F. and Banks D.A. (2008). Mesozoic fluorite veins in NE Spain record regional base metal-rich brine circulation through basin and basement during extensional events. *Chemical Geology*, 257, 139-152.

Oxygen-boron isotope systematics in the Larderello granites

Villa I[1], Fiebig J[2], Gerdes A[2*], Marko L[2]

1 - Institut für Geologie, Switzerland 2 - Goethe-University Frankfurt *gerdes@em.uni-frankfurt.de

We analyzed oxygen and boron stable isotope fractionations on K-feldspar-biotite (Kfs-Bt) pairs of the borehole granites dated by Villa *et al*. [1]. The geological framework is apparently simple: anatectic granites were encountered at depths of 2-4 km b.g.l.; above the granites, a vapour-dominated geothermal field is mined for electricity production. Hydrothermal alteration of the granite is expected and indeed observed, especially near the fractured country rock, but was not pervasive, as magmatic cordierite is preserved. Rb-Sr-^{39}Ar-^{40}Ar analyses indicate that the granites in the eastern part of the geothermal field (Travale-Montieri-Chiusdino) intruded around 3 Ma ago; in the western part (Carboli) a younger granite intruded <1 Ma ago [2]. Pennisi *et al*. [3] reported δ^{11}B of +3-16 ‰ in fluids from Larderello wells, with low B fluids having the highest δ^{11}B. The present stable isotope study attempts to characterize the interaction of minerals from granites in the East with hydrothermal fluids.

The oxygen isotope fractionation δ^{18}O (Kfs-Bt), measured on 1 mg multigrain samples by CO_2 IR laser fluorination, is quite uniform and ranges from 2.3 to 3.5 ‰, closely reflecting magmatic temperatures. We observe neither complete diffusive re-equilibration of the Bt-Kfs pairs below ca. 500 °C, nor pervasive recrystallization at the present-day in-hole temperatures (210 - 330 °C). However, we observe a very high variability in bulk oxygen isotopic compositions, with δ^{18}O (Kfs) ranging from +4 to +12 ‰. The δ^{18}O correlates with no macroscopic indicator (proximity to country rocks, rock fracturing, Sr isotopic variations). Oxygen isotopic signatures suggest a strong heterogeneity of the granitic magma batches, which did not coalesce to form a homogeneous pluton.

B isotope data were acquired by LA-MC-ICP-MS on ca. 15-25 single Kfs and Bt grains for each sample. δ^{11}B ranges from +27 to -1‰ in Bt and +18 to -20 in Kfs and generally correlates negatively with the B content. B and O are related: samples with highest average δ^{11}B have also highest δ^{18}O.

[1] Villa I.M. *et al*. (2006). *J Volcanol Geothermal Res*., 152, 20-50.

[2] Villa I.M. *et al*. (2001). *Water-Rock Interaction*, 10, 1589-1592.

[3] Pennisi M. *et al*. (2001). *Water-Rock Interaction*, 10, 899-902.

4D mapping of fluid distribution in porous sedimentary rocks using X-ray micro-CT differential imaging

Boone M[1*], De Kock T[1], Masschaele B[2], De Schryver T[3], Van Hoorebeke L[3], Cnudde V[1]

1 - UGCT - Dept. Geology and Soil Science, Ghent University *marijn.boone@ugent.be 2 - X-Ray Engineering (XRE) - UGCT, Belgium 3 - UGCT - Dept. of Physics and Astronomy, Ghent University

Where fluids are located and how they behave inside the pore network of rocks, is of crucial importance in many geological fields. For complex sedimentary rocks like limestone with both primary and secondary porosity, a multidisciplinary approach is often needed to characterise the broad pore size distribution and the complex pore geometries, as well as to determine the fluid occupancy in that pore network. In this research differential imaging is applied on a time-lapse X-ray computed microtomography (micro-CT) scan of a porous limestone sample during a fluid infiltration process. The scans were obtained using the Environmental micro-CT (EMCT) set-up at the UGCT facility (www.ugct.ugent.be), which permits to obtain full 3D micro-CT images of the rock with spatial resolution up to 5 µm and a temporal resolution of 1 minute. The limestone sample was placed in an X-ray transparent flow cell and injected with a CsCl solution to enhance contrast. Registration and subtraction of the micro-CT images generates a differential image, which allows the mapping of the fluid distribution inside the rock and also to determine the amount of fluid in the rock. By comparing the differential images during the fluid infiltration process, a detailed progression of the fluid front can be visualized and the change in the amount of fluid in the pore space of the rock monitored over time (Figure 1). This technique allows a detailed study of fluid infiltration processes at the scale of the constituent pore spaces.

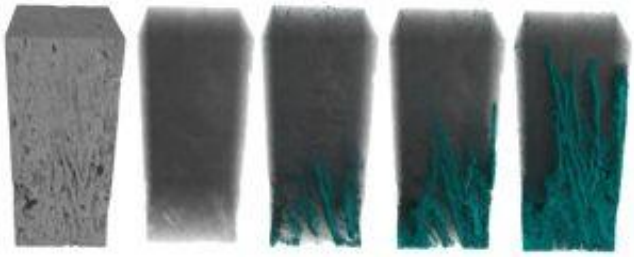

Figure 1: Time lapse fluid uptake visualized using differential micro-CT imaging. 3D rendering of the original limestone (left) followed by 3D differential images showing the progressive migration of the fluid, in blue (right)

Tomographic reconstruction for dummies

Churms C

DebTech De Beers Group. cecil.churms@debeersgroup.com

Many, if not most users of the Computer-assisted Axial Tomography (CAT) technique, view the process of reconstruction as some sort of magic black box. Although this might be a valid approach in some situations, it also leads inevitably to a lack of understanding of either the capabilities or the optimum setup and use of the technique. This paper will attempt to de-mystify the process of tomographic reconstruction using filtered back-projection (even with cone-beam geometry) by highlighting the basic principles and ignoring some of the more complex details or refinements.

Furthermore, algorithms and computer hardware requirements will be presented to enable a researcher with a little experience in programming, to implement a completely functional reconstructor from scratch.

It will be illustrated how such a simple "home-built" reconstructor can be used to understand the operation and optimisation of a tomographic facility more fully, while still yielding high quality results.

Mineral research: recent developments using X-ray- and neutron radiography in South Africa

De Beer F*, Bam L

Necsa *frikkie.debeer@necsa.co.za

The past three years saw the support by the Department of Science And Technology-National Research Foundation (DST-NRF) for the development of research infrastructure in South Africa that benefited the national capacity in the fields of penetrating radiation research through X-Ray- (University of the Witwatersrand, University of Stellenbosch and Necsa) and neutron radiography (Necsa).

The radiography/tomography section at Necsa has the unique opportunity to complement X-ray imaging with neutron imaging and to offer research infrastructure for free to post graduate students and researchers in fields such as anatomy, energy, geosciences, palaeosciences and archaeology to name a few.

The neutron tomography facility (SANRAD) [1], located at the SAFARI-1 Nuclear Research Reactor at Necsa, South Africa, has been exploited successfully in those fields and is currently being upgraded to international standards. Its imaging capabilities are being supported by a separate 225kV micro-focus X-ray tomography facility that was commissioned in 2011 and which is currently extensively being utilised.

The 120kV X-ray- and thermal neutron attenuation coefficients of some compositions, which are common minerals of importance in geo-scientific investigations, are listed in Table 1.

It is evident from Table 1 that the high density compositions have lower attenuation coefficients for neutrons than for X-rays. These compositions are thus more transparent to neutrons as compared to X-rays and therefore thicker samples can be penetrated more effectively. Higher density minerals, bearing elements such as gold, uranium, platinum, etc., imbedded in the matrix of these listed minerals, can thus be detected to reveal physical and morphological information through neutron tomography.

This paper explores several research results from a number of case studies to show the complementary nature as well as the unique radiography/tomography applications where neutrons and X-rays are successfully utilised.

Table 1: List of attenuation coefficients of common minerals for thermal neutrons and X-Rays (120kV)

Mineral Composition	Density (g/cm^3)	Attenuation Coefficient (cm^{-1})	
		Thermal Neutrons (0.005eV)	X-Rays (120kV)
Quartz SiO_2	2.66	0.27	0.69
Biotite: $K(Mg.Fe)_3(OH,F)_2(AlSi_3O_{10})$	2.8 - 3.2 (3.25)	0.57 - 0.72 (0.62)	1.87
K-Feldspar: Orthoclase: $KAlSi_3O_8$	2.55 - 2.63	0.25 - 0.27	1.05
Plagioclase feldspar: Anorthite: $CaAl_2Si_2O_8$	2.76	0.25 - 0.27	0.83
Garnet: Grossular: $Ca_3Al_2Si_3O_{12}$	3.71	0.29 - 0.54 (0.35)	1.29
Orthopyroxene: Orthoferrosilite: $Fe_2Si_2O_6$	3.2 - 4 (4)	0.35 - 0.51 (0.51)	2.64
Clinopyroxene: Hedenbergite: $CaFeSi_2O_6$	3.1 - 3.6 (3.66)	0.32 - 0.40 (0.41)	1.93

[1] De Beer F.C. (2005) *NIM-A*, 542, 1-6.

Dynamic X-ray µCT to monitor frost weathering of rocks

De Kock T[1*], Boone M[1], De Schryver T[2], Masschaele B[3], Cnudde V[1]

1 - UGCT - Dept. Geology and Soil Science, Ghent University *tim.dekock@ugent.be

2 - UGCT - Dept. of Physics and Astronomy, Ghent University 3 - X-Ray Engineering (XRE), Belgium – UGCT

Freeze-thaw cycling in humid environments is generally considered as an effective rock-weathering process to rocks in landscape evolution and built environments. However, the dynamics of the breakdown process are still under debate. The most accepted theory involves pressure exerted by the continuous growth of ice crystals ('ice lenses') in larger pores or cracks while water is withdrawn from smaller pores. Other theories emphasise hydraulic pressure, built up when water is expelled from the freezing site by the volumetric expansion accompanying the water to ice transition.

Despite the many studies, predicting the frost susceptibility of natural stones is still an ambiguous topic. Here, we try to contribute with direct observations on the dynamics involving the freeze-thaw weathering of rocks with X-ray computed tomography (CT).

For this, dynamic X -ray µCT was performed using the Environmental CT (EMCT) established at the UGCT facility (www.ugct.ugent.be), a gantry based system capable of acquiring a full µCT scan in down to one minute. A custom-made freezing cell was developed for this system, allowing for freezing down to 40°C below ambient temperature (Figure 1). The effect of freezing at -5 °C is compared to the effect at -15°C for several freeze-thaw cycles on capillary saturated bioclastic limestone samples. The cylindrical samples have a diameter of 9 mm and are confined within the freezing cell, except for the top surface. They are water saturated by absorption under atmospheric pressure. The obtained resolution for dynamic scans is ± 10 µm.

Preliminary results show that cracks develop preferentially near the top surface and that minimal temperature has an important effect. Whilst samples frozen at -5 °C merely show surface scaling after 15 cycles, samples frozen to -15 °C develop cracks along flaws after 5 cycles. Challenges at this point include the rendering and presentation of dynamic scans, visualization of crack initiation at sub-voxel resolution and incorporating the effect of sample saturation on damage process.

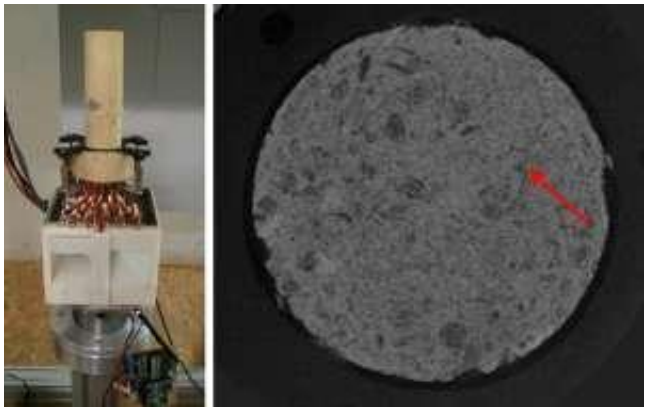

Figure 1: Custom made freezing cell (left); transversal slice with scaling crack (right).

Imaging and understanding of iron ore granulation using X-ray microtomography

Evrard M[1], Contreras R[2], Pirard E[1*]

1 - University of Liège *eric.pirard@ulg.ac.be 2 - Centre for Research in Metallurgy

Most iron ores cannot be directly fed into blast furnaces because their particle size distribution will negatively impact the blast furnace permeability and hence the overall efficiency of the ore reduction process. The finest fraction (typically <6.3 mm) has to undergo a sintering process, wherein a mixture of iron ore, coke and flux (limestone, olivine and other minor components) is heated, partially fused and transformed into pieces of sintered material with acceptable size, porosity and strength characteristics for the blast furnace. The preparation of an adequate mixture involves a granulation process, which is the subject of this study. Sintering, and hence granulation of iron ores, is particularly important in Europe, where supplied iron ores show a downward trend in quality (finer particles, broader size range, lower grades with higher variability). In addition, an increasing fraction of non-sintered material (return fines) is being added to the mix to optimize the resource efficiency while maintaining sinter quality.

In the field of sintering, microgranules (or micropellets) are considered as being composed of a nucleus (a particle in the range of 1 to 2 mm) surrounded by layers of the finest ore particles (typically the <250 µm fraction). A series of experiments and 3D imaging tests have been performed in this study to better understand the granulation mechanisms.

Microgranules are formed by mixing iron ore with water in a small rotating drum. Several parameters can be tuned during the granulation process, including size and proportion of nucleating particles, size and proportion of fines, water addition, rotating speed and total duration, amongst others.

Simple experiments using a single ore type (dominantly goethitic or hematitic) and water additions have been carried out systematically to better understand the kinetics of granulation. X-ray microtomography and subsequent 3D image analysis is used to identify and quantify the number of nuclei (when present), to measure the porosity and identify layering or cracks in the microgranule.

Compared with previous studies on iron ore pellets [1, 2, 3], this work focuses on imaging prior to sintering. It also uses higher resolution micro-CT and definitely provides a better insight into granulation as compared with data from 2D imaging of polished blocks, for example, fewer artefacts in apparent porosity due to sample preparation, a good discrimination among components of the granule, and clear identification of the nuclei.

This work is part of a larger European project (IMSIMI - Improved Sintering Mix) aiming at an optimal use of challenging input materials through carefully monitored preparation phases (mixing, granulation, etc.) and better understanding of their impact on the sintering process.

[1] Farber L., Tardos G. and Michaels J.N. (2002). Use of X-ray tomography to study the porosity and morphology of granules. *Powder Technology*, 132, 57-63.

[2] Shatokha V., Korobeynikov I., Maire E. and Adrien J. (2009). Application of 3D X-ray tomography to investigation of structure of sinter mixture granules. *Ironmaking and Steelmaking*, 36 (6), 416-420.

[3] Shatokha V., Korobeynikov I., Maire E., Gremillard L. and Adrien J. (2010). Iron ore sinter porosity characterisation with application of 3D X-ray tomography. *Ironmaking and Steelmaking*, 37(5), 313-319.

Combined X-ray diffraction (XRD) and computed tomography (CT) analysis in Earth sciences

König U[1*], Götz D[1], Fransen M[1], Pöllmann H[2]

1 - PANalytical.B.V., Almelo, Netherlands *uwe.konig@panalytical.com 2 - Martin Luther University, Halle-Saale, Germany

In this contribution, we will show examples of the strength of the combination of X-ray diffraction, X-ray imaging and Computed Tomography (CT) results on solid objects from earth science applications.

New developments – especially in detector technology – allow integration of these techniques on one laboratory X-ray diffraction system.

By combining phase analysis with density and microstructure information a complete picture of the sample is obtained. Results can be correlated with macroscopic material properties such as porosity and pore size, mineral distribution, graphitization or the visualization of transition zones.

Examples from mineralogical applications and from building material analysis will be discussed.

Application of XCT in determining the 3-D environment of PGM and sulphide minerals in Merensky and UG2 Reefs, Bushveld Complex

McCall M[1*], Du Plessis A[1], Miller J[1], Basson I[2], Smith D[3]

1 - Stellenbosch University *15804100@sun.ac.za 2 - TECT Geological Consulting 3 - Northam Platinum

Platinum group minerals (PGM) in the Bushveld Complex are known to be intimately associated with sulphides and chromite. The relationship between these phases is crucial to understanding mechanisms of platinum group element (PGE) concentration within mineralised reefs. Our current understanding of this relationship is based on 2-D imaging (principally scanning electron microscopy, SEM). However, recent studies have highlighted how 3-D imaging via X-ray computed tomography (XCT) can extend our understanding of relationships between these phases. In this study, 2-D surface imaging using SEM was combined with high-resolution (micron -scale) XCT analysis of 25mm block mounts to investigate the relationship between PGM grains, sulphides and chromite in different reef samples. The combination of 2-D and 3-D imaging was necessary in order to accurately identify different mineral phases and to delineate their grain boundaries. Many PGM grains were found to be of significant size (100-200 microns diameter) while their grain shape was extremely irregular (Figure 1). This irregularity in shape appears to lead to an underestimation of grain size using 2-D imaging (Figure 1). Moreover, grain boundary relationships do not appear to be so straight forward with PGM grains being partially immersed in the sulphide grains rather than just on the boundary or at junctions between sulphides with chromite or silicates. While the generally small grain-size of most PGM is problematic in conventional XCT analysis, the new generation of micro-XCT, especially in combination with 2-D imaging using SEM and appropriate image processing software can circumvent this problem.

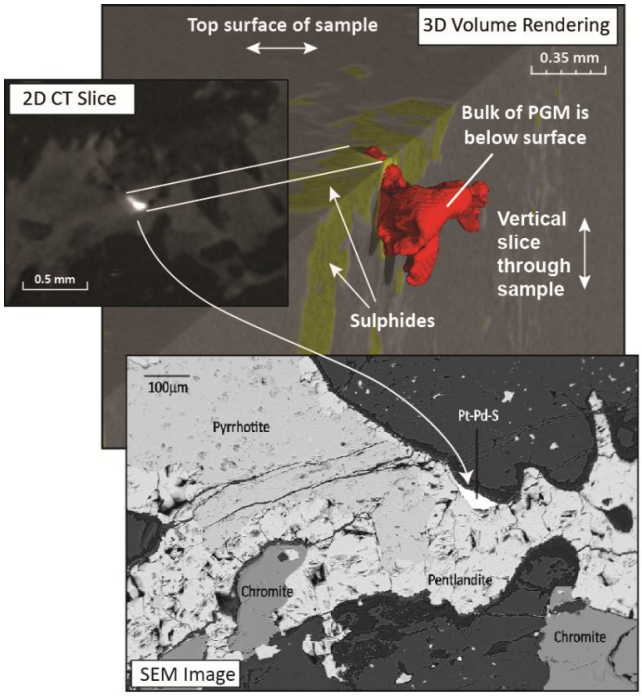

Figure 1: 2-D CT slice correlated with SEM image and 3-D volume rendering of highlighted PGM (Pt-Pd-S) in red within pentlandite (green). Voxel resolution of XCT images is 10µm. The PGM grain is situated on the boundary of a pentlandite grain in the SEM image but partially within the pentlandite in the 3-D volume. The PGM volume was extracted to expose the full extent of the grain whilst cutting a vertical slice through the remaining rock volume.

Towards effective and rapid registration of SEM images and micro-CT scans with commodity graphics processing hardware

Shipman W[1*], Chetty D[2], Nel A[1]

1 - University of Johannesburg *shipman.william@gmail.com 2 - Mineralogy Division, Mintek, Randburg, South Africa

X-ray micro-tomography (micro-CT) provides three-dimensional information about the distribution of minerals within an ore sample [1]. Backscattered electron (BSE) images from a scanning electron microscope (SEM) with energy dispersive X-ray (EDX) detector provide accurate location and allow mineral identification on a polished section of an ore sample. Combining the BSE and micro-CT imaging modalities can enhance the interpretation of X-ray micro-CT images and verify the accuracy of the interpretation. In order to correlate both sets of data, a registration of the BSE and micro-CT images must be undertaken.

Registration has proved to be computationally challenging [2], owing to excessive processing time requirements. Graphics processing units (GPUs) offer a low-cost solution to this challenge as they are massively parallel processors that provide substantial computing power and high-speed memory [3]. This talk describes a GPU-accelerated registration algorithm and demonstrates its use on an *in situ* copper ore sample. This algorithm builds on the work of Latham *et al.* [2] by exploring massively parallel multi-start and evolutionary optimisation algorithms to maximise the correlation between the BSE image and the micro-CT scan.

BSE images with sizes up to 2000x2000 pixels have been registered in under 20 minutes, producing correlation coefficients ranging from 0.91 for an 820x860 pixel BSE image, to 0.95 for a 2000x2000 BSE image. In each test, 250 iterations of the optimisation algorithm were performed at each of the four scales used in the multi-scale registration. Figure 1 shows the results achieved after registering the 2000x2000 pixel BSE image to the micro-CT scan.

These results were obtained using a mixture of old and new GPUs. A single high-end GPU is approximately 5 times faster than the maximum theoretical speed that a top-of-the-range workstation central processing unit can achieve, while costing less than one quarter of the price. The results show that two high-end GPUs are required to achieve speeds similar to those reported here. These results also show that accurate registrations can be achieved rapidly without requiring the use of costly workstations or computer clusters.

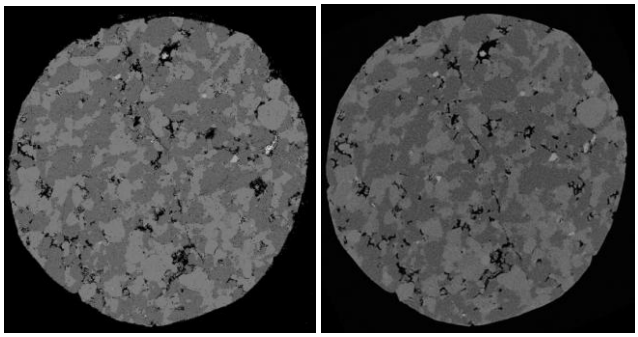

Figure 1: Target BSE image (left) and the plane through the micro-CT scan that most closely matches the BSE image (right).

[1] Ketcham R. and Carlson W. (2001). Acquisition, optimization and interpretation of X-ray computed tomographic imagery: applications to the geosciences. *Computers and Geosciences*, 27, 381-400.

[2] Latham S., Varslot T. and Sheppard A. (2008). Image registration: Enhancing and calibrating X-ray micro-CT imaging. *The Proceedings of the International Symposium of the Society of Core Analysts*, Abu Dhabi, UAE.

[3] Owens J.D. *et al.* (2005). A Survey of General-Purpose Computation on Graphics Hardware, in *Proceedings of Eurographics 2005*.

X-ray microtomography imaging of disequilibrium tourmaline growth by diffusion-limited aggregation

Valentini L[1*], Parisatto M[1], Artioli G[1], Perugini D[3]

1 - University of Padua *luca.valentini@unipd.it 2 - University of Perugia

The development of a disequilibrium growth pattern in tourmaline nodules occurring in aplitic rocks (Capo Bianco, Elba Island, Italy) is investigated by non-invasive 3D imaging, using X-ray microtomography. The reconstructed 3D images reveal the irregular morphology of the nodules, which consist of branches that extend radially from the core. The morphology of the tourmaline nodules is analysed quantitatively by calculating the associated fractal dimension, using a box-counting algorithm. The values of the fractal dimension are compared with those calculated for a virtual tourmaline nodule, simulated by means of a diffusion-limited aggregation (DLA) model. The fractal dimension of both the natural and simulated samples varies proportionally to the size of the nodules and tends asymptotically to the value 2.5, in agreement with the theoretical value of a fully developed DLA cluster. The results suggest that the tourmaline nodules formed by a disequilibrium magmatic process, in an undercooled environment, in which slow chemical diffusion induced the irregular growth of tourmaline, in the form of branching aggregates. Furthermore, this study proves that the development of disequilibrium textures in magmatic rocks can be adequately assessed by non-invasive 3D imaging using X-ray microtomography.

In situ phase mapping by X-ray diffraction microtomography: applications to cement materials

Valentini L[1], Artioli G[1*], Dalconi M[1], Parisatto M[1], Voltolini M[2], Ferrari G[3]

1 - University of Padua *gilberto.artioli@unipd.it 2 - Lawrence Berkeley Lab 3 - Mapei S.p.A.

This contribution illustrates recent advances in the assessment of the time-dependent mineral assemblage present in hydrating cement, by non-invasive 3D imaging. In recent years, the improvement of X-ray tomographic imaging techniques provided researchers with an excellent tool for accessing the 3D microstructural information of both rocks and man-made materials such as cement. However, conventional X-ray absorption tomography imaging may be affected by limitations in phase selectivity, due to poor resolution of sub-micrometre features and low compositional contrast between phases characterized by similar X-ray attenuation. These limitations may be addressed by the use of a recent imaging method, named X-ray diffraction microtomography (XRD-CT). This method provides 3D phase maps by tomographic reconstruction of diffraction patterns collected at different combinations of rotation and translation steps of the analysed sample. XRD-CT scans can be performed *in situ*, and provide time-resolved images of the 3D phase assemblage evolving by dissolution-precipitation reactions. Quantitative image analysis by means of radial distribution functions provides information on the nucleation mechanisms of the reaction products.

Qualitative and quantitative investigation of microstructures within porous rocks by using very high resolution X-ray micro-CT

Zacher G[1*], Halisch M[2], Westenberger P[3], Paul T[1]

1 - GE Sensing &Inspection Technologies GmbH, phoenix|x-ray
*gerhard.zacher@ge.com 2 - Leibniz Institute for Applied Geophysics 3 - FEI Visualization Sciences Group

In recent years high resolution X-ray Computed Tomography (CT) for geological purposes has contributed increasing value to the quantitative analysis of rock properties. Especially spatial distribution of pores, mineral phases and fractures are important for the evaluation of reservoir properties. The possibility to visualize a whole plug volume in a non-destructive way and to use the same plug for further analysis is undoubtedly the most valuable feature of this type of rock analysis and is a new area for routine application of high resolution X-ray CT. All presented geological CT volume evaluations were performed with GE's Phoenix Nanotom, a 180 kV/15W nanofocus CT system tailored specifically for extremely high-resolution scans with voxel-resolutions down to <300 nm.

The first sample shows a typical reservoir rock scanned with 1 µm voxel size to characterize the pore space and to extract information about the distribution of mineral components (Figure 1). The segmented *in-situ* porosity could be easily used for fluid flow modelling purposes, to predict permeabilities and complex flow processes within these structures.

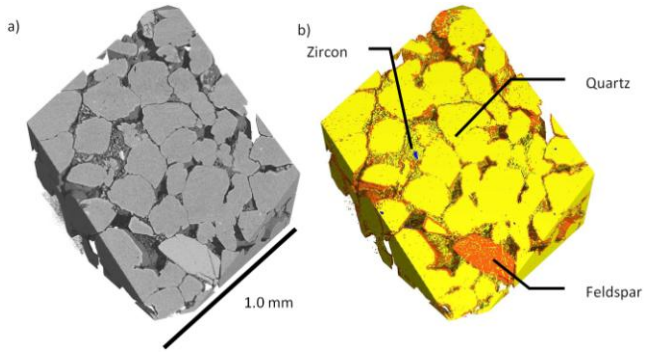

Figure 1: 3D visualization with greyscale (a) and after segmentation (b) of different mineral types.

Second, a very porous pyroclastic rock data set has been analysed at a resolution of 5 µm with the Avizo software tool XLab Hydro (Figure 2). The resulting velocity field can be visualized whereas the colour mapping visualizes the velocity's magnitude.

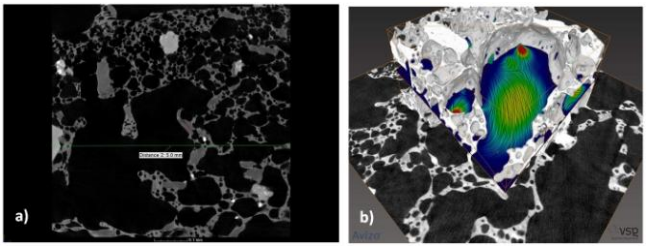

Figure 2: (a) 2D image through the reconstructed volume of a pyroclastic rock (view width: 5 mm). The right hand image (b) visualizes in 3D the results of fluid flow modelling performed by Avizo software.

Today's high-resolution X-ray CT with its powerful tubes and great detail detectability lends itself naturally to geological applications. Those include the non-destructive interior examination and textural analysis of rocks and their permeability and porosity, the study of oil occurrences in reservoir lithologies, and the analysis of morphology and density distribution in sediments – to name only a few.

Mineral analysis of Witwatersrand Basin ore using micro-focus X-ray tomography

Bam L

Necsa. lunga.bam@necsa.co.za

The application of Micro-Focus-X-Ray Computed Tomography (µXCT) in the geosciences as non-destructive probe has shown much potential for the characterization of minerals within rock matrices. The X-rays interact with these minerals resulting in an attenuated X-ray beam that contains information about the energy dependence of the attenuation coefficient of these minerals within the rock. This information is used to quantify rock composition and to discriminate between minerals based on, not only their densities but also their differences in their energy dependent X-ray attenuation. Using tomography enhances, through better statistics, mineral discrimination using attenuation coefficient properties of these minerals. Physical properties such as morphology, distribution, shape and sizes become possible.

The aim of this project is to study the distribution of gold and pyrite using sphericity and roundness. For this project ten samples (11.4mm in size) were analysed, which contained more than enough gold particles to give good statistics. The image analysis results emphasize the shapes and sizes of gold particles and pyrite as they reflect material composition, grain formation, transportation and depositional environments. The linear correlation of gold and pyrite with respect to sphericity and roundness observed in the results will be discussed as well.

CT-scan images as a tool for the evaluation of soil development

Bittar S M B[1*], Heck R J[2]

1 - Universidade Federal Rural de Pernambuco - UFRPE *schulze@depa.ufrpe.br 2 - University of Guelph

X-Ray Computed Tomography (XRCT) images of dry, undisturbed soil samples were used to evaluate incipient soil evolution in 15 technosols, 0-15 years old, located in areas of overburden material (~200 km^2), derived from gypsum mining in the Araripe Basin, NE Brazil. The parent material is a mix of sedimentary rock (siltstone, marl, limestone and shale) that overlaps the gypsum layers, top soil and tailings, deported and accumulated using trucks and tractors in small plateaus which are 30-40 meters high. Soil constituents include rock fragments, soil aggregates, pores and organic matter (OM). The spatial variability (expressed as 3D semivariograms) of the respective radiodensities (X-Ray attenuation) of these principal constituents formed the basis of our investigative approach. Pores and OM show similar behaviour. As a rule, the radiodensities showed rock >soil aggregate >pore, while the variability was soil aggregate >rock >pore.

The XRCT used was an EVS/GE MS8x-130, with a tungsten tube, operated at 120kV and 155mA, with a copper filter, 3500 mS and 720 projections. The GE Reconstruction Utility Software was used to standardize darkness and brightness, (air = 0 HU; water = 1000 HU) and to make scan projection adjustments and reconstruction of the final 3D volume (60µm voxel size). A Gaussian filter was applied and a subvolume (40x40x25 mm) was extracted using Micro View Software. Finally, the segmentation was made using ImageJ Software, containing the plug-in CT Segmentation SD Variant. During the analysis, image slices showing solid ("solid-images") and pores ("pore-images") were generated, and to identify areas in the images corresponding to rocks and soil. First, "seeds" that have characteristics of rocks and "seeds" with soil characteristics were identified (plug-in Pure Voxel Extraction). Given the nature of the parent material, the parameters used to generate these "seeds" were: size >2 mm (33 voxels) and coefficient of variation equal to 0.02. Starting from these "seeds", using the plug-in Region Growing Seed, areas of rocks and soil were generated. To separate pores from soil aggregate areas, the "pore-images" were subtracted. Finally, 3D semivariograms and histograms (radiodensity) for rock, soil and soil aggregate images were made and statistically analyzed, using the Kruskal-Wallis test Step-wise Step-down Multiple Comparisons at 5% significance level.

Statistical data indicate that: (1) Variation in the Rock Radiodensity creates subsets of technosols, but whose significance is uncertain as they are unrelated in age or location. Probably, this result reflects the variation inherent to the parent material associated with sample size (Ø = 6 cm); (2) Soil Radiodensity (soil aggregate + pore), although there are certain discrepancies, grouped soils of between 6-12 years old. The discrepancies doubtless happen because the pores in the incipient stage of soil formation, especially macrospores, are more prominent than soil aggregates. Additionally, the pore development depends on the parent material (mineralogy, friability, granulometry); (3) Soil Aggregated Radiodensity shows the tendency to form 2 subsets: <6 and 6-12 years old. Taking into account the question of representivity of samples, we can consider that this variable provides a good indicator of soil evolution; (4) Rock Semivariogram is a poor indicator of soil evolution, but it is good to show the parent material mixture; (5) Soil Semivariogram shows soil subsets with <4, 6-9 and >9 years old, in short, it is a very good variable to indicate soil evolution; (6) Soil Aggregate Semivariogram also has a tendency to group soils of the same age, but not as good as the Soil Semivariogram.

In conclusion, the best variable used as a tool for the studied soils was the Soil Semivariogram, followed by Soil Aggregated Radiodensity. Indeed this is a preliminary work since only a thin superficial slice of soil was analyzed. Nevertheless, this approach seems to be promising in the study of the development of the Neossolos soil type of Brazil.

The use of X-ray computed tomography to study microwave induced cracks in sphalerite ore particles

Charikinya E[1], Bradshaw S[1], Du Plessis A[2*]

1 - Department of Process Engineering, Stellenbosch University 2 - Stellenbosch University *anton2@sun.ac.za

3D imaging and analysis of a multiphase particulate system by X-ray computed tomography provides detailed information of interest in the analysis of hydrometallurgical operations. X-ray micro CT is now widely accepted as a method to study particle damage during comminution operations and in investigating the nature of particle breakage [1, 2]. For example, it is possible to investigate the internal damage and cracks of ore particles of different sizes and this study utilises the technique to study microwave induced thermal cracks in sphalerite-bearing ore. Tomographic analysis was conducted on fine (-5+4.75) mm, medium (-16+9.5) mm, and large (-25+19) mm ore particles before and after microwave treatment, at voxel resolutions of 5 µm, 15 µm and 25 µm, respectively. Image segmentation, thresholding and spatial registration techniques were then applied to study the microwave induced crack patterns in the ore particles.The results showed considerable micro crack formation with the ore particles. The crack patterns showed cracks propagating across all mineral phases, with no evidence of grain boundary fracture (Figure 1).

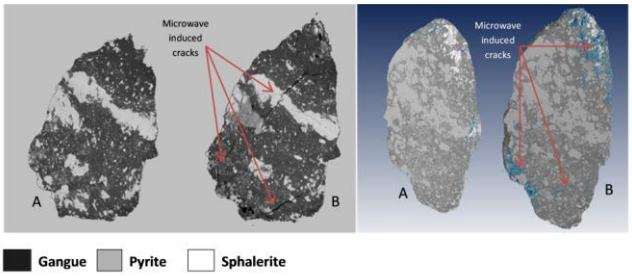

Figure 1: Left image shows a 2D slice image of a medium sized sphalerite ore particle (-16+9.5) mm; right image is a cropped 3D view of a medium sized sphalerite ore particle showing cracks in blue, gangue, pyrite and sphalerite in dark grey, light grey and white, respectively (A- untreated, B-microwave treated).

[1] Ghorbani Y. *et al.* (2011). Use of X-ray computed tomography to investigate crack distribution and mineral dissemination in sphalerite ore particles. *Minerals Engineering*, 24(12), 1249-1257.

[2] Kodali P. *et al.* (2011). Particle damage and exposure analysis in HPGR crushing of selected copper ores for column leaching. *Minerals Engineering*, 24(13), 1478-1487.

Dual energy X-ray computed tomography applied to sulphides in gold ores

Du Plessis A*, Miller J

Stellenbosch University *anton2@sun.ac.za

X-ray micro computed tomography (CT) is a well-established technique that is growing in popularity in the Earth Sciences to visualize the 3D distribution of ore minerals and their associations with non-ore minerals, for example platinum minerals or gold particles within sulphide groups. One limitation of CT images is the potential for different mineral phases to look identical due to poor (absorption) contrast. For example, in a recent study [1], the sulphides were all classed as one phase, though their discrimination was not of interest in that study. The image contrast and hence quality is dependent on various factors, such as the sample type, scanner type and settings, and the presence of artefacts in the images. Post-processing of data using image segmentation methods can assist in extracting useful information. However, the use of standard X-ray absorption CT is inherently limited in sensitivity even when all the above has been optimized and can result in some important mineral phases remaining indistinguishable from each other. Dual energy CT is used widely in medical imaging but is still in its infancy in industrial laboratory CT, with few reported examples in the literature. The difference between two successive scans of the same object (correlated voxel by voxel subtraction of grey values) at two different X-ray energies can highlight features that might have only very small differences in X-ray absorption, hence not clearly discriminated in a single scan. By subtracting these scans from one another, small differences can be highlighted, which can be applied to enhance mineral discrimination for some types of minerals.

In this paper, the imaging capabilities of dual energy micro CT of a gold-bearing ore are presented, with a focus on discrimination of different types of sulphide minerals. An example is shown in Figure 1 of CT slice images containing various sulphide phases: pyrrhotite, chalcopyrite and pentlandite, amongst others. The images correspond to low energy, high energy and a dual energy subtracted image from the aligned volumes. Ignoring the edge effects (vertical red lines), it is clear that specific features have enhanced contrast (red). In both low and high energy scans the difference between pyrrhotite and chalcopyrite is visible, while the dual energy seems to highlight pentlandite, amongst others. Other highlighted particles will be discussed, as well the location of gold relative to the sulphides in this ore type.

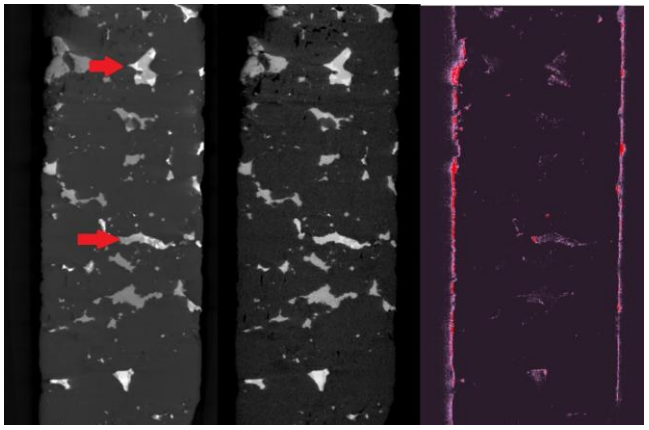

Figure 1: CT slice images of a gold ore sample at low energy (left), high energy (middle), dual energy (right - false colour contrast enhanced). The sulphide minerals are clear in both low and high energy scans, and two of these are indicated by red arrows. Both of these indicated sulphides contain pyrrhotite and chalcopyrite well discriminated by absorption contrast (as dark and light grey). The dual energy image seems to highlight pentlandite, shown in bright red, amongst other minerals.

[1] Godel B. M., Barnes S.J., and Barnes S.-J. (2013). Deposition mechanisms of magmatic sulphide liquids: Evidence from high-resolution X-ray computed tomography and trace element chemistry of komatiite-hosted disseminated sulphides. *Journal of Petrology*, 54(7), 1455-1481.

Development of a simple and fast drill core analysis method with X-ray micro-CT

Le Roux S*, Du Plessis A, Miller J

Stellenbosch University *lerouxsg@sun.ac.za

Even though X-ray micro computed tomography (microCT) is rapidly gaining popularity in the geological sciences as an analytical tool, its main focus is currently academic research. However, with the increased availability of CT service facilities, routine analyses are now also possible. One such possibility is scanning drill core samples for exploration companies to perform a quick ore grade analysis. It is possible to perform quantitative grade analysis on these scans through segmentation and volumetric quantification, however the technique has not been used widely due to various limitations. These limitations include the difficulties experienced in resolving the small particles typical of low ore grades, the inability to distinguish between different ore minerals due to their having similar X-ray absorption properties, as well as the possibility of incorrect conclusions being drawn as a result of image artefacts.

This research aims to develop a rapid technique for mineral exploration in general, to quantify ore grade of both drill core and chippings, working within the limitations mentioned above. By working within the limitations, i.e., samples with relatively high grade, large particle sizes, and ideal scan geometry and size for best scan quality, the results obtainable are comparable with other techniques, while being much faster and without the need for specialised and time-consuming sample preparation.

Calibration standards were used to identify specific mineral types present in the samples in order to quantify the mineral of interest. The cylindrical shape of the core samples contributed toward the quality of the results due to the fact that the X-ray pathway through the core remains constant during specimen rotation providing a more accurate representation of the sample with minimal artefacts. Core sample sizes of approximately 80 mm in length and 35 mm diameter were scanned at 60 microns voxel resolution at 15min per scan, which could allow a scan rate of about 0.4 m of core per hour, making the method cost efficient.

The method was tested on typical drill cores of different types of deposits. Typical data generated in such a drill core "routine" analysis are presented. The method is aimed not at replacing standard laboratory chemical analysis, but providing a fast non-destructive grade estimate and providing additional information not available using other techniques. An example is presented in Figure 1, where a banded iron formation (BIF) drill core was scanned in order to identify different density phases in the core. The CT scan identified the distribution of more dense mineral particles in the core which were not visible on the surface. The 3D analysis results have been utilized to provide quantitative values for average ore grade, association of ore grade with other phases, grade spatial distribution in one or more directions, and particle size distributions.

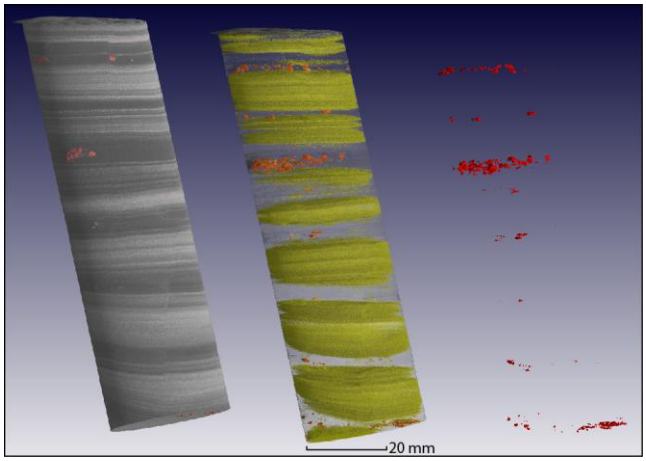

Figure 1: CT scan analysis of a single drill core of a BIF deposit identifying different banded features. The image demonstrates the how the banded structures of the sample can be identified and visualized in 3D space. The grey and white layers indicate the layered variation in density of the core where the white layers (hematite) are denser than the darker grey layers (silicates). The more dense layers are highlighted in yellow alongside the densest mineral particles indicated in red. These layers are separated in the analysis process and quantified to determine the grade of the sample. The most dense particles (barite) occupy 0.02 vol% (red), yellow layers 51.18 vol% and the least dense layers are 48.8 vol% of the drill core sample.

Synchrotron-based micro X-ray diffraction investigations of cement-clay interfaces

Dähn R[1*], Schaub P[1], Pattison P[2], Jenni A[3], Mäder U[3], Wieland E[1]
1 - Paul Scherrer Institut *rainer.daehn@psi.ch 2 - EPFL 3 - University Bern

Synchrotron-based micro X-ray diffraction (microXRD) is a powerful tool for spatially resolved micro-scale investigations of retention processes in heterogeneous systems. Interpretation of the diffraction patterns produced by "real" samples such as polymineralic aggregates, soil nodules or cements is still a challenging task since they are complex images in which many crystal grains from different structures can contribute. The quality of the diffraction data ranges from almost perfect individual single crystals to microfine powders or even non-crystalline materials. The challenge of analyzing these complex diffraction patterns, in order to extract the maximum information concerning both the spatial distribution and the crystal structure type associated with each of the many diffracting grains in heterogeneous, polycrystalline samples will be highlighted exemplarily on a cement-clay interface.

Cement-based materials and argillaceous rocks play an important role in multi-barrier concepts developed worldwide for the safe disposal of radioactive wastes in deep geological repositories. An approximately 180 million year old marine clay-rich sediment (Opalinus Clay) was identified and selected as the first-priority host-rock for the disposal of high-level radioactive waste in Switzerland. Both materials, i.e., Opalinus Clay and cement used for construction of the repository, are heterogeneous mineral assemblages with discrete nano- to micro-scale particles. Hardened cement paste (HCP) consists of mainly calcium (aluminium) silicate hydrates, portlandite, calcium aluminates, and some minor phases such as calcite and hydrotalcite, in a hyper-alkaline environment (pH >11), whereas Opalinus Clay (OPA) is a mineral assemblage consisting mainly of illite, illite-smectite mixed layers, kaolinite, quartz and calcite in near neutral conditions. Cement-clay interface samples were taken from a long-term Cement/OPA-Interaction experiment ("CI-project") in the Mont Terri Rock Laboratory (St-Ursanne, Switzerland) and compared with samples from a natural analogue (Maqarin, Jordan). In order to extract the maximum information concerning both the spatial distribution and the crystal structure type associated with each of the many diffracting grains in heterogeneous, polycrystalline samples, an approach has been developed in which microXRD was applied to thin sections that were rotated in the X-ray beam. The data analysis, performed on microXRD patterns collected from a filled vein of a cement-clay interface from a natural analogue (Maqarin), and a sample from a two-year-old altered interface between cement and argillaceous rock (CI), demonstrates the potential of this method. Whereas in the study on the Maqarin natural analogue sample crystalline C-S-H phases in the form of 11Å tobermorite were observed, no crystalline C-S-H phases were observed in the two years altered samples from the cement-clay field experiment in the Mont Terri rock laboratory.

Pressure-induced reversible transformation of amorphous calcium carbonate (ACC) into an "aragonitic" form

Fernandez-Martinez A[1], Waychunas G[2*], Kalkan B[2], Clark S[3]
1 - Université Joseph Fourier 2 - Lawrence Berkeley National Laboratory
*gawaychunas@lbl.gov 3 - Macquarie University

Amorphous calcium carbonate, known as ACC and having composition of approximately $CaCO_3 \cdot H_2O$, is commonly found during the first stages of biomineral formation as a metastable precursor phase of crystalline $CaCO_3$ polymorphs. It may also be the first forming precipitate in inorganic reactions involving carbonate nucleation at interfaces, such as during mineral trapping reactions. We have examined the high pressure structural properties of ACC up to 20.6 GPa using a combination of X-ray total scattering, Reverse Monte-Carlo analysis and Raman spectroscopy. A structural transition from the 'vaterite-like' local order previously reported for ACC at ambient pressure to an 'aragonitic' form of ACC has been found to occur at a pressure of ~9.8 GPa. The structural characteristics of the high pressure phase are compatible with a local order similar to that of aragonite: a Ca-O coordination number of ~8.5, close to the ideal coordination number of 9 for aragonite, and a higher proportion of Ca-CO_3 complexes linked with bidentate ligands with respect to the ambient pressure state, which has 50% monodentate and 50% bidentate ligands. The transition appears to be reversible upon decompression, although there may be some hysteresis. The fact that the structure is hydrated and that dehydration is not observed during the compression process suggests that water is a key element in the reversibility of the transition. A novel procedure was used to extract the density changes in the ACC as a function of pressure. To our knowledge, this is the first reversible amorphous-amorphous phase transition found for an amorphous ionic system. The scattering and density experiments were performed using a diamond anvil cell system on beamline 12.2.2 at the Advanced Light Source at Lawrence Berkeley National Laboratory.

Minimising measurement uncertainty and improving limit of detection in gold bearing ores from concentrations predicted from linear regression

Fraser A

Allan Fraser &Associates. allan@allanfraserandassociates.co.za

This study shows that the close observances of experimental design criteria in gold assays minimises the uncertainty in measurement in gold predicted from a regression model. Minimising the uncertainty in measurement in gold has cost implications in the real-world of gold mining. Gold has high economic value and high accuracy and reliability are required in gold assays. Even small measurement uncertainty in gold assays will have a marked economic significance when taking into consideration the large volumes of gold bearing ore, base metal or tailings being processed. This becomes apparent when processing of, for example, 100 000 tons of tailings material with a 0.52 g/t concentration of gold. In this study, the improvement made to measurement uncertainty at a 95% confidence level on 0.52 g/t gold is ±0.09 g/t. In 100 000 tonnes of tailings this equates to 52±9 Kg of gold. In comparison to an existing method at Antech Laboratories a broader uncertainty at 51±12 Kg is obtained. The difference between the improved method and the Antech Laboratories method is 3 Kg of or 105 oz. of gold. With the price of gold at US$1245/oz., (January 2014) this difference equates to US$137 800. Improving measurement uncertainty is therefore of real benefit in terms of economics. The accuracy of gold analytical data also has implications on evaluation of ore reserves. Poor accuracy combined with large measurement uncertainty may result in either an underestimation or overestimation of gold reserves in a deposit and may produce spurious recovery values. Gold is often found in base metal concentrates and has a direct influence on their selling price. Where gold values are at trace level, knowledge of the minimum quantifiable quantity of gold is of importance. After tailings have been processed to remove gold by treatment with cyanide, the levels of gold would be appreciably lower than before treatment. Mining companies calculate the recovery of gold by comparing the gold content before and after treatment. Therefore, better knowledge of the minimum quantifiable amount of gold would give more reliable recovery values. It would also benefit exploration companies to have better resolution of low level gold in defining a tailings dump or low grade gold deposit.

Calorimetric studies of boron minerals: danburite ($Ca[B_2Si_2O_8]$) and olenite $NaAl_3Al_6[(BO_3)_3Si_6O_{18}O_3(OH)]$)

Grevel K[1*], Dachs E[2], Benisek A[2], Majzlan J[1]

1 - Jena University *klaus-dieter.grevel@rub.de 2 - Salzburg University

Experimental thermodynamic data for all borosilicates including the minerals of the tourmaline group are very limited. Consequently, van Hinsberg *et al.* [1] list the inclusion of tourmaline in thermodynamic modeling packages based on careful thermodynamic measurements as a key research question about tourmaline that should be addressed in future.

In this study, we present low- and high-temperature heat-capacity (C_P) data for natural danburite ($Ca[B_2Si_2O_8]$) and the tourmaline end member olenite (ideally, $NaAl_3Al_6[(BO_3)_3Si_6O_{18}O_3(OH)]$) which we obtained synthetically. Standard entropies were derived from these measurements.

Danburite was chosen to check the applicability of the physical property measurement system (PPMS) method [2] to boron minerals. The standard entropy of the natural, pure sample (Charcas, Mexico) was derived from low-temperature heat capacity measurements using a PPMS in the temperature range 5 K <T <300 K: S^0_{298} (danburite) was obtained to 153.9 ± 0.8 $JK^{-1}mol^{-1}$. This value agrees very well with S^0_{298} (danburite) = 154.8 ± 2.1 $JK^{-1}mol^{-1}$ obtained by adiabatic calorimetry [3]. Additionally, DSC measurements with a Perkin Elmer Diamond DSC in the temperature range 280 K <T <760 K were performed to check the reproducibility of the PPMS measurements around ambient temperature. The heat capacity curve was fitted to the experimental values:

$C_P(T) = 367.24 - 1289.57 \cdot T^{-0.5} - 0.2047593 \cdot 10^8 \cdot T^{-2} + 0.3213486 \cdot 10^{10} \cdot T^{-3}$.

Analytical data on an olenite sample prepared at 2.5 GPa, 600°C in a piston cylinder device, show excess boron and water relative to the theoretical formula $NaAl_3Al_6[Si_6O_{18}](BO_3)_3O_3(OH)$, coupled with deficiencies in Si, Al, and Na. Thus, a provisional structural formula was derived as $(Na_{0.65}[]_{.35})(Al_{2.72}[]_{0.28})(Al_{5.4}2Si_{0.58})[Si_{3.73}B_{2.27}O_{18}](BO_3)_3(OH)_{3.87}O_{0.13}$ [4]. The standard entropy of a similar sample (No. V 81, [5]) was obtained to 574.2 ± 2.0 $JK^{-1}mol^{-1}$ assuming the composition of the first sample [4]. The C_P curve can be described by the polynomial: $C_P(T) = 1198.85 + 2809.47 \cdot T^{-0.5} - 0.1201668 \cdot 10^9 \cdot T^{-2} + 0.1915016 \cdot 10^{11} \cdot T^{-3}$.

[1] van Hinsberg V.J., Henry D.J. and Marschall H.R. (2011). *Can. Mineral*. 49, 1-16.

[2] Dachs E. and Bertoldi C. (2005). *Eur. J. Mineral.*, 17, 251-261.

[3] Zhdanov V.M., Turdakin V.A., Arutyunov V.S., Semenov Y.V. Malinko S.V. and Khodakovskiy I.L. (1977). *Geochem. Int.* 14 (6), 135-141.

[4] Schreyer W., Wodara U., Marler B., Aken P. van, Seifert F. and Robert J.L. (2000). *Eur. J. Mineral.*, 12, 529-541.

[5] Wodara U. (1996). Unpublished Diploma Thesis, Ruhr-Universität Bochum, 99+xii p.

Chemical environment of iron in mineral fibres determined by XAS experiments

Gualtieri A[1*], Pollastri S[1], D'Acapito F[2], Trapanati A[2], Quartieri S[3]
1 - University of Modena and R.E. Italy *alex@unimore.it 2 - GILDA beamline, ESRF, France 3 - Università degli Studi di Messina, Messina, Italy

Mineral fibres are ubiquitous on Earth; asbestos is the major class of natural fibres worldwide. It includes chrysotile and amphibole asbestos minerals. All amphibole asbestos minerals are banned worldwide whereas chrysotile is banned only in those countries that adopt the indication of the International Agency for Research on Cancer (IARC), which includes chrysotile in Group 1 "substance carcinogenic to humans". Chrysotile asbestos is actually still largely used in many countries that deny the ban of chrysotile asbestos as they consider only amphibole asbestos minerals hazardous to human health (*the amphibole hyphothesis*). The chrysotile ban litigation is still an open issue mainly because revealing the relationship between asbestos and human toxicity is a very difficult task. The determination of the toxicity of mineral fibres should be the outcome of a well pondered assemblage of chemical-physical, mineralogical-structural, and biological information put together to draw a general picture of the complex mechanism. The mineralogical phase characterization in terms of molecular structure, chemical composition, surface reactivity and physical properties is a crucial preparatory step to the understanding of the mechanism of bio-toxicity in its entirety.

In this work, we present the results of XAS experiments (XANES and EXAFS) conducted at the GILDA beamline (ESRF, Grenoble, France) on selected mineral fibres in order to determine the oxidation state of the iron and to obtain information about its chemical environment. The investigated samples correspond to the major classes of mineral fibres of economic and social importance: three chrysotile species including the UICC standard, Balangero and Valmalenco (Italy), crocidolite UICC standard, amosite from Penge (South Africa), anthophyllite UICC standard, tremolite from Val d'Ala and the zeolite erionite from Jersey valley (Nevada USA). The iron content (wt%) of the samples was determined by microprobe analysis: the three chrysotile samples show an iron content of about 2 wt%; crocidolite and amosite about 38 wt%; anthophyllite 10 wt%; tremolite 2.50 wt%; erionite 0.09 wt%.

Phenomenology of the alpha-beta transition of (ultra)-high purity cristobalite

Hess K-U*, Hrynio P, Schmahl W W, Dingwell D B
Ludwig-Maximilians-Universität *hess@lmu.de

The characterisation of cristobalite has recently renewed the attention of the volcanological and applied mineralogical communities. High levels of cristobalite in respirable volcanic ash raise concerns about health effects, whereas the room temperature stabilized beta-cristobalite ceramic powder has great potential for use in production of engineering ceramic materials due to its high resistance.

For this study we prepared cristobalite by using milled ultra-high purity glassy precursor material for 3D fibre optics applications and heated the glass for 12 hours in platinum crucibles at fixed temperatures of 1400°C, 1500°C and 1600°C in air. The fused silica ranged from the "type 1" to the "type 4" category with defined impurity contents (Cl, OH, Al and Alkalis) down to ppm or even ppb level. The synthesis products were examined with a heat compensated standard high temperature differential scanning calorimeter from Netzsch (404 C/3/F Pegasus). The effects of different heating and cooling rates and heating cycles have been evaluated (following Smykatz-Kloss) by the determination of the alpha-beta transformation of cristobalite through: a) the extrapolated onset temperature of inversion -TI- b) the width of the inversion temperature interval c) the shape of the inversion peak, and d) the hysteresis between TI during heating and cooling.

For heating and cooling rates higher than 1 °C/min (as been used in conventional differential scanning calorimetry) reproducible, but artificially broadened peaks in the heat flow curve are observed. For lower heating and cooling rates the true inversion dynamics is revealed in an "inversion temperature range" indicated by individual peaks relating to differently ordered domains; generally the individual peaks position and areas are reproducible during heat cycling. However, sometimes some peaks are growing at the expense of the others. A so far undescribed feature is that during slow cooling the individual peaks resolved by heating collapse to a single broad peak, indicating a difference in the transformation process during the inversion from the tetragonal low-temperature (alpha) form to the cubic high temperature (beta) form. All cristobalites synthesized from high purity glasses are characterized by different inversion temperatures (relating to the specific kind of impurity), but independent of the applied temperature. All new cristobalites show equal or higher degree of "order" than synthesized crystals by conventional routes (such as transforming amorphous silica gel or quartz).

The new high purity cristobalites will enable a concise understanding of structure-property relationships of tectosilicates with an alpha-beta transition behavior.

PLSR – a new tool for quantitative analysis of XRD data

König U*, Degen T

PANalytical.B.V., Almelo, Netherlands *uwe.konig@panalytical.com

Quantitative phase analysis using X-ray diffraction (XRD) has become a standard tool for process optimization and quality control in industrial environments such as mining, metals production or building material industries.

A common method is the Rietveld quantification using structural information to extract/predict information from the full pattern using physical models and fitting techniques. Sometimes this approach is stretched to its limits. That usually happens, when no realistic physical model is available, or when the model is either too complex or doesn't fit to reality.

In such cases there is one very elegant way out: multivariate statistics and Partial Least-Squares Regression (PLSR). This technique is rather popular in spectroscopy as well as in a number of science fields like biosciences, proteomics and social sciences.

PLSR as developed by Herman Wold [1] in 1960 is able to predict any defined property *Y* directly from the variability in a data matrix *X*. In the X-ray powder diffraction the rows of the data matrix used for calibration are formed by the individual scans and the columns are formed by all measured data points.

We will explain the method PLSR and compare it to other statistical methods used in XRD such as Principal Component Analysis (PCA). During the presentation a number of case studies such as the Fe^{2+} determination in iron ore sinter, the crystallinity of pharmaceutical compounds, the flyash content in cement or the amount of FeO in production samples from ilmenite smelting will be discussed and demonstrated.

[1] Wold H. (1966). Estimation of principal components and related models by iterative least squares. In P.R. Krishnaiaah (Ed.). *Multivariate Analysis*. pp.391-420 New York: Academic Press.

Validation of X-ray powder diffraction data for cement manufacturing process control

Loubser M[1*], Ntuane P[2], Verryn S[3], Grote W[4]

1 - PPC Ltd. *maggi.loubser@ppc.co.za 2 - XRD Analytical and Consulting cc, Pretoria 3 - University of Pretoria

A PANalytical CubixPRO was installed at the Hercules Factory during the commissioning of its new Vertical Roller Mill. The instrument was calibrated by PANalytical during commissioning. X-ray Powder Diffractometry is a new process control tool in the PPC group and thorough validation had to be done before the data could be integrated in the normal process control toolbox. No literature references could be found regarding a scientific validation method for XRD as process control tool.

As a first step, two clinker samples were analysed using the Rietveld Refinement method by the Hercules laboratory using the Hercules Cubi'X (Highscore+ Roboriet software), by the centralised Group Laboratory Services on a Bruker D5000 diffractometer with Topaz software and by the University of Pretoria, using a PANalytical X'Pert PRO and third party software, Autoquan/BGMN (GE Inspection Technologies). The differences among the three analyses seemed very large, and in order to find reasons for this, a certified reference material, CRM 2686, was analysed by all three laboratories.

Again, the data did not show good agreement for various reasons: the samples were pulverized before splitting to protect the integrity of the Free Lime and Periclase. In retrospect this was an error, because the phases seem to be particle size dependent and the sample may not have been split representatively.

An additional concern was that the crystallographic data of the phases used for the Rietveld determination influenced the quantification. The point counting data did not correspond well - the correct method would have been to crush a clinker to 1-2mm, homogenize and then mount for point counting but this was omitted in the attempt to homogenise the sample.

A fresh (~10Kg) sample of clinker was collected and screened between 6.3 - 12.5mm. The purpose was to present a more homogenous sample for analysis. The sample will not necessarily be representative of the entire Hercules clinker, but should be more homogenous. After riffle splitting, two portions were taken and packaged as is. The remainder of the clinker was ground to <75µm, homogenized and split using a rotary splitter, sealed and distributed. A 30g portion was removed from each split for homogeneity testing.

In addition the Hercules data were sent to each participating laboratory as raw data, which could be imported into any software and was refined using the above mentioned software and Rietveld refinement strategies. The results will be presented in this paper.

The automatic soft press (ASP100), a revolutionary improvement for quantitative X-ray diffraction of heterogeneous mineral mixtures

Meier R[1*], Campbell I[1], Bruzenak L[1], Götz D[2]

1 - FLSmidth *roger.meier@flsmidth.com 2 - PANalytical B.V.

The development in various industries towards more advanced processes and materials in combination with the recent X-ray diffraction technology asks for more and more quantitative full pattern XRD analysis at different stages of the process. The indispensible preconditions for a reproducible, repeatable and accurate result are the 'perfect' sample preparation, where the highest focus is required to minimize the human factor and to eliminate as far as possible the preferred orientation of the crystallites of different mineralogical phases during sample preparation. The last one of the most critical steps in the process is the pressing of the powder into a sample holder. There are various methods available to compact the sample in the predefined space of the XRD sample holders like:

- Front loading
- Back loading
- Side loading
- Filling the sample into a transmission holder

Up to today most of these methods are, with the exception of back loading, hardly automated and introduce therefore a strong pronounced human factor into the process. This human factor results in many cases in an insufficient reproducibility of the analytical results. On the other hand the back loading method causes, in particular in automated set-ups, a high degree of preferred orientation of plate or stick shaped crystals. The analysts are subsequently struggling with the compromise between repeatability and preferred oriented samples, which influences the quality of the attainable analytical results.

A recent development of the automatic soft press machine (ASP100) opens an opportunity to combine optimal reproducibility, user-friendly operation and lowest preferred orientation, resulting in the best analytical results.

The unique soft press applies a four core step approach consisting of holder and bottom presentation, pouring of a defined sample amount, levelling including random crystal orientation and soft pressing of the sample. This approach results in a very statistical oriented presentation of the sample with a perfect defined surface and sample height. The subsequent XRD measurement shows the perfect data for a full pattern quantitative data analysis with the highest obtainable repeatability, reproducibility and accuracy, the ideal precondition for a reliable analytical result.

This article will demonstrate the revolutionary method and its advantages based on examples of different complex samples by comparing the various, in XRD mostly used, sample preparation methods. The in-depth data interpretation of the achieved results clearly proves the capabilities of the soft press in science, quality and process control.

Routine mineralogical analysis of zircon and rutile intermediate products by the standardless XRD method

Rakgalakane B*, Spicer E

Richards Bay Minerals *ben.rakgalakane@gmail.com

Ilmenite, rutile and zircon are present in economic concentrations in heavy mineral sands as important sources of Fe, Ti and Zr for various industrial uses. The beach sands of northern KwaZulu-Natal, along the Zululand Indian Ocean coastline in South Africa, are mined for these minerals.

Ilmenite is the main component in the magnetic fractions produced by subjecting the heavy mineral concentrate (HMC) to successive stages of high and low intensity magnets. It is used as the smelter feed stock where it is processed at high temperatures to produce titania slag and high purity pig iron. The non-magnetic fraction of the HMC is purified and upgraded at the mineral separation plants to produce high grades of rutile and zircon products. For the metallurgists to reach the targeted zircon and rutile grades, intermediate product streams are periodically sampled and analyzed to enable the precise control of the separation circuits. However, the analysis of these intermediates by traditional methods such as X-ray fluorescence has been difficult due to the scarcity in the market of the certified calibration standards with suitable matrices and concentration ranges.

An automated X-ray diffraction (XRD) method was developed and commissioned for the robotic laboratory for the routine analysis of rutile and zircon intermediate product steams. The samples are fed to the auto-mill and press equipment and analyzed for mineral content on a Thermo Fisher XRF-XRD Workstation that is part of an automated Robotic configuration. Parameters such as milling time and scan acquisition time were optimized, preliminary results were evaluated for method and instrument variability and validated against wet chemical methods. The XRD method is standardless, robust and easily maintainable and measurable with regard to normal X-ray tube drift and stability.

Gold mineralization of the Sinilga deposit (Subpolar Ural, Russia)

Sokerina N*, Kuznetsov S, Piskunova N, Shanina S, Isaenk S[1]

Institute of Geology Komi Science Center UB of RAS *sokerina@geo.komisc.ru

Thermobarogeochemical studies are most relevant to gold-quartz-sulfide type deposits. Ore occurrence Sinilga is an example of such mineralization, which is associated with the Narodinsky granite massif. Host rocks are low graphitic shales related to the Puyva Formation of the Middle Riphean. Gold and non-gold containing quartz veins are widespread here. The mineral composition of gold-sulphide ores has been studied and fluid inclusions have been analysed in the quartz. Using the method of atomic force microscopy (AFM), some growth characteristics of quartz crystals were obtained.

We have studied the fluid inclusions in gold-bearing and non-gold-containing quartz veins. Gold-bearing vein quartz of two generations was investigated: vein quartz (generation 1) and rock crystals (generation 2).

In the non-gold containing quartz, only vein quartz was considered.

It was found that in non-gold-containing vein quartz the homogenization of fluid inclusions frequently occurs at 290-325 °C.

The eutectic temperature of the water-salt solution occurs at -33±2 and - 42.5±1.5° C. Salinity of inclusions varies from 12 to 22 weight % (NaCl equivalent).

In the gold-bearing vein quartz of the first generation the homogenization of fluid inclusions occurs at temperatures 290-390°C. Eutectic temperature of the water-salt solution occurs at - 22.5±0.5°C. Salinity of inclusions varies from 9.5 to 17.5 weight % (NaCl equivalent).

Some of the inclusions include liquid carbon dioxide; the homogenization temperature of carbon dioxide varies from 1 to 25° C.

In the gold-bearing vein quartz of the second generation the homogenization of fluid inclusions occurs at temperatures of 260-290° C. The eutectic temperature of the water-salt solution is - 23±1°C. Salinity of inclusions varies from 7 to 12 weight % (NaCl equivalent). Some of the inclusions include liquid carbon dioxide; the homogenization temperature of carbon dioxide varies from - 7 to 25°C.

The gas composition of individual inclusions was studied by Raman spectroscopy; using gas chromatography, gross analysis is done.

Chromatographic analysis in the main confirms the Raman spectroscopy data. Some differences relate to the content of carbon monoxide. As mentioned above, it was not detected by Raman spectroscopy. At the same time, gas chromatography showed the small contents of this gas in each analyzed sample. It is due to the procedure of the chromatographic analysis: in spite of using the pyrolysis method that minimizes synthesis of the separate gases during heating, to completely eliminate this phenomenon is not possible. According to the chromatographic analysis, the average values of ratios CO_2/CH_4 were determined. Its maximum value correlated with the first generation of gold-bearing vein quartz, and –the minimum value correlated with vein quartz of the barren veins (49.8 and 18.3 respectively).

To investigate growth surfaces, weused atomic force microscopy (AFM)., The growth surfaces of the rhinestone crystals were studied. The resulting images show the basic mechanism of layer-by-layer growth of quartz crystals initiated by screw dislocations. It is the first time when using AFM on rhombohedron faces of quartz crystals that we have received successive images of dislocational growth spirals, compiled from growth steps of elementary height (step height is 6 to 8 Å, which is close to the unit cell parameter *c*).

The concentration of such spirals (screw dislocations) on the rhombohedron faces is about 10^6 cm^{-2}. Capture of the fluid and solid inclusions on the initial crystal formation stage (normal growth mechanism) is considered as the main cause of dislocation origin.

High dislocation density in these crystals suggests that this stage of their formation was characterized by high speeds.

Acknowledgement: The investigation was carried out with the financial support of the Programs of the UrB and FEB RAS № 12-P-5-1027, Scientific School 4795.2014.5, RFBR 14-05-00592a, Basic Research Project of UrB RAS 12-5-6-016-ARCTIC.

Applications of Mineralogic® in the minerals industry

Tonzetic I

Indigo Research Laboratories. igor.zeljko@gmail.com

Mineralogic® is the latest technology in the offering of what has come to be known in industry as "autoSEM" instrumentation. The Mineralogic® system is manufactured by Carl Zeiss, and favours image processing and image analysis during the automatic measurement runs to discriminate between particulate samples and mounting media. Unlike other available systems, analysis times are requested and not analysis counts. The analysis involves a parallel two stream approach where image processing/image analysis forms one stream and energy dispersive X-ray analysis forms a second stream (similar to more traditional technologies). The X-ray analysis and image analysis can then be recombined to form a higher order classification that can increase confidence in mineral/maceral/material identification. This allows for a certain degree of mineral variety classification whereby for instance, a hematite spectral assignation occurring in a mineral grain of a specific shape may be assigned the classification of "specularite". The Mineralogic® system also allows for a degree of correlative microscopy whereby it is possible to "georeference" or correlate images from different technologies (light microscopy, cathodoluminescence, secondary electron images etc.) with those seen in the autoSEM to facilitate mineral identification (especially magnetite/hematite distinction). The applications of Mineralogic® in the minerals industry further include the analysis of coal macerals (organic analogues of minerals), iron ore sinters (materials derived from pre-treatment of iron ore before feeding to a blast furnace), heavy mineral sands, Cu-Co-Ni sulphide ores, manganese ore, precious metal ores and minerals present in coal ash. With improved image processing capabilities, the possibility of using alternative sample preparation pathways to enhance the final image analysis is made apparent. Furthermore, this range of image processing and image analysis options available to the user is presented with a view to possibly distinguishing minerals that are mineralogically the same but may have adverse side effects based on their morphologies (for instance quartz/asbestos that can be easily inhaled *vs.* quartz/asbestos which cannot). The granulation of quartz cemented sandstones providing accurate particle size analyses may prove of interest to Oil &Gas companies. Lastly, the benefits of allowing the operator to setup stage parameters include the use of non-instrument-specific sample block holders.

Coupled XRF and XRD analyses for efficient and rapid characterization of geological materials: applications for the mineral exploration and mining industry

Uvarova Y[1*], Cleverley J[1], Baensch A[2]

1 - CSIRO *yulia.uvarova@csiro.au 2 - Olympus NDT

Portable X-ray fluorescence (pXRF) spectrometry has numerous applications in a wide range of studies, including: non-destructive analyses in the alloy metals industry, particularly scrap metal sorting and material identification; archaeometry; environmental sciences for conducting contamination characterization, removal, and remedial operations at hazardous waste sites; archaeology; non-invasive analysis of museum artefacts; rapid screening of toxic elements in various products, goods and media; and soil analysis and agriculture. In the last decade, pXRF analysis has emerged as an important analytical technique for exploration and mining. Portable XRF offers rapid and cost-effective analysis of geologic samples and provides data of high quality and accuracy where appropriate calibration and quality assurance/quality control protocols are followed. Conversely, until now powder X-ray diffraction (XRD) has been a technique that is used mainly in research. With the advancement in hardware technology, namely X-ray tubes, detectors and processors, and more powerful and sophisticated software packages, X-ray diffraction (XRD) has become a qualitative and quantitative tool for the identification of crystalline materials, and has tremendous potential applications in exploration and mining. With the current progress in development and implementation of automated algorithms for data processing, XRD has the potential to become a routine technique for analysis of geologic materials. Ultimately, combined portable XRF and XRD instrument analyses will allow rapid chemical and mineralogical characterization of a sample, which in turn allows discrimination of lithologies, hydrothermal alteration and ore types. Coupled portable XRF-XRD analyses will pioneer a new paradigm in greenfields and brownfields exploration and geometallurgy. Here, we give an example of the application of coupled pXRF-pXRD analysis and software packages for data processing currently available on the market to a set of geologic samples. The samples chosen for this study are core pulps obtained from a core from a diamond drill hole at the Brukunga pyrite mine, South Australia, closed in the 1970s and currently being used as a Deep Exploration Technologies Cooperative Research Centre Drilling Testing and Training Facility. The rocks intersected by the drill hole are metasediments of the Nairne Pyritic Formation composed of fine-grained greywackes, quartzites and siltstones and pyrite- and pyrrhotite-bearing beds siltstones of Cambrian age. The drill hole intersected the main ore body from 130 to 280 m, and a number of thin zones with pyrite-pyrrhotite veins. The rocks of the Nairne Pyritic Formation are intruded by dolerite dikes. In this study we analyzed a set of core pulps by pXRF, conventional lab assay and lab-based and portable powder XRD. The corresponding diamond drill core was logged and the analytical data were interpreted in light of the logging data, showing exceptional agreement between data obtained with lab analyses and portable instruments. The current study illustrates that combined pXRF-pXRD analysis can be performed on a large set of complex geological samples and the techniques complement each other. Our study also shows the viability and usefulness of portable XRD analysis that is currently underused.

Investigations of XRD standards for the analysis of amorphous content

Verryn S[1*], De Villiers J[2]

1 - XRD Analytical and Consulting cc, Pretoria. *sabine.verryn@xrd.co.za

2 - Department of Materials Science and Metallurgical Engineering, University of Pretoria

Phase quantification using X-Ray Powder Diffraction (XRD) relies on the diffraction of crystalline phases, and the amount of amorphous phases present in a sample has to be determined indirectly. Two principal methods are in use: measurement of the intensity of the broad amorphous peak calibrated using standard additions, or the use of a known amount of an internal standard. The broad peak, however, is not always present and its peak is of variable intensity. The most reliable method is considered to be the internal standard method. For this investigation 50:50 mixtures of well crystallized standard phases were prepared using the following materials: Si (NIST Standard), Si (Aldrich 99% pure), ZnO (Associated Chemical Enterprises 99% pure, annealed at 700 degrees for 4 hours), Fe_2O_3 (Promark chemicals 97% pure 1% LOI), Al_2O_3 (Koch-Light Laboratories 4N+), Fe_3O_4 (Aldrich 99.99%), Rutile (Merck). Independently weighed samples were prepared in triplicate and micronized in a McCrone micronizing mill. A back loading method was used for preparation for XRD analysis. They were scanned using a PANalytical X'Pert Pro powder diffractometer with X'Celerator detector and variable divergence- and fixed receiving slits with Ni filtered Cu-Kα and Fe filtered Co-Kα radiation. Phase contents were determined using the Rietveld method employing 3 different software programs. One phase was defined as the standard and calculations of the (negligible) amorphous contents are highly variable between different Rietveld programs, between different mixtures as well as between different X-ray wavelengths. A small standard deviation in results within groups of the triplicate analyses rules out weighing or sample preparation errors (SD ~ 0.28-0.4%). Preferred orientation correction does not have a major effect on the quantification, but micro-absorption correction gives variable results. There seems no correlation between mass absorption coefficient differences of phases within a mixture and amorphous content. In conclusion: treat the results with circumspection.

Effects of heat treatment on red gemstone spinel: a single-crystal X-ray, Raman and photo-luminescence study

Widmer R[1*], Malsy A[2], Armbruster T[1]

1 - University of Bern *remo.widmer@students.unibe.ch 2 - Gubelin Gem Lab Luzern

A red Burmese (Myanmar) spinel $MgAl_2O_4$ (a = 8.0919(1) Å) containing ca. 0.5 wt. % of each Cr_2O_3 and V_2O_3 was heated in air for 30 d at 600 °C and 650 °C, 5 d at 700°C, and 72 h at temperatures ranging from 750 °C to 1100 °C. The natural and quenched samples were examined by single-crystal X-ray diffraction (XRD), Raman- and photoluminescence spectroscopy. XRD results display the evolution of the cell parameter a, oxygen positional parameter u and bond lengths T-O and M-O, all of which are dependent on the degree of Mg, Al disorder: $^{T}(Mg_{1-x}Al_x)^{M}(Al_{2-x}Mg_x)O_4$ (evaluated by the inversion parameter x according to [1]). The natural spinel has x = 0.157(2) and reaches x = 0.284(4) after water quenching from 1100 °C (quenching in air: x = 0.264(4)). With increasing heat treatment above 700 °C the Raman bands (250 - 900 cm^{-1}) of quenched samples become significantly broadened. An additional band at 727 cm^{-1} assigned to Al-O stretching within AlO_4 tetrahedra [2] occurs first at 800 °C. At room temperature photoluminescence spectra are dominated by a strong R line at 684.5 nm accompanied by poorly resolved N lines: N1 (687 nm), N2 (688 nm), and N3 (689 nm) [3]. The R line is characteristic of the local Cr^{3+} cation surrounding of a completely ordered $MgAl_2O_4$ spinel with x = 0 (normal spinel). N lines are caused by different Mg, Al environments of Cr^{3+}. With increasing inversion the R line decreases in intensity and the N lines become prominent leading to strongly broadened overlapping peaks with a maximum slightly shifted towards higher wavelengths.

The lowest treatment temperature at 600 °C of quenched Burmese spinel indicated decrease of unit cell volume and increase of the inversion parameter to x = 0.199(4). Although, red spinels from the Mogok area (Myanmar) were previously estimated to have formed above 700 °C [4], extrapolation of unit-cell and oxygen-parameter values of heat-treated samples suggest a "closing temperature" of intra-cation-exchange between octahedral and tetrahedral sites for the natural (untreated) spinel at ca. 400 °C.

[1] Andreozzi G.B., Princivalle F., Skogby H. and Della Giusta A. (2000). *American Mineralogist*, 85, 1164-1171.
[2] Cynn H., Sharma S.K., Cooney T.F. and Nicol M. (1992). *Physical Review B*, 45, 500-502.
[3] Mikenda W. and Preisinger A. (1981). *Journal of Luminescence*, 26, 67-83.
[4] Yui T-F., Zaw K. and Wu C-M. (2008). *Ore Geology Reviews*, 24, 192-199.

Rietveld quantification of hydrated slag-fly ash cements

Witzke T[1*], Füllmann T[1], Schöler A[2], Winnefeld F[2], Lothenbach B[2]

1 - PANalytical *thomas.witzke@panalytical.com 2 - EMPA, Switzerland

X-ray diffraction analysis in combination with the Rietveld method enables the quantification of hydrated cementitious systems containing cement, blast-furnace slag and fly ash. The aim of the analysis approach is to determine all occurring crystalline phases and to distinguish between the amorphous contents originating from blast-furnace slag, fly ash and amorphous or ill-crystalline phases formed during the hydration reaction. The investigation of the time dependent decrease of the amorphous blast-furnace slag and fly ash content enables to follow the reaction of these materials and to determine the overall degree of reaction. In order to quantify the different amorphous contents, internal and external standard methods as well as hkl-approaches can be applied. In this study different multi-component cements including clinker, blast-furnace slag, fly ash and limestone were investigated at hydration times of up to 91 days.

High-temperature reaction calorimetry: techniques and applications

Xu H

Los Alamos National Laboratory. hxu@lanl.gov

High-temperature reaction calorimetry is a powerful and versatile tool for measuring thermodynamic properties of natural minerals and synthetic materials. Determination of phase equilibria of minerals is essential for understanding the related geological processes. Studying phase stability and its underlying structural mechanisms is important for designing robust materials for various applications. In this talk, I will first give an overview on the types of high-temperature calorimeters (especially solution calorimeters) and recent progresses in their technological improvements. Then I will present examples of their applications to a variety of materials including minerals, glasses, nanoparticles, and ceramics used for nuclear waste disposal. Particular focus will be given to measurements of the enthalpies of formation, phase transition, order-disorder, and mixing in solid solutions. Complementary results from structural characterization of the materials (e.g., by synchrotron X-ray and neutron diffraction) will also be presented to illustrate structure-stability relations.

A high repeatability electron probe microanalysis of olivine: new analytical protocol with detection limits down to 3 µg/g level

Batanova V[1*2], Sobolev A[1,2], Kuzmin D[3]

1 - ISTerre, Grenoble, France *valentina.batanova@ujf-grenoble.fr 2 - Vernadsky Institute, Moscow, Russia 3 - V.S.Sobolev Institute, Novosibirsk, Russia

Olivine comprises over 50% of the upper mantle of the Earth; it is the common mineral of the ultramafic and basaltic volcanic rocks, mantle peridotites and inclusions in diamond. Composition of olivine provides crucial information on the composition and origin of primary mantle-derived melts and their sources [1, 2]. Of special importance are minor and trace elements in the concentration range over 10 µg/g: Ni, Mn, Ca, Al, Cr, Co, Ti, Zn, P, Na, which are analysable by EPMA [2, 3]. In the current paper we will present ae new analytical protocol for EPMA analysis of these elements, which yields analytical uncertainty of better than 10 µg/g (2 standard errors) and detection limits from 3 to 10 µg/g (based on 3 standard errors of background variation).

The analytical protocol built up on the new JEOL JXA 8230 EPMA in ISTerre, UJF, Grenoble, France. The instrument is equipped with five WDS and one SDD EDS, has a tungsten source gun, and is housed in an environment with controlled temperature (22+/-0.3 degrees C) and humidity (50+/-3%).

The analytical conditions are the following: acceleration voltage 25kV, 900 nA beam current, WDS recording for trace elements (Ni, Mn, Ca, Al, Cr, Co, Ti, Zn, P, Na) and EDS recording for Si, Mg, Fe, total counting time 12 minutes, ZAF correction. Instrumental drift during analytical sessions is monitored by repeated measurements of olivine standards. For trace elements this protocol yields detection limits from 3 to 10 µg/g and average analytical uncertainty of individual analysis of 10 µg/g (2 standard errors). For contents of Fo in olivine analytical uncertainty is about 300 µg/g (2 standard errors).

Comparison of EPMA and LA ICP-MS data for the large range of olivine compositions suggests that accuracy of EPMA is similar to analytical uncertainty noted above. For elements with a concentration over 100 µg/g the obtained EPMA repeatability and accuracy are better than those of LA ICP-MS. For the concentration of elements between 50-100 µg/g both methods show similar repeatability and accuracy; and for concentration between 10-50 µg/g LA ICP-MS yields better repeatability and accuracy. Spatial resolution of EPMA, however, is significantly better: 3-5 µm compared to 30-50 µm for LA ICP-MS. This makes our new EPMA protocol of great advantage for measurement of zoned or small olivine grains.

[1] Sobolev *et al.* (2005). *Nature*, 434, 590-597.

[2] Sobolev *et al.* (2007). *Science*, 316, 412-417.

[3] De Hoog *et al.* (2010). *Chemical Geology*, 270, 196-215.

Quality control: QEMSCAN from a different angle

Lombard A*, Youlton B

SGS South Africa *annegret.lombard@sgs.com

QEMSCAN is traditionally used as an analytical tool for assessing the bulk mineralogy and mineral characteristics of ores and plant products. From a trade point of view, conformity assessments are used to verify products' compliance with requirements of applicable standards and technical regulations for export and import. This is usually done by means of chemical analyses in the case of geological materials. This method however, can create more questions than answers. In this case study the quality control on a supply chain for a sulphide concentrate was tested by a combination of X-ray diffraction analyses (XRD), QEMSCAN bulk modal analysis (BMA) and particle map analysis (PMA) and chemical assays. The following was then assessed: 1) Are the submitted samples comparable, or 2) If inconsistencies are observed, can they be attributed to sampling errors, salting or any other process that would change the characteristics of the material. The bulk modal mineralogy, grain sizes, liberation characteristics and chemical compositions of the samples were specifically compared. Where inconsistencies were noted, a mathematical simulation was then used to determine if they could be attributed to sampling errors, salting or alteration of the material or if a sample swap had taken place.

Calculation of diffraction free spectra using a double-detector µ-EDXRF system

Nikonow W*, Rammlmair D

Federal Institute for Geosciences and Natural Resources *wilhelm.nikonow@bgr.de

A problem in qualitative and quantitative EDXRF analysis on crystalline samples is diffraction. When the Bragg equation ($n\lambda=2d*\sin(\theta)$) is satisfied, diffraction appears, depending on the crystal lattice, the incident angle and energy of the X-ray beam. Diffraction creates peaks in the spectrum that may superimpose element peaks. Quantification of a spectrum containing diffraction peaks is problematic and may lead to higher contents of elements underlying a diffraction peak. The target of this work is to quantify the effect of diffraction peaks by comparing the diffraction-minimized spectra to the original in order to acquire information for balancing time and accuracy of EDXRF measurements.

Within the µ-EDXRF spectrometer M4 Tornado from Bruker Nano the incident polychromatic beam (Rh-Tube, 50keV 600µA; polycapillary lens spot size 17µm) hits the sample in a 51° angle in moving direction, whereas two detectors are mounted in the 90° and 270° positions, each with a 51° take-off angle. Due to the polychromatic beam (0-50 keV) the Bragg equation fits for numerous lattice planes of minerals. In order to minimize or eliminate the effect of diffraction, samples are mapped separately for each detector and a spectrum is saved for each measuring point in a data-cube. For each point the regions of interest for selected elements of both spectra are compared and the minimum of both detectors is calculated using hyperspectral software, commonly used in remote sensing (Figure 1).

By this calculation element peaks remain, whereas diffraction peaks of one or the other detector are corrected by the value of the other one, except for the very special case of a crystal lattice plane lying parallel to the sample surface resulting in diffraction peaks on both detectors and therefore occurring in the minimum-spectrum, too.

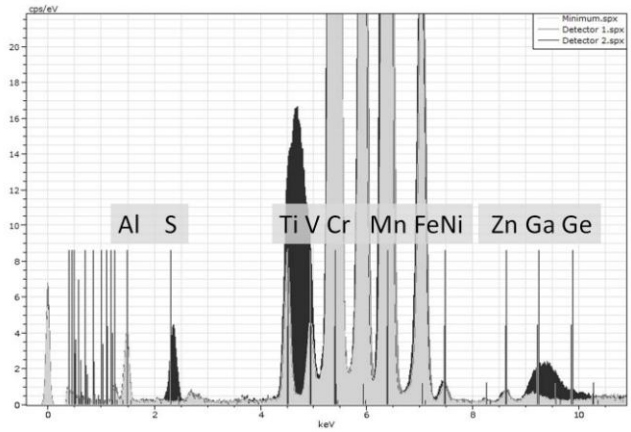

Figure 1: Chromite spectra showing diffraction peaks superimposed on S Kα, Ti Kα, Ni Kα and Ga Kα (Detector 1: grey), (Detector 2: dark grey) and a diffraction-free minimum-spectrum (light grey). High Ti-content in chromite is not uncommon and therefore may be not questioned in this sample, but it can be traced back to diffraction by this method.

Hyperspectral evaluation of the minimum signals for the selected elements is used to obtain phase maps undisturbed by the diffraction generated pseudo-element distribution of a single detector system.

By generating a diffraction-free minimum data cube of full spectra for each measuring point, quantification of selected targets or minerals can be obtained by fundamental parameter calculation with the M4 Tornado software.

Low voltage quantitative microanalysis with a WDS electron microprobe equipped with a FE column

Outrequin M*, Hombourger C

CAMECA *michel.outrequin@ametek.com

Thanks to its precision, its reproducibility and its stability, the Electron Microprobe is a well suited technique to accurately analyze nearly all chemical elements to concentration levels down to a few 10's of ppm, with a spatial resolution of about 1 µm, which is relevant to microstructures in a wide variety of materials and mineral specimens.

With the development of the Schottky emitter and its implementation as an electron source in the Electron Microprobe, small features are commonly analyzed down to sub-micrometre scale. Thanks to the high brightness of the Schottky emitter, a fine focused electron beam can be achieved with both high and stable beam currents even at low accelerating voltages (≤10 keV).

Since X-rays are generated from a much larger diameter than the diameter of the incident electron beam, it is necessary to optimize the two interdependent parameters, accelerating voltage and beam diameter, in order to take full advantage of the FEG electron source for X-ray analysis. The electron beam diameter increases with decreasing the electron beam energy. The interaction volume - within which scattered electrons generate X-rays - decreases with the electron energy as it will be shown on Monte Carlo simulation run with the program CASINO [1]. Thus a small beam diameter is not always synonymous with a small interaction volume and optimized conditions are obtained when the analytical spatial resolution is primarily limited to the diameter of the X-ray emission volume in a specific material.

The ability to accurately quantify precipitate phases on the micrometre and sub-micrometre scale when working at low beam energy with high spatial resolution will be illustrated in such examples as dunite, an igneous rock locally enriched in Platinum, acquired on the CAMECA SXFiveFE. The analytical resolution determined from X-ray maps will be presented.

Acknowledgements: The authors acknowledge Ph. De Parseval et B. Abily from GET for sharing samples.

[1] Drouin D. *et al*. (2007). *Scanning*, 29, 92-101.

Advanced EDS and µXRF analysis of Earth and planetary materials using spectrum imaging, computer-controlled SEM and an annular SDD

Salge T[1], Tagle R[1], Hecht L[2], Mohr-Westheide T[2], Reimold U[2,3], Ferrière L[4], Ball A[5], Kearsley A[5], Smith C[5], Jones C[5], Patzschke M[6*]

1 - Bruker Nano GmbH, Berlin, Germany 2 - Museum für Naturkunde Berlin 3 - Humboldt University Berlin 4 - Naturhistorisches Museum, Vienna, Austria 5 - Natural History Museum, London, UK 6 - Vale S/A, Santa Luzia, Brazil
*maxpatzschke@hotmail.de

Introduction: A combination of energy-dispersive X-ray spectrometry (EDS) on scanning electron microscopes (SEM) with benchtop micro X-ray fluorescence spectrometry (µXRF) enhances data generation for Earth and Planetary science samples.

Methods: Improvements for EDS and µXRF are a result of silicon drift detector (SDD) technology and data processing provided by spectrum imaging techniques. µXRF allows the distribution of elements with Z>10 and trace elements (down to the low µg/g range) to be displayed with a spatial resolution >25 µm. Samples with sizes up to 20x16 cm (~18 thick sections) can be analyzed with the M4 Tornado µXRF system within ~4 hours in one run. The large area µXRF scans can be utilized in locating regions of interest for further high-resolution SEM studies. Using SEM-EDS, minerals in large areas can be classified by automated feature analysis with stage control. This analysis option combines morphological classification with chemical analysis. Analyzing only features of interest by selecting grey scale thresholds in a BSE micrograph reduces measurement and evaluation time. All grains <4 µm in diameter can be classified throughout an entire thin section within <2 hours using a BSE pixel resolution of ~1 µm. The spatial resolution for element analysis can be enhanced to the sub-µm scale by using low accelerating voltages (<7 kV). Extended atomic databases improve the identification and quantification of low energy X-ray lines.

A new type of EDS detector, the annular XFlash QUAD 5060F, is placed between the SEM pole piece and the sample and has a very large solid angle (1.1 sr). It is ideally suited for the analysis of topographically complex, three-dimensional samples. X-rays are collected from four separate detector segments and signals are processed in parallel by four detection units allowing high count rates at low dead-time. Even at the lowest beam current (<10 pA), a sample can be investigated without carbon coating under high vacuum. Compared to low vacuum analysis, this approach reduces hydrocarbon contamination and avoids beam skirting effects.

Applications: (1) Sudbury Igneous Complex: The existence of high demand elements in samples from an offset dike can be determined by µXRF. SEM-EDS analysis of features at the sub-µm scale provides new insights for sulfide, telluride and arsenide deposit models. (2) ICDP Drill Core BARB5: µXRF and EDS analysis of Archean spherule layers in the Barberton Greenstone Belt provide information of the early impact record on Earth. PGE-sulpharsenides (Ø = 0.6-1.4 µm) can be classified by feature analysis using an accelerating voltages of 6 kV at 100 nm BSE pixel resolution. (3) Mocs historic meteorite: µXRF studies reveal lead enrichment along cracks. EDS using the annular SDD indicates contamination of lead as a result of old polishing and soot by heating with coal-fired furnaces. (4) Tissint Martian meteorite: EDS studies with the annular SDD display a thin coating and local enrichment of carbon and nitrogen.

Conclusions: SDD technology, advanced data processing and the possibility to analyze samples more or less non-destructively and with little prior preparation will stimulate new approaches for Earth and Planetary sciences as well for biological and cultural heritage investigations.

Multiscale phase mapping by LIBS and µ-EDXRF: a comparison

Rammlmair D*, Meima J A

Federal Institute for Geosciences and Natural Resources (BGR)
*dieter.rammlmair@bgr.de

Geologists are generally faced with the problem of adequate sample selection in complex rock types such as ores, sediments, metamorphic rocks, etc., to extract best possible information at minimum investigation effort.

Acquisition of comparable information at variable scale helps to optimize sampling strategies and helps to reduce areas for detailed investigations. Ffour systems were applied to drilling cores from Merensky Reef (Bushveld Complex, SA) in the m-, dm-, and cm scale, with sampling point resolutions of 200µm, 60µm, 17µm, and 4µm spot size, respectively, namely: (1) a LIBS (laser induced breakdown spectroscopy) core scanner and (2) microscope from LTB (Laser Technik Berlin), (3) an EDXRF Tornado M4 microscope from Bruker Nano, and (4) for comparison and validation, a SEM-MLA Quanta from FEI.

SEM-MLA requires polished sections (e.g. 3 cm by 3 cm). To avoid time consuming point by point mapping, spectra are collected in the centers of grains classified on the base of segmented BSE image grey values, and are compared to the spectra of a data base to attribute a phase colour to the selected grain.

LIBS and EDXRF collect single spectra for each measuring point of the grid for a given step size. Whilst LIBS requires minimum sample preparation such as split cores (max. sampling area 100 cm by 2.5 cm, with. 3 spectra/sec) and small morphological differences show little effect, EDXRF is sensitive regarding the focus point and operates on cut or polished surfaces (measuring area 20 cm by 12 cm).

LIBS spectra collected by an Echelle-spectrograph with CCD-detector (285-960 nm, resolution 28-94 pm) on the basis of a Nd:YAG 200mJ 1064 laser with spot sizes of 200µm and 50 mJ in the LIBS core scanner, or 60µm and 10 mJ in the LIBS-microscope, provide a large quantity of spectral peaks from which the most significant (non overlapping) are selected for element maps.

EDXRF spectra were collected sequentially by two detectors (180°) in a 90° arrangement to the Rh Tube (50 kV 600µA without filters) and 51° incident and takeoff angles. The minima of each channel of the two detectors were calculated to extract diffraction free element distribution patterns.

For both LIBS and EDXRF-min data sets, the spectral angle mapper algorithm of the ENVI hyperspectral software was applied to extract phase distribution maps.

The phase distribution maps obtained with LIBS, EDXRF and SEM-MLA correspond well on the basis of characteristic minerals of an appropriate grain size. Basic chemical, textural and mineralogical information is obtained by LIBS on a large scale (e.g. drill core), providing information on anomalous portions which can easily be investigated in more detail with the EDXRF microscope for pinpointing areas of interest for polished sections and accurate SEM-MLA and microscopic investigation.

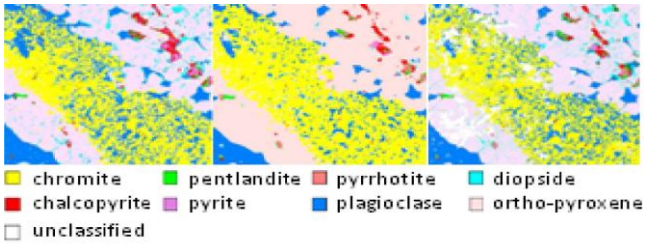

Comparison of phase maps from LIBS, EDXRF and MLA-SEM

The use of QEMSCAN X-ray elemental peak intensity ratios to distinguish isochemical minerals

Tonzetic I

Indigo Research Laboratories. igor.zeljko@gmail.com

QEMSCAN instrumentation falls under the category of what has now come to be known as "autosems" and is in essence an integrated, automated image analysis system based on a Scanning Electron Microscope as its operating platform, with up to four light-element X-Ray detectors attached. It is an instrument that can simultaneously utilise both Backscatter Electron (BSE) brightness and Energy Dispersive (EDS) X-Ray Spectra in the creation of digital mineral images. Off-line data mining, interrogation and graph-plotting is possible with iExplorer software [1].

The aim of this paper is to present a robust way for differentiating minerals with similar chemical elements from each other where QEMSCAN might traditionally have difficulty in doing so.

Over and above the fact that QEMSCAN uses EDS spectra and BSE values to identify mineral phases, it is also able to use what it terms "formulas" which can be written as X/X+Y where X and Y are two separate elements. These formulas were traditionally of limited value though since mineral categories were typically made by collecting EDS spectra and subsequently buffering these identification rules. There was no way to guess the appropriate formula ratios to help define or delineate mineral categories. Prior to 2007, Intellection Pty Ltd had been subdividing Ti minerals of Heavy Mineral Sands into 10 Fe/Fe+Ti fractional groupings/classes, though most analyses were simply classified as "ilmenite" in part because the heavy mineral sands industry dealt with "liberated particles" and in part because there was no way to justify separating the different formulas into different minerals. In early 2009, the author began plotting percentile elemental ratios for selected elemental groupings on histograms to see if specific peaks would form for specific minerals. Abundance histograms per entry were then constructed showing separate peaks for isochemical minerals (in this instance taken to mean minerals that have different ratios of similar elements). The ranges of the separate peaks were then used for primary mineral identification and were successfully used to distinguish the minerals mentioned below:

1.) ferropseudobrookite ($FeTi_2O5$) from ilmenite ($FeTiO_3$) in heavy mineral beach sands (as seen in Figure 1);

2.) orthopyroxene ($(Mg,Fe)SiO_3$) from olivine ($(Mg,Fe)_2SiO_4$) in basic igneous rocks;

3.) muscovite ($KAl_2(AlSi_3O_{10})(OH)_2$) from orthoclase ($KAlSi_3O_8$) in acidic igneous rocks; and

4.) pyrite (FeS_2) from pyrrhotite ($Fe_{1-x}S$) in economic sulphide ores.

Possibly the single most important benefit of this development is that elemental peak intensity ratio histograms provide the opportunity for the provenancing or fingerprinting of sediments if they are used in an analogous way to the best-fit matching of x-ray spectra.

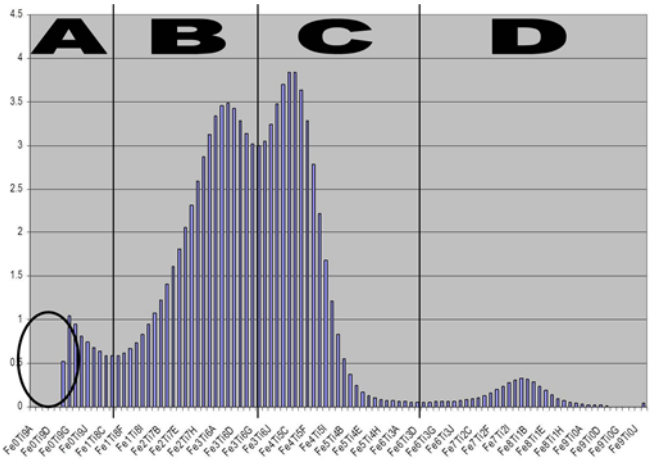

Figure 1. Histogram of QEMSCAN x-ray elemental peak ratios for Fe/Fe+Ti present within analysed heavy mineral sands. Circle presents missing rutile definition. Peaks are represented by the following: (A) - Rutile; (B) - Ferropseudobrookite; (C) - Ilmenite; (D) - Ulvospinel

[1] Tonžetić I.Ž. and Dippenaar A. (2011). An alternative to traditional iron-ore sinter phase classification. *Minerals Engineering*, 24 (12), 1258-1263.

A TES microcalorimeter EDS-SEM system for silicates and other minerals

Uehara S*, Shirose Y, Yamaguchi K

Kyushu University *uehara@geo.kyushu-u.ac.jp

Introduction

A field emission scanning electron microscope (FE-SEM) with a superconductor transition edge sensor (TES) microcalorimeter energy dispersive X-ray spectrometer (EDS) detector was installed in the HVEM Laboratory, Kyushu University, Japan. The FE-SEM is an ULTRA55 (Carl Zeiss Inc.). Furthermore, TES (SII Nano Technology Inc.) is a new commercial tool for chemical analysis using an electron microprobe [1, 2]. These analysis methods are very useful for specimens with microstructure in submicron range. However, a quantitative chemical analysis method has yet to be established. The basic data of FE-SEM with TES-EDS and the preliminary experiment for quantitative analysis using *M* lines of rare earth elements has been partly reported [3]. Further in this study, we investigated silicates and other minerals.

Experimental

The analytical conditions were as follows; accelerating voltage is 5 kV, condenser aperture is 60 or 120 μm, current mode is high and spectra were obtained for 60, 300, 450, 600, or 1800 seconds in live time. TES detector was maintained at 160 mK and energy resolution is 15 eV. Three sets of standard specimens were used: Astimex MINM25-53 mounts (serial number 96-048), JEOL rare earth standard and JEOL sulfide standard for EPMA analysis. Natural serpentinized peridotites were also investigated using this system.

Results

For quantitative analysis, we could apply a calibration curve method, using standard specimens with known chemical compositions. Linear calibration curves were obtained for intensity versus weight % in plots of Si, Mg (Figure 1), Ca, and Fe in Mg-Fe-Ca-Al-silicates (olivine, diopside, pyrope, almandine, and chlorite) and other minerals (periclase, quartz, hematite, magnetite, calcite, and dolomite). Characteristic X-rays were selected for *K* lines of Na to Ca, and *L* lines of transition metals. The errors are about 5 relative % in each element using a linear calibration curve method.

Further, some sulfides (marcasite, pentlandite, sphalerite, stibnite, cinnabar, etc.) were also investigated. Chemical analysis under lower accelerating voltage will be useful for submicron scale minerals in serpentinite analysis.

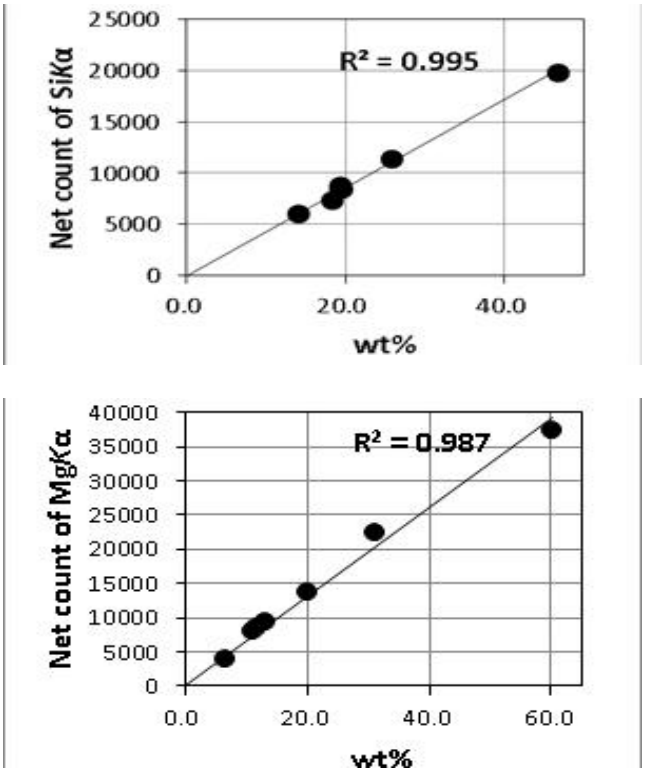

Figure 1: Linear calibration curves for Si and Mg obtained by TES-EDS.

[1] Tanaka *et al*. (2005). *Journal of Surface Analysis*, 12, 122-126.
[2] Tanaka *et al*. (2006). Surface and Interface Analysis, 38, 1646-1649.
[3] Uehara *et al*. (2012). *Journal of Mineralogical and Petrological Sciences*, 107, 105-109.

Proximal core scanning combining laser surfometry and hyperspectral imaging

Decamp X, Pirard E*, Dislaire G

University of Liège *eric.pirard@ulg.ac.be

This study investigates the potential of combining hyperspectral imaging and laser surfometry to identify and quantify lithologies in mining and petroleum exploration. Indeed, automatic core logging is becoming increasingly important in mineral exploration to estimate more efficiently ore deposit reserves with a geometallurgical approach. With this in mind, this research brings mineralogical, grain size and geological textures data during automatic core scanning.

Laser surfometry (obtained by triangulation) is acquired by a camera/laser system arranged with a 30° angle allowing a topography acquisition of a 1cm width groove resulting from a previous scratch-test. The output image owns a 20X20 µm pixel resolution and a 2 µm z-axis resolution. Two hyperspectral cameras, covering VNIR and SWIR spectral wavelengths (400-2500nm), provide hyperspectral data acquisitions. These cameras are linked thanks to mirrors and lenses that enable to study the same area at the same time.

For this research, a drill core (30cm long - sawed in half) has previously undergone a semi-automatic scratch-test which is almost non-destructive but nevertheless producing a 1cm width scratch where optical measurements have been led.

Laser surfometry allows to isolate potential fractures and especially to calculate an estimation of the rock grain size using watershed algorithms. These results are extremely important because of their contribution to later calibrations and corrections during hyperspectral acquisitions and hyperspectral data processing. Hyperspectral IR acquisitions provide reflectance spectra of rocks and, by end member selection, demixion algorithms, spatial and spectral classification, allow to identify and quantify several lithologies and mineral species.

Preliminary results permit us to map core topography, classify rock grain size and create core surface mappings such as lithological data and geological micro-structures.

Regolith characterisation by spaceborne and drillcore spectral sensing data

Laukamp C*, Gonzalez-Alvarez I, Salama W

CSIRO *carsten.laukamp@csiro.au

Extensive regolith cover imposes a challenge for mineral exploration over regolith-dominated terrains, such as large parts of Australia, Brazil, India, West Africa and China. Spatial mineralogical characterisation of the regolith is critical for mineral exploration targeting, for example, in order to distinguish transported from residual material or to identify bedrock lithologies [1].

This paper presents a case study from the Au prospective Albany-Fraser Orogen (AFO) in Western Australia. Publically available, precompetitive ASTER mineral maps [2], covering the eastern Biranup Zone of the northeastern AFO, were compared with hyperspectral drill core logging data, acquired using a HyLogging™ system. A detailed regolith profile was interpreted from the HyLogging™ data, consisting of, from bottom to top, saprock, lower ferruginous and upper kaolinitic saprolite, overlain by a mottled zone, silicified sandstones (Permian bedrock or silcrete), and a lateritic duricrust and gravel at the top of the sequence. A comparable regolith stratigraphy was described by independent, stratigraphic logging [3].

Remote sensing data over the same area identified an erosional saprolite and exposed bedrock-dominated terrain that comprises weathered Proterozoic or potentially Mesozoic bedrock and their transition into lower saprolite. Al-clays are mainly represented by Al-poor smectites (e.g. montmorillonite) and/or white micas without kaolinite. However, upper saprolite can contain kaolinite, shown as a halo surrounding the bedrock or lower saprolite. The abundance of iron oxides can vary considerably in this erosional regime. Bedrock has an intermediate to high iron oxide abundance, with goethite being the dominating iron oxide type. Outcrops of potentially Permian bedrocks (i.e. Paterson Formation) are surrounded by the highest iron oxide contents, especially where they form mesas. Beyond this erosional regime, dune fields and flat depositional environments next to levelled plateaus where interpreted from the ASTER mineral maps.

The ASTER mineral maps enable a spatially comprehensive evaluation of the regolith mineralogy at the district scale. The combination with hyperspectral drill core logging technologies, such as HyLogging™, support the evaluation of the mineral maps, and illustrates that remote sensing data provide not just an image of the Earth's surface, but significant insights on regolith units characterization and stratigraphy. The proposed regolith block model provides an overview over the major regolith-geomorphological landforms of the study area, and can be generated for any other areas of interest in Australia [4] and elsewhere. This enables the comparison of regolith systems from a regional to continental scale.

[1] Cudahy T.J., Caccetta M., Cornelius A. *et al.* (2005). Regolith geology and alteration mineral maps from new generation airborne and satellite remote sensing technologies. MERIWA Report 252, 114 p.

[2] Cudahy T., Caccetta M., Hewson R., *et al*. (2012). Satellite ASTER Geoscience Map of Australia. v1. (DOI. 10.4225/08/51400D6F7B335).

[3] Salama W., González-Álvarez I., Anand R.R. and Abdat T. (2013). Regolith Characterization in the Northeast Albany-Fraser Orogen and Southeast Yilgarn Craton Margin: Stratigraphy, Mineralogy and Geochemistry in the Neale Tenement. CSIRO report EP 139620, 52 p.

[4] Laukamp C. (2013). Regolith landform mapping at the Oldfield well (Laverton Region, Western Australia) using ASTER. IGARSS 2013, 21.-26. July, Melbourne, Australia. IEEE Explore Volume, 4 p.

Quantitative mineralogy of fine particles in slurry from multispectral imaging

Leroy S, Dislaire G, Barnabe P, Pirard E*
University of Liège *eric.pirard@ulg.ac.be

Mineral processing, especially in its final stages, relies heavily on the differential behavior of particles in pulps. In order to monitor hydrocyclones and flotation cells in almost real time, it is important to develop at line particle characterization providing information on particle distribution but also mineralogy. A sampling device has been established based on a flow cell with variable wall spacing linked to a high pressure peristaltic pump. This setup allows for dispersion and dilution of the mineral slurry into the cell. Depending on the ore or gangue minerals to be controlled, particles can be imaged either in diffuse reflectance or in transmittance mode.

A simple multispectral imaging module has been designed to acquire images at eight different wavelengths. The design is based on a series of dichroic filters thereby avoiding any moving part and enabling a very fast acquisition of multispectral images. Imaging artifacts due, among others, to specular reflectance from the glass window are minimized.

Multispectral classification is used to outline particles appearing in the field of view and to qualify their main mineral component. In particular, areas reflecting a meaningful and discriminative spectrum are identified and compared to a multispectral database. The database is continuously enriched through testing of pure mineral particles under similar pulp conditions (dilution, grain size, etc.).

Results of final classification are compared to the modal analysis obtained from polished blocks and conventional reflected light microscopy. The technology developed in this work sets the basis for at line monitoring of ore slurries with reasonably simple mineralogy. Extension of the spectral range is being considered for future developments.

Hyperspectral core imaging applied to drillcore from the La Colosa project, Colombia

Linton P[1*], Jahoda R[1], Montoya P[1], Harris P[2], Pendock N[2]
1 - AngloGold Ashanti *plinton@anglogoldashanti.com 2 - Geospectral Imaging

This paper describes the acquisition, data processing and results of hyperspectral image data collected on drillcore from AngloGold Ashanti's La Colosa porphyry gold project in Colombia. A Specim sisuROCK hyperspectral core imaging system was deployed during three separate imaging campaigns between 2009 and 2012 to collect image data from 257 exploration drillholes totalling 101000 metres of core. Acquisition rates of between 1500 and 2000 metres per day were routinely achieved. The sisuROCK comprised a VNIR-SWIR pushbroom camera collecting 256 spectral bands between 1000 and 2500nm at a spectral resolution of ~6nm and a spatial resolution of ~1mm per pixel, which was supplemented by a RGB linescan camera for colour imagery (in the third campaign only) at a spatial resolution of ~90 microns per pixel. Hyperspectral data were corrected to reflectance, continuum corrected, and spectral indices calculated from absorption features. Spectral indices included both depths and wavelength positions of absorptions, ratios of absorption depths, and band ratios. The spectral indices formed the basis of a series of Boolean decision trees which were used to map the presence of minerals in each image pixel. The data, in conjunction with geological logging, have been applied to mapping of regolith, mapping of alteration mineralogy, and for geometallurgy.

Total iron ore characterisation by combining hyperspectral imaging, Raman spectroscopy and X-ray fluorescence mapping

Ramanaidou E[1*], Nguyen J[2], Mathian M[3], Carey R[4], Honey F[4], Goodey N[4], Wells M[1]

1 - CSIRO *erick.ramanaidou@csiro.au 2 - UWA 3 - Poitiers University 4 - Corescan

Chinese and Japanese steel mills will, before long, require iron ore with detailed chemical, mineralogical, metallurgical and environmental properties. To meet these requirements a combination of techniques is essential. Although hyperspectral analyses by the CSIRO HyLogging™ System of iron ore cores and chips is now routinely used by BHP Billiton Iron Ore in Western Australia for banded iron-formation (BIF) hosted iron ores and channel iron deposits (CID), more information can be gained by adding extra sensors such as hyperspectral imaging, Raman spectroscopy and XRF detectors. The current HyLogging™ System provides point analysis reflectance spectra and a RGB high resolution image. Hyperspectral imaging using the Corescan System™ provides, in addition, a full spectral image at a 0.5 mm pixel resolution, but also a surface topography image thanks to an array of laser beams. Raman spectroscopy adds the ability of detecting and quantifying quartz and magnetite (or maghemite) as well as characterising the hematite and goethite composition, such as aluminium substitution. Micro X-ray fluorescence mapping using a BRUKER Tornado M4 system provides chemical information at a 100 µm scale that cross validates the mineralogical techniques.

Raman fingerprint of spinels

Andreozzi G[1*], D'Ippolito V[1], Lottici P[2], Bersani D[2]

1 - Sapienza University of Rome *gianni.andreozzi@uniroma1.it 2 - University of Parma

Although there has been a large amount of experimental and theoretical work on spinel in literature, a comparative study of Raman shift and relative intensity variations in spinel is lacking.

Synthetic and natural spinel single crystals having compositions approaching spinel end-members $MgAl_2O_4$, $CoAl_2O_4$, $FeAl_2O_4$, $ZnAl_2O_4$, $MgCr_2O_4$ and $ZnCr_2O_4$ were investigated by Raman spectroscopy in the 100-900 cm^{-1} range using the excitation of the blue 473.1 nm line of a diode pumped Nd:YAG laser. Notably, the $FeAl_2O_4$ Raman spectrum is here presented for the first time.

Each studied end-member exhibits a Raman fingerprint with at least one peculiar peak in terms of Raman shift and relative intensity (Figure 1). The chromates exhibit the A_{1g} mode at 680 cm^{-1}, more intense than the other modes and localized at lower frequencies than the aluminates, in agreement with the heavier atomic mass of Cr with respect to Al. For aluminate spinels the more intense and diagnostic peak in the spectrum is: E_g at 405 cm^{-1} for $MgAl_2O_4$, $F_{2g}(2)$ at 516 cm^{-1} for $CoAl_2O_4$, $F_{2g}(3)$ at 660 cm^{-1} for $ZnAl_2O_4$, and A_{1g} at 750 cm^{-1} for $FeAl_2O_4$.

The discrimination between natural and synthetic spinels is quite successful. Synthetic spinels usually show high cation disorder due to their high temperature thermal history, which causes a broadening of the bands and the occurrence of a new peak at ca. 720 cm^{-1} with an A_{1g} mode behavior, not predicted by the group theory.

Results obtained allow discrimination and identification of different spinels from their characteristic Raman fingerprint. Moreover, a detailed Raman study can give information about the cation disorder and then about spinel thermal history.

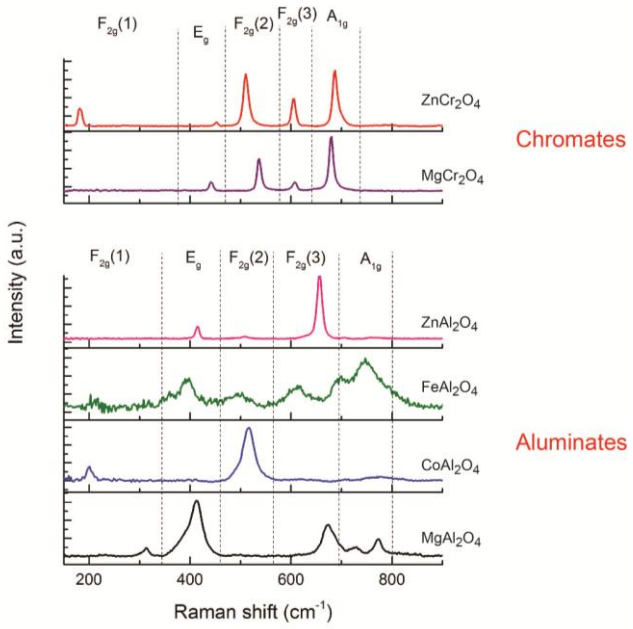

Figure 1: Raman fingerprint of spinel end members

Cation exchange in clinotobermorite: preliminary results

Bonaccorsi E

University of Pisa, Italy elena.bonaccorsi@unipi.it

Cement is commonly used in landfills to stabilize waste materials which contain heavy metals and / or radioactive elements, despite that the behavior of the cement matrix during the process of alteration is very little known. The CSH, mainly responsible for the mechanical strength of the hardened cement, is a substantially amorphous or semi-amorphous compound, with a compositional ratio Ca/Si ranging between 0.6 and 2.0. The detailed study of the incorporation of heavy metals in this material and of its thermal behavior is difficult due to the lack of long-range order. On the other hand, in the same range of chemical composition of the CSH, several crystalline phases exist, whose structure has been solved and described in detail in recent years. Such phases occur also in crystalline state in certain types of cement. Among these phases, the members of the tobermorite group are definitely the most representative. The incorporation of various metals (Zn, Co, Sr, Pb, etc.) in the structure of tobermorite has been investigated by several authors, and the products of such incorporation have been so far characterized with spectroscopic methods. Ziegler *et al.* (2001) hypothesised that Zn-enriched metastable phases formed in treated synthetic tobermorite. They used XAFS (X-ray Absorption Fine Structure) spectroscopy and found that a high concentration of Zn gave rise to a hemimorphite-like phase, whereas low Zn concentration corresponded to intercalation of Zn in the interlayer space of tobermorite. Tommaseo & Kersten (2002) studied the hydration product of tricalcium silicate in presence of zinc oxide. Their EXAFS data suggested that Zn-centred tetrahedra could substitute the end-chain tetrahedra.

Our goal is to build a crystal-chemical model for the Ca-Zn cation-exchange reaction in C-S-H through a detailed study of the effects due to the incorporation of Zn within the well-known crystal structure of clinotobermorite (Merlino *et al.*, 2001). Preliminary single crystal X-ray diffraction results indicated that (1) for autoclaved products at high temperature (150°C) the exchange product is essentially hemimorphite; and (2) for mild-treatment, at 70-80°C, a significant amount of Zn partially substitutes the Ca cations in the interlayer space of clinotobermorite (Figure 1). The bad quality of the exchanged single crystal prevented an acceptable structural refinement, but the Fourier synthesis clearly indicated an additional electron maximum at approximately 1 Å from Ca, with reasonable bond-distances with four neighbour oxygen atoms, which could correspond to 0.3 Zn. The final chemical formula for the exchanged phase, obtained through EDS analyses and X-ray diffraction data, is approximately $Ca_{4.7}Zn_{0.3}Si_6O_{17}\cdot 5H_2O$.

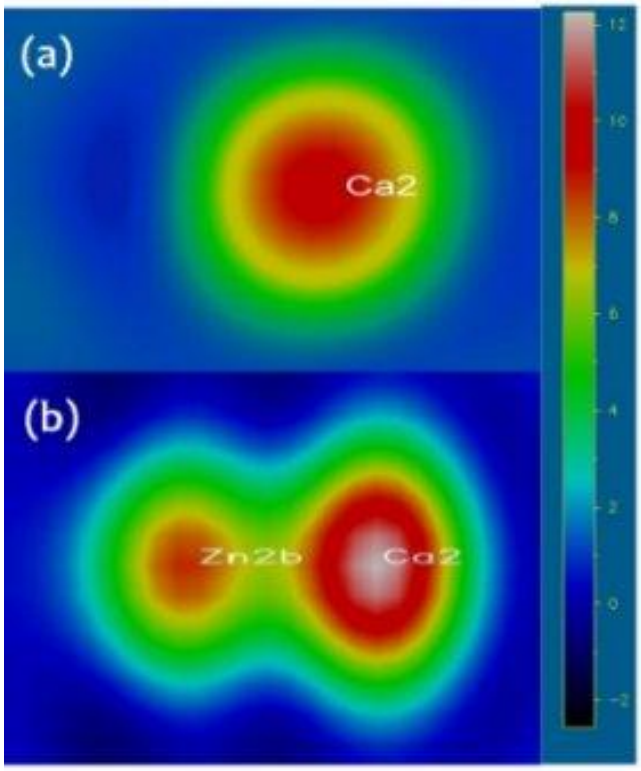

Figure 1: Electron density map in the structural cavity of clinotobermorite (a) for an unexchanged crystal and (b) for a Zn-exchanged crystal.

Crystal structure refinement of the iron ore sinter phases SFCA and SFC and their quantification using powder XRD data

De Villiers J*, Liles D

University of Pretoria *johan.devilliers@up.ac.za

Iron ore sinters are extensively used in ironmaking and they consist of predominant hematite, magnetite and calcium ferrite phases. The calcium ferrite phases are commonly denoted as SFCA (silico-ferrite of calcium and aluminium) and they are important bonding phases that impart improved strength and reducibility to the sinters. Measurement of their quantities is therefore important to assess the extent of the sintering reaction and to correlate the phase quantities with strength and reducibilty indices. For the phase quantification by the Rietveld method, accurate structure data is a prerequisite.

The structure of SFCA has been determined by Hamilton *et al.* [1] and has been used extensively for the quantification of this phase. Additional structure analysis of the magnesium-rich phase was published by Sugiyama *et al.* [2] using the reduced cell choice to describe the SFCAM structure.

Powder XRD data of pure synthesized SFCA do not quite match the calculated patterns, especially in the low-angle region. The calculated patterns show very high intense peaks that do not match the experimental pattern. This normally necessitates an extensive preferred orientation correction which affects the phase quantification, and this motivated a re-examination of the structure.

Crystals of SFCA and aluminium-poor SFC were grown from synthetic mixtures of the constituent oxides and homogenized by successive reaction and regrinding. The homogenized mixtures were then heated to 1300°C for SFCA and 1240°C for SFC, kept at temperature for 14 hours and the slow cooled at 0.5°C/minute. Microprobe analysis gave $Ca_{2.30}Mg_{0.31}Al_{1.67}Si_{0.88}Fe_{8.76}O_{20}$ for SFCA and $Ca_{2.50}Si_{0.65}Fe_{10.85}O_{20}$ for SFC.

Full reflection sphere data were collected for the two phases and the similarity with the Hamilton *et al.* and Sugiyama *et al.* structures was established. However, additional sites of electron density necessitated their inclusion in the structure. This indicated some minor positional disorder in both the SFCA and SFC structures. Final R-factors for the structures are 0.030 and 0.028 respectively.

Comparison of the powder data of SFCA with the calculated pattern from Hamilton *et al* and this study shows that good correspondence is obtained from this structure analysis. This is shown in Figure 1 below. Use of these structure data should lead to a better quantification of the sinter phases.

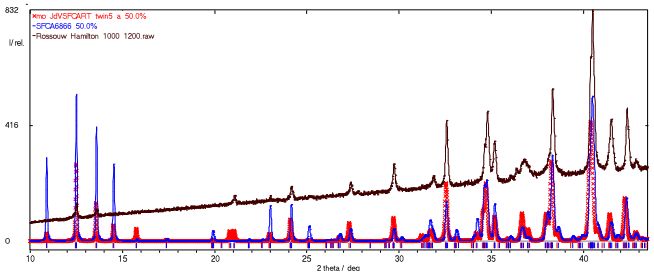

Figure 1: Powder XRD pattern of SFCA with the superimposed calculated patterns; SFCA Hamilton *et al*, blue solid line and this study, red crosses. Better correspondence is apparent, especially in the low-angle region.

[1] Hamilton J.D.G., Hoskins B.F., Mumme W.G. Borbidge W.E., and Montague M.A. (1989). *N. Jb. Miner. Abh.*, 161, 1-26.

[2] Sugiyama K., Monkawa A. and Sugiyama T. (2005). *ISIJ International*, 45, 560-568.

Structure refinement of legrandite and paradamite: crystal chemistry and hydrogen bonds

Jinnouchi S[1], Yoshiasa A[1*], Sugiyama K[2], Miyawaki R[3]

1 - Kumamoto University *yoshiasa@sci.kumamoto-u.ac.jp 2 - Tohoku University
3 - National Museum of Nature and Science

Legrandite, $Zn_2AsO_4(OH)H_2O$ and paradamite, $Zn_2AsO_4(OH)$, are zinc arsenate minerals and have a color between pale yellow and yellowish brown. Related minerals of legrandite and paradamite are adamite, $Zn_2AsO_4(OH)$, and so on with different structures. We performed the structure refinement of legrandite and paradamite Oujela Mine, Mapimi, Durango, Mexico, by (RAPID) RIGAKU single-crystal structure analysis system. We determined the hydrogen position by difference Fourier method. We revealed the detail hydrogen bond using bond valence calculation and hydrogen positions and compared crystal structures of these. The structure of legrandite is constituted by two AsO_4 tetrahedrons, ZnO_6 octahedron and three ZnO_5 trigonal dipyramids that have large unique distortion. AsO_4 tetrahedron, ZnO_5 trigonal dipyramid and ZnO_6 octahedron constitutes the unique framework. The structure of paradamite is constituted by AsO_4 tetrahedron and two ZnO_5 trigonal dipyramid that have large unique distortion. In legrandite, 5 coordination of trigonal dipyrmids have a distance to be expected from ionic radii but interatomic distance of Zn(3)-O(1) has extraordinary distance. Two OH groups bond to Zn1 and Zn2, Zn3 and Zn4 make the $ZnO_3(H_2O)_2$ trigonal dipyramid that is bonded to two H_2O group in legrandite. In paradamite, Zn1 and Zn2 make $ZnO_3(OH)_2$ and $ZnO_4(OH)$ trigonal dipyramid. Hydrogen atoms make a lot of hydrogen bonding in legrandite and paradamite. Crystal structure of legrandite has a tunnel structure continuous that is only parallel to c axis and similar structure is observed in paradamite only parallel to a axis. There are path of proton-conduction in these direction and we conjecture that these proton-conductivity have large anisotropy of one dimension.

Synthesis and crystal chemistry of manganese containing perovskites: ternary perovskites $Ca(Fe,Mn,Ti)O_{3-\delta}$ and $Ca_3(Fe,Mn,Ti)_3O_{8-\delta}$ phases

Stöber S[1*], Redhammer G[2], Pöllmann H[3]

1 - Institut für Geowissenschaften und Geographie *stefan.stoeber@geo.uni-halle.de
2 - Universität Salzburg FB Materialforschung und Physik Abt. Mineralogie 3 - MLU

With the improvement of iron rich CAC cement properties due to intergrinding and sintering of Mn - secondary raw materials and cement raw meal, perovskite phases contain significant concentrations of Mn^{3+}/Mn^{4+} ions, dependent on the oxygen fugacity (fO_2). Brownmillerite phases, structurally described as oxygen deficient perovskites, can compensate certain amounts of Mn^{4+} due to incorporation of additional oxygen, but will become unstable and dissolve into Alumina rich Iron - Manganese - brownmillerites $Ca_2(Al,Mn,Fe)_2O_{5+\delta}$ and perovskites $Ca(Mn,Ti,Fe)O_{3-\delta}$.

Beside the typical layer sequence of tetrahedra (t) - octahedra (o) in brownmillerite type structure, different stacking sequences can be stabilized due to the variation of fO_2. These structures are built up of different sequences like oo or too. In order to investigate these phases, samples with the chemical compositions $Ca_2Al_2O_5$-$Ca_2Fe_2O_5$-$Ca_2Mn_2O_5$ and $CaFeO_{3-\delta}$ - $CaMnO_{3-\delta}$ - $CaTiO_3$ were synthesized either as powders by sol - gel methods or as single crystals.

The crystal structures were refined using neutron diffraction techniques at the BENSC E6 of the Helmholtz - Centre Berlin for Materials and Energy, the manganese valences were determined by iodometric titration. The valence state of iron was determined by Mössbauer - spectroscopy.

The phases with the chemical composition $Ca(Fe,Mn,Ti)O_{3-\delta}$ with $ABO_{3-\delta}$ type structure crystallize predominately in space group *Pnma*. With the incorporation of trivalent iron the space group changed to *I4/mcm* and finally into Pm3m. The phase transition is also dependent on the temperature level, which was proofed by high temperature XRD.

Phase with the chemical composition $Ca_3(Fe,Mn,Ti)_3O_{8+\delta}$ (n = 3 $A_3B_3O_{8+\delta}$) were only synthesized purely in a narrow range as long as enough iron filled the tetrahedrally coordinated sites in the crystal structure.

$(Cs,K)_3DySi_6O_{15}$: a novel framework structure type based on Si_6O_{15} rings

Wierzbicka-Wieczorek M[1*], Göckeritz M[1], Kolitsch U[2], Lenz C[3], Giester G[3]

1 - Friedrich-Schiller University, Jena, Germany
*maria.wierzbicka-wieczorek@uni-jena.de 2 - Naturhistorisches Museum, Wien, Austria 3 - Universität Wien, Austria

The silicate $(Cs_{9.19}K_{5.81})Dy_5Si_{30}O_{75}$, simplified $(Cs,K)_3DySi_6O_{15}$, is one of 12 silicates obtained during an ongoing detailed study focusing on the synthesis, structural and optical properties of novel silicates containing Sm^{3+}, Tb^{3+}, Dy^{3+} and Pr^{3+} cations. It was synthesised using a high-temperature flux method in air (T_{max} = 950 °C) forming colourless, acicular crystals.

Its structure was solved based on single-crystal X-ray intensity datasets collected at room temperature on a Bruker AXS APEX2 diffractometer with Mo*K*α radiation in space group *R*32 with unit cell parameters *a* = 13.896(2), *c* = 35.623(7) Å, *V* = 5957.2(17) $Å^3$, to *R*(*F*) = 4.41% for 4517 reflections. The asymmetric unit contains three Dy sites, three mixed Cs/K sites, five Si and 14 O sites. $(Cs_{9.19}K_{5.81})Dy_5Si_{30}O_{75}$ represents a novel crystal structure type with a mixed-framework architecture based on roughly circular Si_6O_{15} rings and isolated DyO_6 octahedra (mean Dy-O distance is 2.23 Å). Due to the connectivity of the Si_6O_{15} rings, additional, more irregular rings are formed that are built from six SiO_4 tetrahedra and one DyO_6 octahedron. Above and below these latter rings, the Cs/K sites are located. $(Cs_{9.19}K_{5.81})Dy_5Si_{30}O_{75}$ conforms to the PME ('polyhedral microensembles') type A-1, which is characterized by sharing each corner of MO_6 octahedra with a SiO_4 tetrahedron [1].

The known silicates containing $[Si_6O_{15}]^{6-}$ units crystallize in monoclinic, orthorhombic or trigonal crystal systems and show various structural topologies. Among the eight silicates present in the ICSD and the recently reported compound $(Cs,K)_3SmSi_6O_{15}$ [2], only one silicate, namely $Cs_3DySi_6O_{15}$ (space group $R\bar{3}m$, a = 13.996, c = 7.178 Å) [3] shows a similar rhombohedral unit cell (with *c*/5) and an apparently closely related atomic arrangement. However, we consider the reported structure model for $Cs_3DySi_6O_{15}$ doubtful since except for Dy (one site) all Cs, Si and O atoms (one, one and three sites, respectively) are "disordered" (Si-Si = 0.73 Å, Cs-Cs = 0.99 Å); in addition all O sites show anomalously elongate displacement ellipsoids.

PL spectra of $(Cs_{9.19}K_{5.81})Dy_5Si_{30}O_{75}$ were obtained from randomly oriented crystals at room temperature using a Horiba Jobin Yvon LabRAM-HR 800 spectrometer with 473 nm laser-excitation. Rather weak luminescence emissions are interpreted to be intra 4*f*-transitions of Dy^{3+} cations. Low luminescence efficiency is attributed to self-quenching effects due to occupancy of the REE octahedral site solely by Dy^{3+}. The strongest emission is the $^4F_{9/2} \rightarrow {}^6H_{13/2}$ transition, observed in the visible-yellow spectral range at 570 nm.

[1] Ilyushin G.D. and Blatov V.A. (2002). *Acta Crystallogr*., B58, 198-218.

[2] Wierzbicka-Wieczorek M., Göckeritz M., Lenz C. and Giester G. (2014). Synthesis, structural and optical characterizations of $(Cs,K)_3SmSi_6O_{15}$, 22nd Annual Conference of the German Crystallographic Society, 17 - 20 March 2014, Berlin, Book of Abstracts, Poster MS05-P04.

[3] Zhao X., Li J., Chen P., Li Y., Chu Q., Liu X., Yu J. and Xu R. (2010). *Inorg. Chem*., 49, 9833-9838.

Structural investigations on $Ca_2Mg(NO_3)_6 \cdot 12H_2O$, a new hydrous nitrate retrieved from chimney deposits of a combined heat and power plant

Kahlenberg V*, Tessadri R, Haefeker U

Institute of Mineralogy and Petrography, University of Innsbruck

*volker.kahlenberg@uibk.ac.at

In contrast to the large group of natural carbonates the number of nitrate minerals is rather limited. Although compounds such as niter (KNO_3) or nitratine ($NaNO_3$) can form large exploitable deposits of thousands or even billions of tons (Chuquicamata district, Chile) the occurrence of most of the natural nitrates including nitrocalcite ($Ca(NO_3)_2 \times 4H_2O$) or nitromagnesite ($Mg(NO_3)_2 \times 6H_2O$) is restricted to caves with very special conditions of formation. In the field of applied mineralogy, on the other hand, both phases have attracted much more interest. For example, both compounds are among the most common deterioration agents responsible for salt attack of buildings and monuments. To the best of our knowledge no intermediate synthetic or natural hydrous Ca-Mg-nitrate has been reported so far.

Starting point for this study was a routine X-ray powder diffraction phase analysis of a series of samples which were obtained from incrustations of an exhaust gas chimney of a combined heat and power plant located in Malchow/Germany. What seemed to be a routine X-ray powder diffraction job turned into an interesting crystallographic problem. Phase analysis using the current version of the PDF-4 database showed the existence of a small amount of anhydrite as well as bassanite. However, the majority of the peaks could not be attributed to any phase or phase mixture contained in the powder diffraction file. A re-examination of the residual under a petrographic microscope revealed that the sample contained a large number of colourless transparent crystals. A single-crystal of good optical quality was further studied by X-ray single-crystal diffraction (performed at 25°C). Structure solution was also used to establish the chemical composition: $Ca_2Mg(NO_3)_6 * 12H_2O$. The presence of water as well as nitrate moieties in the structure was confirmed by micro-Raman spectroscopy. Basic crystallographic data are as follows: trigonal symmetry, space group *R* -3, a=10.5583(5) Å, c=19.5351(10) Å, V=1885.98(16)Å^3, Z=3, R(|F|)=0.0248 for 744 reflections with I>2s(I). Principal structural building units are columns containing an alternating sequence of $Mg(H_2O)_6$-octahedra and CaX_9 tricapped trigonal prisms. (X:H_2O molecules, O atoms from the nitrate groups). Linkage between the polyhedra of a single column as well as between neighbouring columns is provided by hydrogen bonding.

Using the result of the structural investigation a quantitative phase analysis of the incrustations based on the Rietveld method could be accomplished.

Jahn-Teller effect in tourmaline

Ertl A[1*], Tillmanns E[2]

1 - Naturhistorisches Museum *andreas.ertl@a1.net 2 - Universität Wien, Institut für Mineralogie und Kristallographie

After checking the structural data of different Cu^{2+}- and Mn^{3+}-rich tourmalines, we found the first tourmaline worldwide, in which the Jahn-Teller effect seems to be well established. The studied blue Cu-rich tourmaline was synthesized at the Institute of Mineralogy and Petrography, Novosibirsk, Russia (Lebedev *et al*. [1]; further characterisations by Vereshchagin *et al*. [2]). The Cu-richest zone (~14 wt% CuO) of a synthetic tourmaline crystal, with a = 15.849(1), c = 7.087(1) Å (R = 2.5%), has the formula $\sim{}^{X}(Na_{0.8}[]_{0.2})\ {}^{Y}(Cu_{1.8}Al_{1.2})\ {}^{Z}Al_6\ {}^{T}(Si_{5.2}Al_{0.4}B_{0.4})O_{18}\ (BO_3)_3\ {}^{V}(OH)_3\ {}^{W}[(OH)_{0.6}F_{0.4}]$ (Ertl *et al*. [3]). The *Y*O_6 octahedron of this, as far as we know, Cu-richest tourmaline is mainly occupied by Cu. Two of the six (Cu,Al)-O distances are significantly enlarged: Cu-O1 with 2.031(2) Å and Cu-O3 with 2.170(2) Å. The other (smaller) distances are Cu-O2 (2x) with 1.949(1) Å and Cu-O6 (2x) with 1.952(1) Å. The proportion of the average of the two enlarged distances to the average of the other distances gives a value of ~1.077, which is the highest value known so far for Cu-rich tourmalines. We conclude that the Jahn-Teller effect seems to be verified for this investigated tourmaline sample which is not surprising, because this tourmaline is the only known sample with a Cu-dominant octahedrally-coordinated Y site. However, since all oxygen atoms of the YO_6 octahedron are corner- or edge-connected to other coordination polyhedra and since the YO_6 octahedron has only a Cu^{2+} occupation of about 60% the Jahn-Teller effect is by far not as pronounced as in other copper-bearing compounds.

Acknowledgments: This work was funded by the Austrian Science Fund (FWF) projects no. P23012-N19 and no. P-26903-N19.

[1] Lebedev A.S., Kargalcev S.V. and Pavlychenko V.S. (1988.In: Proc. Gen. & Exper. Mineral. Growth and properties of crystals. Novosibirsk, Nauka. (in Russian).
[2] Vereshchagin O.S., Rozhdestvenskaya I.V., Frank-Kamenetskaya O.V., Zolotarev A.A. and Mashkovtsev R. I. (2013). *Am. Mineral*., 98, 1610-1616.
[3] Ertl A., Vereshchagin O.S., Giester G., Meyer H.-P., Ludwig T., Rozhdestvenskaya I.V. and Frank-Kamenetskaya O.V. (2013). *Mitt. Österr. Miner. Ges*., 159, 53.

The structure and crystal chemistry of harkerite and sakhaite

Evans R[1], Groat L[1*], Grew E[2]

1 - University of British Columbia *groat@mail.ubc.ca 2 - School of Earth and Climate Sciences, University of Maine

Harkerite, c. $Ca_{48}Mg_{16}[AlSi_4(O,OH)_{16}]_4(BO_3)_{16}(CO_3)_{16}(H_2O, HCl)_2$, and sakhaite, c. $Ca_{48}Mg_{16}(BO_3)_{32}(CO_3)_{16}(H_2O, HCl)_2$, are rare complex borate-carbonate minerals typically found in calcareous skarns formed at low pressure and high temperature, but have also been reported from a deep-seated, granulite facies complex. These two minerals form a substitution series where aluminosilicate pentamers, $AlO_4(SiO_3)_4$, replace groups of four disjoint borate triangles, $(BO_3)_4$; in harkerite, one half of the borate groups are replaced by aluminosilicate pentamers. Substitution of additional CO_3 for BO_3 of up to 4 per formula unit has been reported in both sakhaite and harkerite. Interstitial H_2O or HCl occur within the cavities of some $(BO_3)_4$ groups not replaced by aluminosilicate pentamers, from 2 per formula unit up to the highest reported 15 per formula unit. The overall composition may be described by the general formula

$Ca_{48}Mg_{16}[AlSi_4(O,OH)_{16}]_x(BO_3)_{32-4x-y}(CO_3)_{16+y-w}(OH)_{2w}(H_2O,HCl)_z$.

Sakhaite has cubic symmetry at least up to x = 1.5, space group *Fd-3m*, with unit cell a = 14.7 Å (Z = 1), while harkerite (x = 4) has rhombohedral symmetry, space group *R-3m*, unit cell a = 10.4 Å, c = 51.3 Å (Z = 3/2); the 3-fold rotational axis of this latter cell corresponds to a doubling of the body diagonal in the cubic unit cell. Disorder of the borate, silicate, carbonate and interstitial H_2O/HCl groups leads to strong cubic pseudosymmetries in harkerite and intermediate sakhaite-harkerite compositions. Compositions with x >4, i.e. with total Si >B, have not yet been reported but a B-free harkerite end-member is believed to be possible by analogy with the structurally and topologically homeotypic tychite $[Na_6Mg_2(CO_3)_4(SO_4)]$.

We decided to study the crystal chemistry of the sakhaite-harkerite series to (1) fully define harkerite; (2) characterize symmetry and crystal structures across the series; (3) identify and characterize new members of the family; (4) study the roles of OH, H_2O, and HCl molecules in the crystal structure; (5) define the stability range(s) of the series, and (6) study mineral associations and parageneses. This study has been inititated the refinement of the crystal structure of a sakhaite from Yakutia in Russia in space group *Fd*-3*m* to $R1$ = 3.1%; we have also recently initiated our study of harkerites from the Cascade Slide in New York state but the correct symmetry is not yet clear.

A natural barium zeolite related to zeolite ZK-5 from the Gun claim, Yukon Canada

Peterson R[1*], Farber G[2], Evans R[3], Groat L[3], MacNeil L[1], Joy B[1], Witzke T[4]

1 - Department of Geological Sciences, Queens University, Kingston, Ontario *peterson@queensu.ca 2 - Mineralien, Samswegen, Germany 3 - University of British Columbia 4 – PANalytical

A natural zeolite mineral, ideally, $Ba_{42}Si_{66}Al_{30}O_{192}Cl_{25}(OH)_{34}$ is described from the Gun claim, just south of the Itsi Range, Yukon Territory, Canada. The zeolite occurs as equant grains up 200 microns across, enclosed within large gillespite crystals. The mineral is transparent, has a vitreous luster and is non-fluorescent. It has a white streak and Mohs hardness of approximately 5½. It is brittle with no observed cleavage. The calculated density based upon the empirical formula and single-crystal unit cell dimension is 3.37 g/cm^3. The mineral is optically isotropic (n= 1.598) Electron-microprobe analyses (average of 11): SiO_2 28.30, P_2O_5 1.61, Al_2O_3 11.75, TiO_2 0.05, FeO 0.27, CaO 0.21, BaO47.61, Na_2O 0.15, K_2O 0.21, Cl 6.64 and a total of 96.80%.The empirical formula (based on 192 O *apfu*) is $Ba_{41.1}Ca_{0.5}Fe_{0.5}Na_{0.6}K_{0.6}Si_{62.4}Al_{30.6}P_{3.0}O_{192}Cl_{24.8}\cdot 33.4(OH)$. The zeolite is cubic, *Im3m*, a=18.5502(4) Å, V = 6383.3(2) Å^3 and Z= 1.The ten most intense lines in the X-ray powder diffraction pattern are [d_{obs} in Å(*I*)(*hkl*)]: 4.39(70)(411), 4.16(26)(420), 3.798(25)(422), 3.288(34)(440), 3.189 (100)(433), 3.100(22)(442), 3.016(72)(611), 2.803(42)(622), 2.629(31)(710), 2.529(28)(721), 3.323(46)(800), 2.287(59)(741).

The crystal structure (R_1 = 4.0% for 1531 $F_o > 4sF$) is a three dimensional framework of silicon-, aluminium- and phosphorous-containing tetrahedra that created an open framework consisting of a large cubo-octahedral cavity connected by channels made of double 8-membered rings and double 6-membered rings. The framework is the same as that observed for zeolite ZK-5 (KFI). The phase has been submitted for recognition as a new mineral species.

Valletta mine: a treasure trove of new minerals in the Western Alps

Cámara F[1*], Ciriotti M[2], Bittarello E[1]

1 - University of Torino - CrisDi, Italy *fernando.camaraartigas@unito.it 2 - Associazione Micromineralogica Italiana

The Valletta Fe-Mn deposit is located in the Briançonnais Zone of the Cottian Alps. It is the remains of an old mining operation, probably an open pit, at 2536 m asl, active in 1455 in the Saluzzo Marquisate. For more than 5 centuries it was abandoned until a recognition exploration by G.C. Piccoli, who noticed the presence of mineral phases in quartzite and quartz veins difficult to classify. As in previous occasions, the collaboration among mineral collectors and academia researchers led to a detailed study of the mineral phases in the collected samples and soon it was evident that a forgotten and unknown treasure had been unearthed. Since then we have recognized a great number of new mineral compositions and its characterization has led to new approved mineral species, grandaite $Sr_2Al(AsO_4)_2(OH)$ (space group $P2_1/m$, a 7.5764(5), b 5.9507(4), c 8.8050(6) Å, β 112.551(2)°, V 366.62(4) Å^3, Z 2; IMA-CNMNC no. 2013-059, [1]) and braccoite $NaMn^{2+}{}_5[Si_5As^{5+}O_{17}(OH)](OH)$ (triclinic, space group $P\bar{1}$, a 9.7354(4), b 9.9572(3), c 9.0657(3) Å, α 92.691(2)°, β 117.057(4)°, γ 105.323(3)°, V 740.37(4) Å^3, Z 2 ; IMA 2013-093 [2]). But many others are on the run: we have observed a large solid solution among vanadates and arsenates of the arsenbrackebuschite group, including compositional changes among Ba, Sr and Ca members and proposals for new mineral species are being submitted to IMA-CNMNC. Within these series we have observed a triclinic modification (triclinic, space group $P\bar{1}$, a 6.1187(3), b 9.3705(4), c 14.2503(9) Å, α 99.914(5)°, β 112.433(5)°, γ 89.983(4)°, V 785.39(7) Å^3, Z 4). We have also recognized unknown Mn-Fe oxides that deserve appropriate studies. The description of the mineral treasure trove has become an exciting experience.

[1] Cámara F., Ciriotti M.E., Bittarello E., Nestola F., Massimi F., Radica F., Costa E., Benna P., and Piccoli G.C. (2014). *Mineralogical Magazine* (in press).

[2] Cámara F., Bittarello E., Ciriotti M.E., Nestola F., Radica F. and Marchesini M. (2013). Braccoite, IMA 2013-093. CNMNC Newsletter No. 18, December 2013, page 3256; *Mineralogical Magazine*, 77, 3249-3258. doi:10.1180/minmag.2013.077.8.15.

Microstructural evolution of carbonaceous material during natural graphitization process: an integrated HRTEM, micro-Raman and XRD study

Nakamura Y[1*], Madhusoodhan S[2], Toyoshima T[2]

1 - Graduate School of Science &Technology, Niigata University *f12e059g@mail.cc.niigata-u.ac.jp 2 - Niigata University

Structural evolution of Carbonaceous Material (CM) assumes a key role as a thermal indicator, however, it is also well known that many factors such as fluid activity, shear stress and presence of catalysts can affect natural graphitization. In this study, we present a detailed microstructural study on the evolution of CM to judge the influence of these factors by combining SEM, HRTEM, micro-Raman spectroscopy, XRD and carbon isotope analysis. A typical progressive metamorphic terrane of very low to high grade metamorphic rocks located in the central part of Hokkaido, Japan was selected for this purpose. We divided the study area into four metamorphic zones based on the metamorphic temperature estimates by Illite Crystallinity data, Raman Spectra on Carbonaceous Material thermometry and the previous petrologic studies; zone Ia (200 ~ 300 °C), zone Ib (300 ~ 400 °C), zone IIa (400 ~ 500 °C) and zone IIb (500 ~ 650 °C). The morphological characteristics of CM change from porous structure in zone Ia and Ib to lathy shape in zone IIa, and finally into hexagonal platy graphite at the boundary of zone IIa and IIb. The structural parameters in XRD, micro-Raman spectroscopy and microstructures are mainly reflected by various crystallographic characterization of CM, can be classified into two important components in microstructures; Local molecular orientation (LMO) and amorphous domain. Changes of G band FWHM, R1 ratio, FWHM of *d002* spacing are mainly reflected by transformation of LMO from turbostratic to graphitic structures, whereas, change of D1 band FWHM, D3 and D4 bands in Raman band are reflected by decreasing of amorphous domain in microstructures. In particular, *d002* spacing in XRD study is most sensitive indicator for "heterogeneity of microstructures" during natural graphitization. The *d002* spacing splits into two peaks between combinations of coaly material (~ 3.5 Å) and turbostratic structure (~ 3.43 Å) in zone Ib, and turbostratic structure and graphitic structure (< 3.36 Å) in zone IIa. Fully ordered graphite (< 3.36 Å) with heterogeneous structures already appeared at around 400 °C as reported by previous studies, however, those microstructures of CM have retained turbostratic structures until zone IIb. Thus, we should consider natural graphitization as a heterogeneous crystallization process affected by not only the peak metamorphism but also other factors such as fluid activity, catalytic effect from amorphous to graphitic structure. The appearance of heterogeneous structure in this study corresponds to the boundary of the dehydration reaction of chlorite. These data suggest that ambient influences such as devolatilization process strongly affect crystallization of CM during prograde metamorphism, and that is the reason why natural graphitization cannot explain thermodynamic relationship between peak temperature and duration of heating.

Hydrothermal synthesis and crystal structure of $NaMg_3(AsO_4)(HAsO_4)_2$ and $Na(Zn_{2.5},Na_{0.5})(AsO_4)(H_{1.25}AsO_4)_2$, two new members of the alluaudite-group compounds

Wittwer A*, Djordjevic T

Institut für Mineralogie und Kristallographie, Universität Wien *a.wittwer@gmx.at

$NaMg_3(AsO_4)(HAsO_4)_2$ (**1**) and $Na(Zn_{2.5},Na_{0.5})(AsO_4)(H_{1.25}AsO_4)_2$ (**2**) were synthesised during an on-going research on natural and synthetic arsenates, with a focus on their structural and spectroscopic classification.

Single crystals of **1** and **2** were prepared under hydrothermal conditions from the mixtures of $NaNO_3$, $Mg(OH)_2$/ZnO, As_2O_3 in a 1:2:1 molar ratio, respectively (Teflon vessels, stainless steel autoclaves filled up to approximately 70% of their inner volume with distilled water, T_{max} = 473 K, 12 days). **1** and **2** crystallised as transparent, prismatic, colourless crystals up to 135/160 µm in length. **2** crystallized together with twinned, pseudo-hexagonal crystals of $NaZnAsO_4$ (Andratschke *et al*. [1]) (yield 93 %) up to 205 µm in length.

The crystal structures of **1** and **2** were determined using single-crystal X-ray diffraction data (CCD area detector for **1** and Dectris PILATUS 300K Pixel Detector for **2**, Mo*K*α radiation, 293 K, $2\theta_{max}$ = 65/80°, respectively). They crystallise in the space group *C*2/*c*: *a* = 11.978(2)/12.500(3), *b* = 12.373(3)/12.497(3), *c* = 6.7467(13)/6.8507(14) Å, *β* = 112.67(3)/113.98(3) °, *V* = 922.6(4)/977.8(4) Å^3, *Z* = 4. Their crystal structures were refined starting from the atomic coordinates of the mineral o'danielite, $Na(Zn,Mg)_3H_2(AsO_4)_3$ (Keller and Hess [2]). The refinement yielded for the 1449/634 observed reflections with $F_o^2 \geq 4\sigma(F_o^2)$ $R_1(F)$ is 0.0227/0.0476 (Sheldrick [3]). For non-hydrogen atoms anisotropic displacement parameters were refined; the H atoms were found from a difference Fourier map and refined as riding atoms, with restraints on the O-H bond distances of 0.82(2) Å. U_{iso}(H) values were fixed at 1.2 U_{eq}(O).

The compounds **1** and **2** belong to the alluaudite-group: natural and synthetic compounds adopting general formula *A*2*A*2'*A*1*A*1'*A*1"$_2$*M*1*M*2$_2$[*X*O$_4$]$_3$, where *A* are large cations, *M* are distorted octahedral centers and *X* = P^{5+}, As^{5+} (Hatert *et al*. [4]). In some synthetic materials, instead of monovalent cations, protons can also be incorporated leading to compounds with general formula $AM_3(XO_4)(HXO_4)_2$, with *A* = H^+, Na^+, K^+, Ag^+, Cd^{2+} (Stojanović *et al*. [5] and references therein). In alluaudites *A* sites may be either vacant or partially filled, depending on the cation substitution. The structure is composed of chains of variously distorted MO_6 edge-sharing octahedra running in the [101] direction. Each *X*, situated in slightly deformed tetrahedron, shares common O atoms and OH groups from octahedral chains and links them in layers normal to the *b*-axis. There are two such kinds of layers per unit cell. The adjacent half-unit-cell layers are linked sharing common oxygen atoms to form a heteropolyhedral 3D framework, which generates two crystallographically distinct types of parallel channels along *c*-axis. In **1** and **2**, these are filled with Na^+ and H^+ ions, the latter forming strong hydrogen bonds O-H···O inside the channel (O2-H2···O3 = 2.500(2) and 2.511(8) Å, for **1** and **2**, respectively and O3-H3···O2 = 2.511(6) Å for 2.

Acknowledgments: Financial support of the Austrian Science Foundation (FWF) (Grant V203-N19) is gratefully acknowledged.

[1] Andratschke M., Range K.J. and Klement U. (1993). The Crystal Structure of $NaZnAsO_4$. *Z Naturforsch B*, 48, 965-968.

[2] Keller P. and Hess H. (1988). Die Kristallstrukturen von O'Danielit, $Na(Zn,Mg)_3H_2(AsO_4)_3$, und Johillerit, $Na(Mg,Zn)_3Cu(AsO_4)_3$. *Neues Jb Miner Monat*, 9, 395-404.

[3] Sheldrick G.M. (2008). A short history of SHELX. *Acta Crystallogr A*, 64, 112-122.

[4] Hatert F., Keller P., Lissner F., Antenucci D. and Fransolet A.M. (2000). First experimental evidence of alluaudite-like phosphates with high Li-content: the $(Na_{1-x}Li_x)MnFe_2(PO_4)_3$ series (x = 0 to 1). *Eur J Mineral*, 12, 847-857.

[5] Stojanović J., Đorđević T. and Karanović L. (2012). Structural features of two novel alluaudite-like arsenates $Cd_{1.16}Zn_{2.34}(AsO_4)_{1.5}(HAsO_4)(H_2AsO_4)_{0.5}$ and $Cd_{0.74}Mg_{2.76}(AsO_4)_{1.5}(HAsO_4)(H_2AsO_4)_{0.5}$. *J Alloy Compd*, 520, 180-189.

Reinvestigation of the crystal structure of liberite, Li_2BeSiO_4

Yang Z[1*], Miyawaki R[2], Yang Z[1]

1 - Institute of Geology and Geophysics,Chinese Academy of Sciences *yangzhm@mail.iggcas.ac.cn 2 - National Museum of Nature and Science

Liberite, Li_2BeSiO_4, is a rare mineral species, which is known only from Xianghualing tin-polymetallic orefield, Hunan Province, P.R. China. The crystal structure was previously solved in space group *P*1*n*1 (#7) from X-ray Weissenberg photographs of crystals, with *a* = 4.68, *b* = 4.95, *c* = 6.13 Å, β = 90°20′, *V* = 142 Å^3, Z = 2, R_{0kl} = 0.07 and R_{h0l} = 0.085. However in the formerly reported parameters there are errors, which resulted in unacceptable values of bond distances and angles. Among them the Li(1)-O lengths range from 1.470 to 2.463 Å by recalculation, and the edge-lengths of $Li(1)O_4$ tetrahedra range from 2.784 to 3.278 Å. The value of bond-length distortion (BLD) is up to 17.32, and the edge-length distortion (ELD) is 4.10. In a statistical study based on 59 selected LiO_4 tetrahedra, 85% of the values scatter over the range 0 ~ 5 BLD and ELD. The structure of liberite should be re-examined. In this study we have conducted a structural reinvestigation on the original liberite sample.

The mineral formed during the skarn stage and is associated with fluorite, dolomite, cassiterite, lepidolite, natrolite, eucryptite, hsianghualite, and scheelite. Liberite appears as minute monoclinic mineral aggregates. The empirical formula by calculation can be expressed as: $(Li_{1.82}Be_{0.18}Ca_{0.01}Na_{0.01}Mg_{0.01})_{\sum 2.03}Be_{1.00}(Si_{0.94}\ Al_{0.01})_{\sum 0.95}O_4$.

Single-crystal X-ray data for liberite were collected using monochromatic Mo*K*a-radiation on a Rigaku RA-Micro7HF diffractometer with a Saturn 724+ CCD detector. The crystal structure for liberite was refined in space group *P*1*n*1, with *a* = 4.7022(9), *b* = 4.9443(10), *c* = 6.1026(12) Å, β = 90.09(3)°, *V* = 141.88(5) Å^3, to *R*1 = 0.024, w*R*2 = 0.064. The refined formula is Li_2BeSiO_4.

This study confirms that liberite has the wurtzite structure. Be and Si atoms in liberite are completely ordered in sites. The structure of this mineral consists of a framework of BeO_4, SiO_4 and LiO_4 tetrahedra, in which all linkages are by corner-sharing only. The structure of liberite also shows that SiO_4 and BeO_4 tetrahedra form 6-membered rings. The 6-membered rings form a framework with channels for Li ions. The channel looks like a tunnel in a direction, suggesting a presage for ionic conduction of Li.

Mean Li-O distances are 1.984Å in $Li(1)O_4$ and 1.973 Å in $Li(2)O_4$ tetrahedra for liberite, which are close to 1.96(3) Å of the calculated mean Li-O distances from 95 LiO_4 tetrahedra. The value of BLD in liberite is 0.67 for Li(1), and 1.19 for Li(2). The value of ELD is 2.80 for $Li(1)O_4$ terahedra and 2.51 for $Li(2)O_4$ terahedra. These values are within the range of 0-5 BLD and ELD. This study indicates that the incorrect atomic coordinates in the formerly reported structure resulted in unacceptable values of bond distances and angles.

Borate polytypes used to interpret geological conditions of formation

Grice J

Canadian Museum of Nature jgrice@mus-nature.ca

Crystal structures of the three polytypes of veatchite, $Sr_2B_{11}O_{16}(OH)_5 \cdot H_2O$, are determined by X-ray, single-crystal studies [1]. The crystal structures have two layer types with similar fundamental building blocks: **A** layer FBB = 3Δ2□:<Δ2□>-<2Δ□> and **B** layer FBB = 3Δ2□,1Δ:<Δ2□>-<2Δ□>,Δ [2]. Polytypes of veatchite do not coexist and are therefore expected to be unique to a particular environment. To date there is only one occurrence of veatchite-1*A*, Emet, Turkey. Here the borate minerals are intercalated with lacustrine playa lake sediments. Veatchite-1*A* partially replaced colemanite by low temperature diagenetic alteration. Veatchite-1*M* occurs at Reyershausen, Germany and Yorkshire England. Both of these are marine potash deposits and they have undergone high temperature metamorphism. Veatchite-2*M* occurs in sediment buried playa lakes at Lang, Four Corners, and Billie, California. It also occurs in the marine evaporates of Inder, Kazakhstan, Russia and Sussex, New Brunswick, Canada. All five of these deposits have been subjected to moderate temperatures and folded under pressure. From these observations it appears temperature and pressure control the occurrence of each polytype but precise parameters are not known.

Hilgardite, $Ca_2B_5O_8Cl{\bullet}H_2O$, has a zeolite-type framework structure consisting of cross-linked (010) layers of borate sheets having the fundamental building block (FBB) = 2Δ3□:<Δ2□>-<Δ2□>. These layers are polar and the orientation, plus number of layers in a sequence determine the polytype. To date three hilgardite polytypes have been described; hilgardite-1*A*, -3*A* and -4*M*. Two polytypes are identified in the Sussex New Brunswick potash deposits, hilgardite-1*A* and -3*A*. The Millstream deposit occurs as an isolated, inner basin during evaporite formation. Borate formation from this marine environment was during the last stages of evaporation. Simple Mg-Ca borates precipitated from this highly saline brine. It underwent subsequent minor folding and all hilgardite samples are the hilgardite-1*A* polytype. The Penobsquis deposit occurs as an open fore-basin. This larger, less saline basin also precipitated borate minerals during the final stages of evaporation. The borate assemblage here is much more complex with borate minerals that have essential Ca, K, Fe, Mg and Sr. This deposit was subjected to major folding and recrystallization. Both hilgardite-1*A* and -3*A* occur here. Polytype -3*A* is concentrated in areas of maximum folding and it is proposed that pressure is the main control of hilgardite polytypes. Sr substitution has no effect on polytype formation [3].

[1] Grice J.D. and Pring A. (2012). *American Mineralogist*, 97, 489-495.

[2] Grice J.D., Burns P.C. and Hawthorne F.C. (1999). *Canadian Mineralogist*, 37, 731-762.

[3] Grice J.D. and Rowe R. (2014). *Mineralogical Magazine*, 78, p. 235-252.

Interpretation of staurolite twins in terms of the pseudo-eigensymmetry of crystallographic orbits

Marzouki M[1,2], Souvignier B[2], Nespolo M[1*]

1 - Université de Lorraine *massimo.nespolo@crm2.uhp-nancy.fr 2 - Radboud Universiteit Nijmegen

Staurolite is an enigmatic mineral characterized by a high degree of pseudo-symmetry, which frequently occurs twinned. It gives two twins with different occurrence frequency, the 90º or Greek cross (lower frequency) and the 60º or Saint Andrews cross (higher frequency). To date no explanation has been found for their different occurrence frequency. We have analyzed the structure of staurolite in terms of the pseudo-eigensymmetry of the crystallographic orbits building this structure [1]. The union of the crystallographic orbits based on oxygen atoms has a pseudo-cubic eigensymmetry which contains the twin operations of both twins: the operations restore, with good approximation, the whole set of oxygen atoms, which justifies the high frequency of twinning of this mineral but does not discriminate between the two twins. On the other hand, a subset of the tetrahedral cations has a pseudo-eigensymmetry which contains the twin operation of the Saint Andrews cross, but not that of the Greek cross. Also, a subset of the octahedral cations has a pseudo-eigensymmetry which contains the twin operation of the Greek cross and a larger subset has an eigensymmetry which contains the twin operation of the Saint Andrews. The substructure approximately restored by the twin operation is thus more extensive for the Saint Andrews cross, which justifies its higher occurrence frequency.

[1] Marzouki M.A., Souvignier B. and Nespolo M. (2014). *IUCrJ*, 1, 39-48

The crystal structures of kimuraite-(Y) and lokkaite-(Y)

Miyawaki R[1*], Momma K[1], Matsubara S[1], Tahara T[2], Nakai I[2]

1 - National Museum of Nature and Science *miyawaki@kahaku.go.jp 2 - Tokyo University of Science

The crystal structures of kimuraite-(Y) [$Y_2Ca(CO_3)_4$•$6H_2O$: orthorhombic, *I2cb*, *a* = *9.2673(7)*, *b* = 24.0435(2), *c* = 6.0537(2) Å, *V* = 1348.88(11) Å^3, *Z* = 4] and lokkaite-(Y) [$Y_4Ca(CO_3)_7$•$9H_2O$: orthorhombic, *C2mb*, *a* = 9.23346(18), *b* = 39.2328(7), *c* = 6.11166(11) Å, *V* = 2213.97(7) Å^3, *Z* = 4] were solved and refined with single crystal XRD data to *R* = 0.0389 for 1215 and 0.0858 for 2542 reflections, respectively. The crystal structure was solved by the charge flipping method. A racemic twin model was suggested. The crystal structures of kimuraite-(Y) and lokkaite-(Y) consist of two layers, a flat Ca layer and a corrugated Y layer (Figure 1). The Y-corrugated layer is isostructural with that in the crystal structure of tengerite, $Y_2(CO_3)_3$·nH_2O. The difference in the stacking sequence of layers is reflected in the difference in the interval of cell dimension, i.e., the b length. The close structural relation was verified among kimuraite-(Y), lokkaite-(Y) and tengerite-(Y). The Y sites are coordinated by 9 O atoms to form YO_9 polyhedra. The Ca sites form CaO_8 polyhedra with carbonate ions and water molecules. The bond-valence calculations suggested that the Nd substitute for a part of Ca in the flat Ca layer. The smaller heavy REEs are usually dominant following Y in a Y-mineral. The unusual Nd-rich chemistry in kimuraite-(Y) is possibly attributed to the crystallographic character of Nd-Ca substitution.

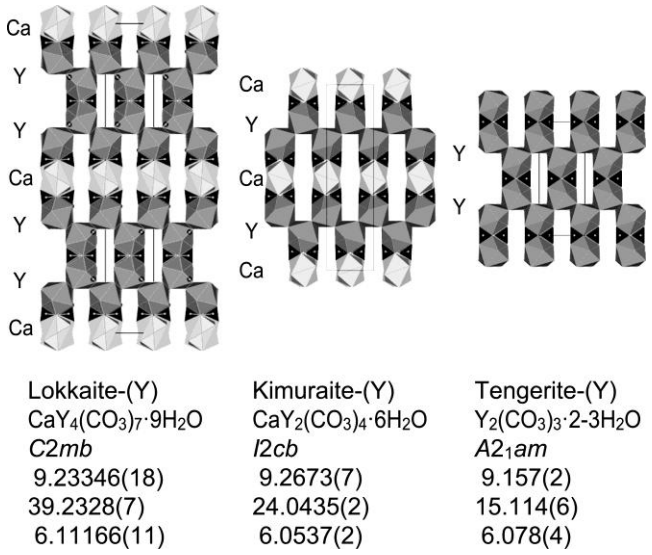

Figure 1: A comparison of stacking sequencies of the flat Ca- and corrugated Y-layers in the crystal structures of lokkaite-(Y), kimuraite-(Y) and tengerite-(Y). The layers are connected by the wedged carbonate ion (black triangle) between the corner-sharing polyhedra.

Structural diversity of layered Pb oxychloride minerals: crystal structure of "chubutite" phase, $Pb_7O_6Br_2$

Siidra O

Saint-Petersburg State University siidra@mail.ru

Lead oxychlorides can be found as secondary minerals in oxidation zones of mineral deposits. Their structures may accommodate a wide range of elements, including As, S, V, Mo, P, Si, I, *etc*., which results in interesting chemical and structural diversity. Of particular interest are minerals with layered PbO-derivative structures, which are structurally related to the Aurivillius phases. The crystal structures of Litharge (α-PbO)-related layered lead oxyhalides are based upon the O-Pb layers alternating with the *X* sheets of X^- ions (*X* = Cl, Br, I). The relationships between the structures of litharge and its oxyhalide derivatives can be conveniently described in terms of structural units based upon OPb_4 oxocentered tetrahedra [1].

The structural data are available for a number of 'pure' Pb oxyhalides without additional cations and anions: $Pb_3O_2X_2$ (X=Cl, Br, I) (mendipite), $Pb_5O_2Cl_6$, $Pb_{13}O_{10}X_6$ (X=Cl, Br), $Pb_{31}O_{22}X_{18}$ (X = Cl, Br) and $Pb_9O_4Br_{10}$. "Lorettoite" and "chubutite" phases correspond to the following chemical composition of $Pb_7O_6Cl_2$. Both of these phases are not valid mineral species to date [2]. Crystal structure of $Pb_7O_6Cl_2$ is unknown. Recently we have succeeded to obtain perfect crystals of $Pb_7O_6Br_2$ (**1**) from lead oxyhalide melt. The structure of **1** is monoclinic, P21/c a = 13.494(2), b = 12.482(2), c = 8.102(1), β = 107.173(4). The structure of **1** is based on highly corrugated layers unprecedented for layered Pb oxyhalides. The crystal chemical reasons for such structural architecture in **1** are discussed. Structural relationships between different oxide-halide ratio in PbO-PbX_2 (X = Cl, Br) system are reviewed.

[1] Krivovichev S.V., Mentré O., Siidra O.I., Colmont M. and Filatov S.K. (2013). Anion-centered tetrahedra in inorganic compounds. *Chemical Reviews*, 113, 6459-6535.

[2] White J.S. (1979). Lorettoite discredited and chubutite reviewed. *American Mineralogist*, 64, 1303-1305.

Crystal chemistry of quintinite – the natural Mg-Al-CO_3-layered double hydroxide

Zhitova E[1*], Krivovichev S[1], Zolotarev A[1], Yakovenchuk V[2], Ivanyuk G[2]

1 - St. Petersburg State University *zhitova_es@mail.ru 2 - Apatity, Nanomaterials Research Centre, KSC, RAS

Quintinite $[Mg_4Al_2(OH)_{12}](CO_3)(H_2O)_3$ is a member of the quintinite group of the hydrotalcite supergroup [1]. Quintinite and hydrotalcite are very close chemically and differ in the Mg:Al ratio, which is equal to 3:1 for hydrotalcite and 2:1 for quintinite. Quintinite was described as a new mineral species by Chao and Gault [2] on samples from Mont St-Hilaire (Canada) as 3*T* polytype (*P*$3_1$12 or *P*$3_2$12, *a* = 10.558, *c* = 22.71 Å) and from Jacuperanga (Brazil) as 2*H* polytype (*P*$6_3$22, *a* = 10.571, *c* = 15.139 Å). The crystal structure determination for *hydrotalcite* from Vezna, Czech Republic with the Mg:Al close to 2:1 was carried out by Allmann and Jepsen [3] in the space group is *R*-3*m* (*a* = 3.054, *c* = 22.81 Å). Crystal structure of quintinite-2*H* (*P*-62*m*, *a* = 5.283, *c* = 15.150 Å) was solved by Arakcheeva *et al*. [4] on the crystal from Jacuperanga and originally reported as the crystal structure of *manasseite*.

Within recent years, we have studied *hydrotalcites* or *manasseites* samples from different Russian deposits (Kovdor (Kola Peninsula); Bazhenovo and Mariinskoe (Middle Urals); Rudnogorskoe (Irkutsk reg., Ilim)). Dozens of the studied samples appeared to be quintinite with Mg:Al ≈ 2:1. The Mg-Al ratios were determined by wavelength dispersion spectrometry and in many cases confirmed by layer stoichiometry obtained crystal-structure solution [5, 6]. There are four polytypes of quntinite (Table 1), and their diversity is owing to the different degree and patterns of Mg-Al cation ordering inside and in between the octahedral layers [7, 8].

	2*H*-3*c*[6*R*]	1*M*	2*H*	2*H*-1*c*
Crystal system	Trigonal	Monoclinic	Hexagonal	Trigonal
Space group	*R*32	*C*2/*m*	*P*6_3/*mmc*	*P*-3*c*1
a (Å)	5.2745(6)	5.266(2)	3.0446(9)	5.2720(6)
b (Å)	= *a*	9.114(2)	= *a*	= *a*
c (Å)	45.364(10)	7.766(3)	15.178(5)	15.113(3)
β (°)	-	103.17(3)	-	-
V(Å^3)	1093.0(3)	362.9(2)	121.84(6)	363.76(8)
Z	3	1	1	2

Studying of constant succession of natural phases results in the following sequence of polytypes: 2*H*→2*H*-1*c*→1*M* that can be attributed to the increase of temperature or crystal growth velocity.

Acknowledgments: This work was supported by the Russian Foundation for Basic Research (project no.14-05-31229).

[1] Mills S.J., Christy A.G., Génin J-M.R., Kameda T. and Colombo F. (2012). *Mineral. Mag.*, 76, 1289-1336.

[2] Chao G.Y. and Gault R.A. (1997). *Canad. Mineral.*, 35, 1541-1549.

[3] Allmann R. and Jepsen H.P. (1969). *Neues. Jahr. Mineral. Monat.*, 544-551.

[4] Arakcheeva A.V., Pushcharovskii D.Yu., Atencio D. and Lubman G.U. (1996). *Crystallogr. Rep.*, 41, 972-981.

[5] Krivovichev S.V., Yakovenchuk V.N., Zhitova E.S., Zolotarev A.A., Pakhomovsky Ya.A. and Ivanyuk G.Yu. (2010). *Mineral. Mag.*, 74(5). 821-832.

[6] Krivovichev S.V., Yakovenchuk V.N., Zhitova E.S., Zolotarev A.A., Pakhomovsky Ya.A. and Ivanyuk G.Yu. (2010). *Mineral. Mag.*, 74(5). 833-840.

[7] Krivovichev S.V., Yakovenchuk V.N. and Zhitova E.S. (2012). MAAM II (Ed. S.V.Krivovichev) Springer. 87-91.

[8] Zhitova E.S., Yakovenchuk V.N., Krivovichev S.V., Zolotarev A.A., Pakhomovsky, Ya.A. and Ivanyuk, G.Yu. (2010). *Mineral. Mag.*, 74(5), 841-848.

Crystal structure and chemistry of Na-deficient Y-dominant analogue of hainite/götzenite

Zolotarev A[1*], Krivovichev S[1], Lyalina L[2], Selivanova E[2]

1 - St. Petersburg State University *aazolotarev@gmail.com 2 - Geological Institute of the KSC RAS, Apatity

The crystal structures of hainite and götzenite [1-4] as members of the rosenbuschite group [5] are based upon the HOH modules: the H-layer is heterogeneous (consisting of octahedra linked to the Si_2O_7 groups); the O-layer is an octahedral layer. Here we present structural data for the new cation-deficient Y-dominant analogue of hainite/götzenite. The mineral was found in the nepheline-feldspar pegmatite, in the contact zone of large essexite xenolith and nepheline syenite of the Sakharjok massif, Kola Peninsula, Russia.

The crystal structure was studied on a Bruker DUO CCD diffractometer (MoKα X-radiation). Mineral is triclinic, space group *P*-1, *a* = 9.4024(8), *b* = 5.5623(5), *c* = 7.3784(6) Å, α = 89.919(2), β = 101.408(2), γ = 96.621(2)°, V = 375.65(6) Å^3 (refined on the basis of 5115 unique reflections (R_{int} = 0.0425)). The structure was solved and refined with the ShelXS and ShelXL [6] to R_1 = 0.057.

The structure of the mineral studied differs from the structure of hainite by the composition and structure of the O layer formed by the M2, M4 and M5 sites. In the studied mineral, the M4 site is vacant, with only 35% occupancy by Na. The M1 site is preferentially occupied by the Y^{3+} cations and has a sevenfold coordination, which is different from the octahedral (sixfold) coordination of the M1 site in hainite occupied by Ca. The occupation of the M1 site by trivalent ions results in a significant re-arrangement of cation packing in the interlayer, which is manifested in different polyhedral structure of the M1-M3 H-layer. In general, the difference between the crystal structures of the studied mineral and hainite is the result of the coupled cation substitution that can approximately be described by the scheme: $Y^{3+} + \square \rightarrow Ca^{2+} + Na^{+}$, where the $Y^{3+} \rightarrow Ca^{2+}$ substitution occurs at the M1 site, and the $\square \rightarrow Na^{+}$ substitution occurs at the M4 site. Thus, sample studied is the Na-deficient Y-analogue of hainite with Y content approximately 2.5 times higher than in hainite. Structural formula of mineral can be written as $(Y_{0.82}Ca_{0.61}REE_{0.24}Mn_{0.20}Zr_{0.13})_{2.00}$ $(Ca_{1.00}\square_{1.00})_{2.00}$ $(Ca_{1.92}REE_{0.08})_{2.00}$ $(\square_{0.65}Na_{0.35})_{1.00}$ $(Ti_{0.68}Nb_{0.19}Zr_{0.13})_{1.00}$ $(Si_2O_7)_2$ $F_2F_{1.94}$

[1] Atencio D., Coutinho J.M.V., Ulbrich M.N.C., Vlach S.R.F., Rastsvetaeva R.K. and Pushcharovsky D.YU. (1999). Hainite from Poços de Caldas, Minas Gerais, Brazil. *Can. Mineral.*, 37, 91-98.

[2] Bulakh A.G. and Kapustin Yu. L. (1973). Götzenite from the alkaline rocks of the Tur'yev Peninsula, Kola Peninsula. *Zap. Vses. Mineral. Obschhest.*, 102(4), 464-466.

[3] Cannillo E., Mazzi F. and Rossi G. (1972). Crystal structure of götzenite. *Sov. Phys. Crystallogr.*, 16, 1026-1030.

[4] Johan Z. and Cech Z. (1989). New data on hainite, $Na_2Ca_4[(Ti,Zr,Mn,Fe,Nb,Ta)_{1.5}\square_{0.5}](Si_2O_7)_2F_4$ and its crystal chemical relationship with götzenite, $Na_2Ca_5Ti(Si_2O_7)_2F_4$. *C.R. Acad. Sci. Paris.*, 308(II), 1237-1242.

[5] Christiansen C.C., Johnsen O. and Makovicky E. (2003). Crystal chemistry of the rosenbuschite group. *Can. Mineral.*, 41, 1203-1224.

[6] Sheldrick G.M. (2008). SHELXS, SHELXL. *Acta Cryst.* A64, 112-122.

Order-disorder high-temperature phase transition in kogarkoite

Avdontceva M*, Zolotarev A, Krzhizhanovskaya M, Krivovichev S

St. Petersburg State University *margarita.avdontceva@spbu.ru

Kogarkoite, Na_3SO_4F, was first described by L.N. Kogarko (1961), from alkaline rocks of the Lovozero alkaline massif, Kola peninsula, Russia. Later it was found in hot-springs deposits at Mt. Princeton, Colorado, and named in honor of L.N. Kogarko [1]. Synthetic analogue of kogarkoite was first reported by de Marignac (1859).

In our study, synthetic crystals of kogarkoite were prepared by evaporation from aqueous solutions of sodium sulfate and sodium fluoride at 25°C. Thermal behavior of synthetic kogarkoite was studied by high-temperature X-ray powder diffraction method using a Rigaku Ultima IV ($CuK\alpha_{1+2}$ radiation, 40 kV/30 mA, Bragg-Brentano geometry, PSD D-Tex Ultra) diffractometer with a high-temperature attachment in the temperature range of 25-700 °C with the 30-40 degree steps. Thin powder sample was deposited on a Pt sample holder (20x12x2 mm^3) from an ethanol suspension. The unit cell parameters were calculated using the program package Topas 4.2 (Bruker). It was observed that the diffraction pattern of kogarkoite changed dramatically in between 100 and 125°C that was assigned to the monoclinic-to-trigonal phase transition.

The crystal structure of synthetic kogarkoite was studied by single crystal X-Ray diffraction analysis by means of the Bruker Kappa Apex Duo diffractometer equipped with the CCD detector at room temperature and at 150 °C using low-temperature Oxford Cobra Plus system. The room-temperature crystal structure is monoclinic, $P2_1/m$, a = 18.065(3), b = 6.958(1), c = 11.446(1) Å, β = 107.711(1)°. The structure is based upon face-sharing [FNa_6] octahedra, which form triplets further linked into a three-dimensional framework by sharing corners. The SO_4 tetrahedra are located in the framework cavities [2]. The high-temperature modification of kogarkoite is trigonal, $R\bar{3}m$, a = 6.94(1), c = 24.58(4) Å. The structure of high-temperature modification has the same framework of fluorine-centered octahedra. However, in contrast to the room-temperature modification, SO_4 tetrahedra in the framework cavities are disordered with different orientations of tetrahedra observed at the same time.

Therefore, the $P2_1/m \rightarrow R\bar{3}m$ phase transition in kogarkoite is associated with the disorder of sulfate tetrahedra in the cavities of the antiperovskite-type framework formed by face- and corner-sharing FNa_6 octahedra.

[1] Pabst A. and Sharp W.N. (1973). *Amer. Mineral.*, 58, 116.

[2] Krivovichev S.V. (2008). *Z. Kristallogr.*, 228, 109.

Crystal chemistry of uranyl arsenates and phosphates from the Rabejac deposit, Lodève, France

Dal Bo F[1*], Hatert F[1], Baijot M[1], Philippo S[2]

1 - University of Liège *fdalbo@ulg.ac.be 2 - National Museum of Natural History (Luxembourg)

Located on the meridional border of the Central Massif, France, the Permian sedimentary basin of Lodève is well-known for its abundance of uranium minerals species. The uranium ore is mainly located in Autunian, Saxonian and Thuringian sandstones, pelites and conglomerates. This basin can be divided in several mining districts such as Mas d'Alary, Saint-Jean-de-la-Blaquière, les Mares, Usclas-du -Bosc, Riviéral, La Plane and Rabejec. The district of Mas d'Alary is the type locality of two uranyl sulfates: deliensite and leydetite. The district of Riviéral is the type locality of a rare uranyl arsenate named metalodèvite, and the distric of Rabejac has provided three new uranyl mineral species: fontanite, rabejacite and seelite.

The Rabejac deposit is also well-known for the occurence of many uranyl arsenates and phosphates. However, detailed chemical and crystallographic data on these minerals are still missing. Electron-microprobe analyses were performed on metauranocircite, nováčekite, uranospinite, and single-crystal X-ray diffraction measurements were performed on zeunerite and arsenuranospathite. Zeunerite, is tetragonal, $P4/nnc$, with a = 7.183(1), c = 20.872(2) Å and V = 1076.1(1) Å³. Arsenuranospathite, is orthorhombic, $Pnn2$, with a = 29.926(1), b = 7.132(1), c = 7.186(1) Å, and V = 1533.9 (1) Å³.

As the other members of the autunite group, the basic structural unit of zeunerite and arsenuranospathite is the corrugated autunite-type sheet. This sheet consists of corner-sharing UO_6 square bipyramids and $T^{5+}O_4$ tetrahedra (T^{5+} = As or P), and shows the composition $[(UO_2)(T^{5+}O_4)]^-$. The negative charge of the sheets is balanced by mono-, di- or trivalent cations and H_2O molecules located in the interlayer space. The interlayer space of zeunerite is occupied by one Cu atom occuring in a Jahn-Teller distorted octahedron, which connects together two successive uranyl arsenate sheets. The Cu atom shares two long bonds with the $(UO_2)^{2+}$ uranyl cation and four shorter bonds with H_2O molecules (O3) positioned in a square planar arrangement. One symmetrically independent H_2O molecule (O5) also occurs in the zeunerite interlayer space. Four of these molecules are connected to each other by H-bonding to form a square-planar group. The oxygen shared by the UO_6 square bipyramids and AsO_4 tetrahedra (O4) is also connected by H-bonding to the independent H_2O group (O5). The structure of natural zeunerite is identical to that of synthetic zeunerite and to that of torbernite.

The interlayer arrangement of arsenuranospathite is far away more complicated than in other minerals from the autunite group, with one Al atom and eleven symmetrically independent H_2O molecules. These water molecules can be divided in to three sets: the first set contains three H_2O molecules which form an octahedron around Al atoms; the second set contains four H_2O molecules connected in square-planar groups by H-bonding; and the third set contains four H_2O groups. Al atoms are completely isolated from the uranyl arsenate sheets while the H_2O molecules from the first set show H-bonds with oxygens occuring in the uranyl arsenate sheets. Arsenuranospathite is isostructural with the P-analogue mineral named uranospathite.

Crystal structure of the natural eulytite

Li G[1*], Xiong M[2], Yang G[3]

1 - China University of Geosciences *liguowu@126.com 2 - China University of Geosciences (Beijing) 3 - China University of Geosciences (Wuhan)

Eulytite ($Bi_4(SiO_4)_3$) is one of the rarest silicate minerals of bismuth in a nature. It occurs in the Chaobuleng Skarn iron polymetallic deposit, Dongwuqi, inner Mongolia Autonomous Region,China. It occurs together with rhodontie and tremolite. Single crystals generally range from 0.07-0.15mm in size and are attached to tremolite fibers in the geodes or cracks. It has a habit with form tetrahedron {111} and triakistetrahedron {211} combination form.

The crystal structure of nature eulytite was solved using the single-crystal X-ray diffraction with CCD detector. The structural refinement has led to a reliability factor of R1=0.021 (wR2=0.041) for 341 independent reflections. The mineral was found to crystallize in the cubic system, space group I43d and the lattice parameters: a=10.116(2) Å, V=1035.21Å ^{3}, Z=4, $D_{calc.}$=7.136 g/cm^3. The structure is characterized by the existence of one general position (48e) for oxygen anions and two positions 16c and12b occupied by Bi and Si cations, respectively. The positional parameters and anisotropic displacement parameters are presented in Tables 1 and 2. Although all Si-O distances are identical (1.604(5)Å), the O-Si-O angles ranging from 107.32(15)°to 113.87(31)°, show that $[SiO_4]^{4-}$ tetrahedra are rather distorted. Bismuth cations are located in octahedral sites with corresponding mean distances of Bi-O equal to 2.126 to 2.553 Å. The structure consists of edge-shared Bi octahedra linked at the corners to independent $[SiO_4]^{4-}$ tetrahedra units. It could be viewed as built up from independent $[SiO_4]^{4-}$ tetrahedra, lying along rods parallel to the axis and to [001].

Table 1. Positional parameters in fractional coordinates for eulytite

Atom	Wyck.	Occ.	x	y	z
Bi1	16c	0.911	0.91491(3)	0.91491(3)	0.91491(3)
Si1	12b		1.00000	3/4	5/8
O1	48e		0.9389(5)	0.8680(5)	0.7115(5)

Table 2. Anisotropic displacement parameters [Å^2] for eulytite

Atom	U_{11}	U_{22}	U_{33}	U_{12}	U_{13}	U_{23}
Bi1	0.00197(14)	0.00197(14)	0.00197(14)	-0.00020(8)	-0.00020(8)	-0.00020(8)
Si1	0.0026(10)	0.0026(10)	0.0004(15)	0.00000	0.00000	0.00000
O1	0.014(3)	0.008(2)	0.004(2)	0.005(2)	-0.0020(18)	0.0008(16)

Crystallographic examination of tsugaruite

Matsushita Y[1*], Momma K[2], Miyawaki R[2], Sato A[1], Kaise M[1], Kitazawa H[1]

1 - National Institute for Materials Science (NIMS) *matsushita.yoshitaka@nims.go.jp 2 - National Museum of Nature and Science

Tsugaruite ($Pb_4As_2S_7$) is one of the rare sulfosalt minerals reported in 1987 for the first time [1]. Even now it is found at the original locality (Yunosawa Mine, Tsugaru-gun, Aomori Prefecture, Japan) only, and also its crystal structure has not been reported yet. Here we report its crystal structure using a single crystal diffraction method (RIGAKU AFC11R Varimax + Saturn CCD system, MoKa). A single crystal for this study was picked up from an original type specimen. Observed cell parameter is orthorhombic, a = 15.147(2) Å, b = 38.146(5) Å, c = 8.0568(11) Å, V = 4655.2(11) Å^3, corresponding to first reported parameter. Diffraction pattern suggests that the structure may belong to one of space group: Pnnm or Pnn2. Using Pnn2 space group, R1 value is drop down to ~7.5 %. The structure is basically formed by PbS substructure unit. However, it has some discussable points from crystallochemical point of view. Detail of the crystal structure will be presented.

[1] Shimizu M., Miyawaki R., Kato A., Matsubara S., Matsuyama F. and Kiyota K. (1998). Tsugaruite, $Pb_4As_2S_7$, a new mineral species from the Yunosawa mine, Aomori Prefecture, Japan. *Mineralogical Magazine*, 62 (6), 793-799.

Epitaxial intergrowths of wiluite and grossular: a single-crystal X-ray diffraction study and modular interpretation

Panikorovskii T*, Zolotarev A, Krivovichev S

St. Petersburg State University *taras.panikorovsky@spbu.ru

Wiluite has the general chemical formula $Ca_{19}(Al,Mg,Fe,Ti)_{13}(B,Al,\square)_5(O,OH)_{10}O_{68}$ (Groat *et.al.* [1]) and belongs to the vesuvianite group. In contrast to other minerals of the group, it contains an essential B content [B >2.5 apfu (atoms per formula unit)]. Wiluite usually has the space group *P4/nnc* (references [1-5]) and has often been found in the association with grossular.

Similar to other vesuvianite-group minerals, wiluite has a modular structure and may be considered as containing one-dimensional domains extracted from the crystal of grossular (Figure 1).

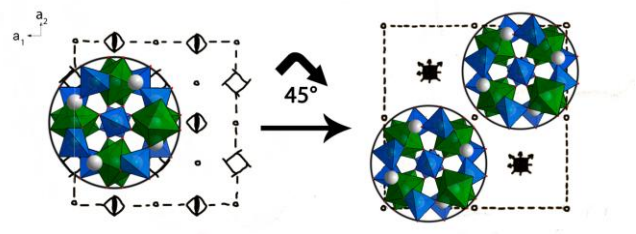

Figure 1: One-dimensional domains in the structure of grossular (left) and vesuvianite-group minerals (right). Note that, in the vesuvianite structure, the domains are rotated by 45° around their axes compared to the garnet structure.

In this work, we have studied epitaxial intergrowths of wiluite and grossular using single-crystal X-ray diffraction on the Excalibur Eos single-crystal difractometer. The CrysAlisPro (2012) program was used for the reciprocal space reconstruction. The observed mutual orientation of the wiluite and grossular unit cells is shown in Figure 2. It is obvious that this orientation coincides with that that can be seen in Figure 1: the *a* axis of the wiluite structure is parallel to the [110] direction in the structure of garnet, i.e. the (001) planes of the two structures are parallel to each other and rotated relative each other by 45°. Thus, the observed epitaxy has a direct crystal chemical nature and is based upon structural similarities between the two structures.

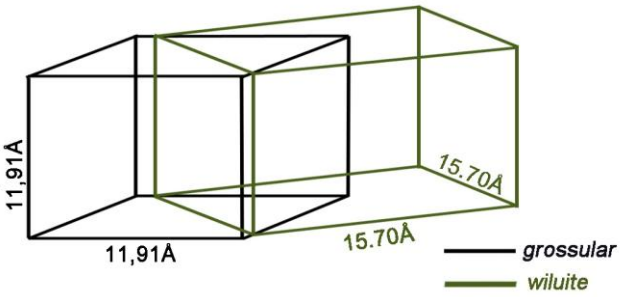

[1] Groat L.A., Hawthorne F.C., Ercit T.S. and Grice J.D. (1998). *Can. Mineral*., 36, 1301-1304.

[2] Groat L.A., Evans R.J., Cempírek J., McCammon C. and Houzar S. (2013). *Amer. Mineral*., 98, 1330-1337.

[3] Kurazhkovskaya V.S., Borovikova E.Yu., Alferova M.S. (2005). *Proc. RMO* 134(4), 45-54 (in Russian).

[4] Bellatreccia F., Cámara F., Ottolini L., Della Ventura G., Cibin G. and Mottana A. (2005). *Can. Mineral*. 43, 1457-1468.

[5] Balassone G., Talla D., Beran A., Mormone A., Altomare A., Moliterni A., Mondillo N., Saviano M., Petti C. (2011). *Per. Mineral*., 80, 369-384.

Oscillatory chemical zoned chlorite in Pyrenean thrust fault

Trincal V[1], Buatier M[1*], Charpentier D[1], Lanari P[2], Lacroix B[3], Munoz M[4]

1 - ChronoEnvironnement, UFC Besançon, France *martine.buatier@univ-fcomte.fr 2 - Institute of Earth Sciences, University of Bern, Switzerland 3 - University of Michigan, Ann Arbor, Michigan, USA. 4 - Laboratoire ISTerre, Grenoble, France

Oscillatory compositional zoning in minerals has been observed in hydrothermal magmatic and metamorphic environments and has been commonly attributed to changing chemical or physical conditions during crystal growth. Chemical zoning is common in solid solution minerals however it has been rarely described in phyllosilicates.

The present study describes oscillatory zoning in chlorite from pelitic samples from the Pic de Port Vieux thrust sheet, a minor thrust sheet associated to Gavarnie thrust fault zone (Central Pyrenees). The Pic de Port Vieux Thrust sheet comprises a 1-20 meter thick layer of Triassic red pelite to sandstone and mylonitized Cretaceous limestone. The thrust sheet is affected by faults and cleavage; the important deformation product is a set of veins filled by quartz and chlorite [1].

Chlorite fills extension veins, crack-seal shear veins and is also present in open cavities. The chlorites filling the open cavities occur as pseudo-uniaxial plates arranged in rosette-shaped aggregates. These aggregates appear to have developed as a result of radial growth of the chlorite platelets.

Detailed observations (SEM, TEM images) and analyses (microprobe analyses) were focused on these chlorite aggregates. Oscillatory zoning is well imaged from Backscattered Scanning Electron Microscopic images and X-ray Mapping. According to point and microprobe X-ray images, these chlorites display oscillatory chemical zoning with alternating iron-rich and magnesium-rich bands. The chlorite composition ranges from Fe rich pole $([Si_{2.62}Al_{1.38}O_{10}](Al_{1.47}Fe_{1.87}Mg_{2.61})\ (OH)_8)$ to Mg rich pole $([Si_{2.68}Al_{1.31}O_{10}](Al_{1.45}Fe_{1.41}Mg_{3.06})\ (OH)_8)$.

Temperature maps are derived from standardized microprobe X-ray images using the program *XMapTools* [2]. The (Fe^{3+}/Fe_{tot}) value in chlorite is directly measured using µXANES spot analyses collected at the Fe-K edge. These analyses permit an estimation of temperature and redox state of the fluid from which chlorite precipitated.

All these data will permit to discuss the origin of the oscillatory zoning in chlorite and to determine if this type of zoning can be attributed to an external control of cyclic change in temperature, pressure or fluid composition or to a growth mechanism resulting in differential incorporation of Mg or Fe related to matrix and kinetic effects.

[1] Grant N.T. (1992). Post-emplacement extension within a thrust sheet from the central Pyrenees. *Journal of the Geological Society*, 149, 775-792.

[2] Lanari P., Vidal O., De Andrade V., Dubacq B., Lewin E., Grosch E.G., Schwartz S., 2014. XMapTools: A MATLAB©-based program for electron microprobe X-ray image processing and geothermobarometry. *Computers & Geosciences*, 62, 227-240.

The anion framework in garnet: occupancy of its voids, connection of the coordination polyhedra and its influence on cation exchange and mobility

Amthauer G*, Rettenwander D

University of Salzburg, Department of Materials Research and Physics, Salzburg, Austria. *georg.amthauer@sbg.ac.at

"Garnet" is the common name for a large number of natural and synthetic metal oxide and fluoride phases. Conventional oxide garnets have the general formula $A_3B_2C_3O_{12}$ and crystallize in the cubic space group [1]. The O^{2-} ions in the general crystallographic positions 96h form an oxygen-atom framework with interstices occupied by the A cations, such as Ca^{2+}, Fe^{2+}, Y^{3+}, La^{3+}, etc. in the 8-fold coordinated position 24c (point symmetry 222), the B cations, such as Al^{3+}, Fe^{3+}, Zr^{4+}, Sn^{4+}, Sb^{5+}, etc. in the 6-fold coordinated position 16a (point symmetry -3), and the C cations, such as Li^{+}, Al^{3+}, Fe^{3+}, Ga^{3+}, Ti^{4+}, Si^{4+}, etc. in the four-fold coordinated 24d position (point symmetry -4). In addition to these cation sites, there are other interstices within the oxygen framework that are empty in the conventional garnet structure [2], e.g. (i) the six-fold coordinated 16b positions with point symmetry 32, (ii) the six-fold coordinated 48g positions with point symmetry 2, and (iii) an additional four-fold coordinated 96h position with point symmetry 1. In some cases these interstices can be filled by "excess" cations, giving rise to compositions with nonstandard garnet stoichiometries, such as the excellent solid-state Li-ion conductors $Li_7La_3Zr_2O_{12}$ [3].

In our contribution the cation distribution of chemically very different compounds with garnet structure will be presented based on the model of Hellner *et al*. [2]. Experimental data of the temperature dependent cation exchange in garnets with compositions $Y_3Fe_{5-x}Ga_xO_{12}$ and $Y_3Fe_{5-x}Al_xO_{12}$ [4] will be discussed with special regard to the connection of the coordination polyhedra and possible diffusion pathways. A model of the mobility of Li^{+} in Li-oxide garnets and its dependence on the positions of the main elements as well as on the dopant ions will be presented and related to ion conductivities of those garnets.

[1] Menzer G.Z. (1928). *Kristallogr*., 69, 300.

[2] Hellner E., Gerlich R., Koch E. and Fischer W. (1979). Physics Data; Fachinformationszentrum Energie, Physik, Mathematik: Karlsruhe, Germany,16-1, p.1-16.

[3] Murugan R., Thangadurai V., Weppner W. (2007). *Angew. Chem*., 119, 7925.

[4] Nitsche R., Tippelt G. and Amthauer G. (2003). *J. Material Science*, 29, 2903.

The WURM project – a web-based freely available database of computed physical properties for minerals

Caracas R[1*], Bobocioiu E[2]

1 - CNRS *razvan.caracas@ens-lyon.fr 2 - ENS de Lyon

We present an update of the WURM database.

The WURM project aims to build a freely accessible web-based database of computed physical properties for minerals. The database provides various physical properties for each mineral: the crystal structure used in the calculation, the dynamical charges and the dielectric tensors, the refractive index, the Raman spectra with both peak position and intensity and the infrared spectra with peak position. Additional information comprises the parameters of the calculation, to ensure reproducibility of the results.

The vibrational information makes up the bulk of the database and constitutes the major computational effort. For each vibrational mode in the zone-center we determine the frequency, the symmetry assignment, the atomic displacement patterns, and the Raman tensors. The Raman spectra are represented as both single crystal and powder with different possible laser polarizations. For the infrared modes we give both the TO and the LO components.

The database is freely available on the web at http://www.wurm.info and is highly interactive. Jmol-powered applets incorporated in the website allow the quick visualization of the crystal structure and of the atomic displacement patters of all vibrational modes.

All the results are exclusively obtained from first-principles calculations performed using the local density approximation of density functional theory and density functional perturbation theory in the ABINIT implementation [http://www.abinit.org], based on planewaves and pseudopotentials.

Fe^{2+}-Ti^{4+} vs. Fe^{2+}-Fe^{3+} charge-transfer and short-range order in single chains of face-sharing octahedra: ellenbergerite and dumortierite

Chopin C[1*], Khomenko V[2]

1 - Ecole normale superieure - CNRS *chopin@geologie.ens.fr 2 - Academy of Science of Ukraine

In zoned pyrope megacrysts from the Dora-Maira ultrahigh-pressure terrain, new, dark-violet colour varieties of the hexagonal, high-pressure silicate ellenbergerite, $(Mg,Ti,Zr,\square)_2Mg_6Al_6Si_8O_{28}(OH)_{10}$, extend the range of known Fe contents for this mineral from 0-0.1 to 0-0.4 atom pfu, for Ti contents commonly in the range 0.2-0.4 pfu. The new varieties show an extremely intense pleochroism, colourless for **E**|**c** to deep Prussian blue for **E**//**c**, as compared to colourless to lilac or reddish purple for classical Fe-poor ellenbergerite. These features were the incentive for an electronic absorption spectroscopic study and a reappraisal of the interpretation of the charge transfers (CT), colour and ordering schemes in this group and the structurally related borosilicate dumortierite. Both structures are characterized by the presence of infinite single chains of face-sharing, partly vacant octahedra along the 6-fold screw axis and pseudo-hexad axis, respectively, in which the Fe and Ti atoms are partitioned [1].

In the spectra of Fe-poor ellenbergerite, the presence of a single Fe^{2+}-Ti^{4+} CT band near 19000 cm^{-1} was taken as evidence for complete short-range ordering of Mg(Fe), Ti and vacancies in the octahedral single chain [2]. The **E**//**c** spectra of Fe-rich ellenbergerite show the same absorption band near 19000 cm^{-1} but consistently flanked by another CT band near 14000 cm^{-1} , the intensity of which increases with total Fe content. The latter is similar to the 12400 cm^{-1} CT band observed as the single feature in **E**//**c** spectra of the isostructural (Ti-free and Fe-bearing) phosphoellenbergerite, and clearly assigned to Fe^{2+}-Fe^{3+} CT in the octahedral single chain [2].

The same colour pattern occurs in the dumortierite group, with red Fe-poor, Ti-rich crystals showing a single CT band near 20000 cm^{-1}, blue Ti-poor crystals showing a single CT band near 16500 cm^{-1}, and violet Fe- and Ti-rich crystals showing a combination of the two bands [3]. In the light of the new data, we reinterpret the dumortierite colour scheme as due to both Fe^{2+}-Fe^{3+} (16500 cm^{-1}) and Fe^{2+}-Ti^{4+} (20000 cm^{-1}) CT, rather than to Fe^{2+}-Ti^{4+} CT only with two extreme types of Fe-Ti dimers [- ¤ - Fe^{2+} - Ti^{4+} - ¤ -] and [- M - Fe^{2+} - Ti^{4+} - ¤ -]. We discuss the implications in terms of energy and of short-range ordering of vacancies in the octahedral single chains of the ellenbergerite and dumortierite groups. Optical spectroscopy appears as a very sensitive structural probe of minor or trace elements.

[1] Evans R.J. and Groat L.A. (2012). Structure and topology of dumortierite and dumortierite-like materials. *Can. Mineral.*, 50, 1197-1231.

[2] Chopin C. and Langer K. (1988). Fe^{2+}-Ti^{4+} charge transfer between face-sharing octahedra: polarized absorption spectra and crystal chemistry of ellenbergerite. *Bull. Minéral.*, 111, 17-27.

[3] Platonov A.N., Langer K., Chopin C., Andrut Mo. and Taran M.N. (2000). Fe^{2+}-Ti^{4+} charge-transfer in dumortierite. *Eur. J. Mineral.*, 12, 521-528.

An in situ and ex situ SXRD and TEM microscopy study of CuXSZ and CuXZnYSZ thin films

Di Benedetto F[1*], Cinotti S[2], Carlà F[3], Felici R[3], Foresti M[2], Guerri A[2], Innocenti M[2], Lavacchi A[4], Montegrossi G[5]

1 - Università Firenze - Dip. di Scienze della Terra, Italy *francesco.dibenedetto@unifi.it 2 - Università Firenze - Dip. Chimica, Italy 3 - ESRF, France 4 - CNR-ICCOM, Italy 5 - CNR.IGG, Italy

Metal sulfide semiconductors with technological application in the photovoltaic field were prepared by electrodeposition. In particular, we used the E-ALD (Electrochemical Atomic Layer Deposition) to grow CuS and Cu-Zn sulfides on Ag substrates. With the aim of performing a chemical, morphological and structural characterization of the grown films, a TEM (Transmission Electron Microscope) study, for morphology and composition at the nanometer level, and SXRD (Surface X-Ray Diffraction) investigations, for the structural information, were undertaken. SXRD measurements have been performed at the ID03 beamline of ESRF (Grenoble). In particular, an in-situ experiment of crystal growth was attempted and this allowed to investigate the growth mechanism of CuS thin films. The growth of the film was monitored by following the evolution of the Bragg peak and monitoring the presence of powder diffraction rings. No shifts of the Bragg peaks were observed during the film growth, indicating a homogeneous growth process from the first layers. The intensity of the Bragg peak starts to be appreciable from the 15th deposition cycle, suggesting that the material crystallizes with low symmetry and a large elementary cell. Owing to the fact that the SXRD analysis is performed investigating the reciprocal space of the electrode over which the chalcogenide film is growing, the extraction of the Miller indices of the chalcogenide films is difficult. In order to check the possibility for a model to represent the actual chalcogenide film structure obtained by E-ALD, a procedure to derive the expected Miller indices of many models for the chalcogenide films on a silver single crystal has been implemented.

No shifts in the Bragg peak position are observed comparing CuS and Cu-Zn sulfides, suggesting a similar crystalline structure. Analysis of these data are still in progress but all the samples show a high crystallinity, proposing E-ALD as method to grow structurally ordered thin films.

Multianalytical investigation of Fe- and Zn-bearing kuramites for solar cell production

Di Benedetto F[1*], Cinotti S[2], D'Acapito F[3], De Luca A[2], Foresti M[2], Guerri A[2], Innocenti M[2], Lavacchi A[4], Montegrossi G[5], Romanelli M[1]

1 - Università Firenze - Dip. di Scienze della Terra, Italy *francesco.dibenedetto@unifi.it 2 - Università Firenze - Dip. di Chimica, Italy 3 - CNR-IOM-OGG @ ESRF, France 4 - CNR-ICCOM, Italy 5 - CNR-IGG, Italy

In the present study, we report the results of a multianalytical study (SEM/EDS, XRD, Electron Paramagnetic Resonance, SQUID magnetometry, X-ray Absorption Spectroscopy and Diffuse Reflectance Spectroscopy) carried out on different materials belonging to the Cu-Zn-S and Cu-Fe-Zn-Sn-S systems, related to the kesterites, Cu2ZnSn(S,Se)4, in the light of their potential application to solar cell production. In recent years, in fact, kesterites attracted a worldwide interest because they encompass reduced production costs and low environmental risks.

Samples are obtained by two different synthetic routes. Fe- and Zn-bearing kuramite nanoparticles are obtained through solvothermal syntheses, whereas Cu-Zn-S thin films analysed in the present study were realised through the E-ALD (Electrochemical Atomic Layer Deposition) technique.

Both Fe- and Zn- bearing nanokuramite samples crystallise in a tetragonal pseudocubic structural arrangement, affine to that of the ZnS sphalerite. The pseudocubic arrangement is confirmed by the EXAFS results, according to which we can attribute the lack of tetragonal reflections to the random occupancy of cations (Cu, Sn). From a microanalytical point of view, nanocrystals exhibit different particle morphologies, accompanied by own characteristic chemical compositions. That is, Fe appears inhomogeneously distributed within the powders, whereas Zn appears more regularly distributed over the lattice.

As far as thin films are concerned, a wide degree of heterogeneity, involving the morphological organisation of the films, as well as their phase composition, is revealed. E-ALD is proposed to operate a progressive and conventional coverage of the Ag (111) surface through a nanometric polycrystalline film consisting of oriented microcrystals. The insertion of a unit of ZnS in the deposition sequence apparently induces the formation of nanowhiskers on the film surface. From a structural point of view, Cu and Zn follow completely different paths in the crystallisation of the film. The XAS data, in fact, point to a poorly ordered low coordinated structure for Cu as in the mineral chalcocite. Conversely, Zn forms a crystalline structure in excellent agreement with the sphalerite model compound.

The first descriptions of the crystal structure of natural mullite and a related mineral named sillimullite

Fischer R X[1*], Tikhonova V[1], Birkenstock J[1], Fischer L[2], Herrmann K[3], Mengel K[3], Schneider H[1,4]

1 - Universität Bremen *rfischer@uni-bremen.de 2 - Universität Hannover 3 - TU Clausthal 4 - Universität Köln

The mineral name mullite was first proposed in 1924 by Bowen and Greig [1] who discovered crystals with a chemical composition of $3Al_2O_3{\cdot}2SiO_2$ in natural rocks of the Isle of Mull (Scotland). At that time synthetic analogues were already known to occur in ceramic materials. Since then the mineral mullite was frequently found in other locations as well and its synthetic counterpart became one of the most important phases in conventional and advanced ceramics. Its importance is documented by more than 4500 papers on mullite with many crystal-structure descriptions as summarized in [2]. Surprisingly, there is no crystal-structure refinement of the natural mineral, though there is no paucity of suitable specimens. Here we present our results on single-crystal studies of the mineral mullite and a new mineral named sillimullite, intermediate between sillimanite and mullite.

All minerals described here were found in the Eifel area (Germany) in the basalt quarry Caspar at the Ettringer Bellerberg near Mayen The chemical composition of natural mullites is close to a composition of $Al_{4+2x}Si_{2-2x}O_{10-x}$ with an *x*-value close to 0.25 (3/2-mullite) representing the number of oxygen vacancies per unit cell. Essentially all of these mullites contain Fe^{3+} replacing Al, and minor amounts of Mg and Ti. The crystal structures were refined by single-crystal methods and the results are compared with crystal structures of synthetic mullite.

Another crystal with an acicular shape was found in the same locality. The chemical compositions derived from the microprobe results and the crystal-structure refinements are $Al_{7.84}Fe_{0.18}Ti_{0.03}Mg_{0.03}Si_{3.92}O_{19.96}$ and $Al_{8.28}Fe_{0.20}Si_{3.52}O_{19.76}$, corresponding to *x*-values of 0.02 and 0.12, respectively, assigning Fe, Ti, and Mg to the Al site. The first composition is close to a stoichiometric sillimanite (with Fe,Ti, and Mg incorporated) and the second composition is between sillimanite and mullite. The deviation is assumed to be caused by exsolution of amorphous SiO_2 from the crystal structure detected by the microprobe but not affecting the diffraction data. It crystallizes in the orthorhombic space group *Pnam* with $a = 7.5127(4)$ Å, $b = 7.6823(4)$ Å, $c = 5.785(3)$ Å, $V = 333.88(4)$ Å^3, $Z = 1$. It has a complete Si/Al ordering like sillimanite but with neighboring double chains of SiO_4 and AlO_4 tetrahedra having an offset of ½ parallel **c** relative to each other causing the change of the space-group setting from *Pbnm* (sillimanite) to *Pnam*. Difference Fourier calculations and refinements with anisotropic displacement parameters revealed the formation of oxygen vacancies and triclusters as known in the crystal structures of mullite. Final refinements converged at R1 = 5.9% for 1024 unique reflections with $F_o > 4\sigma(F_o)$. Fe was found to reside predominantly in the octahedral site and with minor amounts in one of the T* sites. Mg and Ti were not considered in the refinements. Therefore, the crystal studied here can be considered to represent a new mineral intermediate between sillimanite and mullite, named sillimullite. In this respect, it is revolutionizing current knowledge on sillimanite and mullite type compounds. As a rare mineral it might be just a curiosity, but it implies that compounds similar, but significantly different to mullite do exist and might represent an interesting alternative to this important class of ceramic materials.

[1] Bowen N.L. and Greig J.W. (1924). *J. Amer. Ceram. Soc.*, 7, 238.

[2] Fischer R.X. and Schneider H. (2005). in: H. Schneider,S. Komarneni (Eds). Mullite, Wiley-VCH, Weinheim 1.

Ammonium exchanged zeolites

Fischer R X[1*], Wang L[1], Hölzen H[1], Birkenstock J[1], Spieß I[1], Baur W H[2]

1 - Universität Bremen *rfischer@uni-bremen.de 2 - Western Springs

Zeolites belong to the most important classes of materials with main applications as catalysts, e.g., in oil refinery, adsorbents and as ion exchangers, e.g., for the softening of water with a production of more than 1 million metric tons per year just as an additive to laundry detergents. Similarly, it is used for drying and purifying gasses, cleaning up nuclear wastes, adsorbing odors, and even for clotting blood applied to large open wounds. Zeolites in their classical descriptions are aluminosilicates with a framework structure enclosing cavities occupied by large ions and water molecules, both of which have considerable freedom of movement, permitting ion-exchange and reversible dehydration. NH_4 zeolites, where the ammonium ion represents the charge-compensating cation, play an important role as precursor materials in the production of H-zeolites. The hydrogen zeolites in turn represent the actual catalysts with their protons acting as Brønsted acids.

Single crystals of natural zeolites provide an ideal system for crystal chemical studies while many of their synthetic counterparts are available as fain-grained powder materials only. In our systematic studies of NH_4-exchanged zeolites we are presenting here first results from single-crystal studies on the chabazite-type mineral willhendersonite and merlinoite compared with synthetic NH_4-A.

All zeolites are represented in their standardized settings as defined in [1, 2] and contained in [3] together with about 1,500 structure descriptions of natural zeolites and more than 4,500 entries of synthetic zeolites. That way, all details in their framework structures can be directly compared and discussed.

A special focus is on the evaluation of occupancy factors of the nonframework cations and species. They are very often statistically distributed over several sites being mutually exclusive due to short distances not allowing simultaneous occupation. Site occupancy factors are evaluated using Boolean satisfiability techniques as introduced in [4].

[1] Baur W.H. and Fischer R.X. (2000). Zeolite-type crystal structures and their chemistry. Subvolumes B, C in Landolt-Börnstein, Numerical data and functional relationships in science and technology, New Series, Group IV: Physical Chemistry, Volume 14, Microporous and other framework materials with zeolite-type structures, eds. W.H. Baur, R.X. Fischer, Springer-Verlag, Berlin, 2000, 2002.

[2] Fischer R.X. and Baur W.H. (2006). Zeolite-type crystal structures and their chemistry. Subvolumes D, E, F, G in Landolt-Börnstein, Numerical data and functional relationships in science and technology, New Series, Group IV: Physical Chemistry, Volume 14, Microporous and other framework materials with zeolite-type structures, eds. R.X. Fischer, W.H. Baur, Springer-Verlag, Berlin, 2006, 2009. 2013, 2014.

[3] Baur W.H. and Fischer R.X. (2010). ZeoBase, a new kind of crystal structure database. In Proc. *16th Int. Zeolite Conf. 2010*. Sorrento, Italy: A. De Frede.

[4] Soeken M., Drechsler R. and Fischer R.X. (2013). *Jahrestagung der Deutschen Kristallographischen Gesellschaft. Z. Kristallogr.* (2013) *Suppl.*

High temperature behaviour, phase transition and structural investigations on a sulfate apatite

Kahlenberg V[1*], Botta C[2], Többens D[3], Bykov M[4], van Smaalen S[4]

1 - Institute of Mineralogy and Petrography, University of Innsbruck *volker.kahlenberg@uibk.ac.at 2 - RHI AG, Technology Center Leoben 3 - Helmholtz-Zentrum Berlin für Materialien und Energie 4 - University of Bayreuth, Laboratory of Crystallography

The apatite family comprises a large series of natural and synthetic compounds with the general crystal chemical formula $M1_6M2_4(ZO_4)_6X_2$, which mainly adopt the hexagonal space group $P6_3/m$. The most common composition corresponds to $Ca_{10}(PO_4)_6(OH,F)_2$, known as "calcium phosphate apatite". However, as indicated by the general formula, extensive substitutions can occur on the different cation and anion sites in mineral samples.

Polycrystalline material of a sulfate apatite with chemical composition $Na_6Ca_4(SO_4)_6F_2$ or $(Na_2Ca_4)Na_4(SO_4)_6F_2$ has been synthesized by solid state reactions. Basic crystallographic data are as follows: hexagonal symmetry, a = 9.3976(1) Å, c = 6.8956(1) Å, V = 527.39(1) Å^3, Z = 1, space group $P6_3/m$. For structural investigations the Rietveld method was employed. Thermal expansion has been studied between 25 and 600°C. High temperature (HT) powder diffraction data as well as thermal analysis indicate that the apatite-type compound undergoes a reconstructive phase transition in the range between 610 and 630°C. Single-crystals of the HT-polymorph were directly grown from the melt. Structural investigations based on single-crystal diffraction data of the quenched crystals performed at -100°C showed orthorhombic symmetry (space group $Pna2_1$) with a = 12.7560(8) Å, b = 8.6930(4) Å, c = 9.8980(5) Å, V = 1097.57(10) Å^3 and Z = 2. The lattice parameters of both modifications are related by the following *approximate* relationships: $\boldsymbol{a}_{HT} \approx 2\boldsymbol{c}_{RT}$, $\boldsymbol{b}_{HT} \approx -(\frac{1}{2}\boldsymbol{a}_{RT} + \boldsymbol{b}_{RT})$, $\boldsymbol{c}_{HT} \approx \boldsymbol{a}_{RT}$. The HT-modification is isotypic with the corresponding potassium compound $K_6Ca_4(SO_4)_6F_2$. The pronounced disorder of the sulphate group even at low temperatures has been studied by maximum entropy calculations. Despite the first-order character of the transformation clusters of sulfate groups surrounding the fluorine anions can be identified in both polymorphs.

Spectroscopic study of $Mg(Ga_{2-}Cr_X)O_4$, $Mg(Ga_{2-}Al_X)O_4$ and $Mg(Ga_{2-X}Fe^{3+}{}_X)O_4$ spinels

Lenaz D[1*], Skogby H[2], Hålenius U[2]

1 - University of Trieste *lenaz@units.it 2 - Swedish Museum of Natural History

We report results from single crystal XRD, ^{57}Fe Mössbauer spectroscopy and optical absorption spectroscopy studies on synthetic spinels in the $MgGa_2O_4$-$MgCr_2O_4$, $MgGa_2O_4$-$MgFe^{3+}{}_2O_4$ and $MgGa_2O_4$-$MgAl_2O_4$ series. A total of 15 crystals with variable Cr/Ga ratios, 11 with variable Fe^{3+}/Ga ratios and 8 with variable Al/Ga-ratios obtained in some 35 different synthesis runs were investigated.

The object of the study was to obtain information on cation ordering between the octahedral (M) and tetrahedral (T) sites in related spinels series containing M-cations with very different octahedral site preferences. An additional object was to explore the local real structure around ^{M}Cr and hence evaluate the influence of next-nearest atoms on the local structure.

Mössbauer spectra acquired at room-temperature indicate that Fe occur solely in the ferric state. For samples with a magnesioferrite component up to 62 %, the spectra are dominated by a somewhat asymmetric absorption doublet, consistent with Fe^{3+} occurring at both the octahedral and tetrahedral sites. For samples with a magnesioferrite component from 74 %, the spectra display magnetic splitting. Towards the magnesioferrite end-member, the magnetic fields increase from 33.8 to 45.6 T for the tetrahedral sites and from 39.2 to 48.0 T for the octahedral site.

Pure magnesium gallate crystals show a cell edge equal to 8.2780 (2) Å and an oxygen positional parameter of 0.2567 (2). The relationships between cell edge dimensions and $MgGa_2O_4$-fractions in the $MgAl_2O_4$ - $MgGa_2O_4$ and the $MgFe_2O_4$-$MgGa_2O_4$ series are almost linear with R^2-values equal to 0.994 and 0.998, respectively. This is due to the fact that Mg, Ga, Fe^{3+} and Al can be accommodated at both T and M sites and consequently show disorder over the two structural sites. The relation between cell edge and Mg-chromite content of the $MgCr_2O_4$ - $MgGa_2O_4$ is best approximated by a 2nd order polynomial with an R^2 equal to 0.954 due to the strict ordering of Cr at the M site. In this case there is a small increase in cell edge dimension for low-Cr values due to the Mg-Ga exchange among the M and T sites, and a steeper increase at higher Cr-contents.

Optical absorption spectra of $MgCr_2O_4$ - $MgGa_2O_4$ solid solution crystals are characterised by two absorption bands at ~17500 and ~23500 cm^{-1} caused by spin-allowed *d-d* transitions in $^{M}Cr^{3+}$. The energy shifts of these two bands along the compositional range are very small, ~40 and 270 cm^{-1}, respectively. This demonstrates that the local $^{M}Cr^{3+}$-O distance varies with less than 0.001 Å within this spinel series. This is in strong contrast to the situation in the $MgCr_2O_4$-$MgAl_2O_4$ series, where local $^{M}Cr^{3+}$-O distance varies with ~0.020 Å and it reflects the smaller difference in cation radii between $^{VI}Cr^{3+}$and $^{VI}Ga^{3+}$ (0.005 Å) as compared to $^{VI}Cr^{3+}$ and $^{VI}Al^{3+}$ (0.080 Å).

Optical absorption spectra of $MgAl_2O_4$-$MgFe_2O_4$ solid solution crystals show a set of absorption bands at ~10000, ~17950, ~19060, ~21180, ~22080, ~25420 and ~27000 cm^{-1} caused by electronic transitions in $^{M}Fe^{3+}$. The intensities of the absorption bands are linearly correlated with the square of the sample $^{M}Fe^{3+}$ thus demonstrating that they are caused by electronic transitions in exchange coupled pairs or clusters of $^{M}Fe^{3+}$-cations.

Acknowledgements: Funding provided by the project SE-TAF-3188 performed at the Swedish Museum of Natural History within SYNTHESYS (http://www.synthesis.info/). SYNTHESIS receives funding from the European Community - Research Infrastructure Action under the FP7 "Capacities" Specific Programme and SE-TAF-785 program.

Crystal structure and properties of boron-doped mullite – investigations at ambient, high-pressure, and high-temperature conditions

Lührs H[1*], Kalita P E [2], Lipinska K [2], King S P [3], Hanna J V [3], Söllradl S [4], Konzett, J[5] Schneider H [1], Fischer R X [1]

1 - Universität Bremen, Germany *hluehrs@uni-bremen.de 2 - University of Nevada, Las Vegas, USA 3 - University of Warwick, UK. 4 - FRM II, Garching, Germany. 5 - Universität Innsbruck, Austria.

Despite its rareness as a natural mineral, mullite is one of the most important synthetic compounds for advanced structural and functional ceramic materials. The crystal structure of mullite ($Al_2[Al_{2+2x}Si_{2-2x}]O_{10-x}$, 0.2 <x <0.9) can incorporate a large variety of foreign cations [1]. The influence of boron on the crystal structure and selected properties of mullite was investigated under ambient, high-pressure, and high-temperature conditions.

Based on powder neutron diffraction and ^{11}B MAS-NMR data the crystal structure of B-mullite (Figure 1) was solved yielding the following substitution mechanism: 2 Si^{4+} + $O^{2-} \rightarrow$ 2 B^{3+} + vac [2]. The structure model allows a crystal chemical explanation for the anisotropic behavior of lattice parameters [3-5]. Whereas lattice parameters *a* and *b* show minor changes only, a linear relationship between lattice parameter *c* and the amount of boron in the crystal structure was established on the basis of prompt gamma activation analyses (PGAA) and Rietveld refinements. According to this relationship single-phase mullite with 15% replacement of silicon by boron can be produced, higher amounts of boron in the mullite structure lead to the formation of alumina impurities in the respective samples.

The incorporation of boron results in a strong reduction (16 %) of the volume thermal expansion coefficient, making B-mullites a potential candidate for technical applications in the temperature range below 1000°C [4]. Moreover, it was shown by in situ high-pressure synchrotron X-ray diffraction experiments that the formation of additional oxygen vacancies reduces the mechanical stability of the B-mullite structure. The increasing anisotropy of lattice parameters under pressure is explained by a rotation of the octahedra and the increasing inclination angle ω between the octahedral axes of neighboring AlO_6 octahedra in the **ab**-plane [6].

Single-phase B-mullite with 40% replacement of silicon by boron was synthesized at 10 kbar and 875°C [7]. Based on XRD, ^{11}B MAS NMR, and PGAA data, it was shown that some aluminum in the AlO_4 tetrahedra is replaced by boron as well in addition to the established silicon-boron substitution mechanism.

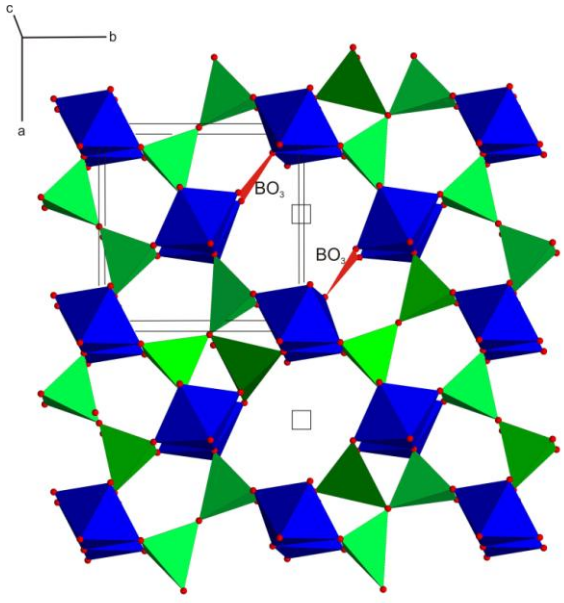

Figure 1: Crystal structure of B-mullite showing the Si-B substitution mechanism. Square = oxygen vacancy.

[1] Schneider H. (2005). in *Mullite*, H. Schneider and S. Komarneni, Editors. WILEY-VCH: Weinheim. p. 70-93.

[2] Lührs H., *et al*. (2013). *Z Kristallogr*, 228(9), 457-466.

[3] Griesser K.J. *et al*. (2008). *Miner Petrol*, 92(3-4), 309-320.

[4] Lührs H. *et al*. (2012). *Mater Res Bull*, 47, 4031-4042.

[5] Zhang G.M. *et al*. (2010). *J Europ Ceram Soc*, 30(12), 2435-2441.

[6] Kalita P.E. *et al*. (2014). subm. to *J Am Ceram Soc*.

[7] Lührs H., *et al*. (2013). *Cryst Res Technol*, 49, 21-31.

Ion exchange in epistolite-group minerals: chemical and structure aspects

Lykova I[1*], Pekov I[1], Chukanov N[2], Zubkova N[1], Yapaskurt V[1], Zolotarev A[3]

1 - Moscow State University *innalykova@mail.ru 2 - Institute of Problems of Chemical Physics 3 - St. Petersburg State University

We carried out first systematic experimental studies of the ion-exchange properties of epistolite-group minerals lomonosovite $Na_4Ti_4(Si_2O_7)_2O_4{\cdot}2Na_3PO_4$, murmanite $Na_4Ti_4(Si_2O_7)_2O_4{\cdot}4H_2O$ and epistolite $Na_4Ti_4(Si_2O_7)_2O_4{\cdot}4H_2O$ with different salt solutions (0.01 - 1 N concentration) in the temperature range of 30-150°C. The duration of experiments ranged from 1 hour to 7 days.

All three heterophyllosilicates show strong affinity for chalcophile elements. Na exchanges for Ag (up to 9.3, 3.7 and 4.7 *apfu* Ag in Ag-exchanged forms of lomonosovite, murmanite and epistolite respectively), Cu (up to 1.9, 0.8 and 0.6 *apfu*) and Zn (up to 0.4, 0.8 and 0.8 *apfu*). In all cases the P content in the cation-exchanged forms of lomonosovite remains the same as in initial lomonosovite (1.9-2.0 *apfu*). Unlike aluminosilicate zeolites, epistolite-group members poorly exchange Na for lithophile elements (K, Rb, Cs, Ca, Sr). For alkali and alkali-earth cations, negative correlation between ionic radius and exchange degree was observed. We assume that the involvement of alkali cations in the ion-exchange reactions with P-bearing heterophyllosilicates requires preliminary hydrolysis and partial leaching of PO_4^{3-} from the interlayer space.

The reaction of ion exchange of murmanite with Ag^+ follows the first order kinetic model up to 70-80% conversion. The rate of the process is described by the equation $k\ (h^{-1}) = 10^{7.64\pm0.60}\ \exp[-(12.2\pm0.9)\times10^3/RT]$. The average heat release value in the temperature range 39.4-72°C is 230 Jg^{-1}. The cation exchange is limited by processes in solid state, most probably binding of silver.

The crystal structures of cation-exchanged forms of lomonosovite and murmanite were studied by single-crystal X-ray diffraction data. In the Ag-exchanged forms of murmanite the main structural *HOH* block remains unchanged. Ag^+ cations occupy two crystallographically non-equivalent positions: one in the heteropolyhedral (*H*) and one in the octahedral (*O*) layer, corresponding to the positions of Na in initial murmanite. Unit-cell parameter *c* of the Cu-exchanged form of lomonosovite decreases significantly as compared to the initial lomonosovite, while parameters *a* and *b* remain almost unchanged. There is one Cu site corresponding to one of the three Na sites in the interlayer space of the initial lomonosovite and two Na sites: one fully occupied in the interlayer space and one half-occupied in the *O* layer. The Na site in the *H* layer and the third one in the interlayer space of the initial lomonosovite are vacant in its Cu-exchanged form. The crystal structure of Ag-exchanged form of lomonosovite is characterized by the increased unit cell parameter *c* and doubled parameter *b* as compared to the original lomonosovite. One of two PO_4-tetrahedra has two orientations of one of the apices with half-occupied O, which leads to a double *b* parameter. Ten (*pfu*) large-cation sites, statistically occupied by Ag and Na, correspond to the Na sites in the initial lomonosovite: six in the interlayer space, two in the *H* and two in the *O* layers. Ag strongly replaces Na in sites in the interlayer space and in the *O* layers whereas sites in the *H* layers remain filled mainly by Na.

Our studies unambiguously show that ion exchange reactions in heterophyllosilicates occur in nature: Na exchanges for chalcophile elements, Zn, Pb and Cd. Two new Zn heterophyllosilicates, vigrishinite $Zn_2Ti_{4-x}Si_4O_{14}(OH,H_2O)_8$, $x<1$, and zvyaginite $NaZnNb_2Ti[Si_2O_7]_2O(OH,F)_3(H_2O)_{4+x}$ were recently discovered by us in a hydrothermally altered peralkaline pegmatite at Mt. Malyi Punkaruaiv, Lovozero alkaline complex, Kola Peninsula, Russia. No doubt that they were formed as a result of natural cation exchange reactions of murmanite and epistolite, respectively, with low-alkaline hydrothermal solutions enriched in Zn^{2+}, mobilized from dissolved earlier sphalerite.

Vigrishinite and zvyaginite cannot be described with the small, epistolite-type unit cells due to the distortion of the *HOH* block caused by the differences in ionic radii between Na^+ and Zn^{2+}. The *a* and *b* parameters of their large unit cells correspond to the *ab* face diagonals of the epistolite-type unit cell. Vigrishinite contains the main part of Zn in the *H* layer and additional low-occupied Zn sites in the interlayer space, whilst zvyaginite contains Zn in the *O* layer.

Crystal chemistry of hydroxide perovskites

Najorka J*, Welch M

1 - Natural History Museum, London *j.najorka@nhm.ac.uk

"Hydroxide perovskites" have the general formula $BB'(OH)_6$ or $B(OH)_3$ ($B = B'$) for which $B = M^{1+}$, M^{2+} or M^{3+} and $B' = M^{3+}$, M^{4+} or M^{5+}. As well as several naturally-occurring phases, synthetic analogues have recently been used as precursors to the preparation of protonated perovskites, as well as being studied as ionic transport media in their own right.

Their structure topology (Figure 1) is a three-dimensional framework of corner-linked $B(OH)_6$ and $B'(OH)_6$ octahedra in which all oxygens form OH groups, and the *A*-site cavity is empty. We have studied the effects of composition on solid solution behaviour in three $Cu_x M^{2+}_{(1-x)}Sn(OH)_6$ binary series for M^{2+} = Zn, Mn, Co. Miscibility gaps between cubic and tetragonal phase exist in all three binaries between x = 0.5-0.8 (Cu-Zn), x = 0.6-0.9 (Cu-Co) and x = 0.8-0.9 (Cu-Mn) (Figure 2, $Cu_xZn_{(1-x)}Sn(OH)_6$). For the Cu-Zn and Cu-Co systems, we provisionally interpret this behaviour in terms of a critical threshold for avoidance of $Cu(OH)_6$-$Sn(OH)_6$-$Cu(OH)_6$-$Sn(OH)_6$ quartets in the cubic phase near the 50:50 composition, that may arise from an amplified local Jahn-Teller distortion of these quartets, driving a tetragonal distortion, that cannot be tolerated. Contrasting with the wide compositional range of the cubic phase, the Cu-rich tetragonal phase accepts only 0.05-0.15 M^{2+} substitution. Other parameters, such as a different *d*-electron configuration, may mitigate the distortion or result in different clustering of $Cu(OH)_6$ octahedra in the Cu-Mn system.

The results of single-crystal and powder XRD studies and vibrational spectroscopy will be reported and an overview given of the major structural trends of this over-looked, but potentially widely significant, topology.

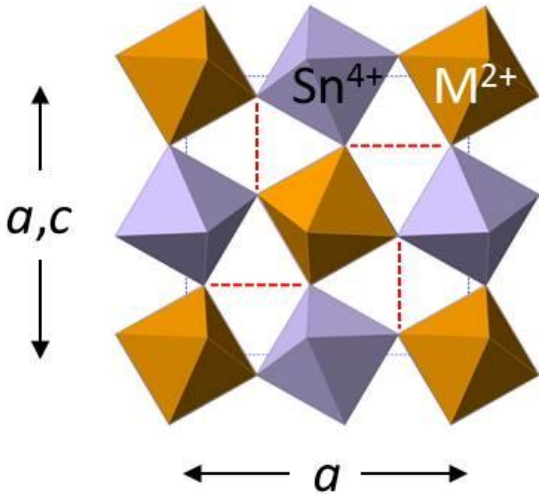

Figure 1: Structure topology of hydroxystannate perovskite. Red dashed lines show hydrogen bonded linkages

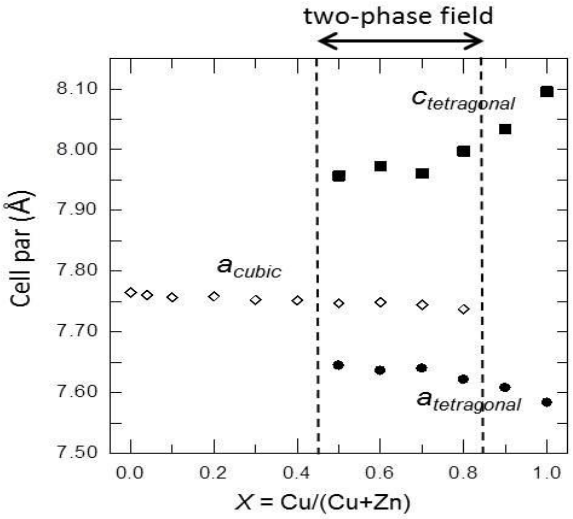

Figure 2: Lattice parameters of the $Cu_xZn_{(1-x)}Sn(OH)_6$

Marshallsussmanite, a new pyroxenoid mineral of the pectolite group from the Wessels mine, Kalahari Manganese Field, South Africa

Origlieri M J*, Downs R T, Yang H

University of Arizona. *moriglie@email.arizona.edu

Marshallsussmanite is a new pyroxenoid mineral species (IMA2013-067) with ideal chemistry $NaCaMnSi_3O_8(OH)$. Marshallsussmanite forms transparent pink bladed crystals up to 2.1 cm in association with sérandite and calcite at the Wessels mine, Kalahari Manganese Field, South Africa. In a separate assemblage, marshallsussmanite occurs with pectolite, aegirine, and apophyllite-(KOH). The average of 19 standardized electron probe microanalyses yielded an empirical chemistry of $Na_{0.906}Ca_{0.953}Mg_{0.007}Mn_{1.071}Si_3O_8(OH)$ when normalized to 9 O atoms. Unit cell parameters obtained from single crystal X-ray diffraction are a = 7.7834(4), b = 6.9373(4), c = 6.8496(3) Å, α = 90.680 (3)°, β = 94.329(3)°, γ = 102.854(3)°, V = 359.40(4) Å^3. The mineral is triclinic with space group P-1 and Z = 2. The mineral is a single chain silicate, with a chain repeat of three SiO_4 tetrahedra (dreier chain). Crystal structure refinement shows distinct ordering of Na, Ca, and Mn into separate sites. Marshallsussmanite is an ordered intermediate between pectolite, $NaCa_2Si_3O_8(OH)$, and sérandite, $NaMn_2Si_3O_8(OH)$; and is isostructural with tanohataite, $LiMn_2Si_3O_8(OH)$, all four of which constitute the pectolite group. Marshallsussmanite has an especially strong hydrogen bond between two non-bridging oxygen atoms on the silicate chain with R(O-H-O) = 2.458 Å. The mineral name honors collector Marshall I. Sussman, of Oro Valley, Arizona, who bought the mineral to the attention of the senior author.

Na-K interdiffusion in potassium-rich alkali feldspar: composition dependence and diffusion anisotropy

Schaeffer A-K[1], Abart R[1*], Petrishcheva E[1], Habler G[1], Rhede D[2]

1 - Department of Lithospheric Research, University of Vienna

*rainer.abart@univie.ac.at 2 - Helmholtzzentrum Potsdam, German GFZ, Potsdam

Na-K interdiffusion in potassium-rich alkali feldspar was investigated using cation exchange between gem-quality disordered alkali feldspar from the Eifel (XOr = 0.85) and NaCl-KCl or NaBr-KBr salt melt. Single crystals of the feldspar were machined to plates with 3 by 3 by 1 millimetre edge length and the large faces polished. Plates with the polished faces in seven different crystallographic directions were prepared. The plates were sealed in quartz glass tubes together with salt mixtures with different K/Na proportions. A 40-fold molar excess of alkali cations in the salt as compared to the feldspar was applied to ensure constant composition of the salt melt during cation exchange. The experiments were done at about 1 bar pressure, temperatures of 800°C to 1000°C, and for run durations from 2 to 64 days. Cation exchange produced chemically altered zones at the grain surfaces, which extended further into the grain interior with time. The transition between altered and pristine domains of the feldspar corresponds to diffusion fronts, which were analyzed along profiles perpendicular to the polished grain surfaces. The full diffusivity tensor and its composition dependence were determined from combining the information obtained from the diffusion fronts along the seven different directions. Na-K interdiffusion turned out to be composition dependent with a pronounced increase of the Na-K interdiffusion coefficient at XOr >0.95 and a more subtle composition dependence at 0.65 <XOr <0.95. A pronounced diffusion anisotropy was found with the principle axes of the diffusivity tensor parallel to the crystallographic [101] direction (fastest diffusion) and in the direction within the (010) plane that is perpendicular to [101] (slowest diffusion). The principle axis of the diffusivity tensor that corresponds to intermediate diffusion coefficients is parallel to [010]. The activation energy for Na-K interdiffusion is about 280 kJ/mol for diffusion parallel to [010] and about 180 kJ/mol for diffusion parallel to (001). Diffusion anisotropy becomes successively less pronounced with increasing temperature. Exceptionally sharp diffusion fronts develop at the polished (010) faces, i.e. along the [010] direction. This phenomenon is probably related to lattice distortion, which is localized at the sharp diffusion fronts due to the composition dependence of the lattice parameters. Comparison of our direct determinations of the Na-K interdiffusion coefficient with predictions obtained from interdiffusion models for ionic crystals that employ experimentally determined tracer diffusion coefficients for sodium and potassium yield good qualitative agreement. Discrepancies in terms of absolute values are probably due to the fact that the tracer diffusion coefficients were determined by bulk exchange methods, which are biased by diffusion in the fastest diffusion direction and cannot reveal the underlying diffusion anisotropy.

Compositional and structural diversity in pyroxenoids revisited: a new dreier-chain silicate $Na_{1.5}Y_{0.5}CaSi_3O_9H$

Welch M[1*], Mitchell R[2], Kampf A[3], Chakhmouradian A[4], Spratt J[1]

1 - Natural History Museum,London *mdw@nhm.ac.uk 2 - Lakehead University 3 - Natural History Museum of Los Angeles County 4 - University of Manitoba

The structure of an unusual new Y- and REE-rich hydrous pyroxenoid of the pectolite-serandite-cascandite group has been determined by single-crystal XRD to R_1 = 0.038, wR_2 = 0.068, GoF = 1.132. It is monoclinic, space group $P2_1/a$, with unit-cell parameters a 15.5026(2) Å, b 7.0233(1) Å, c 6.9769(1) Å, beta 95.149(1)°, V 756.58(2) Å^3 (Z = 4). All crystals examined have the monoclinic 2M polytype structure, which has not been observed in pectolite-group pyroxenoids, all of which are the 1T triclinic polytype. The average empirical formula obtained by EMPA on a single crystal (n = 14) based on 9 anions (8 O + OH) *pfu* is tightly constrained as $Na_{1.54(2)}$ $Ca_{0.74(1)}$ $Mn_{0.15(1)}$ $Fe_{0.07(1)}$ $Y_{0.38(1)}$ $Nd_{0.008(1)}$ $Sm_{0.008(1)}$ $Gd_{0.020(1)}$ $Tb_{0.005(1)}$ $Dy_{0.036(1)}$ $Ho_{0.008(1)}$ $Er_{0.022(1)}$ $Tm_{0.003(1)}$ $Yb_{0.014(1)}$ $Si_{3.00(1)}$ O_9 H [(Y + REE) = 0.51]. Refined site-scattering values of the three metal sites are M(1) = 19.6 e, M(2) = 28.1 e, M(3) = 10.9 e. Y and REE are assigned to the electron-rich M(2) site; M(1) = Ca; M(3) = Na. The calculated site-scattering values based upon the empirical composition agree closely with these refined values. The ideal structural formula of the new pyroxenoid is $^{M(3)}Na\ ^{M(2)}(Na_{0.5}\ Y_{0.5})\ ^{M(1)}Ca\ Si_3\ O_9$ H, and is displaced from pectolite by the substitution ½ [Na Y Ca_{-2}] at M(2). An alternative ordering scheme $^{M(3)}Na\ ^{M(2)}(Ca_{0.5}\ Y_{0.5})^{M(1)}(Na_{0.5}\ Ca_{0.5})\ Si_3\ O_9$ H is incompatible with the refined site-scattering values. Bond-valence analysis confirms the proposed ordering scheme. The highly constrained composition of the new pyroxenoid suggests a strong coupling between composition and structure. Yttrian pectolite with up to 0.16[Na Y Ca_{-2}] substitution is the 1T triclinic polytype and occurs as a distinct phase in rocks with the new pyroxenoid. The structure and crystal chemistry of $Na_{1.5}Y_{0.5}CaSi_3O_9H$ (e.g. Figure 1) will be described and the implications for compositional and structural diversity in pyroxenoids discussed.

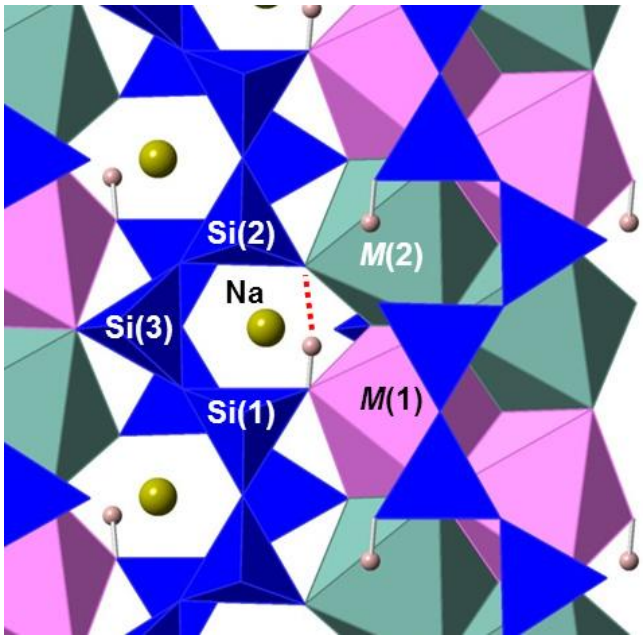

Figure 1: View of part of the crystal structure of $Na_{1.5}Y_{0.5}CaSi_3O_9H$ projected onto (102) showing the environment of the O-H...O bridge. M(1) = Ca, M(2) = $Na_{0.5}Y_{0.5}$. The chain/ribbon extension is parallel to the y axis.

High temperature C2/c clinoenstatite single crystals: detail structure and transition mechanism

Yoshiasa A[1*], Nakatsuka A[2], Okube M[3], Katsura T[3]

1 - Kumamoto University *yoshiasa@sci.kumamoto-u.ac.jp 2 - Yamaguchi University 3 - Okayama University

The high-temperature clinoenstatite (HT-CEn) is one of the important MgSiO3 pyroxene polymorphs. The single-crystals of C2/c HT-CEn are firstly synthesized by rapid pressure-temperature quenching from 15-16 GPa and 900-1900 °C [1]. The high pressure and high temperature experiments were carried out with a Kawai-type multi-anvil apparatus. The samples were quenched by rapidly releasing the oil pressure load and/or by blow out of anvil cell gasket. The space group of C2/c is strictly determined by Weissenberg photographs and synchrotron radiation. Single-crystal X-ray diffraction experiments were performed at ambient conditions using a four circle diffractometer. A total of 9383 reflections were measured and 766 independent reflections were used for the structure refinements. Final reliability factors converged smoothly to R = 0.029. The HT-CEn single crystal was formed by the isosymmetric phase transition from HP-CEn. HT-CEn type single-crystals cannot be frozen without pressure. The single-crystal diffraction analysis shows the unusual bonding distances frozen in this metastable structure. The degree of kinking of the silicate tetrahedral chains is 175° for HT-CEn. The chain angle for HP-CEn is substantially smaller (135°) and the angle for L-CEn turned to the opposite direction at 200°. The degree of kinking increases by being curved more than 180° in the transition from HT-CEn to L-CEn. When the cooling rate and quenching route are satisfactory, HT-CEn crystals are quenched as a metastable structure formed at a middle stage of the transition from HP-CEn to L-CEn. Metastable HT-CEn may be found in a shock-metamorphosed meteorite.

[1] Yoshiasa A. *et al.* (2013). *Acta Cryst. B*, 69, 541.

The vibrational entropy of solid solutions

Benisek A*, Dachs E

Salzburg University *artur.benisek@sbg.ac.at

The excess vibrational entropy, defined as the deviation of the vibrational entropy of a solid solution composition from that of the corresponding mechanical mixture of the end members, is found to depend on bond length changes that occur with compositional variations. The bond length changes itself, depending on the elasticity of the substitution polyhedra in the end member structures in such a way, that the elastically stiffer substitution polyhedron forces the softer one to fit to its size. In cases, where the smaller substitution polyhedron is elastically softer, its bond lengths are expected to be strongly enlarged by adaption to the stiffer and larger substitution polyhedron resulting in positive excess heat capacities and thus positive excess vibrational entropies. On the other hand, if the larger polyhedron is elastically softer, its bond lengths are forced by the stiffer and smaller substitution polyhedron to become shorter and this may result in negative excess vibrational entropies [1]. Based on an empirical relationship that uses the differences of end member volumes and bulk moduli, the maximum excess vibrational entropy of various solid solutions has been estimated. This delta *V* vs. delta *K* approach (see equation below) has been applied to binary alloys, silicate solid solutions and the NaCl-KCl binary. A comparison of calculated and calorimetrically determined excess vibrational entropies of these binaries is compiled in Figure 1 below.

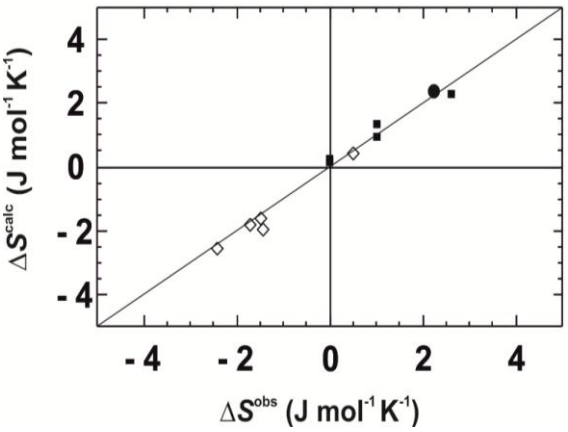

Figure 1: Calculated versus measured maximum excess vibrational entropies. Data are from binary alloys (open symbols), silicate solid solutions (closed squares) and the NaCl-KCl binary (closed circle).

The ΔV vs. ΔK approach:

$$\Delta_{max}S^{exc} = (\Delta V + m\,\Delta K)\,f$$

$\Delta_{max}S^{exc}$ is the maximum excess vibrational entropy. ΔV and ΔK are the differences of volumes and bulk moduli of the end members A and B, i.e., $\Delta V = V_A - V_B$ and $\Delta K = K_A - K_B$, where the end member A has a larger volume than B.

ΔK has a positive or negative value depending on which end member (larger or smaller) is elastically stiffer distinguishing between positive or negative $\Delta_{max}S^{exc}$. The parameters of this equation were determined to be $m = 1.089\ 10^{-16}$ J mol^{-1} Pa^{-2} and $f = 2.505\ 10^{5}$ Pa K^{-1}[1].

[1] Benisek A. and Dachs E. (2012). A relationship to estimate the excess entropy of mixing: Application in silicate solid solutions and binary alloys. *J. Alloys Compounds*, 527, 127-131.

Tokyoite and As-rich tokyoite: new occurrence in the manganese ore of the Postmasburg Manganese Field, South Africa

Costin G*, Fairey B, Tsikos H

2 - Department of Geology, Rhodes University, Grahamstown, *g.costin@ru.ac.za

Samples with As-rich tokyoite were retrieved from an exploration drill core from south-west of Bruce iron ore mine, Postmasburg Manganese Field, South Africa. The samples consist of a fine black matrix, made of various proportions of hematite, braunite and hausmannite, which contains abundant vugs filled by K-feldspar, quartz, sérandite-pectolite, tokyoite, As-rich tokyoite, noélbensonite, witherite, baryte, albite and minor aegirine, natrolite, paragonite, strontianite, piemontite, barytocalcite and calcite. As-rich tokyoite, tokyoite and noélbensonite are often associated and occur in the centre of the vugs, in fine aggregates of 0.1 to 1 mm in size, whereas the individual As-rich tokyoite grains are usually of 20-200 micron in size. The outer walls of the vugs are lined with K-feldspar (adularia habit), witherite or serandite. In hand specimen, the As-rich tokyoite is reddish brown. In thin sections, it has a dark red to pinkish dark red colour, more intense than tokyoite, which is reddish brown, whereas the noélbensonite has a lighter, honey-brown colour.

EBSD results shows a monoclinc lattice of As-rich tokyite with $P2_1/c$ space group, structure identical with that of gamagarite with cell parameters a= 9.121 Å, b= 7.838 Å, c= 7.838 Å, α=90º, β=90º, γ=112.7º, density 4.691 g/cm^3. The Raman spectrum of As-rich tokyoite was compared to spectra of arsenbrackebuschite and arsentsumebite (Figure 1).

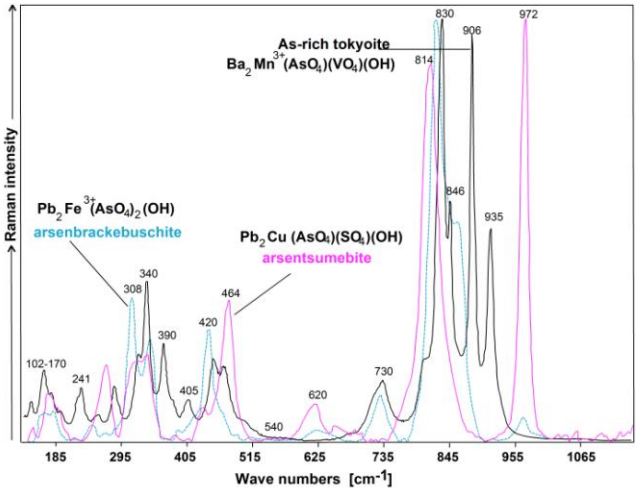

Figure 1: Raman spectrum of As-rich tokyoite, compared with the Raman spectra of arsenbrackebuschite and arsentsumebite.

The four outstanding peaks between 800 and 930 cm-1, a pair between 810-860 cm-1, and a pair between 870 and 930 cm-1, could suggest that the $(VO_4)^{3-}$ and $(AsO_4)^{3-}$ groups in our sample may be ordered and such, they may occupy two distinct crystallographic positions, as in arsentsumebite (AsO_4 vs. SO_4) or in bushmakinite (PO_4 vs. VO_4). Until XRD data will become available, we can speculate that the formula of As-rich tokyoite is rather $Ba_2Mn^{3+}(AsO^4)(VO_4)(OH)$ instead of $Ba_2Mn^{3+}((As,V)O_4)_2(OH)$, which might have been inferred from the analogue tokyoite formula $Ba_2Mn^{3+}(VO_4)_2(OH)$. The 1:1 ratio of As and V apfu calculated from the EPMA data also strongly supports the interpretation of $(VO_4)^{3-}$ and $(AsO_4)^{3-}$ tetrahedrons occupying distinct positions in the As-rich tokyoite lattice. An average of 15 EPMA analyses of As-rich tokyoite shows (wt%): BaO=48.695, As_2O_5=19.920, V_2O_5=14.421, Mn_2O_3=12.289, SiO_2=0.134, Al_2O_3=0.017, Fe_2O_3=0.256, K_2O=0.011, PbO=1.270, CaO=0.033, SrO=1.033, SO3=0.007, P_2O_5=0.027. Normalization to 8.5 Oxygen gives a total cation content equal to 4.997. The H_2O was not analysed. However, indirect evidences for the presence of (OH) consist of: a) Hydrogen bonding bands in Raman spectrum, b) lower totals of the microprobe analyses (~98%), as well as c) similitude with other phases from the brackebuscite group. As-rich tokyoite most probably formed from Ba, V and As hydrothermal fluids interacting with Mn minerals, such as braunite. EBSD, Raman and EPMA data show that As-rich tokyoite is a mineral belonging to the brackebuschite mineral group, with probable formula $Ba_2Mn^{3+}(AsO_4)(VO_4)(OH)$.

TEV – a program for the determination of the thermal expansion tensor from diffraction data

Kahlenberg V*, Langreiter T

Institute of Mineralogy and Petrography, University of Innsbruck

*volker.kahlenberg@uibk.ac.at

TEV (*T*hermal *E*xpansion *V*isualization) is a user-friendly program for the calculation of the thermal expansion tensor a_{ij} from diffraction data. Unit cell parameters determined from temperature dependent data collections can be provided as input. An intuitive graphical user interface enables fitting of the evolution of individual lattice parameters to polynomials up to third order. Alternatively, polynomial representations obtained from other fitting programs or from the literature can be entered. The polynomials and their derivatives are employed for the calculation of the tensor components of a_{ij} in the infinitesimal limit following the approach described in [1]. The tensor components, eigenvalues, eigenvectors as well as their angles with the crystallographic axes can be evaluated for individual temperatures. Values of the tensor in specific directions parallel to either [uvw]s of the crystal lattice or vectors (hkl) of reciprocal space can be calculated. Finally, the 3-D representation surface for the second rank tensor and 2-D sections can be plotted and saved in a bitmap (PNG) format.

TEV is written in JAVA. A prerequisite for working with TEV is the installation of the JAVA runtime environment version 7 which can be downloaded from the following link: http://www.java.com/en/download/. The distribution contains an EXE-file for Windows users and a system independent JAR-file for running the software under Linux and Mac OS X. Furthermore, three test files containing temperature dependent data sets from hexagonal, monoclinic and triclinic compounds and a short manual are included.

[1] Paufler P. and Weber T. (1999). On the determination of linear thermal expansion coefficients of triclinic crystals using X-ray diffraction. *Eur. J. Mineral.*, 11, 721-730.

Anomalous thermal expansion behaviour of quartz and calcite

Mirwald P, Tappert R, Stalder R*

University Innsbruck *roland.stalder@uibk.ac.at

Quartz and calcite play an outstanding role in geosciences and technology. An expansion study between -100 to +200° C at 1 atm has been conducted on quartz and calcite using Raman and IR-spectroscopy. Figure 1 below shows the temperature dependence of the Raman band of quartz at 128 cm^{-1} and that of the IR band of calcite at 740 cm^{-1}.

The striking similar expansion behaviour of both minerals suggests a thermal anomaly in the range of 50°C, where structural changes are not accompanied by changes in the crystallographic symmetry. In case of quartz, volumetric precision data confirm this finding [1]. The results show, that this phenomenon seems to be related to the oxidic composition of these materials, since corresponding Raman data on BN and cryolite (Na_3AlF_6) show no thermal effect, thus supporting our hypothesis.

The thermal expansion anomalies reported here imply an extension towards high pressure. Considering recent observations of high pressure anomalies in quartz, cordierite and water [2, 3, 4], these new observation are a further indication that oxygen-bearing compounds are prone to PVT anomalies that are not directly relatable to phase transitions.

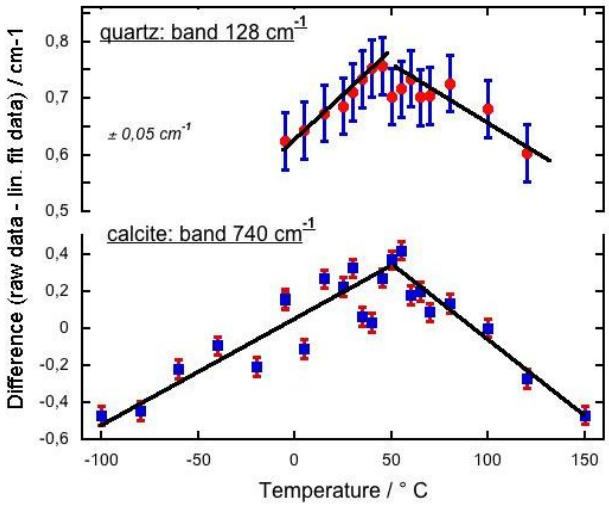

Figure 1: Temperature dependence of the Raman band of quartz at 128 cm^{-1} and the IR band of calcite at 740 cm^{-1}

[1] Kosinski J.A. *et al.* (1992). Proc. ESTEC, Paris, 397.

[2] Mirwald P.W. and Loerting T. (2011). Tagung DGK; DMG; ÖMG, Salzburg p.91.

[3] Miletich R. *et al.* (2014). *Am. Min.* 99, 749-493. 124715,1-6.

[4] Mirwald P.W. (2005). *J. Chem. Phys.*, 123.

Crystal chemistry of a silica clathrate mineral that is isostructural with the structure H gas hydrate

Momma K[1*], Ikeda T[2], Nagase T[3], Kuribayashi T[4], Honma C[5], Nishikubo K[5], Takahashi N[6], Takada M[5], Matsushita Y[7], Miyawaki R[1], Matsubara S[1]

1 - National Museum of Nature and Science *k-momma@kahaku.go.jp 2 - AIST 3 - Tohoku University Museum 4 - Tohoku University. 5 - Unaffiliated 6 - Natural History Museum and Institute, Chiba 7 - National Institute for Materials Science (NIMS)

Melanophlogite, chibaite, and another silica mineral have recently been found in the Boso Peninsula, Chiba Prefecture, Japan. These minerals are clathrate compounds of silica that contain hydrocarbon molecules in their cage-like framework structures. These silica minerals are isostructural with three types of natural gas hydrates. The framework topology of melanophlogite is the same as the structure I (sI) gas hydrate, and that of chibaite is the same as the structure II (sII) gas hydrate. Another silica mineral is isostructural with the structure H gas hydrate. The framework type code **DOH** is assigned to this topology by the Structure Commission of the International Zeolite Association.

The silica minerals occur as small veins in sandstone and mudstone of the Miocene Hota Group, at Arakawa, Minami-boso City, Chiba Prefecture, Japan. The Hota Group is a series of forearc sediments distributed in the Boso Peninsula, which encompasses the entirety of Chiba Prefecture and forms the eastern edge of Tokyo Bay. The Hota Group deposited near the plate margin by the Paleo-Izu arc and the triple junction of the Pacific, Philippine Sea and North America plates. It is composed mainly of tuffaceous siltstone with tuffaceous and volcaniclastic sandstones.

The DOH-type mineral exhibits platy-like shapes parallel to the {001} face, and it is epitaxially intergrown over euhedral chibaite crystals. The optical axis (*c* axis) of the DOH-type mineral is parallel with the <111> axis of chibaite. The grain size of individual crystal is about 0.01 mm to 0.05 mm in thickness and 0.05 mm to 0.3 mm in diameter. It is colorless, has vitreous lustre and white streak, and the Mohs hardness is 6.5 - 7. The empirical chemical formula excluding hydrocarbons, obtained by means of an electron microprobe (WDS mode, 15 kV, 5 nA, 1 μm beam diameter), is $Na_{0.01}(Si_{0.98}Al_{0.02})_{\sum 1.00}O_2$, z = 34. These constituents compose 87-89 wt% (average: 88.35 wt%), and the difference represents hydrocarbon molecules. The calculated density is 2.04 g cm^{-3}. A Raman peak attributable to C-H stretching mode of CH_4 was observed at 2904 cm^{-1}, and broad peaks of C_2H_6 or larger hydrocarbons were observed in the range of 2850-3050 cm^{-1}. Powder X-ray diffraction data were collected by the Debye-Scherrer method with synchrotron radiation (λ = 0.49957 Å) using an imaging plate at the BL15XU, SPring-8. The refined unit cell parameters are a = 1.38725(3) nm, c = 11.2694(3) nm, V = 1.87818(8) nm^3, and the space group is *P*6/*mmm*. Single-crystal X-ray diffraction studies were carried out using a Rigaku R-Axis Rapid II equipped with the curved imaging plate microdiffractometer with monochromatized Cu Kα radiation. The crystal structure was refined by SHELXL-97 software and converged to R_1 = 4.37% ($I_o > 2\sigma(I_o)$), wR_2 = 13.59%, GOF = 1.128 (Figure 1). The refined number of carbon atoms at guest sites is 17.5 per unit cell, which is in good agreement with the number estimated by the difference in the total wt% of the chemical analyses (17 per unit cell).

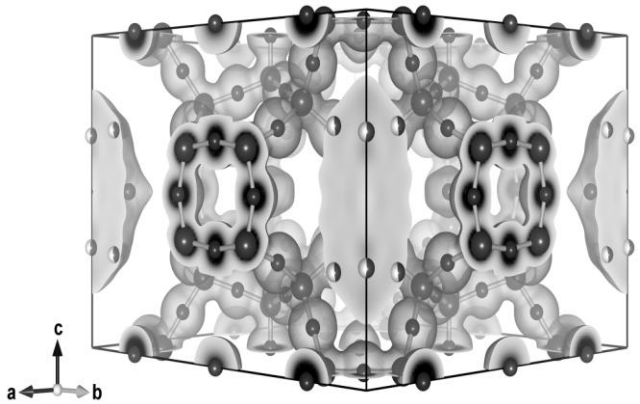

Figure 1: Electron density distributions (isosurface level: 0.5 Å^{-3}) in the **DOH**-type silica clathrate mineral calculated by the maximum entropy method, superimposed on the refined structural model.

Phase transition between high- and low-temperature orthopyroxene in the $Mg_2Si_2O_6$ - $Fe_2Si_2O_6$ system

Ohi S*, Miyake A

Kyoto University *shugo-ohi@kueps.kyoto-u.ac.jp

Pyroxene is one of the most important rock-forming minerals not only for its abundant occurrence, but also for various paragenesis, which provide information on the thermal history of pyroxene-bearing rocks. In the system $Mg_2Si_2O_6$-$CaMgSi_2O_6$, there had been the controversy about the appearance and stability of the orthopyroxene (Opx) phase near 1400 °C other than protopyroxene (Ppx) since the discovery by Foster and Lin [1]. In recent years, Ohi *et al*. [2] observed the isosymmetric phase transition between low-temperature Opx (LT-Opx) and high-temoperature Opx (HT-Opx) at 1170 °C by high-temperature X-ray powder diffraction (HT-XRD) experiments. They concluded that Opx, the phase near 1400 °C was HT-Opx. The purpose of the present study is to research the transition temperature between Fe-bearing LT-Opx and HT-Opx and the stability field of HT-Opx in the $Mg_2Si_2O_6$- $Fe_2Si_2O_6$ system by HT-XRD.

The starting material for HT-XRD were natural Opx of composition Fs_{10} (Morogoro, Tanzania), Fs_{14} (Bamble, Norway) and Fs_{37} (Ibaragi, Japan) as well as synthetic Opx of composition Fs_{20} and Fs_{30}. Opx (Fs_{20}) was synthesized from gel, which was placed in a one-atmosphere gas mixing (H_2-CO_2) furnace to maintain the furnace oxygen fugacity near the iron-wüstite buffer and heated at 1415 °C for 3 days. Opx (Fs_{30}) was synthesized from gel which was loaded in a Pt capsule surrounded by a Ni-NiO capsule and placed in a Boyd-England type piston-cylinder apparatus at 1350 °C, 1GPa for 2 hours. HT-XRD experiments were performed by using a multiple-detector system with HTK 16N (Anton Paar GmbH) high temperature chamber at the BL-4B2 beam line of the Photon Factory (PF), High Energy Accelerator Research Organization (KEK) in Tsukuba, Japan. Temperature calibration was made according to transition temperature between a-b quartz (573 °C) and low-high temperature orthoenstatite (1120 °C). Ar+H_2(1%) gas passed through the chamber to prevent the oxidation of Fe.

The peak profiles of HT-XRD experiments showed that the transition temperature of natural Opx (Fs_{10}) was 1136-1169 °C, that of natural Opx (Fs_{14}) was 1120-1137 °C, that of synthetic Opx (Fs_{20}) was 1069-1103 °C and that of synthetic Opx (Fs_{30}) 1036-1061 °C. Although, the phase transition was not observed in natural Opx (Fs_{37}) from 800 to 1200 °C, the volume thermal expansion coefficient of natural Opx (Fs_{37}) increased at around 1000 °C. This change of Opx (Fs_{37}) shows that the transition may occur above 1200 °C, because [2] also observed it bellow transition temperature between HT-Opx and LT-Opx.

In the present study, the transition between LT- and HT-Opx occurred around 1100 °C. It means that the stability field of Opx in $Mg_2Si_2O_6$- $Fe_2Si_2O_6$ system proposed by Huebner [3] was divided into LT-Opx and HT-Opx. On the other hand, the HT-XRD experiments with natural Opx showed that the transition temperature between LT- and HT-Opx was higher with increasing Fe contents, whereas those with natural Opx showed that the transition temperature was lower. This discrepancy of the transition temperature between natural and synthetic Opx might be influenced by minor elements in natural Opx such as Na, Al, Ca and Mn, or from Mg-Fe distribution between M1 and M2 site.

[1] Foster and Lin (1975). *EOS*, 56, 470.

[2] Ohi *et al*. (2008). *American Mineralogist*, 93, 1682-1685.

[3] Huebner (1980). *Reviews in Mineralogy*, 7, 213-288.

Florencite from gold bearing black shale from Lena gold province, Eastern Siberia, Russia

Palenova E[1*], Belogub E[1,2], Lebedeva S[1], Shtenberg M[1], Mironov A[1], Khvorov P[1]

1 - Institute of Mineralogy UB of RAS *palenova@mineralogy.ru 2 - South Ural State University

Florencite $(Ce,La)Al_3(PO_4)_2(OH)_6$ is the general concentrator of TR elements in black shale from Kopylovsky, Kavkaz and Krasny gold deposits located in the Lena gold province, Eastern Siberia. The Lena gold province belongs to Patom highland. The Lena gold province occurs within the Patom Highlands orogen, a deformed Neoproterozoic passive margin sequence on the southern margin of the Siberian craton. Dozens of gold ore deposits including the famous Sukhoy Log are in the region [1]. The studied Kopylovsky, Kavkaz and Krasny gold deposits are located within the carbon-bearing carbonaceous terrigenous Neoproterozoic rocks. Arcosic and quartz sandstone, siltstone, carbon-clayey and clayey shales, metamorphosed under sericite-chlorite subfacies of green-schist facies are the host rocks. Apatite is the main allogenic accessory mineral. Accessory rutile, tourmaline, and epidote occur both as clasts and as newly formed crystals and rims of regeneration in all the lithologic rock types. Florencite-Ce is the most important authigenic accessory mineral in shale. It isclosely associated with minor monazite, xenotime, allanite, goyazite, jarosite, and gorseixite.

Florencite forms green, brownish-green zonal, sectorial, and mosaic rhombohedral crystals 0.01 - 0.1 up to 1 mm in size. Ce prevails in A-site, but additional La, Nd, Pr, Sm as well Ca, Sr, Th, Pb, Ba, K are common. In the phosphate site S, Si, and As occur. There is also admixture of Fe^{3+} in the Al^{3+} site.

Lattice parameters of florencite calculated from the base of 17 reflexes using a least square method are a_0=6.98(7)-6.99(5) Å, c_0=16.25(8)-16.30(9) Å. Reflexes of (00n) are asymmetric with shoulders reflecting the increase of c_0 owing to chemical inhomogenity.

The Mössbauer spectra contain two doublets, which correspond to two nonequivalent positions for Fe^{3+}. The first doublet shows an isomeric shift 0.60-0.67 mm/s, quadrupole splitting of 1.07-1.09 mm/s, halfwidth of 0.48-0.55 mm/s, and occupations of 15.83-26.20 % of Fe^{3+}. Dominating second doublets (73.80-84.17 % Fe^{3+}) shows an isomeric shift of 0.54-0.56 mm/s, quadrupole splitting of 0.61-0.66 mm/s, and a halfwidth of 0.44-0.65 mm/s. The presence of two position for Fe^{3+} in the structure of the jarosite-like minerals reflect the change of local symmetry according to heterovalent substitution of interlayer cations or anion groups [2].

In the IR spectra of florencite, besides bands of $(PO_4)^{3-}$ and $(HPO_4)^{2-}$ vibration (613, 904, 1032, 1082, 1213 sm^{-1}) there are bands connected to H_2O and OH^- vibrations (1649, 1687, 2852, 2922, 2933, 3282, 3484 sm^{-1} [3, 4]. The Raman spectra bands of $(PO_4)^{3-}$ and $(HPO_4)^{2-}$ are also present (396, 452, 528, 605, 974, 1012, 1099 $см^{-1}$). 1778 & 2920 cm^{-1} weak bands can be explained by H_2O vibration [4]. Probably, replacing $H_2O \rightarrow OH^-$ compensates heterovalent cation substitution in the interlayer.

So, florencite from black shale from the Lena gold province is characterized by wide isomorphism and local structure and chemical heterogeneity.

Acknowledgement: Work is supported by Urals Branch of RAS, project No 14-5-IP-56.

[1] Large R.R., Maslennikov V.V., Robert F., Danyushevsky L.V. and Chang Z. (2007). Multistage sedimentary and metamorphic origin of pyrite and gold in the giant Sukhoi Log Deposit, Lena gold province, Russia. *Econ Geol*, 102, 1233-1267.

[2] Belogub E.V. and Nikandrova N.K. (2011). Mössbauer spectroscopy of Pb-bearing minerals from the Jarosite Group. *Geol Ore Deposit*, 53, 649-656.

[3] Repina S.A., Popova V.I., Churin E.I., Belogub E.V. and Khiller V.V. (2011). Florencite-(Sm) - $(Sm,Nd)Al_3(PO_4)_2(OH)_6$: a new mineral species of the alunite-jarosite group from the Subpolar Urals. *Geol Ore Deposit*, 53, 564-574.

[4] Frost R.L., Yunfei X., Scholz R. and Tazava E. (2013). Spectroscopic characterization of the phosphate mineral florencite-La - $LaAl_3(PO_4)_2(OH,H_2O)_6$, a potential tool in the REE mineral prospection. *J Mol Struct*, 1037, 148-153.

The study on genesis and characteristics of babingtonite in vesicles of Emeishan amygdaloidal basalt from southern Sichuan

Zhang L[1*], Li D[1], Zhu Y[2]

1 - College of Earth Sciences, Guilin University of Technology *zljpgig@glut.edu.cn
2 - Guilin Cuiyuan Jade Company, Guilin

Five different types of amygdaloid complexes were found in vesicular basalt from Puge county, south Sichuan, mainly including babingtonite amygdaloid complex, chlorite amygdaloid complex, quartz amygdaloid complex, calcite amygdaloid complex and asphalt(bitumen) amygdaloid complex. The babingtonite amygdaloid complexes are spheroidal with 5-8mm diameter. A commonly recognized mineral sequence of the amygdaloid complex from the wall inward is quartz → brunsvigite → babingtonite. The babingtonite crystals are black and lamellar, and are composed of five pinacoids. X-ray micro-diffraction measurements indicated that babingtonite is triclinic, space group P. Chemical composition analyses show that babingtonite ontains SiO_2=53.55%, CaO=18.84%, Fe_2O_3=13.65%, FeO=9.68%, MgO=1.44% and H_2O, 1.74%, FeO/ Fe_2O_3=0.709, and brunsvigite includes SiO_2=33.17%, Al_2O_3=13.03%, Fe_2O_3=8.45%, FeO=13.06%, MgO=18.82%, H_2O=12.12% and CaO=0.87%, FeO/ Fe_2O_3=1.55. The evolution of mineral associations in babingtonite amygdaloid complexes suggested that the mineralizing fluids in late stage basalt changed from Mg- and Fe-rich to Si- and Ca-rich. Babingtonite crystallized in a transitional environment between acidulous and weak reducing and alkalescence and weak oxydic.

Keywords: babingtonite and chlorite; FeO/ Fe_2O_3 ratio;genesis; amygdaloid complex; Emeishan basalt; Puge county in south Sichuan

Mean bond length variation in crystal structures: a bond valence approach

Bosi F

Sapienza University of Rome. ferdinando.bosi@uniroma1.it

The distortion theorem of bond valence theory e.g., [1] is based on the non-linear correlation between bond valence and bond length. This theorem predicts that mean bond length <<em>D> increases with increasing deviation of the individual bond lengths from their mean value, according to the equation <<em>D> = (D' + ΔD), where D' is the mean length found in a polyhedron having equivalent bonds and ΔD is the distortion index [2].

For a given atom, D' is expected to be very similar from one structure to another, whereas <<em>D> should vary as a function of ΔD. However, in several crystal structures, <<em>D> varies *without* any significant contributions from ΔD. For example, in the spinel and garnet structures, undistorted polyhedra (ΔD = 0) show a large range of <<em>D> values: <<sup>IVZn-O> (1.950-1.980 Å) and <<sup>VIAl-O> (1.887-1.929 Å), respectively.

In accord with the bond valence theory, <<em>D> variation can be described by a new equation: <<em>D> = (D_{RU} + ΔD_{top} + ΔD_{iso} + ΔD_{aniso}+ ΔD_{elec}), where D_{RU} is a constant related to the type of cation and coordination environment, ΔD_{top} is the distortion relative to the way the atoms are linked (bond topology), ΔD_{iso} is an isotropic effect of compression (or stretching) in the bonds produced by steric strain and represents the same increase (or decrease) in all the bond lengths in the coordination sphere, ΔD_{aniso} is the distortion produced by compression and stretching of bonds in the same coordination sphere, ΔD_{elec} is the distortion produced by electronic effects (if present, it can be combined with ΔD_{aniso} because they lead to the same kind of distortions). Each D-index in the new equation corresponds to an algebraic expression containing experimental and theoretical bond valences.

On this basis, the ΔD index defined by Allmann [2] is a result of both the distortion theorem and the bond topology according to the relation: ΔD = (ΔD_{top} + ΔD_{aniso} + ΔD_{elec}). Also the mean bond length D' is not a constant, but a result of the compression (or stretching) of bond lengths according to the relation D' = (D_{RU} + ΔD_{iso}).

In conclusion, the deficiencies present in the bond valence theory in predicting mean bond lengths can be overcome, and the observed variations of <<em>D> in crystal structures can be explained by a unified model.

[1] Brown (2009). *Chem Rev*, 109, 6858-6919.

[2] Allmann (1975). *Monatsh Chem*, 106, 779-793.

Crystal chemistry of transition elements and defects in minerals

Calas G[1*], Allard T[1,2], Balan E[1,3], Galoisy L[1], Juhin A[1,2]

1 - Institute of Mineralogy, University Pierre and Marie Curie, Paris
*georges.calas@impmc.upmc.fr 2 - CNRS 3 - IRD

Minerals provide a large wealth of information on their formation conditions and further evolution, through substituted trace and minor elements/isotopes and structural defects. These impurities also give specific properties to industrial minerals, such as their coloration. Spectroscopic approaches are the basis of chemically selective crystal chemistry. They provide a unified view on the behavior of these minor elements in systems of geological, environmental or technological interest.

We will present information on element location in crystal lattice, including oxidation state, charge compensation and relaxation processes. This information is possible by combining spectroscopic, diffraction and microscopic techniques, coupled with simulation tools. Application to the location of Cr and V in colored minerals will be presented, in relation with their formation conditions and the origin of their color.

Radiation-induced defects may be directly detected by spectroscopic techniques and then used to trace short-lived uranium daughter elements in minerals such as quartz and clay minerals. The high specific area of clays makes them sensitive to ground-level radiation doses. By an adequate experimental calibration, it is possible to trace the past transfer of radionuclides in the geosphere, helping to model uranium-bearing fluid migration during U-deposit formation or for the investigation of natural analogues of geologic repositories for nuclear wastes.

New data on the crystal-chemistry of arrojadite: an HT study

Cámara F[1*], Ciriotti M[2], Bittarelo E[1], Alvaro M[3]

1 - University of Torino - CrisDi, Italy *fernando.camaraartigas@unito.it 2 - Associazione Micromineralogica Italiana 3 - University of Padova

Arrojadite group minerals are very complex orthophosphates, with monoclinic symmetry. Ideally arrojadite has formula $A_2B_2Ca_1Na_{2+x}M_{13}Al(PO_4)_{11}(PO_3OH_{1-x})W_2$, where *A* sites are occupied by Ba, Sr, Pb, Na, K plus vacancy; the *B* site is occupied by divalent Fe, Mn, Mg, (Zn, Li) plus vacancy; the *W* site can be occupied by OH or F [1]. Their classification was approved by IMA-CNMMN and published by [1]. Their structure was described as *C*2/*c* by [2] and [3], and later revised by [4] who showed that the correct space group is actually *Cc* on the basis of new single-crystal X-ray diffraction data (SCXRD) and Raman spectroscopy. Recently the *Cc* model has been questioned [5] although very recent spectroscopic evidences confirm the lower singony [6].

The collaboration with AMI led us to examine new samples of arrojadite with compositions never described so far. In particular, we found the occurrence of a specimen with Mg dominant at the M group cation site coming from the locally known "Costa Balzi Rossi" locality, close to the village of Isallo (Liguria, Italy). This sample has *a* 16.3944(4), *b* 9.9477(2), *c* 24.4435(7) Å, β 105.661(3)°, and *V* 3838.41(16) Å^3 and SCRDX data confirms that Mg is dominant in most of the *M* sites. Another specimen from Hagendorf (Germany) revealed to be F and (Na,Ba) dominant at W and A sites respectively. The relative proposals for new mineral names are being prepared to be submitted soon to IMA-CNMNC. Both samples show structural models in *Cc* s.g. which have the presence of residual density reproducing the *C*2/*c* model. This has been observed for other specimens, among them the arrojadite-(NaFe) from Nickel Plate (USA) studied also by [3] and [5].

Due to the controversy related to the choice of the *C*2/*c* versus *Cc* space groups, we performed annealing experiment of an arrojadite-(KFe) sample from Rapid Creek, Yukon (Canada). The natural crystal has *Cc* symmetry without any residue of density in the Fourier difference maps. A single crystal (0.080 0.30 0.35mm radius) was placed in a sealed and vacuumed quartz vial together with a Pt crucible containing iron-wüstite buffer and annealed at 650 °C for 24 hours. The vial was dropped into water and the crystal was studied by SCXRD at the same conditions used for the natural crystal. The results of structure refinement in the *Cc* space group showed the presence of disorder in a similar fashion to that found for natural samples coming from Nickel Plate. Therefore, the annealing clearly promotes the disorder of cations leading to an apparent centre of symmetry.

Acknowledgments: M.A. has been supported by ERC grant #307322 to F.N.

[1] Chopin C., Oberti R. and Cámara F. (2006). *Am. Mineral*., 91, 1260-1270.

[2] Krutik V.M., Pushcharovskii D.Y., Pobedimskaya E.A., Belov N.V. (1979). *Kristallografiya*, 24, 743-750.

[3] Merlino S., Mellini M., Zanazzi P.F. (1981). *Acta Crystallogr*. B37, 1733-1736.

[4] Cámara F., Oberti R., Chopin C., Medenbach O. (2006). *Am. Mineral.* 91, 1249-1259.

[5] Kallfaß C., Hocha C., Schiera H., Simon A., Schubert H. (2010). *Z. Naturforsch*., 65b, 1427-1433.

[6] Frost R.L., Xi Y., Scholz R., Frota Campos Horta L. (2013). *Spectrochimica Acta Part A: Molecular and Biomolecular Spectroscopy*, 109, 138-145.

Thermal expansion in bafertisite

Cámara F[1*], Arletti R[2], Sokolova E[3], Hawthorne F[3]

1 - University of Torino - CrisDi, Italy *fernando.camaraartigas@unito.it 2 - University of Torino - NIS Torino 3 – University of Manitoba, Winnipeg, Canada

Bafertisite, ideally $Ba_2Fe^{2+}{}_4Ti_2(Si_2O_7)_2O_2(OH)_4$, is a Ti-disilicate layered mineral with the TS (Titanium-Silicate) block, a central trioctahedral (O) sheet and two adjacent heteropolyhedral (H) sheets of [5-7]-coordinated polyhedra and Si_2O_7 groups [1, 2]. The topology of the H sheet dictates two translation vectors, t_1 and t_2 (~ 5.5 and ~ 7 Å, respectively; t_1 ^ t_2 close to 90°). The structure of bafertisite was described by [3] as monoclinic cell, *Cm*, *a* = 10.6, *b* = 13.64, *c* = 12.47 Å, β= 119.5° Z = 8. Bafertisite belongs to Group -II minerals with Ti = 2 *apfu* in the H sheets and linkage 2 of H and O sheets in the TS-block: two Si_2O_7 groups link to two octahedra of the O sheet adjacent along t_2.

We have studied a sample of manganoan bafertisite from Darai-Pioz (Tajikistan) with composition $(Ba_{1.9}Na_{0.1})(Fe^{2+}{}_{1.8}Mn^{2+}{}_{1.6}\ Fe^{3+}{}_{0.4}\ Zr^{4+}{}_{0.1})(Ti_{1.9}Nb_{0.1})(Si_2O_7)_2O_2(F_{2.2}OH_{1.8})$ on a very thin sample (0.15 X 0.07 x 0.01). Careful inspection of lattice parameters revealed a triclinic symmetry, with lattice constants: *a* = 10.695(1), *b* = 13.788(1), *c* =12.551(1) Å, α = 90.210(1), β = 119.860(1), γ = 89.994(1), V =605.2(3) Å^3. Structure was therefore solved and refined in space group *C*-1, with the mirror plane imposed as a twin operation and agreement factor was as low as 2.8% for 4716 observations.

The thermal behaviour of bafertisite from Darai-Pioz (Tajikistan) was studied by an *in-situ* synchrotron radiation X-ray powder diffraction experiment. The data were collected in transmission geometry with a fixed wavelength of (0.8279 Å) at MCX beamline at Elettra synchrotron light source (Trieste-Italy). The sample was heated from RT to 700°C with a thermal gradient of 5°C/min. Diffraction patterns were collected every 25°C on a translating image plate. Full profile Rietveld refinements were performed to follow the evolution of cell parameters with temperature.

Lattice parameters expands showing α_{V300}=3.02(18). The observed lattice expansion anisotropy is 1:1.09:1.22. At ca. 600°C β angle starts widening and crosses 120°. Contemporaneously *c* lattice parameters start decreasing while expansion increases within (001). The contraction of the [001] direction leads the cell volume variation that show negative thermal expansion (NTE) at T >600 °C. Preliminary data point to a NTE driven by differential shift among the TS-block and a change in the coordination of Ba in the intermediate layer that brings closer the TS-blocks in order to achieve satisfactory coordination.

[1] Sokolova E. (2006). *Can. Mineral.*, 44, 1273-1330.

[2] Sokolova E. and Cámara, F. (2013). *Can. Mineral.*, 51(6), in press.

[3] Guan Ya.S., Simonov V.I., and Belov N.V. (1963). Doklady Akademii Nauk SSSR, *Earth Sciences*, 149, 123-126.

The structural architecture of tellurium oxycompounds

Christy A[1*], Mills S[2], Kampf A[3]

1 - Australian National University *andrew.christy@anu.edu.au 2 - Museum Victoria
3 - Natural History Museum of Los Angeles County

Tellurium is one of the rarest elements in the Earth's crust. Nevertheless, there are about 160 Te mineral species described to date. This is an anomalous diversity, given that such a number of species is more typical of much more abundant elements such as Ce or Ni, present in the crust at the tens of ppm level. We are investigating why this is so, as part of a broader study of tellurium mineralogy and geochemistry.

We surveyed the coordination behaviour of Te, while refining bond-valence parameters for Te–O bonds (Mills and Christy [1]). Te^{VI} coordination was almost always 6 (rarely 4 or 5). Conversely, Te^{VI} could have any number of oxygens from 3–12 within our cutoff distance of 3.5 Å. The Te^{IV} cation typically has a stereochemically active lone pair, so its polyhedra are asymmetric. Te^{IV}–O distances can usually be separated into short "primary" bonds facing away from the lone pair, and longer "secondary" bonds; both subsets fit the same bond valence-bond distance relationship. In Christy and Mills [2], we established that the volumes of 40 $Te^{IV}O_6$ polyhedra are also highly flexible, ranging from 80–180% of the 12.83 $Å^3$ expected for a regular octahedron, as a function of lone pair stereoactivity and the distribution of oxygens around the lone pair.

Now, we examine the types of structural building unit formed by Te–O polyhedra in about 700 structures for which good-quality refinements are available in the ICSD. Only the stronger "primary" bonds are considered for Te^{IV}, of which there are usually 3–5. Te–O polyhedra polymerise readily. Apart from monomeric anions, they form finite oligomers, rings, chains, layers and frameworks, analogous to those of the silicates. In fact, the diversity is greater than found for silicate anions, for several reasons:

1. Te may occur as Te^{IV}, Te^{VI} or both, in a given structure.

2. Both oxidation states, particularly Te^{IV}, show a range of coordination numbers and geometries. Examples of Si in coordination other than tetrahedral are rare.

3. Te^{IV} and Te^{VI} polyhedra can share not just corners but edges, unlike SiO_4 tetrahedra.

4. A given oxygen may be coordinated by three Te^{IV}. This option is not available to Si or Te^{VI}, where the high bond valence ($^5/_6$–1 valence units) limits the oxygen coordination to two.

The resulting wide range of tellurate building units is illustrated using selected examples, mineralogical where possible. We note particularly the frequent occurrence of structures that are nanoporous, containing potentially exchangeable species in large channels, the tendency of tellurate groups to link to other high-valence cations such as Ti^{IV} and Mo^{VI} to form more complex heteropolyanions and frameworks, and the ability of the neutral molecule $Te^{VI}(OH)_6$ to form crystalline adducts with ions and small polar molecules, held together only by hydrogen bonds. The latter weakly-bound compounds do not occur as minerals, but are of interest as solid electrolytes, given their high ionic mobility.

Structures for enough secondary Te minerals are known to at least pose the questions of whether, as for silicates, the degree of polymerisation correlates with paragenetic sequence or with the proportions of "network-forming" and "network-modifying" cations.

[1] Mills S.J. and Christy A.G. (2013). Revised values of the bond valence parameters for Te^{IV}–O, Te^{VI}–O and Te^{IV}–Cl. *Acta Crystallographica*, B69, 145–149.

[2] Christy A.G. and Mills S.J. (2013). The effect of lone-pair stereoactivity on polyhedral volume and structural flexibility: application to Te^{IV}–O octahedra. *Acta Crystallographica*, B69, 446–456.

Crystal chemistry of mineral-like M1-M2-H-arsenates ($M1^{2+}$ = Mr^{2+}, Ba^{2+}, Cd^{2+}; M2 = Mg, $Fe^{2+,3+}$,Co^{2+}, Ni^{2+}, Cu^{2+}, Zn^{2+})

Djordjevic T

Institut für Mineralogie und Kristallographie, Universität Wien.
tamara.djordjevic@univie.ac.at

Synthesis of mineral-like arsenates should add significant new knowledge relative to the crystal chemistry of these complex materials, and also a framework for understanding the structural relationships within these classes of compounds. A better knowledge of the solid-state chemistry of arsenic compounds can be expected to have important implications in studies of water contamination and the health of individuals in affected areas. The crystal-chemical study on synthetic arsenate minerals has demonstrated that mineral-like structures are not rare among M1-M2-H-arsenates (see Table 1). This system counts fifteen compounds, of which with the exception of $CdCu(OH)(AsO_4)$, all others have been hydrothermally synthesized in the course of the present study.

Table 1. Mineral like M1-M2-H-arsenates ($M1^{2+}$ = Sr, Ba, Cd; M2 = Mg^{2+}, $Fe^{2+,3+}$, Co^{2+}, Ni^{2+}, Cu^{2+}, Zn^{2+}).

Chemical formula	S.G.	Mineral-group	Reference
$SrCo_2(AsO_4)(AsO_3OH)(OH)(H_2O)$	$P2_1/a$	tsumcorite	Mihajlović &Effenberger, 2004, [5]
$BaMg_2(AsO_4)_2{\times}2H_2O$	*C*2/*m (?)*	tsumcorite	in preparation
$SrNi_2(AsO_4)(AsO_3OH)(OH)(H_2O)$	*C*2/*m (?)*	tsumcorite	in preparation
$SrZn(OH)(AsO_4)$	$P2_12_12_1$	adelite	in preparation
$SrCo(OH)(AsO_4)$	$P2_12_12_1$	adelite	Đorđević, 2007
$CdCo(OH)(AsO_4)$	$P2_12_12_1$	adelite	Đorđević, 2007, [1]
$CdCu(OH)(AsO_4)$	$P2_12_12_1$	adelite	Effenberger, 2002, [4]
$BaCo_3(AsO_4)_2(OH)_2$	*C*2/*c*	bayldonite	in preparation
$BaCu_3(AsO_4)_2(OH)_2$	*C*2/*c*	bayldonite	in preparation
$SrFe_2(AsO_4)_2(OH)_2$	*C*222	carminite	in preparation
$Sr_2Mg(AsO_4){\times}2H_2O$	*P*-1	talmesite	Đorđević, 2013, [3]
$BaZn_2(AsO_4)_2{\times}H_2O$	$P2_1$	paracelsian	Đorđević, 2011, [2]
$Cd_{0.74}Mg_{2.76}(AsO_4)(HAsO_4)$	*C*2	alluaudite	Stojanović *et al*., 2012, [6]
$Cd_{0.77}Co_{2.73}(AsO_4)(HAsO_4)$	*C*2	alluaudite	in preparation
$Cd_{1.16}Zn_{2.34}(AsO_4)(HAsO_4)$	*C*2	alluaudite	Stojanović *et al*., 2012, [6]

New mineral-like compounds can represent either novel structure types that could be topologically related to some minerals, or known structure types with interesting crystal-chemical properties. An overview of the structural hierarchy for such compounds will be presented.

Acknowledgments: Financial support of the Austrian Science Foundation (FWF) (Grant V203-N19) is gratefully acknowledged.

[1] Đorđević T. (2007). Mitt. Österr. Mineral. Gesellschaft, 153, MinPet 2007, Meran, Italy, September 2007, 40.

[2] Đorđević T. (2011). *European Journal of Mineralogy*, 23, 437-447.

[3] Đorđević T. (2013). Mitteilungen der Österreichischen Mineralogischen Gesellschaft 159, MinPet 2013, Graz, Austria, September 2013, 50.

[4] Effenberger H. (2002). *Z. Kristallogr., Suppl. Issue*, 19, 85.

[5] Mihajlović T. and Effenberger H. (2004). *Mineral. Mag.*, 68, 757-767.

[6] Stojanović J., Đorđević T. and Karanović Lj. (2012). *J. Alloys Compd*., 520, 180-189.

Al/Si-disordered anorthite ($An_{92.0}Ab_{3.4}$) occurring in an anorthite megacryst from Miyake-jima, Japan

Echigo T[1*], Hoshino M[2], Kimata M[3], Shimizu M[3], Matsui T[4], Nishida N[3]

1 - Shiga University *echigo@edu.shiga-u.ac.jp 2 - Institute for Geo-Resources and Environment, AIST 3 - University of Tsukuba 4 - Kagoshima University

The crystal chemistry of anorthite with the low content of albite ($An_{92.0}Ab_{3.4}$), part of a rapid cooled, anorthite megacryst occurring in 1940 ejecta from Miyake-jima volcano, Japan, has been investigated using single-crystal X-ray diffractometer and electron microprobe analyzer with wavelength dispersive X-ray spectroscopy (EMPA-WDS). The structure was refined in space group *P*-1 and cell parameters, a = 8.182(6) Å, b = 12.883(4) Å, c = 7.092(4) Å, α = 93.19(4) °, β = 115.91 °(4), γ = 91.18 °(4). The final weighted R-factor is 3.77 % for 1549 reflections. Averaged T-O distances are 1.681 Å for T_1(0), 1.674 Å for T_1(m), 1.677 Å for T_2(0) and 1.680 Å for T_2(m), indicating each Al occupancy of 0.501, 0.453, 0.472, and 0.496, respectively. These occupancies suggest that the present anorthite exhibits the highly disordered (Q_{OD} = 0.06) Al/Si-distribution in the tetrahedral framework, having the lattice parameter c of some 7 Å. Twice this parameter corresponds directly to the c-axis determined in the completely Al/Si ordered anorthites (c ~ 14 Å). Chemical composition of the refined crystal obtained by EMPA-WDS is $(Ca_{0.93}Na_{0.03}Fe_{0.02}Mg_{0.01}\square_{0.01})$ $Al_{1.94}Si_{2.06}O_8$. The extra-framework site-populations consist of the following two: (1) A(000) site occupied by Ca (86 %), Na (8 %), Fe^{2+} (4 %) and □(2 %), and (2) A(zi0) site by Ca (100 %). The Al/Si tetrahedral framework is so pseudo-face-centered in symmetry (*C*-1) that both extra-framework-site cations and the same-site defect appear to reduce the symmetry of the overall structure to *P*-1. Although this Al/Si disordered anorthite can be interpreted as a metastable phase, the observed chemical non-stoichiometry may stabilize such a metastable structure by introducing -Si^{4+}-O-Si^{4+}- bonds into the tetrahedral framework and anti-phase-boundary.

Ferric iron within olivine in a lherzolite xenolith from Oku district, Oki-Dogo Island, Shimane Prefecture, Japan

Ejima T[1*], Akasaka M[2], Ohfuji H[3]

1 - AIST *olivinefe3@yahoo.co.jp 2 - Shimane University 3 - Ehime University

Occurrence and distribution of ferric iron within olivine in a lherzolite xenolith from Oki-Dogo Islands, Japan, was investigated using ^{57}Fe Mössbauer spectroscopy, X-ray FeL_b/FeL_a-intensity ratio method, X-ray powder diffraction (XRD), Raman spectroscopy and transmission electron microscopy (TEM) analysis.

A lherzolite xenolith consists of olivine, orthopyroxene and clinopyroxene. The olivine grains are nearly homogeneous in composition, with Fo contents of 80.7-81.9 mol%. Pure olivine grains were separated from the fresh core of the lherzolite xenolith under a binocular microscope to perform X-ray diffraction and ^{57}Fe Mössbauer analyses. The site occupancies of Fe in the M1 and M2 sites refined using X-ray Rietveld method are 0.151 and 0.206 apfu, respectively. The Mössbauer spectrum of the separated olivines consists of two doublets assigned to Fe^{2+} at the M1 and M2 sites and a doublet attributed to Fe^{3+} at the octahedral site. The populations of Fe^{3+} in the olivine derived from the Mössbauer method and FeL_β/FeL_α-intensity ratios are 0.02 and 0.03 atoms per formula unite (apfu), respectively.

At the contact of the lherzolite xenolith with host olivine basalt, olivine has brownish outermost rim. In the brownish rim, hematite and magnetite with nano-scale were found using Raman spectroscopy. Thus, it is suggested that the lherzolite xenolith underwent high temperature oxidation in a process of the transportation from the mantle to the surface or near surface by alkaline olivine basaltic magma. The Fe^{3+} within olivine in the lherzolite xenolith might have formed by annealing in this process.

Survey of bond lengths in the solid state for atoms bonded to oxygen: results and applications

Gagne O*, Hawthorne F

1 - University of Manitoba, Winnipeg, Canada *olivier.c.gagne@gmail.com

A complete survey of bond lengths is done for all atoms of the Periodic Table of Elements bonded to oxygen. The Inorganic Crystal Structure Database (ICSD) is used to analyse over 135,000 crystal structures, from which a total of 33,343 coordination polyhedra and 188,462 bond distances are collected after passing a rigorous filtering process. The data is organized into the one hundred thirty-six (136) ions and four hundred seventy-three (473) different configurations (coordination numbers) that result. First, the bond length distributions are visually inspected. This leads to (1) the observation and visual interpretation of known phenomena (e.g. Jahn-Teller effect), and (2) the isolation of new phenomena, as subtleties in the bond length distributions of specific ions become more evident and allow us to examine the underlying principles giving rise to these distributions. Next, different applications of the data are investigated. The completeness of the survey allows the reassessment of important parameters of the solid state: ionic radii, and bond-valence parameters. Of the 473 ionic radii derived in this study, 329 revisions are made to Shannon's list of radii [1] (of which 176 were estimates), and 144 new ionic radii are derived. Next, a systematic evaluation of all bond-valence parameters published to date is done for oxides. Furthermore, using a new method of derivation, 136 new pairs of bond-valence parameters are obtained. In comparison to the previous-best published bond-valence parameters, an overall average decrease in the r.m.s.d. to the valence-sum rule of 20.7% is observed (12.55% when weighted) for the 33,343 coordination polyhedra using the new parameters. New equations to describe the bond-length to bond-valence relation are also investigated. From an optimization between the experimental and *a priori* bond-valences of 54 carefully-selected crystal structures, roughly 20 relatively simple equations were selected for testing. Following a rigorous evaluation, the current exponential equation was found to be a viable choice in describing the relation. Finally, bond-length and bond-valence ranges are assigned to the 473 configurations of the atoms. The bond length ranges are a useful aid in the refinement of crystal structures. The assignment of a bond-valence range to the ions in turn allows *a priori* analysis of site occupancy in crystal structures, when used in conjunction with their calculated set of "ideal" bond-valences.

[1] Shannon R.D. (1976). *Acta Crystallographica*, A32, 751-767.

Garnet: the rainbow mineral relations between structure and garnet colorations

Galoisy L

Mineralogical Institut (IMPMC) Paris, France laurence.galoisy@upmc.fr

Garnets are remarkable by their colors and shades from green to orange and red. Naturally multi-faceted, these quite complex minerals form wide solid-solutions with each other and captivate people with their incomparable range of colors which are largely controlled by the crystal chemistry of substituted transition elements. The variations of colors and hues of garnets are related to the presence of coloring agents such as Fe, Mn, Cr, V, Ti substituted in the structure of garnet solid-solutions between various end-members $A_3B_2(SiO_4)$. Spectroscopic techniques demonstrate how the nature and concentration of transition elements explain the color variation.

On another hand, natural garnets are used as gemstones since Ages. Also used as historical symbols, they are part of legends in all countries. Of bright colors and clear transparency, this mineral has attracted a large number of jewelers, mineral collectors, artists, but also painters, since the dawn of time. Even in architecture and sculpture are found adornments made of garnets. On an archeological point of view, the hardness of this mineral has protected historical garnets as it enhances the resistance to alteration. Thus, this gemstone can travel through time without noticeable weathering and can be used to trace ancient trading routes and understand the origin and nature of garnet used in ornaments.

This presentation will discuss the crystal-chemical factors that produce the myriad colors of this fascinating mineral and emphasize some aspects of garnets as important cultural heritage.

Bond topology, bond-valence theory and structure stability

Hawthorne F

University of Manitoba, Winnipeg, Canada frank.hawthorne@umanitoba.ca

We conventionally represent a crystal structure as (1) a space group, (2) a set of unit-cell dimensions, and (3) a list of atom coordinates (and displacement parameters), and we use these parameters, together with various theories and/or computational techniques from Physics and Chemistry, to calculate various properties of the crystal, particularly those related to energy. This general approach is extremely successful in understanding the physical properties of materials and attests to the significance of the underlying theory. However, what this underlying theory does not do is explain the origin of translational (and quasi-crystal) symmetry in crystals, *i.e.*, a crystal is an emergent property within a system of interest; it can be interpreted by such theories from a reductionist viewpoint where emergence is input into the calculation via boundary conditions, but it cannot be interpreted from a constructionist viewpoint. Moreover, crystal structure can seem surprisingly insensitive to major variations in electron delocalization and corresponding variations in physical properties. This suggests that if we wish to understand why crystal structures have the atom arrangements that they do, we should not seek this understanding *via* calculations involving the sharing of electrons between atoms. It is here than bond topology and bond-valence theory are important. Bond-valence theory is based on three theorems: (1) The valence-sum rule; (2) the loop rule; (3) the valence-matching principle, and it is important to realize that these theorems are topological in nature; they are not based on any physical idea of a chemical bond. Bond valences may be calculated from bond lengths *via* parameterized bond-valence curves. However, it is important to realize that that bond-valence theory is not dependent on experimental bond-valence curves. The crucial theorem affecting structure stability, the valence-matching principle, relates to the Lewis acidity and Lewis basicity of structural components which, in turn, are dependent on average coordination number (a bond-topological property) and formal charge. *A priori* bond valences may be calculated by solving the equations inherent in the valence-sum rule and the loop rule, *i.e.*, may be calculated from bond topology and formal charge of the constituent ions, and show good agreement with the "experimental" bond-valence, *i.e.*, those calculated from the experimental bond-lengths and experimental bond-valence curves.

Structural complexity and phase transformations in the $Cu_4(OH)_6(SO_4)(H_2O)_n$ system: hydrogen bonding, the Ostwald Step Rule and Shannon information

Krivovichev S[1*], Hawthorne F[2], Williams P[3]

1 - St. Petersburg State University *skrivovi@mail.ru 2 – University of Manitoba, Winnipeg, Canada 3 - University of Western Sydney

The $Cu_4(OH)_6(SO_4)(H_2O)_n$ system includes four crystalline phases, all of which are known as minerals: langite (n = 2), wroewolfeite (n = 2), posnjakite (n = 1), and brochantite (n = 0). Dabinett and others [1] reported on the synthesis of wroewolfeite (n = 2) and its sequential transformation to posnjakite (n = 1) and brochantite (n = 0) that follow the Ostwald Step Rule. Brochantite seems to be the only thermodynamically stable phase in the system, wroewolfeite, langite and posnjakite being metastable reaction products. The $Cu_4(OH)_6(SO_4)(H_2O)_n$ phases are important from both mineralogical and environmental points of view, as they form as oxidation products of primary Cu sulfide minerals and are known as corrosion products of copper and copper alloys, e.g. copper tubes and brass monuments. They have been the subject of extensive crystal chemical, spectroscopic and thermodynamic studies. However, despite many efforts, details of hydrogen bonding in the structures of these phases were unknown. We have used density functional theory (DFT) to model hydrogen positions in the structures and to elucidate the hydrogen bonding system by means of the CRYSTAL14 program package [2]. This allows a more detailed picture of the structurally complex atomic arrangements in the $Cu_4(OH)_6(SO_4)(H_2O)_n$ system and an investigation of their evolution in the course of phase transformations. We have also used Shannon information theory [3, 4] to show quantitatively that the Ostwald phase transformation sequences correspond to increasing complexity of the crystalline phases calculated as amounts of structural and topological information encoded in their atomic arrangements. The levels of complexity of particular phases and their constituents in the $Cu_4(OH)_6(SO_4)(H_2O)_n$ system are strongly influenced by Jahn-Teller distortion of the octahedral coordination geometries of Cu^{2+} cations.

[1] Dabinett T.R., Humberstone D., Leverett P. and Williams P.A. (2008). *Pure Appl. Chem.*, 80, 1317-1323.

[2] Dovesi R., Orlando R., Civalleri B., Roetti C., Saunders V.R. and Zicovich-Wilson C.M.Z. (2005). *Kristallogr.*, 220, 571-573.

[3] Krivovichev S.V. (2013). *Mineral. Mag.*, 77, 275-326.

[4] Krivovichev S.V. (2014). *Angew. Chem. Int. Ed.*, 53, 654-661.

Understanding of the depolymerization's processes in lithium borates: structural determination and role of the superstructural units

Lelong G*, Rousse G, Baptiste B
IMPMC University Pierre and Marie Curie *gerald.lelong@impmc.upmc.fr

Boron is a crustal element of major geochemical and mineralogical interest, being enriched in the Earth crust by orders of magnitude relative to primitive mantle. Its complex crystal chemistry, including the coexistence of two coordination states and the presence of complex structural superunits, explains the mineral diversity of borates and borosilicates, a unique primary source of boron. Indeed, the structural diversity offered by borates is impressive, as boron oxides can be built upon triangular BO_3 units, tetrahedral BO_4 units, or both. The connectivity between these building units is also extremely diverse and may give rise to isolated units, dimers, chains, rings and so on. The iconic Li_2O-B_2O_3 system has been studied for more than 50 years and it illustrates perfectly the great complexity of boron crystal chemistry. About ten single phase compositions are reported in this binary, some of them presenting also temperature- or pressure-induced polymorphism. Having a good knowledge of crystal structure helps in modeling and predicting the properties of Li-borates. It is also a necessary step as a reference for Li- borate glasses and melts, whose local structure is not so easily accessible.

Most of the lithium borate crystals do not melt congruently, which make them difficult to synthesize. However we successfully synthesized a whole series of lithium borates crystals on a large range of lithium concentration. By coupling single crystal X-ray diffraction and X-ray powder diffraction with Rietveld refinements, we have solved the crystal structure of $Li_6B_4O_9$ and $Li_3B_{11}O_{18}$. In view of these two new crystal structures, we will present a complete overview describing, in the Li_2O-B_2O_3 binary, the processes related to the depolymerization of the borate network caused by the addition of Li_2O.

Molecular-like medium-range order and mineral species in K-feldspars by multinuclear NMR

Sánchez-Muñoz L[1*], Sanz J[2], Sobrados I[3], Gan Z[4]
1 - ICV-CSIC *lsm@icv.csic.es 2 - ICMM-CSIC, Madrid, Spain 3 - ICMM-CSIC, Madrid, Spain 4 - NHMFL, Tallahassee, FL, USA

The structures, polymorphism and mineral species of K-rich feldspars $(K>Na)AlSi_3O_8$ are currently described with periodic "ideal" average structures from Bragg diffraction maxima obtained by reciprocal-space techniques. Substitutional order-disorder of framework Si and Al cations in tetrahedral T sites is supposedly associated with positional disorder of cavity alkali cations in a single M site. Here, "real" structure data are obtained by high-resolution magic-angle spinning multi-nuclear magnetic resonance spectroscopy (^{29}Si, ^{27}Al and ^{23}Na spectra at 9.4 and ^{27}Al, ^{39}K and ^{23}Na spectra at 19.6 T), from natural specimens and synthetic samples along the order-disorder series. The "ideal" and "real" structure coincides only in the perfectly long-range ordered triclinic end-member (low microcline). Long-range disordered structures (either with monoclinic or triclinic symmetry by X-ray diffraction), show triclinic-like short-range distortions, four sets of T sites for framework atoms, two sets of M sites for alkali atoms, respect for the Loewenstein's rule (Al-O-Al avoidance), and Al-O-(K,Na) multi-site correlations. Specific molecular-like order schemes at the medium-range scale are proposed to define the K-feldspar mineral species by considering the number of Al atoms per four-membered rings of tetrahedra, with "…-2-0-2-0-…" chains for microcline and orthoclase where ($t_1O > t_2m > t_2O \gg t_1m$), and with "…-1-1-1-1-…" chains for "valencianite" and sanidine, in which ($t_1O > t_2m \gg t_2O \gg t_1m$). "Valencianite" shows strong additional constraints of charge dispersion effects involving deficiency of Si atoms in Q^4 (4Si,0Al), (1Si,3Al) and (0Si,4Al) environments. This constraint is almost absent in sanidine. These molecular-like features have not been described by average structure models owing to the lack of resolving power of the reciprocal-space techniques when disorder exists.

From chemical composition to structure topology in Ti silicates with the TS block: new developments

Sokolova E

University of Manitoba. elena_sokolova@umanitoba.ca

New developments in the crystal chemistry will be considered for titanium disilicate minerals that contain the TS (Titanium-Silicate) block, a central trioctahedral (O) sheet and two adjacent heteropolyhedral (H) sheets of [5-7]-coordinated polyhedra and Si_2O_7 groups [1]. The general formula of the TS block is $A^P_2B^P_2M^H_2M^O_4(Si_2O_7)_2X_{4+n}$, where M^H_2 and M^O_4 = cations of the H and O sheets; M^H = Ti, Nb, Zr, Mn, Ca + REE, Ca; M^O = Ti, Zr, Nb, Fe^{2+}, Mg, Mn, Ca, Na; A^P and B^P = cations at the peripheral (*P*) sites = Na, Ca + REE, Ca, Ba, Sr, K; X = anions, O, OH, F, and H_2O groups; $X_{4+n} = X^O_4 + X^P_n$, n = 0, 1, 1.5, 2, 4. There are three topologically distinct TS blocks based on three types of linkage of H and O sheets. In the crystal structures of TS-block minerals, TS blocks either link directly or alternate with intermediate (**I**) blocks. The **I** block consists of alkali and alkaline-earth cations, oxyanions (PO_4), (SO_4) and (CO_3), and H_2O groups. There are four groups of TS-block structures, based on the topology and stereochemistry of the TS block: Groups I, II, III and IV, where Ti (+ Nb + Zr + Mg + Mn) = 1, 2, 3 and 4 *apfu*, respectively. In a TS-block structure, four types of self-linkage between adjacent TS blocks occur.

There are thirty-one *basic* TS-block structures and five *derivative* TS-block structures [2]. A *basic structure* has the following four characteristics: (1) There is only one type of TS block; (2) The two H sheets of the TS block are identical; (3) There is only one type of **I** block or it is absent; (4) There is only one type of self-linkage of TS blocks. *Basic structures* obey the general structural principles of [1]. A *derivative structure* has one or more of the three following characteristics: (1) There is more than one type of TS block; (2) There is more than one type of **I** block; (3) There is more than one type of self-linkage of TS blocks. A *derivative structure* is related to two or more *basic structures* of the same Group: it can be derived by adding these structures via sharing of the central O sheet of the TS blocks of adjacent structural fragments of *basic structures*.

Two new topological aspects are considered here.

(1) In many Ti-silicate minerals, Ti ⇔ Nb substitution is common (r $[^{[6]}Ti^{4+}]$ = 0.605, r $[^{[6]}Nb^{5+}]$ = 0.64 Å). Hence, where I refer to TiO_6 octahedra, I include $(Ti,Nb)O_6$ and $(Nb,Ti)O_6$ octahedra and four groups of TS-block structures have been defined on the content of Ti (+ Nb) in the TS block [1]. Here, I consider topological aspects of the Ti ⇔ Nb substitution in the TS block.

(2) Ba plays an important but yet not understood role in the TS-block structures: all five derivative structures and thirteen basic structures contain Ba as an essential **I**-block cation. Here I consider how the topology of the cation layers in the **I** block affects the topology of the TS block.

[1] Sokolova E. (2006). From structure topology to chemical composition. I. Structural hierarchy and stereochemistry in titanium disilicate minerals. *Canadian Mineralogist*, 44, 1273-1330.

[2] Sokolova E. and Cámara F. (2013). From structure topology to chemical composition. XVI. New developments in the crystal chemistry and prediction of new structure topologies for titanium disilicate minerals with the TS block. *Canadian Mineralogist*, 51(6).

Iron spectroscopy in minerals and glasses: experiment and theory

Vercamer V[1,2*], Lelong G[1], Hijiya H[2], Juhin A[1,3], Calas G[1], Galoisy L[1], Brouder C[1,3], Arrio M[1,3], Glatzel P[4]

1 - IMPMC - UPMC *vincent.vercamer@impmc.upmc.fr 2 - AGC 3 - CNRS 4 - ESRF

As iron is the most abundant transition element, understanding the crystal chemistry of Fe^{2+} and Fe^{3+} in minerals and glasses remains an important issue. A direct approach may be to investigate the spectroscopic properties of both oxidation states of iron, by quantifying the influence of Fe-site geometry and by constraining different experimental spectroscopic data by simulations. We will present an extensive set of data on the spectroscopic properties of 12 Fe^{2+} and Fe^{3+} minerals, using two kinds of techniques: synchrotron-based high-resolution X-ray spectroscopy (Resonant Inelastic X-ray Scattering (RIXS), X-ray Absorption Spectroscopy with High Energy Resolution Fluorescence Detection (HERFD)) and optical absorption spectroscopy. The reference compounds investigated contain Fe^{2+} and Fe^{3+} in 4-, 5- and 6-coordination and various site geometries: gillespite ($^{[4]}Fe^{2+}$), staurolite ($^{[4]}Fe^{2+}$), grandidierite ($^{[5]}Fe^{2+}$), siderite ($^{[6]}Fe^{2+}$), hypersthene ($^{[6]}Fe^{2+}$), rodolicoite ($^{[4]}Fe^{3+}$), ferriorthoclase ($^{[4]}Fe^{3+}$), yoderite ($^{[5]}Fe^{3+}$), grattarolaite ($^{[5]}Fe^{3+}$), andradite ($^{[6]}Fe^{3+}$), acmite ($^{[6]}Fe^{3+}$) and hematite ($^{[6]}Fe^{3+}$). Experimental data are well reproduced by Ligand Field Multiplet (LFM) calculations, which enable to relate the spectroscopic properties to the local crystal field. This sheds light on the chemical, geometrical and ligand field dependence of the spectroscopic behavior of iron. The set of parameters obtained will be used to discuss the surrounding of Fe^{2+} and Fe^{3+} in glasses.

First archaeometrical data of glass from Sarno necropolis (9th - 6th century BC)

Arletti R

University of Torino - NIS Torino. rossella.arletti@unito.it

The archaeometrical data on a set of 35 glass beads coming from two ancient necropoles, situated near the modern city of Sarno (near Naples), are reported in this work. The glass samples are dated from the 9th to 6th century BC. The chemical analyses were obtained by Electron Microprobe (EMPA), for major and minor elements, and by LA-ICPMS for trace elements. The chemical data indicate that both natron and plant ash glass are present in the sample set. The natron glass beads are mainly copper blue and turquoise, cobalt blue and iron black. The cobalt blue samples show very high Al_2O_3 (~6.60 wt.%) and MgO (~4 wt.%) levels associated to trace elements such as Ni and Zn, that indicate the use of cobaltiferous alums as source of colorant [1]. Furthermore they exhibit a very low amount of CaO (1.3-3 wt. %), K_2O and P_2O_5 (0.2-0.6 wt.% and 0.03 wt.% respectively). The question about what kind of fluxing agent was used to produce these glasses has been object of great debate. Gratuze and Picon [2] and Reade *et al.* [3] underlined the differences between the 2nd millennium BC cobalt blue glass and the 1st millennium BC ones. The latest contain low amount of K_2O (<0.5 wt. %) and P_2O_5 (<0.1 wt.%) as the earlier, but show also low levels of CaO (3-4 wt.%). These chemical characteristic strongly suggested the use of natron. The Sarno cobalt blue glasses were hence probably produced with natron and the high amount of MgO can be related to the use of cobaltiferous alums. The iron black samples exhibit similar chemical characteristics as regards CaO, K_2O and P_2O_5, consistent with the use of natron, as also observed for coeval black glass from France [2] and Italy [4]. Moreover, these beads are rich in FeO (10-14 wt. %), responsible for the black coloration. The majority of the plant ash glass samples are colorless and high antimony levels are found (Sb_2O_3 ~ 0.40 wt. %). The trace elements analysis shows that the plant ash and the natron glass samples (excluding the cobalt blue and the iron black) are characterized by a high Sr concentration, suggesting the use of a coastal sand as vitrifying raw material [5]. The natron cobalt blue and iron black samples exhibit the lowest amounts of Sr (~75 ppm), that could indicate the use of a limestone-bearing sand as vitrifying agent. There is no chronological distinction among the samples: the presence of natron glass and plant ash glass overlaps each other in a span of time from the 8th to the 6th century BC.

[1] Shortland A.J. and Tite M.S. (2000). Raw materials of glass from Amarna and implications for the origins of Egyptian glass. *Achaeometry* 42, 1, 141-151.

[2] Gratuze B. and Picon M. (2006). Utilisation par l'industrie verriers des sels d'aluns des oasis égyptiennes au début du premier millénaire avant notre ère. In: Colloque International- L'alun de Méditerranée- 4-8 Juin 2003 (ed. Brun, J. P.), Institut Français de Naples, Naples.

[3] Reade W. *et al*. (2005). Innovation or continuity? Early first millennium BCE glass in the Near East: cobalt blue glasses from Assyrian Nimrud. In: Annales du 16e Congrès de l'Association International pour l'Histoire du Verre-London 2003 (ed. H. Cool), 23-7.

[4] Henderson J. and Arletti R. (Personal communication).

[5] Freestone I.C. (2006). Glass production in Late Antiquity and Early Islamic period: a geochemical perspective. In: Geomaterials in Cultural Heritage, edited by Maggetti, M. and Messiga, B., London.

Hyperspectral monitoring of marble in buildings: a case study of the Santa Maria del Fiore (Florence, Italy) facades

Di Benedetto F[1*], Suzuki A[2], Xinhue G[2], Vettori S[3], Costagliola P[1], Benvenuti M[1], Rimondi V[1], Camaiti M[4], Pecchioni E[1], Carretti E[5], Moretti S[1]

1 - Università Firenze - Dip. di Scienze della Terra, Italy
*francesco.dibenedetto@unifi.it 2 - Università Firenze - Italy 3 - CNR-ICVBC, Italy 4 - CNR-IGG, Italy 5 - Università Firenze - Dip. di Chimica, Italy

Hyperspectral instruments, discriminating materials on the basis of their different patterns of wavelength-specific absorption, might be employed in the characterization of the components in exposed stone surfaces, and therefore contribute to understand their conservation state. A portable radiometer (ASD-FieldSpec Pro spectroradiometer), which continuously and rapidly acquires punctual reflectance spectra in the 350-2500 nm spectral range, has the potential to be used for monitoring the state of conservation of stone surfaces through the monitoring of the relative abundance of some components considered precursor symptoms of decay. Major advantages of this technique include its non-destructive and non invasive nature.

In this study, gypsum is considered as a damage symptom in marble facades of ancient buildings. A method to unravel qualitative and semi-quantitative information on the degree of the alteration of the calcite to gypsum is proposed. This method is based on the spectral decomposition in individual spectral components assigned to calcite and gypsum, during the analysis of spectra of synthetic mixtures of microcrystalline calcite and gypsum. Advantages, perspectives and limits of the methods are discussed. Furthermore, a case study is considered. The analysis of 24 areas of white Carrara marble was carried out on the facades of the Santa Maria del Fiore (Florence, Italy) cathedral, a UNESCO world heritage monument. The preliminary analysis of the data are presented and discussed.

A database for the provenance study of chalcedony

Gliozzo E[1*], Angelini I[2]

1 - Department of Environment, Earth and Physical Sciences, University of Siena, Italy *gliozzo@unisi.it 2 - Dept. of Geosciences, University of Padua, Italy

Despite their importance, in terms of preciousness, aesthetic properties, mysterious virtues, commercial trade and social destination, chalcedony studies still remain largely unaddressed in the field of archaeometry.

Microcrystalline α-quartz and moganite were identified as the components of three engraved gemstones (Early Roman Empire period) found in central Paris [1]. Carnelians, sardonyxes, chalcedonies, jaspers, quartzes and agates from Crypta Balbi (Rome, Italy), worked between the end of Republican age and the seventh century AD, were further identified [2], as well as quartz gems from the Guarrazar treasure (seventh century AD-[3]; [4]) and carnelians from Vigna Barberini, on the Palatine hill at Rome [5]. More attention has been paid to engraving techniques of hard gems such as quartz [6, 7].

The worldwide occurrence of quartz and chalcedony and their composition, frequently lacking in characteristic fingerprints, deeply undermines the possibility of tracing their origin. Three different methodologies have been approached so far in order to investigate the provenance of chalcedony and jasper. Laser-ablation inductively coupled plasma mass spectrometry [8]; proton-induced X-ray and gamma-ray emission analyses [5, 9], and the determination of the quartz:moganite ratio [5, 10].

Due to the lack of a wide reference database, the results obtained so far did not allow a clear differentiation among Indian, sub-Saharan African, German, Turkish, etc. chalcedonies. Therefore, a systematic sampling of both raw materials and archaeological materials has been undertaken. The collection has been expanded to materials found in Italy, Libya, and Sudan and a methodological protocol has been established for their investigation. The quartz:moganite ratios obtained by X-ray powder diffraction and Raman spectroscopy were combined with trace elemental data obtained on the same samples and on reference samples by laser ablation mass spectrometry. The investigations led to the creation of new reference groups and provided robust arguments for the discrimination of these materials against the Indian chalcedonies.

The results obtained verified the effectiveness of the analytical procedure followed for the study of these materials, thus indicating the way to go for the enlargement of the existing database. In terms of provenance, the results obtained for the materials under examination provided new tiles for the reconstruction of ancient trade routes.

[1] Smith D.C. and Robin S. (1997). *JRS*, 28, 189-193.
[2] Andreozzi G.B. *et al.* (1996). *Zeitsch. Deut. Gemmol. Gesel.*, 4, 49-72.
[3] Calligaro T. *et al*. (2000). *NIMB*, 161-3, 769-774.
[4] Guerra M.F. *et al*. (2007). *Archaeometry*, 49, 53-74.
[5] Gliozzo E. *et al*. (2011). *Archaeometry*, 53, 469-489.
[6] Sax M. and Meeks N.D. (1995). *Archaeometry*, 37, 25-36.
[7] Rosenfeld A. *et al*. (2003). *JAS*, 30, 227-238.
[8] Insoll T. *et al.* (2004). *JAS*, 31, 1161-73.
[9] Theunissen R. *et al*. (2000). *World Archaeology*, 32, 84-105.
[10] Pretola J.P. (2001). *JAS*, 28, 721-39.

Late antique glass products in northern Apulia (southern Italy)

Gliozzo E[1*], Turchiano M[2], Turbanti I[1]

1 - Department of Environment, Earth and Physical Sciences, University of Siena, Italy *gliozzo@unisi.it 2 - Department of Humanities and Cultural Heritage University of Foggia, Italy

This contribution reviews the results obtained from the study of Late Antique (4^{th} - 5^{th} century AD) glass materials found in two main archaeological sites of northern Apulia (Italy): Faragola and Herdonia. Moreover, new data have been here provided for Herdonia, adding thirty new samples to the dataset already available from our previous research.

The measurements (XRF, ICP-MS, ICP-OES, INAA, SEM-EDS, EMPA, XAS at the Cu-K, Fe-K and Mn-K edges) were performed on a total of 94 samples: transparent, opaque, colourless, naturally coloured or intentionally coloured (red, orange, yellow, amber, green, blue, white and blackish).

As for glass forming agents, it was established that different types of calcareous sands were used as the source of silica (network former), also providing the stabilizing agent. A natron-type soda source served as the network modifier; however, the use of a sodium-rich plant ash and the recycling process were hypothesized for the production of red and orange tesserae.

For colouring agents, it was possible to determine that colourless vessels were achieved using a very pure sand source as well as by the introduction of Mn as a decolouriser. The orange and yellow tesserae were coloured by metallic copper, cuprite and Pb antimonates, respectively. Cu^{2+} and Pb antimonates were responsible for the opaque green colours. The dark green and yellow portions of the marbled tesserae were respectively comparable to the tesserae comprising only one of these colours. Cu^{2+} together with Ca antimonates likely produced light blue tesserae, whereas cobalt was used to produce dark blue tesserae. These contexts were of particular help in defining the glass technology used for red and blackish glasses. In the former, the XAS investigations identified both metallic (28%) and oxidized (72%, with a $^{+1}$ charge) Cu phases. In the latter, XANES results indicated the coexistence of Fe^{2+} and Fe^{3+}, while Mn was in the $^{2+}$ state.

As for provenance, the relationship that most Faragola tesserae showed with the products from Syria-Palestine was rather convincing. Conversely, the comparison with HIMT glasses and Levantine products was significant but inconclusive for the study of the tesserae. In the former case, the comparison did not seem appropriate for any element (especially Mn); in the latter case, only a small group of tesserae perfectly matched the compositional range of Levantine products. It was impossible to tell whether the raw materials originated from Egypt, or from the Syro-Palestinian coast or more northern Levantine sources. Nevertheless, our results showed the wide distribution of the tesserae among reference groups, suggesting diverse supply channels. Moreover, the presence of a secondary workshop was hypothesized, especially for tessera production.

As far as the Herdonia collection, several samples showed compositional similarities with the HIMT group while others were more similar to the Levantine glasses, thus suggesting an import of raw glass or artefacts from the Syro-Palestinian coast.

Insights into the smoothing and burnishing of ceramic surfaces

Ionescu C[1*], Hoeck V[2], Crandell O[1], Šarić K[3]

1 - Babes-Bolyai University *corina.ionescu@ubbcluj.ro 2 - Paris Lodron University, Salzburg, Austria 3 - University of Belgrade, Serbia

From the onset of pottery making in Late Palaeolithic-Early Neolithic times, until the present, people have tried various methods to improve and ornament the surface of ceramic objects. Among these methods smoothing, as well as plain and pattern burnishing, gives an even surface. This study focuses on the effects of smoothing and pattern burnishing on the surface of black ceramic ware produced today in NE Romania. Smoothing is done with a wet cloth or hand, at the end of the hand or wheel shaping of the object. Burnishing is done with a water-worn pebble, at the so-called 'leather-stage' of drying. The surface of the fired pot shows a smooth background with a pattern of shiny strips.

Optical microscopy and scanning electron microscopy reveal that both finishing methods result in diminishing surface irregularities by pushing the larger aplastic particles into the still plastic ceramic body. Nevertheless, in detail, there are specific surface and subsurface changes. Smoothing creates a surface which is even yet still has small irregularities (Figure 1a). Beneath, the phyllosilicate lamellae are oblique-oriented to the surface. Burnishing overlaps the previous smoothed surface and forms a thin and more compact layer (Figure 1b). Within this layer, the phyllosilicate lamellae are parallel-oriented to the surface (Figure 1b). Upon firing, whereas smoothing gives a matte and dull appearance due to diffuse reflection of light, burnishing will create lustre due to specular reflection of the light.

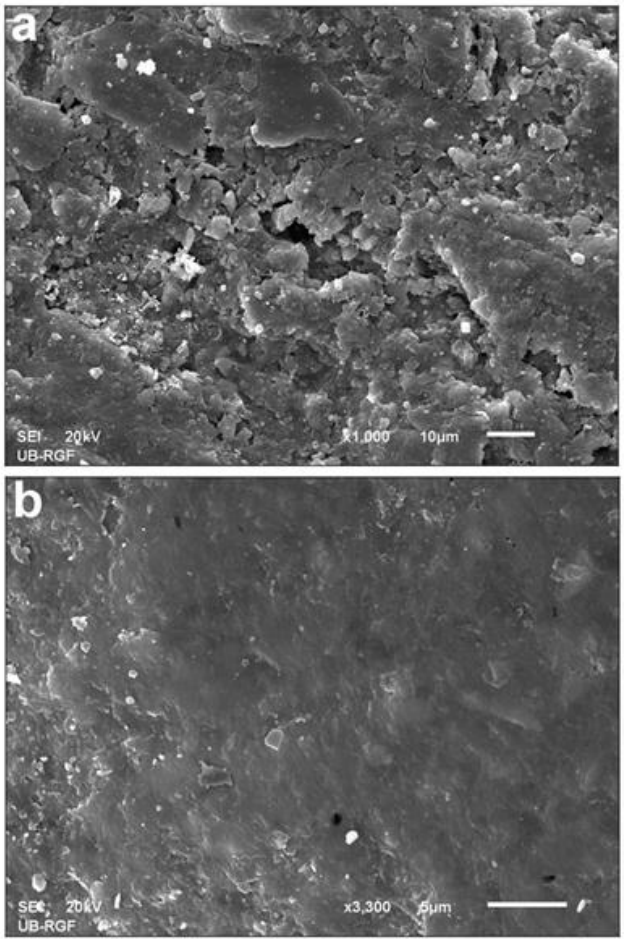

Figure 1: Secondary electron images of smoothed (a) and burnished (b) surfaces.

The results of this study can be used to infer surface treatments, particularly in cases of fragmentary wares, as well as to identify ceramic production centres at archaeological sites.

Acknowledgements: This study was financed by the PN-II-ID-PCE-2011-3-0881 project granted by the Romanian Ministry of Education and Research. Part of the SEM analyses was provided through project 176016, granted by the Serbian Ministry of Education, Science and Technological Development.

Provenance analysis of calcite-alabaster vessels from Qaṭna by NAA

Köster T

Eberhard Karls Universität Tübingen, IANES/Curt-Engelhorn-Centre for Archaeometry. tina.koester@uni-tuebingen.de

Vessels made from 'calcite-alabaster' (also known as 'Egyptian Alabaster' or 'travertine') appear in Egypt and in the region of Mesopotamia and Iran in the late 4th millennium B.C. During the 2nd millennium B.C. these vessels were a tangible part of exchange systems which linked kingdoms of the Eastern Mediterranean and Mesopotamia. The provenance analysis of their raw material may provide insights into the nature of trade, dependency on source regions and the trend of imitating foreign products. Concerning the origin of 'calcite-alabaster', archaeometric analyses have the potential to contribute valuable information, complementing archaeological and philological studies. It is widely assumed that the 'calcite-alabaster' vessels found in Bronze Age contexts in the Levant were manufactured in Egyptian workshops, from material originating in one of the nine well-known ancient Egyptian 'calcite-alabaster' quarries. This assumption is mainly based on the strong typological similarities in vessel forms and the long history of stone vessel manufacture in Egypt. However, a limited number of vessels discovered at Levantine sites have a Levantine form or display slight, but marked distinctions from the bulk of vessels known from Egypt itself. Furthermore, deposits of travertine are known outside Egypt. Since the production of objects imitating Egyptian forms and motives in Levantine workshops is clearly indicated by other object classes, the possible manufacture of 'calcite-alabaster' vessels in Levantine workshops should be considered. In this case, the raw material processed in those workshops might have originated outside of Egypt. An initial result of this study was the development of a procedure to differentiate between 'calcite-alabaster' deposits. This involved the application of neutron activation analysis (NAA) to determine 25 trace elements selected based on geochemical reasoning, e.g., the mechanism (e.g. inclusion, occlusion) of trace element integration during the genesis of this material. Then the number of elements primarily used in the interpretation routine was further decreased by the application of principal component analysis. Two of the 28 geologic deposits studied stuck out due to markedly higher concentrations of certain elements and could thus be distinguished fairly well from the other deposits. However the majority of the deposits require a multi-step procedure to differentiate between geological samples from various deposits. Consequently an iterative interpretation routine was developed.

This routine was subsequently implemented to study the provenance of 68 'calcite-alabaster' vessels, discovered in 2 Bronze Age grave contexts at Qaṭna. In particular, by comparing the concentrations of mainly 6 to 8 elements in bivariate plots, for each archaeological sample, it was possible to exclude step-by-step several of the geological deposits studied. From this the following observations resulted. While an Egyptian provenance of the raw material could not be excluded for the majority of the vessels studied, several vessels are distinguished by marked difference in trace element concentrations from the Egyptian sources (Figure 1). Interestingly, not all of these anomalous vessels can be typologically classified as 'non-Egyptian'. At the same time not all typologically 'Levantine' vessels belong to this chemically different group. Furthermore, the chemically anomalous vessels are not a chemically homogenous group. This demonstrates that the typology of a 'calcite-alabaster' vessel cannot be used as a clear indicator of the raw material origin. In the presented case, the chemically anomalous vessels suggest that Egypt was not the only source for 'calcite alabaster', but rather that deposits in other regions also need to be considered.

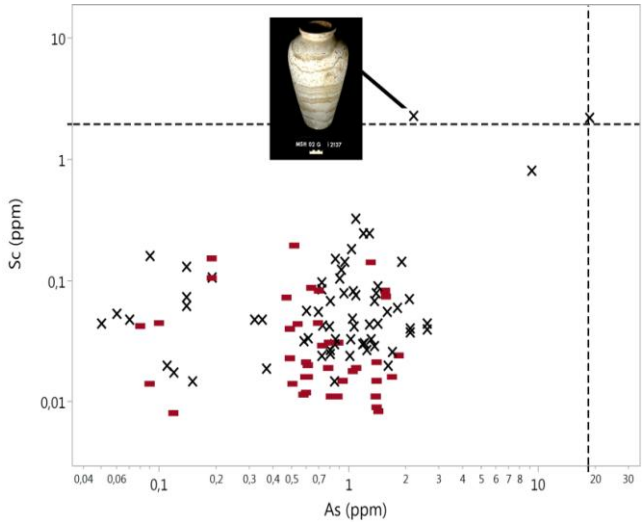

Figure 1: Sc versus As discrimination diagram for 'calcite-alabaster' originating from Egyptian deposits (horizontal bars) and archaeological 'calcite-alabaster' samples (x). Dotted lines represent the maximum elemental concentration of the deposits multiplied by ten. The photo shows a 'calcite-alabaster' jar from the Royal Hypogeum at Qaṭna.3748

Firing experiments on clay-sand mixtures and comparison of results with ceramic artifacts from a Bronze Age settlement (Hejőpapi, NE-Hungary)

Kristály F

University of Miskolc, Institute of Mineralogy and Geology. askkf@uni-miskolc.hu

A Celtic settlement (La Tène period, LT B2 - LT C1 transition) with a large cemetery was excavated in the summer of 2008 at Hejőpapi (Borsod-Abaúj-Zemplén County, NE-Hungary). The cemetery was unusually rich in ceramic vessels as burial objects, indicating significant local pottery making. Ceramic artefacts, various in size and shape, recovered from the cemetery are of two different types: well preserved and highly deteriorated vessels. Based on this the assumption was made that the reason of deterioration was technological and not mineral alteration. This led to the question of whether the burial pottery was purposely produced by low temperature and short time firing?

The area, situated on the river Tisza's plain, has several well sorted clay and sand strata beneath the soil cover. In the vicinity of the settlement clay and sand extracting holes were also excavated. Samples of both materials were taken to test the shaping, drying and firing properties of clay and clay-sand mixtures. Mineralogy and chemistry of raw materials were determined in details: illitic, with R0 illite/smectite, montmorillonite and minor chlorite, low calcite and CaO and rich in K_2O and Na_2O. Firing temperatures were set at the major thermal transformations according to thermal analysis of raw clay. Mineralogy by means of Rietveld-refinement based quantitative XRD of fired test pieces was performed. Results were used to describe the mineralogical transformations for the clay and mixtures and to determine the major differences between mixtures at different temperatures.

Archeomineralogical research was done on selected pottery from the second group, since it accounts for most of vessels. Firing temperatures were found to be low to very low for the second group. A smectite rehydration - recrystallization was also determined. This group was found to be made from the local clays and sand, and fired at temperatures below the crystallization of Ca- and Mg-silicates. A graphitic vessel was also found and investigated by non-destructive XRD. This vessel is presumed to be made of local raw material, but with a higher firing temperature.

Weathering of rocks in polluted urban atmosphere – mechanisms of processes on rain-washed and sheltered surfaces

Wilczynska-Michalik W[1*], Michalik M[2]

1 - Pedagogical University, Institute of Geography, Krakow, Poland
*wanda.michalik@post.pl 2 - Institute of Geological Sciences, Jagiellonian University

High concentrations of particulate and gaseous atmospheric pollutants have caused accelerated weathering of building stones in Kraków (S Poland). For a long time salt weathering was a dominant process of rock decay. Crystallization of salts in pore spaces was the reason of high rate of destruction of rocks. Recent concentration of SO_2 is significantly lower than in the last decades of 20th century but particulate matter concentration is permanently high.

The aim of the study was to compare mechanisms of weathering of rocks in different environments. Samples of Middle Triassic dolomite were collected from walls exposed to rain-washing (wet and dry depositional environment) and walls completely sheltered from rain (dry depositional environment).

On the walls exposed to rain two contrasting zones are present. Fragments exposed to intensive washing are devoid of secondary minerals and subject to dissolution. Less intensively washed surfaces are covered by black brittle gypsum-rich crust composed of platy gypsum crystals. Newly formed non-stoichiometric 'protodolomite' occurs within black crust. Other sulphates occur rarely. Black color is related to dark dust particles and organic pigment dispersed between gypsum crystals.

On surfaces of sheltered walls dark grey crust has developed. It is composed of loosely packed agglomerations of gypsum crystals with abundant dust particles derived from soil (quartz, mica, feldspars) and of industrial origin. Small amount of authigenic calcite, halite and whewellite occur in this crust.

Concentration of various elements is different in the black crust from rain-washed walls in comparison with the grey crust on sheltered walls. Higher concentrations of these elements in the grey crust are related to higher amount of dust which is systematically removed from rain-washed surfaces. Values of $\Delta^{34}S_{CDT}$ and $\Delta^{18}O_{SMOW}$ in gypsum from both groups of samples are very similar.

Crystallization of gypsum from rainwater is important in the formation of black gypsum crust on rocks exposed to rain-washing. This mechanism is accompanied by reactions of sulphur-containing components from the atmosphere with Ca ions from the rock. The presence of 'protodolomite' is additional evidence of dissolution of dolomite. Downward movement of solution is the reason for the folded surface of the crust. Dust particles deposited on the rock surface are removed during subsequent rain-washing. Adsorption of sulphur-containing components on dry surfaces of walls between periods of precipitation is probably negligible in the black crust formation.

Deposition of dust particles and adsorption of sulphur-containing components are the most important factors in grey crust formation. Condensation of water vapour on sheltered walls causes significant moisture retention on the surface and facilitates both deposition of dust and formation of sulphate anions and gypsum crystallization. The rate of sulphate anion formation is increased by the catalytic role of metal-containing dust particles and soot. Hyphal filaments and spider webs also play a role in the binding of crust components.

Self-cleaning photocatalytic coating and hybrid organic-inorganic strengthening products for the protection and conservation of calcarenites from Sabucina (Italy, Sicily)

Barone G[1], Mazzoleni P[1*], Raneri S[1], Alfieri I[2], Bergamonti L[2], Lorenzi A[2], Predieri G[2]

1 - University of Catania, Department of Biological, Geological and Environmental Sciences *pmazzol@unict.it 2 - University of Parma, Department of Chemistry

In recent years, research projects on coating and strengthening products for the protection and conservation of building stones has been increased. In particular, cheap, eco-friendly, reversible, compatible and high activity products are under testing in order to verify their efficiency and applicability on stones. In this work we present the results obtained on the Sabucina Stone, a calcarenite outcropping in Central Sicily and widely used as building and replaced stone, by applying TiO_2 nanoparticle coatings and hybrid organic-inorganic strengthening products. The durability of the studied calcarenite determined by its structural, textural and porosimetric features, requires an integrated preservation and conservation of stone both in terms of surface protection and structural strengthening.

First we tested self-cleaning photocatalytic coatings based on TiO_2 nanoparticles obtained by the sol-gel process at different pH values. Photocatalytic activity of theTiO_2 coatings on Sabucina Stone was assessed under daylight and ultraviolet irradiation, monitoring methyl orange (MeO) and methyl blue (MB) dye degradation as a function of time. To evaluate the effect of the treatment, colorimetric and water absorption tests were performed. Moreover, in order to verify the action of coating in inhibiting degradation processes, aging tests were carried out by evaluating stone resistance to salt crystallization.

Second, a network based on aluminium and silicon oxides with epoxidic functional groups have been used with strengthening aims. In order to test the effectiveness of the hybrid organic-inorganic strengthening product, colorimetric, water adsorption, compressive strength and aging tests have been performed. Finally, the performance of a hydrophobic coating applied in association with the strengthener was verified by colorimetric and water adsorption tests.

The results obtained show good photodegradation rates for titania nanosols and good protection properties, especially using the basic pH preparation. With reference to hybrid organic-inorganic strengthening products and hydrophobic coatings, preliminary tests highlight promising applications to the preservation of calcarenites.

Geochemical modelling of ancient ceramics: in search of technology and sources

Ionescu C[1], Hoeck V[2*]

1 - Babes-Bolyai University 2 - Paris Lodron University, Salzburg *volker.hoeck@sbg.ac.at

An ancient ceramic is a multicomponent system consisting of a clayey matrix and various clasts. It can be approached as an 'artificial' rock. The clasts may be various minerals, rocks, fossils or older potsherds. Tempering material, clay processing (washing), firing processes and burial alteration bear a significant influence on the overall final ceramic composition.

A wide range of mineralogical-petrological, physical and chemical methods are used for compositional, technological and provenance studies of ancient ceramics. In combination with mineralogy, the geochemistry allows classification and grouping, inferences on the nature of clay and temper and various processes such as clay treatment, firing and burial changes.

In particular for provenance studies, not only the major elements (SiO_2, Al_2O_3, Fe_2O_3, MgO, CaO, TiO_2, Na_2O, K_2O, P_2O_5 including LOI) but also the minor, trace and rare earth elements are important. Figure 1 shows the influence of LOI in discriminating ceramics from raw clay based on chemistry. The geochemical data can be handled in a similar way as is done for rocks, e.g. plotted in bivariate, ternary, REE and spider diagrams. The selection of the variables and the discriminating diagrams is not random and depends on basic information - mineralogy. The handling of chemical data is specific for each ceramic type.

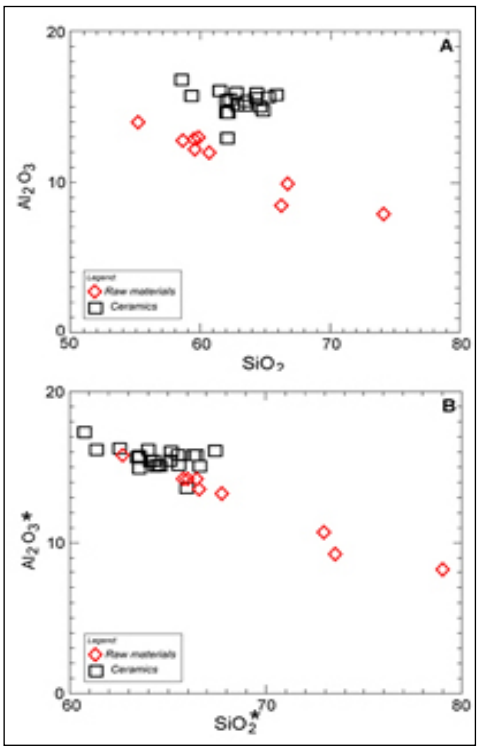

Figure 1: Influence of LOI on the handling of chemical data. A. Original data, B. Data recalculated on LOI-free basis.

Ceramics are made of common materials found in the continental realm, e.g. mudstones ('clays') and temper. Consequently, the overall chemistry can be normalized to the upper continental crust or average continental shale compositions.

Many ceramics are made of clays and non-plastic temper material thus forming a mixture of at least two sources. On the other hand, washing of clays separates out some non-plastics from the original raw material composition giving rise to an artificial un-mixing process. Geochemistry can be used to model these processes to a certain extent.

Acknowledgements: This study was financed by the PN-II-ID-PCE-2011-3-0881 project granted by the Romanian Ministry of Education and Research.

EPR study of heated carbonate-rich illitic clay

Ionescu C[1*], Hoeck V[2], Gruian C[1], Simon V[1]

1 - Babes-Bolyai University *corina.ionescu@ubbcluj.ro 2 - Paris Lodron University Salzburg

In order to establish whether electron paramagnetic resonance (EPR) spectroscopy can be used for evaluating the firing temperature of clay-based ceramic objects, the EPR response of heated clay was investigated. The clay consists of the minerals illite, muscovite, quartz, calcite, as well as clinochlore, K-feldspar, plagioclase, altered biotite, dolomite and Fe-oxyhydroxides.

Briquettes of 4 x 4 x 1 cm size were modelled from the clay and heated between 400°C and 1200°C, with 2 hours soaking time. Samples of red ceramic vessels fired from the same clay in a workshop in NE Romania were used for comparison. The aims of the study were: i) to define the relation between the resonance signal characteristics on one side, and temperature and mineral composition of thermally treated clay on the other side, and ii) to demonstrate the relevance of EPR studies in archaeometry, in particular for ancient ceramic technology.

The manganese- and iron-bearing minerals were identified by electron microprobe analysis (EMPA) in the ceramic vessels. The most important carriers of MnO are: clinochlore, Fe-oxyhydroxides, calcite and dolomite. FeO is found in Fe-oxyhydroxides, clinochlore, carbonates, muscovite, altered biotite and illite. As newly-formed phases, small and isolated Fe-rich minerals (hematite), gehlenite, clinopyroxene and a glass phase were also identified by XRD and EMPA.

The EPR spectrum recorded for the raw clay shows a weak resonance line at 1607 Gauss (g ~4.18), and a strong sextet of hyperfine signals between ~3200 and ~3750 Gauss (g ~2) magnetic field, respectively. The comparison of the EPR spectrum with the mineralogy, mineral chemistry and chemical composition of the raw clay suggests that the recorded signals are due most likely to Mn^{2+} and Fe^{3+} ions, and to structural defects in Mn and Fe-bearing phases. The first signal at g ~ 4.18 is assigned to Fe^{3+} located in orthorhombic positions and the substitution of Fe^{3+} for Al^{3+} in the structure of clay minerals. The hyperfine sextet is due to Mn^{2+} ions located in an environment with octahedral symmetry. The doublets of the 'forbidden transitions' in the interspace of the hyperfine lines are typical for Mn^{2+} in calcite and dolomite. Resonance signals at g ~ 2 can also be assigned to Fe^{3+} ions located in octahedral sites.

In the heated samples, oxidation of Mn^{2+} (EPR active) to Mn^{3+} (EPR silent) or Mn^{4+}, and Fe^{2+} (EPR silent) to Fe^{3+} (EPR active) respectively, combined with changes in their environment, produces the resonance signals. The dominating hyperfine sextet, at g @ 2 due to Mn^{2+}, is replaced at T >700ºC by a large signal, mainly due to Fe^{3+}. The gradual destruction with temperature of the carriers such as Fe-oxyhydroxides, clinochlore, calcite, dolomite, altered biotite, illite and muscovite, as well as the formation of new minerals and glass are the main mineralogical processes influencing the width of the resonance signals.

The EPR signals recorded from raw and heated carbonate-rich illitic clay show systematic changes as a result of a complex interaction of several factors: i) primary mineralogical composition of the material, ii) heating atmosphere, iii) specific phase transformations at various temperatures, iv) distribution of paramagnetic species within various phases and v) the local environment for each paramagnetic ion. Heating of clay, as long as it is in crystalline state, has a trend toward the narrowing of the resonance signal as opposed to the broadening evolution of the signal at temperatures where amorphous/vitreous structure prevails.

As most of the carbonate-rich clays used for traditional ceramics contain small amounts of Mn and Fe, an EPR study can be useful in interpretation of a firing temperature range. A broader signal with remnants of the hyperfine sextet will indicate a temperature around 700°C, whereas the lack of these remnants in a broad signal would suggest temperatures over 1000°C. The results of this study can be used in conjunction with mineralogical and microstructural data for the investigation of technological conditions such as firing temperature and atmosphere related to archaeological ceramic objects.

Acknowledgements: This study was financed by the PN-II-ID-PCE-2011-3-0881 project granted by the Romanian Ministry of Education and Research.

Building-sandstone biodeterioration in polluted urban conditions: a case study from Wrocław, SW Poland

Kryza R[*], Prell M, Kosior G, Samecka-Cymerman A, Brudzinska-Kosior A, Pietrzykowska K

University of Wroclaw *ryszard.kryza@ing.uni.wroc.pl

Building-stone biodeterioration is a serious problem in the preservation and conservation of historical monuments, especially in polluted environmental conditions. We present geochemical results from sandstones collected from architectural monuments in Wroclaw and comparative data from their potential source quarries in the Cretaceous deposits of SW Poland.

The study sites, seven in the city (WR) and seven in the quarries (QU) were selected where architectural stone was found to be covered with moss (*Tortula muralis* Hedw) and lichen (*Lecanora saxicola*). The samples were collected as borehole cores, 8 and 18 mm in diameter and 6-8 cm long. The sandstones studied, representing quartz arenites with subordinate clayey matrix, are noticeably weathered, usually within an up to ca. 10 mm thick subsurface zone that passes gradually into less altered substrate. 28 samples from 14 borehole cores (surface and interior specimens) - seven from Wroclaw and seven from quarries, were analyzed for major and trace elements at the Acme Lab, Canada (4A, 4B, 1DX analytical procedures).

Distinct differences are observed in element distributions, in particular when comparing the weathered subsurface zones of sandstones from the city with those from the quarries (see selection of data for two representative cores from Wroclaw and Zerkowice quarry in the Table 1; surface samples - s, 0-1 cm deep, interior samples - i, 4-5 cm deep; trace elements in ppm).

Table 1. Element distributions in two representative cores WR and QU

Samples		Co	Ni	Zn	Pb	As	U	Th
WR	MM-s	11.4	0.4	10	191.5	2.2	0.4	1.7
	MM-i	3.7	0.3	1	2.2	0.5	0.3	1.1
QU	ZER-s	3.4	0.9	4	1.5	0.5	0.3	1.4
	ZER-i	5.1	1.0	2	0.8	0.5	0.2	1.1

The altered subsurface zones of architectural sandstone from the city show clearly elevated parameters and components, e.g. Fe_2O_3, CaO, P_2O_5, TOT/C and LOI. Most spectacular is the enrichment of the altered subsurface zones of the sandstones from the city in heavy metals: Pb, Zn, Co and Ni. The main factor controlling the distribution patterns of elements in weathered building stones seems to be the polluted atmosphere of the urban area. The potential role of living organisms (moss and lichen) will be described in a separate paper.

Acknowledgements: The study was supported from the Research Project 2011/01/N/ST10/03925 of the National Centre of Science, NCN, Poland, and University of Wroclaw grants 1164/M/KEBOŚ/13 and 1017/S/ING/13.

Formation sequence and deliquescence of the mixed salt darapskite

Latrille C[1*], Blanc C[1,2], Le Caer S[1,2,3]

1 - CEA *christelle.latrille@cea.fr 2 - DEN, DPC, SEARS, LISL, F-91191 Gif-sur-Yvette, France. 3 - DSM, IRAMIS, SIS2M UMR 3299 CNRS/CEA, Laboratoire de Radio

Darapskite, $Na_3(NO_3)(SO_4).H_2O$ is a widespread mineral encountered in evaporites and nitrate deposits, in atmospheric particulate matter, in efflorescence of monuments masonry or outcome from industrial processes of waste treatment.

This mixed salt is reported associated with pure sodium sulfate and nitrate salts in the nitrate deposits and in efflorescence. Solubility studies of the binary system $NaNO_3$+Na_2SO_4 in H_2O identified the darapskite as the stable mineral phase over a portion of the solubility isotherm. Mineral synthesis leads to the physico-chemical conditions of stability but the reaction mechanisms remain unclear. To span this gap, we may consider that the sequence of mineral formation depends on the approach used to evidence this. Drying a saturated solution or hydrating the salt until deliquescence may result in various ways to reach the stable product, due to different initial hydrations of the salts. Deliquescence refers to the formation of an aqueous solution by the adsorption of water by hygroscopic salt minerals. The relative humidity at which salts deliquesce is dependent on temperature and is characteristic of each salt mineral or assembly of salt minerals. $NaNO_3$ being more hygroscopic than Na_2SO_4, it deliquesces at lower relative humidity and produces aqueous solution which can initiate Na_2SO_4 dissolution below its deliquescence point. Conversely, it is unclear if the darapskite dissolution is congruent. To clarify the mechanism of darapskite formation, mixtures of Na_2SO_4 and $NaNO_3$ salts have been placed in conditions of controlled relative humidity. The influence of the sulfate and nitrate proportion on the darapskite formation is tested by adding salts to excess in the mixture. Mineralogical determinations by XRD, IR and SEM/EDS were performed on these mixtures, at varying levels of moisture content. Synthesis performed by drying saturated solution leads to formation of pure darapskite. Its deliquescence is studied and its transformation products are determined.

Proto-Byzantine glassware from the Roman Amphitheatre of Catania (Italy): archeometric characterization through geochemical data

Quartieri S[1*], Di Bella M[1], Sabatino G[1], Giacobbe C[2], Spigo U[3]

1 - University of Messina, Italy, Department of Physics and Earth Sciences *squartieri@unime.it 2 - University of Insubria, Italy, Dept. of Science and High Technology 3 - Parco Archeologico delle Isole Eolie, Italy

Twenty-five glassy samples, including fragments of objects, glass drops and glass scoria coming from Proto-Byzantine glassware recovered during excavations of the Catania Roman Amphitheatre, were analysed for major, minor and trace elements using different analytical techniques, namely SEM-EDS, EMPA and LA-ICP-MS. Two groups of natron-based silica-lime glasses were identified: high iron, manganese and titanium (HIMT) glass (specifically subdivided in HIMT1 and HIMT2 types) and Levantine I type.

The geochemical signatures of HIMT raw materials, with a high abundance of HREE relative to LREE, suggest the use of an impure sand, particularly enriched in heavy minerals and/or in mafic phases. Furthermore, the noticeable difference in all the HFS elements (Zr, Nb, Ta, Ti, Hf, Th) contents showed by the two sub-groups of samples - the enriched HIMT and the depleted Levantine I - allows us to propose these elements as discriminators between the two categories.

Mineralogy, swelling mechanism, and swelling inhibition in swelling sandstones and tuffs

Wangler T[1*], Siegesmund S[2], Wedekind W[2], Flatt R[1]

1 - ETH Zürich Institute for Building Materials *wangler@ifb.baug.ethz.ch 2 - Geoscience Center of the University of Göttingen

Hydric and hygric expansion of sandstones and tuffs used in historic buildings and monuments can be a major contributor to their degradation when subjected to moisture cycles. The source of this expansion can be related to swelling of the clay fraction of rocks containing clay minerals, or a disjoining pressure in the microporosity, or both [1]. In rocks where the swelling is due to the clay-bearing fraction, swelling inhibitors consisting of alkyl- or polyamines exchange with the native cations in the clay interlayer and can reduce subsequent swelling significantly [2]. In this work, we test a mono-, a di- and a poly-alkylamine and demonstrate their effectiveness on several German and Mexican sandstones and tuffs that have previously been characterized mineralogically [3]. These rocks were selected for this study based on their relatively high hydric expansion and their content of swelling clay minerals. Linear dilatation experiments pre- and post-treatment show a decrease in hydric expansion of 30-50%. One Mexican tuff proved to be immune to these treatments, which is likely the result of a swelling mechanism related to the microporosity of the zeolite in the matrix rather than the swelling of the clay fraction.

[1] Ruedrich J. *et al*. (2011). Moisture expansion as a deterioration factor for sandstone used in buildings. *Environ. Earth Sci.*, 63, 1545-1564.

[2] Wangler T. and Scherer G.W. (2009). Clay swelling inhibition mechanism of α,ω-diaminoalkanes in Portland Brownstone. *J. Mater. Res.*, 24, 1646-1652.

[3] Wedekind W. *et al*. (2013). Weathering of volcanic tuff rocks caused by moisture expansion. *Environ. Earth Sci.*, 69, 1203-1224.

Copper and bronze in North-Eastern Italy from the Chalcolithic to the Final Bronze Age: chemistry and origin of the metals

Angelini I[1*], Artioli G[1], Nimis P[1], Addis A[1], Villa I[2]

1 - Department of Geoscience, University of Padua, Italy *ivana.angelini@unipd.it 2 - Institut für Geologie, Switzerland

Thanks to several research projects developed in collaboration with Italian Cultural Heritage Offices, Museums and archaeologists from different Universities, numerous prehistoric metals finds from north-eastern Italy have been analysed in recent years. The majority of the objects studied are weapons (axes, swords, etc.), ingot fragments and ornaments (pins, torques, etc.). They can be dated from the Chalcolithic to the Final Bronze Age (Italian chronology), based on excavation stratigraphies and/or their typology. The aim of the archaeometric analyses is the identification of the nature of the metals, the investigation of the manufacturing technologies and the determination of the metal provenance. Moreover, we want to verify the potential systematic changes in any of these aspects with the age of the finds.

The chemical and textural characterization of the finds was performed on micro-samples by SEM-EDS, EPMA and metallographic etching. In addition, lead isotopes analyses were carried out by mass spectrometry. To identify the origin of the metals, the data were compared with existing literature data and with the additional in-house data on geochemical tracers (lead isotopes and trace elements) produced by our group for most copper deposits in the Western Alps and Italian Eastern Alps (http://geo.geoscienze.unipd.it/aacp/welcome).

The results confirm the previously observed changes in the metal composition from the Chalcolithic (pure copper and arsenical copper) to the Bronze Age ("fahlerz" alloy and tin bronze). Moreover, several consistent variations in the contents of minor elements (Fe, Ni, Sb, etc.) have been noted in particular finds, suggesting changes in smelting technologies (high Fe content) and the exploitation of different ore sources. A few objects made with copper ores of south-eastern Alpine origin have been positively identified since the Chalcolithic (Fig. 1). An Italian Alpine origin has also been proved for numerous objects dated from the Early to the Final Bronze Age, although the data also indicate wide circulation of copper metal from ore sources outside the Alps. Further evidence for the use of copper ores from the Italian Eastern Alps during the Chalcolithic and the Bronze Age is provided by our chemical, mineralogical and isotopic analyses of copper slags from Trentino and Alto Adige (Northern Italy).

In the talk, a review of the complex picture that has emerged from these studies will be presented and discussed.

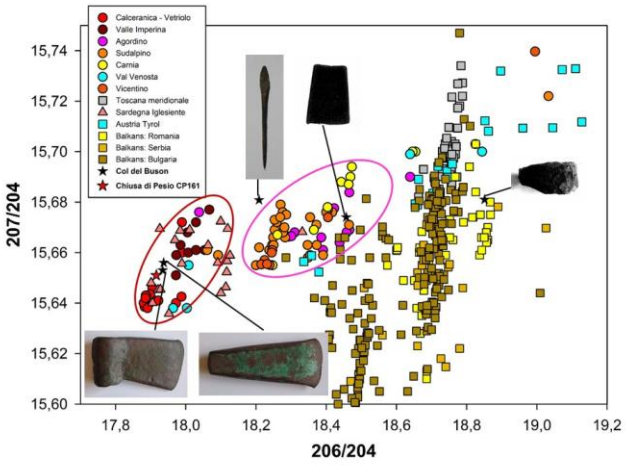

Figure 1: Lead isotope data for some Chalcolithic objects from the Col del Buson hoard, (Belluno, north-eastern Italy). Data for copper ore fields from the Italian eastern Alps (outlined), Austrian Tyrol, Tuscany, and the Balkans are shown for comparison.

The Phalaborwa Complex – a forgotten mineral treasure

Fraser A

Allan Fraser &Associates. allan@allanfraserandassociates.co.za

INTRODUCTION

The Phalaborwa Complex is situated in the province of Limpopo, South Africa about 550 kilometres from Johannesburg. The geology of the Complex is that of intrusive, ultramafic alkaline and carbonatitic rocks emplaced into Archaean gneisses [1]. The age of emplacement has been determined as 2060.6 ±0.5 Ma [2]. The carbonatite at Phalaborwa is unique in that it contains appreciable amounts of copper. Other economic minerals mined are magnetite, uraninite-thorianite and baddeleyite whilst the ultramafic rocks of the complex host apatite and vermiculite [3]. Foskor had been mining phosphate at Phalaborwa since the mid-1950s and it was only in the 1964 that copper mining began in haste by the Palabora Mining Company at a large conspicuous carbonatite koppie known as Loolekop. Palabora Mine's open pit reached its final depth of 754 meters below the original outcrop in April 2002 [2]. Underground mining commenced soon after the closure of the open pit.

COLLECTABLE MINERALS

In the 1980s the then Pit Superintendent at Palabora mine, John Gliddon, collected perhaps thousands of specimens from the pit and in particular from the dolerite dykes. It is likely that all of the specimens from Phalaborwa in collections worldwide are from those originally recovered by John Gliddon. Attractive specimens and related minerals in a variety of habits and combinations were found. The collectable minerals from the Phalaborwa Complex can be divided into two groups: the minerals associated with the dolerite dykes and those of the intrusive rocks. The zeolites from the Phalaborwa Complex are arguably the most attractive found in Africa, a continent not known for their occurrence [3]. Today the Phalaborwa Complex produces virtually no mineral specimens and this is partly due to the 'block cave' mining method used as well as the highly mechanised nature of modern mining.

Minerals Associated with Dolerite Dykes

The Complex is hosted by swarms of dolerite dykes of possible younger age than the emplacement itself. The age of the dyke swarm is unknown [2]. It is in these dykes that most of the collectable minerals have been found. The dykes are between a few centimetres to up to 50 meters in width [2, 3]. Within the narrower fractures and openings zeolite minerals are found as a chalky coating on the host rock but where the cavities are larger, a host of different zeolite minerals are found. One cavity opened was 1.8 meters in size and was lined with prehnite and apophyllite [3]. Other finds included zeolites such as mesolite, analcime, chabazite, heulandite, laumontite and natrolite. White balls of datolite are often found included in apophyllite.

Minerals Associated with Intrusive Rocks

Euhedral baddeleyite crystals occur in the carbonatite with sizes typically of a few millimetres. On perhaps only a few occasions have larger crystals been found, such as the 10 cm crystal now in the collection of Desmond Sacco. Large euhedral magnetite crystals are rare as most are found as 1 - 2 cm on edge with high lustre. Other minerals found are orange-red chondrodite up to 5 millimetres, dark green iowaite as microcrystals [4], rare micro purple cubic fluorite as well as attractive bronze coloured biotite. Crystallised valleriite is rare but a single specimen in the authors collection exhibits euhedral crystals up to 5 mm. Attractive blue brucite has been found with fibrous lizardite. An interesting find during the early stages of mining were specimens of brilliant green chromium fuchsite associated with blue kyanite. Other interesting combinations are fibrous antigorite with chondrodite, clinochlore and magnetite. Minor fibrous fluoborite occurs with magnetite and calcite.

CONCLUSION

Today, very few if any collectable mineral specimens are being recovered from the Phalaborwa Complex. Consequently, the Phalaborwa Complex has to some extent become a 'forgotten' mineral locality by mineral collectors. We are fortunate that the many thousands of mineral specimens saved from the crusher in the past has resulted in our better understanding of the mineralogy of the Complex as well as the preservation of a national heritage.

[1] Bullen W.D., Wilson M.G.C. and Vorster C.J. (1995). The Metallogeny of the Pietersburg and Tzaneen Areas. *Council for Geoscience*. 85 pages.

[2] Johnson M.R., Anhausser C.R. and Thomas R.J. (2006). The Geology of South Africa. *Council for Geoscience and the Geological Society of South Africa.* Pages 291-295.

[3] Glidon J. and Braithwaite R.S. (1991). Zeolites and Associated Minerals from the Palabora Mine Transvaal. *The Mineralogical Record*, 22, 255-262.

[4] Cairncross B. and Dixon R. (1995). Minerals of South Africa. *Geological Society of South Africa*, Johannesburg. 289 pp.

Geology of gold: Edward Dunn, the Australian - South African connection

Henry D*, Birch W

Museum Victoria *dhenry@museum.vic.gov.au

Museum Victoria's gold collection consists of about 2300 mineral specimens. Approximately half are from Victorian localities, 35 % from other Australian States, with the remaining 15% from overseas occurrences. In addition, the Museum has a large collection of rocks and ores from Victorian gold mines.

Almost 30% of Museum's gold specimens are from the collection of Edward J. Dunn, a former Director of the Geological Survey of Victoria. Dunn's collection was acquired by the National Museum of Victoria from his daughter in 1946. The collection contains 625 gold specimens, many of which were photographed by Dunn to illustrate his 1929 book *Geology of Gold* (South Africa, Australia and New Zealand).

Edward Dunn was born in Bristol, England, in November 1844 and emigrated with his family to Goulburn, New South Wales, in 1849. His family moved to the rich mining district of Beechworth in north eastern Victoria in 1856. Dunn's childhood interests in gemstones led to a distinguished career as geologist. Dunn's contributions were recognised by the awarding of the Murchison medal by the Geological Society London in 1905.

In 1871, Dunn moved to the Cape Colony, South Africa, where he was involved in gold and diamond discoveries. Upon his return to Victoria (Australia) in 1886, he set up a practice as a mining surveyor. Dunn had detailed knowledge of gold occurrences, an eye for unusual specimens and excellent contacts within the mining industry. These traits are reflected in his book, *Geology of Gold*, and in the nature of the specimens within his collection. The collection also reflects his travels in South Africa and his work in the Victorian goldfields in Australia.

Count Vargas-Bedemar – 4th president of the Mineralogical Society of Jena/Germany

Kreher-Hartmann B

Friedrich-Schiller-University Jena. cbk@uni-jena.de

Eighteen years after the foundation of the mineral collection in Jena in the former dukedom of Sachsen-Weimar, Johann Georg Lenz (1745-1832), first Professor of Mineralogy at the University of Jena, founded the first geoscientific society, so called "Die Societät für die gesammte Mineralogie zu Jena". The aims of this society were proclaimed in §1 of the statutes: The knowledge of mineralogy should be discussed in public and the collections in Jena should increase. Therefore Lenz, as the founder and director of the society, intended to work together with a president and there should be named ordinary, extraordinary and correspondent members.

During the following 88 years about 2500 persons obtained a diploma of membership and at least more than 3000 persons (professionals such as R.J. Hauy, M. v. Flurl, A.G. Werner, A. Bruce and interested persons like Carl Grosse - alias Duke Vargas-Bedemar, Prince Dimitrij Gallitzin, Maria Paulowna - daughter of Tsar Paul I, H. Struve and J. H. L. Pansner, one of the founders of the Russian Mineralogical Society) contacted the Jena society. Once obtaining membership, they normally sent minerals, rocks and fossils and also literature and maps from all over the world to Jena.

What about the presidents of the Society? The first one, Domokos Teleki, a young Hungarian nobleman, died already in his second year as acting president. He was followed by Prince Dimitrij Gallitzin, a former Russian diplomat, who worked for example in Den Haag and after retired, he lived in Braunschweig/Germany. He donated his huge and spectacular private collection in 1802 to the Society in Jena. Shortly after his death he was followed by Johann Wolfgang von Goethe (1799-1832) as the 3rd president. Goethe used his popularity to get in contact to many people interested in mineralogy. So he corresponded with a man living in Denmark who was the friend of the next Danish king (Chistian VIII). This person was Carl Friedrich August Grosse, who called himself since 1809 Count Vargas-Bedemar. Grosse was born 1768 in Magdeburg/Germany, studied Literature in Göttingen and Halle; during his whole life he was interested in mineralogy and geology. He published a few books, mainly during his stay in Italy from 1792 to 1809. Because of some political affairs he had to leave Italy and went to Denmark. There he came into contact with the King and other persons of the government. He went on excursions through the northern part of Europe. For many years he had been in charge of the mining interests of the Danish government and member of the Danish Society for the Advancement of Science. During this time Goethe supported Bedemar (already being an extraordinary member) to become vice president of the "Mineralogische Societät" in Jena in 1820. Vargas-Bedemar sent many suites of minerals, amongst others lots of zeolites, to Jena. He followed Goethe as president and held this job till he died in Copenhagen in 1847.

The early history of mineralogy in southern Africa (1505-1850)

Master S

EGRI, School of Geosciences, University of the Witwatersrand
sharad.master@wits.ac.za

The history of mineralogy in southern Africa, prior to the famous discoveries of diamonds and gold in the late 19th Century, is relatively unknown. In the late 15th Century (1488-1500), Portuguese explorers discovered the sea route to India via the Cape of Good Hope. In 1505, Pedro de Nhaya wrote about the gold mines of Sofala, Mozambique - the first indication of the mineral wealth of southern Africa. The Portuguese, in Angola and Mozambique, were especially interested in commodities like Au, Ag and Cu, obtaining concessions from the local chiefs. In 1569, Francisco Barreto led a fatally disastrous expedition to conquer the legendary silver mines of the Kingdom of Chicova (Mozambique), along the Zambezi River. In 1575 his successor Vasco Fernandez Homem marched from the coast to the gold mines of Manica (Zimbabwe/ Mozambique) where he agreed on terms to facilitate peaceful commerce. In 1591 Edoardo Lopez reported on the Kingdom of the Congo, and on its Cu and Ag mines, and mentioned the Monts de Cristal, the Sierras de Sol, and the hills of Sal-nitrum or Saltpetre, in Angola.

In 1608 Jean Mocquet visited the gold mines of Mozambique and described how fine mesh nets were used in fast flowing rivers at the foot of gold-bearing mountains, after heavy rainfall, to capture gold nuggets, including one weighing ~15 oz. Francois Pyrard reported seeing, in 1610, a large specimen of pure dendritic gold, a cubit long, "branched like a coral", which had been found in the lower Zambezi River, carefully preserved, and was to be taken to Portugal as a present for the Queen of Spain. In the first, unsubstantiated, report of minerals from the Cape, in 1615 Sir Thomas Roe claimed to have discovered a rock containing quicksilver and vermilion. In 1647, the crew of the wrecked ship Haarlem in Table Bay discovered fresh water supplies, "clean white salt", and "pearls" (probably nacre from abalone shells), and this led directly to the establishment of the Dutch settlement at Cape Town, by the Dutch East India Company. Hondius (1652) reported that the country of the Cimbebas (in Angola) has "numerous crystal mines, quarries, and many other metals". The Governor Jan van Riebeeck enthusiastically pursued a spurious discovery of Ag at the Cape in 1654. In 1681, some Namaquas brought Cu ores to Cape Town, and Governor Simon van der Stel despatched two expeditions to Namaqualand, the second of which (1685-86) he led personally, leaving a team to do trial mining in the Copper Mountains under Bergmeester Friedrich von Werlinckhof, who produced the first mineralogical report in SA history (1686). In 1687-1688, von Werlinckhof and his successors dug shafts and galleries in wasteful pursuit of non-existent Ag ores at Zilvermyn, S. of Cape Town.

In 1719 Peter Kolb gave a basic description of rocks and minerals at the Cape. The first mining scam in SA history, which occurred in 1743-1748, involving a supposed silver mine on the slopes of Simonsberg NE of Stellenbosch, was exposed by gold- and silversmiths. In 1762 Karel Rykvoet produced a mineralogical report on the Cu mines of Namaqualand. The first new mineral discovered in South Africa was prehnite from the Cape, described by Heinrich Klaproth in 1787.

The first meteorite to be found in Southern Africa- the Cape of Good Hope meteorite, was found in the Eastern Cape by John Barrow in 1797. In 1811 Klaproth described further minerals from the Cape- "blue ironstone" (riebeckite?), and fibrous quartz. Friedrich Hesse (1820) described the rocks around Cape Town. In 1837 Dr Hehl published the first catalogue of minerals from South Africa, based on samples collected by Andrew Smith.

The history of the emerald in Brazil

Roeser H[1*], Kay S[2]

1 - Department of Environmental Engineering, Mining School, Federal University of Ouro Preto, Minas Gerais, Brazil *hubert-deamb@em.ufop.br 2 - Senckenberg Museum, Frankfurt, Germany.

Emeralds occur in all 5 continents of our earth. Famous emerald mines are located in Africa (Mozambique, Zimbabwe and Tanzania), India and Russia. From Europe, the occurrences of the Habachtal (Habach Valley) in Austria are known. Emerald from South America was associated, until the mid-sixties of the last century, almost exclusively with Colombia, where the significant emerald mines of Muzo and Gachala are situated. But within the last 40 years, Brazil has almost caught up as an important producer for this gemstone and is now one of the signified emerald producers in South America. Although the first emeralds in Brazil were discovered until in the early 20th Century this gem played an important role in the Brazilian - Portuguese colonial history. Green stones, wrongly interpreted as emeralds, initially gave the impetus during the 16th and 17th century for daring explorations into the uncharted interior of the South American continent. These expeditions were mainly organized by the so-called *"bandeirantes"* from the territory of the present-day state of São Paulo. They came specifically to the territory of today's Minas Gerais state. Time and again, the conquistadores thought they had found the treasured emeralds. On old maps appear "emerald mountains". Indeed, Fernão Dias Paes Leme (1608 - 1681) is heralded in historic accounts as "The Hunter of Emeralds." But, upon thorough examination, all 'finds' of the coveted gems turned out to be just green tourmaline. Significantly for Brazil, large deposits of gold and diamonds were found as well during these forays into the unknown jungle. This quickly led to extensive geological mapping of this territory and its subsequent economic and political independence. Named *"capitania"* at first, today this treasure-rich land is the Brazilian State of Minas Gerais.

It is an interesting twist of fate, that the gemstone, which made the most sensation in Brazilian history, and who had been crucial to the exploration of the interior of the colony, was discovered as one of the last Brazilian gemstones. This happened at the beginning of the 20th Century in *"*Bom Jesus dos Meiras*"* in the State of Bahia.

Today's most important emerald deposits occur in four Brazilian states:

- Bahia (Carnaíba): pegmatite, quartzite, ultrabasic rocks (serpentinites - serpentinitic schists) and within them metasomatically influenced rock.

- Goias (Santa Terezinha de Goias in Campos Verdes) carbonate leading talc schists and rounded bulbous deposits of biotitic schists.

- Minas Gerais (Belmont Mine and Rocha mine at Itabira and the "garimpos" - gem-diggings - "Capoeirana" , "Cantagalo" and "Toco". These emerald mines and occurrences are combined under the name of occurrences of Sta. Maria de Itabira). A basement mainly of granitic - granodioritic gneisses overlain by a volcano - sedimentary sequence of mica schist's, pelitic gneisses, with various types of amphibolites, schists and phyllites of ultrabasic - ultramafic nature.

- Tocantins (Monte Santo). Meta-ultramafic rocks of the formation "Xambioá" in contact with nepheline syenites of the "Monte Santo" Suite.

Looking ahead at the next 100 years: the centennial and the Kirwin Collection at the Royal Ontario Museum

Tait K

Royal Ontario Museum ktait@rom.on.ca

The Royal Ontario Museum (ROM) in Toronto, Canada is celebrating its centennial year this year. Looking forward to the next 100 years, the ROM is acquiring a large private collection from Bangkok, Thailand. At just over 25,000 pieces, this new collection will be incorporated into the museum's growing mineral and ore collections. Doug Kirwin is an exploration geologist with over 35 years of experience and has an excellent eye for not only aesthetic samples, but educational and collector pieces as well. His unprecedented access to mines grew this collection representing approximately 574 deposits, from 47 countries.

Asia is particularly well represented as with the outstanding suite of minerals from the Mogok area in in Myanmar and the Luc Yen region of Vietnam. Another highlight is an extensive suite of minerals from the alkalic intrusive rocks of Russia's Kola Peninsula.

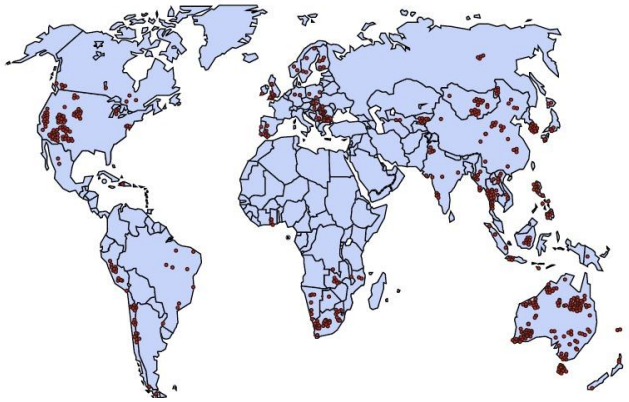

In order to make room for this large collection, the ROM has been fundraising to completely renovate the collection storage space, to build a classroom/boardroom with wireless capabilities, to digitize the collection and make thousands of images accessible online, a broader audience that just in Canada. The "Rock of Ages gala" at the ROM was a sold-out ticketed event that kicked off this fundraising campaign that was anchored by several large donations from the mining community and private donors. Plans are now underway to upgrade the collection space currently with compact storage and Delta-style cabinetry and build a low rH storage area for humidity sensitive material.

We anticipate the Kirwin collection can be used to develop any number of educational entry points. Its most immediate use in terms of the Centre of Earth and Space is to develop university-level and continuing-education level training. There is no question that this collection has significant teaching potential for training future and existing geologists, but it cannot be overlooked that there is equal and arguably broader potential to have our general visitor understand the natural world they live in and connect to certain places, colours, textures that are represented in these specimens.

Mineral species resource information – preliminary investigation and its relative problems

Yang L*, Cao X, Ye Q, Wang Y, Fu C, Dong J, Geng Z, Jiang N

The Geological Museum of China *liangfeng_yang@hotmail.com

Using the IMA-CM mineral species catalogue of 4,782 kinds of valid mineral species, each valid mineral species was searched for in the Chinese scientific community open literature database such as CNKI, WanFang, etc., and then the results were analyzed and summarized. The preliminary achievement shows that more than 900 kinds of mineral species are found in China. These mineral species specimens are scattered in the large or small diverse kinds museums throughout China; and most of them are kept in the Geological Museum of China (GMC). Among these, 116 kinds were new minerals. In the GMC's mineral specimen database, including more than 1,500 kinds of mineral species from all over the world, about 400 kinds of mineral specimens were found from China; more than 90 kinds are new minerals species found from China. More than 70 of these new mineral species were included in IMA-CM mineral species catalogue. On the other hand, the initial use of minerals in China is ancient, mainly used in Chinese medicine, Taoism, jewellery accessories, mineral pigments and smelting areas. Mineral medicine records in China exist dating as far back as 4,000 years ago. The earliest record about mineral resources in ancient China is "Shan Hai Jing", written before 475 BC, which may be the first systematic book in the world about rough mineral information. More than 70 kinds of minerals were recorded in that book. To better reflect the Chinese mineral species resource information, and to provide a reference for mineralogical studies and archaeological research, based on GIS technology, the Chinese mineral species resource geographic information system was established. Its data includes the IMA-CM mineral species catalogue, new minerals first discovered from China, mineral species discovered in China, medicinal minerals, GMC stored minerals species specimens from China, main aesthetic minerals from China.

Problems: (1) due to various reasons, many mineral species specimens were not collected and stored in museums; (2) most of the units, including museums, pay little attention to collect different and series mineral species specimens, but rather collect the aesthetic and showy minerals; (3) various reasons make the information about Chinese new minerals in IMA-CM mineral species catalogue incomplete and inaccurate; (4) information of ancient Chinese minerals is messy and insufficient; but study on geographic information of mineral species, including ancient Chinese mineral, would enrich medicinal mineral research and geo-archaeology research.

Acknowledgements: This paper was financially supported by the Land and Resource Ministry, China (Ministry Budget Project, 1211131181003).

Microminerals from the Bushveld Complex, South Africa

Atanasova M[1*], Cairncross B[2], Windisch W[3]

1 - Council for Geoscience *mtg@geoscience.org.za 2 - University of Johannesburg 3 - Self-employed

The Bushveld Complex is world famous for its spectacular geology and platinum-chromium deposits [1]. It covers an area of approximately 65 000 km^2 and is therefore the largest layered complex in the world.

The Bushveld Complex lithostratigraphy comprises four subdivisions, the Rooiberg Group (acidic rhyolites, dacite and basaltic andesite), Rustenburg Layered Suite, Rashoop Granophyre Suite and the Lebowa Granite Suite. The Rustenburg Layered Suite consists of the Marginal Zone norite, overlain by Lower Zone pyroxenite and harzburgite. The overlying Critical Zone contains the spectacularly layered pyroxenite, anorthosite, chromitite, norite and the platinum-bearing Merensky Reef, the largest known resource of platinum-group elements (PGE's) in the world that also contains substantial amounts of nickel, copper, cobalt, and gold. The Main Zone and the Upper Zone consists of gabbronorite and diorite. Granophyres and granites overlie the Rustenburg Layered Suite. At least ten chromitite seams occur throughout the Critical Zone. Titaniferous magnetite occurs as layers close the top of the Rustenburg Layered Suite, as well as small cross-cutting intrusives within the Main Zone. These contain substantial reserves of vanadium ore.

What is less well known is the array of secondary microminerals that occur within the Bushveld Complex - most of these do not contain platinum or chromium [2]. These minerals are important for at least two reasons: 1) they record the physico-chemical alteration and changes that the Bushveld Complex underwent after its original intrusion, and 2) the minerals, some of which are extremely rare, add to the mineralogical database of minerals for South Africa as a whole. Examples of these include spectacular erythrite from Kruisrivier, parisite from Boekenhouthoek, koechlinite from Vergenoeg and bastnäsite-(Ce) from Slipfontein.

These microminerals originated either during metamorphism of the country rocks by the intruding Bushveld magma when invading fluids concentrated gold, silver, lead, zinc and aluminium, or during later alteration events. Hydrothermal action produced the mineralized veins of silver-galena-sphalerite ore that intersect gabbro at Argent, 80 km east of Johannesburg. Furthermore, hydrothermal deposits, related to acid magmatism, formed several ore bodies of considerable importance west and north of Bella-Bella [3], for example, cassiterite deposits in sandstone and shale in the Rooiberg area and the Buffalo Fluorspar Mine that was a major producer of fluorite from a stockwork of veins in granite of the Lebowa Granite Suite. A unique volcanic complex located 60 km north-east of Pretoria, enriched with fluorite, magnetite and hematite, contains the largest fluorite deposit on Earth, the Vergenoeg ore body. Vergenoeg is famous for its goethite stalactites and rare microminerals such as gearksutite, prosopite and nitrocalcite.

[1] Cawthorn R.G. *et al.* (2006). The Bushveld Complex. In: Johnson, M.R., Anhaeusser, C.R. and Thomas, R.J. (Eds.), The Geology of South Africa. Geological Society of South Africa, Johannesburg / Council for Geoscience, Pretoria, 261-281.

[2] Atanasova M. *et al.* (in press). Microminerals of the Bushveld Complex. Popular Geoscience Series. Council for Geoscience, Pretoria, South Africa.

[3] Crocker I.T. *et al.* (2001). The fluorite, cassiterite and sulphide deposits associated with the acid rocks of the Bushveld Complex. *Memoir 90*, Council for Geoscience, Pretoria, 152 pages.

X-ray diffraction: a didactic tool in the construction of geoscience collections

Bittar S M B[1*], de Brito Barreto S[2], Xavier P S[1]

1 - Universidade Federal Rural de Pernambuco *schulze@depa.ufrpe.br 2 - Universidade Federal de Pernambuco

The Interactive Rock and Mineral Museum (MIMR) of the Federal Rural University of Pernambuco (UFRPE) in Northeast Brazil, was created in 2007. The central principle of the MIMR is to develop, preserve and protect the amazing amount of mineral and rock samples found in the Geological Laboratory of the Agronomic Department of UFRPE. In the past, some of these samples were part of reference collections acquired through purchase or donations, but the lack of infrastructure and trained staff resulted in the loss of these collections and any records of them. Some didactic collections were prepared as a way of utilizing these samples and to help in the teaching and learning process. Most of these collections can be used by students in practical classes and, as a result, the term interactive was proposed for the Museum. The main collections existing in MIMR are: (1) Systematic Classification of Minerals, made up of more than 60 samples representative from different classes; (2) Rocks from the Earth's Crust, with 40 samples that represent the most important kinds of igneous, metamorphic and sedimentary rocks; (3) Fossils from Araripe Basin in northeast Brazil, consisting of 100 described and cataloged examples, some of which are displayed in a special showcase; (4) A collection of Gypsum from Araripe Basin, including different varieties with unusual color and crystal formation; (5) Didactic Kit of Main Rock Constitution Minerals made up of 17 samples numbered and packed in a plastic box, an explanatory folder and a magnet hand, a glass slide, a porcelain plate and a bottle dropper with HCl (10%), that can be useful in sample descriptions and identification; (6) Physical Properties of Minerals, which consists of 8 sets illustrating proprieties such as: hardness, diaphaneity, fracture, cleavage, luster, color, streak and crystal habit; (7) Texture and Structure of Rocks, nowadays with more than 60 samples; (8) Didactic Kit of Rocks, made up of 14 samples numbered and packed in a plastic box and accompanied by an information sheet. The first three collections are permanent exhibitions, and cannot be touched by visitors to the museum. The others are used in normal classes and also in activities involving elementary school students. Although the MIMR has organized these collections described above, an amazing number of samples in its technical reserve still need to be identified. In order to identify these mineral samples, and subsequently add them to the MIMR collections, a new methodology using student participation was introduced in 2011. The idea is to use practical classes for the students to describe the physical properties and try to identify the mineral using the mineral identification key. First of all, the sample is described to at least three different students who then try to identify the mineral. However, some samples cannot be identified through the macroscopic descriptions or even with stereomicroscope assistance. So students get a small piece of mineral which they crush and prepare to make the X-ray diffraction analysis. Finally they identify the mineral, using the usual procedure that compares the strongest peaks with those which have been previously recorded. As a result, more than 40 samples were introduced into the MIMR, and a new special collection is being developed. The collection aims to create a virtual database with the mineral picture, its physical properties and the X-ray diffraction pattern. This new didactic tool will undoubtedly enhance the MIMR's collection.

Museum of minerals and rocks: geoscience cultural heritage in northeast Brazil

de Brito Barreto S[1*], Rodrigues da Silva T[2], Bittar S M B[3], Jussara P[1]

1 - UFPE/Department of Geology *sandradebritobarreto@gmail.com 2 - UFPE/Department of Mining Engineering 3 - Universidade Federal Rural de Pernambuco

The Museum of Minerals and Rocks, at the Federal University of Pernambuco, was inaugurated in 1968. This Museum gathers collections of two older museums of geosciences, built in the 1950s in two educational institutions in geosciences, Escola de Geologia do Recife and Instituto de Geologia, both located in the city of Recife, state of Pernambuco. The collection consists of minerals and rocks nowadays numbering about 5,000 samples. The mineral and rock collections show the development of the scheelite and industrial minerals mines on skarns and pegmatites. These mines are situated in the northeast of Brazil, in the region of Borborema Province, especially Rio Grande Norte and Paraíba states. The mineral and rock collections consist of reference collections bought for the beginning of geoscience education on that time. The development of teaching and research in geosciences allowed the creation of teaching collections and collections intended for the museum.

Throughout the history of the museum, into the collection were incorporated various scientific instruments produced in the first half of the twentieth century, which nowadays are part of a collection consisting of about 100 pieces including goniometers, thermometers, refractometers, compensators, scales and microscopes of various models, produced primarily on metal and glass, wood, plastic and resin components. These objects of S&T come from the divisions of Mineralogy, Petrology and Paleontology of the former Institute of Geology (1957), from the offices of professors of Geology and Mining Engineering, from the laboratory of Mineralogy Optics, Department of Geology, from the former laboratory of X-rays diffraction analyses and from the classroom mineralogy of UFPE. The vast majority have German origins and the collection is quite heterogeneous when it comes to manufacturers. We identified several European houses such as Ernst Leitz (Wertzlar - Germany), Carl Zeiss - (Winkel - Germany), Hertel & Reuss (Kassel - Germany), Stoe & Cie (F. Rheinheimer Heidelberg - Germany), Nonius (Delf - Netherlands) and to a lesser extent, North American (Eimer & Amend - New York), Japanese (Rigaku Denki Co. Ltd.), and Brazilian manufacturers (Asca - RJ / SP / RS), among others. Recently, the museum in 2013 had a donation of a collection of geophysical instruments named after Profesor Helmo Rand, who was a pioneer in teaching and research of geophysics in the northeast of Brazil. The collection includes 245 documents (scientific books, literature, periodicals, photographic registers of field trips and meetings) and 25 instruments (altimeters, scintillation, resistivity, magnetometers, geophone, seismographs, arms and precision balance). The instruments are manufactured mostly in USA and secondarily Sweden, Germany and Japan. This is a very significant collection in the fields of mineralogy, petrology and geophysics, especially when it comes to training of geologists, mining engineers and natural historians. This paper expects to be a way to present its collection to the geoscience community and to value this cultural heritage.

The historical mineral collections of the University of Liège, Belgium

Hatert F

University of Liège fhatert@ulg.ac.be

The Laboratory of Mineralogy, University of Liège, possesses a mineral collection mainly consisting of old and historical samples, preserved since the middle of the 19th Century. The first entries in the collection are reported by Gustave Dewalque (1826-1905), who was Geology Professor from 1857 to 1897. A nice meteorite collection was built at that time, with 3 Belgian samples (Tourinnes-la-Grosse, Lesves, and St-Denis-Westrem) and several famous European meteorites (Ensisheim, L'Aigle, Château-Renard, Orgueil, Juvinas).

In 1891, Giuseppe Cesàro (1849-1939), born in Naples, Italy, was appointed to the mineralogy chair. Cesàro was a great mathematician and crystallographer; he can be considered as the founder of the mineralogy and crystallography school of Liège. He was teacher of mathematics for the King Leopold III of Belgium, and was the mentor of the famous crystallographer J.D.H. Donnay. The Cesàro collection mainly consists of calcite crystals collected in Belgian limestone quarries; the morphology of these samples was investigated by Cesàro, who annotated all crystal faces. Many calcite samples were collected in the Rhisnes quarry, in which Cesàro described a new morphology: the isoscelohedron, for which Rhisnes can be considered as the "type locality".

In 1939, the Mineralogy Institute bought the complete collection of the famous French mineralogist Henri Léon Ungemach (1879-1936), from Strasbourg. The Ungemach collection is a first-rank collection, since it is mainly constituted by old historical European samples, many of which were collected in famous mines like Freiberg (Germany) or Sainte-Marie-aux-Mines (France). During the Second World War, the collection was seriously damaged by fire, but the majority of these unique samples are still preserved.

Henri Buttgenbach (1874-1964) was mineralogy Professor from 1921 to 1945. After the Second World War, he decided to rebuild the collection, and received samples from many international museums and universities. He was responsible for several prospecting campaigns in Katanga, Congo, where he found and described many new copper- and uranium-bearing mineral species. The holotypes of these species, for example fourmarierite, sharpite, cornetite, and buttgenbachite, are a significant part of our mineral collection.

Finally, more recent samples were also introduced in the collection, resulting from the research projects of Joseph Mélon (1898-1991), André-Mathieu Fransolet (1947-), and Frédéric Hatert (1974). These samples contain many holotypes, as for examples those of viséite, vantasselite, graulichite-(Ce), ferrorosemaryite, and qingheiite-(Fe^{2+}). These historical samples are actually not accessible to the public; however, in a few months, they will be exhibited in a new and secure room.

Mineral collection of the Fossa Magna Museum, Itoigawa, Niigata, Japan. The candidate venue of the next M&M8 in 2016

Miyajima H

Fossa Magna Museum. mac314@mac.com

Introduction

Preparation for the next M&M8-2016 conference has already begun in Itoigawa City, Niigata Prefecture, Japan. We would like to introduce the outline of Itoigawa, and the characteristic mineral collection in Fossa Magna Museum, Itoigawa.

Itoigawa is located 220 km northwest of Tokyo. Its land is mountainous especially in the south with 2,766 meters vertical drop, and faces the Sea of Japan in the north. It is situated at the northern end of the great fault, Itoigawa-Shizuoka Tectonic Line (ISTL), which geologically separates Northeast and Southwest Japan. The western region of ISTL is characterized by the serpentinite melange with high-P/T type schists and various fragments of Palaeozoic accretionary complexes composed of greenstone, limestone, chert and mudstone, etc. The fascinating minerals recognized here were identified from jadeitite, albitite, nephrite and rodingite in the serpentinite melange. It should be emphasized that many Sr-dominant minerals are found in this area.

Most famous mineral from Itoigawa

The most famous mineral from Itoigawa is jadeite of gem quality. Use of the jadeite of this area had started about 7,000 years ago. This is the oldest Jadeite culture in the world. Ancient jadeite artifacts such as carved beads and large pendants have been excavated in several hundred localities, mostly in graveyards, all over Japan. It is now widely accepted that these jadeite artifacts originated from Itoigawa area. The jadeite of Itoigawa was no longer used after the middle of the 8th century, and was forgotten till 1938. The reasons are unknown. Jadeite boulders exceeding 100 tons have been recovered from the river bed in Jade Gorge, which has been designated as a Natural Monument of the Nation. There are various colors in jade from Itoigawa. Green jade is not Cr-bearing jadeite but Fe-bearing omphacite. Lavender color jade is Ti-bearing jadeite. Black jade is jadeitite containing with tiny graphite. Blue jade is Ti-rich omphacite.

New minerals from Itoigawa

Six new minerals are discovered from Itoigawa, and these are all Sr-dominant silicates: ohmilite, strontio-orthojoaquinite, itoigawaite, rengeite, matsubaraite, clinozoisite-(Sr). Ohmilite [1] and strontio-orthojoaquinite [2] were discovered from magnesioriebeckite-bearing albitite. Itoigawaite [3], rengeite [4] and matsubaraite [5] occurred in jadeitite. Clinozoisite-(Sr) [6] was discovered in diaspore prehnite rock. Itoigawaite, Sr-analogue of lawsonite, shows very beautiful blue.

Minerals from Japan first found in Itoigawa

Jadeite, Xonotlite, Edenite, Eckermannite, Benitoite, Leucosphenite, Stronadelphite, Shandite, Tausonite, Lamprophyllite, Thomsonite-Sr, Preiswerkite

Jadeite was first discovered from Itoigawa in Japan [7]. Five species of these are Sr-dominant minerals.

Rare minerals from Japan first found in Itoigawa

Stronalsite, slawsonite, kosmochlor, omphacite, celsian, banalsite, Sr-analogue of margarite, corundum, epidote-(Sr), strontianite. Five species of these are Sr-dominant minerals. Kosmochlor, Cr-analogue of jadeite, shows bright green. Although this mineral was discovered in 1977, the first discovery of kosmochlor from terrestrial rocks, regrettably it has not yet been not published.

[1] Komatsu M. *et al*. (1973). *Mineralogical Journal*, 7, 298-301.

[2] Chihara K. *et al*. (1974). *Mineralogical Journal*, 7, 395-399.

[3] Miyajima H. *et al*. (1999). *Mineralogical Journal*, 63, 906-916.

[4] Miyajima H. *et al*. (2001). *Mineralogical Journal*, 65, 111-120.

[5] Miyajima H. *et al*. (2002). *European Journal of Mineralogical*, 14, 1119-1128.

[6] Miyajima H. *et al*. (2003). *Journal of Mineralogical and Petrological Sciences*, 98, 118-129.

[7] Kawano Y. (1939). *Journal of Japanese Association of Mineralogy, Petrology and Economic Geology*, 22, 195-201.

Afwillite to willemseite: biographical and mineralogical insights into South African type-minerals named after South Africans

Moitsi E, Cairncross B*

University of Johannesburg. *brucec@uj.ac.za

South Africa is home to 68 type minerals (as of March 2014). Of these, 36 are named after people, 15 after their type-locality, 15 after chemical composition and 2 species are acronyms [1, 2]. Of the 36 named after people, only one third are named after South Africans *per se*. "South Africans" are defined here as South African citizens (i.e., born in South Africa) or individuals who have either lived substantive periods in the country and/or made significant contributions to South African mineralogy and/or geology.

The geological settings and main mineralogical aspects of these type-minerals will be presented, together with geobiographical insights into the individuals after whom the minerals were named, highlighting some of their achievements that resulted in minerals being named in their honour. Some were (are) academics (cairncrossite, geversite*,mathiasite*, mountainite*, willemseite*), some leaders in related industries (afwillite*, hawthorneite, liebenbergite*, merenskyite*), one mineral dealer (colinowensite), one medical doctor, an expert on the Kalahari manganese field minerals (vonbezingite) and one the wife of the discoverer of the type-species (clairite). (*= deceased).

The first mineral named after a South African was in 1925 and most recently as 2013. The Transvaal Supergroup (Kalahari Manganese Field), kimberlites and the Bushveld Complex and a cave deposit are host to the type-minerals named after South Africans. In recent times, most of the research related to quantifying type-species from South Africa, has taken place either in Europe or the USA, notwithstanding co-authorship by South Africans. In the past 22 years, non-academics have been responsible for discovering the three most recent type-minerals (1992-2013).

Table 1. South African mineral type-species named after South Africans, listed chronologically.

MINERALS	DATE	Mineralogy
Afwillite	1925	$Ca_6Cu_3(SO_4)_3(OH)_{12}.2H_2O$
Mountainite	1957	$KNa_2Ca_2[Si_8O_{19}(OH)].6H_2O$
Geversite	1961	$PtSb_2$
Merenskyite	1976	$(Pd,Pt)(Te,Bi)_2$
Willemseite	1968	$(Ni,Mg)_3(Si_4O_{10})(OH)_2$
Liebenbergite	1973	$(Ni,Mg,Fe,Co)_2SiO_4$.
Clairite	1983	$NH_2Fe_3(SO_4)_4(OH)_3.3H_2O$
Mathiasite	1983	$(K,Ca,Sr)(Ti,Cr,Fe,Mg,Zr)_{21}O_{38}$
Hawthorneite	1989	$Ba(MgTi_3Cr_4Fe_4)O_{19}$

[1] Daltry V.D.C. (1997). Mineralogy of South Africa: Type-mineral species and type-mineral names. Handbook 15, Council for Geoscience / Geological Survey of South Africa, Pretoria, South Africa, 114 pages.

[2] Gait R.I. (2002). African type-minerals: minerals first described from African localities. *Rocks & Minerals*, 77, 25-30

Formation of phosphates in ceramic pots: subsidies for understanding the origin of phosphor in ceramic fragments in archaeological dark earth soils

Rodrigues S[1], Costa M[1*], Pöllmann H[2], Göske J[3]

1 - Federal University of Pará *marcondeslc@gmail.com 2 - Martin-Luther University 3 - Zentrum für Werkstoffanalytik Lauf

High concentrations of phosphorous in the ceramic fragments found within so-called 'archaeological dark earth' (ADE) in the Amazon region- Brazil is well known but its origin is still controversial. Most of the studies suggest that phosphorous originates from food preparation by cooking. However, some researchers propose soil contamination during burial as cause of the high amount of phosphorous in ceramics. In order to investigate if P-enrichment is due to contamination by cooking, six ceramic pots were produced according to the techniques employed by traditional populations. The raw materials (clay and temper) and the pots producing by cording (firing about 600°C) were characterized by X-ray diffraction (XRD) for mineralogy and by ICP-OES and ICP-MS for bulk chemical composition. Afterward the pots were set in contact (200 h, 220h, 240h, 260h, 280h and 300 h) with P and Ca-rich solutions (0,3 wt.%) at the temperature around 110 °C in order to simulate cooking conditions. The chemical analyses show that calcium and phosphate were incorporated within the pot walls including the lid. The XRD analyses detected variscite, an aluminium phosphate, but no Ca minerals. Possibly Ca and most of P were not in contact with the fired clay body long enough to form crystalline phases. An example could be the amorphous Ca-Al phosphates already described in several ceramic fragments from ADE. Another example could be the crystalline solid solution (crandallite- goyazite) from other sites in Amazon. In conclusion, the presence of phosphor in ceramic fragments from ADE can be a product of food cooking, insofar as the Ca-P solution may well represent the water solution coming from fish and meal cooking.

Key words: variscite, calcium, phosphor, cooking, XRD analysis

Mineralogical witnesses of the Brazilian gold rush in museums and churches along the Estrada Real in Minas Gerais

Roeser H[1*], Leonardo Brabosa G[1], Maria Margarete M[2], Kay S[3]

1 - Mining School, UFOP, Ouro Preto, Brazil *hubert-deamb@em.ufop.br

2 - Inconfidencia Museum, Ouro Preto, Brazil 3 - Senckenberg Museum, Frankfurt, Germany

Green stones, wrongly interpreted as emeralds, initially gave the impetus during the 16th and 17th century for daring explorations into the interior of the Portuguese colony of Brazil. These expeditions were organized by the so-called "bandeirantes" from the territory of the present-day state of São Paulo. They found large deposits of gold and later diamonds in the "capitania" of Minas Gerais, today the Brazilian State with the same name. The subsequent gold rush lasted until the mid-18th Century.

Over time, they constructed a path, which became known as the "Estrada Real" (Imperial way). It goes from Paraty (or the second younger possibility: Rio de Janeiro) via Ouro Preto to the diamond fields of Diamantina.

Along this road you can see the results of the gold rush in many historical cities until today. The largest are: Paraty - Rio de Janeiro - Tiradentes - São Jão del Rey - Brabacena - Ouro Preto - Mariana - Sabará - Diamantina. Hundreds of gold-decorated churches and many museums (e.g. the Gold Museum in Sabara) bear witness to this glorious time. The city of Ouro Preto owes its foundation, its wealth and its name from the gold.

In addition to many others in the region, two main institutions preserve in Ouro Preto the memory of this gold rush time: the Mineralogical Museum of the School of Mines, founded in 1876, and the *Museu da Inconfidência*. In the first one, the former Governor´s Palace, today Mining School, we find the mineralogical evidence, in the second one the testimonies of cultural and social traditions of that epoch.

In the showcases of the first one, many gold samples are drawn from gold-rock as well as placer gold. In between them, a classical gold quartz vein sample with the paragenesis of covellite, pyrite and gold from the Ouro Fino Mine near Bento Rodrigues in the neighbourhood of Ouro Preto. In addition, the famous specimens of the black gold are exposed. The gold nuggets are black because fine skins of iron oxide surround them. They gave the city its name Ouro Preto = Black Gold. Other rarities are the palladium gold (Au,Pd) and palladium-containing minerals [atheneite - $(PdHg)_3As$; arsenopalladinite $(Pd_8(As,Sb)_3$; stibiopalladinite (Pd_5Sb_2)] from the area.

The other museum, also located in the city´s downtown opened in 1944. The building, which today houses documents of the regional history, was created to be the Chamber of Deputies and public jail in the colonial time.

It contains many things from the gold mining and industry. One room is devoted exclusively to the gold rush time. In it are exhibited a model of an old gold mine, old mining tools, such as miner's lamps and picks but also equipment for the gold processing such as melting pots, gold-scales and others. In addition, the museum shows many daily utilitarian objects that represent the cultural and social realities of the gold rush era.

Moreover, the city has other witnesses of the gold rush, 6 other museums, 14 Baroque churches, chapels and many historical monuments. Due to its historical significance and good preservation, the city was in 1980 recognized by UNESCO as an International Monument of Mankind.

Integration of process mineralogy into the undergraduate education of mineral processors at Hacettepe University

Celik I[1], Can M[2], Bradshaw D[2*]

1 - Hacettepe University, Dept. of Mining Engineering, Ankara, Turkey 2 - Julius Kruttschnitt Minerals Research Centre, University of Queensland *d.bradshaw@uq.edu.au

The field of 'process mineralogy' combines an understanding of the mineral treatment together with the characteristics of the minerals and their effects on the economics of the process. It is becoming increasingly important and it has been recognised that there are appropriately educated and trained people at all levels. At Hacettepe University in Ankara Turkey, where Mineral Processing is part of the Mining Engineering Department, there has always been the inclusion of some geological foundation in the curriculum, such as the 2nd year course in classical Mineralogy and Petrography, but until 2013 no explicit course in process mineralogy. The development of expertise in process mineralogy strengthened in the department in the early 2000s with some applied research focused on diagnosing reasons for poor flotation performance in a nearby operation. In 2003, an optical system, Clemex was obtained and Dr David Sutherland, a specialist Process mineralogist from CSIRO, Australia joined the department as a visiting academic. The successful application of process mineralogy to solving this and other problems led to it being included in more post graduate projects and short courses being offered at a post graduate level and to Industry. However, because many of the graduate engineers went directly to industrial metallurgical positions, they required this knowledge as part of their undergraduate engineering degree and in 2013 process mineralogy was introduced as a formal course for third year students at Hacettepe University.

The goal of the undergraduate course is to teach students to identify and scope the questions that need to be answered and which tools should be used. They are taught how to manipulate the data accordingly. Real world examples are given from the stage of exploration of an ore body, laboratory testing, plant design and optimization, plant auditing and finally the tailings treatment. The course evaluation from the students was excellent and they felt that it gave them the competency needed as a foundation for their careers and the decisions that they would need to make in the future. It is expected that this course will go from strength to strength, equipping the Hacettepe University graduates and thereby strengthening the Mining Industry as a whole.

Mineralogy for metallurgists and process engineers – an integral part of Mintek's graduate development programme

Chetty D[1], Mngomezulu A[2]

1 - Mineralogy Division, Mintek, Randburg, South Africa *deshc@mintek.co.za 2 - Executive management, Mintek, Randburg, South Africa

Mintek, formerly known as the Council for Mineral Technology, undertakes research investigations and testwork towards serving the minerals beneficiation sector both in South Africa and globally. As such, the technical staff complement at Mintek comprises, chiefly, scientists, metallurgists and engineers. In order to help new graduate recruits adjust to the Mintek environment, and obtain a broad, practical understanding of organisational activities, Mintek has initiated an annual graduate development programme (GDP), for its new graduate recruits, which involves rotation amongst its various divisions. This builds skills within, and knowledge of, the organisation, so that new graduate recruits can ultimately make informed decisions regarding their career paths, particularly within the Mintek context of activities.

Given the highly specialised nature of process mineralogy at Mintek, an interactive course has been devised as part of the GDP to help the graduates understand what process mineralogists do, how they do it, and importantly, why they do things in a certain manner. X-ray diffraction (XRD), optical and scanning electron microscopy (SEM), automated SEM and other mineralogical techniques are covered, in the context of the quality and type of information obtained, and how this information can be used to benefit metallurgical operations. Emphasis is placed on case studies involving mineralogical applications in comminution, physical separation, flotation, hydrometallurgy and pyrometallurgy to show the importance of mineralogy in decision-making for beneficiation operations. Common misconceptions and assumptions are discussed, as is the data quality versus cost versus turnaround time triangle, in highlighting the importance of effective communication in project management. The course thus aims to engender better understanding between metallurgists/process engineers and process mineralogists in facilitating future client-supplier relationships, since the majority of graduates become the clients of the process mineralogist in beneficiation projects.

The GDP is into its third year, and positive feedback has been received from the mineralogy course, which promises more effective beneficiation project outcomes, but also improved staff retention within the organisation as a whole.

Is geometallurgy teachable? A challenge for a new Erasmus Mundus master course

Pirard E*, Leroy S

University of Liège. *eric.pirard@ulg.ac.be

Within a few years' time, geometallurgy has become a sesame password for everyone concerned with the technical optimization of mining and metallurgical operations. Most often, it is being used abusively to designate any kind of advanced ore characterisation prior to mineral processing operations while in fact it should clearly refer to a multidisciplinary integration of geological, mining, metallurgical, environmental and economic information into a single orebody model.

In order to instil the best available geometallurgical practices in the professional world, it seems essential to break the traditional cleavages among disciplines and educate a new generation of engineers. The Erasmus Mundus EMerald "Master in Georesources Engineering" program, initiated by four European universities under the coordination of University of Liège, has been designed to exactly tackle this challenge. It is not surprising that this program has been set up by universities having a long tradition in mixing a double perspective of geology and engineering (Nancy; Luleå; Liège and Freiberg). Geometallurgy requires both an excellent understanding of the natural variability and complexity of an ore and a comprehensive overview of the techniques available to extract and concentrate any valuable material.

The course program has been designed to achieve a right balance between knowledge of mineral resources (geology, resource characterisation, reserve estimation, modelling) and processing (comminution, preconcentration, leaching, waste disposal, etc.). It also includes a broader view on life cycle analysis and urban mining. A series of professional seminars, suggested by an industrial advisory board, shed light on strategic issues, economic and environmental challenges, corporate social responsibilities, etc.

Mobility and multicultural experience is an added-value of the Erasmus Mundus experience which definitely contributes to breeding engineers for tomorrow.

Celebrating IYCr – developing a low cost workshop for science centres

Reinhardt T

University of KwaZulu-Natal - Science and Technology Education Centre.
reinhardtt2@ukzn.ac.za

Every year Science Centres around South Africa are faced with the challenge to design activities revolving around "International year" themes. Specific sciences on which an "International Year" focuses need to be promoted to learners.

The Science and Technology Education Centre (STEC) at the University of KwaZulu-Natal, which includes the Geology Education Museum, planned to carry out a crystallography workshop to promote the International Year of Crystallography at the Science Centre itself and at Science Festivals. One of the requirements for the workshop was that we would be able to complete the workshop within 60-90 minutes. It also needed to be low cost, not computer-dependant, hands-on and suitable for South African higher-grade learners.

Research on the International Year of Crystallography website revealed that the education material offered was not always suitable for the age group we wanted to target or they were too time-consuming such as the crystal growing activities. We therefore decided to design our own workshop around the theme. As crystallography includes many different aspects such as symmetry and crystal structures we needed to focus on a particular facet.

What we wanted the learners to appreciate is that minerals have a three-dimensional crystal structure and that the crystal structure in combination with the chemical composition determines what type of mineral it is. We also wanted them to understand the process of how one obtains information about crystal structures.

Mineralogy and in this case the understanding of crystal structures of minerals covers abstract concepts of chemistry were learners are requested to understand atomic or molecular structures in three-dimensions, concepts that learners and even University students have difficulties to grasp. It has long been recognized that physical three-dimensional models of crystal structures are useful tools to help learners visualize these structures. We therefor decided to let them rebuild the crystal structure model of an "unknown" crystal and compare the model to a variety of other structures in order to determine what the unknown crystal is. Ball-and-stick models are routinely used in teaching at high school or university level, and ball-and-stick kits are available to build these models in groups. Unfortunately, such models come at a price. As one of our requirements was low cost we decided to use coloured sweets and toothpicks to build the models.

This workshop has been introduced at Scifest Africa in Grahamstown. The learners' response to this workshop is evaluated using a feedback questionnaire. Our future plan is to set up this workshop in other Science Centres around South Africa.

Teaching the future generation about mining and minerals – the introduction of mining and mineral processing as a topic in the South African school curriculum

Toerien R

University of Cape Town. trnren001@myuct.ac.za

When was the first time you heard about the mining industry? When was your first encounter with rocks and minerals? Why and how did you become a mineralogist? These are questions that can easily be taken for granted, but play an important role in educating a next generation in mining and mineralogy.

The mining industry is one of the biggest industries in South Africa, and has been so for a long time, yet learning about this industry generally only happens once you leave school. And only if you choose to study further in this field or happen to find a job in the industry.

This situation changed somewhat when the South African school curriculum was revised in the early 2000's and 'Mining and Mineral Processing' was included as a topic in the school science syllabus. For the first time in 2007 Grade 11 students (16/17 year olds) learned about one of the biggest industries in their country.

This new focus represented a fundamental shift from the previous curriculum as it makes the link between science, society and the environment explicit and aims to bring science into the homes of people. Students at school are now learning about extracting rocks from the earth and processing minerals to make useful products. The environmental impact of these industries is given priority, and students are beginning to think about how to work in an environmentally responsible way. In addition, the introduction of an applied topic opened up career opportunities for young people in South Africa.

This presentation will highlight many of the benefits and some of the challenges of introducing industry-related content into a school curriculum. It will tell the story of how a tertiary education institution and the mining industry worked together to support teachers to teach about mining at school level in South Africa (Figure 1).

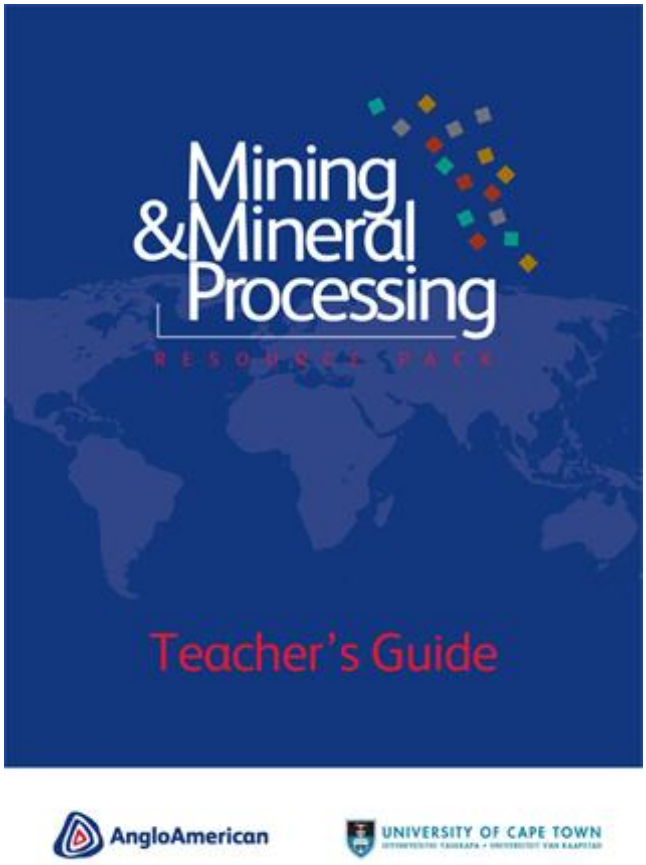

Figure 1: Cover from the teacher's guidebook

Waimirite-(Y), orthorhombic YF_3 from Pitinga Mine, Presidente Figueiredo, Amazonas, Brazil

Atencio D[1*], C. Bastos Neto A[2], P. Pereira V[2], T.M.M. Ferron J[2], M.V. Coutinho J[1], B. Andrade M[3], Domanik K[4]

1 - Inst.Geociências - USP, Brazil *datencio@usp.br 2 - Inst. Geociências - UFRGS, Brazil 3 - Inst. Física - USP - São Carlos, Brazil 4 - Lunar and Planetary Laboratory, Arizona, USA

Waimirite-(Y), orthorhombic YF_3 (IMA 2013-108), occurs in thin hydrothermal veins crosscutting the albite-enriched granite facies of an A-type Madeira granite (~1,820 Ma), Pitinga mine, Presidente Figueiredo, Amazonas, Brazil. Directly associated minerals are dickite and quartz. Other minerals in granite are "alkali feldspar", albite, riebeckite, biotite, muscovite, cryolite, zircon, polylithionite, cassiterite, pyrochlore group minerals, "columbite", thorite, lead, galena, fluorite, "xenotime", gagarinite-(Y), fluocerite-(Ce), genthelvite-helvite, topaz, "illite", kaolinite and "chlorite" [1]. The mineral occurs as thin veins (up to 3 cm thick) of platy crystals up to about 1 μm in size. Forms: not determined, but synthetic YF_3 displays pinacoids, prisms and bipyramids [2]. Colour: pale pink. Streak: white. Lustre: nonmetallic. Transparent or translucent. Density (calc.) = 6.092 g/cm^3 using the empirical formula. It is biaxial, mean n = 1.54 - 1.56. Microprobe (WDS) analyses (24): F 29.27, Ca 0.83, Y 37.25, La 0.19, Ce 0.30, Pr 0.15, Nd 0.65, Sm 0.74, Gd 1.86, Tb 0.78, Dy 8.06, Ho 1.85, Er 6.38, Tm 1.00, Yb 5.52, Lu 0.65, Al 0.10, Fe 0.07, Si 0.12, total 95.77 wt%. The empirical formula (based on 4 *apfu*) is $(Y_{0.78}Dy_{0.09}Er_{0.07}Yb_{0.06}Ca_{0.04}Gd_{0.02}Ho_{0.02}Nd_{0.01}Sm_{0.01}Tb_{0.01}Tm_{0.01}Lu_{0.01}Si_{0.01}Al_{0.01})_{\Sigma 1.15}F_{2.85}$. The simplified formula requires: Y 60.93, F 39.07, total 100.00 wt%. Orthorhombic, *Pnma*, *a* 6.386(1), *b* 6.877(1), *c* 4.401(1) Å, *V* 193.28(7) Å^3, Z 4 (powder data), *a*:*b*:*c* = 0.929:1:0.640. X-ray powder diffraction data [d in Å (I) (hkl)]: 3.707 (26) (011), 3.623 (78) (101), 3.438 (99) (020), 3.205 (100) (111), 2.894 (59) (210), 1.937 (33) (131), 1.916 (24) (301), 1.862 (27) (230). The name is for the Waimiri-Atroari Indian people of Roraima and Amazonas. Type material is deposited in the collections of the Museu de Geociências, Universidade de São Paulo, Brazil, specimen number DR919, and the Museu de Mineralogia Luiz Englert, Universidade Federal do Rio Grande do Sul, Brazil, specimen number 3620. The synthetic orthorhombic YF_3 has previously been obtained and its crystal structure was studied [3, 4]. The Y ion is coordinated by 9 F ions to give a slightly deformed trigonal prism with atoms opposite each of the lateral faces. Eight of the nearest neighbours lie at distances between 2.281 and 2.310 Å. The ninth distance is 2.538 Å.

[1] Bastos Neto A. *et al*. (2009). *Canadian Mineralogist*, 47, 1329-1357.

[2] Qian W. *et al*. (2010). *Cryst Eng Comm*, 12, 99-206.

[3] Zalkin A. and Templeton D.H. (1953). *Journal of the American Chemical Society*, 75, 2453-2458.

[4] Cheetham A.K. and Norman N. (1974). *Acta Chemica Scandinavica*, A28, 55-60.

Rruff.info/IMA

Downs R

University of Arizona. rdowns@u.arizona.edu

At the 2006 Kobe IMA meeting, the IMA council authorized the RRUFF project to produce an interactive website of the IMA approved mineral names and selected properties on behalf of the IMA outreach committee. This website is found at RRUFF.info/ima and contains the names and formulas of the CNMNC approved minerals, as well as links to the American Mineralogist Crystal Structure Database for structural data, the RRUFF project database for selected laboratory measurements of chemical, crystallographic and spectroscopic properties, and an extensive suite of pdfs of relevant articles from the literature. In this presentation, new data fields will be introduced, including cell parameters especially useful for searches on minerals without reported crystal structure data, enhanced chemical searches that include valence states and string recognition, and locality age dating that is being integrated into the website as part of the mineral evolution project that is led by Dr Bob Hazen. In addition, in order to promote private use of the IMA list of minerals, the software for the database has included an option to create links from the RRUFF.info/ima page to any independent database that will accept queries based on mineral names. These new features will be presented and their uses will be reviewed.

Gatedalite, a new Zr-rich braunite group mineral from Långban, Sweden

Hålenius U[1*], Bosi F[2]

1 - Swedish Museum of Natural History *ulf.halenius@nrm.se 2 - Sapienza University of Rome

A new Zr-rich braunite group mineral, gatedalite $ZrMn^{2+}_2Mn^{3+}_4SiO_{12}$, occurs as very rare, small (≤ 60 μm), rounded, grains in hausmannite-impregnated skarn at the Långban Fe-Mn deposit, central Sweden. Associated minerals are Mn-bearing calcite, hausmannite, jacobsite, Mn-bearing phlogopite, tephroite, långbanite, pinakiolite and oxyplumboromeite.

Gatedalite crystals are grey-colored opaque with a submetallic luster, brittle tenacity and greyish brown streak. The mineral has a Mohs hardness of approximately 6, and a calculated density of 4.78 g/cm^3. It is tetragonal, space group $I4_1/acd$, with the unit cell-parameters a = 9.4668(6) Å, c = 18.8701(14) Å, V = 1691.1(2) Å^3, Z = 8. The crystal structure of gatedalite (Figure 1) was refined to an R1 index of 3.53% using 1339 unique reflections collected with MoKα X-radiation. The strongest lines of the calculated powder diffraction pattern are [d, Å (hkl) I]: 2.730 (224) 100, 2.367 (040) 12, 2.155 (235) 6, 1.6735 (440) 12, 1.6707 (048) 29, 1.4267(264) 16, 1.4233 (2.2.12) 10.

Crystal chemical analysis of the holotype gatedalite (IMA 2013-091) resulted in the empirical formula: $(Zr^{4+}_{0.49}Mn^{2+}_{0.47}Ca_{0.02}Zn_{0.01}Ce^{3+}_{0.01})_{\sum 1.00}(Mn^{3+}_{4.44}Fe^{3+}_{0.59}Mn^{2+}_{0.50}Mg_{0.48}Al_{0.01})_{\sum 6.01}Si_{0.99}O_{12}$. Gatedalite is related to braunite ($Mn^{2+}Mn^{3+}_6SiO_{12}$) by the coupled substitution $^{M1}Zr^{4+}_1{}^{M2\text{-}4}Mn^{2+}_2{}^{M1}Mn^{2+}_{-1}{}^{M2\text{-}4}Mn^{3+}_{-2}$. The mineral is named in honour of the Swedish amateur mineralogist Kjell Gatedal (b 1947).

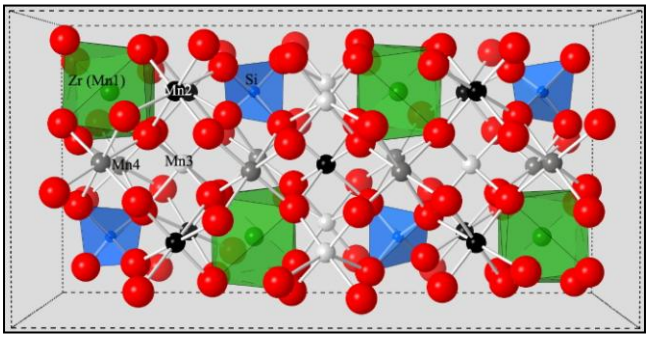

Figure 1: The crystal structure of gatedalite projected on [100]

A new nomenclature scheme for the alluaudite supergroup

Hatert F[*], Baijot M, Dal Bo F

1 - University of Liège, Belgium *fhatert@ulg.ac.be

The alluaudite supergroup consists of phosphates and arsenates, divided in two groups: The alluaudite group, characterized by monoclinic species with unit-cell parameters a ~ 12, b ~12.5, c ~ 6.5 Å, β ~ 114°, space group $C2/c$, and the wyllieite group, in which phosphates show similar unit-cell parameters with space group $P2_1/n$. Alluaudite-type phosphates, as well as minerals of the wyllieite group, occur in rare-element granitic pegmatites, whereas alluaudite-type arsenates are more frequently observed in ore deposits or in volcanic fumaroles.

The alluaudite structure is based on kinked chains of edge-sharing octahedra stacked parallel to {101}. These chains are formed by a succession of M(2) octahedral pairs linked by highly distorted M(1) octahedra. Equivalent chains are connected in the b direction by the $P(1)O_4$ and $P(2)O_4$ tetrahedra, to form sheets perpendicular to [010]. These interconnected sheets produce channels parallel to the c axis, which contain large sites generally occupied by large Na of Ca atoms. The wyllieite structure is topologically identical to the alluaudite structure, but due to an ordering provoked by significant amounts of Al, the space group is modified and the M(2) and X(1) (=A(1)) sites are split into M(2a)-M(2b) and X(1a)-X(1b) positions, respectively.

The crystal-chemical formula of alluaudites is $A(2)'A(1)M(1)M(2)_2[(P,As)O_4]_3$; it becomes $X(2)X(1a)X(1b)M(1)M(2a)M(2b)(PO_4)_3$ in wyllieites. In pegmatites, the large X and A sites are generally occupied by Na and Ca, while the octahedral M sites contain Mn, Fe^{2+}, Mg, Fe^{3+}, or Al. In arsenates, more exotic cations occur in the structure, as for example Zn or Cu, due to the unusual geochemistry of the environment in which these minerals crystallize.

The nomenclature of phosphates of the alluaudite group [1] uses the content of the M(2) site to determine the root name: alluaudites (Fe^{3+} dominant), hagendorfites (Fe^{2+} dominant), and varulites (Mn dominant). A prefix ferro- or mag- is then added to indicate if Fe or Mg are dominant on the M(1) site, instead of Mn.

A careful re-calculation of ca. 100 analyses of natural phosphates of the alluaudite group indicates that this nomenclature scheme is very difficult to apply. In pegmatites, many samples are completely oxidized, leading to a composition $[]NaMnFe^{3+}_2(PO_4)_3$ corresponding indeed to alluaudite. But compositions for which Fe^{2+} or Mn are predominant on M(2) are extremely rare; even the chemical analyses of type hagendorfite and varulite show a significant amount of Fe^{3+} on M(2).

Since alluaudite is produced by oxidation of hagendorfite, following the mechanism $Na^+ + Fe^{2+} = [] + Fe^{3+}$, we can easily obtain the ideal formula of parent hagendorfite: $Na_2MnFe^{2+}Fe^{3+}(PO_4)_3$. The ideal composition of varulite becomes $Na_2Mn_2Fe^{3+}(PO_4)_3$. In this new nomenclature scheme, we allow a valency-imposed double site occupancy on M(2), in order to take into account the extremely complex crystal chemistry of this group. Several new root-names will be defined in the near future, in order to complete the existing nomenclature of the alluaudite supergroup.

[1] Moore P.B. and Ito J. (1979). Alluaudites, wyllieites, arrojadites: crystal chemistry and nomenclature. *Mineralogical Magazine*, 43, 227-235.

New polyoxometalate minerals from the western United States

Kampf A[1*], Hughes J[2], Nash B[3], Marty J[4]

1 - Natural History Museum of Los Angeles County *akampf@nhm.org 2 - University of Vermont 3 - University of Utah 4 - unaffiliated

The field of polyoxometalate (POM) chemistry has been extremely active over the last few decades as POM clusters have proven to have a remarkable array of technological and biochemical uses. Thousands of POM compounds are now known and hundreds of new ones are synthesized each year. However, there are very few known POM or POM-like minerals. Best known are the pascoite family minerals, which contain the decavanadate cluster anion $[V_{10}O_{28}]^{6-}$, an isopolyanion. Over the last several years, our studies of the secondary mineralization in U-V deposits of western Colorado and eastern Utah have yielded many new members of the pascoite family, including the first protonated decavanadates, gunterite, $Na_4[H_2V_{10}O_{28}]\cdot 22H_2O$, and rakovanite, $Na_3[H_3V_{10}O_{28}]\cdot 15H_2O$, and first mixed-valence (V^{4+}-V^{5+}) decavanadate, nashite, $Na_3Ca_2[V^{4+}V^{5+}{}_9O_{28}]\cdot 24H_2O$. One these U-V deposits, the Packrat mine in Colorado, has also yielded four new phases containing the POM-like heteropolyanion, $[As^{3+}As^{5+}{}_6V^{4+}{}_{2+x}V^{5+}{}_{10-x}O_{51}]^{(11+x)-}$ (x = 0 to 1), which is new to science. Investigation of the secondary mineralization at the Ophir Hill Consolidated mine in western Utah (not a U-V deposit) has revealed the new mineral ophirite, $Ca_2Mg_4[Zn_2Mn^{3+}{}_2(H_2O)_2(Fe^{3+}W_9O_{34})_2]\cdot 46H_2O$, which contains the heteropolyanion $[Zn_2Mn^{3+}{}_2(H_2O)_2(Fe^{3+}W^{6+}{}_9O_{34})_2]^{12-}$, composed of a $[Zn_2Mn^{3+}{}_2(H_2O)_2]^{10+}$ octahedral layer sandwiched between opposing tri-lacunary $(Fe^{3+}W^{6+}{}_9O_{34})^{11-}$ Keggin anions. Ophirite is the first known mineral to contain a lacunary defect derivative of the Keggin anion, a heteropolyanion that is well-known in synthetic phases.

Walking in a tellurium wonderland

Mills S[1*], Christy A[2], Kampf A[3]

1 - Geosciences, Museum Victoria *smills@museum.vic.gov.au 2 - Centre for Advanced Microscopy, Australian National University 3 - Mineral Sciences Department, Natural History Museum of Los Angeles County

The Mojave Desert in the United States Southwest contains thousands of old mines and prospects, the vast majority of which were never economically profitable. However, a few deposits, though they produced little ore, are now recognized as world-class localities for secondary minerals, especially those that contain tellurium (Te). Tellurium is an unusual element in that its cosmic abundance is greater than that of any other element with an atomic number >40, as measured by relative number of atoms in C1 chondrite. Nevertheless, Te is one of the rarest elements in the Earth's crust (0.4–10 ppb) and also in seawater (up to 0.0009 ppb). It is thus 3-5 orders of magnitude less abundant than even-number elements that are nearby in the periodic table, such as tin and barium, and is, in fact, rarer than platinum or gold.

Given this fact, it is remarkable that thirteen new Te secondary minerals have been described from the Otto Mountain deposit alone. Study of these new phases has enabled us to understand much more about the role that Te plays in the environment, and has shown us the incredible diversity of Te oxysalt crystal structures. Using a number of dating techniques, we are also searching for links between the formation ages of these minerals and climatic fluctuations during the Quaternary.

As part of this project, we have also refined the bond-valence parameters for Te^{IV}–O, Te^{VI}–O and Te^{IV}–Cl [1] and established that the volumes of $Te^{IV}O_6$ polyhedra are also highly flexible, as a function of lone pair stereoactivity and the distribution of oxygens relative to the lone pair [2].

Acknowledgements: This study has been funded by The Ian Potter Foundation grant "tracking tellurium" to SJM, which we gratefully acknowledge.

[1] Mills S.J. and Christy A.G. (2013). Revised values of the bond valence parameters for Te^{IV}–O, Te^{VI}–O and Te^{IV}–Cl. *Acta Crystallographica*, B69, 145–149.

[2] Christy A.G. and Mills S.J. (2013). The effect of lone-pair stereoactivity on polyhedral volume and structural flexibility: application to Te^{IV}–O octahedra. *Acta Crystallographica*, B69, 446–456.

Do you know what it means to manage the IMA list of minerals and other related stuff

Pasero M

Dept. of Earth Sciences, University of Pisa. marco.pasero@unipi.it

Since the birth of the IMA (1958) and the CNMMN (1959), then CNMNC (2006), one of the major tasks of the officers was the creation and the maintenance of a list of valid mineral species, which could register all decisions taken month after month by the Commission itself (approval of new mineral species and inheritance of old ones, discreditations, redefinitions, renaming, etc.). This goal was initially pursued with the publication of the *Glossary of Mineral Species* by Michael Fleischer, the first chairman of the CNMMN. After Fleischer's retirement the job was continued by Joseph A. Mandarino, another chairman of the CNMMN. The latter editions of *Glossary* were issued after Mandarino stepped down from his position within the Commission, and survive until now as publications independent from IMA. As a matter of fact, in recent years an official voice of the CNMNC on new minerals was lacking. Therefore it was decided at the CNMNC meeting in Budapest (August 2010) to set up and keep updated, in a simple and dynamical way, a comprehensive list of all valid mineral species. The starting point was a list compiled as an extract of the *Mineral* database by E. Nickel and M. Nichols, posted to the CNMNC website with several restrictions because the above database was a commercial product. The IMA List of Minerals was launched in September 2012 as a pdf which is freely available from the CNMNC website, and is intended as a work in progress, being updated on a regular basis as soon as notice on newly approved minerals, and other information on the status of valid minerals, is made available.

The amount of information contained in the list is low if compared to most Internet sites devoted to minerals, some of which are really attractive. In the IMA List of Minerals there are no photographs, nor any other frills, just the name, the ideal chemical formula, the IMA status, the IMA number, the type locality (country) and up to a pair of references. The rationale of the list is to present first-hand and up-to-date information on valid minerals, their formulae and their names, and it should be intended as the primary source for the other databases.

A short outline of the current IMA List of Minerals and of its evolution during the last two years, as well as other recent actions taken by the CNMNC executive in the frame of general classification and nomenclature issues, will be presented and discussed.

A redefinition of Claringbullite to $Cu_4ClF(OH)_6$; the importance of type material and group/series based studies

Rumsey M[1*], Welch M[1], Origlieri M[2], Cressey G[1], Kampf A[3], Burgio L[4], Spratt J[1], Humphreys-Williams E[1], Kirk C[5]

1 - Natural History Museum, London, UK *m.rumsey@nhm.ac.uk 2 - University of Arizona, Tucson, Arizona, USA 3 - Natural History Museum of Los Angeles County 4 - Victoria and Albert Museum, London, UK 5 - Loughborough University, Loughborough, UK

There is currently wide cross-disciplinary interest in the structural chemistry of substituted copper hydroxyhalides having the paratacamite/herbertsmithite, kapellasite/haydeeite and claringbullite groups on account of their potential applications in solid-state science. Most notably, the herbertsmithite and kapellasite structures are natural examples of synthetic "Kagome magnets" in which a fully ordered magnetic state is prevented and a magnetically frustrated disordered configuration is stabilised.

As part of a re-evaluation of the structural systematics of naturally-occurring substituted copper hydroxyhalides, we determined the crystal structure of what appeared to be a new mineral of composition $Cu_4ClF(OH)_6$ from the Ojuela Mine in Mexico that was isostructural with claringbullite. Electron microprobe analyses yielded: CuO, 78.23 wt%; Cl, 8.50 wt% and F, 5.21 wt%, while H_2O calculated on the basis of structural considerations as 13.07 wt%, brought the total to 100.9 wt%. Water content was also determined empirically by CHN analysis to confirm calculations. A charge balanced formula, based on 8 anions, is $Cu_{4.00}Cl_{0.98}F_{1.12}(OH)_{5.90}$. The material is hexagonal, space group $P6_3/mmc$, a = 6.6674(2) Å, c = 9.1747(3) Å, V = 353.21(2) Å^3 (Z = 2). The crystal structure was solved by direct methods and refined to R_1 = 0.033, wR_2 = 0.078. The structure is composed of sheets of edge-sharing Jahn-Teller-distorted $CuCl_2(OH)_4$ octahedra forming triplets around channels occupied by F ions running ||[001]. Sheets are connected *via* $Cu(OH)_6$ triangular prisms in which the Cu site is split into three sub-sites with one-third occupancy, each site lies almost within a rectangular face and has $Cu(OH)_4$ coordination. The O-H bonds of the $CuCl_2(OH)_4$ octahedron are directed into the channels towards F atoms, which are H-bond acceptors. As such, the structure of the new mineral was analogous to those of claringbullite (widely published at the time having composition $Cu_4Cl(OH)_7$) and barlowite $Cu_4BrF(OH)_6$. The new mineral was approved by the IMA and a paper was drafted for publication.

During preparation of a second paper all isostructural members were studied with the goal of creating a claringbullite group to establish compositional boundaries and identify all potential end-members. It became clear that no claringbullite of composition $Cu_4Cl(OH)_7$ could be found, so as a final attempt to obtain a chemical analysis corresponding to published claringbullite, the two co-type specimens were restudied. However, both types and all other specimens analysed were found to be of composition $Cu_4ClF(OH)_6$, identical to the newly approved mineral species rather than the published $Cu_4Cl(OH)_7$.

As a consequence, the new mineral is to be withdrawn/discredited and a redefinition of claringbullite will be submitted to the IMA-CNNMN. It is fortunate that the compositional equivalence was found prior to publication. The study has highlighted the importance of access to type materials for research and the need to study all compositional members of an isostructural group when defining any new end-member as technological advances may have made even recent publications erroneous.

Unusual Tl(I)-rich sulphate mineral assemblage from Tolbachik volcano, Kamchatka

Siidra O

Saint-Petersburg State University. siidra@mail.ru

Thallium (Tl) is an exceptionally rare element in both mantle and crustal rocks. Depending upon the chemical environment, thallium could exhibit either lithophile or chalcophile behaviour. Fifty-three thallium minerals are known to date and the majority of these minerals belong to sulphides and sulphosalts (CNMMN 2013). Studies of gases from active volcanic areas show their enrichment in thallium owing to highly volatile behaviour of the element at high and medium temperatures during magma degassing. High Tl concentrations are even used as a tracer for preindustrial volcanic eruptions. The Great Fissure Tolbachik eruption (GFTE) that occurred in 1975-1976 on Kamchatka peninsula, Russia, was followed by exceptional fumarolic activity and formation of many unique assemblages of mineral species. No Tl minerals from the Tolbachik volcano have been reported so far. Moreover, Tl oxysalt minerals were unknown from volcanic exhalations before this study. Tl enrichment of fumarolic gases at Tolbachik might be explained by subduction of Tl-bearing marine sediments and Pacific oceanic plate under Kamchatka with subsequent magma degassing. Recent investigation of Tolbachik samples collected from fumaroles in 1977 lead to the discovery of three new thallium sulphate and vanadyl-sulphate minerals, which are reported in the current contribution: markhininite, $TlBi(SO_4)_2$; karpovite, $Tl_2VO(SO_4)_2(H_2O)$ and evdokimovite, $Tl_4(VO)_3(SO_4)_5(H_2O)_5$. Crystal structures of three thallium sulphate minerals are unique. However they reveal close structural relationships of all heteropolyhedral units observed in markhininite, karpovite and evdokimovite. All Tl sulphate minerals from Tolbachik volcano provide a good example of correlation of the degree of stereochemical activity of lone-pair and presence/strength of Lewis bases.

A nomenclature for the Atacamite Family

Williams P[1*], Downes P[2], Grice J[3], Hibbs D[4], Kampf A[5], Leverett P[1], Malcherek T[6], Schlüter J[6], Sciberras M[1], Welch M[7]

1 - University of Western Sydney *p.williams@uws.edu.au 2 - Western Australian Museum 3 - Canadian Museum of Nature 4 - Sydney University 5 - Natural History Museum of Los Angeles County 6 - Universität Hamburg 7 - Natural History Museum, London

The Atacamite Family is defined here as comprising those species that possess the stoichiometry $M_2X(OH)_3$ or $M_4X_2(OH)_6$, where M is either a particular metal ion or a combination of different metal ions, usually possessing a divalent charge, and X is a halide. So far, only Members of the Family with X = Cl have been reported to occur in Nature. Known members of the Family and its Groups are set out below as a basis for discussion.

ATACAMITE FAMILY

ATACAMITE GROUP; orthorhombic, space group *Pnam*

Atacamite, $Cu_2Cl(OH)_3$

Kempite, $Mn_2Cl(OH)_3$

Hibbingite, $Fe_2Cl(OH)_3$

BOTALLACKITE GROUP; monoclinic, space group $P2_1/m$

Botallackite, $Cu_2Cl(OH)_3$

Iyoite, $CuMnCl(OH)_3$

PARATACAMITE GROUP

Paratacamite, $Cu_3CuCl_2(OH)_6$; trigonal, space group *R*-3

Clinoatacamite, $Cu_3CuCl_2(OH)_6$; monoclinic, space group $P2_1/n$

Anatacamite, $Cu_3CuCl_2(OH)_6$; triclinic, space group *P*-1

Paratacamite -(Ni), $Cu_3(Ni,Cu)Cl_2(OH)_6$; trigonal, space group *R*-3

Paratacamite -(Mg)-, $Cu_3(Mg,Cu)Cl_2(OH)_6$; trigonal, space group *R*-3

HERBERTSMITHITE GROUP; trigonal, space group *R*-3*m*

Herbertsmithite, $Cu_3ZnCl_2(OH)_6$

Gillardite, $Cu_3NiCl_2(OH)_6$

Leverettite, $Cu_3CoCl_2(OH)_6$

Tondiite-, $Cu_3MgCl_2(OH)_6$

KAPELLASITE GROUP; trigonal, space group *P*-3*m*1

Kapellasite, $Cu_3ZnCl_2(OH)_6$

Haydeeite, $Cu_3MgCl_2(OH)_6$

Misakiite, $Cu_3MnCl_2(OH)_6$

Centennialite, $Cu_3CaCl_2(OH)_6{\cdot}nH_2O$ (n ~ 0.7)

The reasons for the groupings will be discussed. It should be noted that the scheme recognises the relationships of a number of known species. In this connection, paratacamite, clinoatacamite and anatacamite are homeotypic species structurally related through slight distortions. The Family name is chosen because atacamite was the first member to be described [1]. A summary of the naming of the mineral (originally "cuivre muriaté de Pérou"), chemical analyses and physical properties is given by [2]. Finally, a number of known synthetic compounds that would belong to the Family and may be identified in Nature in the future are mentioned.

[1] de La Rochefoucauld F.A.F. *et al*. (1788). Examen d'un sable vert cuivreux du Pérou. Mémoires de l'Académie des Sciences de l'Institut de France for 1786, 465-466.

[2] Palache C. *et al*. (1951). The System of Mineralogy. John Wiley and Sons, New York, Volume 2, pp. 69-73.

Recent characterization of new microlite-group mineral species

B Andrade M[1*], Atencio D[2], Ellena J[1]

1 - São Carlos Institute of Physics USP Brazil *mabadean@terra.com.br 2 - Inst.Geociências - USP Brazil

The microlite mineral group is part of the pyrochlore supergroup, whose nomenclature was recently published [1]. Betafite, elsmoreite, pyrochlore and roméite are the other mineral groups of the pyrochlore supergroup. When the pyrochlore supergroup nomenclature scheme was approved, only four species, namely hydroxykenomicrolite $(\square,Na,Sb^{3+})_2Ta_2O_6(OH)$ (cesstibtantite discredited), oxystannomicrolite $Sn_2Ta_2O_6O$ (stannomicrolite discredited), oxystibiomicrolite $(Sb^{3+},Ca)_2Ta_2O_6O$ (stibiomicrolite discredited) and fluornatromicrolite $(Na,Ca,Bi)_2Ta_2O_6F$ had been completely described. The latter, i.e. fluornatromicrolite, was published only in 2011 due to the approval process of the nomenclature scheme. Hydrokenomicrolite $(\square,H_2O)_2Ta_2(O,OH)_6(H_2O)$ and fluorcalciomicrolite $(Ca,Na,\square)_2Ta_2O_6F$ were approved in 2011 and 2013, respectively. In 2013, oxynatromicrolite $(Na,Ca,U)_2(Ta,Nb)_2O_6(O,F)$ and hydroxycalciomicrolite $Ca_{1.5}Ta_2O_6(OH)$ were approved. The names oxycalciomicrolite, kenoplumbomicrolite and hydromicrolite refer to minerals that must be completely described in order to be approved as valid species. Microlite-group minerals occur as octahedral and rhombododecahedral crystals. The crystals are typically colorless, yellow, green, reddish and translucent, with vitreous to resinous luster, and their densities are approximately 6.2 g/cm³. Microlite species are cubic, belong to space group Fd-3m, and exhibit a = 10.42 to 10.52 Å as a unit-cell parameter. The only exception is hydroxycalciomicrolite, in which the presence of P-lattice is confirmed by the large number of weak reflections observed by X-ray diffraction. As a result, its space group is $P4_332$ and the unit-cell parameters are a = 10.4211(8) Å, and V = 1131.72(15) Å³.

[1] Atencio D. *et al*. (2010). *Canadian Mineralogist*, 48, 673-698.

Silicocarnotite, an old and potentially new mineral from the Negev Desert, Israel

Galuskin E[1*], Kusz J[1], Gfeller F[2], Galuskina I[1], Vapnik Y[3], Dulski M[1], Dzierżanowski P[4]

1 - University of Silesia, Poland *evgeny.galuskin@us.edu.pl 2 - University of Bern, Switzerland 3 - Ben-Gurion University of the Negev, Israel 4 - University of Warsaw, Poland

Silicocarnotite (silico-carnotite) is a historical name used for more than 100 years to describe the artificial and synthetic phases with composition close to $Ca_5(PO_4)_2(SiO_4)$ [1-11]. The crystal structure of silicocarnotite from slag [*Pnma*, a = 6.737(1), b = 15.508(2), c = 10.132(1) Å] was first reported in 1971 [12]. Potentially a new mineral, silicocarnotite $Ca_5(PO_4)_2(SiO_4)$ occurs as micro- and nano-symplectitic intergrowth with rankinite in pyrometamorphic gehlenite rocks of the Hatrurim Basin, one of the outcrops of the Hatrurim Complex, in the Negev Desert, Israel [13, 14]. Single grains (~0.05 mm) of silicocarnotite [*Pnma*, a = 6.7230(1), b = 15.4481(2), c = 10.0847(2) Å] were found in gehlenite rocks that have been used by hominins for axe and adze production. Localities of gehlenite rock known as "Paleolithic factories" were discovered on the eastern slope of the Har-Parsa Mt and also near the Hatrurim junction, located between Arad and the Dead Sea [15]. Associated with silicocarnotite minerals are pseudowollastonite, rankinite, flamite-like mineral, andradite-schorlomite, fluorapatite, gehlenite, larnite, magnesioferrite, kalsilite. Gehlenite rocks were formed by high temperature metamorphism of an unknown protolith at sanidinite facies. In larnite rocks of the Hatrurim Complex, ternesite, $Ca_5(SiO_4)_2(SO_4)$ [*Pnma*, a = 6.8428(1), b = 15.3921(2), c = 10.1836(1)Å] isostructural with silicocarnotite is a common mineral. Ternesite may contain up to 40% of the silicocarnotite end-member. The content of the ternesite end-member in silicocarnotite does not exceed 10 %.

Acknowledgements: Investigations were partially supported by the National Sciences Center (NCN) of Poland by decision no. DEC-2012/05/B/ST10/00514

[1] Carnot A. and Richards A. (1883). Comptes rendus hebdomadaires des séances de l'Académie des Sciences, 97, 316-320.

[2] Kroll V.A. (1911). *J. Iron and Steel Ins*., 84, 126-187.

[3] Riley D.P. and Segnit E.R. (1949). *Min.Mag*., 28, 496-504.

[4] Trömmel G. and Zaminer C. (1959). Archiv für das Eisenhüttenwesen, 30, 205.

[5] Keppler U. (1968). *N.Jahr.Min.Mon*., 320-330.

[6] Gualtieri A.F. *et al*. (2007). *J. Hazardous Materials*, 152, 563-570.

[7] Radev L. *et al*. (2009). *Centr. Eur. J.Chem*., 7, 721-730.

[8] Gomes S. *et al*. (2011). *Crys.Growth and Design*, 11, 4017-4026.

[9] Martinez I.M. *et al*. (2012). *J. Am. Cer. Soc*., 95, 1112-1117.

[10] Roh H.-S. *et al*. (2012). *Mater. Let*., 70, 37-39.

[11] Yu H. *et al*. (2013). *Optics Communications*, 289, 103-108.

[12] Dickens B. and Brown W.E. (1971). *Tscher. Min. Petr.Mitt*.16, 1-27.

[13] Bentor Y.K. (ed) (1960). Israel. In: Lexique Stratigraphique International, Asie. CNRS, Paris, Volume III, Section 10.2.

[14] Gross S. (1977). *Geol. Surv. Israel Bull*., 70, 1-80.

[15] Vapnik Y. and Vardi J. (2012). In: Stracher G.B., Prakash A. and Sokol E.V. (eds) Coal and Peat Fires: A Global Perspective. Elsevier, Amsterdam, 2, 189-201.

Uranian garnet from pyrometamorphic rocks of the Hatrurim Complex, Jordan. Problem of crystal chemical formula of elbrusite

Galuskina I[1*], Galuskin E[1], Utsunomiya S[2], Nakamatsu Y[2], Murashko M[3], Vapnik Y[4]

1 - University of Silesia, Poland *irina.galuskina@us.edu.pl 2 - Kyushu University, Fukuoka, Japan 3 - ZAO "Systematic Mineralogy", S-Petersburg, Russia 4 - Ben-Gurion University of the Negev, Israel

The crystal-chemical formula of uranian garnet, elbrusite $Ca_3(U^{6+}Zr)(Fe^{2+}Fe^{3+}_2)O_{12}$ [1], discovered in xenoliths of the Upper Chegem Caldera, Northern Caucasus, does not fit to the end-member formula [2]. In the new classification of the garnet supergroup, the new end-member formula, proposed for elbrusite, is: $Ca_3(U^{6+}_{0.5}Zr_{1.5})(Fe^{3+})_3O_{12}$ [3]. In elbrusite from the Caucasus, the U content often exceeds 0.5 apfu (up to 0.7 apfu) [1]. The Uranium excess was proposed to combine in the yafsoanite-like end-member - $Ca_3U^{6+}_2Fe^{2+}_3O_{12}$ [3], which in this case does not correspond to very oxidative conditions during mineral formations in altered xenoliths of the Upper Chegem Caldera [1].

Recently, in pyrometamorphic spurrite rocks of the Hatrurim complex in the Siwaqa area, Jordan, uranian garnet with UO_3 contents exceeding 38 wt.% was found, with composition perfectly fitting to the crystal-chemical formula: $Ca_3UZrFe_2AlO_{12}$. According to the EBSD and Raman spectroscopic data, elbrusite from Jordan is fully metamict. Attempts to recover its structure under laser beam heating had failed and led to crystallization of vorlanite $CaUO_4$, and garnet with composition $Ca_{1.5}Zr_{1.5}(Fe^{3+}, Al)_5O_{12}$ (a = 12.25Å, EBSD).

The composition of uranian garnet from Jordan can be described as a sum of two end-members $1/3\{Ca^{2+}_3\}[U^{6+}_2](Fe^{2+}_3)O_{12}$ + $2/3\{Ca^{2+}_3\}[U^{6+}_{0.5}\ Zr_{1.5}](R^{3+}_3)O_{12}$ = $\{Ca^{2+}_3\}[U^{6+}_{1.0}\ Zr_{1.0}](Fe^{2+}R^{3+}_2)O_{12}$, where R^{3+} = Fe^{3+}, Al, i.e. 33.3% of yafsoanite and 66.7% of elbrusite end-members. We suggest U in elbrusite structure is stabilized as U^{5+}, i.e. elbrusite from Jordan fits to the $\{Ca^{2+}_3\}[U^{5+}Zr](Fe^{3+}_3)O_{12}$ end-member. Our suggestion is based on the following facts: 1) minerals containing oxidized iron Fe^{3+} (srebrodolskite, magnesioferrite) are in association with elbrusite; 2) U^{5+} has very similar ionic radius to U^{6+} and it is incorporated exclusively in the octahedral site in the garnet structure; 3) preliminary data of EELS investigation indicate the U-oxidation state in elbrusite from the Caucasus generally close to 5+; 4) thermodynamic calculations point out the possibility of stable state U^{5+} in the garnet structure [4].

Acknowledgments: Investigations were partially supported by the National Sciences Center (NCN) of Poland by decision no. DEC-2012/05/B/ST10/00514

[1] Galuskina *et al*. (2010). *American Mineralogist*, 95, 1172-1181.

[2] Hawthorne (2002). *The Canadian Mineralogist*, 40, 699-710.

[3] Grew at al. (2013). *American Mineralogist*, 98 (4), 785-810.

[4] Rak *et al*. (2013). *Journal of Physics: Condensed Matter*, 25, 1-10.

New minerals in the Boa Vista pegmatite field, Minas Gerais, Brazil – césarferreiraite and correianevesite

Scholz R[1*], Chukanov N[2], Pekov I[3]

1 - Universidade Federal de Ouro Preto *r_scholz_br@yahoo.com 2 - Institute of Problems of Chemical Physics, Russian Academy of Science 3 - Faculty of Geology, Moscow State University

Brazil is an important source of pegmatite minerals, especially gemstones, industrial minerals and rare mineral species. The Eastern Brazilian Pegmatite Province, located in Minas Gerais is the most important. In the last decade, the expansion of mineralogical and geological studies in the Brazilian pegmatites gave support to the description of a number of new minerals. As part of a detailed mineralogical study of the pegmatites located in the Boa Vista pegmatite field (BVP, two new minerals were described and approved by the IMA CNMNC in 2013, namely césarferreiraite (IMA 2012-099) and correianevesite (IMA 2013-007).

Césarferreiraite, $Fe^{2+}Fe^{3+}_2(AsO_4)_2(OH)_2{\bullet}8H_2O$, is a new laueite-group mineral of triclinic symmetry, from the Eduardo pegmatite mine, Conselheiro Pena municipality. Intimately associated minerals are pharmacosiderite, scorodite and earlier arsenopyrite, and probably césarferreiraite replaces the latter. Chemical composition is: FeO 11.50, Fe_2O_3 25.56%, CaO 15.41%, As_2O_5 33.51%, H_2O(calc.) 26.01%, total 100.12. The empirical formula is $Fe^{2+}_{0.98}Fe^{3+}_{1.96}[(AsO_4)_{1.79}(PO_4)_{0.31}](OH)_{1.52}{\bullet}8.08H_2O$. The IR spectrum confirms the presence of OH and H_2O. Unit-cell parameters refined from powder data indexed by analogy with related laueite-group minerals (space group: *P*-1) are: a = 5.383(2) Å, b = 10.363(3) Å, c = 6.878(2) Å, α = 96.42(4)°, β = 109.19(3)°, γ = 102.30(2)°, V = 347.1(2) Å^3, and Z = 1. Césarferreiraite is the arsenate analogue of ferrolaueite and the second arsenate, after maghrebite, belonging to the laueite group. The general formula of laueite-group minerals is $M1M2_2(TO_4)_2(OH)_{2\text{-}3}{\cdot}8\text{-}7H_2O$ where *M*1 is typically a bivalent cation, *M*2 = Fe^{3+} or Al, *T* = P or As. Bivalent state of iron in *M*1 of césarferreiraite is confirmed by excellent Gladstone-Dale compatibility.

Correianevesite, ideally $Fe^{2+}Mn^{2+}_2(PO_4)_2{\bullet}3H_2O$, is a new reddingite-group mineral. It occurs in a phosphate-rich granite pegmatite outcropped by the Cigana mine, Conselheiro Pena, Rio Doce valley. Associated minerals are triphylite, hureaulite, lithiophilite, frondelite, rockbridgeite, eosphorite, hureaulite, vivianite, fairfieldite, leucophosphite, cyrilovite and phosphosiderite. The Mössbauer spectrum shows the presence of two states for Fe^{2+} and one state for Fe^{3+} occupied in the ratio $Fe1^{2+}$:$Fe2^{2+}$:Fe^{3+} = 39:55:6. The chemical composition is: MnO 29.21%, FeO 21.74%, Fe_2O_3 1.54%, P_2O_5 34.59%, H_2O 12.6%, total 99.68%. Correianevesite is orthorhombic, space group *Pbna*, a = 9.4887(2) Å, b = 10.1149(2) Å, c = 8.7062(2) Å, V = 835.60(3) Å^3, Z = 4. Taking into account Mössbauer spectroscopy data and the results of the crystal structure refinement, the refined crystal-chemical formula can be written as $(Fe^{2+}_{0.72}Mn^{2+}_{0.20}Fe^{3+}_{0.08})(Mn_{1.48}Fe^{2+}_{0.52})(PO_4)_2\ (H_2O,OH)_3$. Both IR and Raman spectra confirm the presence of H_2O and acidic OH groups. The presence of acidic OH groups is due to the asymmetric polarization of H_2O molecules that form strong hydrogen bond Ow(2)-H(2)···O(1) (with the distance Ow(2)···O(1) of 2.539 Å) and act as proton donors according to the dynamic acid-base equilibrium $AsO_4^{3-} + H_2O \leftrightarrows HAsO_4^{2-} + OH^-$.

It is important to note that landesite, a member of the reddingite group, and correianevesite cannot be distinguished by electron microprobe analysis, but landesite is characterized by much higher values of refractive indices as a result of high Fe^{3+} content. Correianevesite and Fe-bearing reddingite can be easily distinguished by means of Mössbauer spectroscopy.

Acknowledgements: This study was supported by the RFBR, grant no. 14-05-00276-a; CNPq ,grants No. 306287/2012-9, 306287/2012-9 and No. 402852/2012-5. R. Scholz is also grateful to CAPES (Coordenação de Aperfeiçoamento de Pessoal de Nível Superior) program Apoio a Eventos no Exterior (AEX).

$Be_{1-x}(Cr,Ti)_3O_{6-y}(OH)_y$, an unusual new mineral from Verbier (Switzerland)

Widmer R[1*], Meisser N[2], May E[2], Armbruster T[1]

1 - University of Bern *remo.widmer@students.unibe.ch 2 - University of Lausanne

The new mineral $Be_{0.47}(Cr_{1.57}Ti_{1.02}Fe_{0.27}Al_{0.08}V_{0.05})O_{6-y}(OH)_y$ (a = 9.933(2), b = 8.458(2), c = 4.5106(8) Å, space group *Pnma*), is the Cr-dominant analogue of the kyzylkumite-like mineral $Be_{1-x}(V,Ti)_3O_6$ from Norway [1] It occurs near Verbier, Valais (Switzerland) as a primary phase associated with Cr-bearing muscovite in quartzite, crosscut by mm-sized quartz and albite veins. Other primary minerals include quartz, apatite, monazite-(Ce), pyrite, a tennantite-tetrahedrite group mineral, and a new Th, Ca-rich mineral. These late alpine-stage veins, ~10 million years old [2], are located in small quartzite lenses embedded in Triassic gypsum and tectonically admixed carboniferous black shale. The new mineral probably formed due to retrograde decomposition of alpine greenschist facies Cr-bearing muscovite associated with late stage Na-rich hydrothermal activity. Results of fluid inclusion microthermometry and oxygen-isotope fractionation in albite veins, in a close-by similar geological setting, suggest crystallization conditions between 270 °C and 320 °C under a pressure of 1 kb to 2.5 kb [3].

The structure of $Be_{1-x}(Cr,Ti)_3O_{6-y}(OH)_y$ is of the norbergite type and was refined from single-crystal X-ray data to $R1$ = 0.0338. In contrast to $Be_{1-x}(V,Ti)_3O_6$ from Norway, $Be_{1-x}(Cr,Ti)_3O_{6-y}(OH)_y$ from Verbier occurs as idiomorphic crystals, is untwinned, but displays severe structural disorder indicated by strongly streaked reflections parallel to b*. Transition metal ions (Cr, V, Fe, Ti) occupy octahedrally coordinated positions. Be partially occupies tetrahedral sites comparable to Si in norbergite *sensu stricto* $Mg_3(SiO_4)(F,OH)_2$. The amount of Be vacancies and possible hydroxylation in $Be_{1-x}(Cr,Ti)_3O_{6-y}(OH)_y$ is related to the octahedral M^{3+}/M^{4+} ratio and the availability of Be in the fluid.

[1] Raade G. and Balic-Zunic T. (2006). The crystal structure of $(Be,\square)(V,Ti)_3O_6$, a mineral related to kyzylkumite. *Canadian Mineralogist*, 44, 1147-1158.

[2] Marshall D., Meisser N., and Taylor R.P. (1998). Fluid inclusion, stable isotope and Ar-Ar evidence for the age and origin of gold-bearing quartz veins at Mont Chemin, Switzerland, *Mineralogy and Petrology*, 62: 147-165.

[3] May E. (2008). Albites et albitisation dans l'unité de la Pierre Avoi (Zone de Sion Courmayeur) à Verbier (Valais, Suisse): étude combinée des inclusions fluides et des isotopes stables. Unpublished Master Thesis, University of Lausanne.

Metaborate minerals from the Fuka Mine, Okayama Prefecture, Japan

Kobayashi S*, Ando T, Kanayama A, Kusachi I

1 - Okayama University of Science *kobayashi@das.ous.ac.jp

From the Fuka mine, Okayama Prefecture, Japan (34°46'N, 133°26'E), metaborate minerals such as calciborite [1] CaB_2O_4, uralborite [2] $CaB_2O_2(OH)_4$, nifontovite [3] $Ca_3B_6O_6(OH)_{12}\cdot 2H_2O$, frolovite [4] $CaB_2(OH)_8$, pentahydroborite [5] $CaB_2O_4\cdot 5H_2O$ and hexahydroborite [6] $CaB_2(OH)_8\cdot 2H_2O$ were confirmed. The minerals were formed as pyrometasomatic products of limestone. The minerals are characterised by a constant molar ratio $CaO : B_2O_3 = 1 : 1$. Among the minerals, calciborite shows the highest B_2O_3 content. This contribution reviews the metaborate minerals from the Fuka mine.

Optical and physical properties of the metaborate minerals from Fuka are as follows. The crystal system of calcibolite is orthorhombic, and uralborite, nifontovite and hexahydroborite are in the monoclinic system, whereas frolovite and pentahydroborite are triclinic. The colors of the minerals are colorless, white, yellow and red-brown. Refractive indices (a, b, g) and birefringence are 1.502 - 1.672 (1.502 - 1.605, 1.505 - 1.654, 1.509 - 1.672) and 0.007 - 0.078, respectively. Vickers and Mohs hardness are 151 (25g load) - 372 (50g load) kg/mm^2 and 2.5 - 4.5, respectively. Measurement densities are 1.84 - 2.88 g/cm^3. The molecular numbers of water within the minerals vary from 0 for the calciborite to 6 H_2O in the molecule of hexahydroborite. The refractive indices, birefringence, hardness and density of calciborite were relatively high, but these values decreased with increase in water content. From the mode of occurrence, it is very likely that metaborate minerals from the Fuka mine were formed by a reaction of boron-bearing fluids with limestone.

[1] Kobayashi S. *et al*. (2014). *Jour. Min. Petro. Sci.*, 113 (in print).
[2] Kusachi I. *et al*. (2000). *Jour. Mineral. Petrol. Sci.*, 95, 43 - 47.
[3] Kusachi I. and Henmi C. (1994). *Mineral. Mag.*, 58, 279 - 284.
[4] Kusachi I. *et al*. (1995). *Mineral. Jour*., 17, 330 - 337.
[5] Fujiwara T. *et al*. (1982). *Chigaku Kenkyu*, 33, 11-20 (in Japanese).
[6] Kusachi I. *et al*. (1999). *Mineral. Jour*., 21, 9 - 14.

Anorthite megacryst from Take-shima, Kagoshima Prefecture, Japan: oscillatory zoning and micro inclusions

Matsui T[1*], Arakawa Y[2], Kimata M[2], Nishida N[2], Hoshino M[3], Echigo T[4]

1 - Kagoshima University *matsui@edu.kagoshima-u.ac.jp 2 - University of Tsukuba 3 - National Institute of Advanced Industrial Science and Technology 4 - Shiga University

We investigate the mineralogy of micro inclusions in anorthite megacrysts that are found as phenocrysts of about 1 cm in maximum diameter in the basaltic lavas from Take-shima, Kagoshima Prefecture, Japan. Back-scattered electron (BSE) images, compositional mapping, and line analysis by electron probe microanalyzer (EPMA) clearly show compositional oscillatory zoning in the megacryst. The anorthite content of the megacryst is about 94 mol% at the most. Because a trifling amount of Fe and excess Si are detected by EPMA, minor end-members of $FeAl_2Si_2O_8$, $CaFeSi_3O_8$ and $[]Si_4O_8$ are incorporated into the present megacryst. The anorthite megacrysts show slight optical zoning. Zonal arrangement of the micro inclusions of opaque minerals and bubbles are common in the specimens. The textural feature studied under an optical microscope seems to be consistent with the chemical zonation observed in the BSE images and compositional mapping. From BSE images and qualitative analyses, four types of micro inclusions of opaque minerals can be recognized within the megacryst: (1) Fe bearing vesicular fragment, (2) Fe bearing solid thin plate which fills cracks in the host megacryst, (3) Fe bearing solid particle, and (4) Fe bearing particle with Cu and S rich parts and cavities.

The four types of micro inclusions strongly suggest a wide variation in redox environment of the host magma, however, presence of the compositional oscillatory zoning implies oscillation in pressure, temperature or vapor pressure occurred at a certain narrow range around melting point of anorthite. Though further investigation is required for completely understanding the formation of the anorthite megacryst from Take-shima, this new work provides fundamental information about the history of magmatic systems related to anorthite megacryst formation under island arcs.

Formations of minerals solidified with micro carbon-bearing grains

Miura Y

Yamaguchi University moonyas@hotmail.com

Crystalline minerals with larger sizes are mainly formed by igneous differentiation over long geological processes of active Earth with the global water system. On the other hand, volatile elements including carbon generated by extreme conditions with rapid processes are easily isolated from original rocks by liquid and vapor contributions. The purpose of this paper is mainly to elucidate formation of carbon-bearing solidified materials through rapid vaporization by extreme conditions of meteoritic impact, earthquake and volcanic processes [1-4]. For changes in material state, previous mineral change is based on microscopic observation between solid and solid through other states of fluids and vapor conditions as follows [2]:

Crystal (A) ⇒ *(mineralization with vapor, liquid and/or solid)* ⇒ ***Crystal (B)***, (1)

where crystals (A) and (B) suggest minerals from original crystal (A) to final crystal (B), respectively, through common crystallization. Mineralogical sciences mainly describe expression (1) for productive mineral species on global water-system of Earth by considerable contribution of vapor, liquid and/or vapor states. This is mainly because terrestrial minerals are special products with wide variety compared with limited mineral species on extraterrestrial bodies of the airless and waterless Moon, Asteroids and some planets. For solidified materials from other material states, primordial Earth and extraterrestrial bodies contain solidified materials with volatile elements, mainly because they have localized systems of air and water as follows [1, 2]:

Solid (A) ⇒ *(Extreme vapor-liquid condition by quenching)* ⇒ ***Solid (B),*** (2)

where solids (A) and (B) express solidified material (A) to other solid (B), respectively, with remnant volatile elements through extreme conditions. Solidified materials (A) and (B) expressed by equation (2) contain usually crystalline minerals (A) and (B) respectively with volatile elements shown as amorphous or mixed solids, where carbon-bearing materials are relatively representative elements remaining through extreme conditions. Carbon-bearing solids examples are nano-grains of carbon-bearing materials interpreted as quenched products changed from original solid including crystalline minerals [1-4]. Present laboratory work using rapid injection with carbon dioxides to crystalline solids under dry and wet conditions, obtained the following three products: a) new minerals replaced by carbon, b) carbon-bearing layered products by wet condition, and c) carbon-bearing irregular deposition by dry condition. Natural examples of micro-grains with carbon-bearing solids are obtained in this study at impact craters of the Ries and the Barringer, impact-related structures of the Libyan glass-Africa, Akiyoshi and Takamatsu-Japan, meteoritic explosion-related grains of the Nio-Yamaguchi, Shungai-Russia and Chelyabinsk-Russia, volcano-related depositions of the Lengai-Africa, Shimonoseki- and Hagi-Yamaguchi-, and Hamada-Japan, and earthquake-related carbon of Hiroshima-Japan. Carbonaceous and lunar meteorites with carbon-deposited solids are microscopically obtained by the analytical electron microscopy (FE-ASEM) for comparative and systematic study.

[1] Miura Y. and Fukuyama S. (1999). *Journal. Materials Proc. Tech*. (Elsevier), 85, 192-193.

[2] Miura Y. (2006). Int. Mineral. Assoc. (Kobe) Vol. ISBN 1348-6543, p.163.

[3] Cresswell R., Miura Y. and J. Rucklidge *et al*. (1994). *Nuclear Instr. Methods Phys. Res. Sect. B (NIM-B)* (Elsevier), 92, 505-509.

[4] Miura Y. and Fukuyama S. (1998). *Rev. High Press. Sci. Tech*., 7, 1306-1308.

Stability and spectroscopy of Mg sulfate minerals under Martian conditions. Role of hydration on sulfur isotope partitioning

Bobocioiu E[1], Caracas R[2*]

1 - ENS de Lyon 2 – CNRS * razvan.caracas@ens-lyon.fr

We study hydrated magnesium sulfate minerals from first-principles calculations based on density-functional theory. We determine the heat of hydration for $MgSO_4 \cdot nH_2O$, we compute the Raman and infrared spectra for several phases, and we calculate the S isotope partitioning as a function of hydration. We find that epsomite and meridianiite, with n=7 and n=11 water molecules per $MgSO_4$ unit, respectively, are particularly stable with respect to other individual or combinations of hydration states. The Raman spectra of all phases present clear SO_4 features that are easily identifiable. We use this to show one can use the vibrational spectroscopic information as an identification tool in a remote environment, like the Mars surface. We discuss the character and atomic displacement pattern of all vibration modes. We compute the S^{34}/S^{32} partitioning and find that hydration favors enrichment in lighter S isotope S^{32} with respect to the heavier S^{34}, which is accumulated in the less hydrous structures. We show for the first time that the signature of the S^{34}/S^{32} partitioning could be observed by in situ spectroscopy on the surface of Mars. Moreover, this can be related to the diurnal cycle of hydration and dehydration and hence it can improve the modeling of the water circulation on Mars.

Space weathering simulations through controlled growth of iron nanoparticles on olivine surface

Filip J[1*], Čuda J[1], Kohout T[2], Britt D[3], Bradley T[3], Tuček J[1], Skála R[2], Kletetschka G[2], Kašlík J[1], Zbořil R[1]

1 - RCPTM/Palacký University, Olomouc *jan.filip@upol.cz 2 - Institute of Geology, AS CR, v.v.i., Prague, Czech Republic 3 - Department of Physics, University of Central Florida, USA

Airless planetary bodies are directly exposed to space weathering. The main spectral effects of space weathering are darkening, reduction in intensity of silicate mineral absorption bands, and spectral slope increase towards longer wavelengths (reddening). Production of nanophase metallic iron ($npFe^0$) during space weathering plays a major role in these spectral changes.

A laboratory procedure for controlled production of $npFe^0$ in silicate mineral powders has been developed [1]. The method is based on two-step thermal decomposition of low-iron olivine in ambient air followed by reduction in hydrogen atmosphere. Through this process, a series of olivine powder samples was prepared with various amount of $npFe^0$ in 7-20 nm size range and quantitative spectral changes were evaluated. Amount of $npFe^0$ was estimated from saturation magnetization measurement.

Main results:

1. Linear trend is observed between the amount of $npFe^0$ and 1 µm band center position.
2. Logarithmic trend is observed between amount of $npFe^0$ and darkening, shallowing of 1 µm olivine absorption band, and reddening.
3. Similar logarithmic trend between reddening and duration of space weathering has been proposed by [2]. If this assumption is correct, then amount of $npFe^0$ increases linearly with time.
4. The 1 µm band width at half depth generally decreases with increasing amount of $npFe^0$, but no reliable fit was found.
5. Olivine sample with the additional population of larger $npFe^0$ particles follows similar spectral trends as other samples, except for the reddening trend. This is interpreted that larger, ~40-50 nm sized, $npFe^0$ particles do not contribute to the slope change as efficiently as smaller $npFe^0$ fraction.

Compared to fresh olivine, our olivine samples with artificially introduced, ~5-20 nm sized $npFe^0$ particles exhibit all spectral characteristics of lunar-type space weathering. From a quantitative point of view a linear trend is observed between the amount of $npFe^0$ and 1 µm band center position, and a logarithmic trend is observed between amount of $npFe^0$ and darkening, shallowing of 1 µm olivine absorption band and reddening. The 1 µm band width at half depth generally decreases with increasing amount of $npFe^0$, but no reliable fit was found. Through comparing our results with space weathering observations [2], we conclude that the $npFe^0$ concentration increases linearly with time.

[1] Hapke B. *et al*. (1975) *Moon*, *13*, 339-353.

[2] Brunetto R. *et al*. (2006) *Icarus*, *180*, 546-554.

The planetary materials database

Lafuente B[1*], Downs R[1], Blake D[2], Stone N[1], Pires A[1]

1 - University of Arizona *barbaralafuente@email.arizona.edu 2 - NASA Ames Research Center

The web pages of the RRUFF project (http://rruff.info/) [1] have been an essential tool for the identification and further characterization of minerals. This open database, which receives more than 80,000 visits per week from geologists, mineralogists and the general public worldwide, includes X-ray diffraction (XRD), Raman, infrared (IR) and electron microprobe data of more than 4,000 mineral samples. The experience acquired from the development and maintenance of the RRUFF project has motivated the creation of a new and more interactive database of properties and descriptive measurements of terrestrial planetary analog materials, the *Planetary Materials Database* (PMD). Terrestrial analog data are used by the broader Space Science/Astrobiology community to understand planetary geologic processes, to interpret returned data from present and past missions and to evaluate future mission and instrument concepts prior to their selection for flight. The PMD fills an existing need to archive data obtained in terrestrial laboratories using a variety of instrumental techniques and to make them available in a useful form to the worldwide science community. The PMD will be used to archive and access this data, as well as to provide reference patterns, spectra and other information used by the Space Science and Astrobiology community.

Although the RRUFF project provided the initial inspiration for the PMD, RRUFF was built with a rigid software structure that prevented the addition of new features without extensive reprogramming. The PMD software was developed in part to overcome this limitation. The PMD software platform will be useful for many if not most types of scientific data, allowing database customization according to the particular needs of the users. The database structure was created and is maintained by the University of Arizona. Sample data will be first uploaded from the laboratories who initiated the PMD archive project (University of Arizona, NASA-Ames and Indiana University) and which have extensive databases and existing instruments for on-going data acquisition. Additional data will be uploaded as they are made available from other institutions and research teams.

PMD will be made available to other database developers, and is intended to be a universally accessible, downloadable and citable database, providing measured diffraction patterns, spectra, chemistry, metadata, etc., suitable for use by the Space Science community and the public in general. In follow-on work, we will equip the PMD with interactive web applications for the quantitative analysis of mineralogical and geochemical data.

Acknowledgement: We gratefully acknowledge the support from the NASA NNX11AP82A, Mars Science Laboratory Investigations.

[1] Downs R.T. (2006). 19th General Meeting of the International Mineralogical Association. O03-13.

Raman spectra of coexisting graphite and feldspar crystals from the Morasko meteorite

Majzner K[1*], Slaby E[2], Karwowski Ł[3], Muszyński A[4], Simon K[5], Kruszewski Ł[2]

1 - Faculty of Chemistry, Jagiellonian University *majzner@chemia.uj.edu.pl

2 - Institute of Geological Sciences, Polish Academy of Sciences 3 - Faculty of Earth Sciences, University of Silesia, Wroclaw, 4 - Institute of Geology, Adam Mickiewicz University, Poznan, 5 - Department of Geochemistry, GZG of Georg-August-University

The Morasko meteorite, found in 1914 within an area located north of Poznań (central-west Poland), is classified as an IAB-MG octahedrite [1]. Its troilite-graphite nodules contain alkali feldspar, pyroxene, and numerous accessory minerals. Feldspar crystals, although ternary, are of almost pure sodium ($Ab_{95.75}An_{4.2}Or_{0.05}$) composition. Plagioclase is a minor phase in the nodules and up to 0.2 mm in size. It fills empty spaces in troilite-graphite matrix forming a complex mosaic, which resembles intergrowths of several minerals. Some albite crystals show potassium-rich ($Or_{96.8}Ab_{3.0}An_{0.2}$) antiperthitic texture. Many of them are strongly enriched in iron (up to 2.15 wt %). The iron-rich domains also demonstrate significant enrichment in trace elements, primarily transition elements. This may indicate that growing feldspar crystals incorporated numerous tiny inclusions. The main phase coexisting with feldspar is graphite. Raman spectra from feldspar and accompanying graphite have been collected to study their structure and phase interrelationship. No area examined by Raman is mono-mineralic and inclusion-free. Raman microspectroscopy allows detailed analysis of chemical composition and distribution of selected compounds in the sample. The collected spectra are dominated by graphite. In this study G and D band analysis has been used to examine crystallinity of the Morasko meteorite. The D band (~1348 cm^{-1}) gives information about disordered/amorphous carbon (A_{1g} symmetry). The G band (~1580 cm^{-1}) is an indication of presence of monocrystalline graphite (E_{2g} symmetry). In the investigated sample the G band has been observed. It implicates the presence of graphite as the main component of the Morasko iron nodules. The D band was also observed. Its intensity is dependent on the degree of disorder in graphite symmetry. Appearance of feldspar seems to increase disorder in graphite symmetry (raised intensity of the D band). Additionally, Raman results provide information about distribution of minerals such as albite (285, 476, 513 cm^{-1}) and pyroxene (339, 663, 683, 1013 cm^{-1}).

Acknowledgement: The work has been funded by NCN 2011/01/B/ST10/04541.

[1] Karwowski Ł., Kryza R., Muszyński A., Pilski A.S., (2012). Outline of the mineralogy of the Morasko meteorite. In: Muszyński *et al.* (eds.): Morasko - the largest meteorite shower in Europe. Bogucki Wydawnictwo Naukowe. Poznań.

Mixed solidified materials formed on the Moon and extraterrestrial bodies

Miura Y

Yamaguchi University. yasmiura50@gmail.com

Mineral identification of the collected lunar Apollo samples has been applied by using numerous standard database systems of the terrestrial minerals and rocks from forty five years ago (1969). Proposed formation models of the Moon are mainly derived through analysis of several collected samples from Apollo sites, as explained by well-crystallized minerals formed on Earth with global air and liquid systems [1-4]. The main purpose of the present paper is to shed light on poorly-understood extraterrestrial mineral-bearing assemblages composed of volatiles and poor-crystalline materials.

Minerals of the lunar rocks are formed in water-depleted environments, and hence display the least variety of mineral species compared with other celestial bodies (e.g. Earth, the Moon, asteroid meteorites). Earth, with its rich water-environment, has many minerals with water, ca. 48%, among nine volatiles-bearing mineral groups. The lunar rocks formed by rapid quenching process contain solidified materials with main elements mixed with minor volatiles, calcium (Ca) and rare-earth elements (REE) based on data analyses of high-speed impact images and the published compositional data [1, 2]. The present analysed data suggest that impact-related compositions for floated surface rocks are produced from Ca- and REE-rich solids with carbon-fixed processes.

Solidified textures of the lunar rocks are characterized by voids-rich solids quenched from vapour, liquid and solid states to void, amorphous solids and crystalline grains as state-changes on the airless and waterless Moon. In fact, reported data of porosity and density indicate that lunar rocks are similar in tendency to meteorites with anomalous voids-rich textures of regolith soils. The present data are well consistent with volatile-bearing reservoirs of the interior of the shallow underground after impact processes on fragile surface-rocks combined with carbon-bearing compounds. Atomic bonds formed by rapid cooling are easily broken by the ion-sputtering melting process, compared with slow-cooled magmatic minerals, for example. Present experimental data of secondary ion-peaks sputtered on various targets of mineral-rocks are increased at impacted meteorites and the Moon breccias combined with carbon-bearing solids.

Cyclic processes of carbon-bearing materials are observed at global and local sites of active Earth (as a water-based planet) and biological systems in general. On the Moon, different and quasi-cyclic processes of carbon-bearing materials found at meteoritic impact sites and within lunar rocks are considered to be still forming in open-like systems of the airless Moon, related to continuous meteoritic impacts as a result of volatile injection during such impacts. Possible microscopic relicts of carbon-bearing materials as different activities are expected to be checked in detail during future missions planned on the Moon [3, 4].

[1] Miura Y. and Fukuyama S. (1999). *Journal. Materials Proc. Tech.* (Elsevier), 85, 192-193.

[2] Miura Y. (2006). Int. Mineral. Assoc. (Kobe) Vol. ISBN 1348-6543, p.163.

[3] Miura Y. and Fukuyama S. (1998). *Rev. High Press. Sci. Tech*., 7, 1306-1308.

[4] Miura Y. (2010). Int. Mineral. Assoc. (Budapest) XO150G.

Crystal-chemical analyses of Martian minerals in Gale crater

Morrison S[1*], Downs R T[1], Blake D F[2], Bish D L[3], Vaniman D T[4], Ming D W[5], Morris R V[5], Morookian J M[6], Achilles C N[3], Rampe E B[5], Bristow T F[2], Chipera S J[7], Treiman A H[8], Crisp J A[6], Farmer J D[9], Gellert R[10], Sarrazin P C[11], Des Marais D J[2], Stolper E M[12], Yen A S[6], Wilson M A[2], Spanovich N[6], Anderson R C[6], MSL Team[6]

1 - University of Arizona *shaunnamm@email.arizona.edu 2 - NASA ARC 3 - Indiana University 4 - PSI 5 - NASA JSC 6 - JPL-Caltech 7 - CHK Energy 8 - LPI 9 - Arizona State University 10 - University of Guelph 11 - in-Xitu 12 - Caltech

The CheMin instrument on the Mars Science Laboratory (MSL) rover *Curiosity* performed X-ray diffraction analyses on soil and rock samples in Gale crater [1]. The first series of experiments wre performed on scooped soil at the Rocknest sand shadow. The second and third series of analyses focused on the Sheepbed mudstone member at the base of the Yellowknife Bay Formation; the first drilled mudstone site was John Klein and the second was Cumberland. CheMin is entering a campaign to analyze minerals at a new site known as the Kimberly, and these results will also be presented if they are available.

Crystalline phases from each of these samples were identified. Subsequently, their abundances and unit-cell parameters were refined with the Rietveld method [2, 3]. The relationships between unit-cell dimensions and composition for each major crystalline phase were modelled using hundreds of unit-cell parameters from minerals with known chemical compositions obtained from literature data. These crystal-chemical systematics were applied to the refined unit-cell parameters of each of the major phases observed in the Gale crater samples, and their chemical formulae were estimated. The compositions of the minor phases, assumed to be ideal, were combined with those of the major phases to estimate the bulk crystalline composition for each sample. All of the samples contained both crystalline and amorphous materials. The amorphous compositions were estimated for each sample by subtracting the chemistry of the crystalline component from the bulk chemical composition measured by APXS.

Plagioclase, pyroxene and olivine group minerals make up the greatest proportion of the samples. However, significant magnetite and smectite, correlated with diminished olivine, was observed for the John Klein and Cumberland mudstones. The mineralogical and amorphous compositions of the Rocknest soil indicate a basaltic source with global and regional components, similar to that proposed for Gusev crater and Meridiani Planum. The drilled mudstone samples exhibited mafic silicate mineral compositions similar to those of the aeolian-formed Rocknest deposit. In contrast, the mudstone mineral assemblage includes aqueously-formed phyllosilicates, and is therefore considered a potentially habitable fluvio-lacustrine environment.

[1] Blake *et al.* (2013) *Science*, 27, 341, DOI: 10.1126/science.1239505.
[2] Bish *et al.* (2013) *Science*, 27, 341, DOI: 10.1126/science.1238932.
[3] Vaniman *et al.* (2013) *Science*, 24, 343, DOI: 10.1126/science.1243480.

New data on trace element composition of feldspars from the Morasko meteorite

Moszumańska I[1*], Slaby E[1], Wirth R[2], Karwowski Ł[3], Muszyński A[4], Simon K[5], Majzner K[6]

1 - Institute of Geological Sciences, Polish Academy of Sciences *i.moszumanska@twarda.pan.pl 2 - GeoForschungsZentrum Potsdam 3 - Faculty of Earth Sciences, University of Silesia 4 - Institute of Geology, Adam Mickiewicz University 5 - Department of Geochemistry, GZG of Georg-August-University 6 - Faculty of Chemistry, Jagiellonian University

The Morasko meteorite, found in 1914 within an area located north of Poznań (central-west Poland), is classified as an IAB-MG octahedrite [1]. Its matrix, composed of kamacite and taenite, contains frequent troilite-graphite inclusions (nodules). The nodules appear to be free of any indications of shock deformation. They comprise a range of accessory minerals, silicates and phosphates among others. Feldspars found within silicates, although ternary, are of almost pure sodium ($Ab_{95.75}An_{4.2}Or_{0.05}$) composition. Plagioclase is a minor phase in the nodules and is up to 0.2 mm in size. It fills empty spaces in troilite-graphite matrix forming a complex mosaic, which resembles intergrowths of several minerals. Raman spectra from such areas are dominated by carbonaceous material. The relationship between feldspar and C-rich phases suggests a sequential or simultaneous formation process. At some locations plagioclase coexists with pyroxene crystallizing in voids. TEM bright-field images of such albite reveal perfectly twinned crystals without any signs of changes and shock deformation. Some albite crystals show potassium-rich ($Or_{96.8}Ab_{3.0}An_{0.2}$) antiperthitic texture, many of them are strongly enriched in iron (up to 2.15 wt %). Albite with orthoclase antiperthites frequently forms a mosaic of differently oriented crystals. The mosaic contains numerous inclusions of carbonaceous material.

Plagioclase trace-element composition has been determined by LA ICP MS. Feldspar strongly enriched in potassium was too small to perform a reliable analysis. None of the Na-rich crystals was inclusion-free. Careful data processing allowed assigning some of the element concentrations to albite only. Albite trace element composition indicates crystallization from a melt strongly depleted in LILE elements, but phosphorus. The compatible trace element content of rubidium, barium and strontium in feldspar is low, varying between: Rb = 11-16 ppm, Ba = 86-2 ppm, Sr = 5-1 ppm. Phosphorus content attains 240 ppm. REE are below detection limits. Phosphates accompany feldspars and seem to crystallize in equilibrium or, more likely, sequentially. LA ICP MS analysis of iron-rich domains in feldspar shows elevated concentrations of Sc, Ti, V, Cr, Mn, Sb, As, Bi. They fluctuate around 3700-4500 ppm and may imply that tiny crystals of accessory phases had crystallized prior to feldspar nucleation and were enclosed by growing feldspar. Explanation of this fact may be different. Within un-shocked meteorite parts veins of late iron-phosphide melt have been found. Drops of such melt may be present in the late crystallizing phases; also may postdate crystallization process from silicate melt. Feldspars and phosphates appear to be the last phases growing from differentiated silicate melt and terminating the crystallization process.

Acknowledgement: The work has been funded by NCN 2011/01/B/ST10/04541.

[1] Karwowski Ł., Kryza R., Muszyński A. and Pilski A.S. (2012). Outline mineralogy of the Morasko meteorite. In: Muszyński *et al*. (eds.): Morasko - the largest meteorite shower in Europe. Bogucki Wydawnictwo Naukowe. Poznań.

Challenges in asteroidal science: deciphering the origin of chondrites

Russell S[1*], Hezel D[2], Claydon J[1], Vacarro E[1]

1 - Natural History Museum, London, U.K. *sarr@nhm.ac.uk 2 - University of Köln, Germany

Chondritic meteorites are sedimentary rocks formed from the accretion of material from the solar system's protoplanetary disk. They have experienced varying amounts of thermal and aqueous alteration, with the "type 3" chondrites believed to represent the least altered samples. The main components of chondrites: chondrules, calcium-alumimium-rich inclusions (CAIs), metal, and fine-grained matrix provide a record of the environmental conditions at this time in the solar system's history. However, the record they provide is a fuzzy one, and full of surprises.

The study of chondrites poses many questions including:

1. How did chondrules and CAIs form, and why are they present in differing amounts in asteroidal materials?
2. When did chondritic components form?
3. What was the extent of isotopic mixing and unmixing in the early solar system?
4. What is the relationship between matrix, chondrules, CAIs and metal?
5. Where and when did aqueous alteration take place?
6. Was the formation of the solar system similar to that of other planetary systems?

We are starting to make headway with some of these questions. A relationship between the composition of the matrix and chondrules suggest that chondrules formed in a region local to asteroid accretion. In contrast, since the abundance of CAIs is correlated to the meteorite's bulk Al abundance, CAIs were probably exotic components, scattered into the asteroid accretion region [1]. Recent Fe isotope data (e.g., [2, 3]) showed that chondrules did not undergo Rayleigh fractionation when they formed, so melting must have taken place in a region with a high dust/gas ratio. This suggests that chondrule formation was linked to asteroidal accretion.

Over the next decade the NASA Osiris Rex mission and the JAXA Hayabusa 2 mission will both visit, and bring back material from, asteroids that we believe are similar to the parent bodies of these meteorites. The geological perspective they will provide will enable us to answer some of these outstanding questions and give us an opportunity to study the minor planets from which we believe these enigmatic samples originated.

[1] McKeegan K. *et al*. (1998). *Science*, 280 414-418.
[2] Hezel D. *et al*. (2010). *EPSL* 296, 423-433.
[3] Alexander C. *et al*. (2008). *Science* 320 1617-1619.

TEM and chemical-composition study of phosphates from NWA 2975 shergottite: equilibrium or sequential crystallization?

Slaby E[1*], Wirth R[2], Förster H-J[2], Moszumańska I[1], Kruszewski Ł[1]

1 - Institute of Geological Sciences, Polish Academy of Sciences, Poland
*e.slaby@twarda.pan.pl

2 - GeoForschungsZentrum Potsdam, Germany

Previous studies reported the joint occurrence of merrillite and chlorapatite in Martian NWA 2975 shergottite [1, 2], together with zoned pyroxene, maskelynite, other accessory minerals, and glass pockets. Both phosphates are REE-substituting minerals, with the REE content of merrillite exceeding that of apatite by two orders of magnitude. While apatite is a volatile-bearing mineral, merrillite is anhydrous. Both phases are thought to have been precipitated from residual magmas either as a result of sequential crystallization, simultaneous crystallization at equilibrium with major phases, or at local melt pockets [3].

Phase-relationship examination (BSE, EPMA, CL) confirms that merrillite actually represents unique intermediate merrillite-□????ferromerrillite solid solution poor in Y and REE and that chlorapatite was misidentified for fluorapatite rich in Cl and OH, but equally poor in the lanthanides. Both phosphates are spatially displaced. Four foils have been cut for HR TEM study, including one from a vein enriched in glassy material. Both phosphates have been indexed and their structures are compatible with merrillite and apatite. Both reveal planar deformation effects and mosaicism of several, variably distorted and undistorted sub-domains indicative of shock-induced deformation, thus suggesting that both phases formed prior to the shock event. Quenched, very porous melt drops of phosphate composition, containing silica and volatiles (with F dominant over Cl) occur in merrillite, but not in apatite. Other textures in merrillite remind of a bubble-rich quenched amorphous fluid. In apatite cracks, crystallization of restitic, F-enriched and Cl-free melt is observed. Tiny tile-shaped crystals (identified as apatite) nucleate on the crack's walls and grow in parallel-oriented piles. The composition of host apatite shows the presence of both F and Cl.

A silica-rich vein of glassy material contains fragments of mainly pyroxene and apatite. The contact of the glass with these grains does not show any evidence for *in-situ* melting. The glass is partly crystallized. Parallel-oriented plates of triangular habit and pure SiO_2 composition occur within amorphous material. The glass composition (paucity of P, Ca etc.) precludes that both apatite and merrillite might have crystallized from it.

EDS spectra of amorphous inclusions in merrillite as well as of two apatite generations support the presence of volatiles in the melt during the formation of both phosphate minerals. The Cl activity tended to decrease during progressive crystallization. Phosphate-liquid partitioning used for reconstruction of melt composition implies that the REE are not preferentially incorporated into merrillite relative to apatite. Combined information from TEM, compositional analysis and recalculated melt composition implies that both phosphates crystallized in equilibrium rather than that they precipitated sequentially.

Acknowledgement: The work has been funded by NCN 2011/01/B/ST10/04541.

[1] Wittke J. H. *et al*. (2006). *Lunar Planet. Sci*. 37, #1368.

[2] He Q. *et al*. (2011). *Lunar Planet. Sci*. 42, #1648.

[3] Jolliff B.L. *et al*. (1993). GCA 57, 4069-4094.

Experimental insight into Noachian clay-forming environments on Mars

Farsang S*, Tosca N

University of St Andrews, Scotland, UK *sf57@st-andrews.ac.uk

Clay minerals are an important component of the ancient sedimentary record on Mars. The layer silicates, in addition to carbonates, sulfates, and other alteration minerals, together carry critical information regarding the chemical conditions present during the interaction between primary basalt and liquid water. However, we know comparatively little about how the total secondary mineral assemblages may have responded to primary geochemical parameters on Mars, most notably the presence/absence of oxygen, variable CO_2, and temperature

The main aim of this project is to understand the processes that form, transform and distribute clay minerals through the Martian crust. Considerable previous work has been conducted on Martian basalt alteration processes and products but most have focused primarily on short-duration acidic conditions as opposed to circum-neutral pH conditions that probably characterized Noachian environments on Mars. Here we focus on long-term basalt alteration experiments and monitor the dominant secondary mineral phases as a function of pH, oxidative conditions and CO_2 content.

As a starting material, we use well-characterized Columbia River basalt, which has a similar chemical composition to many basalts on Mars. Several sets of experiments were performed with variable (temperature: 25-85°C, initial pH: 3.00-5.75, Oxic/anoxic) combinations likely to exist in shallow surface and subsurface environments on Mars. Both unaltered basalt and mineral assemblages formed from the alteration experiments were analysed. The bulk composition of the unaltered basalt was determined using X-ray fluorescence (XRF). The altered basalt was examined by XRF and electron probe microanalyzer (EPMA) and then the alteration phases were physically separated and Fourier transform infrared spectroscopy (FTIR) and powder X-ray diffraction (XRD) was performed on them. XRD analyses on the separated clay fraction were conducted in the air-dried, ethylene glycol solvated and heated states. Aqueous solutions were sampled for two months (1 sample/week) and continuously monitored for pH and Eh. Major cation chemistry was analyzed by inductively coupled plasma mass spectrometry (ICP-MS) and anion chemistry was analyzed by spectrophotometry. Major variations between secondary mineral assemblages as a function of geochemical parameters will be presented.

Environmental implications of mineralogical and geochemical features in lower-middle Triassic rocks and potential analogies with early stages of evolution on Mars

Galán-Abellán A B[1], Barrenechea J F[2], López-Gómez J[1], De la Horra R[3], Borruel-Abadía V[1], Luque F J[2], Alonso-Azcárate J[4], Martínez-Frías J[1*]

1 - Inst. Geociencias (CSIC-UCM). Madrid. Spain *j.m.frias@igeo.ucm-csic.es 2 - Dept. Cristalografía y Mineralogía, UCM, Spain 3 - Dept. Estratigrafía, UCM. Madrid. Spain 4 - Fac. C.C. Ambientales. Toledo. Spain

The end of the Paleozoic is characterized by the largest biotic crisis ever recorded in marine and terrestrial sedimentary rocks and the damaged environmental conditions persisted during Early Triassic times.

These palaeoenvironmental conditions have been recently studied in continental sedimentary rocks of the Iberian Ranges (Spain) using mineralogical, geochemical and sedimentological criteria [1, 2]. The sedimentological analysis indicates that the siltstones and sandstones of the Lower-Middle Triassic rocks (Cañizar Fm.) correspond to braided fluvial systems frequently affected by aeolian reworking, in an arid to semi-arid climate. The lack of any fossil remains in the lower and middle parts of the unit is indicative of conditions unsuitable for life development. The presence in all the studied sections of small amounts of early diagenetic Sr-rich aluminium phosphate-sulphate minerals (APS) has been interpreted as an indirect evidence of acid conditions in the meteoric waters that promoted precipitation shortly after sedimentation. These minerals belong to the group of alunite and jarosite, which have been reported in rocks from Mars [3]. These well-characterized Iberian geological settings, and early-diagenetic processes, could be useful to assess environmental and habitability conditions at some Martian sites.

[1] Galán Abellán *et al*. (2013). *Sed. Geol*., 289, 169-181.
[2] Galán Abellán *et al*. (2013). *J. Sed. Research*, 83, 406-426.
[3] Klingelhöfer *et al*. (2004). *Science*, 306, 1740-1745.

Experimental make-up of a regolith simulant from CI carbonaceous chondrite composition: mineralogical features and significance for sampling of C-type asteroids

Martínez-Frías J[1*], Rodriguez-Losada J[2], Ortega C[3], Carrera M[3]

1 - IGEO (CSIC-UCM) *j.m.frias@igeo.ucm-csic.es 2 - Facultad de Ciencias, ULL, Tenerife, Spain 3 - AVS, Guipúzcoa, Spain

In accordance with the project "Breadboard of a sampling tool mechanism for low gravity bodies (ESA ITT AO/1-7061/12/NL/HB" and the theoretical estimations regarding the main features of the target asteroid, a regolith simulant (RS) was made in order to match ESA requirements. The final mixture was made trying to obtain a general mineralogical composition similar to that of CI chondrites. This final mixture (CAB-JMF-AVS regolith simulant) includes primary mineralogical phases as well as secondary phases (generated by the aqueous alteration of the primary ones). Most minerals correspond to pure phases that were specifically used for obtaining the final mixture. Sepiolite (extremely pure) and mantle-related basalt (mainly composed of olivine and pyroxene) were sampled from selected outcrops in Madrid and Tenerife, respectively. After mixing and sieving (granulometric selection; <32 mm) the material to obtain the different simulant fractions, various assessments regarding sample preparation and later analytical issues were also performed. More than 270 measurements were made, including 23 simple compression tests, and for the rest triaxial tests, taking into account different configurations. In accordance with the Mohr-Coulomb combined circle and failure line method, angle of friction values obtained for the three subtests range from 19.21 to 39.84. Experimental cohesion values (kp/cm^2) that correspond to this final compositional make-up of the regolith simulant and general test configurations range from 1.61 to 3.22.

Ti-metal sand grains with acritarchs in ferruginous palaeosol from the Libyan Desert Glass area, Egypt: implications for a regional reservoir of cometary debris

Andreoli M[1*], Bamford M[2], Block D[2], De Beer F[1], di Martino M[3], Gallino R[4], Gucsik A[5], Hudson Lamb D[1], Huotari S[6], Jinnah Z[2], Kramers J[5], Mouri H[5], Ntsoane T[1], Pischedda V[7], Sigalas J[2], Stengel I[8], Straker C[2], Ziegler A[2], Zinner E[9]

1 - Necsa, South Africa *marco.andreoli@necsa.co.za 2 - University of the Witwatersrand 3 - INAF Observatorio astronomico di Torino 4 - Università di Torino 5 - University of Johannesburg 6 - University of Helsinki 7 - Université de Lyon 8 - Polytechnic of Namibia 9 - Washington University

The recent identification of a 30 g diamondiferous stone named Hypatia from the Libyan Desert Glass area of SW Egypt (see other abstracts in this conference) as a comet fragment holds significant promise to further understand the nature of comets. Scientists have searched for cometary particles in space (with probes), in the upper atmosphere as interplanetary dust particles (IDP), and in Antarctica as ultra-carbonaceous micrometeorites. Despite these efforts, the mass of recovered samples is generally less than a few micrograms. In the present study we tested the possibility that additional comet fragments may be found in the ferruginous gritty sandstone bedrock in the area where Hypatia was found. For this we crushed and milled a ~1 kg sample of this sandstone to a fine pulp which was digested in *aqua regia* to remove the abundant Fe-oxides. A ~25 ml scoop of quartz-rich pulp was dissolved in HF leaving a small residue of fine grained minerals (mainly undigested quartz, zircon, and rutile) in addition to two mm-size grains (called Romulus and Remus) and a few smaller black grains a few tenths of a mm in the long axis. Advanced microanalytical techniques subsequently applied to these grains (SEM with EDS; microfocus x-ray tomography; nano-SIMS, electron microprobe; microRaman spectroscopy) revealed that they consisted of Ti-metal locally coated by black carbonaceous films and filaments up to ~0.3 mm in length. Under high magnification, the Ti-metal grains consist of a great number of much smaller, ~30 to 50 micrometre wide, interconnected Ti-metal grains that range in shape from rounded to wavy and elongated. As a consequence, tomographic scans of the grain called Romulus show textures typical of crystallization under microgravity conditions. The grains host occasional veinlets of TiN, while occasional blebs of Al_2O_3 and complex, Cu-bearing alloys may occur in between grains. Zn and rarer, submicrometer Ag were also observed. Finally, both grains are partly coated by black carbonaceous films from which emanate smooth and delicate, tendril-like filaments up to 0.3 mm in length. While the Raman spectrum of this carbon compares to that of thermally metamorphosed organic material, not unlike shungite, the isotopic composition of the titanium grains does not show the anomalies characterizing some grains of extrasolar origin. Having discarded the first two possibilities, for a number of reasons, including the fact that no Ti-metal has ever been found on Earth or in meteorites, we conclude that Romulus and Remus were hosted in the comet before its explosion. The carbonaceous material represents acritarchs, i.e. thermally processed, fossilized Oligocene lichens/algae that exploited the Ti-metal grains after they had been reworked in the arenaceous beds of the Libyan Desert Glass area. We thus conclude that the Cenozoic sediments in this sector of SW Egypt represent an untapped reservoir of cosmic material that should be studied to complement deep space sampling missions. From our data we also conclude that the rare Ti-metal grains found in IDPs may not have necessarily a presolar, interstellar origin as previously speculated [1]. Instead, they support results from the Stardust mission to the Wild 2 comet, namely that such bodies were formed from material that underwent extreme heating (>1700°C), probably near the young Sun, before being ejected to the outer realms of the solar system.

[1] Rietmeijer FJM *et al.*, 1990, Proc. Lunar Planet. Sci. Conf. 20: 323-333.

Mineral inclusions found in the Hypatia stone (Libyan Desert Glass area)

Belyanin G[1*], Kramers J[1], Andreoli M[2]

1 - University of Johannesburg *gbelyanin@gmail.com 2 - Necsa, South Africa

The carbon-rich, microdiamond-bearing Hypatia stone was found in 1996 by Aly A. Barakat in the Libyan Desert Glass area, southwest Egypt. It is an extremely hard yet very brittle and heavily fractured black material coated with light brownish desert varnish. Based on a multidisciplinary approach, Kramers *et al.* [1] proposed that Hypatia might be a remnant of a cometary nucleus fragment and that most likely it was once part of a bolide, which broke up and exploded in the atmosphere causing the formation of the Glass.

We report the first results of a mineralogical and mineral-chemical study of the inclusions in the stone, and discuss these comparing them to meteoritic matter as well as carbonados (see review in [2]). Among secondary minerals that fill in prominent cracks that cut the stone in numerous directions, calcite and clay minerals are the most common; they may indicate that the stone was at or near surface during periods of much wetter climate in the area of presently extreme desert. However, inclusions of different types occur inside the carbonaceous matrix. Two of them (often associated with each other) are prevalent - iron sulphide (troilite) and nickel phosphide, whereby the former is in all cases much finer grained (< 1 µm) than the latter (up to 50-100 µm, see Figure 1). Although never found in terrestrial rocks, phosphides have been reported from iron meteorites and achondrites, with iron-rich varieties being the most common. Nickel-rich end-members (i.e., very high Ni/Fe ratio) have never been described from any terrestrial or meteoritic material, thus making the Hypatia case unique. Other minerals that have been observed as inclusions are metallic aluminium (in a single ~50 µm grain) and silver (5 µm), as well as silicon carbide, which occurs as grains up to ~5 µm in size. So far, no silicate grains have been observed as genuine inclusions.

The occurrence of metallic aluminium lends support to the proposal of Andreoli *et al.* [3] that a grain of metallic titanium found in associated sediments also originates from the cometary body. Further, the inclusions bear witness to an extremely reducing and cold environment at their formation. The latter is indicated by the occurrence of pure Ni-phosphides, which are formed at much lower temperature than iron-rich species [4]. The strange assortment of minerals suggests that they were incorporated randomly from ambient dust as the main cometary body agglomerated. Silicon carbide commonly occurs in carbonaceous chondrites as preserved presolar grains similar in size to those found in Hypatia (but in much lower concentration). We speculate that the non-carbon minerals in the stone are dominated by presolar matter.

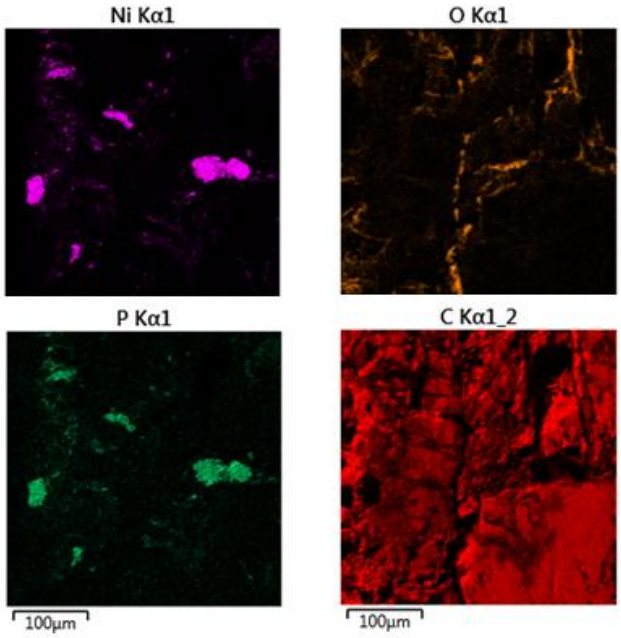

Figure 1: EDS maps for Ni, O, P and C showing the occurrence of nickel phosphide. Notice the lack of oxygen in the phase.

[1] Kramers J.D. *et al.* (2013). *Earth and Planetary Science Letters*, 382, 21-31.

[2] McCall G.J.H. (2009). *Earth-Science Reviews*, 93, 85-91.

[3] Andreoli M.A.G. *et al.* (2014). IMA2014 abstracts volume.

[4] Geist V. *et al.* (2005). *Crystallography Research Technology*, 40, 52-64.

HP behaviour of bloedite at low and high T: insights to the knowledge of the ice planets

Comodi P[1*], Stagno V[2], Zucchini A[1], Fei Y[3], Prakapenka V[4]

1 - Dipartimento di Fisica e Geologia, Università di Perugia, Italy *paola.comodi@unipg.it 2 - Carnegie Institution of Washington, USA 3 - Geophysical Laboratory, Carnegie Institution of Washington, US 4 - Argonne National Laboratory, University of Chicago, US

Bloedite [$Na_2Mg(SO_4)_2 \cdot 4H_2O$], $P2_1/a$ space group, Z=2, *a*=11.129(1), *b*=8.247(1), *c*=5.5395(3) Å, β=100.88(1)º, contains (001) sheets with waved infinite chains of alternated $MgO_2(H_2O)_4$ and $NaO_4(H_2O)_2$ octahedra sharing vertices, interconnected through SO_4 tetrahedra and hydrogen bonds. The knowledge of the release of water from its structure as a function of P and T is of great interest to planetary scientists, as it can explain the presence of subsurface oceans and the cryovolcanism phenomena observed from Voyager data on Galilean icy satellites (Europa, Ganymede).

We performed in situ synchrotron X-ray powder diffraction experiments on natural bloedite at P up to 10 GPa and T from ~100 K to ~570 K using diamond anvil cell technique at GSECARS, Advanced Photon Source (Argonne, USA).

The calculated thermal expansion coefficients at low T, from 300 to 120 K, are a_a = 0.7(2) 10^{-5} ; a_b = 1.4(3) 10^{-5}; a_c = 4.4 (4) 10^{-5} K^{-1}; a_V = 5.8 (7)10^{-5} K^{-1}, and the calculated thermal expansion coefficients at relatively high T, from 300 to 480 K, are a_a = 2.5(3) 10^{-5}; a_b = 2.5(3) 10^{-5}; a_c =3.7 (4) 10^{-5} K^{-1}; a_V = 8.3 (6)10^{-5} K^{-1}. Both compression and expansion behaviours of bloedite are strongly anisotropic, with the c parameter more deformed with respect to a and b.

At T higher than 430 K, at room pressure, the evolution of lattice parameters show a sharp discontinuity, with a strong contraction of the cell volume and all lattice parameters, which may be associated to the loss of two water molecules, in agreement with thermogravimetric data. They showed, at ambient P, three endotherms at 410 K, 500 K and 1000 K, with weight losses of approximately 11%, 11% and 43%, related to partial dehydration, full dehydration and sulphate decomposition, respectively. Increasing T at 10.4 GPa, the lattice parameters increase continuously up to 480 K; then a sharp decrease in volume cell and of c lattice parameter is observed.

The following equation of state $V = V0 (1 - 2.5 \cdot 10^{-2} \Delta P + 7.0 \cdot 10^{-5} \Delta T)$ may be derived, taking into account the bulk modulus measured by Comodi *et al.* [1] that allows to estimate P-T conditions, which leave the volume cell of bloedite unchanged with respect to V_0 (P is in GPa, T in K). Starting from the thermal model of Ganymede where a surface T is assumed of 110 K and a constant thermal gradient of 6 - 7 K/km, we measured that bloedite remains stable up to about 40 -50 km of depth where it starts to lose two water molecules. The effect of pressure on the dehydration is relatively low.

The fluid phase may determine a change on the rheology of layer and a contrast in material properties with different viscosity and may represent a detachment level. This way the complex structure observed on Ganymede's surface may be interpreted. Moreover, features on Europa and Ganymede related to cryovolcanic activity, namely the eruption of aqueous solution or partly crystallized slurry derived from partial melting of ice-bearing materials, may be associated to differential dehydration of the hydrous sulphate phases.

[1] Comodi *et al.* (2014). *Am. Mineral.* 99, 511-518.

Farringtonite, a rare phosphate mineral from the Springwater pallasite

Fowler-Gerace N[1], Tait K[2*], Hyde B[2]

1 - University of Toronto, Canada 2 - Royal Ontario Museum, Toronto, Canada, *ktait@rom.on.ca

Only 98 pallasites are currently known out of the over 45,000 meteorites in the world's collections. They are often considered to be some of the most beautiful meteorites, being composed of an intriguing mixture of olivine set in an iron-nickel alloy matrix. One of such meteorites is the Springwater pallasite which was originally discovered in 1931 in a farmer's field in Saskatchewan, Canada. In 2009 meteorite hunters surveyed over 1,000 acres of land using powerful metal detecting devices and successfully located an additional 100 kg of meteorite fragments. The largest mass recovered then, which is now the main mass (52.8 kg), resides at the Royal Ontario Museum, Toronto, Canada. We have cut open the main mass for display with a low-loss diamond wire saw, and after the initial cut, we took a second thin slice (25 x 18 x 1.5 cm thick) for study. We applied a grid pattern to the meteorite and sliced the meteorite up in 3 x 5 cm 'tiles' and performed a systematic investigation of the pallasite, including a crystal structure determination, chemistry and spectroscopy of the minerals, with particular attention to the phosphate mineralogy.

Farringtonite is the dominant phosphate in the Springwater pallasite (70%) next to stanfieldite (29%) ($Ca_4Mg_5(PO_4)_6$ and minor merrillite (~1%) ($Ca_9NaMg(PO_4)_7$. Although a major phase in the Springwater pallasite, it has only been found in a handful of other pallasites and never on Earth. Based on the mean values of all analyses, the empirical formula (normalized to eight oxygen atoms) is calculated to $(Mg_{2.82}Fe_{0.15}Mn_{0.01})P_{2.01}O_8$; this can be simplified as $Mg_5(PO_4)_2$. The smaller farringtonite grains are observed every centimeter or two, while the larger grains are much more widely spaced. Farringtonite occurs in rounded clots that are generally millimeters, occasionally up to centimeters, in width, always adjacent to and partially or fully encompassing olivine crystals. Blebs of Fe-Ni alloy and troilite (FeS) commonly occur within farringtonite clots or between farringtonite and olivine. Along some farringtonite boundaries with olivine, dark grey vermiform features are observed; in other cases, the farringtonite-olivine interface hosts grid-like arrays of euhedral chromite crystals. Farringtonite is also observed in contact with schreibersite, $(Fe,Ni)_3P$ and phosphoran olivine.

The crystal structure of farringtonite has been determined by least-squares refinement of single-crystal X-ray diffraction data to $P2_1/n$, with a = 7.5988(4), b = 8.2433(4), c = 5.0818(3) β = 94.039(2), Z =2, R_1 = 1.31%, wR_2 = 4.65%. Raman spectra were collected with a Horiba LabRAM Aramis micro-Raman spectrometer at the Royal Ontario Museum. A 3 x 3 mm region of a polished section was mapped in 25 µm steps using a 532 nm, 50 mW laser filtered to 10% power to prevent sample damage, averaging spectra over 2 repetitions of 3 seconds each. The farringtonite spectrum shows strong peaks at 980, 1025, and 1070 wavenumbers and weaker peaks at 131, 170, 319, 353, 420, 473, 500, 577, 620-655, 1111, and 1149 wavenumbers. Phosphorous-rich olivine and phosphorous-poor olivine could be differentiated by Raman spectroscopy.

Assessing the paleomineralogy of the Hadean Eon: what was the role of impacts?

Hazen R

Carnegie Institution of Washington, Washington D.C., USA, rhazen@ciw.edu

Hazen [1] suggested that the Hadean Eon, encompassing Earth's first 550 million years, was a time of limited mineralogical diversity. Prebiotic Earth's near-surface environment may have held no more than approximately 420 different rock-forming or accessory mineral species that were widely distributed and/or volumetrically significant. This relative Hadean mineralogical parsimony is a consequence of the limited modes of mineral paragenesis prior to 4 Ga compared to the last 3 billion years. Dominant Hadean Eon mineralizing processes include the evolution of a diverse suite of intrusive and extrusive igneous lithologies; hydrothermal alteration over a wide temperature range, notably serpentinization; authigenesis in marine sediments; and diagenesis and low-grade metamorphism in near-surface environments. A significant difference in Hadean mineralization compared to subsequent periods relates to impact processes, including shock mineralization, creation of hydrothermal zones, and excavation of deep metamorphosed terrains.

The Hadean Eon may have been notably lacking in mineralization generated by plate tectonic processes, such as subduction zone volcanism and associated fluid-rock interactions, which result in massive sulfide deposition; convergent boundary orogenesis and consequent extensive granitoid-rooted continental landmasses; and the selection and concentration of incompatible elements in complex pegmatites, with hundreds of accompanying minerals. The dramatic mineralogical consequences of life are reflected in the absence of Hadean biomineralization; for example, the lack of extensive carbonate deposits and the associated restricted development of skarn and cave minerals prior to 4 Ga. Most importantly, it was not until after the establishment via photosynthesis of significant near-surface redox gradients that supergene alteration, redox-controlled ore deposition, and subaerial weathering in an oxidizing environment could diversify Earth's near-surface mineralogy. These post-Hadean processes may be responsible for more than 4000 of the more than 4800 approved mineral species. Any scenario for life's origins that invokes minerals as agents of molecular synthesis, selection, protection, or organization must take into account the limited mineralogical repertoire of the time.

This analysis may be applied equally to mineral evolution on Mars, which may have progressed no farther than that of Earth's Hadean Eon. Recent mineralogical results from the Mars Science Lander are consistent with this model of Earth's Hadean mineralogy.

[1] Hazen R.M. (2013). *American Journal of Science*, 313, 807-843.

High-pressure mineralogy of planetary ice and gas

Hemley R

Carnegie Institution of Washington, Washington D.C., USA, rhemley@ciw.edu

Studies of a broad range of molecular systems as a function of pressure and temperature are revealing a rich new 'mineralogy' of the planetary systems, including ice and gas giants and their satellites, as well as those of newly discovered exoplanets including super-Earths and mini-Neptunes. Understanding hydrogen, and hydrogen-rich systems in extreme environments is obviously crucial in view of its cosmic abundance. These systems are also of fundamental interest due to the quantum character and electronic structure of hydrogen, which gives rise to intriguing if not unique properties of these systems at multi-megabar pressures. With recent improvements in techniques, the range of extreme conditions over which hydrogen can be studied experimentally has been significantly extended, and the material has been studied under static pressures reaching well above 300 GPa using synchrotron infrared, Raman, and other optical spectroscopies, and new phases are documented. Additional studies of ices have been performed using new neutron diffraction techniques, including H_2O to megabar pressures. These new studies of planetary ice and gas systems at extreme conditions reveal a richness of phenomena that provides an essential baseline for planetary modeling that complements both Earth and space-based observations.

Si isotope fractionation between metal and silicate at high-temperature and high-pressure conditions – implications for early metal core segregation in terrestrial planets

Kempl J[1*], Vroon P[2], Frost D[3], Kowalski P[4], and van Westrenen W[2]

1 - Technical University of Delft, The Netherlands, *j.kempl@tudelft.nl 2 - VU University Amsterdam, NL 3 - BGI Bayreuth, Germany 4 - Forschungszentrum Juelich, Germany

The largest differentiation event in Earth and other terrestrial planets was the process of early metal core segregation from a silicate mantle. With the invention of Multi-Collector (MC) ICP-MS, silicon stable isotope compositions of terrestrial and extraterrestrial materials could be analysed aiming at constraining models of planetary core formation. The identification of a small offset between the silicon stable isotopic composition of the Bulk Silicate Earth (BSE) and primitive meteorites suggests that Earth's metallic core contains a significant amount of silicon [1].

Quantitative links between this isotopic offset and core composition models require accurate knowledge of Si stable isotope fractionation between metal and silicate at high pressures (*HP*) and high temperatures (*HT*). To date only a few experimental constraints on Si isotope fractionation in high-pressure, high-temperature (*HPT*) metal-silicate systems exist [e.g., 2-5]. Recent studies of Si isotope fractionation in *HPT* metal-silicate systems suggest that Si isotope fractionation is mainly a temperature driven process [1, 5, 6]. In particular, little is known about the Si stable isotope fractionation behaviour at *higher pressure* conditions.

In this study we present Si isotope fractionation data obtained in metal-silicate *HPT* systems (Figure 1). Our simplified metal-silicate system contains $Fe_{83}Si_{17}$ and a silicate (diopside and forsterite) and was exposed to 9 GPa and 2150 ºC in a Multi-Anvil-Press at BGI Bayreuth, Germany. In a time-dependent experimental series both metal and silicate were molten. Si isotopes were analysed with a ThermoFinnigan Neptune MC-ICPMS in dry-plasma mode at VU University Amsterdam.

We compare our data with earlier, lower-pressure data and show that (1) Si-coordination influences the fractionation of Si stable isotopes and (2) the pressure dependence of Si isotope fractionation is either negligible or slightly negative.

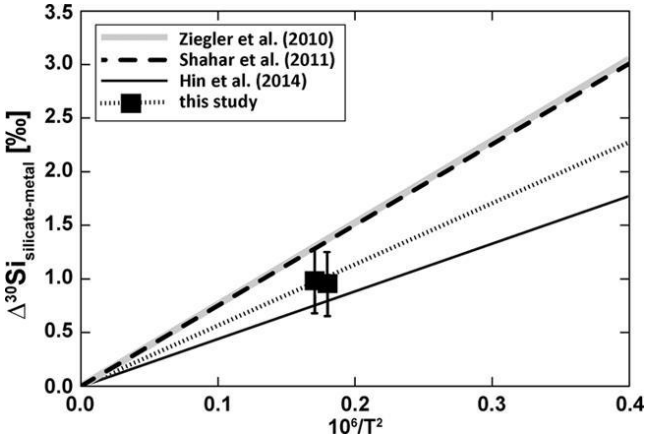

Figure 1: Temperature dependence of equilibrium Si isotope fractionation between metal and silicate in a pressure range between 1 and 9 GPa. Studied systems reached isotopic equilibrium either in solid, partially molten, or completely molten state.

[1] Georg *et al*. (2007). *Nature* 447, 1102-1106.

[2] Shahar *et al*. (2009). *EPSL* 288, 228-234.

[3] Kempl, J. *et al*. (2013). *EPSL* 368, 61-68.

[4] Hin *et al*. (2014). *EPSL* 387, 55-66.

[5] Shahar *et al*. (2011). *Geochim. Cosmochim. Acta* 75, 7688-7697.

[6] Ziegler *et al*. (2010). *EPSL* 295, 487-496.

Indications from noble gas data on the presolar mineral content of comet Hypatia

Kramers J[1*], Andreoli M[2], Belyanin G[1]

1 - University of Johannesburg *jkramers@uj.ac.za 2 - Necsa, South Africa

The carbonaceous and diamond-bearing 30 g stone found in 1996 in the southwestern desert of Egypt (the Libyan Desert Glass strewnfield) has a unique and bewildering noble gas content [1]. For argon, krypton and xenon this portrays a mixture between terrestrial-atmospheric and extraterrestrial gases (with the former dominant), while helium and neon in Hypatia appear to be wholly extraterrestrial. This difference probably reflects adsorption of atmospheric gases onto the carbonaceous matter of the body before it impacted and became transformed into an impermeable, mostly glassy state. This glassy matrix contains atmospheric gas inclusions for which the pressure can be estimated at a megabar or more from the amount of argon released from them.

On the basis of isotope ratios, it is possible to unravel the mixture of atmospheric and extraterrestrial (ET) noble gas constituents, and to make comparisons of the ET noble gases with what is known from the Asteroid Belt via chondritic meteorites. In the latter, up to 8 noble gas components have been identified from differences in element and isotope abundance ratios [2]. Most of these are hosted in presolar minerals condensed in interstellar space. However, one component named "Q", and which is the most abundant in chondrites, is hosted in chondritic organic matter and is thought to have been captured by adsorption within the early solar nebula. The ET noble gas content in Hypatia differs from that in chondrites in a number of ways:

(i) The overall abundance of noble gases in Hypatia is 10 to 100 times lower than in the chondritic matrix (which includes organic matter and presolar grains);

(ii) the "Q" component, dominant in chondrites, appears to be absent in Hypatia. These two differences can be explained by low temperatures (<70K) and pressures ($<10^{-8}$ bar), and thus absence of noble gases to be adsorbed, in the early solar nebula at >50 AU distance from the sun. This is the zone where the Kuiper Belt, the source of comets, is today. It follows that the ET noble gases in Hypatia should be essentially made up by the components trapped in presolar mineral grains;

(iii) The only ET noble gas component in Hypatia that can be recognized from chondrite studies is "G" (identified by anomalies in neon, krypton and xenon isotope ratios) which (in chondrites) is hosted in presolar silicon carbide grains and originates from S-process nucleosynthesis in the asymptotic giant branch (AGB) stage of stars. The discernible presence of this component is in accord with SiC grains having been observed in Hypatia [3]

(iv) A noble gas component that is fairly ubiquitous in chondrites, "HL" which is produced in supernova explosions and hosted in presolar diamonds, is completely absent in Hypatia, which implies some heterogeneity in the early solar nebula with respect to the population of presolar mineral grains.

(v) A further ET noble gas component, or mixture of components, about 20 times more abundant than "G" does not fit to any component or mixture of components described from chondrites. This appears to be devoid of helium and neon and we speculate here that it is a pre-nebula adsorbed component, associated with the most common, probably presolar mineral association of Hypatia, namely iron sulphide and nickel phosphide [3], which also has not been described from chondrites. The retention of an adsorbed noble gas component in Hypatia would indicate that no thermal processing has taken place as the cometary nucleus formed, and presolar mineral inclusions were preserved unchanged.

[1] Kramers J.D. *et al.* (2013). *Earth and Planetary Science Letters*, 382, 21-31.

[2] Ott U. (2002). Noble gases in meteorites - Trapped components. *Rev. Mineral. Geochem*. 47, 71-100.

[3] Belyanin, G. *et al*. (2014). IMA 2014 abstracts volume.

Shock-produced reidite and TiO_2-II in the Xiuyan crater, China

Chen M

Guangzhou Institute of Geochemistry, Chinese Academy of Sciences, Guangzhou, China, mchen@gig.ac.cn

The Xiuyan crater of China is a simple crater measuring 1.8 km in diameter and that is 150 m deep, occurring in a Proterozoic metamorphic terrain composed of gneiss, granulite, amphibolite, and marble [1]. It is an impact crater formed before 0.05 Ma ago. At the bottom of the crater, an impact breccia lens 188 m thick lies under lacustrine sediments. Previous investigation of the strongly shock-metamorphosed gneiss and granulite fragments from the impact breccia revealed abundant coesite crystallized from shock-produced SiO_2 melt [2]. Here, we report two other high-pressure polymorphs - reidite and TiO_2-II - that occur in moderately shock-metamorphosed gneiss fragments from the impact breccia.

The intact gneiss is composed of quartz, feldspar and amphibole, as well as the accessory minerals zircon, rutile and magnetite. Both quartz and feldspar have been mostly transformed into diaplectic glasses. Amphibole is mostly decomposed to oxides. Based on the classification of shock stages, the moderately shock-metamorphosed gneiss belongs to shock stage II corresponding to a shock pressure of 35-45 GPa and shock temperature of 300-900 $^{\circ}$C [3,4]. Zircon was strongly deformed. Reidite was found in about 20 % of zircon grains and mainly occurs as multiple sets of lamellae less than 1 mm in thickness (Figure 1a). Some thin layers of reidite up to 5 micrometres thick are also observed along planar fractures and irregular fractures in zircon. Compositions of reidite are identical to zircon. Rutile was broken into small pieces. The fine-grained clasts of rutile less than 2 mm in size have been transformed to TiO_2-II (Figure 1b). Some thin layers of TiO_2-II about 1.5 micrometers thick are observed along irregular fractures in coarse clasts of rutile. About 30 % of rutile in the rock has been transformed to TiO_2-II. It appears that both transitions of zircon to reidite and rutile to TiO_2-II are solid-state processes, which could correspond to a martensitic-like mechanism and thermally activated phase transformation. The formation of both reidite and TiO_2-II had, at least partially, involved diffusion-controlled growth. This study indicates that the shocked minerals in this crater might adopt different mechanisms of high-pressure phase transformations depending on the P-T conditions.

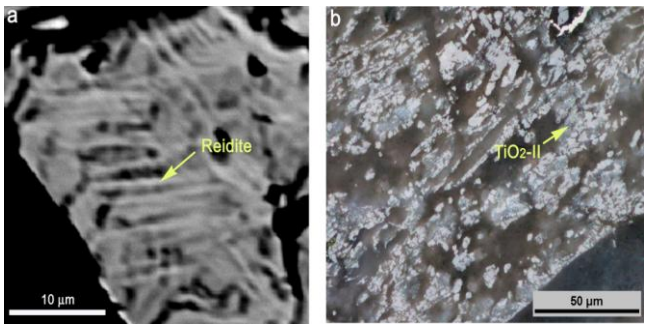

Figure1. a) Lamellar reidite in zircon, BSE image. b) TiO_2-II, Plane-polarized reflected light.

Acknowledgement: This research was supported by NNSF of China (41172044) and GIG CAS 135 Project (Y234071001).

[1] Chen M. *et al*. (2010). *Chinese Sci Bull*, 55, 1777-1781.

[2] Chen M. *et al*. (2010). *Earth Planet Sci Lett* 297, 305-313.

[3] Stöffler D. (1971). *J Geophys Res*, 76, 5541-5551.

[4] Grieve R.A.F. *et al*. (1996). *Meteorit Planet Sci*, 31, 6-35.

Highly variable response of baddeleyite to shock metamorphism in shergottite NWA 5298 and implications for planetary chronology

Darling J[1*], Moser D[2], Barker I[2], Tait K[3], Chamberlain K[4], Schmitt A[5]

1 - University of Portsmouth, U.K., *james.darling@port.ac.uk 2 - University of Western Ontario, London, Canada 3 - Royal Ontario Museum, Toronto, Canada

4 - University of Wyoming, USA 5 - University of California, Los Angeles, USA

In order to fully understand the precious archive that meteorites provide, it is critical to separate the effects of shock metamorphism that occurs during ejection from the mineralogical record of endogenic crustal processes.

Here we show that in the case of the highly shocked shergottite NWA 5298, this evolution can be resolved by combining electron beam microstructural techniques (CL, EBSD) with in-situ U-Pb SIMS analyses. We focus upon the effects of shock metamorphism on the U-Pb systematics of baddeleyite (ZrO_2) - a micrometer-scale phase common to many shergottites. Unlike zircon, the relationship of shock heating and deformation with retention of radiogenic Pb is poorly known.

Baddeleyite grains from a single polished thin-section show a wide array of deformation microstructures. These include fracturing, varying degrees of amorphization and granulation, plastic deformation, and recrystallization due to post-shock fluids: reflecting local variations in shock pressures and waste heat. SIMS U-Pb isotope analyses of these grains reveal variable degrees of age resetting, broadly correlated with microstructure and preservation of primary igneous CL zonation. Degree of Pb loss (as much as 80%) is also broadly correlated with degree of growth of post-shock zircon reaction rims. The zircon reaction-rims are linked to release of Si-rich fluids during quenching of shock melt pockets during transit to space.

These findings, contrary to the results of shock loading experiments [1], indicate that baddeleyite U-Pb ages can be reset under certain shock metamorphic pathways. The U-Pb data are thus useful for determining both the primary age of the meteorite assemblage and bracketing the time of its Earthward launch.

[1] Niihara *et al*. (2012). *EPSL*, 341-344, 195-210.

Archean spherule layers in the Barberton Mountain Land: a consortium study on Earth's early impact record

Fritz J[1*], Mohr-Westheide T[1], Reimold W U[1,2], Schmitt R[1], Hofmann A[3], Koeberl C[4,5], McDonald I[6], Luais B[7], Salge, T[8], Tagle R[8], Schulz T[4], Mader D[4], Hoehnel D[1]

1 - Museum für Naturkunde, Berlin, Germany, *joerg.fritz@mfn-berlin.de 2 - Humboldt University Berlin, Germany 3 - University of Johannesburg, South Africa 4 - University of Vienna, Austria 5 - Museum for Natural History Vienna, Austria 6 - Cardiff University, Cardiff, U.K. 7 - CRPG-CNRS, Nancy, France 8 - Bruker Nano GmbH, Berlin, Germany

Introduction: The marine meta-sedimentary sections in the Barberton Mountain Land (BML) were subject to an ICDP drilling campaign in 2012. The Archean lithologies of the BML contain spherule layers interpreted as the oldest known traces of impact cratering events on Earth [1, 2]. So far, three to four (S1-S3; possibly S4) impact event layers (maybe more [3]) have been identified in the time interval 3.5 to 3.2 Gyr. During that time the Moon, and by implication the Earth, experienced a substantially higher impact flux than today [4]. The Earth's sedimentary record allows investigating the frequency of impacts and the types of projectiles involved in the late stages of the Heavy Bombardment period [5].

Methods and overview: In a consortium study we are investigating a 2 meter core section of the ICDP BARB 5 drill core hosting 5 spherule occurrences. Before cutting the obtained quarter core into subsections for further analysis high spatial resolution (~25 µm spot size) X-ray elemental maps of the up to 20 cm long quarter-core sections were obtained. After cutting and sample preparation we have begun to conduct SEM, EMPA, Raman spectroscopy, instrumental neutron activation analysis, and LA-ICP-MS studies for a detailed petrographic and geochemical characterization of the samples. This is aimed at discrimination of the primary characteristics related to the impact event and the secondary characteristics that developed during (re)deposition, diagenesis, tectonic displacement, and metamorphism [3, 6]. Remarkable differences in the occurrence of "primary characteristics" such as occurrence of Ni-rich chromite and zircon, and platinum group element abundances raise questions whether any of these occurrences in one layer can be considered diagnostic for a specific event or rather depends on modifications after (re)emplacement of the impact ejecta (Mohr-Westheide *et al*., this meeting).

Issues related to locally extremely high Ir enrichments of up to four times the Ir concentration in chondrites [6] are addressed by localizing and identifying the phases that host the Platinum Group Elements (refer to McDonald *et al*. & Mohr-Westheide *et al*., this meeting).

Future work will target possible isotope fractionation processes during the impact event by conducting isotopic studies of volatile elements (Ge) of the spherule layers. The five spherule-bearing horizons in the BARB-5 drill core present a complex succession that will provide new insights into the "primary" characteristics and "secondary" modification of these deposits.

[1] Lowe D.R. *et al*. (2003). *Astrobiology* 3, 7-47.

[2] Lowe D.R. and Byerly G.R. (1986). *Geology* 14, 83-86.

[3] Hoffmann A. *et al*. (2006). *GSA Special Paper* 405, 33-56.

[4] Neukum G. *et al*. (2001). *Space Sci. Rev.* 96, 55-86.

[5] Fritz J. *et al*. (in press) *Planet. Spac. Sci.*.

[6] Koeberl C. and Reimold W.U. (1995). *Precambr. Res.* 74, 1-33.

Mineralogical evidence of shock and related thermal phenomena in the Vredefort Dome, South Africa

Gibson R L

University of the Witwatersrand, Johannesburg, South Africa, roger.gibson@wits.ac.za

The 90-km-wide Vredefort Dome represents the deeply exhumed central uplift of an originally ca. 250-300-km-wide, 2.02 Ga impact structure. The Dome presents an opportunity to study both the effects of shock wave interaction and impact processes in a variety of rocks on a broad range of scales, and to consider the little-explored realm of thermal effects of giant impacts, in which shock-induced heating affects already significantly pre-heated rocks that may have also remained buried for a significant period after the impact. Such knowledge is invaluable in the search for other exhumed giant impact structures.

Field evidence for the impact includes abundant melt breccias - kilometer-long dykes of impact-melt rock, and ubiquitous pseudotachylitic breccia vein/dyke occurrences - as well as shatter cones and complex faulting, with or without folding, at a variety of scales (mm to km). Unequivocal impact phenomena are restricted to the central uplift, and most lie at $R \leq 30$ km from the center of the dome.

Microscopic evidence of the impact includes coesite and stishovite and PDF in quartz and PF as well as granular shock texture in zircon, as well as an array of microtextures that are interpreted as annealed shock-induced features after diaplectic glasses and/or shock melts. Coesite and stishovite are associated with thin pseudotachylitic breccia veins, signifying an origin by shock compression for the latter. Other evidence of localised shock effects in the vicinity of thin veins has been documented; however, the timing and mechanism of formation of larger veins remains controversial.

Whilst early mineralogical studies in the Dome noted the lack of glass in PDF in quartz and concluded that the rocks experienced post-shock annealing, the extent of this annealing was originally severely underestimated. In recent years, estimation of the post-impact metamorphic conditions has assisted in constraining the maximum P_{shock} by allowing assessment of the relative contributions to the post-impact T by the pre-impact geotherm and shock heating. This evidence indicates that the central uplift was characterised by a ca. 40 °C/km *lateral* post-impact thermal gradient, with peak post-shock T increasing from ~ 300 °C at R = 25 km to ≥ 1000 °C at $R \leq 5$ km. The high post-shock T in the central parts of the Dome has created an unusual metamorphic granofels zone, the outer limits of which are inferred to coincide with the limits of wholesale diaplectic feldspar glass formation at P >30 GPa (the glass now being completely recrystallised to <50 µm aggregates). The sustained high post-shock T for up to 1 Ma after impact in these rocks also led to local anatexis of appropriate lithologies.

Throughout the Dome, and even in the granofels zone, evidence indicates that shock effects remain highly heterogeneous, down to the microscopic scale.

Shear-induced ringwoodite formation in the Martian basalt Dar al Gani 670: a microstructural investigation

Greshake A[1*], Fritz J[1], Wirth R[2]

1 - Museum für Naturkunde, Berlin, Germany, *ansgar.greshake@mfn-berlin.de 2 - Helmholtz Centre Potsdam, GFZ German Research Center for Geosciences, Potsdam, Germany

The Martian meteorite Dar al Gani 670 is an olivine-phyric shergottite mainly composed of mm-sized olivine megacrysts set into a fine-grained basaltic groundmass of dominantly pigeonite and maskelynized plagioclase [1]. During impact ejection from Mars, the rock experienced strong shock metamorphism. Shock effects include planar and irregular fractures, strong mosaicism, and planar deformation features in olivine, intense fracturing and polysynthetic twinning in pyroxene, maskelynitized plagioclase, and shock-melt veins and pockets [2]. The meteorite contains a ~1.3 mm sized, almost euhedral olivine grain that was sheared along a shock-melt vein cutting through the crystal. From the olivine-vein interfaces thin, ~1-3 µm wide lamellae oriented along distinct crystallographic orientations extend into the olivine megacryst. These lamellae are often more Fe-rich than the host olivine and are separated from each other by thin zones of more Mg-rich material. Raman spectroscopy and electron backscattered diffraction attest that the lamellae in the sheared olivine contain blocky crystals of ringwoodite, the spinel-structured high-pressure polymorph of olivine. Stereographic projection pole figures reveal special orientation relationships between ringwoodite and olivine: $<001>_{ol}$ parallel with $<110>_{rw}$ and $<100>_{ol}$ parallel with $<111>_{rw}$. Due to their narrow width, the nature of the Mg-rich zones between the ringwoodite crystals remains unclear. To exploit the microstructural characteristics of this interstitial material, the ringwoodite crystals and the olivine host, foils were cut from the respective phases with the focused ion beam technique (FIB) and studied by transmission electron microscopy (TEM). The TEM studies document an increasing density of lattice defects in the olivine host crystal towards the shock melt vein. These defects are typically concentrated in distinct, sometimes band-like domains. Blocky ringwoodite crystals occurring close to the vein-olivine interface show an even higher density of lattice defects. At the direct vein-olivine contact the ringwoodite crystals display curved irregular outlines and appear to be partly to almost completely dissolved by the hot melt. At this contact the melt crystallized to several nm-sized pyroxenes + ferrite (alpha-Fe) and FeS spheres. The narrow Mg-rich zones interstitial to the partly dissolved defect-rich ringwoodites are composed of 50 to 100 nm sized crystallites that nucleate on the ringwoodite crystal surfaces and grow into the interstitial zones. These tiny grains have random orientations and are almost defect-free. Selected area diffraction patterns prove that the small grains are olivine, wadsleyite, and ringwoodite, all occurring next to each other in the same thin zone. The findings indicate that the high density of lattice defects in olivine very likely developed during brittle shearing. Hot melt injected along the shear plane provided the temperatures required for the olivine-ringwoodite transformation, which preferentially occurred in regions with high defect concentrations. The hot melt almost completely dissolved ringwoodite that grew directly at the olivine-melt vein interface. Additionally, the melt migrated along particular (maybe less defect-rich) crystal planes into the olivine host and partially dissolved the growing ringwoodite grains. Almost defect-free ringwoodite, wadsleyite, and olivine grains occurring interstitial to the partially dissolved ringwoodites document crystallization during decreasing pressure and low stress.

[1] Folco L. and Franchi I.A. (2000). *Meteorit. Planet. Sci*., 34, p. A54.

[2] Greshake A. *et al*. (2013). *Earth Planet. Sci. Lett*., 375, 383-394.

Luminescence-based laboratory astromineralogy: past, present and future

Gucsik A[1*], Pakovi T[2]

1 - University of Johannesburg, South Africa *argu1986@hotmail.com

2 - Micromatlab Hungary Kft., Hungary

The formation mechanism of diamond in the planetary nebula [1], low-temperature crystallization of forsterite in the Solar System [2-4], shock metamorphism of the Martian rocks and their analogous materials [5, 6], spectral properties of the refractory minerals in the primitive chondrites, shock-wave barometry and degree of space weathering of fine-grained astromaterials are still poorly understood.

Scanning Electron Microscope-Cathodoluminescence (SEM-CL) microscope and spectrscope provide an adequate background for the analysis of different Earth and Planetary materials that require the non-destructive, easy-to-use, and relatively rapid analysis. In this case, SEM-CL would provide a powerful method for the study of the the above-mentioned samples, which can aid to understand more about the crystallization environment of minerals in the Early Solar System, for instance.

The purpose of this abstract is to summarize of results on the new scientific field, luminescence-based laboratory astromineralogy, mentioning its future perspectives.

[1] Gucsik A. *et al*. (2012). *Microscopy and Microanalysis*, 18, 1285-1291.

[2] Gucsik A. *et al*. (2013). *Meteoritics and Planetary Science*, 48, 2577-2596.

[3] Nishido H. *et al*. (2013). *Geochronometria*, DOI 10.2478/s13386-013-0116-7.

[4] Gucsik A. *et al*. (2012). *Journal of Luminescence*, 132, 1041-1047.

[5] Gavin P. *et al*. (2013). *Journal of Geophysical Research*, 118, E004185.

[6] Kayama M. *et al*. (2012). *Journal of Geophysical Research Planets*, 117, E09007.

Projectile-target interaction during cratering in nature and experiment

Hecht L[1*], Ebert M[1], Hamann C[1], Deutsch A[2], Kenkmann T[3], Wirth R[4]

1 - Museum fürNaturkunde Berlin, Berlin, Germany, *lutz.hecht@mfn-berlin.de 2 - Institut für Planetologie, WWU Muenster, Germany 3 - Institut für Geo- und Umweltnaturwissenschaften, ALU Freiburg, Germany 5 - Deutsches GeoForschungsZentrum Potsdam, Germany

Chemical traces of extraterrestrial material in impactites are important for the detection and identification of projectiles that impacted the Earth. Little is known, however, about the mixing processes between meteoritic material and terrestrial impactites during cratering. Our recent studies have been focused on the interaction of iron meteorites with SiO_2-rich targets. In the framework of the MEMIN (Multidisciplinary Experimental and Modeling Impact Research Network) research group investigations hypervelocity impact experiments have been performed with sandstone and quartzite targets and Campo del Cielo iron meteorite and Co-Cr-V-Mo-W-rich steel projectiles [1,2]. For comparison, young and pristine impact melts from the Wabar craters (Saudi Arabia) have been studied [3]. In this case an iron meteorite (IIIAB) impacted a quartz-rich sand target about 300 years ago.

In nature and experiments droplets of molten projectile are mechanically mixed into partially or completely molten target material. During mingling of melts, Fe and some lithophile elements like Cr and V are strongly partitioned into the silicate target melt. Thereby projectile droplets become smaller and are relatively enriched in siderophile elements (Ni, Co, Mo, W). Inter-element ratios of projectile tracer elements within the contaminated target melts differ strongly from the original ratios of the projectile. The fractionation results from differences in the reactivity of the respective elements with oxygen during interaction of metal melt with silicate melt. Our results indicate that the principles of projectile-target interaction and associated fractionation do not depend on impact energies (at least for the selected experimental conditions) and water-saturation of the target. Mass transfer of some elements from the projectile melt to the target melt is enhanced in case of non-porous targets (quartzite). Examples are given were increasing meteoritic element enrichment in target melts occurs when approaching projectile melt droplets, which documents the element transfer process. Due to strong iron enrichment liquid immiscibility between an iron-rich ultrabasic (L_{Fe}) and a highly polymerized silica-rich (L_{Si}) melt is induced during cooling. Various emulsion textures are developed depending on the mass ratio between different melts. The quenched impact melt is finally composed of three coexisting melts with projectile droplets located within an emulsion of L_{Fe} and L_{Si}.

[1] Ebert M. *et al*. (2013). *Meteorit Planet Sci*, 48, 134-149.

[2] Ebert M. *et al*. (2014). *Geochim Cosmochim Acta (in press).*

[3] Hamann C. *et al*. (2013). *Geochim Cosmochim Acta*, 121, 291-310.

Formation process of maskelynite in meteorite analyzed by cathodoluminescence spectroscopy and microscopy

Kayama M[1*], Nishido H[2], Sekine T[3], Tomioka N[4], Kaneko S[5], Miyahara M[3], Ohtani E[5], Ozawa S[5], Katoh Y[3], Ninagawa K[2]

1 - Department of Earth and Planetary Systems Science, Graduate School of Science, Hiroshima University, Japan, *kayama0127@gmail.com 2 - Okayama University of Science, Japan 3 - Hiroshima University 4 - Institute for Study of the Earth's Interior, Okayama University 5 - Tohoku University, Japan

Maskelynite, an amorphous product after feldspar due to an impact event, is common in stony meteorites that have experienced shock metamorphism and is used as a shock barometer, by the refractive index method, the paragenetic assembly of high-pressure phases, and recently Raman and cathodoluminescence (CL) spectroscopy. Recent scientific interests have focused on such impact history to interpret evolution of the Solar System (e.g., Giant impact and the late heavy bombardment on the Moon and the Earth), but it has been uncertain whether maskelynite is produced by shock-induced amorphization of plagioclase in a solid-state reaction or by quenching from shock-induced dense melts of plagioclase at high pressures. CL spectroscopy and microscopy provide useful information on existence and distribution of lattice defects produced by destruction or distortion of atomic linkages with high-spatial resolution, which should be more informative to clarify vitrification of feldspar. In this study, CL analysis of maskelynite in meteorites, as well as diaplectic glasses (produced without melt) derived from dynamic and static high-pressure experiments has been conducted to interpret the formation process of maskelynite from feldspar.

Maskelynite in Martian meteorites (Dhofar 019, Shergotty, Zagami and NWA 2975), lunar meteorites (NWA4734) and L6 chondrites (Yamato-790729 and Tenham) were employed for CL spectroscopy and microscopy. Single crystals of sanidine from the Eifel, Germany and albite from Minas Gerais, Brazil were selected as starting materials for high-pressure experiments using a propellant gun and a diamond anvil cell.

CL spectroscopy of maskelynite in the present meteorites commonly reveals emission bands at 330 and 380 nm. Similar UV and blue emissions are also detected in CL spectra of diaplectic glasses recovered from high-pressure experiments using both a propellant gun and diamond anvil cell. Deconvolution of CL spectra obtained from these maskelynites and the recovered diaplectic glasses successfully separate the UV to blue emission bands into Gaussian components at 3.88, 3.26 and 2.95 eV, which have been undetectable in unshocked feldspars. The emission components are, therefore, characteristic CL signals of maskelynite and diaplectic glass from the high-pressure experiments and may be responsible for the pressure-induced defect centers in octahedral and tetrahedral coordination of Si and Al atoms. The emission intensities increase with an increase in the induced pressures from 10.0 to 40.1 GPa for the dynamic experiments and 21 to 35 GPa for the static experiment, but the intensities of the diaplectic glasses recovered from the dynamic experiments are lower than that from the static experiments in spite of the comparable pressure conditions. This may be due to difference of duration time of the induced pressure.

CL images of the lunar and Martian meteorites indicate that the maskelynite occurring in melt pockets or shock veins shows bright CL emission, but that in contact with or located near them has a dark or dull emission. This might be explained by formation of large amounts of defects during rapid quenching process from the dense melt for the former and by elimination of the defect centers due to the effect of annealing of shock metamorphism above given temperature without melting, for the latter. On the other hand, maskelynite far from melt pockets or shock veins has higher CL intensities than that located near the melt occurrences, but lower than that occurring in them. Furthermore, distribution of their CL intensities is quite homogeneous under the CL microscope. These facts imply that the post-shock temperature effects may have almost no effect on the CL character of maskelynite if the temperature exceeds annihilation temperature of the defect center or the melting point. CL spectroscopy and microscopy allow us to distinguish maskelynite originating from solid-state reaction and quenching from dense melts.

Mapping the distribution of projectile material in Archaean impact spherule layers using LA-ICP-MS

McDonald I[1*], Fritz J[2], Mohr-Westheide T[2], Reimold W U[2,3], Koeberl C[4,5], Simonson B[6]

1 - Cardiff University, Cardiff, U.K., *mcdonaldi1@cardiff.ac.uk 2 - Museum für Naturkunde Berlin, Berlin, Germany 3 - Humboldt University Berlin, Germany 4 - Dept. of Lithospheric Research, University of Vienna, Austria 5 - Natural History Museum Vienna, Austria 6 - Dept. of Geology, Oberlin College, Oberlin, USA

Impact spherule-rich layers have been recognised within early-mid Archaean greenstone belts (Barberton in South Africa and in the Pilbara of Western Australia [1]) and in the late Archaean platform sequences of the Griqualand West and Hamersley basins [2]). The layers carry elevated levels of platinum-group elements (PGE), in chondritic proportions for the most immobile PGE, and may be characterised by extraterrestrial Cr isotopes [2, 3]. Three late Archaean layers (Jeerinah-Monteville, Paraburdoo-Reivilo and Dales Gorge-Kuruman) can be correlated between the two basins [4] indicating that impact spherules were widely (possibly globally) distributed. Levels of extraterrestrial component (ETC), represented by PGE and Cr concentrations, vary from <1% to >100% in some layers [e.g., 1-3]. The cause of this variation and the carrier phases for PGE and Cr in the spherule layers are poorly known. The aim of this work is to understand the distribution of these trace elements and how these might relate to primary condensation or low temperature remobilization processes.

The ICDP-BARB 5 core section available for this study likely relates to the S3 spherule layer of the Barberton belt. S3 and the late Archaean Paraburdoo-Reivilo layer are both characterised by extremely high ETCs which make them ideal candidates for trace element mapping of the distribution of projectile material by time resolved laser ablation ICP-MS. Preliminary results have been reported from Paraburdoo-Reivilo spherules [5]. Results for the S3 layer are reported for the first time.

Mg, Cr and Fe are depleted in the spherules and maps for V and Mg (Figure 1) effectively define the outlines of spherules and surrounding matrix for both spherule layers. In both layers, sulphides occur but are PGE-poor and do not host former projectile material (Figure 1). Chromium in Reivilo is associated with small particles (possibly spinels) in spherules and more broadly distributed in the matrix, whereas it is mainly present in the matrix of the S3 layer (Figure 1). At Reivilo, maps for high temperature PGE (Os, Ir, Ru, Rh and Pt) show single or clustered pixels that reflect tiny (<20 µm) PGE-rich particles within spherule interiors; similar to maps produced by [5] for the matching Paraburdoo layer. Pd and Au are always found in the matrix at Reivilo. In contrast, high temperature PGE maps for S3 indicate that these elements are not located within the spherules but are present in Cr-rich areas of the matrix. It is not known whether this is a primary feature or reflects remobilization of the PGE and Cr, possibly related to the more extensive metamorphism and deformation that all of the Barberton spherule layers have experienced in comparison with Reivilo and the other late Archaean layers.

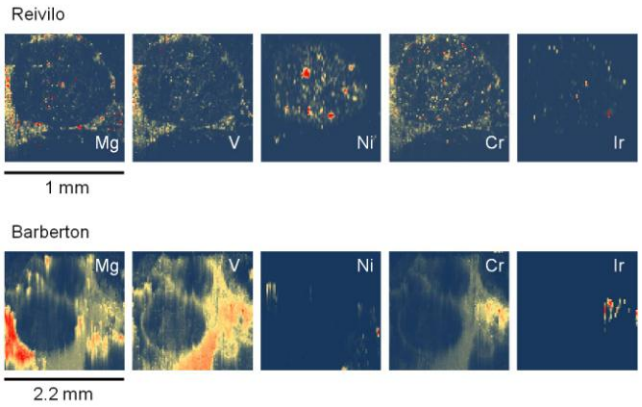

Figure 1: LA-ICPMS element maps. Note the scale and resolution change. Laser beam diameters and pixel sizes: 12 micrometers (Reivilo) and 25 micrometers (Barberton).

[1] Glass B. and Simonson B.M. (2010). *Elements*, 8, 3-48.

[2] Simonson B.M. *et al.* (2009). *Precambr. Res.*, 175, 51-76.

[3] Kyte F.T. *et al.* (2003). *Geology*, 31, 283-286.

[4] Hassler S. *et al.* (2011). *Geology*, 39, 307-311.

[5] Goderis S. *et al.* (2013). *Earth Planet. Sci. Lett.*, 376, 87-98.

ICDP drill core BARB5: first petrographic results of the Archean Impact Spherule Layer Consortium

Mohr-Westheide T[1*], Fritz J[1], Reimold W U[1,2], Schmitt R-T[1], Hofmann A[3], Koeberl C[4,5], McDonald I[6], Luais B[7], Tagle R[8], Salge T[8], Schulz T[4], Mader D[4], and Hoehnel D[1]

1 - Museum für Naturkunde, Berlin, Germany, *tanja.mohr-westheide@mfn-berlin.de

2 - Humboldt University Berlin, Berlin, Germany 3 - University of Johannesburg, South Africa 4 - University of Vienna, Austria 5 - Natural History Museum Vienna, Austria 6 - Cardiff University, Cardiff, U.K. 7 - CRPG-CNRS, Nancy, France 8 - Bruker Nano GmbH Berlin, Germany

Archean spherule layers (ca. 3.47-3.2 Ga) in the Barberton Greenstone Belt (BGB) represent the oldest known impact deposits on Earth [1, 2]. Primary signatures in the spherule layers may elucidate the impact event(s) and the projectiles involved. A comprehensive study of sedimentary, petrographic, mineralogical, and geochemical characteristics of spherule layers in ICDP drill core BARB5 from the Barite Valley Syncline of the BGB is being carried out.

Four ca. 4 cm thick layers with densely packed, 0.3-2 mm sized spherules are separated by shale intercalations in a 20 cm core interval (511.29-511.51 m). All spherule beds are comprehensively altered to quartz-phyllosilicate-K-feldspar-Mg-siderite-barite-calcite assemblages. Sulfide mineralization (mainly py, cpy, and gersdorffite) increases in abundance from lowermost layer 1 to uppermost layer 4. Only layers 2-4 contain zircon and nickel-rich chromium-spinel. SEM-EDX analyses indicate that spinel has distinct, multiple types of zonation with respect to Fe, Ni, Zn, and Cr contents. Spinel aggregates representing shattered precursor crystals frequently show marginal Zn-enrichment on all fragments.

Neutron activation analysis of spherule layer and shale show distinctly elevated contents of siderophile elements (Ni, Co, Ir, and Os), and of Cr and Au over the whole sample section. The lowest contents were found in bottom layer 1, with ca. 0.3-10 ppb Ir, 7-22 ppm Co, and 120-470 ppm Ni. Highest amounts were found in spherule layer 2 with ca. 600 ppb Ir, 250 ppm Co, and 3800 ppm Ni, and at the top of layer 3 with 730 ppb Ir, 530 ppm Co, and 5400 ppm Ni. In other parts of the section Ir concentration is in the 150-400 ppb range.

The presence of four closely spaced but well separated spherule beds is suggestive of aquatic deposition after a single impact event, with multiphase currents having affected sedimentation. Preliminary petrographic and geochemical findings indicate strong hydrothermal overprint for all lithologies in the studied section of the BARB5 core. Primary characteristics include spherule size, shapes, and presence of Ni-rich chromite (projectile related formation), as well as zircon (terrestrial source). Sulfide mineralization is of secondary origin. High Zn concentrations frequently observed along cataclased spinel grains are likely related to late overprint. High abundances of the siderophile elements and PGEs are thought to reflect extraterrestrial components. As already observed by [3], these abundances are on the same level, or even exceeding, the contents of these elements in chondritic meteorites.

[1] Lowe D.R. *et al.* (1989). *Science*, 245, 959-962.

[2] Lowe D.R. *et al.* (2003). *Astrobiology*, 3, 7-47.

[3] Koeberl C. and Reimold W.U. (1995). *Precambr. Res.*, 74, 1-33.

The 2014 census of African impact structures

Reimold W U[1*2] and Koeberl C[3,4]

1 - Museum für Naturkunde Berlin, Berlin, Germany, *uwe.reimold@mfn-berlin.de 2 - Humboldt University Berlin, Germany 3 - University of Vienna, Austria 4 - Natural History Museum, Vienna, Austria

After more than 50 years of dedicated impact cratering research on Earth the overall tally of confirmed impact structures, as currently listed in the Earth Impact Database (University of New Brunswick) is 185. Many more possible structures have been proposed - worldwide, but confirmation of their origin by hypervelocity impact must still be obtained. This can only be achieved through either (1) finding of meteorite debris, (2) detection of chemical traces of the projectile in impact breccias, especially impact melt rock, (3) presence of shatter cones or (4) of bona fide shock metamorphic microdeformation features in shocked target rock or breccia constituents. The African record has recently been comprehensively reviewed by us [1]. To date, it comprises a mere 19 confirmed impact structures (only 5 more than 20 years ago when the last review was compiled), as well as one location with abundant shatter cones in the High Atlas mountains of Morocco, near the village of Agoudal, which is obviously the remnant of an impact structure. However, 49 sites of proposed but not yet confirmed structures were listed, some of which represent excellent targets for further studies (although in most of these cases, local conditions involving civil strife or landmine deposits render this hazardous). In addition, a total of 28 structures have been dismissed so far as not being of impact origin. This overall record strongly indicates that impact cratering research has taken hold in Africa, with considerable progress having been made with respect to promotion of such studies, as well as with detailed research contributions that not only have been of parochial interest but that, in part, have fertilized international science with regard to impact cratering, but also, inter alia, regional geology and geophysics, environmental science, metamorphism, and geoheritage promotion and conservation.

[1] Reimold W.U. and Koeberl C. (2014). *Journal of African earth Sciences*, 93, 57-175 (Open Access).

Eutectic metal + troilite + Fe-Mn-Na phosphates + Al-free chromite assemblage in shock-produced chondritic melt of the Yanzhuang chondrite

Xie X[1*], Chen M[1], Zhai S[2], Wang F[1]

1 - Guangzhou Institute of Geochemistry, Chinese Academy of Sciences, Guangzhou, China, *xdxie@gzb.ac.cn 2 - School of Earth and Space Sciences, Peking University, Beijing, China

Fe-Mn phosphates usually do not occur in ordinary chondrites [1], but some Fe-Mn phosphates were reported in iron and pallasite meteorites [2], and a new Fe-Na phosphate mineral galileiite $NaFe_4(PO_4)_3$ was found in troilite nodules in iron meteorites of the IIIA and IIIB groups [3]. More recently, we studied the mineralogy of a large eutectic metal-troilite nodule in the heavily shocked Yanzhuang H6 chondrite and found several tens of Fe-Mn-Na phosphate globules (up to 10~12 μm in diameter) and two chromite crystals (35~45 μm in size) in troilite of this nodule. Electron microprobe and Raman spectroscopic analyses show that a few phosphate spherules have the composition of Na-bearing graftonite $(Fe,Mn,Na)_3(PO_4)_2$, and the majority of them corresponds to two phosphate minerals: Mn-bearing galileiite $Na(Fe,Mn)_4(PO_4)_3$ and a possible new phosphate phase of $Na_2(Fe,Mn)_{17}(PO_4)_{12}$ composition. Chromite crystals in this eutectic nodule are Al-free in composition that is different to the Al-rich chromite in the Yanzhuang chondritic host. It is assumed that such eutectic crystalline metal + troilite + Fe-Mn-Na phosphates + Al-free chromite assemblage was identified for the first time in the shock-produced melt of chondritic meteorites.

The Yanzhuang meteorite is classified as a petrological type H6 chondrite, and is considered to be one of the most heavily shocked and severely reheated chondrites described so far [4]. It was shocked to a peak pressure of some tens of GPa and a peak temperature of ~2000 ºC [5]. All minerals in melt regions were melted after pressure release to form a chondritic melt due to very high post-shock heat that brought the chondrite material above its liquidus. The volatile elements P and Na released from original whitlockite and plagioclase along with the elements Cr and Mn released from original chromite were concentrated into the shock-produced Fe-Ni-S-O melt at high temperatures. During cooling, microcrystalline olivine and pyroxene first crystallized from the chondritic melt, and metal-troilite eutectic intergrowths and silicate melt glass finally solidified at about 950-1000ºC. On the other hand, P, Mn and Na in the Fe-Ni-S-O melt combined with Fe and crystallized as Fe-Mn-Na phosphates within troilite, while Cr combined with Fe and crystallized as Al-free chromite also within troilite.

[1] Fuchs (1969). *Meteorite Research* (ed. P.M. Millman), pp.683-695.

[2] Olsen and Fredriksson (1966). *Geochim. Cosmochim. Acta*,30, 459-470.

[3] Olsen and Steele (1997). *Meteorit. Planet. Sci.*, 32, A155-A156.

[4] Xie X. *et al*. (1991). *Meteoritics*, 26, p. 411.

[5] Chen (1992). *Ph.D thesis*, Institute of Geochemistry, Chinese Academy of Sciences, Beijing, 95pp.

Shock experimental investigation of the formation mechanism for maskelynite

Fritz J[1*], Greshake A[1], Fernandes V[1], Reimold WU[1,2], Wünnemann K[1]

1 - Museum für Naturkunde Berlin, Berlin, Germany, *joerg.fritz@mfn-berlin.de 2 - Humboldt University Berlin, Berlin, Germany

Introduction: Diaplectic glasses of plagioclase (maskelynite) and silica are characterized by the lack of flow structures and vesicles [1]. These glasses retain the original grain boundaries and chemical zonation of the original mineral grains, from which they formed via shock. Diaplectic glasses have lower density (refractive indices) than the crystalline phases, and higher densities compared to thermally quenched glasses, of identical composition. Two shock metamorphic mechanisms, by which diaplectic glasses form from their crystalline precursors, have been proposed: (1) a kind of solid-state transformation without melting [2], and (2) a combination of shock melting and subsequent quenching at high confining pressure [3, 4].

Method: To clarify this we have conducted a series of shock recovery experiments at 20-45 GPa shock pressures and ambient temperature, using plagioclase of different chemical compositions ($An_{55;}$ An_{94}). In addition, a series of samples was shocked at different initial temperatures of 293 and 77 K. The shock metamorphic effects in the samples were characterized by optical microscopy including refractive index measurements and Raman spectroscopy. Compositions of mineral grains used were determined by EMPA.

Results: The plagioclase samples subjected to the same shock pressures but different initial temperatures of 293 and 77 K displayed an identical degree of shock metamorphic overprint. Shock experiments with An_{94} showed that maskelynite was present in samples shocked to ~24 GPa - at lower shock pressures compared to plagioclase with lower An content [5].

Discussion: These results advocate that diaplectic glasses from by static failure of the crystal lattice due to overpressure, i.e., physical crushing. Melting of plagioclase during shock seems unrelated to diaplectic glass formation, because one would expect that higher shock pressures (thus higher shock induced heating) would be required to melt samples shocked at initial temperatures of 77 K compared to those shocked at 293 K, which is not observed [also 5]. Additionally, we observe that An-rich plagioclase transforms to maskelynite at lower shock pressure than An-poor plagioclase. This trend is opposite to the melting behaviour of plagioclase where melting temperatures increase with increasing An content. Instead, this trend seems related to the physical stability of plagioclase. With increasing An content more Si is replaced by Al and the Si-O bounds are weaker compared to Si-O bounds in the lattice structure of tectosilicates [6, 7].

[1] von Engelhardt W. *et al*. (1967). *Contr. Mineral. Petrol.*, 15, 93-102.

[2] Stöffler D. (1967). *Contrib. Mineral. Petrol.*, 16, 51-83.

[3] Langenhorst F. (1994). *Earth Planet. Sci. Conf.*,128, 683-698.

[4] Chen M. and El Goresy A. (2000). *Earth Plamnet. Sci. Conf.*, 179, 489-502.

[5] Stöffler D. *et al*. (1986). *Geochim. Cosmochim. Acta*, 50, 889-903.

[6] Fritz J. *et al*. (2011). *Int. J. Impact Eng.*, 38, 440-445.

[7] Matson D.W. *et al*. (1986). *Amer. Mineral.*, 71, 694-704.

Cathodoluminescence properties of forsterite in the Tagish Lake meteorite

Gyollai I[1], Gucsik A[2*], Ninagawa K[3], Izawa M[4], Nishido H[3]

1 - University of Vienna, Vienna, Austria 2 - University of Johannesburg, South Africa, *argu1986@hotmail.com 3 - Okayama University of Science, Japan 4 - University of Winnipeg, Canada

Introduction: The Tagish Lake meteorite fell by fireball event in January 2000 [1]. This meteorite is an intermediate between CM and CI chondrites, the original pre-atmospheric weight was 200 kg [1], and the meteorite was classified as a CI2 chondrite [2]. Tagish Lake is brecciated, matrix-dominated material, which contains chondrules with less than 1 mm diameter, altered Calcium-Aluminium-rich (CAIs) up to 2 mm in diameter, magnetite, invidual grains of olivine, Ca-Fe-Mn carbonates (mainly mixture of magnesite and siderite), Fe-Ni sulfides including pyrrhotite [1].

Results: The analyzed chondrule is a less altered intermediate between granular and barred texture chondrules. The mesostasis is composed of both phyllosilicates and carbonaceous material. In both types of chondrules, olivines show zoned mosaicism, which may correspond to inhomogeneity.

The major part of the selected grain is composed of a mineral-fragment rich groundmass, which contains a strongly altered forsterite chondrule. Cathodoluminescence spectral features have broad luminescence centres at 400-460, 600-650 and 700 nm. In some parts of the selected grain, peak intensities at 600-700 region are relatively high. After correction of CL spectra, a peak at 400 nm, shoulders at 600-650 and 700-800 nm can be identified. In energetic CL spectra, broad shoulders occur in the 0-2 eV region, and a broad peak appears in the 2.5-3.5 eV region.

Discussion: The broad luminescence center at 400 nm corresponds to structural defect. The variation of luminescence intensity in chondrule determines chemical inhomogenity due to low degree of thermal metamorphism [3]. At duller red luminescence centers, the olivine has fayalitic component, whereas light luminescent patches are pure forsterites.

The fractures in chondrules are non-luminescent, which is driven by either enrichment of divalent Fe due to terrestrial weathering, or shock-driven lattice defect. The blue luminescence centres int several areas are addressed as intrinsic defect centres. This defect centre is associated with either Al^{3+} substitution for Si^{4+} ions or lattice deformation due to Ca and Ti ions [3, 4].

The broad emission at 650 nm is assigned to Mn^{2+} impurity centre in M2 position of forsterite [3]. The broad emission bands at 720 nm and also in the higher wavenumber range are attributed to Cr^{3+} activator in the M1 and M2 sites and interstitial positions of forsterite [3].

The activation energies for red emissions are centered at 0.8 and 1.74 eV, where the 1.74 eV peak corresponds to Cr^{3+}, 1.94 Mn^{2+}. The activation energies in the blue region appears as a broad band at 3.15 eV, the FWHM of which is 1 eV, which corresponds to defect centre [3].

Conclusion: The CL zonation corresponds to thermal quenching, chemical inhomogenities in chondrules. The blue CL emission is caused by lattice defect. The CL properties of Tagish Lake forsterite depend on distribution of activator elements (Cr, Mn), quenching element (Fe^{2+}), and crystal lattice defect.

[1] Brown P.G. *et al*. (2000). *Science*, 290/5490, 320-325.

[2] Grady M.M. *et al*. (2002). *Meteorit. And Planet.* Sci., 37, 713-735.

[3] Nishido H. *et al*. (2013). *Geochronometria* 40/4, 239-243.

[4] Steele I.M. (1986). *Amer. Min*., 71, 966-970.

Characterization of impact-induced brittle deformation: Ries meteorite crater, Germany

Hossain M*, Kruhl J

Technical University Munich, Germany, *sakawat@juniv.edu

Shock waves of the Ries (Figure 1) meteorite impact caused fragmentation of the target rock far beyond the range and style typical for regional brittle deformation. In horizontal and vertical directions fracture patterns vary systematically with increasing distance from the impact centre. Quantification of fracture patterns with different fractal-geometry methods shows that impact fragmentation largely follows power laws, but to variable extent on different scales and at different locations. *Box counting* of limestone fracture patterns in a ca. 114 m long and 9 m high vertical section at the crater margin shows two different power-law relationships. They are interpreted as resulting from two different pattern-forming processes: pre-impact compaction of the sediment and impact-induced deformation. The strong pattern anisotropy and its spatial variation are quantified by the *Mapping of Rock Fabric Anisotropy (MORFA)* method [1]. The pattern's local systematic variation is interpreted as resulting from shatter-cone style fractures on the dm- to m-scale [2]. The regular variation of complexity and orientation of the fracture patterns seems to be typical for impact-related fragmentation [3].

Fragment size distributions (FSD) and fracture patterns of boulders collected inside the crater show power-law relationships over one order of magnitude, most likely resulting from material excavation through non-ballistic ejection during the impact. The two different power-law relationships for the FSD and fracture patterns of the Ries drill cores, however, demonstrate two subsequent pattern-forming processes. Probably, the first one is related to shock-wave fragmentation, the second one to elastic rebound of the transient crater floor from a depth of ca. 4.5-5 km. Whereas the box-counting dimension (D) of the fragmentation patterns do not vary with depth, the D-values of the two different power-law relationships for FSD of the drill cores decrease. Only at greatest depth of ca. 1200 m the higher D-value is clearly increased. This can be related to stress localization with enhanced comminution [4]. In general, fractal geometry - specifically when based on automated procedures - proves a powerful tool for quantifying and analysing complex rock structures.

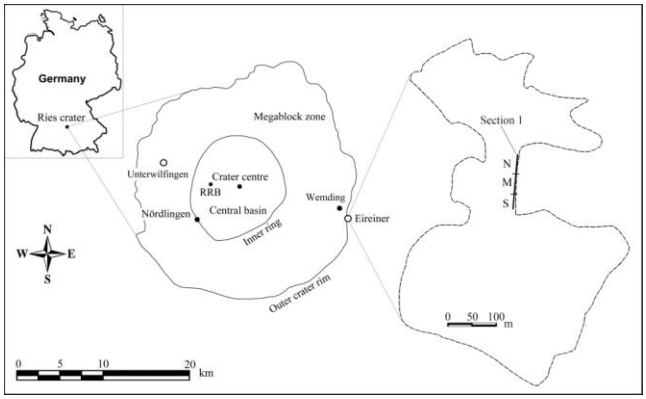

Figure 1: Ries impact area with crater outline, crater centre, location of Ries research borehole RRB, boulder sample location (Unterwilflingen) and position of Eireiner quarry. Boundary of the quarry: dashed line. Total length of section-1 (quarry wall): 114.03 m; general height: 9 m. N, M and S: north, middle, and south part, as used for quantification [3].

[1] Peternell M. *et al.* (2011). *Journal of Structural Geology*, 33, 609-623.

[2] Osinski G.R. and Pierazzo E. (2013). Impact Cratering, pp. 45-64.

[3] Hossain M.S. and Kruhl J.H. (2014), *Pure and Applied Geophysics*, submitted.

[4] Buhl, E. *et al.*, 2013, *Journal of Structural Geology*, 56, 20-33.

Genesis of Vredefort pseudotachylitic breccias

Mohr-Westheide T[1*], Reimold WU[1,2], Tagle R[3], Mader D[4], Koeberl C[4,5]

1 - Museum für Naturkunde Berlin, Germany, *tanja.mohr-westheide@mfn-berlin.de 2 - Humboldt University Berlin, Germany 3 - Bruker Nano GmbH, Berlin, Germany 4 - University of Vienna, Austria 5 - Natural History Museum Vienna, Austria

Generation of pseudotachylitic breccias (PTB) in impact structures has been controversial [1], with debate of genesis by friction melting, shock compression melting, decompression melting, combination of these processes, and - as of late - intrusion of allochthonous impact melt. Resolving this requires detailed multidisciplinary analysis to characterize the nature of these breccias. PTB are the most prominent impact-induced deformation phenomenon in the central uplift of the Vredefort Impact Structure - the Vredefort Dome [2, 3]. We present chemical data (INAA, XRF and EMPA) for mm to several m wide PTB from granitic and mafic (dioritic) host rocks and compare with compositions of the respective host rocks. µ-XRF spectrometry (M6 Jetstream, Bruker) was used for comparison of compositions of PTB and granitic host rock in a 71 x 52 cm slab from a PTB occurrence on Leeukop Hill.

EMP analysis of PTB groundmass in comparison to XRF bulk chemical analysis of PTB and their host rocks revealed that PTB generally display close chemical relationships to the adjacent host rock. For example, comparing the chondrite-normalized REE abundance patterns shows that pairs of PTB and respective host rock samples plot generally together. This is in agreement with the general PTB/host rock XRF data systematics from this and earlier studies.

In granitic environments, the refractory behavior of quartz seems to be the main reason for the slight chemical differences between PTB and host rock. The µ-XRF derived element distribution maps for the slab from Leeukop Hill show very similar chemical compositions for the granitic host rock and the melt breccia. This confirms that melt was formed from material of the same composition and that mm to dm wide breccia veinlets are of local origin. In larger occurrences, admixture of a small component of precursor material from a somewhat wider (say, 50-100 m) source volume is possible.

Chemical investigations of PTB in mafic host rocks revealed that the elements associated with plagioclase and/or hydrous ferromagnesian minerals are enriched in PTB veins. PTB seemingly occur preferentially in amphibole-rich host rock portions of intermediate gneisses, which confirms the macroscopic observations of [4, 5]. In addition, the veins selected for analysis do not provide textural evidence for shearing/faulting. PTB of up to 1 m width all contain clast populations that represent local lithologies only, with distinct differences between clast population and host rock mineral abundances likely the result of different mechanical behavior and different melting temperatures of the various minerals.

[1] Mohr-Westheide T. and Reimold W.U. (2011). *Meteorit. Planet. Sci.*, 46, 543-555.

[2] Dressler B.O. and Reimold W.U. (2004). *Earth-Science Rev.*, 67, 1-60.

[3] Reimold W.U. and Gibson R.L. (2006). *Geol. Soc. Amer. Spec. Pap.* 405, pp. 233-253.

[4] Reimold W.U. and Colliston W.P. (1994), *Geol. Soc. Amer. Spec. Pap.* 293, 177-196.

[5] Reimold W.U. (1991). *N. Jhrb. Min.*, 161, 151-184.

Cathodoluminescence characterization of luminescent minerals in E-chondrite Yamato 86004

Ninagawa K*, Mishima M, Tsuchiya Y, Kusano N, Yoshida E, Ohgo S, Nishido H

Okayama University of Science, Japan, *kninagawa@dap.ous.ac.jp

Cathodoluminesence (CL) is the emission of light from the materials excited with an electron beam, and its appearance could be attributed to impurities such as transition metal and rare earth elements, and to structural defects in the lattice. The applications of the CL for geological materials have been developed to clarify calcite cementation, secondary growth of quartz, and radiation damage of rock-forming minerals.

According to [1] the enstatite in metamorphosed EL chondrites displays a distinctive magenta CL with emission bands in the blue and red regions, whereas the enstatite in metamorphosed EH chondrites shows a blue CL. We have been examining CL features of the constituting minerals in the E chondrite Yamato 86004 (EH melt rock, [2]) by means of the Luminoscope (ELM-3: American Technologies) for color CL imaging and an SEM-CL for CL spectroscopy. SEM-CL analysis was conducted using a SEM (JEOL: JSM-5410) combined with a grating monochromator (Oxford: Mono CL2) to measure CL spectra ranging from 300 to 800 nm in 1nm steps at room temperature.

Figure 1 shows an overview CL color image collected from the whole area of Yamato 86004 with the Luminoscope. Three CL phases were recognized from the center to the outer rim as follows, blue, red and black, of which the non-luminescent area corresponds to fusion crust. This suggests that the heating during atmospheric entry might cause such CL zonation in the spherical meteorite. Peripheral grains give different CL spectral peaks in the red emission region at 630 nm and 650 nm, respectively. The former can be assigned to an impurity center of divalent Mn ion in forsterite, and the latter to the same center in enstatite [3].

At high-magnification, some enstatite grains have domain texture of CL emission with a red core in blue matrix. It demonstrates lack of compositional heterogeneity in this grain based on BSE information. The intensity ratios of red emission at 650 nm to blue emission at 435 nm are almost 1.0 for red core and 0.1-0.2 for blue matrix. The red-CL area includes iron grains, suggesting reductive activity during the formation of zoned enstatite.

Furthermore, we found several grains exhibiting a characteristic yellow-CL emission in this meteorite. The chemical analysis from EDS reveals that these grains with yellow CL have mainly Zr and Si, suggesting zircon. It may be the first time that zircon was found in enstatite chondrite, whereas zircon has been reported from eucrite [4]. CL spectra of the zircon grains in Yamato 86004 and terrestrial zircon in granodiorite from Okayama Japan have similar CL emission bands at 480 nm and 580nm, which are assigned to an impurity center of trivalent Dy ions commonly found in plutonic zircon.

Figure 1: An overview CL color image collected from the whole area of Yamato 86004 with the Luminoscope.

[1] Zhang Y. *et al.* (1996). *Meteoritics & Planetary Science*, 31, 87-96.

[2]. Lin Y. and Kimura M. (1998). *Meteoritics & Planetary Science*, 33, 501-511.

[3] Ninagawa K. *et al.* (2000). 25th Symposium on Antarctic Meteorites (NIPR, Tokyo), 114-116.

[4] Misawa K. *et al.* (2005). *Geochim. Cosmochim. Acta*, 69, 5847-5861.

Pseudotachylitic breccias in impact structures: the case of PTB in Siljan, Sweden

Reimold WU[1*2], Fischer L[1,3], Müller J[4], Schmitt RT[1]

1 - Museum für Naturkunde Berlin, Berlin, Germany, *uwe.reimold@mfn-berlin.de 2 - Humboldt University Berlin, Germany 3 - University of Potsdam, Potsdam, Germany 4 - Freie Universität Berlin, Berlin, Germany

The type locality for pseudotachylitic breccia (PTB - often confused with pseudotachylite = friction melt) is the Vredefort Dome, the deeply eroded central uplift structure of the Vredefort impact structure on the Kaapvaal craton of South Africa. Similar conspicuous breccias also occur in the Sudbury impact structure, as well as - though to a lesser degree - at the somewhat smaller Araguainha (Brazil), Dhala (India), Carswell and Charlevolix (Canada) and Siljan (Sweden) impact structures. In the latter case, a 600 m drill core from alkali granite of the central uplift structure revealed a >40 m wide breccia zone between 220 and 263 m depth, another of ca 15 m width between 544 and 559 m depth, as well as numerous other, millimeter to centimeter, PTB intersections (altogether an aggregate of PTB intersections of >60 m). Textural observations including sharp, often straight vein margins and rip-off clasts are suggestive of an associated although limited shear component upon breccia genesis. The clast population is derived mainly from the alkali granite host rock and xenoliths of granodioritic to dioritic compositions, but also contains a gabbro component that is, however, not intersected in the drill core. Dolerites do, though, occur in surface outcrops on the central uplift. Locally, clasts can be linked directly to adjacent host rock, testifying to frequent very small lateral movements. Chemical analysis shows that the PTB display a similar chemical variation to that of the granitoid host rocks. It also confirms that alkali granite and xenoliths form the major precursor component for the melt, but a more mafic component is required to model the overall melt rock composition, especially with respect to Ti, Fe, and Mg contents. Shock metamorphism of granitoid clasts and host rocks at and around breccia occurrences in this drill core is of similar degree to that of the other core sections. This lack of enhanced shock degree at the breccia occurrences suggests that the Siljan PTB is likely not derived by shock compression/decompression in the early phase of cratering. Our preferred genetic mode is decompression melting plus/minus friction melting during the slightly later modification phase of cratering - in analogy to our thinking regarding the formation of the massive PTB occurrences of the Vredefort Dome or the occurrences at Dhala.

Infrared imaging of drill core from the Barberton Greenstone Belt

Ashworth L*, Harris P

GeoSpectral Imaging, Johannesburg, South Africa, *luisa@geospectral.co.za

Hyperspectral imaging of drill core obtained during the ICDP-funded Barberton drilling project "Peering into the cradle of life" was conducted in 2013. Volcanic and plutonic ultramafic and mafic units, and chert from the Onverwacht Group, as well as Figtree Group shales and greywackes were scanned using a shortwave infrared (SWIR) sensor, measuring between 1000 and 2500 nm, and a high-resolution RGB camera. Spectral data sets generated during the processing of the infrared data include classification and false colour composite images, maps indicating the distribution of dominant spectral features in the drill core, and mineral maps. In addition to this, a comprehensive set of digital data was generated, which can be used to identify down-hole trends in the spectral and mineralogical data. Classification images based on spectral variation in the samples show that major lithological units in each of the drill cores can be identified spectrally. These results are corroborated by spectral feature extractions. While major rock-forming silicates such as pyroxene and olivine could not be mapped in the SWIR, a variety of AlOH, MgOH-, and FeOH-bearing phases such as clays, phyllosilicates, amphiboles and carbonates were effectively mapped in all five of the Barberton cores. These mineral assemblages highlight areas of significant alteration, influencing sampling for further geochemical studies. In addition to this, the wavelength position of certain spectral features can be monitored as an indicator of compositional variation in a given phase, which can then be tested by conventional geochemical techniques such as electron microprobe analysis. The hyperspectral and RGB image dataset can be used as a comprehensive base dataset for any further studies, both geochemical and mineralogical, which are to be undertaken on the Barberton drill cores at any stage in the future.

Unraveling the 3.4 Ga sulfur cycle from the study of pyrite from the Buck Reef Chert drill core

Eickmann B[1*], Agangi A[1], Meffre S[2], Wing B[3], Hofmann A[1]

1 - Department of Geology, University of Johannesburg, Johannesburg, South Africa, *beickmann@uj.ac.za 2 - CODES and School of Earth Sciences, University of Tasmania, Hobart, Australia 3 - Department of Earth and Planetary Sciences, McGill University, Montreal, Canada

The well-preserved Paleoarchean volcano-sedimentary succession of the Barberton Greenstone Belt represents an ideal target site for studying interactions between the geosphere and biosphere on early Earth. Although most of the cherts in the Onverwacht Group (3540 to 3300 Ma) can be associated with active, low-temperature hydrothermal activity, this might not be the case for the Buck Reef Chert (BRC), for which a hydrothermal influence is debated. The BRC is a sequence of thinly interstratified carbonaceous, ferruginous and pure chert layers, which are interpreted to have formed in a shallow to sub-wave base marine platform setting. Although sulfide minerals are common in Archean cherts and throughout the BRC, their origin and paragenetic history remain poorly constrained.

Here we present petrographic, major and trace element analyses, Pb-Pb ages, as well as multiple sulfur isotope data on paragenetically different sulfide minerals from a new ICDP (International Continental Scientific Drilling Program) drill core (BARB3) from the BRC in order to shed new light on sulfide genesis and its link to syn-sedimentary processes, diagenesis and metamorphic overprints of the BRC. Sulfide minerals occur in all facies, but are more abundant in black carbonaceous cherts. Pyrite is the dominant sulfide mineral, occurring either finely dispersed or as nodules in the chert matrix, or in later veins, in which it is associated with pentlandite, chalcopyrite, sphalerite and millerite. The morphology of the sulfides ranges from euhedral to anhedral, indicating that all sulfides were formed after sedimentation. Laser ablation ICP-MS compositional maps indicate relatively constant concentrations in the pyrite nodules, but marked compositional variations between the nodules and pyrite in the matrix. Multiple sulfur isotope data enable abiogenic and biogenic processes to be distinguished, providing further constraints on the origin of the sulfides.

Lead isotope analyses (^{204}Pb, ^{206}Pb, ^{207}Pb, ^{208}Pb), performed on the matrix and nodule pyrite, indicate good preservation with likely Pb remobilization in only a few spot analyses. Two groups of analyses were distinguished based on their chemical composition. One group (both nodule and matrix) has low U and Th, the other group (mostly matrix) has high U and Th. The best age approximation for the low-U and -Th group of analyses was obtained using Stacey and Kramers' [1] model with μ (^{238}U/^{204}Pb) = 11.7, which gives a model age of 3355 ±20 Ma. These ages appear to be approximately 95 Ma younger than the underlying felsic rocks of the Hooggenoeg Formation (zircon U-Pb 3451 ±5 Ma [2]), but overlap with some ages obtained in the overlying Kromberg Formation (zircon Pb-Pb 3334 ±3 Ma [3] and 3416 ±5 Ma [4]).

[1] Stacey J.S. and Kramers J.D. (1975). *Earth and Planetary Science Letters*, 26, 307-221.

[2] de Vries S.T. *et al*. (2006). *Precambrian Research*, 149, 77-98.

[3] Byerly G.R. *et al*. (1996). *Precambrian Research*, 78, 125-138.

[4] Kröner A. *et al*. (1991). *Earth and Planetary Science Letters*, 103, 41-54.

Geochemistry of BARB5 – insights into an early Archaean environment that potentially contains traces of early biosphere

Galic A[1], Mason P R D[1*], Vroon P Z[2], Strauss H[3], Montinaro A[3], Heubeck C[4], Drabon N[5]

1 - Utrecht University, Utrecht, The Netherlands, *p.mason@uu.nl 2 - Vrije Universiteit Amsterdam, The Netherlands 3 - Institut für Geologie und Paläontologie, Westf. Wilhelms-Universität Münster, Münster, Germany 4 - Freie Universität Berlin, Berlin, Germany 5 - Stanford University, USA

Recent scientific drilling in the Barberton Greenstone Belt has sampled some of the earliest well-preserved volcanic and sedimentary rocks of Archean age. The BARB5 core drilled in 2012 by the ICDP-funded Barberton Greenstone Belt drilling project intersects siliclastic and felsic volcaniclastic rocks of the 3.26- 3.23 Ga Middle Mapepe Formation in the Fig Tree Group. Here we use a chemostratigraphic approach to identify the nature of sedimentation and provide constraints on the environment of deposition for this core which potentially contains traces of an early biosphere. The core traversed roughly 400 m of stratigraphic length of siltstone, sandstone and conglomerate together with chert, carbonate, barite and volcaniclastic ash. Siltstones at the base of the core represent a deep water basin, shallowing upwards through an alluvial fan to a shallow-water platform with chemical sedimentation at the top. The rocks are depleted in TiO_2, K_2O, P_2O_5, Al_2O_3, Na_2O and enriched in Fe_2O_3, MnO, CaO and MgO relative to PAAS. Major and trace element data reveal remarkable heterogeneity and diversity in processes across only 400 m of stratigraphic depth. Cr/Th and La/Th ratios reveal variable proportions of source material weathered from high-Mg basalt and TTG. A distinctive layer of detrital heavy minerals including diverse sulfides indicates weathering of mineralized crust, that may also be the source of reworked barite. Carbonate chemistry links fine grained bedded carbonate to late stage carbonate veining. Silification is absent at most depths and cherts occur as distinctive layers in shale and ash horizons. Cryptic alteration has affected only the most highly mobile elements including alkali metals, Sr and Ba. Many other elements including redox sensitive tracers such as Fe, Mo, V and U appear immune to alteration and are consistent with fully anoxic conditions in the Palaeoarchean. Some transition metals like Ti, V, Cr, Ni or Cu show a decreasing trend towards the top of the core. REE elements show LREE enrichment with a positive Eu anomaly when normalized to chondritic values. HREE are unfractionated which might be an indication of mafic source or granitic source with unfractionated pattern. The wealth of information provided here will provide a critical framework for the interpretation of sedimentary and geochemical processes in early Archean basins as well as potential life signatures using more advance stable isotope studies in future.

Microbial iron and sulfur cycling in an early Archean basin: evidence from the Barberton Greenstone belt drilling project

Galic A[1*], Stausberg N[1], Mason P[1], Vroon P[2], Whitehouse M[3], Strauss H[4], Montinaro A[4]

1 - Utrecht University, Utrecht, The Netherlands, *a.galic@uu.nl 2 - Vrije Universiteit Amsterdam, The Netherlands 3 - Laboratory for Isotope Geology, Swedish Museum of Natural History, Stockholm, Sweden 4 - Institut für Geologie und Paläontologie, Westfälische Wilhelms-Universität Münster, Münster, Germany

The Archean oceans were anoxic and ferruginous, and despite being S-poor contain abundant sedimentary pyrite from both deep and shallow water settings. Fe and S isotopes in pyrite can be used to give insight into the sources, mixing and (bio) geochemical redox processes affecting both of these elements in the Earth's early surface environment. Here we present bulk Fe isotopes and pyrite Fe and multiple S isotopes from the rocks of the Middle Mapepe Formation (3.26-3.23 Ga) of the Fig Tree Group, sampled by the BARB5 drill core of the ICDP Barberton Greenstone Belt drilling project in South Africa. Fourty-three whole rock samples spanning deep and shallow basinal settings were analysed for bulk δ^{56}Fe by MC-ICPMS. An additional 160 *in situ* pyrite measurements were made for δ^{56}Fe and multiple S isotopes (32, 33, 34, 36) by SIMS. Bulk rock δ^{56}Fe varies from 0.42‰ to -0.46‰, with an average value of ca. 0 ‰. More negative values were observed deeper in the core where deposition occurred in deep anoxic environment with Fe derived mainly from the water column. Slightly more positive values were observed in shallower water alluvial fan deposits at the core top. We interpret the variability as a result of mixing between Fe derived from the water column and detrital Fe minerals weathered from the hinterland. A mass weighted average of 0‰ for the Barb5 core is close to the igneous average. Heterogeneity was observed in multiple S and Fe isotopes in single grains and between the grains from different lithologies. Multiple S isotopes vary from -13.‰ to 6 ‰ for δ^{34}S, -2 ‰ to 4 ‰ for Δ^{33}S and from -5 ‰ to 1 ‰ for Δ^{36}S. Correlations indicate intensive mixing of different S sources together with the presence of microbial or abiotic sulfate reduction in the basin. A negative excursion in d^{56}Fe and d^{34}S corresponds to a litharenite unit interbedded with chert, barite and carbonate and volcanic ash deposits. We interpret this as related to Fe drawdown from the basin during increased sulfide production due to microbial sulfate reduction. In summary, our results indicate mixing of different sulfur and iron sources in the basin that overprints primary photolytic variability for sulfur isotopes.

Deep-time, data-driven discovery in mineralogy: evidence for the co-evolution of life and minerals

Hazen R[1*], Liu X[1], Sverjensky D[2], Downs R[3], Golden J[3], Hystad G[3], Pires A[3], Fox P[4], Grew E[5], Kah L[6]

1 - Carnegie Institution of Washington, Washington D.C., USA *rhazen@ciw.edu 2 - Johns Hopkins University 3 - University of Arizona 4 - Rensselaer Polytechnic Institute 5 - School of Earth and Climate Sciences, University of Maine 6 - Department of Earth and Planetary Sciences, University of Tennessee

Discovery in geochemistry relies principally on induction and deduction approaches to reasoning that focus on observation, modeling, and predictive explanations of known natural patterns and phenomena. However, these powerful methods are inherently inefficient at discovering new complex patterns that require multivariate analysis of large datasets or synthesis of diverse types of data. Recognition of such gradual global processes as oxidation of the oceans and atmosphere, diversification of near-surface mineralogy, and co-evolution of the terrestrial geosphere and biosphere may require decades of integration of geo- and bioscience data. Accordingly, we are developing a deep-time data infrastructure that links trace element and isotope data for rocks and minerals to paleoenvironment, paleobiology, proteomics, and thermochemical data resources. The potential now exists for an alternative "abductive" approach to investigate Earth's co-evolving geo- and biosphere [1-4].

Earth's near-surface environment has evolved as a consequence of selective physical, chemical, and biological processes - an evolution that is preserved in the mineralogical record. Recent studies of mineral diversification through time reveal correlations with major geochemical, tectonic, and biological events, including large changes in ocean chemistry, the supercontinent cycle, the increase of atmospheric oxygen, and the rise of the terrestrial biosphere. Data on trace element distributions [5] and species diversification [6-8] reveal significant temporal changes in Earth's near-surface oxidation state. Growing data resources also point to new opportunities for applying multivariate statistical methods and adapting visualization strategies for deep-time data. Ultimately, we envision an integrated deep-time data infrastructure - a new kind of open-access "scientific instrument" that may facilitate transformation of current Earth Science paradigms.

[1] Fayyad *et al.* (1996). *AI Magazine* Fall 1996, 37-54.

[2] Hey *et al.* [Eds.] (2009). *The Fourth Paradigm: Data-Intensive Scientific Discovery*. Redland, WA: Microsoft External Research.

[3] Hazen R. *et al.* (2011). *Amer. Mineral.*, 96, 953-963.

[4] Keller and Schoene (2012). *Nature*, 485, 490-493.

[5] Golden *et al.* (2013). *Earth Planet. Sci. Lett.*, 366, 1-5.

[6] Hazen R. *et al.* (2012). *Amer. Mineral.*, 97, 1013-1042.

[7] Hazen R. *et al.* (2013). *Amer.Mineral.*, 98, 2007-2029.

[8] Hazen R. (2013). *Amer. J. Sci.*, 313, 807-843.

Preliminary results from the 3.4 Ga Buck Reef Chert BARB3 core, Barberton drilling project

Hofmann A[1*], Vroon P[2], Bekker A[3], Harris C[4], Ledevin M[5], Arndt N[5]

1 - University of Johannesburg, Johannesburg, South Africa, *ahofmann@uj.ac.za 2 - University of Amsterdam, The Netherlands 3 - University of California Riverside, USA 4 - University of Cape Town, South Africa 5 - Université Joseph Fourier, Grenoble, France

As part of the ICDP-funded Barberton drilling project a single drill core (BARB3) with a total length of 899 m was obtained from the c. 3.4 Ga Buck Reef Chert (BRC). The BRC is an unusually thick (up to 350 m) sequence of predominantly chemical sedimentary rocks. It overlies a shallow intrusive to extrusive sequence of dacitic volcanic rocks of the Hooggenoeg Formation and is separated from ultramafic lapillistone of the Kromberg Formation by a >150 m thick ultramafic sill. Drilling commenced in the ultramafic body at an angle of c. 45° and c. 200 m of serpentinized peridotite were intersected. The remaining c. 700 m of the core include a variety of predominantly chemical sedimentary rocks and minor intrusive mafic to intermediate igneous rocks. The base of the BRC was not intersected.

The chemical sedimentary rocks are characterized by two dominant lithofacies, thinly bedded, relatively pure chert and a variably silicified, irregularly laminated siderite-rich rock. Subordinate facies include sandstone with sand- to granule-sized particles of chert and carbonaceous chert in the lower part, black carbonaceous chert throughout the succession typically containing aluminosilicates and sulfides of different generations, and rare thin beds of jasper in the middle part. Stratiform and cross-cutting veins filled with botryoidal chert and quartz ± carbonate are common and are particularly abundant in the lower part.

Major and trace element data of different chert facies as well as C, O, and S isotope data of carbonate, organic matter and chert will be presented for a first-order characterisation of the interplay between oceanic, environmental and hydrothermal conditions in this shallow-marine Palaeoarchaean setting. An outlook on follow-up petrological, mineralogical and geochemical studies will be given that will provide insights into the habitat of early life, geochemical cycles and marine/hydrothermal conditions 3.4 Ga ago.

Mesoarchean oceanic floor environment at sedimentary sequences in Dixon Island-Cleaverville formations, Pilbara Australia: result of the DXCL drilling project

Kiyokawa S[1*], Ito T[2], Ikehara M[3], Yamaguchi K[4], Naraoka H[5], Onoue T[6], Horie K[7], Aihara Y[5], Miki T[1]

1 – Department of Earth and Planetary Sciences, Graduate School of Sciences, Kyushu University, Japan, *kiyokawa@geo.kyushu-u.ac.jp 2 - Ibarai University, Japan. 3 - Kochi University, Japan 4 - Toho University, Japan 5 - Kyushu University 6 - Kumamoto University, Japan 7 – NIPR, Japan

The 3.2-3.1 Ga Dixon Island (DX)-Cleaverville (CL) formations are well-preserved black shale to banded iron formation (BIF) sequences that are only affected by low-grade metamorphism without intensive deformation. We performed two DXCL drilling projects: DXCL-1 in 2007 and DXCL-2 in 2011 ([1, 2]. These drilling projects selected two sites: the CL site for the CL Formation, and the DX site for the upper DX Formation. The DXCL result shows upward coarsening and upward thickening black shale-BIF sequences, representing an oceanic small depression environment that is identified by an accreted immature island arc setting [3, 4].

The DX Formation contains well preserved hydrothermal ocean floor surface stratigraphy which consists of 1) an altered komatiite and rhyolite sequence with a hydrothermal organic rich vein system, 2) a black chert sequence and 3) a white-red chert sequence. The CL Formation contains a black shale, siderite banded iron formation, magnetite BIF and black chert fragment-bearing rhyolite pyroclastic beds. The estimated sedimentation rate from the DX Formation (3195±15 Ma) to the CL Formation (3108±13 Ma) is 2-8 cm/1000year.

Through detailed stratigraphic reconstruction, thin section observation, and detailed analyses of C and S isotopes, we identified several important data. Most of the core samples of black shale and chert below BIF show similar contents of organic carbon and ^{13}C isotope values (around -30per mil). $\delta^{34}S$ shows heavy values (around -5 to +30per mil). There is a very weak sulfur MIF signal (< 0.2%) in the black shale sequence.

Results of lithological observation indicate that this sequence represents well-stratified quiet conditions and the environment was anoxic and stagnant, partly being influenced by hydrothermal activity from the ocean floor. Sulfate reducing bacteria might have inhabited an anoxic closed bottom - lower sequence of the water column. This also indicates that ocean sulfur isotopes at this time may have resembled modern ocean values (~20 per mil). At areas on the ocean surface, cyanobacteria may have bloomed, resulting in abundant organic matter at the ocean floor.

The thick organic-rich black shale may have triggered the deposition of iron beds. The stratigraphy of the black shale - BIF sequence quite resembles other iron formations (eg. Hamersley BIF). Therefore we suggest that the DX-CL formations contained an oxygen production system around 3.2-3.1 Ga in time. These geological results indicate that, at this time, partial oxygenation began to occur at anoxic oceanic conditions, with wide cyanobacteria activity at the surface of the ocean with development of iron formations.

[1] Yamaguchi K., Kiyokawa S., Ito T., Ikehara M., Kitajima F. and Suganuma Y. (2009). *Scientific Drilling*, no. 7, 34-37.
[2] Kiyokawa S., Koge S., Ito T., Ikehara M., Kiyajima F., Yamaguchi K.E., and Suganuma Y. (2012). Geological Survey of Western Australia, Record 2012/14, 39p.
[3] Kiyokawa S., Ito T., Ikehara M. and Kitajima F. (2006). *Geological Society of America Bulletin*, vol. 118, no. 1/2, 3-22.
[4] Kiyokawa S., Ito, T., Ikehara, M., Yamaguchi, K.E., Koge S. and Sakamoto R. (2012). *The Island Arc*. v.21, 2, 66-78.

Reconstruction of 3.2Ga sea floor environment: in situ and whole-rock analysis of carbon and sulfur isotope of DXCL project

Miki T[1*], Kiyokawa S[1], Naraoka H[1], Takahata N[2], Ishida A[2], Ito T[3], Ikehara M[4], Yamaguchi K[5], Sakamoto R[6], Sano Y[2]

1 - Department of Earth and Planetary Sciences, Graduate School of Sciences, Kyushu University, Kyushu, Japan, *we.re.ten0r.capt.m1ckey@gmail.com 2 - Atmosphere and Ocean Research Institute, The University of Tokyo, Japan 3 - College of Education, Ibaraki University, Japan 4 - Graduate School of Integrated Arts and Sciences, Kochi University, Japan 5 - Faculty of Science, Toho University/NASA Astrobiology Institute, Japan 6 - Mitsui Oil Exploration CO., LTD.

In the Pilbara Coastal Greenstone Terrane in Western Australia, the Dixon Island and Cleaverville Formations of 3.2-3.1 Ga age are exposed. The DXCL Drilling Project was performed both in 2007 and 2011 for the purpose of the high-resolution reconstruction of the change of past sedimentary environment in this area, and four core samples (DX, CL1, CL2, and CL3) were acquired. Through these cores, except for CL3, previous study revealed carbon isotopic ratio (=$\delta^{13}C$) with about -30‰ and sulfur isotopic ratio (=$\delta^{34}S$) of sulfide in black shale from DX core obtained by whole-rock analysis with wide range of fluctuation and very high values ($\delta^{34}S$=-10.1～+26.8‰, n=93: unpubl. data). This is dissimilar to the previously reported sulfur isotopic ratio of sedimentary sulfides of the early Archean ($\delta^{34}S$=-16.8～+8.7‰, n=351: [1]).

In this study, we evaluated the change of carbon and sulfur isotopic ratios through the whole DXCL cores. Moreover, in order to clarify the cause of positive shift and dispersion, we performed in situ analysis with NanoSIMS focusing onto minute spherical pyrites observed in the DX core.

Three cores (CL2: 44.4m, CL1: 66.1m, CL3: 200m to the top) were collected from the Cleaverville Formation which consists of lower Black Shale Member and upper Banded Iron Formation Member. DX core (100.40m) of the upper part of Dixon Island Formation is composed of black shale, gray chert, and alternated pyrite layers. Especially, the DX core contains the layer of tens-hundreds of μm sized, euhedral pyrites and the layer of the minute spherical pyrites (about 10 μm in diameter) which are fulfilled with silica. Their morphology and occurrence suggest that the minute spherical pyrites were formed at an early stage of sedimentation.

We did whole-rock analysis of sulfur isotope using EA-IRMS system (FISONS, NA 1500NCS and Thermo Finnigan, DELTA plus XL) at Kyushu University. In situ analysis of sulfur isotopes was performed using Cameca NanoSIMS50, at the Atmosphere and Ocean Research Institute, Tokyo University. Carbon isotope analysis was performed using Thermo Finnigan Delta Plus Advantage (EA/IRMS) at the Center for Advanced Marine Core Research, Kochi University.

As results of in situ analysis, minute spherical pyrites were revealed to have 5-10‰ isotopic fractionation in the inner structure, showing distribution that area of high value is in ring-shape on the inside and area of low value is in the outer side and the central part of the crystal. Besides, CL3 core (n=27) showed $\delta^{34}S$=+1.33 ～ +21.52‰, $\delta^{13}C_{org}$=-30.79～-28.57‰, C_{org} =0.09～1.65wt%.

In this analysis, most of carbon isotopic data had values between -30 to -28‰ in about 400 m forming the Dixon Island to Cleaverville formations. The carbon isotope values indicate that the same kind of carbonaceous material was deposited on the seafloor and they correspond to photosynthetic bacteria such as cyanobacteria. Besides, pyrites formed in organic-rich anoxic marine sediment. Particularly, when closed system to sulfate was formed, Rayleigh type isotopic fractionation would be promoted by sulfate reducing bacteria. As a result, the feedback occurred; bacteria must use remaining isotopically heavier sulfate because they metabolize isotopically lighter sulfate at first and pyrites isotopically heavier than contemporary seawater sulfate (+10±3‰: [2]) formed on the inside of pyrite shell. Although generally, in case sulfate reducing bacteria are concerned, sulfur isotopic ratios of sulfides are expected to have negative values. However, in this study, +20‰ or more were observed in these sequences. It is possible that sedimentary sulfides at that time were in a condition that they had high sulfur isotopic ratio for some reason, for example, Dixon Island was in an environment that $\delta^{34}S$ of sulfate locally exceeded +20‰, which was different from that of ordinary open sea.

[1] Strauss H. (2003). Sulphur isotopes and the early Archean sulphur cycle. Precambrian Research, 126, 349-361.

[2] Ueno Y., Ono S., Rumble D. and Maruyama S. (2008). Quadruple sulfur isotope analysis of ca. 3.5Ga Dresser Formation: New evidence for microbial sulfate reduction in the early Archean. *Geochimica et Cosmochimica Acta*, 72, 5675-5691.

Multiple sulfur isotopes reveal insights into environmental conditions and early sulfur metabolism some 3.5 Ga ago in the Barberton Greenstone Belt

Montinaro A[1], Strauss H[1*], Mason P[2], Galić A[2]

1 - Westfälischen Wilhelms-Universität Münster, Germany *hstrauss@uni-muenster.de
2 - Utrecht University, Utrecht, The Netherlands

The Barberton Greenstone Belt, South Africa (3.55-3.23 Ga), was drilled in 2011 by the multinational and multidisciplinary ICDP project "Peering into the Cradle of Life", that aims at investigating under which environmental conditions life emerged and evolved on our planet. In this study, multiple sulfur isotopes are used in order to trace early sulfur metabolisms on Earth as well as to characterize the prevailing environmental conditions. Iron speciation is also used in order to define the depositional environment of the sedimentary rocks, because iron proxies are a strong tool for constraining the redox conditions in ancient oceans.

We studied ICDP drill core BARB5, drilled in the Barite Syncline, specifically through the Mapepe Formation of the Fig Tree Group. The lowest part is mostly composed of carbonaceous siltstone and calcareous litharenite; the middle part of chertarenite and conglomerate; the upper part of litharenite interbedded with chert and carbonate.

Total sulfur abundances range from 0.01 to 3.03 wt.% (highest values in the lowest part). Each lithology is characterized by a different sulfur isotopic composition. The carbonaceous siltstone and calcareous litharenite display $\delta^{34}S$ values between -1.0 and 2.3‰; the chertarenite and conglomerate between -1.3 and 3.4‰; the litharenite interbedded with chert and carbonate between -6.5 and 3.4‰. Carbonaceous siltstone and calcareous litharenite yielded $\Delta^{33}S$ values between 0.02 and 2.33‰; chertarenite and conglomerate between -0.38 and 1.86‰; litharenite interbedded with chert and carbonate between -0.32 and 0.30‰. Sequential iron extraction data indicate Fe_{tot} concentration between 3.3 and 13.5 wt.%, with no discernible stratigraphic variation. Fe_{carb} values are high, in agreement with the abundant carbonate observed in thin-section, and varies between 1.0 and 8.6 wt.%. Fe_{ox} concentrations are low, ranging from below detection limits to 0.6 wt.%. Fe_{mag} varies between 0.2 and 4.6 wt.%. The Fe_{py}/Fe_{HR} ratios range between below detection limits and 0.63, while Fe_{HR}/Fe_{tot} ratios vary between 0.37 and 1.00.

Clearly, $\Delta^{33}S$ values in carbonaceous siltstone and calcareous litharenite reflect mass-independent isotope fractionation, hence an atmospheric signature. Data define a mixing line between two different pathways of S in pyrite: one reflecting the derivation from elemental sulfur (carrying positive $\Delta^{33}S$) and the other revealing pyrite formation following the bacterial reduction of atmospheric sulfate (carrying negative $\Delta^{33}S$). In contrast, litharenite interbedded with chert and carbonate displays rather small $\Delta^{33}S$ values but a substantial variability in $\delta^{34}S$. They show an extremely attenuated mass-independent fractionation signal, visible from the slope of -0.8 between $\Delta^{33}S$ and $\Delta^{36}S$ that is typical for Archean sulfides. In addition, iron speciation results point on an anoxic and ferruginous, but not to a sulfidic ocean during deposition, indicating that ocean water was enriched in dissolved Fe^{2+} but low in sulfate.

The environment of formation of BIFs from the ~2.4 Ga Manjeri Formation, Belingwe Greenstone Belt, Zimbabwe

Orberger B[1*], Morgan R[2], Hofmann A[3]

1 - Eramet Group, where, France, *beate.orberger1@orange.fr 2 - Université Paris Sud, Paris, France 3 - University of Johannesburg, Johannesburg, South Africa

The presence of nano-hematite inclusions within quartz crystals of chert of the oxide-facies Spring Valley Member (Manjeri Formation, Belingwe Greenstone Belt) banded iron formation indicate that oxygenated conditions, produced by photosynthetic bacteria in a sheltered basin and giving rise to stromatolitic carbonates, were already developed by 2.7 Ga, well before the purported Great Oxygenation Event. The deeper, more reduced facies of the Jimmy Member, consisting of cherty iron formation, sulphidic shales and massive sulphides, indicate that oxygenated conditions were restricted to the shallow water. Precipitation of the chemical sediments were from a mixed marine-hydrothermal fluid as shown by Eu/Eu* values of 2.46 (Spring Valley Member) and 2.40 (Jimmy Member). Ankerite in the Spring Valley Member and Jimmy Member, and siderite (Spring Valley Member only) form lenses with euhedral sulphides or veins that cross-cut the chert matrix. Samples with the greatest proportion of carbonates also have the largest negative $d^{13}C$ values (Spring Valley Member: -10.12 ‰; Jimmy Member: -8.58 ‰) suggesting recycling of organic matter during carbonate formation. Carbonate coexistence of ankerite and siderite occurs in veins, is replacive and resemble alteration zones of possibly volcanogenic massive sulphide deposition related to volcanism that ultimately gave rise to the thick pile of Ngezi Group basalts and komatiites overlying the Manjeri Formation. This study indicates that depositional environments can be deciphered with careful application of mineralogical investigations and REE+Y studies, which may see through post-depositional alteration events common in the Archaean rock record.

Stromatolitic carbonates of the Pongola Supergroup, South Africa: a unique record of surface conditions 3 billion years ago

Siahi M[1*], Hofmann A[2], Hegner E[1], Master S[3], Mayr C[1]

1 – Earth Sciences, LMU, Munich, Germany, *mehrnazsiahy56@yahoo.com 2 - University of Johannesburg, Johannesburg, South Africa 3 - Geosciences, University of the Witwatersrand, Johannesburg, South Africa

Sedimentary carbonates are extremely rare in the geological record older than 2.9 billion years, probably reflecting specific environmental and/or physico-chemical conditions of the oceans not conducive for carbonate precipitation. Rare occurrences of stromatolite-bearing dolomite are present in the c. 3.0 Ga Nsuze Group, Pongola Supergroup, the oldest well preserved successions of epicratonic volcanic and sedimentary rocks on Earth [1].

Three different stratigraphic sections of carbonates 2 - 25 m thick were observed in the Nsuze Group exposed in the White-Umfolozi Inlier of KwaZulu-Natal and investigated sedimentologically, petrographically and geochemically. The carbonates are intercalated with shallow-marine siliciclastic deposits locally containing mafic-ultramafic ash-fall deposits. They consist essentially of dolomite, with minor calcite and ankerite. Secondary silicification and a detrital component are common. Detritus includes abundant carbonate-replaced pyroclastic material and terrigeneous material.

Sedimentological investigations revealed different, in part cyclically-stacked sedimentary facies that were deposited in a tide-dominated, deep subtidal to supratidal shallow marine environment. Different types of organo-sedimentary structures are present, including stratiform stromatolite, domical thrombolite and oncolite. Conical and columnar stromatolites were observed in one section. The presence of a variety of these structures suggests formation by different types of bacteria under different physico/chemical conditions. Carbonaceous matter is preserved, but does not delineate microbial structures due to dolomitisation and recrystallization, the latter associated with greenschist facies metamorphism.

C, O, and Sr isotope analyses are in agreement with previous studies [2]. $\delta^{18}O_{PDB}$ values range from -19.7 to -12.0 ‰, reflecting alteration during metamorphism and/or hydrothermal activity. $\delta^{13}C_{PDB}$ values range from 0.1 to 2.3 ‰ similar to, but slightly more positive, than Phanerozoic marine carbonates. $^{87}Sr/^{86}Sr$ ratios ranges from 0.710 to 0.752, which can be explained, in part, by isotopic exchange with non-carbonate fraction during alteration and, possibly, by high continental influx into the epicontinental setting in which the carbonates were deposited.

[1] Mason T.R. and von Brunn V. (1977). *Nature*, 266, 47-49.

[2] Veizer J., Clayton R.N., Hinton R.W., von Brunn V., Mason T.R., Buck S.G. and Hoefs J. (1990). *Geochim. Cosmochim. Acta*, 54, 2717-2729.

Carbonaceous material characterization of the 3.2 Ga Mapepe Fm, Fig Tree Group, Barberton Greenstone Belt, South Africa (BARB5 drill core, ICDP project, Cradle of Life): new insights from micro Raman spectroscopy analysis

Storme J-Y*, Javaux E J

University of Liège, Belgium, *jystorme@ulg.ac.be

Raman spectra of carbonaceous material (CM) from 30 samples of the BARB 5 drill core (ICDP project, Cradle of Life) were used to characterize thermal maturity, metamorphic grade and metamorphic temperature that have affected rocks of the middle Mapepe Formation (Fig Tree Group, BGB, South Africa). Raman analyses were performed with a Renishaw In via Raman spectrometer coupled to a Leica DM 2500 confocal microscope and with an Ar-ion-50 mW monochromatic 514.5 nm laser source. Laser excitation was adjusted to an on-sample intensity of ca. 2mW (measured with a Coherent Lasercheck Analyser) and focused through a 50x objective to obtain a 1-2 µm spot size. Acquisitions were obtained with an 1800/mm grating with an air cooled (-70°C) 1024x256 pixel CCD array detector. This method enabled a 2000 cm^{-1} spectral detection range. Beam centering and Raman spectra calibration were performed daily on a Si-Al microprocessor chip with a characteristic Si Raman band at 520.5 cm^{-1}. Spectra were manipulated with Wire 3.4™ software. Point analysis measurements were made in static mode (fixed at 1150 cm^{-1}), spectra were collected from 10 different points in each sample, and each spectrum was acquired at 1x10 s running time. Peak parameters (G, D_1, D_2, D_3, D_4-bands; FWHM-D_1, FWHM-D_2; I_G, I_{D1}, I_{D2}, I_{D3}, I_{D4}; A_G, A_{D1}, A_{D2}, A_{D3}, A_{D4}) were obtained by fitting spectra (2-10 spectra by sample) with mixed Lorentzian-Gaussian curves.

Two peaks characteristic of disordered CM were observed in the samples. The G bandsis located at ~1597± 5 cm^{-1} (n=300; ±2σ) and results from in plane vibrations in ordered graphite. The D band (D for disordered) is located at ~1351± 2 cm^{-1} (n=300; ±2σ). The presence of well-developed D_3 and D_4 bands with D_1 band that is more intense than G band (FWHM-D_1 ~60 cm^{-1}) are indicative of rather poorly ordered CM that is typically encountered in lower greenschist-facies. Thermal maturity of CM was evaluated by comparing FWHM-G with G-position. The values fall in the range of those of the ~1.9 Ga Gunflint chert, ~2.7 Ga Tumbiana Fm or ~3.5 Ga Strelley Pool and Apex cherts which indicate that samples have experienced sub-greenschist to lower greenschist facies metamorphism. Another Raman thermal maturity "proxy" consisting in the relation between A_{D1}/A_G and I_{D1}/I_G ratios, which vary systematically with increasing metamorphic grade in metapelites, shows that the CM studied has a crystallinity equivalent to that of the chlorite-zone shales corresponding to lower greenschist facies or less. A tentative geothermometry based on 65 analyses is also proposed for the Mapepe Formation. Four different geothermometers involving R_1, R_2, R_{A1}, R_{A2} parameters were investigated giving a range of mean temperatures evolving from 210°C to 355°C. This range of temperature is in line with the temperature expected for a lower greenschist-facies metamorphism.

Even if all these Raman characterization parameters described above do not allow to elucidate the origins of CM, the parameter FWHM-D_1 plotted against I_{D1}/I_G ratio could, however, give some information about the precursor carbonaceous material of the sample. The values obtained for the Mapepe Formation could be compared to those of the Tumbiana Fm, Strelley Pool Fm and Apex chert but are different from those of the Gunflint chert.

Acknowledgement: This work was supported by EU FP7-ERC StG ELiTE.

Organic-bound trace metals and unconventional isotopic systems as new approaches for reconstructing Earth's early biosphere

Ciscato E[1*], Vance D[1], Bontognali T[1], Poulton S[2]

1 - ETH Zürich, Switzerland *emily.ciscato@erdw.ethz.ch 2 - University of Leeds, Leeds, U.K.

The rock record provides evidence for a dynamic early Earth characterized by continental growth, the formation of mountain ranges, glaciations, intense volcanic and hydrothermal activity, atmospheric oxygenation, and primitive biogeochemical cycles. The application of well-established isotopic systems has been instrumental in elucidating the interplay between environmental changes and the evolution of the early biosphere. Here we seek to extend this approach to the abundance and isotopic systems of organic-bound trace metals.

Metalloproteome analyses suggest that trace metals (e.g., Cu, Mo, Zn, Ni, Fe) were selectively utilized by different metabolisms and organisms at different times throughout the evolution of Earth's biosphere.

We aim to test hypotheses related to variations in trace metal bioavailability through time and the influence of this on biological evolution. Our approach is to extract trace metals from organic matter (kerogen) preserved in a suite of rocks (mostly organic-rich shales) spanning the past 3.5 billion years, and to characterize their abundances and isotopic compositions. This will provide an extensive chronological record of metal bioavailability and isotopic fractionation, to be interpreted with respect to biotic utilization and the evolution of different metabolisms, organisms and environments from the Archean onwards. Coupling of non-traditional trace metal stable isotope geochemistry with traditional C and S geochemical analyses will enable parallel development of our novel tracers with more well-established techniques.

Ultimately, we seek to understand whether the results from bioinformatics can indeed be a starting point for geochemical investigations and if the development of trace metal proxies can be successfully applied to advance our knowledge on the origins of life and its evolution.

Crystal chemistry and genesis of oxalate and polycyclic aromatic hydrocarbon minerals: organic mineral evolution

Echigo T[1*], Kimata M[2]

1 - Shiga University. Japan. *echigo@edu.shiga-u.ac.jp 2 - University of Tsukuba, Japan

The crystal chemistry and genesis of both oxalate and polycyclic aromatic hydrocarbon (PAH) minerals were studied in detail because they are the most typical ionic and molecular organic minerals, respectively. These studies have revealed that the cations and oxalate anions ($C_2O_4^{2-}$) in oxalate minerals are strongly bonded to form fundamental building blocks (FBBs) in their crystal structures and that FBBs in PAH minerals are individual PAH molecules and these are loosely bonded by weak intermolecular interactions. In addition, carbon isotope ratios of karpatite ($C_{24}H_{12}$) and idrialite ($C_{22}H_{14}$) from West Coast (California, USA) were analyzed and suggested that these PAH minerals derive their origins from hydrothermally alternated biogenic organic substances in oceanic sediments (hydrothermal petroleum).

Hazen *et al.* [1] divided the history of mineral evolution into three broad eras: (1) the era of planetary accretion (>4.55 Ga), (2) the era of crust and mantle reworking (4.55 to 2.5 Ga) and (3) the era of bio-mediated mineralogy (2.5 Ga to present). Considering the evolution of organic minerals according to Hazen's historical division, whewellite ($CaC_2O_4{\cdot}H_2O$), which is the most typical ionic organic mineral, appears to have emerged in the first era because it was found in Murchison meteotire. Three structural components of whewellite, Ca^{2+} ion, oxalate anion and electro-neutral water molecule (H_2O^0) are strongly tied by both ionic and hydrogen bonds to form the stable framework structure. The early emergence of whewellite in the history of organic mineral evolution can be attributed to the structural stability of the ionic mineral. On the other hand, karpatite and idrialite that derived from biogenic organic substances seem to emerge in the third era because they were only found in Cenozoic epithermal mercury deposits. Although coronene molecules were detected in Murchison meteorite, they could not crystallize into karpatite due to both the low concentration and the weak intermolecular attraction of van der Waals interaction. Thus the late emergence of karpatite and idrialite in the history of organic mineral evolution can be attributed to the weak attraction between the FBBs of the molecular minerals. In conclusion, it is suggested that differences in chemical bonding among these crystal structures significantly affect the evolution of organic minerals.

[1] Hazen R.M. *et al*. (2008). Mineral Evolution. *American Mineralogist*, 93, 1693-1720.

Fluid inclusion record of chert vein formation in the Barberton Greenstone Belt, South Africa

Farber K[1*], Dziggel A[1], Meyer F M[1], Prochaska W[2]

1 - Institute of Mineralogy and Economic Geology, RWTH Aachen
*farber@iml.rwth-aachen.de 2 - Department for Applied Geosciences and Geophysics, University of Leoben, Austria

Strongly silicified volcano-sedimentary sequences are a common feature in Archaean greenstone belts. In the Onverwacht Group in the Barberton Greenstone Belt, South Africa, silicification has been interpreted as a result of fluid circulation in shallow sub-seafloor convection cells [1]. This study uses fluid inclusion microthermometry and crush-leach analyses to constrain (1) the conditions of chert formation, and (2) the sources and the physico-chemical evolution of interacting fluids.

Silicified ultramafic rocks, overlying banded cherts and chert veins of the Mendon Formation were investigated. The veins are either stratiform or crosscutting, and many of them contain coarse crystalline quartz in their interior. Primary fluid inclusions occur as intragranular clusters in the coarse-grained vein interiors. Most samples contain homogeneous 2-phase (L+V) inclusions at room temperature with a relatively constant vapor fraction. Two samples of the banded cherts additionally contain 3-phase inclusions with H_2O (L) and CO_2 (L+V). The inclusions in aqueous intragranular clusters have a salinity of 3-11 mass% NaCl equiv. Homogenization into the liquid phase occurs at 150-200°C.

Crush-leach analyses show compositional differences between the coarse crystalline vein interiors and the microcrystalline chert veins. The element ratios in the vein interiors partly follow the seawater evaporation trend, but are more similar to metamorphic fluid. In contrast, the fluid composition in the chert veins and the banded cherts is consistent with Archaean and Proterozoic seawater [2]. In addition, the samples show a range in Cl/Br ratios and resemble organic-rich fluids such as those observed in oilfield brines. This suggests that the commonly observed carbonaceous matter in cherts of the Mendon Formation represents material that originated in biogenic processes in the Archaean ocean [3].

Independent temperature estimates indicate greenschist facies conditions (250-350°C). Combined with the microthermometric data, the depth of vein formation is estimated at ~5-8 km, arguing against a shallow water deposition. This, likely, means that the crystalline interiors formed during a later fluid infiltration event. Thus, the crystalline parts of chert veins are not suited for Archaean seawater reconstruction. The microcrystalline veins, however, still appear to retain the original signature of the fluid that was trapped during shallow water deposition, and indicate that both Archaean seawater and hydrothermal fluid have been involved in the alteration.

[1] Hofmann A. and Harris C. (2008). *Chemical Geology*, 257, 224-242.

[2] Foriel J. *et al*. (2004). *Earth and Planetary Science Letters*, 228(3), 451-463.

[3] Hofmann A. and Bolhar R. (2007). *Astrobiology*, 7(2), 355-388.

SPONSORS AND EXHIBITORS INFORMATION

35TH International Geological Congress

The 35th International Geological Congress, the *"World Cup of Geoscience"* of the IUGS; will be hosted in Cape Town in August 2016; only the third time on the African Continent. It is an ideal opportunity to showcase the geological heritage of Africa and its incredible variety of mineral resources.

Advanced Laboratory Solutions (Bronze Sponsor)

Advanced Laboratory Solutions is a leading laboratory supplier in Southern Africa, providing testing solutions in Quality Control and Research/Development. Our Mineralogy Solutions include Scanning Electron Microscopy (SEM), Transmission Electron Microscopy (TEM), EPMA/Microprobes, Raman Microscopy, 3D X-ray Microscopy and Sample Preparation to name but a few.
Our Quality Products are supported by a proficient Technical and Application Support team, who drive on-site training and workshops to ensure our customers get the highest return on their investments.

African Mineral Standards (Silver Sponsor)

AMIS is committed to assisting mineral laboratories and mining companies worldwide monitor assay laboratory performance; through the development, production and supply of a broad range of quality matrix matched, multi-element - Certified Reference Materials.
AMIS CRM's are samples with known grades made from real ore, whose properties have been characterised by international laboratories and which have been independently certified. Since commencement in 2004 AMIS has made CRM's out of raw materials from mines and exploration projects in 21 countries on 6 continents.
AMIS is an ISO 9001:2008 certified company.
Contact us at www.amis.co.za if you want CRM's made for your mine or project.

Africore

Africore is today one of the oldest established companies in South Africa manufacturing and supplying geological and exploration equipment and services to the industry. We design, manufacture and erect core sheds, core logging facilities and core storage facilities. We provide a full supply and logistics service as well as outsourcing for all your needs.

Anglo American (Sponsor - Session: Process Mineralogy and Geometallurgy (EG7))

Our founder Sir Ernest Oppenheimer said, our purpose is to "create value for our shareholders, but to do so in such a way as to create a real and lasting contribution in the communities in which we operate." It's a way of doing business that unites the company to this day.

Behre Dolbear

Behre Dolbear consulting services provide independent technical expertise to all participants in the mining sector. We operate globally covering base and precious metals, coal, iron ore, industrial minerals and more. Behre Dolbear has served its clients for over 100 years and welcomes an opportunity to learn more about your requirements.

Bruker (Sponsor - Pre-conference Workshop: Phase quantification by XRD and Session: Computed tomography (MA1))

Bruker is one of the world's leading analytical instrumentation companies. We cover a broad spectrum of advanced solutions in all fields of research and development. Today, worldwide more than 6,000 employees are working on this permanent challenge, at over 90 locations on all continents. www.bruker.com

Cameca

World leader in SIMS, EPMA and APT, CAMECA supports the geological research community with high-end microanalytical instruments:

- **SXFive:** world-standard EPMA
- **IMS 1280-HR:** Ultra High Sensitivity SIMS with tenth-permil precision
- **NanoSIMS 50L:** high spatial resolution SIMS
- **LEAP® Atom Probe:** 3D imaging and analysis with atomic resolution.

Carl Zeiss Limited - South Africa (Silver Sponsor)

Represented in South Africa since 1926, and a wholly owned subsidiary of Carl Zeiss Germany since 1974, Zeiss has a long history in this country.
Zeiss microscopes, electron microscopes and histology sample preparation and remote digital imaging equipment, can be found in operation throughout Southern Africa – from the routine veterinarian or rural clinic to state of the art research facilities, modern hospital, laboratories and industry.
Contact details: 363 Oak Avenue, Ferndale, 2125. Tel# 011 8869510.
Fax# 011 8869592. E.mail: info.za@zeiss.com. www.zeiss.co.za.

Continental Instruments

Lab Crystals Specializes in Thin Section Preparation of Rocks & Minerals. Fastest, Reliable & Cost effective services. Easy Collection of Rock samples & dispatch of thin sections globally. State of the art facilities and knowledgeable staff. The most dedicated Team committed to quality. Also available: Mortar & Pestles (Agate). www.labcrystals.com.

Corescan

Corescan is a global services company, specializing in automated mineralogical/ textural analysis of drill core and rock chips for mining, oil and gas and geotechnical applications. Corescan provides turn-key core logging services, both at regional bureaus and on-site coreshed or mine/drilling locations, using specialist geoscientists and advanced hyperspectral imaging technology.

De Beers (Sponsor - Session: Cratons and Diamonds (DE1))

De Beers was established in 1888 in Kimberley, South Africa. It strives to be the leading company in diamond exploration, mining, grading, valuation and sales of rough diamonds, marketing and the retailer of premium diamond jewellery and the iconic Forevermark diamond brand. Present in more than 20 countries, employing 20 000 'Diamond People' worldwide, De Beers has mining operations in South Africa and Canada; and in partnership with the Government in Botswana and Namibia. The Company has discovered about half the kimberlites known and joins the fraternity of exploration professionals in the quest to find more in the future. /
De Beers is committed to safe working practices and achieving 'zero harm' in the workplace. The equity in diamonds depends on respect for our environment, ecology and the community in which employees live and work. De Beers seeks to promote economic, environmental and social development in the counties where the company operates. For an insight into our diamond world visit: www.debeersgroup.com and www.diamondroute.co.za.

De Bruyn Spectroscopic Solutions

The Company's Analytical Chemist, Jan De Bruyn, has over 50 years' experience in the service of Anglo American Corporation, Anglo Vaal Iscor and the Atomic Energy Corporation. The main emphasis as Research Chemist is the development and application of advanced chemical analysis methods for Spectroscopy and manufacturing of CRM's. DE BRUYN SPECTROSCOPIC SOLUTIONS was established in 2002 by Jan De Bruyn. The laboratory is fully equipped to provide our clients with the best service and support. We provide reliable Certified Aqueous CRM's, Analysis, instrumentation supplies and consumables for Spectroscopy. We are conforming to the Protocol for ISO 2005: 17025/34/35. De Bruyn Spectroscopic Solutions is well known for our REE Analysis, PGM Analysis, Geological, Metallurgical and water Analysis. DE BRUYN SPECTROSCOPIC SOLUTIONS manufacture Certified Aqueous CRM's. All 'ULTRASPEC' CRM's will be accompanied by a Certificate of Analysis, traceable to 'NIST' standards. DE BRUYN SPECTROSCOPIC SOLUTIONS manufactures and distributes the "ULTRASPEC" CRM range and "ULTRAPURE" acids and Distilled water for Aqueous and Inorganic analysis. We customize CRM's to clients' specifications. Through the efforts of highly specialised group of dedicated professionals. DE BRUYN SPECTROSCOPIC SOLUTIONS is committed to ensuring complete customer satisfaction for the services it provides and the goods it manufactures.
www.ultraspec.biz. Cell: 082 354 7730. Fax: 086 530 3357

Department of Science & Technology (Platinum Sponsor - Bursaries)

The Department of Science and Technology's vision is to create a prosperous society that derives enduring and equitable benefits from science and technology.
Its mission is to develop, coordinate and manage a national system of innovation that will bring about maximum human capital, sustainable economic growth and improved quality of life.
The Department of Science and Technology provides leadership to develop the National System of Innovation primarily by implementing the 2002 National Research and Development Strategy and the 2008 Ten-Year Innovation Plan for South Africa. Its role includes managing and coordinating the National System of Innovation through policy formulation and resource allocation, and working closely with all its stakeholders, e.g. business, science councils, agencies and service delivery departments. The Department's efforts are aimed at, among other things, growing high-level science, technology and innovation human capital, developing science and technology infrastructure, encouraging research in emerging domains, establishing technologies and innovations to stimulate new industries, and driving indigenous innovations in established industries. For more information, go to www.dst.gov.za.

Elements

Elements - An International Magazine of Mineralogy, Geochemistry, and Petrology is published bimonthly by 17 mineralogical and geochemical societies. Each issue explores a theme of broad interest in the mineral sciences. Visit booth 76 to find out about incoming thematic issues and about the publications of some of our participating societies.

FEI (Silver Sponsor)

With more than 60 years of microscopy innovation and leadership, FEI enables customers to find meaningful answers to questions that accelerate breakthrough discoveries, increase productivity, and ultimately change the world. FEI designs, manufactures, and supports the broadest range of high-performance microscopy workflow solutions that provide images and answers in the micro-, nano-, and picometer scales.

GIA (Sponsor - Post-conference Workshop: Gem diamonds: treatments, synthetics and its identification)

GIA is a global public benefit institute that ensures the public trust in gems and jewellery through research, education, gemmological laboratory services and instrument development. An independent organization established in 1931 that now operates in 14 countries, GIA created the International Diamond Grading System™ and the 4Cs of diamond quality - Colour, Cut, Clarity and Carat Weight. In 2008, GIA established a gemmological laboratory in Johannesburg and later expanded its gem and jewellery education programmes.

Geo Explore Store

Geo-Explore Store was formed in April 2009 to offer a one stop geological and exploration supply outlet for Africa.
Based on 15 years of experience in the exploration market, and headed by a geologist, the company is able to assist with a broad range of equipment needs.
Our PDF catalogue is hosted on our web site for your convenience, if you cannot find what you need there please feel free to contact us.
We are based in Johannesburg but have representation , and ship, throughout Africa.
Should there be any questions please do not hesitate to contact us.
Denis Blewett, 0827447594 cell, 0865807392 fax, denis@geoexplorestore.co.za.

GeoSpectral Imaging

GeoSpectral Imaging specialises in the automated scanning of drill core using imaging sensors operational across the visible and infrared wavelength ranges of the electromagnetic spectrum. We generate a comprehensive set of image and data products for the purposes of geological characterisation, geometallurgy and geotechnical logging in the mining/exploration industries.

The Geological Society of South Africa (GSSA)

(USB Abstract Volume, Delegate Conference Bags Sponsor and Bursary Support)

The Geological Society of South Africa (GSSA) is a not-for-profit Scientific and Professional Society for earth scientists first established in 1895, and since regarded as the professional home for southern African geoscientists in academia, industry and government. It is the largest and oldest Society of its kind in southern Africa, and publishes a scientific journal, the South African Journal of Geology, as well as a quarterly news journal, Geobulletin. While the Society is focused on the African continent, the membership of the Society is global. New members from around the world are welcome to apply for membership.

Max Planck Institute for Chemistry Mainz / International Association of Geoanalysts

The open-access database GEOROC is a comprehensive collection of published whole rock and mineral analyses of volcanic rocks and mantle xenoliths from various geological settings. IAG (International Association of Geoanalysts) promotes the interests and supports the professional needs of those involved in the analysis of geological and environmental materials.

IMA 2018

The XXII General Meeting of the International Mineralogical Association will be held from 13-17 August 2018 in Melbourne, Australia. Join us for what will be an outstanding conference with interesting field trips and opportunities to explore new technologies, present new research and engage with your international colleagues. For more information, visit www.ima2018.com.

IMP

IMP has been providing complete solutions for the mining, analytical, biological, industrial and metallurgical industries since 1987.

Our innovative solutions include:

- Analytical laboratory equipment
- Automated robotic laboratories
- Biological laboratory equipment
- Industrial laboratory equipment
- General laboratory equipment
- Sampling systems
- Sample transport systems
- In-line on-line analysers
- Transportable and mobile laboratories
- Stand-alone laboratory equipment
- Calibration and services.

Innov X Africa (Silver Sponsor)

Innov X Africa is the African distributor for Olympus Innov X.
Olympus Innov-X is an innovative company involved in X-Ray Fluorescence (XRF) instrumentation.
Our systems perform fast, accurate chemical analysis in seconds to identify, differentiate and quantify most materials by elemental composition.
The Olympus Innov-X Analyser family includes, on-line liquid Analysers, Handheld and Bench top units suitable for the analysis of liquids, powders, ore, solids or slurry and the world's first truly portable x-ray diffraction (XRD) instrument the "TERRA".
Our DELTA Hand held XRF with integrated GPS and GIS software, has been widely accepted as the new standard in the geologist's tool box for instant geochemistry out in the field. The instruments are used in an array of applications such as exploration, mining, grade control, forensics, scrap metal, glass recycling, toxic metals in toys and the list goes on. For more information visit us at www.innovxafrica.co.za.

Johannesburg Convention Bureau

Africa's second largest city that's growing at an unprecedented rate – continuously transforming itself. Johannesburg is the financial and industrial capital of South Africa, the economic powerhouse of Africa and was founded in the heydays of one of the world's biggest and richest gold rushes - earning it the name of **Egoli meaning 'place of gold'.**
Johannesburg offers plethora of cultural, leisure, sporting, fashion, lifestyle activities, legendary shopping, dining, entertainment and nightlife - complimented by fabulous weather.
Johannesburg Convention Bureau is responsible for promoting the City as a business events destination, providing diverse innovative options and ensuring that patrons leave with memorable experiences that last a lifetime.

Micron Scientific (Bronze Sponsor)

Micron Scientific has been a leader in the area of Material Characterization since 1990. We provide sales, service and applications support for instrumentation that address a range of applications in analysis and research relating to Material Characterisation. Systems supplied are used to measure particle size, shape, zeta potential, protein charge, molecular weight, mass, and conformation, rheological properties, stability and for chemical identification, advancing the understanding of dispersed systems. These instruments are used by both industry and academia, in sectors ranging from pharmaceuticals and biopharmaceuticals to bulk chemicals, mining, cement, polymers, and the environment.

The Mineralogical Association of Canada (Sponsor - Sessions: Pegmatites and pegmatite mineralogy (GP10) and The Geology of Gems and their Geographical Origin (GP12))

The Mineralogical Association of Canada is a non-profit scientific organization formed to promote and advance the knowledge of Mineralogy. We publish the Canadian Mineralogist, an international journal of mineralogy, crystallography, petrology, geochemistry and ore deposits, international authorship, readership, editorship; great book reviews, thematic issues, short course volumes and special publications.

The Mineralogical Association of South Africa (MINSA)
(Bursaries Support)

The Mineralogical Association of South Africa, or MINSA as it is more commonly called, was formed in 1979 as a specialist division of the Geological Society of South Africa (GSSA) with the primary aim of promoting interaction between mineralogists, particularly in the fields of mineralogy, petrology and geochemistry. Over the years it has grown to more than just pure mineralogy so that nowadays applied mineralogy also forms a strong focus.
The prime objective of the Association is the organisation of field excursions, symposia, workshops and laboratory visits of interest to members.
The planning and organisation of all events is undertaken by a committee made up of a Chair, Vice-Chair, Secretary and three elected members together with usually 20-25 co-opted committee members drawn from industry and academia throughout South Africa, all of whom give of their time on a voluntary basis. Should anyone be interested in joining MINSA, a membership form can be downloaded from the Minsa website at http://www.minsoc.org.za.

Mintek (Silver Sponsor and Lanyards Sponsor)

For 80 years, Mintek has been at the forefront of minerals and metallurgical research and development. Today, this centre of technological excellence, with its teams of highly trained and experienced scientists, engineers, researchers and specialists, continues to build South Africa's resources and capacity by providing advanced technology for the more effective extraction, utilisation and beneficiation of our mineral wealth. Our expertise lies in:

- integrated piloting facilities for process development, including commination, flotation, physical separation, leaching, smelting, metal recovery and purification
- analytical services
- certified reference materials
- mineralogical investigations
- novel/advanced materials
- mineral economic studies.

Mintek – Your partner in unlocking mineral wealth.

National Research Foundation (Platinum Sponsor - Bursaries)

Global Research. Global Reach.
The National Research Foundation (NRF) leads the way in building local and international links for researchers and research institutions.
Working closely with the Department of Science and Technology, the NRF's International Relations and Cooperation (IRC) directorate plays a critical role in proactively facilitating and enhancing international scientific collaboration among individual scientists, higher education institutions, research bodies and scientific and professional associations in South Africa and abroad.
IRC maintains a broad focus in the following areas:

- **Overseas Cooperation (OC)**

Promoting South Africa's science links on a global front through intergovernmental and interagency agreements; facilitation of joint research; and ensuring capacity building in key areas.

- **Africa Cooperation (AC)**

Promoting continental and regional scientific collaboration to address socioeconomic and sustainable growth issues in Africa.

• **Multilateral and Strategic Initiatives (MSI)**
- *Secretariat for the International Council for Science (ICSU)*
Promoting South African involvement in ICSU organisations to address common concerns such as capacity development, data, science and technology in developing countries, ethics and freedom in the conduct of science.
-*Knowledge Interchange and Collaboration (KIC)*
Providing mobility funds for local researchers interact with the global scientific community as well as bring the international research community to South Africa.

Contact: Dr Aldo Stroebel (Executive Director International Relations and Cooperation). Michael Nxumalo (Director: International Relations and Cooperation *Africa Cooperation)*
Email: michael@nrf.ac.za.
Dr Sepo Hachigonta (Director: Multilateral and Strategic Initiatives *Multilateral and Strategic Initiatives)*
Email: sepo.hachigonta@nrf.ac.za.
Prudence Makhura (Director: International Relations and Cooperation *(Overseas Corporation)*
Email: prudence.makhura@nrf.ac.za.

Nikon (Bronze Sponsor)

Nikon Metrology offers the broadest range of metrology solutions for applications ranging from miniature electronics to the largest aircraft. Nikon Metrology's innovative measuring and precision instruments contribute to a high performance design-for-manufacturing process that allows manufacturers to deliver premium quality products in a shorter time. http://www.nikonmetrology.com.

PPC (Sponsor - Pre-conference Workshop: Applied Mineralogy of Cement and Concrete)

PPC Ltd, the leading supplier of cement in Southern Africa was established in 1892 in Hercules, Pretoria. PPC has eight cement manufacturing facilities and three milling depots in South Africa, Botswana, Zimbabwe and Rwanda that can produce around eight million tons of cement products each year. PPC also produces aggregates, metallurgical-grade lime, burnt dolomite and limestone. Since 2012 we have expanded to Ethiopia, Rwanda, DRC and Mozambique. Each facility has its own quality assurance laboratory with additional support by Group Technical Services.

PANalytical (Bronze Sponsor - Pre-conference Workshop: Phase quantification by XRD)

PANalytical is the world's leading supplier of analytical instrumentation and software for X-ray diffraction (XRD), X-ray fluorescence spectrometry (XRF), near-infrared (NIR) spectroscopy and pulsed fast thermal neutron activation (PFTNA). This combination of analysis techniques can provide customers with tailor-made analytical solutions for the characterization of a wide range of products such as cement, metals, nanomaterials, polymers and many more.
PANalytical's systems are used for scientific research and development, for industrial process control applications and for semiconductor metrology.

PerkinElmer South Africa

PerkinElmer Inc., a global leader focused on improving the health and safety of people and the environment is represented in Southern Africa through a direct operation based in Midrand, with support offices in Cape Town, Port Elizabeth and Durban. Our offices support the business across all Southern African countries in the following key markets: academia, mining and mineral testing, chemical and petrochemical analysis, pharmaceutical applications, and food and beverage safety testing.

Our new head office in Midrand is home to a staff compliment of 34 sales, support and back office staff members. It also houses our technical and customer knowledge centre with conference, training and instrumentation demonstration facilities.

PerkinElmer provides solutions in the following areas:

- Molecular Spectroscopy -UV, UV/Vis, FT-IR, FT-NIR, Fluorescence
- Atomic Spectroscopy - AA, ICP-OES and ICP-MS
- Chromatography - GC, GC custom, GC/MS, LC/MS, HPLC/UHPLC
- Thermal and Elemental Analysis – DTA, DSC, TGA, TMA and DMA
- Hyphenated Systems – TGA/IR, TGA/MS, TGA/GC-MS
- Mass Spectrometry - GC/MS, LC/MS, TOF/MS, GC/MS/MS, ICP-MS
- Informatics

Contact details: PerkinElmer South Africa (Pty) Ltd, Building 21, Thornhill Office Park, 94 Bekker Road, Midrand , South Africa. Tel: +27 11 564 2400.
Email: info.za@perkinelmer.com.

Society of Economic Geologists

The Society of Economic Geologists is a worldwide Society with more than 7000 members in over 100 countries. In addition to quarterly Newsletters and 8 issues a year of the prestigious journal Economic Geology, the Society publishes many special issues, guidebooks and specialist compilations, both in book and as CD's and organizes numerous education and training courses. Popular compilations include the 100th Anniversary Volume which contains all the papers in Economic Geology covering 100 years. The SEG stand here at IMA provides an opportunity to sign up for membership, or to order any of the publications.

SGS (Silver Sponsor)

SGS is the world's leading inspection, verification, testing and certification company. SGS is recognised as the global benchmark for quality and integrity. With more than 75 000 employees, SGS operates a network of over 1 500 offices and laboratories around the world. We provide competitive advantage, drive sustainability and deliver trust. At SGS, we are continually pushing ourselves to deliver innovative services and solutions that help our customers move their businesses forward.

SGS Minerals Services is the global leader in testing, consulting and on-site services for the mining and minerals sector. With metallurgical, analytical, mineralogical and environmental technical expertise, we support clients worldwide from offices in Canada, USA, Chile, Brazil, Australia, Peru, Russia and South Africa.

SMM Instruments (Bronze Sponsor)

SMM Instruments (Pty) Ltd is a socially progressive company and prides itself on having excellent people in all spheres of its activities. Continuous local and international training, coupled with an emphasis on teamwork, ensures a high level of staff motivation and positive customer orientation. Our head office in Johannesburg is based in Kyalami Business Park. We have two branches, one in Durban and the other in Cape Town. All our offices are fully equipped with professional Sales Staff, Service Engineers and Application Specialist. As a company working together in a team environment, our main goal is to provide solutions to virtually every need of the Analytical and Laboratory community. We have signed exclusive international agency agreements, and we have Specialised Sales Staff and Experienced Service Engineers to ensure that solutions to application problems are readily available and enable us to service and support our entire range of instruments throughout Sub-Saharan Africa as well as locally. We have employed qualified application specialist to cater for customers' individual needs, while international specialists from the various manufacturing companies are regularly on hand to augment the service.
The company's impressive product portfolio features world renowned process and analytical equipment for industries such as:
• Mining • Chemical • Research • Academia • Agriculture • Petrochemical
• Pharmaceutical • Food and Beverage • Medical and Surgical.

The South African National Convention Bureau

The South African National Convention Bureau acts as a ‘one stop solution’ for independent information and assistance, giving neutral advice on all aspects of hosting and organising any business event in South Africa. Meeting and incentive planners will have ease of access to any and all information they require on the destination, simplifying their processes and making turnaround time significantly quicker.
South Africa has the proven capacity and world-class infrastructure to successfully host major international business events and meetings. Our strength relies on the diversity of our destination, not only in terms of our welcoming people and rich culture, but our ability to deliver the dynamic, flexible and value-for-money attributes of a major global business events destination with all the world-class infrastructure, without compromising on the authentic, distinctly ‘African’ business and leisure environment.

Springer (Bronze Sponsor)

Looking to publish your research? Learn about our print and electronic publication services, including Open Access! Get high-quality review, maximum readership and rapid distribution. Come to our booth or find us online: springer.com/authors. Editors Elodie Tronche and Annett Buettner will be available to discuss book projects.
You can also browse key titles in your field and buy (e)books at discount prices. With Springer you are in good company.
http://www.springer.com/earth+sciences+and+geography/geochemistry?SGWID=0-1733513-0-0-0.

The Stellenbosch University

The Stellenbosch University's Central Analytical Facilities provides a high quality, fast turnaround service for academics and industrial clients, making optimal use of top of the range analytical equipment and techniques.
Services relevant to the mining industry include: XRF, LA-ICP MS, X-ray microCT & SEM, amongst others.
Please see www.sun.ac.za/caf and contact us today for a quote for your analytical requirements.

UIS Analytical Services (Bottled Water Sponsor)

UIS Analytical Services (Pty) Ltd is an independent testing laboratory company offering a wide range of analytical techniques and consulting services, with focus on analysis for the mining industry and environmental samples (water analysis).
Many of our methods are SANAS (South African National Accreditation System) ISO/IEC 17025 accredited, comparable with international standards and procedures. In addition to our minerals, metals and other inorganic analysis on all material and XRF analysis on mostly mineral ores, the company can provide a comprehensive set of analysis according to SANS 241 for water.
The laboratories provide analytical services and expertise unrivaled by other laboratories in Southern Africa, as it is staffed with advanced degree chemists, technicians and highly trained laboratory assistants to provide an exemplary and personalised service. The personnel's strong multi-skilled technical backgrounds, combined with high personal standards and experience in a variety of analytical specialities, ensure that our laboratories stay in the forefront of technology to provide superior results.
Our modern facilities, comprising over 1500 square meters at the head office in Centurion and 700 square meters at the Kimberley branch, include centrally situated laboratories with ample sample preparation, analysis and storage space.
For a truly South African service by a fully South African company, contact us for your analytical needs.
We also have several partnerships to offer you a truly one-stop services. This includes access to XRD analysis, organic analysis, bulk sample preparation and metallurgical testing of metals.
We also have a company movie for a quick overview - http://youtu.be/MakIirz6xWY.

United Spectrometer Technologies

United Spectrometer Technologies CC (“US TECH”) is a Leading supplier of Scientific Analytical equipment within Africa for the mining, mineral and industrial industries. Our mission is to supply high-integrity, **reliable analytical instrumentation** throughout Africa. Our Scientific Analytical equipment lines performs a critical role for user identifying key ore bodies and acid-consuming minerals more quickly, which supports our mission and increased production efficiencies for our customers. Our product range includes products like **THERMO SCIENTIFIC Niton (Portable XRF); Analytik-Jena (Analytical Spectrometers)** and PANalytical (Spectroscopy Products).

Wirsam Scientific

Wirsam Scientific was established in 1968. Throughout its proud history Wirsam has entrenched itself as one of the leading suppliers of laboratory instrumentation. The company is categorised into Microscopy, Analytical, Material Testing, Petrochemical and General Laboratory Instrumentation divisions. Wirsam has fully equipped workshops providing complete sales and service capabilities.

XRD (Nickel Sponsor)

ZETECH (Nickel Sponsor)

List of Sponsors

Organisation	Sponsorship Details
Department of Science & Technology	Platinum Sponsor - Bursaries
National Research Foundation	Platinum Sponsor - Bursaries
AMIS	Silver Sponsor
Carl Zeiss	Silver Sponsor
FEI Australia	Silver Sponsor
Joburg Convention Bureau	Silver Sponsor
Innov-X Africa	Silver Sponsor
MINTEK	Silver Sponsor and Lanyard Sponsor
SGS South Africa	Silver Sponsor
Advanced Laboratory Solutions	Bronze Sponsor
Nikon Metrology	Bronze Sponsor
SMM Instruments	Bronze Sponsor
Springer-Verlag GmbH	Bronze Sponsor
PANalytical / Micron Scientific	Bronze Sponsor
XRD Analytical & Consulting	Nickel Sponsor
Zetech	Nickel Sponsor
UIS Analytical Services	Branded Bottled Water
Geological Society of South Africa	USB Abstract Volume, Delegate Conference Bags and Bursary funding
Geological Society of America	Bursary funding
IMA	Bursary Funding
Mineralogical Association of South Africa	Bursary Funding
Mineralogical Association of Canada	Pegmatites and Pegmatite Mineralogy Session &The Geology of Gems and their Geographic Origin Session
Anglo American	Process Mineralogy and Geometallurgy Session
Bruker AXS GmBH	Quantitative Phase Analysis XRD Workshop
Bruker MicroCT	Computed Tomography - Pushing Frontiers in Imaging of the Third and Fourth Dimensions Session
Carl Zeiss	Trade Symposium: Spanning the 2D and 3D Worlds
De Beers	Cratons and Diamonds Session
FEI	Trade Symposium: Automated Mineralogy & Petrology workshop for Geometallurgy
GIA Education & Laboratory	Gem Diamonds: Treatment, Synthetics and it's IdentificationWorkshop
PANalytical	Quantitative Phase Analysis XRD Workshop
PPC	Applied Mineralogy of Cement and Concrete Workshop

Author	Page number
Abart R	208, 245, 251, 249, 250, 339
Abbondanzi F	141
Abegunde O	158
Abratis M	171, 237
Achilles C N	384
Ackerman L	74
Addis A	361
Afanasyev V	30, 70
Agangi A	271, 402
Agashev A	23, 30
Ageeva O	249
Agheem M H	253
Agrosì G	278
Aiglsperger T	212
Aihara Y	405
Akai J	154, 186
Akai K	186
Akasaka M	343
Akiyama S	186
Alaabed S	80
Al-Ali S	57
Albrecht-Schmitt T	182
Aldieri E	177
Alekssev E	182
Alfieri I	357
Alfonso P	267
Allard T	345
Alonso-Azcárate J	387
Altermann W	153
Altree-Williams A	131
Alunno S	91
Alvarado Ávila A	58
Alvaro M	346
Amaike Y	52
Amaya-Perea Z	58
Ames D	101, 73
Amoako F	154
Amores Casals S	195
Amponsah-Dacosta M	149
Amthauer G	333, 66
Anason M	264
Andersen J	57, 195
Andersen T	192
Anderson R C	384
Ando T	380
André A	129
Andreeva E	88
Andrejkovičová S	8
Andreoli M	5, 6, 389, 392
Andreozzi G	174, 253, 313
Andrews L	113
Angeli N	110
Angelica R	191
Angelini I	355, 361
Angerer T	128
Anicin I	66
Annabi-Bergaya F	170
Aomar E	97
Arakawa Y	380
Aranovich L	224
Arbaret L	132
Arenholz E	166
Arias D	134
Arletti R	138, 142, 346, 353
Armbruster T	139, 141, 308, 381
Arndt N	39, 192, 229, 404
Arrio M	352
Artioli G	189, 191, 296, 361
Ashwal L	232
Ashworth L	254, 402
Atanasova M	365
Atencio D	372, 377
Atzei D	174
Avdeenko A	224
Avdontceva M	330
Ayora C	143, 147, 179
Azer M	209
Azzaro A	280
B Andrade M	377, 372
B. Silva P	261
Bach W	197
Bačík P	86, 218
Badra L	97
Baensch A	307
Bai J	158
Baibatsha A	63
Baijot M	131, 252, 262, 330, 373
Bailau R	139
Bailly L	129

Bajda T 164
Bakker R 33
Bakos F 91
Balan E 50, 345
Balassone G 98
Balboni E 179
Ball A 312
Bam L 293, 298
Bambi A C J M 195
Bamford M 389
Banaszak M 240
Banchi B 163
Banno Y 213
Baptiste B 351
Barata C 8
Barbanson L 97, 100
Barker I 393
Barnabe P 316
Barnes S 101, 108, 73, 103
Baron A 38
Baron M 213
Barone G 172, 242, 357
Barrenechea J F 387
Barrese E 175, 176
Barry P 21, 107
Bartoli D 163
Bartsch C 78
Basson I 295
Batanova V 39, 310
Bau M 105
Baur W H 336
Beaudoin G 73
Beausir B 45
Becker M 114, 115, 121, 152, 156
Bekker A 404
Belfortini C 150, 175
Belluso E 7, 175, 176, 177, 178
Bellver Baca M 120
Belmonte D 48
Belogub E 92, 96, 344
Belpoggi F 176
Belser P 142
Beltrán G 58
Belviso C 7
Belyanin A 32
Belyanin G 5, 126, 167, 389, 392
Belyatsky B 211
Benisek A 302, 341
Benko Z 106
Benna P 37
Benvenuti M 159, 242, 353
Berbeleac I 84
Bergamonti L 357
Berger A 59
Berkesi M 55
Berkh K 91
Bermanec V 84, 262, 264, 266
Bernier F 59
Berryman E 271, 277
Bersani D 318
Bethke M 235
Beukes N 125, 215, 288
Beurlen H 260
Bilal E 71
Bindi L 39
Birch W 257, 362
Birkenstock J 335, 336
Bish D 7, 379
Bittar S M B 298, 365, 366
Bittarello E 325, 346
Blaauwbroek N 197
Blake D 383, 384
Blamey N 95
Blanc C 359
Blancher S 120
Blattmann T 161
Blichert-Toft J 229
Blignaut L 122, 125, 215
Blinov I 96
Block D 5, 389
Bloise A 175, 176, 178
Bobocioiu E 333, 382
Boev B 66
Boeva N 103
Boffa Ballaran T 40
Bogush I 26
Boixet L 92
Bonaccorsi E 317
Boni M 97, 98, 99
Boniface N 204

Bonilla-Pérez A 58
Bonnet J 129
Bons P 237
Bontognali T 408
Boone M 149, 292, 293
Borisov A 39
Bornefeld M 113
Borruel-Abadía V 387
Borzdov Y 46
Bosch F 66
Bosi F 253, 345, 373
Bosse V 286
Botha T 104
Botta C 334
Boudreaux A 255
Boullier A 192
Boyce A 89, 90
Bradley D 208
Bradley T 382
Bradshaw D 1, 369
Bradshaw S 299
Brady A 57, 197
Brancucci M 156
Brand A 284
Brandmeier M 240
Branquet Y 97, 134, 256
Brantut N 49
Breeding C M 278, 282, 283
Brenker F 32, 52
Brey G 25, 31, 20
Bristow T F 379
Britt D 377
Broadhurst J 152, 156
Brooks W 58
Broom-Fendley S 57, 195
Broska I 53, 218
Brouder C 352
Bruand E 248, 272, 273
Brudzinska-Kosior A 358
Brugger J 88, 101, 131, 135
Brunet F 49, 59, 216
Bruzenak L 305
Bryzgalov I 19
Buatier M 6, 100, 332
Buccianti A 159
Büchel G 185
Buchholz T 257
Buchriegler J 117
Buda G 215
Bunno M 213
Burda J 214, 238
Burgio L 375
Burns P 179
Buxton M 121
Bybee G 255
Bykov M 336
C. Bastos Neto A 372
Cabral A 102, 289
Cai Y 18
Cairncross B 116, 365, 367
Calas G 241, 345, 352
Caldeira R 42
Calin N 264
Calzaferri G 142
Cama J 151, 150
Camaiti M 348
Cámara F 37, 325, 346
Cameron D 89
Campbell I 305
Campisi T 141
Can M 369
Cannas C 172
Cao X 364
Capacci 163
Capella S 175, 177, 178
Cappelletti P 7
Caraballo M 143
Caracas R 45, 333, 382
Caratto V 150, 175
Carbone C 159
Cardoso A 8
Carey R 317
Carlà F 334
Carrera J 151, 179
Carrera M 388
Carretti E 353
Carvalho P 171
Case B 174
Castañeda Gómez A 58
Castellano Calvo A 249

Castillo Hernandez J 145
Castillo J 144, 145, 146, 148
Castillo-Oliver M 196
Catalano M 175
Caterina R 176
Cauzid J 129
Cavailhes T 6
Cavalcante F 7
Cavallo A 176
Cawthorn G 102, 229, 232, 236
Celik I 369
Cempirek J 284, 73
Cepedal A 92, 93, 134
Cerantola V 43
Cesarano M 7
Chaerun S K 183
Chakhmouradian A 335
Chamberlain K 393
Charikinya E 299
Charles N 97
Charpentier D 6, 332
Charusiri P 95
Charykova M 172
Chassé M 241
Chen C 129, 132, 205
Chen F 181
Chen H 199
Chen M 393, 398
Chen Y 97
Cheng H 204
Cheng Y 155
Chetty D 58, 115, 295, 369
Chida Y 95
Chipera S J 384
Chistyakova S 109, 230
Chopin C 334
Choulet F 97, 100
Chovan M 91
Christy A 13, 347, 374
Chudy T 73
Chukanov N 338, 378
Chumakov A 43
Churms C 292
Ciftci E 80, 133
Cinotti S 334, 335
Cioaca M 81, 173
Ciobanu C 130
Ciriotti M 325, 346
Ciscato E 408
Clark S 301
Clark W 58
Clarke C 6
Claydon J 385
Cleverley J 307
Cloete M 6
Cnudde V 149, 292, 293
Cobic A 262,264
Cody G 164
Coelho G 132
Coetze G 229
Colás V 133
Coltorti M 141
Comodi P 43, 48, 390
Compagnoni R 177
Connolly J 219
Consani S 159
Cook N 87, 130
Copuroglu O 189
Cordier C 192
Cordier P 45
Cormier L 241
Costa M 191, 368, 70
Costagliola P 159, 172, 242, 353
Costin G 81, 84, 236, 250, 341
Couture R 147
Cramer T 58
Crandell O 355
Cremisini C 174
Cressey G 375
Crisp J A 384
Croce A 176
Cronwright M 256
Crouzet C 218
Crowley Q 238
Čuda J 382
Cui X 183
Curetti N 37
Contreras R 294
Curry J 272
Cvetkovic V 66

da Costa M 11
da Fonseca Martins G O 60
d'Acapito F 163, 242, 303, 335
Dachs E 302, 341
Daghino S 177
Dähn R 301
Dairou J 218
Dal Bo F 131, 254, 330, 373
Dalconi M 189, 191, 296
Dan S 66
Danisi R 138, 141
Dare S A S 73, 103
Darling J 393
Dars H 253
Davey J 231
Davies A 74
Davies R 74
Davila G 150
Dawes W 57, 195
Day J 107
Dazas B 16
De Ascenção Guedes R 286
De Beer F 293
de Brito Barreto S 266, 365, 366
De Giudici G 172
de Kock M 288
De Kock T 149, 292, 293
De la Horra R 387
De Luca A 335
De Min A 42
de Moura O 262
De Pourcq K 179
de Saint Blanquat M 269
De Schryver T 292, 293
de Souza Gonçalves V F 60
de Vaux D 118
De Villiers J 307, 319
De Vito C 259
de Wit F 157
Decamp X 315
Deegan F 54
DeFlaun M 145
Degen T 304
Dekura H 47
del Campo A 262
Della Giustina M 207, 224
Deloule E 50
Delville A 16
Demaiffe D 279, 283
Demouchy S 45
Depmeier W 1, 172, 182
Des Marais D J 384
Deutsch A 396
Devaux A 142
Deveaud S 256, 270, 259
D'Haenens-Johansson U F 278, 282
Di Bella M 359
Di Benedetto F 159, 163, 172, 186, 242, 334, 335, 353
Di Giuseppe D 141
di Martino M 389
Di Piazza S 187
Diaconu G 71
Dias P 265
Diaz J 58
Diedericks V 144
Diko Makia L 163
Dilek Y 28
Ding H 185, 187
Ding J 35
Dingwell D B 233, 303
D'Ippolito V 318
Dislaire G 315, 316
Djafar A 183
Djordjevic T 326, 347
Do Cabo V 63
Dohmen R 202
Domanik K 372
Domenech C 81
Dong H 184
Dong J 364
Downes P 376
Downs R 372, 383, 404
Downs R T 339, 384
Drabon N 403
Druguet E 269
du Plessis A 121, 295, 299, 300
Dubinina E 224
Dubrovinsky L 43
Dulski M 139, 377

Dultz S	9	Falus G	51
Dumitras D	71, 81, 173, 264	Fan D	44
Dunlevey J	209	Fancsik T	51, 55
Dutrow B	272, 274	Fanlo I	133, 135
Duvenhage M	111	Fantauzzi M	174
Dyussembayeva K	63	Farber G	324
Dzierżanowski P	377	Farber K	273, 409
Dziggel A	273, 404	Farina G	163
Dzvinamurungu T	120	Farmer J D	384
Eagle R	257	Farsang S	387
Ebert M	396	Faryad S	245, 246, 247
Echigo T	348, 380, 408	Favero-Longo S	177
Eglinton T	161	Fedortchouk Y	20
Eickmann B	402	Fehér B	62, 136
Eiler	197	Fei Y	39, 390
EIMF T	26	Felici R	334
Ejima T	348	Feneyrol J	283
Elburg M	192, 237	Feng T	133
Ellena J	377	Fernandes V	399
Elliott T	200	Fernández J	262
Ellmies R	63	Fernandez-Martinez A	301
Elsen J	188	Ferrage E	16
Enea F	275	Ferrari G	189, 191, 296
Eng P	161	Ferraris C	37
Ennaciri A	100	Ferreira Filho	224, 207
Erambert M	192	Ferrero S	219
Ermolina O	92	Ferretti M	150, 175
Ertel-Ingrisch W	233	Ferrière L	312
Ertl A	323	Feuillie C	164
Estrada C	164	Fiebig J	291
Etschmann B	88, 101, 131, 135	Figueira B	70
Ettinger K	245	Filip J	144, 382
Evans M	6	Fiore S	7
Evans R	323, 324	Fiorentini M	101, 108
Evrard M	294	Fischer L	335, 401
Evstigneeva T	103	Fischer R	225, 335, 336, 337
Faccini B	141	Fisher D	29
Fagan A	279	Fisher P C	103
Fairey B	341	Flatt R	9, 360
Faithfull J	21	Flores V	207
Falk E	197	Fois E	138
Fallick A	279	Foresti M	335, 335
Fallick T	283	Förster H-J	381
Fallon E	82	Fourie J	155, 180
Falster A	257, 255, 258	Foustoukos D	164

Fowler M 248, 272
Fowler-Gerace N 390
Fox P 404
Franco Victoria J 58
Franke H 78
Fransen M 294
Fransolet A 264
Franz G 271
Franzen C 180
Franzidis J 152, 156
Fraser A 302, 361
Frei D 293
Freitag R 78
Fressengeas C 45
Frimmel H 86
Fritz J 394, 395, 397, 399
Frost B 262
Frost D 40, 392
Fu C 364
Fubini B 177
Fuertes-Fuente M 92, 93
Fujiwara T 136
Fukuhara H 154
Fukui H 38, 243
Füllmann T 308
Fyfe S 87
Gäbler H 78, 259
Gabo J 64, 93, 112
Gadas P 215
Gaetani G 49
Gaggero L 150, 175
Gagne O 349
Gaillard F 221, 226
Gál P 62
Galán-Abellán A B 387
Galbiatti H 102
Galí S 79, 81, 150, 198
Galic A 403, 406
Gallino R 389
Galoisy L 241, 345, 349, 352
Galuskin E 139, 377, 378
Gan Z 351
Gao J 44
Gao S 66, 133
Gao W 66
Garate-Olave I 265, 267
García-Casco A 79
Garcia-Gutierrez M 179
Garcia-Rios M 151
Garuti G 82, 110
Gasc J 49
Gauert C 74, 105, 266
Gaupp R 185
Gawęda A 214, 238
Gazaleeva G 122
Gazzano E 177
Gellert R 384
Geng Z, Jiang N 364
Genin J 13, 14
George L 130
Gerdes A 20, 25, 31, 238, 259, 269, 282, 292, 294, 296
Gervilla F 133, 135
Gerya T 225
Gfeller F 139, 382
Ghigo D 177
Ghinet C 71
Ghosh, S 219
Giacobbe C 359
Gibsher A 42
Gibson R L 394
Giester G 321
Gigli L 142
Gil-Crespo P 265
Giuffrida A 172
Giuli G 159
Giuliani G 278, 279, 280, 281, 283
Giustetto R 7
Glatzel P 347
Gleixner G 185
Gliozzo E 354
Gloaguen E 256, 288
Göckeritz M 316
Godel B 108
Goed R 258
Goeske J 70
Goguelin A 120
Golden J 404
Goldmann S 78

Goldstein S 197
Golonka J 214
Golunova M 223
Gomez- Arias A 145, 148
Gonçalves A O 195
Gonzalez-Alvarez I 94, 277, 315
Goodey N 317
Goodrich C 107
Gori C 253
Göske J 368
Götz D 294, 305
Gout C 7
Grand' Homme A 286, 269
Grassi L 258
Graupner T 259
Greau Y 50
Greenway G 146
Greshake A 395, 399
Grevel K 302
Grew E 323, 404
Greyling L 114
Grice J 327, 376
Griffin W 22, 26, 28, 29, 50, 196
Griffiths T 245, 250
Groat L 73, 279, 284, 323, 324
Grobler D 234
Groppo C 177
Grote W 299
Gruian C 358
Gryffenberg L 58
Gualtieri A 175, 176, 178, 188, 298
Guatame-Garcia A 121
Gubelin S 280
Gucsik A 271, 389, 395, 399
Guégan R 100
Guerin O 14
Guerri A 334, 335
Guidry J 257
Guillou-Frottier L 256
Guimarães F 265
Gumiaux C 256
Gunn G 57, 195
Guo X 41
Gutzmer J 119, 291
Guyot F 218
Guzzo P 266
Gyollai I 399
Habler G 208, 245, 249, 250, 339
Hadher A 80
Haefeker U 322
Haeger T 285
Hagemann S 128
Hagiwara A 93
Hålenius U 253, 337, 373
Halisch M 297
Hamann C 396
Han R 155
Han Z 158
Händel M 162
Hanf D 117
Hanfland M 43
Hanley J 101
Hanna J V 337
Harlov D 220
Harlow G 200
Harris C 6, 254, 404
Harris J 26
Harris P 114, 153, 316, 402
Harrison S 156
Hart E 248, 273
Hartai É 136
Hassan M 214
Hatert F 131, 254, 264, 265, 330, 366, 373
Hatton C 29
Hauck S 106
Hauri E 49
Havelocova M 67
Hawthorne F 346, 349, 350
Hayashi K 51
Hazen R 164, 391, 404
He H 79, 162, 165, 170
He Z 165
Hecht L 219, 233, 235, 312, 396
Heck R J 298
Heeschen K 78
Hegner E 407

Heidi H 31
Heinrich C 86
Heinrich W 271, 277
Heistek R 240, 391
Henderson G 243
Henjes-Kunst F 259, 291
Henning W 66
Henry D 272, 274, 362
Hentschel R 237
Hering D 180
Hermann J 50
Herrmann K 335
Hertwig A 198, 201, 202
Hess K-U 233, 303
Heubeck C 403
Heuser D 208
Hezel D 385
Hibbs D 376
Higo Y 39
Hijiya H 352
Hirao N 52
Hiraoka N 243
Hochella Jr. M 143
Hoeck V 355, 358, 357
Hoefer C E 20
Hoefer H 25
Hoefer H E 20
Hoehnel D 394, 397
Hofmann A 126, 271, 394, 397, 402, 404, 403, 407
Hofmann C 202
Hofmeister W 285
Hoinkes G 216, 246
Hollanders S 188
Holtz F 269
Hölzen H 336
Hombourger C 311
Honey F 317
Honma C 343
Honour V 230
Horie K 405
Horn H 58
Horng C 132
Horstwood M 195
Horváth A 215
Hoshino M 62, 321, 380, 400
Hou T 235
Houssou N 89
Houta N 18
Howarth G 21, 107
Howell D 29, 32
Hrynio P 303
Huang A 132
Huang F 66, 133
Huang J 33, 50
Huang K 129, 132
Huang W 44
Huang Y 133
Huang Zh 28
Hudson Lamb D 389
Hudson M 87
Hughes H 21
Hughes J 374
Humphreys M 230
Humphreys-Williams E 375
Hung S 183
Hunt L 26
Huotari S 389
Hušková I 144
Hutchison M 52
Hyde B 390
Hystad G 404
Iaia T 163
Iancu A 264
Ichangi D 280, 281
Ihlen P 260
Ikeda T 343
Ikehara M 405
Imai A 64, 65, 89, 93, 95
Ingrin J 50
Innocenti M 163, 334, 335
Inoue T 51
Ionescu C 355, 358, 357
Isaenk S 306
Ishibashi J 136
Ishida A 205, 405
Ishihara Y 93
Ismailova L 43
Ito T 405
Ivanyuk G 329

Izawa M 399
Jackson S 101
Jacob D 285
Jacobs T 114
Jacobson M I 264
Jahn S 36
Jahoda R 114, 316
Janák M 53, 218
Jang C 160
Janicka U 164
Janney P 22
Janots E 59, 286
Jardine M 121
Javaux E J 407
Jedlicka R 245
Jeffries T 225
Jégo 132
Jenni A 301
Jia Y 158
Jiang W 129, 132
Jinnah Z 389
Jinnouchi S 320
Johanson B 87, 104
Johnson C 257
Jones A 32
Jones C 312
Jordan N 180
Joy B 324
Juanerio J 112
Juhin A 345, 352
Junge M 105, 109
Jussara P 366
Kabeya F 76
Kachlík V 246
Kadarusman A 183
Kaden R 70
Kah L 404
Kahlenberg V 322, 336, 342
Kaise M 331
Kalichini M 114
Kalita P E 337
Kalkan B 301
Kamada S 38, 52
Kamenetsky M 249
Kamenetsky V 249
Kampf A 340, 347, 374, 375,
Kanayama A 380
Kaneko S 396
Kantor A 43
Kanzaki M 243
Karampelas S 280
Karimova A 53
Karki B 46
Karwowski Ł 383, 385
Kašlík J 144, 382
Kassenova A 63
Kastner A 185
Katoh Y 396
Katsura T 340
Kaufmann F 235
Kavecsanszki D 59, 196
Kawamoto T 199, 222, 220
Kay S 363, 368
Kayama M 396
Kearsley A 312
Keatley A 75
Kelemen P 197
Kempl J 189, 392
Kenkmann T 396
Kerr A 21
Ketcham R A 2
Khalo M 149
Khan T 253
Khomenko V 334
Khvorov P 344
Kimata M 348, 380, 408
King S P 337
Kinnaird J 104, 124, 234, 254
Kirk C 375
Kis A 215
Kiseeva K 227
Kiseleva I 19
Kiss G 82
Kitajima K 198
Kitazawa H 331
Kiyokawa S 405
Klausen M 288
Kleebe H 68, 67
Kleespies P 284
Kletetschka G 382

Klimm K 41
Kloetzli U 251
Klötzli U 238
Klügel A 197
Knapp N 41
Knieß R 75
Knippenberg S 202
Knoper M 120
Kobayashi S 380
Kobayashi T 199
Kobussen A 26
Koch-Müller M 277
Kodera P 91, 86
Koeberl C 394, 397, 398, 3400
Koenig A 87
Koga K 49
Koglin N 289
Kohn S 50
Kohout T 382
Koizumi T 227
Kojonen K 104
Kolařík J 144
Kolitsch U 157
Kolitsch U 321
Kon Y 61
Konc Z 55
Kong F 199
König U 14, 15, 294, 304
Konrad-Schmolke M 275
Konzett J 213, 337
Korsakov A 246
Kosior G 358
Köster T 355
Kothe E 154, 185
Kotouček M 72
Kotova O 122
Kotzé E 105
Kovacs I 50, 51, 55
Kovaleva E 245
Kowalski P 392
Kozlik M 287
Kraemer D 105
Kramers J 5, 126, 167, 169, 389, 392
Krasheninnikov S 39
Kreher-Hartmann B 362
Kristály F 62, 136, 137, 165, 215, 35
Krivovichev S 140, 329, 330, 332, 350
Krivovichev V 172
Kruhl J 400, 35
Krupskaya V 19
Kruszewski Ł 383, 386
Krymsky R 211
Kryza R 358
Krzhizhanovskaya M 330
Kudo H 154
Kuhn K 75
Kuleci H 245, 251
Kuligin S 30
Kullerud K 218
Kumagai Y 199
Kunihiro T 201
Kupenko I 43
Kuribayashi T 343
Kusachi I 384
Kusano N 401
Kusiak M 277
Kusz J 139, 377
Kuzmin D 39, 42, 310
Kuznetsov S 306
Kuzyura A 225
Kyser K 98
L. Gomes C 261
Labaume P 6
Lacroix B 332
Lafuente B 383
Laguerta E 112
Lalomov A 19, 126
Lambert C 260
Lambert-Smith J 90
Lanari P 332
Landman B 153
Lang K 72
Langreiter T 342
Lanson B 16
Lanson M 59
Lapen T 208
Lasobras E 133
Latapie L 243

Latrille C 359
Lattanzi P 159
Latypov R 109, 230
Laukamp C 315
Laurent O 238
Laurora A 141
Lavacchi A 334, 335
Lavina B 37
Lawrence D 90
Lázaro M 133
Le Caer S 359
Le Roux S 300
Leal Gomes C 265
Leardini L 142
Lebedeva S 344
Leclère H 6
Ledevin M 404
Lee N 164
Lehmann B 58, 78
Lekgau 149
Lelong G 241, 351, 352
Lenaz D 42, 337, 230, 231
Lenz C 321
Leonardo Brabosa G 368
Leonenko N 122
Lerat J 6
Lermi A 80
Leroy S 316, 370
Leskó M 85
Leverett P 170, 376
Lewis J 79
Lexa J 86
Lezzerini M 176
Li D 344
Li G 331
Li J 31, 184
Li K 131
Li P 50
Li X 199
Li Y 167, 169, 185
Liang X 79, 165
Lightfoot P C 73
Liles D 319
Lima A 256
Lin J 41
Lin L 95
Lin W 155
Link K 280
Linton P 114, 316
Lipinska K 337
Liptai N 51
Litvin Y 225
Litvinenko A 285
Liu D 170, 173
Liu J 41, 66, 166, 167, 169
Liu P 165
Liu R 66
Liu X 399
Lockington J 130
Logue A 6
Lombard A 166, 310
Longridge L 230, 231
Lopez A 202
López-Gómez J 387
Lorenzi A 357
Lothenbach B 308
Lottici P 318
Loubser M 304
Lowers H 87
Loye E 60, 63
Lu A 2, 167, 169, 183, 185, 187
Lu J 83, 184
Lu X 184
Luais B 394, 397
Lucchetti G 156, 187, 159
Luffi P 250
Lührs H 337
Lundgaard K 229
Luque F J 387
Luquot L 151
Lyalina L 329
Lykova I 338
M. R. Neiva A 171, 261
M.V. Coutinho J 372
Ma C 239
MacDonald N 266
Macías F 143
MacNeil L 324
Mádai F 137

Mader D 394, 397, 400
Mäder U 301
Madhusoodhan S 38, 325
Madingoana I 134
Magson J 110
Mahmoud B 80
Maila P 232
Mainza A 115
Majodina O 6
Majzlan J 91, 154, 168, 171, 302
Majzner K 383, 385
Makhubela T 167
Malatji T 236
Malcherek T 376
Maleke M 145
Malferrari D 141
Malkovets V 22, 30, 42
Malsy A 308
Malvoisin B 218
Manaka T 61
Manecki M 164
Manyeruke T 235
Manyeruke T D 233
Mao H 39
Mao Z 41
Maresch W 3, 198, 201, 202
Marescotti P 156, 159, 187
Maria de Lima Correia A 266
Maria Margarete M 368
Marin V 156
Marincea S 71, 81, 262
Mariotti M G 187
Marko L 287, 291
Marschall H 200, 274, 275
Martelat J 280, 281
Martesheva A 96
Martin R 259, 260, 262
Martin T 75
Martínez Abad I 134
Martínez-Frías J 387, 388
Martin-Izard A 92, 93
Martins Pimentel M 207
Martra G 142
Marty J 374
Marzec K 139
Marzoli A 42
Marzouki M 327
Mason P 403, 406
Mason P R D 403
Masschaele B 149, 292, 293
Massonne H 68
Massuyeau M 221, 226
Master S 363, 407
Mata J 42
Mather K 52
Mathian M 317
Mathieu S 278
Matsubara S 328, 343
Matsui T 348, 380
Matsushita Y 331, 343
Mattioli M 91
Matveev S 52
Mauk J 127, 87
May E 379
Mayachar G 219
Mayer F 68
Mayes W 146
Mayr C 407
Mazzei F 156
Mazzoleni P 172, 242, 357
McCall M 295
McCammon C 41, 43
McCarthy T 6
McClelland W 198
McCubbin F 242
McDonald A 104
McDonald I 21, 231, 394, 397
McDonald J 30
McGladrey A 98
McIntyre C 161
McLoughlin A 122
McMillan N 272
McNeill J 27, 52
Medas D 172
Meffre S 402
Mei F 167, 169
Mei Y 101
Meier R 305
Meima J 75, 312

Meisser N 379
Melchakova L 19
Melcher F 58, 109, 259, 287
Melegy A 67
Melgarejo Draper J C 249, 269, 195, 196
Melleton J 256, 288
Mendonça A 128
Meng F 167
Meng L 66
Meng Y 37
Mengel K 335
Ménot R 250
Menzies A 87
Métrich N 241
Meyer F M 409, 273
Meyer H 274
Meyer N 152
Miao M 11
Mibe K 38, 220, 222
Michalik M 168, 356
Migdisova N 211
Mihaly J 51, 55
Mikhail S 32
Mikhno A 246
Miki T 405
Milesi V 218
Miller J 121, 295, 299, 300
Mills S 13, 347, 374
Ming D W 384
Minnaar H 260
Mirabueno M 199
Miranda Figueiro B 11
Mironov A 344
Mirwald P 344
Mishima M 401
Mishra G 123
Misra S 209
Missana T 179
Mitchell R 340
Miura Y 381, 384
Miyahara M 396
Miyajima H 200, 367
Miyake A 343
Miyawaki R 213, 320, 326, 328, 331, 343
Mizutani S 38
Mngomezulu A 369
Modreski P 262
Mogessie A 106
Mohanlal K 118
Mohr-Westheide T 312, 394, 397, 400
Moitsi E 367
Mollai H 83
Molnar F 106, 87
Moloantoa K 146
Momma K 213, 323, 326, 343
Mondillo N 98
Monie P 283
Montegrossi G 163, 186, 242, 334, 335
Monteleone B 49
Montinaro A 403, 406
Montoya P 114, 316
Moore K 59, 196
Moretti S 353
Morgan R 252, 406
Moriyama T 62
Morizet Y 221, 226
Morookian J M 384
Morris R V 384
Morrison S 384
Moser D 393
Mosinyi D 166
Mösser-Ruck R 129
Moszumańska I 239, 385, 386
Moulton B 243
Mouri H 118, 123, 169, 226, 389
MSL Team 384
Mubarok M Z 183
Muedi R 149
Muehlenbachs K 26, 27
Mueller M 68
Mulaba A 134
Mulaba-Bafubiandi A 152
Müller A 254, 260, 261
Müller J 401
Munnik F 117
Munoz M 59, 332
Munteanu M 81, 236
Murashko M 378

Murphy T 170
Musco M 42
Musi L 175
Muszyński A 383, 385
Muzondo T 118
Mxinwa T 226
Nagase T 343
Nagashima M 141
Najorka J 338
Nakai I 328
Nakai S 136
Nakamatsu Y 378
Nakamura E 22, 201
Nakamura Y 325
Nakatsuka A 340
Naraoka H 405
Nardi A 147
Nasdala L 52
Nash B 374
Nasreddinov Z 285
Nazzareni S 43, 91
Ndikumana A 76
Ndongani F 153
Neacsu A 173
Negulescu E 84, 250
Nel A 295
Német C 55
Németh B 55
Németh C 51, 55
Németh N 62
Nespolo M 327
Nestola F 52
Neto B 98
Netterberg F 6
Neumann R 60
Neuville D 243
Newton A 87
Nex P 254
Ngothai Y 131
Nguyen J 317
Ni P 33, 35
Niedermann S 66
Nielsen P 149
Nielsen T F D 233
Nieto F 79, 98
Nieto J 143
Nikandrov A 15
Nikandrov S 15
Nikandrova N 15
Nikonow W 311
Nimis P 361
Ninagawa K 396, 399, 403
Nishida N 348, 380
Nishido H 396, 399, 401
Nishihara Y 44
Nishikubo K 343
Nkomo T 123
Noda K 64, 112
Noell U 75
Novoselov K 92, 96
Nowak S 117
Nowell G 27
Ntsoane T 389
Ntuane P 404
Nuertai M 18
Nyamai C 280, 281
Nziza L 76
Obeid M 209
Oberthür T 78, 105, 109, 259
O'Brien P 219
Ochoa Gutierrez L 58
Ogata T 89
Ogorodova L 19
Ohfuji H 348
Ohgo S 401
Ohi S 343
Ohira I 52
Ohnenstetter D 278, 279, 283
Ohtani E 38, 52, 396
Ojo A 145
Okrugin V 88, 135
Okube M 340
Okuchi T 56
Okujeni C 158
Okunlola O 267
Okuno M 199
O'Leary J 49
Oliveira G 98
Olivier P 269
Olivo G 98

Ona-Nguema G 13
O'Neill H 40
Onoue T 405
Opitz A 156
Orberger B 120, 252, 406
O'Reilly S 26, 50
Origlieri M 375, 339
Orihashi Y 216
Ortega C 388
Ossa Ossa F 126
Ostendorf J 296
Ota T 22, 201
Ottley C 27
Oty U 146
Outrequin M 311
Ouyang B 184
Ovtcharova M 290
Ozawa S 396
P. Pereira V 372
Pacella A 174
Padrones J 64
Page A 230
Pakkanen L 87
Pakovi T 395
Palenova E 96, 344
Pan Y 18
Panetta D 156
Panikorovskii T 332
Paradis S 99
Pardi L A 186
Pardieu V 281
Parisatto M 296
Parsons I 3
Pascoe R 57
Pasero M 375
Passaglia E 141
Passaponti M 186
Patkó L 51, 55
Pattison P 301
Patzschke M 312
Paul T 297
Pavicevic M 66
Pearce C 166
Pearson G 27, 52
Pearson N 50
Pecchioni E 353
Pedro G 267
Peiffer S 146
Pejovic V 66
Pekov I 338, 378
Pendock N 114, 316
Perchiazzi N 176
Perchuk A 222
Percy E 98
Peréz Estébanez M 188
Perito B 186
Pernet-Fisher J 21, 107
Perotto S 177
Perraki M 247
Pertsev A 249
Perucchi A 55
Perugini D 296
Pervov V 196
Pesquera A 265
Pesquera-Perez A 268
Peterson R 319
Petitgirard S 43
Petrikis J 168
Petrishcheva E 339
Pfänder J 237
Philander C 115
Philippo S 330
Piazolo S 29
Pichavant M 132, 270
Piervittori R 177
Pieterse L 76
Pietrzykowska K 358
Pignatelli I 278
Pillay K 115
Pimentel M 224
Pintér Z 51, 55
Pirard E 116, 294, 315, 316, 370
Perugini D 296
Pires A 383, 404
Pischedda V 5, 389
Piskunova N 306
Pivin M 279
Plessen B 277
Ploetze M 8, 56, 161

Podda F 172
Pogge von Strandmann P 200
Pohjolainen E 87
Pokhilenko L 22, 23, 30
Pokhilenko N 22, 23, 30, 70, 170
Poli C 163
Pollastri S 176, 188, 301
Pöllmann H 11, 14, 15, 70, 191, 294, 320, 368
Portella Y 110
Posthumus J 145, 148
Posukhova T 30
Poulton S 408
Prakapenka V 41, 390
Predieri G 357
Prell M 358
Prencipe M 48
Pretorius D 116
Prichard H M 103
Princivalle F 42
Pring A 131
Prins C 118
Prochaska W 409
Proenza J 79, 81, 212
Proyer A 216, 247
Prucek R 144
Pugnaloni A 176
Puhakka E 12
Puhr B 216
Purchase M 111
Purevjav N 56
Putro S 89
Qiao S 31
Qin S 44
Qiu J 179
Quaghebeur M 149
Quartieri S 138, 142, 303, 359
Raic S 106
Raith J 287
Rakgalakane B 113, 305
Ramakoloi N 106
Ramanaidou E 317
Ramboz C 132
Rammlmair D 75, 311, 312
Rampe E B 384
Raneri S 357
Ravna E 218
Recham N 218
Reddy S 108
Redhammer G 320
Reguer S 8
Reid D 114, 149, 152
Reid D L 4
Reimanis I 68
Reimold W U 312, 394, 397, 398, 399, 400, 401
Reinhardt T 370
Reith F 101
Ren M 209
Renno A 117
Renzulli A 91
Rettenwander D 333
Reutsky V 46
Rhede D 250, 251, 277, 332
Richards J 117
Rimoldi B 176
Rimondi V 159, 242, 353
Rinaudo, C 178
Robb L 88, 230
Robert J 210
Robert J-L 16, 17, 19
Roberts J 119
Robinson P 31
Robinson P T 28
Roccotiello E 187
Rocha F 8
Roda-Robles M 268
Roda-Robles M E 265, 267
Rodrigues da Silva T 366
Rodrigues S 368
Rodríguez Ramos R 202
Rodriguez-Losada J 388
Roelofse F 110, 232
Roelofse F 266
Roeser H 368, 363
Roetting T 151
Rogerson M 146
Rollinson G 57
Romanelli M 163, 186, 242, 335
Romer R 27, 232, 233

Roper A 170
Roqué-Rosell J 79
Rose D 118
Rose-Koga E 49
Rossi A 174
Rosso K 166
Rousse G 351
Rozendaal A 76, 77, 115, 127
Rubat du Merac M 68
Ruby C 13
Rumsey M 375
Russell S 385
Ryabov V 107
Rybacki E 251
Sabatino G 359
Săbău G 84, 250
Sadek Ghabrial D 210
Safonov O 24, 223, 227, 244
Saing S 94
Sakamaki T 38, 52
Sakamoto R 404
Salama W 315
Salge T 312, 397, 394
Salmona P 156
Samecka-Cymerman A 358
Samoylovich M 32
Sánchez-Muñoz L 262, 351
Sándorné Kovács J 51
Sanematsu K 61
Sanguineti E 150, 175
Sano Y 205, 405
Santana M 77
Santoro L 99
Santos A 171
Santos R 64, 112
Sanwani E 183
Sanz J 16, 351
Sarafian A 274
Šarić K 355
Sarrazin P C 384
Sato A 331
Sato T 181
Saul J M 284
Sauzeat L 192
Scancarello G 163
Schaeffer A-K 339
Schaltegger U 290
Schampera B 9
Schannor M 233, 235
Scharf O 117
Scharneck Y 113
Schaub P 301
Schersten A 89
Schertl H 198, 201, 248
Schertl H-P 202, 275
Schlüter J 376
Schmahl W W 303
Schmidt C 36
Schmitt A 31, 393
Schmitt R 394
Schmitt RT 397, 401
Schmitz S 52
Schneider H 335, 337
Schnellrath J 280
Schöler A 303
Scholten L 36
Scholz R 262, 280, 378
Schopf A 68
Schouwstra R 118, 119
Schulz T 394, 397
Schuster R 216
Schwarz D 280
Schwarz-Schampera U 77, 78, 197
Sciberras M 376
Scott T 75
Seabra Gome A 289
Secco M 189
Seenivasan K 7
Seifert T 291
Sekine T 396
Selivanova E 324
Senzani F 152
Seppala A 12
Setiawan I 65
Seto Y 44
Severson M 106
Seydoux-Guillaume A-M 286
Shafei B 147
Shah M T 253
Shahab A 9

Shanina S 306
Sharma V 144
Sharygin V 139
Shaybekov R 111
Shcherbakova E 15
Shelembe R 169
Shi G 202
Shi L 166
Shi Z 166
Shibazaki Y 39
Shimaki Y 201
Shimizu M 348
Shinjoe H 214
Shipman W 295
Shirose Y 268, 314
Shiryaev A 24, 244
Shtenberg M 344
Shu Q 20, 25
Shur M 222
Siad A 158
Siahi M 407
Sibley S 29
Sieber M 31
Siegesmund S 360
Sigalas J 5, 389
Siidra O 328, 376
Silva D 256
Silva M 171
Silversmit G 52
Simmons W 257, 260, 255, 258
Simon K 383, 385
Simon P 254
Simon V 358
Simonson B 397
Singh M 185
Sinmyo R 43
Sisson V 208
Sitnikova M 58, 78, 259
Sizaret S 97, 132
Sizun J 6
Skála R 382
Skoda R 262
Skogby H 53, 54, 337
Skvortsova V 32
Slaby E 244, 383, 385, 386
Slezak P 98
Smart K 27
Smit K 25, 282
Smith B 119, 217
Smith C 312
Smith D 295
Snegirev O 70
Snyman Q 118
Sobolev A 39, 211, 310
Sobolev N 4, 21
Sobrados I 16, 351
Soderlund U 288
Sokerina N 306
Sokolova E 346, 352
Sokolova M 30
Solc R 9
Soler J 150
Soler J M 151
Solimano M 156
Söllradl S 335
Song C A 160
Song W 160
Sorokina E 285
Soufek M 84, 262, 264
Southworth R 32
Souvignier B 327
Spanovich N 384
Spasevski L 84
Speich L 202
Spetsius Z 26
Spicer E 113, 304
Spieß I 336
Spigo U 359
Spratt J 340, 375
Srikantappa C 34
Stachel T 25, 26
Stagno V 39, 390
Stalder R 53, 211, 213, 342
Stanley C 104
Stausberg N 403
Steenfelt A 27
Smith D 295
Steenkamp N C 119
Steinhardt P 39
Stengel I 6, 389

Stern R 25, 282
Stöber S 320
Stock M 230
Stolper E M 384
Stone N 383
Storey C 248, 272, 273, 275
Storme J-Y 407
Stracke A 27
Straker C 389
Strauss H 403, 406
Stricker K 68
Stubbs J 161
Su H 10, 11, 158
Subias I 133, 135
Sugiyama K 320
Sushchevskaya N 211
Suzuki A 353
Sverjensky D 164, 404
Sweetapple M 94
Swinden S 60, 63
Sýkorová I 67
Szabó C 51, 55
Szakáll S 62, 136, 137, 165
T.M.M. Ferron J 372
Tabacchi G 138
Tagle R 312, 394, 397, 400
Tahara T 323
Tait K 364, 390, 393
Takács Á 87
Takada M 343
Takahashi N 343
Takahashi R 64, 65, 89, 94, 95
Takahata N 405
Takamasa A 136
Takashi Y 41
Tan D 170, 173
Tan W 79
Tang C 162
Tange Y 39
Tanhua-Tyrkkö M 12
Tani K 64
Tappe S 27
Tappert R 342
Tarchi M 163
Tatarinova D 223
Tauler E 79
Taupin V 45
Taylor L 21, 107
Tegner C 229
Tessadri R 321
Thalhammer O 110
Theron S 117, 275
Thomas R 260
Thu K 198
Tibane V 153
Tikhonova V 335
Tillmanns E 323
Tindell T 89
Titkov S 24
Többens D 336
Toerien R 371
Tomasic N 262, 264
Tomatis M 177
Tomioka N 56, 396
Tonzetic I 306, 313
Topa B 85
Topolska J 164
Török K 55
Torres E 147
Tosca N 387
Totsche K 162
Tourigny G 89
Toyoda S 136
Toyoshima T 325
Tranberg J 104
Trapanati A 298
Trcera N 59
Tredoux M 110, 111, 212
Treiman A H 384
Treloar P 90
Trincal V 332
Troll V 54
Trubač J 74
Trubkin N 103
Trumbull R 31, 273
Tsikos H 125, 341
Tsuchiya J 47
Tsuchiya T 47
Tsuchiya Y 401
Tsuchiyama A 186

Tsujimori T 201, 204
Tsujino N 44
Tsunogae T 227, 228
Tsutsui S 38
Tuček J 144, 377
Tudryn A 252
Tuersun M 18
Tunega D 9
Turbanti I 354
Turchiano M 354
Turci F 174, 177
Tychkov N 70
Uchida A 136
Uehara S 268, 314
Uenver-Thiele L 40, 41
Uher P 86
Ujihara H 64
Ulmer P 56
Upton B 21
Usuki T 203
Utsunomiya S 378
Uvarova Y 307
Vacarro E 385
Váczi T 85, 87, 215
Vafeas N 217
Valentini L 189, 191, 296
Valizer P 15
Valley J 198
Valter M 56
van Blerk J 6
Van Cappellen P 147
Van Deventer J 190
van Heerden E 144, 145, 146, 148
Van Hoorebeke L 292
Van Lichtervelde M 269, 287
van Reenen D 223, 224, 227, 228
van Rooy L 6
van Smaalen S 336
van Westrenen W 392
Vance D 408
Vander Kaaden K 242
Vanhanen E 87
Vaniman D T 384
Vapnik Y 377, 378
Vasilyev P 40
Vavilov M 30
Vekemans B 52
Veksler I 233, 235, 236
Vercamer V 352
Verchovsky A 32
Verplanck P 143
Verryn S 304, 307
Vettori S 353
Vezzalini M 138, 141, 142
Viani A 188
Vidal O 126
Viereck L 171, 237
Vigasina M 19
Vigh T 85
Vigliaturo R 178
Viljoen F 106, 116, 118, 119, 120, 122, 123, 125, 226
Villa I 291, 361
Villanova-de-Benavent C 79, 81, 212
Villaros A 256, 270
Vincze L 52
Vitillo J 142
Voegelin A 168
Vojtko P 218
Voltolini M 296
Vroon P 392, 403, 404
Vroon P Z 403
Všianský D 72
Vukmanovic Z 108
Vymazalová A 103
Wabo H 288
Wade B 130
Walde D 128
Wall F 57, 59, 60, 61, 63, 195, 196
Walle M 81, 86
Walliser A 117
Wamunyu A 280, 281
Voltolini M 296
Wan M 146
Wang C 79, 167, 169
Wang F 398
Wang G 33, 35
Wang H 18, 185, 187
Wang J 133
Wang L 69, 336

Wang M 236
Wang R 83, 184, 263
Wang T 33
Wang W 278, 282, 283
Wang X 33
Wang Y 364
Wang Z 166
Wangler T 360, 9
Wansbury N 102
Wanty R 143
Watanabe K 89, 93
Watanabe Y 61, 62
Watenphul A 36
Waychunas G 161, 301
Webber K 255, 258
Wedekind W 360
Wei H 95
Wei J 162
Weis F 54
Weiss S 180
Weiss Y 27
Weist A 185
Weiszburg T 85, 215
Welch M 338, 340, 375, 376
Wells M 317
Wessels M 161
Westenberger P 297
Westraad J 5
Whitehouse M 207, 403
Widmer R 308, 379
Wieczorek A 162
Wiedenbeck M 90, 273
Wieland E 301
Wierzbicka-Wieczorek M 321
Wiesmaier S 233
Wilczynska-Michalik W 168, 356
Williams P 145, 170, 350, 376
Wilson A 229, 236, 289, 290
Wilson M A 384
Wilson R 229
Windisch W 365
Wing B 403
Winnefeld F 308
Wirth R 109, 252, 271, 385, 386, 395, 396, 250
Wise M 260
Wittwer A 326
Witzke T 157, 308, 324
Wong Y 132
Woodland A 40, 41
Woodman J 99
Woodruff L 127
Wörner G 240
Wu I C 158
Wu S 181, 182
Wu X 41, 44, 95
Wu Z 44
Wunder B 219, 271, 277
Wünnemann K 399
Xavier P S 365
Xia D 44
Xia Q 50
Xiao Y 41
Xie X 69, 398
Xing H 10
Xinhue G 353
Xiong F 239
Xiong M 331
Xu H 309
Xu J 95
Xu X 155
Xu X Z 28
Yablokova D 135
Yakovenchuk V 324
Yamaguchi K 314, 405
Yang D 66
Yang G 331
Yang H 339
Yang J 31, 239
Yang J S 28
Yang L 364
Yang X 185, 187
Yang Z 160, 326
Yao Y 236
Yapaskurt V 223, 333
Yaxley G 40
Ye Q 364
Yen A S 384
Yilmaz T 35
Yin R, Zhang A 263

Yonezu K 64, 89, 122
Yoshiasa A 320, 340
Yoshida E 401
Yoshikawa M 199
Yoshino T 38
Youbi N 42
Youlton B 124, 310
Yu W 173
Yuan G 158
Yuan P 170, 173
Yuan W 173
Yudovskaya M 104, 234
Yui T 203, 252
Yupaskurt V 222
Yurimoto H 51
Zabotina M 96
Zaccarini F 82, 91, 109, 110
Zacher G 297
Zack T 276
Zaczek-Pedroza K 54
Zagorsky V 262
Zajzon N 62, 136, 137, 165, 215
Zaw K 61
Zbořil R 144, 382
Zeh A 238, 274, 289, 290
Zhai S 398
Zhang B 10, 11, 158
Zhang L 344
Zhang R 83
Zhang Z 20
Zhang Zh M 28
Zhao C 35
Zhao J 131
Zhao R 133
Zhao W 169
Zhao Z 158
Zhitova E 329
Zhong Y 79
Zhou Q 162
Zhu J 162
Zhu T 184
Zhu Y 185, 342
Ziegenrücker R 117
Ziegler A 389
Ziemann M 219
Zinner E 389
Zoleo A 163
Zolotarev A 329, 330, 332, 338
Zotti M 187
Zubkova N 338
Zucchini A 48, 340
Zudin N 24